

36 Copin



SATURN

MPR-SAT-FE-68-3

JUNE 25, 1968

(NASA-TM-X-61038) SATURN V LAUNCH VEHICLE
FLIGHT EVALUATION REPORT: AS-502 APOLLO 6
MISSION (NASA) 637 6

478-79430

Unclass
00/15 025707

SATURN V LAUNCH VEHICLE FLIGHT EVALUATION REPORT-AS-502 APOLLO 6 MISSION

FACILITY FORM 602

[REDACTED] (ACCESSION NUMBER) _____ (THRU) _____

637 (PAGES) _____ 20 (CODE) _____

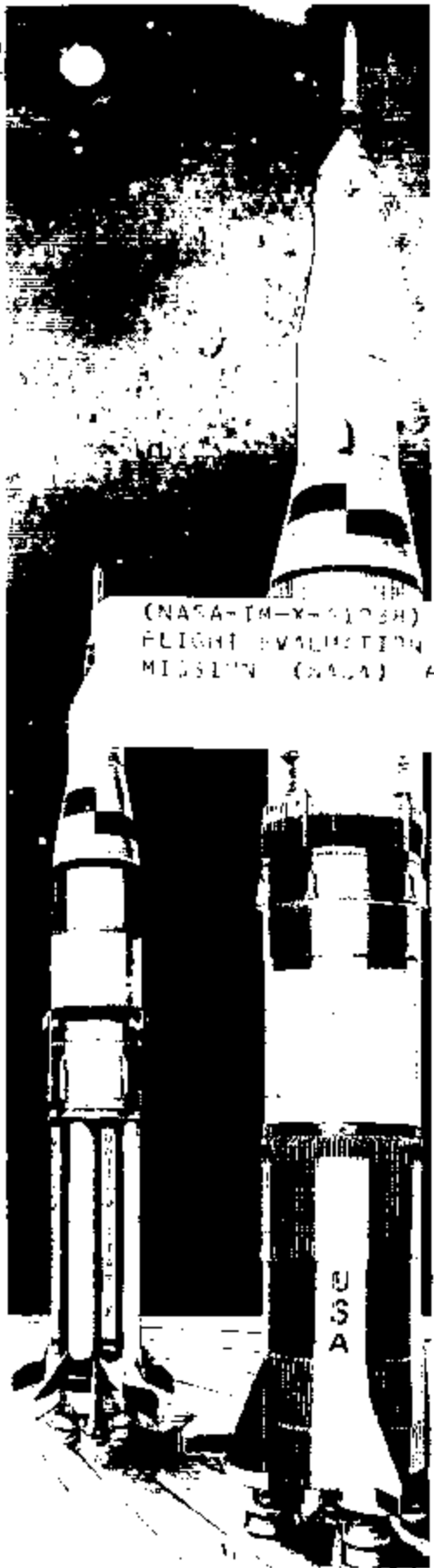
TMX-61038 (NASA CR OR TMX OR AD NUMBER) _____ 3 (CATEGORY)

[REDACTED]

PREPARED BY
SATURN V FLIGHT EVALUATION WORKING GROUP



NATIONAL AERONAUTICS AND SPACE ADMINISTRATION



;

1

30 Copies

GEORGE C. MARSHALL SPACE FLIGHT CENTER

MPR-SAT-FE-68-3

**SATURN V LAUNCH VEHICLE
FLIGHT EVALUATION REPORT - AS-502
APOLLO 6 MISSION**

**PREPARED BY
SATURN V FLIGHT EVALUATION WORKING GROUP**



AS-502 Launch Vehicle

MPR-SAT-FE-68-3

SATURN V LAUNCH VEHICLE FLIGHT EVALUATION REPORT - AS-502
APOLLO 6 MISSION

BY

Saturn Flight Evaluation Working Group
George C. Marshall Space Flight Center

ABSTRACT

Saturn V AS-502 (Apollo 6 Mission) was launched at 07:00:01 Eastern Standard Time on April 4, 1968, from Kennedy Space Center, Complex 39, Pad A. The vehicle lifted off on schedule on a launch azimuth of 90 degrees east of north and rolled to a flight azimuth of 72 degrees east of north.

The actual trajectory parameters of the AS-502 were close to nominal until the premature shutdown of two engines in the S-II stage. After this occurred, the trajectory deviated significantly from the nominal throughout the remainder of the mission.

Nine of the sixteen primary objectives of this mission were completely accomplished, six partially accomplished, and one (S-IVB restart) was not accomplished. One of the two secondary objectives was completely accomplished, and one partially accomplished.

Any questions or comments pertaining to the information contained in this report are invited and should be directed to:

Director, George C. Marshall Space Flight Center
Huntsville, Alabama 35812
Attention: Chairman, Saturn Flight Evaluation
Working Group, R-AERO-F (Phone 876-4575)

TABLE OF CONTENTS

Section		Page
	TABLE OF CONTENTS	iii
	LIST OF ILLUSTRATIONS	xiii
	LIST OF TABLES	xxvii
	ACKNOWLEDGEMENT	xxxii
	ABBREVIATIONS	xxxiii
	MISSION PLAN	xxxvi
	FLIGHT TEST SUMMARY	xxxviii
1	INTRODUCTION	
	1.1 Purpose	1-1
	1.2 Scope	1-1
2	EVENT TIMES	
	2.1 Summary of Events	2-1
	2.2 Sequence of Events	2-2
3	LAUNCH OPERATIONS	
	3.1 Summary	3-1
	3.2 Prelaunch Milestones	3-1
	3.3 Countdown Events	3-1
	3.4 Propellant Loading	3-4
	3.4.1 RP-1 Loading	3-4
	3.4.2 LOX Loading	3-4
	3.4.3 LH ₂ Loading	3-5
	3.4.4 Auxiliary Propulsion System Propellant Loading	3-5

TABLE OF CONTENTS (CONTINUED)

Section		Page
	3.4.5 S-IC Stage Propellant Load	3-6
	3.4.6 S-II Stage Propellant Load	3-6
	3.4.7 S-IVB Stage Propellant Load	3-6
	3.5 S-II Insulation Purge and Leak Detection	3-8
	3.6 Ground Support Equipment	3-8
4	TRAJECTORY	
	4.1 Summary	4-1
	4.2 Tracking Data Utilization	4-2
	4.2.1 Tracking During the Ascent Phase of Flight	4-2
	4.2.2 Tracking During Orbital Flight	4-2
	4.3 Trajectory Evaluation	4-3
	4.3.1 Ascent Trajectory	4-3
	4.3.2 Orbital Trajectory	4-8
5	S-IC PROPULSION	
	5.1 Summary	5-1
	5.2 S-IC Ignition Transient Performance	5-2
	5.3 S-IC Main Stage Performance	5-5
	5.4 S-IC Engine Shutdown Transient Performance	5-7
	5.5 S-IC Stage Propellant Management	5-10
	5.6 S-IC Pressurization System	5-10
	5.6.1 S-IC Fuel Pressurization System	5-10
	5.6.2 S-IC LOX Pressurization System	5-14
	5.7 S-IC Pneumatic Control Pressure System	5-14
	5.8 S-IC Purge System	5-16
	5.9 S-IC Camera Ejection and Purge System	5-16
6	S-II PROPULSION	
	6.1 Summary	6-1
	6.2 S-II Chillover and Buildup Transient Performance	6-2

TABLE OF CONTENTS (CONTINUED)

Section		Page
6.3	S-II Main Stage Performance	6-9
6.4	S-II Stage Shutdown Transient Performance	6-19
6.5	S-II Propellant Management	6-22
6.6	S-II Pressurization Systems	6-26
6.6.1	S-II Fuel Pressurization System	6-29
6.6.2	S-II LOX Pressurization System	6-30
6.7	S-II Pneumatic Control Pressure System	6-34
6.8	Camera Ejection System	6-35
6.9	Helium Injection System	6-35
7	S-IVB PROPULSION	
7.1	Summary	7-1
7.2	S-IVB Chilldown and Buildup Transient Performance for First Burn	7-2
7.3	S-IVB Main Stage Performance for First Burn	7-4
7.4	S-IVB Shutdown Transient Performance for First Burn	7-11
7.5	S-IVB Coast Phase Conditioning	7-11
7.6	S-IVB Chilldown and Attempted Restart for Second Burn	7-15
7.7	S-IVB Main Stage Performance for Second Burn	7-28
7.8	S-IVB Shutdown Transient Performance for Second Burn	7-28
7.9	S-IVB Stage Propellant Utilization	7-28
7.10	S-IVB Pressurization System	7-34
7.10.1	S-IVB LiF ₂ Tank Pressurization System	7-34
7.10.2	S-IVB LOX Pressurization System	7-39
7.11	S-IVB Pneumatic Control System	7-50
7.12	S-IVB Auxiliary Propulsion System	7-51

TABLE OF CONTENTS (CONTINUED)

Section		Page
8	HYDRAULIC SYSTEMS	
	8.1 Summary	8-1
	8.2 S-IC Hydraulic System	8-2
	8.3 S-II Hydraulic System	8-2
	8.4 S-IVB Hydraulic System (First Burn)	8-9
	8.5 S-IVB Hydraulic System (Coast Phase)	8-12
	8.6 S-IVB Hydraulic System (Second Burn)	8-12
9	STRUCTURES	
	9.1 Summary	9-1
	9.2 Total Vehicle Structures Evaluation	9-2
	9.2.1 Longitudinal Loads	9-2
	9.2.2 Bending Moments	9-5
	9.2.3 Vehicle Dynamic Characteristics	9-8
	9.2.4 S-IC Fin Dynamics	9-17
	9.3 Vibration Evaluation	9-19
	9.3.1 S-IC Stage and Engine Evaluation	9-19
	9.3.2 S-II Stage and Engine Evaluation	9-29
	9.3.3 S-IVB Stage and Engine Evaluation	9-35
	9.3.4 S-IVB Stage Forward Skirt Dynamics	9-39
	9.3.5 Instrument Unit Evaluation	9-41
9A	133 SECOND TRANSIENT	
	9A.1 Summary	9A-1
	9A.2 Instrument Unit	9A-1
	9A.2.1 Mechanical Versus Electrical Disturbance	9A-2
	9A.2.2 Pressure, Flowrate, and Temperature Measurements	9A-10
	9A.2.3 Radio Frequency (RF) Measurements	9A-13
	9A.2.4 ST-124M-3 Stabilized Platform Subsystem and Control Subsystem Analysis	9A-13
	9A.2.5 Structures and Dynamics	9A-15
	9A.3 S-IVB Stage	9A-15
	9A.4 S-II Stage	9A-22
	9A.5 RF Systems	9A-22

TABLE OF CONTENTS (CONTINUED)

Section		Page
	9A.6 Emergency Detection System (EDS)	9A-22
10	GUIDANCE AND NAVIGATION	
	10.1 Summary	10-1
	10.1.1 Flight Program	10-1
	10.1.2 Instrument Unit Components	10-1
	10.2 Guidance and Navigation System Description	10-2
	10.2.1 Instrument Unit System Description	10-2
	10.2.2 Flight Program Description	10-2
	10.3 Guidance Intelligence Errors	10-7
	10.4 Navigation and Guidance Scheme Evaluation	10-9
	10.4.1 Inertial Platform and Navigation Parameter Comparisons	10-9
	10.4.2 Flight Program Evaluation	10-10
	10.4.3 Orbital Guidance	10-17
	10.4.4 Orbital Routines	10-20
	10.4.5 Event Sequencing	10-20
	10.5 Guidance System Component Evaluation	10-20
	10.5.1 LVDC Performance	10-20
	10.5.2 LVDA Performance	10-20
	10.5.3 Ladder Outputs	10-21
	10.5.4 Telemetry Outputs	10-21
	10.5.5 Discrete Outputs	10-21
	10.5.6 Switch Selector Functions	10-21
	10.5.7 ST-124M-3 Inertial Platform Performance	10-21
11	CONTROL SYSTEM	
	11.1 Summary	11-1
	11.2 Control System Description	11-2
	11.3 S-IC Control System Evaluation	11-3
	11.3.1 Liftoff Clearances	11-5
	11.3.2 S-IC Flight Dynamics	11-8
	11.4 S-II Control System Evaluation	11-25
	11.4.1 Attitude Control Dynamics and Stability	11-25
	11.4.2 Liquid Propellant Dynamics and Their Effects on Flight Control	11-33

TABLE OF CONTENTS (CONTINUED)

Section		Page
11.5	S-IVB Control System Evaluation	11-36
11.5.1	S-IVB Control System Evaluation Before and During First Burn	11-36
11.5.2	Control System Evaluation During Parking Orbit	11-45
11.5.3	Control System Evaluation During Restart Attempt	11-54
11.5.4	Control System Evaluation After Restart Attempt	11-54
11.6	Instrument Unit Control Components Evaluation	11-58
11.6.1	Control-EDS Rate Gyros/Control Signal Processor Analysis	11-58
11.6.2	Flight Control Computer Analysis	11-58
12	SEPARATION	
12.1	Summary	12-1
12.2	S-IC/S-II Separation Evaluation	12-3
12.2.1	S-IC Retro Motor Performance	12-3
12.2.2	S-II Ullage Motor Performance	12-3
12.2.3	S-IC/S-II Separation Dynamics	12-3
12.3	S-II Second Plane Separation Evaluation	12-7
12.4	S-II/S-IVB Separation Evaluation	12-14
12.4.1	S-II Retro Motor Performance	12-14
12.4.2	S-IVB Ullage Motors	12-15
12.4.3	S-II/S-IVB Separation Dynamics	12-15
12.5	S-IVB/IU/Spacecraft Separation Evaluation	12-21
13	ELECTRICAL NETWORKS	
13.1	Summary	13-1
13.2	S-IC Stage Electrical System	13-2
13.3	S-II Stage Electrical System	13-5
13.4	S-IVB Stage Electrical System	13-9
13.5	Instrument Unit Electrical System	13-15

TABLE OF CONTENTS (CONTINUED)

Section		Page
14	RANGE SAFETY AND COMMAND SYSTEMS	
	14.1 Summary	14-1
	14.2 Range Safety Command Systems	14-1
	14.3 Command and Communications System	14-2
15	EMERGENCY DETECTION SYSTEM	
	15.1 Summary	15-1
	15.2 System Description	15-1
	15.3 System Evaluation	15-1
	15.3.1 General Performance	15-1
	15.3.2 Propulsion System Sensors	15-3
	15.3.3 Flight Dynamics and Control Sensors	15-3
	15.3.4 EDS Sequential Events	15-5
	15.4 Interface Considerations	15-5
16	VEHICLE PRESSURE AND ACOUSTIC ENVIRONMENT	
	16.1 Summary	16-1
	16.2 Surface Pressures and Compartment Venting	16-1
	16.2.1 S-IC Stage	16-1
	16.2.2 S-II Stage	16-5
	16.2.3 S-IVB Stage	16-9
	16.3 Base Pressures	16-12
	16.3.1 S-IC Base Pressures	16-12
	16.3.2 S-II Base Pressures	16-12
	16.4 Acoustic Environment	16-19
	16.4.1 External Acoustics	16-19
	16.4.2 Internal Acoustics	16-20
17	VEHICLE THERMAL ENVIRONMENT	
	17.1 Summary	17-1
	17.2 S-IC Base Heating and Separation Environment	17-1
	17.2.1 S-IC/S-II Separation	17-8

TABLE OF CONTENTS (CONTINUED)

Section		Page
	17.3 S-II Base Heat Shield and Separation Environment	17-11
	17.4 S-II/S-IVB Separation Environment	17-22
	17.5 Vehicle Aeroheating Thermal Environment	17-23
	17.5.1 S-IC Stage Aeroheating Environment	17-23
	17.5.2 S-II Stage Aeroheating Environment	17-33
	17.5.3 S-IVB Stage Aeroheating Environment	17-36
	17.5.4 Instrument Unit Aeroheating Environment	17-39
	17.6 Vehicle Orbital Heating Environment	17-42
	17.6.1 S-IVB Orbital Heating	17-42
	17.6.2 IU Orbital Heating	17-46
18	ENVIRONMENTAL CONTROL SYSTEM	
	18.1 Summary	18-1
	18.2 S-IC Environmental Control	18-1
	18.3 S-II Environmental Control	18-7
	18.4 S-IVB Environmental Control	18-11
	18.4.1 Ascent Powered Flight Phase	18-11
	18.4.2 Parking Orbit Phase	18-12
	18.5 IU Environmental Control	18-13
	18.5.1 Thermal Conditioning System	18-15
	18.5.2 Gas Bearing Supply System	18-21
19	DATA SYSTEMS	
	19.1 Summary	19-1
	19.2 Vehicle Measurements Evaluation	19-1
	19.2.1 S-IC Stage Measurement Analysis	19-2
	19.2.2 S-II Stage Measurement Analysis	19-4
	19.2.3 S-IVB Stage Measurement Analysis	19-6
	19.2.4 Instrument Unit Measurement Analysis	19-6
	19.3 Airborne Telemetry Systems	19-6
	19.3.1 S-IC Stage Telemetry System	19-14
	19.3.2 S-II Stage Telemetry System	19-16
	19.3.3 S-IVB Stage Telemetry System	19-16
	19.3.4 Instrument Unit Telemetry System	19-17

TABLE OF CONTENTS (CONTINUED)

Section		Page
	19.4 Airborne Tape Recorders	19-17
	19.4.1 S-IC Stage Recorder	19-17
	19.4.2 S-II Stage Recorders	19-17
	19.4.3 S-IVB Stage Recorder	19-20
	19.4.4 Instrument Unit Recorder	19-20
	19.5 RF Systems Evaluation	19-21
	19.5.1 Telemetry Systems RF Propagation Evaluation	19-21
	19.5.2 Tracking Systems RF Propagation Evaluation	19-24
	19.5.3 Command Systems RF Evaluation	19-28
	19.5.4 Television Propagation Evaluation	19-31
	19.6 Optical Instrumentation	19-31
	19.6.1 Onboard Cameras	19-31
	19.6.2 Ground Engineering Cameras	19-32
20	VEHICLE AERODYNAMIC CHARACTERISTICS	
	20.1 Summary	20-1
	20.2 Vehicle Axial Force Characteristics	20-1
	20.3 Vehicle Static Stability	20-4
	20.4 Fin Pressure Loading	20-4
21	MASS CHARACTERISTICS	
	21.1 Summary	21-1
	21.2 Mass Evaluation	21-1
22	MISSION OBJECTIVES ACCOMPLISHMENT	22-1
23	FAILURES, ANOMALIES AND DEVIATIONS	
	23.1 Summary	23-1
	23.2 System Failures and Anomalies	23-1
	23.3 System Deviations	23-1

TABLE OF CONTENTS (CONTINUED)

Section		Page
24	SPACECRAFT SUMMARY	
24.1	Summary	24-1
24.2	Spacecraft Performance Evaluation	24-1
Appendix		
A	ATMOSPHERE	
A.1	Summary	A-1
A.2	General Atmospheric Conditions at Launch Time	A-1
A.3	Surface Observations at Launch Time	A-1
A.4	Upper Air Measurements	A-1
A.4.1	Wind Speed	A-1
A.4.2	Wind Direction	A-2
A.4.3	Pitch Wind Component	A-2
A.4.4	Yaw Wind Component	A-2
A.4.5	Component Wind Shears	A-3
A.5	Thermodynamic Data	A-3
A.5.1	Temperature	A-3
A.5.2	Pressure	A-3
A.5.3	Density	A-4
A.5.4	Optical Index of Refraction	A-4
A.6	Comparison of Selected Atmospheric Data for all Saturn Launches	A-4
B	AS-502 VEHICLE DESCRIPTION	
B.1	Summary	B-1
B.2	S-IC Stage	B-1
B.2.1	S-IC Configuration	B-1
B.3	S-II Stage	B-5
B.3.1	S-II Configuration	B-5
B.4	S-IVB Stage	B-9
B.4.1	S-IVB Configuration	B-9
B.5	IU	B-12
B.5.1	IU Configuration	B-12
B.6	Spacecraft	B-14
B.6.1	Spacecraft Configuration	B-14

LIST OF ILLUSTRATIONS

Figure		Page
4-1	Ascent Trajectory Position Comparison	4-4
4-2	Ascent Trajectory Earth-Fixed Velocity Comparison	4-5
4-3	Ascent Trajectory Space-Fixed Velocity Comparison	4-6
4-4	Ascent Trajectory Acceleration Comparison	4-7
4-5	Dyanmic Pressure and Mach Number Versus Range Time	4-8
4-6	AS-502 Acceleration Due to Venting	4-9
4-7	AS-502 Ground Track	4-11
5-1	S-IC Start Box Requirements	5-3
5-2	S-IC Engine Buildup Transients	5-4
5-3	S-IC Steady State Operation	5-6
5-4	S-IC Engine Shutdown Transient Performance	5-9
5-5	S-IC Fuel Ullage Pressure During Countdown	5-12
5-6	S-IC Fuel Ullage Pressure During Boost	5-13
5-7	S-IC Helium Bottle Pressure for Fuel Pressurization	5-13
5-8	S-IC LOX Ullage Pressure	5-15
5-9	S-IC Pneumatic Control Regulator Outlet Pressure	5-17
5-10	S-IC Control Sphere Pressure	5-17
5-11	S-IC Camera Ejection System	5-18
5-12	S-IC Predicted Camera Ejection and Purge Sphere Pressure	5-19
6-1	S-II LH ₂ and LOX Recirculation Systems	6-3
6-2	S-II Thrust Chamber Temperature	6-4
6-3	S-II Engine Start Tank Performance	6-5
6-4	S-II Start Box Requirements	6-7
6-5	S-II LH ₂ and LOX Recirculation System Performance	6-8
6-6	S-II Engine Thrust Buildup	6-10

LIST OF ILLUSTRATIONS (CONTINUED)

Figure		Page
6-7	S-II Steady State Operation	6-13
6-8	S-II J-2 Engine Diagram	6-16
6-9	S-II Injector after 28 Second Test at High ASI Mixture Ratio	6-16
6-10	S-II Engine No. 2 Performance Shift	6-17
6-11	S-II Engine No. 2 Cutoff Performance	6-18
6-12	S-II Engine No. 2 Gas Generator Performance at Shutdown	6-20
6-13	S-II Engine No. 3 Performance at Shutdown	6-21
6-14	S-II Engine Shutdown Transient	6-23
6-15	S-II Stage Thrust Decay	6-23
6-16	S-II Stage PU Valve Position	6-24
6-17	S-II LOX Probe/Tank Mismatch	6-27
6-18	S-II LH ₂ Probe/Tank Mismatch	6-27
6-19	S-II Mass at Ignition and Cutoff	6-28
6-20	S-II Fuel Tank Ullage Pressure	6-29
6-21	S-II Fuel Pump Inlet Conditions	6-31
6-22	S-II LOX Tank Ullage Pressure	6-32
6-23	S-II LOX Pump Inlet Conditions	6-33
6-24	S-II Recirculation Valves Receiver and Regulator Outlet Pressures	6-34
6-25	S-II Camera Ejection Pressures	6-36
7-1	S-IVB Start Box and Run Requirements - First Burn	7-3
7-2	S-IVB Thrust Chamber Temperature - First Burn	7-5
7-3	S-IVB Start Tank Performance	7-6
7-4	S-IVB Buildup Transient - First Burn	7-7
7-5	S-IVB Steady State Performance - First Burn	7-8
7-6	S-IVB Shutdown Transient Performance - First Burn	7-12
7-7	S-IVB CVS Performance - Coast Phase	7-13
7-8	S-IVB Ullage Conditions - Coast Phase	7-14

LIST OF ILLUSTRATIONS (CONTINUED)

Figure		Page
7-9	S-IVB Engine Start Tank Temperature and Pressure - Coast Phase	7-16
7-10	S-IVB Start Box and Run Requirements - Restart Attempt	7-17
7-11	S-IVB Thrust Chamber Chilledown Performance - Restart Attempt	7-18
7-12	S-IVB Start Tank Pressure - Restart Attempt	7-19
7-13	S-IVB Engine Control Helium Sphere Pressure - Restart Attempt	7-20
7-14	S-IVB Fuel Turbine Inlet Temperature - Restart Attempt	7-21
7-15	S-IVB GG Chamber Pressure - Restart Attempt	7-22
7-16	S-IVB Engine Environmental Charges During J-2 Engine Anomaly	7-24
7-17	S-IVB Environmental Conditions During J-2 Performance Shift	7-25
7-18	S-IVB Summary of Environment Effects	7-26
7-19	S-IVB Pumps Performance During Restart Attempt	7-27
7-20	S-IVB J-2 Engine ASI Schematic	7-29
7-21	S-IVB J-2 Engine Injector Schematic	7-29
7-22	S-IVB PU Mass Sensor Volumetric Nonlinearity	7-31
7-23	S-IVB Ignition and Cutoff Best Estimate Mass* - First Burn	7-32
7-24	S-IVB PU Valve Positions - First Burn	7-33
7-25	S-IVB LOX Coarse and Fine Mass Data	7-34
7-26	S-IVB Servo Bridge	7-35
7-27	Failure Modes of S-IVB PU Probes	7-35
7-28	S-IVB LH ₂ Ullage Pressure - First Burn and Orbit	7-37
7-29	S-IVB LH ₂ Ullage Pressure - Restart Attempt	7-38
7-30	S-IVB Fuel Pump Inlet Conditions - First Burn	7-40
7-31	S-IVB Fuel Pump Inlet Conditions - Restart Attempt	7-41

LIST OF ILLUSTRATIONS (CONTINUED)

Figure		Page
7-32	S-IVB LOX Tank Ullage Pressure - First Burn and Orbit	7-42
7-33	S-IVB LOX Tank Ullage Pressure - Restart Attempt	7-44
7-34	S-IVB LOX Pump Inlet Conditions - First Burn	7-46
7-35	S-IVB LOX Pump Inlet Conditions - Restart Attempt	7-47
7-36	S-IVB Cold Helium Supply Decay	7-48
7-37	S-IVB Cold Helium Pressurization Schematic	7-49
7-38	S-IVB Pneumatic Control Performance - First Burn	7-52
7-39	S-IVB Pneumatic Control Performance - Coast Phase	7-53
7-40	S-IVB Pneumatic Control Performance - Restart Attempt	7-54
7-41	S-IVB APS Propellant Predictions - Module No. 1	7-56
7-42	S-IVB APS Propellant Predictions - Module No. 2	7-56
7-43	S-IVB Helium Bottle Pressure - Module No. 1	7-58
7-44	S-IVB Helium Bottle Pressure - Module No. 2	7-58
7-45	S-IVB Chamber Pressure, APS Engine No. 2 - Module No. 2	7-59
8-1	S-IC Hydraulic System Performance	8-3
8-2	S-II Hydraulic System Performance	8-5
8-3	S-II Engines No. 2 and 3 Hydraulic System Temperature	8-6
8-4	S-II Engine No. 2 Actuator Forces	8-7
8-5	S-II Engine No. 2 Actuator Commands and Positions	8-8
8-6	S-II Engines No. 2 and 3 Hydraulic Reservoir Levels	8-9
8-7	S-IVB Hydraulic System Performance - First Burn	8-11
8-8	S-IVB Hydraulic System Performance - Coast Phase	8-12
8-9	S-IVB Hydraulic System Pressure During Attempted Restart	8-13
8-10	S-IVB Hydraulic System Performance During Attempted Restart	8-14
8-11	J-2 Engine Hydraulic Component Locations	8-15

LIST OF ILLUSTRATIONS (CONTINUED)

Figure		Page
9-1	Longitudinal Structural Dynamic Response Due to Thrust Buildup and Release	9-3
9-2	Slow Release Rod Loads During Release	9-4
9-3	Longitudinal Acceleration Time History	9-5
9-4	Longitudinal Loads at Maximum Bending Moment and Inboard Engine Cutoff	9-6
9-5	Longitudinal Acceleration During S-IC Thrust Cutoff (OECO)	9-7
9-6	Longitudinal Loads Subsequent to S-II Engines Out	9-8
9-7	Lateral (Pitch) Structural Dynamic Response During Thrust Buildup and Release	9-9
9-8	Maximum and S-II Engines Out Bending Moment	9-10
9-9	First Longitudinal Modal Frequencies and Accelerations During S-IC Powered Flight	9-11
9-10	Longitudinal Oscillation Trends, 110 to 140 Seconds	9-13
9-11	S-IC Maximum Individual Engine and Composite Chamber Pressure Oscillations	9-14
9-12	F-1 Engine Chamber Pressure and Structural Acceleration Response at S-IC Gimbal Plane During Time of High Longitudinal Oscillations	9-15
9-13	Longitudinal Loads at Time of Maximum Longitudinal Oscillation	9-18
9-14	First Longitudinal Mode Shapes During S-IC Powered Flight	9-19
9-15	Lateral Modal Frequencies and Accelerations During S-IC Powered Flight	9-20
9-16	Pitch and Yaw Mode Shapes During S-IC Powered Flight	9-21
9-17	S-IC Fin Vibration Response and Bending and Torsional Modal Frequencies	9-22
9-18	S-IC Vibration and Strain Measurements at Fin, Fin and Fairing, F-1 Engine, and Thrust Structure	9-23

LIST OF ILLUSTRATIONS (CONTINUED)

Figure		Page
9-19	S-IC Vibration and Strain Measurements at Intertank, LOX Tank, and Forward Skirt	9-24
9-20	S-IC Stage Structure Vibration Envelope	9-25
9-21	S-IC Stage Engine Vibration Envelope	9-26
9-22	S-IC Stage Components Vibration Envelope	9-27
9-23	S-II Stage Structure Vibration Envelopes at Forward Skirt Stringers and Interstage Frames	9-30
9-24	S-II Stage Structure Vibration Envelopes at Aft Skirt Stringers and Interstage Frames	9-31
9-25	S-II Stage Structure Vibration Envelope at Thrust Cone Longerons, Engine 1 Bear, and Engine 1 Gimbal Pad	9-32
9-26	S-II Stage Component Vibration Envelopes	9-33
9-27	S-IVB Acoustics, Vibration and Dynamic Strain Measurements	9-35
9-28	S-IVB Stage Vibration Envelopes	9-36
9-29	S-IVB Forward Skirt Dynamic Strain	9-40
9-30	Pressure Differential Across S-IVB Forward Skirt Panels	9-41
9-31	Time Slices of Dynamic Strain Output Showing Wave Forms	9-42
9-32	S-IVB Forward Skirt RMS Strain Amplitudes	9-43
9-33	Instrument Unit Vibration Envelopes	9-44
9-34	AS-502 Versus AS-501 Inertial Gimbal Vibrations	9-46
9A-1	First Instrument Unit Measurements Affected by the 133 Second Disturbance	9A-3
9A-2	Location of Earliest Events That Were Noted at 133 Seconds	9A-4
9A-3	Composite Electrical Effects	9A-11
9A-4	Sublimator Inlet Water Differential Pressure	9A-12
9A-5	S-IVB Strain Gage Locations	9A-16
9A-6	Axial Strain, Aft Skirt Station 2821	9A-17
9A-7	Axial Strain, Forward Skirt Station 3145, Side Gages	9A-18

LIST OF ILLUSTRATIONS (CONTINUED)

Figure		Page
9A-8	Axial Strain, Forward Skirt Station 3145, Top Gages	9A-19
9A-9	S-IVB Forward Skirt Strains Bar Chart Showing Strain Changes at 133 Seconds Through DECO	9A-20
9A-10	"Quick Look" Assessment, ALOTS 70 MM Film, 133 to 135 Seconds	9A-23
9A-11	Simplified EDS Power and Auto-Abort Interface	9A-24
10-1	Navigation, Guidance, and Control System Block Diagram	10-3
10-2	Platform Gimbal Configuration	10-4
10-3	Velocity from Postflight Trajectory Minus ST-124M-3 Platform Measured Velocity	10-8
10-4	Predicted and Measured Accelerations in Parking Orbit	10-12
10-5	Composite Pitch Steering Angle (Not Rate Limited) Referenced to Local Horizontal	10-15
10-6	Actual and Nominal Velocities-to-be-Gained	10-16
10-7	Commanded Attitude Angles (Rate Limited) During Boost Phase	10-18
10-8	Attitude Timeline - Liftoff to Spacecraft Separation	10-19
10-9	Accelerometer Pickup Signals During Liftoff	10-22
10-10	Envelope of Maximum Deviations of the Gyro and Accelerometer Servo Amplifier Outputs	10-24
11-1	Engines, Actuators and Nozzle Arrangement	11-4
11-2	Surface Wind Speeds	11-6
11-3	Liftoff Vertical Motion and Soft Release Forces	11-7
11-4	Holddown Post Clearances (Position 1)	11-9
11-5	Liftoff Trajectories of Fin Tip A	11-10
11-6	S-IC Center Engine Trajectories and Plume Angles	11-11
11-7	Pitch Plane Dynamics During S-IC Burn	11-12
11-8	Yaw Plane Dynamics During S-IC Burn	11-13
11-9	Roll Plane Dynamics During S-IC Burn	11-14
11-10	Free Stream Angle-of-Attack During S-IC Burn	11-16

LIST OF ILLUSTRATIONS (CONTINUED)

Figure		Page
11-11	Pitch and Yaw Plane Wind Velocity During S-IC Burn	11-17
11-12	Oscillograms of IU Control Sensors During S-IC Transient	11-18
11-13	Oscillograms of Engine Position and S-IC Sensors During S-IC Transient	11-19
11-14	Predominate Slosh Frequencies During S-IC Burn	11-21
11-15	S-IC Propellant Slosh Amplitudes at the Wall During S-IC Burn	11-22
11-16	S-II and S-IVB Propellant Slosh Amplitudes During S-IC Burn	11-23
11-17	S-IC Engine Deflection Response to Propellant Slosh	11-24
11-18	Pitch Plane Dynamics During S-II Burn	11-26
11-19	Yaw Plane Dynamics During S-II Burn	11-27
11-20	Roll Plane Dynamics During S-II Burn	11-28
11-21	Pitch and Yaw Steering Misalignment Correction During S-II Burn	11-31
11-22	S-II Engine No. 2 Pitch and Yaw Actuator Response to the External Compression Load at 319 Seconds and to the Consequent Command at 320 Seconds	11-32
11-23	S-II LH ₂ and LOX Slosh Amplitudes During S-II Burn	11-34
11-24	S-IVB LH ₂ Slosh Amplitude at the Probe During S-II Burn	11-35
11-25	Predominant Slosh Frequencies During S-II Burn	11-35
11-26	S-II Engine Deflection Response to Propellant Slosh	11-37
11-27	S-IVB Pitch Actuator Excitation During S-IC Burn	11-38
11-28	Pitch Plane Dynamics During S-IVB First Burn	11-40
11-29	Yaw Plane Dynamics During S-IVB First Burn	11-41
11-30	Roll Plane Dynamics During S-IVB First Burn	11-42
11-31	S-IVB LOX Slosh Frequency and Height at the Probe	11-44
11-32	S-IVB LH ₂ Slosh Frequency and Height	11-44
11-33	Pitch Control Dynamics Following S-IVB First Burn	11-45
11-34	Yaw Control Dynamics Following S-IVB First Burn	11-47

LIST OF ILLUSTRATIONS (CONTINUED)

Figure		Page
11-35	Roll Control Dynamics Following S-IVB First Burn	11-48
11-36	Pitch Control Dynamics During 20 Degree Pitch Down Maneuver	11-49
11-37	Pitch Control Dynamics During Pitch and Roll Maneuvers	11-51
11-38	Yaw Control Dynamics During Pitch and Roll Maneuvers	11-52
11-39	Roll Control Dynamics During Pitch and Roll Maneuvers	11-53
11-40	S-IVB Pitch Attitude Errors and Rates During Attempted Second Burn	11-55
11-41	S-IVB Yaw Attitude Errors and Rates During Attempted Second Burn	11-56
11-42	S-IVB Roll Attitude Errors and Rates During Attempted Second Burn	11-57
11-43	Pitch, Yaw, and Roll Dynamics at Loss of Control	11-59
11-44	S-IVB/IU Tumble Rate History	11-60
12-1	S-IC Retro Motor Thrust	12-5
12-2	S-IC/S-II Relative Velocity and Separation Distance During First Plane Separation	12-6
12-3	S-IC/S-II Clearance Distance and Longitudinal Acceleration During First Plane Separation	12-8
12-4	S-IC Pitch and Yaw Angular Dynamics Following S-IC/S-II Separation	12-9
12-5	S-II Angular Dispersions During S-IC/S-II First Plane Separation	12-10
12-6	Interstage/S-II Relative Velocity and Separation Distance During Second Plane Separation	12-11
12-7	S-II Angular Dispersions During Second Plane Separation	12-12
12-8	Lateral Clearance Distance and Interstage Body Rates During Second Plane Separation	12-13
12-9	S-II Retro Motor Thrust	12-17
12-10	S-IVB Ullage Motor Thrust	12-17

LIST OF ILLUSTRATIONS (CONTINUED)

Figure		Page
12-11	S-II/S-IVB Relative Velocity and Separation Distance	12-18
12-12	S-II/S-IVB Longitudinal Accelerations	12-19
12-13	S-II Angular Dispersions During S-II/S-IVB Separation	12-20
12-14	S-II and S-IVB Angular Dispersions During S-II/S-IVB Separation	12-20
12-15	S-II/S-IVB Separation Clearance	12-22
12-16	Relative Motion During Spacecraft Separation	12-22
13-1	S-IC Power Generation and Distribution Systems Block Diagram	13-2
13-2	S-IC Stage Voltage (on Bus 1D10) and Current (at the Battery)	13-3
13-3	S-IC Stage Voltage (on Bus 1D20) and Current (at the Battery)	13-3
13-4	S-II Power Generation and Distribution Systems Block Diagram	13-5
13-5	S-II Stage Main DC Bus Voltage and Current	13-7
13-6	S-II Stage Instrumentation Bus Voltage and Current	13-7
13-7	S-II Stage Recirculation DC Bus Voltage and Current	13-8
13-8	S-II Stage Ignition DC Voltage	13-8
13-9	S-IVB Power Generation and Distribution Systems Block Diagram	13-9
13-10	S-IVB Stage Forward Battery No. 1 Voltage, Current, and Temperature	13-11
13-11	S-IVB Stage Forward Battery No. 2 Voltage, Current, and Temperature	13-12
13-12	S-IVB Stage Aft Battery No. 1 Voltage, Current, and Temperature	13-13
13-13	S-IVB Stage Aft Battery No. 2 Voltage, Current, and Temperature	13-14
13-14	Instrument Unit Power Generation and Distribution Systems Block Diagram	13-16
13-15	IU Battery 6D10 Voltage, Current, and Temperature	13-17
13-16	IU Battery 6D20 Voltage, Current, and Temperature	13-17

LIST OF ILLUSTRATIONS (CONTINUED)

Figure		Page
13-17	IU Battery 6D30 Voltage, Current, and Temperature	13-18
13-18	IU Battery 6D40 Voltage, Current, and Temperature	13-18
13-19	Currents and Voltages Associated with 133.3 Second Transient	13-20
15-1	EDS Functional Diagram	15-2
15-2	Q-Ball ΔP Versus Flight Time	15-5
16-1	S-IC Engine Fairing Compartment Pressure Differential	16-2
16-2	S-IC Engine Fairing Pressure Loading	16-3
16-3	S-IC Compartment Pressure Differential	16-6
16-4	S-IC Compartment Pressure Loading	16-7
16-5	S-II Compartment Pressure Loading	16-8
16-6	S-II LH ₂ Sidewall Insulation Differential Pressure	16-10
16-7	S-IVB Forward Compartment Differential Pressure	16-11
16-8	S-IVB Aft Skirt and Interstage Differential Pressure	16-11
16-9	S-IVB Aft Skirt and Interstage Pressure Loading	16-12
16-10	S-IC Base Pressure Differentials	16-13
16-11	S-IC Base Heat Shield Pressure Loading	16-14
16-12	S-II Heat Shield Aft Face Pressures	16-16
16-13	S-II Base Heat Shield Forward Face and Thrust Cone Pressures	16-16
16-14	S-II Base Heat Shield and Thrust Cone Pressures	16-17
16-15	S-II Base Heat Shield Pressures	16-18
16-16	Vehicle External Overall Sound Pressure Level at Liftoff	16-19
16-17	Vehicle External Sound Pressure Spectral Densities	16-21
16-18	Vehicle External Overall Fluctuating Pressure Level	16-23
16-19	Vehicle External Fluctuating Pressure Spectral Densities	16-25
16-20	S-IC Internal Acoustic Environment	16-27
16-21	S-II Internal Acoustics	16-28

LIST OF ILLUSTRATIONS (CONTINUED)

Figure		Page
Figure		Page
16-22	S-IVB Forward Skirt Acoustic Levels	16-29
16-23	S-IVB Aft Skirt Acoustic Levels	16-29
17-1	S-IC Base Heat Shield Thermal Environment	17-3
17-2	F-1 Engine Thermal Environment	17-3
17-3	S-IC Base of Fin D Total Heating Rate	17-4
17-4	S-IC Heat Shield Thermal Environment	17-5
17-5	S-IC Thermal Environment Effect of M-31 Loss on Heat Shield Temperatures at OECD	17-7
17-6	Thermal Environment, Temperature Under Insulation on Inboard Side of Engine No. 1	17-8
17-7	S-IC/S-II Separation Thermal Environment	17-9
17-8	S-II Heat Shield Aft Face Heating Rates and Surface Temperature	17-12
17-9	S-II Thrust Cone Total Heating Rates	17-14
17-10	S-II Thrust Cone Total and Radiation Heating Rates	17-17
17-11	S-II Heat Shield Forward Face Temperature	17-18
17-12	Engine Compartment Gas Temperature	17-19
17-13	S-II Heat Shield Aft Face and Thrust Cone Surface Temperatures	17-21
17-14	S-IC Aerodynamic Heating	17-24
17-15	S-IC Engine Fairing Aerodynamic Heating	17-25
17-16	S-IC Fin Aerodynamic Heating	17-26
17-17	S-IC Body Aerodynamic Heating	17-27
17-18	Forward Location of Separated Flow	17-29
17-19	S-IC Thermal Environment	17-30
17-20	S-IC Thermal Environments Aerodynamic Heating Indicator (AHI)	17-31
17-21	S-IC Thermal Environment Fin Skin Temperatures	17-32
17-22	S-II LH ₂ Feedline Fairing Total Heating Rates	17-34
17-23	S-II Ullage Motor Fairing and Aft Skirt Total Heating Rates	17-35

LIST OF ILLUSTRATIONS (CONTINUED)

Figure		Page
17-24	S-II Structural Temperatures	17-36
17-25	S-II Forward Skirt Skin and Insulation Temperatures	17-37
17-26	S-IVB Aeroheating Environment	17-38
17-27	S-IVB Protuberance Aeroheating Environment	17-40
17-28	S-IVB LH ₂ Heating During Boost	17-42
17-29	IU Inner Skin Temperatures for Ascent	17-43
17-30	S-IVB APS Fairing Temperature	17-45
17-31	S-IVB APS Propellant Control Module Temperature	17-46
17-32	IU Inner Skin Temperature in Earth Orbit	17-47
18-1	S-IC Environmental Control Systems Forward Compartment Canister Conditioning System	18-3
18-2	S-IC Forward Skirt Canister Temperatures	18-4
18-3	S-IC Environmental Control System and Compartment Temperatures	18-5
18-4	Container Equipment Mount Temperature	18-10
18-5	S-II Engine Compartment Conditioning System Transducer Locations	18-11
18-6	LOX and LH ₂ Chilldown Inverter Temperatures	18-13
18-7	IU Environmental Control System Schematic Diagram	18-14
18-8	Schematic of Thermal Control Using Water Coolant Valve	18-16
18-9	Temperature Control Parameters	18-17
18-10	Sublimator Water Inlet Performance	18-18
18-11	IU AS-502 Sublimator Startup Characteristics	18-19
18-12	TCS GN ₂ Supply Pressure and Temperature	18-21
18-13	Component Temperatures	18-22
18-14	GBS Pressure Regulation Performance	18-23
18-15	GBS GN ₂ Supply Pressure and Temperature	18-24
19-1	CT4 and GBI Telemetry Coverage	19-22
19-2	GBI Telemetry Coverage	19-23
19-3	VHF Telemetry Coverage Summary	19-25
19-4	AZUSA/GLOTRAC Coverage Summary	19-29

LIST OF ILLUSTRATIONS (CONTINUED)

Figure		Page
19-5	C-Band Radar Coverage Summary	19-30
20-1	Average Base Differential Pressure	20-2
20-2	Forebody Axial Force Coefficient, Based on Wind Tunnel Tests	20-3
20-3	Vehicle Total Aerodynamic Axial Force	20-3
20-4	S-IC Fin Pressure Differential	20-5
21-1	Total Vehicle Mass, Center of Gravity, and Mass Moment of Inertia During S-IC Stage Powered Flight	21-18
21-2	Total Vehicle Mass, Center of Gravity, and Mass Moment of Inertia During S-II Stage Powered Flight	21-19
21-3	Total Vehicle Mass, Center of Gravity, and Mass Moment of Inertia During S-IVB Stage Powered Flight	21-20
A-1	AS-502 Launch Time Scalar Wind Speed	A-5
A-2	AS-502 Launch Time Wind Direction	A-6
A-3	AS-502 Launch Time Pitch Wind Speed Component (W_x)	A-7
A-4	AS-502 Launch Time Yaw Wind Speed Component (W_z)	A-8
A-5	AS-502 Launch Time Pitch (S_x) and Yaw (S_z) Component Wind Shears	A-10
A-6	Relative Deviation of AS-502 Temperature and Density From PAFB (63) Reference Atmosphere	A-12
A-7	Relative Deviation of Pressure and Absolute Deviation of the Index of Refraction from the PAFB (63) Reference Atmosphere, AS-502	A-13
B-1	Saturn V Apollo Flight Configuration	B-2
B-2	S-IC Stage Configuration	B-3
B-3	S-II Stage Configuration	B-6
B-4	S-IVB Stage Configuration	B-10
B-5	Instrument Unit Configuration	B-13
B-6	Apollo Space Vehicle	B-16

LIST OF TABLES

Table		Page
2-1	Time Base Summary	2-1
2-2	Significant Event Times Summary	2-3
2-3	Sequence of Switch Selector Events	2-6
2-4	Unscheduled Switch Selector Events	2-19
3-1	AS-502 Milestones	3-2
3-2	S-IC Stage Propellant Mass at Ignition Command	3-7
3-3	S-11 Stage Propellant Mass at S-IC Ignition Command	3-7
3-4	S-IVB Stage Propellant Mass at S-IC Ignition Command	3-8
3-5	Ground/Vehicle Interface Events	3-9
4-1	Summary of AS-502 Orbital C-Band Tracking Stations	4-3
4-2	S-11 Engine No. 2 Premature Cutoff Conditions	4-9
4-3	Comparison of Significant Trajectory Events	4-10
4-4	Comparison of Cutoff Events	4-11
4-5	Comparison of Separation Events	4-12
4-6	Stage Impact Location	4-13
4-7	Parking Orbit Insertion Conditions	4-14
5-1	S-IC Stage Engine Startup Event Times	5-4
5-2	S-IC Engine Performance Deviations	5-7
5-3	S-IC Velocity and Time Deviation Analysis at OECO (Simulation Versus Predicted)	5-8
5-4	Comparison of S-IC Stage Flight Reconstruction Data with Trajectory Simulation Results	5-9
5-5	S-IC Cutoff Impulse	5-10
5-6	S-IC Stage Propellant Mass History	5-11
5-7	S-IC Residuals at Outboard Engine Cutoff	5-11
6-1	S-11 Engine Start Sequence Events	6-9
6-2	S-11 Engine Performance Deviations (ESC +60 Seconds)	6-11
6-3	S-11 Flight Reconstruction Comparison with Simulation Trajectory Match Results	6-12
6-4	S-11 Engine No. 2 Performance Shift and Cutoff	6-15

LIST OF TABLES (CONTINUED)

Table		Page
6-5	S-II Cutoff Impulse	6-22
6-6	S-II Stage Propellant Mass History	6-26
6-7	S-II Helium Mass	6-35
7-1	S-IVB Engine Start Sequence Events - First Burn	7-7
7-2	S-IVB Steady State Performance - First Burn (ESC +60 Second Time Slice)	7-9
7-3	Comparison of S-IVB Stage Flight Reconstruction Data - First Burn	7-10
7-4	S-IVB Simulation Burn Time Deviations	7-10
7-5	S-IVB Cutoff Impulse - First Burn	7-12
7-6	S-IVB Engine Start Sequence - Second Burn Attempt	7-16
7-7	S-IVB Stage J-2 Engine Failure to Restart	7-23
7-8	S-IVB Stage Propellant Mass History	7-31
7-9	S-IVB Pneumatic Helium Bottle Mass	7-55
7-10	S-IVB APS Propellant Consumption	7-57
8-1	S-IVB Hydraulic System Pressures	8-10
9-1	Maximum Modal Accelerations at 5.5 Hertz for 110 to 140 Seconds Range Time	9-16
9-2	S-IC Stage Vibration Summary	9-28
9-3	S-II Vibrations, Vehicle Structure	9-34
9-4	S-IVB Vibration Summary	9-37
9A-1	List of IU Measurements with 133 Second Response	9A-5
9A-2	133 Second Transient Survey, IU Stage	9A-9
10-1	Inertial Platform Velocity Comparisons	10-9
10-2	Guidance Comparisons (Navigation System)	10-11
10-3	Rate Limited Steering Command Times	10-17
10-4	Start and Stop Guidance Commands	10-17
11-1	Summary of Liftoff Clearances	11-5
11-2	AS-502 Misalignment Summary	11-6
11-3	Maximum Control Parameters During S-IC Burn	11-10

LIST OF TABLES (CONTINUED)

Table		Page
11-4	S-IC Dynamic End Conditions*	11-20
11-5	Maximum Control Parameters During S-II Burn	11-29
11-6	Maximum Control Parameters During S-IVB Burn	11-39
11-7	APS Impulse Requirements	11-43
12-1	Separation Event Times	12-2
12-2	S-IC Retro Motor Performance	12-4
12-3	S-II Retro Motor Performance	12-14
12-4	S-IVB Ullage Motor Performance	12-16
13-1	S-IC Stage Electrical System Battery Performance During Flight	13-4
13-2	S-II Stage Battery Consumption	13-6
13-3	S-IVB Stage Battery Consumption	13-15
13-4	Instrument Unit Battery Consumption	13-19
14-1	CCS Command History, AS-502	14-3
15-1	Performance Summary of Thrust OK Pressure Switches	15-4
15-2	Discrete EDS Events	15-6
15-3	Switch Selector EDS Events	15-7
16-1	S-II Acoustic Noise Levels Comparison of AS-501 and AS-502 Data	16-28
17-1	Retro Motor Plume Heating	17-22
17-2	APS Orbital Temperatures	17-44
18-1	S-IC Environmental Control System Canister Temperatures	18-2
18-2	S-IC Environmental Control System Aft Compartment Temperatures	18-4
18-3	S-II Forward Thermal Control System AS-501 and AS-502 Prelaunch and Flight Data	18-8
18-4	S-II Aft Thermal Control System AS-501 and AS-502 Prelaunch and Flight Data	18-9
18-5	S-II Engine Compartment Temperature Data Comparison of AS-501 and AS-502 Flights	18-10

LIST OF TABLES (CONTINUED)

Table		Page
18-6	Forward and Aft Skirt Component Temperature*	18-12
18-7	IU TCS Flowrates and Coolant Pressure Data	18-20
19-1	Vehicle Measurements Summary	19-2
19-2	Measurements Waived/Scrubbed Prior to Launch	19-3
19-3	Measurement Malfunctions During Flight	19-7
19-4	Measurements with Improper Range	19-11
19-5	Questionable Measurements	19-13
19-6	Launch Vehicle Telemetry Links	19-15
19-7	Tape Recorder Summary	19-18
19-8	AS-502 Onboard Tracking Systems	19-27
21-1	Total Vehicle Mass, S-IC Burn Phase, Kilograms	21-3
21-2	Total Vehicle Mass, S-IC Burn Phase, Pounds Mass	21-4
21-3	Total Vehicle Mass, S-II Burn Phase, Kilograms	21-5
21-4	Total Vehicle Mass, S-II Burn Phase, Pounds Mass	21-6
21-5	Total Vehicle Mass, S-IVB First Burn Phase, Kilograms	21-7
21-6	Total Vehicle Mass, S-IVB First Burn Phase, Pounds Mass	21-8
21-7	Total Vehicle Mass, S-IVB Second Burn Phase, Kilograms	21-9
21-8	Total Vehicle Mass, S-IVB Second Burn Phase, Pounds Mass	21-10
21-9	Flight Sequence Mass Summary	21-11
21-10	Mass Characteristics Comparison	21-14
22-1	Mission Objectives Accomplishment Summary	22-2
23-1	Summary of Failures and Anomalies	23-2
23-2	Summary of Deviations	23-5
A-1	Surface Observations at AS-502 Launch Time	A-2
A-2	Systems Used to Measure Upper Air Wind Data, AS-502	A-3
A-3	Maximum Wind Speed in High Dynamic Pressure Region	A-9
A-4	Extreme Wind Shear in High Dynamic Pressure Region	A-11

LIST OF TABLES (CONTINUED)

Table		Page
A-5	Selected Atmospheric Observations for Sixteen Saturn Vehicle Launches at Kennedy Space Center, Florida	A-14
B-1	S-IC Significant Configuration Changes	B-5
B-2	S-II Significant Configuration Changes	B-9
B-3	S-IVB Significant Configuration Changes	B-12
B-4	IU Significant Configuration Changes	B-14

ACKNOWLEDGEMENT

This report is published by the Saturn Flight Evaluation Working Group-- composed of representatives of Marshall Space Flight Center, John F. Kennedy Space Center, and MSFC's prime contractors--and in cooperation with the Manned Spacecraft Center. Significant contributions to the evaluation have been made by:

George C. Marshall Space Flight Center

Research and Development Operations

Aero-Aerodynamics Laboratory
Astrionics Laboratory
Computation Laboratory
Propulsion and Vehicle Engineering Laboratory

Industrial Operations

John F. Kennedy Space Center

Manned Spacecraft Center

The Boeing Company

Douglas Aircraft Company

International Business Machines Corporation

North American Rockwell/Rocketdyne Division

North American Rockwell/Space Division

ABBREVIATIONS

AEDC	ArnoId Engineering Development Center	EBW	Exploding bridge wire
ANT	Antigua	ECO	Engine cutoff
APS	Auxiliary propulsion system	ECP	Engineering change proposal
ASC	Ascension Island	ECS	Environment control system
ASI	Augmented spark igniter	EDS	Emergency detection system
BDA	Bermuda	EMR	Engine mixture ratio
CAL	Goldstone, California	ESC	Engine start command
CCS	Command and communications system	FCM	Flight combustion monitor
CDDT	Countdown demonstration test	FM/FM	Frequency modulation/frequency modulation
CG	Center of gravity	GBI	Grand Bahama Island
CIF	Central instrumentation facility	GFCV	GOX flow control valve
CM	Command module	GG	Gas generator
CO	Cutoff	GLOTRAC	Global tracking
CRO	Carnarvon	GRR	Guidance reference release
CSM	Command and service module	GSE	Ground support equipment
CT4	Cape telemetry 4	GSFC	Goddard Space Flight Center
CVS	Continuous vent system	GTI	Grand Turk Island
CYI	Grand Canary Island	GYM	Guaymas
DEE	Digital events evaluator	HAW	Hawaii
		HFCV	Helium flow control valve

IECO	Inboard engine cutoff	OAT	Overall test
IGM	Iterative guidance mode	ODOP	Offset frequency doppler
IRIG	Inter range instrumentation group	OECO	Outboard engine cutoff
IU	Instrument Unit	PAM/FM/FM	Pulse amplitude modulation/frequency modulation/frequency modulation
LES	Launch escape system		
LET	Launch escape tower	PCM	Pulse code modulation
LM	Lunar module	PCM/FM	Pulse code modulation/frequency modulation
LTA	Lunar module test article		
LUT	Launch umbilical tower	PMR	Programmed mixture ratio
LV	Launch vehicle	PMRS	Programmed mixture ratio shift
LVDA	Launch vehicle data adapter	PSD	Power spectral density
LVDC	Launch vehicle digital computer	PTCS	Propellant tanking computer system
MAB	Materials analysis branch	PJ	Propellant utilization
MCC-H	Mission control center-Houston	PWS	Potable water system
MFV	Main fuel valve	RACS	Remote analog calibration system
MILA	Merritt Island Launch Area	RED	Redstone (ship)
ML	Mobile launcher	RET	Transition Reynolds number
MLV	Main LOX valve	RF	Radio frequency
MOV	Main oxidizer valve	RJ-1	Ground hydraulic fluid (kerosene)
MR	Mixture ratio	RMR	Reference mixture ratio
MSC	Manned Spacecraft Center	RMS	Root mean square
MSFC	Marshall Space Flight Center	RP-1	S-IC stage fuel (kerosene)
NPSP	Net positive suction pressure	RPM	Revolutions per minute

RPS	Revolutions per second	VAB	Vehicle assembly building at KSC
R/S	Range safety	VCO	Voltage controlled oscillators
RSS	Root sum square	VSWR	Voltage standing wave ratio
SA	Swing arm		
SAR	Start arm retract		
SC	Spacecraft		
SLA	Spacecraft LM adapter		
SM	Service module		
SMC	Steering misalignment correction		
SPS	Service propulsion system		
SRSCS	Secure range safety command system		
SS	Switch selector		
SS/FM	Single sideband/frequency modulation		
STCSV	Start tank control solenoid valve		
STDV	Start tank discharge valve		
SV	Space vehicle		
TAN	Tananarive		
TEL4	Cape telemetry 4		
TMR	Triple modular redundant		
TSM	Tail service mast		
TVC	Thrust vector control		

MISSION PLAN

AS-502 (Apollo 6 Mission) was the second flight vehicle of the Saturn V Apollo flight test program. The basic purpose of the flight was to demonstrate the compatibility and performance of the launch vehicle and the Apollo Command and Service Modules (CSM) for a future manned flight.

The AS-502 vehicle was launched from Launch Complex 39, Pad A at Kennedy Space Center (KSC) on a launch azimuth of 90 degrees, then rolled to a flight azimuth of 72 degrees. The S-IC and S-II stage powered flight times were to be approximately 147 and 368 seconds, respectively. First S-IVB stage powered flight time was to be approximately 138 seconds terminating with insertion into a 185.2 kilometer (100 n mi) circular parking orbit of the S-IVB and spacecraft. Vehicle weight at parking orbit insertion was to be approximately 127,000 kilograms (280,000 lbm). Approximately 15 seconds after first burn cutoff, the S-IVB was to align with the local horizontal, then the vehicle was to roll 180 degrees to obtain a position III down configuration. In this configuration the vehicle would be subjected to a 20 degree pitch-down and a 20 degree pitch-up maneuver, then roll 180 degrees again to obtain the original position I down configuration. These maneuvers were to produce information on the S-IVB restart bottle repressurization and propellant slosh excitation while qualifying these maneuvers for manned flight. On manned flights these maneuvers may be used to orient the astronauts for landmark tracking.

Chilldown and reignition sequencing were to begin between Hawaii and California during the second revolution and continue across the continental United States. After the restart preparation was initiated, an orientation maneuver was to be performed to yield the high apogee elliptical orbit after second burn. The S-IVB was to be reignited over KSC, near the end of the second revolution for translunar injection boost, and aimed at a target simulating the moon. This was in order to preclude hitting the moon while verifying launch vehicle guidance technique.

The S-IVB second burn, which was to be approximately 316 seconds, was to terminate with the injection of the S-IVB/IU/CSM into an elliptical orbit with an apogee radius of approximately 528,024 kilometers (285,110 n mi). Following S-IVB second cutoff, the vehicle was to coast on a simulated lunar trajectory for about 3 minutes before separation. A pitch rotation of approximately 155 degrees was to be accomplished during this coast to position the CSM for retrograde burn. After this rotation, the Spacecraft Lunar Module Adapter (SLA) panels were to open to free the CSM. Following CSM separation, the S-IVB was to be oriented to give satisfactory attitude

for ground communications. Four minutes and 40 seconds after S-IVB second cutoff, the Service Module Service Propulsion System (SPS) was to begin a 254-second retrograde burn to retard the CSM onto an earth intersecting ellipse having an apogee altitude of approximately 22,204 kilometers (11,989 n mi).

About two hours after separation, the S-IVB was to be aligned by ground command with the local horizontal to test the ground command capability near the limit of S-IVB stage active lifetime. The S-IVB was to reenter the atmosphere over the Pacific Ocean on the return leg of the high apogee ellipse.

After SPS first cutoff, the CSM was to coast in the 22,204 kilometer (11,989 n mi) apogee orbit for about 6 hours, oriented to cold soak the heat shield, approximating lunar return thermal conditions. During descent portion of the orbit, the second SPS burn was to accelerate the CSM to the approximate lunar return velocity of 11,125 m/s (36,500 ft/s) with an inertial flight path entry angle of -6.5 degrees. The service module was to be jettisoned before reentry. The command module was to enter the atmosphere approximately 4 minutes after SPS cutoff and splash down near Hawaii at approximately 9 hours and 50 minutes after liftoff.

FLIGHT TEST SUMMARY

The second Saturn V Apollo space vehicle, AS-502 (Apollo 6 Mission), was launched at Kennedy Space Center (KSC), Florida on April 4, 1968 at 07:00:01 Eastern Standard Time (EST) from Launch Complex 39, Pad A. This was the second mission to use a Saturn V launch vehicle with an unmanned block I Command Service Module (CSM020), and a Lunar Module Test Article (LTA-2R). Nine of the sixteen primary objectives were completely accomplished, six partially accomplished, and one (S-IVB restart) was not accomplished. One of the two secondary objectives was completely accomplished, and one partially accomplished.

The launch countdown was completed without any unscheduled countdown holds. Ground systems performance was highly satisfactory. The relatively few problems encountered in countdown were overcome such that vehicle launch readiness was not compromised.

The vehicle was launched on an azimuth of 90 degrees east of north and after 11.1 seconds of vertical flight, (which included a small yaw maneuver for tower clearance) AS-502 began to roll into a flight azimuth of 72 degrees east of north. Actual trajectory parameters of the AS-502 were close to nominal until the premature shutdown of two engines on the S-II stage. After this premature shutdown, the trajectory deviated significantly from the nominal throughout the remainder of the mission. Space-fixed velocity at S-IC Outboard Engine Cutoff (OECO) was 7.28 m/s (23.89 ft/s) greater than nominal. At S-II Engine Cutoff (ECO) the space-fixed velocity was 102.36 m/s (335.82 ft/s) less than nominal and the altitude was 6.39 kilometers (3.95 n mi) higher than nominal. At S-IVB velocity cutoff command the space-fixed velocity was 48.94 m/s (160.56 ft/s) greater than nominal. The altitude at S-IVB velocity cutoff command was 0.79 kilometers (0.42 n mi) lower than nominal and the surface range was 498.46 kilometers (269.15 n mi) longer than nominal. Parking orbit insertion conditions deviated considerably from nominal because of anomalies that occurred during the powered portion of flight. The space-fixed velocity at insertion was 48.16 m/s (158.00 ft/s) greater than nominal and the flight path angle (elevation of space-fixed velocity vector from local horizontal) was 0.378 degree less than nominal. These conditions produced an orbit which was quite elliptical with an eccentricity 0.0138 greater than nominal. The resulting apogee of the parking orbit was 171.54 kilometers (92.63 n mi) higher than nominal, and the perigee was 12.17 kilometers (6.57 n mi) less than nominal. The S-IVB stage failed to reignite. Shortly after the attempted reignition, the spacecraft separated from the launch vehicle on ground command to the spacecraft. The S-IVB stage reentered due to orbital decay on April 25, 1968.

S-1C propulsion systems performed satisfactorily. In general, all performance flight data fell close to the nominal predictions. Average engine thrust reduced to standard sea level conditions from 35 to 38 seconds was 0.20 percent lower than predicted and average specific impulse was 0.10 percent lower than predicted. The vehicle first longitudinal structural mode frequency coupled with the engine response to the oxidizer suction lines resonant frequency within the 110 to 140 second period. This resulted in a vehicle longitudinal oscillation termed "POGO". Inboard Engine Cutoff (IECO) and Outboard Engines Cutoff (OECO) occurred 0.11 and 0.85 seconds later than predicted, respectively. An intentional fuel level cutoff of the outboard engines and a LOX level cutoff of the inboard engine were planned and attained, demonstrating the adequacy of these cutoff modes. All the subsystems except the camera ejection system and the control pressure system performed as expected. The camera ejection system ejected only one of the four film cameras and the control pressure system sphere pressure decayed unexpectedly after separation.

The S-II propulsion system performed satisfactorily during the first 169 seconds of operation following Engine Start Command (ESC). Engine thrust, at 60 seconds after ESC, was only 0.43 percent below prediction and specific impulse 0.08 percent above predictions. At 319 seconds a sudden performance shift was exhibited on engine No. 2 with thrust decreasing approximately 33,806 Newtons (7600 lbf). The engine continued performance at the reduced level until 412.3 seconds. By 412.92 seconds the dropout of thrust OK switches indicated engine No. 2 cutoff, and at 414.18 seconds engine No. 3 also cut off. Postflight evaluation of telemetered data led to the conclusion that the engine No. 2 Augmented Spark Igniter (ASI) fuel line failed and ultimately caused failure of the engine. Since the flight, testing at Marshall Space Flight Center (MSFC) and the engine manufacturer's facility has substantiated this conclusion. The testing reveals that an oxidizer rich mixture, caused by a fuel leak, creates very high temperatures and rapidly erodes the injector. Because of this erosion the LOX dome of engine No. 2 eventually failed, opening the LOX high pressure system and causing Engine Cutoff (ECO). A modification of the ASI propellant feedlines (both fuel and LOX) and their installation is being accomplished. Interchanged LOX prevalve control wiring connections between engines No. 2 and 3 solenoids caused the premature cutoff of engine No. 3. When engine No. 2 cutoff, the LOX prevalve on engine No. 3 was commanded closed. Individual check-out of the prevalve wiring during prevalve timing checks is planned for future vehicles. S-II burn time was 425.31 seconds which is 37.81 seconds longer than predicted. The extended burn time was caused by the premature cutoff of engines No. 2 and 3. Loss of the two engines reduced propellant consumption approximately 40 percent and required a longer burn time to reach propellant-depletion. The S-II propulsion subsystems met all performance requirements.

The S-IVB J-2 engine operated satisfactorily throughout the operational phase of first burn. However, a total performance shift of 2.3 percent decrease in thrust occurred during first burn from 684 to 702 seconds.

The engine continued to operate at the shifted performance level and had a normal shutdown. S-IVB first burn time was 166.52 seconds which was 28.95 seconds longer than predicted due to the two engines out condition on the S-II stage. Stage performance during first burn deviated from the predicted at the 60 second time slice by -0.08 percent for thrust and 0.06 percent for specific impulse. The LOX mass measuring side of the Propellant Utilization (PU) system malfunctioned during orbit prior to the attempted restart. The LOX mass measuring system malfunction caused a 100 percent LOX load indication prior to and during the restart attempt. The probable cause of the erroneous 100 percent LOX mass indication may have been due to shorting of the inner and outer elements of the LOX PU probe from metallic debris that could have been in the LOX tank. Also, an intermittent short in the cable shield between the mass probe and the PU electronics assembly may have occurred. Engine restart conditions were within limits even though main chamber second ignition failed to occur. Results thus far indicate that a leak in the Augmented Spark Igniter (ASI) fuel supply system probably occurred during first burn. Additional engine tests have essentially verified the performance shift and the restart failure. A modification of the ASI propellant feedlines (both fuel and LOX) and their installation is being accomplished. All subsystems operationally met all performance and stage requirements. However, there were two unexpected deviations which are discussed in Section 7.

In general, the hydraulic systems performed satisfactorily in that the vehicle remained stable during all portions of guidance-controlled powered flight. No hydraulic system problems occurred during S-IC powered flight. S-II hydraulic systems performed within predicted limits, and operated satisfactorily until 280 seconds. At this time, the S-II engine No. 2 yaw actuator delta pressure transducer began to deviate significantly from expected values. From 319 seconds until engine No. 2 cutoff, both the pitch and yaw actuators showed apparent side loads from the engine. After engine No. 2 cutoff, the yaw actuator performance indicates that it locked up. The engine No. 3 system performed normally until engine shutdown when the system pump stopped operation and the pressures decayed. The engine No. 1 and engine No. 4 hydraulic systems performed normally throughout S-II powered flight. The S-IVB hydraulic system performed within predicted limits during liftoff, boost, and first burn. During engine restart preparation and restart attempt, the system failed to produce hydraulic pressure. System temperatures observed during S-IVB first burn indicated the existence of a cryogenic fuel leak which led to the freezing of the hydraulic fluid and system blockage. During the restart attempt, measurements indicated that both the main and the auxiliary hydraulic pumps cavitated during operation and virtually no system pressure was produced.

The AS-502 flight vehicle experienced considerably more structural activity than AS-501; however, this activity did not reach sufficient magnitude to pose a threat to the launch vehicle structural integrity. Thrust buildup and vehicle release transients, resulted in maximum longitudinal and lateral (pitch plane) dynamic load factors of ± 0.4 and ± 0.08 g,

respectively, at the command module. The maximum steady-state bending moment condition, 9.89×10^6 N-m (7.29×10^5 lbf-ft), was experienced at 66.6 seconds. The maximum longitudinal loads were experienced at 144.72 seconds (IECO) at a rigid body acceleration of 4.8 g. Although the 4.8 g IECO condition was greater than the 4.63 g design value, no mainline structural problems were encountered during this phase of flight. Thrust oscillation-structural dynamic response coupling (POGO) was evident during the 110 to 140 second region of S-IC range time. The longitudinal dynamics of the launch vehicle induced lateral accelerations of 0.65 g peak at the LTA. Oscillations in the first longitudinal mode during the 110 to 140 second time period exceeded that experienced during AS-501 flight by approximately a factor of three. Maximum response occurred in the 5.2 to 5.5 hertz bandwidth. Fin bending and torsional modes compared well with analytical predictions. Fin vibrations exceeded the range of the accelerometers but the modal frequencies did not coalesce and flutter did not occur. S-IC, S-IVB and Instrument (IU) vibrations were as expected. S-II stage vibrations were as expected, except that forward skirt vibrations exceeded the sine and random criteria at liftoff. No adverse effects were noted. S-IVB forward skirt experienced limited amplitude panel flutter. The stress amplitudes encountered due to flutter were about three times higher than those of AS-204 but were still within a tolerable level.

At approximately 133 seconds abrupt changes of strain, vibration, and acceleration measurements were indicated in the S-IVB, IU, Spacecraft/Lunar Module Adapter (SLA), LTA, and Command and Service Module (CSM). Photographic coverage, Airborne Light Optical Tracking System (ALOTS), and ground camera film showed pieces separating from the area of the SLA. There were no known structural failures noted on the launch vehicle.

The performance of the guidance and navigation system was as predicted from liftoff to 412.9 seconds. When engine No. 2 cut off a discrete signal was recognized by the IU indicating a single engine failure. However, since only single engine failures were considered in constructing the flight program, no program action was taken for engine No. 3 failure. With the discrete signal and loss in acceleration the program entered a guidance mode where guidance and navigation computations were made based on a thrust change for the single engine failure which was 50 percent of the total actual change. This mode (artificial tau) lasted until the IU sensed an acceleration change due to S-II Programmed Mixture Ratio (PMR) shift. Guidance computations responded to variations in altitude and velocity caused by the decrease in thrust during the S-II burn period. The control system responded well to the guidance commands for the remainder of the boost period. Due to the two-engine-out perturbation, flight path angle and velocity were not optimum at the time guidance commanded S-IVB ECO. This resulted in an overspeed of 48.9 m/s (160 ft/s). A parking orbit which was acceptable though off nominal was achieved. All orbital guidance maneuvers were satisfactorily performed. IU commands were properly executed for S-IVB restart, but the engine did not reignite.

When acceleration test conditions were not met, Time Base 7 (T7) was initiated and a cutoff command was issued to the S-IVB stage.

The AS-502 Flight Control Computer (FCC), Thrust Vector Control (TVC), and Auxiliary Propulsion System (APS) satisfied all requirements for attitude control and stability of bending and propellant slosh modes in both the boost and orbital coast modes of operation. During liftoff, all vehicle clearance requirements were met. During first stage boost the control system was required to correct for a steady-state roll attitude error of approximately -0.5 degree. This roll torque was not observed on AS-501, as the attitude error was essentially null after about 50 seconds. Control system performance was consistent with events which occurred during S-II boost. The performance shift of engine No. 2 at 319 seconds was evidenced in the TVC as well as in the FCC parameters. However, this performance shift caused no control problems and resulted only in a new steady-state trim condition. The FCC and TVC responded satisfactorily to the perturbations caused by the shutdown of engines No. 2 and 3. This shutdown resulted primarily in a large pitch plane disturbance during which the pitch rate built up to a maximum of 2.8 deg/s (nose-up) and the pitch attitude error reached a maximum of 13.4 degrees. A maximum engine deflection of 5.95 degrees was required to stabilize the attitude excursions. At S-II/S-IVB separation, the guidance computer switched to the S-IVB coast mode for 0.3 second. The 7.4 degrees pitch attitude error caused a full-on APS pitch-engine firing of 0.3 second duration to correct the attitude. At 0.3 second after separation, the guidance computer switched to the S-IVB burn mode. The pitch attitude error was trimmed out by the TVC after S-IVB stage J-2 engine ignition. Control system performance was nominal for the remainder of S-IVB first burn. Orbital attitude control requirements required considerably more APS activity than anticipated. The APS system was required to overcome a 50 degrees nose-up from local horizontal attitude and a 1 deg/s nose-up angular rate to align the vehicle along the local horizontal. The vehicle was subsequently exercised through a sequence of four maneuvers as follows: 180 degrees roll, 20 degrees pitch down, 20 degrees pitch up, and 180 degrees roll. The pitch and roll maneuvers were planned to produce information on the S-IVB restart bottle repressurization and propellant slosh excitation while qualifying these maneuvers for manned flight. Each maneuver was executed as planned. No appreciable effect was noted on the restart bottle conditions. LH₂ sloshing was not appreciable during any of the maneuvers. Significant LOX sloshing existed at the initiation of each pitch maneuver; however, the initial amplitude was not sustained due to high damping. An auxiliary hydraulic pump failure prevented the S-IVB stage J-2 engine from being centered at the time of second S-IVB ESC. The engine position at ESC was approximately 1.5 degrees in pitch and -2.3 degrees in yaw. Appreciable attitude errors resulted from this engine position during restart attempt; however, vehicle control was maintained by the APS system following the switch from thrust vector to coast mode control. Subsequent to spacecraft separation the APS system maintained control until APS module I fuel depletion at approximately 21,953 seconds. Vehicle attitude rates began to build up significantly following module III fuel depletion (22,602 seconds) and continued

to increase as indicated by reduced radar data until a tumble rate of 180 deg/s was recorded by the ninth day following launch.

Launch vehicle separation systems performed satisfactorily. Separation and associated sequencing occurred as planned with adequate clearance between stages. All ullage and retro motor performance was satisfactory. The S-IC retro motor data indicate that some parameters were either above normal or possibly above the maximum limits but caused no problem. Spacecraft separation was initiated by ground command to the spacecraft during the maneuver to separation attitude. Even though there was a possible momentary interference between a SLA panel and the CSM at the separation plane, the momentary interference was not detrimental to the separation.

In general, launch vehicle electrical systems performed satisfactorily. Battery voltages and currents were satisfactory and battery temperature remained within acceptable limits. S-IC battery No. 2 experienced a sharp current rise and voltage drop after S-IC/S-II separation which lasted for 11 seconds; however, tape recorder performance was not impaired. A similar anomaly was experienced by Battery No. 1 on the AS-501 flight. Disturbances were experienced on the S-II main and instrumentation batteries during the engine No. 2 and 3 shutdown period. A current surge was experienced on the IU 6D10 battery at the time of the 133 second transient.

Data indicated that the redundant Secure Range Safety Command Systems (SRSCS) on the S-IC, S-II, and S-IVB stages were ready to perform their functions properly on command if flight conditions during the launch phase had required vehicle destruct. The system properly safed the S-IVB SRSCS on command from KSC. The performance of the command and communications system in the IU was very good.

The space vehicle Emergency Detection System (EDS) was flight tested in the automatic abort closed-loop configuration on AS-502. Launch vehicle measurements indicated that no EDS limits were exceeded and the system functioned properly. There were some anomalies indicated in the spacecraft.

The vehicle internal, external and base region pressure environments were generally in good agreement with the predictions and compared well with the AS-501 data. The pressure environment was well below the design level. The measured acoustic levels were also generally in good agreement with the predictions and with AS-501 data.

The vehicle thermal environment was generally less severe than that for which the vehicle was designed. One exception was the S-IC forward skirt thermal environment which exceeded design after S-IC/S-II separation. Loss of M-31 to the level of the crushed core on the S-IC base heat shield was visually observed on this flight via the television cameras which viewed the heat shield. This was a repeat of an AS-501 anomaly and no adverse effects were noted. The effect of the premature shutdown of engines No. 2

and 3 on the S-II heat shield and base region environment was minor. With the exception of abrupt spikes due to the engine anomalies, the base region thermal data compared favorably with AS-501 data.

The S-IC canister conditioning system and the aft environmental conditioning system performed satisfactorily during the AS-502 countdown with only one canister and one ambient temperature measurement dropping below the minimum requirement. The S-II thermal control and compartment conditioning system maintained temperatures within the design limits throughout the prelaunch operations. Temperatures monitored on the S-IVB aft skirt components were slightly cooler than on the AS-501 flight but within design limits. Temperatures of all components mounted on the forward skirt cold plates were within design limits at liftoff. The IU Environmental Control System (ECS) performed well throughout the flight. Coolant temperatures, pressures, and flowrates remained within the predicted ranges and design limits for the duration of the flight data. One specification deviation was observed which was expected. At 11,670 seconds, the platform gas bearing pressure differential was 0.069 N/cm² (0.1 psig) above the 10.7 N/cm² (15.5 psig) maximum allowable and remained there throughout the remainder of the flight period for which data is available (33,780 seconds).

There were 2758 telemetered measurements active at the start of the AS-502 automatic countdown sequence. Of the 2758 measurements, 58 failed in flight, resulting in an overall system reliability of 97.9 percent. The Airborne Telemetry System operated satisfactorily, including preflight calibrations and inflight calibration. Tape recorder performance was good; however, due to the extended burn time of the S-II and S-IVB stages, the S-IC/S-II separation data playback was not recovered from the S-II, S-IVB, and IU recorders. This was because insufficient playback time was programmed to cover the anomalous situation caused by the S-II two-engines-out condition. Performance of the RF systems was good. Approximately 2 seconds of real time data on all S-IC stage telemetry links were lost due to a data dropout at 146.0 seconds. This condition was also noted on AS-501 and appears to be related to S-IC IECC. Ground camera coverage was good as evidenced by 84 percent system efficiency. However, only two of the six onboard film cameras were recovered. Three of the cameras on the S-IC stage failed to eject and one of the S-II cameras was not recovered due to a weak recovery beacon signal.

SECTION 1
INTRODUCTION

1.1 PURPOSE

This report provides the National Aeronautics and Space Administration (NASA) Headquarters, and other interested agencies, with the launch vehicle evaluation results of the AS-502 flight test. The basic objective of flight evaluation is to acquire, reduce, analyze, evaluate and report on flight test data to the extent required to assure future mission success and vehicle reliability. To accomplish this objective, actual flight malfunctions and deviations must be identified, their causes accurately determined, and complete information made available so that corrective action can be accomplished within the established flight schedule.

1.2 SCOPE

This report presents the results of the early engineering flight evaluation of the AS-502 launch vehicle. The contents are centered on the performance evaluation of the major launch vehicle systems, with special emphasis on failures, anomalies, and deviations. Summaries of launch operations and spacecraft performance are included for completeness.

The official MSFC position at this time is represented by this report. It will not be followed by a similar report unless continued analysis or new information should prove the conclusion presented herein to be significantly incorrect. Final stage evaluation reports will, however, be published by the stage contractors. Reports covering major subjects and special subjects will be published as required.

SECTION 2
EVENT TIMES

2.1 SUMMARY OF EVENTS

Range zero time, the basic time reference for this report, is 7:00:01 Eastern Standard Time (EST) (12:00:01 Universal Time [UT]). This time, by definition, is based on the nearest second prior to S-IC tail plug disconnect, which occurred at 7:00:01.74 EST. Range time is calculated as the elapsed time from range zero time and unless otherwise noted is the time used throughout this report.

Guidance Reference Release (GRR) occurred at -16.85 seconds and start of Time Base 1 (T₁) occurred 17.54 seconds later at 0.69 second. The times noted above were established by the Digital Events Evaluator (DEE-6) except for T₁ which was determined by the Launch Vehicle Digital Computer (LVDC). First motion of the vehicle was established by ground cameras as having occurred at 0.38 second.

Range time for each time base used in the flight sequence program and the signal for initiating each time base are presented in Table 2-1.

Table 2-1. Time Base Summary

TIME BASE	RANGE TIME SEC (HR:MIN:SEC)	SIGNAL START
T ₀	-16.85	Guidance Reference Release
T ₁	0.69	IU Umbilical Disconnect Sensed by LVDC
T ₂	144.95	S-IC IECD Sensed by LVDC
T ₃	148.41	S-IC OICD Sensed by LVDC
T ₄	576.33	S-II ECD Sensed by LVDC
T ₅	747.30	S-IVB ECD (Velocity) Sensed by LVDC
T ₆	11,287.73 (3:08:7.73)	Restart Equation Solution
T ₇	11,630.33 (3:13:50.33)	Commanded ECD based on Thrust Criteria not being met

Start of T₂ was initiated approximately 0.23 seconds after S-IC inboard engine cutoff. Two redundant LOX level cutoff sensors were located on the S-IC stage 180 degrees apart. The system was designed so that the sensor which first detected the cutoff level would initiate Inboard Engine Cutoff (IECO) by means of redundant circuitry and cutoff solenoids. Only one sensor circuit, however, was wired to provide the LVDC interrupt signal which would initiate T₂. IECO was achieved at 144.72 seconds by means of the cutoff circuit which did not have the LVDC interrupt capability. The second circuit subsequently sensed cutoff level and initiated T₂ via the LVDC interrupt at 144.95 seconds. The reason why the level sensors detected cutoff level at different times is not known at this time and the problem is under investigation. Because of the time discrepancy, both times are listed in Table 2-2.

Failure to restart the S-IVB engine terminated T₆ early and started T₇ at 11,630.33 seconds. The flight sequence program normally commands engine cutoff and initiates T₇ based on velocity attained. On AS-502, however, engine cutoff was commanded and T₇ initiated because thrust criteria were not being met due to the S-IVB stage restart failure.

A summary of significant events for AS-502 is given in Table 2-2. The most significant deviations from nominal predicted times occurred in guidance and navigation events because of perturbations to the Guidance and Navigation System occasioned by the premature shutdown of two S-II stage engines. A more detailed discussion of these problems is contained in paragraph 10.4.

2.2 SEQUENCE OF EVENTS

Table 2-3 lists the sequence of switch selector events. Terminology in this table agrees with the terminology in document 40M33622C "Interface Control Document Definition of Saturn SA-502 Flight Sequence Program." Eight events, including S-II engine start, were not verified because of telemetry dropout during S-IC/S-II staging, although subsequent events indicate that these events did in fact occur. Additionally, 21 orbital events and 10 events in T₇ were not verified because of station visibility constraints and loss of data due to flight perturbations. Probable times for all but two of these events were derived from the flight program. Times were also derived for six switch selector functions which were verified to ± 0.5 seconds by compressed data. Four switch selector events (Fuel Injection Temperature OK Bypass Reset, Flight Control Computer Switch Point No. 5, Point Level Sensor Arming and Cutoff S-IVB Velocity) were missed at the end of T₆ due to the early start of T₇.

Table 2-4 lists the unscheduled switch selector events, which are dependent upon vehicle orientation and position and therefore variable, and also ground commanded events, which have been verified from available data.

Table 2-2. Significant Event Times Summary

EVENT	RANGE TIME		TIME FROM BASE	
	ACTUAL (SEC)	ACT-PRED (SEC)	ACTUAL (SEC)	ACT-PRED (SEC)
1. Guidance Reference Release	-16.85	-0.75	-17.54	-0.39
2. S-IC Engine Start Sequence Command	-8.77	0.02	-9.46	0.39
3. Range Zero	0.00	-	-	-
4. All Holddown Arms Released	0.36	0.0	-0.33	0.0
5. First Motion	0.38	-0.23	-0.31	0.14
6. IU Umbilical Disconnect, Start of Time Base 1 (T ₁)	0.69	-0.37	T ₁	-
7. Begin Yaw Maneuver	1.9	-0.2	1.2	0.2
8. End Yaw Maneuver	9.8	-1.3	9.1	-0.9
9. Begin Pitch and Roll Maneuver (Tilt and Roll)	11.1	-0.5	10.4	-0.2
10. End Roll Maneuver	31.3	0.7	30.6	1.1
11. Mach 1 Achieved	60.5	-1.3	59.8	-0.9
12. Occurrence of Max Dynamic Pressure (Max Q)	75.2	-4.8	74.5	-4.4
13. End Pitch Maneuver (Tilt Arrest)	140.9	-2.7	140.2	-2.4
14. S-IC Inboard Engine Cutoff (IECO) (Solenoid Activation)	144.72	0.11	-	-
15. S-IC Inboard Engine Cutoff Sensed by LVDC, Start of Time Base 2 (T ₂)	144.95	0.34	T ₂	-
16. S-IC Outboard Engine Cutoff (OECO) (Sensed by LVDC), Start of Time Base 3 (T ₃)	148.41	0.85	T ₃	-
17. S-IC/S-13 Separation Command to Fire Separation Devices and Retro Motors	149.08	0.82	0.67	-0.03
18. S-II Engine Start Command	149.76	0.80	1.35	-0.05
19. S-II Second Plane Separation Command	179.06	0.80	30.65	-0.05
20. Launch Escape Tower (LET) Jettison Command	184.77	0.81	36.36	-0.04
21. Initiate Iterative Guidance Mode (IGM) Phase 1	190.95	1.39	42.54	0.54
22. Initiate Steering Misalignment Correction (SMC)	211.99	1.76	63.58	0.34

Table 2-2. Significant Event Times Summary (Continued)

EVENT	RANGE TIME		TIME FROM BASE	
	ACTUAL (SEC)	ACT-PRED (SEC)	ACTUAL (SEC)	ACT-PRED (SEC)
23. S-II Stage Engine No. 2 Out	412.92	-	264.51	-
24. S-II Stage Engine No. 3 Out	414.18	-	265.77	-
25. Guidance Sensed Engine Mixture Ratio (EMR) Shift, Inflate IGM Phase 2	490.76	78.03	342.35	77.18
26. Initiate Chi Freeze	517.7	7.47	369.3	7.02
27. S-II Engine Cutoff (ECO) (Sensed by LVDC), Start of Time Base 4 (T ₄)	576.33	58.64	T ₄	-
28. S-II/S-IVB Separation Command to Fire Separation-Devices and Retro Motors	577.08	58.59	0.75	-0.05
29. S-IVB Engine Start Sequence Command	577.28	58.59	0.95	-0.05
30. Stop Chi Freeze	582.9	55.8	6.6	-2.8
31. Initiate Iterative Guidance Mode, Phase 3	584.78	57.67	8.45	-0.97
32. Pitch Command Nose-up Attitude	644.02	-	67.69	-
33. Initiate Chi Bar Steering	712.3	85.8	136.6	27.2
34. Initiate Chi Freeze	746.4	93.67	173.07	35.03
35. S-IVB Velocity Cutoff Command (ECO)	747.04	87.78	T ₅ -0.26	-0.06
36. S-IVB Engine Cutoff Sensed by LVDC Start of Time Base 5 (T ₅)	747.30	87.84	T ₅	-
37. Coast Period On	748.55	87.79	1.25	-0.05
38. Parking Orbit Insertion	757.04	87.78	9.74	-0.06
39. Maneuver to Local Horizontal	762.30	87.84	15.00	0.00
40. Initiate 180° Roll to Place Position III Down	837.30	87.84	90.00	0.00
41. Initiate 20° Pitch Down Maneuver	3207.30	87.84	2460.00	0.00
42. Initiate 20° Pitch Up Maneuver	5427.30	87.84	4680.00	0.00
43. Initiate 180° Roll to Place Position I Down	5787.30	87.84	5040.00	0.00
44. Initiate S-IVB Restart Sequence and Start of Time Base 6 (T ₆)	11,287.73	211.12	T ₆	-
45. S-IVB Engine Restart Command	11,614.69	211.08	326.95	-0.05

Table 2-2. Significant Event Times Summary (Continued)

EVENT	RANGE TIME		TIME FROM BASE	
	ACTUAL SEC	ACT-PRED SEC	ACTUAL SEC	ACT-PRED SEC
46. S-IVB ECO Command and Start of Time Base 7 (~7)	11,630.33	-97.66	T ₇	-
47. Coast Period On	11,631.50	-97.79	1.17	-0.03
48. Maneuver to Separation Attitude	11,650.33	-97.76	20.00	0.00
49. End Cold Soak Attitude and Spacecraft Separation Command*	11,666.02	-	35.69	-
50. LV-LTA/CSM Physical Separation*	11,667.82	-240.27	37.49	-142.51
51. Execute Maneuver A*	16,201.0	-	4570.7	-
52. S-IVB LOX Tank Vent Valves Open*	22,023.30	-	10,392.97	-
53. S-IVB LH ₂ Tank Vent Valves Open*	22,024.21	-	10,393.88	-
* Ground Command				

Table 2-3. Sequence of Switch Selector Events

FUNCTION	STAGE	RANGE TIME	TIME FROM BASE	
		ACTUAL (SEC)	ACTUAL (SEC)	ACT-PRED (SEC)
1. Start of Time Base 1 (T ₁)	IU	0.69	-	-
2. Auto-Abort Enable Relays, RESET	IU	5.64	4.95	-0.05
3. Sensor Bias, ON	IU	6.86	5.17	-0.03
4. Multiple Engine Cutoff, ENABLE	S-IC	14.65	13.96	-0.04
5. Telemeter Calibrate, ON	S-IC	25.44	24.75	-0.05
6. Telemetry Calibrator In-Flight Calibrate, ON	IU	27.66	26.97	-0.03
7. Telemeter Calibrate, OFF	S-IC	30.46	29.77	-0.03
8. Launch Vehicle Engines EDS Cutoff, ENABLE	IU	30.66	29.97	-0.03
9. Telemetry Calibrator In-Flight Calibrate, OFF	IU	32.64	31.95	-0.05
10. Fuel Pressurizing Valve (HFCV) No. 2, OPEN & Tape Recorder, RECORD	S-IC	50.14	49.45	-0.05
11. Start Data Recorders	S-II	74.74	74.05	-0.05
12. Cooling System Electrical Assembly, Power, OFF	IU	75.66	74.97	-0.03
13. Telemetry Calibrator In-Flight Calibrate, ON	IU	90.66	89.97	-0.03
14. Telemetry Calibrator In-Flight Calibrate, OFF	IU	95.65	94.96	-0.04
15. Fuel Pressurizing Valve (HFCV) No. 3, OPEN	S-IC	95.95	95.26	-0.04
16. Flight Control Computer Switch Point No. 1	IU	105.66	104.97	-0.03
17. Telemeter Calibrate, ON	S-IC	115.66	114.97	-0.03
18. Regular Calibrate Relays, ON	S-IVB	119.85	119.16	-0.04
19. Telemeter Calibrate, OFF	S-IC	120.66	119.97	-0.03
20. Flight Control Computer Switch Point No. 2	IU	120.84	120.15	-0.05
21. Regular Calibrate Relays, OFF	S-IVB	124.84	124.15	-0.05
22. Start First PAM-FM/FM Calibration	S-II	130.36	129.67	-0.03
23. Fuel Pressurizing Valve (HFCV) No. 4, OPEN	S-IC	134.16	133.47	-0.03
24. Fast Record, ON	S-IVB	135.16	134.47	-0.03

Table 2-3. Sequence of Switch Selector Events (Continued)

FUNCTION	STAGE	RANGE TIME	TIME FROM BASE	
		ACTUAL (SEC)	ACTUAL (SEC)	ACT-PRED (SEC)
25. Stop First P/M-FM/FM Calibration	S-II	135.34	134.65	-0.05
26. Tape Recorder Record, ON	IU	135.55	134.86	-0.04
27. LOK Tank Strobe Lights, OFF	S-IC	135.74	135.05	-0.05
28. S-IC Two Engine Out Auto-Abort Inhibit, ENABLE	IU	135.95	135.26	-0.04
29. S-IC Two Engine Out Auto-Abort Inhibit	IU	136.17	135.48	-0.02
30. Excess Rate (P,Y,R) Auto-Abort Inhibit, ENABLE	IU	136.34	135.65	-0.05
31. Excess Rate (P,Y,R) Auto-Abort Inhibit	IU	136.54	135.85	-0.05
32. Two Adjacent Outboard Engines Out Cutoff, ENABLE	S-IC	136.76	136.07	-0.03
33. Inboard Engine Cutoff, ENABLE	S-IC	136.96	136.27	-0.03
34. Inboard Engine Cutoff Backup, ENABLE	S-IC	137.14	136.45	-0.05
35. Inboard Engine Cutoff Interrupt 1520		144.95		
36. Start of Time Base 2 (T ₂)		144.95		
37. S-II Ordnance, ARM	S-II	145.03	0.08	-0.02
38. Separation and Retro EBW Firing Units, ARM	S-IC	145.20	0.25	-0.05
39. Separation Camera, ON	S-IC	145.42	0.47	-0.03
40. Camera Lights, ON	S-II	145.51	0.56	-0.04
41. Telemetry Measurement Switch Over	S-IC	145.70	0.75	-0.05
42. Outboard Engines Cutoff, ENABLE	S-IC	145.91	0.96	-0.04
43. Outboard Engines Cutoff-Interrupt 1520		148.41		
44. Start of Time Base 3 (T ₃)		148.41		
45. Camera Motor, ON	S-II	148.49	0.08	-0.02
46. S-II LP2 Recirculation Pumps, OFF	S-II	148.66	0.25	-0.05
47. S-II Ullage, TRIGGER	S-II	148.87	0.47	-0.03
48. S-IC/S-II Separation	S-II	149.08	0.67	-0.03
49. Camera Event Mark	S-II	149.17	0.77	-0.03

Table 2-3. Sequence of Switch Selector Events (Continued)

FUNCTION	STAGE	RANGE TIME	TIME FROM BASE	
		ACTUAL (SEC)	ACTUAL (SEC)	ACT-PRED (SEC)
50. Switch Engine Control to S-II; S-II Engine Out Indication "A", ENABLE; S-II Aft Interstage Separation Indication "A", ENABLE	IU	149.26*	0.85*	-0.05
51. S-II Engines Cutoff, RESET	S-II	149.36*	0.95*	-0.05
52. Engines Ready Bypass	S-II	149.46*	1.05*	-0.05
53. Prevalves Lockout, RESET	S-II	149.56*	1.15*	-0.05
54. S-II Engine, START	S-II	149.76*	1.35*	-0.05
55. Camera Event Mark	S-II	149.86*	1.45*	-0.05
56. S-II Engine Out Indication "B", ENABLE and S-II Aft Interstage Separation Indication "B", ENABLE	IU	150.06*	1.65*	-0.05
57. Engines Ready Bypass, RESET	S-II	150.26*	1.85*	-0.05
58. Q-Bell Power, OFF	IU	150.76	2.35	-0.05
59. S-II Hydraulic Accumulators, UNLOCK	S-II	151.38	2.97	-0.03
60. Chilldown Valves, CLOSE	S-II	154.76	6.35	-0.05
61. S-II Start Phase Limiter Cutoff, ARM	S-II	155.08	6.67	-0.03
62. Activate PU System	S-II	155.26	6.85	-0.05
63. S-II Start Phase Limiter Cutoff Arm, RESET	S-II	156.07	7.67	-0.03
64. Stop Data Recorders	S-II	159.78	11.38	-0.02
65. Fast Record, OFF	S-IVB	159.96	11.56	-0.04
66. Tape Recorder Record, OFF	IU	160.17	11.77	-0.03
67. S-II Aft Interstage Separation, ON	S-II	179.06	30.65	-0.05
68. Camera Event Mark	S-II	179.16	30.75	-0.05
69. Camera Event Mark	S-II	180.16	31.75	-0.05
70. Launch Escape Tower Jettison "A", ON	IU	184.77	36.36	-0.04
71. Launch Escape Tower Jettison "B", ON	IU	184.98	36.57	-0.03
72. Camera Eject No. 1	S-II	186.37	37.97	-0.03
73. Camera Eject No. 2	S-II	186.97	38.56	-0.04
74. Camera Eject No. 3	S-II	187.46	39.06	-0.04

* Derived Times

Table 2-3. Sequence of Switch Selector Events (Continued)

FUNCTION	STAGE	RANGE TIME	TIME FROM BASE	
		ACTUAL (SEC)	ACTUAL (SEC)	ACT-PRED (SEC)
75. Flight Control Computer Switch Point No. 3	IU	209.76	61.36	-0.04
76. Start Second PAM-FM/FM Calibration	S-II	330.26	181.85	-0.05
77. Stop Second PAM-FM/FM Calibration	S-II	335.27	186.86	-0.04
78. Flight Control Computer Switch Point No. 4	IU	339.76	191.35	-0.05
79. Telemetry Calibrator In-Flight Calibrate, ON	IU	353.26	201.85	-0.05
80. Telemetry Calibrator In Flight Calibrate, OFF	IU	355.27	206.87	-0.03
81. Measurement Control Switch No. 2, ACTIVATE	S-II	361.06	212.66	-0.04
82. Start Third PAM-FM/FM Calibration	S-II	420.98	272.58	-0.02
83. Stop Third PAM-FM/FM Calibration	S-II	425.97	277.56	-0.04
84. S-II LH2 Step Pressurization	S-II	468.36	319.95	-0.05
85. Regular Calibrate Relays, ON	S-IVB	477.26	328.85	-0.05
86. Telemetry Calibrator In-Flight Calibrate, ON	IU	477.47	329.07	-0.03
87. Regular Calibrate Relays, OFF	S-IVB	482.28	333.87	-0.03
88. Telemetry Calibrator In-Flight Calibrate, OFF	IU	482.46	334.05	-0.05
89. Charge Ullage Ignition, ON	S-IVB	482.88	334.48	-0.02
90. S-II/S-IVB Ordnance, ARM	S-II	483.06	334.65	-0.05
91. Tape Recorder Record, ON	IU	483.27	334.87	-0.03
92. Fast Record, ON	S-IVB	483.46	335.05	-0.05
93. Start Data Recorders	S-II	483.67	335.26	-0.04
94. S-II LOX Depletion Sensor Cutoff, ARM	S-II	483.88	335.47	-0.03
95. S-II LH2 Depletion Sensor Cutoff, ARM	S-II	484.06	335.65	-0.05
96. Cutoff S-II J-2 Engines-Interrupt 1520		576.33		
97. Start of Time Base 4 (T4)		576.33		
98. Redundant S-II Cutoff SS	S-II	576.41	0.08	0.08

Table 2-3. Sequence of Switch Selector Events (Continued)

FUNCTION	STAGE	RANGE TIME	TIME FROM BASE	
		ACTUAL (SEC)	ACTUAL (SEC)	ACT-PRED (SEC)
99. Start Recorder Timers	S-II	576.50	0.18	0.08
100. Prevalves Close, OFF	S-IVB	576.61	0.28	0.08
101. S-IVB Engine Cutoff, OFF	S-IVB	576.70	0.37	0.07
102. Engine Ready Bypass	S-IVB	576.79	0.46	-0.04
103. LOX Chilldown Pump, OFF	S-IVB	576.88	0.56	-0.04
104. Fire Ullage Ignition, ON	S-IVB	576.98	0.65	-0.05
105. S-II/S-IVB Separation	S-II	577.08	0.75	-0.05
106. S-IVB Engine Start Interlock Bypass, ON	S-IVB	577.18	0.85	-0.05
107. S-IVB Engine Start, ON	S-IVB	577.28	0.95	-0.05
108. Flight Control Computer S-IVB Burn Mode On "A"	IU	577.40	1.07	-0.03
109. Flight Control Computer S-IVB Burn Mode On "B"	IU	577.49	1.16	-0.04
110. S-IVB Engine Out Indication "A", ENABLE	IU	577.88	1.55	-0.05
111. S-IVB Engine Out Indication "B", ENABLE	IU	578.09	1.77	-0.03
112. Fuel Chilldown Pump, OFF	S-IVB	578.48	2.15	-0.05
113. LOX Tank Flight Pressure System, ON	S-IVB	580.08	3.75	-0.05
114. Fuel Injection Temperature OK Bypass	S-IVB	580.30	3.97	-0.03
115. S-IVB Engine Start, OFF	S-IVB	580.48	4.15	-0.05
116. First Burn Relay, ON	S-IVB	582.08	5.75	-0.05
117. Emergency Playback Enable, ON	S-IVB	584.09	7.77	-0.03
118. Fast Record, OFF	S-IVB	585.28	7.95	-0.05
119. PU Activate, ON	S-IVB	585.30	8.97	-0.03
120. Charge Ullage Jettison, ON	S-IVB	586.09	9.77	-0.03
121. Fire Ullage Jettison, ON	S-IVB	589.08	12.75	-0.05
122. Fuel Injection Temperature OK Bypass, RESET	S-IVB	590.29	13.95	-0.05
123. Ullage Charging, RESET	S-IVB	591.88	15.55	-0.05

Table 2-3. Sequence of Switch Selector Events (Continued)

FUNCTION	STAGE	RANGE TIME	TIME FROM BASE	
		ACTUAL (SEC)	ACTUAL (SEC)	ACT-PRED (SEC)
124. Ullage Firing, RESET	S-IVB	592.09	15.76	-0.04
125. Tape Recorder Record, OFF	IU	595.18	18.85	-0.05
126. Emergency Playback Enable, OFF	S-IVB	597.58	21.25	-0.05
127. Telemetry Calibrator In-Flight Calibrate, ON	IU	598.68	22.35	-0.05
128. Telemetry Calibrator In-Flight Calibrate, OFF	IU	603.70	27.38	-0.02
129. Regular Calibrate Relays, ON	S-IVB	608.10	31.77	-0.03
130. Regular Calibrate Relays, OFF	S-IVB	613.08	36.75	-0.05
131. Engine Pump Purge Control Valve Enable, ON	S-IVB	746.91	T ₅ -0.39	6.61
132. Cutoff S-IVB Engine (Velocity)	S-IVB	747.04	T ₅ -0.26	-0.06
133. Cutoff S-IVB Engine-Interrupt 1520		747.30		
134. Start of Time Base 5 (T ₅)	S-IVB	747.30		
135. Redundant S-IVB Cutoff S5	S-IVB	747.38	0.08	0.08
136. Point Level Sensor Disarming	S-IVB	747.47	0.18	0.08
137. S-IVB Ullage Engine No. 1, ON	S-IVB	747.57	0.27	-0.03
138. S-IVB Ullage Engine No. 2, ON	S-IVB	747.66	0.36	-0.04
139. S-IVB Ullage Thrust Present Indicator, ON	IU	747.87	0.57	-0.03
140. First Burn Relay, Off	S-IVB	747.97	0.67	-0.03
141. PU Activate, OFF	S-IVB	748.15	0.86	-0.04
142. LOX Tank Flight Pressure System, OFF	S-IVB	748.36	1.06	-0.04
143. Coast Period, ON	S-IVB	748.55	1.25	-0.05
144. Engine Pump Purge Control Valve Enable, ON	S-IVB	748.75	1.45	-0.05
145. PU Fuel Boiloff Bias Cutoff, ON	S-IVB	748.97	1.67	-0.03
146. Flight Control Computer S-IVB Burn Mode Off "A"	IU	750.76	3.46	-0.04
147. Flight Control Computer S-IVB Burn Mode Off "B"	IU	750.97	3.67	-0.03
148. Aux. Hydraulic Pump Coast Mode, ON	S-IVB	751.15	3.85	-0.05

Table 2-3. Sequence of Switch Selector Events (Continued)

FUNCTION	STAGE	RANGE TIME	TIME FROM BASE	
		ACTUAL (SEC)	ACTUAL (SEC)	ACT. PREP. (SEC)
149. Aux. Hydraulic Pump Flight Mode, OFF	S-IVB	751.37	4.07	-0.03
150. S-IVB Engine Out Indication "A" Enable, RESET	IU	757.27	9.97	-0.03
151. S-IVB Engine Out Indication "B" Enable, RESET	IJ	757.43	13.15	-0.05
152. Telemetry Calibrator In-Flight Calibrate, ON	IL	759.45	12.15	-0.05
153. Regular Calibrate Relays, ON	S-IVB	759.66	12.26	-0.04
154. Telemetry Calibrator In-Flight Calibrate, OFF	IU	764.47	17.17	-0.03
155. Regular Calibrate Relays, OFF	S-IVB	764.65	17.35	-0.06
156. SS/FM Transmitter, OFF	S-IV3	769.26	21.96	-0.04
157. SS/FM Group, OFF	S-IVB	769.46	22.16	-0.04
158. LH2 Tank Continuous Vent Valve Open, ON	S-IVB	805.25	58.95	-0.05
159. LH2 Tank Continuous Vent Valve Open, OFF	S-IVB	808.26	60.96	-0.04
160. S-IVB L11age Engine No. 1, OFF	S-IVB	835.25	87.95	-0.05
161. S-IVB L11age Engine No. 2, OFF	S-IVB	835.35	98.05	-0.05
162. S-IVB L11age Thrust Present Indication, OFF	IU	835.56	88.26	-0.04
163. Emergency Playback Enable, ON	S-IVB	835.75*	88.45*	-0.05
164. Tape Recorder Playback Reverse, ON	IU	836.45	89.15	-0.05
165. Emergency Playback Enable, OFF	S-IVB	908.75*	167.45*	-0.05
166. Slow Record, ON	S-IVB	909.45*	162.15*	-0.05
167. Slow Record, OK	S-IVB	919.45*	172.15*	-0.05
168. Tape Recorder Playback Reverse, OFF	IU	920.45*	173.15*	-0.05
169. Engine Pump Purge Control Valve Enable, OFF	S-IVB	1349.85	632.05	-0.05
170. Slow Record, ON	S-IVB	2360.75*	1613.45*	-0.05
171. Slow Record, OFF	S-IVB	2392.75*	1645.45*	-0.05
172. Recorder Playback, ON	S-IV3	2392.95*	1645.65*	-0.05

* Derived Times

Table 2-3. Sequence of Switch Selector Events (Continued)

FUNCTION	STAGL	RANGE TIME	TIME FROM PASS	
		ACTUAL (SEC)	ACTUAL (SEC)	ACT-PRED (SEC)
173. Recorder Playback, OFF	S-IVB	2560.75*	1813.45*	-0.05
174. Slow Record, ON	S-IVB	2560.95*	1813.65*	-0.05
175. Slow Record, ON	S-IVB	2570.95*	1823.65*	-0.05
176. Telemetry Calibrator In-Flight Calibrate, ON	LU	3340.75	2593.45	-0.05
177. Regular Calibrate Relays, ON	S-IVB	3340.95	2593.65	-0.05
178. Telemetry Calibrator In-Flight Calibrate, OFF	LU	3345.77	2598.47	-0.03
179. Regular Calibrate Relays, OFF	S-IVB	3345.96	2598.67	-0.04
180. Telemetry Calibrator In-Flight Calibrate, ON	LU	5385.75*	4638.45*	-0.05
181. Slow Record, ON	S-IVB	5385.95*	4638.65*	-0.05
182. Regular Calibrate Relays, ON	S-IVB	5386.15*	4638.85*	-0.05
183. Telemetry Calibrator In-Flight Calibrate, OFF	LU	5390.75	4643.45	-0.05
184. Regular Calibrate Relays, OFF	S-IVB	5391.15	4643.85	-0.05
185. Slow Record, OFF	S-IVB	5417.95	4670.65	-0.05
186. Recorder Playback, ON	S-IVB	5418.35	4671.05	-0.05
187. Recorder Playback, OFF	S-IVB	5774.75	5027.45	-0.05
188. Slow Record, ON	S-IVB	5775.15	5027.85	-0.05
189. Slow Record, ON	S-IVB	5785.15	5037.85	-0.05
190. Telemetry Calibrator In-Flight Calibrate, ON	LU	6340.75	5593.45	-0.05
191. Regular Calibrate Relays, ON	S-IVB	6340.95	5593.65	-0.05
192. Telemetry Calibrator In-Flight Calibrate, OFF	LU	6345.76	5598.46	-0.04
193. Regular Calibrate Relays, OFF	S-IVB	6345.96	5598.66	-0.04
194. Slow Record, ON	S-IVB	7907.75*	7160.45*	-0.05
195. Slow Record Off	S-IVB	7939.77	7192.48	-0.02
196. Recorder Playback, On	S-IVB	7939.97	7192.67	-0.03
197. Recorder Playback, OFF	S-IVB	8210.55	7463.25	-0.05
198. Slow Record, ON	S-IVB	8210.75**	7463.45**	-0.05

* Derived Times

** Verified to ±0.5 by Compressed Data

Table 2-3. Sequence of Switch Selector Events (Continued)

FUNCTION	STAGE	RANGE TIME	TIME FROM BASE	
		ACTUAL (SEC)	ACTUAL (SEC)	ACT-PRED (SEC)
199. Slow Record, ON	S-IVB	8220.75	7473.45	-0.05
200. Regular Calibrate Relays, ON	S-IVB	8980.75	8233.45	-0.05
201. Telemetry Calibrator In-Flight Calibrate, ON	TU	8980.95	8233.65	-0.05
202. Regular Calibrate Relays, OFF	S-IVB	8985.75	8238.45	-0.05
203. Telemetry Calibrator In-Flight Calibrate, OFF	TU	8985.95	8238.65	0.05
204. Slow Record, ON	S-IVB	10,410.75*	9663.45*	-0.05
205. Slow Record, OFF	S-IVB	10,442.75*	9695.45*	-0.05
206. Recorder Playback, ON	S-IVB	10,442.95*	9795.65*	-0.05
207. Recorder Playback, OFF	S-IVB	10,707.75*	9960.45*	-0.05
208. Slow Record, ON	S-IVB	10,707.95*	9960.65*	-0.05
209. Slow Record, ON	S-IVB	10,717.95*	9970.65*	-0.05
210. Aux. Hydraulic Pump Flight Mode, ON	S-IVB	10,822.25**	10,074.95**	-0.05
211. Aux. Hydraulic Pump Coast Mode, OFF	S-IVB	10,822.45**	10,075.15**	-0.05
212. LOX Chilldown Pump, ON	S-IVB	10,872.25**	10,124.95**	-0.05
213. Fuel Chilldown Pump, ON	S-IVB	10,877.25**	10,129.95**	-0.05
214. Provalves Close, ON	S-IVB	10,877.25**	10,139.95**	-0.05
215. Telemetry Calibrator In-Flight Calibrate, ON	TU	11,260.75	10,513.45	-0.05
216. Regular Calibrate Relays, ON	S-IVB	11,260.95	10,513.65	-0.05
217. Telemetry Calibrator In-Flight Calibrate, OFF	TU	11,265.75	10,518.45	-0.04
218. Regular Calibrate Relays, OFF	S-IVB	11,265.95	10,518.65	-0.04
219. Begin Restart Preparations - Time Base Backup 1536	S-IVB			
220. Start of Time Base 5 (T ₆)		11,287.73		
221. S-IVB Ullage Engine No. 1, ON	S-IVB	11,287.90	0.17	-0.03
222. S-IVB Ullage Engine No. 2, ON	S-IVB	11,288.01	0.27	-0.03
223. S-IVB Ullage Thrust Present Indication, ON	TU	11,288.19	0.40	-0.04

* Derived Times

** Verified to ±0.5 by Compressed Data

Table 2-3. Sequence of Switch Selector Events (Continued)

FUNCTION	STAGE	RANGE TIME	TIME FROM BASE	
		ACTUAL (SEC)	ACTUAL (SEC)	ACT-PRED (SEC)
224. LH ₂ Tank Vent Valve Boost Close, ON	S-IVB	11,288.49	0.75	-0.05
225. LOX Tank Vent Valve Boost Close, ON	S-IVB	11,288.69	0.96	-0.04
226. LH ₂ Tank Continuous Vent Valve Close, ON	S-IVB	11,288.89	1.15	-0.05
227. C-Band Transponders No. 1 and No. 2, ON	IU	11,289.09	1.35	-0.05
228. LH ₂ Tank Vent Valve Boost Close, OFF	S-IVB	11,290.49	2.75	-0.05
229. LOX Tank Vent Valve Boost Close, OFF	S-IVB	11,290.69	2.96	-0.04
230. LH ₂ Tank Continuous Vent Valve Close, OFF	S-IVB	11,290.91	3.18	-0.02
231. Fuel Chilldown Pump, ON	S-IVB	11,293.69	5.95	-0.05
232. LOX Chilldown Pump, ON	S-IVB	11,298.69	10.95	-0.05
233. Prevalves Close, ON	S-IVB	11,308.69	20.95	-0.05
234. LOX Tank Repressurization Control Valve Open, ON	S-IVB	11,387.69	99.95	-0.05
235. Telemetry Calibrator In-Flight Calibrate, ON	IU	11,436.00	148.27	-0.03
236. Telemetry Calibrator In-Flight Calibrate, OFF	IU	11,440.99	153.25	-0.05
237. LH ₂ Tank Repressurization Control Valve Open, ON	S-IVB	11,487.70	199.96	-0.04
238. SS/FM Group, ON	S-IVB	11,496.90	208.26	-0.04
239. SS/FM Transmitter, ON	S-IVB	11,496.21	208.48	-0.02
240. Regular Calibrate Relays, ON	S-IVB	11,556.19	268.45	-0.05
241. Regular Calibrate Relays, OFF	S-IVB	11,561.20	273.46	-0.04
242. PU Valve Handover Position, ON	S-IVB	11,574.69	286.96	-0.04
243. Prevalves Close, OFF	S-IVB	11,603.90	316.16	-0.04
244. S-IVB Restart Alert	IU	11,604.69	316.96	-0.04
245. S-IVB Engine Cutoff, OFF	S-IVB	11,613.29	325.56	-0.04
246. Engine Ready Bypass	S-IVB	11,613.51	325.77	-0.03
247. LH ₂ Tank Repressurization Control Valve Open, OFF	S-IVB	11,613.69	325.95	-0.05

Table 2-3. Sequence of Switch Selector Events (Continued)

FUNCTION	STAGE	RANGE TIME	TIME FROM BASE	
		ACTUAL (SEC)	ACTUAL (SEC)	AGI-PREFD (SEC)
248. Fuel Chilledown Pump, OFF	S-IVB	11,613.90	326.27	-0.03
249. LOX Chilledown Pump, OFF	S-IVB	11,614.09	326.36	-0.05
250. LOX Tank Repressurization Control Valve Open, OFF	S-IVB	11,614.51	326.77	-0.03
251. S-IVB Engine Start, OK	S-IVB	11,614.69	326.95	-0.09
252. S-IVB Engine Out Indication "A", ENABLE	TU	11,615.49	327.75	-0.05
253. S-IVB Engine Out Indication "B", ENABLE	TU	11,615.70	327.96	-0.04
254. S-IVB Ullage Engine No. 1, OFF	S-IVB	11,617.69	329.95	-0.05
255. S-IVB Ullage Engine No. 2, OFF	S-IVB	11,617.79	330.05	-0.05
256. S-IVB Ullage Thrust Present Indication, OFF	TU	11,617.99	330.26	-0.04
257. Flight Control Computer S-IVB Burn Mode On "A"	TU	11,622.29	334.55	-0.05
258. Flight Control Computer S-IVB Burn Mode On "B"	TU	11,622.49	334.76	-0.04
259. Fuel Injection Temperature OK Bypass	S-IVB	11,622.69	334.96	-0.05
260. LOX Tank Flight Pressure System, ON	S-IVB	11,622.90	335.17	-0.03
261. Coast Period, OFF	S-IVB	11,623.09	335.36	-0.04
262. S-IVB Engine Start, OFF	S-IVB	11,623.30	335.56	-0.04
263. Second Burn Relay, ON	S-IVB	11,625.29	337.55	-0.05
264. PU Activate, ON	S-IVB	11,627.50	339.77	-0.03
265. PU Valve Hardover Position, OFF	S-IVB	11,627.69	339.95	-0.05
266. Fuel Injection Temperature OK Bypass, RESET	S-IVB	***		
267. Flight Control Computer Switch Point No. 5	TU	***		
268. Point Level Sensor Arming	S-IVB	***		
269. Cutoff S-IVB Velocity	TU	***		
270. Start of Time Base 7 (T7) (ECO)	S-IVB	11,630.33		
271. Redundant S-IVB Cutoff	S-IVB	11,630.41	0.08	0.08

*** Started new time base before these events could take place

Table 2-3. Sequence of Switch Selector Events (Continued)

FUNCTION	STAGE	RANGE TIME	TIME FROM BASE	
		ACTUAL (SEC)	ACTUAL (SEC)	ACT-PRFD (SEC)
272. LOX Tank Vent Valve, OPEN	S-IVB	11,530.51	0.18	-0.02
273. Point Level Sensors Disarming	S-IVB	11,530.60	0.27	-0.03
274. LH2 Tank Vent Valve, OPEN	S-IVB	11,530.70	0.37	-0.03
275. Second Burn Relay, OFF	S-IVB	11,531.08	0.75	-0.05
276. LOX Tank Flight Pressure System, OFF	S-IVB	11,531.29	0.96	-0.04
277. Coast Period, ON	S-IVB	11,631.50	1.17	-0.03
278. PL Activate, OFF	S-IVB	11,631.70	1.38	-0.02
279. PI Inverter and DC Power, OFF	S-IVB	11,531.80	1.47	-0.03
280. LOX Chidown Pump Purge Control Valve Open, OFF	S-IVB	11,531.89	1.56	-0.04
281. Flight Control Computer S-IVB Burn Mode Off "A"	IU	11,533.78	3.46	-0.04
282. Flight Control Computer S-IVB Burn Mode Off "B"	IU	11,634.00	3.67	-0.03
283. Aux. Hydraulic Pump Flight Mode, OFF	S-IVB	11,634.18	3.85	-0.05
284. Telemetry Calibrator In-Flight Calibrate, ON	IU	11,634.39	4.07	-0.03
285. Regular Calibrate Relays, ON	S-IVB	11,634.58	4.25	-0.05
286. Telemetry Calibrator In-Flight Calibrate, OFF	IU	11,639.38	9.06	-0.04
287. Regular Calibrate Relays, OFF	S-IVB	11,639.59	9.26	-0.04
288. SS/FM Transmitter, OFF	S-IVB	11,639.80	9.48	-0.02
289. SS/FM Group, OFF	S-IVB	11,639.98	9.65	-0.05
290. LOX Tank Vent Valve, CLOSE	S-IVB	11,640.28	9.95	-0.05
291. LOX Tank Vent Valve Boost Close, ON	S-IVB	11,643.29	12.97	-0.03
292. LOX Tank Vent Valve Boost Close, OFF	S-IVB	11,645.28	14.96	-0.04
293. LH2 Tank Vent Valve, CLOSE	S-IVB	11,750.28	119.95	-0.05
294. LH2 Tank Vent Valve Boost Close, ON	S-IVB	11,753.29	122.96	-0.04
295. LH2 Tank Vent Valve Boost Close, OFF	S-IVB	11,755.28	124.95	-0.05
296. LV/SC Separation Sequence Start	IU	11,810.28	179.95	-0.05

Table 2-3. Sequence of Switch Selector Events (Continued)

FUNCTION	STAGE	RANGE TIME	TIME FROM BASE	
		ACTUAL (SEC)	ACTUAL (SEC)	ACT. PREF. (SEC)
297. Switch PCM to Low Gain Antenna (Fail Safe)	IU	12,830.28*	1199.95*	-0.05
298. Switch CCS to Low Gain Antenna	IU	12,830.48*	1200.15*	-0.05
299. LH ₂ Tank Continuous Vent Valve Open, ON	S-IVB	12,830.68*	1200.35*	-0.05
300. LH ₂ Tank Continuous Vent Valve Open, OFF	S-IVB	12,832.68*	1202.35*	-0.05
301. Telemetry Calibrator In-Flight Calibrate, ON	IU	12,940.50*	1310.25*	-0.05
302. Regular Calibrate Relays, ON	S-IVB	12,940.78*	1310.45*	-0.05
303. Telemetry Calibrator In-Flight Calibrate, OFF	IU	12,945.58*	1315.25*	-0.05
304. Regular Calibrate Relays, OFF	S-IVB	12,945.78*	1315.45*	-0.05
305. Switch PCM to High Gain Antenna	IU	17,030.28	5399.95	-0.05
305. Switch CCS to High Gain Antenna (Fail Safe)	IU	17,030.49	5400.17	-0.03
307. Telemetry Calibrator In-Flight Calibrate, ON	IU	17,140.59	5510.25	-0.04
308. Regular Calibrate Relays, ON	S-IVB	17,140.79	5510.45	-0.04
309. Telemetry Calibrate In-Flight Calibrate, OFF	IU	17,145.58	5515.25	-0.05
310. Regular Calibrate Relays, OFF	S-IVB	17,145.78	5515.45	-0.05
311. LH ₂ Tank Continuous Vent Valve Close, ON	S-IVB	No Data	-	-
312. LH ₂ Tank Continuous Vent Valve Close, OFF	S-IVB	No Data	-	-
* Derived Times				

Table 2-4. Unscheduled Switch Selector Events

EVENT	STAGE	RANGE TIME (SEC)	TIME FROM BASE (SEC)	REMARKS
Water Coolant Valve, OPEN	IU	102.29	Tj+33.49	Tj+181.60 LVDC function
Water Coolant Valve, CLOSED	IU	1084.08	Tj+336.78	LVDC function
C-Band Transponder NO. 1 and NO. 2, ON	IU	3580.80	Tj+2833.51	
C-Band Transponder NO. 1, OFF	IU	3580.87	Tj+2833.57	NO. 2 Active
C-Band Transponder NO. 1 & NO. 2, ON	IU	5821.51	Tj+5074.21	
C-Band Transponder NO. 1, OFF	IU	5821.58	Tj+5074.28	NO. 2 active
Water Coolant Valve, OPEN	IU	5891.18	Tj+5143.83	LVDC function
C-Band Transponder NO. 1 & NO. 2, ON	IU	5925.51	Tj+5178.21	
C-Band Transponder NO. 2, OFF	IU	5925.58	Tj+5178.28	NO. 1 active
Water Coolant Valve, CLOSED	IU	6191.65	Tj+5444.35	
C-Band Transponder NO. 1 & NO. 2, ON	IU	6637.21	Tj+5889.91	
C-Band Transponder NO. 1, OFF	IU	6637.28	Tj+5889.98	NO. 2 active
Water Coolant Valve, CLOSED	IU	7995.44	Tj+7248.15	LVDC function
C-Band Transponder NO. 1 & NO. 2, ON	IU	11,069.04	Tj+10,321.74	
C-Band Transponder NO. 2, OFF	IU	11,069.11	Tj+10,321.81	NO. 1 active
C-Band Transponder NO. 1 & NO. 2, ON	IU	11,650.44	Tj+20.12	
C-Band Transponder NO. 1, OFF	IU	11,650.54	Tj+20.21	NO. 2 active
C-Band Transponder NO. 1 & NO. 2, ON	IU	11,658.68	Tj+28.35	
C-Band Transponder NO. 2, OFF	IU	11,658.75	Tj+28.42	NO. 1 active
C-Band Transponder NO. 1 & NO. 2, ON	IU	11,699.13	Tj+68.80	
C-Band Transponder NO. 1, OFF	IU	11,699.20	Tj+68.87	NO. 2 active
C-Band Transponder NO. 1 & NO. 2, ON	IU	11,707.33	Tj+77.00	
C-Band Transponder NO. 2, OFF	IU	11,707.40	Tj+77.00	NO. 1 active
C-Band Transponder NO. 1 & NO. 2, ON	IU	11,722.60	Tj+92.28	
C-Band Transponder NO. 1, OFF	IU	11,722.69	Tj+92.36	NO. 2 active
C-Band Transponder NO. 1 & NO. 2, ON	IU	11,850.66	Tj+220.33	
C-Band Transponder NO. 2, OFF	IU	11,850.73	Tj+220.40	NO. 1 active
Water Coolant Valve, OPEN	IU	12,203.47	Tj+573.74	LVDC function
Hydraulic Pump Coast Mode, OFF	S-IYB	14,961*	Tj+3331	Ground command
Hydraulic Pump Flight Mode, ON	S-IYB	14,961*	Tj+3331	Ground command
Telemetry Calibrator, ON	IU	15,004*	Tj+3374	Ground command
Regular Calibrator Relays, ON	S-IYB	15,004*	Tj+3374	Ground command
Hydraulic Pump Coast Mode, OFF	S-IYB	15,037*	Tj+3407	Ground command
Hydraulic Pump Flight Mode, ON	S-IYB	15,037*	Tj+3407	Ground command
Hydraulic Pump Flight Mode, OFF	S-IYB	15,060*	Tj+3430	Ground command
Telemetry Calibrator, OFF	IU	16,173*	Tj+4543	Ground command
Regular Calibrator Relays, OFF	S-IYB	16,173*	Tj+4543	Ground command

*Ground Transmittal times used because pulse times not available

Table 2-4. Unscheduled Switch Selector Events (Continued)

EVENT	STAT	RANGE TIME (SECF)	TIME FROM CASE (SECF)	REMARKS
Execute Maneuver A	TU	16,201*	T7+4571	Ground command
C-Band Transponder NO. 1 & NO. 2, ON	TU	16,266.45	T7+5156.12	
C-Band Transponder NO. 1, OFF	TU	16,285.52	T7+5156.19	NO. 2 active
Slow Record, ON	S-IVB	16,528.87	T7+5298.49	Commanded
Slow Record, OFF	S-IVB	16,529.72	T7+5299.39	Commanded
Recorder Playback, ON	S-IVB	16,930.62	T7+5300.29	Commanded
C-Band Transponder NO. 1 & NO. 2, ON	TU	16,971.01	T7+5340.56	
C-Band Transponder NO. 2, OFF	TU	16,971.06	T7+5340.75	NO. 1 active
C-Band Transponder NO. 1 & NO. 2, ON	TU	17,234.54	T7+5604.21	
C-Band Transponder NO. 1, OFF	TU	17,234.61	T7+5604.28	NO. 2 active
Water Coolant valve, CLOSED	TU	17,314.29	T7+5640.96	LVSC function
C-Band Transponder NO. 1 & NO. 2, ON	TU	17,555.17	T7+5924.85	
C-Band Transponder NO. 2, OFF	TU	17,555.25	T7+5924.92	NO. 1 active
Recorder Playback, OFF	S-IVB	21,997.42	T7+10,257.09	Commanded
LOX Tank Flight Pressure System, ON	S-IVB	22,021.49	T7+10,391.16	Commanded
Coast Period, OFF	S-IVB	22,022.39	T7+10,392.06	Commanded
LOX Tank Vent Valve, OPEN	S-IVB	22,023.30	T7+10,392.97	Commanded
LH2 Tank Vent Valve, OPEN	S-IVB	22,024.21	T7+10,393.88	Commanded
C-Band Transponder NO. 1 & NO. 2, ON	TU	22,170.39	T7+10,540.06	
C-Band Transponder NO. 1, OFF	TU	22,170.46	T7+10,540.13	NO. 2 active
C-Band Transponder NO. 1 & NO. 2, ON	TU	22,594.88	T7+10,964.56	
C-Band Transponder NO. 1, OFF	TU	22,594.95	T7+10,964.63	NO. 2 active
C-Band Transponder NO. 1 & NO. 2, ON	TU	22,611.17	T7+10,980.84	
C-Band Transponder NO. 2, OFF	TU	22,611.25	T7+10,980.93	NO. 1 active
C-Band Transponder NO. 1 & NO. 2, ON	TU	22,674.50	T7+11,044.48	
C-Band Transponder NO. 1, OFF	TU	22,674.87	T7+11,044.55	NO. 2 active
C-Band Transponder NO. 1 & NO. 2, ON	TU	22,754.56	T7+11,124.23	
C-Band Transponder NO. 1 & NO. 2, ON	TU	22,754.63	T7+11,124.30	NO. 1 active
C-Band Transponder NO. 1 & NO. 2, ON	TU	22,963.27	T7+11,332.94	
C-Band Transponder NO. 1, OFF	TU	22,963.34	T7+11,333.01	NO. 2 active
C-Band Transponder NO. 1 & NO. 2, ON	TU	23,026.89	T7+11,396.57	
C-Band Transponder NO. 2, OFF	TU	23,026.97	T7+11,396.64	NO. 1 active
C-Band Transponder NO. 1 & NO. 2, ON	TU	23,122.70	T7+11,492.43	
C-Band Transponder NO. 1, OFF	TU	23,122.83	T7+11,492.50	NO. 2 active

*Ground Transmittal Times used because pulse times not available

SECTION 3

LAUNCH OPERATIONS

3.1 SUMMARY

The Saturn AS-502 was the second flight vehicle of the Saturn V Apollo flight program. The basic purpose of the flight was to demonstrate the compatibility and performance of the launch vehicle and the Apollo Command and Service Modules (CSM) for manned flight.

The launch countdown for AS-502 was completed without any unscheduled countdown holds and the vehicle was successfully launched at 07:00:01 Eastern Standard Time (EST) April 4, 1968.

Ground systems performance was highly satisfactory. The relatively few problems encountered in countdown were overcome such that vehicle launch readiness was not compromised.

Launch damage to the complex and support equipment was minor. Modifications to the ground systems were effective in reducing the amount of blast damage below that sustained during AS-501 launch.

3.2 PRELAUNCH MILESTONES

A chronological summary of events and preparations leading to the launch of AS-502 is contained in Table 3-1.

3.3 COUNTDOWN EVENTS

The launch countdown for AS-502 was picked up at -24 hours at 1:00:00 EST April 3, 1968 and proceeded to -8 hours with no holds. At this point the scheduled six hour hold period was initiated. The count was resumed from -8 hours at 23:00:00 EST April 3, 1968, and culminated in the successful launch of the vehicle at 07:00:01 EST April 4, 1968.

Only four significant problems developed during the launch countdown. All these problems were resolved before the end of the scheduled six hour hold period. The items are stated below in chronological order:

- a. Several LH₂ vent bubble caps were found to have cracks exposing the vehicle vent system directly to the atmosphere.

Table 3-1. AS-502 Milestones

DATE	EVENT
February 21, 1967	S-IVB Stage Arrival
March 3, 1967	S-IC Stage Arrival
March 20, 1967	Instrument Unit Arrival
March 29, 1967	Erection of Launch Vehicle (LV) with S-II Spacer
May 4, 1967	LV Electrical Interface Mate Test with S-II Spacer
May 19, 1967	LV Guidance & Control Tests with S-II Spacer
May 24, 1967	S-II Stage Arrival
May 29, 1967	LV Propellant Dispersion Test with S-II Spacer
May 29, 1967	LV Power Transfer Test with S-II Spacer
May 31, 1967	LV Emergency Detection System (EDS) Test with S-II Spacer
June 1, 1967	LV Flight Sequence and Exploding Bridge Wire (EBW) Functional Test with S-II Spacer
June 8, 1967	LV Sequence Malfunction Test with S-II Spacer
June 13, 1967	LV Plugs-In Overall Test (OAT) No. 1 with S-II Spacer
June 29, 1967	De-erection of the LV through S-II Spacer
July 6, 1967	Completed S-II LH ₂ Tank Inspection
July 13, 1967	Erection of LV with S-II Flight Stage
July 24, 1967	LV Electrical Interface Mate Test
July 24, 1967	LV Switch Selector Functional Test
August 8, 1967	LV EDS Test

Table 3-1. AS-502 Milestones (Continued)

DATE	EVENT
August 10, 1967	LV Flight Sequence and EBW Functional Test
August 11, 1967	LV Power Transfer Test
August 11, 1967	LV Propellant Dispersion Test
August 30, 1967	LV OAT No. 2, Plugs Out
December 10, 1967	Erection of Spacecraft (S/C)
December 11, 1967	Swing Arm Compatibility Test
December 21, 1967	LV OAT No. 1, Plugs In (Waivered)
December 27, 1967	LV Combined Guidance and Control System Tests
December 29, 1967	LV OAT No. 2, Plugs Out
January 4/5, 1968	LV Mission Control Center-Houston (MCC-H) Interface Test Vehicle Assembly Building (VAB)
January 16, 1968	Space Vehicle (SV) OAT No. 1, Plugs In
January 24, 1968	SV OAT No. 2, Plugs Out
January 29, 1968	SV Swing Arm OAT
February 2, 1968	Ordnance Installation
February 6, 1968	Transferred Launcher Umbilical Tower (LUT)/Vehicle to Pad
March 8, 1968	SV Flight Readiness Test (FRT) Completed
March 22, 1968	RP-1 Load
March 31, 1968	SV Countdown Demonstration Test (CDDT) Completed
April 4, 1968	Vehicle Launched on Schedule at 07:00:01 EST

- b. The S-II stage, BP-1 transmitter (PCM/FM Link) failed and had to be replaced.
- c. An electronics package in the S-IC stage RP-1 loading system required replacement and re-calibration.
- d. The S-IC Ground Support Equipment (GSE) stage power supply required replacement.

3.4 PROPELLANT LOADING

3.4.1 RP-1 Loading

The RP-1 system completed all operations from CDDT through launch satisfactorily. There were no delays or questionable items during loading other than one minor anomaly. During adjust level drain in CDDT, a time delay relay malfunctioned and required replacement.

The level adjust operation in both CDDT and the launch countdown left the flight mass within 0.01 percent of the intended value. Kennedy Space Center (KSC) mass readout indicated that 610,197.4 kilograms (1,345,255 lbm) of RP-1 were onboard the S-IC stage at ignition.

3.4.2 LOX Loading

The LOX system supported CDDT and launch satisfactorily. Minor problems during CDDT were corrected without impact on the launch. There were no hardware failures nor propellant leaks during launch countdown. The LOX automatic loading sequence was initiated at -6 hours 29 minutes with S-IVB slow fill and terminated at -3 hours 7 minutes. Approximately 3418.2 m³ (903,000 gal) of LOX were consumed during CDDT and launch countdown. At launch, about 1703.4 m³ (450,000 gal) were onboard AS-502 and flight LOX mass was within specifications.

Two of the minor anomalies encountered during final LOX loading are as follows:

- a. During the S-IC final fast fill sequence, the speed of the LOX transfer pump was manually adjusted raising the flowrate from 0.524 m³/s (8300 gpm) to a desired level of 0.590 m³/s (9350 gpm) in order to avoid a loading delay. The need for this manual adjustment had been anticipated and was covered in the released loading procedure.
- b. Level shifts were experienced by the S-IC LOX and RP-1 recorders associated with the automatic Propellant Tanking Computer System (PTCS) during LOX loading. The shifts had no effect on the operation of the PTCS. The exact cause of the shifts has not yet been established, but investigation will continue.

3.4.3 LH₂ Loading

The LH₂ system performed satisfactorily throughout CDDT and launch countdown. The prelaunch fill sequences were performed with no anomalies or delays. Preconditioning of the S-II stage was initiated at -6 hours 25 minutes and was continued through -3 hours successfully cooling down the S-II stage. Automatic loading was initiated at -2 hours 58 minutes with transfer line chilldown and terminated at -1 hour 31 minutes.

During CDDT approximately 1041.0 m³ (275,000 gal) of LH₂ were consumed. This included losses from three S-II preconditioning runs, vehicle boil-off, and drain volume not returned to the storage tank. Launch countdown consumed 1748.9 m³ (462,000 gal) from the LH₂ facility. At launch LH₂ flight mass was within specifications.

The following anomalies were noted:

- a. Water entered the vehicle vent system at the burn pond after the replenish sequence was terminated during CDDT and launch countdown. This also occurred during AS-501 loading operations and was attributed to siphoning action through the standpipes initiated by rapid closing of the stage vent. The AS-502 problem may have been caused by insufficient helium purge resulting in cold piping, thus allowing the helium to contract once the purge was terminated. This contraction could result in lowering of the pressure and initiation of the siphoning action.
- b. After both CDDT and the launch countdown, several LH₂ vent bubble caps were cracked which exposed the vehicle vent system directly to the atmosphere. These cracks are attributed to localized overheating coupled with rapid cooling by the splashing water in the pond.
- c. The debris valve in the LH₂ fill line was not closed until 12 seconds. This compromises the integrity of the fill line by raising the possibility that debris may enter the line during launch.

3.4.4 Auxiliary Propulsion System Propellant Loading

There were no problems encountered during propellant loading of the Auxiliary Propulsion System (APS). Propellants consumed during loading were as follows:

a. Module 1

(1) Oxidizer System (Nitrogen Tetroxide, N₂O₄)

- (a) Volume loaded 67,219.7 cm³ (4102 in.³) at 299.8°K (80°F).
- (b) Volume off-loaded 6096.0 cm³ (372 in.³) at 297.0°K (75°F).
- (c) Volume removed with bubble bleed during burp firing 458.8 cm³ (28 in.³) at 304.5°K (88.5°F).
- (d) Volume removed with bubble bleed during countdown 622.7 cm³ (38 in.³) at 302.6°K (85°F).

- (2) Fuel System (Mono Methyl Hydrazine, MMH)
 - (a) Volume loaded 67,219.7 cm³ (4102 in.³) at 300.6°K (81.5°F).
 - (b) Volume off-loaded 1442.1 cm³ (88 in.³) at 301.5°K (83°F).
 - (c) Volume removed with bubble bleed during countdown 622.7 cm³ (38 in.³) at 302.0°K (84°F).

b. Module 2

- (1) Oxidizer System (Nitrogen Tetroxide, N₂O₄)
 - (a) Volume loaded 67,219.7 cm³ (4102 in.³) at 300.9°K (82°F).
 - (b) Volume off-loaded 6096.0 cm³ (372 in.³) at 300.9°K (82°F).
 - (c) Volume removed with bubble bleed during burp firing 344.1 cm³ (21 in.³) at 305.9°K (91°F).
 - (d) Volume removed with bubble bleed during countdown 491.6 cm³ (30 in.³) at 302.0°K (84°F).
- (2) Fuel System (Mono Methyl Hydrazine, MMH)
 - (a) Volume loaded 67,219.7 cm³ (4102 in.³) at 299.3°K (79°F).
 - (b) Volume off-loaded 1442.1 cm³ (88 in.³) at 300.1°K (80.5°F).
 - (c) Volume removed with bubble bleed during countdown 458.8 cm³ (28 in.³) at 300.9°K (82°F).

3.4.5 S-IC Stage Propellant Load

Initial propellant loads were obtained from the KSC weight and balance log and compared with the continuous level sensor data. This comparison showed the LOX load to be 1103 kilograms (2432 lbm) greater, and the fuel load 1259 kilograms (2777 lbm) less than the KSC loads. The propulsion performance reconstruction utilizing an RPM match was able to follow the continuous level sensor data for both LOX and fuel with an accuracy of ±1.27 centimeters (±0.5 in.). The reconstruction also matched the residuals calculated from level sensor and line pressure data indicating that the propellant loads calculated from the level sensor data are accurate. The reconstructed LOX load is 0.08 percent above KSC indicated values, and the reconstructed fuel load is 0.20 percent below KSC indicated values. Both are well within the predicted three sigma limits of ±0.5 percent. Total propellants onboard at ignition command are shown in Table 3-2.

3.4.6 S-II Stage Propellant Load

The percentage of flight mass onboard the S-II stage just before each tank pressurizing time was indicated by the PTCS to be 99.96 percent for LH₂ and 100.02 percent for LOX. Table 3-3 presents the S-II stage propellant load at S-IC ignition command.

3.4.7 S-IVB Stage Propellant Load

The PTCS indicated flight mass onboard the S-IVB stage just prior to individual tank pressurization was 100.08 percent for LH₂ and 99.98 percent

Table 3-2. S-IC Stage Propellant Mass at Ignition Command

PROPELLANT	UNITS	MASS REQUIREMENTS		MASS INDICATIONS		MASS DEVIATIONS	
		PREDICTED PRIOR TO LAUNCH	LOADING TABLE AT IGNITION ^{1,2}	LEVEL SENSOR DATA	BEST ESTIMATE	BEST EST MINUS PREDICTED	BEST EST MINUS IGNITION
LOX	kg lbm	1,427,032	1,428,039	1,429,142	1,429,155	2123	1116
		3,145,067	3,148,286	3,150,718	3,150,749	4601	2462
RP-1	kg lbm	611,318	610,197	608,958	608,949	-2369	-1248
		1,347,727	1,343,255	1,342,478	1,342,503	-5224	-2752
Total	kg lbm	2,038,350	2,038,236	2,038,080	2,038,104	-246	-132
		4,493,794	4,493,541	4,493,196	4,493,251	-541	-290
						-0.01	-0.01

¹ Based on LOX density of 1137.3 kg/m³ (71.0 lbm/ft³) and RP-1 density of 802.5 kg/m³ (50.1 lbm/ft³).

² Based on LOX density of 1136.8 kg/m³ (70.97 lbm/ft³) and RP-1 density of 801.0 kg/m³ (50.035 lbm/ft³).

³ KSC propellant mass readouts are same as loading table data at ignition.

Table 3-3. S-II Stage Propellant Mass at S-IC Ignition Command

PROPELLANT	UNITS	PREDICTED PRIOR TO LAUNCH	PJ SYSTEM	LEVEL SENSOR DATA	ENGINE FLOW INTEGRAL (BEST ESTIMATE)	PJ SYSTEM MINUS PREDICTED	BEST EST. MINUS PREDICTED
LOX	kg lbm	357,940	358,318	360,663	359,770	379	1930
		789,123	789,959	795,125	793,157	836	4034
LH ₂	kg lbm	69,164	68,964	69,505	69,380	-200	216
		152,480	152,039	153,237	152,957	-441	477
Total	kg lbm	427,104	427,283	430,168	429,150	179	2046
		941,603	941,998	948,356	946,114	395	4511
						0.04	0.48

for LOX. Table 3-4 lists the S-IVB propellant load at S-IC ignition command. Simulation-trajectory match results were used in conjunction with the listed data to determine the best estimate values. The best estimate propellant masses are 0.46 percent higher for LOX and 0.07 percent lower for LH₂ than the predicted values. These deviations were well within the required loading accuracy.

3.5 S-II INSULATION PURGE AND LEAK DETECTION

The S-II insulation purge and leak detection system performed effectively during prelaunch operations. It was necessary to activate auxiliary back purge in the sidewall insulation during terminal count; however, detailed inspection by operational television failed to identify any leak in the external insulation surface. Data recorded during this time indicated an interconnection developed between the sidewall and feedline elbow flow circuits in terminal count following the LH₂ fill sequence. Reevacuation of the common bulkhead was accomplished at -1 hour 33 minutes without compromise to the purge system.

3.6 GROUND SUPPORT EQUIPMENT

Ground systems performance was highly satisfactory. The swing arms, hold-down arms, tail service masts, propellant tanking systems, and all other ground equipment functioned well in support of AS-502 launch. Table 3-5 gives the start times for some of the pertinent ground/vehicle interface events. There were relatively few anomalies, and launch damage was light in most areas. Detailed information of ground equipment performance, problems encountered during launch preparations, and blast damage to the complex and equipment is given in Apollo/Saturn V Ground Systems Evaluation Report AS-502, Kennedy Space Center, May 1968.

Table 3-4. S-IVB Stage Propellant Mass at S-IC Ignition Command

PROPELLANT	UNITS	PREDICTED PRIOR TO LAUNCH	PU INDICATED (CORRECTED)	LEVEL SENSOR (EXTRAPOLATED)	FLOW INTEGRAL	BEST ESTIMATE	PU INC. MINUS PREDICTED	BEST EST. MINUS PREDICTED
LOX	kg	87,555	87,730	88,401	88,109	88,960	75	405
	lbm %	191,246	193,412	194,593	194,424	194,140	166 0.09	894 0.46
LH ₂	kg	19,268	19,269	19,309	19,245	19,254	1	-14
	lbm %	42,479	42,482	42,569	42,429	42,246	3 0.01	31 0.07
Total	kg	106,823	106,999	107,710	107,434	107,314	75	391
	lbm %	235,725	235,894	237,162	236,853	236,386	169 0.07	805 0.36

Table 3-5. Ground/Vehicle Interface Events

EVENT		RANGE TIME HR:MIN:SEC
Arm 3, S-II Aft (Access) (Start Arm Retract [SAR])		-00:26:06.74
Arm 9, Egress Arm (SAR)		-00:26:06.40
C-Ball Cover (Start Cover Retract)		-00:04:46.57
Arm 1 S-IC Intertank (SAR)		-00:00:26.27
Arm 2, S-IC Forward (SAR)		-00:00:21.42
Launch Commit	Initiate Release System	-00:00:00.12
	Arm Liftoff Switches	00:00:00.18
Holddown Arm Release, Primary (Pneumatic)		00:00:00.36
Liftoff Switches (Position II-IV), Primary (1 inch)		00:00:00.55
Arm 8, CM/SM Arm (SAR)		00:00:00.60
Arm 7, IU/S-IVB Forward (SAR)		00:00:00.60
Tail Service Masts (3), Primary (Pneumatic)		00:00:00.75
Arm 4, S-II Intermediate (SAR)		00:00:00.83
Arm 5, S-II Forward (SAR)		00:00:00.91
Arm 6, S-IVB Aft (SAR)		00:00:00.92

Two problems associated with the S-II stage oriented pressurization and servicing system were as follows:

- a. The system experienced an excessive loss of helium during CDDT and the launch countdown. Replacement of two relief valves, suspected as sources of leakage, did not reduce the loss of helium during launch countdown. Troubleshooting of this system will continue.
- b. S-II engine start tank temperatures, although within required limits at launch, were colder than expected. Helium used to condition the start tanks is prechilled by the GSE LH₂ heat exchanger. An analysis of the engine servicing system will be performed to isolate this problem.

Overall damage to the launch complex and support equipment was less than occurred at AS-501 launch. Modifications incorporated to reduce blast damage below that experienced on the previous launch were effective. Some conditions of damage revealed by post launch damage assessment are as follows:

- a. RP-1 System. The mast cutoff valve in tail service mast 1-2 opened at liftoff causing activation of the Ansel fire chemical system in Mobile Launcher (ML) Room 4A. This resulted in the RP-1 distributor cabinet being filled with fire extinguishing powder.
- b. LOX System. Thirty one cables on level 30 sustained varying degrees of burn damage. The jacket of a section of vacuum-insulated piping near level zero was dented.
- c. Environmental Control System (ECS). Launch damage was approximately the same as was experienced during the launch of AS-501; however, the ECS ducts were more extensively damaged. The horizontal ducts on level zero and the first 6 meters (approximately 20 ft) of vertical ducting were completely destroyed. The second 6-meter section of ducting also suffered extensive blast damage and the supporting structure was broken loose and severely warped.
- d. Holddown Arms. The holddown arm hoods were warped. Arm 3 hood was warped extensively. Grouting between the holddown arm bases and the LUT deck prevented recurrence of the AS-501 flame damage to arm interior components.
- e. Swing Arms. Damage was somewhat more widespread than for AS-501 launch but fewer major components were affected. Lower swing arms, particularly arm 1, sustained the greater damage. There were fires in the lower hinge areas of arms 4 and 6 resulting from hydraulic oil leakage through loosened "B" nuts.
- f. S-IC stage oriented mechanical GSE. Storage racks on LUT levels 60, 100 and 120 sustained varying amounts of engine exhaust damage. One rack was completely destroyed but the others are considered repairable.

SECTION 4

TRAJECTORY ANALYSIS

4.1 SUMMARY

Actual trajectory parameters of the AS-502 were close to nominal until the premature shutdown of two engines on the S-II stage. After this premature shutdown, the trajectory deviated significantly from the nominal throughout the remainder of the mission.

Space-fixed velocity at S-IC Launch Vehicle Digital Computer (LVDC) sensed Outboard Engine Cutoff (OECO) was 7.28 m/s (23.89 ft/s) greater than nominal. At S-II LVDC sensed Engine Cutoff (ECO), compared to nominal cutoff, the space-fixed velocity was 102.36 m/s (335.82 ft/s) less than nominal and the altitude was 6.39 kilometers (3.45 n mi) higher than nominal. At S-IVB velocity cutoff command, compared to nominal cutoff, the space-fixed velocity was 48.94 m/s (160.56 ft/s) greater than nominal; the cause of this overspeed is discussed in Section 10. The altitude at S-IVB velocity cutoff command was 0.79 kilometers (0.42 n mi) lower than nominal and the surface range was 498.45 kilometers (269.15 n mi) longer than nominal.

Parking orbit insertion conditions deviated considerably from nominal because of anomalies that occurred during the powered portion of flight. The space-fixed velocity at insertion was 48.16 m/s (158.00 ft/s) greater than nominal and the flight path angle (elevation of space-fixed velocity vector from local horizontal) was 0.378 degree less than nominal. These conditions produced an orbit which was quite elliptical with an eccentricity 0.0138 greater than nominal. The resulting apogee of the parking orbit was 171.54 kilometers (92.63 n mi) higher than nominal, and the perigee was 12.17 kilometers (6.57 n mi) less than nominal.

The S-IC stage broke up at approximately 397 seconds at an altitude of 28.9 kilometers (15.6 n mi) according to photographic coverage. At this time the actual surface range and altitude as determined from a theoretical free flight simulation, were within 0.10 kilometers (0.05 n mi) and 1.42 kilometers (0.76 n mi), respectively, of nominal. The free-flight trajectory indicates S-II stage impact of 436.82 kilometers (235.86 n mi) further downrange than the nominal impact point.

The S-IVB stage failed to reignite. Shortly after the attempted reignition, the spacecraft separated from the launch vehicle on ground command to the spacecraft. The S-IVB stage reentered due to orbital decay on April 26, 1968.

4.2 TRACKING DATA UTILIZATION

4.2.1 Tracking During the Ascent Phase of Flight

Tracking data were obtained during the period from the time of first motion through parking orbit insertion.

Postflight trajectory for the initial portion of flight was established from a least squares curve fit of optical tracking data and was merged with a best estimate trajectory. The best estimate trajectory utilized telemetered guidance velocities as the generating parameters to fit data from GLOTRAC Station I and five different C-Band radar tracking stations. These data points were fit through a guidance error model and constrained to the insertion vector obtained from the orbital solution. Comparison of the best estimate trajectory with data from all the tracking systems yielded reasonable agreement.

GLOTRAC Segment I data is a best estimate fit of the data from the various GLOTRAC sites. GLOTRAC Segment I provided data up to 480 seconds. Comparisons between these data and the trajectory show maximum differences of 300 meters (984 ft) in the vertical component, 20 meters (66 ft) in the crossrange component, and 100 meters (328 ft) in the downrange component. The vertical component is the least accurately determined by the GLOTRAC system. These GLOTRAC data were received too late to be considered in the establishment of the trajectory, but are helpful in ascertaining the validity of the trajectory. The GLOTRAC Segment I data were the only precision tracking data available after 230 seconds. Comparisons with the GLOTRAC Station I and Offset Frequency Doppler (ODOP) data show deviations which are considerably less than those obtained from the GLOTRAC Segment I data.

4.2.2 Tracking During Orbital Flight

Table 4-1 presents a summary of the C-Band radar stations furnishing data for use in determining the orbital trajectory. There were also considerable S-Band tracking data available during the orbital flight which were not used in determining the orbital trajectory due to the abundance of C-Band radar data.

The orbital trajectory was obtained by taking the insertion conditions and integrating them forward at the desired time intervals. The insertion conditions, as determined by the Orbital Correction Program (OCP), were obtained by a differential correction procedure which adjusted the estimated insertion conditions to fit the C-Band radar tracking data in accordance with the weights assigned to the data. After all the C-Band radar tracking data were analyzed, some stations and passes were eliminated completely from use in the determination of the insertion conditions.

Table 4-1. Summary of AS-502 Orbital C-Band Tracking Stations

STATION	TYPE OF RADARS	REV 1	REV 2	REV 3	REV 4	REV 5	REV 6	REV 7
Insertion Ship	FPS-16M	X						
Tananarive	FPS-16M	X	X					
Carnarvon	FPQ-6	X	X	X	X			
Hawaii	FPS-16M		X	X	X	X	X	X
California	FPS-16M	X						
White Sands	FPS-16M	X	X	X	X			
Merritt Island	TPQ-1B		X	X*				
Patrick	FPQ-6		X	X*				
Grand Bahama	TPQ-1B		X		X			
Bermuda	FPS-16M		X	X				
Antigua	FPQ-6			X*				
Canary Island	MPS-26	X						

* Tracked Spacecraft After S-IVB/CSM Separation

Final GLOTRAC Segment I data were received for the interval where the attempted S-IVB stage reignition occurred. These data were received too late to be considered in the establishment of the trajectory; however, comparisons of the trajectory with these data help to indicate the validity of the trajectory. After the GLOTRAC data became reliable (about 11,590 seconds), the maximum deviations were about 270 meters (886 ft) in the vertical component, 175 meters (574 ft) in the crossrange component, and 125 meters (410 ft) in the downrange component.

4.3 TRAJECTORY EVALUATION

4.3.1 Ascent Trajectory

Actual and nominal altitude, surface range, and cross range for the ascent phase are presented in Figure 4-1. The actual and nominal total earth-fixed velocities, and the elevation angles (elevation of earth-fixed velocity vector from the local horizontal) of the velocity vectors are shown in Figure 4-2. Actual and nominal space-fixed velocity and flight path angle during ascent are shown in Figure 4-3. Comparisons of total inertial accelerations are shown in Figure 4-4.

The combined burn time of the S-IC, S-II, and S-IV3 first burn was 87.61 seconds longer than nominal; the S-IC burned 0.85 seconds longer than nominal, the S-II burned 57.81 seconds longer than nominal, and the S-IVB burn was 28.95 seconds longer than nominal. The abnormally long S-II burn was the result of the premature cutoff of the two engines,

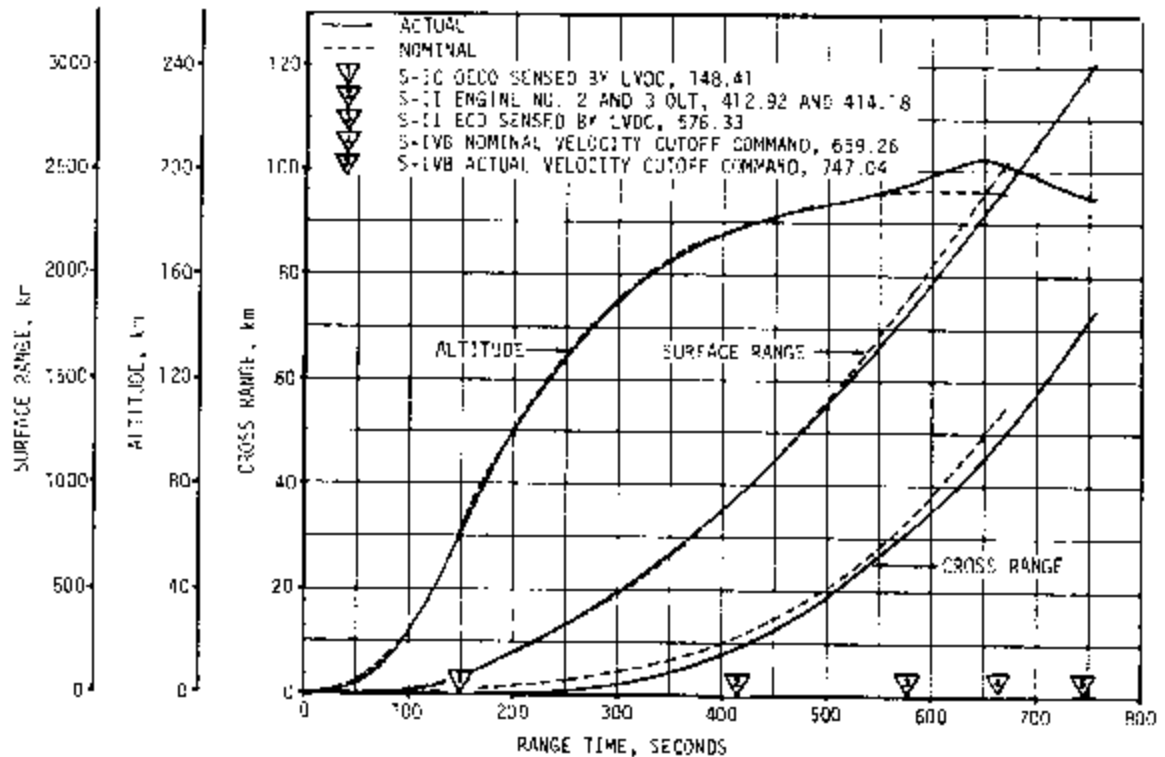


Figure 4-1. Ascent Trajectory Position Comparison

causing the S-IVB to burn longer in attempting to arrive at the proper end conditions. The accuracy of the trajectory at S-IVB cutoff is estimated to be ± 1.0 m/s (3.3 ft/s) in velocity, and ± 500 meters (1,640 ft) in altitude.

Mach number and dynamic pressure are shown in Figure 4-5. These parameters were calculated using measured meteorological data to an altitude of 50.2 kilometers (27.1 n mi). Above this altitude the measured data were merged into the U.S. Standard Reference Atmosphere.

Comparisons of the actual S-II engine No. 2 premature cutoff conditions, with their corresponding nominal conditions, are shown in Table 4-2. Actual and nominal values of parameters at significant trajectory event times, cutoff events, and separation events are shown in Tables 4-3, 4-4, and 4-5, respectively. The heading angle is the azimuth of the space-fixed velocity measured east of north.

Until the S-II engine premature shutdown, the altitude was slightly lower than nominal, the surface range was close to the nominal, and the total inertial acceleration was less than nominal.

The theoretical free-flight trajectory simulation data for the discarded S-IC and S-II stages were based on initial conditions obtained from the final postflight trajectory at separation. The simulation was based

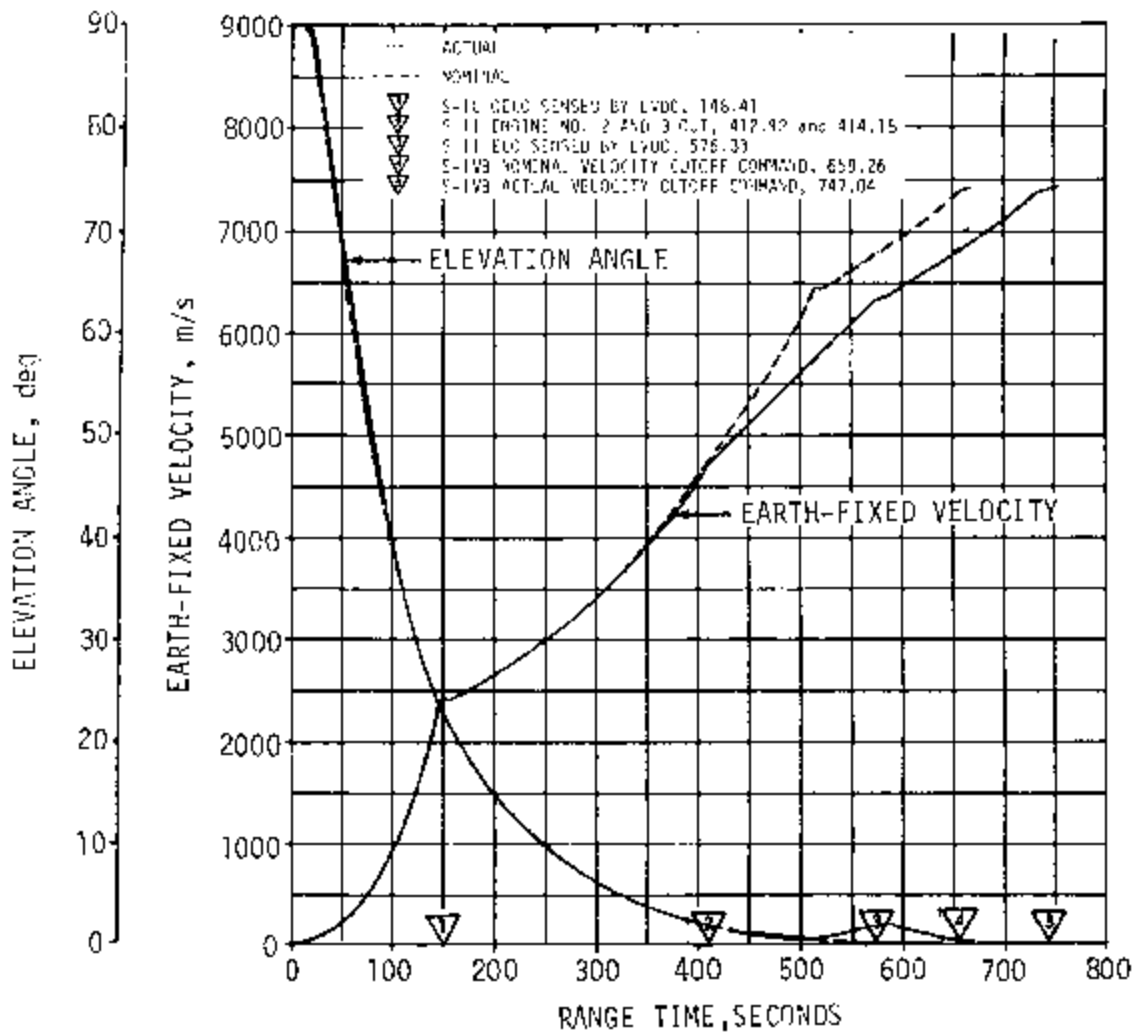


Figure 4-2. Ascent Trajectory Earth-Fixed Velocity Comparison

upon the separation impulses for both stages and nominal tumbling drag coefficients due to lack of tracking data for both stages. Photographic coverage of the S-IC stage indicated that the stage broke up at 397 seconds within 0.10 kilometer (0.05 n mi) surface range, and 1.42 kilometers (0.76 n mi) altitude of nominal. Table 4-3 presents the significant parameters and their deviations from nominal; including Max Q, maximum acceleration, apexes of spent stages, and maximum earth-fixed velocities. A summary of impact times and locations for the S-IC and S-II stages is presented in Table 4-6. Since there was no tracking or photographic coverage of the discarded S-II stage, its impact was simulated as noted above.

Spacecraft separation was initiated on ground command to the spacecraft after it was ascertained that the S-IVB stage had failed to reignite. The trajectory conditions at spacecraft separation are presented in Table 4-5.

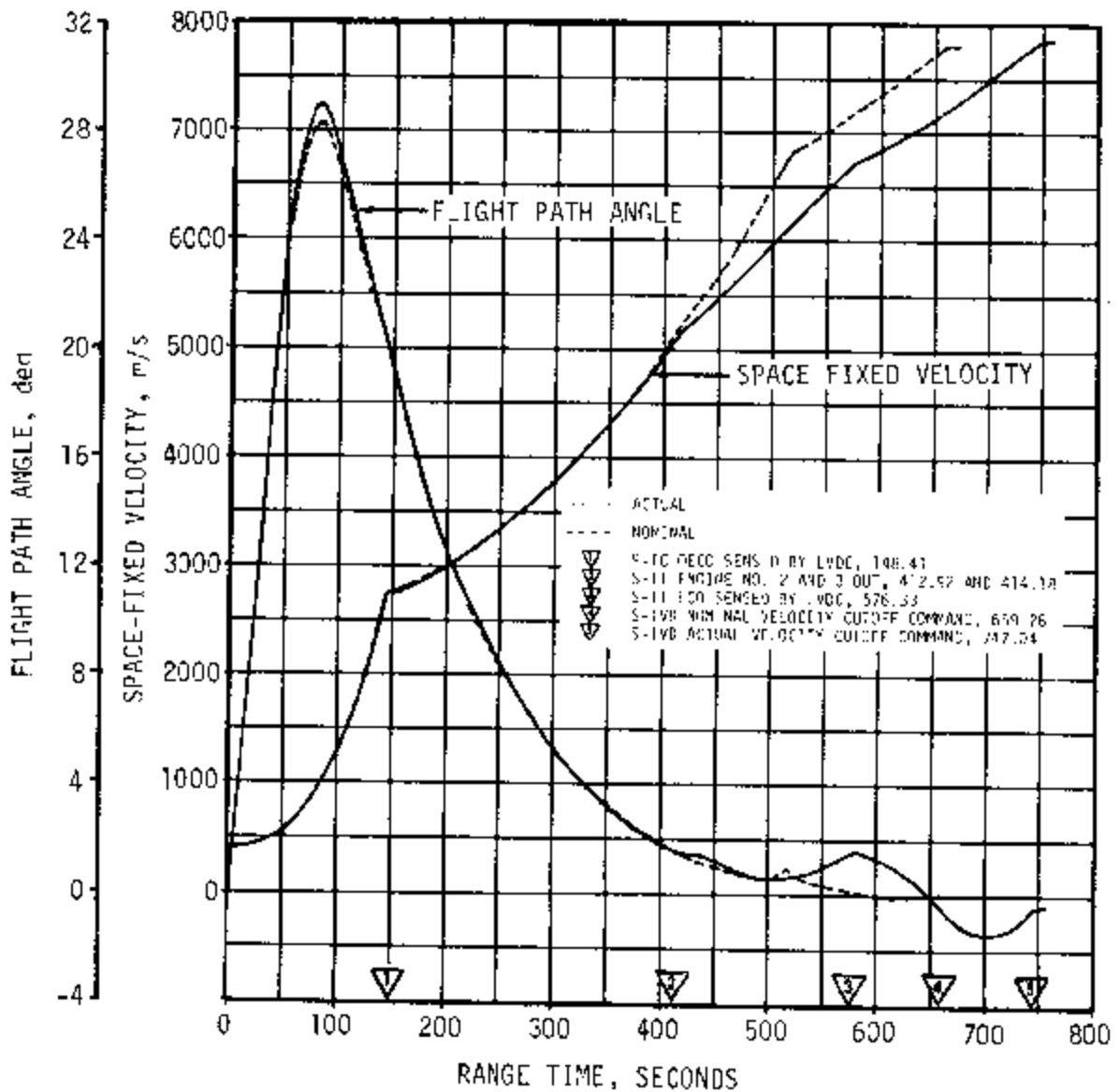


Figure 4-3. Ascent Trajectory Space-Fixed Velocity Comparison

As a result of the S-IVB failure to reignite for second burn, the S-IVB stage remained in orbit after spacecraft separation instead of flying the high apogee (lunar distance) orbit planned.

The S-IVB stage reentered on April 26, in the ocean between the east coast of Africa and the west coast of India.

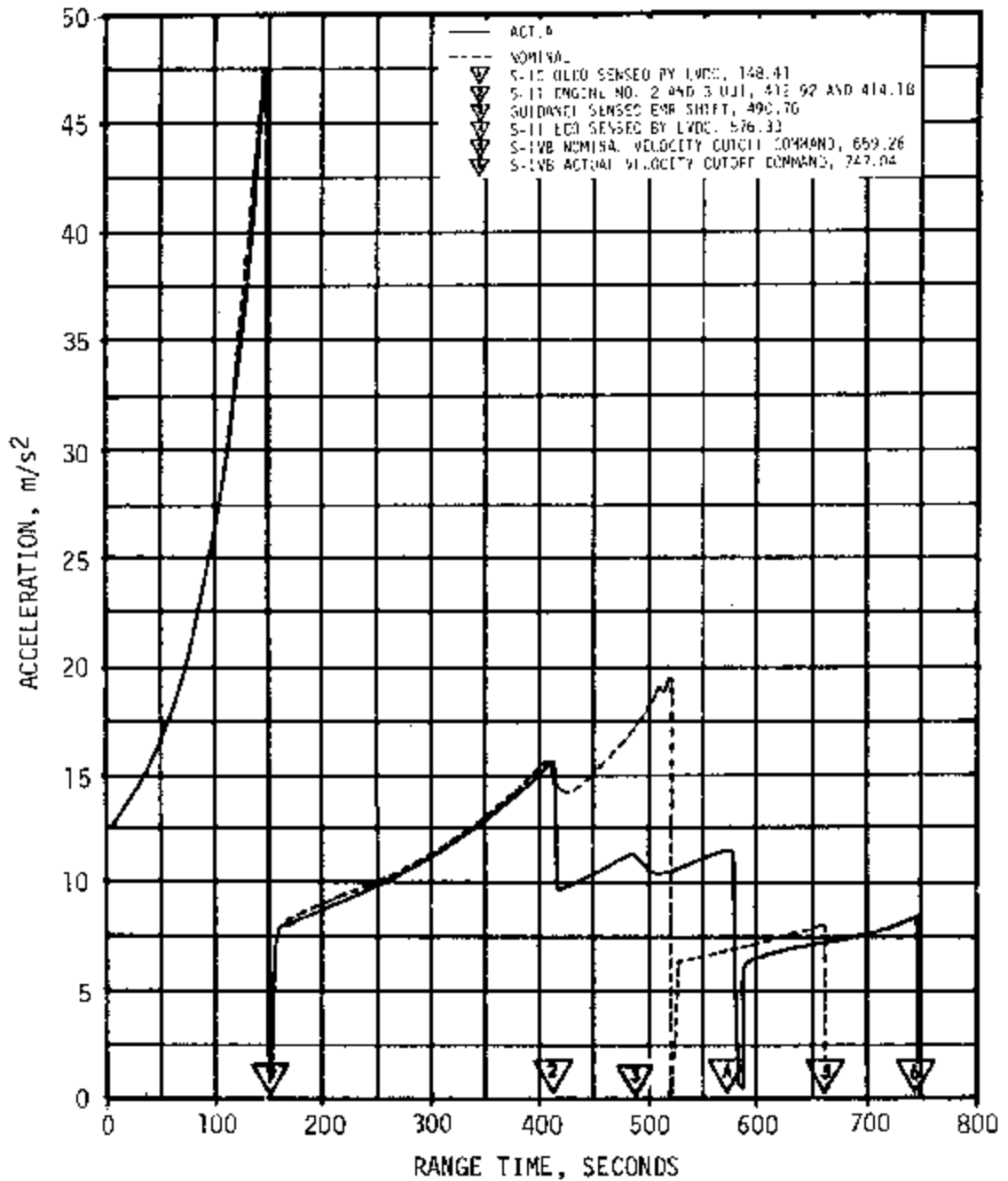


Figure 4-4. Ascent Trajectory Acceleration Comparison

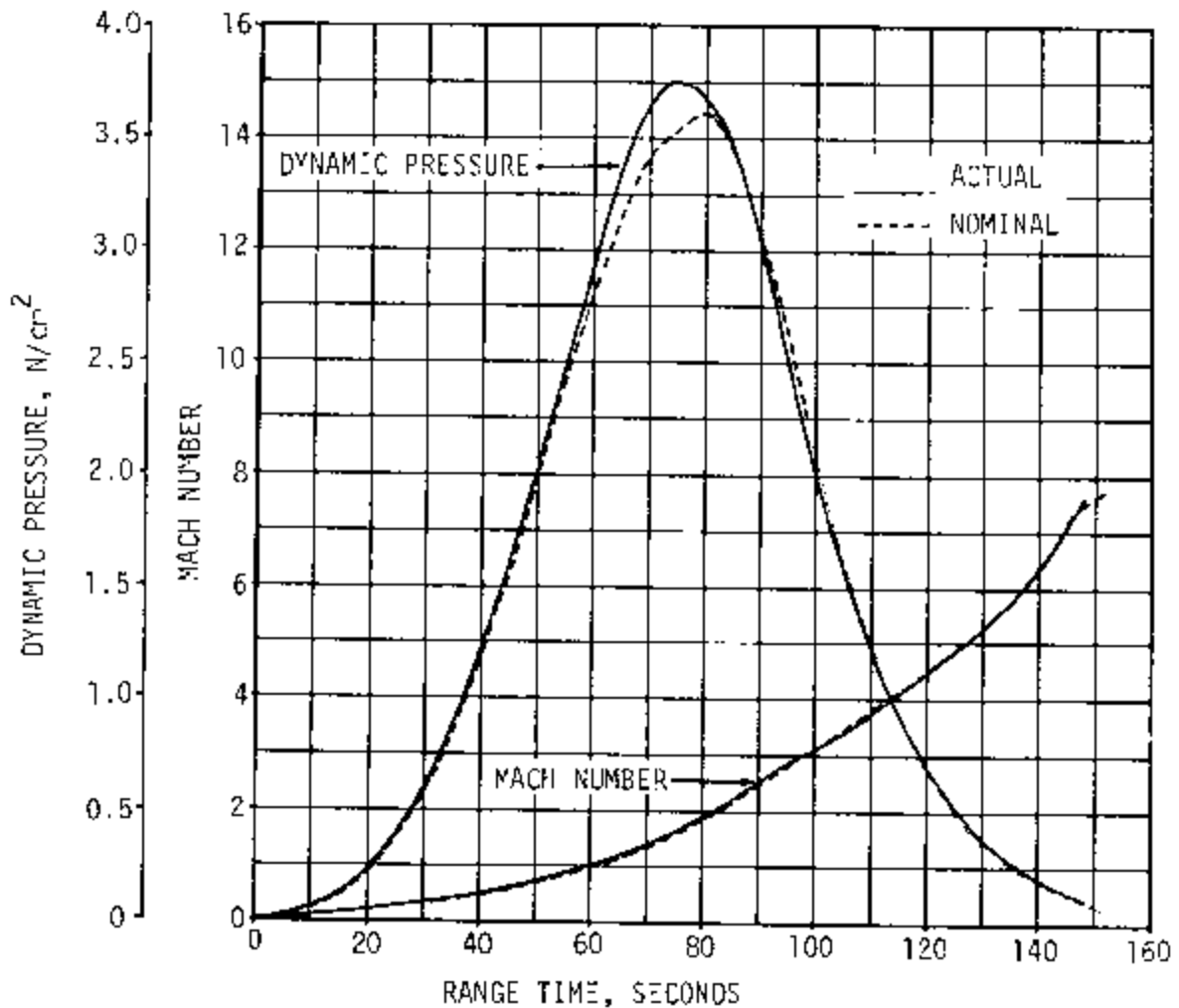


Figure 4-5. Dynamic Pressure and Mach Number Versus Range Time

4.3.2 Orbital Trajectory

The acceleration due to venting during parking orbit is presented in Figure 4-6. These accelerations were obtained by differentiating the telemetered guidance velocity data and removing accelerometer biases and the predicted effects of drag.

A family of values for the insertion parameters was obtained depending upon the combination of data used and the weights applied to the data. The solutions that were considered reasonable had a spread of about ± 500 meters (1,640 ft) in position components and ± 1.0 m/s (3.3 ft/s) in velocity components. The actual and nominal parking orbit insertion parameters are presented in Table 4-7.

The ground track of the first two revolutions in parking orbit for the AS-502 vehicle is given in Figure 4-7.

Table 4-2. S-II Engine No. 2 Premature Cutoff Conditions

PARAMETER	ACTUAL	NOMINAL	ACT-NOM
Range Time, sec	412.9		
Altitude, km (n mi)	177.26 (95.71)	177.80 (96.00)	-0.54 (-0.29)
Surface Range, km (n mi)	933.27 (503.93)	936.43 (505.63)	-3.16 (-1.70)
Space-Fixed Velocity, m/s (ft/s)	5,153.74 (16,906.63)	5,183.31 (17,005.61)	-30.17 (-98.98)
Flight Path Angle, deg	1.611	1.647	-0.036
Heading Angle, deg	78.706	78.607	0.099
Cross Range, km (n mi)	8.87 (4.79)	11.41 (6.16)	-2.54 (-1.37)
Cross Range Velocity, m/s (ft/s)	92.30 (302.82)	82.86 (271.85)	9.44 (30.97)

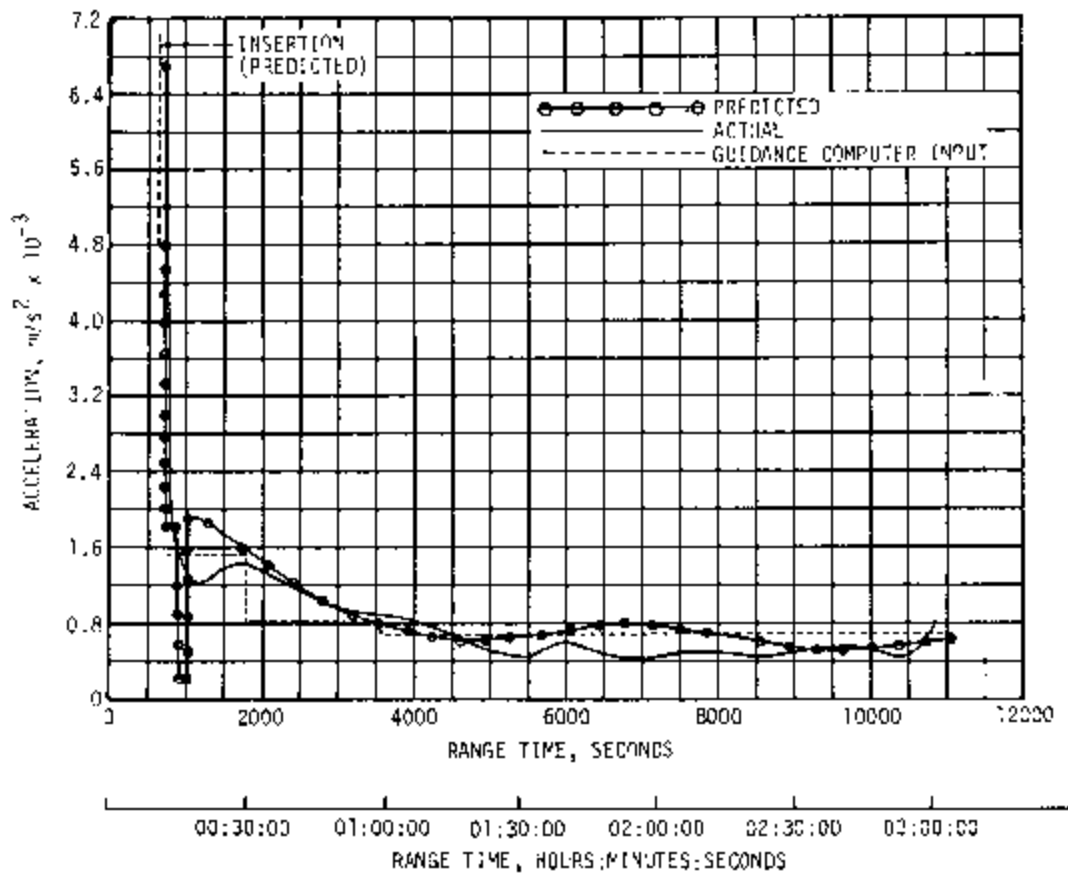


Figure 4-6. AS-502 Acceleration Due to Venting

Table 4-3. Comparison of Significant Trajectory Events

EVENT	PARAMETER	ACTUAL	NOMINAL	ACT-NOM	
First Motion	Range Time, sec	0.38	0.61	-0.23	
	Total Inertial Accel, g/s^2 (ft/s^2)	10.51 (35.43)	10.55 (34.71)	0.22 (0.72)	
Mach 1	Range Time, sec	53.50	51.80	-1.30	
	Altitude, km (n mi)	7.14 (3.86)	7.37 (3.98)	-0.23 (-0.12)	
Maximum Dynamic Pressure	Range Time, sec	75.20	79.98	-4.78	
	Dynamic Pressure, N/cm^2 (lb/ft^2)	3.755 (784,248)	3.896 (793,129)	-0.143 (31,119)	
	Altitude, km (n mi)	12.00 (6.48)	13.54 (7.37)	-1.64 (-0.89)	
Maximum Total Inertial Acceleration:	S-IC	Range Time, sec Acceleration, m/s^2 (ft/s^2)	144.72 47.34 (153.87)	144.61 47.34 (155.2)	0.11 -0.64 (-1.44)
	S-II	Range Time, sec Acceleration, m/s^2 (ft/s^2)	413.00 5.68 (51.44)	517.59 19.39 (53.62)	-104.69 -3.71 (-12.18)
	S-IVB	Range Time, sec Acceleration, g/s^2 (ft/s^2)	747.04 8.32 (27.33)	659.26 8.00 (26.25)	87.78 0.33 (1.08)
Apex: S-IC Stage	Range Time, sec	257.13	250.81	6.32	
	Altitude, km (n mi)	169.57 (59.16)	109.25 (56.99)	60.32 (31.17)	
S-II Stage	Surface Range, km (n mi)	315.62 (173.36)	314.88 (170.62)	0.74 (0.94)	
	Range Time, sec Altitude, km (n mi)	655.13 202.50 (129.42)	560.61 90.73 (102.99)	94.52 11.87 (6.41)	
Break-up of S-IC Stage	Surface Range, km (n mi)	2291.67 (1237.51)	1767.66 (954.46)	524.21 (283.05)	
	Range Time, sec Altitude, km (n mi)	397. 28.93 (15.50)	397. 27.48 (14.84)	0. 1.45 (0.76)	
Maximum Earth-Fixed Velocity: S-IC	Surface Range, km (n mi)	512.22 (330.57)	512.12 (330.52)	0.10 (0.05)	
	Range Time, sec Velocity, m/s (ft/s)	149.08 2396.54 (7862.66)	149.24 2386.02 (7825.15)	-0.84 10.52 (34.51)	
S-II	Range Time, sec Velocity, m/s (ft/s)	517.08 6325.43 (20,752.72)	518.57 6431.50 (21,100.72)	-8.51 -106.07 (-348.00)	
	Range Time, sec Velocity, m/s (ft/s)	757.04 7438.82 (24,425.58)	669.26 7387.56 (24,237.40)	87.78 51.26 (168.18)	

Table 4-4. Comparison of Cutoff Events

PARAMETER	ACTUAL	NOMINAL	ACT-NOM	ACTUAL	NOMINAL	ACT-NOM
	S-IC ECG (SOLENOID ACTIVATION)			S-IC OCG (LVDC SENSED)		
Range Time, sec	144.72	144.61	0.11	148.41	147.56	0.85
Altitude, km (n mi)	56.07 (30.28)	55.60 (30.02)	0.47 (0.26)	59.44 (32.10)	58.33 (31.50)	1.11 (0.60)
Surface Range, km (n mi)	75.38 (40.70)	75.58 (40.81)	-0.20 (-0.11)	83.16 (44.90)	81.82 (44.18)	1.34 (0.72)
Space-Fixed Velocity, m/s (ft/s)	2620.74 (8598.23)	2638.54 (8656.63)	-17.80 (-58.40)	2752.56 (9030.71)	2745.28 (9006.82)	7.28 (23.89)
Flight Path Angle, deg	20.145	20.251	-0.106	19.667	19.844	-0.177
Heading Angle, deg	75.131	75.582	-0.451	75.005	75.495	-0.490
Cross Range, km (n mi)	-0.12 (-0.06)	0.59 (0.32)	-0.71 (-0.38)	-0.13 (-0.07)	0.65 (0.35)	-0.78 (-0.42)
Cross Range Velocity, m/s (ft/s)	-3.05 (-10.03)	17.17 (56.33)	-20.22 (-66.34)	-3.77 (-12.37)	18.17 (59.61)	-21.94 (-71.98)
	S-II ECG (LVDC SENSED)			S-IVB ECG (VELOCITY CUTOFF COMMAND)		
Range Time, sec	576.33	517.69	58.64	747.04	659.26	87.78
Altitude, km (n mi)	195.09 (105.34)	188.70 (101.89)	6.39 (3.45)	190.71 (102.98)	191.50 (103.40)	-0.79 (-0.42)
Surface Range, km (n mi)	1810.62 (977.66)	1500.43 (810.17)	310.19 (167.49)	2943.03 (1589.11)	2444.57 (1319.96)	498.46 (269.15)
Space-Fixed Velocity, m/s (ft/s)	6725.67 (22,065.85)	6828.03 (22,401.67)	-102.36 (-335.82)	7839.85 (25,721.29)	7790.91 (25,560.73)	48.94 (160.56)
Flight Path Angle, deg	1.600	0.786	0.814	-0.400	-0.001	-0.399
Heading Angle, deg	83.388	81.607	1.781	90.237	87.192	3.045
Cross Range, km (n mi)	30.60 (16.52)	23.56 (12.72)	7.04 (3.80)	70.92 (38.29)	52.47 (28.33)	18.45 (9.96)
Cross Range Velocity, m/s (ft/s)	172.47 (565.85)	156.77 (514.34)	15.70 (51.51)	296.81 (973.79)	256.93 (842.95)	39.88 (130.84)

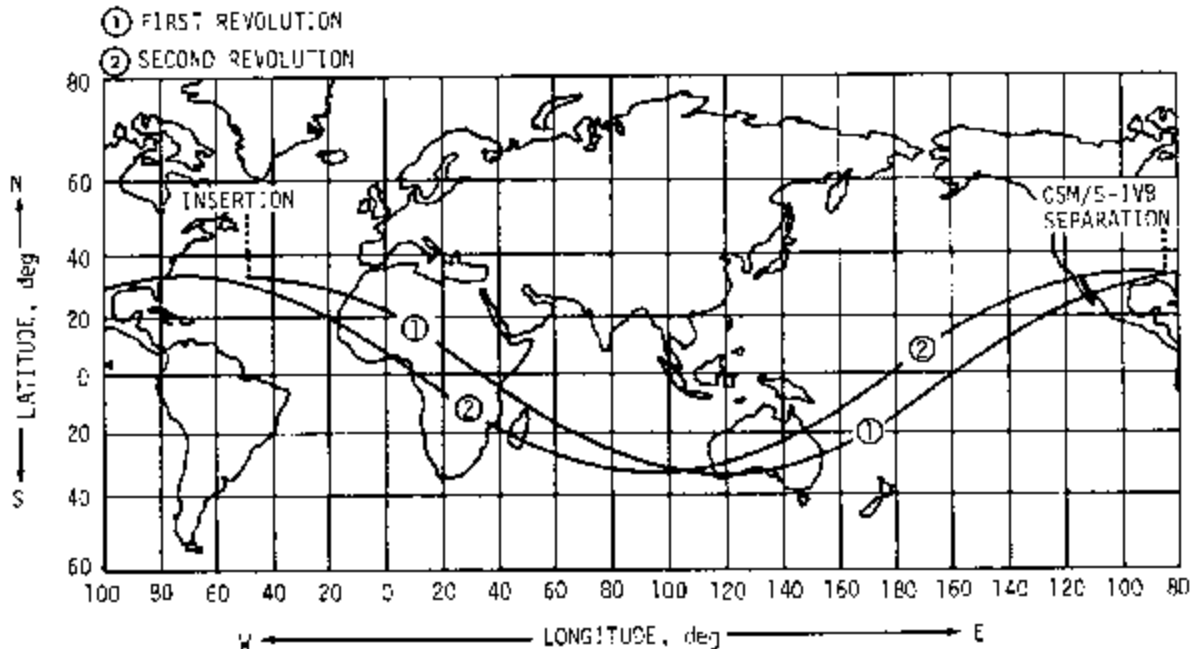


Figure 4-7. AS-502 Ground Track

Table 4-5. Comparison of Separation Events

PARAMETER	ACTUAL	NOMINAL	ACT-NOM
S-IC/S-II SEPARATION COMMAND			
Range Time, sec	149.08	148.26	0.82
Altitude, km (n mi)	60.08 (32.44)	59.05 (31.88)	1.03 (0.56)
Surface Range, km (n mi)	84.65 (45.71)	83.51 (45.09)	1.14 (0.62)
Space-Fixed Velocity, m/s (ft/s)	2,765.14 (9,071.98)	2,755.03 (9,038.81)	10.11 (33.17)
Flight Path Angle, deg	19.530	19.725	-0.195
Heading Angle, deg	74.996	75.491	-0.495
Cross Range, km (n mi)	-0.13 (-0.07)	0.66 (0.36)	-0.79 (-0.43)
Cross Range Velocity, m/s (ft/s)	-3.81 (-12.50)	18.26 (59.91)	-22.07 (-72.41)
Geodetic Latitude, deg North	28.843	28.833	0.010
Longitude, deg East	-79.780	-79.788	0.008
S-II/S-IVB SEPARATION COMMAND			
Range Time, sec	577.08	518.49	58.59
Altitude, km (n mi)	195.25 (105.43)	188.78 (101.93)	6.47 (3.50)
Surface Range, km (n mi)	1,815.52 (980.33)	1,505.90 (813.12)	309.62 (167.18)
Space-Fixed Velocity, m/s (ft/s)	6,728.65 (22,075.62)	6,834.44 (22,422.70)	-105.79 (-347.08)
Flight Path Angle, deg	1.597	0.778	0.819
Heading Angle, deg	83.416	81.639	1.777
Cross Range, km (n mi)	30.74 (16.60)	23.70 (12.80)	7.04 (3.80)
Cross Range Velocity, m/s (ft/s)	172.83 (567.03)	157.33 (516.17)	15.50 (50.86)
Geodetic Latitude, deg North	32.144	31.747	0.397
Longitude, deg East	-62.136	-65.377	3.241

Table 4-5. Comparison of Separation Events (Cont)

S-IVB/CSM PHYSICAL SEPARATION			
PARAMETER	ACTUAL	NOMINAL	ACT-NOM
Range Time, sec	11,667.82	11,908.09	-240.27
Altitude, km (n mi)	196.21 (105.94)	661.31 (357.08)	-465.10 (-251.14)
Space-Fixed Velocity, m/s (ft/s)	7,846.32 (25,742.52)	10,574.07 (34,691.83)	-2,727.75 (-8,949.31)
Flight Path Angle, deg	-0.281	14.360	-14.641
Heading Angle, deg	96.440	115.139	-18.699
Geodetic Latitude, deg North	31.993	21.412	10.581
Longitude, deg East	-85.117	-45.680	-39.437

Table 4-6. Stage Impact Location

PARAMETER	ACTUAL	NOMINAL	ACT-NOM
S-IC STAGE IMPACT			
Range Time, sec	528.93	507.80	21.13
Surface Range, km (n mi)	635.38 (343.08)	638.06 (344.52)	-2.68 (-1.44)
Cross Range, km (n mi)	3.79 (2.05)	10.19 (5.50)	-6.40 (-3.45)
Geodetic Latitude, deg N	30.201	30.151	0.050
Longitude, deg E	-74.314	-74.272	-0.042
S-II STAGE IMPACT			
Range Time, sec	1,251.24	1,151.52	99.72
Surface Range, km (n mi)	4,648.43 (2,509.95)	4,211.61 (2,274.09)	436.82 (235.86)
Cross Range, km (n mi)	152.16 (82.16)	130.49 (70.46)	21.67 (11.70)
Geodetic Latitude, deg North	31.205	31.850	-0.645
Longitude, deg East	-32.182	-36.722	4.540

Table 4-7. Parking Orbit Insertion Conditions

PARAMETER	ACTUAL	NOMINAL	ACT-NOM
Range Time, sec	757.04	669.26	87.78
Space-Fixed Velocity, m/s (ft/s)	7,842.09 (25,728.64)	7,793.93 (25,570.64)	48.16 (158.00)
Flight Path Angle, deg	-0.377	0.001	-0.378
Inclination, deg	32.567	32.561	0.006
Eccentricity	0.0741	0.0003	0.0138
Apogee*, km (n mi)	360.10 (194.44)	188.56 (101.81)	171.54 (92.63)
Perigee*, km (n mi)	173.15 (93.49)	185.32 (100.06)	-12.17 (-6.57)
Altitude, km (n mi)	190.19 (102.69)	191.51 (103.41)	-1.32 (-0.72)
Period, min	89.84	88.23	1.61
Geodetic Latitude, deg North	32.730	32.653	0.077
Longitude, deg East	-49.388	-54.709	5.321

*Based on a spherical earth of radius 6,378.165 km (3,443.934 n mi).

SECTION 5

S-IC PROPULSION

5.1 SUMMARY

The S-IC propulsion system consists of the engines, oxidizer system, fuel system, pneumatic control pressure system, and the camera ejection and purge system. Five F-1 engines provide the thrust to propel the Saturn V launch vehicle during first stage boost. The F-1 engine is a single-start, 6,770,193 Newton (1,522,000 lbf) fixed-thrust, bipropellant rocket system using liquid oxygen as the oxidizer, and RP-1 as fuel, turbopump bearing coolant, and control system fluid. Liquid oxygen is stored in a cylindrical tank having a capacity of 1342 m³ (47,405 ft³), allowing for a usable oxidizer supply of 1,489,960 kilograms (3,284,000 lbm). RP-1 (kerosene) fuel is stored in a tank having a capacity of 827 m³ (29,221 ft³), allowing for a usable fuel supply of 646,823 kilograms (1,426,000 lbm). Pressurized Gaseous Nitrogen (GN₂) is used as a source of pneumatic pressure for propellant system valve actuation and engine purging. During flight, GN₂ is used to purge the film camera and television camera lenses and to eject the film cameras.

S-IC propulsion systems performed satisfactorily. In general, all performance flight data as determined from the propulsion reconstruction analysis fell close to the nominal predictions. Average engine thrust reduced to standard sea level conditions from 35 to 38 seconds was 0.20 percent lower than predicted. Average reduced specific impulse was 0.10 percent lower than predicted, and reduced propellant consumption rate was 0.07 percent less than predicted.

The vehicle first longitudinal structural mode frequency coupled with the engine response to the oxidizer suction lines resonant frequency within the 110 to 140 second period. This resulted in a vehicle longitudinal oscillation termed "POGO".

Inboard Engine Cutoff (IECO) (solenoid activation signal) occurred 0.11 seconds later than predicted. Outboard Engines Cutoff (OECO) occurred 0.85 second later than predicted, primarily due to lower than predicted average fuel flowrate. An intentional fuel level cutoff of the outboard engines was planned and attained, demonstrating the adequacy of this cutoff mode. An inboard engine LOX level cutoff was planned and attained, demonstrating the adequacy of this cutoff mode.

The usable LOX residual at OEEO was 11,673 kilograms (25,735 lbm) of LOX compared to the usable 8544 kilograms (18,837 lbm) predicted and the usable fuel residual at OEEO was zero, as predicted. The higher than expected LOX residual was primarily due to a slightly higher than expected loading mixture ratio.

All the subsystems except the camera ejection system and the control pressure system performed as expected. The camera ejection system ejected only one of the four film cameras. It appears that the system pneumatic supply pressure tubing failed during S-IC/S-II separation. The control pressure system performed satisfactorily during powered flight. After separation, however, the sphere pressure decayed unexpectedly. This decay may be due to a failure of the pneumatic lines to solenoid valves that control the LOX vent and relief valves. The planned correction for both of these problems on S-IC-3 and subsequent stages will be the substitution of stainless steel tubing for the aluminum tubing that was used on S-IC-1 and S-IC-2.

5.2 S-IC IGNITION TRANSIENT PERFORMANCE

The fuel pump inlet preignition pressure and temperature were 30.4 N/cm^2 (44.1 psia) and 274°K (33°F), respectively. These fuel pump inlet conditions were within the F-1 engine model specification limits (start box requirements) as shown in Figure 5-1. The preignition temperature at the fuel pump inlet was considerably lower than the fuel bulk temperature of 294°K (70°F). Similarly, the LOX pump inlet preignition pressure and temperature were 55.4 N/cm^2 (80.4 psia) and 96°K (-287°F), respectively. The LOX pump inlet conditions were also within the F-1 engine model specification limits as shown in Figure 5-1. The fuel and LOX ullage pressures were 19.1 N/cm^2 (27.7 psia) and 17.2 N/cm^2 (24.9 psia), respectively, at ignition.

The engine startup sequence was normal. A 1-2-2 start was planned and attained. Engine position starting order was 5, 1-3, 2-4. Two engines are considered to start together if their combustion chamber pressures reach 69 N/cm^2 (100 psig) in a 100-millisecond time period. Figure 5-2 shows the thrust buildup of each engine indicative of the successful 1-2-2 start. The major events during engine startup sequence are listed in Table 5-1.

The best estimate of propellants consumed during the period between ignition and holddown arms release were 38,901 kilograms (85,765 lbm) as compared to 38,923 kilograms (85,810 lbm) by the reconstruction analysis. These consumptions are more than the predicted consumption of 38,846 kilograms (85,643 lbm). The more than predicted holddown consumption resulted in best estimate liftoff propellant loads of 1,398,599 kilograms (3,083,382 lbm) for LOX and 600,604 kilograms (1,324,104 lbm) for fuel.

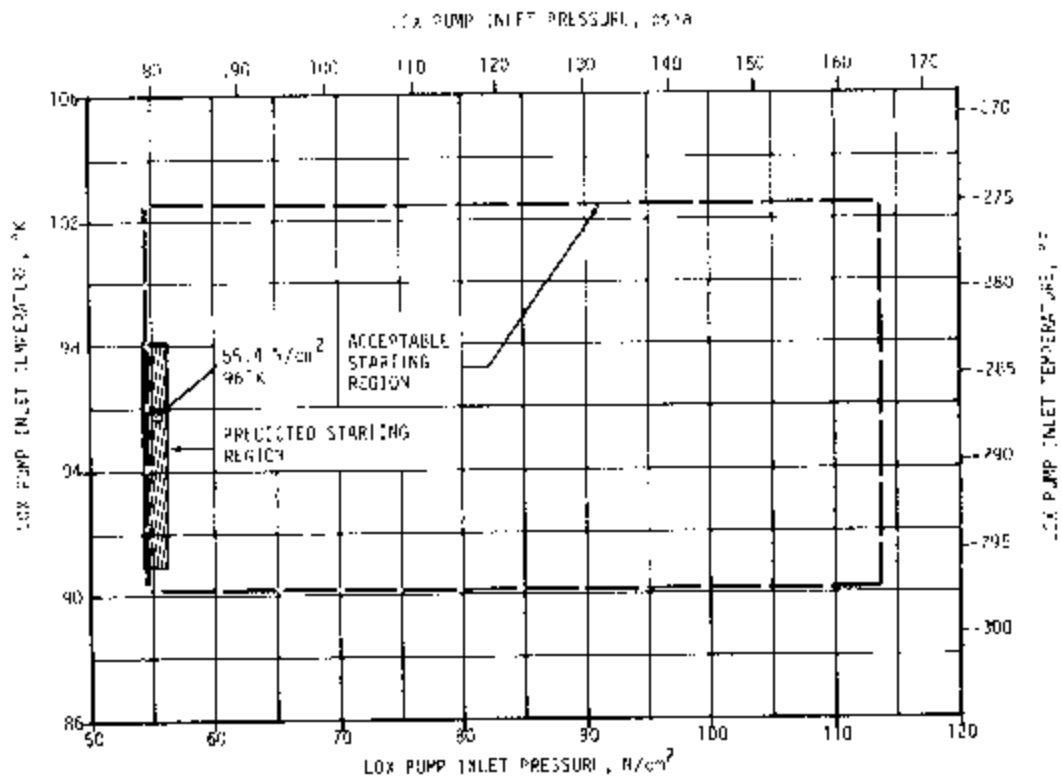
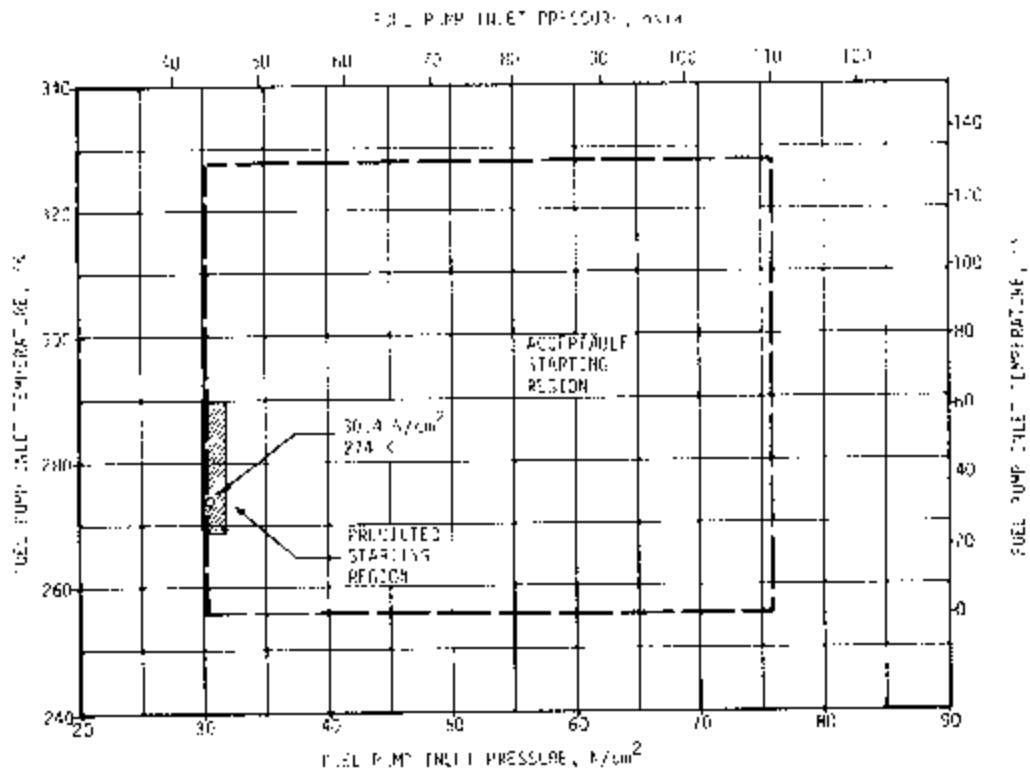


Figure 5-1. S-IC Start Box Requirements

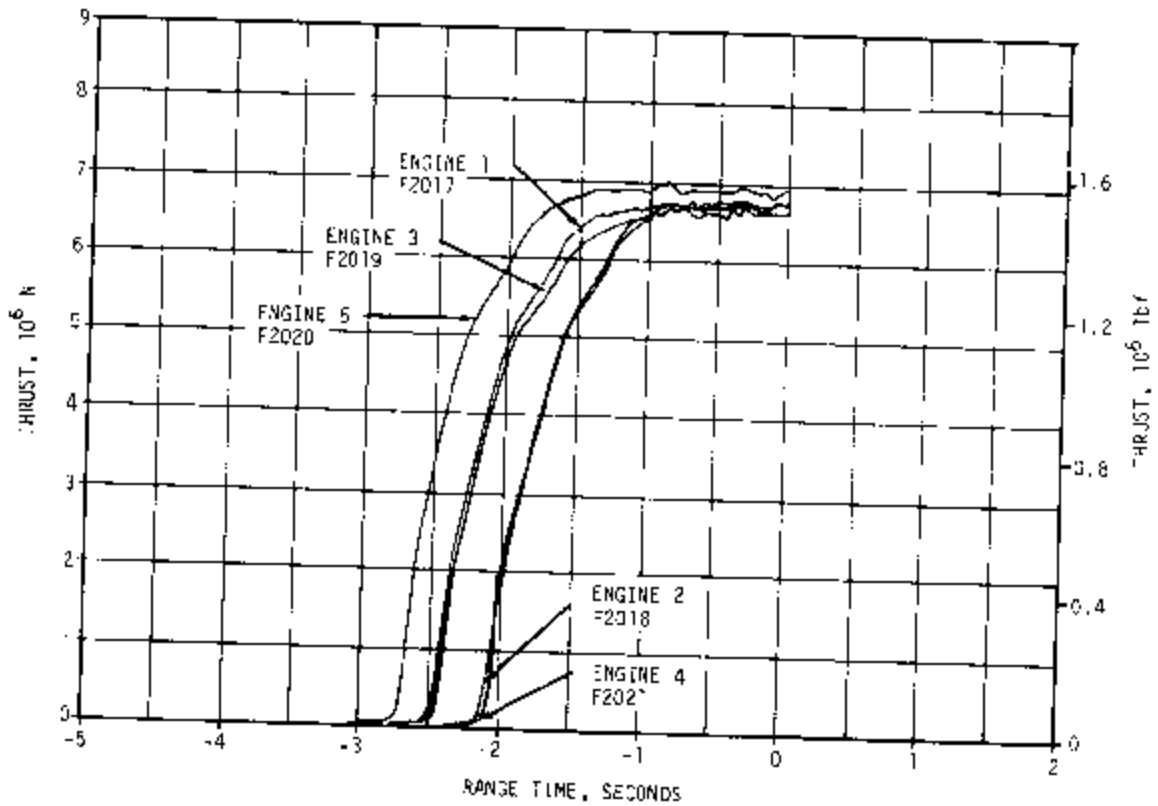


Figure 5-2. S-IC Engine Buildup Transient

Table 5-1. S-IC Stage Engine Startup Event Times

EVENT	RANGE TIME, SECONDS				
	ENGINE 1	ENGINE 2	ENGINE 3	ENGINE 4	ENGINE 5
Start Solenoid Energized	-5.949	-5.979	-5.739	-5.489	-5.959
MLV 1 Starts Open	-5.787	-5.811	-5.587	-5.341	-5.811
MLV 2 Starts Open	-5.793	-5.827	-5.579	-5.345	-5.797
Thrust Chamber Ignition	-2.800	-2.430	-2.760	-2.410	-3.020
MFV 1 Starts Open	-2.659	-2.281	-2.617	-2.265	-2.885
MFV 2 Starts Open	-2.651	-2.289	-2.617	-2.259	-2.887
Final Thrust OK	-1.693	-1.287	-1.621	-1.319	-1.985
All Engines Running	-1.291				
Launch Commit	0.115				

NOTE: Times taken from data sampled 500 times per second.

5.3 S-IC MAIN STAGE PERFORMANCE

The F-1 engine has a single bellshaped thrust chamber with an expansion area ratio of 10:1. The thrust chamber is cooled regeneratively by fuel which passes through tubes that form the thrust chamber wall. A double walled extension nozzle, utilizing turbopump turbine exhaust gases for inner wall coolant, is used to increase the expansion area ratio from 10:1 to 16:1. The propellants are supplied to the thrust chamber by a direct drive turbopump driven by exhaust gases from a gas generator.

Two analytical techniques were employed in evaluating S-IC stage propulsion system performance. The primary method, propulsion reconstruction analysis, utilized telemetered engine and stage data to compute longitudinal thrust, specific impulse, and stage mass flowrate. In the second method, flight simulation, a six-degree-of-freedom trajectory simulation was utilized to fit propulsion reconstruction analysis results to the trajectory. Using a differential correction procedure, this simulation determined adjustments to the reconstruction analysis of thrust and mass flow histories to yield a simulated trajectory which closely matched the observed postflight trajectory. S-IC stage propulsion performance, as determined by reconstruction was completely satisfactory.

Performance parameters compared well with the nominal predictions over the entire flight as shown in Figure 5-3.

Average engine thrust, reduced to standard sea level conditions, at a 35 to 38 second time slice was 0.20 percent lower than predicted, as shown in Table 5-2. Individual engine deviation from predicted thrust ranged from 0.86 percent lower (engine No. 2) to 0.33 percent higher (engine No. 4). Average engine specific impulse was 0.10 percent lower than predicted. Individual engine deviations from predicted specific impulse ranged from 0.30 percent lower (engine No. 2) to 0.04 percent higher (engines No. 3 and 4).

Reduced to sea level ambient pressure, the stage average longitudinal thrust for the flight from propulsion reconstruction was 0.53 percent lower than predicted, and the stage average longitudinal specific impulse as reconstructed was 0.17 percent higher than predicted.

Flight simulation showed that the stage average specific impulse was 0.68 percent greater than predicted. The flight simulation results were used in an attempt to explain the time and velocity deviations at OECO. To explain the velocity deviation, an error analysis was made to determine the contributing parameters and the magnitude of the velocity deviation caused by each of these parameters. Table 5-3 lists the various error contributors and the cutoff velocity and time deviations associated with each.

▽ S-IC IEGG SOL ACT. 1, 186.72
 ▽ S-IC OEGG SENSED BY LVCC, 5 PART OF 3, 148.41

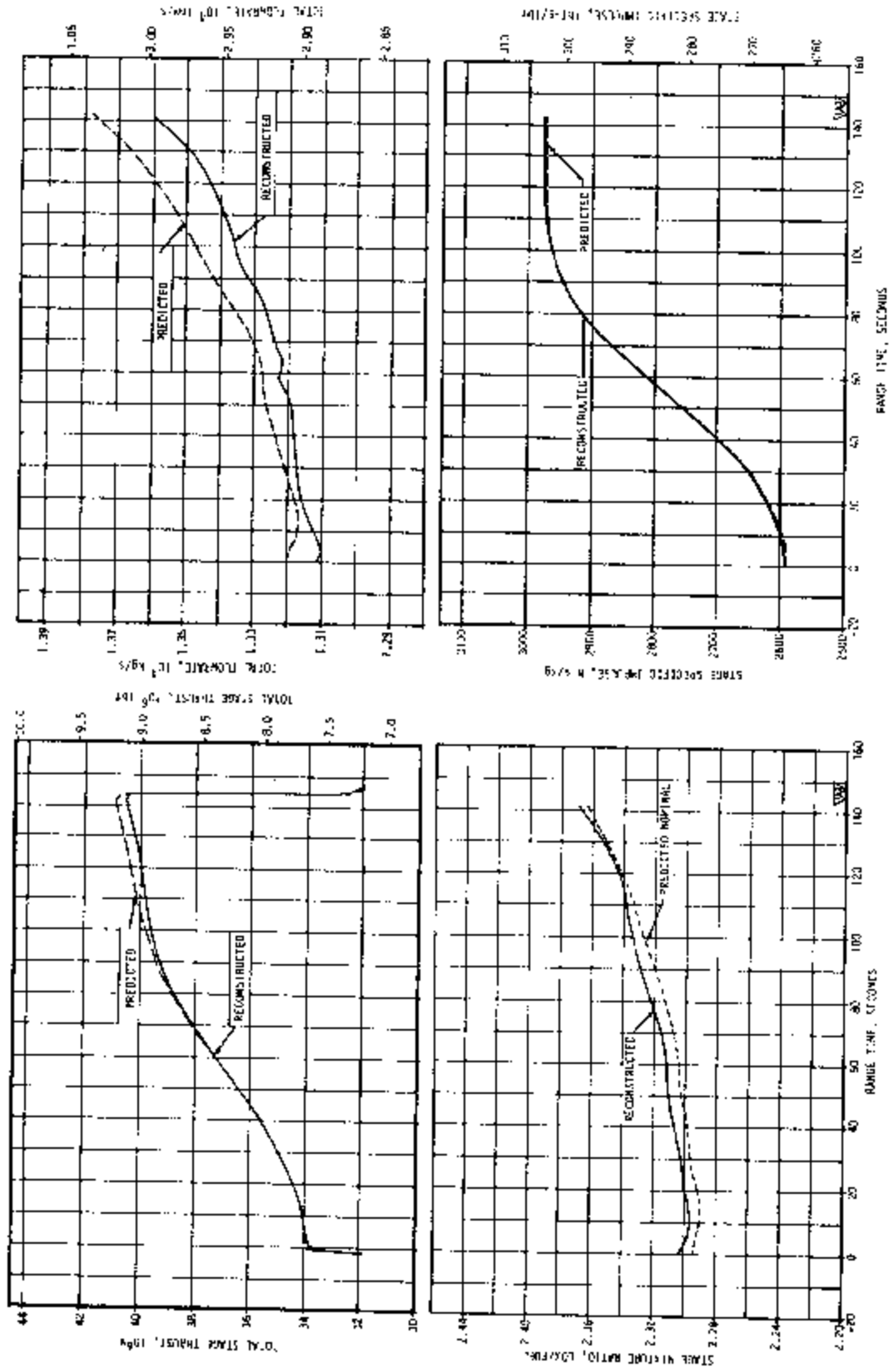


Figure 5-3. S-IC Steady State Operation

Table 5-2. S-IC Engine Performance Deviations

PARAMETER	ENGINE	PREDICTED	RECONSTRUCTION ANALYSIS	DEVIATION PERCENT	AVERAGE DEVIATION PERCENT
Thrust 10^3 N (10^3 lbf)	1	6739 (1515)	6757 (1519)	0.26	-0.20
	2	6752 (1518)	6695 (1505)	-0.86	
	3	6784 (1525)	6766 (1521)	-0.26	
	4	6690 (1504)	6712 (1509)	0.33	
	5	6761 (1520)	6730 (1513)	-0.46	
Specific Impulse N-s/kg (lbf-s/lbm)	1	2576 (262.7)	2577 (262.8)	0.04	-0.10
	2	2598 (264.0)	2590 (264.1)	-0.30	
	3	2591 (264.2)	2586 (263.7)	-0.19	
	4	2580 (263.1)	2581 (263.2)	0.04	
	5	2590 (264.1)	2588 (263.9)	-0.08	
Total Flowrate kg/s (lbm/s)	1	2616 (5766)	2521 (5779)	0.23	-0.07
	2	2598 (5728)	2586 (5702)	-0.45	
	3	2618 (5772)	2616 (5768)	-0.07	
	4	2593 (5716)	2500 (5733)	0.30	
	5	2610 (5755)	2601 (5734)	-0.36	
Mixture Ratio LOX/Fuel	1	2.27	2.27	0.0	-0.002
	2	2.26	2.28	0.00	
	3	2.24	2.23	-0.45	
	4	2.27	2.28	0.44	
	5	2.27	2.27	0.0	
NOTE: Analysis was reduced to standard sea level conditions (standard pump inlet conditions) at liftoff plus 35 to 38 seconds.					

Table 5-4 presents a summary of the flight simulation results, reduced to sea level ambient pressure conditions, on the average values and deviations of longitudinal thrust, propellant flowrate, and vehicle longitudinal specific impulse.

The vehicle first longitudinal structural mode frequency coupled with the engine response to the oxidizer suction lines resonant frequency within the 110 to 140 second period. The S-IC stage engines experienced chamber pressure oscillations building up to a maximum at approximately 125 seconds of 5.5 to 6.9 N/cm² (8 to 10 psid) peak-to-peak. The "POGO" phenomenon is discussed in detail in paragraph 9.2.3.1.

5.4 S-IC ENGINE SHUTDOWN TRANSIENT PERFORMANCE

Inboard engine cutoff was initiated by LOX level indication and occurred at 144.72 seconds (solenoid activation signal). Outboard engine cutoff was initiated by fuel level and occurred at approximately 148.41 seconds (start of Time Base 3 [T₃]). This was 0.85 seconds later than the predicted time of 147.56 seconds. The late OECO was primarily caused by lower than predicted average fuel flowrate.

Table 5-3. S-IC Velocity and Time Deviation Analysis at OEEO
(Simulation Versus Predicted)

VELOCITY DEVIATION (EARTH-FIXED)	
CONTRIBUTING ERROR FACTORS	DEV. (ACT-PRED) ΔV (m/s)
Liftoff Weight Increase.....(0.16 Percent)	-10.63
Total Propellant Flowrate Decrease..(0.68 Percent)	-20.52
Axial Force Coefficient Difference	6.02
Meteorological Data Difference	- 8.92
Late IEEO	2.93
Late OEEO	38.68
Total Contribution	7.56
Observed	<u>7.73</u>
Difference (Observed - Total Contribution)	0.17
TIME DEVIATION	
CONTRIBUTING ERROR FACTORS	DEV. (ACT-PRED) Δt (sec)
Initial Fuel Underloading.....(2369 kg)	- 0.60
Fuel Flowrate Decrease	1.84
Late IEEO	- 0.08
Residual Differences.....(30 kg)	- 0.01
Total Contribution	1.15
Observed	<u>0.85</u>
Difference (Observed - Total Contribution)	- 0.30

Thrust decay of the F-1 engines is shown in Figure 5-4. The decay transient was normal. The oscillations which occur near the end of "tailoff" are characteristic of the engine shutdown sequence.

The total stage impulse from OEEO to separation was indicated by engine analysis to be greater than predicted. Telemetered guidance data also indicated the cutoff impulse was greater than expected, as shown in Table 5-5. These deviations are within the acceptable range considering the difference between the actual and predicted vehicle mass.

Table 5-4. Comparison of S-IC Stage Flight Reconstruction Data With Trajectory Simulation Results

PARAMETERS	UNITS	PREDICTED	RECONSTRUCTION	RECONSTRUCTION DEVIATION FROM PREDICTED	FLIGHT SIMULATION	SIMULATION DEVIATION FROM PREDICTED
Average * longitudinal thrust	N (lbf)	34,692,927.0 7,748,826.0	34,508,047.0 7,757,718.0	-0.53%	34,692,422.0 7,799,167.0	0.004%
Vehicle mass at hold-down arm release	kg (lbm)	2,782,972.0 6,135,402.0	2,785,005.0 6,135,886.0	0.07%	2,784,235.0 6,138,167.5	0.16%
Average mass loss rate	kg/s (lbm/s)	13,372.25 29,480.89	13,275.90 29,277.17	-0.69%	13,283.86 29,281.49	-0.68%
Average * specific impulse	N-s/kg (lbf-s/lbm)	2694.25 264.54	2598.57 264.98	0.17%	2672.00 266.35	0.68%

*Parameters reduced to sea level ambient pressure.

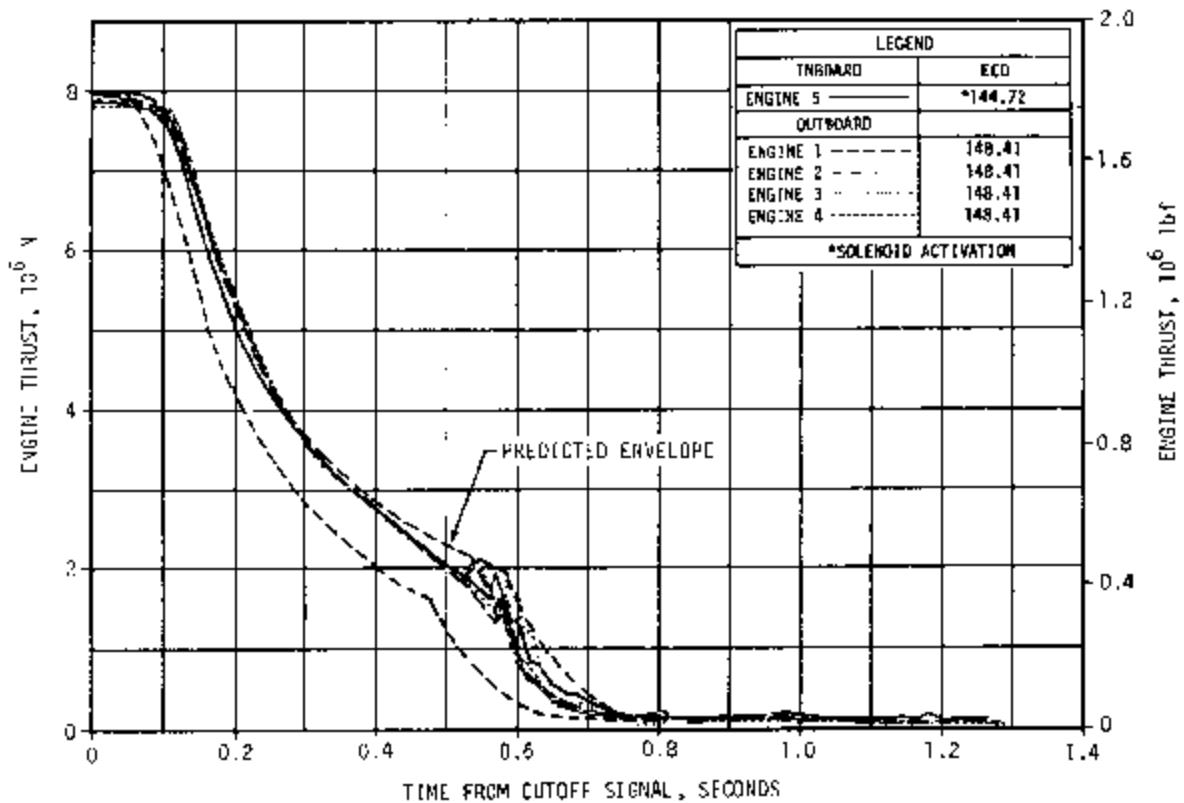


Figure 5-4. S-IC Engine Shutdown Transient Performance

Table 5-5. S-IC Cutoff Impulse

PARAMETER	PREDICTED	FLIGHT		PERCENT DEVIATION FROM PREDICTED	
		ENGINE	GUID. DATA	ENGINE	GUID. DATA
Cutoff N-s Impulse (lbf-s)	8,975,026 2,017,666	10,755,582 2,417,951	9,141,331 2,055,053	19.84	1.95
Velocity m/s Increase (ft/s)	10.89 35.73	13.14 43.11	11.17 36.65	20.66	2.57

5.5 S-IC STAGE PROPELLANT MANAGEMENT

S-IC stage uses an open loop method for achieving Propellant Utilization (PU). The propellants loaded were 2123 kilograms (4681 lbm) greater than predicted for LOX and 2369 kilograms (5224 lbm) less than predicted for fuel. This loading resulted in the desired propellant level cutoff signals. Since the S-IC stage uses an open loop method for achieving propellant utilization, the usable propellant residual deviations are the result of propellant loading and performance prediction inaccuracies. A summary of the propellants remaining at major event times is presented in Table 5-6 and the residuals are presented in Table 5-7. An inboard engine LOX level cutoff was planned and attained, demonstrating the adequacy of this cutoff mode. An intentional fuel level cutoff of the outboard engines was planned and attained, demonstrating the adequacy of this cutoff mode.

5.6 S-IC PRESSURIZATION SYSTEMS

5.6.1 S-IC Fuel Pressurization System

The fuel pressurization system maintains sufficient fuel tank ullage pressure to meet the minimum Net Positive Suction Pressure (NPSP) requirements of the engine fuel turbopump during engine start and flight. In addition, this system helps provide fuel tank structural capability by keeping a positive pressure head at all points inside the tank. The fuel tank is protected from overpressurization with a pressure relief system design which requires a double failure mode to occur to exceed the tank design pressure. Before engine ignition the fuel tank is pressurized with helium from a ground source. During flight, the tank is pressurized with gaseous helium obtained by using the F-1 engine heat exchanger to heat helium which is supplied from storage bottles located in the LOX tank. The helium pressurization system satisfactorily maintained the required ullage pressure in the fuel tank during flight. The Helium Flow Control Valves (HFCV) opened as programmed and the fifth flow control valve was not required. In Section 2, Event Time Tables, these valves are designated "Fuel Pressurizing Valves." The heat exchangers performed as expected.

Table 5-6. S-IC Stage Propellant Mass History

EVENT	PROPELLANT		RECONSTRUCTED		LEVEL SENSOR DATA		BEST ESTIMATE		
	LOX	FUEL	LOX	FUEL	LOX	FUEL	LOX	FUEL	
Master Ignition	kg (lbm)	1,427,032 3,145,067	811,318 1,797,727	1,429,151 3,155,739	698,938 1,542,478	1,429,182 3,150,718	698,938 1,542,478	1,429,155 3,150,740	698,949 1,542,503
Holddown Arm Release	kg (lbm)	1,035,679 2,279,150	522,825 1,159,001	1,308,590 2,883,363	600,576 1,324,044	1,397,537 3,081,151	522,715 1,158,350	1,394,595 3,083,382	522,504 1,158,104
IECC	kg (lbm)	46,709 103,018	21,142 46,610	55,477 122,306	23,540 51,845	54,259 119,621	23,357 51,693	55,486 122,325	23,567 51,956
Decel	kg (lbm)	23,522 51,827	11,202 24,698	26,483 58,428	11,357 25,038	28,122 61,992	11,519 25,395	26,650 58,755	11,305 24,924
Separation	kg (lbm)	21,178 46,689	9,905 21,824	24,622 54,282	10,232 22,557			24,035 52,988	10,106 22,290

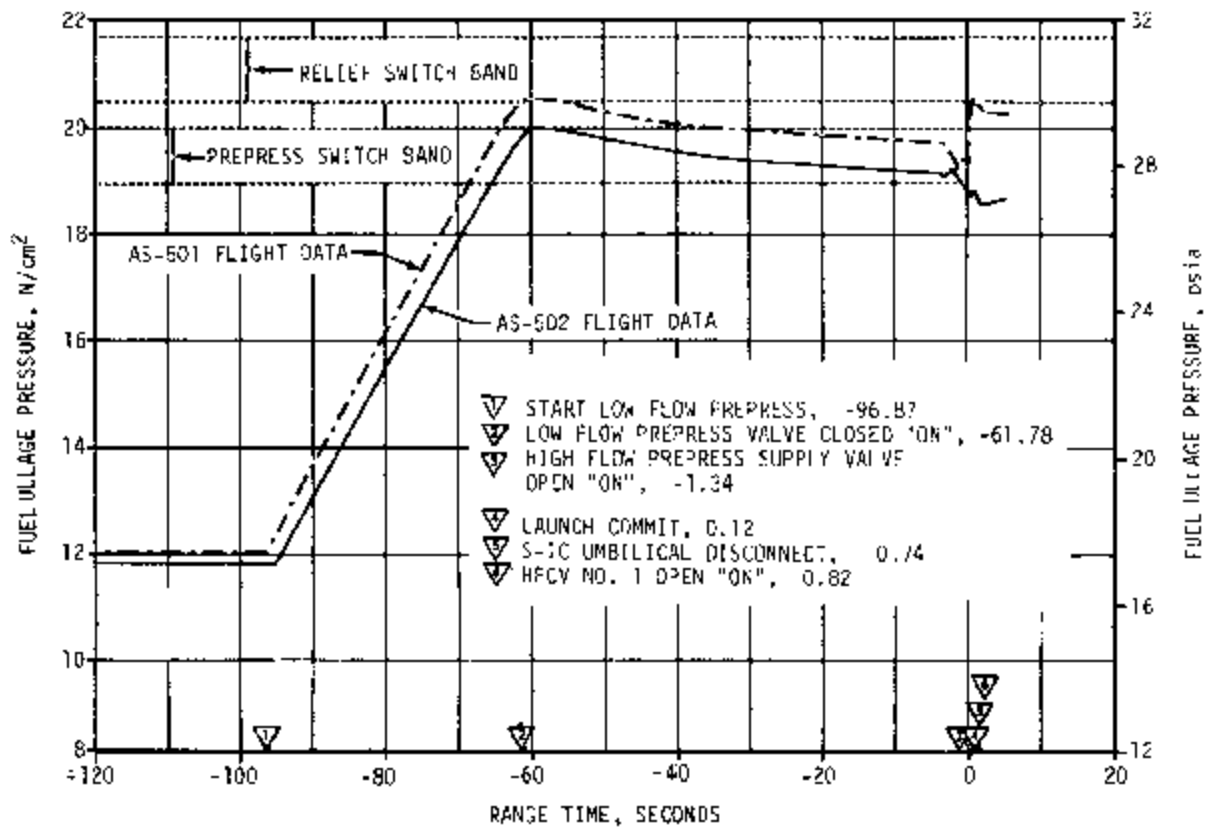
NOTE: Values do not include pressurization gas (GOX) so they will compare with level sensor data.

Table 5-7. S-IC Residuals at Outboard Engine Cutoff

PROPELLANTS		PREDICTED	ACTUAL	DEVIATION
LOX RESIDUALS *				
Usable Mainstage	kg	8544**	11,673	3129
	(lbm)	18,837	25,735	6898
Thrust Decay and Unusable***	kg	14,978	14,978	0
	(lbm)	33,020	33,020	0
FUEL RESIDUALS				
Usable Mainstage	kg	0	0	0
	(lbm)	0	0	0
Thrust Decay and Unusable	kg	11,202	11,305	103
	(lbm)	24,698	24,924	226
<p>* Does not include GOX pressurization gas. ** LOX bias. *** Includes 150 kilograms (330 lbm) in LOX interconnect lines and 14,828 kilograms (32,690 lbm) in LOX suction ducts.</p>				

The low flow prepressurization system was commanded on at -96.87 seconds and performed satisfactorily, providing ullage pressure as shown in Figure 5-5.

The fuel high flow prepressurization supply valve of the Ground Support Equipment (GSE) was opened at -1.34 seconds and maintained the ullage pressure within the band. At 0.82 seconds the No. 1 HFCV of the onboard pressurization system was opened. The flow overlap between the onboard and the prepressurization systems seen on AS-501 did not occur for this flight. HFCV No. 1 was signalled to open by umbilical disconnect instead of launch commit, eliminating the flow overlap between the two systems. HFCV's No. 2, 3, and 4 were commanded open by the switch selector within acceptable times as shown in Table 2-3. These flows held the ullage pressure within the operating band as shown in Figure 5-6. The fifth HFCV was not required to operate since ullage pressure was maintained above the fifth HFCV switch actuation pressure. Helium bottle pressure as shown in Figure 5-7 stayed within expected limits. The heat exchangers performed within the expected performance limits.



NOTE: ALL TIMES REFER TO AS-502 DATA
TIME BASE FOR AS-501 AND AS-502 DATA IS NOT THE SAME

Figure 5-5. S-1C Fuel Ullage Pressure During Countdown

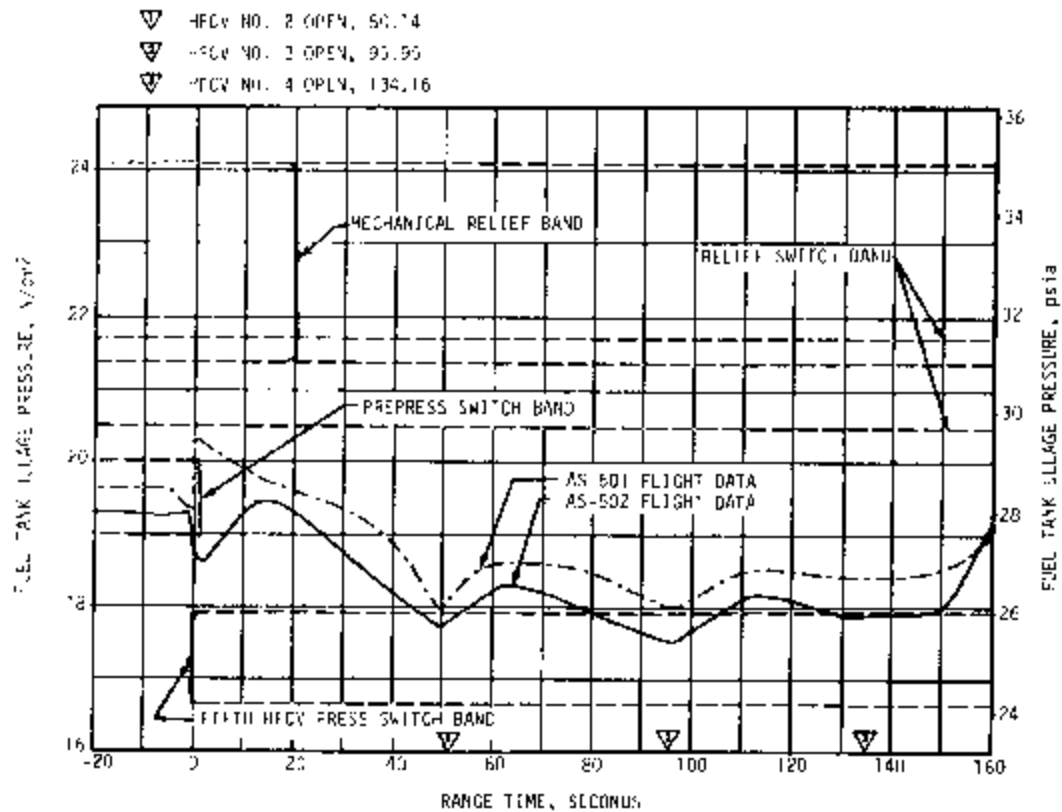


Figure 5-6. S-IC Fuel Ullage Pressure During Boost

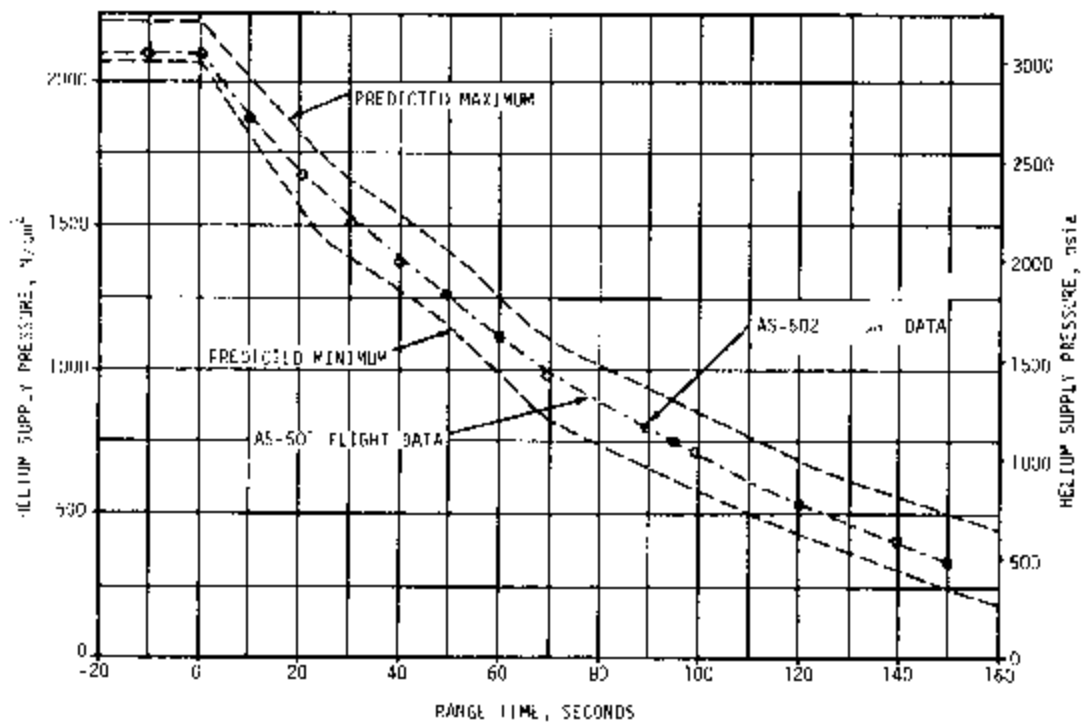


Figure 5-7. S-IC Helium Bottle Pressure for Fuel Pressurization

5.6.2 S-IC LOX Pressurization System

The LOX pressurization system provides and maintains sufficient LOX tank ullage pressure to meet the minimum NPSP requirements of the LOX turbo-pump during engine start and flight. In addition, the pressure provides additional LOX tank structural capability by keeping a positive pressure head at all points inside of the tank. This system also protects the LOX tank from overpressurization. Before engine ignition, the oxidizer tank is pressurized with helium from a ground source. During flight, the tank pressurization is accomplished with Gaseous Oxygen (GOX) obtained by using F-1 engine heat exchangers to convert oxygen from liquid to gas.

The LOX pressurization system performed satisfactorily and all performance requirements were met. The ground prepressurization system maintained ullage pressure within acceptable limits until launch commit. The onboard pressurization system subsequently maintained ullage pressure within the GOX Flow Control Valve (GFCV) band during the flight. The heat exchangers performed as expected.

The prepressurization system was initiated by opening of the ground supply valve at -66.65 seconds. The ullage pressure increased until it entered the switch band zone which resulted in terminating the flow at approximately -58.84 seconds. The ullage pressure increased approximately 1.34 N/cm^2 (1.95 psi) above the prepressurization switch setting to 18.75 N/cm^2 (27.2 psia). This overshoot is similar to that seen on AS-501.

The LOX tank ullage pressure history is shown in Figure 5-8. During flight, the ullage pressure was maintained within required limits by the GFCV throughout the flight and followed the anticipated trend. The GFCV reached full open at 120 seconds and remained open until the end of flight. The maximum GOX flowrate during full open position of the valve was 25.85 kg/s (57 lbm/s). After IECCO, the GOX flow requirements for the remaining four engines increased until OECCO.

5.7 S-IC PNEUMATIC CONTROL PRESSURE SYSTEM

The pneumatic control pressure system uses pressurized GN_2 as a source of pneumatic pressure for propellant system valve actuation and engine purging. GN_2 is supplied by a ground source to the stage GN_2 fill system and to individual ground controlled, stage pneumatic valves during stage system test, checkout, static firing, and prelaunch operations. Late in the prelaunch operation, the stage GN_2 system is charged to flight storage pressure. The pneumatic control pressure system on the S-IC stage performed satisfactorily during the 148 second flight. The actual pneumatic control regulator outlet pressure measured 521 N/cm^2 (755 psia) as shown in Figure 5-9. The control pressure system succeeded in actuating the prevalues after engine cutoff. All instrumented pre-values indicated closed positions.

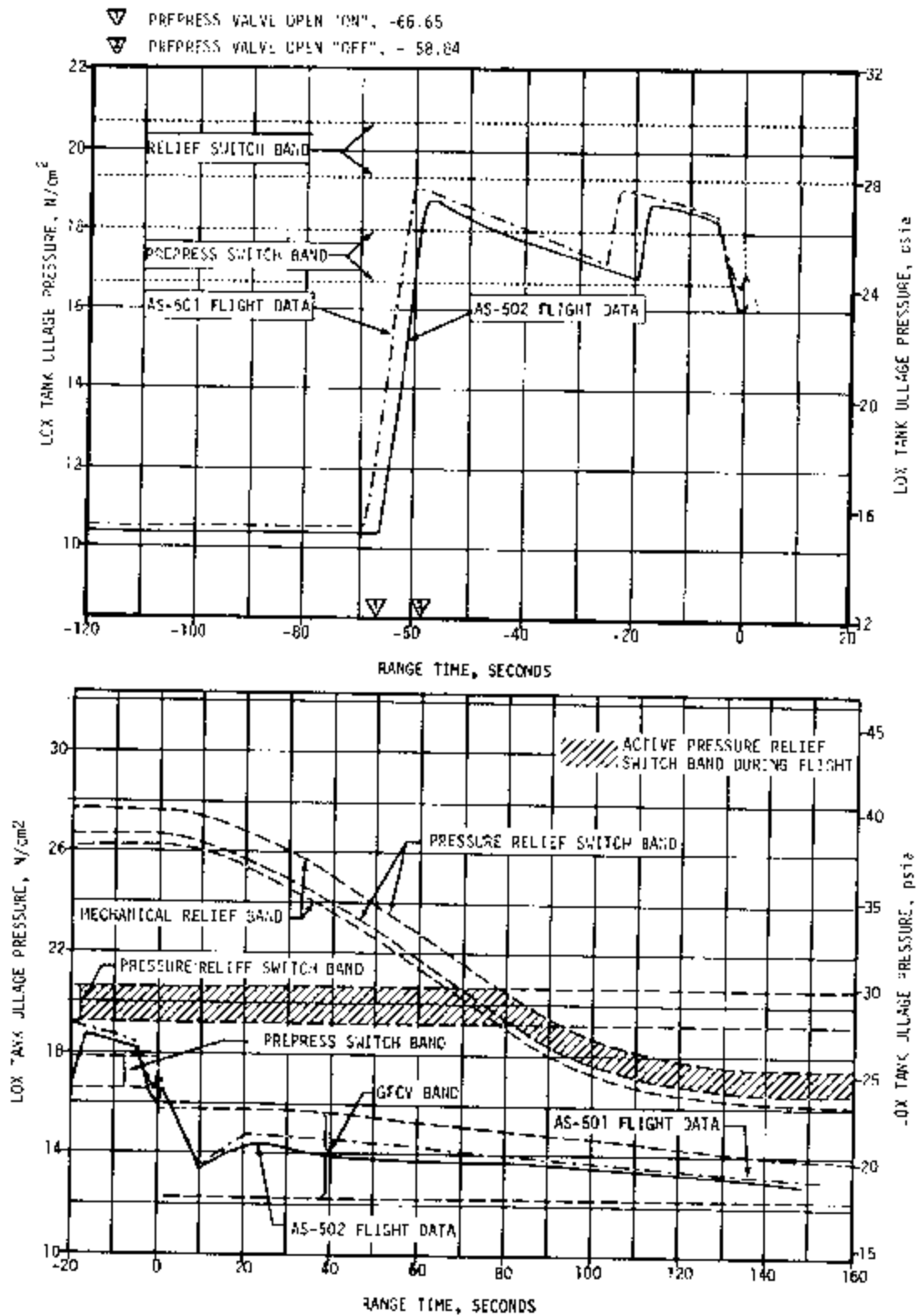


Figure 5-8. S-IC LOX Ullage Pressure

The control sphere pressure decreased to 1793 N/cm² (2600 psia) during prevalve actuation and then leveled off for about 2 seconds as shown in Figure 5-10. At this time, approximately 157 seconds, the sphere pressure started decaying rapidly. It is suspected that the pneumatic lines to the solenoid valves that control the LOX tank vent and relief valves burst during the severe environments imposed by S-IC/S-II separation. A thermal analysis of the pneumatic lines was conducted assuming twice the design separation environment. Data from AS-501 and AS-502 flights indicate that the separation environment may be of this magnitude. The thermal study indicated that the 6061-T6 aluminum tubing would reach a temperature of 739°K (870°F) 3 seconds after separation. With a 517 N/cm² (750 psia) pressure in the lines, the ultimate stress of the lines is exceeded at 544°K (700°F). Flow analysis indicated that a broken line would have a maximum flowrate of 0.067 kg/s (0.147 lbm/s), while the average flowrate out of the sphere was 0.086 kg/s (0.19 lbm/s). The difference between these two values is attributed to fuel tank vent valve cycling and other system demands.

ECP 441 has been approved and the 6061-T6 aluminum lines to the solenoid valves that control the LOX tank vent and relief valves will be replaced with stainless steel lines for AS-503 and subsequent vehicles. This will eliminate the possibility of line rupture due to high temperatures.

5.8 S-IC PURGE SYSTEM

The turbopump LOX seal, gas generator actuator housing, and radiation calorimeter purge systems performed satisfactorily during the 148 second flight. The LOX dome and Gas Generator (GG) LOX injector purge system also met all requirements.

5.9 S-IC CAMERA EJECTION AND PURGE SYSTEM

The camera ejection and purge system utilizes GN₂ to perform its function during flight. The GN₂ is supplied by a ground source to the onboard system. During flight GN₂ from the system's storage sphere is used to purge the separation viewing cameras lenses, to eject the two separation viewing cameras, and to eject two LOX viewing cameras. A schematic of the camera ejection system is shown in Figure 5-11.

The system ejected only one of the four film cameras. The camera frame rate measurement for separation camera No. 1 went to zero at 174.25 seconds, indicating ejection of that camera. Frame rates for the remaining three cameras did not change, indicating that there was neither ejection nor sufficient motion of the capsules within the ejection tubes to disconnect the electrical plug.

A study of possible system failure modes was conducted to determine the most probable cause of failure. These analyses indicate the most probable reason for failure to eject three of the four cameras was inadequate bottle pressure at ejection command due to failure of the purge system line very near the purge system solenoid valve (see Figure 5-11).

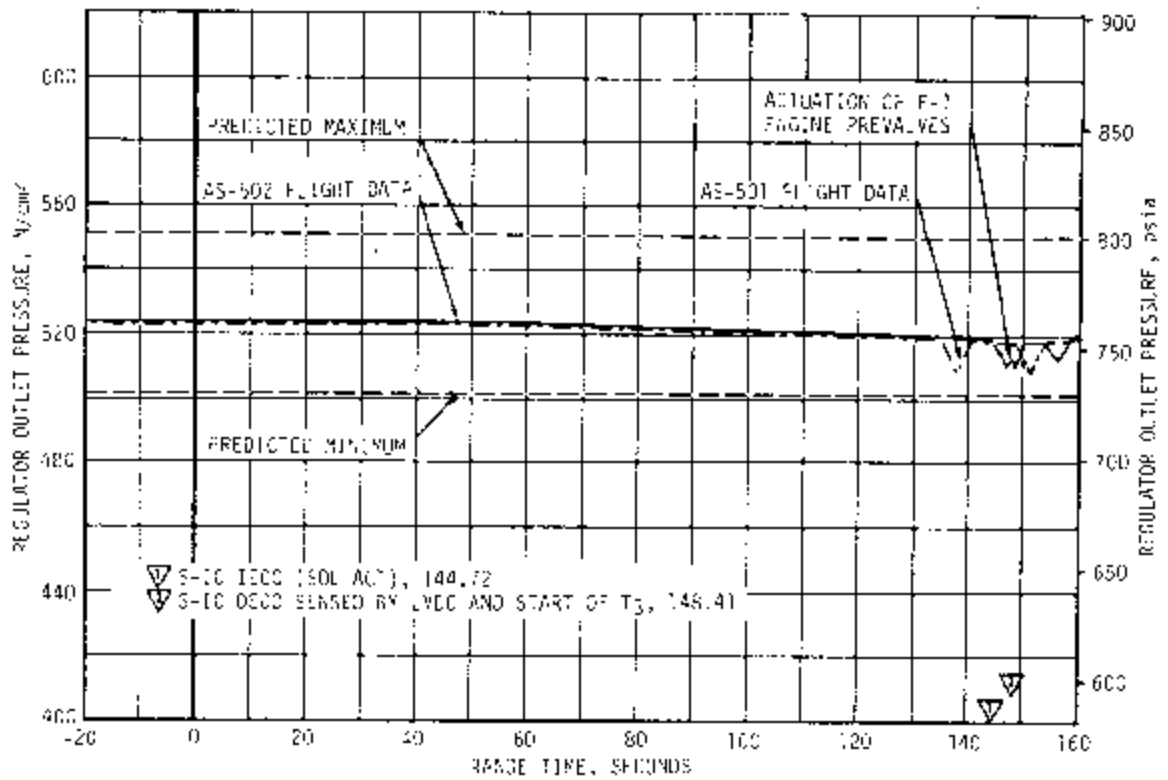


Figure 5-9. S-IC Pneumatic Control Regulator Outlet Pressure

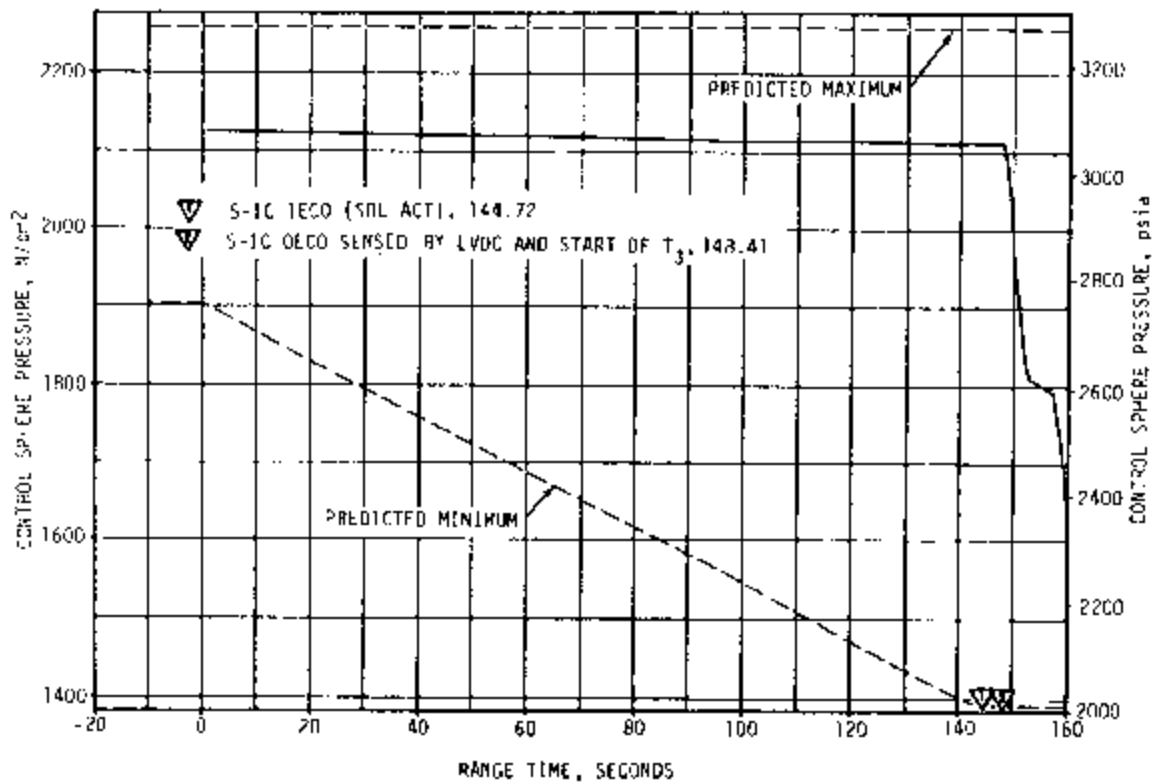
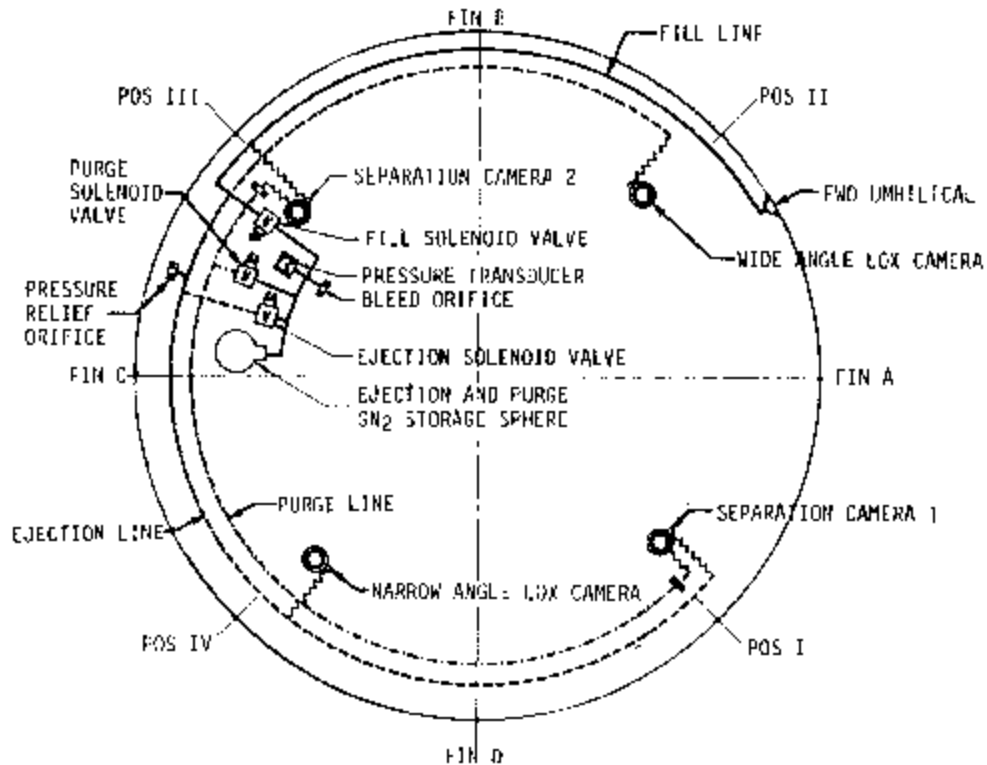


Figure 5-10. S-IC Control Sphere Pressure



FORWARD COMPARTMENT LOOKING AFT

Figure 5-11. S-IC Camera Ejection System

No flight measurement of bottle pressure was made. Ground measurements showed bottle pressure to be 1688 N/cm² (2450 psia) just prior to liftoff. Figure 5-12 shows the minimum predicted sphere pressure for normal operation compared to the predicted pressure assuming failure of the purge line.

If the system operates normally, bottle pressure at ejection command is approximately twice that required for camera ejection as demonstrated by ground ejection tests. However, with a purge line failure, bottle pressure at ejection command would be below the required pressure for ejection.

The following improvements to the camera ejection system have been proposed:

- a. The aluminum purge system lines in the vicinity of the suspected failure will be replaced with stainless steel lines.
- b. The lines in this same area will be redesigned and provided with improved supports to reduce the probability of vibration damage.

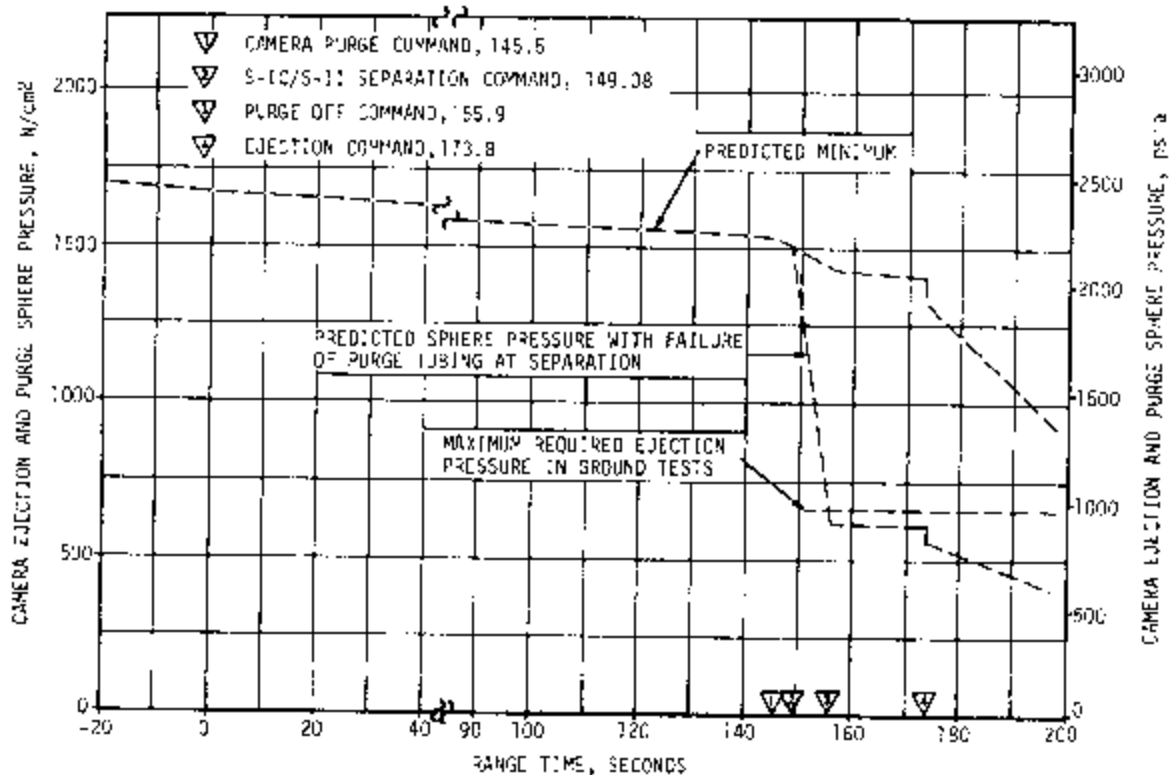


Figure 5-12. S-IC Predicted Camera Ejection and Purge Sphere Pressure

- c. Cabling to the thrusters which open the camera doors will have additional insulation installed as protection from S-II ullage motor heating.
- d. Flow balancing orifices in the purge system will be relocated closer to the purge solenoid valve to prevent excessive bottle blowdown in the event of purge line breakage downstream of the orifices.
- e. Orifices will be added to the ejection lines. In the event that one of the ejection lines fails, sufficient pressure will be maintained in the second line for ejection of two of the cameras.

SECTION 6

S-II PROPULSION

6.1 SUMMARY

The S-II propulsion system consists of five single-start liquid bipropellant J-2 engines, Liquid Oxygen (LOX) and Liquid Hydrogen (LH₂) propellant systems, propellants management, pressurization, pneumatic control pressure, recirculation and camera ejection systems. The five engines are functionally independent but are clustered and controlled to form an integrated mainstage propulsion system for the S-II stage.

The S-II propulsion system performed satisfactorily during the first 169 seconds of operation following Engine Start Command (ESC). Engine thrust, as determined by reconstruction analysis and telemetered propulsion measurements at 60 seconds after ESC, was only 0.43 percent below prediction. Total propellant flowrate was 0.53 percent below and specific impulse 0.08 percent above predictions at this time slice.

At 319 seconds a sudden performance shift was exhibited on engine No. 2 with thrust decreasing approximately 33,806 Newtons (7600 lbf). The engine continued performance at the reduced level until 412.3 seconds. By 412.92 seconds the dropout of thrust OK switches indicated engine No. 2 cutoff, and at 414.18 seconds engine No. 3 also cut off. Postflight evaluation of telemetered data led to the conclusion that the engine No. 2 Augmented Spark Igniter (ASI) fuel line failed and ultimately caused failure of the engine. Since the flight, testing at Marshall Space Flight Center (MSFC) and the engine manufacturer's facility has substantiated this conclusion. The testing reveals that an oxidizer rich mixture, caused by a fuel leak, creates very high temperatures and rapidly erodes the injector. Because of this erosion the LOX dome of engine No. 2 eventually failed, opening the LOX high pressure system and causing Engine Cutoff (ECO). A modification of the ASI propellant feedlines (both fuel and LOX) and their installation is being accomplished.

Interchanged LOX prevalve control wiring connections between engines No. 2 and 3 solenoids caused the premature cutoff of engine No. 3. When engine No. 2 cutoff the LOX prevalve on engine No. 3 was commanded closed. An individual checkout of the prevalve wiring during prevalve timing checks is planned for future vehicles.

S-II burn time, from engine ignition (Start Tank Discharge Valve [STDV] open) to ECO (start of Time Base 4 [T₄]) was 425.31 seconds which is 57.81 seconds longer than predicted. The extended burn time was caused by the premature cutoff of engines No. 2 and 3. Loss of the two engines reduced propellants consumption approximately 40 percent and required a longer burn time to reach propellants-depletion.

The propellants management subsystem met all performance requirements. However, the Propellant Utilization (PU) mixture ratio step, as sensed by the Launch Vehicle Digital Computer (LVDC), occurred 77.23 seconds later than predicted after ESC because of the two engines out condition. Propellant loading was 0.48 percent above the predicted. Residual propellants remaining in tanks at ECO were 3412 kilograms (7523 lbm) compared to the prediction of 3264 kilograms (7195 lbm), with no 0.5 second time delay incorporated. The discrepancy in residuals was caused by liquid level measurement errors that developed from "tilted" liquid level surfaces after engines No. 2 and 3 cutoff.

The performances of the LOX and LH₂ tank pressurization systems were satisfactory. The premature loss of two engines supplying GOX through heat exchangers to the LOX tank caused the ullage pressure to decrease below the regulator band late in the flight. LOX pump inlet Net Positive Suction Pressure (NPSP), however, was more than adequate throughout the flight.

The engine servicing system operated satisfactorily with the exception that the engine start tanks were chilled more than expected but within required limits. The exact cause of these low temperatures is not known. However, detailed analyses are being conducted of the Ground Support Equipment (GSE) LH₂ heat exchanger and engine purge and loading operations in order to isolate the problem.

Both LH₂ and LOX recirculation systems performed satisfactorily and met the required engine pump inlet and/or discharge conditions at ESC. However, there were some deviations of the LH₂ pump inlet temperatures and the LOX pump discharge temperatures prior to ESC. Potential system changes being considered at this time for AS-503 include improvements to the LH₂ system insulation and increased helium flow from the LOX helium injection system.

6.2 S-II CHILLDOWN AND BUILDUP TRANSIENT PERFORMANCE

During the S-IC boost phase the LOX and LH₂ recirculation subsystems, shown in Figure 6-1, chill the ducts, turbopumps and other engine components. Prior to engine start the recirculation systems are shut down. This opens the LH₂ prevalues, shuts down the LH₂ recirculation pumps and stops LOX helium (He) injection. Engine start signal is then received by the engine electrical controller which causes the propellant valves to open in the proper sequence. The controller also energizes spark plugs in the Gas Generator (GG) and thrust chamber, ignites the

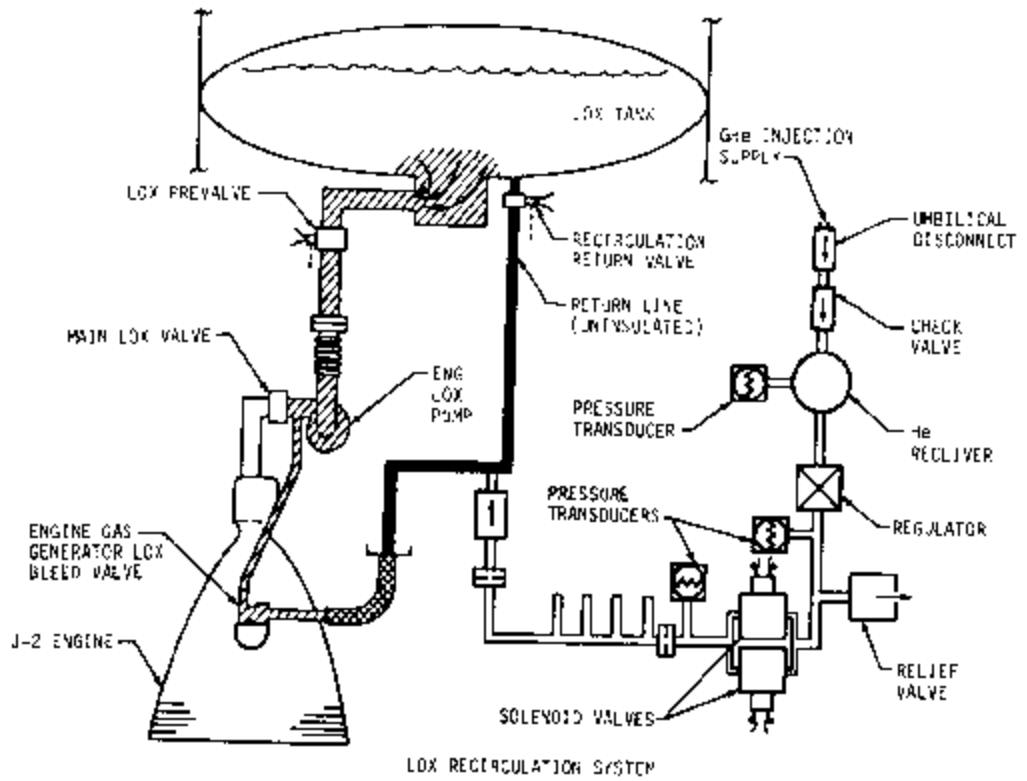
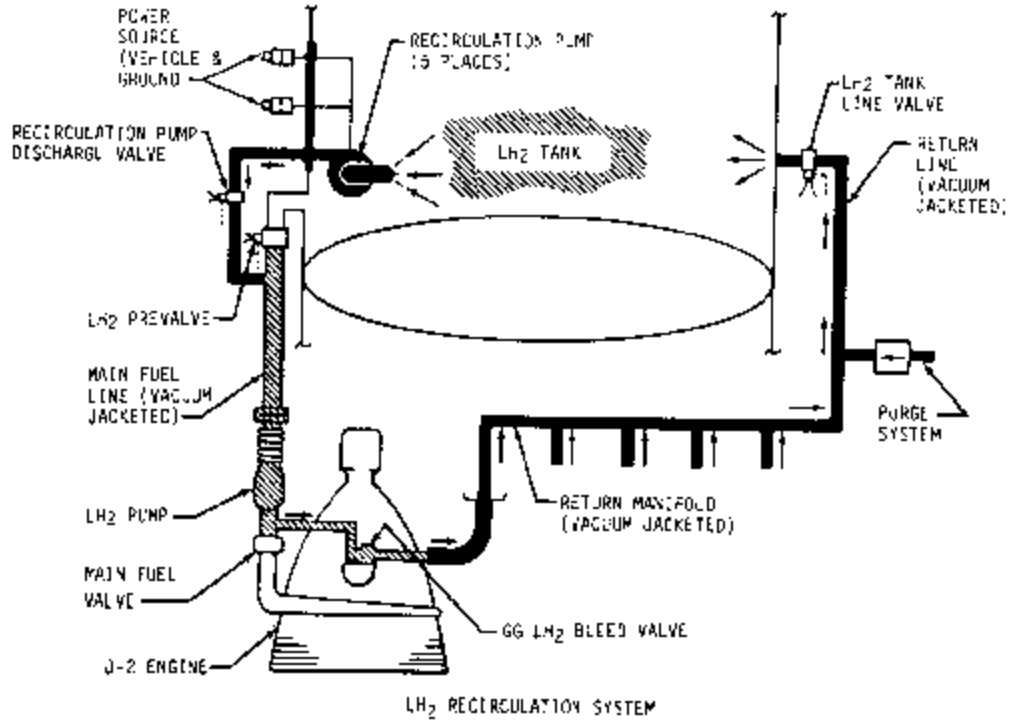


Figure 6-1. S-II LH₂ and LOX Recirculation Systems

propellant and also causes Gaseous Hydrogen (GH₂) to be released from the start tank. GH₂ provides the initial drive for the turbopumps which deliver propellant to the GG and the engine. After propellant ignition, gas generator output accelerates the turbopumps and engine thrust increases to main stage operation at which time the spark plugs de-energize and the engine is in steady-state operation.

The engine servicing and recirculation operations were performed satisfactorily although there were some deviations. Thrust chamber temperatures, as shown on Figure 6-2, lie near the cold edge of the prediction band and are approximately 5.6°K (10°F) colder than for AS-501. Engine servicing procedures and the GSE LH₂ heat exchanger are being evaluated to determine the cause for the low temperatures.

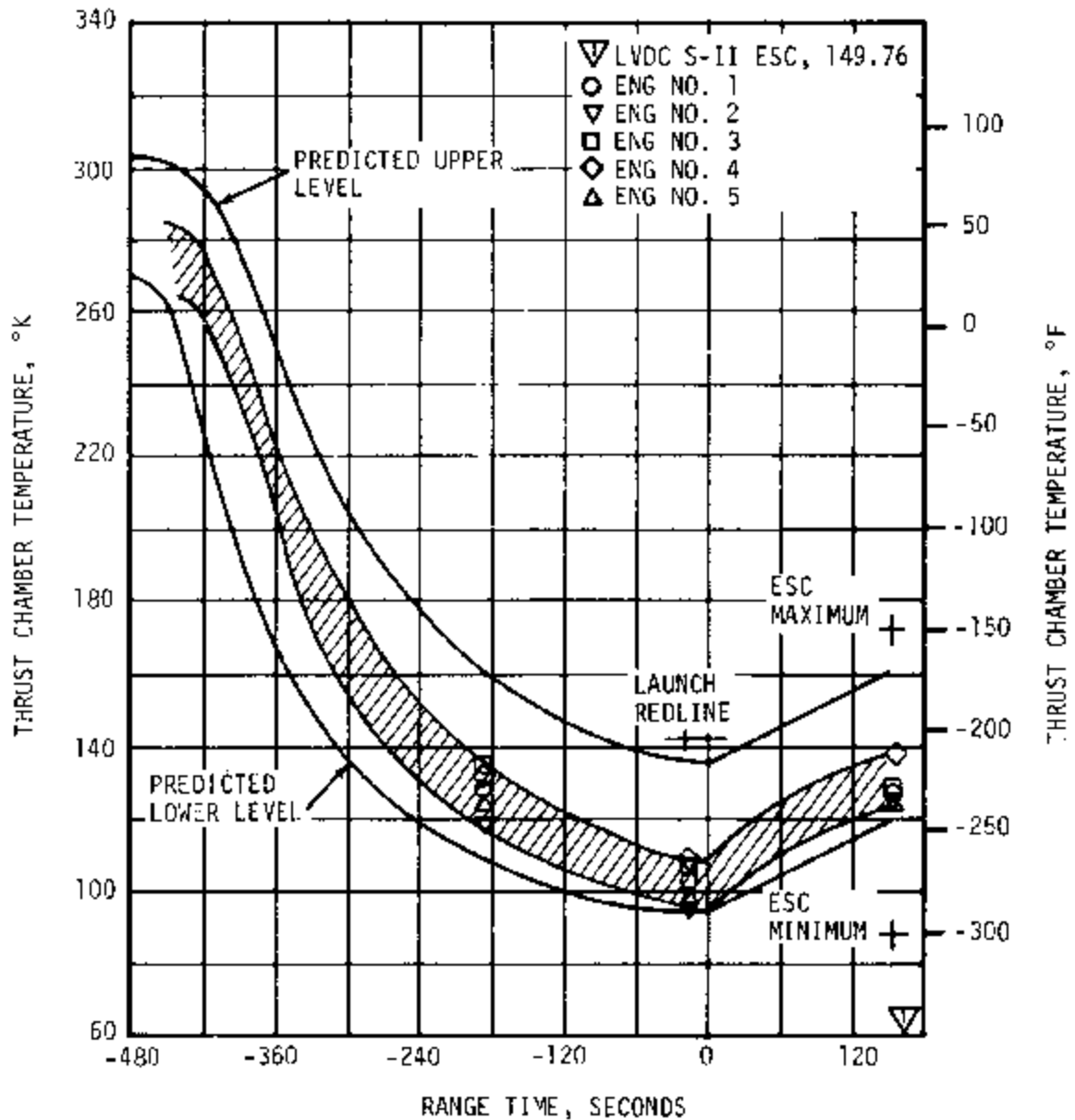


Figure 6-2. S-II Thrust Chamber Temperature

Thrust chamber warmup rates during the S-II boost ranged from 8.7 to 12.5°K/min (15.6 to 22.4°F/min) and closely paralleled the predicted rate. These warmup rates were nearly the same as those experienced on AS-501, confirming the conclusion that AS-501 results should be considered "normal". The AS-501 report recommendation to accommodate the warmup rate was satisfied and the maximum allowable engine start temperature was increased from 161 to 172°K (-170 to -150°F). Thrust chamber temperatures at engine start ranged from 125 to 138°K (-235 to -210°F), well within the 88 to 172°K (-300 to -150°F) requirement.

Both temperature and pressure conditions of the J-2 engine start tanks were within the required prelaunch and engine start boxes. The range of data points were near the cold temperature and high pressure side of the boxes as shown in Figure 6-3. Chillydown temperatures ranged from 90 to 105°K (-298 to -271°F), (lower than predicted), and analyses are being conducted to determine the reason for increased chilling. Start tank pressures, 808 to 815 N/cm² (1171 to 1180 psia), were lower than for AS-501, as planned. The lower pressures were intended to increase tank temperatures but the increased chillydown offset this planned increase.

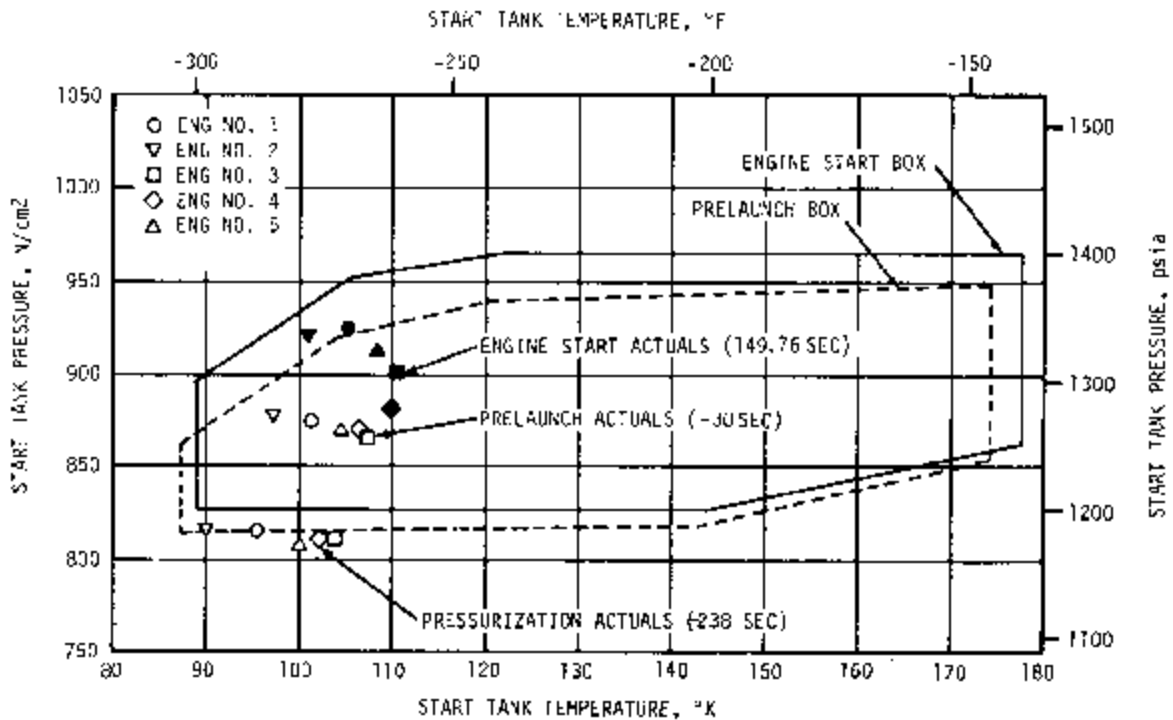


Figure 6-3. S-II Engine Start Tank Performance

Prelaunch start tank warmup rates ranged from 16.1 to 19.0 N/cm²/min (23.4 to 27.5 psi/min) and 1.1 to 1.9°K/min (2.0 to 3.5°F/min). The warmup rates during the S-IC boost were 10.0 to 14.8 N/cm²/min (14.5 to 21.4 psi/min) and 0.9 to 1.6°K/min (1.6 to 2.8°F/min). These rates are higher than experienced on AS-501 and are the result of very cold initial start tank temperatures. Engine No. 4 start tank indicated a considerably lower warmup rate and it is suspected to have had a small leak. During S-II engine operation, the start tanks refilled as designed. However, at approximately 413.5 seconds engine No. 2 start tank pressure started to decay probably caused by the failure of the start tank refill line.

A change to the start tank servicing system is being considered which would increase the launch facility start tank vent system line size from 2.54 to 3.81 centimeters (1 to 1.5 in.) from the stage umbilical to the main vent line. This would increase start tank temperatures approximately 11.1°K (20°F).

All engine helium tank pressures were within the required prelaunch and engine start limits. At -276 seconds, engine No. 5 helium tank pressure decreased below the redline of 2000 N/cm² (2900 psia) to a minimum of 1985 N/cm² (2884 psia). At -240 seconds, the pressure increased to 2035 N/cm² (2950 psia); this was caused by erratic operation of the GSE pressurization regulator.

Helium tank temperature during prelaunch chilldown ranged from 103 to 110°K (-274 to -263°F), approximately 7°K (12.6°F) lower than those exhibited on AS-501. Engine servicing procedures and the GSE LH₂ heat exchanger are being evaluated to determine the cause of these low temperatures.

During the S-IC boost the helium tank pressure increase due to warmup rates was approximately 4 N/cm² (5.8 psi) higher than that for AS-501; the rates were 21.9 to 39.2 N/cm²/min (31.8 to 56.7 psi/min).

The LH₂ and LOX recirculation systems performed satisfactorily. At S-II ESC the predicted engine pump inlet conditions were obtained as shown on Figure 6-4. However, during prelaunch operations difficulties were experienced in maintaining engines No. 3, 4 and 5 pump discharge temperatures below the launch redlines. As shown in Figure 6-5 the LOX pump discharge temperatures of engines No. 3 and 4 and the LH₂ pump discharge temperatures on engines No. 3 and 5 were above the prediction bands most of the time from -210 seconds until just before ESC at 149.76 seconds. These same difficulties were experienced during the Countdown Demonstration Test (CDDT) at which time it was demonstrated that these temperatures decreased substantially after tank pressurization. Accordingly, the CDDT prelaunch maximum temperature redline for engines LOX pumps discharge was increased from 96.5 to 97.6°K (-286 to -284°F) and the time was changed from between -100 and -50 seconds to a constraint at -22 seconds. Similarly, the maximum LH₂ pump discharge temperature redline, between -52 and -30 seconds, was changed to a constraint at -30 seconds and increased from 21.8 to 22.3°K (-420.5 to -419.5°F) for engine No. 5

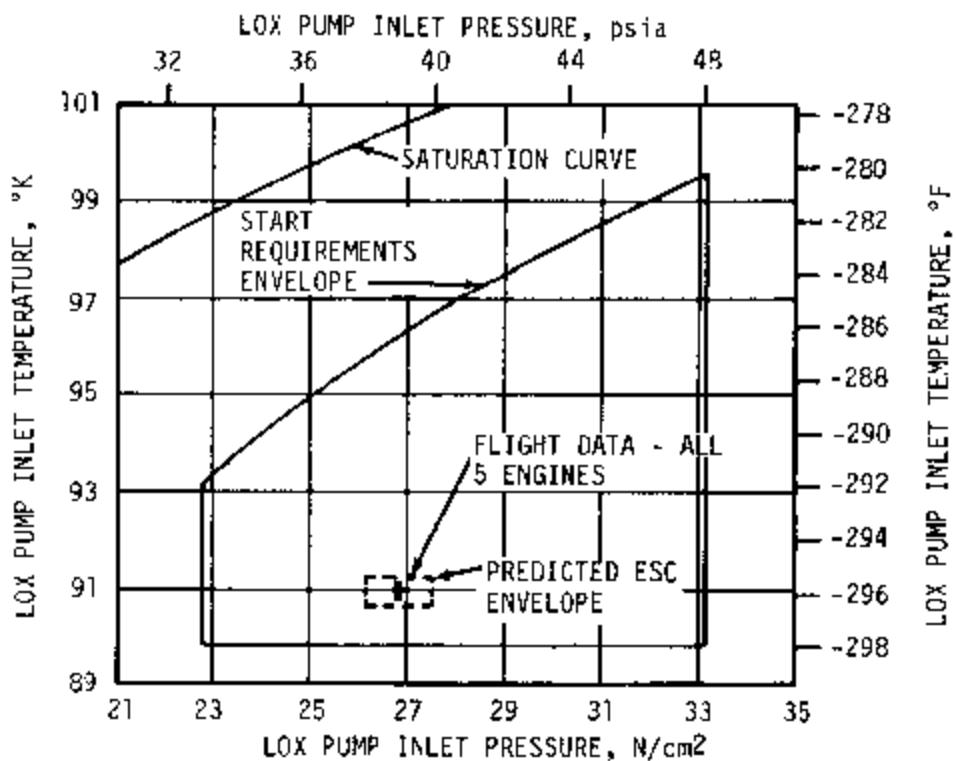
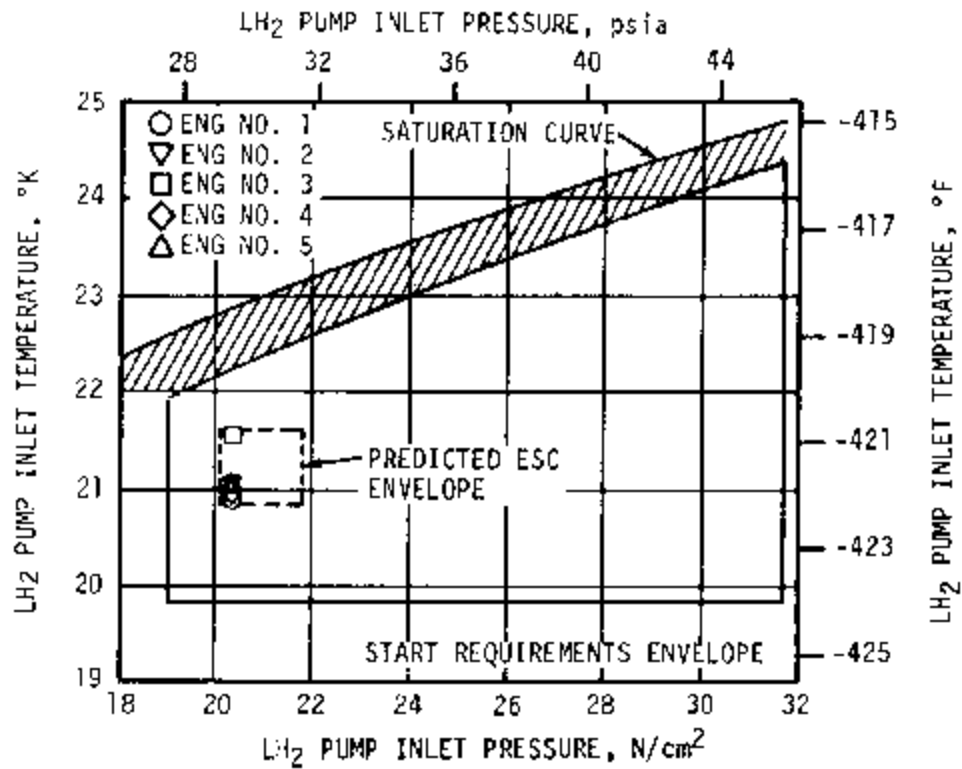


Figure 6-4. S-II Start Box Requirements

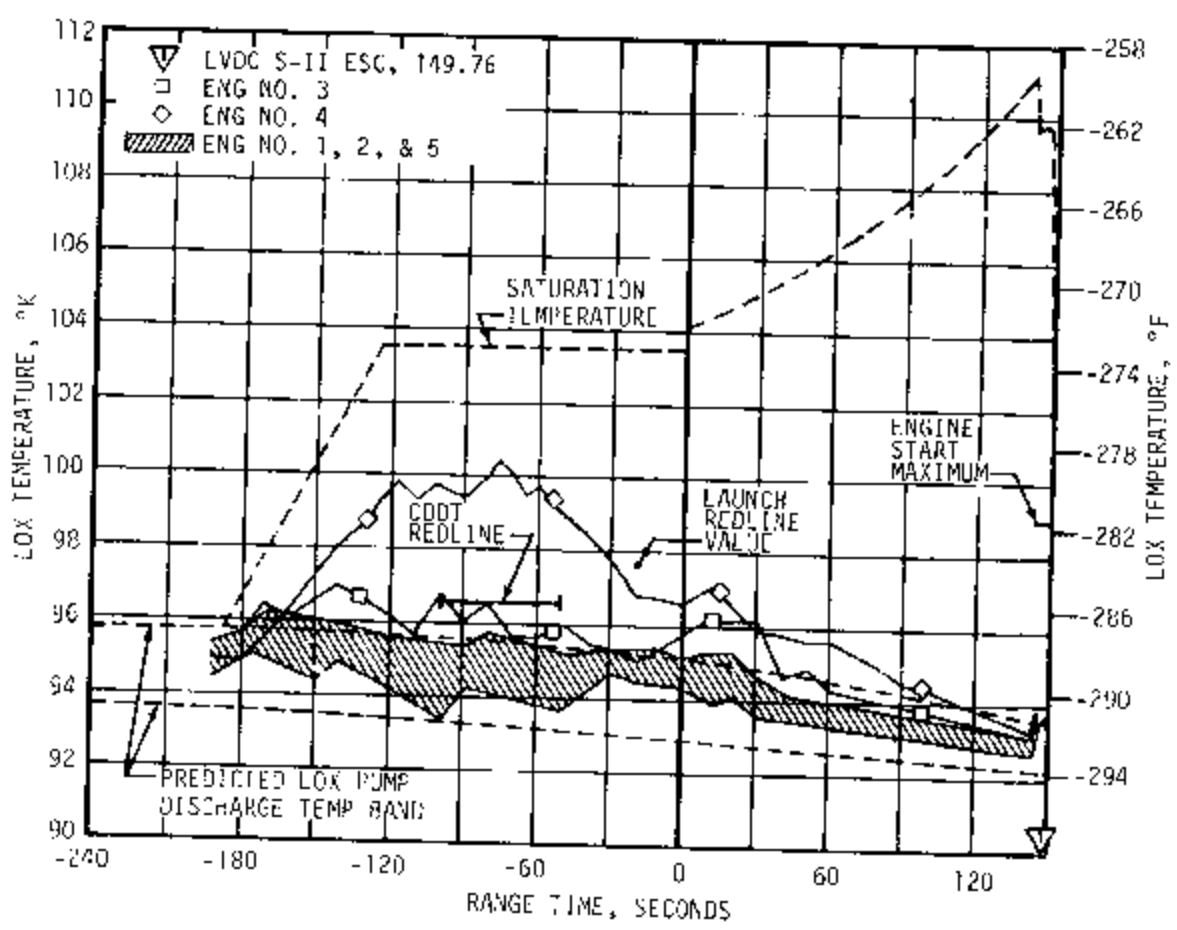
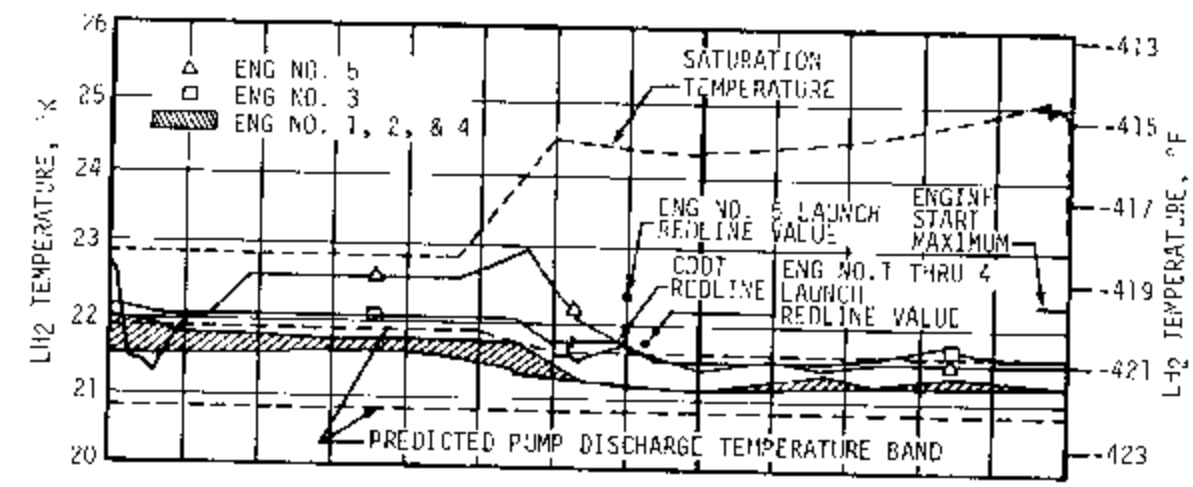


Figure 6-5. S-II LH₂ and LOX Recirculation System Performance

providing that a cooling trend prevails. Engines No. 1 through 4 red-line limits were maintained at 21.8°K (-420.5°F) maximum but changed to a constraint at -22 seconds. Recommended changes to the LOX recirculation system are presented in paragraph 6.9. Changes under consideration for the LH₂ recirculation system are:

- a. Insulate all bare flanges of the LH₂ return manifolds.
- b. Provide additional insulation on J-2 engine components.
- c. Retrofit improved evacuation valves on the LH₂ feed and recirculation vacuum jacketed lines.

The thrust buildup profile of each J-2 engine is shown in Figure 6-6. All engine performance parameters were within the predicted thrust buildup envelope. Major engine start event times are summarized in Table 6-1. The S-II stage engine start was commanded by the LVDC at 149.76 seconds and the engine buildup transient commenced at 151.02 seconds (average) when the STDV opened. S-II mainstage, average time for engines to reach 90 percent thrust, occurred at 153.08 seconds, 2.06 seconds after STDV. The engine thrust levels stabilized between 870,000 and 900,000 Newtons (195,500 and 202,200 lbf) prior to PU system activation at 155.26 seconds.

Table 6-1. S-II Engine Start Sequence Events

EVENT	TIME OF EVENT IN RANGE TIME, SECONDS				
	ENGINE 1	ENGINE 2	ENGINE 3	ENGINE 4	ENGINE 5
Engine Start Command	149.76	149.76	149.76	149.76	149.76
Mainstage Control Solenoid	150.98	150.98	150.98	150.98	150.98
Start Tank Discharge Valve Open	151.020	151.026	151.011	151.011	151.020
90 Percent Thrust	153.57	152.93	153.03	153.02	152.86
Main LOX Valve Open	153.778	153.778	153.778	153.778	153.737
Mainstage OK	153.79	153.74	153.74	153.74	153.71

6.3 S-II MAIN STAGE PERFORMANCE

Each of the five J-2 engines is a high performance, 1,000,850 Newtons (225,000 lbf) thrust rated engine, using LOX and LH₂ at a mixture ratio of 5.5:1 (can vary to as low as 4.5 for the desired propellant utilization at stage cutoff). It features a tubular wall, bell-shaped thrust chamber (27.5:1 expansion ratio), and two independently driven, direct-drive turbopumps powered in series by a single gas generator. After the initial start transient the engines operate at a high mixture ratio

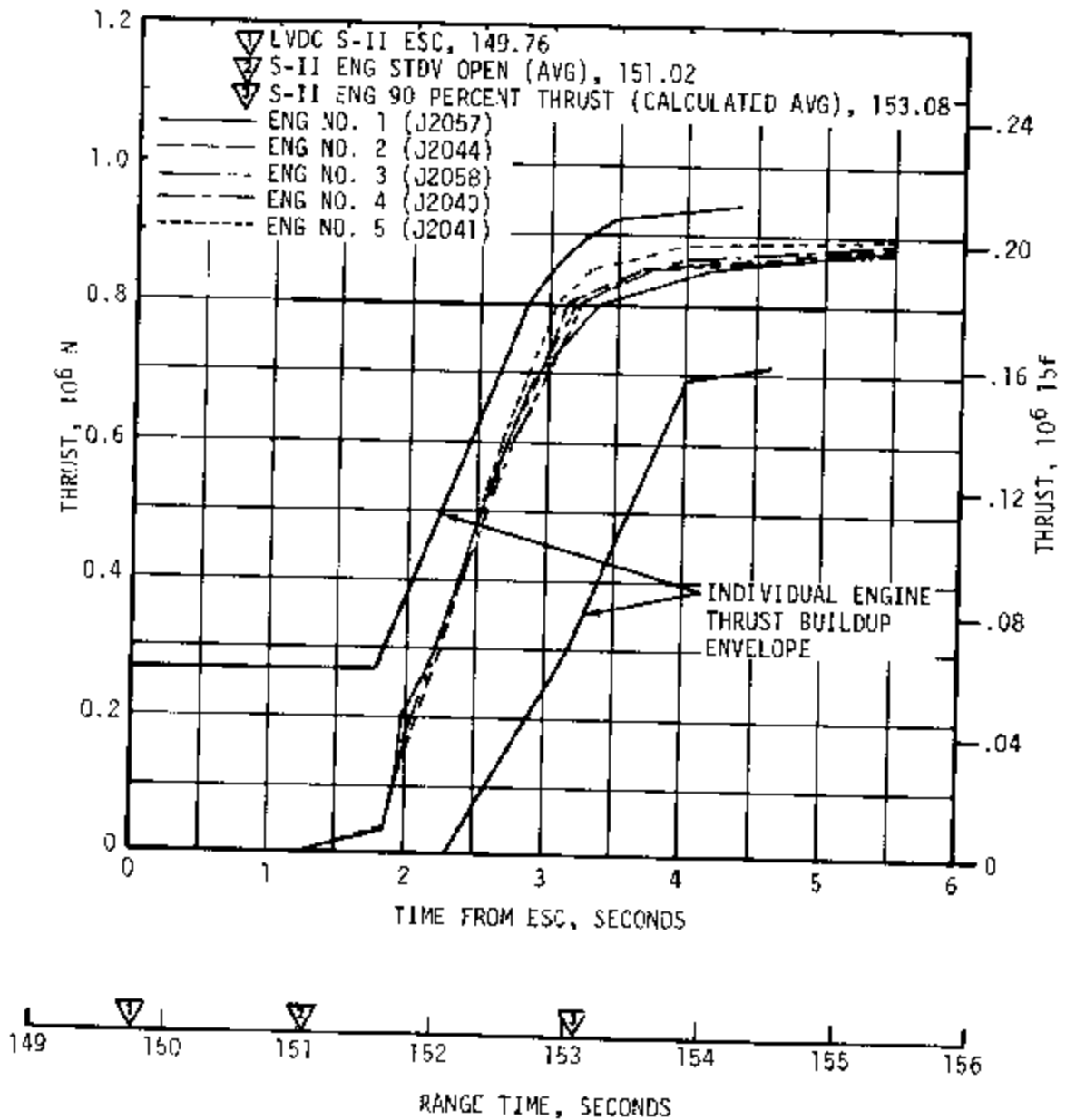


Figure 6-6. S-II Engine Thrust Buildup

until Engine Mixture Ratio (EMR) shift. At this time the EMR is changed to the Reference Mixture Ratio (RMR) until ECD.

Two analytical techniques were employed in evaluating S-II stage propulsion system performance. The primary method, propulsion reconstruction analysis, utilized telemetered engine and stage data to compute longitudinal thrust, specific impulse, and stage mass flowrate. The second method, flight simulation, utilized a six-degree-of-freedom trajectory simulation to adjust propulsion reconstruction analysis results to fit the observed trajectory. Adjustments to the reconstruction analysis of thrust and mass flow histories were determined using a

differential correction procedure which yielded a simulated trajectory closely matching the observed postflight trajectory.

Average engine thrust, as determined from reconstruction analysis, at a time slice of ESC +60 seconds was 0.43 percent below predicted as shown in Table 6-2. Individual engine deviations from predicted thrust ranged from 1.36 percent lower (engine No. 2) to 0.28 percent higher (engine No. 3). Average engine specific impulse was 0.08 percent greater than predicted. Individual engine deviations from predicted specific impulse ranged from 0.02 percent lower (engine No. 4) to 0.17 percent greater (engine No. 3) than predicted. Predicted average performance characteristics of the S-II stage engine system are presented in Table 6-3 for the total flight and for the high and reference mixture ratio burn times. Total flight averages are considerably below predictions because of the premature cutoff of engines No. 2 and 3. During the high mixture ratio burn, however, average thrust and mass loss rate were only 0.25 and 0.33 percent below the predicted, respectively.

Table 6-2. S-II Engine Performance Deviations (ESC + 60 Seconds)

PARAMETER	ENGINE	PREDICTED	RECONSTRUCTION ANALYSIS	PERCENT DEVIATION FROM PREDICTED	AVERAGE PERCENT DEVIATION FROM PREDICTED
Thrust N (lbf)	1	1,007,215 (226,432)	1,003,323 (226,657)	0.39	-0.43
	2	1,009,212 (226,681)	995,489 (223,796)	-1.35	
	3	1,002,077 (225,277)	1,004,548 (225,900)	0.28	
	4	1,006,036 (226,167)	1,005,031 (225,901)	-0.10	
	5	1,015,589 (226,989)	1,012,325 (227,716)	-0.55	
Specific Impulse N-s/kg (lbf-s/lbm)	1	4139.7 (422.5)	4145.3 (423.1)	0.14	0.08
	2	4153.5 (423.9)	4157.4 (424.3)	0.09	
	3	4135.8 (422.1)	4142.7 (422.8)	0.17	
	4	4135.8 (422.1)	4134.3 (422.0)	-0.02	
	5	4165.2 (425.2)	4166.2 (425.2)	0.0	
Flowrate kg/s (lbm/s)	1	243.7 (535.9)	241.8 (533.1)	-0.52	-0.53
	2	242.6 (535.2)	239.2 (527.4)	-1.46	
	3	242.7 (533.7)	242.2 (534.3)	0.11	
	4	243.0 (535.8)	242.7 (535.0)	-0.15	
	5	244.2 (538.5)	242.9 (535.9)	-0.55	
Mixture Ratio LOX/Fuel	1	5.57	5.50	-1.26	-0.59
	2	5.59	5.50	-0.72	
	3	5.63	5.56	-1.24	
	4	5.47	5.46	-0.37	
	5	5.30	5.31	0.19	
NOTE: Analysis is at ESC plus 60 seconds.					

Flight simulation showed the stage time averaged specific impulse during the high mixture ratio step operation to be 0.09 percent greater than predicted, in good agreement with the reconstruction analysis. Detailed results are presented in Table 6-3.

The S-II stage propulsion system performance is presented in Figure 6-7. A shift from normal performance occurred at approximately 319 seconds. The performance change is evidenced by a thrust decrease of 33,806 Newtons (7600 lbf). This has been attributed to an ASI fuel line leak on engine No. 2. At approximately 413 seconds a large step decrease in stage performance was evidenced by a reduction of stage thrust to 3,002,535 Newtons (675,000 lbf) and a change of propellants flowrate from 1213 to 730.3 kg/s (2675 to 1610 lbm/s). This abrupt change in performance, approximately 40 percent, was caused by the shutdown of engines No. 2

Table 6-3. S-II Flight Reconstruction Comparison With Simulation Trajectory Match Results

PARAMETERS	UNITS	PREDICTED				RECONSTRUCTION ANALYSIS				PERCENT DEV. FROM PRED.	
		HIGH MIXTURE RATIO	REFERENCE MIXTURE RATIO	*TOTAL FLIGHT AVERAGE	** HIGH MIXTURE RATIO (5 ENGINES)	HIGH MIXTURE RATIO (3 ENGINES)	REFERENCE MIXTURE RATIO (3 ENGINES)	*TOTAL FLIGHT AVERAGE	HIGH MIXTURE RATIO	F-IG MIXTURE RATIO	TOTAL FLIGHT AVERAGE
Average Longitudinal Stage Thrust	N (lbf)	5,037,538 (1,132,489)	4,219,923 (946,681)	4,306,591 (1,080,570)	5,025,021 (1,129,673)	2,993,799 (673,036)	2,468,395 (554,920)	4,118,566 (925,863)		-0.25	-14.31
Average Vehicle Mass Loss Rate	kg/s (lbf/s)	1212.7 (2673.5)	995.6 (2204.1)	1152.6 (2541.0)	1208.7 (2664.7)	724.6 (1597.4)	603.0 (1321.8)	994.9 (2193.4)		-0.33	-13.68
Average Stage Longitudinal Specific Impulse	N-s/kg (lbf-s/lbf)	4154.1 (423.6)	4220.8 (430.4)	4170.8 (425.3)	4157.0 (423.9)	4131.5 (421.3)	4161.6 (419.8)	4139.4 (422.1)		0.07	- 0.75
S-II FLIGHT - TRAJECTORY MATCH											
PARAMETERS	UNITS	PERCENT DEV. FROM PRED.				PERCENT DEV. FROM PRED.					
		**HIGH MIXTURE RATIO (5 ENGINES)	HIGH MIXTURE RATIO (3 ENGINES)	REFERENCE MIXTURE RATIO (3 ENGINES)	*TOTAL FLIGHT AVERAGE	HIGH MIXTURE RATIO	REFERENCE MIXTURE RATIO	*TOTAL FLIGHT AVERAGE	HIGH MIXTURE RATIO	TOTAL FLIGHT AVERAGE	
Average Longitudinal Stage Thrust	N (lbf)	5,041,292 (1,133,333)	3,003,500 (675,217)	2,476,393 (556,718)	4,137,911 (928,895)	0.07		-14.04			
Average Vehicle Mass Loss Rate	kg/s (lbf/s)	1212.3 (2672.7)	726.7 (1607.2)	601.4 (1325.8)	997.9 (2200.0)	-0.03		-13.42			
Average Stage Longitudinal Specific Impulse	N-s/kg (lbf-s/lbf)	4156.0 (424.0)	4132.5 (421.4)	4117.8 (419.9)	4140.4 (422.2)	0.05		- 0.73			

* Time duration is measured from the occurrence of 90 percent thrust until ECO Command.
 ** Average prior to performance shift of engine no. 2 at approximately 319 seconds range time.

and 3 and is discussed in subsequent paragraphs. Stage thrust dropped below the predicted value for a two engines out condition after engines No. 2 and 3 cutoff. Approximately 33 percent of this performance loss was caused by a reduction of axial acceleration that reduced engine LOX inlet pressure but the remaining effect has not been determined at this time. Analyses by the engine and stage manufacturers are in progress to determine whether data was in error or if an engine/stage performance deviation occurred. Current information indicates that all pressures for engines No. 4 and 5 dropped excessively due to an instrumentation bus change observed in a 47 ampere surge at the time of engines No. 2 and 3 cutoff. Because of the low consumption rate of propellants after cutoff of the two engines the Programmed Mixture Ratio (PMR) shift was delayed 77.23 seconds and was not sensed until 490.76 seconds. The two engine out condition also extended burn time 57.81 seconds to 425.31 seconds with ECO, initiated by LOX depletion, sensed by the LVDC at 576.33 seconds.

A chronological list of events that are believed to have led to the failure of engine No. 2 are discussed briefly in Table 6-4. Postflight data analysis led to the conclusion that the ASI fuel line, shown in Figure 6-8, had cracked at approximately 225 seconds and continued to leak progressively until 319 seconds. Since the flight, testing at Marshall Space Flight Center (MSFC) and the engine manufacturer's facility has substantiated this theory. The testing simulated an ASI fuel line failure by reducing the fuel supply, creating an ASI 9.5 LOX/LH₂ mixture ratio. The high mixture ratio produced abnormally high temperatures in the main injector which caused severe erosion to occur, as evidenced in Figure 6-9. Further indications of the ASI fuel leak are reflected by local decreases of engine compartment, engine instrumentation packages, and engine No. 2 hydraulic actuator return fluid temperatures (discussed in paragraph 17.3) and evidence of cryogenic impingement on the No. 2 yaw actuator pressure transducer, as discussed in paragraph 8.3.

The first indicator of abnormal behavior was a gradual decrease in chamber pressure of engine No. 2 starting at 260 seconds. The rate of decay was approximately 0.07 N/cm²/s (0.10 psi/s). At 318.9 seconds there was a sudden change of engine No. 2 performance. At this time, fuel flowrate started to increase and was followed by a general engine performance decrease at 319 seconds as shown in Figure 6-10. The increase in fuel flowrate is probably due to thrust chamber tube damage resulting from injector debris produced by the high ASI mixture ratio operation preceding this time. This damage resulted in the side loads shown by the actuator AP. MSFC testing demonstrated this type of tube bundle damage. Main thrust chamber pressure decreased 15.8 N/cm² (22.9 psi) with proportionate reductions of pump discharge, main injection and GG injection pressures. During this performance shift however, fuel injection and turbine inlet temperatures abnormally increased indicating that a fuel leak had developed between the flowmeter outlet and the engine fuel manifold discharge. Following the performance shift, engine No. 2 stabilized and continued operation at

Table 6-4. S-II Engine No. 2 Performance Shift and Cutoff

RANGE TIME, SECONDS	EVENT AND/OR PREVAILING CONDITION
225	Cryogenic leak in engine compartment indicated; engine compartment and engine No. 2 yaw actuator return fluid temperatures began to decrease (see paragraphs 17.3 and 8.3)
260 to 318	Chamber pressure decays at rate of 0.07 N/cm ² /s (0.10 psi/s).
280	Cryogenic impingement on pressure transducer believed to have occurred. Engine No. 2 yaw actuator ΔP transducer indicated an abnormal pressure ramp (see paragraph 8.3)
318.9	An increase in LH ₂ flowrate occurred.
319	Engine No. 2 LH ₂ flowrate increased and engine performance decreased; a tube bundle leak is believed to have been the cause.
412.3	Engine No. 2 chamber and fuel injection pressures began a gradual decrease.
412.6	Engine compartment heating spike occurs (see paragraph 17.3)
412.7	LOX dome failed; the LOX high pressure system opened and the engine performance decayed rapidly.
412.9	Mainstage OK pressure switches deactivate when LOX injection pressure decayed below switch setting and initiated ECO sequence.

the reduced level until 412.3 seconds. Immediately after this time, as indicated in Figure 6-11, the LOX pump discharge pressure began to decrease, followed by a rapid increase of LOX flowrate at 412.6 seconds, indicating that the LOX high pressure system had failed. It has been concluded that the LOX dome failed from erosion caused by a hot oxidizer-rich ASI mixture ratio. Failure of the LH₂ high pressure system was also indicated at 412.6 seconds by a large flowrate increase. Engine failure was definitely evidenced by the rapid decay of thrust chamber pressure, main LOX and LH₂ injection pressures, and propellant pump discharge pressures at 412.7 seconds. Mainstage thrust OK pressure switches opened and initiated an engine shutdown sequence at 412.92 seconds. These anomalies

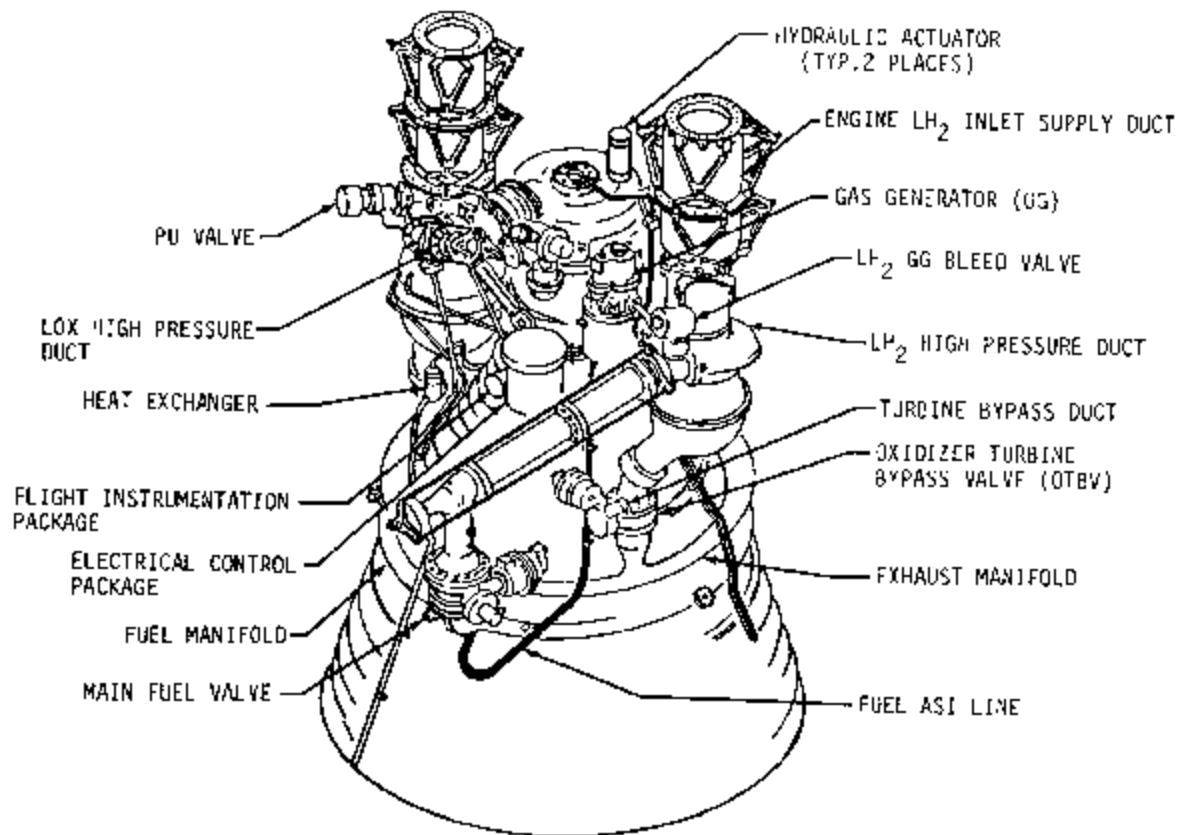


Figure 6-8. S-II J-2 Engine Diagram

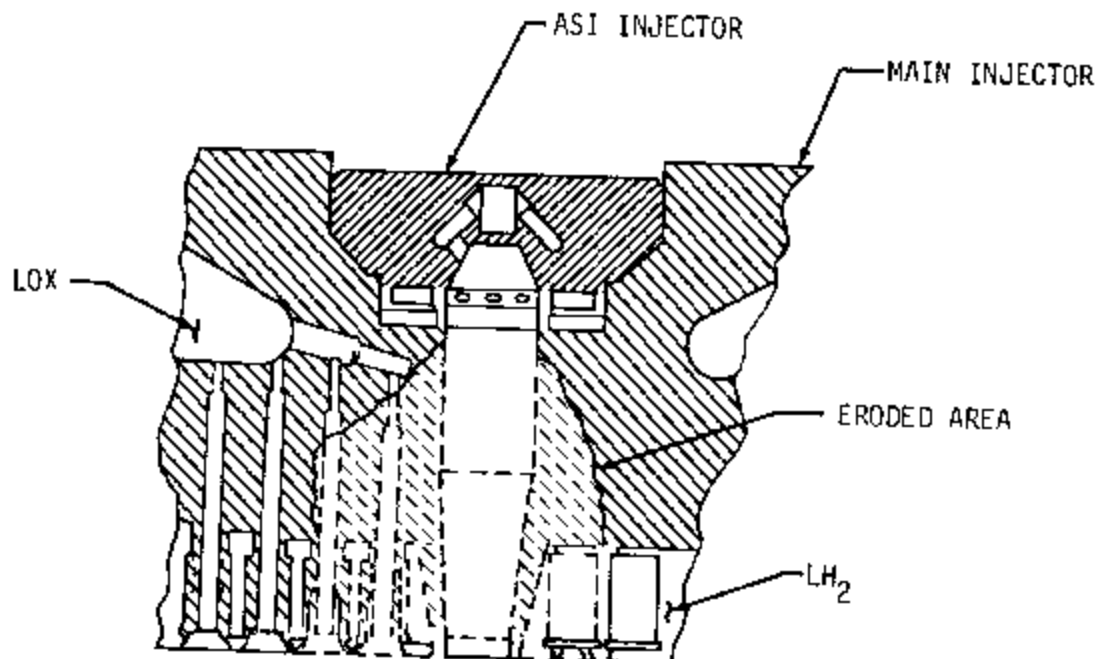


Figure 6-9. S-II Injector After 28 Second Test at High ASI Mixture Ratio

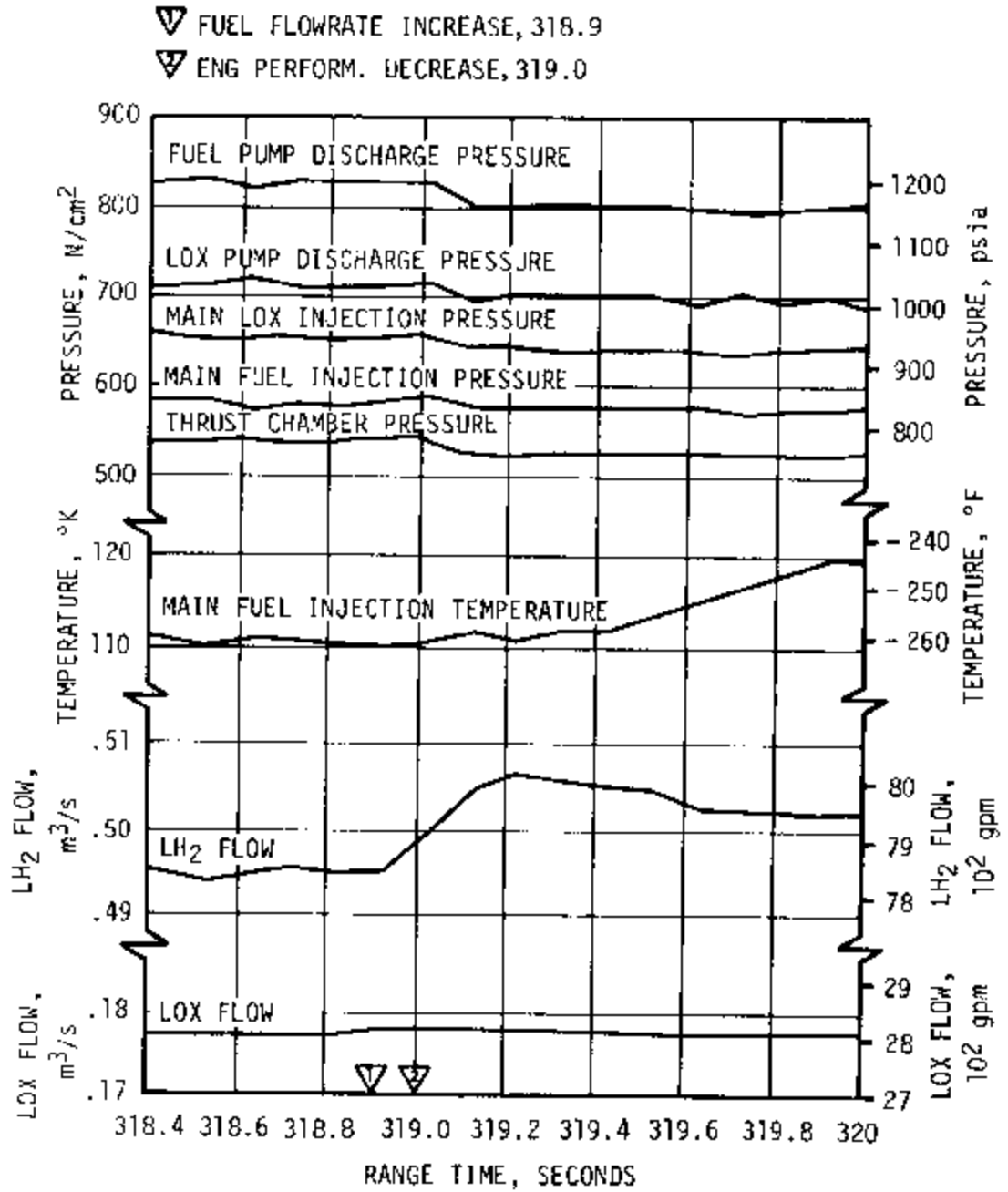


Figure 6-10. S-II Engine No. 2 Performance Shift

- ▽ LOX DOME FAILURE 412.7
- ▽ S-II ENG NO. 2 OUT 412.92
- LH₂ PUMP DISCHARGE PRESSURE
- LOX PUMP DISCHARGE PRESSURE
- ▽ MAIN LOX INJECTION PRESSURE
- MAIN FUEL INJECTION PRESSURE
- ▲ THRUST CHAMBER PRESSURE
- ▲ LH₂ INLET PRESSURE
- ▼ LOX INLET PRESSURE
- ◇ LOX FLOW
- LH₂ FLOW

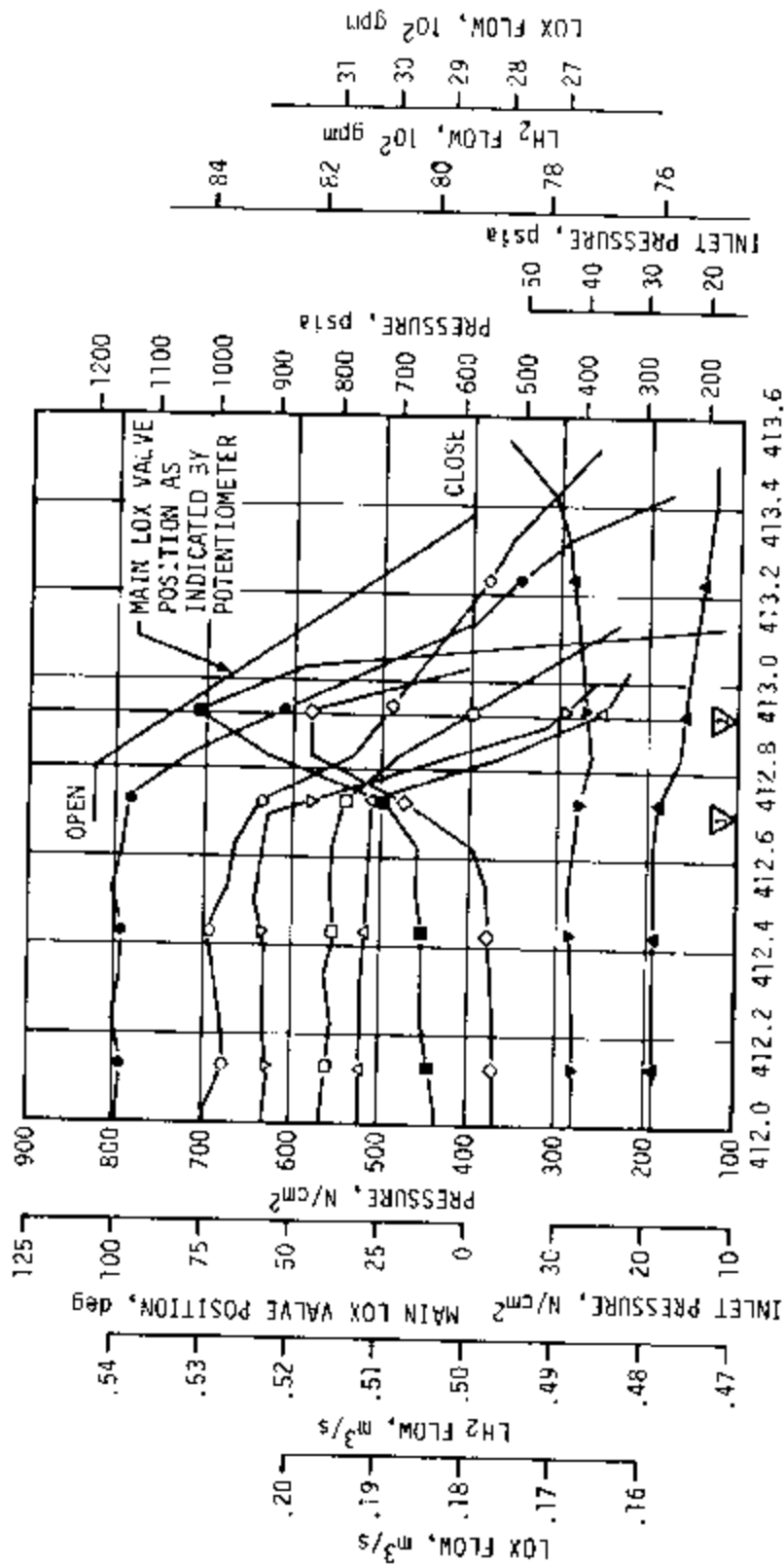


Figure 6-11. S-II Engine No. 2 Cutoff Performance

are apparently the effect of the ASI system failure. As previously stated, testing at MSFC has reproduced the failure characteristics exhibited by engine No. 2 and it has been concluded that the ASI fuel line failure did indeed initiate engine No. 2 failure. It has been recommended that the ASI fuel line and installation be improved by redesign.

Other engine parameters that reflect the cutoff characteristics of engine No. 2 are shown in Figure 6-12. The GG LOX and fuel inlet pressures start to decrease rapidly at 412.7 seconds. This is the same time that the main LOX and fuel injector pressures similarly decayed.

Engine No. 3 was shutdown prematurely when its LOX prevalve was inadvertently closed by the shutdown of engine No. 2. The sequence of events and changes of engine parameters are shown in Figure 6-13. This figure shows the decreases in main LOX injector and thrust chamber pressures and LOX flowrate that resulted from the closure of the LOX pre-valve. Approximately 0.60 second later, the engine No. 3 mainstage OK pressure switches actuated normally when the main LOX injector pressure had dropped to the switch setting band of 262 to 362 N/cm² (380 to 525 psia).

Engine No. 3 cutoff resulted from a wiring harness installation error; the control harnesses for engines No. 2 and 3 LOX prevalve solenoids were interchanged. (Plug 206W17P7 was misconnected to receptacle 206A507J1 instead of 206A508J1 and plug 206W17P8 was misconnected to 206A508J1.) To prevent this from recurring the harnesses for subsequent stages are to be either reinspected and/or redesigned. Also, revisions to the engine checkout program are to provide for individual engine prevalve timing checkout since the simultaneous checkout of all prevalves currently employed at KSC does not detect an error of the type experienced on AS-502.

6.4 S-II STAGE SHUTDOWN TRANSIENT PERFORMANCE

The normal S-II engine shutdown sequence is initiated by a LOX low level indication. Five level sensors are located at the bottom of the propellant tank and engine shutdown is initiated when any two probes of the LOX tank detect a dry condition. This condition initiates the cutoff signal and causes the engine propellant valves to close in the proper sequence resulting in engine thrust decay and the cutoff sequence is complete. A similar system is provided for the LH₂ tank to provide for a safe shutdown should LH₂ depletion occur first.

S-II ECO for AS-502 was initiated by LOX liquid level and ECO was sensed at 576.33 seconds. This corresponds to 425.31 seconds of S-II stage burn time. Engine cutoff transients for engines No. 1, 4, and 5 were normal but engines No. 2 and 3 had cut off earlier at 412.92 and 414.18 seconds, respectively. Thrust decay characteristics for engines No. 4 and 5 are shown on Figure 6-14. Thrust decay rates satisfied separation requirements.

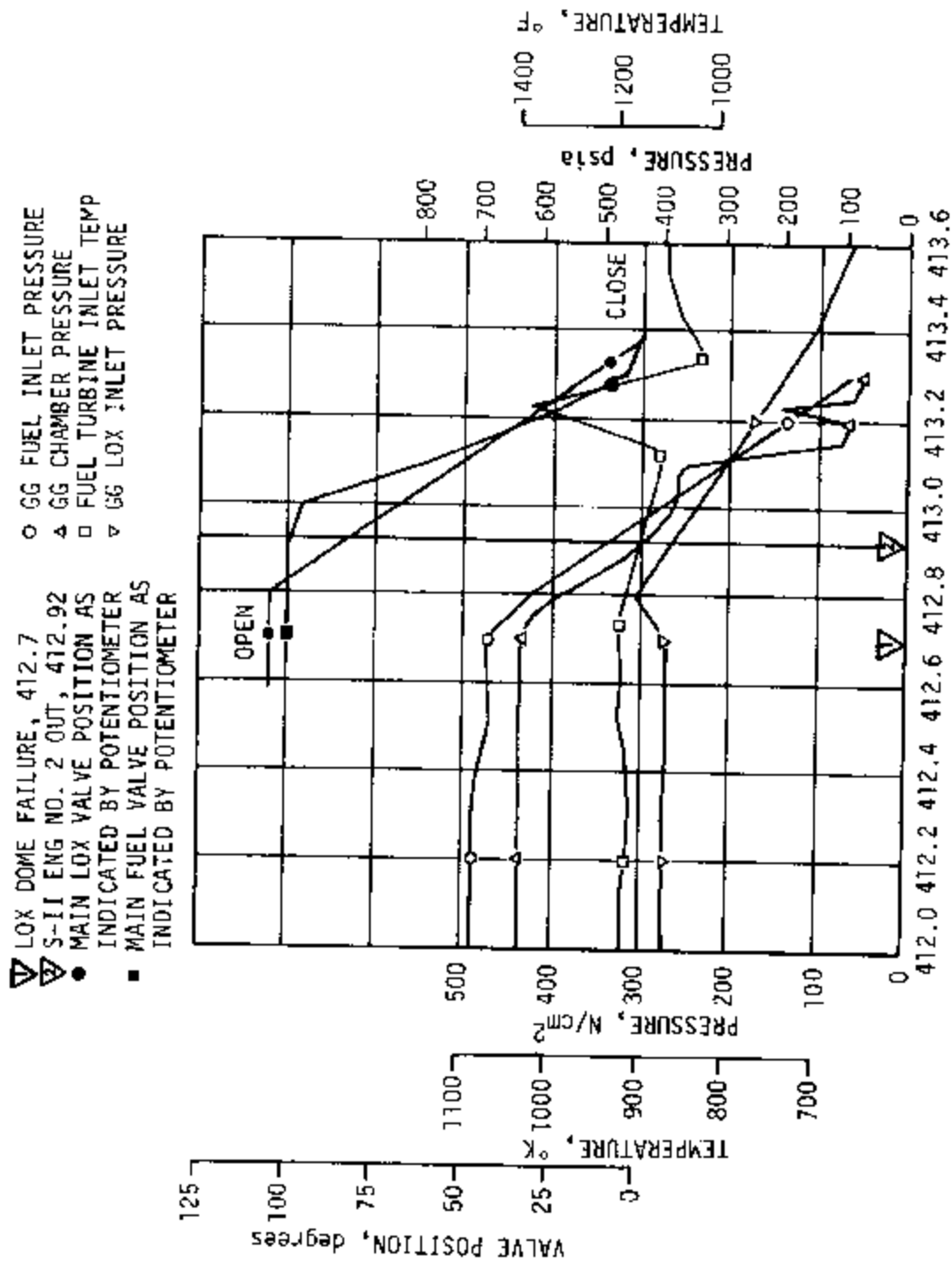


Figure 6-12. S-II Engine No. 2 Gas Generator Performance at Shutdown

- ▽ LOX PREVALVE OPEN (STARTS CLOSED), 413.60
- ▽ LOX PREVALVE CLOSED, 413.79
- ▽ S-II ENG NO. 3 MAINSTAGE OK DE-ENERGIZED SW. NO. 2, 414.13
- ▽ S-II ENG NO. 3 MAINSTAGE OK DE-ENERGIZED SW. NO. 1, 414.18

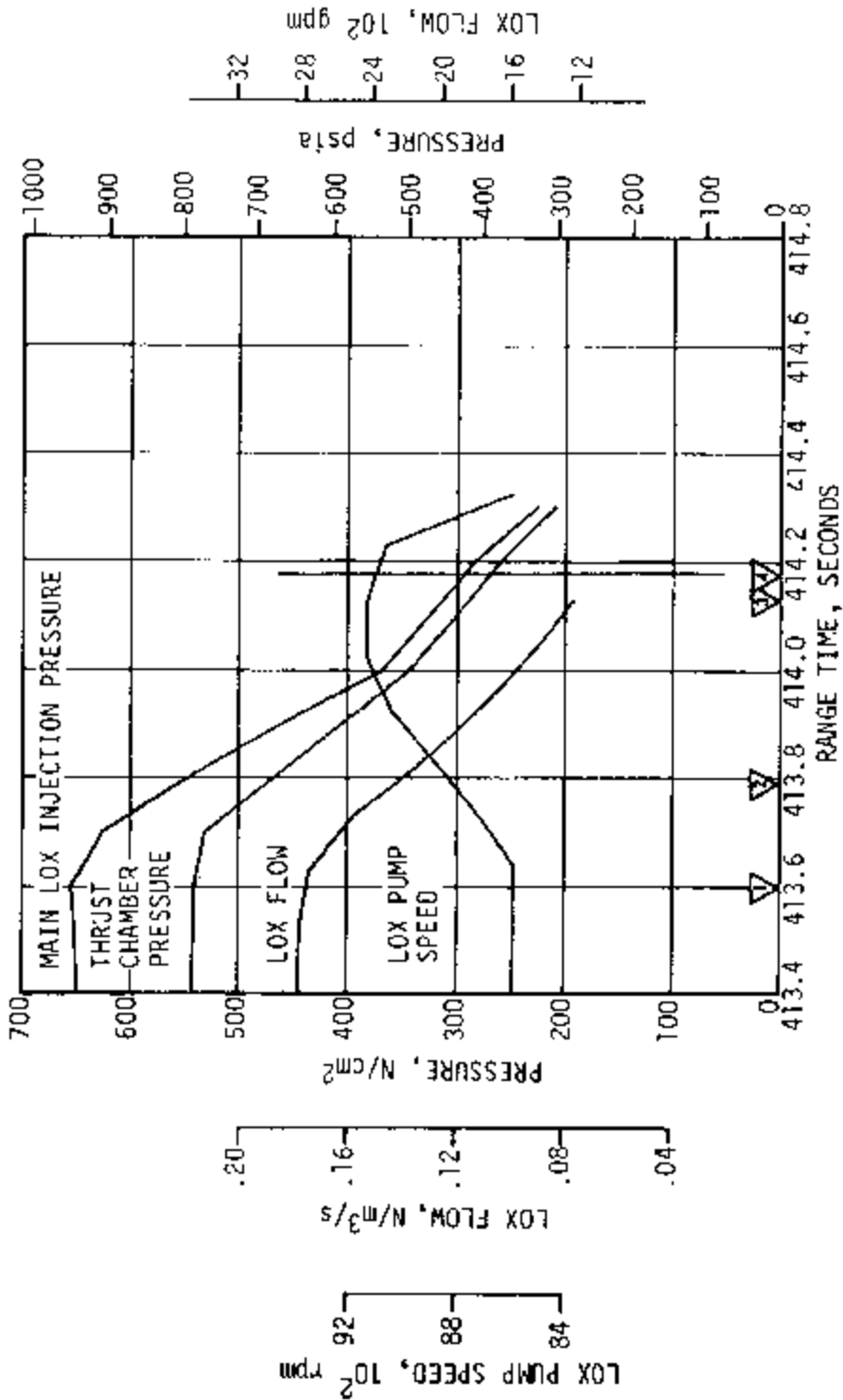


Figure 6-13. S-II Engine No. 3 Performance at Shutdown

Stage engine thrust decay (including a best estimate of engine No. 1) is presented in Figure 6-15. Thrust dropped from 2,354,744 Newtons (529,370 lbf) at ECO to 133,446 Newtons (30,000 lbf) (5 percent thrust) approximately 0.68 seconds later.

The shutdown transient performance, based on telemetered performance data, was determined for the S-II stage. The calculated total engine cutoff impulse was 578,088 N-s (129,960 lbf-s) which corresponds to an equivalent velocity change of 2.74 m/s (8.99 ft/s). Comparisons of flight and predicted values of cutoff impulse and velocity change are presented in Table 6-5. Two reasons may be given to account for the large discrepancies. The most significant reason is that the two engines out condition reduced the S-II stage thrust approximately 40 percent. In addition, thrust performance just prior to ECC was lower than normal and is partially attributed to lower than normal accelerations. The remaining causes of this impulse discrepancy have not been identified at this time.

Table 6-5. S-II Cutoff Impulse

PARAMETER	PREDICTED (5 ENGINES)	FLIGHT (3 ENGINES)		PERCENT DEVIATION FROM PREDICTED	
		ENGINE	GUID. DATA	ENGINE	GUID. DATA
Cutoff N-s Impulse (lbf-s)	1,161,742	578,088	423,849	-50.2	-63.5
	261,171	129,960	95,286		
Velocity m/s Increase (ft/s)	5.53	2.74	2.01	-50.5	-63.7
	18.14	8.99	6.59		

6.5 S-II PROPELLANT MANAGEMENT

The propellant management system controls loading and engine mixture ratios (LOX to LH₂) to ensure balanced consumption of LOX and LH₂. Capacitance probes mounted in the LOX and LH₂ tanks monitor the mass of propellants. At PU activation (5.5 seconds after J-2 ignition) the system senses the LOX to LH₂ imbalance and commands the engine to burn at the high rate engine mixture of 5.5:1. When the excess LOX is consumed the PU system then commands the engine to burn at a mixture ratio of 4.65:1, striving for simultaneous depletion of LOX and LH₂ for maximum stage performance.

The propellant management system satisfactorily performed the functions of propellant loading, mass indication, point sensor level indication, propellant utilization and programmed mixture ratio operation.

The facility Propellant Tanking Control System (PTCS) functioned satisfactorily during S-II loading and replenishment. The best estimates of liquid propellant mass in the tanks at ESC are 69,275 kilograms (152,726 lbm) LH₂ and 359,033 kilograms (791,532 lbm) LOX based on flowmeter integration and the masses remaining at ECO. These propellant

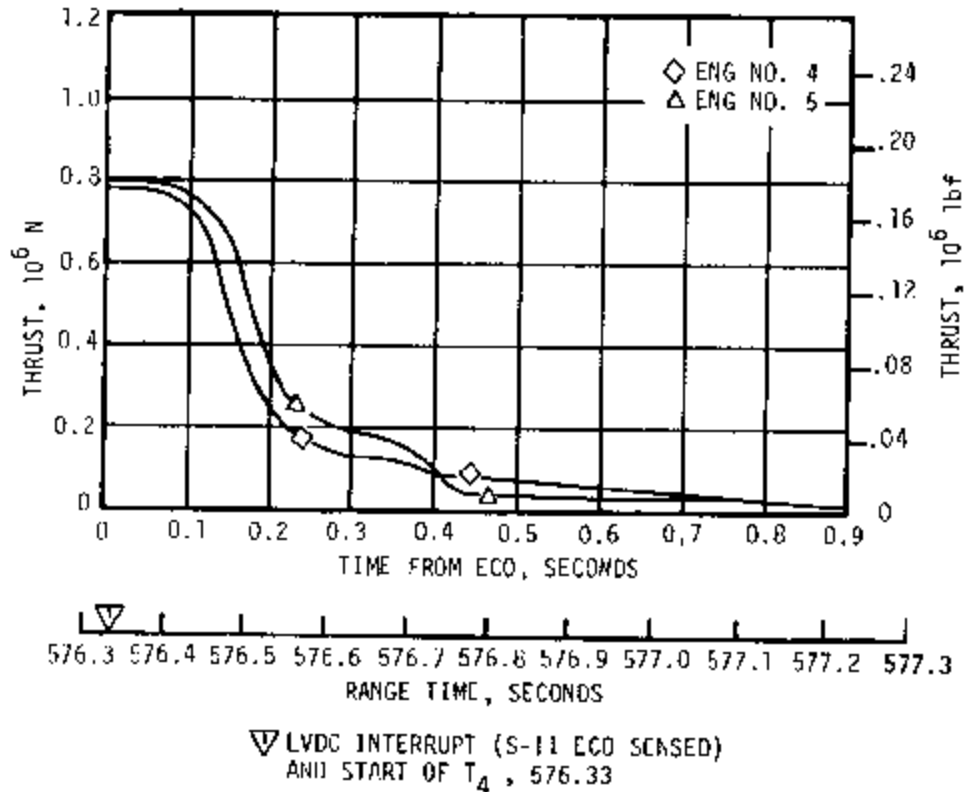


Figure 6-14. S-II Engine Shutdown Transient

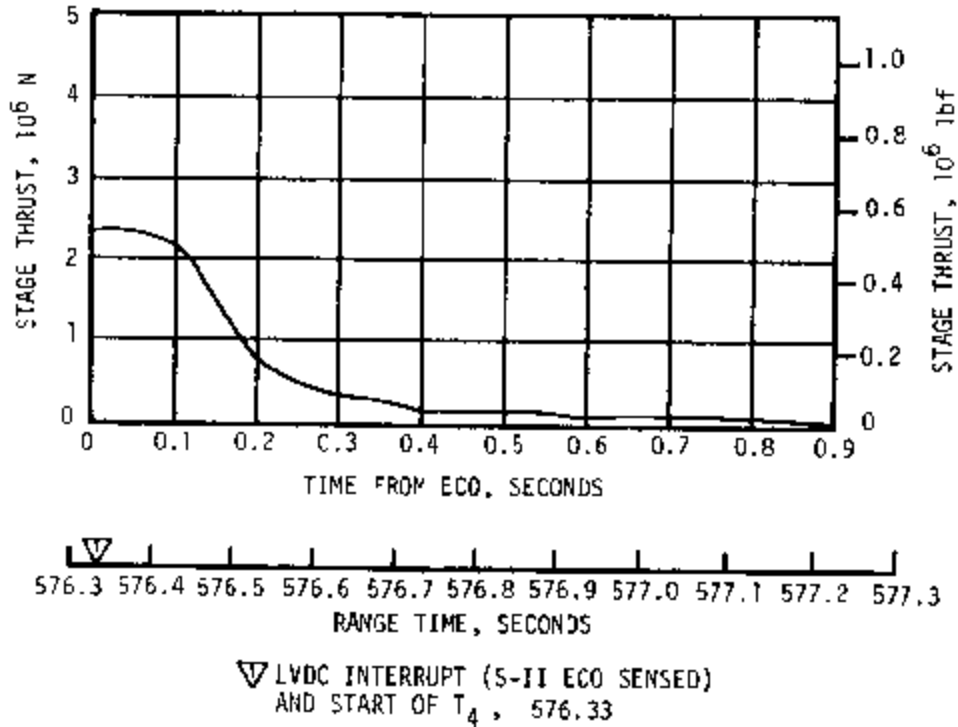


Figure 6-15. S-II Stage Thrust Decay

quantities were 0.51 percent more than predicted for LOX and 0.31 percent more than predicted for LH₂. Best estimate propellant masses at liftoff were 0.48 percent above predicted values.

The "PU Activate" command was received and the PU valves stepped from the nominal engine start position to the full-closed position at 5.5 seconds after ESC as shown in Figure 6-16. This provided a nominal EMR of 5.5 for the first phase of S-II Programmed Mixture Ratio (PMR). Upon shutdown of engines No. 2 and 3 (approximately ESC +263 seconds) the PU valves moved momentarily off the high EMR stop, returning at ESC +268 seconds after an excursion of approximately 5 degrees. No change in EMR or performance resulted since the PU valves are ineffective in this range of travel. At ESC +312.3 seconds the PU valves gradually moved to a position of -24 degrees at ECO, compared to a predicted value of -13.8 degrees. Extrapolation of PU error signal data indicates that this step would have begun at ESC +268 seconds under normal engine operation, which is well within the predicted step time of 250 ±50 seconds.

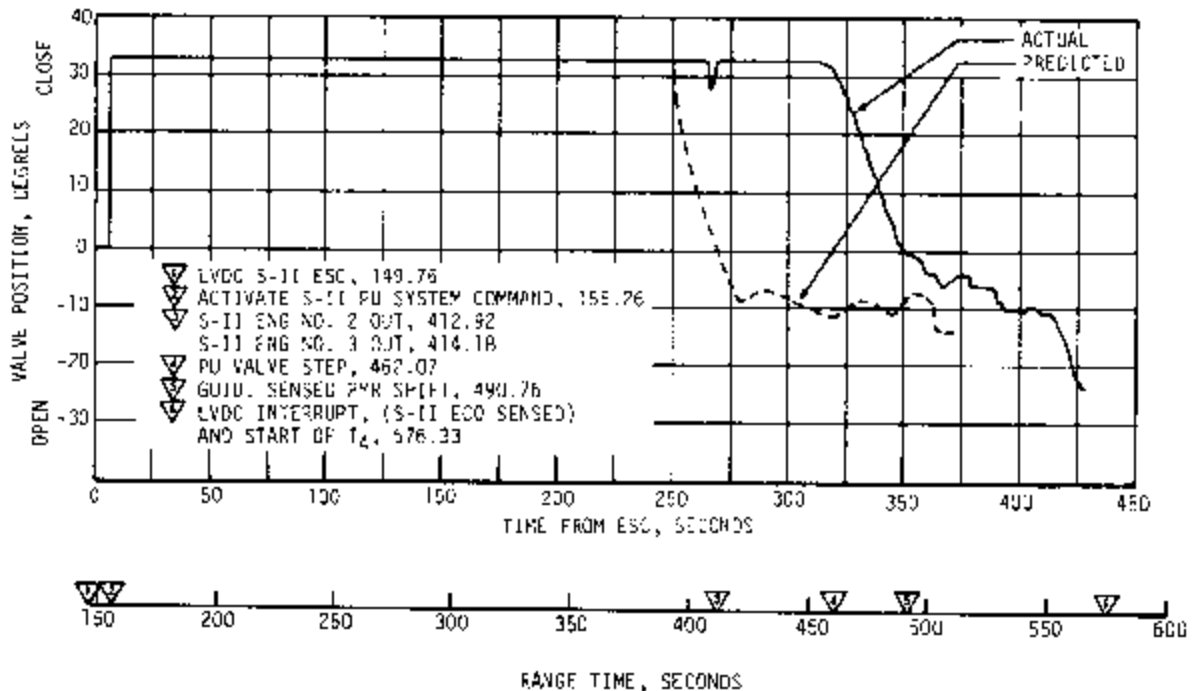


Figure 6-16. S-II Stage PU Valve Position

Other than the temporary excursion that occurred at ESC +263 seconds, the differences between the actual and predicted histories of PU valve position were caused by the changes in liquid surface angle resulting from the early shutdown of engines No. 2 and 3. The initial thrust imbalance at engine failure caused the vehicle to pitch up. This caused a sufficient decrease in the PU error signal to drive the PU valves off the high EMR stop. The flight control system reacted to keep the vehicle on course, the engines gimballed to keep the thrust vector of the remaining

three engines passing through the vehicle Center of Gravity (CG). This maneuver raised the liquid level at the LOX probe and lowered it at the LH₂ probe, increasing the PU error signal sufficiently to return the PU valves to the stop and delay the PMR valve step for 44 seconds. This delay was aggravated by having only three engines burning to consume the increase in LOX error indicated by the PU probes. The tilt of liquid surface was approximately 3 degrees from a plane normal to the vehicle longitudinal axis after attitude recovery by the flight control system, decreasing to approximately 2 degrees at ECO as the remaining propellants were consumed and the vehicle CG moved forward. The difference in LOX burn-off rate between the AS-501 and AS-502 flights is indicated by comparing the rates of change of PU valve angles when PMR occurred for each flight. The ratio of the valve angle slopes between the two flights is about 3/5. Since two of the five engines were shutdown prior to PMR, this is the ratio expected.

Analysis of flight data shows that indicated changes in liquid level due to liquid propellant sloshing were significantly attenuated by the PU system. The PU valve response to the indicated change in propellant levels at 415 seconds (due to shutdown of engines No. 2 and 3) reduced from 89 to 17 deg/volt. Later in the flight after PMR step, changes in propellant levels due to sloshing at frequencies of 0.4 hertz (contribution from LH₂ tank) and 0.6 hertz (contribution from LOX tank) were observed in the PU error signal but were not observed at all in the PU valve response, indicating that slosh dynamics were effectively filtered from commands to the PU valve positioning system. No changes affecting propellant utilization system dynamic performance are recommended for future flights.

The lower than predicted position of the PU valve at ECO was the result of earlier errors in the measurement of LOX level; the previously mentioned LOX surface tilt caused a larger LOX mass to be measured and to be consumed by the engines. At approximately ESC +380 seconds, there was necessarily a deficiency of actual LOX mass in the tanks relative to LH₂ mass. The PU system therefore commanded that less LOX be consumed and reduced the mixture ratio below the 4.65 RMR setting. As ECO was approached, the sensed PU errors became progressively larger based on a percent of propellant remaining. As a result, the PU valves were driven to an unusually low EMR position causing the cutoff residuals to be excessively high. This explanation is supported both by the residuals listed in Table 6-6 and the fact that ECO was initiated by the LOX depletion sensors.

Figures 6-17 and 6-18 show the PU system nonlinearity as determined by comparison of mass data from the PU probes and the engine flowmeters with corrections made for liquid surface tilt. The PU system error at cutoff signal was 373 kilograms (822 lbm) of LH₂ relative to that predicted at the actual LOX cutoff level. This compares to an allowable LH₂ error of ±665 kilograms (±1465 lbm).

Table 6-6. S-II Stage Propellant Mass History

EVENT RF No. T.M.C. SECONDS	UNITS	PREDICTION		PU SYSTEM		CUTOFF POINT PROBE		CUTOFF POINT SENSOR		BEST ESTIMATE	
		LOX	H ₂	LOX	H ₂	LOX	H ₂	LOX	H ₂	LOX	H ₂
S-II Ignition** 151.32	kg (lbm)	357,203 (787,498)	69,059 (152,146)	357,562 (788,334)	68,359 (151,300)	359,045 (791,332)	69,275 (152,726)	359,927 (792,530)	69,400 (153,000)	359,933 (791,747)	69,275 (152,726)
PU Activation 155.26	kg (lbm)	355,871 (784,450)	68,872 (151,837)	365,031 (787,711)	68,446 (151,886)	358,543 (786,040)	68,572 (151,176)	356,845 (784,500)	68,763 (151,800)	356,543 (786,043)	68,572 (151,176)
MR Step 482.50	kg (lbm)	89,631 (197,636)	29,342 (64,761)	49,013 (108,049)	11,955 (26,357)	46,650 (103,370)	11,796 (26,032)	46,534 (102,900)	11,567 (25,590)	46,680 (103,320)	11,796 (26,032)
ESC 576.31	kg (lbm)	1486* (3277)*	1136* (2519)*	1568 (3462)	1105 (2438)	1614 (3574)	1558 (3454)	1574 (3490)	1565 (3460)	1614 (3574)	1562 (3452)
Residuals After Thrust Decay	kg (lbm)	1307 (2897)	1265 (2797)	1513 (3336)	1674 (3670)	1759 (3875)	1678 (3679)	1752 (3856)	1560 (3436)	1674 (3670)	1567 (3456)

* Based on 0.5 second time delay not incorporated for AS 502.
Corrected prediction is 1985 kg (4383 lbm) LOX and 1276 kg (2812 lbm) L₂.

** S-II ignition occurred at STEV OPR, 1.26 seconds after ESC.

NOTE: Range times do not pertain to prediction data. Data only includes liquors in tank.

LOX liquid level initiated engine shutdown sequence and the LVDC sensed ECO at ESC +426.57 seconds. LOX remaining in the tank was 1814 kilograms (4000 lbm) versus 1988 kilograms (4383 lbm) predicted. LH₂ remaining in the tank was 1598 kilograms (3523 lbm) versus 1276 kilograms (2812 lbm) predicted. Cutoff residuals were determined by extrapolation of point sensor data to the time of cutoff signal. A normal 0.5 second ECO time delay (minimize residuals) was not incorporated on AS-502; hence, the predicted residuals, shown above, do not include this delay.

The best estimate of LOX consumption was 357,219 kilograms (787,532 lbm) as compared to a prediction of 355,215 kilograms (783,114 lbm). The best estimate of LH₂ consumption was 67,677 kilograms (149,202 lbm) compared to 67,783 kilograms (149,437 lbm) predicted. These correlations were made from S-II ignition to S-II stage ECO command using data in Table 6-6 without a 0.5 second time delay incorporated.

Table 6-6 presents a comparison of propellant masses as measured by the flowmeters, point sensors, and PU probes. The best estimate of propellant mass is based on the propellant residuals at ECO as indicated by the point sensors, and on integration of the flowmeter data.

The best estimate of launch vehicle total mass at S-II ignition and cutoff, as determined from capacitance probe, point level sensors, flow meters and the trajectory simulation is 643,856 kilograms (1,419,460 lbm) and 210,789 kilograms (464,710 lbm) respectively, as shown in Figure 6-19.

6.6 S-II PRESSURIZATION SYSTEMS

The S-II pressurization system function is to provide the necessary positive pressure to the J-2 engines propellant pumps and to increase the structural capability of the tanks. The system is comprised of tank ullage pressure regulators and vent valves, LOX heat exchangers (integral

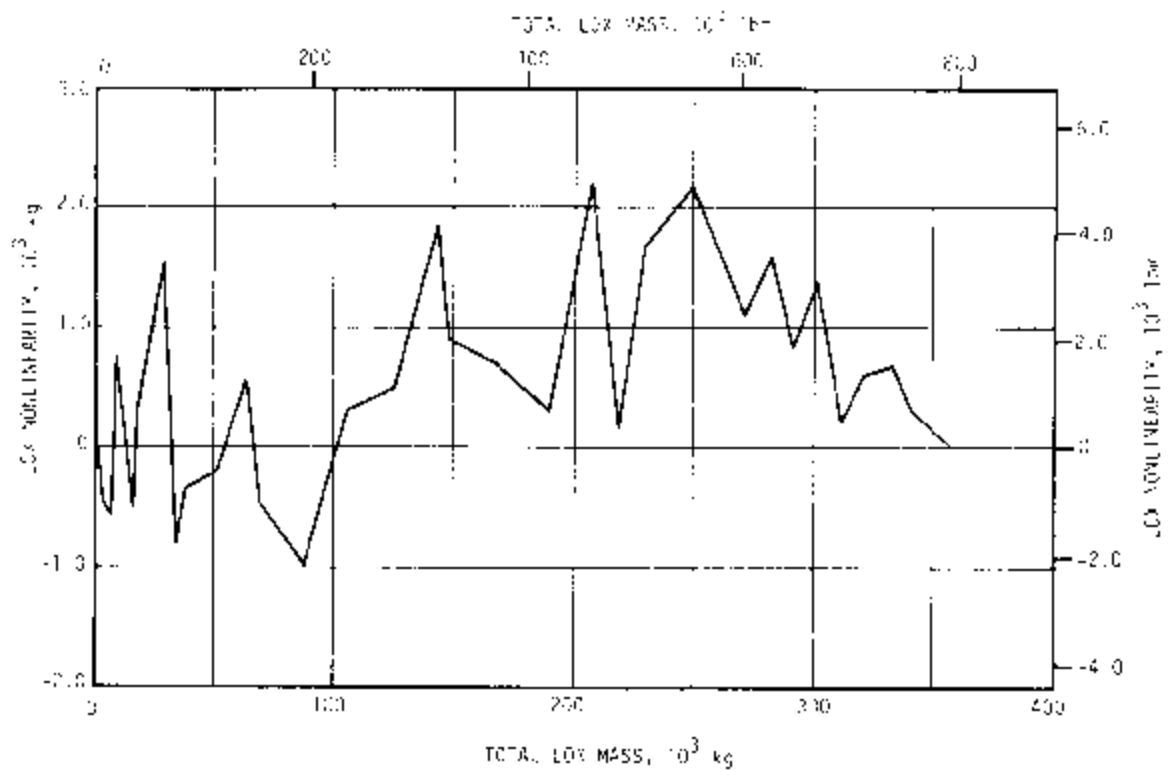


Figure 6-17. S-II LOX Probe/Tank Mismatch

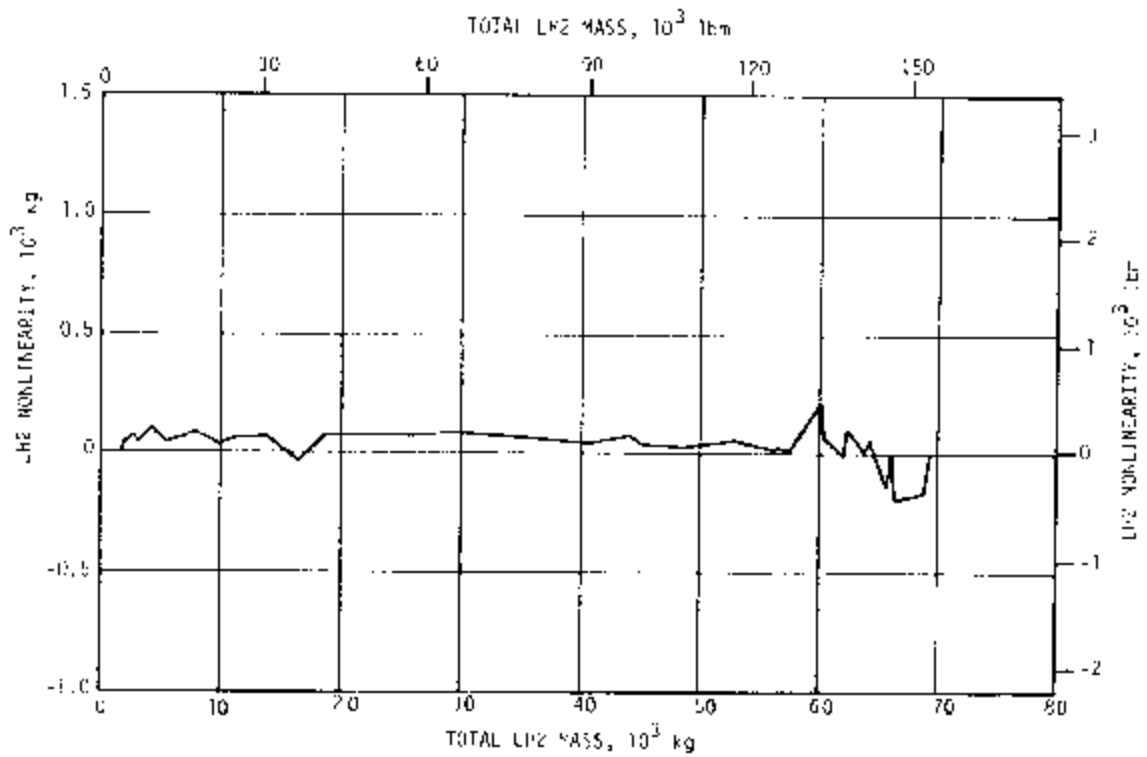


Figure 6-18. S-II LH₂ Probe/Tank Mismatch

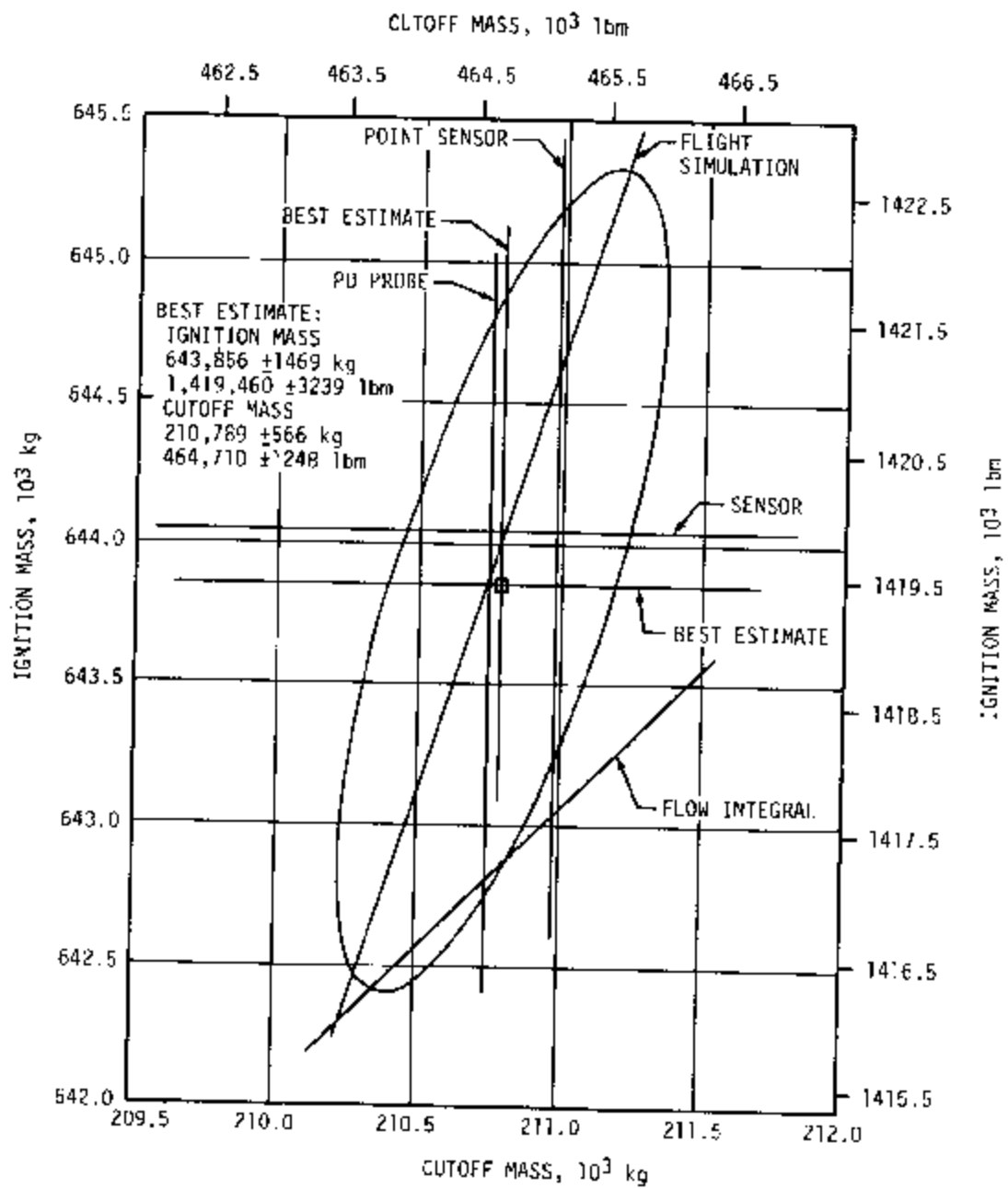


Figure 6-19. S-II Mass at Ignition and Cutoff

part of J-2 engine), interconnecting tubing and manifolds. Prior to launch, the LOX/LH₂ tanks are prepressurized by ground source Gaseous Helium (GHe). During powered flight of the S-II stage, the LOX tank is pressurized by GOX from the LOX heat exchanger. The LH₂ tank is pressurized by GH₂ from the thrust chamber hydrogen injector manifold and pressurization is regulated by the LH₂ pressure regulator and vent valve.

6.6.1 S-II Fuel Pressurization System

The S-II LH₂ tank ullage pressure during S-IC boost was slightly lower, as planned, than for AS-501. Figure 6-20 presents the fuel tank ullage pressure for AS-502 as compared to AS-501 from prepressurization until S-II ECO.

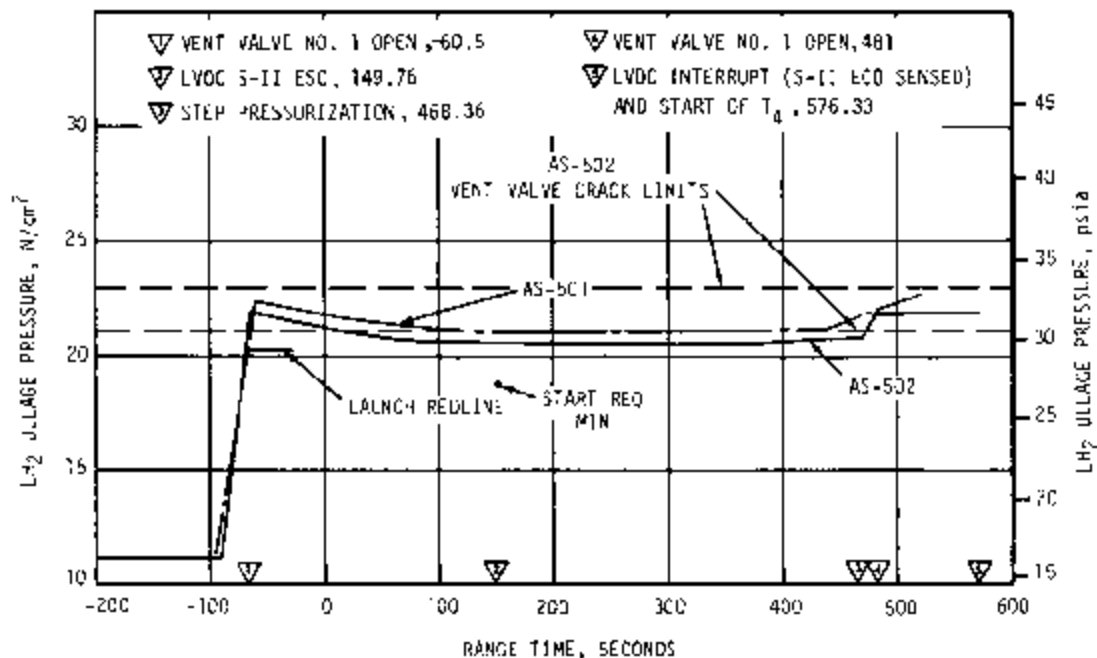


Figure 6-20. S-II Fuel Tank Ullage Pressure

The LH₂ tank vent valves for AS-502 were set to crack between 21.4 and 22.8 N/cm² (31 to 33 psia) as compared to 23.4 to 24.8 N/cm² (34 to 36 psia) for AS-501. During prepressurization the LH₂ tank was pressurized to 22.0 N/cm² (32 psia) in 34 seconds.

"Hi-press" was utilized as recommended after the AS-501 flight and was terminated by the cracking of vent valve No. 1. Vent valve reseal occurred at an ullage pressure of 21.4 N/cm² (31 psia). Ullage pressure decayed approximately 0.7 N/cm² (1 psi) to 20.7 N/cm² (30 psia) at S-II engine start which is well above the minimum requirement of 19.0 N/cm² (27.5 psia).

LH₂ tank pressurization during S-II flight was normal. The regulator controlled the ullage pressure within the regulator band of 19.65 to 20.70 N/cm² (28.50 to 30 psia) up to the time of step pressurization. The ullage pressure increased after step pressurization and at 481 seconds, vent valve No. 1 cracked, controlling the pressure at 22 N/cm² (32 psia) until S-II ECO. Vent valve No. 2 did not open during the entire flight.

Figure 6-21 presents engine inlet data bands consisting of total pressure, temperature and NPSP. The band extremes include data from all five engines during operations; however, after shutdown of engines No. 2 and 3, only data from engines No. 1, 4, and 5 are shown. Engine inlet LH₂ total pressure was obtained by adding calculated dynamic pressure to engine inlet LH₂ static pressure. The total pressure increase after 468.36 seconds was due to the increase in ullage pressure at step pressurization. Engine inlet LH₂ temperature shows a gradual increase which is the effect of stratification. The stratification was well within acceptable limits. Engine inlet LH₂ NPSP, obtained by subtracting the LH₂ vapor pressure from engine inlet LH₂ total pressure, was well above the minimum requirement.

The NPSP increased, as shown on Figure 6-21, after 468.36 seconds as the result of ullage pressure increase at step pressurization. The gradual decrease in available NPSP, commencing at about 500 seconds, was the result of warmer LH₂ entering the fuel pump.

6.6.2 S-II LOX Pressurization System

Figure 6-22 presents the LOX tank ullage pressure, compared to AS-501, from prepressurization until S-II ECO. A pressure decay of only 0.2 N/cm² (0.29 psia) was recorded during S-IC boost as compared to 3.2 N/cm² (4.7 psia) for AS-501. The reduction of pressure decay was due to the prelaunch evacuation of the common bulkhead. The LOX tank was pressurized to the pressure switch setting of 26.5 N/cm² (38.5 psia) in 67 seconds. LOX tank "hi-press" was not utilized since ullage pressure decay was predicted to be negligible with the common bulkhead evacuated. The LOX tank ullage pressure at S-II engine start was well above the S-II engine start requirement of 22.7 N/cm² (33 psia) and above the redline limits at launch.

LOX tank pressurization system performance through S-II boost was adequate to maintain engine NPSP requirements; however, the ullage pressure decreased below the regulator control band lower limit at about the time of EMR shift at approximately 500 seconds, and was 24.0 N/cm² (34.8 psia) at ECO.

The engine heat exchangers supplying the pressurant gas do not have any excess capacity when operating at nominal or low EMR. The regulator attempted to keep pace with the demand by fully opening. However, with only three engines operating, sufficient pressurant gas was not available to maintain the ullage pressure. Although fewer engines were consuming propellant, the LOX and tank surface areas which chill the ullage gas

- ▽ LVDC S-II ESC, 149.76
- ▽ S-II ENG NO. 2 OUT, 412.92
- ▽ S-II ENG NO. 3 OUT, 414.18
- ▽ LVDC INTERRUPT

(S-II ECO SENSED) AND START OF T_4 , 576.33

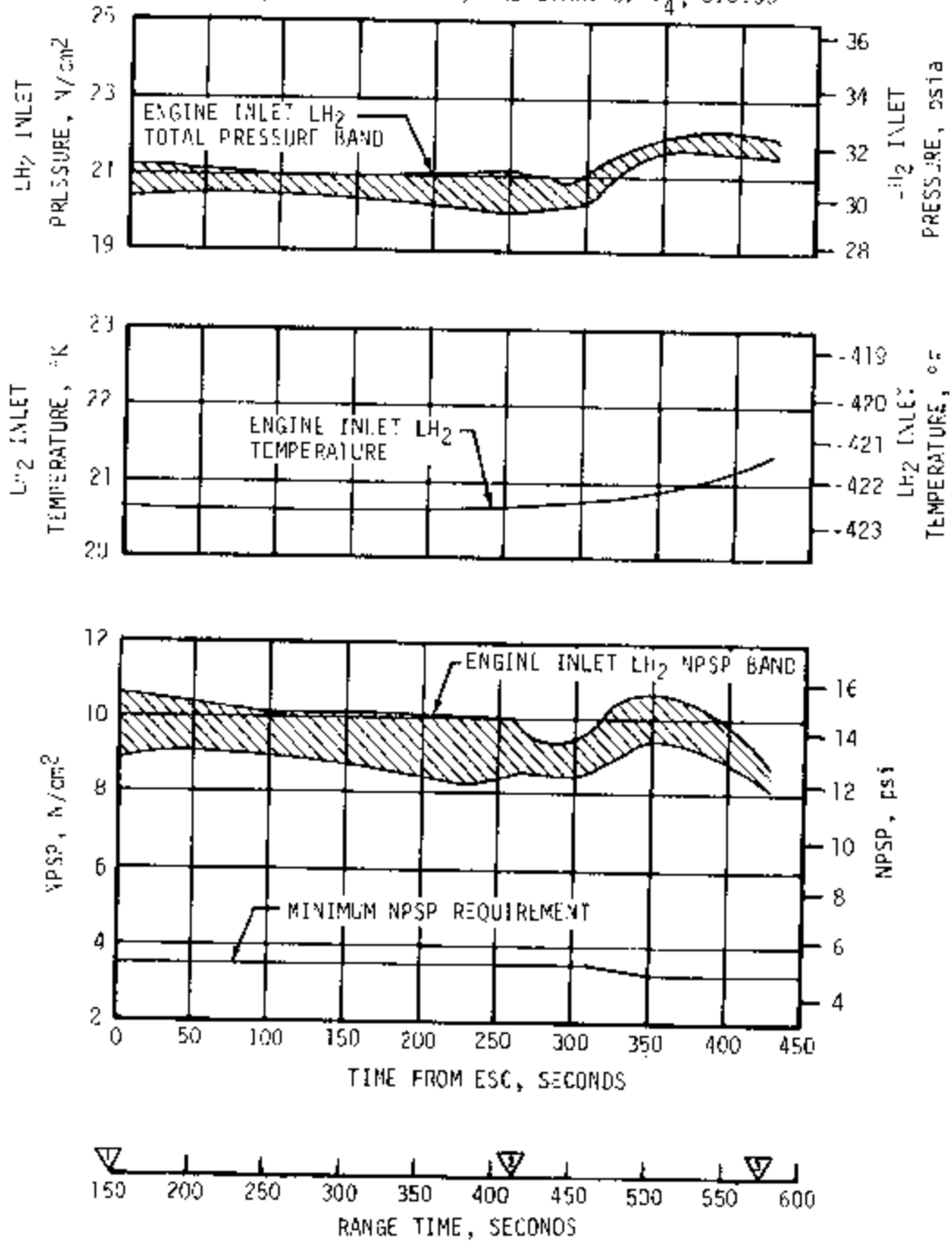


Figure 6-21. S-II Fuel Pump Inlet Conditions

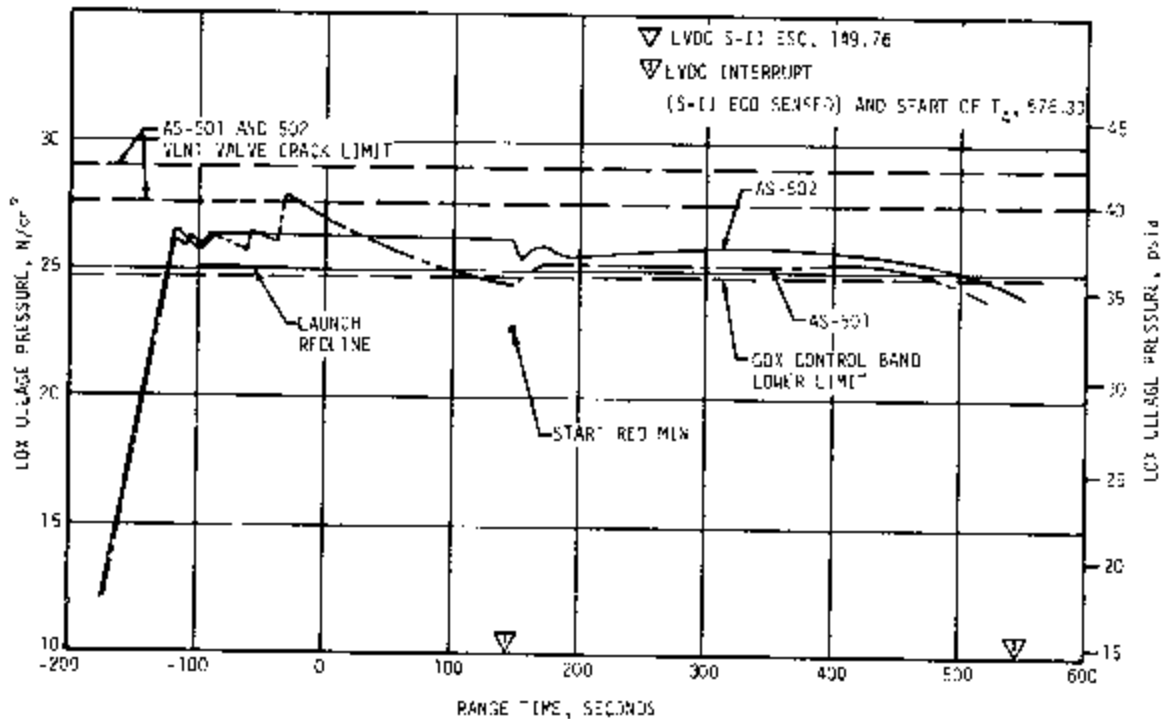


Figure 6-22. S-II LOX Tank Ullage Pressure

did not change. Moreover, the ullage shrinkage created a larger demand of pressurant gases from the remaining engines, resulting in colder heat exchanger outlet temperatures. The data shows that towards S-II cutoff, the heat exchanger exit temperatures were at saturation.

Figure 6-23 presents engine inlet data bands consisting of total pressure, temperature and NPSP. The bands include data from all five engines until the time that engines No. 2 and 3 cut off; thereafter, only data from engines No. 1, 4, and 5 are shown. Engine inlet LOX total pressure was determined by adding the calculated dynamic pressure and head correction for the location of the pressure pickup to the pump inlet LOX static pressure measurement. The abrupt decrease in total pressure at approximately 413 seconds is a direct result of acceleration head loss due to premature cutoff of engines No. 2 and 3. The gradual total pressure loss which occurred toward the end of S-II boost is the combined result of the decrease in liquid head and the decrease in ullage pressure. The gradual increase in liquid temperature toward the end of S-II boost shows that the effect of liquid stratification was well within the acceptable limit.

Engine inlet LOX available NPSP was obtained by subtracting the LOX vapor pressure from engine LOX inlet total pressure. The NPSP was well above the minimum NPSP requirement. The abrupt decrease in available NPSP at 413 seconds is a direct result of the acceleration liquid head lost at the premature cutoff of engines No. 2 and 3. The gradual decrease of available NPSP toward the end of S-II boost is the combined result of a decrease in liquid head, a decrease in ullage pressure, and an increase in liquid temperature caused by stratification.

▽ LVDC S-II ESC, 149.76

▽ LVDC INTERRUPT

▽ S-II ENG NO. 2 OUT, 412.92

(S-II ECO SENSED) AND START OF T₄

S-II ENG NO. 3 OUT, 414.18

576.33

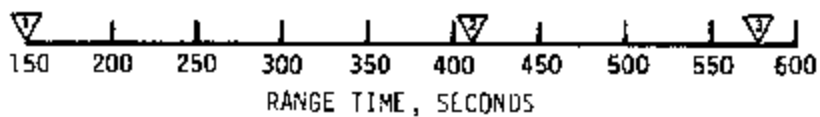
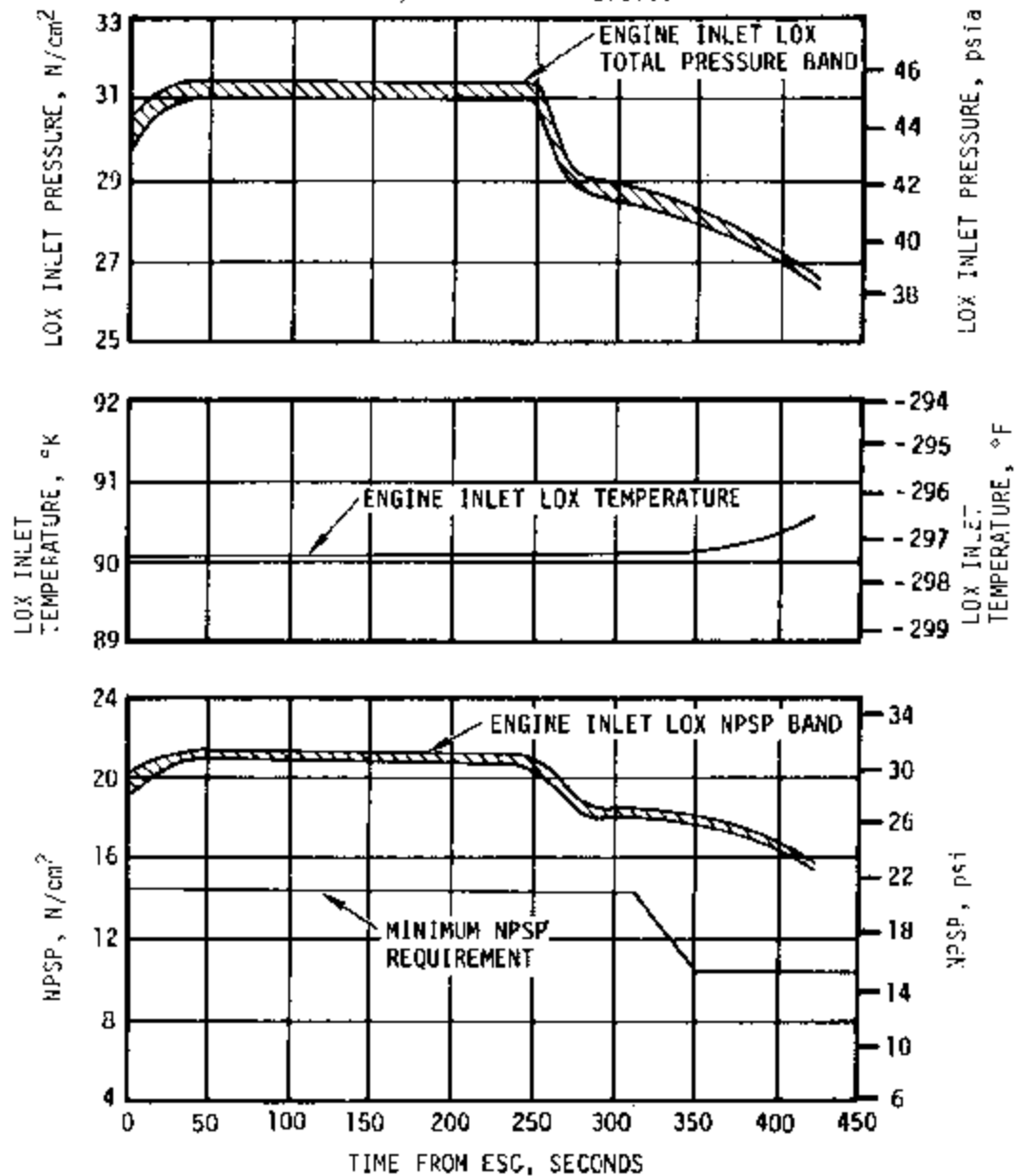


Figure 6-23. S-II LOX Pump Inlet Conditions

6.7 S-II PNEUMATIC CONTROL PRESSURE SYSTEM

The pneumatic control pressure system provides pressurized helium for the actuation of propellant system valves during flight.

Performance of the pneumatic control system was satisfactory. Figure 6-24 shows receiver pressure and regulator outlet pressure of the system from before liftoff until S-II ECO. The receiver pressure and regulator outlet pressure were within the predicted bands throughout the flight. The three step-decreases of pressure represented helium demands for valve actuations. Only the times at which the demands for pre valve closures on engines No. 2 and 3 were made are unusual. Table 6-7 shows the helium mass used by the system.

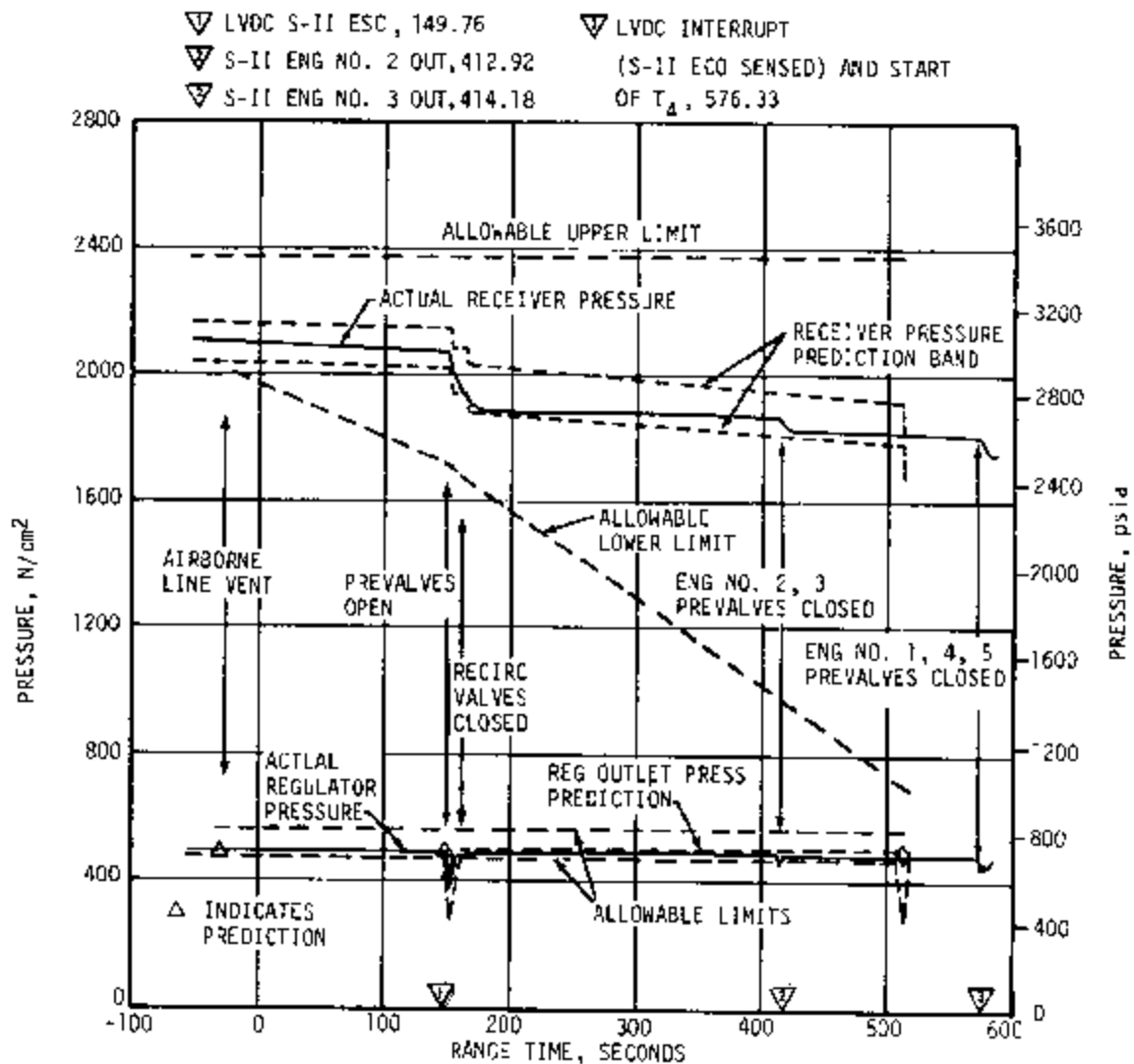


Figure 6-24. S-II Recirculation Valves Receiver and Regulator Outlet Pressures

Table 6-7. S-II Helium Mass

LAUNCH SEQUENCE	PNEUMATIC CONTROL PRESSURE SYSTEM HELIUM MASS READINGS (AS-502)	
	ACTUAL	PREDICTED
Launch Minus 30 seconds	1.71 kg (3.77 lbm)	1.65 to 1.76 kg (3.64 to 3.88 lbm)
S-II Engine Start Command	1.70 kg (3.76 lbm)	1.59 to 1.70 kg (3.50 to 3.76 lbm)
S-II Engines No. 2 and 3 Cutoff	1.56 kg (3.44 lbm)	None
S-II Engine Cutoff Command	1.47 kg (3.25 lbm)	1.47 to 1.60 kg (3.25 to 3.52 lbm)

6.8 CAMERA EJECTION SYSTEM

The function of the camera ejection system is to provide GHe, upon command, to eject the camera cannisters. The camera ejection system consists of two helium spheres, tubing and valves.

The camera ejection system performed satisfactorily. The ejection sequence was programmed to start at $T_3 + 38.0$ seconds and actually started at $T_3 + 37.97$ seconds.

Figure 6-25 indicates a gradual pressure decay of both subsystems. The subsystem located at position III exhibits the greater, but acceptable, rate of decay and lower storage pressure. However, both subsystems had sufficient pressure to eject the cameras. The same pressure drop characteristics were exhibited by the systems during ejection, at which time the pressures decreased 130 N/cm^2 (190 psid). A discussion of camera recovery operations may be found in paragraph 19.6.

6.9 HELIUM INJECTION SYSTEM

The inflight helium injection system supplements natural convection recirculation in the LOX recirculation lines. This system injects helium into the bottom of the return lines to decrease the return line fluid density thereby increasing the recirculation driving force.

In general, performance of the helium injection system was satisfactory. Requirements were met and parameters were in good agreement with predicted values. The supply bottle was pressurized to 2070 N/cm² (3000 psia) prior to liftoff and by ESC was 787 N/cm² (1140 psia). This usage of helium resulted in a helium injection flowrate of 1.67 SCMM (59 SCFM).

As discussed in paragraph 6.2, LOX recirculation was satisfactory except for the prelaunch chilldown of engines No. 3 and 4. Because of the problem experienced in chilling these engines to below the prelaunch redline maximum the following changes are being considered for implementation prior to AS-503 CDDT:

- a. Increase helium injection system total flowrate from 1.13 to 1.70 SCMM (40 to 60 SCFM) to 1.70 to 2.26 SCMM (60 to 80 SCFM) by increasing the primary orifice size.
- b. During checkout, verify that the helium injection flow is distributed evenly to all engines.
- c. Add screens upstream of helium injection orifices.
- d. Delete the solenoid outlet pressure instrumentation and add new pressure measurement downstream of the primary orifice. This measurement will be more sensitive to helium flow distribution while still being representative of total flow conditions.

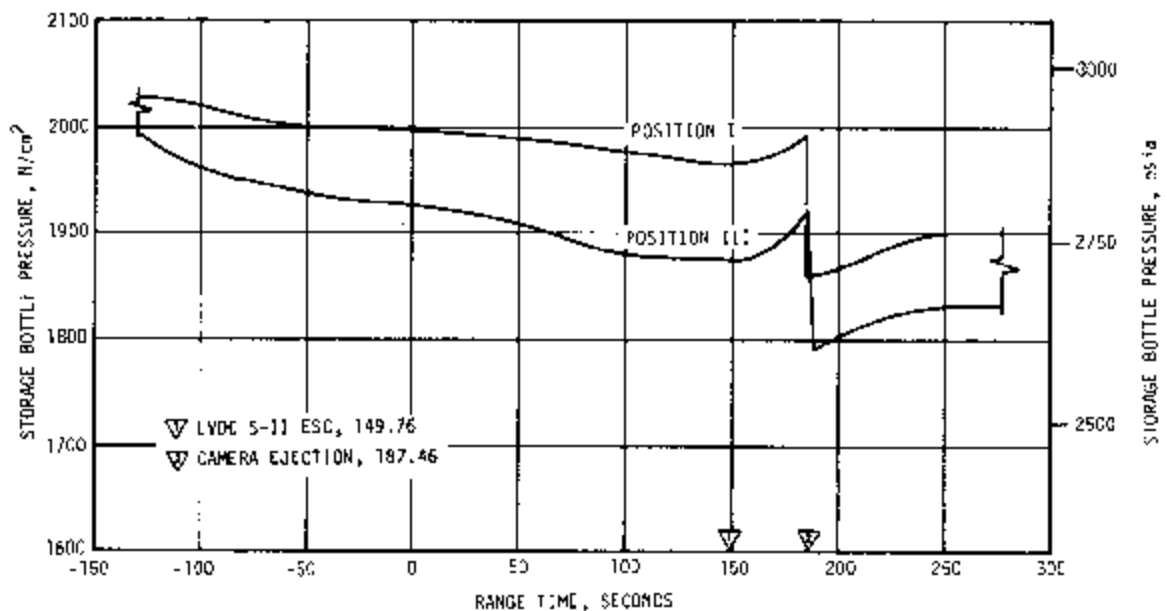


Figure 6-25. S-II Camera Ejection Pressures

SECTION 7

S-IVB PROPULSION

7.1 SUMMARY

The S-IVB stage propulsion system consists of a main and an auxiliary system. The main propulsion system consists of a single, bipropellant J-2 engine, fuel system, oxidizer system, and a propellant management system. The Auxiliary Propulsion System (APS) is provided to control the vehicle attitude during S-IVB operation and position the propellants in the stage during first burn cutoff, parking orbit coast, second burn restart, and cutoff transients. The other systems discussed under this section are the Continuous Vent System (CVS) and the pneumatic control system.

The J-2 engine operated satisfactorily throughout the operational phase of first burn. However, a total performance shift of 2.3 percent decrease in thrust occurred during first burn from 684 to 702 seconds. The engine continued to operate at the shifted performance level and had a normal shutdown. S-IVB first burn time was 166.52 seconds which was 28.95 seconds longer than predicted due to the two engines out condition on the S-II stage. This burn time was computed from Start Tank Discharge Valve (STDV) open (occurred 3.24 seconds after the Launch Vehicle Digital Computer [LVDC] S-IVB engine start sequence command) to the LVDC velocity cutoff command.

The stage performance during first burn, as determined from the propulsion reconstruction analysis, deviated from the predicted at the 60 second time slice by -0.08 percent for thrust and 0.06 percent for specific impulse.

The S-IVB stage first burn Engine Cutoff (ECO) was initiated by the LVDC at 747.04 seconds. The LOX mass measuring side of the Propellant Utilization (PU) system malfunctioned prior to the attempted restart. The LOX mass measuring system malfunction caused a 100 percent LOX load indication prior to and during the restart attempt. The probable cause of the erroneous 100 percent LOX mass indication may have been due to shorting of the inner and outer elements of the LOX PU probe from metallic debris that could have been in the LOX tank. Also, an

intermittent short in the cable shield between the mass probe and the PU electronics assembly may have occurred. Additional tests on cable connector crimping will be conducted along with the evaluation of insulating one or both of the probe elements to prevent shorting by debris.

Engine restart conditions were within limits even though main chamber second ignition failed to occur. Results thus far indicate that a leak in the Augmented Spark Igniter (ASI) fuel supply system probably occurred, resulting in a performance shift and the failure to achieve restart. Additional engine tests have essentially verified the performance shift and the restart failure. A modification of the ASI propellant feedlines (both fuel and LOX) and their installation is being accomplished.

All subsystems operationally met all performance and stage requirements. However, there were two unexpected deviations which are summarized as follows:

- a. Two LOX ullage pressure makeup cycles were required during S-IC boost. The ullage pressure decay requiring two makeup cycles is partially due to ullage cooling, tank geometry response to the vehicle axial acceleration, and possibly vent/relief and/or relief valve intermittent leakage. Investigation is continuing into the LOX ullage pressure decay.
- b. A possible cold helium leak was indicated after first burn ECO. The cause of the leak is still under extensive investigation with special interest into the cold helium system conoseals and joints, the LOX pressurization module, and the cold helium sphere pressure transducer. The conoseals will be changed to 7075 aluminum coated with teflon throughout the cold helium system on subsequent vehicles.

7.2 S-IVB CHILLDOWN AND BUILDUP TRANSIENT PERFORMANCE FOR FIRST BURN

LH2 and LOX recirculation systems are required for proper prestart conditions. With the required prestart conditions, a start is obtained by proper engine sequencing of the engine components with the power obtained from an engine mounted helium control sphere. A hydrogen start tank is employed to spin the turbopumps during the start transient until the Gas Generator (GG) system is operating properly to continue engine start and maintain engine operation. During the start transient and engine operation, the start tank is refilled for another start. The ignition system initiates combustion in the thrust chamber and GG. The system includes four spark plugs, four spark exciters, an ignition chamber, an ASI valve, an ignition detector probe, and the necessary electrical harness and plumbing to join the parts into a system.

The propellant recirculation systems performed satisfactorily, meeting start and run box requirements for fuel and LOX as shown in Figure 7-1.

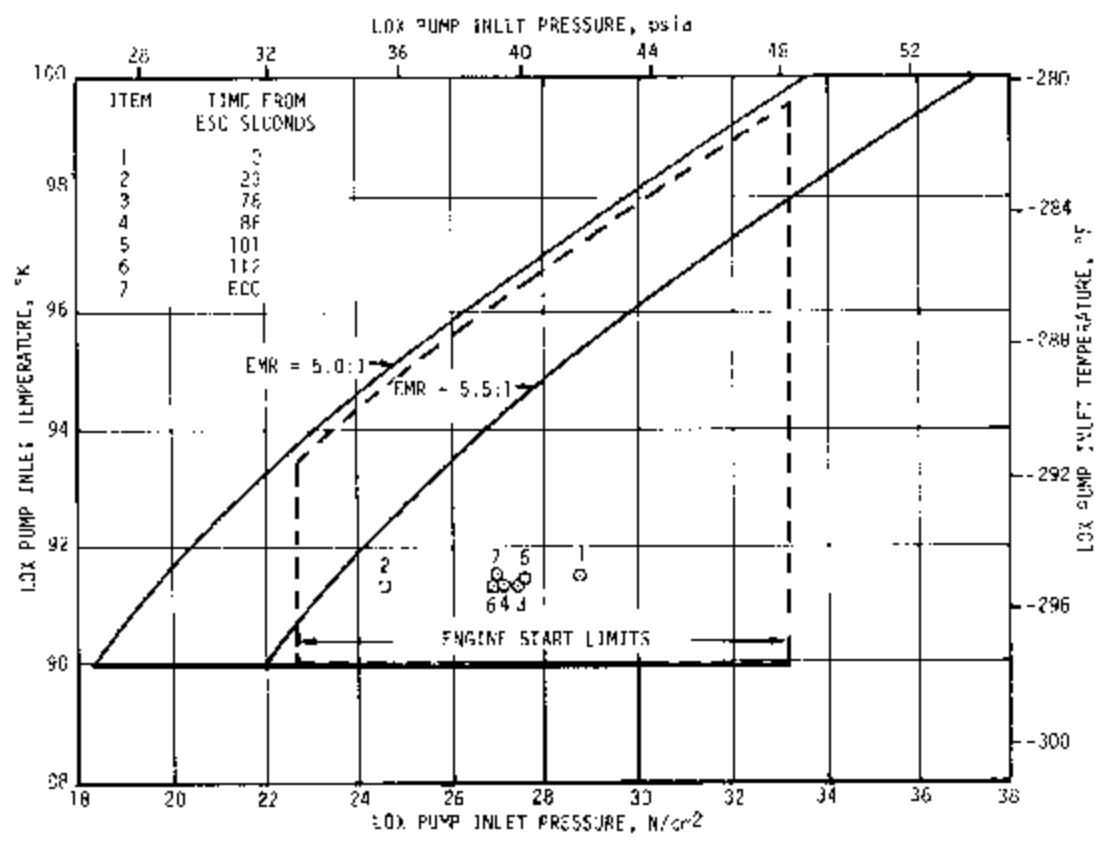
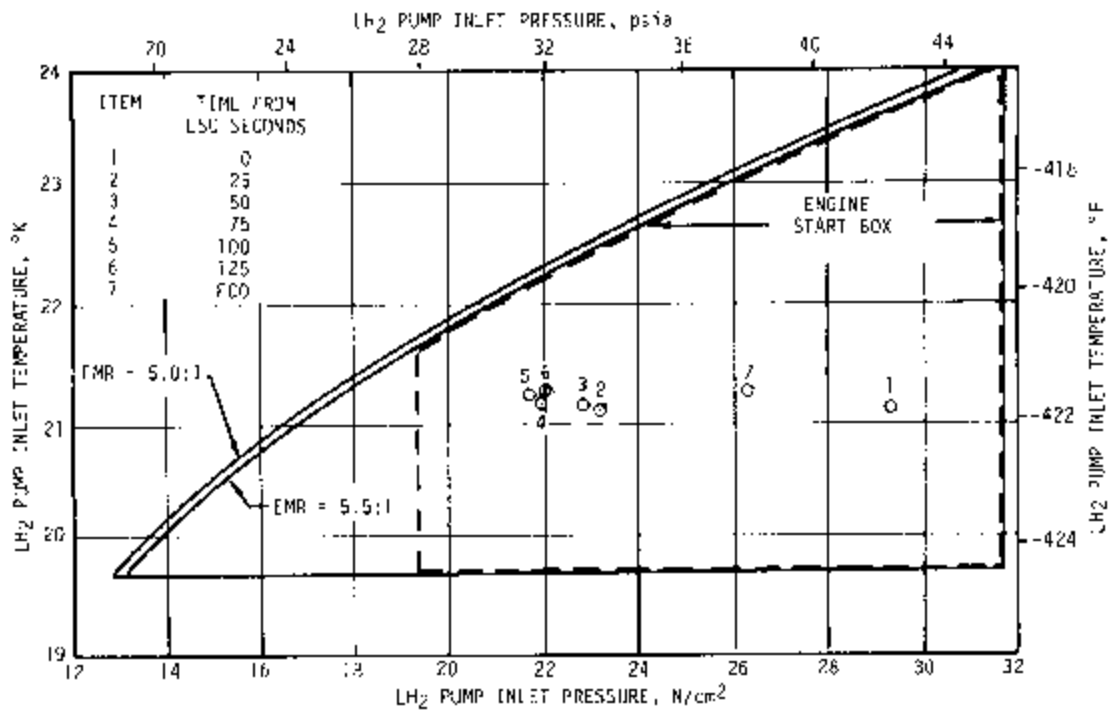


Figure 7-1. S-IVB Start Box and Run Requirements - First Burn

The thrust chamber at launch was well below the maximum allowable redline limit of 167°K (-160°F). At S-IVB first burn Engine Start Command (ESC), the temperature was 159°K (-173°F), which is within the requirement of 167 ±28°K (-160 ±50°F) as shown in Figure 7-2.

The chilldown and loading of the engine Gaseous Hydrogen (G-H₂) start sphere and pneumatic control sphere prior to liftoff were satisfactory. Figure 7-3 shows the start tank performance from first burn ESC. At first burn start command the start tank conditions were within the required S-IVB region for initial start of 913.56 ±51.71 N/cm² and 161 ± 16.7°K (1325 ±75 psia and -170 ±30°F). The discharge was completed and the refill initiated by S-IVB first burn ESC + 3.85 seconds. The refill was satisfactory and in good agreement with the acceptance test. The control bottle pressure and temperatures at liftoff were 2061.6 N/cm² (2990 psia) and 160.6°K (-171°F). Nominal chilldown system performance levels were observed during the chilldown operation. LOX system chilldown, which was continuous from before liftoff until just prior to S-IVB first burn ESC, was satisfactory. At ESC the LOX pump inlet temperature was 91.5°K (-295°F). Nominal chilldown system performance levels were observed during the chilldown operation.

The first burn start transient was satisfactory. The thrust buildup was within the limits set by the engine manufacturer. A faster thrust buildup to the 90 percent level as compared to the acceptance test results was observed on this flight and is shown in Figure 7-4. This buildup was mainly due to the shorter plateau time during main oxidizer valve opening time. A similar thrust buildup was observed on AS-501. Table 7-1 shows the major sequence of events during the buildup transient. The PU system provided the proper null setting of the PU valve during the start transient until system activation. The total impulse from STDV to STDV +2.5 seconds was 802,233 N-s (180,350 lbf-s) compared to 604,651 N-s (135,931 lbf-s) during the same interval for the acceptance test.

7.3 S-IVB MAIN STAGE PERFORMANCE FOR FIRST BURN

The J-2 engine provides the necessary propulsive performance for the S-IVB stage and is a high performance engine utilizing pump-fed propellants. The J-2 engine used on the S-IVB has restart capabilities. At altitude the engine produces a nominal thrust to 1,000,850 Newtons (225,000 lbf) at a LOX to LH₂ ratio of 5.5:1. The engine is capable of operating between 4.5 and 5.5:1 LOX/LH₂ mixture ratio for the desired propellant utilization at stage cutoff. The engine features a tubular-walled, bell-shaped thrust chamber and independently driven, direct-drive turbopumps.

Two analytical techniques were employed in evaluating S-IVB stage propulsion system performance. The primary method, propulsion reconstruction

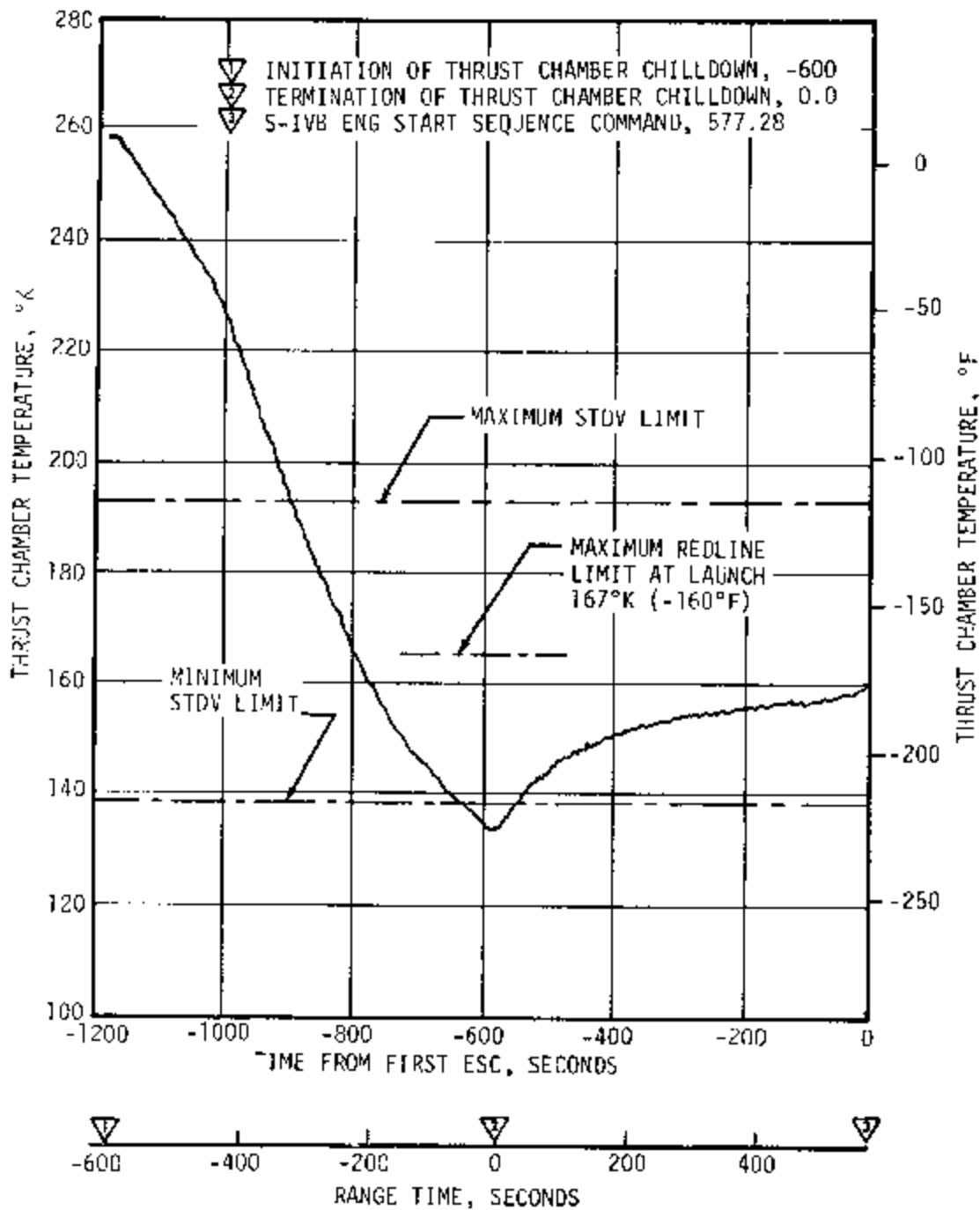


Figure 7-2. S-IVB Thrust Chamber Temperature - First Burn

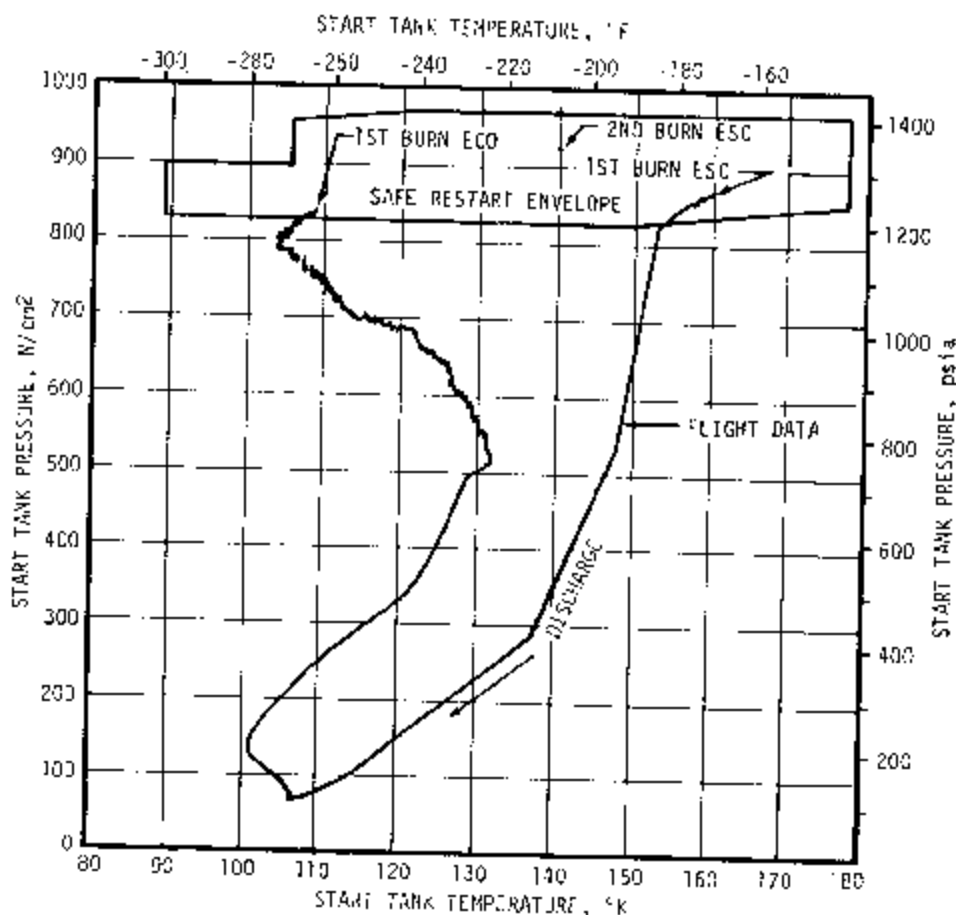


Figure 7-3. S-IVB Start Tank Performance

analysis, utilized telemetered engine and stage data to compute longitudinal thrust, specific impulse, and stage mass flowrate. In the second method, flight simulation, a five-degree-of-freedom trajectory simulation was utilized to fit propulsion reconstruction analysis results to the trajectory. Using a differential correction procedure, this simulation determined adjustments to the reconstruction analysis of thrust and mass flow histories to yield a simulated trajectory which closely matched the observed postflight trajectory.

The propulsion reconstruction analysis showed that the stage performance during mainstage operation was satisfactory. A comparison of predicted and actual performance of thrust, total flowrate, specific impulse, and mixture ratio versus time is shown in Figure 7-5. Table 7-2 shows the specific impulse, flowrates and mixture ratio deviations from the predicted at the 60 second time slice. This time slice performance is

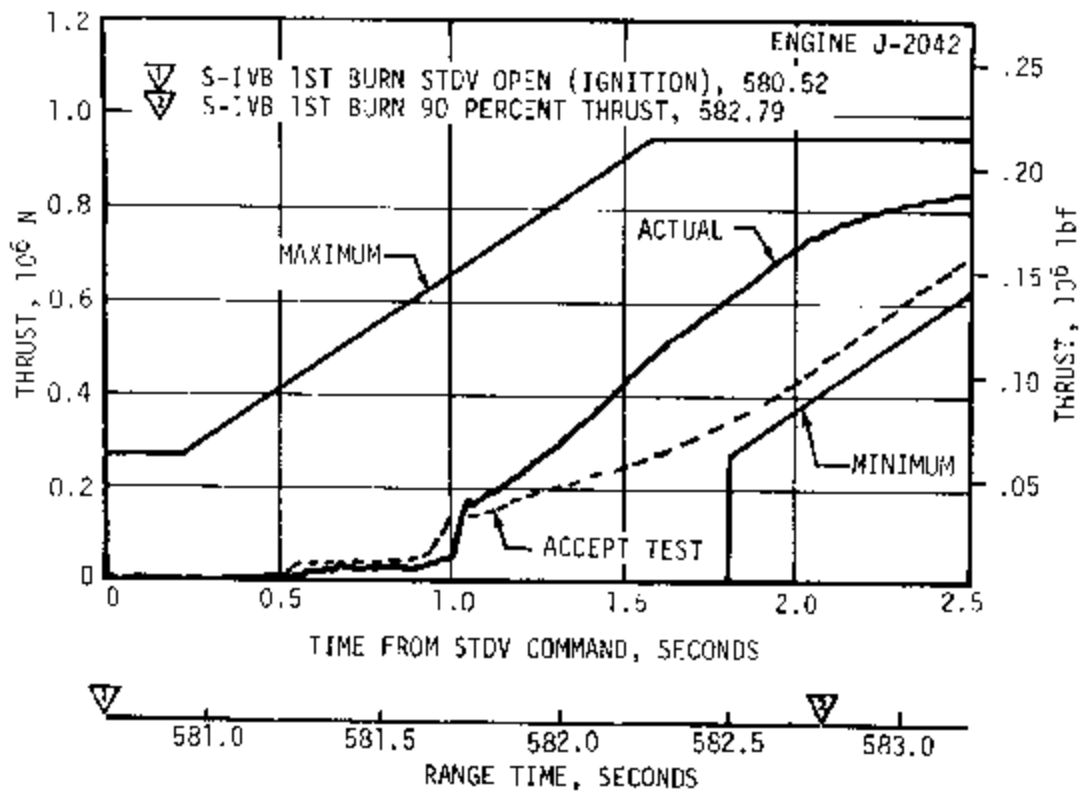
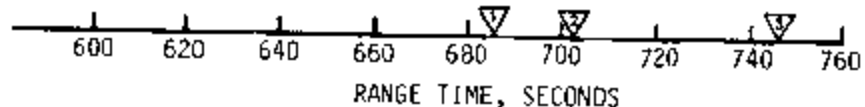
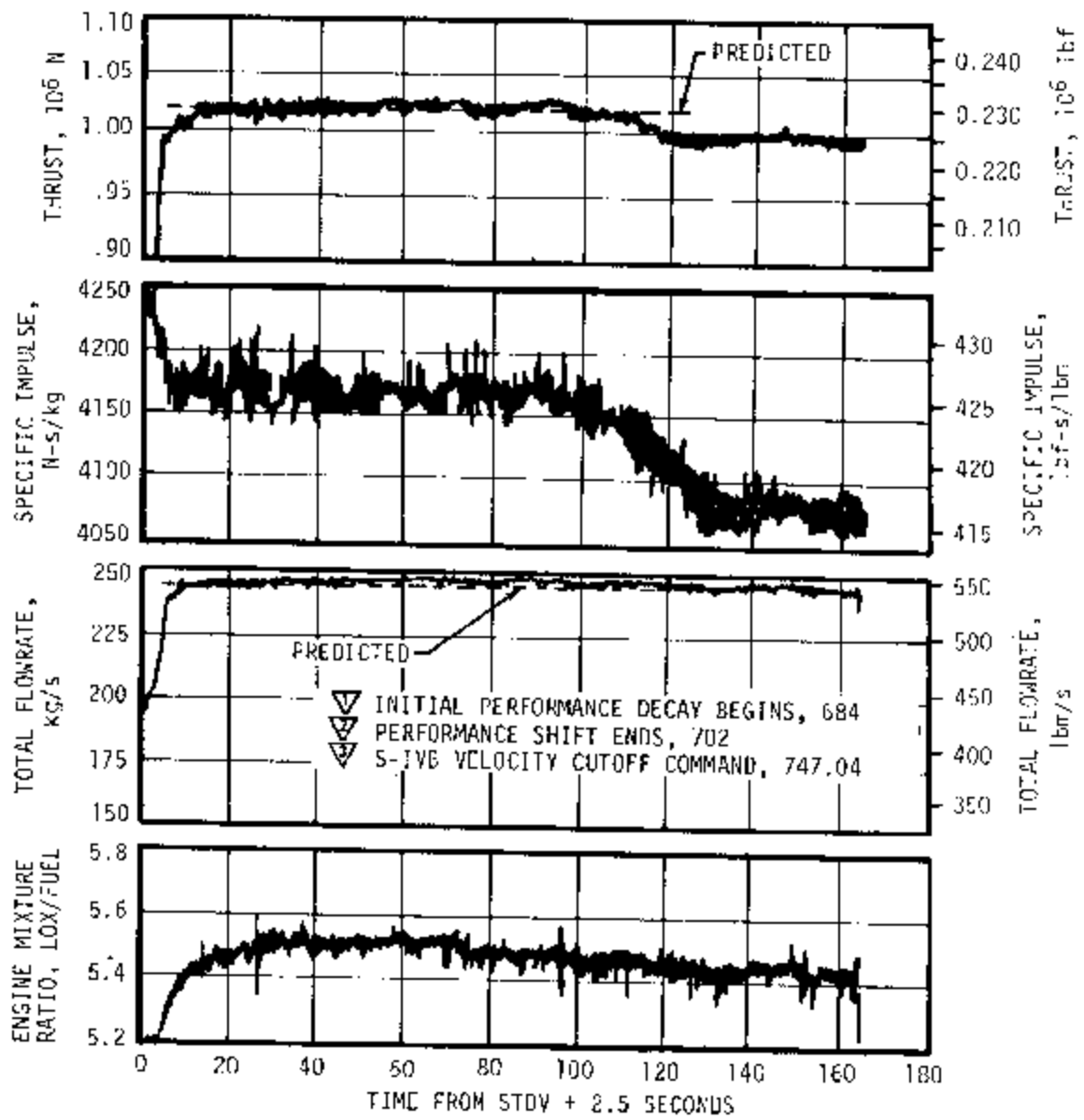


Figure 7-4. S-IVB Buildup Transient - First Burn

Table 7-1. S-IVB Engine Start Sequence Events - First Burn

EVENT	TIME OF EVENT IN RANGE TIME (SECONDS)	
	PREDICTED	ACTUAL
S-IVB Engine Start Sequence Command (ESC)	518.69	577.28
Start Tank Discharge Valve (STDV) Open	521.69	580.52
Mainstage Control Solenoid	521.94	580.75
Mainstage OK	524.10	582.03
Main LOX Valve Open	524.58	582.940
90 Percent Thrust	523.79	582.79



NOTE: THESE DATA DO NOT REFLECT THE TOTAL PERFORMANCE SHIFT AS AFFECTED BY ASI FUEL LEAK.

Figure 7-5. S-IVB Steady State Performance - First Burn

Table 7-2. S-IVB Steady State Performance - First Burn
(ESC +60 Second Time Slice)

PARAMETER	PREDICTED	RECONSTRUCTION	FLIGHT DEVIATION	PERCENT DEVIATION FROM PREDICTED
Thrust N (lbf)	1,018,554 228,980	1,017,771 228,804	-783 -176	-0.08
Specific Impulse N-s/kg (lbf-s/lbm)	4165.5 424.77	4167.8 425.0	2.3 0.24	0.06
LOX Flowrate kg/s (lbm/s)	206.60 455.89	206.33 455.30	-0.27 -0.59	-0.13
Fuel Flowrate kg/s (lbm/s)	37.73 83.19	37.65 83.01	-0.08 -0.18	-0.21
Engine Mixture Ratio LOX/Fuel	5.4804	5.485	0.0046	0.08

the standardized performance which is comparable to engine acceptance tests. The 60 second time slice performance agreed with the predicted by -0.08 percent on thrust and 0.06 percent on specific impulse. The overall propulsion reconstruction average during first burn was -0.77 percent for longitudinal thrust and -0.66 percent in longitudinal specific impulse compared to the predicted.

During first burn operation the engine showed a 2.3 percent drop in thrust from 684 to 702 seconds as shown in Figure 7-5. The most probable cause for this performance shift was an ASI fuel line leak. The suspected ASI fuel line leak is discussed in detail under paragraph 7.6. Engine tests simulating an ASI fuel line failure have been conducted at Marshall Space Flight Center (MSFC) and the engine contractor's test facility which have results compatible with the observed performance shift, a subsequent stabilization, and then a normal shutdown.

The flight simulation analysis showed a decrease of 0.20 percent, compared to the prediction, in specific impulse. Other comparisons are shown in Table 7-3.

The S-IVB burn time was 28.95 seconds longer than predicted. Table 7-4 shows that the primary contributors to the longer burn time were deviations in the preconditions of flight. Another large contributor was the

Table 7-3. Comparison of S-IVB Stage Flight Reconstruction Data - First Burn

PARAMETERS	UNITS	PREDICTED	FLIGHT RECONSTRUCTION	PERCENT DEV. FROM PRED.
		HIGH MIXTURE RATIO FIRST BURN FLIGHT AVERAGE	HIGH MIXTURE RATIO FIRST BURN FLIGHT AVERAGE	HIGH MIXTURE RATIO FIRST BURN FLIGHT AVERAGE
Longitudinal Vehicle Thrust	N (lbf)	1,015,614 228,370	1,007,811 226,565	-0.77
Vehicle Mass Loss Rate	kg/s (lbf/s)	244.73 539.21	243.77 537.41	-0.15
Longitudinal Vehicle Specific Impulse	N-s/kg (lbf-s/lbm)	4158.7 424.31	4130.5 421.19	-0.66
PARAMETERS	UNITS	FLIGHT SIMULATION	PERCENT DEV. FROM PRED.	
		HIGH MIXTURE RATIO FIRST BURN FLIGHT AVERAGE	HIGH MIXTURE RATIO FIRST BURN FLIGHT AVERAGE	
Longitudinal Vehicle Thrust	N (lbf)	1,009,724 226,995	-0.58	
Vehicle Mass Loss Rate	kg/s (lbf/s)	243.31 536.40	-0.34	
Longitudinal Vehicle Specific Impulse	N-s/kg (lbf-s/lbm)	4149.96 423.18	-0.20	

Table 7-4. S-IVB Simulation Burn Time Deviations

CONTRIBUTOR	DEVIATION*	BURN TIME DELTA (SECONDS)	
Preconditions of Flight (S-II/ S-IVB Separation Command)		23.1	
Velocity Magnitude	m/s	-105.79	
(Space Fixed)	ft/s	-347.08	
Flight Path Angle	deg	0.819	
Altitude	Km	6.47	
	n mi	3.50	
Overspeed (ECO)	m/s	48.94	8.1
	ft/s	160.56	
S-IVB Thrust	N	-8830	1.0
	lbf	-1985	
S-IVB Mass Flow	kg/s	0.22	-2.0
	lbm/s	0.48	
S-IVB Initial Mass	kg	5420	2.4
	lbm	1195	
		Explained	32.6
		Unexplained	-3.65

* Observed mass point trajectory (post-flight) minus final operational trajectory (predicted).

overspeed at S-IVB ECO. The total contributors show a burn time deviation of 32.6 seconds. This is 3.65 seconds more than the actual deviation. The additional 3.65 seconds of burn time may be accounted for by uncertainties in preconditions of flight and uncertainties in the thrust average obtained from trajectory reconstruction.

7.4 S-IVB SHUTDOWN TRANSIENT PERFORMANCE FOR FIRST BURN

S-IVB ECO was initiated at 747.04 seconds by a guidance velocity cutoff command which was 87.78 seconds later than predicted for first burn. This later cutoff time was primarily a result of the two engines out on the S-II stage. The ECO transient was satisfactory and agreed closely with the acceptance test and predictions. The total cutoff impulse to 5 and zero percent of rated thrust was 236,543 N-s (53,177 lbf-s) and 264,118 N-s (59,376 lbf-s), respectively. Cutoff occurred with the PU valve in the fully closed position, high Engine Mixture Ratio (EMR).

The Main Oxidizer Valve (MOV) actuator temperature was 156.9°K (-177.5°F) at cutoff. The cutoff impulse was adjusted from these conditions to standard conditions for comparison with the log book values at null PU valve position and 233°K (-40°F) MOV actuator temperature. After these adjustments, the flight values were near the log book values. The thrust during cutoff is shown in Figure 7-6.

Telemetered guidance velocity data indicated the cutoff impulse was greater than expected as presented in Table 7-5. The difference in vehicle mass between the flight and that predicted is the probable cause for the percentage difference in velocity increase.

7.5 S-IVB COAST PHASE CONDITIONING

The CVS performed satisfactorily, maintaining the fuel tank ullage pressure at an average level of 13.6 N/cm² (19.75 psia). Nozzle pressure data, thrust, and acceleration levels for first and second revolutions in the orbit are presented in Figure 7-7. LH₂ ullage conditions during coast are shown in Figure 7-8.

The continuous vent regulator was activated at 806.25 seconds. The tank ullage pressure dropped from 22.1 to 16.8 N/cm² (32.0 to 24.4 psia) in 65 seconds, and then gradually leveled off to 13.6 N/cm² (19.75 psia). Regulation at this level continued, with the expected operation of the main poppet periodically opening, cycling, and reseating as shown in Figure 7-7. CVS thrust and acceleration, also shown in Figure 7-7, were based on venting parameters. The acceleration was computed from the calculated thrust and vehicle mass without consideration of any vehicle drag effects. A different approach for obtaining the thrust and acceleration is discussed in paragraph 10.4.1. Continuous venting was terminated at 11,288.49 seconds, which was 326.20 seconds before second burn ESC. The erroneous CVS readings experienced on AS-501 were not observed on this flight and a further discussion is presented in paragraph 7.10.1.

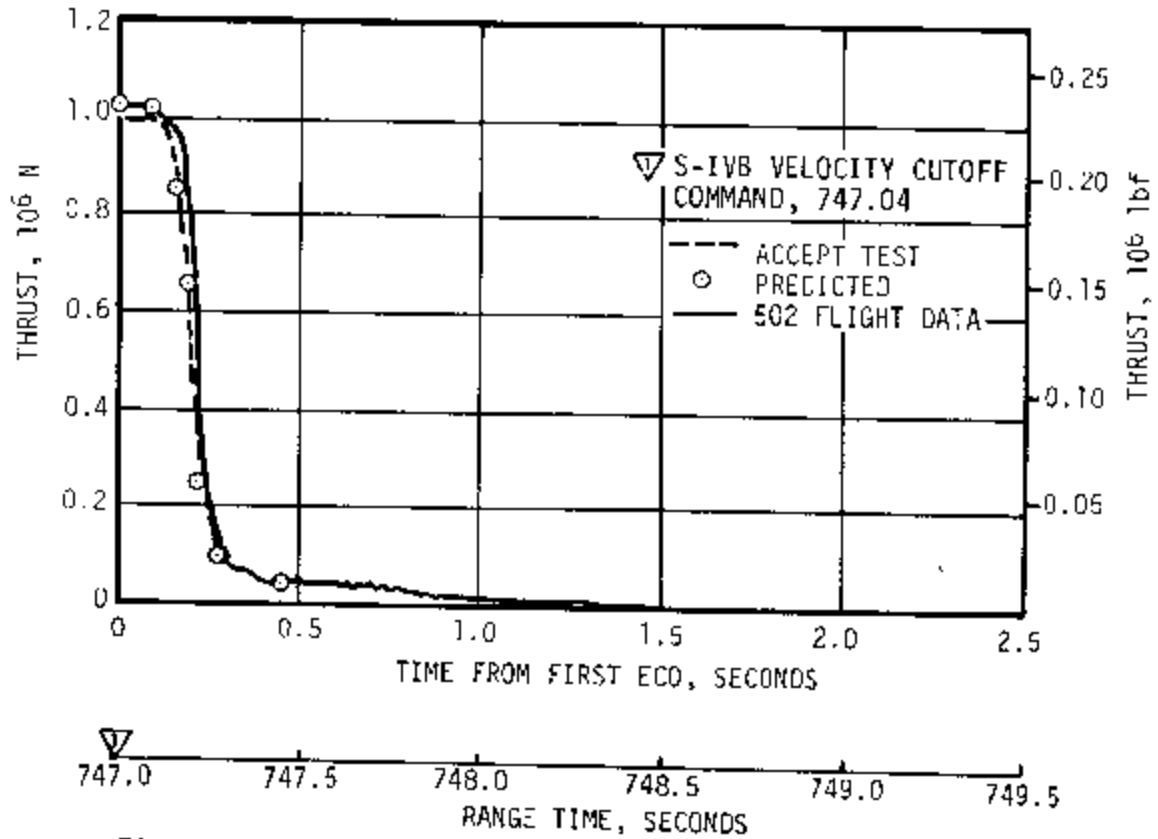


Figure 7-6. S-IVB Shutdown Transient Performance - First Burn

Table 7-5. S-IVB Cutoff Impulse - First Burn

PARAMETER	PREDICTED	FLIGHT		PERCENT DEVIATION FROM PREDICTED	
		ENGINE	GUID. DATA	ENGINE	GUID. DATA
Cutoff N-s	287,177	264,118	300,669	-8.0	4.7
Impulse (lbf-s)	64,560	59,376	67,593		
Velocity m/s	2.26	2.20	2.50	-2.3	10.6
Increase (ft/s)	7.41	7.24	8.20		

Note: The parameters quoted are from velocity cutoff command to zero percent of rated thrust.

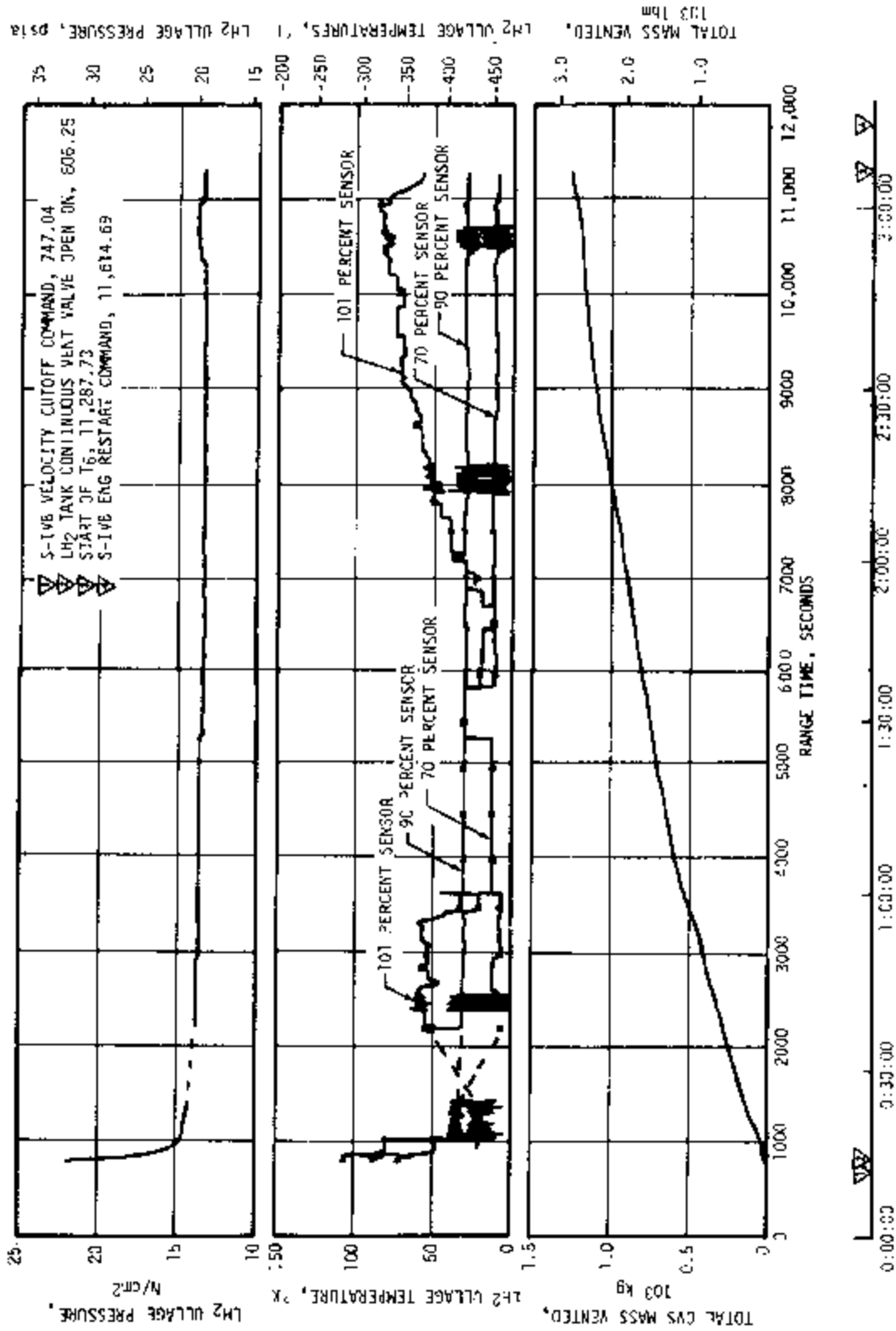


Figure 7-8. S-IVB Ullage Conditions - Coast Phase

Calculations based on estimated temperatures indicate that the mass vented was approximately 1270 kilograms (2800 lbm) and that the boiloff mass was approximately 1360 kilograms (3000 lbm).

Figure 7-9 shows the start tank temperature and pressure during orbital coast for AS-501, 502, and 203. A 180-degree roll maneuver on the AS-502 flight took place at approximately 837.3 seconds. This orientation of the vehicle did not appear to have any effect on the start bottle. Many of the S-IVB pressure sphere temperature measurements during orbit are not considered reliable; however, the temperature reading at second start command was very near that for AS-501.

7.6 S-IVB CHILLDOWN AND ATTEMPTED RESTART FOR SECOND BURN

The S-IVB stage provided adequate conditioning of propellants to the J-2 engine for the restart attempt. The engine start sphere was recharged properly and maintained sufficient pressure during coast to the restart time. The engine control sphere gas usage was as predicted during the first burn and maintained sufficient system pressure for a proper restart.

Table 7-6 showing the major events during the start transient, indicates that all events occurred as required and performance was as predicted until the end of the start bottle blowdown which occurred at approximately ESC +8.5 seconds. At this time, the main engine should have ignited with opening of the MOV, and the GG should have bootstrapped to mainstage operation. The GG was ignited and the MOV opened, however, the main engine did not ignite as evidenced by the lack of an increase in fuel injector temperature. Engine operation was terminated by the Instrument Unit (IU) monitor from lack of sufficient thrust at 11,630.33 seconds.

The propellant recirculation systems performed satisfactorily and met start and run box requirements for fuel and LOX as shown in Figure 7-10. Second burn fuel lead generally followed the predicted pattern and resulted in satisfactory conditions as indicated by the thrust chamber temperatures and the associated fuel injector temperatures shown in Figure 7-11. The LH₂ chilldown system performance for second burn was satisfactory. The LH₂ pump inlet temperature at second burn ESC was 21.9°K (-420.6°F). Second burn LOX pump chilldown was also satisfactory. At S-IVB second burn ESC the LOX pump inlet temperature was 91.7°K (-295°F).

The start tank performed satisfactorily during the second burn blowdown as shown in Figure 7-12. The proper energy input to the turbine was provided for a smooth start. Since there was no ignition of the main chamber for the second start, the start tank did not refill.

Figure 7-13 shows the predicted engine helium control sphere pressure compared to AS-501 for the restart attempt. After the normal post test

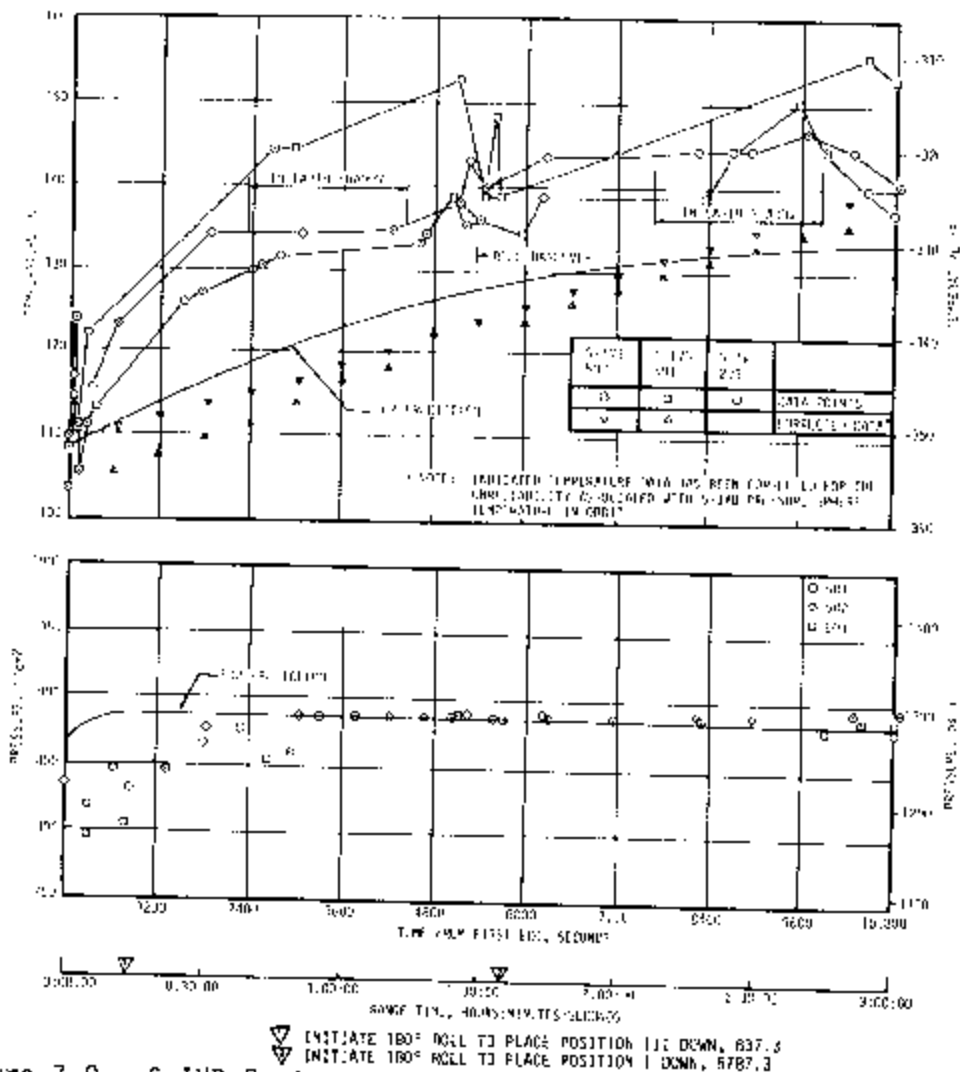


Figure 7-9. S-IVB Engine Start Tank Temperature and Pressure - Coast Phase

Table 7-6. S-IVB Engine Start Sequence - Second Burn Attempt

EVENT	TIME OF EVENT IN RANGE TIME, SECONDS	
	PREDICTED	ACTUAL
S-IVB Engine Restart Command (ESC)	11,403.61	11,614.69
STDY Open	11,411.61	11,622.92
Mainstage Control Sol.	11,411.86	11,623.13
Mainstage OK	11,412.60	Not Attained
Main LOX Valve Open	11,413.58	11,625.20
90 Percent Thrust	11,413.3	Not Attained

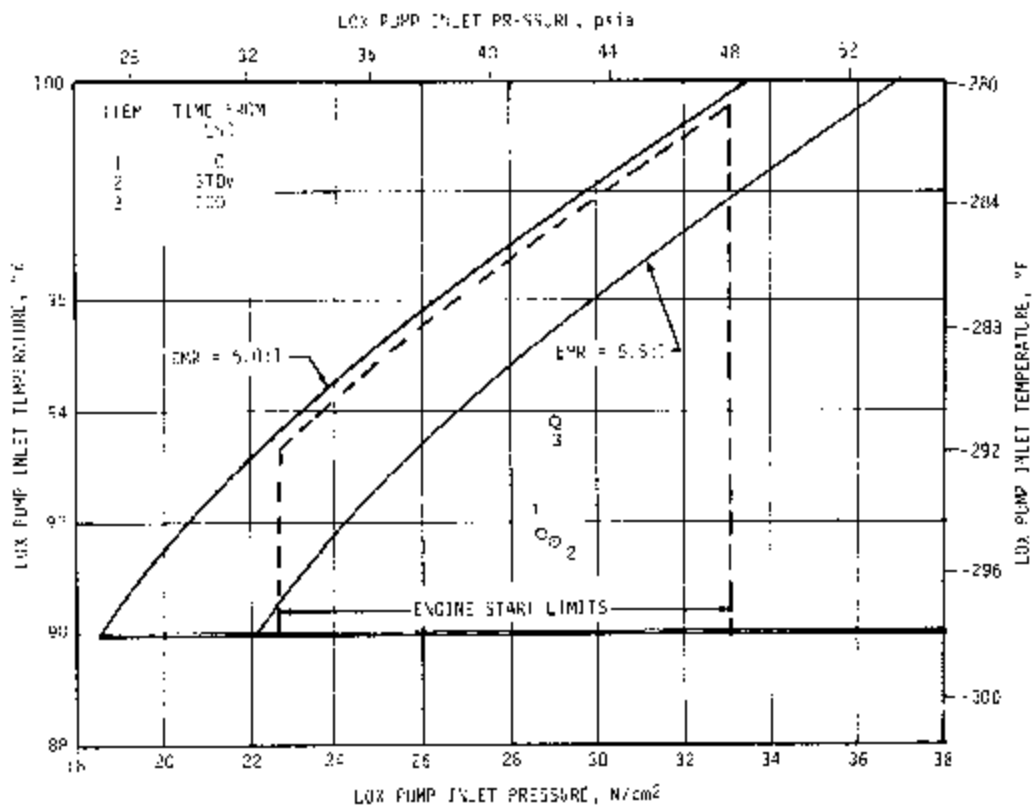
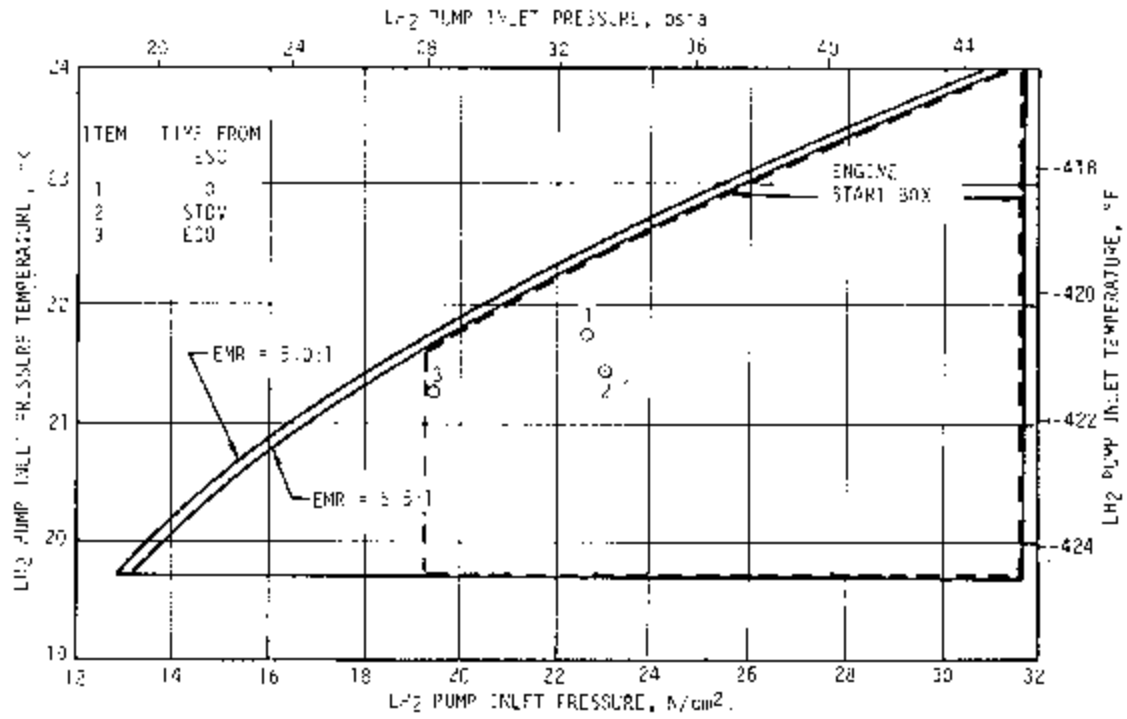


Figure 7-10. S-IVB Start Box and Run Requirements - Restart Attempt

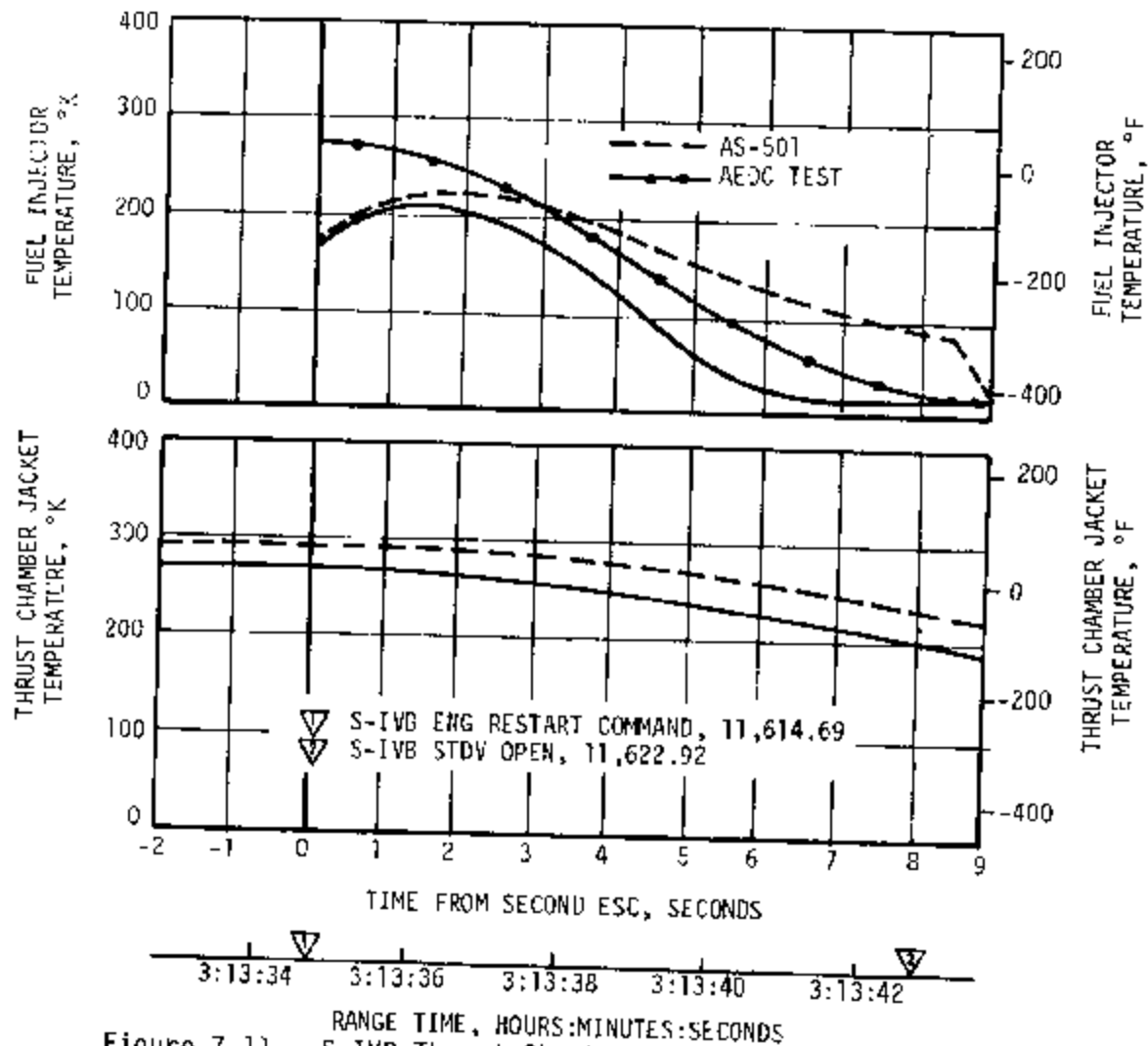


Figure 7-11. S-IVB Thrust Chamber Chilldown Performance - Restart Attempt

1-second blowdown the pressure was 1310 N/cm^2 (1900 psia) at second burn ESC. The pressure decayed more than the predicted 550 N/cm^2 (800 psi) during the second burn fuel lead because of the lower temperature at the injector. The pressure stabilized at 670 N/cm^2 (975 psia) at the end of the blowdown. This pressure would have been sufficient to complete the mission.

During the start of the second burn, the GG experienced a temperature spike as indicated by Figure 7-14. The spike measured 1278°K (1840°F), the upper limit of the temperature bulb, but an expanded plot of fuel turbine inlet temperature suggests the spike actually reached as high as 1389°K (2040°F). The spike resulted from a high start mixture ratio in the GG, which in turn was caused by the failure of the main chamber

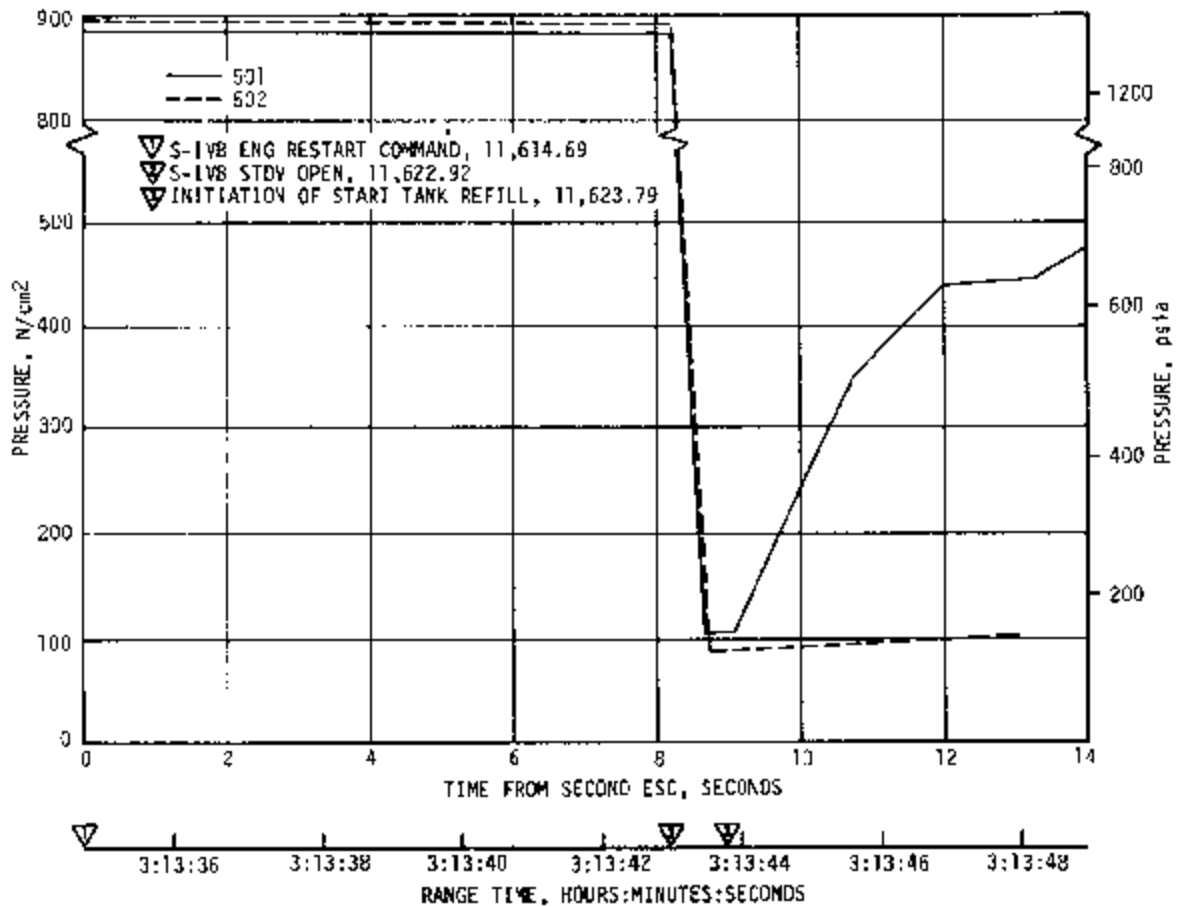


Figure 7-12. S-IVB Start Tank Pressure - Restart Attempt

pressure to rise above 27.57 N/cm² (40 psia). With a low main chamber pressure most of the flow destined for the GG follows the lower pressure drop path to the main chamber, resulting in a low GG total flowrate. However, because the start load of the oxidizer pump is lower than that of the fuel pump, the initial oxidizer flow is less affected than the fuel flow. Thus, the GG chamber pressure, a function of both total flowrate and mixture ratio, is low as shown in Figure 7-15; whereas, the fuel turbine inlet temperature, a function only of GG mixture ratio, is high.

Near engine cutoff command, the GG chamber pressure rose slightly. This fact plus the absence of any unexplained vehicle moment during second burn suggests that the temperature spike did not burn through the GG combustor wall.

Information supporting the suspected ASI fuel line failure is discussed in the following paragraphs. Table 7-7 lists the chronological events which

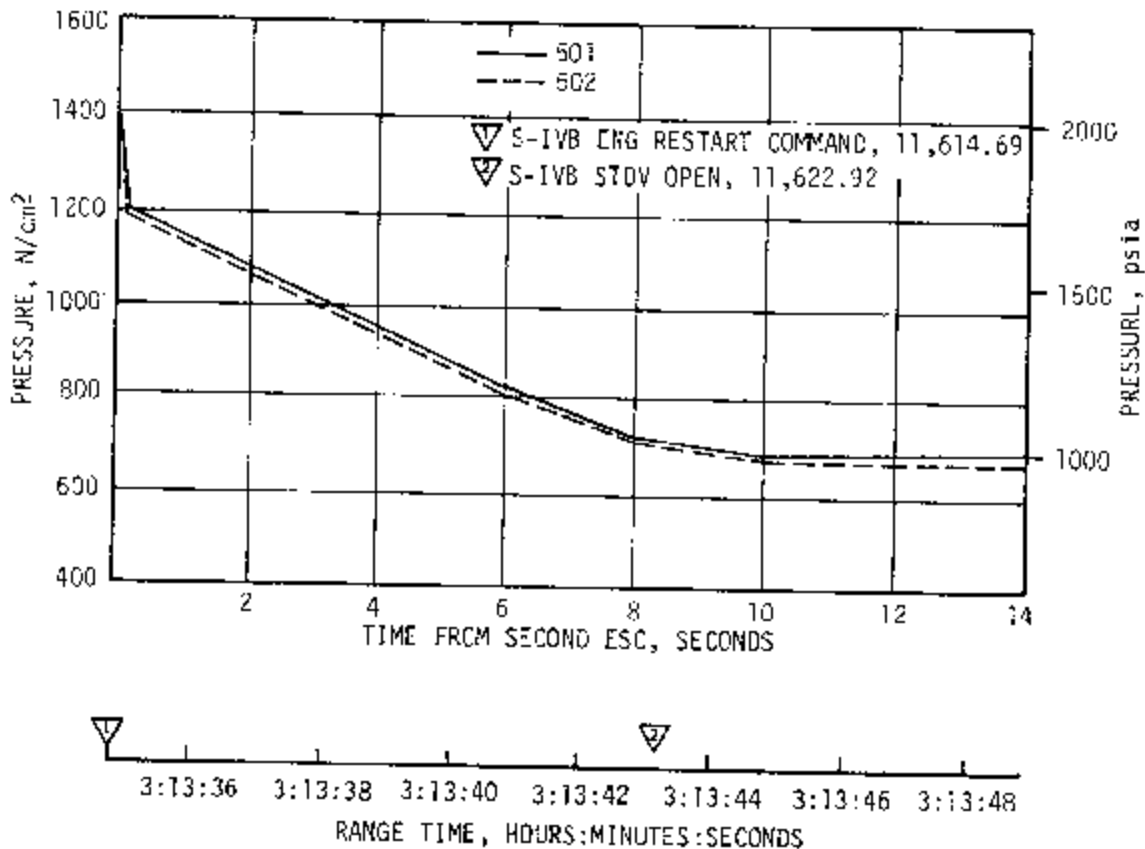


Figure 7-13. S-IVB Engine Control Helium Sphere Pressure - Restart Attempt

led to the failure to restart. The first indication of a problem was engine area chilling of the MOV closing control line at 645 seconds as shown in Figure 7-16. The second indication was the apparent performance shifts indicated during first burn as discussed in paragraph 7.3. During the performance shift at approximately 688 seconds, the yaw actuator experienced an abrupt increase in its cooling rate that cannot be attributed to radiation loss. This may have been due to the impingement of a cold gas on the actuator at this time and is discussed in detail under paragraphs 8.4 through 8.6.

The third indication of a problem during first burn operation was the apparent flash fire at 696 seconds. The thrust structure temperatures decayed from approximately 222 to 216°K (-60 to -70°F) by 696 seconds. At this time, the thrust structure temperature No. 1 showed a rise of approximately 16.7°K (30°F) as shown in Figure 7-17. The heat flux required to obtain the rise rate shown is approximately 1.1 watts/cm² (1 Btu/ft²-s) which was approximately eight times that which can be produced from solar

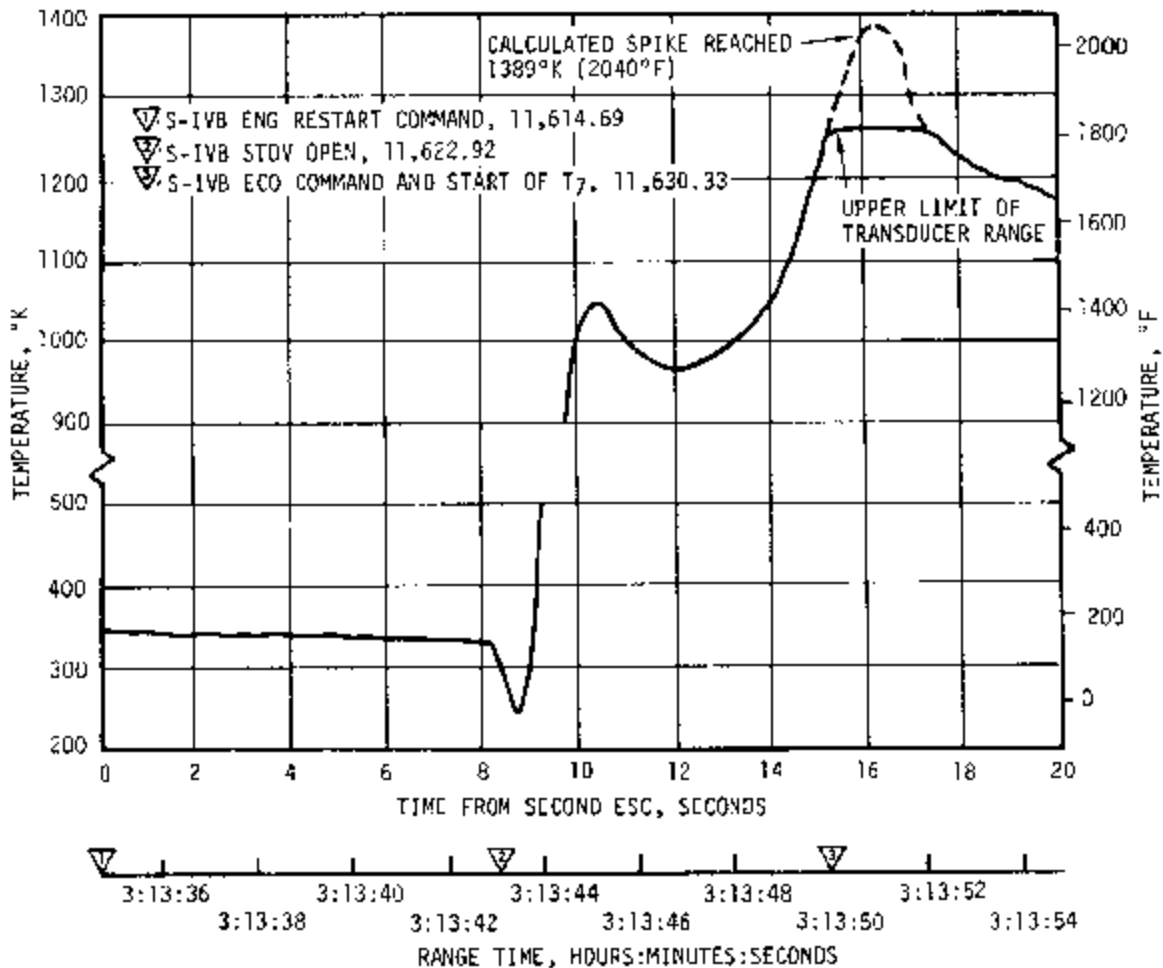


Figure 7-14. S-IVB Fuel Turbine Inlet Temperature - Restart Attempt

heating; therefore, a heat source other than the natural environment was indicated. Figure 7-17 also shows an interstage gas temperature probe which showed a temperature rise at the same time. Its response times were smaller and excursions were larger; however, it does confirm the presence of an additional heat source. Other measurements in the same area also confirm these findings. Figure 7-16 also shows a fire indication between the LOX pump and the start bottle. At approximately 702 seconds these measurements indicated a cooling rate higher than would be expected from radiation to space and the LOX tank, indicating the possibility of a cold gas impinging in the area. After the performance shift, the engine continued to operate at that level until ECO with some chilling in the area of the fire; however, a normal shutdown was still obtained.

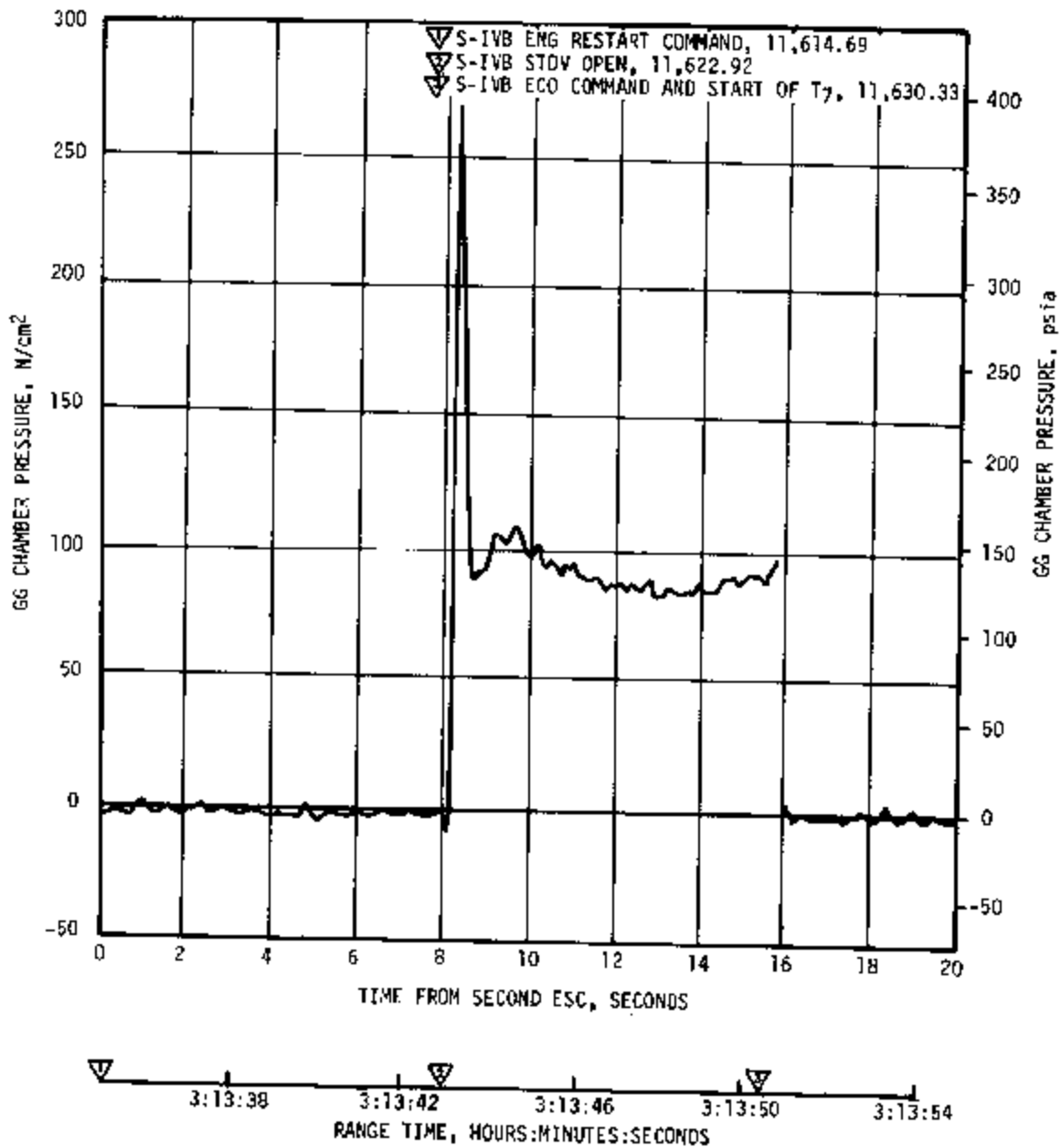


Figure 7-15. S-IVB GG Chamber Pressure - Restart Attempt

During the attempt to start the engine for the second burn, no temperature change was noted on the thrust structure temperature No. 2. However, the thrust structure temperature No. 1 dropped from 194°K (-110°F) at 11,622.92 seconds (the end of fuel lead) to 190°K (-118°F). The engine main LOX pneumatic line surface temperature dropped from 205°K (-90°F) at 11,623 seconds to 169°K (-155°F). The GG fuel inlet line wall temperature rose

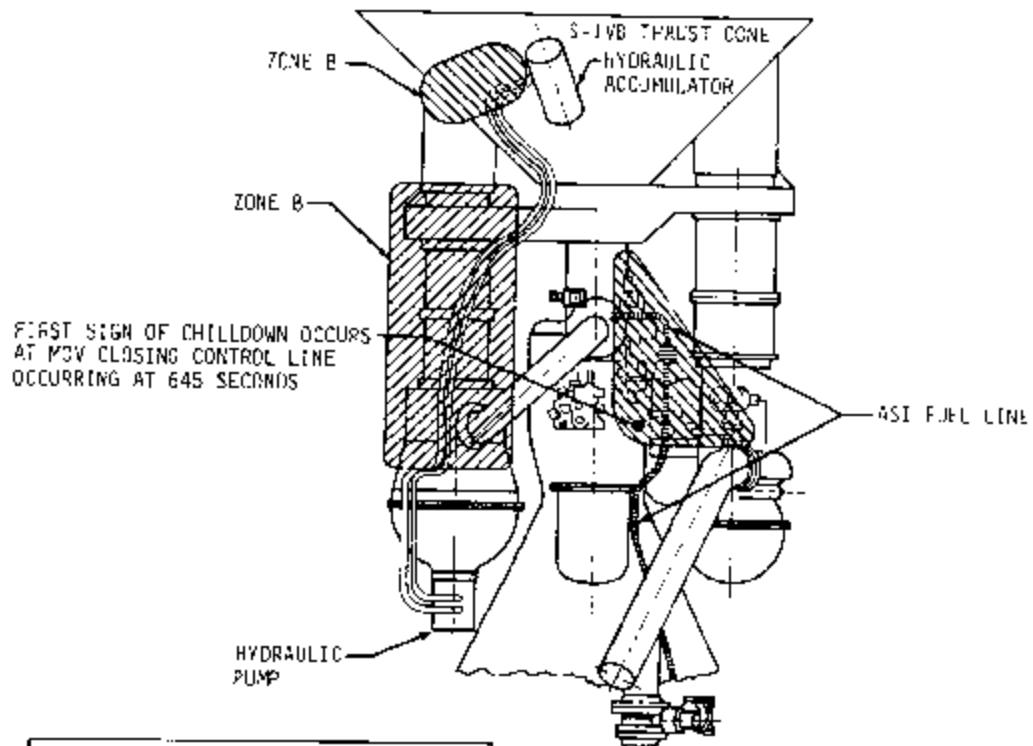
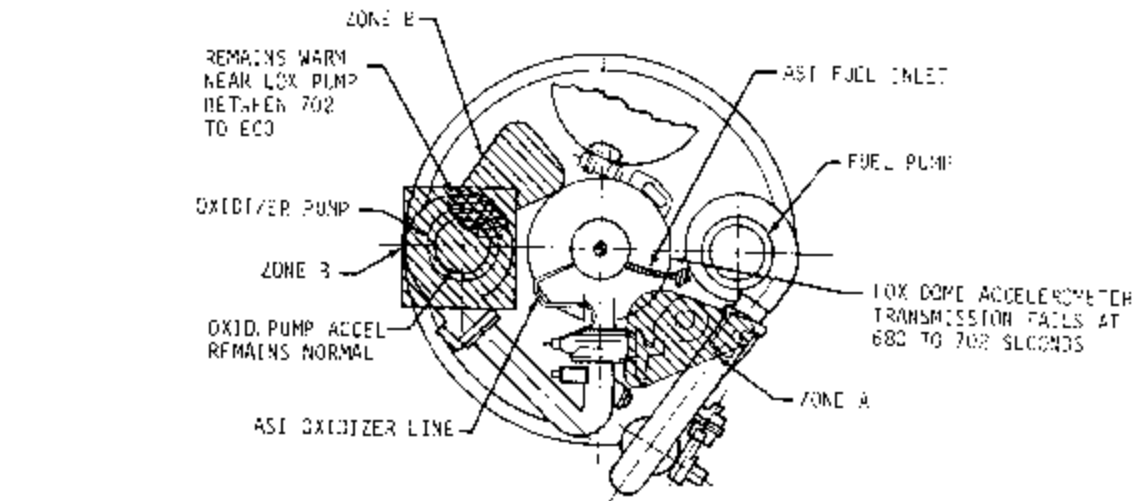
Table 7-7. S-IVB Stage J-2 Engine Failure to Restart

RANGE TIME, SECONDS	EVENT	ANALYSIS
577.28	Engine start (first burn) (LVDC Command)	Normal
645	Start of engine compartment temperature decrease	Cryogenic fuel leakage in upper engine area.
684	Initial performance decay begins (4 psi chamber pressure loss) with engine compartment temperature decreasing more rapidly	Increased leakage in upper engine area.
688	Yaw actuator had abrupt increase in its cooling rate	Impingement of a cold gas on the actuator.
692	Second performance decay begins (12 psi chamber pressure loss)	Performance loss due to leakage of approximately 6-7 lbm/s propellants. (possible both LOX and fuel).
696	Engine compartment heating in vicinity of ASI fuel line and fire indication between LOX pump and start bottle	Possible LOX and fuel leakage from ASI lines.
702	Performance shift ends with general cooling	ASI chamber erosion complete.
747.04	Engine cutoff (velocity cutoff)	Normal
11,622.92	Engine fails to ignite (S ² DV opening)	Lack of ASI ignition.

from 26 to 30°K (-413 to -406°F) at 11,618 seconds and then dropped back to 28°K (-410°F). The engine main LOX valve actuator skin temperature dropped slightly at 11,625 seconds. These locations are shown on a diagram of the engine in Figure 7-18.

Engine reconstruction analysis and engine tests indicated that the initial performance drop during first burn was probably caused by leakage of the ASI fuel line and is substantiated by the chilling experienced near the LH₂ pump as summarized in Figure 7-18. The engine tests simulating an ASI fuel line failure were compatible with the AS-502 observed performance shift, a subsequent stabilization and a normal shutdown. One test conducted at an ASI chamber mixture ratio of 7 resulted in injector damage simulating the performance changes recorded on AS-502 flight.

The propulsion system met all operational requirements during first burn, cutoff transient, and orbital coast. The conditions for restart were nominal, except for a hot start of the GG and lack of main chamber ignition as previously discussed. Figure 7-19 is also presented to verify that pump operation and performance was acceptable up to the time for main chamber ignition. However, the failed ASI system caused the main chamber not to ignite, resulting in the failure to obtain restart for second burn.



CHILL INDICATION - ENGINE ENVIRONMENT		
TIME SPAN	ZONE B	ZONE A
545-645	ENGINE AREA BEGINNING TO CHILL	SOME CHILLING AS TIME APPROACHES 600 SECONDS
660-700 (PERFORMANCE SHIFT)	ENGINE AREA SHOWS RAPID TEMPERATURE RISE	VEHICLE AND ENGINE AREA SHOW RAPID TEMP RISE
700-800	COLD	REMAINS WARM NEAR LOX PUMP AND SOME CHILLING IS REMAINING AREA

Figure 7-16. S-IVB Engine Environmental Changes During J-2 Engine Anomaly

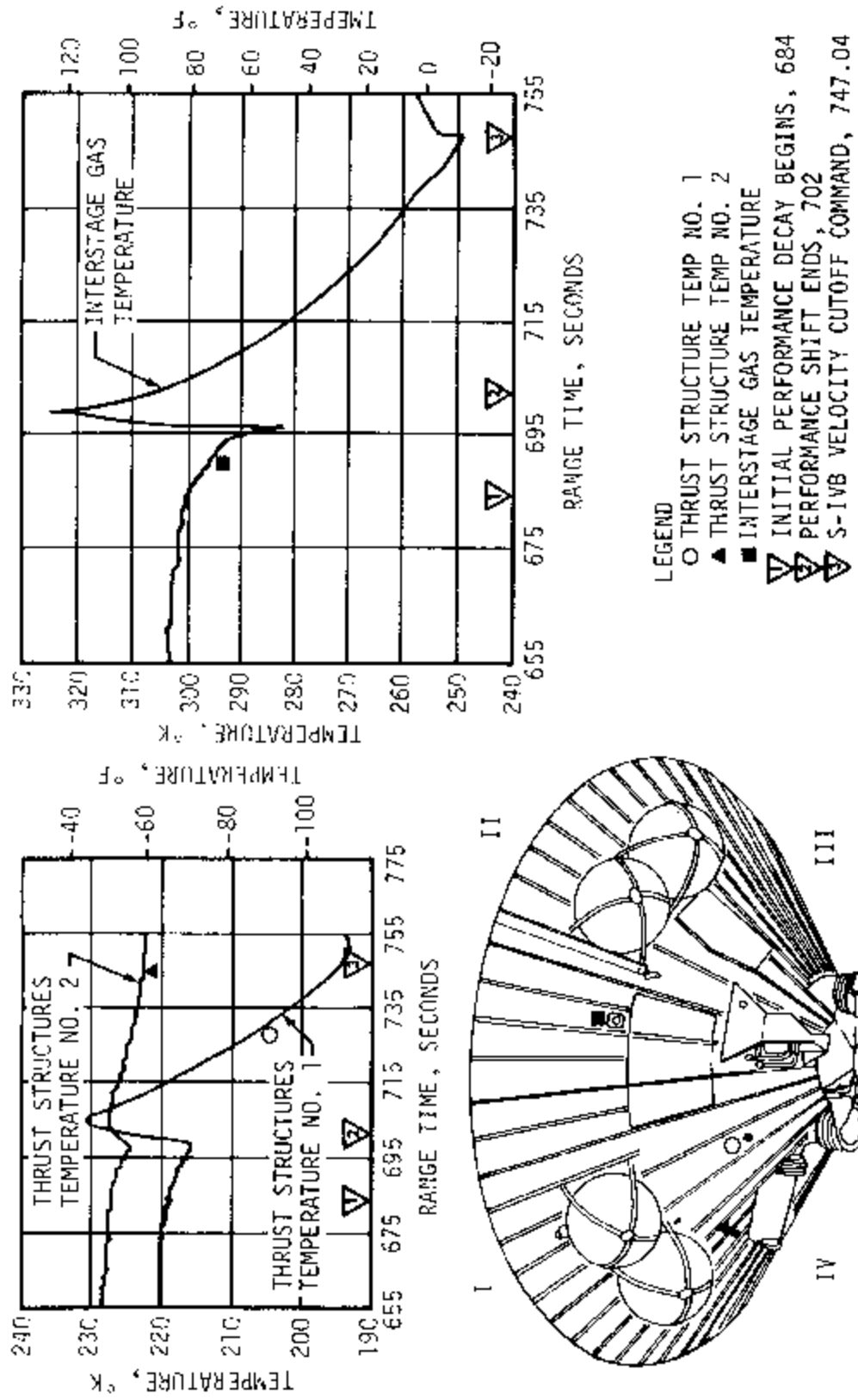


Figure 7-17. S-IVB Environmental Conditions During J-2 Performance Shift

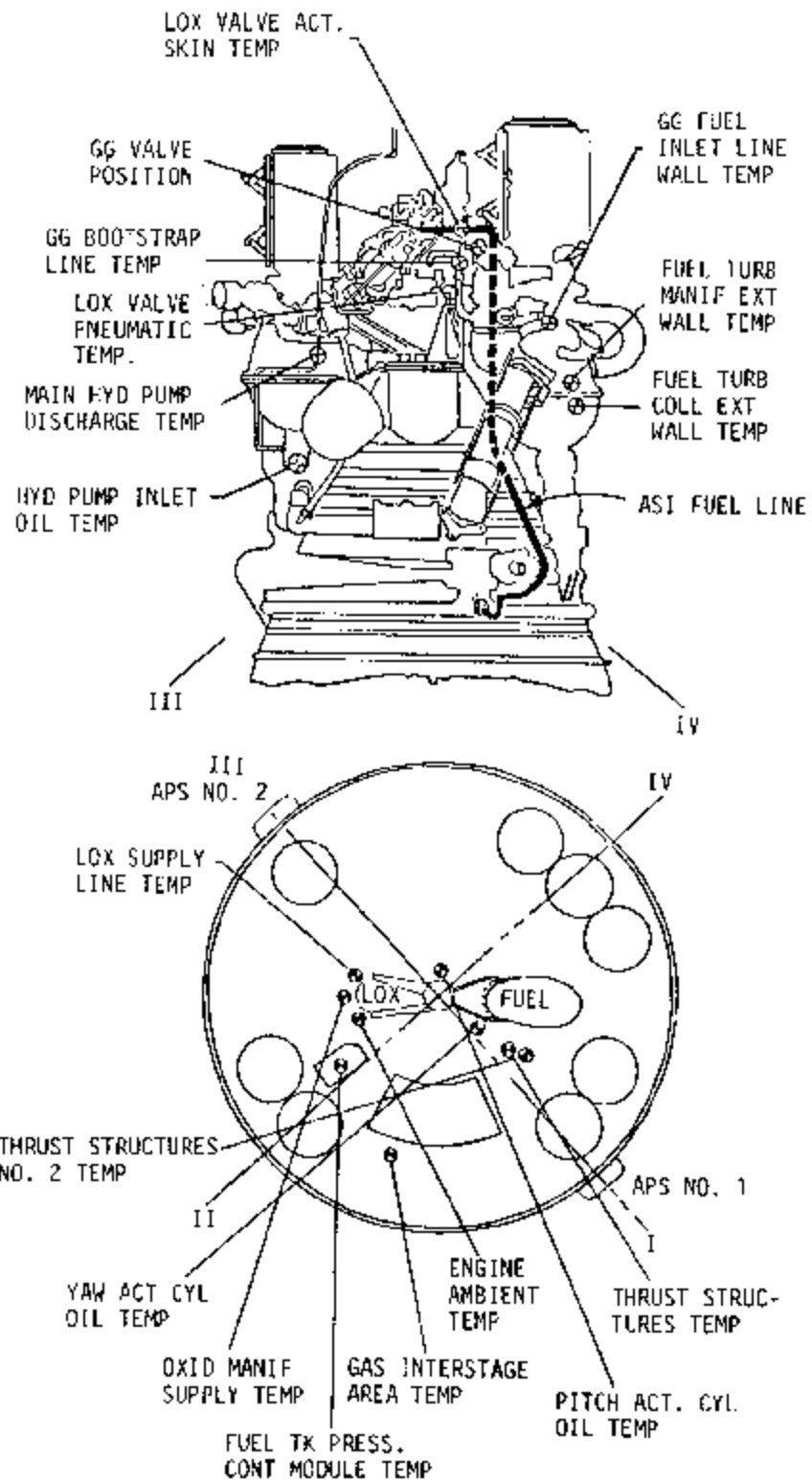


Figure 7-18. S-IVB Summary of Environment Effects

- ▽ S-IVB ENG RESTART COMMAND, 11,614.69
- ▽ S-IVB STOV OPEN, 11,622.92
- ▽ S-IVB FCO COMMAND AND START OF T₇, 11,630.33

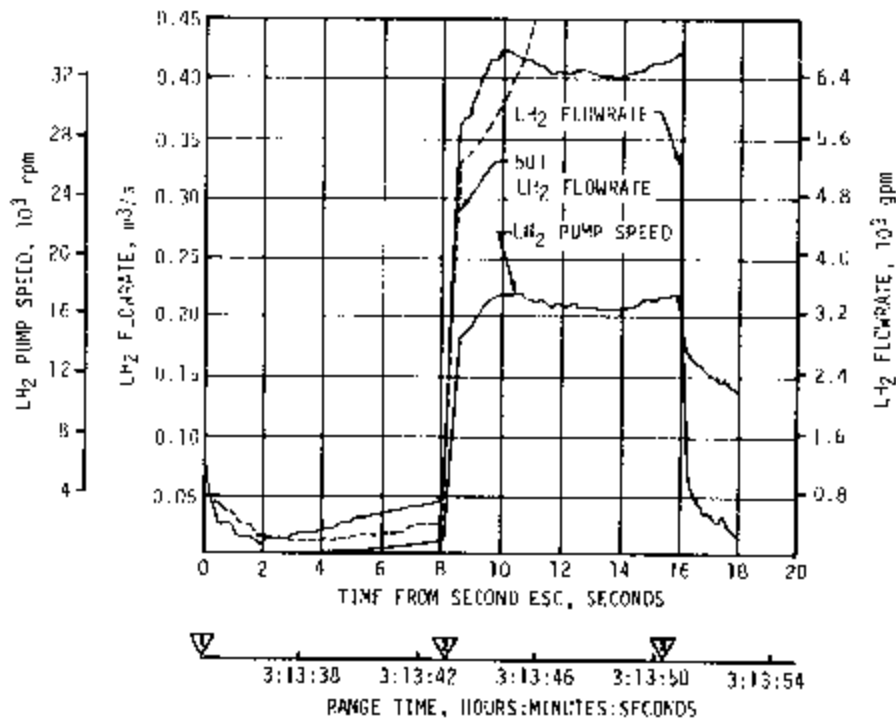
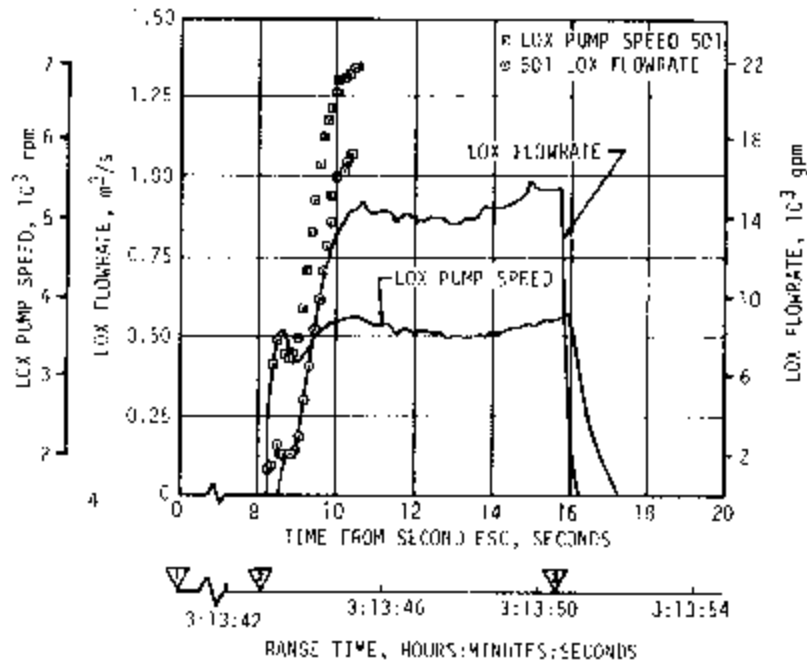


Figure 7-19. S-IVB Pumps Performance During Restart Attempt

The ASI is a small chamber which is center-mounted in the thrust chamber injector. Its purpose is to create and maintain a small ignition flame for thrust chamber ignition. The ASI system is shown in Figure 7-20. Figure 7-21 shows the location of the ASI chamber in the engine injector. At the present time a modification of the ASI propellant feed lines is being made as a result of the flight data and the engine tests made to simulate the failure to restart. A complete report (Rocketdyne No. R-7450-2) titled "J-2 Engine AS-502 (Apollo 6) Flight Report - S-II and S-IVB Stages" will be issued covering the flight performance, S-II failures (common to S-IVB failure), S-IVB failure, verification testing, and the design and modification changes.

7.7 S-IVB MAIN STAGE PERFORMANCE FOR SECOND BURN

(No discussion due to failure to achieve restart.)

7.8 S-IVB SHUTDOWN TRANSIENT PERFORMANCE FOR SECOND BURN

(No discussion due to failure to achieve restart.)

7.9 S-IVB STAGE PROPELLANT UTILIZATION

The primary function of the PU system is to assure simultaneous depletion of propellants by controlling the LOX flowrate to the J-2 engine. By controlling the LOX flowrate to the engine, indicated propellant loading errors and/or deviations from predicted vehicle flight behavior can be corrected and the proper proportion of LOX and LH₂ in the main tanks can be maintained. Other functions accomplished by the propellant utilization system are:

- a. Controlling propellant loading
- b. Maintaining the propellants at any predetermined level during launch countdown.
- c. Providing propellant mass indication signals to the telemetry system.
- d. Providing a signal signifying the depletion of either propellant, thereby initiating ECO.

Components in this system include ground and onboard electronics, continuous capacitance probes, a PU valve, and discrete liquid level sensors.

The PU system successfully accomplished the requirements associated with propellant loading and management during burn. The best estimate propellant mass values at liftoff were 88,060 kilograms (194,140 lbm) LOX and 19,254 kilograms (42,448 lbm) LH₂ as compared to predicted mass values of 87,655 kilograms (193,246 lbm) LOX and 19,268 kilograms (42,479 lbm) LH₂. These values were well within required loading accuracies.

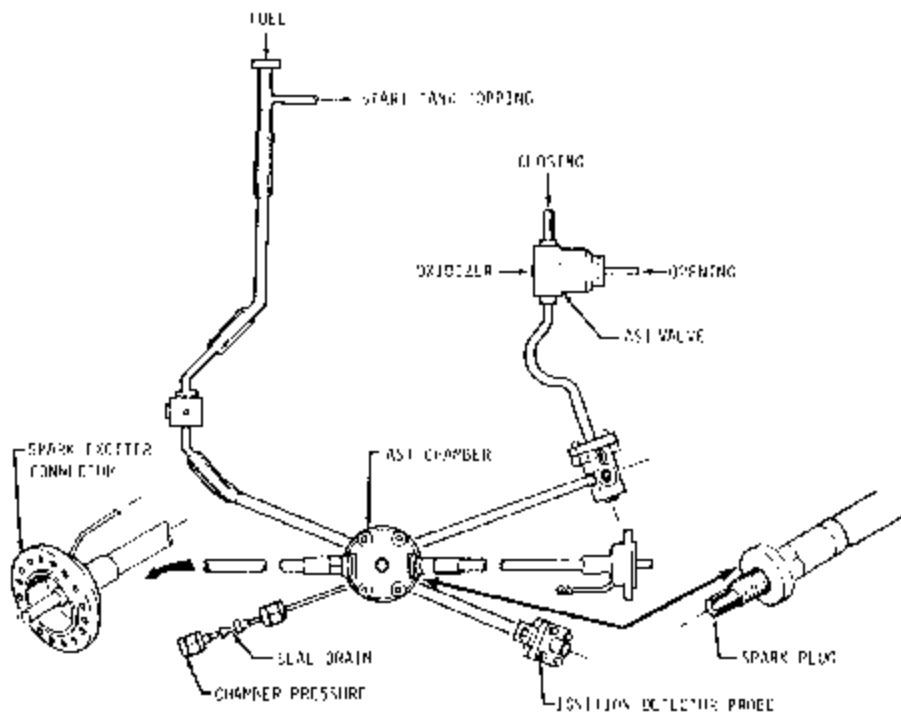


Figure 7-20. S-IVB J-2 Engine ASI Schematic

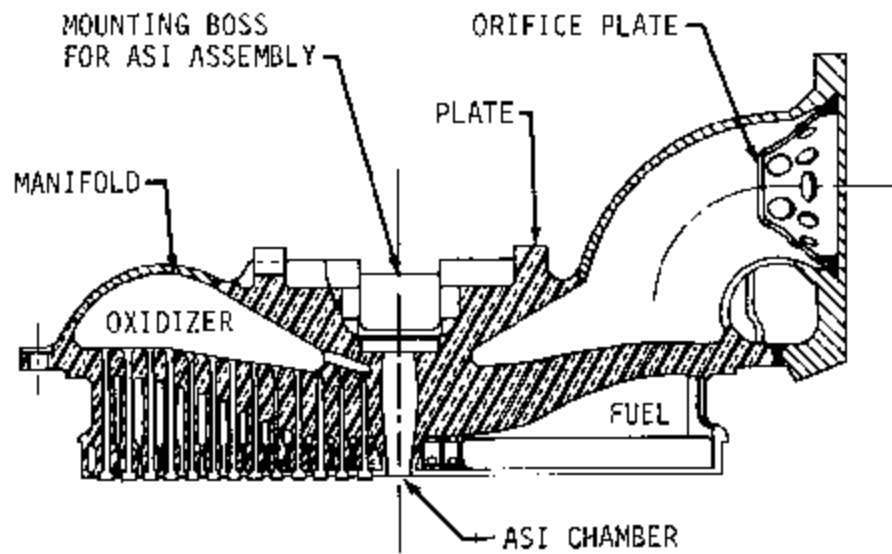


Figure 7-21. S-IVB J-2 Engine Injector Schematic

A comparison of propellant mass values at critical flight events, as determined by various analyses, is presented in Table 7-8. The best estimate full load propellant masses were 0.46 percent higher for LOX and 0.07 percent lower for LH₂ than the predicted values, as shown in Table 3-4 of Launch Operations, Section 3. This deviation was well within the required loading accuracy. The large dispersion in first burn cutoff propellant mass values from predicted was a result of the extended first burn time needed to achieve orbital insertion conditions following the early shutdown of two engines on the S-II stage. Figure 7-22 shows a graphical representation of the PU mass sensor nonlinearities during S-IVB powered flight.

Figure 7-23 is a graphical representation of the best estimate, a statistical weighted average analyses, for ignition and cutoff masses. The third flight stage ignition mass was 160,690 kilograms (354,261 lbm) and the cutoff mass was 120,330 kilograms (265,283 lbm). The five measurement systems used in determining the statistical weighted average best estimate masses were:

- a. PU indicated (corrected).
- b. Flow integral.
- c. PU volumetric.
- d. Level sensor.
- e. Trajectory reconstruction.

Extrapolation of propellant level sensor data to depletion, using the propellant flowrates to depletion, indicated that a LOX depletion would have occurred approximately 2 seconds after second burn velocity cutoff.

The first burn PU valve positions are illustrated in Figure 7-24. During first burn the PU valve was positioned at null for start and remained there until PU activated at first burn ESC +8 seconds. The PU valve was then commanded to the fully closed (high EMR) position at activation and it remained there until ESC +177.9 seconds (749.18 seconds).

Even though the S-IVB PU system functioned normally during Countdown Demonstration Test (CDDT), preflight operation, and first burn, an anomaly of 100 percent indicated LOX mass was experienced during the second orbital revolution. The LOX mass bridge experienced disturbances on nine different occasions which caused the LOX bridge to slew toward the full stop. On each occasion the bridge subsequently recovered except for the last disturbance at 11,091 seconds of flight when the LOX mass bridge

Table 7-8. S-IVB Stage Propellant Mass History

EVENT	PREDICTED		PU INDICATED (CORRECTED)		PU VOLUMETRIC		LEVEL SENSOR (EXTRAPOLATED)		BEST ESTIMATE		FLOW INTEGRAL	
	LOX	LH ₂	LOX	LH ₂	LOX	LH ₂	LOX	LH ₂	LOX	LH ₂	LOX	LH ₂
5-10 LLO kg (lbm)	87,555 193,246	19,268 42,479	87,750 193,412	19,264 42,482	89,129 194,272	19,171 42,266	86,471 194,893	19,309 42,566	86,260 194,190	19,754 42,443	88,784 194,424	19,295 42,429
1st Ignition kg (lbm)	87,655 193,296	19,267 42,477	87,567 193,272	19,246 42,430	88,257 194,122	19,148 42,214	86,401 194,263	19,309 42,566	86,256 194,135	19,255 42,440	88,041 194,097	19,252 42,440
1st LCO kg (lbm)	59,681 131,574	14,112 31,112	59,635 131,235	12,996 28,452	54,243 119,768	12,821 28,235	54,374 119,875	12,988 28,532	54,052 119,166	12,324 28,494	54,202 119,116	12,925 28,494
2nd Ignition kg (lbm)	59,676 131,476	12,779 28,040							53,661 118,745	11,411 25,156	55,518 118,723	11,563 25,472
2nd LCO kg (lbm)	4589 10,118	1267 2793							53,107 117,082	11,304 24,921	53,084 117,030	11,217 24,950

NOTE: Mass in and below the tank.

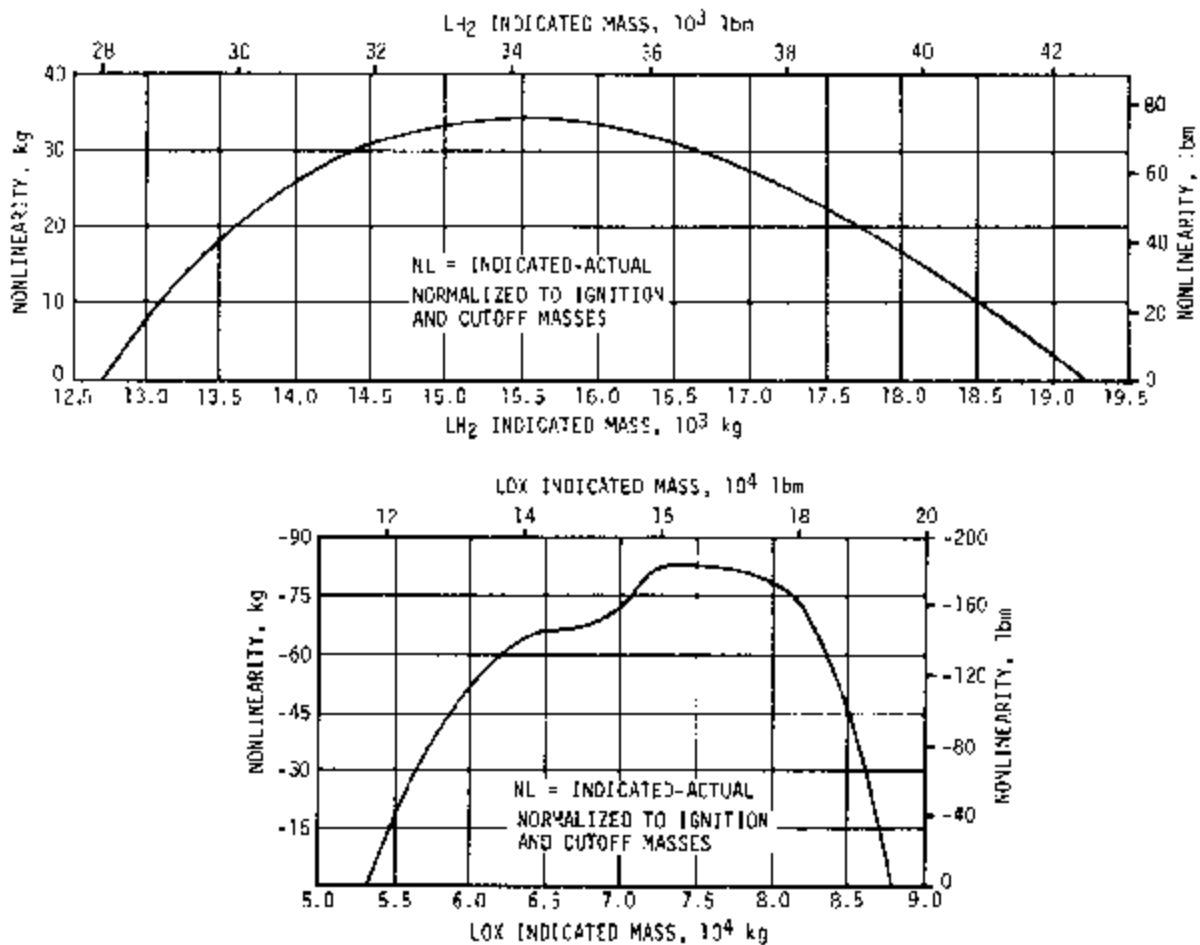
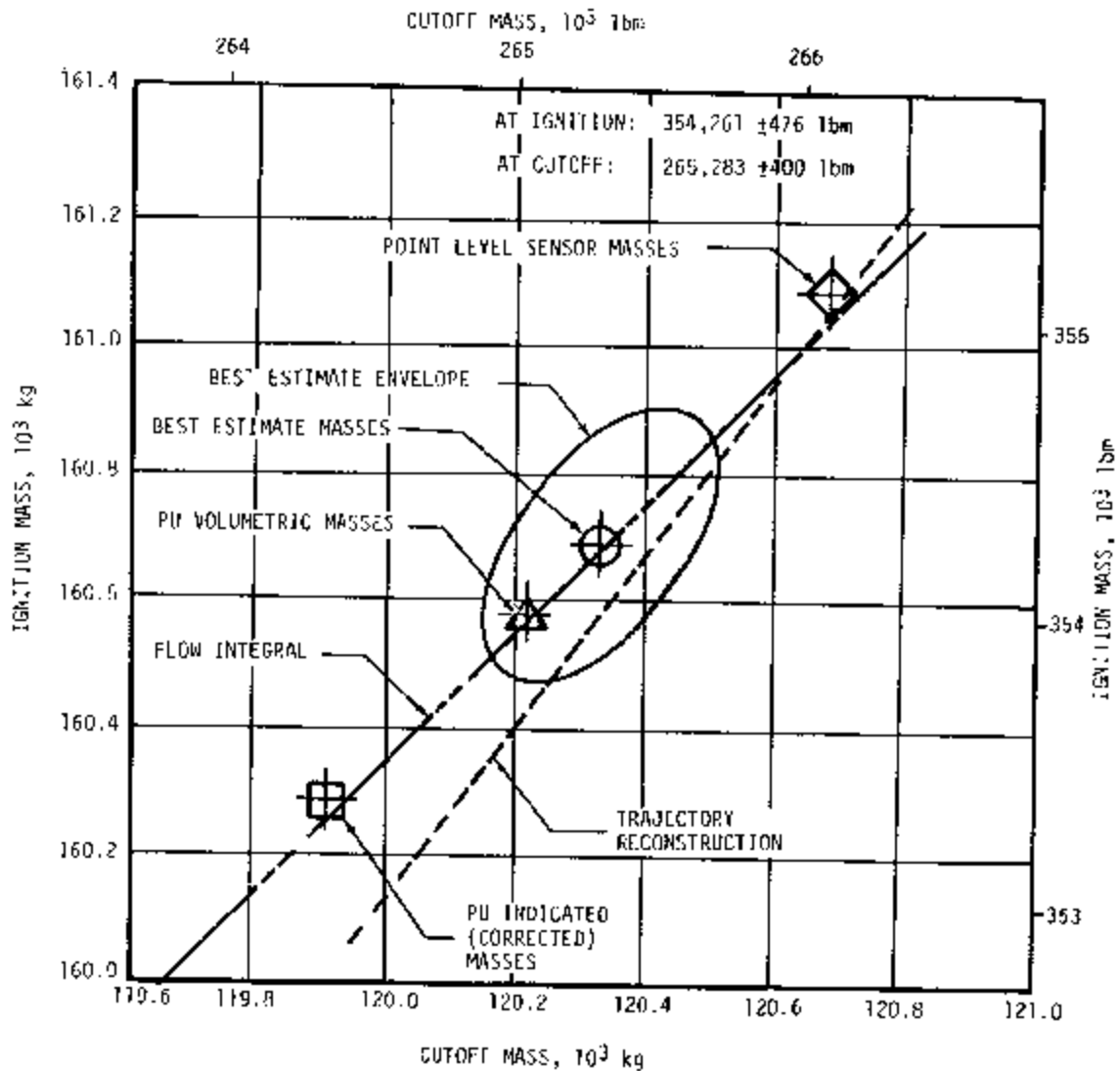


Figure 7-22. S-IVB PU Mass Sensor Volumetric Nonlinearity



* This best estimate is determined by a statistical weighted average method.

Figure 7-23. S-IVB Ignition and Cutoff Best Estimate Mass* - First Burn

slewed to the full mechanical stop and remained there for the remainder of the S-IVB mission. Had second burn restart been attained with the PU system in the malfunctioning mode, the engine would have operated in the high EMR mode until velocity cutoff. The erroneous 100 percent LOX mass bridge indications are shown in Figure 7-25.

At this time there appear to be two possible causes for the PU system anomaly. These causes are:

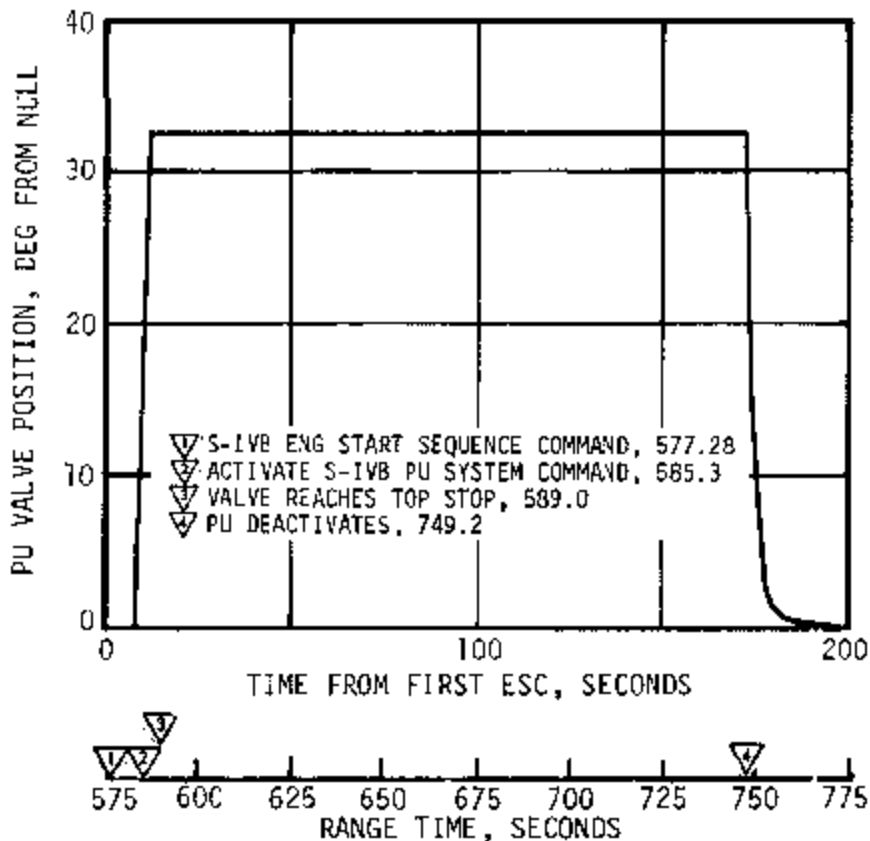


Figure 7-24. S-IVB PU Valve Positions - First Burn

- a. An intermittent cable shield between the mass probe and the PU electronics assembly as indicated by an "X" in Figure 7-26.
- b. Metallic debris of some type in the LOX tank which caused a short between the inner and outer elements of the LOX PU probe. Figure 7-27 shows a cutaway of the PU probe and the possible failure modes.

Debris in the tank during orbital conditions could be distributed anywhere in the tank and possibly lodge between the probe elements. Since the PU system operation was normal during powered flight while the LOX mass probe, its associated cable and PU electronics assembly, were under the highest vibration levels experienced during flight, the possibility of an intermittent cable shield appears remote. Therefore, the most probable cause of the PU system anomaly was metallic debris in the LOX tank shorting the inner and outer element of the LOX probe, thus causing the LOX bridge to slew at a maximum rate to the "over-fill" condition.

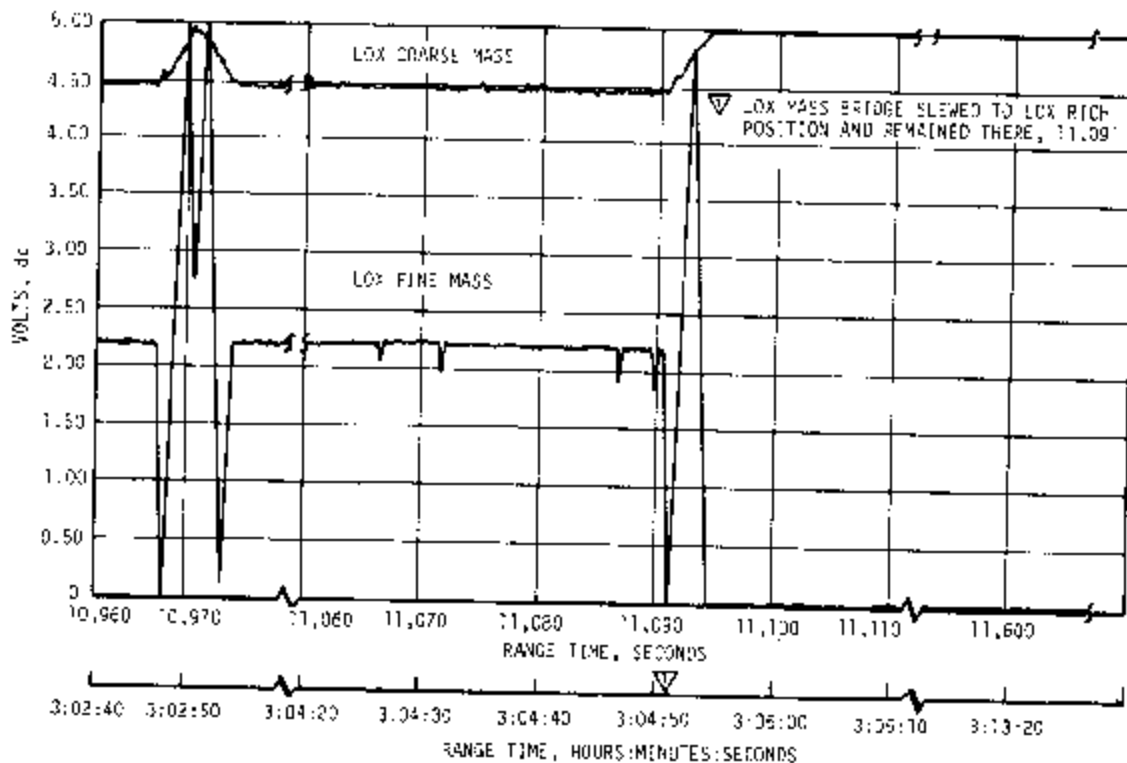


Figure 7-25. S-IVB LOX Coarse and Fine Mass Data

Additional tests will be conducted to check the crimping of the cable connector. The desirability of insulating one or both of the probe elements to prevent shorting by debris is also being considered.

7.10 S-IVB PRESSURIZATION SYSTEM

The functions of the S-IVB pressurization system are to provide the necessary positive pressure to the propellant pumps while also supplying an increased structural capability. The system consists of tank ullage pressure regulators and vent valves. LOX and LH₂ recirculation systems precondition the propulsion feed system prior to starts.

7.10.1 S-IVB LH₂ Tank Pressurization

The fuel pressurization system provides tank pressurization by three methods. Prior to launch, Gaseous Helium (GHe) from a ground source is used. After S-IVB engine start, for both first and second burns, GH₂ for LH₂ tank pressurization is bled from the thrust chamber hydrogen injector manifold. During orbital coast (parking orbit) seven LH₂ tank repressurization GHe storage spheres, attached to the thrust structure,

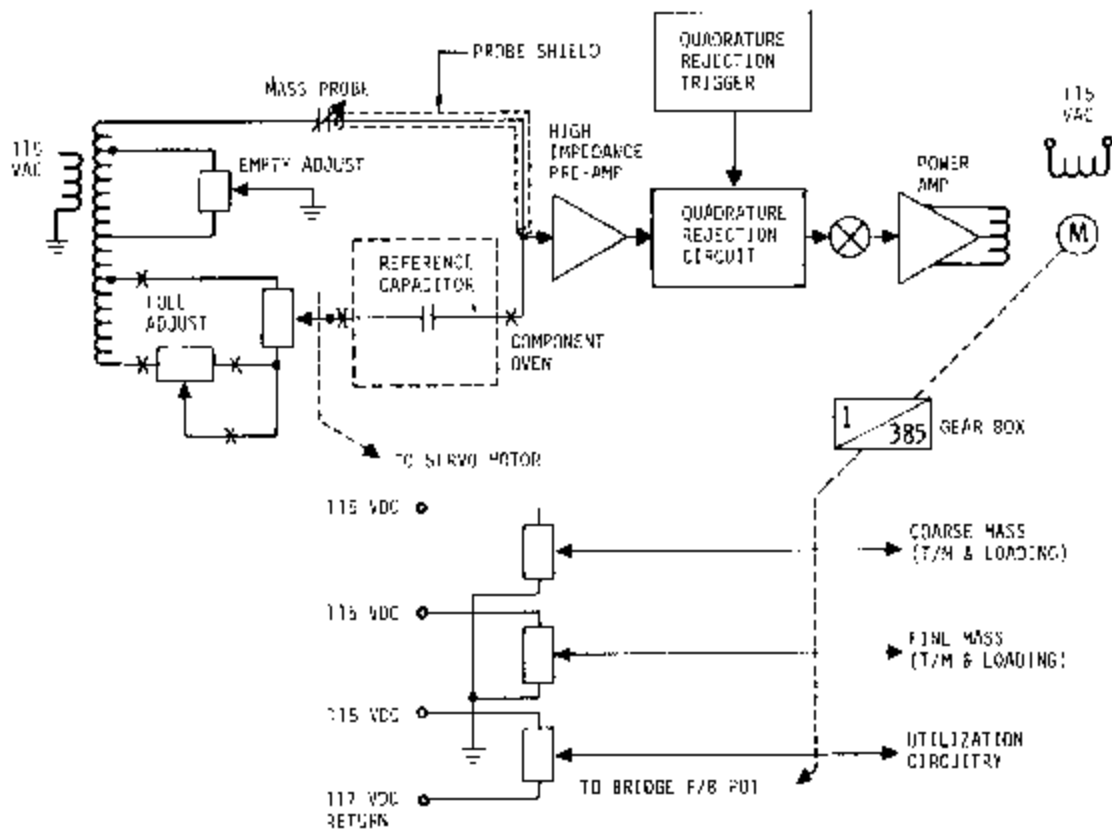
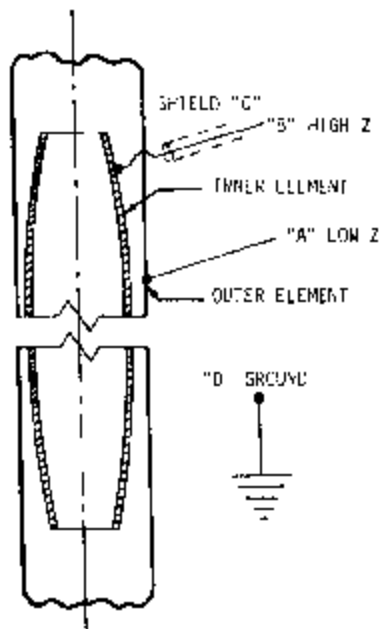


Figure 7-26. S-IVB Servo Bridge



FAILURE MODE	CONDITION BRIDGE WILL GO TO
A SHORTED TO D	EMPTY
B SHORTED TO D	FULL
C SHORTED TO D	SLIGHT SKEW
B SHORTED TO C	EMPTY
C SHORTED TO A	FULL
B SHORTED TO A	FULL (PROBABLE FAILURE)
A OPEN	EMPTY
B OPEN	EMPTY
C OPEN	FULL

Figure 7-27. Failure Modes of S-IVB PU Probes

supply repressurization gas to the LH₂ tank to meet second burn engine start requirements.

The LH₂ pressurization system operationally met all engine performance requirements. The LH₂ pressurization system indicated acceptable performance during S-IVB first burn, coast phase, and second burn attempt. The pressure measurement deviations experienced on AS-501, within the CVS and LH₂ pressurization system, during orbital coast were not experienced on this flight. Relocation of the CVS transducers gave acceptable readings. The sequence of events and associated system performances are discussed in the following paragraphs. The LH₂ tank prepressurization command was received at -96 seconds. The LH₂ tank pressurized signal was received 21 seconds later when the LH₂ tank ullage pressure reached 23.3 N/cm² (33.8 psia). The ullage pressure continued to increase, reaching 25.0 N/cm² (36.2 psia) at S-IVB first burn ESC as shown in Figure 7-28.

During first burn an LH₂ non-propulsive vent occurred at ESC +7 seconds (584 seconds). The average pressurization flowrate was approximately 0.28 kg/s (0.62 lbm/s), providing a total flow of 46.4 kilograms (102 lbm) during first burn. A slight downward shift in pressurization flowrate occurred as a result of the engine performance shift at 696 seconds.

During the repressurization period the LH₂ tank was pressurized from 14.3 to 23.3 N/cm² (20.8 to 33.8 psia). The ullage pressure subsequently decayed, reaching 21.7 N/cm² (31.4 psia). At this time, (ESC -16 seconds) a makeup cycle was initiated, increasing the LH₂ ullage pressure to 22.6 N/cm² (32.8 psia) at second burn ESC as shown in Figure 7-29. Approximately 20.0 kilograms (43.9 lbm) of ambient helium were used in the repressurization operation.

After the stage failed to restart, a decision was made to vent the LH₂ tank in an attempt to gain additional data pertaining to stage safing. The LH₂ tank vent valve was commanded open at 22,024.21 seconds as shown in Figure 7-29.

The LH₂ pump inlet NPSP was calculated from the pump interface temperature and total pressure. These values indicated that the NPSP at first burn ESC was 10.8 N/cm² (22.8 psia). The NPSP then decreased during powered flight to a minimum value of 8.3 N/cm² (12.0 psia) at first burn ECO. At the minimum point, the NPSP was 3.9 N/cm² (5.6 psi) above the required. Throughout the burn, the NPSP had satisfactory agreement with the predicted.

The NPSP at the end of fuel lead prior to second burn was 8.0 N/cm² (11.6 psia) which was 3.7 N/cm² (5.3 psia) above the required. The NPSP increased rapidly after ESC such that it was above the required level

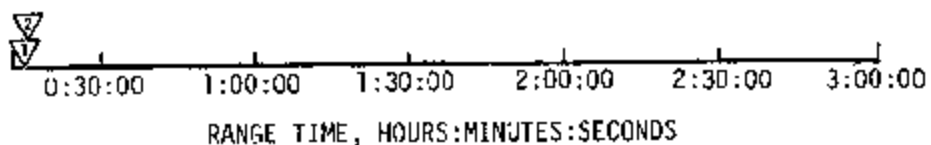
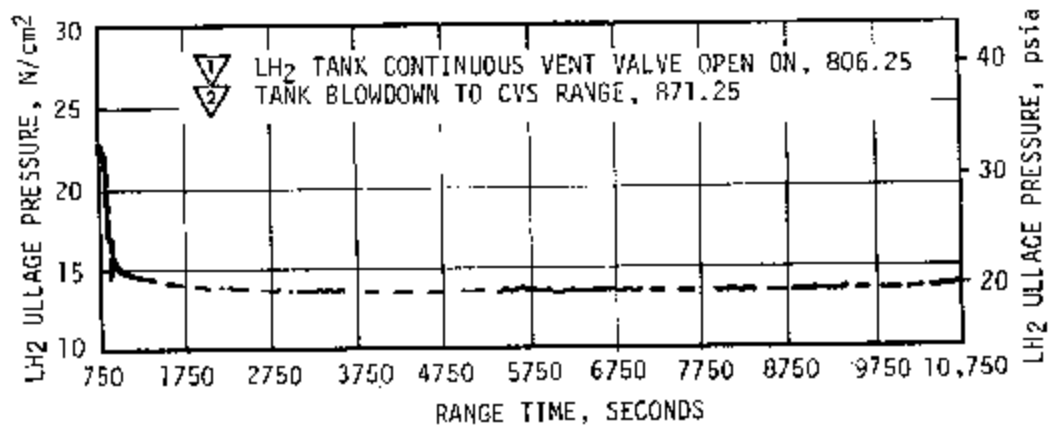
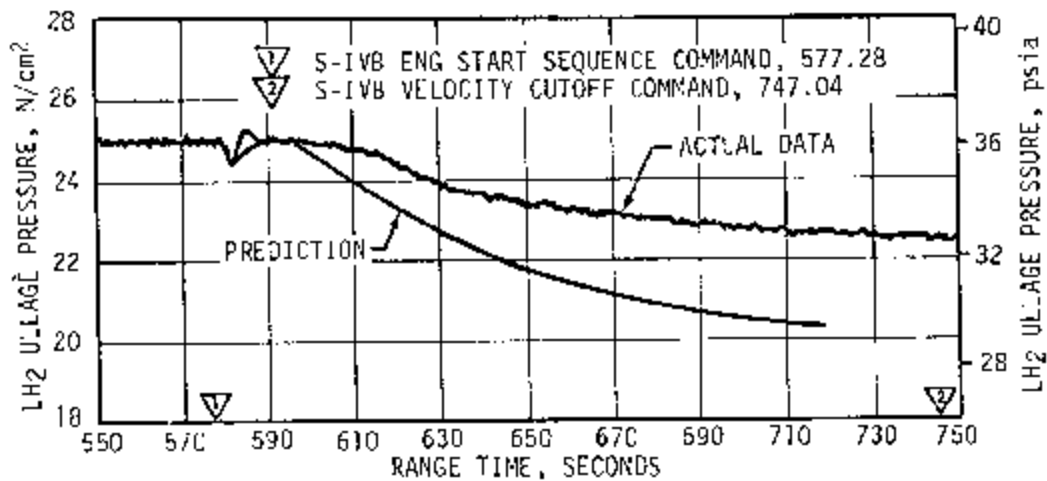
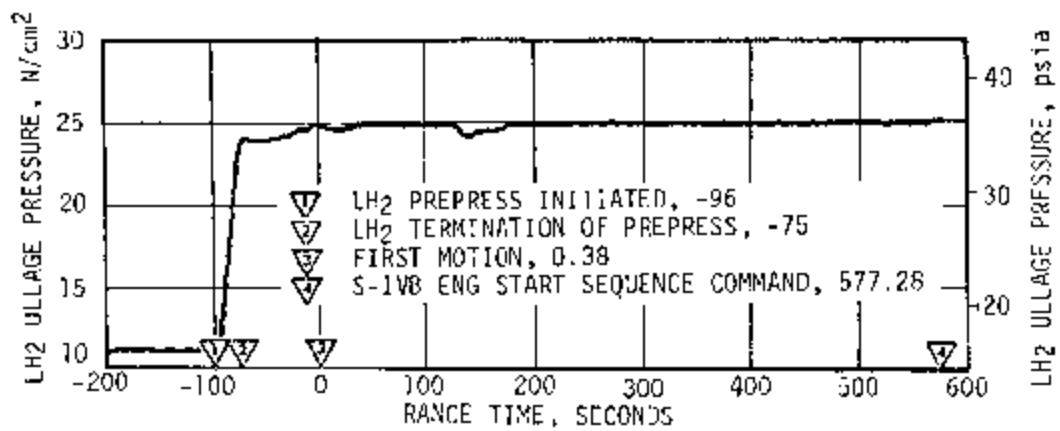


Figure 7-28. S-1VB LH₂ Ullage Pressure - First Burn and Orbit

- ▽ LH2 TANK REPRESS CONTROL VALVE OPEN - DN. 11,487.70
- ▽ LH2 TANK REPRESS TERMINATION, 11,524.69
- ▽ S-IVB ENG RESTART COMMAND, 11,614.69
- ▽ S-IVB ECD COMMAND, 11,630.33
- ▽ LH2 TANK VENT VALVE OPEN, 22,024.21

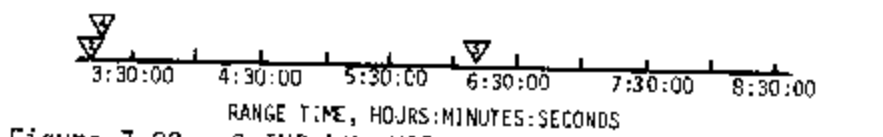
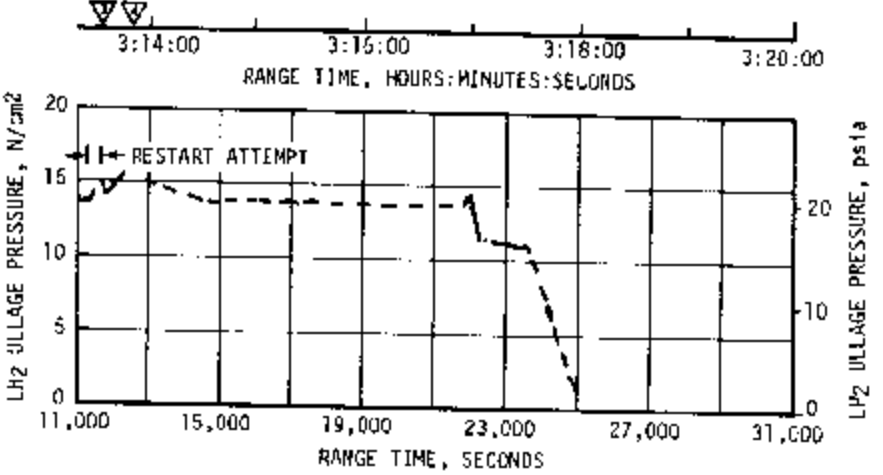
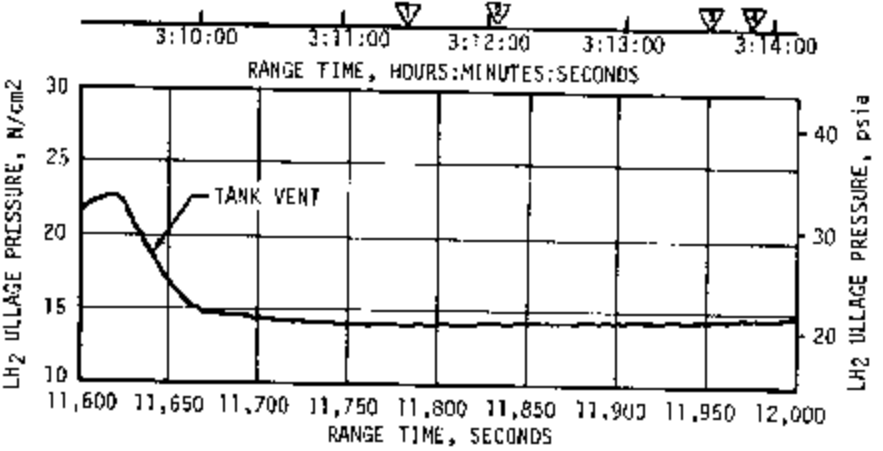
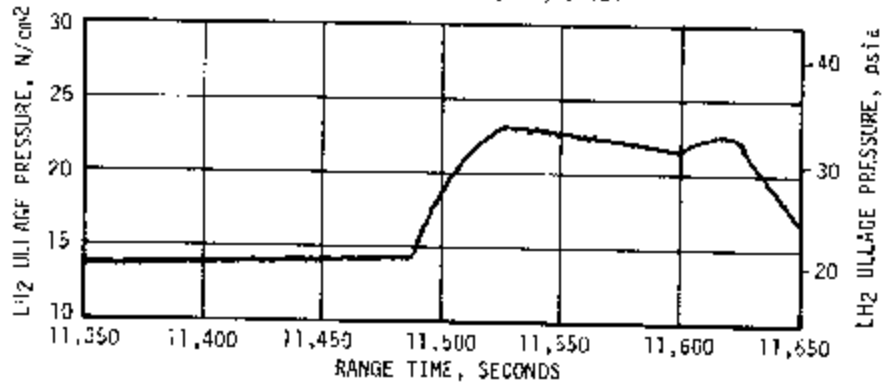


Figure 7-29. S-IVB LH₂ Ullage Pressure - Restart Attempt

during the attempted restart. At second burn ECO the NPSP was 6.0 N/cm^2 (8.7 psia) which was 1.6 N/cm^2 (2.3 psi) above the required. The pump interface total pressure at the end of fuel lead was 22.5 N/cm^2 (32.6 psia). Figures 7-30 and 7-31 summarize the fuel pump inlet conditions for first and second burns, respectively.

7.10.2 S-IVB LOX Pressurization System

The LOX pressurization system provides tank pressurization by three methods. Prior to launch, GHe from a ground source is used. After engine start, for either first or second burn, GHe from eight cold GHe storage spheres located in the LH₂ tank is warmed by a heat exchanger and used for LOX tank pressurization. During orbital coast (parking orbit) ambient GHe, from two high-pressure LOX tank repressurization GHe storage spheres, is utilized to supply engine restart ullage pressure requirements for second burn.

The oxidizer system performed adequately, supplying LOX to the engine pump inlet within the specified operating limits throughout first burn and responded normally during the attempted restart. The available NPSP at the LOX pump inlet exceeded the engine manufacturer's minimum at all times.

LOX tank prepressurization was initiated at -166.5 seconds and increased the LOX tank ullage pressure from ambient to 28.3 N/cm^2 (41.1 psia) within 16.3 seconds as shown in Figure 7-32. Two makeup cycles were required to maintain the LOX tank ullage pressure before the ullage temperature stabilized. The pressurization control pressure switch controlled the pressure between 26.3 and 27.7 N/cm^2 (38.2 and 40.2 psia). At -98 seconds the LOX tank ullage pressure increased from 27.2 to 29.7 N/cm^2 (39.5 to 43.1 psia) due to fuel tank prepressurization, LOX tank vent purge and LOX pressure sense line purge. This caused the vent/relief valve to open, dropping the pressure down to 29.0 N/cm^2 (42.1 psia). The pressure remained at this level until liftoff.

During S-IC boost there was a relatively high rate of ullage pressure decay necessitating two makeup cycles from the cold helium spheres as shown in Figure 7-32. This decay is partially due to ullage cooling and partially due to tank geometry response to the vehicle axial acceleration. There is, correspondingly, a step rise in pressure proportional to acceleration changes at S-IC Inboard Engine Cutoff (IECO) and Outboard Engines Cutoff (OECO). There are also indications that the tank vent/relief and/or relief valve may have experienced intermittent leakage during the period from 105 seconds to S-IC cutoff. Although data are not conclusive, it appears that approximately 0.18 kilograms (0.4 lbm) of ullage gas was lost from the tank during this period. Ullage pressure at S-IC staging was 28.8 N/cm^2 (41.8 psia).

▽ S-IVB ENG START SEQUENCE COMMAND, 577.28
 ▽ S-IVB FIRST BURN STDY OPEN, 580.52
 ▽ S-IVB VELOCITY CUTOFF COMMAND, 747.04

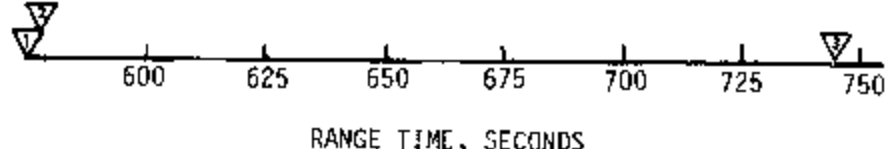
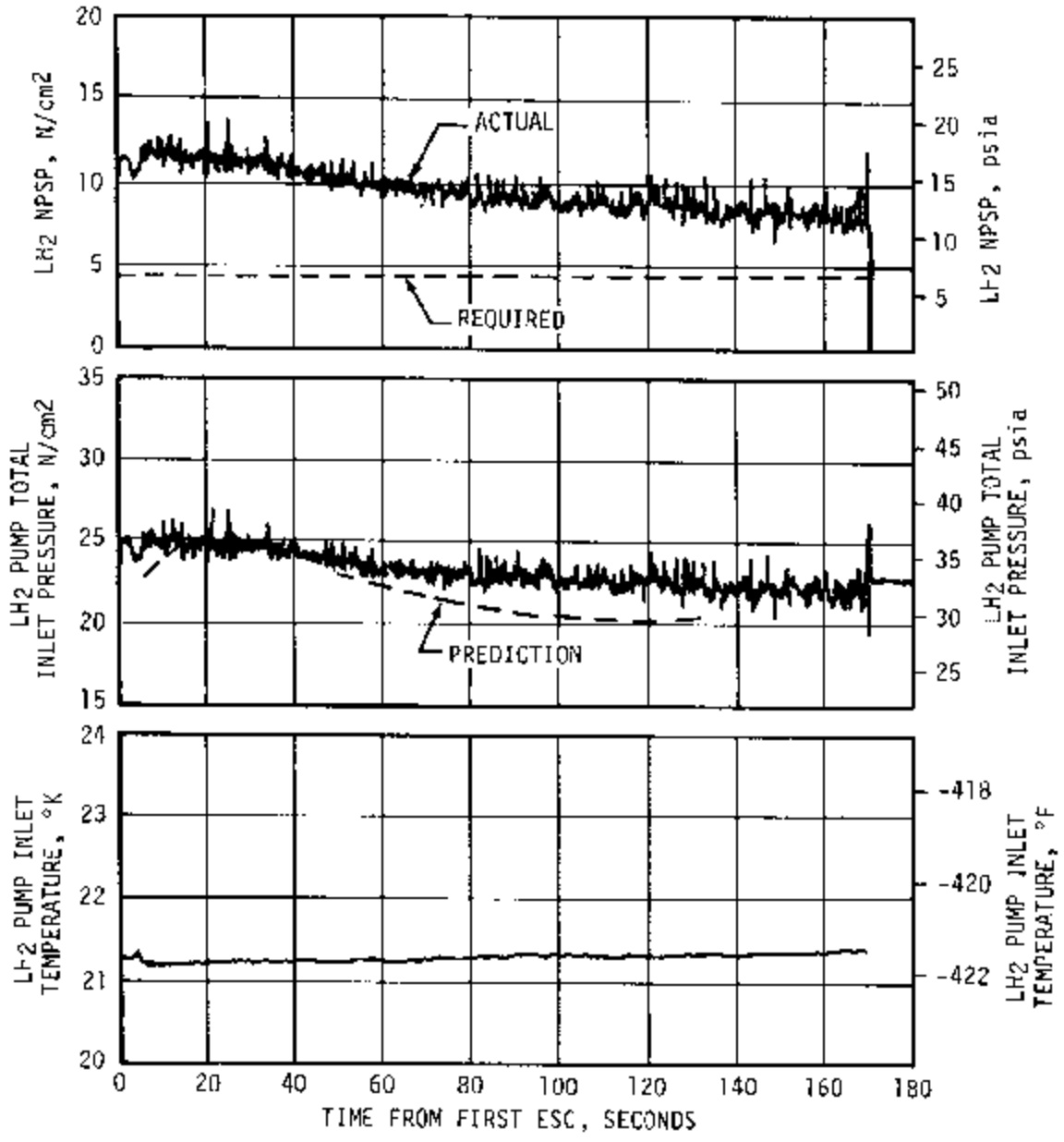


Figure 7-30. S-IVB Fuel Pump Inlet Conditions - First Burn

- ▽ S-IVB ENG RESTART COMMAND, 11,614.69
- ▽ S-IVB STDV OPEN, 11,622.92
- ▽ S-IVB ECO COMMAND AND START OF T₇, 11,630.33

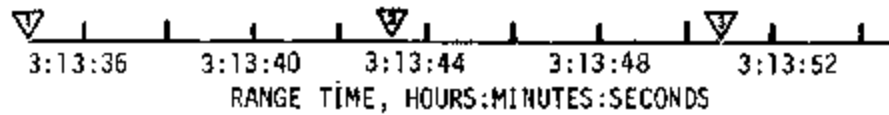
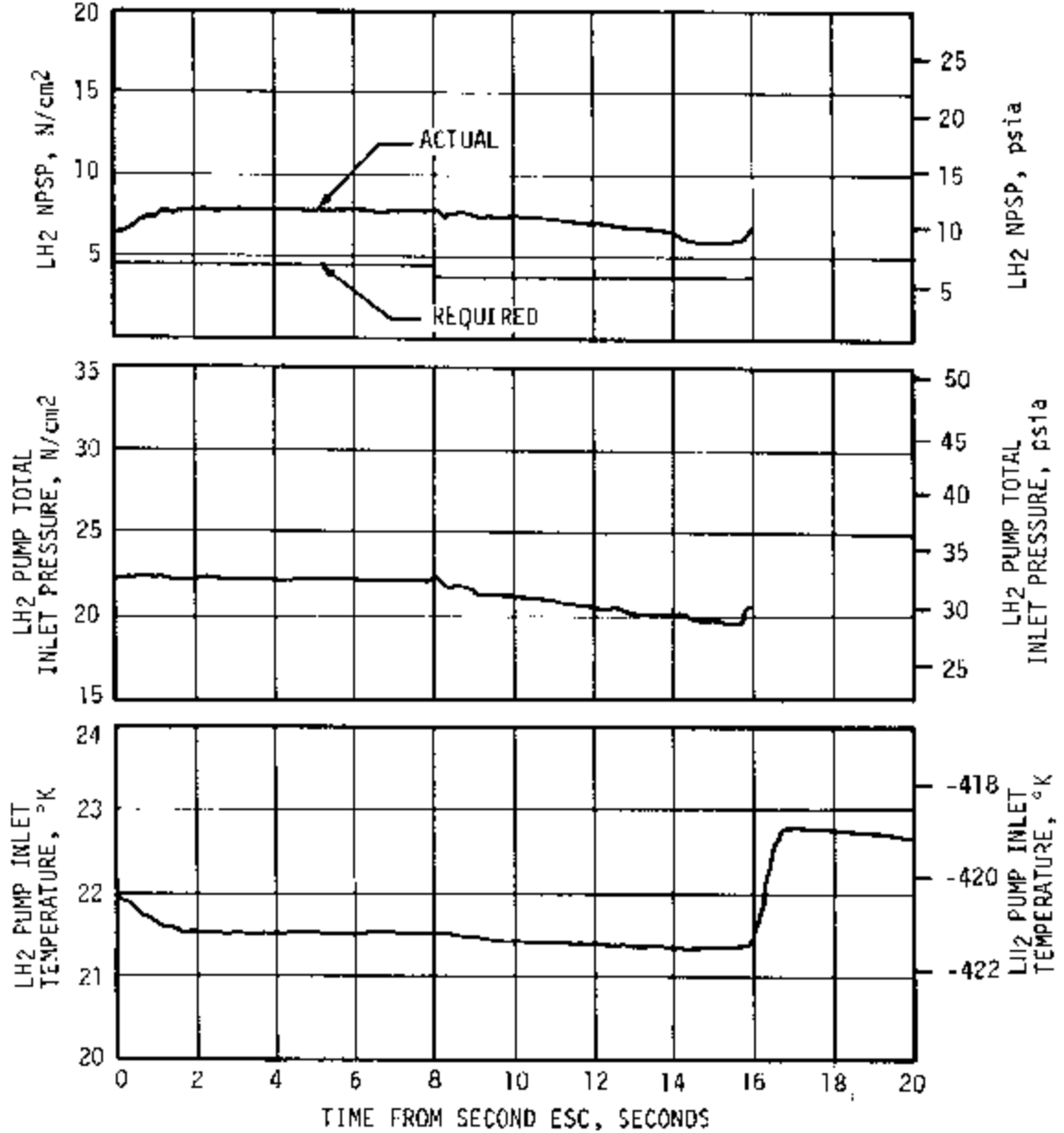


Figure 7-31. S-IVB Fuel Pump Inlet Conditions - Restart Attempt

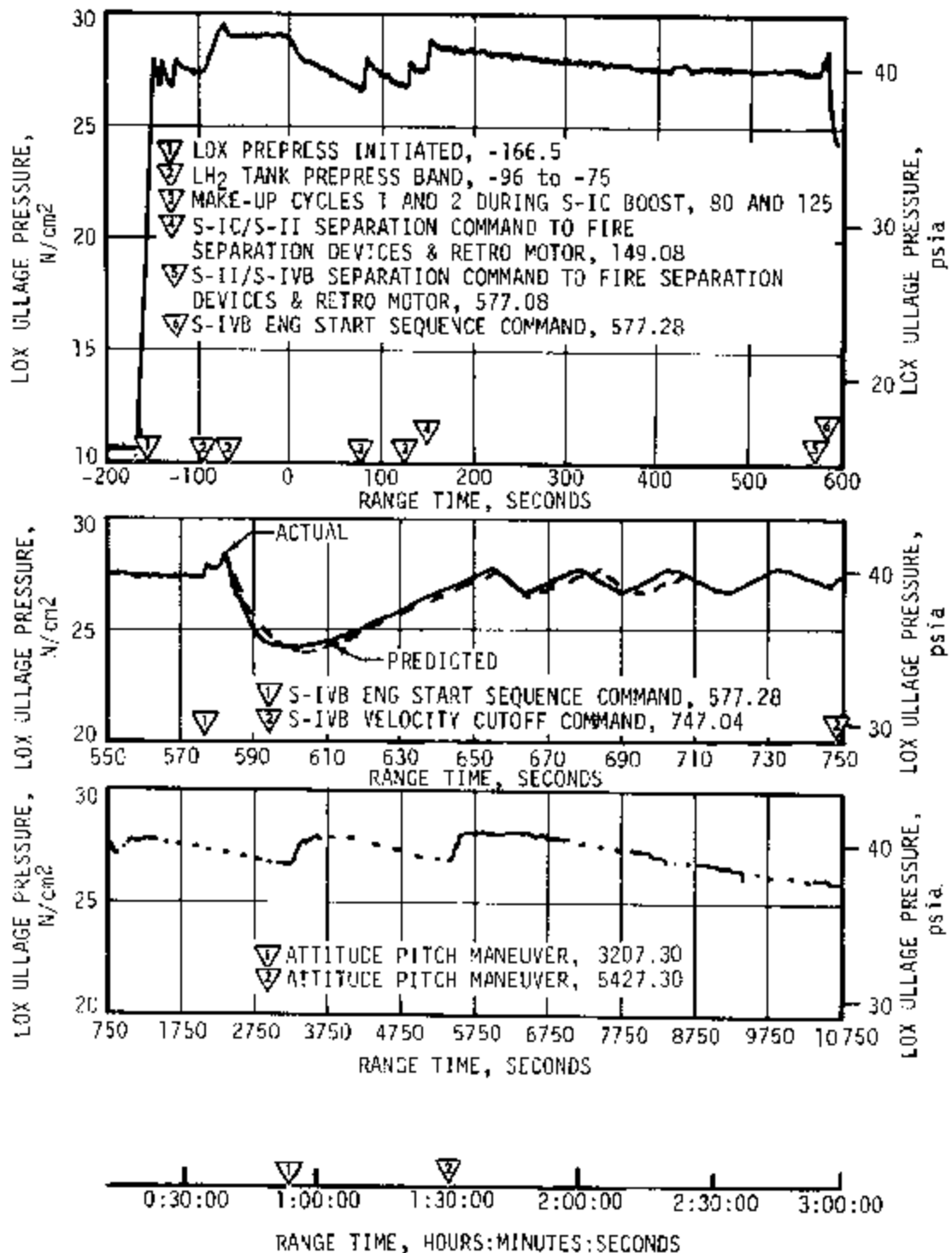


Figure 7-32. S-IVB LOX Tank Ullage Pressure - First Burn and Orbit

During the S-II boost there was a continuing pressure decay, but at a much reduced rate. No makeup cycles were required. Although ullage cooling continued during this period, the major cause of the decay again appears to be response to the vehicle acceleration; there is a step rise in pressure at S-II engines No. 2 and 3 out, and at S-II cutoff.

The LOX tank ullage pressure was 28.8 N/cm^2 (41.8 psia) at ESC, satisfying the engine start requirements as shown in Figure 7-32. During the start transient the ullage pressure decreased to a minimum of 24.2 N/cm^2 (35.1 psia) before the pressurant flowrate became large enough to increase the ullage pressure. During burn the ullage pressure cycled four times. The ullage pressure was sufficient to exceed the minimum NPSP requirements during powered flight.

The LOX tank pressurization flowrate variation was 0.16 to 0.18 kg/s (0.35 to 0.40 lbm/s) during over-control, and from 0.11 to 0.14 kg/s (0.24 to 0.31 lbm/s) during under-control system operation. This variation is normal because the bypass orifice inlet temperature changes as it follows the cold helium sphere temperature. Heat exchanger performance during first burn was satisfactory.

The LOX tank ambient repressurization system satisfactorily raised the tank ullage pressure from 25.7 to 27.7 N/cm^2 (37.3 to 40.2 psia) in 19.7 seconds. Helium consumption during repressurization was 2.4 kilograms (5.3 lbm) with the sphere pressure decaying from 2124 to 1327 N/cm^2 (3080 to 1925 psia). The tank ullage pressure was 28.7 N/cm^2 (41.6 psia) at second ESC, satisfying the engine start requirements.

The LOX tank pressurization system operated nominally considering the boundary conditions during the attempted restart shown in Figure 7-33. The regulator discharge rose rapidly to 276 N/cm^2 (400 psia) and remained at that level until the system was turned off at second ESC +16 seconds. The helium flowrate was 0.16 kg/s (0.35 lbm/s) and the total mass of helium used from the cold helium spheres was 1.3 kilograms (2.9 lbm).

The LOX NPSP calculated at the interface was 17.2 N/cm^2 (24.9 psi) at first burn ESC. The NPSP decreased after start and reached a minimum value of 14.5 N/cm^2 (21.1 psi) at 26 seconds after ESC. This was 0.10 N/cm^2 (0.15 psi) above the required NPSP at that time. The NPSP then increased and followed the LOX tank ullage pressure for the duration of first burn.

The LOX pump static interface pressure during first burn followed the cyclic trends of the LOX tank ullage pressure. Values ranged from 24.1 N/cm^2 (34.9 psia) at 26 seconds after ESC to 28.8 N/cm^2 (41.7 psia) immediately after first burn ESC. The NPSP calculated at the engine

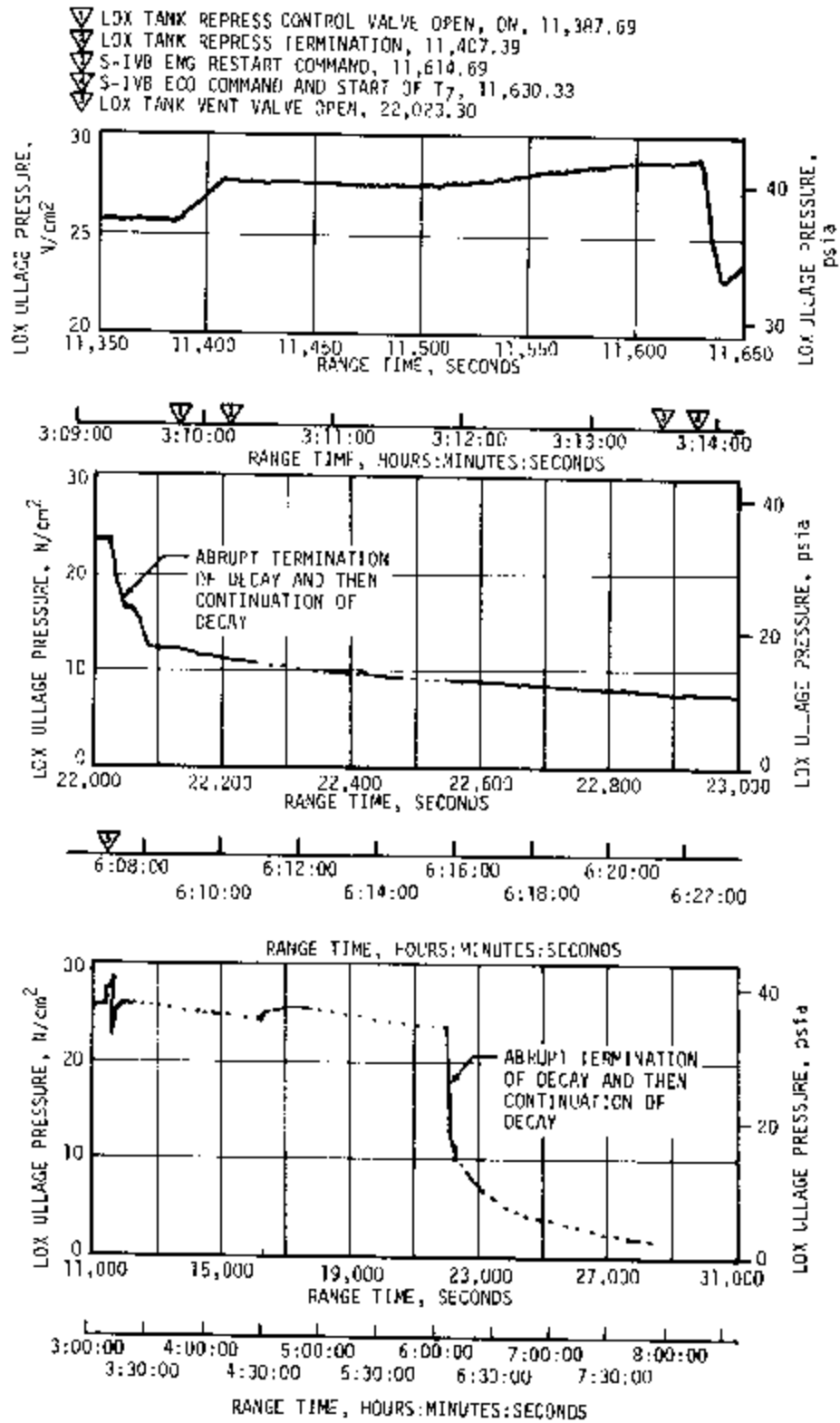


Figure 7-33. S-IVB LOX Tank Ullage Pressure - Restart Attempt

interface was 18.5 N/cm^2 (26.8 psia) at second burn ESC. At all times during second burn attempt, NPSP was above the required level. Figures 7-34 and 7-35 summarize the LOX pump conditions for the first burn and the second burn restart attempt, respectively. The run requirements for first and second burn were satisfactorily met as previously presented.

The cold helium supply was adequate to meet all flight requirements. At first burn ESC the cold helium spheres contained 151 kilograms (332 lbm) of helium at a pressure 2027 N/cm^2 (2940 psia). At the end of the 166.52-second engine burn, the helium mass had decreased to 124 kilograms (273 lbm) at a pressure of 951 N/cm^2 (1380 psia). Following first burn ECO the cold helium sphere pressure data indicated a decay of approximately $2.0 \text{ N/cm}^2/\text{min}$ (2.9 psi/min) as shown in Figure 7-36, resulting in an apparent pressure at second burn ESC of 593 N/cm^2 (860 psia). The cause of this decline is still under extensive investigation; areas of interest include the cold helium system conoseals and joints, the LOX pressurization module, and the cold helium sphere pressure transducer. Figure 7-37 shows these areas of interest. The conoseals will be changed to 7C75 aluminum coated with teflon throughout the cold helium system for AS-503 and subsequent vehicles. Conoseal re-torquing requirements are also being considered.

During the restart attempt the LOX pressurization system was activated for approximately 8 seconds, dropping the cold helium sphere pressure to 572 N/cm^2 (830 psia); mass usage during this period was 1.1 kilograms (2.4 lbm). Following the restart attempt the sphere pressure data continued to decrease, reaching 379 N/cm^2 (550 psia) by 22,023.30 seconds. From this time until loss of stage power the cold helium spheres were dumped overboard through the LOX tank vent valve. Inaccuracy in the sphere pressure data (negative pressure data during the dump as shown in Figure 7-36 invalidates mass calculations during this period.

After the stage failed to restart a decision was made to vent the LOX tank and cold helium spheres in an attempt to gain additional data pertaining to stage safing. The LOX tank vent valve and the cold helium shutoff valves were commanded open at 22,023.30 seconds as shown in Figure 7-33. The cold helium pressure began a smooth blowdown to zero psia and the LOX tank ullage pressure began to blowdown from its 23.8 N/cm^2 (34.5 psia) level. However, at 22,047 seconds with the ullage pressure at 16.5 N/cm^2 (23.9 psia), the pressure decay abruptly terminated, and pressure remained constant until 22,061 seconds at which time the blowdown abruptly resumed and continued as long as data was available. During the period when the ullage pressure remained constant, both the tank vent valve and the cold helium shutoff valves remained open. The reason for this plateau is presently under investigation.

There is a noticeable change in the rate of pressure decay occurring at 22,085 seconds which is coincident with all of the LOX liquid temperature

- ▽ S-IVB ENG START SEQUENCE COMMAND, 577.28
- ▽ S-IVB FIRST BURN STDV OPEN, 580.52
- ▽ S-IVB VELOCITY CUTOFF COMMAND, 747.04

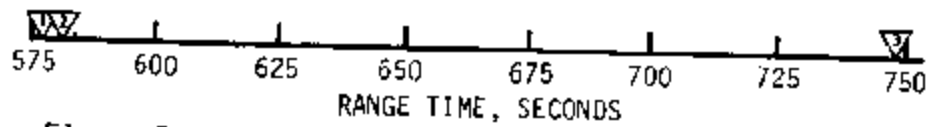
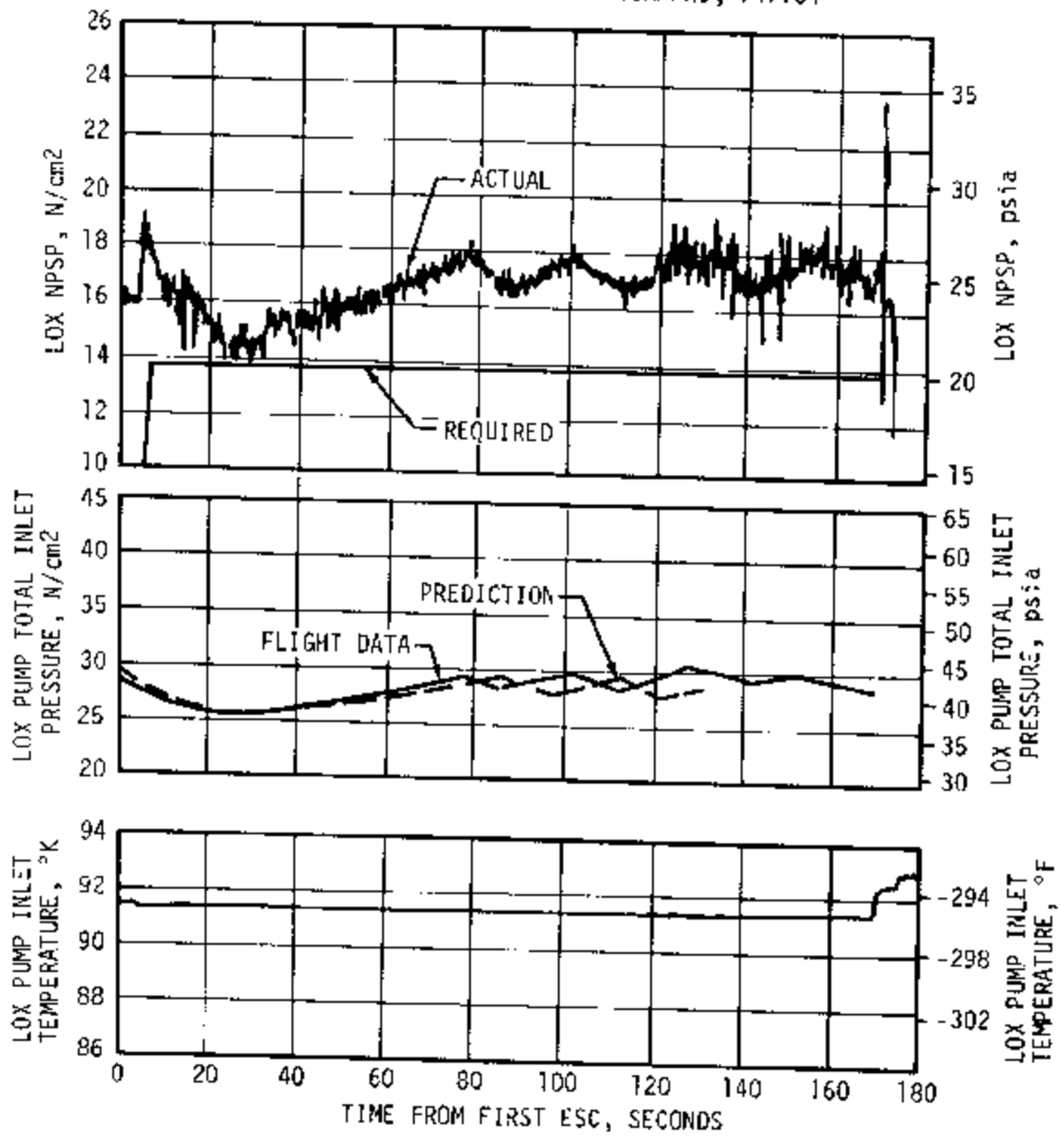


Figure 7-34. S-IVB LOX Pump Inlet Conditions - First Burn

- ▽ S-IVB ENG RESTART COMMAND, 11,614.69
- ▽ S-IVB STDV OPEN, 11,622.92
- ▽ S-IVB ECO Command and Start of T₇, 11,630.33

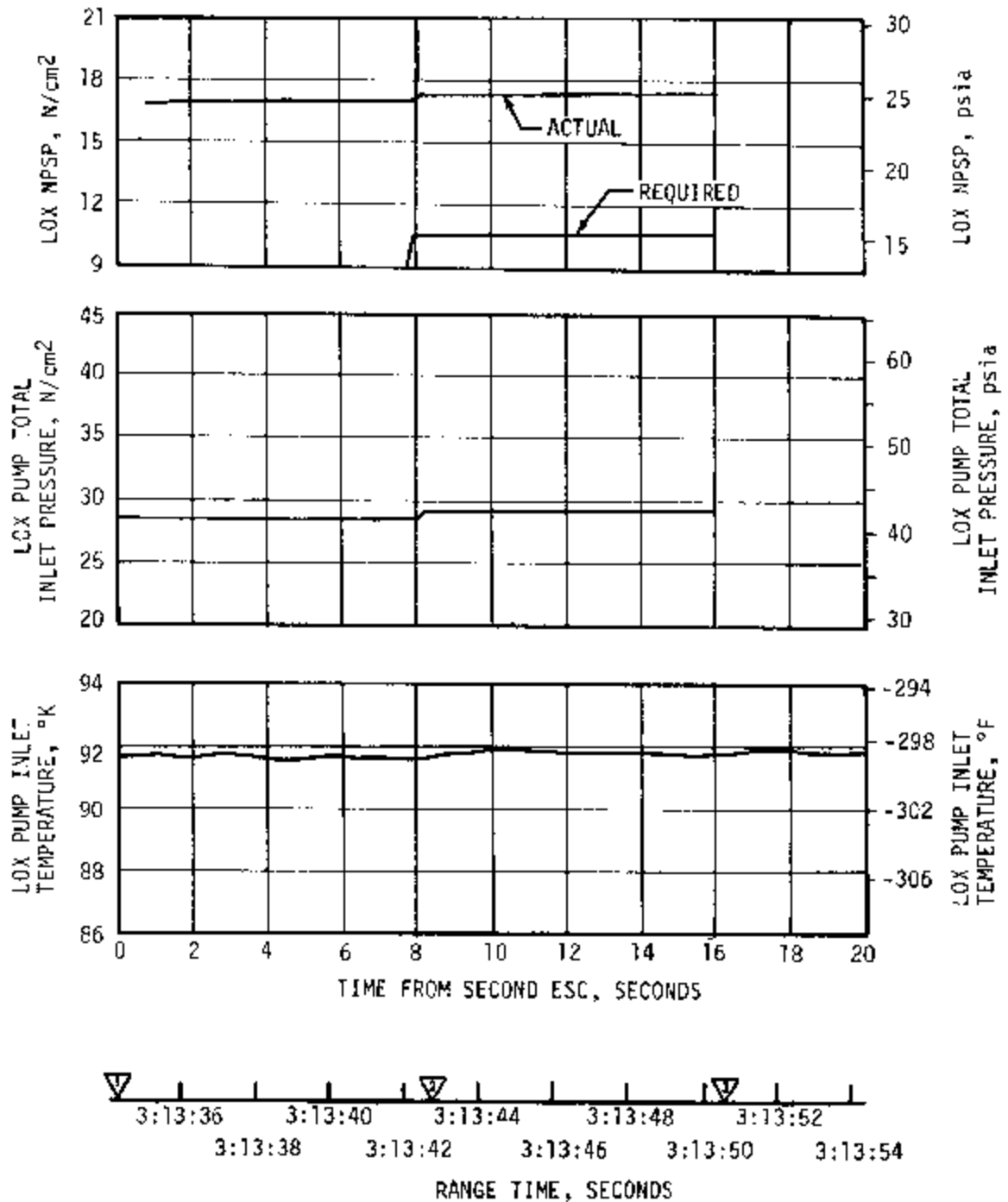


Figure 7-35. S-IVB LOX Pump Inlet Conditions - Restart Attempt

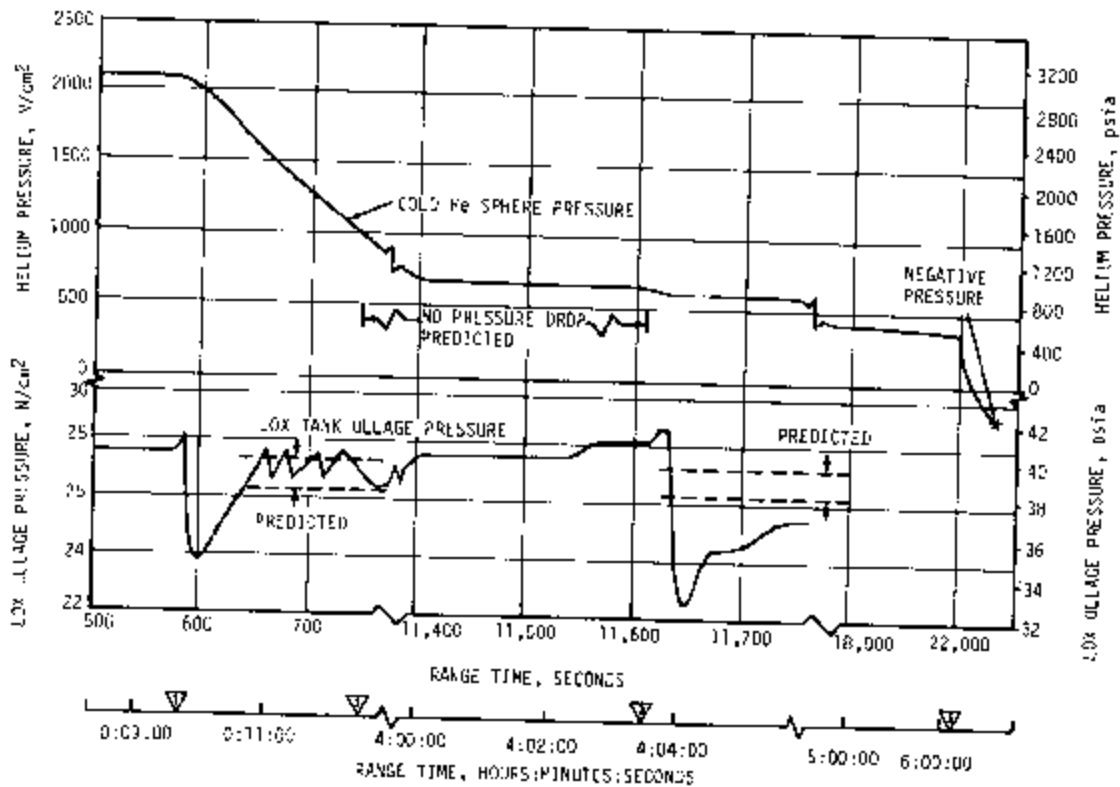
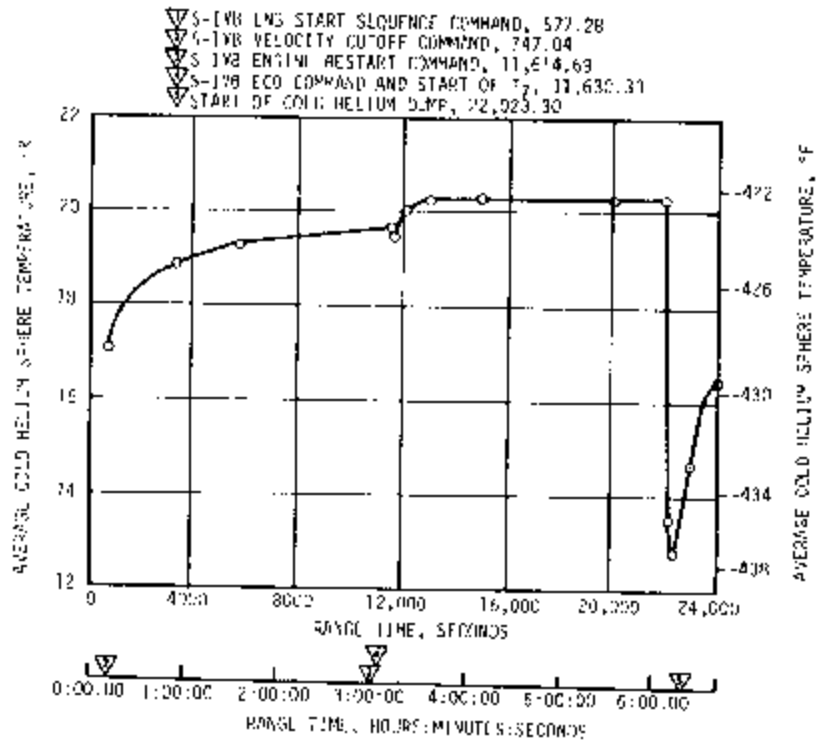


Figure 7-36. S-IVB Cold Helium Supply Decay

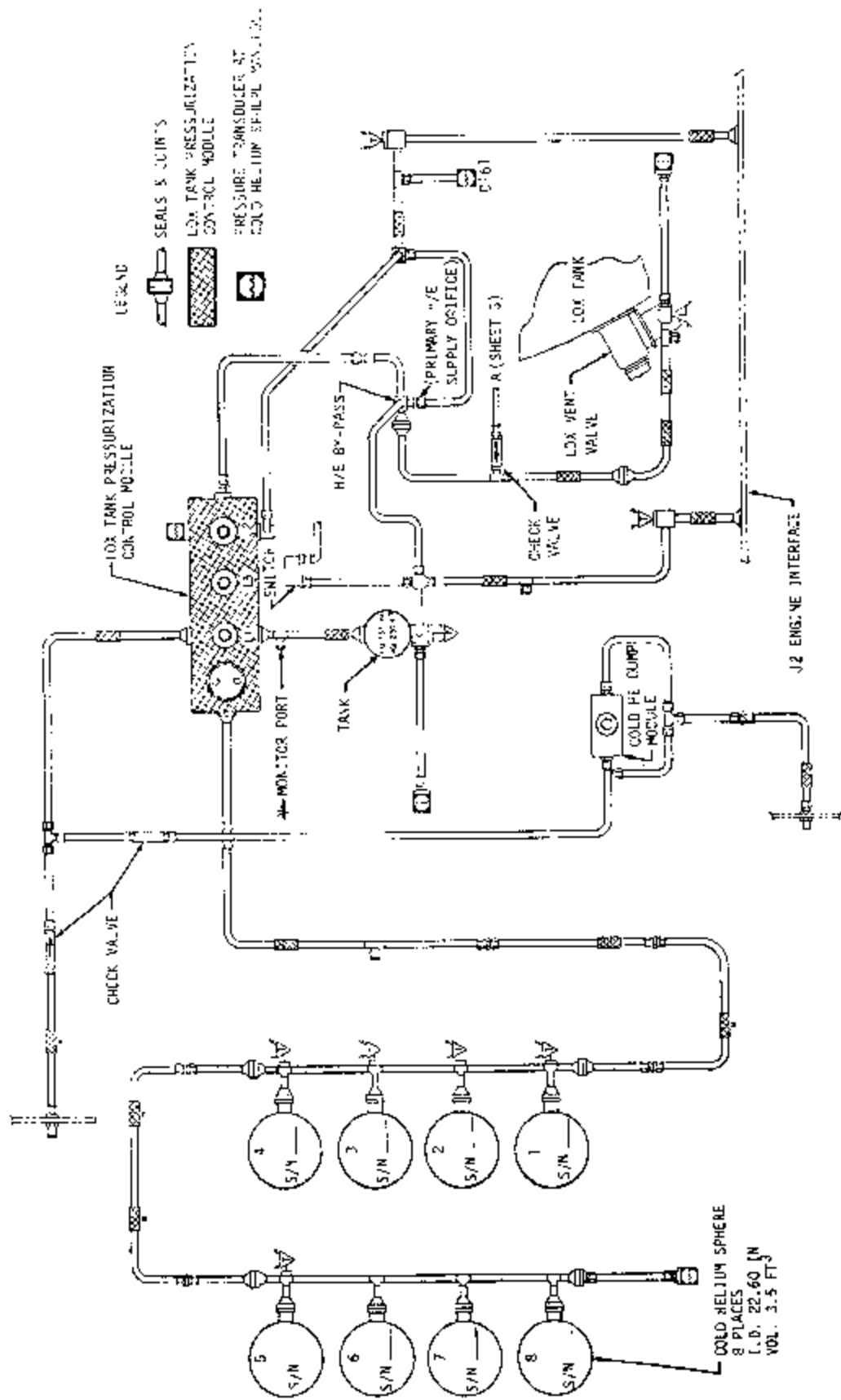


Figure 7-37. S-IVB Cold Helium Pressurization Schematic

measurements converging at 91.7°K (-294.5°F). This is the saturation level correlating with 12.2 N/cm² (17.7 psia). The ullage pressure was indicating 12.5 N/cm² (18.2 psia) at this time, suggesting that LOX boiloff is responsible for the change in the rate of pressure decay.

Although a definitive analysis has not yet been performed, the length of the pressure decay (approximately 11,000 seconds were required to drop the ullage pressure to 0.7 N/cm² [1 psia]) suggests that the vent path is highly restricted from its nominal 103 cm² (16 in.²). At 0.7 N/cm² (1 psi) the flowrate through an opening of this size would be sufficient to vent the tank completely in 500 to 1000 seconds.

Investigation of both the ullage pressure plateau at 16.5 N/cm² (23.9 psia) and the vent line restriction is continuing.

7.11 S-IVB PNEUMATIC CONTROL SYSTEM

The pneumatic control subsystem provides supply pressure for all stage pneumatically operated valves with the exception of J-2 engine valves but including the engine start tank vent valve. A pneumatic power control module regulates filtered ambient helium flowing from the ambient helium sphere loaded to a pressure of 2136 ±68.9 N/cm² (3100 ±100 psia) at 294°K (70°F). The module regulates pressure down to 338 ±17 N/cm² (490 ±25 psia) for operation of the following:

- a. LH₂ directional control valve during ground procedures.
- b. Propulsive vent shutoff valve during powered flight.
- c. LOX and LH₂ fill and drain valves during ground procedures.
- d. J-2 engine GH₂ start subsystem vent-relief valves.
- e. LOX and LH₂ turbopumps turbine purge module.
- f. LOX chilldown pump purge module control.
- g. LOX and LH₂ prevalues.
- h. LOX and LH₂ chilldown shutoff valves.
- i. LOX tank vent-relief valve.
- j. LH₂ propulsive vent valve.

The pneumatic control and purge system performed satisfactorily during all phases of the mission. System performance was nominal during boost and first burn operations. The AS-502 stage incorporated the redesigned

pneumatic actuation control modules, and experienced no discernible leakage as opposed to earlier stages which had significant degrees of leakage. Pneumatic control bottle temperature, pressure, and regulator outlet pressure are shown in Figures 7-38 through 7-40. Bottle masses at various pertinent times are shown in Table 7-9.

7.12 S-IVB AUXILIARY PROPULSION SYSTEM

The APS controls the vehicle attitude during S-IVB operation, and positions the propellants in the stage during first burn cutoff, parking orbit coast, second burn restart, and cutoff transient. Nitrogen tetroxide (N_2O_4) and monomethyl hydrazine (MMH) are the APS propellants. These propellants are hypergolic and require no ignition system. The APS system is composed of two modules located 180 degrees apart on the aft skirt assembly. All requirements are supplied from within the modules except the electrical power signals which are required from the stage. Each module contains three ablatively cooled, 667 Newtons (150 lbf) thrust, attitude control engines; and one ablatively cooled, 311 Newtons (70 lbf) thrust, ullage positioning engine. The attitude control engines control S-IVB roll during engine burn and pitch, yaw, and roll during orbital coast. The ullage positioning engine fires to assure the presence of liquid propellants at the J-2 engine pump inlets during engine chilldown and restart, and to settle the propellants prior to propulsive venting to prevent the loss of liquid propellants through the vent systems.

The APS pressurization systems demonstrated nominal performance throughout the flight and met control system demands as required until APS propellant depletion. The regulator outlet pressures were maintained at 134 N/cm^2 (195 psia). The APS ullage pressures in the tanks were approximately 132 N/cm^2 (192 psia).

The oxidizer and fuel supply systems performed as expected during the flight. The propellant temperatures measured in the propellant control module were as expected. The maximum temperature recorded was 317°K (110°F). The bulk temperatures of the propellants in the bladder ranged from 306 to 311°K (90 to 100°F). The propellant supply pressures were nominal at approximately 131 N/cm^2 (190 psia) during the mission.

The APS engine performance was as expected with the exceptions noted in the following paragraphs:

The propellants were depleted in both modules as a result of disturbances induced during first burn and after attempted restart. Because of the failure to restart, the LOX and LH_2 residuals were much greater than predicted. As a result of this condition and spacecraft separation the vehicle's moments of inertia were larger, and the Center of Gravity (CG) further aft than predicted. With the CG low, the APS pitch and yaw moment arms were shorter than expected, resulting in longer APS burn times.

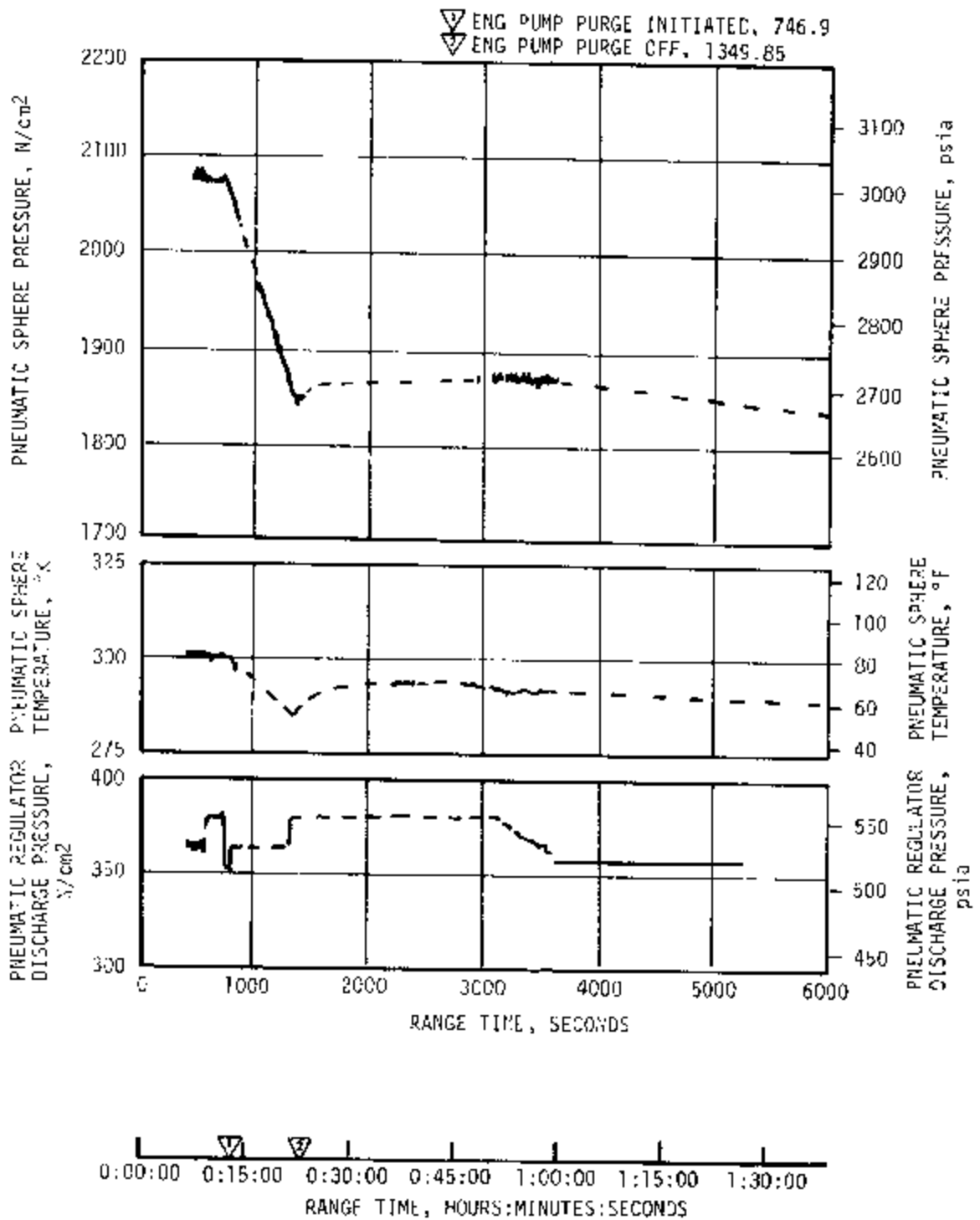


Figure 7-38. S-IVB Pneumatic Control Performance - First Burn

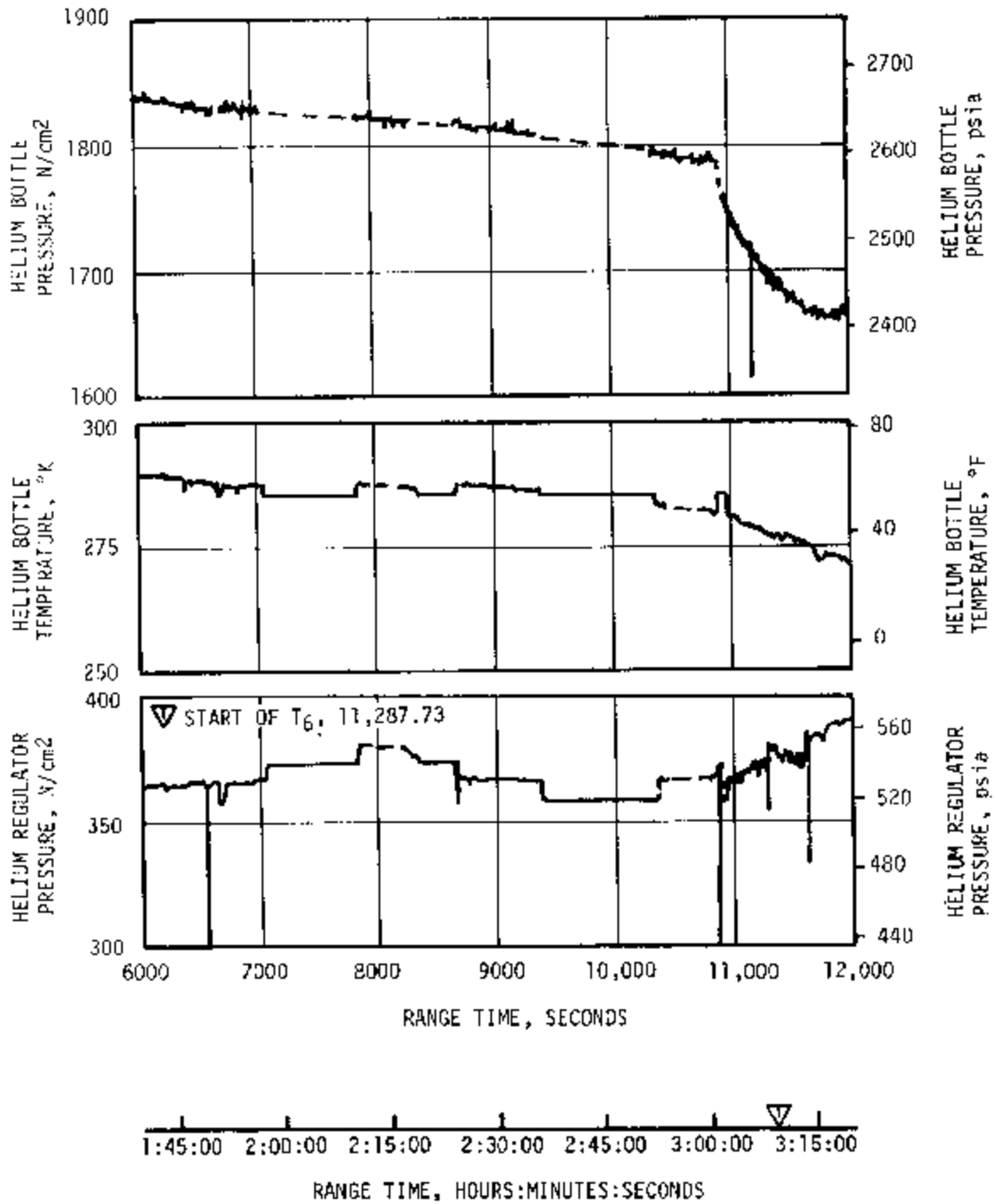


Figure 7-39. S-IVB Pneumatic Control Performance - Coast Phase

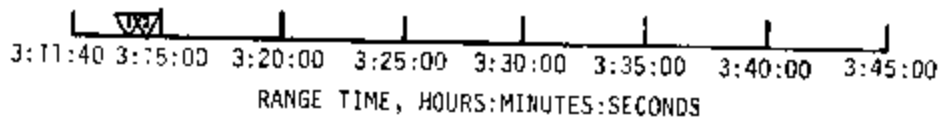
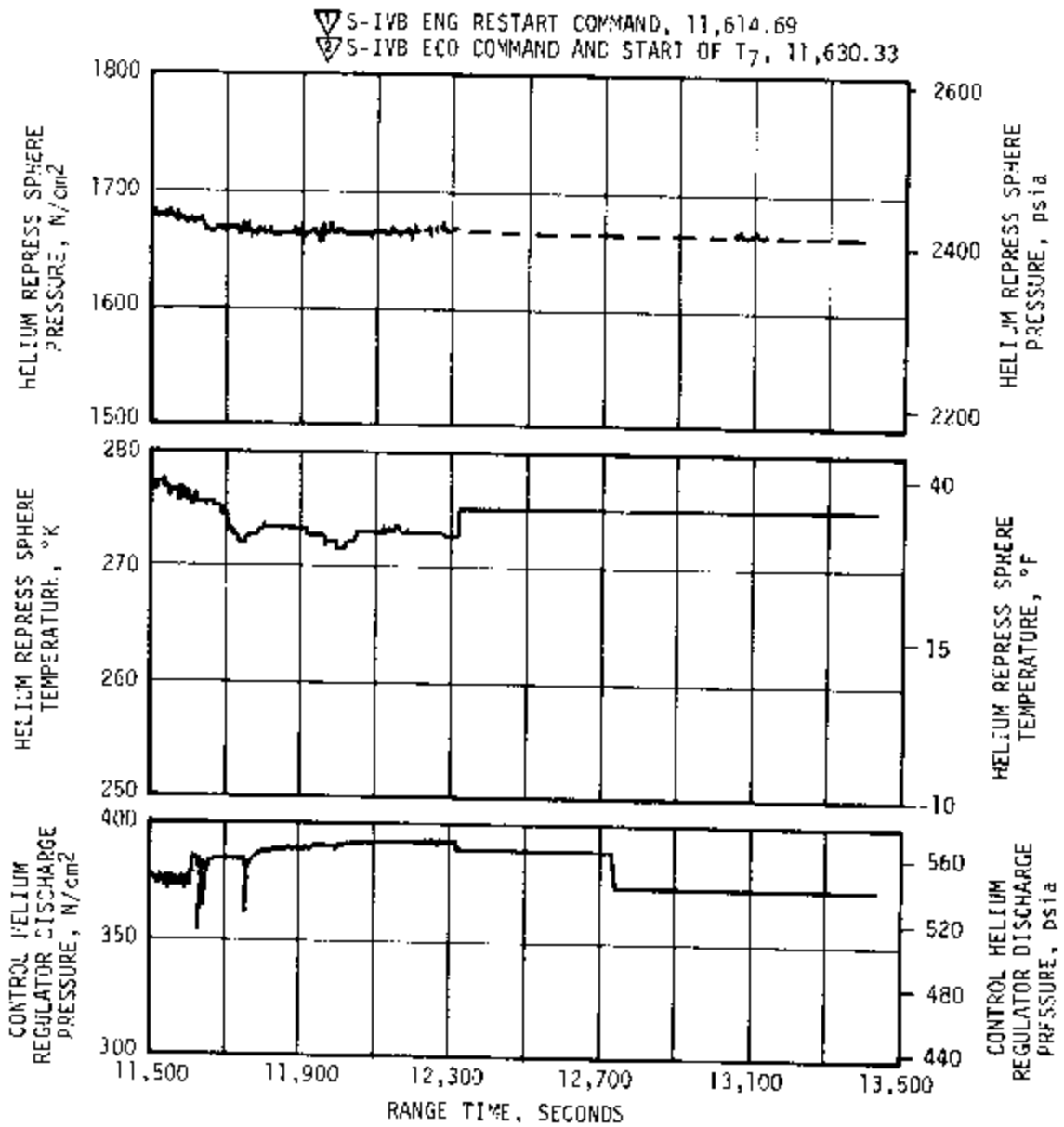


Figure 7-40. S-IVB Pneumatic Control Performance - Restart Attempt

Table 7-9. S-IVB Pneumatic Helium Bottle Mass

TIME	BOTTLE MASS	
	kg	lbm
Liftoff	3.87	8.54
First Burn ESC	3.85	8.48
First Burn ECO	3.85	8.48
3500 sec	3.60	7.94
6500 sec	3.57	7.86
Second Burn ESC 11,614.69 sec, (03:13:34.69)	3.43	7.56
Second Burn ECO 11,630.33 sec, (03:13:50.33)	3.43	7.56
17,500 sec, (04:51:40)	3.42	7.54

The propellants in Module No. 1 (at Position I) were depleted first as shown in Figure 7-41. The fuel was depleted at 21,953 seconds, while the oxidizer was depleted at 22,053 seconds. The fuel was also depleted first in Module No. 2 (at position III) (22,602 seconds) as shown in Figure 7-42. The oxidizer was depleted at 22,634 seconds. The reason the fuel was depleted first in both modules was that the propellants were loaded for a 1.65 EMR to 1.0 EMR while the attitude control engines normally operate at a 1.60 EMR during minimum impulse bit pulsing. This EMR was dropped even further due to the high injector temperatures causing oxidizer vaporization and reduced oxidizer flow. The fuel load for the flight was maximum. Table 7-10 presents the APS oxidizer and fuel consumption at significant events during the flight. The APS helium bottle pressures and propellant quantities derived from the helium bottle pressures are presented in Figures 7-43 and 7-44.

The engine chamber pressures were normal and ranged from 64 to 69 N/cm² (93 to 100 psia) during the initial portion of the flight. However, at approximately 6000 seconds, the chamber pressure of the first pulse in a series of pulses on engine No. III was 41 N/cm² (60 psia). The chamber pressure increased to a nominal value as the series of pulses continued. Figure 7-45 shows an example of this phenomenon. This initial low chamber pressure has been attributed to a high injector temperature as a result of heat soakback of the injector resulting from heavy APS duty cycles following first J-2 burn.

Engine No. III and IIIII had similar low chamber pressures following the long steady state burns on these engines after attempted restart. The

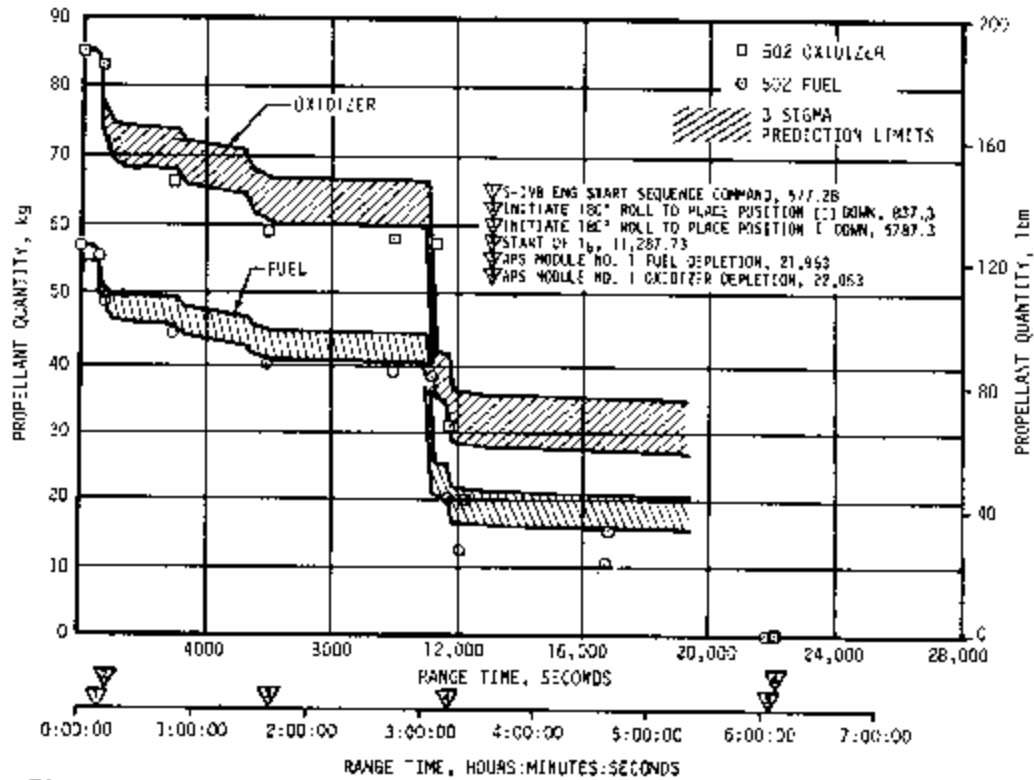


Figure 7-41. S-IVB APS Propellant Predictions - Module No. 1

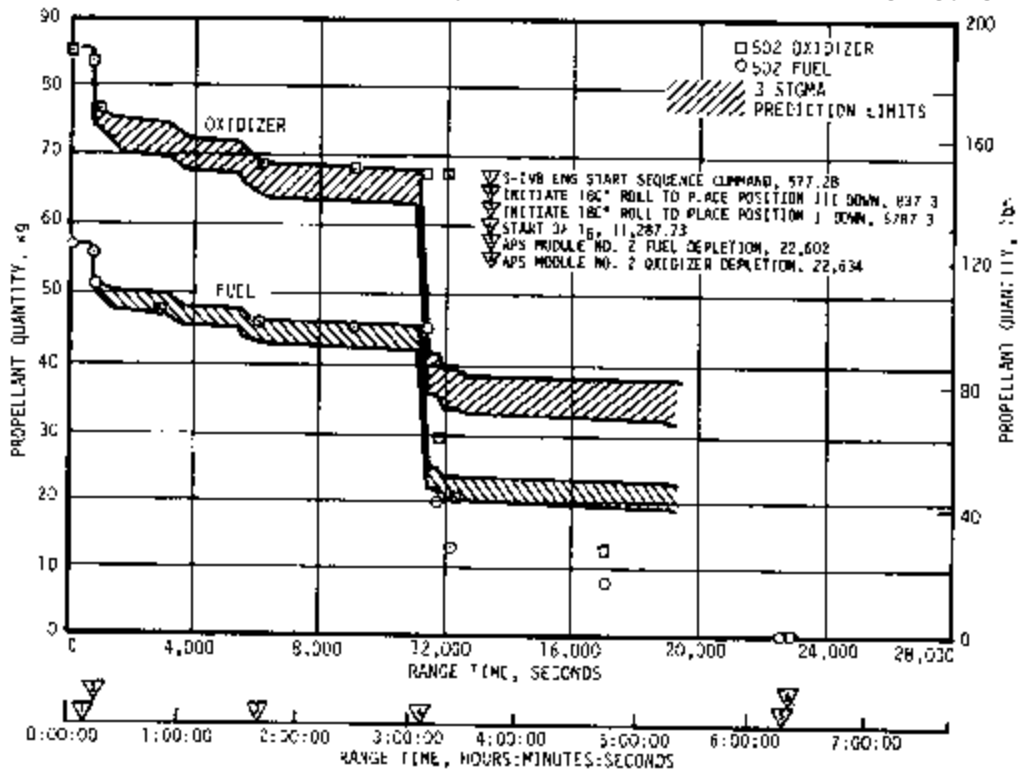


Figure 7-42. S-IVB APS Propellant Predictions - Module No. 2

Table 7-10. S-IVB APS Propellant Consumption

TIME PERIOD	MODULE AT POSITION I				MODULE AT POSITION III			
	OXIDIZER		FUEL		OXIDIZER		FUEL	
	kg	(lbm)	kg	(lbm)	kg	(lbm)	kg	(lbm)
Initial Load	85.6	(188.6)	56.5	(124.4)	86.0	(189.4)	56.6	(124.7)
First J-2 Burn Roll Control	0.7	(1.6)	0.5	(1.0)	0.7	(1.6)	0.5	(1.0)
J-2 ECO to End of First APS Ullaging	12.8	(28.1)	9.8	(21.6)	6.6	(14.5)	5.0	(11.1)
1st and 2nd Earth Revolutions	20.5	(45.3)	12.8	(28.2)	13.0	(28.7)	8.1	(18.0)
Restart Preparations	22.9	(50.5)	17.0	(37.4)	23.4	(51.5)	17.3	(38.1)
Attempted J-2 Restart to Propellant Depletion	28.7	(63.1)	16.4	(36.2)	42.3	(93.1)	25.7	(56.5)

injector temperature of engine No. IIIII increased to a maximum temperature of 406°K (270°F) during this period. Although the injector temperatures of engine No. III could not be obtained at this time because of loss of the measurements, it is thought that its temperature also exceeded 388°K (240°F). Both engines had pulses with chamber pressure as low as 38 N/cm² (55 psia). These were the initial pulses in a series. As the cooler propellants upstream of the injector reached the engine the chamber pressures increased to nominal values.

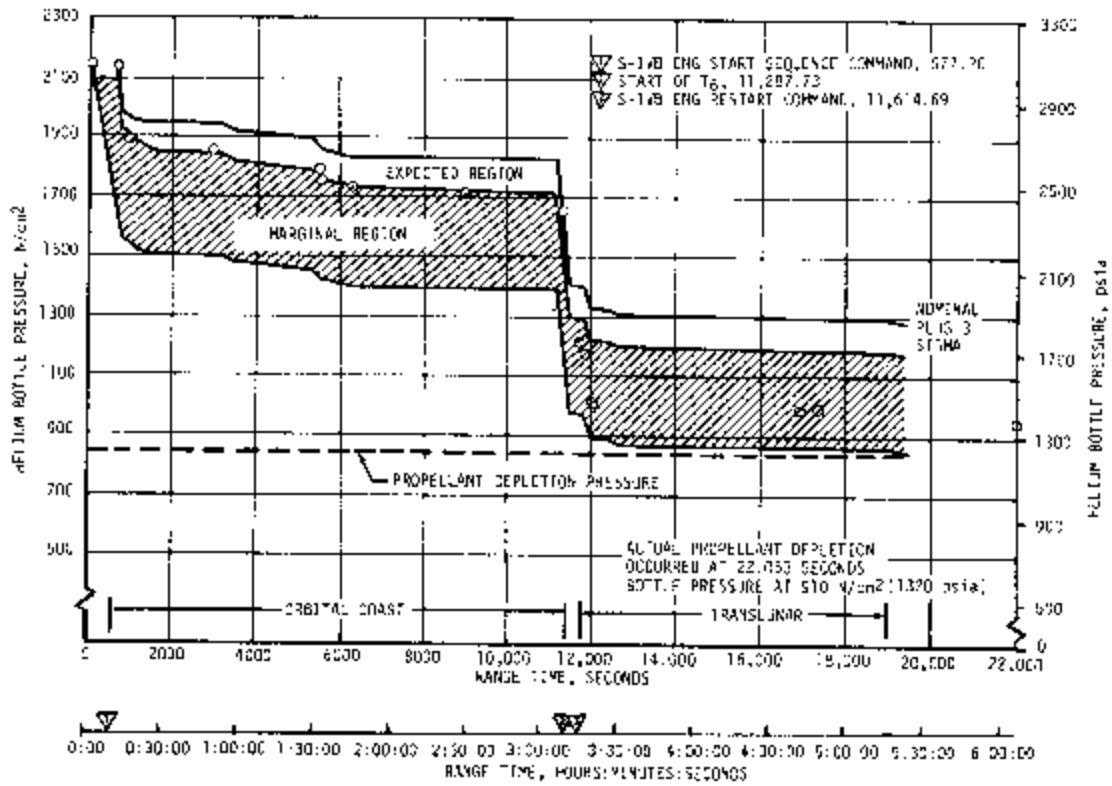


Figure 7-43. S-IVB Helium Bottle Pressure - Module No. 1

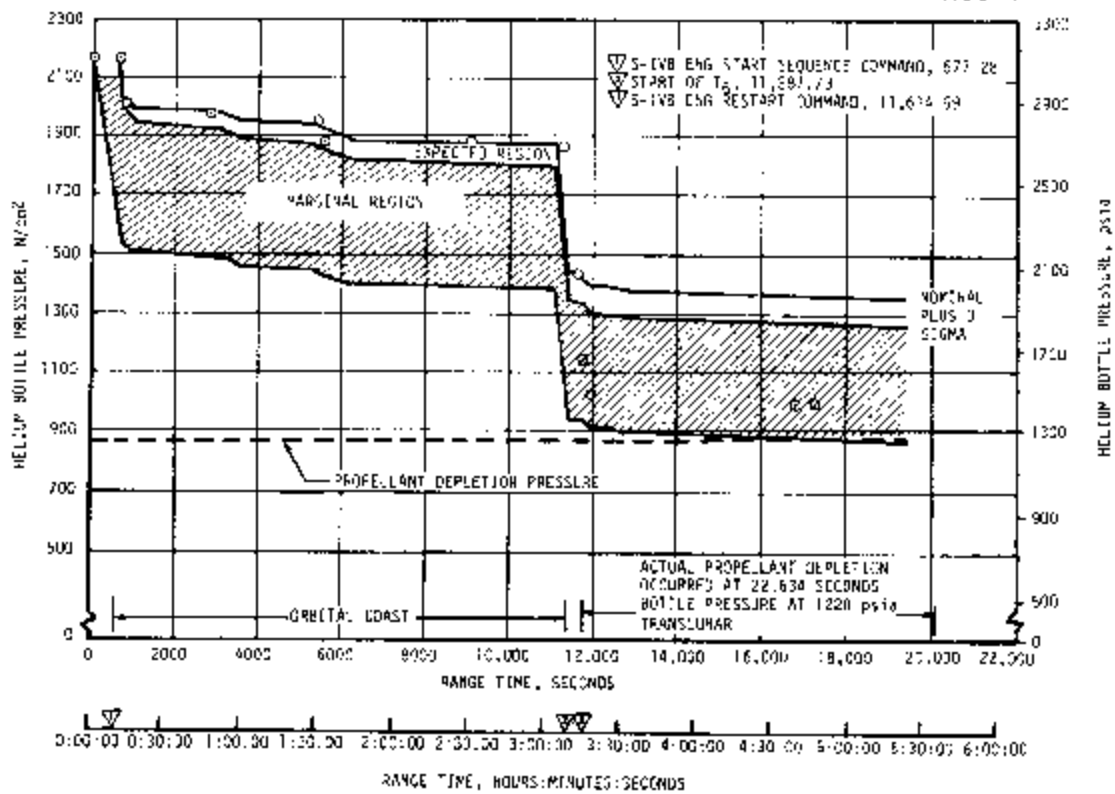
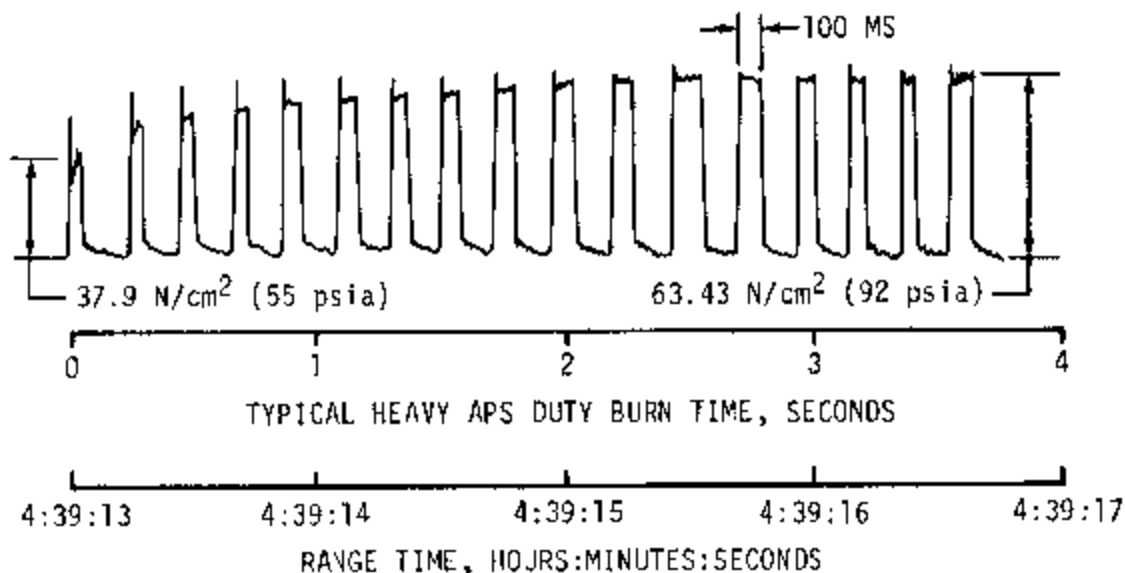
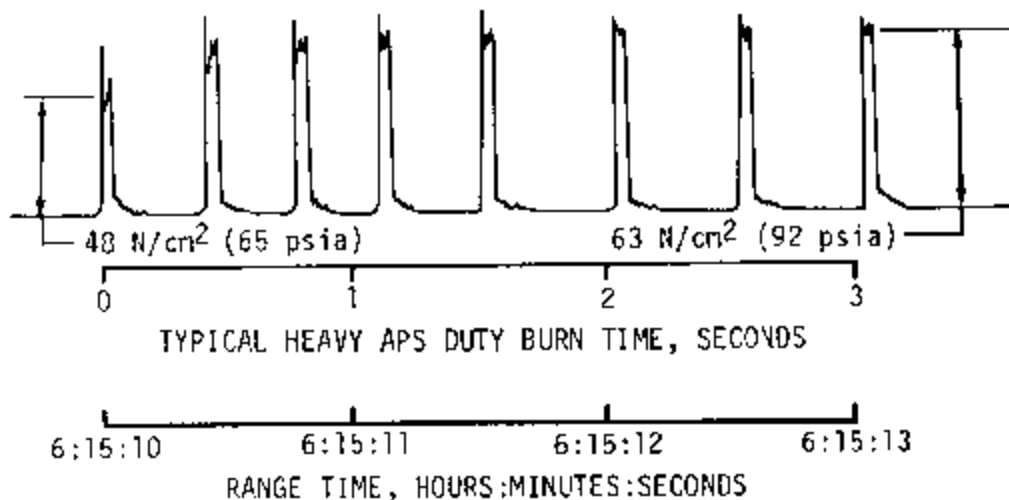


Figure 7-44. S-IVB Helium Bottle Pressure - Module No. 2

The APS ullage engine operation was normal with exception of the slightly extended chamber pressure decrease time of the Module 2 engine (following the second ullage burn cutoff, it required approximately 1 second longer than the Module 1 engine). This extended pressure decrease time did not occur at first ullage burn cutoff.



TYPICAL EXAMPLE OF INITIALLY
LOW CHAMBER PRESSURE
(NO TEMPERATURE DATA ON INJECTOR
WALL OR PROPELLANT MODULES)



INJECTOR WALL TEMP = 357°K (182°F) 22,500 TO 22,550 SEC
OXIDIZER MODULE TEMP = 304°K (87°F) 22,500 TO 22,550 SEC
FUEL MODULE TEMP = 304°K (87°F) 22,500 TO 22,550 SEC

Figure 7-45. S-IVB Chamber Pressure, APS Engine No. 2 - Module No. 2

SECTION 8

HYDRAULIC SYSTEMS

8.1 SUMMARY

The primary purpose of the hydraulic systems on each of the three booster stages is to provide vehicle thrust vector control during powered flight by controlling the thrust vector angle and direction of each of the moveable engines on command from the guidance and control system. In addition the S-IC stage hydraulic system also operates the engine control valves during engine start and shutdown operations. Since the S-IVB stage has only one engine, the Auxiliary Propulsion System (APS) modules provide roll corrections during S-IVB stage flight.

In general, the hydraulic systems performed satisfactorily in that the vehicle remained stable during all portions of guidance-controlled powered flight. No hydraulic system problems occurred during S-IC powered flight. S-II hydraulic systems performed within predicted limits, and operated satisfactorily until 280 seconds. At this time, the S-II engine No. 2 yaw actuator delta pressure transducer began to deviate significantly from expected values. The engine No. 2 yaw actuator showed a cryogenic effect between 280 seconds and 419 seconds. From 319 seconds until engine No. 2 cutoff, both the pitch and yaw actuators showed apparent side loads from the engine. After engine No. 2 cutoff, the yaw actuator performance indicates that it locked up. The engine No. 3 hydraulic system performed normally until engine shutdown when the system pump stopped operation and the pressures decayed. The engine No. 1 and engine No. 4 hydraulic systems performed normally throughout S-II powered flight. S-IVB hydraulic system performed within predicted limits during liftoff, boost, and first burn. During engine restart preparation and restart attempt, the system failed to produce hydraulic pressure. System temperatures observed during S-IVB first burn indicated the existence of a cryogenic fuel leak which led to the freezing of the hydraulic fluid and system blockage. During the restart attempt, measurements indicated that both the main and the auxiliary hydraulic pumps cavitated during operation and virtually no system pressure was produced.

At the present time there are no planned modifications to any of the stage hydraulic systems. The hydraulic system problems that occurred during this flight were related to the engine failures.

8.2 S-IC HYDRAULIC SYSTEM

The hydraulic system supplies high-pressure fluid, RJ-1 (kerosene), from a ground source to each of the five engines to control the engine starting sequence and to the four outboard engines for ground checkout of the Thrust Vector Control (TVC) system. During engine operation, high-pressure control fluid (RP-1) is supplied from the No. 1 fuel discharge of the turbopump assembly through the filter manifold to the servo valve and actuators for TVC. The fluid returns through the checkout valve to the No. 2 fuel inlet of the turbopump assembly. Hydraulic power is also used to close the engine control valves for engine shutdown.

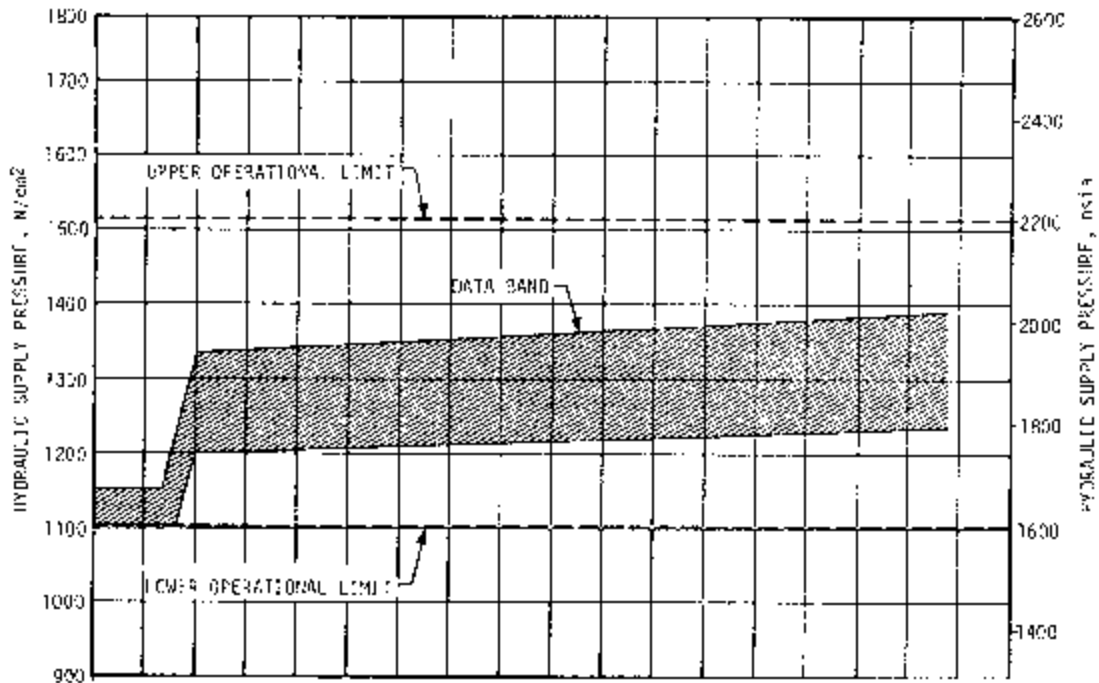
The S-IC stage incorporated four gimbal actuators of the Moog model (60B84500-1) and four of the Hydraulic Research model (50M04050-1). Analysis indicates that all actuators performed as commanded during the flight. The maximum actuator deflection was equivalent to 0.7 degree engine gimbal angle at the initiation of the vehicle roll program. The average hydraulic supply pressure was 1296 N/cm² (1880 psia) and operated in a small band within the operating limits as shown in Figure 8-1. The temperature as depicted by the return actuator fluid was 305°K (90°F) and operated within a narrow band. The maximum hydraulic engine valve opening pressure was 1392 N/cm² (2020 psia) and the maximum supply pressure to the actuators was 1378 N/cm² (2000 psia).

8.3 S-II HYDRAULIC SYSTEM

A complete, separate, and identical hydraulic system for each outboard engine provides power for gimbaling. The major system components include an engine-driven main pump, an auxiliary electric motor-driven pump, two electrically controlled, hydraulically powered servoactuators, and an accumulator reservoir manifold assembly. During S-IC powered flight, S-II hydraulic lockup valves are closed, holding the engines in a null position. After S-IC/S-II stage separation, a signal unlocks the accumulator lockup valves releasing high-pressure fluid to each of the two servoactuators. This fluid provides gimbaling power prior to main hydraulic pump operation. The main hydraulic pump, driven directly from the accessory drive pad of the engine LOX pump, provides actuator power during S-II powered flight.

S-II hydraulic system performance was essentially normal throughout the flight on engines No. 1 and 4, and on engine No. 3 until premature shutdown. System supply and return pressures and reservoir volumes were within predicted ranges. Reservoir fluid temperatures were close to the maximum predicted. Launch pad redlines were met with ample margins at liftoff for all four systems.

Several anomalies were apparent on engine No. 2 system throughout the flight. Actuator and reservoir temperatures of engine No. 2 leveled off



▽ S-IC 1000 (SOLENOID) ACTIVATION, 144.72
 ▽ S-IC 0000 SLEWED BY LYDC, START OF T₂, 148.41

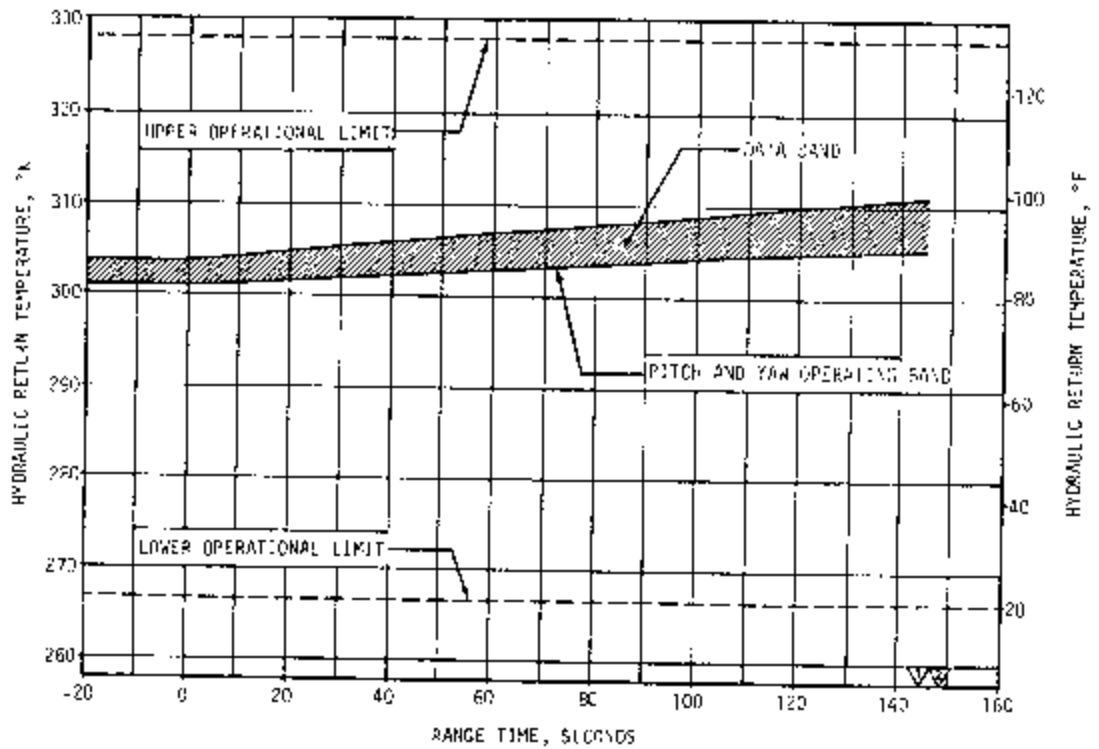


Figure 8-1. S-IC Hydraulic System Performance

early during S-II boost and then decayed while the other three systems rose normally. The differential pressure measurement (indicative of force) on the yaw actuator of engine No. 2 exhibited unusual ramp excursions. Both the pitch and yaw differential pressures increased suddenly at 319 seconds. At engine No. 2 cutoff, the reservoir volume dropped to zero, and the yaw actuator held its position.

Hydraulic system performance for engines No. 1, 3, and 4 is shown in Figure 8-2. Reservoir volumes were within the predicted range prior to cutoff of the respective engines. At engine No. 3 cutoff, the engine No. 3 reservoir volume increased in a normal manner as a result of accumulator depletion following spindown of the main hydraulic pump. Reservoir temperature increase was close to the predicted rate of increase. Temperature data for all four reservoirs and actuators were lost at 415 seconds as discussed in paragraphs 13.3 and 19.2.2. Accumulator pressures (indicative of system supply pressure) were within the predicted range of 2280 to 2620 N/cm² (3300 to 3800 psia) prior to Engine Cutoff (ECO). The decay in engine No. 3 accumulator pressure was normal and resulted from the accumulator depletion. The minimum reservoir volume was 13.0 percent of full versus the redline of 3.0 percent and was within the nominal predicted bands. The hydraulic fluid minimum pressure was 2410 N/cm² (3500 psia). The highest of the three systems fluid temperatures was approximately 306°K (90°F) at 415 seconds and all three were showing a normal upward trend at that time. These were well within the predicted limits as shown in Figure 8-2. Engines No. 1, 3, and 4 actuator forces were well below the predicted maximum of 84,500 Newtons (19,000 lbf). The maximum tensile force was 57,800 Newtons (13,000 lbf), which was exerted by the pitch actuator of engine No. 1. The maximum force in compression was 36,000 Newtons (8000 lbf) which was exerted by the yaw actuator of engine No. 4.

Prior to engine No. 2 cutoff, hydraulic parameters from all four engines followed predicted values except engine No. 2 reservoir and actuator fluid temperatures. Figure 8-3 shows that these temperatures leveled off between 270 and 290 seconds and then decayed. This is unlike the normal, continuous rise characteristic shown by the engine No. 3 reservoir temperature and is attributed to an abnormally low temperature environment in the vicinity of the engine No. 2 hydraulic system.

At 280 seconds, the engine No. 2 yaw actuator differential pressure measurement started a positive ramp increase as shown in Figure 8-4. This indication was apparently not a measure of increasing pressure, but the result of cryogenic fluid coming in contact with the transducer. This effect has been reproduced in tests performed at MSFC and at the S-II stage contractors' test facility. The transducer utilizes two Bourdon tubes to sense pressure difference. In the tests, LN₂ was sprayed on the actuator and caused the instrument to show a pressure difference as shown in Figure 8-4 although no pressure was applied to the actuator. The indication rose, peaked, and then decayed apparently because one of

▽ S-II HYDRAULIC ACCUMULATORS, UNLOCK, 151.38
 ▽ S-II STAGE ENG NO. 3 OUT, 414.78

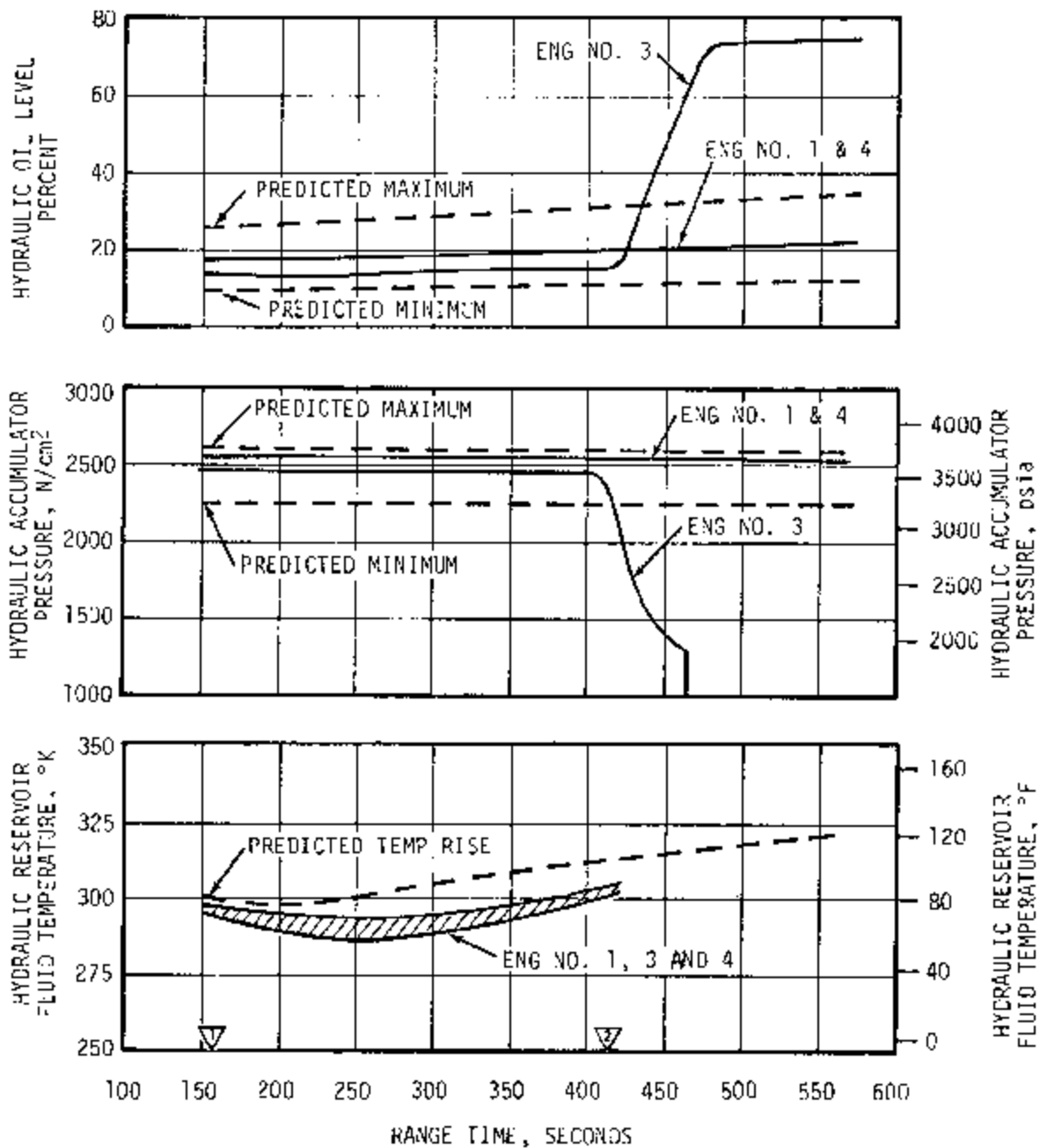


Figure 8-2. S-II Hydraulic System Performance

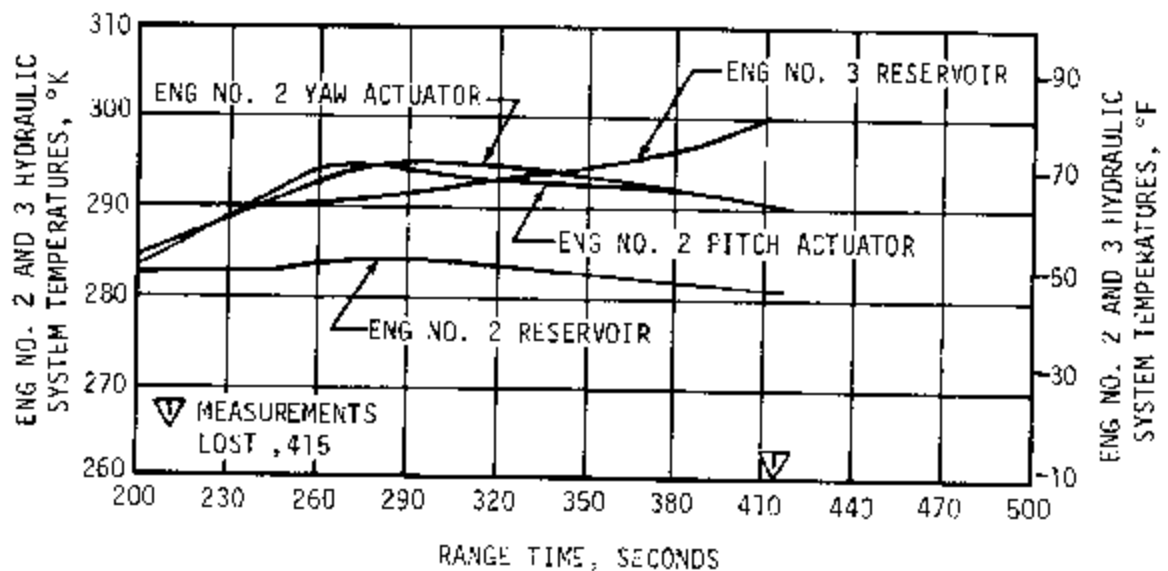


Figure 8-3. S-II Engines No. 2 and 3 Hydraulic System Temperature

the Bourdon tubes was cooled first and then the other. When both tubes had been cooled to the same temperature, indications are that transducer was again able to measure differential pressure.

The ramp increase continued until 319 seconds when the apparent force on the yaw actuator had reached 80,000 Newtons (18,000 lbf). At 319 seconds, the engine No. 2 pitch and yaw actuators showed a step increase in pressure which was apparently caused by a side load on the engine. The apparent force on the yaw actuator rose rapidly to 101,000 Newtons (22,700 lbf) as a constant force of approximately 21,000 Newtons (4700 lbf) was added to the temperature-induced indication. At the same time, the force on the pitch actuator increased to 32,000 Newtons (7000 lbf). These constant forces remained until engine No. 2 cutoff. The total yaw actuator force indication continued to increase from 101,000 Newtons (22,700 lbf) and reached a maximum of 125,000 Newtons (28,000 lbf) at 336 seconds, when it started a decay which reached 13,000 Newtons (3000 lbf) at 416 seconds.

In engine static firing tests conducted at MSFC, these actuator hydraulic pressure changes and engine movements have been reproduced. In the tests, a LOX-rich Augmented Spark Igniter (ASI) mixture ratio was used. This caused the main injector to be eroded. This, in turn, made a hole in the aft portion of the thrust chamber. Expanding gases from this hole created a side thrust which caused effects very similar to those observed in flight as shown in Figure 8-4. The engine failure analysis is described in detail in paragraph 6.3.

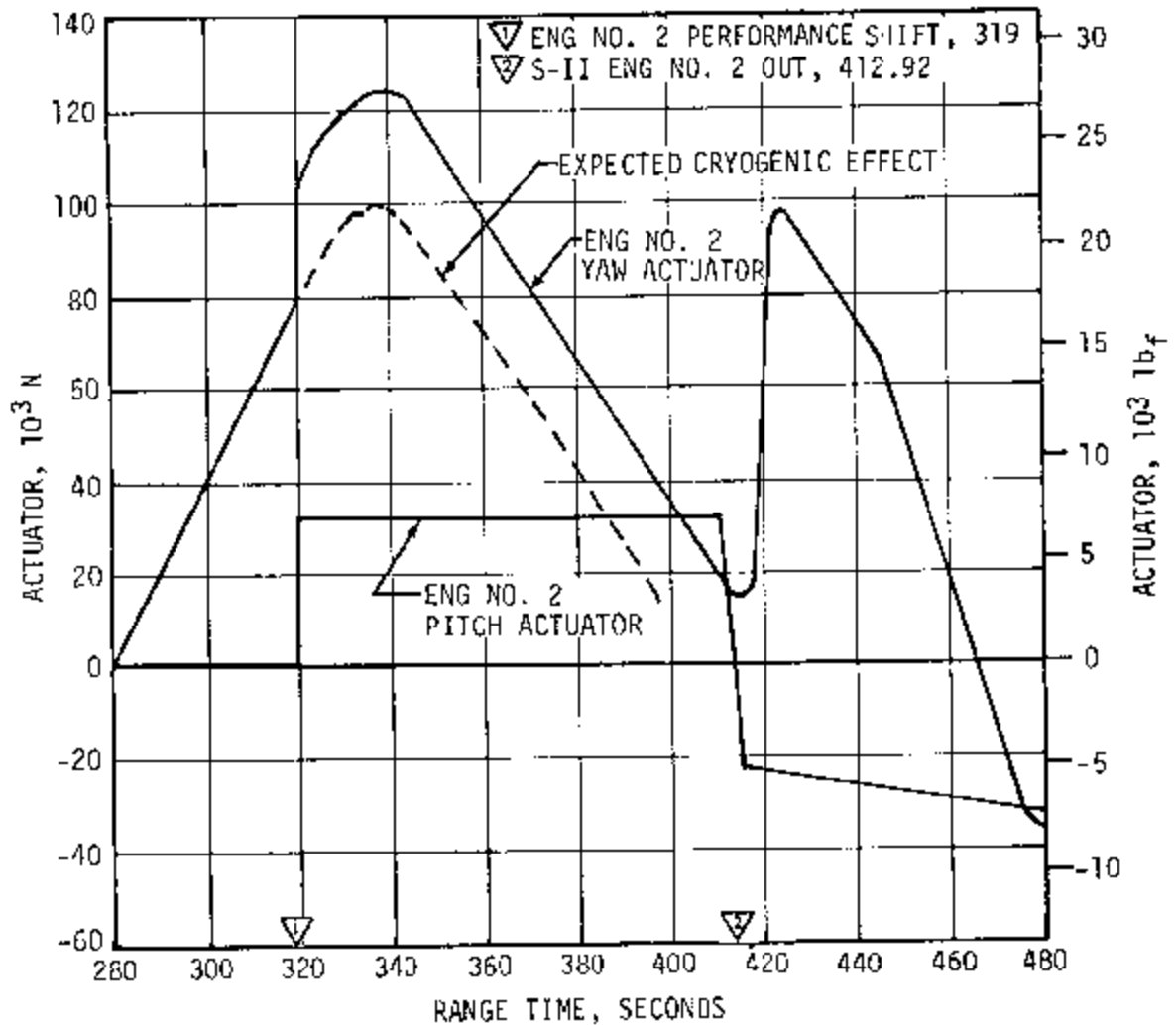


Figure 8-4. S-II Engine No. 2 Actuator Forces

At 423 seconds, the yaw actuator force increased to 98,000 Newtons (22,000 lbf), it then started to decay and finally leveled off at -35,000 Newtons (-8000 lbf) (tensile force) at 478 seconds, where it remained for the duration of S-II flight. The pitch actuator force dropped to -22,000 Newtons (-5000 lbf) at 415 seconds and then decayed to -31,000 Newtons (-7000 lbf) where it remained to the end of S-II flight. After engine No. 2 cutoff, both the pitch and yaw actuator pressure measurements indicated a force which tended to force the engine inboard. This indicated force is still under investigation.

The pitch actuator continued to respond to guidance commands as shown in Figure 8-5 until 480 seconds when the accumulator was empty of fluid. Shortly after engine No. 2 cutoff, the yaw actuator failed to respond to guidance commands. The performance of the yaw actuator indicates that it locked up at this time. The probable causes for this were closure of the

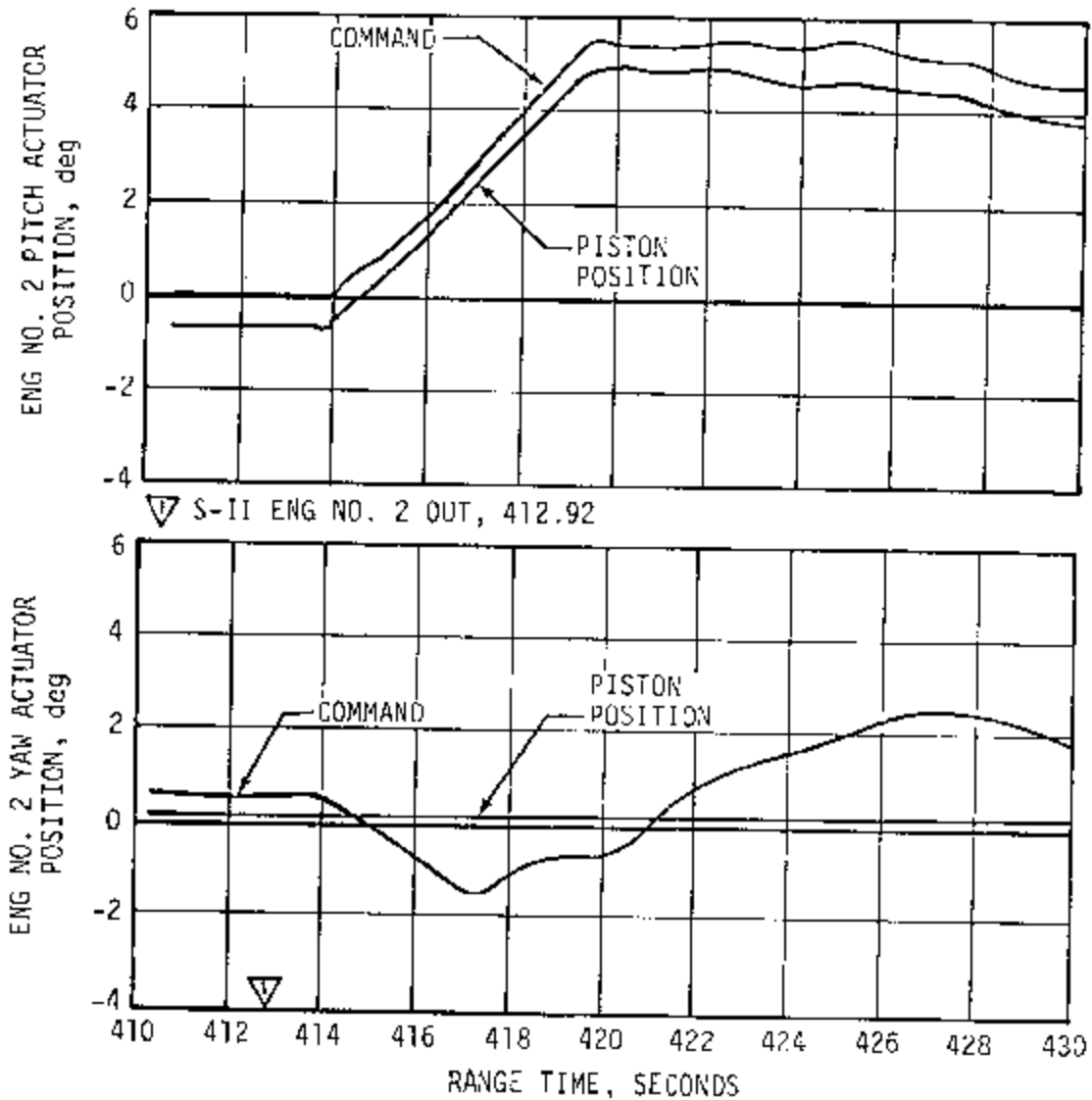


Figure 8-5. S-II Engine No. 2 Actuator Commands and Positions

hydraulic lock valve within the actuator or seizure of the piston. The lock normally closes when the difference between the actuator supply and return pressures decays below 900 to 1200 N/cm² (1300 to 1700 psid). A low differential pressure could have been caused by highly viscous fluid within the actuator or the supply and/or return lines to the actuator, resulting from a low temperature condition. Piston seizure could have resulted from cryogenic fluid spraying on the actuator cylinder. The No. 2 hydraulic reservoir level also appeared to have dropped sharply from 9 percent to zero at ECO. Hydraulic system No. 3 shows the expected reservoir level at this time. The zero volume indication was probably due to a complete loss of reservoir fluid caused by a rupture somewhere in the low pressure side of the system. This is based upon a corresponding

rapid decay in reservoir pressure to zero, accompanied by a slow decay in accumulator pressure which is on the high pressure side of the system. Normally, the reservoir pressure decays to approximately 35 N/cm² (50 psia) after ECO. The cause of the rupture has not been defined, however, an abnormally low temperature environment could have subjected a portion of the system to extreme strains and eventual rupture. The gradual decay in engine No. 2 reservoir volume before engine No. 2 cutoff (Figure 8-6) was probably the result of accumulator gas cooling which resulted in an increase in accumulator oil volume and produced a decrease in reservoir volume.

8.4 S-IVB HYDRAULIC SYSTEM (FIRST BURN)

Engine gimbaling is accomplished by an independent, closed-loop, hydraulic control system consisting of an engine-driven main pump, an auxiliary electric motor-driven pump, two electrically controlled, hydraulically powered servoactuators, and an accumulator reservoir. During S-IC and S-II powered flight and coast, the auxiliary pump is operating to position the J-2 engine in the null position and to pressurize the system. The main hydraulic pump, driven directly from the accessory drive pad of the engine LOX pump, provides the primary actuator power during S-IVB powered flight.

The S-IVB hydraulic system performed within the predicted limits after liftoff with no overboard venting of system fluid as a result of reservoir fluid expansion. Just prior to start of propellant loading, the accumulator was precharged to 1520 N/cm² (2200 psia) at 277°K (40°F). Reservoir

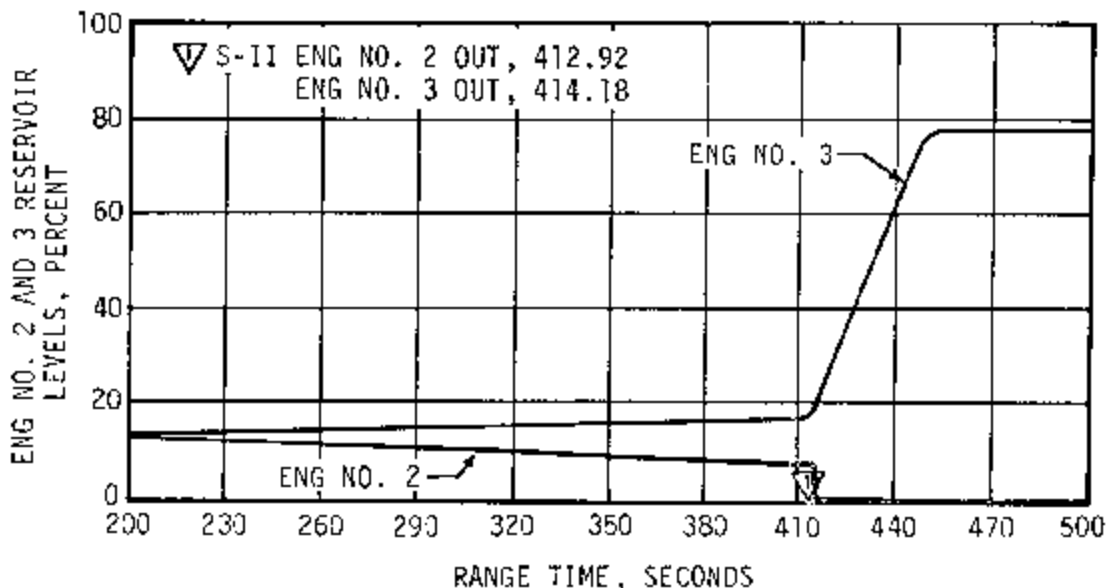


Figure 8-6. S-II Engines No. 2 and 3 Hydraulic Reservoir Levels

oil level (auxiliary pump off) was 78.5 percent at 270°K (26°F). There were no thermal cycles prior to launch. The low Gaseous Nitrogen (GN₂) temperature of 278°K (40°F) resulted in a low accumulator precharge pressure of 1517 N/cm² (2200 psia). This caused approximately 66 percent of the reservoir volume to enter the accumulator after the auxiliary pump was turned on. This effect, coupled with the oil volume shrinkage in the reservoir, resulted in a comparatively low reservoir oil level of 17 percent. Table 8-1 shows minor pressure level variations and compares the liftoff, first burn, parking orbit, and engine restart attempt system pressures.

During S-IC/S-II boost all system fluid temperatures rose steadily (Figure 8-7) when the auxiliary pump was operating and convection cooling was decreasing. Accumulator gas and actuator cylinder temperatures remained low since they are located on the extreme ends of the system. The supply pressure during the first burn was nearly constant at 2482 N/cm² (3600 psia) as compared to the allowable of 2344 to 2517 N/cm² (3400 to 3650 psia). The maximum actuator torque resulting from vehicle attitude command during first burn was in pitch at 12,639 N-m (111,863 lbf-in).

System temperatures did not rise normally during the latter portion of first burn as shown in Figure 8-7. The following characteristics were not experienced on previous flights:

- At 688 seconds the yaw actuator suddenly started to lose temperature at the rate of approximately 0.28 °K/s (0.5 °F/s).
- At 701 seconds the pump inlet oil temperature suddenly jumped 16.6°K (30°F) in 14 seconds and then decreased 8.3°K (15°F) at cutoff.
- The main pump discharge line temperature began to rise normally at the start of engine burn. At 670 seconds it suddenly started to drop and then leveled off at ECO.

Table 8-1. S-IVB Hydraulic System Pressures

PRESSURES	LIFTOFF N/cm ² (psia)	FIRST BURN N/cm ² (psia)	PARKING ORBIT N/cm ² (psia)	AFTER RESTART COMMAND N/cm ² (psia)	ALLOWABLE DURING BURN N/cm ² (psia)
System Oil	2482 (3600)	2482 (3600)			2344 to 2517 (3500 to 3650)
Accumulator GN ₂	2489 (3610)	2489 (3610)	1482 (2100)	2489 (2160)	2344 to 2517 (3500 to 3650)
Reservoir Oil	117 (170)	119 (172)	46 (67)	43 (62)	114 to 128 (165 to 185)
Aux Pump Air Tank	293 (425)	296 (430)	296 (430)	293 (425)	
Aux Pump Motor Air	13.8 (20)	24.8 (35)	24.1 (35)	24.8 (36)	

The values have been corrected to the 293 °K (67 °F).

▽ S-IVB ENG START SEQUENCE COMMAND, 577.28
 ▽ S-IVB VELOCITY CUTOFF COMMAND, 747.04

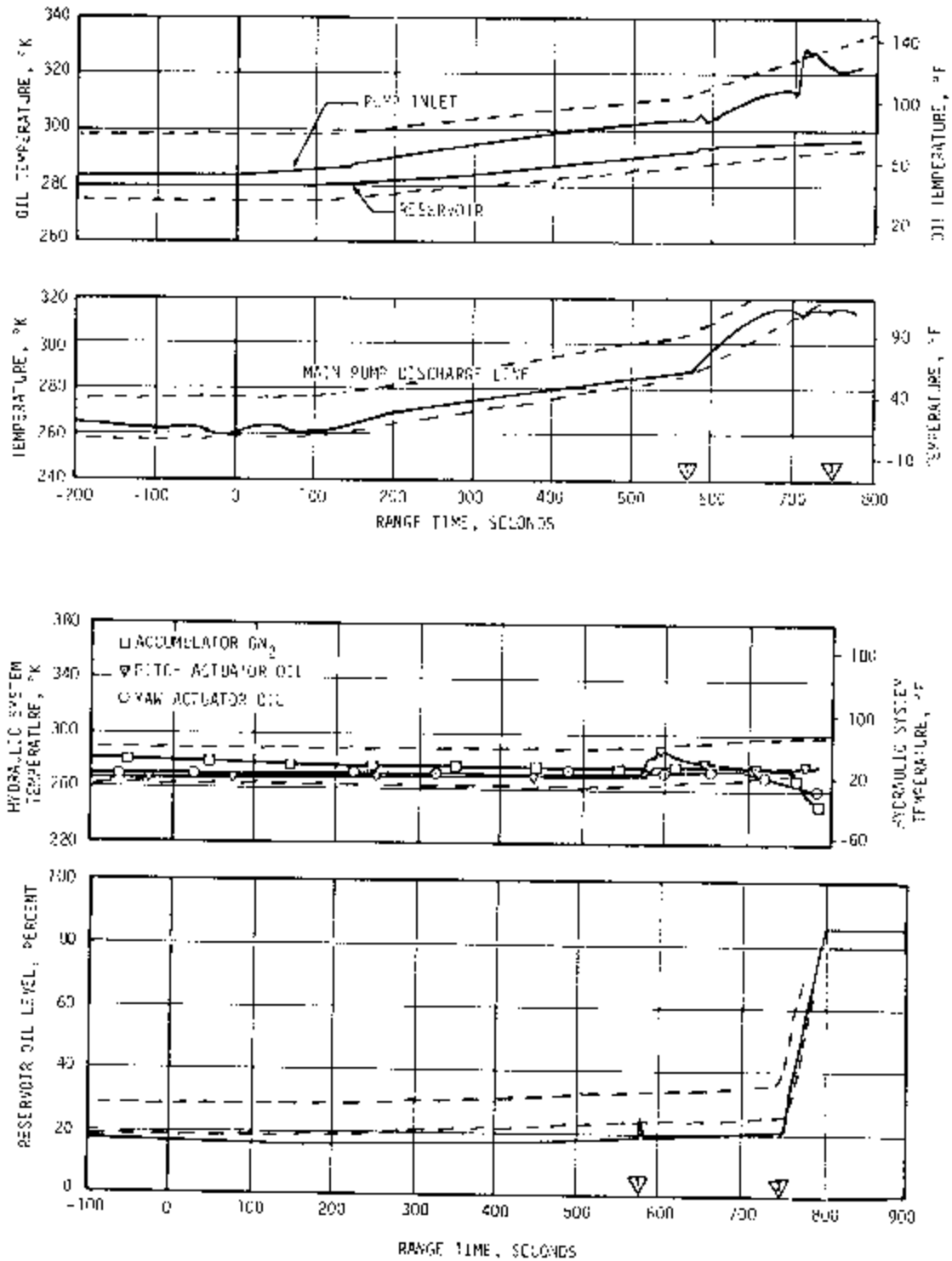


Figure 8-7. S-IVB Hydraulic System Performance - First Burn

8.5 S-IVB HYDRAULIC SYSTEM (COAST PHASE)

During orbital coast there were no thermal cycles of the auxiliary hydraulic pump. After ECO, the pump inlet oil temperature increased from 349 to 358°K (168 to 185°F) due to continued heat transfer from the LOX turbine dome to the pump manifold as shown in Figure 8-8. During the remainder of the coast period this temperature decreased gradually along with other system temperatures. System bleeddown required 57 seconds and accumulator precharge pressure stabilized at 1062 N/cm² (2150 psia).

8.6 S-IVB HYDRAULIC SYSTEM (SECOND BURN)

The auxiliary pump was activated to the flight mode at 10,822 seconds (793 seconds prior to second burn). The pump failed to produce any discernible hydraulic pressure. There was current draw to the pump motor of approximately 12 amperes which is an indication that the pump was cavitating. Normal motor current is 45 amperes. A 6.9 N/cm² (10 psi) reservoir pressure increase occurred approximately 250 seconds later as shown in Figure 8-9, but this was of short duration.

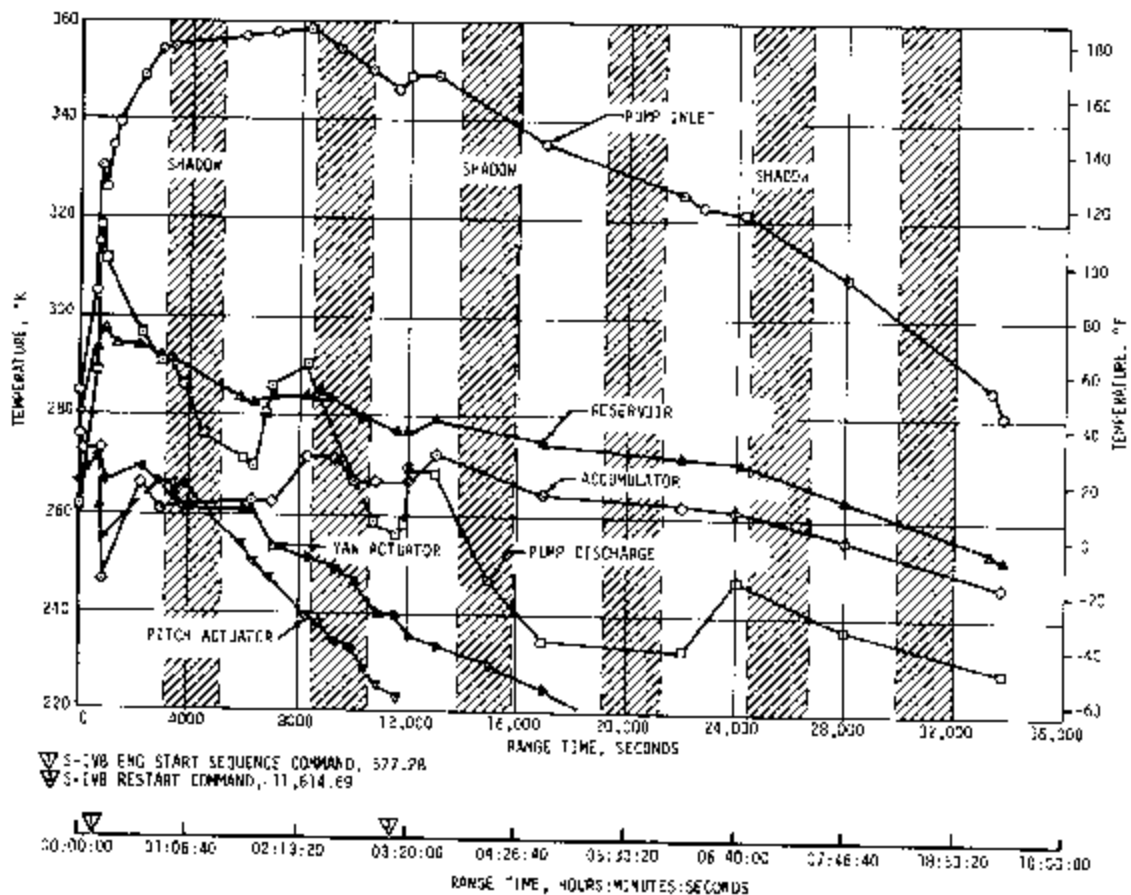


Figure 8-8. S-IVB Hydraulic System Performance - Coast Phase

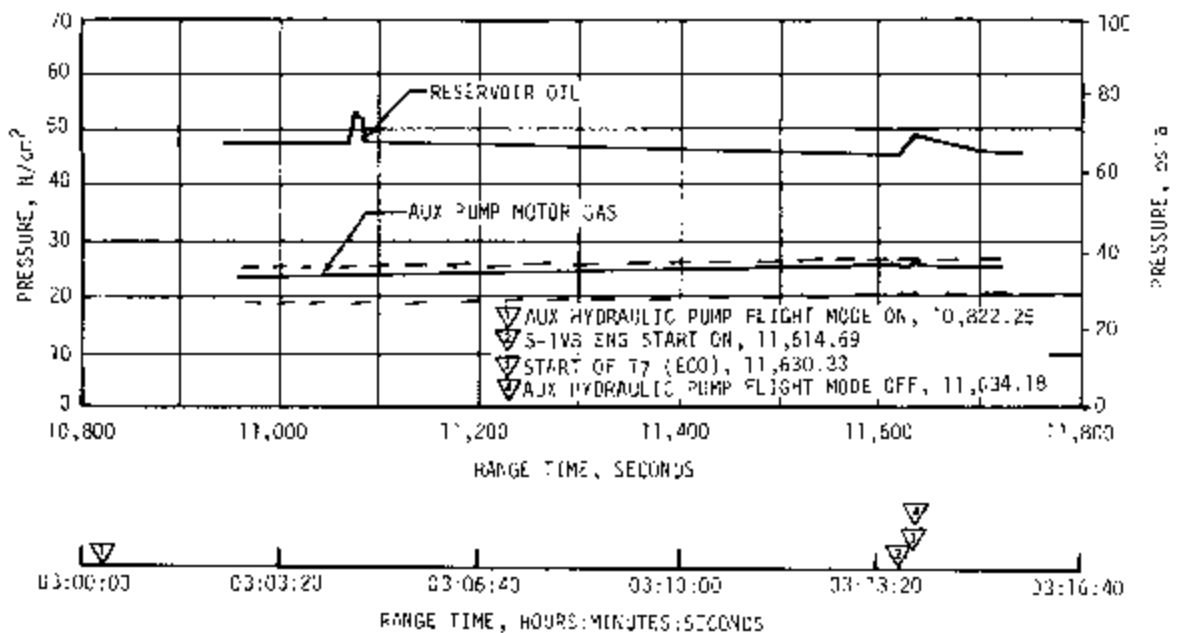


Figure 8-9. S-IVB Hydraulic System Pressure During Attempted Restart

After engine restart command the main engine hydraulic pump failed to produce any measurable hydraulic system pressure. At the start of LOX turbine spin (at approximately 11,622 seconds), after restart engine command, there was a small fluctuation in reservoir oil pressure, the actuators moved slightly and there was a 15°K (27°F) momentary drop in pump inlet oil temperature as shown in Figure 8-10. This indicated that the main pump was turning and moving fluid but was unable to develop system pressure.

It has been concluded that both the auxiliary and main hydraulic pump failures in the period preceding and during second burn attempt were due to cavitation. Since the reservoir oil level and pressure were normal, it is believed that the condition was caused by localized freezing of the pump suction line hydraulic fluid by an impingement from a leaking cryogenic line. The pump suction line runs across the gimbal plane on position III between the accumulator reservoir on the thrust structure and the main hydraulic pump on the LOX turbine dome as shown in Figure 8-11. If this line is subjected to cryogenic freezing, a blockage of oil would result in the line (pour point of MIL-H-5606 oil is 205°K [-90°F]) which would starve the inlets of both pumps, lose inlet pressure head and prevent reservoir fluid from reaching the pumps.

Two attempts were made to start the auxiliary hydraulic pump by ground command with no success. The pump inlet and reservoir oil temperatures continued to sink at approximately the same rates. The pump discharge line temperature measurement which was located near the system thermal switch apparently varied with exposure to solar radiation or earth's shadow. This shows that abnormal system temperature deviations were no longer present after the engine restart attempt.

- ▽ ALX HYDRAULIC PUMP FLIGHT MODE 01, 10,822.25
- ▽ S-IVB ENG START CH, 11,614.69
- ▽ START OF T₂ (FCO), 11,630.33
- ▽ AUX HYDRAULIC PUMP FLIGHT MODE OFF, 11,634.18

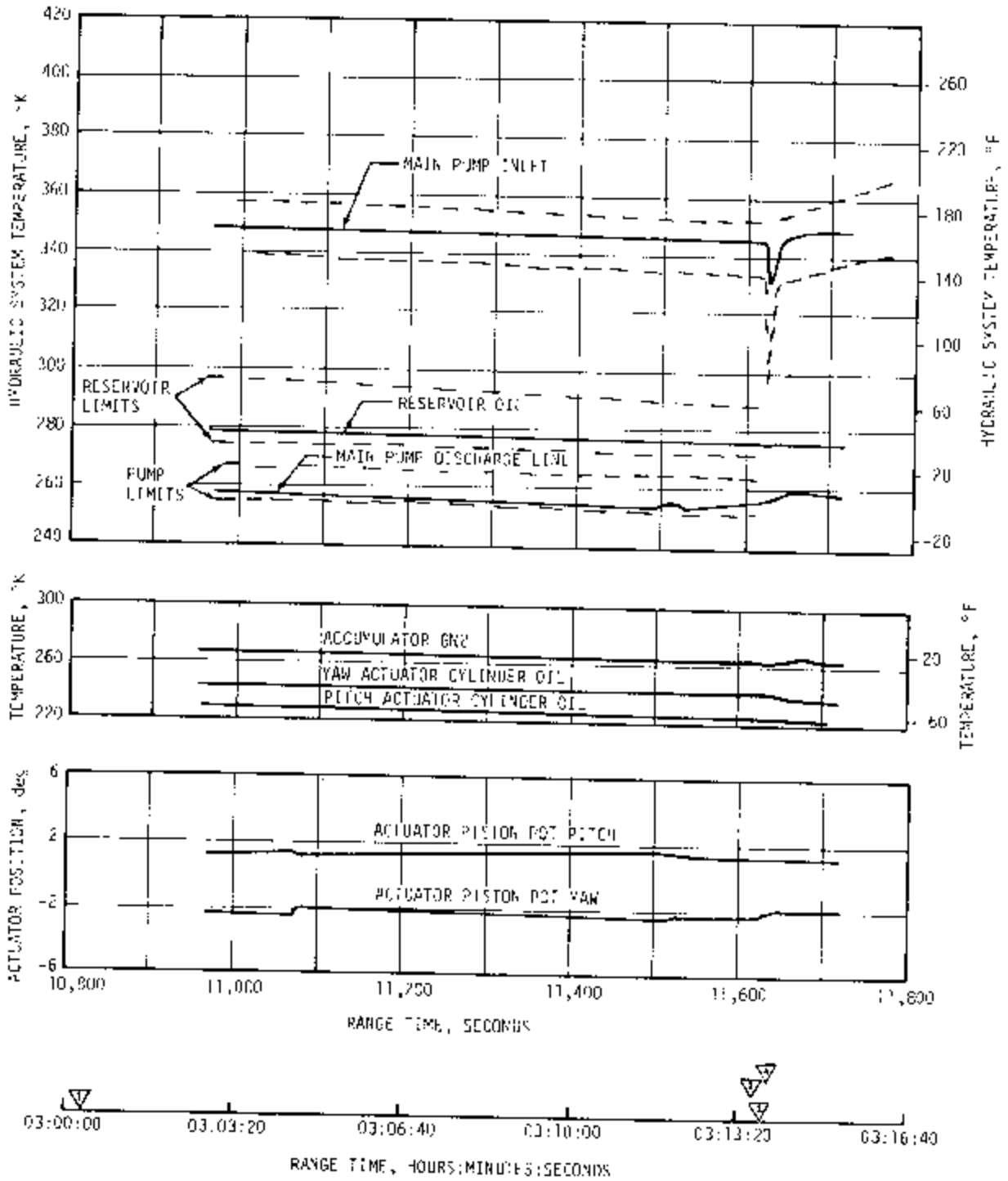


Figure 8-10. S-IVB Hydraulic System Performance During Attempted Restart

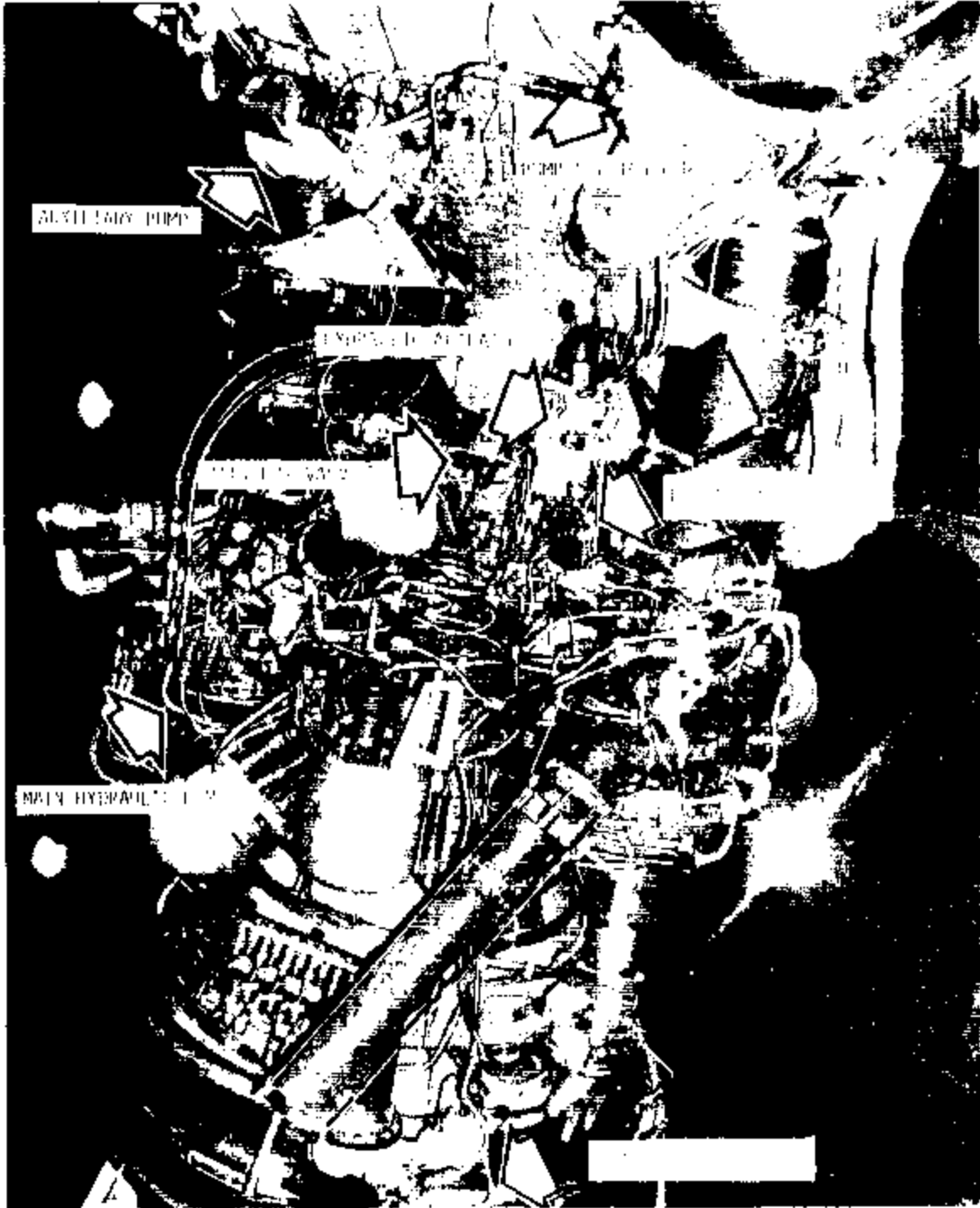


Figure 8-11. J-2 Engine Hydraulic Component Locations

SECTION 9
STRUCTURES

9.1 SUMMARY

The AS-502 flight vehicle experienced considerably more structural activity than the AS-501; however, this activity did not reach sufficient magnitude to pose a threat to the launch vehicle structural integrity. Areas of structural activity included:

- a. A slightly more severe vehicle release transient than on AS-501 (paragraph 9.2.1).
- b. Coupling of longitudinal structural dynamics with thrust oscillations (POGO) (paragraph 9.2.3.1).
- c. Limited amplitude S-IVB panel flutter (paragraph 9.3.4).
- d. A shock response type transient which occurred at 133 seconds (Section 9A).
- e. Inboard Engine Cutoff (IECO) longitudinal acceleration design value exceedance (paragraph 9.2.1).
- f. Premature cutoff of two of the five S-II stage engines (paragraph 9.2.1 and 9.2.2).

The transients, due to thrust buildup and vehicle release, resulted in maximum longitudinal and lateral (pitch plane) dynamic load factors of ± 0.4 and ± 0.08 g, respectively, at the command module. The maximum steady-state bending moment condition, 9.89×10^6 N-m (7.29×10^6 lbf-ft), was experienced at 66.6 seconds. The maximum longitudinal loads were experienced at 144.72 seconds (IECO) at a rigid body acceleration of 4.8 g. Although the 4.8 g IECO condition was greater than the 4.68 g design value, no mainline structural problems were encountered during this phase of flight.

Thrust oscillation-structural dynamic response coupling (POGO) was evident during the 110 to 140 second region of S-IC range time. The longitudinal dynamics of the launch vehicle induced lateral accelerations of 0.65 G_{peak} at the Lunar Module Test Article (LTA). Oscillations in the first longitudinal mode during the 110 to 140 second time period

exceeded that experienced during AS-501 flight by approximately a factor of three. Maximum response occurred in the 5.2 to 5.5 hertz bandwidth.

Fin bending and torsional modes compared well with analytical predictions. Fin vibrations exceeded the range of the accelerometers but the modal frequencies did not coalesce and flutter did not occur. S-IC, S-IVB, and Instrument Unit (IU) vibrations were as expected. S-II stage vibrations were as expected, except that forward skirt vibrations exceeded the sine and random criteria at liftoff. No adverse effects were noted. S-IVB forward skirt experienced limited amplitude panel flutter. The stress amplitudes encountered, due to flutter, were about three times higher than those of AS-204 but were still within a tolerable level.

A pronounced transient was evident at approximately 133 seconds in many measurements on the vehicle. The transient was also reported by Manned Spacecraft Center (MSC) to be present on many of the spacecraft measurements. Details of this transient are discussed in Section 9A.

9.2 TOTAL VEHICLE STRUCTURES EVALUATION

9.2.1 Longitudinal Loads

The vehicle longitudinal dynamic response due to thrust buildup and release is shown in Figure 9-1. The axial dynamic loads derived from strain gage data are shown at the S-IC intertank and forward skirt. Two upper stations, where astronaut comfort is of prime concern, are given in terms of acceleration. The simulated response at the command module is based on measured forcing functions and is presented in lieu of the measured accelerations which were not available.

The measured accelerations shown at the IU were filtered to eliminate localized high frequencies (higher than 6 hertz) so that overall vehicle dynamics could be more accurately established. A frequency analysis of the filtered data indicated a predominance of 3.8 and 4.4 hertz oscillations. Oscillations observed in the axial load plots are not as pronounced as in the acceleration data because of the low frequency limitation (2.4 hertz) of the telemetry system from which the strain data was obtained. The 3.8 and 4.4 hertz oscillations are precisely as predicted for the first two longitudinal modes at the time of vehicle launch.

In general, the AS-502 vehicle longitudinal dynamic response amplitudes at launch were greater than those experienced on the AS-501. Maximum response at the command module was approximately ± 0.4 g (simulated) on AS-502 and ± 0.2 g (simulated) on AS-501.

This increased response was due primarily to changes in the controlled release device characteristics. The time required to clear the controlled release device was 1.17 seconds on AS-501 and 0.54 second on AS-502 with a steady-state acceleration of 1.24 g. The most significant change was the reduction of the number of release rods from 16 for the AS-501 flight

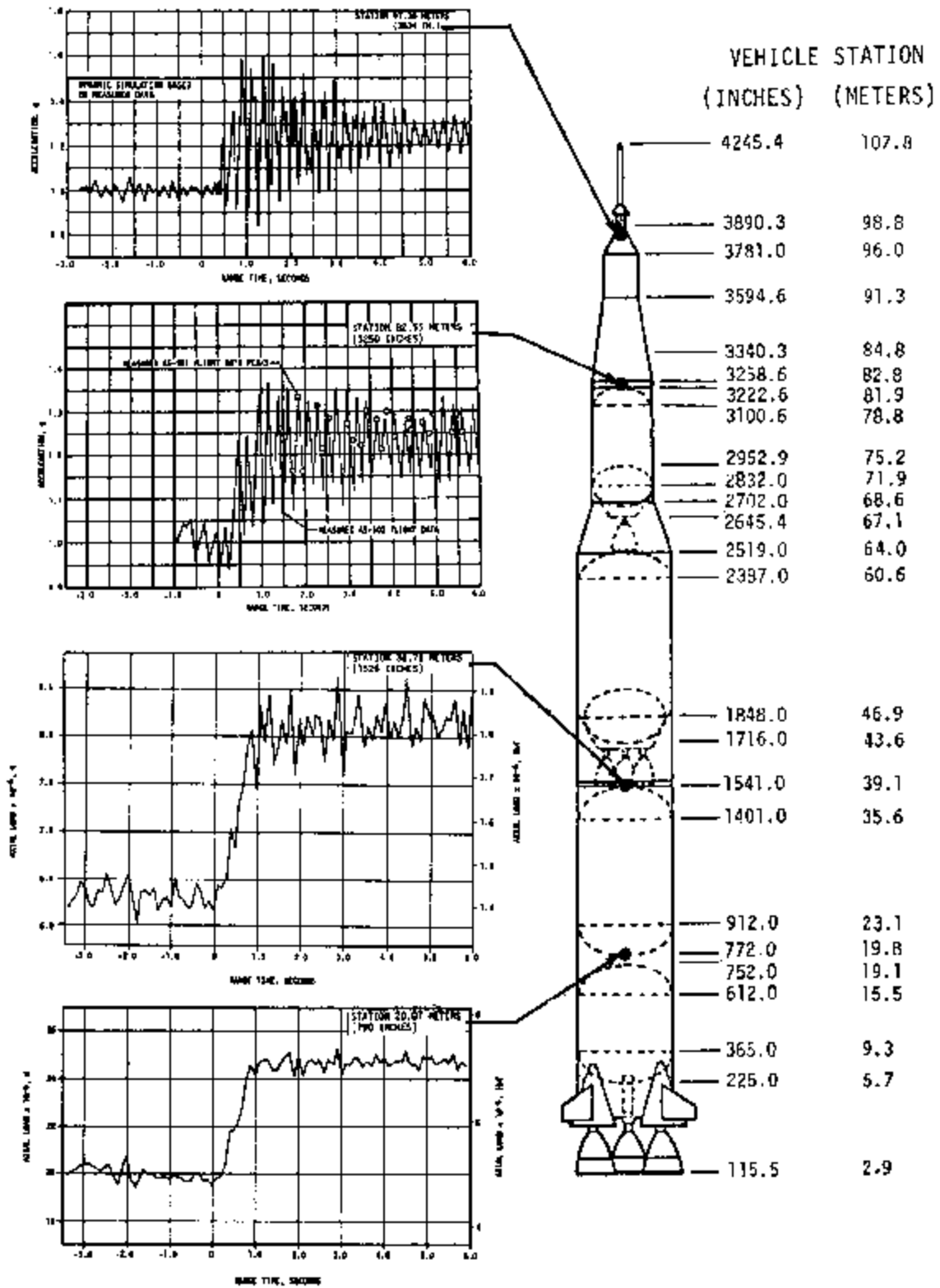


Figure 9-1. Longitudinal Structural Dynamic Response Due to Thrust Buildup and Release

to 12 (6 instrumented) for AS-502. Revised rod lubricating techniques adopted on AS-502 gave rise to the lower release rod maximum force shown in Figure 11-3 (Section 11) which also served to increase the release transient. Still another minor change in the release parameters was the slight decrease in release rod preload shown in Figure 9-2.

In spite of the changes in the controlled release device which increased the dynamic transient due to launch, the response accelerations and corresponding loads throughout the launch vehicle primary structure were well within predicted values. This phase of flight posed no threat to mainline structural integrity.

The vehicle longitudinal acceleration measured during flight is shown in Figure 9-3. The rigid body component of this acceleration was essentially nominal throughout S-IC burn. This acceleration information, along with preflight predicted weight distribution and aerodynamic drag, was used as a basis for longitudinal loads computations. The maximum longitudinal dynamic response subsequent to the release transient was experienced between 110 to 140 seconds and is illustrated by shading in Figure 9-3. This aspect of the flight will be discussed in paragraph 9.2.3.1 of this report. The longitudinal loads which existed at the time of maximum aerodynamic loading (maximum bending moments) and at maximum compression (IECO) are shown in Figure 9-4. These figures illustrate the excellent agreement between measured loads and loads computed from measured flight parameters. The rigid body longitudinal acceleration at time of maximum bending moments (66.6 seconds) was 1.93 g. The maximum longitudinal loads experienced during flight occurred immediately prior to IECO

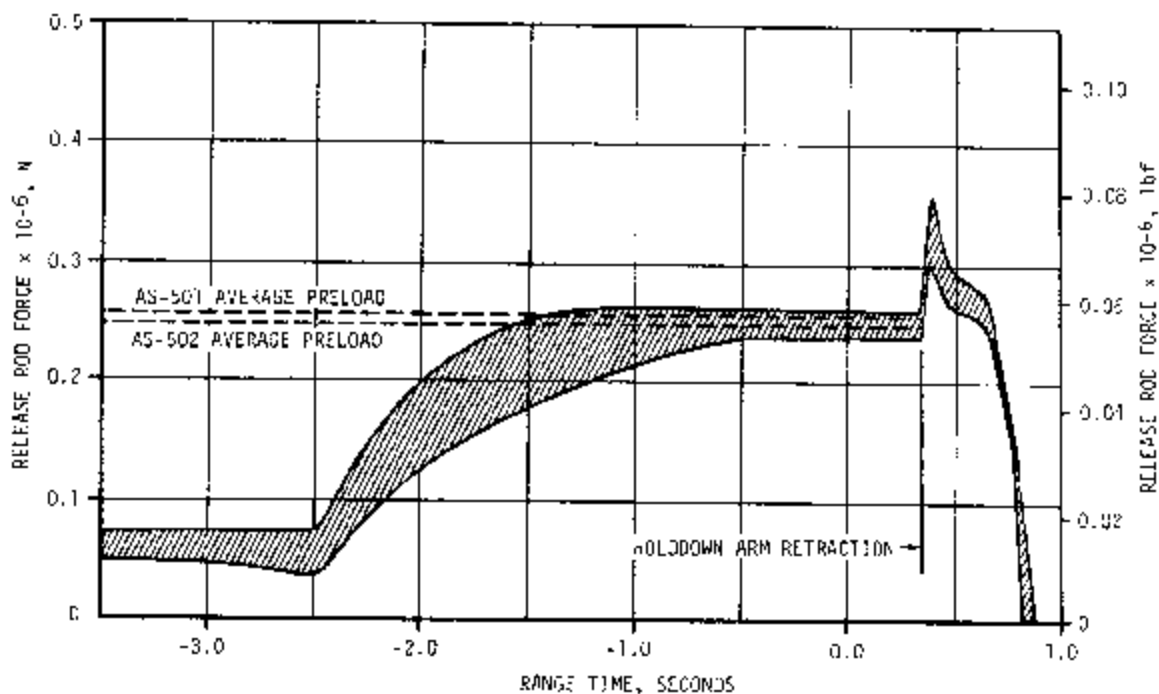


Figure 9-2. Slow Release Rod Loads During Release

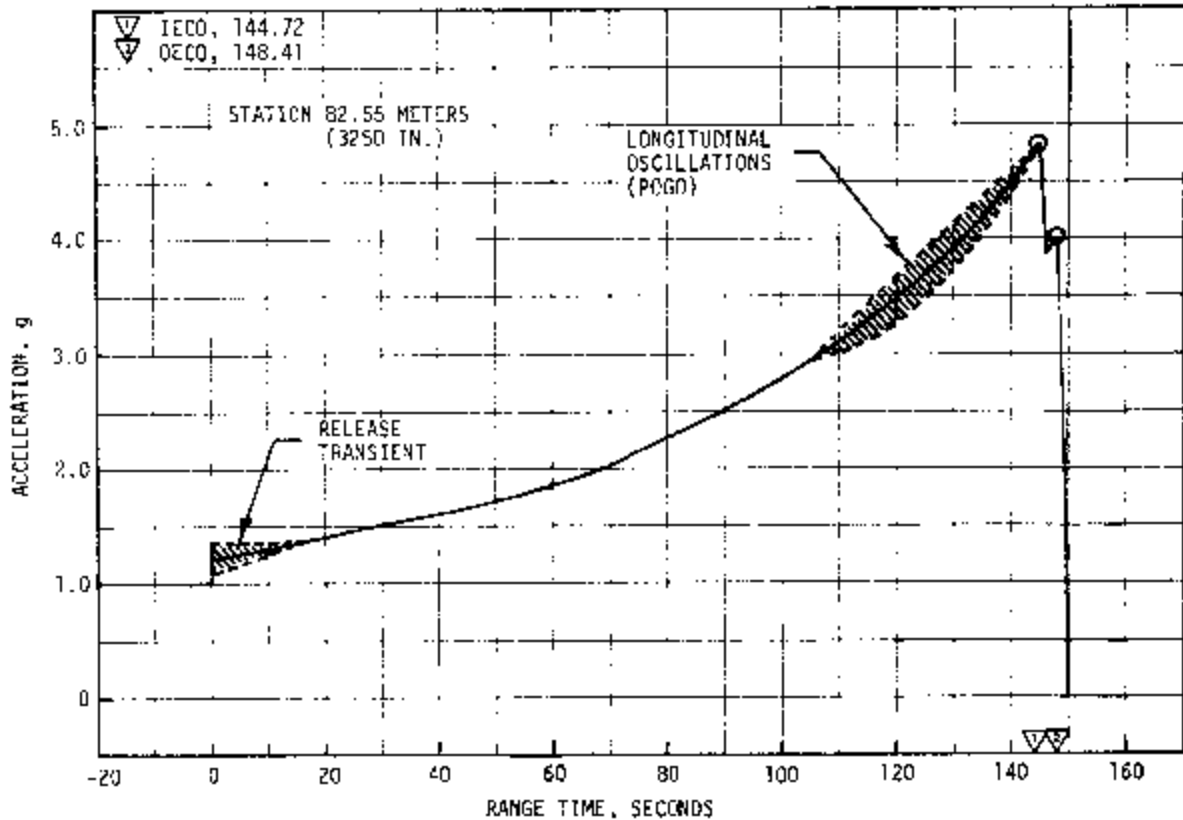


Figure 9-3. Longitudinal Acceleration Time History

(144.72 seconds) at a rigid body longitudinal acceleration of 4.8 g. Although the 4.8 g IECO condition was, as predicted, greater than the 4.68 g design value, no mainline structural problems were expected or encountered during this phase of flight. The higher g level was the result of a longer inboard engine burn to attain LOX level cutoff.

Figure 9-5 shows longitudinal acceleration time histories at the S-IC center engine gimbal block, S-IC intertank region, and the command module during S-IC thrust cutoff (OECO). Due to absence of accelerometer data from the command module, only the dynamic simulation results are presented.

At approximately 413 seconds range time, two of the five S-II engines prematurely cutoff. The longitudinal loads corresponding to this two-engines-out condition are shown in Figure 9-6 and are well below design.

9.2.2 Bending Moments

The lateral transient due to thrust buildup and release is typified by the S-IC intertank and forward skirt load time histories shown in Figure 9-7. The 1 to 2 hertz oscillations apparent in this data are due to the lateral dynamic response, or "twang", at vehicle release. The low frequency load buildup and decay subsequent to 1.5 seconds is a

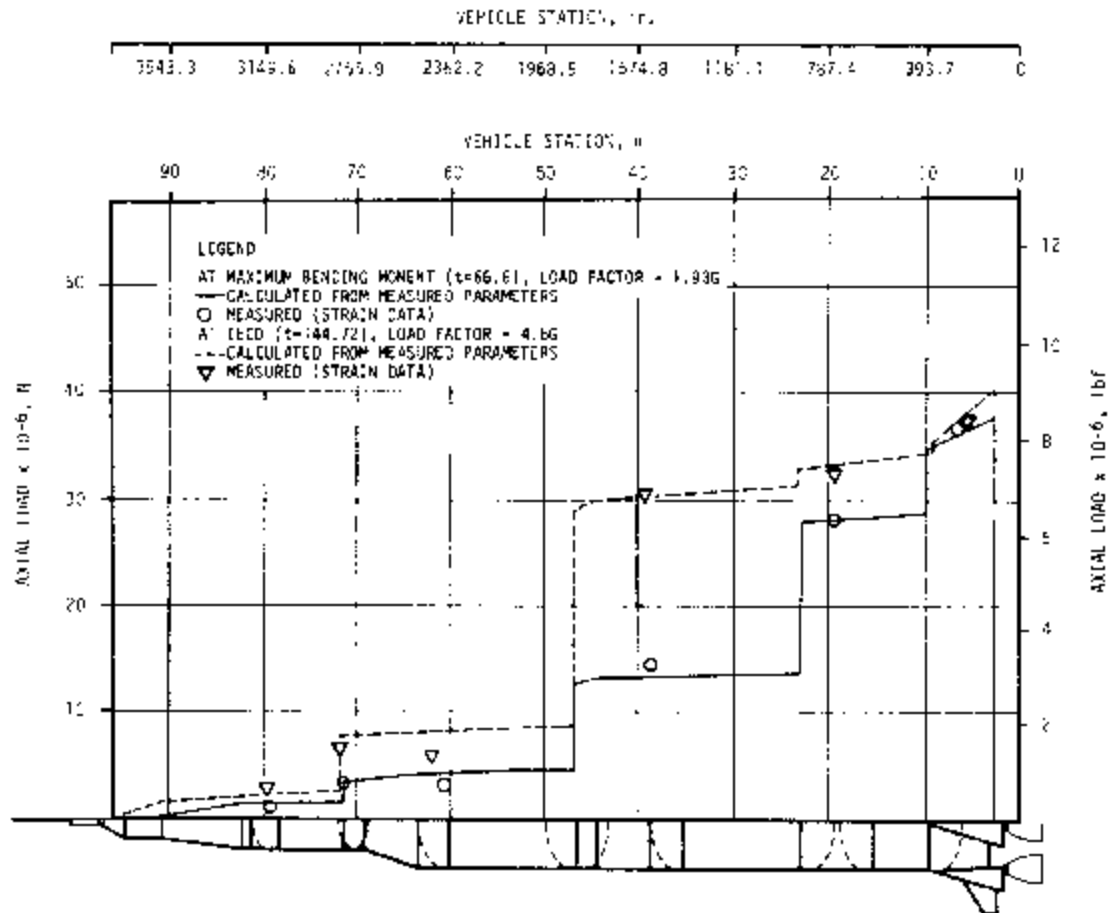


Figure 9-4. Longitudinal Loads at Maximum Bending Moment and Inboard Engine Cutoff

result of the programmed yaw maneuver. The pitch plane dynamic simulation response at the command module during launch is also presented in Figure 9-7. The maximum response acceleration was found to be ± 0.08 g. Measured data at the command module was not available due to questionable flight data.

The conditions which existed during the high aerodynamic loading phase of flight were such as to cause near minimum lateral loads. This is illustrated by a comparison of the maximum AS-502 flight bending moments with design values shown in Figure 9-8. The lateral load factor is also shown. The 9.89×10^6 N-m (7.29×10^6 lbf-ft) maximum bending moment in the S-IC LOX tank at 66.6 seconds was only one third of the design value. The S-II engines which prematurely cut off (Engines No. 2 and 3) were in the upper outboard location and could be expected to produce relatively large bending moments. A conservatively high calculation of these bending moments, shown in Figure 9-8, indicates values well within design envelopes. A comparison with measured strain gage data at one station is shown in the figure.

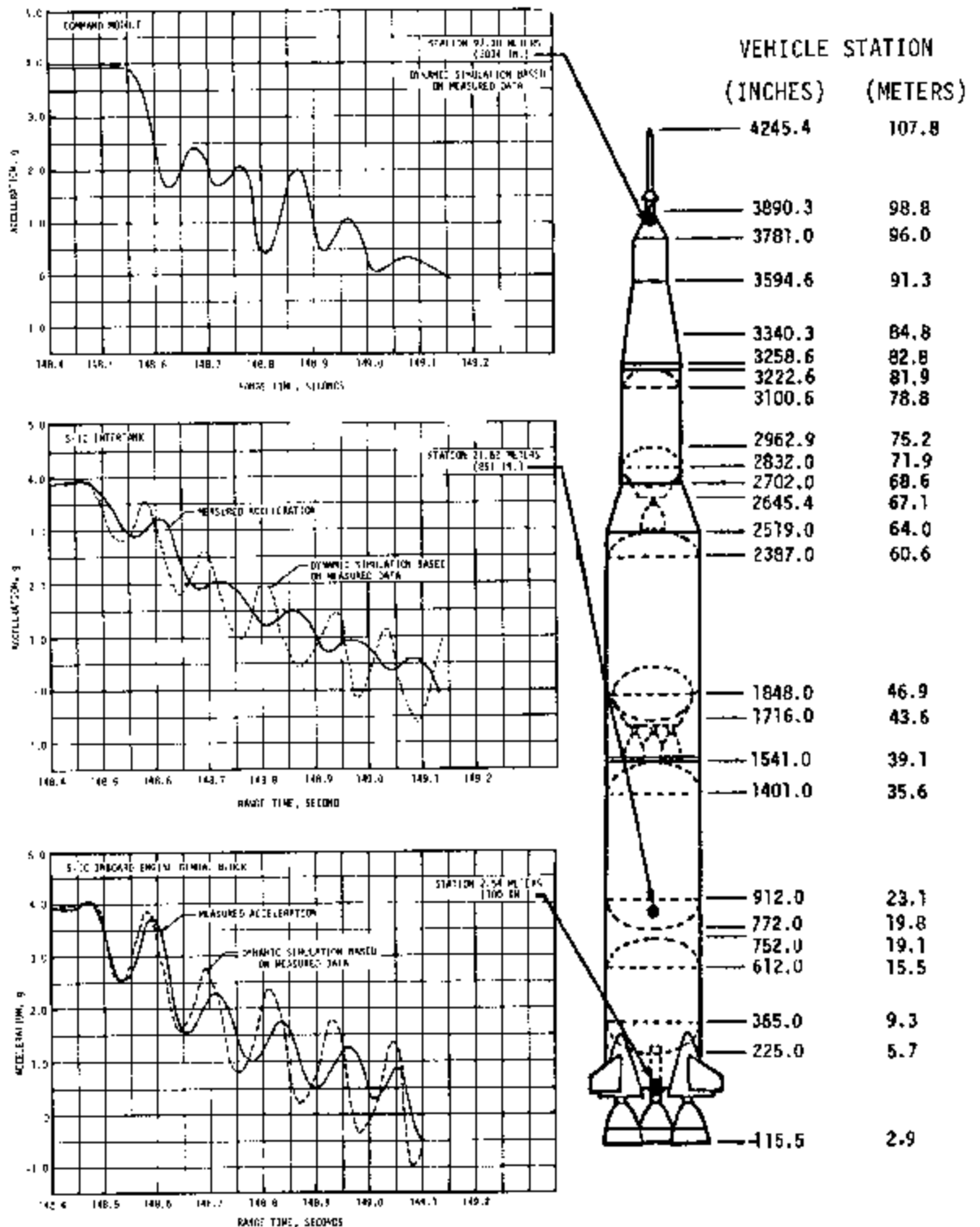


Figure 9-5. Longitudinal Acceleration During S-IC Thrust Cutoff (0ECO)

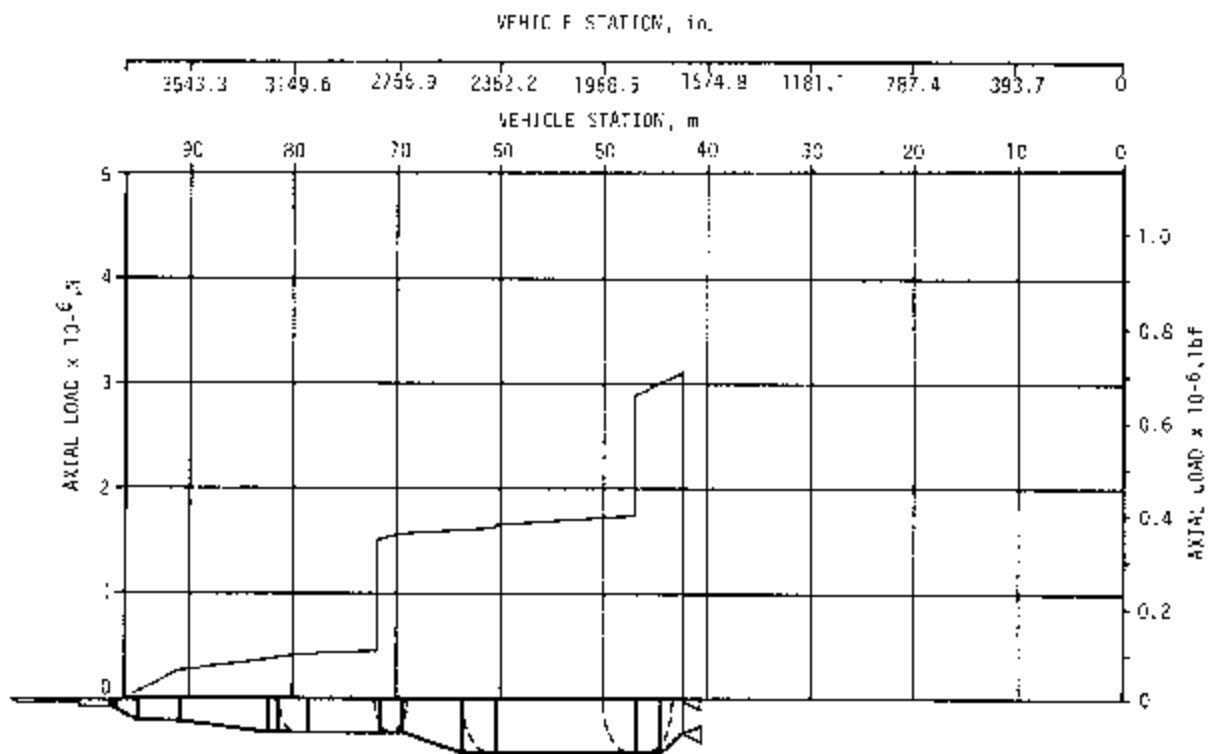


Figure 9-6. Longitudinal Loads Subsequent to S-II Engines Out

9.2.3 Vehicle Dynamic Characteristics

9.2.3.1 Longitudinal Dynamic Characteristics. Frequency versus range time for the first longitudinal mode is compared with the analytical prediction and data from the AS-501 flight in Figure 9-9. Modal amplitude versus range time is also shown. Oscillation in the first longitudinal mode was observed on all longitudinal low frequency instrumentation in the maximum Gpeak regions shown in the lower part of Figure 9-9. The frequency data agree well with both the analytical prediction and the AS-501 data. The data shown in Figure 9-6 of MPR-SAT-FE-68-1 Saturn V Launch Vehicle Flight Evaluation Report AS-501 Apollo 4 Mission is incorrectly identified as being on the IU, when in reality it was obtained from the command module; therefore, it cannot be compared to the AS-501 data shown in Figure 9-9 of this report.

The AS-502 vehicle experienced closed loop structural/propulsion coupling (POGO) in the latter part of the S-1C flight. The POGO phenomenon is a closed loop interaction of the three essential interactive vehicle systems: the vehicle structure, the vehicle suction propellant feed system, and the engine system.

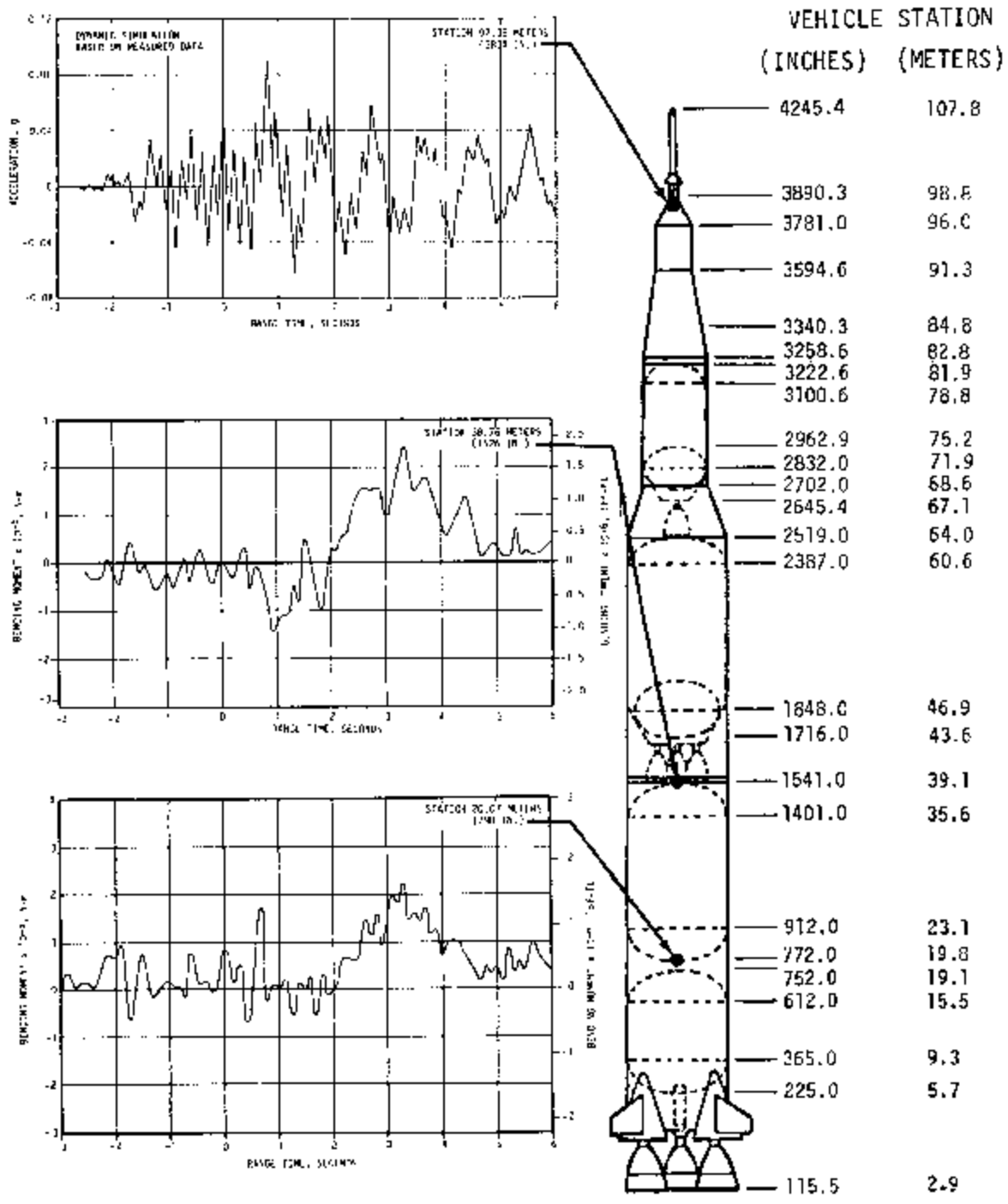


Figure 9-7. Lateral (Pitch) Structural Dynamic Response During Thrust Buildup and Release

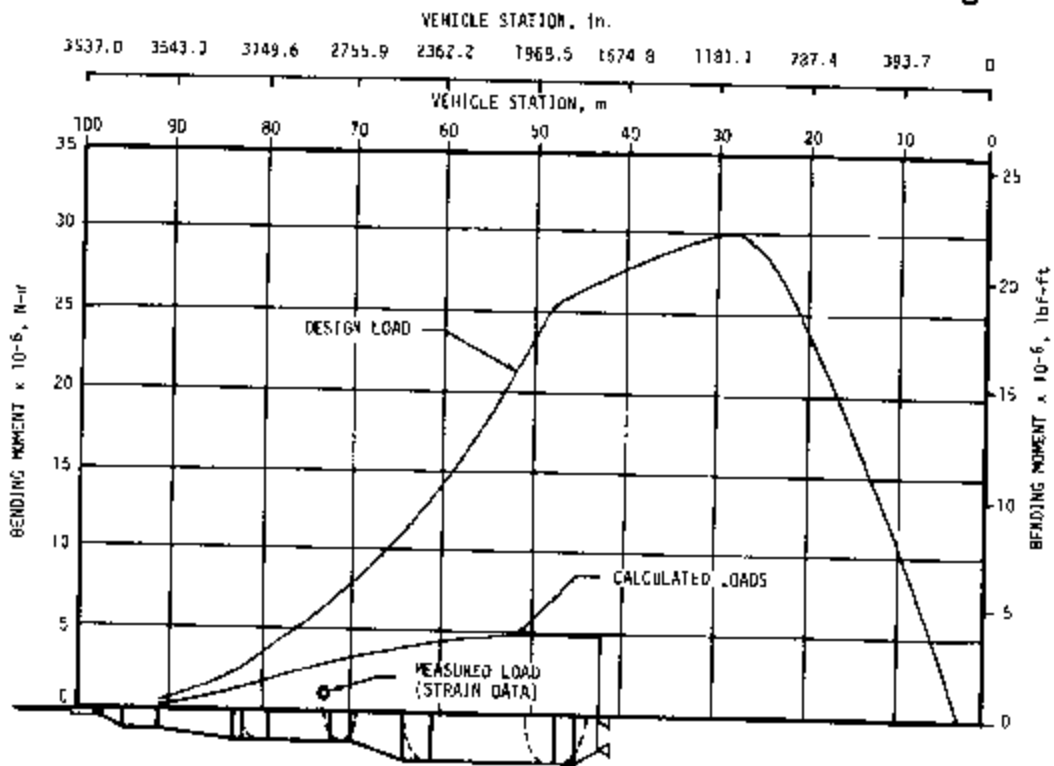
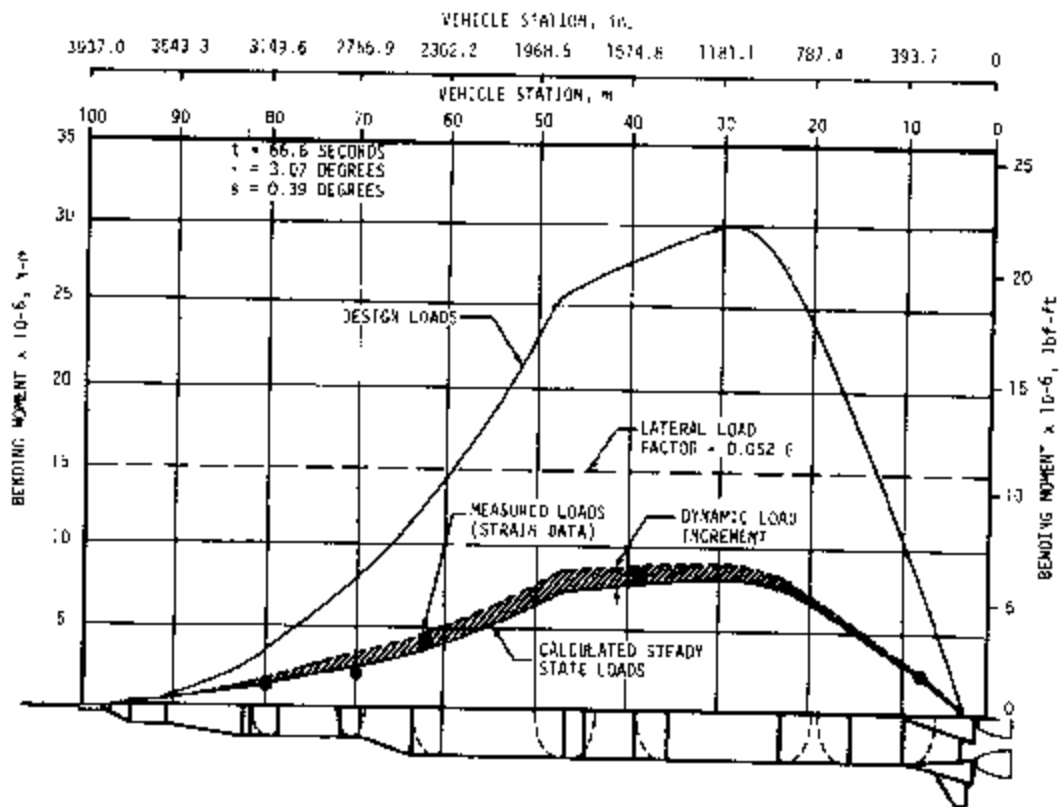


Figure 9-8. Maximum and S-II Engines Out Bending Moment

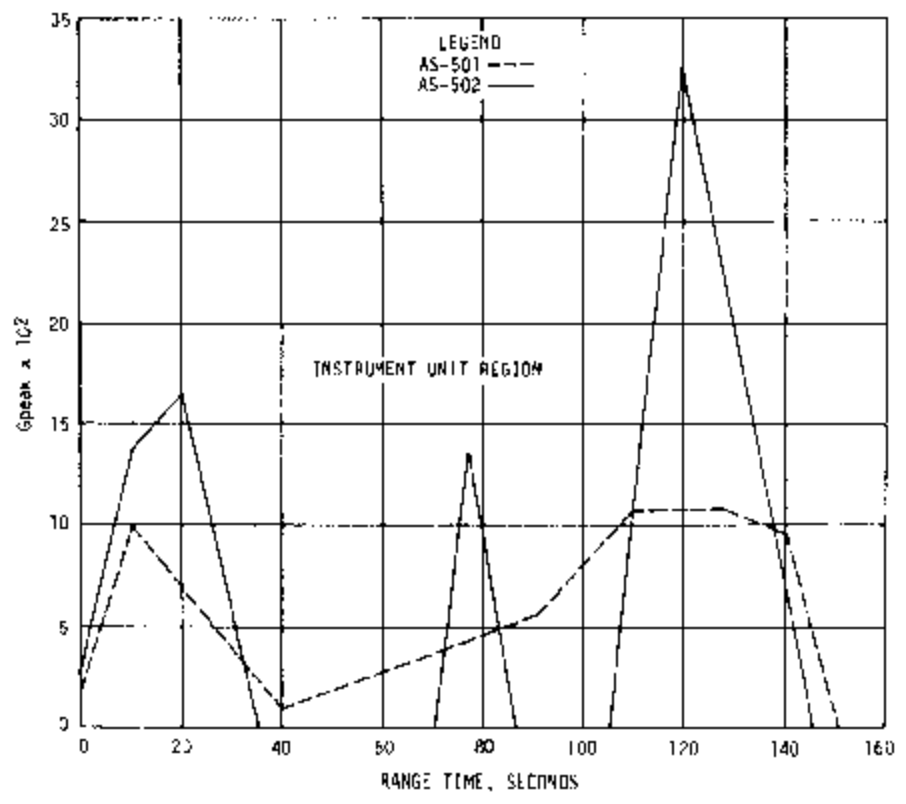
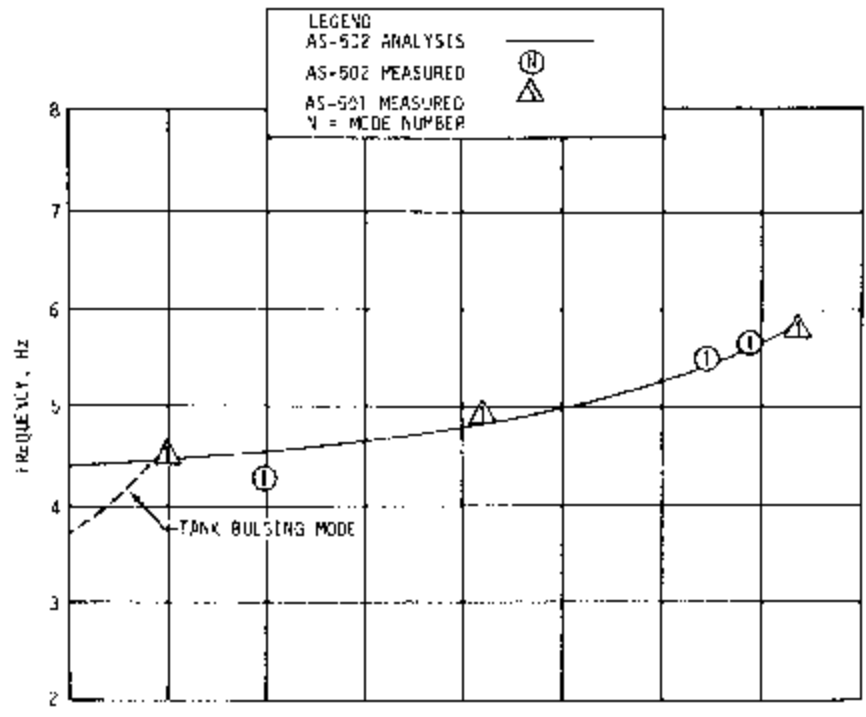


Figure 9-9. First Longitudinal Modal Frequencies and Accelerations During S-IC Powered Flight

The buildup of longitudinal dynamics started about 110 seconds range time. The structural oscillations reached a maximum level of ± 0.18 g at the S-IC gimbal plane and ± 0.65 g at the command module at 125 seconds, then decayed to a negligible level by 140 seconds. This buildup is a result of the coalescence of the first longitudinal frequency of the vehicle with the first LOX line frequency in the frequency range of 5.2 to 5.4 hertz. The frequency coalescence and the resulting structural response buildup is illustrated in Figure 9-10.

All five F-1 engines were essentially in phase on AS-502 and showed a chamber pressure increase from 110 to 125 seconds and then a decrease back within noise level amplitudes at approximately 135 seconds. Figure 9-11 shows the chamber pressures on the individual engines and also a composite chamber pressure for the five F-1 engines.

A major difference observed in the propulsion data of the two vehicles (AS-501 and AS-502) is that all engines exhibited oscillatory thrust at the same frequency and essentially in phase on AS-502; whereas, the AS-501 engines did not show the same engine-to-engine thrust frequency. The buildup in the structural acceleration response at the S-IC gimbal plane and the F-1 engine chamber pressure is shown in Figure 9-12.

Modal amplitudes during the 110 to 140 second region of S-IC range time exceeded those experienced during AS-501 flight by approximately a factor of three as shown in Figure 9-9. Amplitudes at different vehicle stations reached peak levels in this time period at various range times as indicated in Table 9-1. Maximum response occurred in the 5.2 to 5.5 hertz bandwidth. The longitudinal dynamics of the launch vehicle induced lateral accelerations of 0.65 G_{peak} at the LTA. The maximum levels measured in the spacecraft LTA during the 120 to 135 second region were:

- a. Pitch 0.65 G_{peak}
- b. Yaw 0.10 G_{peak}
- c. Longitudinal 0.70 G_{peak}

The combination of steady-state longitudinal acceleration of 3.7 g plus the dynamics at 125 seconds created a relatively critical compression loading condition for the upper portion of the vehicle. This can be best illustrated by a comparison of the combined load (N_c) at 125 seconds with IECD loads.

$$N_c = \frac{BM}{TRZ} + \frac{P}{2TR} - \frac{\Delta PR}{2}$$

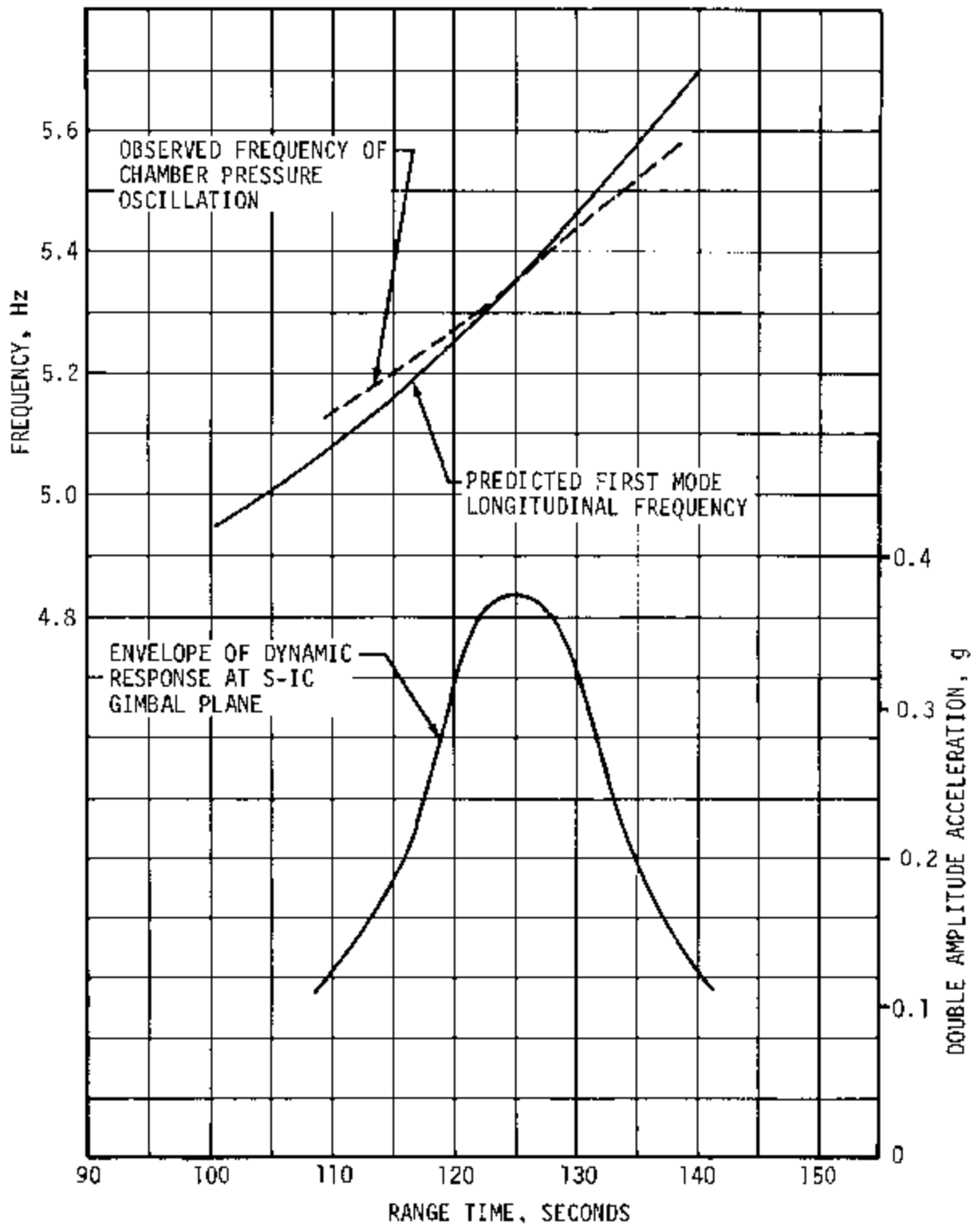


Figure 9-10. Longitudinal Oscillation Trends, 110 to 140 Seconds

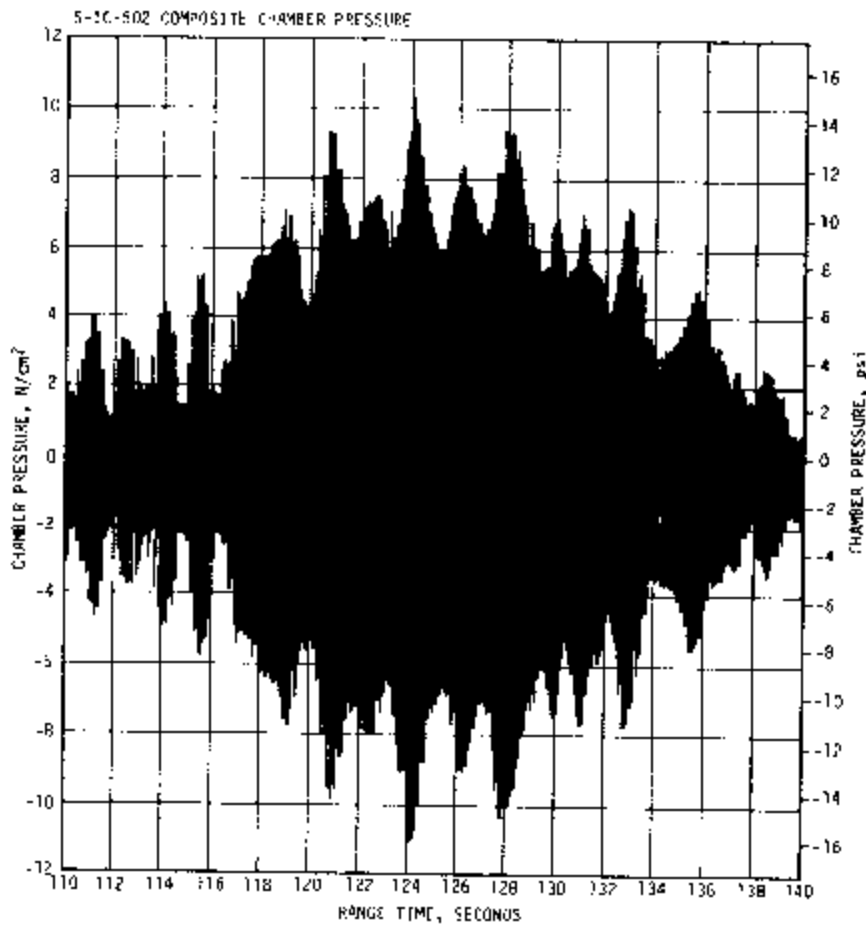
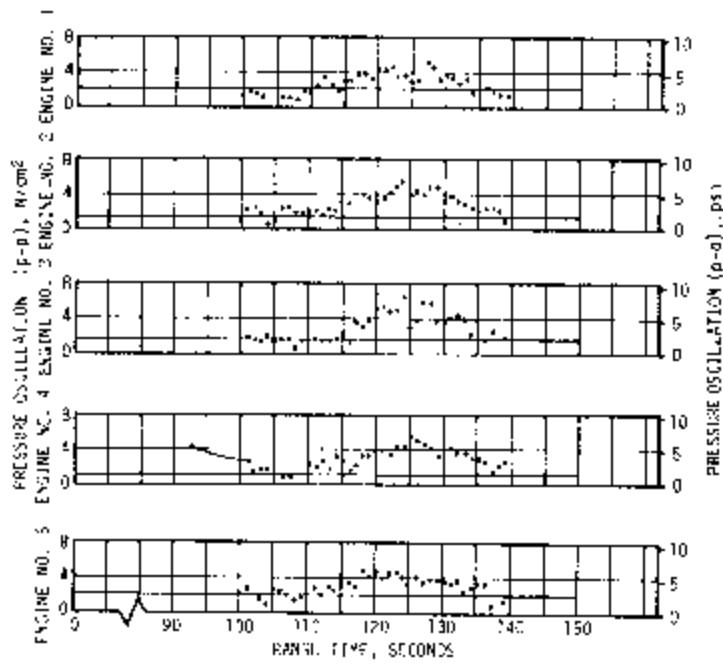


Figure 9-11. S-IC Maximum Individual Engine and Composite Chamber Pressure Oscillations

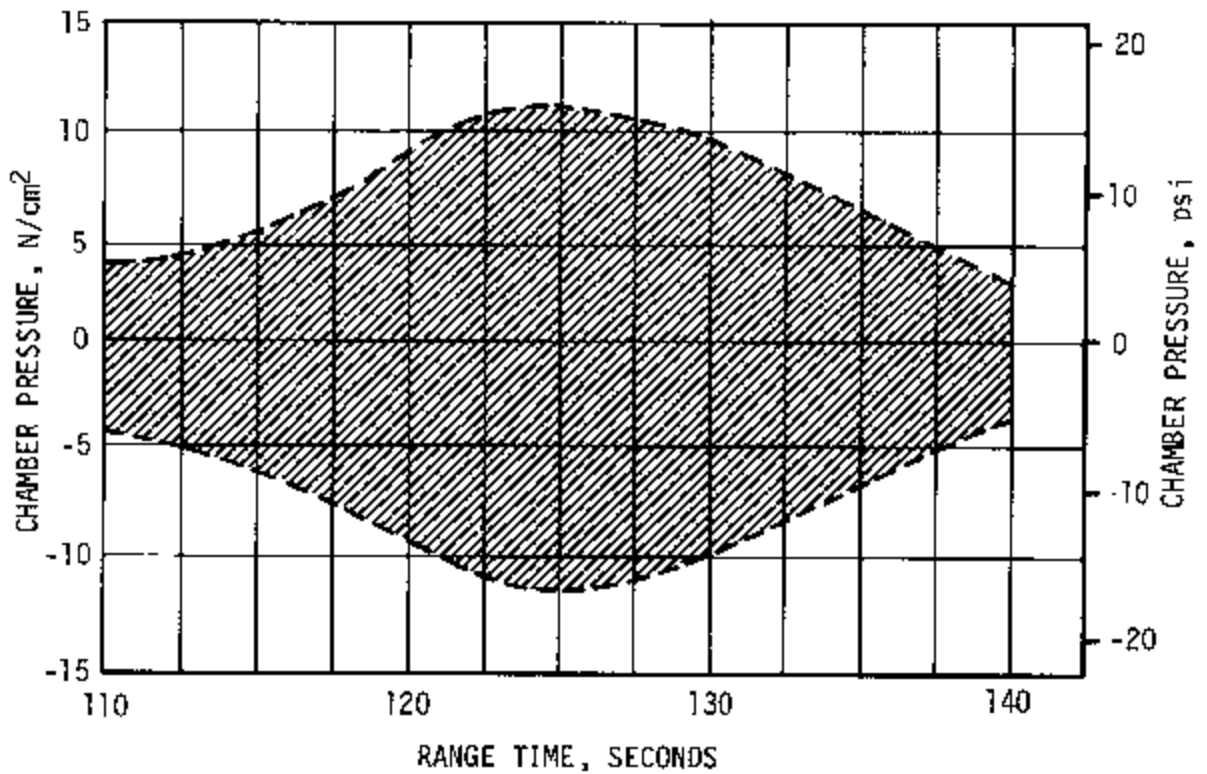
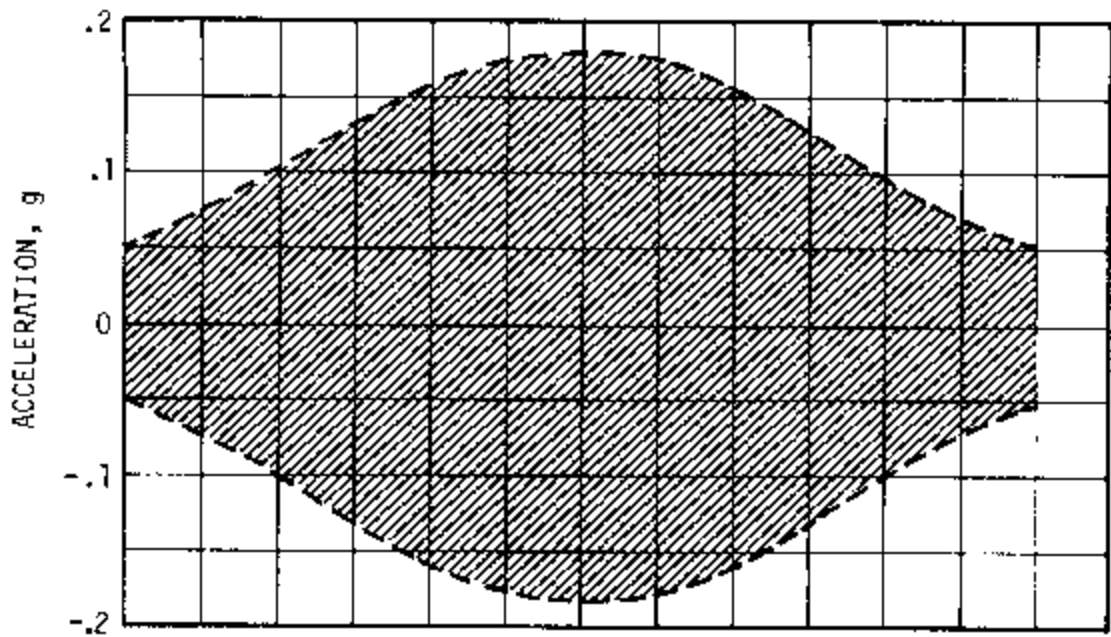


Figure 9-12. F-1 Engine Chamber Pressure and Structural Acceleration Response at S-IC Gimbal Plane During Time of High Longitudinal Oscillations

Table 9-1. Maximum Modal Accelerations at 5.5 Hertz for 110 to 140 Seconds Range Time

INSTRUMENT	VEHICLE STATIONS METERS (IN.)	S-IC RANGE TIME (SEC)	ACCELERATION (GPEAK)
PITCH			
E61-118	16.76 (660)	130	0.03
E59-118	21.67 (853)	132	0.04
A4-120	37.08 (1460)	132	0.03
A6-603	82.55 (3250)	134	0.19
GA7015	88.60 (3488)	134	0.65
CA0007A	97.41 (3835)	134	0.35
LA0012A	107.21 (4221)	130	0.40
LONGITUDINAL			
E90-115	2.92 (115)	120	0.40
E83-115	3.07 (121)	123	0.16
E82-115	3.15 (124)	124	0.18
E57-115	5.31 (209)	120	0.12
E92-117	5.72 (225)	119	0.43
E93-119	19.61 (772)	120	0.18
E58-115	21.62 (851)	128	0.14
GA7011	88.60 (3488)	125	0.70
YAW			
A7-603	82.55 (3250)	133	0.04
GA7013	88.60 (3488)	133	0.10
LA0011A	107.21 (4221)	135	0.12

Where:

- N_C = Circumferential compression shell load (lbf/in.)
- P = Axial load (lbf)
- BM = Bending moment (in.-lbf)
- R = Local vehicle radius (in.)
- ΔP = Gage ullage or venting pressure (lbf/in.²)

The combined compression loads attained the largest relative maximum, compared to IECO loads, in the S-IVB forward skirt and IU. At the IU/spacecraft interface, the limit compression load at 125 seconds was 1103.30 N/cm (630 lbf/in.) compared with 1015.74 N/cm (580 lbf/in.) at IECO. The minimum predicted ultimate capability at this time is 1523.60 N/cm (870 lbf/in.) based on a maximum heating trajectory temperature prediction. AS-502 flight was such that maximum heating was not experienced, and the minimum capability was only degraded to 2084.01 N/cm (1190 lbf/in.). The minimum factor of safety maintained through this condition for AS-502 was well in excess of 1.5. The axial load diagram, steady state plus dynamics, for this condition is presented in Figure 9-13. Lateral loading at this time was slight.

Figure 9-14 shows a comparison of normalized flight data with analytically predicted first longitudinal mode shapes. Mode shape data from the LM analysis have been included on one of the shapes for comparison purposes.

9.2.3.2 Lateral Dynamic Characteristics. Oscillations in pitch and yaw were detectable throughout S-IC powered flight. The frequencies of these oscillations agreed with the analytical predictions as shown in Figure 9-15. The first three vehicle pitch modes were detectable throughout first stage boost. The fourth mode came in very strongly near the end of first stage boost. Spectral analyses were performed to determine modal frequencies using five-second time slices. To obtain maximum acceleration levels, magnetic tape data were filtered using digital filters set at the modal frequency range. The yaw direction acceleration levels were less in the 110 to 140 second region than the pitch or longitudinal levels; however, the first mode response in the yaw direction was generally higher than in the pitch direction throughout first stage flight. Modal data for the second yaw mode were generally hidden by a two cycle noise which existed in the yaw instruments throughout first stage flight. The noise appeared in the S-IC stage and IU measurements. A comparison of normalized flight data with analytically predicted pitch and yaw mode shapes is presented in Figure 9-16.

9.2.4 S-IC Fin Dynamics

Vibration levels on the fins were high at liftoff and in the high dynamic pressure portion of AS-502 flight, but the modal frequencies did not coalesce and there was no evidence of flutter. Figure 9-17 shows that vibration levels were similar to those of AS-501. Levels observed exceeded the range of the instrumentation; however, the range of the instrumentation was below design levels.

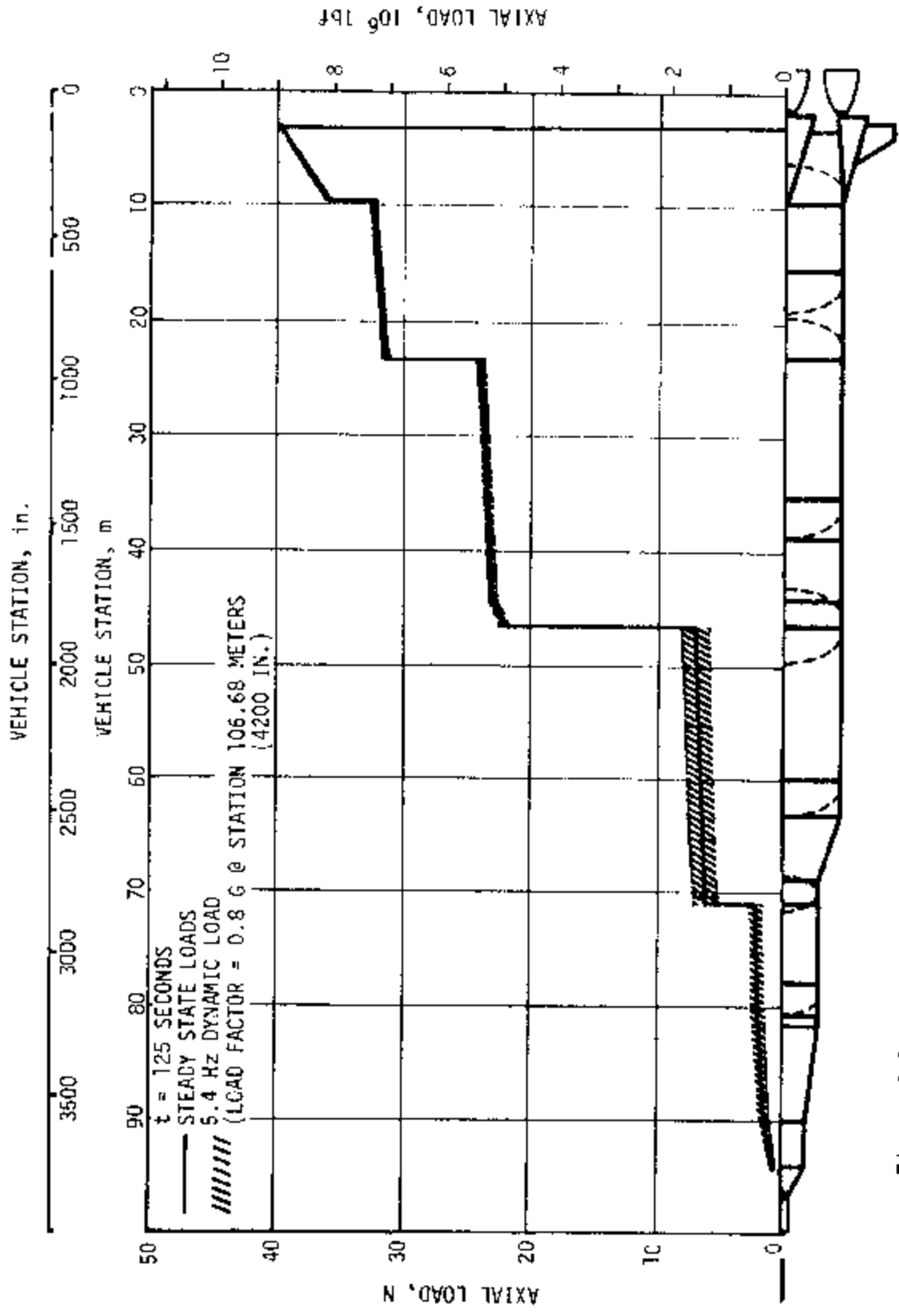


Figure 9-13. Longitudinal Loads at Time of Maximum Longitudinal Oscillation

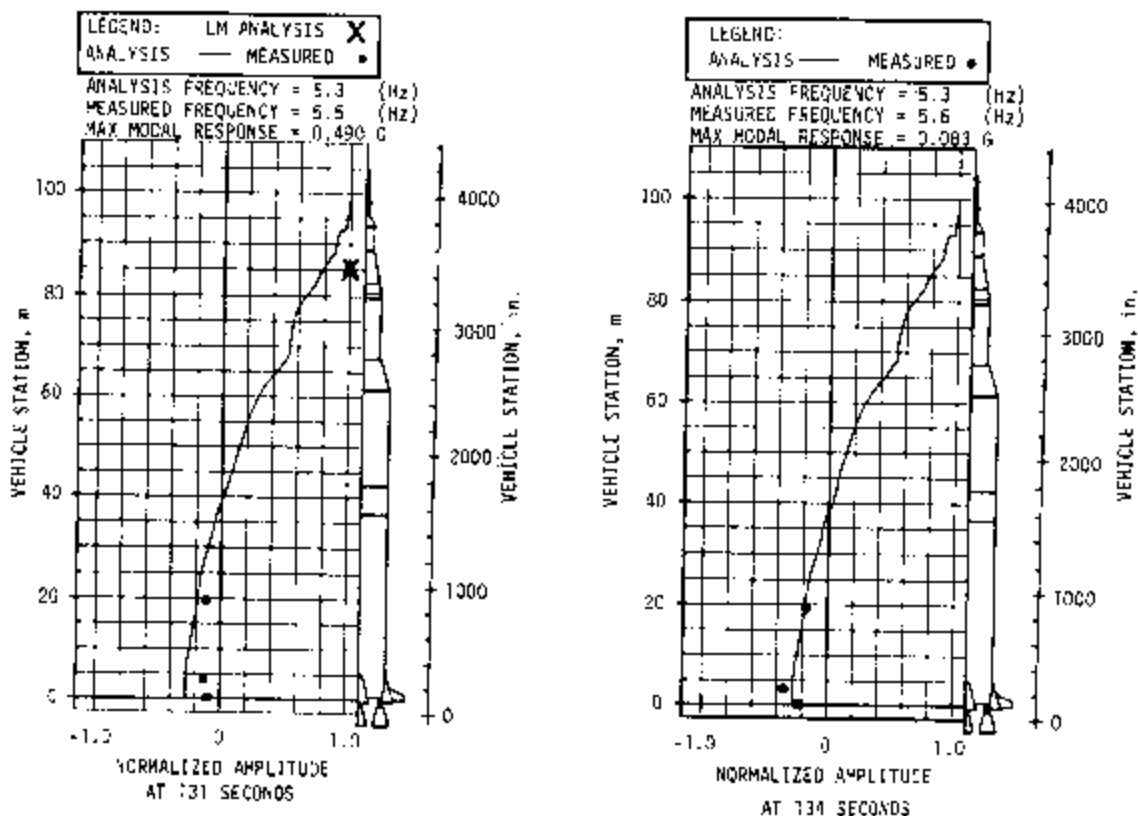


Figure 9-14. First Longitudinal Mode Shapes During S-1C Powered Flight

Measurement range increases were requested after AS-501 flight to determine fin vibration levels. These are to be incorporated into AS-503 instrumentation. Maximum bending moments on the two instrumented fins (Figure 9-18) were approximately 50 percent greater than those encountered during AS-501 flight but were far below design load. Since maximum vehicle angle-of-attack in the high dynamic pressure region occurred in the pitch plane, it is deduced that all four fins experienced approximately equal angles-of-attack, aerodynamic loading, and bending moment.

9.3 VIBRATION EVALUATION

9.3.1 S-1C Stage and Engine Evaluation

The S-1C structure, engine, and component vibration measurements (locations of measurements are shown in Figures 9-18 and 9-19) taken on the S-1C stage are summarized in Figures 9-20 through 9-22 and Table 9-2.

9.3.1.1 S-1C Stage Structure. Vibration levels in the thrust structure at liftoff were similar to static firing levels but were lower during the remainder of AS-502 flight. This trend was expected and is similar to AS-501 flight data. The intertank structure and forward skirt structure

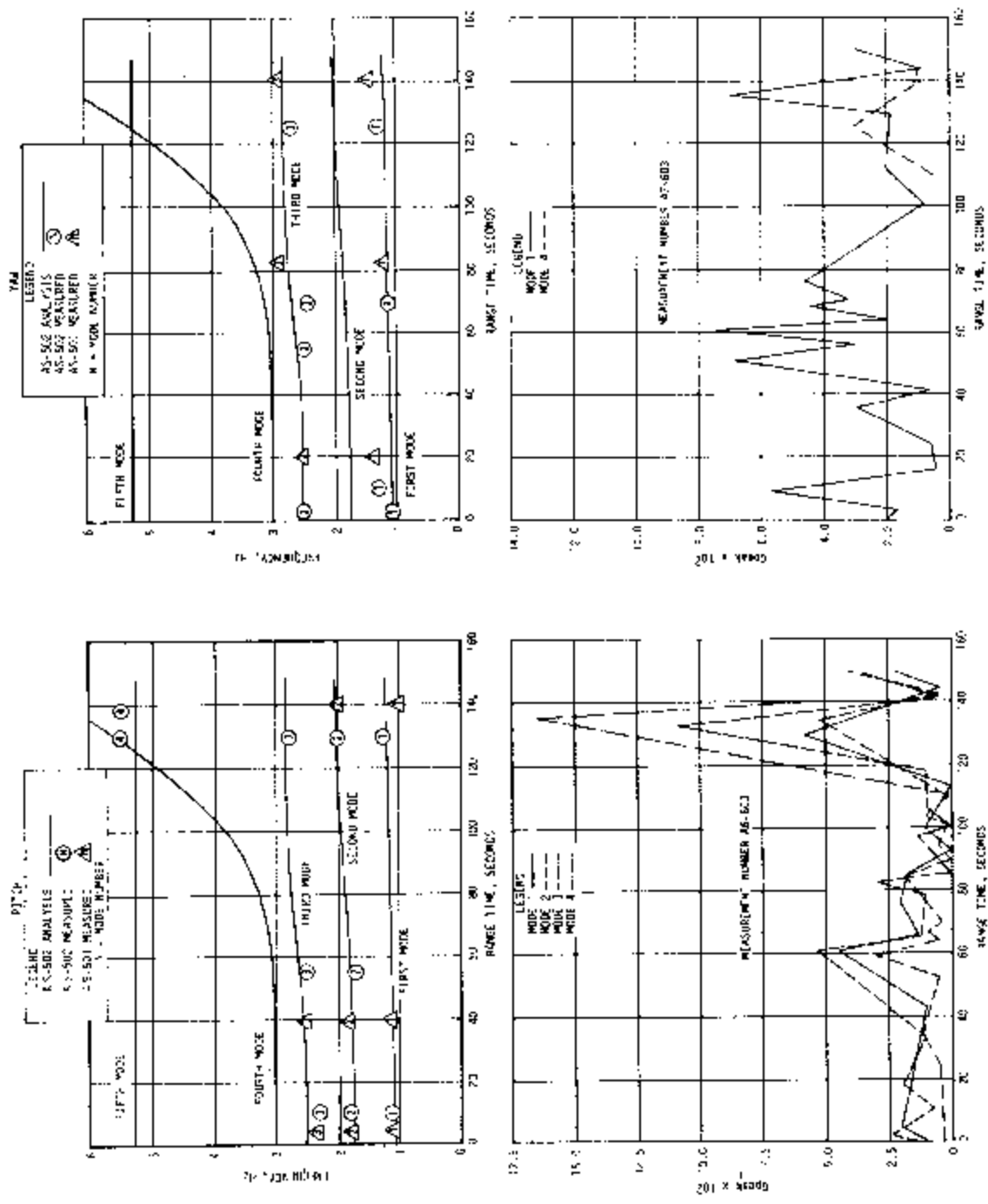


Figure 9-15. Lateral Modal Frequencies and Accelerations During S-IC Powered Flight

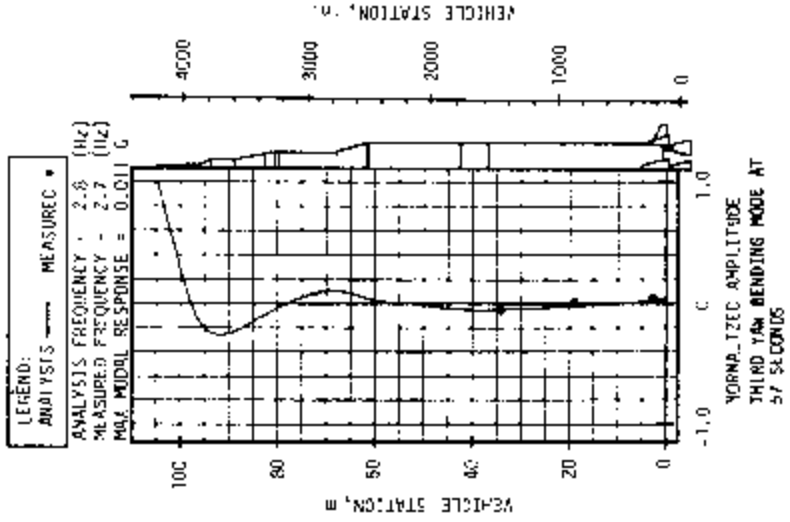
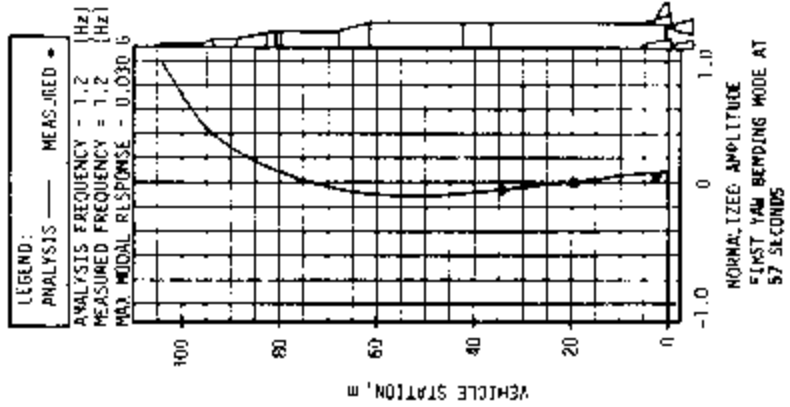
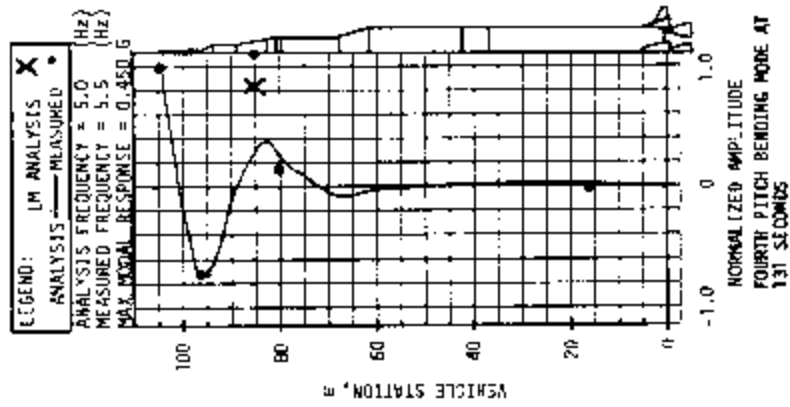


Figure 9-16. Pitch and Yaw Mode Shapes During S-IC Powered Flight

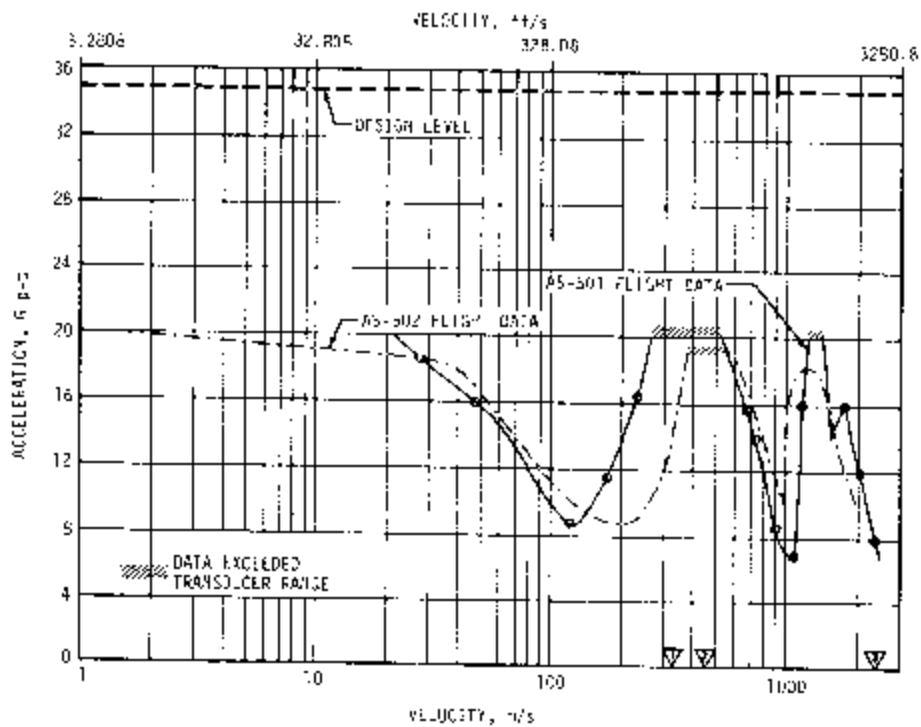
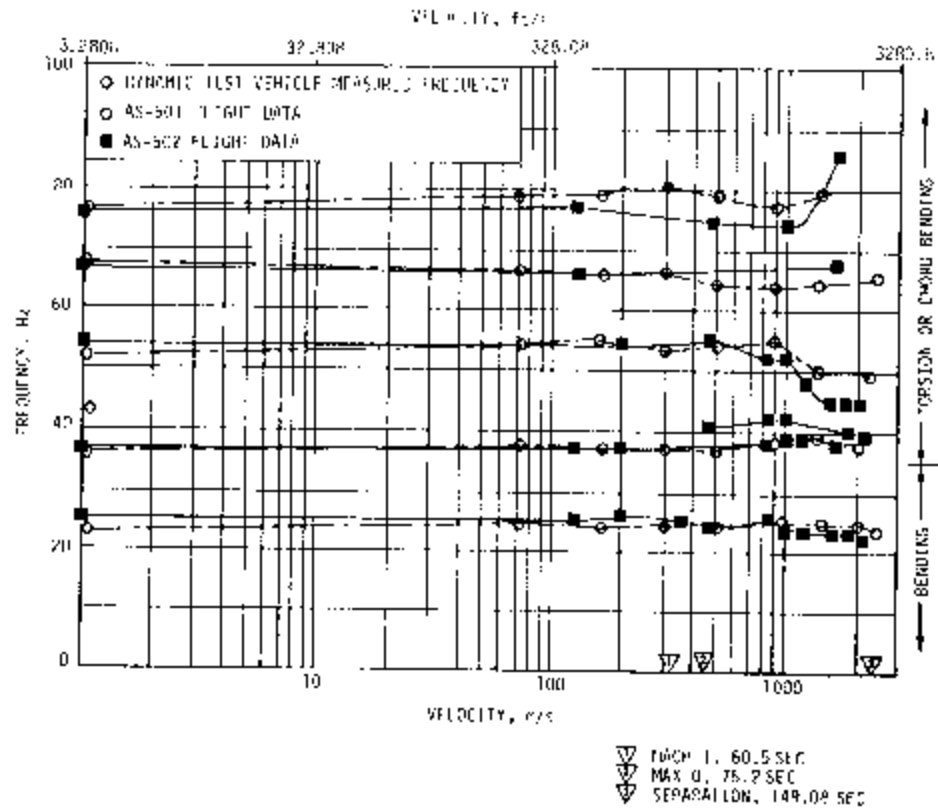


Figure 9-17. S-IC Fin Vibration Response and Bending and Torsional Modal Frequencies

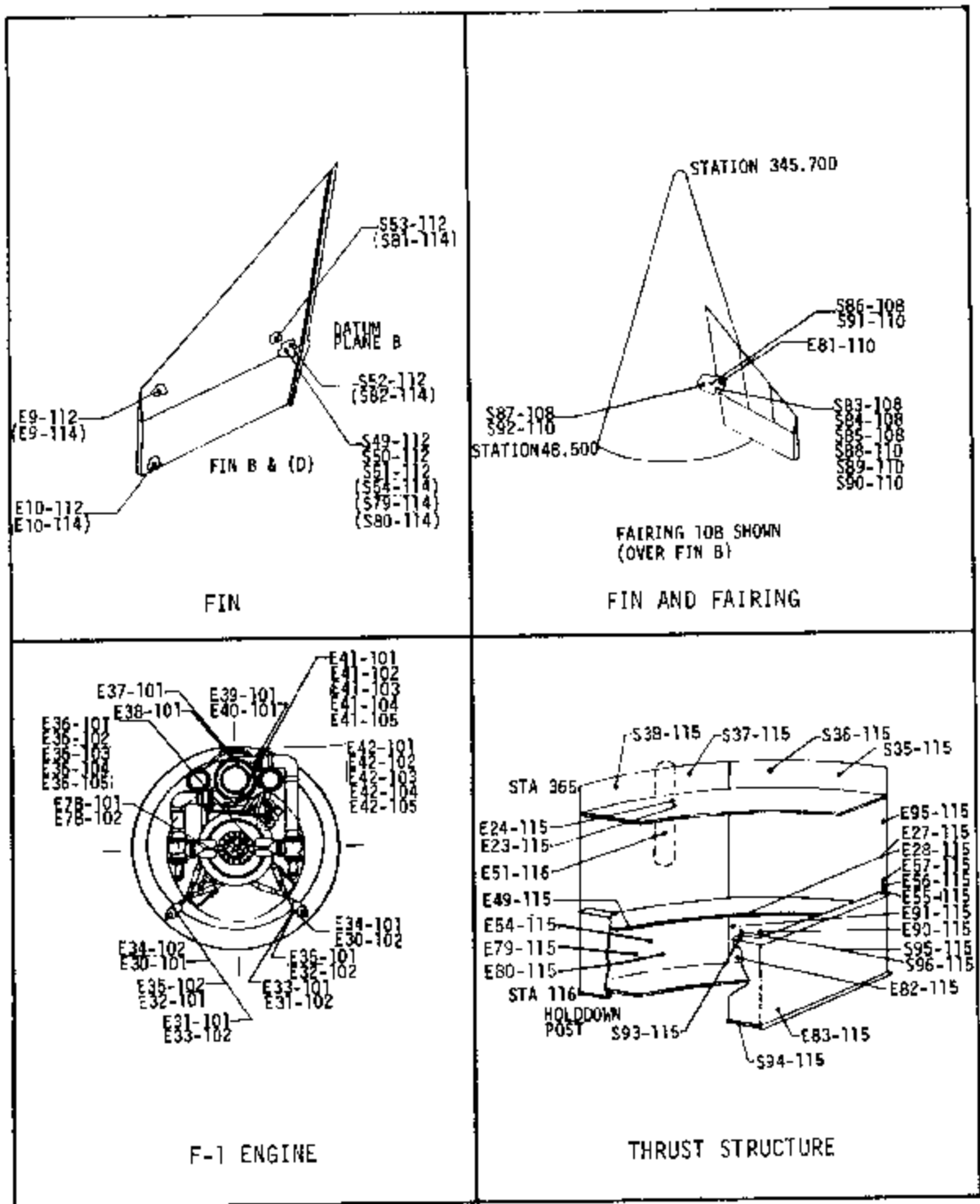


Figure 9-1B. S-IC Vibration and Strain Measurements at Fin, Fin and Fairing, F-1 Engine, and Thrust Structure

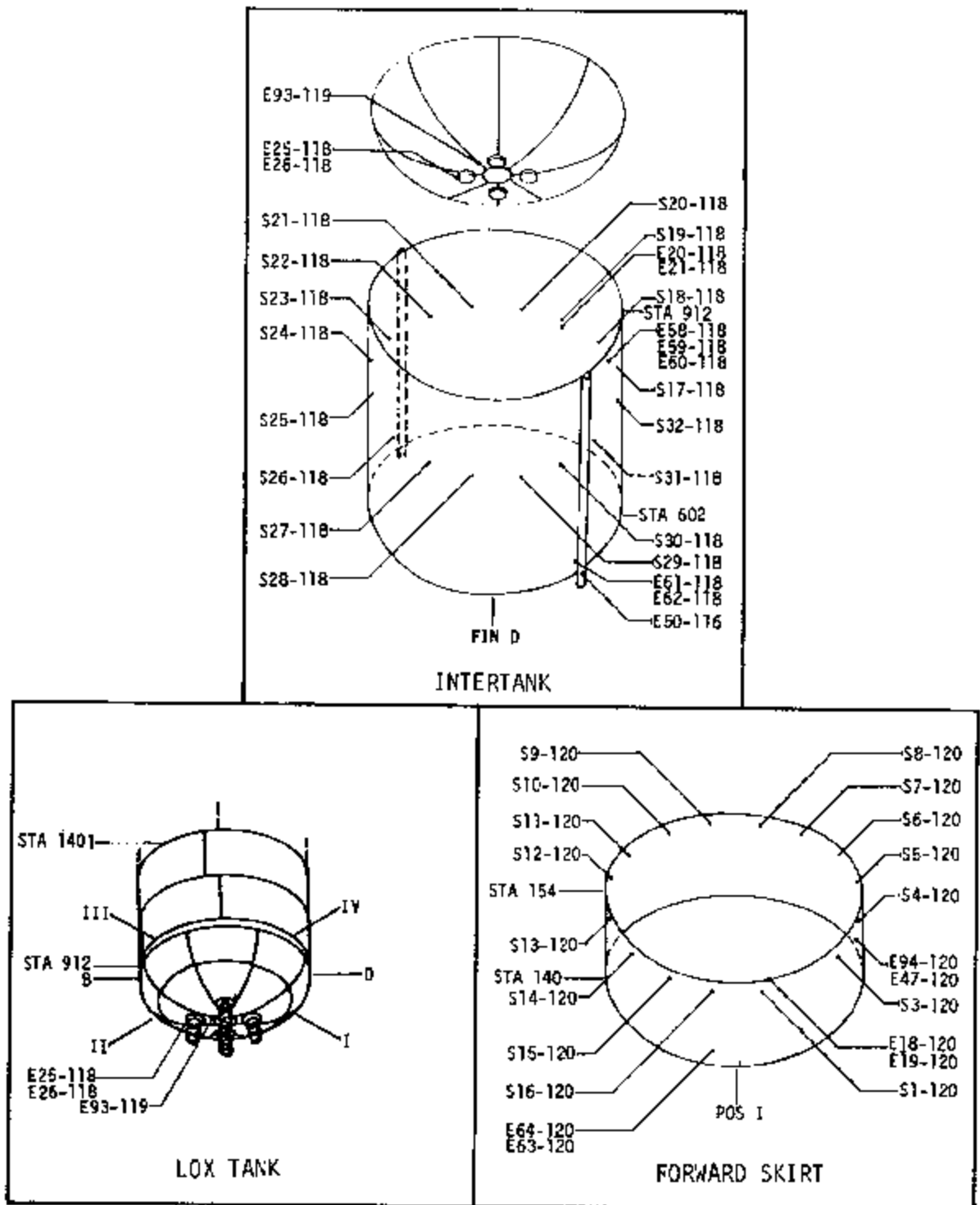


Figure 9-19. S-IC Vibration and Strain Measurements at Intertank, LOX Tank, and Forward Skirt

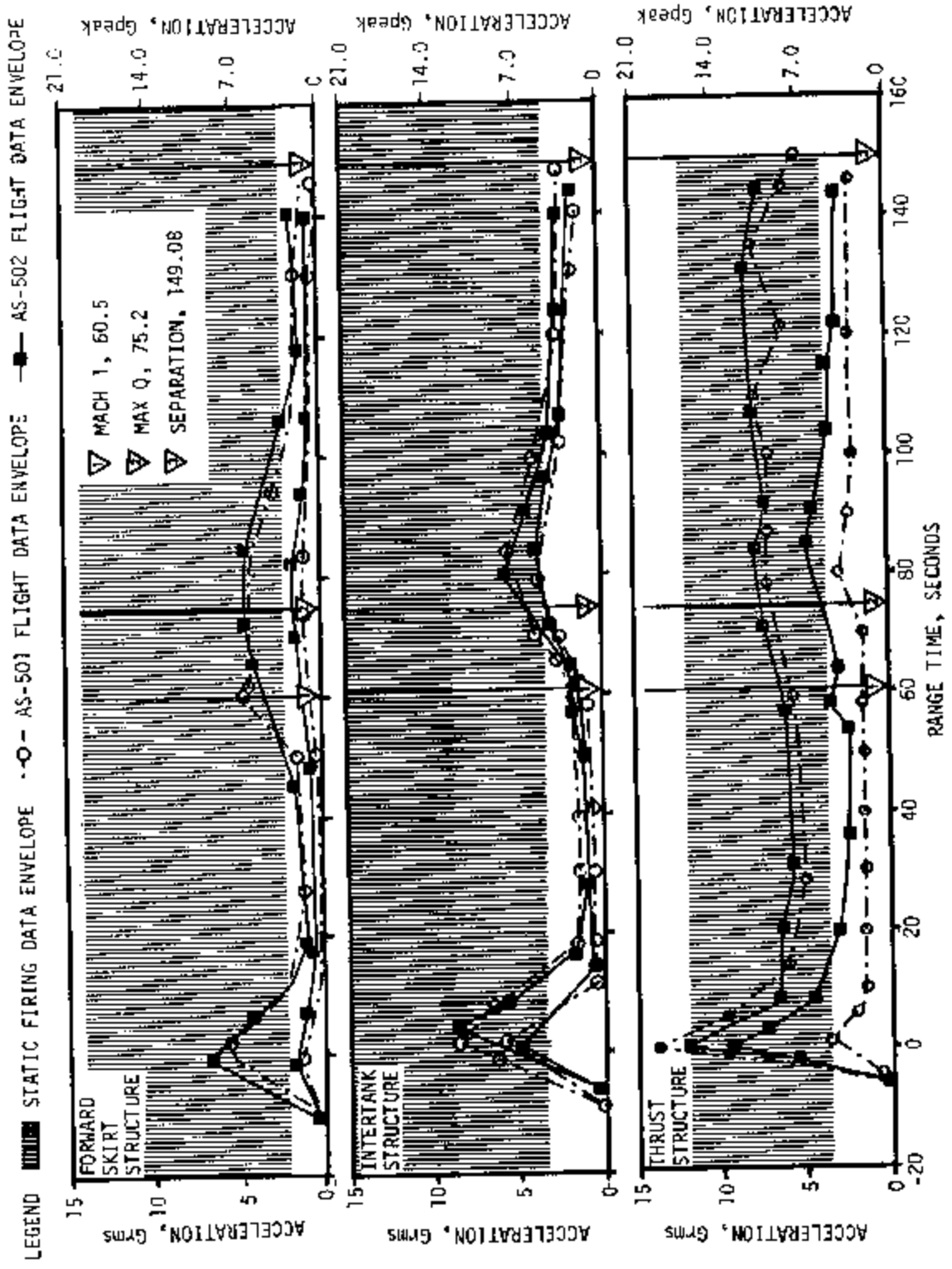
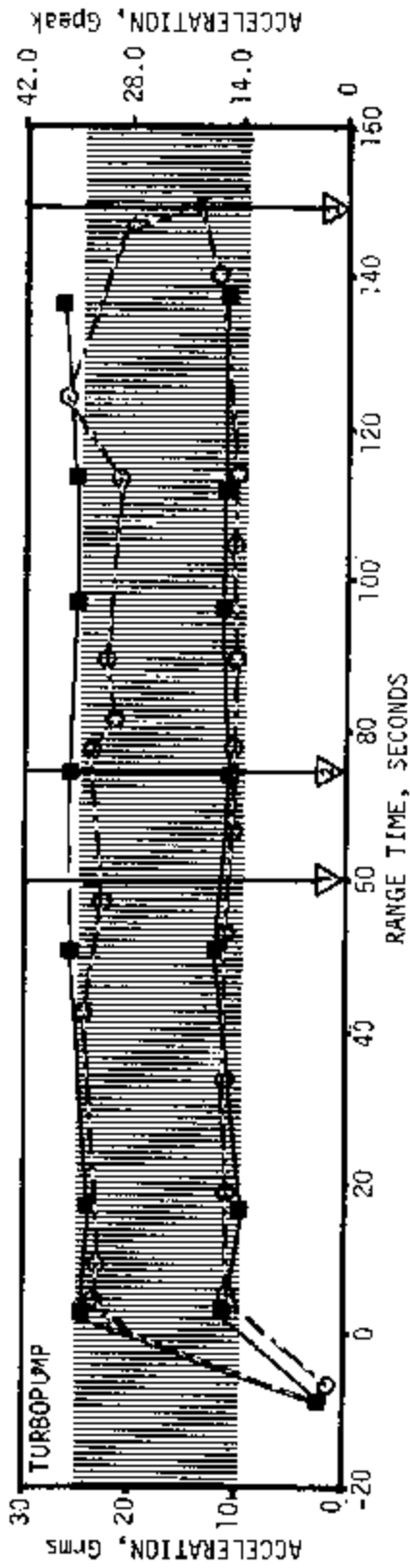


Figure 9-20. S-IC Stage Structure Vibration Envelope



▽ STATIC FIRING DATA ENVELOPE
 -○- AS-501 FLIGHT DATA ENVELOPE
 -■- AS-502 FLIGHT DATA ENVELOPE
 ▽ MACH 1, 60.5
 ▽ MAX Q, 75.2
 ▽ SEPARATION, 149.08

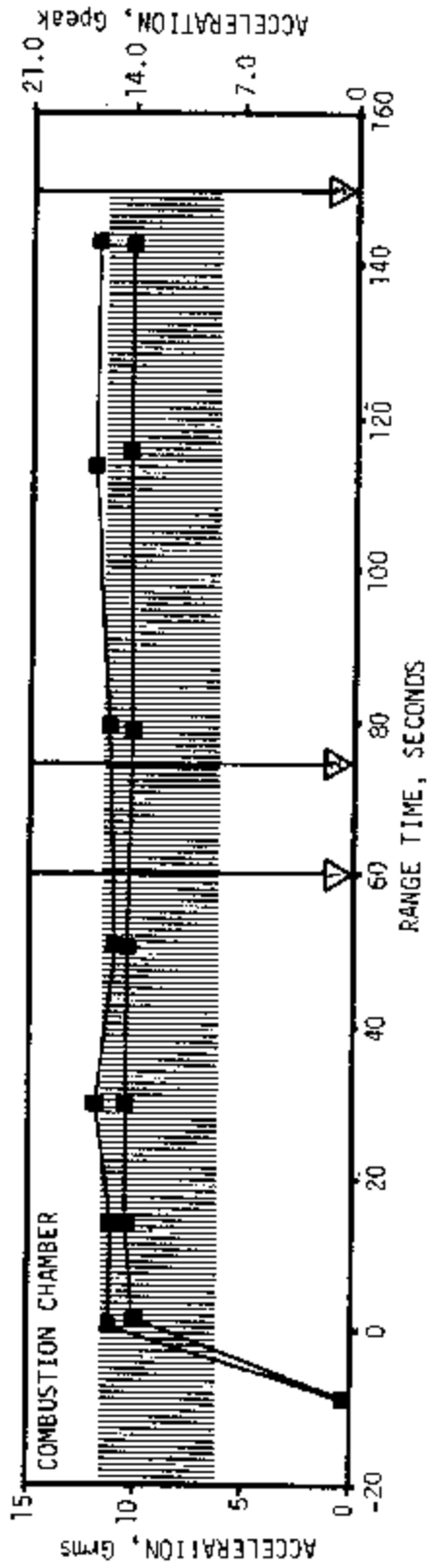


Figure 9-21. S-1C Stage Engine Vibration Envelope

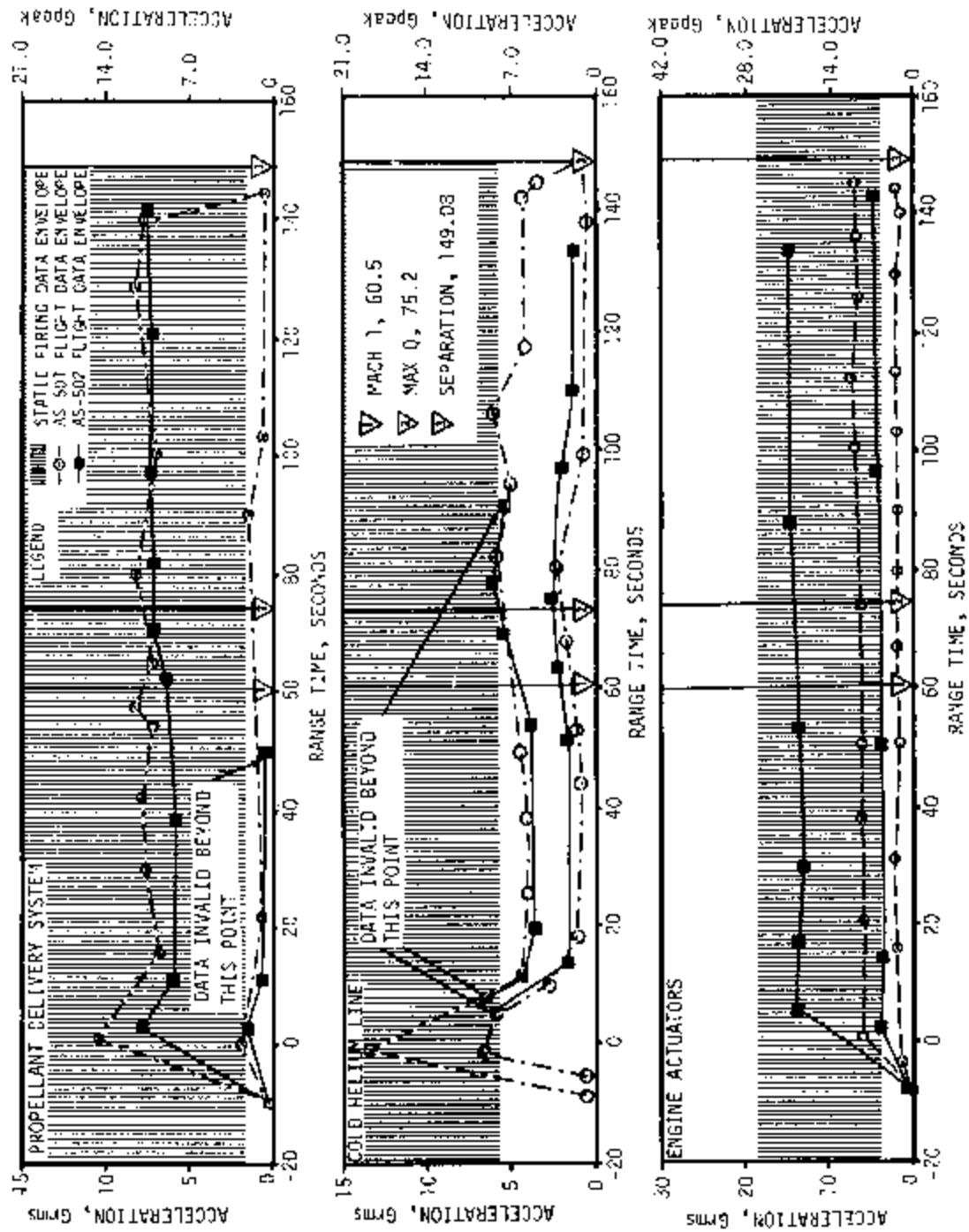


Figure 9-22. S-IC Stage Components Vibration Envelope

Table 9-2. S-IC Stage Vibration Summary

	AREA MONITORED	MAX LEVEL Gms	RANGE TIME (SEC)	REMARKS
Structure	Forward Skirt E18-120, E19-120, E47-120	6.9	-0.2	
	Intertank Structure E20-118, E21-118	8.7	5.7	
	Thrust Structure E23-115, E24-115, E49-115, E79-115, E80-115	13.4	0	The maximum Gms level of 13.4 is 1.27 Gms higher than static firing levels but the spectra are very similar.
Engine	Combustion Chamber E36-101, E36-103, E36-104, E36-105	12.4	20.5	
	Turbopump E41-102, E42-102, E42-103, E42-104	26.7	136.0	
Components	Propellant Delivery System LOX Feed Line and Pressure Volume Compensator Support Bracket E25-118, E26-118, E27-115	10.1	-0.2	
	Cold Helium Line E50-116, E51-116	6.7	9.0	
	Engine Actuators E30-101, E30-102, E31-101, E31-102, E32-101, E32-102, E33-101, E33-102, E34-101, E34-102, E35-102	14.6	17.0	

show vibration levels similar to AS-501 flight data. The levels for launch and throughout AS-502 flight were lower than static firing levels.

9.3.1.2 F-1 Engines. Four of the five F-1 engine combustion chamber vibration measurements yielded valid data. Overall rms levels were higher than static firing data. All five vibration measurements on the combustion chamber of AS-501 were invalid. The engine turbopump vibration levels, although slightly higher during AS-502 flight, were generally comparable to static firing and AS-501 flight levels.

9.3.1.3 S-IC Stage Components. The responses of components on the S-IC, engine actuators, cold helium line, and propellant delivery system are summarized in Figure 9-22 and Table 9-2. The engine actuator measurements showed amplitudes similar to static firing data and somewhat higher than AS-501 flight data. Generally, cold helium line measurements showed levels lower than static firing levels and similar to AS-501 flight levels. All AS-502 flight cold helium data were invalid before 3 seconds. Measurements taken on the propellant delivery system show data similar to the static firing and AS-501 data. The constant level throughout flight indicates that the vibration was a result of flow dynamics and not affected by acoustics. On the vibration isolated panels, the only valid data obtained was from one measurement at launch. This measurement indicated very low level vibrations as expected and therefore is not shown in Figure 9-22.

9.3.2 S-II Stage and Engine Evaluation

S-II structure, engine, and component vibration measurements evaluated on the S-II stage are summarized in Figures 9-23 through 9-26 and Table 9-3. AS-501 data shown for comparison have been updated since release of the AS-501 flight evaluation report. Spectral analyses indicated that the basic AS-502 spectral shapes were the same as for AS-501. The energy is concentrated in narrow bands with major peaks occurring near 100 hertz.

9.3.2.1 S-II Stage Structure. The trends were as expected on the aft skirt, thrust cone, and interstage; however, forward skirt in the liftoff environment on the flame bucket side away from the tower exceeded the sine and random criteria. These exceedances occurred at frequencies near 100 hertz on both AS-501 and AS-502. The exceedances were more pronounced on AS-502 but no adverse effects were noted on either flight.

9.3.2.2 S-II Stage J-2 Engines. The 15 S-II engine vibration measurements (combustion domes, LOX pump, and LH₂ pumps) for AS-501 and AS-502 were considered invalid because of amplifier saturation at frequencies above 3000 hertz.

9.3.2.3 S-II Stage Components. Results were within design levels except for the forward skirt containers which, like the forward skirt structure, exceeded the design criteria for about 1 second during the liftoff period. No failures occurred in the affected equipment.

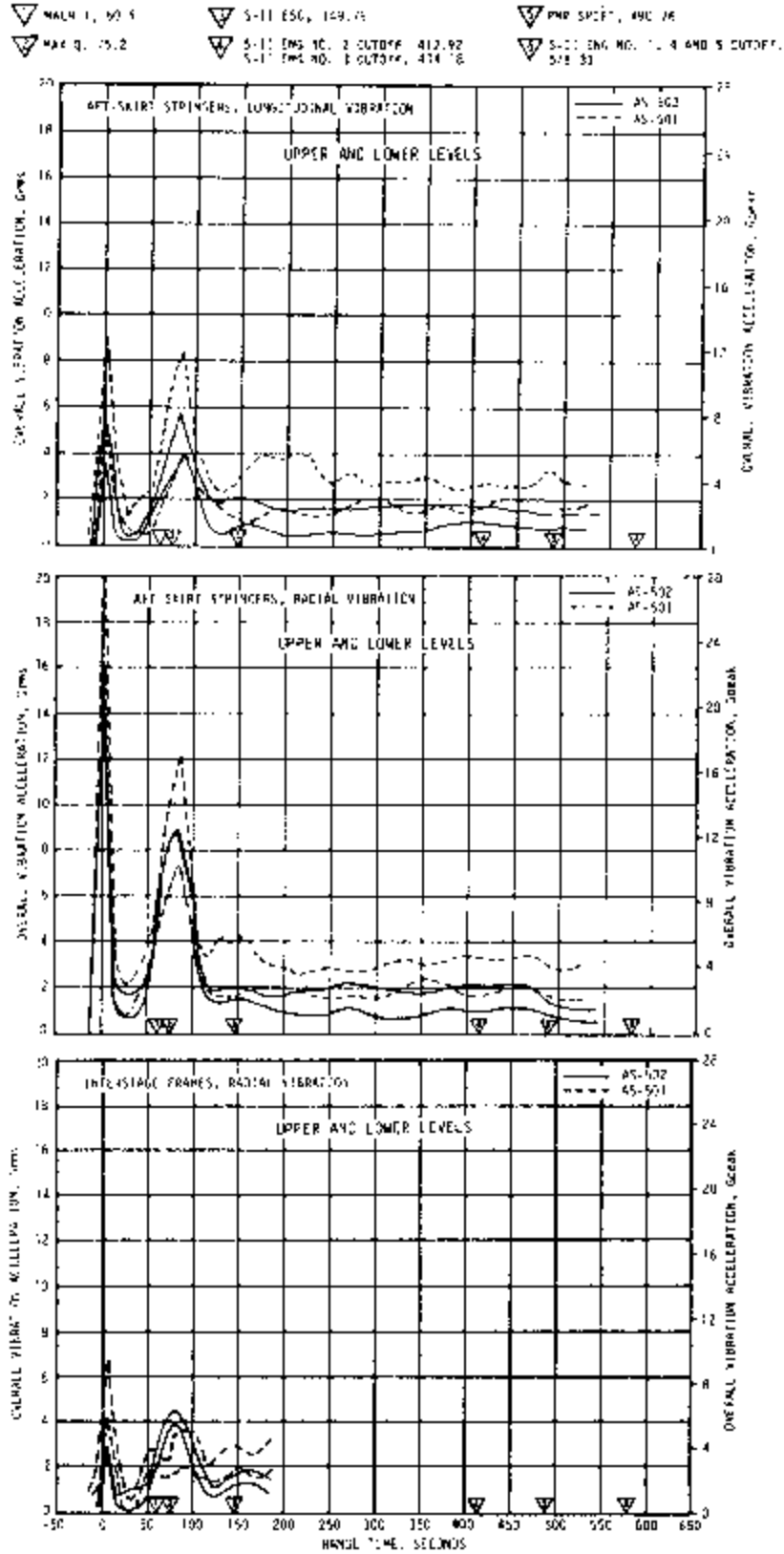


Figure 9-24. S-II Stage Structure Vibration Envelopes at Aft Skirt Stringers and Interstage Frames

Table 9-3. S-II Vibrations, Vehicle Structure

ZONE	NO. OF MEASUREMENTS	S-II 501 AND 502 STATIC FIRINGS	VEHICLE	OVERALL GRMS		
				LIFTOFF	TRANSONIC	MAX. Q
Forward Skirt Containers	8	0.7-2.1	AS-501 AS-502	1.4-8.8	2.1-3.7	2.4-5.1
				2.7-9.0	0.7-2.5	1.1-4.6
Forward Skirt Stringers	10	1.6-4.8	AS-501 AS-502	3.5-11.0	2.3-11.3	3.7-9.2
				3.4-13.1	1.8-7.6	2.7-8.0
Aft Skirt	4	10.1-31.7	AS-501 AS-502	5.5-17.3	3.6-6.2	5.7-12.1
				5.3-14.8	5.2-8.3	5.4-9.4
Interstage	4	Interstage Not Install.	AS-501 AS-502	3.4-5.9	2.0-3.5	2.6-4.5
				3.1-4.8	2.2-3.3	2.8-4.1
Thrust Structure Containers	10	2.2-15.8	AS-501 AS-502	0.8-7.0	0.6-1.8	0.6-2.2
				0.6-2.4	0.4-1.1	0.5-1.4
Thrust Structure Long.	3	4.1-12.3	AS-501 AS-502	1.6-5.1	1.1-2.0	1.2-2.2
				1.0-3.7	0.6-1.6	0.7-1.7
Engine Beams	5	5.4-15.4	AS-501 AS-502	0.9-1.5	0.5-0.9	0.6-1.0
				0.5-1.0	0.3-0.4	0.4-0.5
Gimbal Pad	1	8.8	AS-501 AS-502	1.0	0.9	0.9
				0.4	0.3	0.3
						5.6
						4.5

9.3.3 S-IVB Stage and Engine Evaluation

Nine vibration measurements were made on the structure, twenty-two at components and six on the engine. Measurement locations are shown in Figure 9-27. The maximum composite (50 to 3000 hertz) vibration levels on the structure, forward components, aft components, and engine are summarized in Figure 9-28 and Table 9-4. For comparison purposes, the vibration levels are shown with measurements taken during AS-501 flight.

9.3.3.1 S-IVB Stage Structure and Components. The maximum vibration levels measured on the S-IVB structure were slightly lower on AS-502 than on AS-501. Forward component maximum vibration levels were greater on AS-502 than measured at similar locations during the AS-501 flight. The maximum vibration levels measured at the aft components were 70 percent of those measured at similar locations during the AS-501 flight.

9.3.3.2 S-IVB Stage J-2 Engine. The maximum vibration levels measured on the engine were almost identical to those measured during the first S-IVB burn of the AS-501 flight.

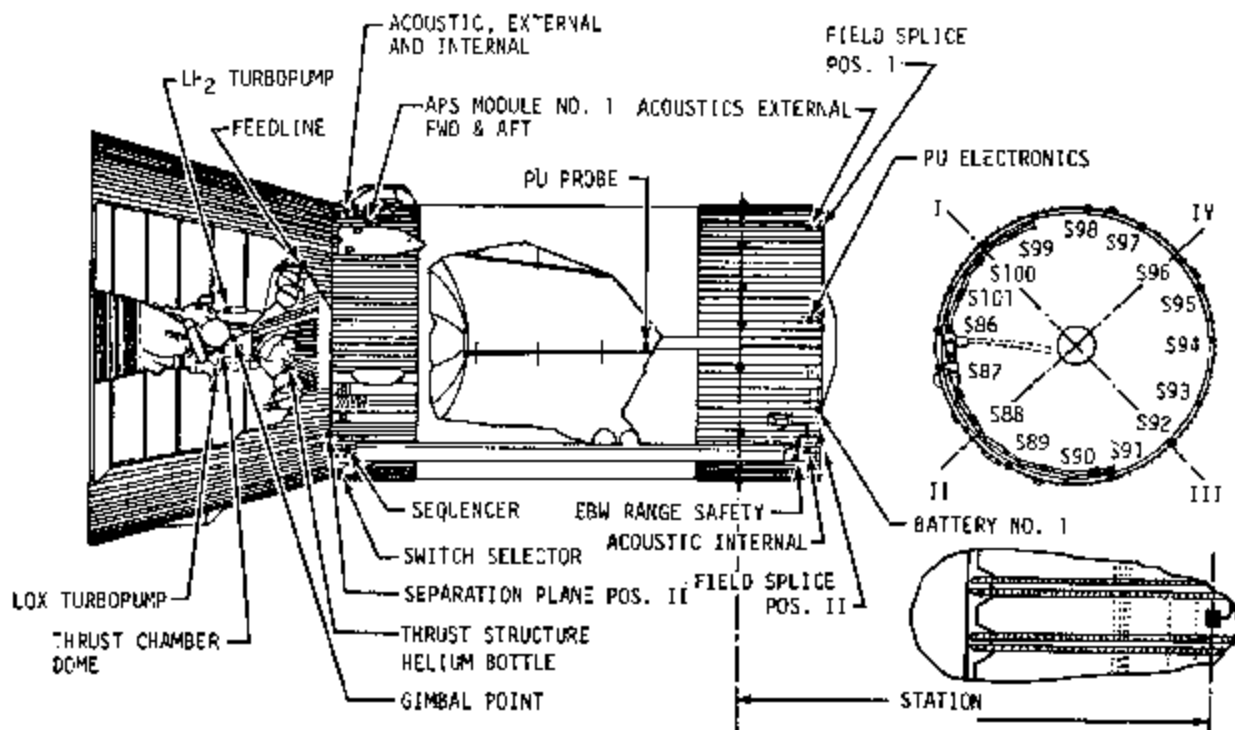


Figure 9-27. S-IVB Acoustics, Vibration and Dynamic Strain Measurements

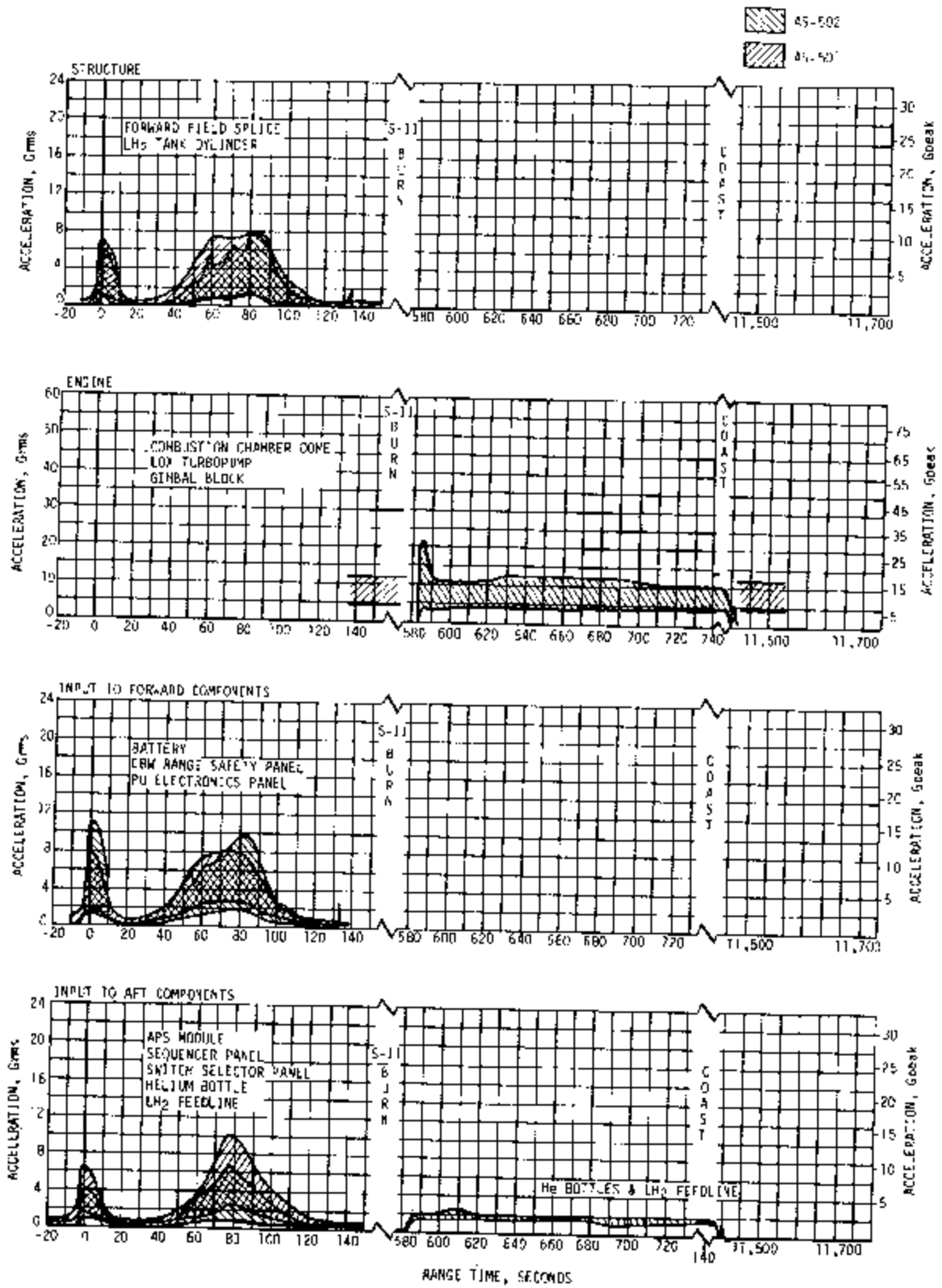


Figure 9-28. S-IVB Stage Vibration Envelopes

Table 9-4. S-IVB Vibration Summary

	AREA MONITORED	MAX LEVEL (Grms)	RANGE TIME (SEC)	REMARKS
Structures	Separation Plane, Pos II - Thrust	0.8	3	The maximum vibration due either to sound pressure at liftoff, turbulence at maximum dynamic pressure, or to J-2 engine operation.
	Field Splice Pos I (1f) - Thrust	0.7	0	
	Field Splice Pos I - Thrust	6.0	89	
	Field Splice Pos I - Pitch	7.6	89	
	Field Splice Pos I - Yaw	4.7	89	
	Field Splice Pos II - Thrust	4.4	80	
	Field Splice Pos II - Pitch	3.0	86	
	Field Splice Pos II - Yaw	8.6	83	
	LH2 PU Probe Input - Radial	6.8	1	
	Component (LH2 Tank)	Gimbal Point - Thrust	4.5	
Gimbal Point - Pitch		5.3	739	
Gimbal Point - Yaw		4.2	739	
Combustion Chamber, Dome - Thrust		9.1	589	
LOX Turbopump - Lateral		2.1	586	
Component (Fwd Skirt)		PU Electronic Panel Input - Thrust	4.3	78
	PU Electronic Panel Input - Radial	10.6	1	
	PU Electronic Panel Response - Radial	5.5	1	
	EBW Range Safety Panel Input - Thrust	3.2	80	
	EBW Range Safety Panel Input - Radial	Invalid		
	EBW Range Safety Panel Response - Radial	2.2	2	
	Battery No. 1 Input - Thrust	2.1	78	

Table 9-4. S-IVB Vibration Summary (Continued)

	AREA MONITORED	MAX LEVEL (Gms)	RANGE TIME (SEC)	REMARKS
Component (Fwd Skirt) (Cont)	Battery No. 1 Input - Radial Battery No. 1 Input - Tangential	4.2 1.9	72 1	
Component (Aft Skirt)	Sequencer Panel Input - Thrust Sequencer Panel Input - Radial Sequencer Panel Response - Radial Switch Selector Panel Input - Thrust Switch Selector Panel Input - Radial Switch Selector Panel Response - Radial APS Mod-1 Aft Attach Point Input - Thrust APS Mod-1 Aft Attach Point Input - Radial APS Mod-1 Fwd Attach Point Input - Radial	5.9 7.8 2.8 4.8 6.6 3.5 2.8 4.2 5.7	78 78 78 83 80 1 80 75 75	Due to a loose connector.
Component (Thrust Structure)	He Bottle Input - Thrust He Bottle Input - Pitch He Bottle Input - Yaw LH2 Feedline Input - Thrust	1.8 2.2 2.1 2.2	589 589 2 2	

9.3.4 S-IVB Stage Forward Skirt Dynamics

Sixteen dynamic strain gage measurements were placed on the AS-502/S-IVB forward skirt for the purpose of investigating possible panel flutter characteristics during the supersonic flight regime. These measurements were located at vehicle station 79.64 meters (3135.5 in.) and placed approximately every 22.5 degrees around the circumference of the skirt section as shown in Figure 9-27. The measurement numbers were S0086-426 through S0101-426. Positioning of each strain gage was such that it was mounted 10.16 centimeters (4 in.) forward of the panel trailing edge. This location was chosen because data was obtained at the same point during earlier wind tunnel tests. The envelopes of the maximum and minimum composite (0 to 800 hertz) strain levels measured at these locations are shown in Figure 9-29. The envelopes from the AS-204 flight are also shown.

The time history of the composite dynamic strain levels from most of the measurements followed the same trend as the acoustic levels measured on the forward skirt shown in Figure 16-18 (Section 16).

Angle-of-attack and differential pressure across the panels are important parameters to consider when assessing panel flutter severity. Figure 11-10 (Section 11) shows the angle-of-attack history for AS-502 and Figure 9-30 shows the differential pressure history. For angles-of-attack smaller than two degrees, all the panels are assumed to be buckled due to axial loads alone. At larger angles-of-attack, a load relief is experienced on the windward side of the vehicle and a higher axial load exists on the leeward side. The panels would be most susceptible to flutter near the critical buckling load of the panel.

The differential pressure time histories across the panels at stations 80.49 meters (3196 in.) and 78.99 meters (3110 in.) are shown in Figure 9-30. The dynamic strain gage location is approximately midway between these stations. These differential pressure loads were calculated by using the internal compartment pressure measurement D0051-411 and external aerodynamic data obtained from the AS-204 flight. The presence of a pressure differential across a panel will tend to decrease the flutter potential and/or suppress the resulting panel flutter stress amplitudes. Angles-of-attack greater than about two degrees will decrease the pressure differential loading on panels on the windward side of the vehicle making conditions more favorable for flutter to occur.

The flight data showed a random response during the liftoff, Mach 1 and Max Q regimes. This response is typical and results from engine acoustics and inflight fluctuating pressures. In the regime after Max Q, 77 seconds $\leq t \leq$ 92 seconds, measurement numbers S-90, S-92, S-93, S-94, S-97, S-100, and S-101 show a complex periodic waveform and a corresponding increase in strain amplitude. These waveforms are characteristic of buckled panel flutter and indicative that panel flutter did occur during flight. Typical examples of these strain time histories are shown in

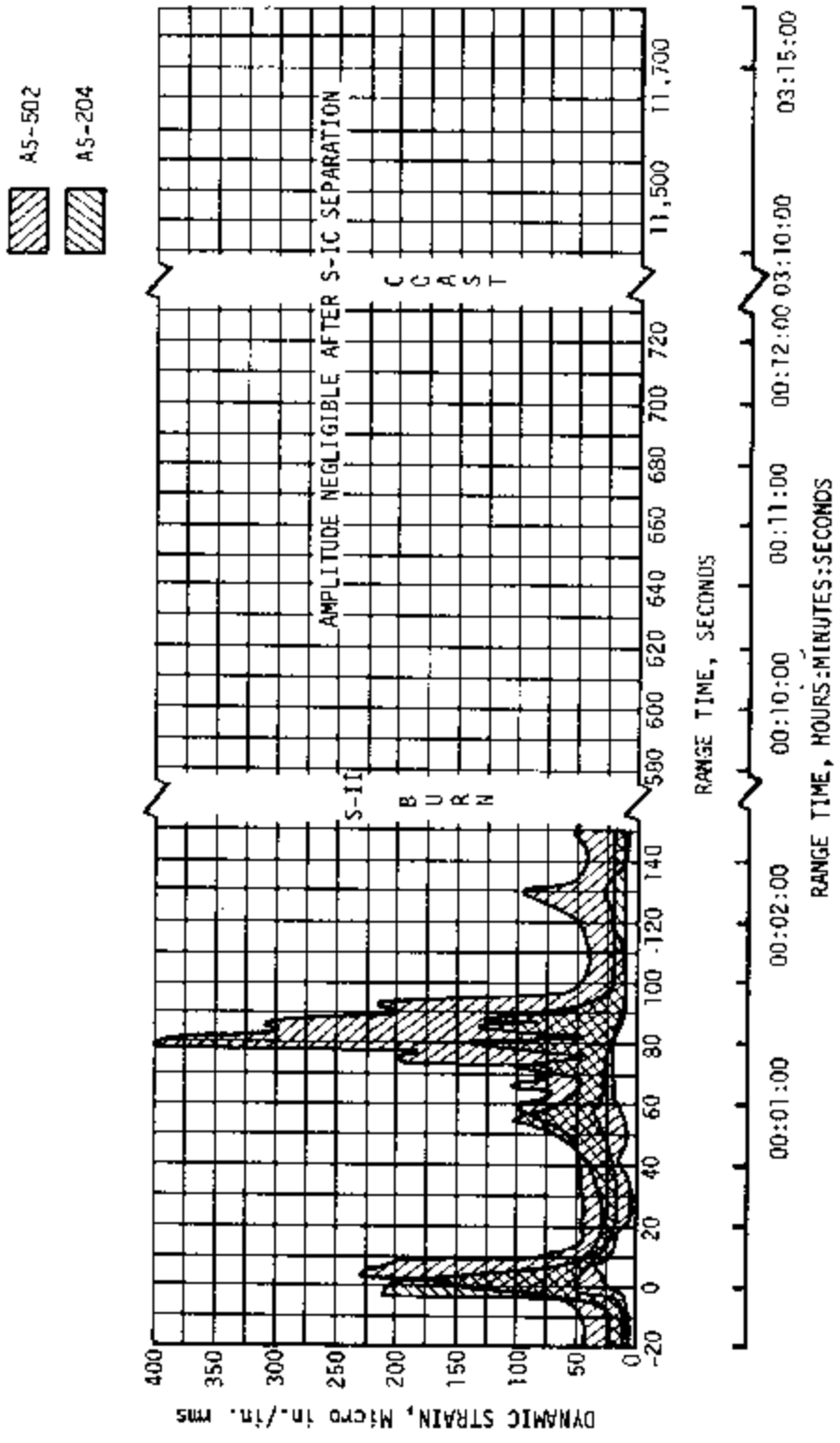


Figure 9-29. S-1VB Forward Skirt Dynamic Strain

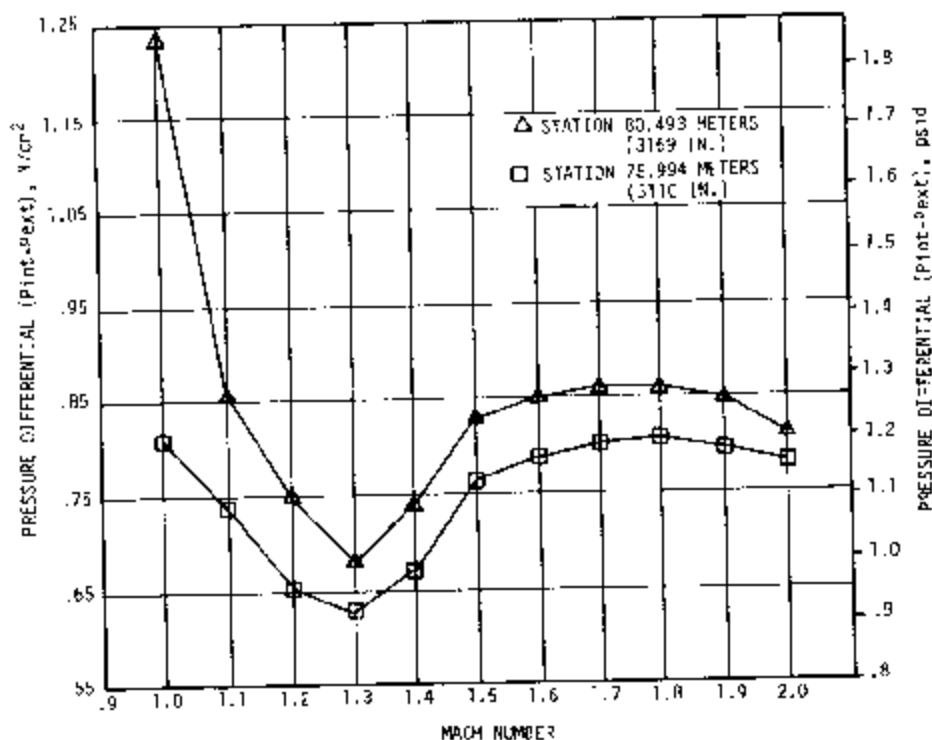


Figure 9-30. Pressure Differential Across S-IVB Forward Skirt Panels

Figure 9-31. S-100 and S-101 exhibited the highest strain amplitudes during flight. These values were 1750 μ in./in. and 2000 μ in./in. of strain and occurred at 88 seconds ($2.2 \leq \text{Mach} \leq 2.4$) and 80 seconds ($1.7 \leq \text{Mach} \leq 1.9$), respectively. The flutter frequency was approximately 150 hertz for S-100 and 300 hertz for S-101. An rms strain history for these respective flutter frequencies is shown in Figure 9-32. The differential pressure across the panels at this time was approximately 0.83 N/cm² (1.2 psid).

It is concluded from these data that panel flutter did occur on the above S-IVB forward skirt panels. The pressure differential across the panels suppressed the stress amplitudes to a tolerable level for the AS-502 flight. Although these flutter amplitudes tended to be suppressed by the very high ΔP , they were about three times higher than those measured on AS-204. Detailed analysis and evaluation of these data will provide guidance for future action with respect to vent area criteria and/or structural fixes.

9.3.5 Instrument Unit Evaluation

Eight measurements were used on the IU for monitoring structural vibration at the upper and lower interface rings. Twenty measurements were used to monitor IU component vibration levels. For comparison purposes, the IU structure and component measurements are shown with those taken during the AS-501 flight. Figure 9-33 shows the Grms time histories of these measurements.

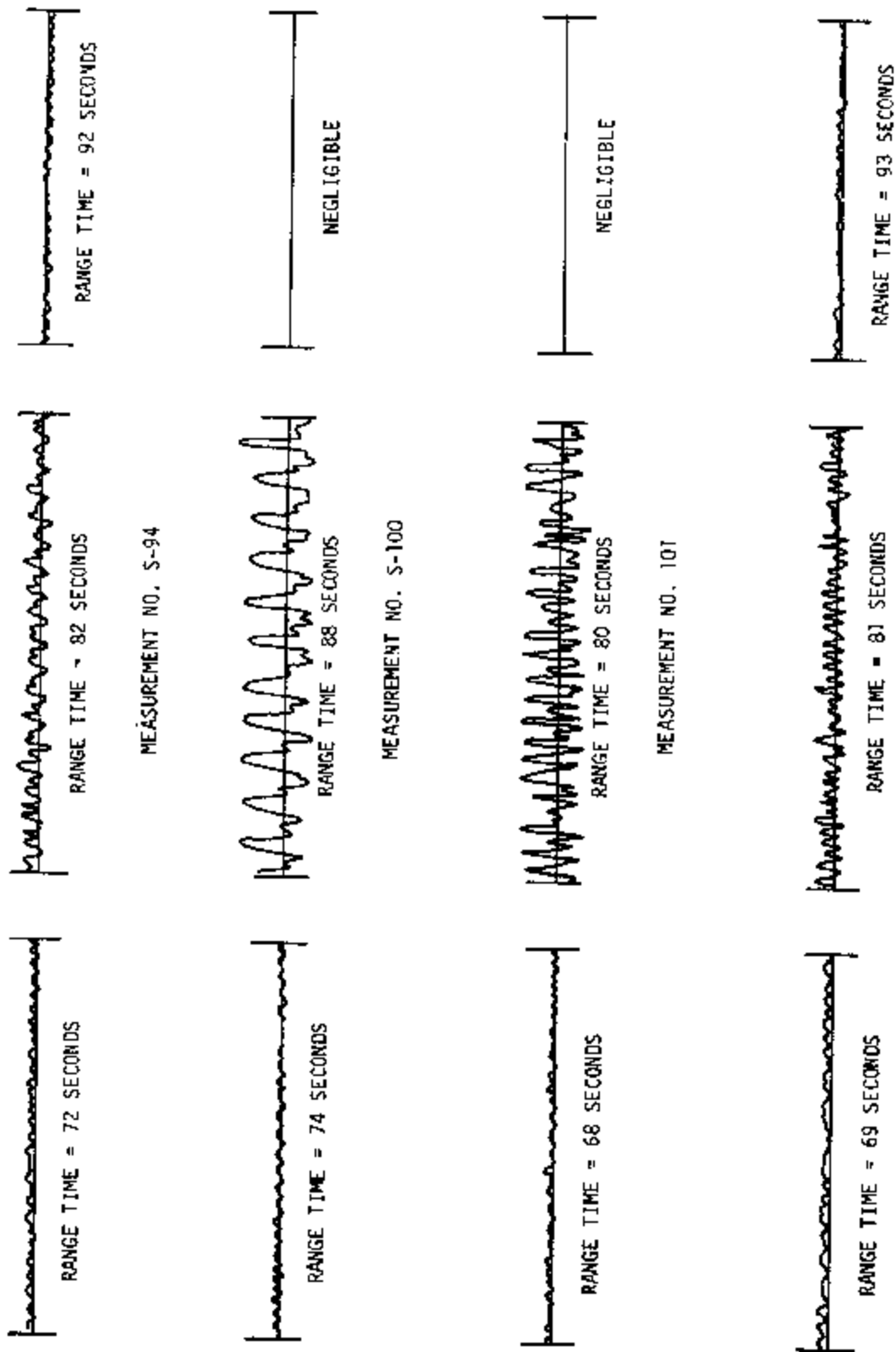


Figure 9-31. Time Slices of Dynamic Strain Output Showing Wave Forms

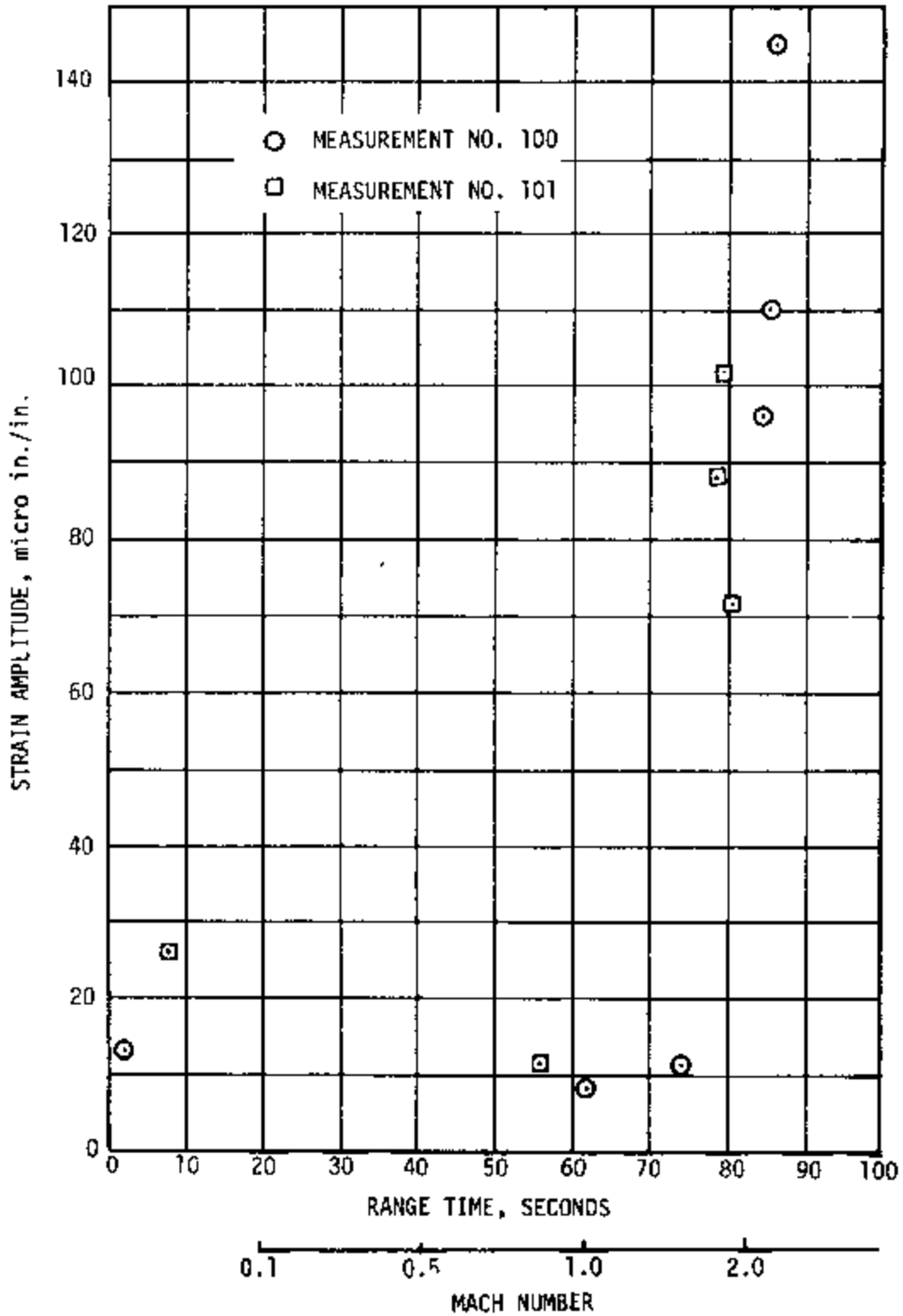


Figure 9-32. S-IVB Forward Skirt RMS Strain Amplitudes

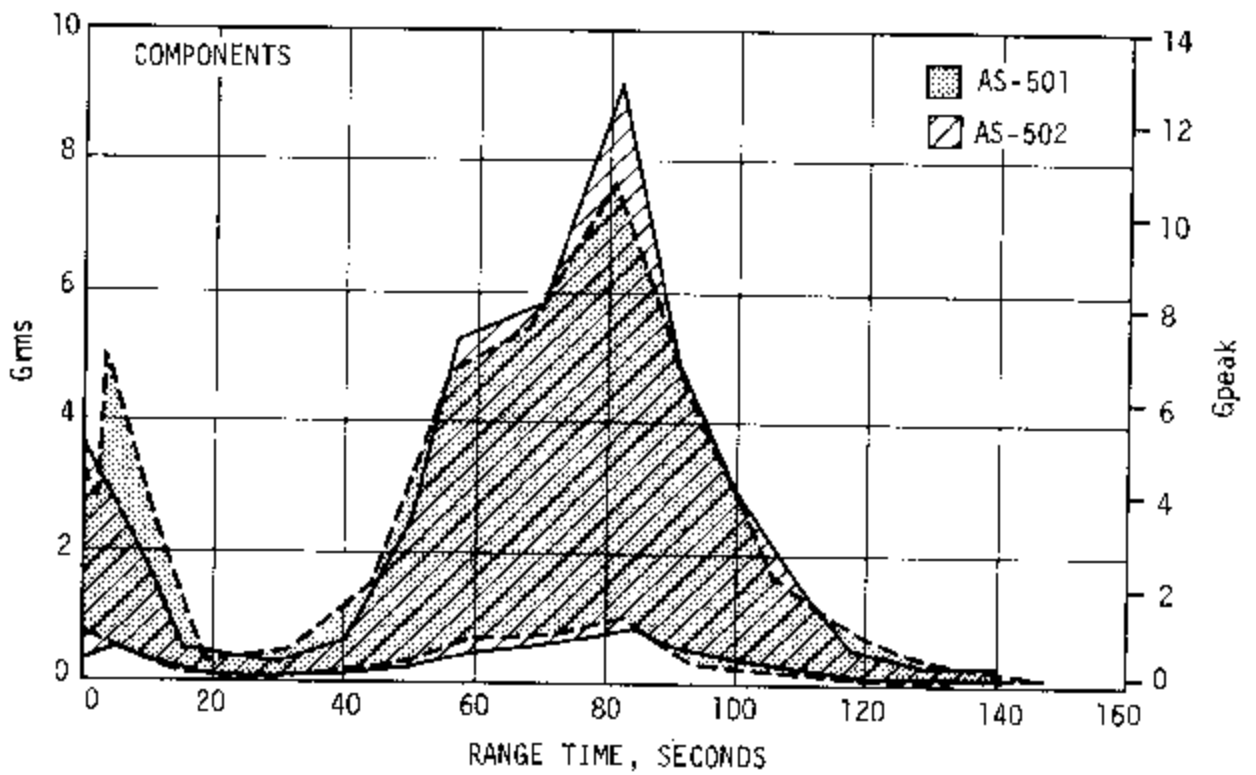
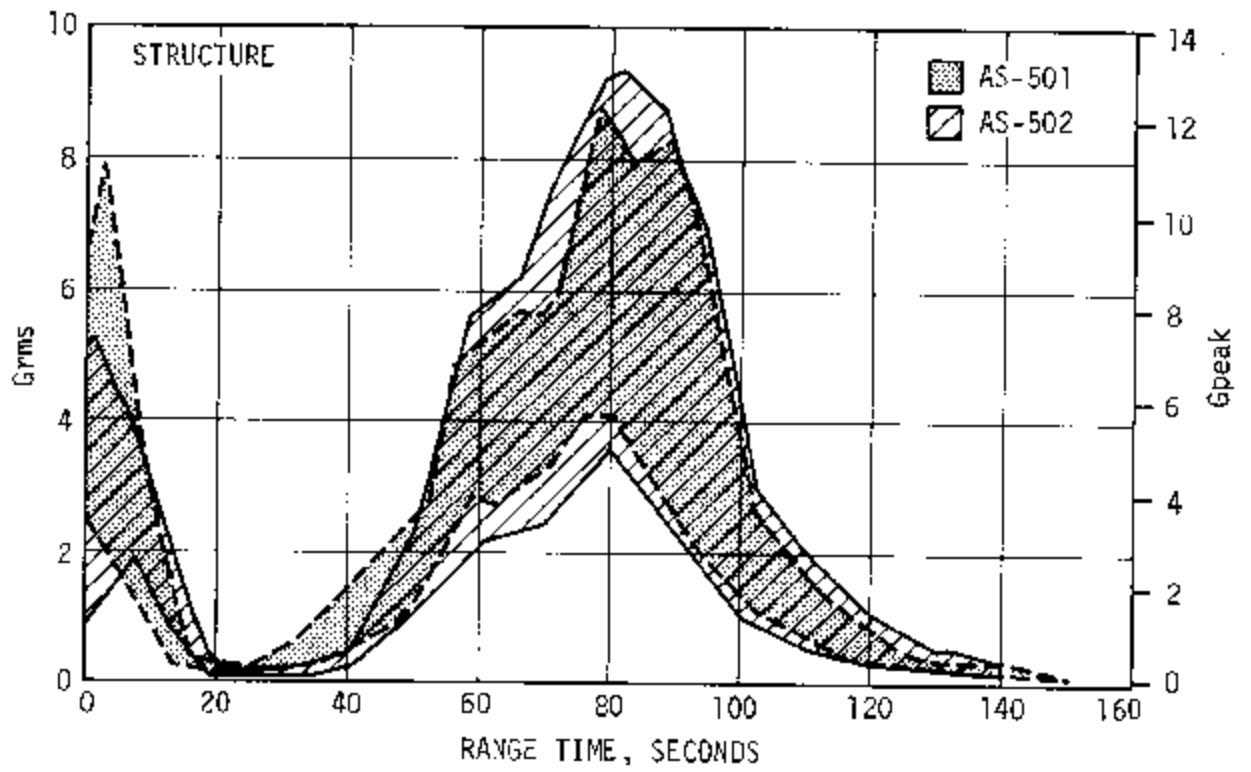


Figure 9-33. Instrument Unit Vibration Envelopes

9.3.5.1 Instrument Unit Structure. The structural vibration levels at liftoff were higher on the AS-501. At Mach 1/Max Q, the levels were higher on AS-502. After S-IC powered flight, the levels became negligible.

9.3.5.2 Instrument Unit Components. The instrument unit component vibration data indicated a broader range of data than that of the structure vibration measurements. This is due to different response characteristics of the various components. The AS-501 component vibration levels exceeded those of AS-502 from liftoff to approximately 56 seconds range time. From 56 seconds range time through maximum in-flight load to approximately 120 seconds range time, AS-502 component level exceeded those of AS-501. The vibration levels during S-II and S-IVB powered flights were negligible.

There were no vibration induced malfunctions of the ST-124M-3 inertial platform on AS-502. Available data indicates that the ST-124M-3 composite vibration levels at liftoff on AS-502 were very near those of AS-501 or the inertial gimbal. The composite levels of the inertial gimbal vibrations are shown in Figure 9-34.

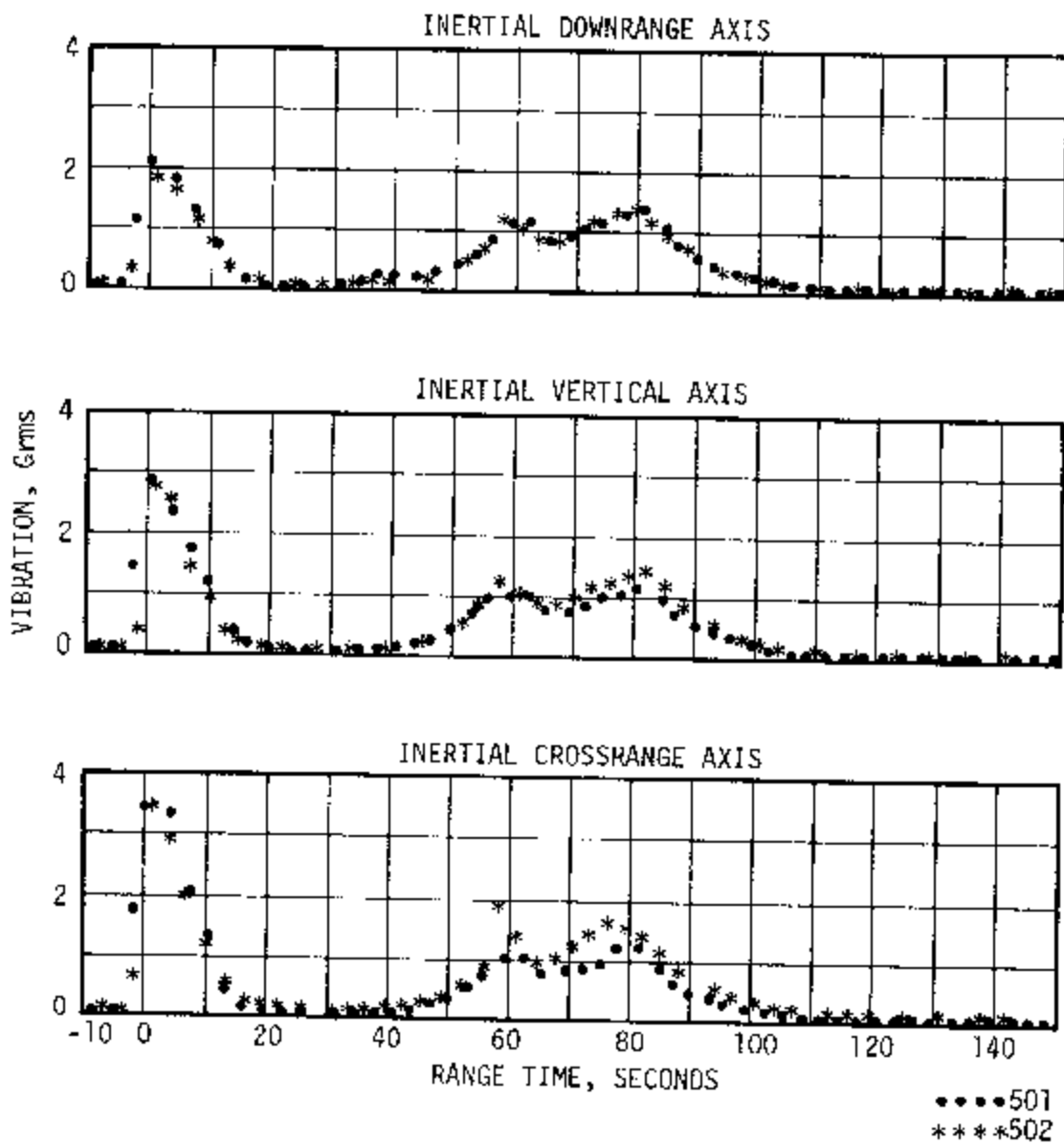


Figure 9-34. AS-502 Versus AS-501 Inertial Gimbal Vibrations

SECTION 9A

133 SECOND TRANSIENT

9A.1 SUMMARY

At approximately 133 seconds abrupt changes of strain, vibration, and acceleration measurements were indicated in the S-IVB, Instrument Unit (IU), Spacecraft/Lunar Module Adapter (SLA), Lunar Module Test Article (LTA), and Command and Service Module (CSM). Photographic coverage, Airborne Light Optical Tracking System (ALOTS), and ground camera film showed pieces separating from the area of the adapter. There were no known structural failures noted on the launch vehicle.

All data from both the launch vehicle and spacecraft relevant to this 133 second anomaly have been investigated by a joint task group at the Manned Spacecraft Center (MSC). The results of this investigation are being published in a separate anomaly report by MSC.

9A.2 INSTRUMENT UNIT

Attempts were made to establish a timeline correlation showing where the disturbance started and its propagation through the vehicle. A timeline of events from each data signal correct to the nearest millisecond would have been necessary in order for the timeline to be valid. Problems associated with the accomplishment of this task are enumerated below:

- a. The primary problem is the interpretation of the start of the event. These differences vary from 1 or 2 milliseconds to as much as 20 milliseconds. Forty-inch-per-second oscillograms were used to aid in this determination.
- b. Delays inherent in the transducer, telemetry link, and receiving station were identified with a step function input at the 10 percent and 90 percent levels; however the input to the various transducers was not necessarily a step function, but a slow changing Direct Current (DC) level followed later by a high frequency shock. This could cause additional undetermined delays up to 20 milliseconds depending upon the Inter Range Instrumentation Group (IRIG) channel and the type of input.
- c. Signals that should have had close correlation did not always show correlation.

- d. Submultiplexed data had a time span over which the event could have occurred.

Despite problems with establishing a meaningful timeline, an IU timeline was made. Figure 9A-1 shows that the single sideband measurements (with the prefix E) responded earliest to the disturbance. This is expected because the transient is readily discernible due to the low level noise and the DC signal level prior to the disturbance and the high (3 kilohertz) response of the vibration measurements. Note that the first measurement to indicate a change was on a Radio Frequency (RF) assembly rather than a hard mounted transducer. It would be expected that the hard mounted transducer would note the shock first. This indication, coupled with relationships of times of vibration measurements on the upper and lower mounting ring, illustrates the difficulty in attempting to locate the source of the disturbance by the use of a timeline. As shown in Figure 9A-2, measurement E14, which is on the upper ring, has a higher G level and precedes E16 which is on the lower ring; however, E39, which is on the upper ring, has a higher G level but occurs after E41 which is on the lower ring. Also, E43, on the ST-124M-3 bracket, preceded all the upper and lower ring measurements as shown in the timeline.

An attempt was made to see which axis was affected first but this resulted in the same type of inconsistencies as listed above. The investigation resulted in a list of all the IU related measurements that exhibited a response at the time of the disturbance. This list is given in Table 9A-1. The indication column of Table 9A-1 briefly describes the data response to the disturbance for each signal. A blip is defined as a small excursion from the nominal that returns shortly to the nominal.

The tolerance column indicates the accuracy of the time but does not account for the problems previously discussed. The adjusted time column takes into account transducer, telemetry, transmission, and receiving station delays in order to show when the transducer actually detected the event. Each of the parameters will not be discussed separately but will be grouped for more meaningful presentation.

9A.2.1 Mechanical Versus Electrical Disturbance

A discussion of the mechanical versus the electrical effects at the time of the disturbance points toward a positive mechanical primary event with most secondary electrical effects readily understood. Table 9A-2 shows the disturbance to be primarily a mechanical shock because the equipment mentioned oscillated at their respective resonant frequency. Measurements A6 and A7 were limited by the telemetry to a 25 hertz response. The equipment would not respond at their resonant frequencies if the disturbance had been purely electrical.

The ST-124M-3 servo loops, in reaction to the shock, drew a higher than normal current from the 56 volt power supply. The supply in turn placed a larger current demand than normal (greater than 9.5 amperes) on the

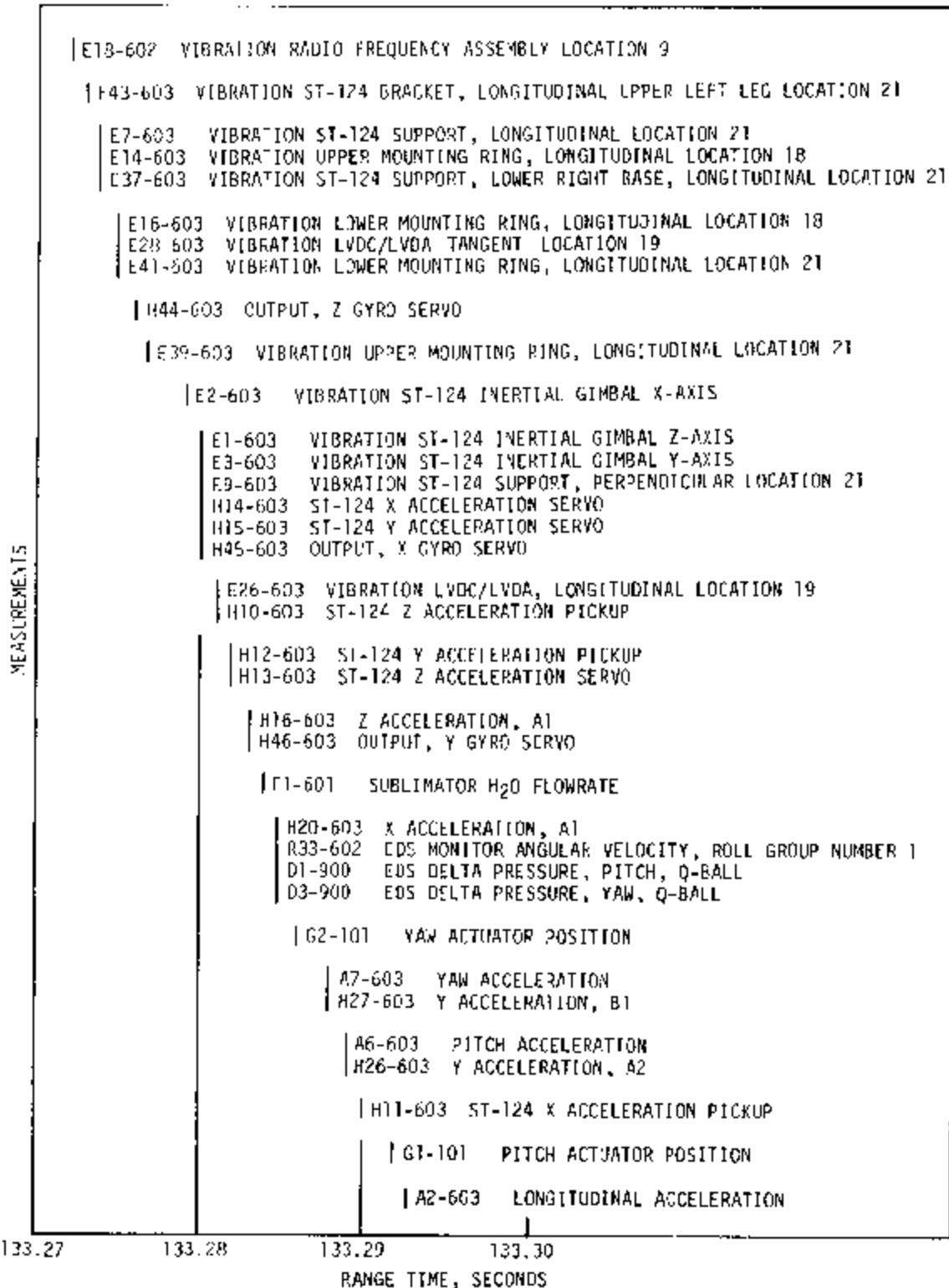


Figure 9A-1. First Instrument Unit Measurements Affected by the 133 Second Disturbance

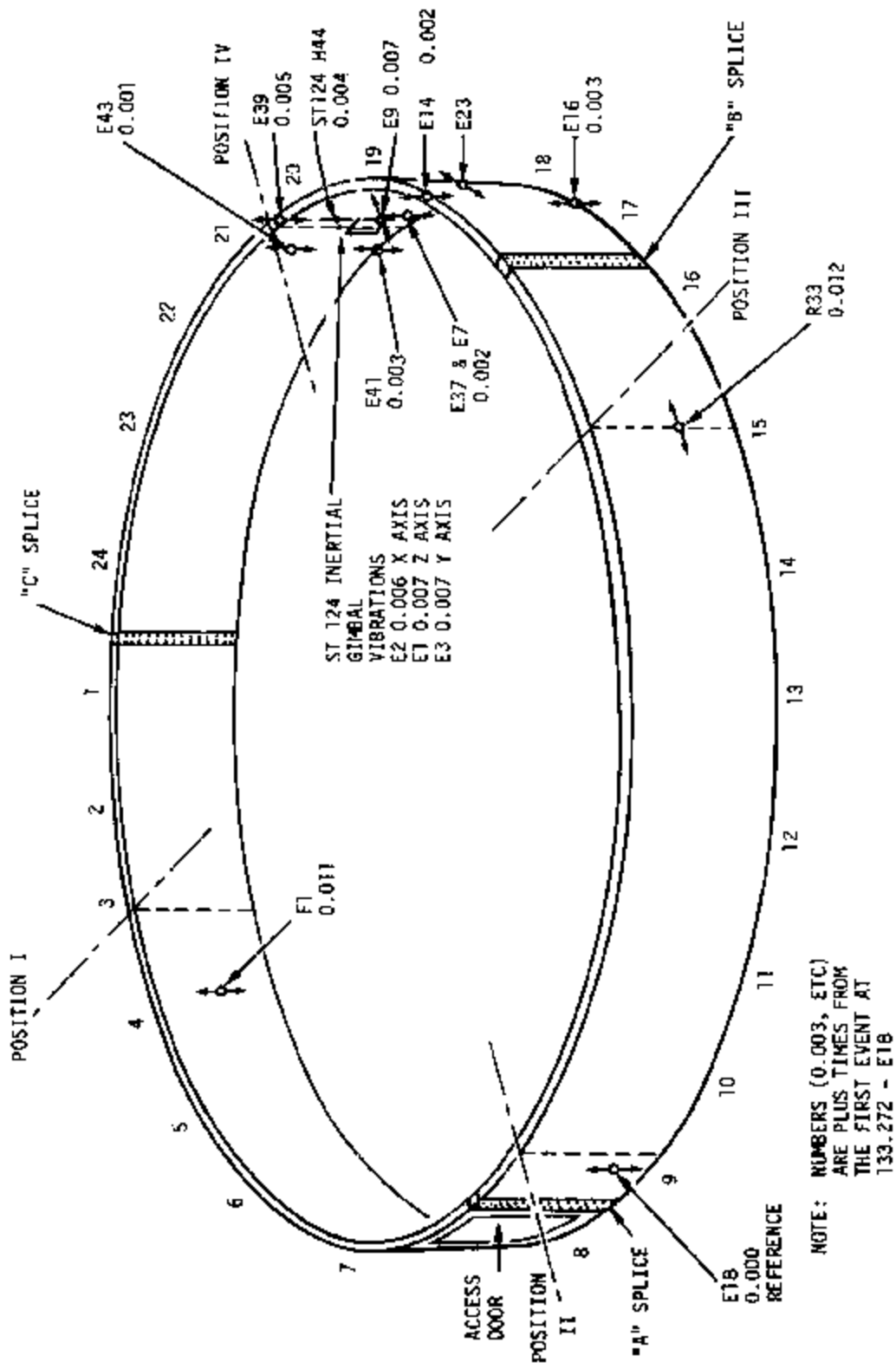


Figure 9A-2. Location of Earliest Events That Were Noted at 133 Seconds

Table 9A-1. List of IU Measurements With 133 Second Response

MEASUREMENT NUMBER	MEASUREMENT NAME	INDICATION	TOLERANCE (MSFC)	RAW DATA TIME (133 SEC+)	ADJUSTED TIME (133 SEC+)
A2-603	Longitudinal Accelerometer	-G(0.06 PP)	+2, -8	0.294	0.293
A6-603	Pitch Accelerometer	+G & Rings	±5	0.295	0.289
A7-603	Yaw Accelerometer	+G & Rings	±5	0.293	0.288
B1-601	Acoustic 23° Off Position I to Position IV	Rings	±20	0.301	0.299
C22-602	Flight Control Computer (FCC) Methanol/Water (M/W) Exit Temperature	+ Blip	+2, -83	0.297	0.296
C36-601	IU Ambient Temperature	Inflection	±1000	0 to 0.1	0 to 0.1
C70-602	FCC Temperature	+ Blip	+50, -100	0.3	0.3
C82-601	Thermal Conditioning System (TCS) GN2 Temperature	- Blip	+50, -100	0.3	0.3
D10-603	Gas Bearing System (GBS) GN2 Regulator Pressure Inlet	Steps Down	+50, -100	0.3	0.3
D18-601	S-IVB M/W Exit Pressure	Rings	+2, -83	0.374	0.373
D24-601	M/W Pumps Inlet Pressure	Steps Up, Levels Off	+50, -100	0.4	0.4
D25-601	GN2 Regulator Inlet Pressure (TCS)	- Blip	+50, -100	0.3	0.3
D43-601	Sublimator Water Inlet Pressure	+ Step	+2, -83	0.307	0.306
E1-603	Inertial Z Axis Gimbal Vibration	12 G PP Rings	±5	0.282	0.280
E2-603	Inertial X Axis Gimbal Vibration	12 G PP Rings	±5	0.281	0.279
E3-603	Inertial Y Axis Gimbal Vibration	20 G PP Rings	±5	0.282	0.280
E7-603	Longitudinal ST-124M Support Vibration	23 G PP Rings	±5	0.276	0.274
E9-603	Perpendicular ST-124M Support Vibration	31 G PP Rings	±5	0.282	0.280
E14-603	Longitudinal Upper Mounting Ring Vibration	47 G PP Rings	±5	0.276	0.274
E16-603	Longitudinal Lower Mounting Ring Vibration	32 G PP Rings	±5	0.277	0.275
E18-602	Longitudinal Radio Frequency (RF) Assembly Vibration (F2 Panel)	9 G PP Rings	±5	0.274	0.272
E26-603	Longitudinal Digital Computer Data Adapter Vibration	4.5 G PP Rings	±5	0.283	0.281
E28-603	Tangent Digital Computer Data Adapter Vibration	5.5 G PP Rings	±5	0.277	0.275
E37-603	Low Right Base ST-124 Support Vibration	7.5 G PP Rings	±5	0.276	0.274
E39-603	Longitudinal Upper Mounting Ring Vibration	16 G PP Rings	±5	0.279	0.277
E41-603	Longitudinal Lower Mounting Ring Vibration	9 G PP Rings	±5	0.277	0.275
E43-603	Upper ST-124M Bracket Vibration	13 G PP Rings	±5	0.275	0.273
F1-601	Sublimator H2O Flowrate	Rings	±5	0.292	0.284
F2-601	Sublimator Bypass M/W	+ Blip	+2, -83	0.348	0.347
F3-601	Cold Plate Inlet Coolant Location 5	+ Blip	+2, -83	0.356	0.355
F4-603	Cold Plate Inlet Coolant Location 20	+ Blip	+2, -83	0.448	0.447
F5-603	ST-124M Shroud Inlet Coolant	+ Blip	+2, -83	0.373	0.372

Table 9A-1. List of IU Measurements With 133 Second Response (Continued)

MEASUREMENT NUMBER	MEASUREMENT NAME	INDICATION	TOLERANCE (MSFC)	RAW DATA TIME (133 SEC+)	ADJUSTED TIME (133 SEC+)
F6-602	Flight Control Computer	+ Blip	+2, -83	0.547	0.546
F7-601	Cold Plate Location 4	+ Blip	+2, -83	0.389	0.388
F8-603	Adapter/Computer M/W Inlet	+ Blip	+2, -83	0.397	0.396
F9-602	IU Exit Coolant	- Blip	+50, -100	0.4	0.4
F10-601	S-IVB Inlet Coolant	- Blip	+50, -100	0.4	0.4
F11-603	ST-124M Shroud Coolant	+ Blip	+50, -100	0.3	0.3
G1-101	Pitch Actuator Position	- Blip	+0, -8	0.293	0.292
G1-102	Pitch Actuator Position	+ Blip	+0, -8	0.384	0.383
G1-103	Pitch Actuator Position	+ Blip	+0, -8	0.294	0.293
G1-104	Pitch Actuator Position	+ Blip	+0, -8	0.295	0.294
G2-101	Yaw Actuator Position	- Blip (Small)	+0, -8	0.287	0.286
G2-102	Yaw Actuator Position	+ Blip	+0, -8	0.295	0.294
G2-103	Yaw Actuator Position	+ Blip (Small)	+0, -8	0.298	0.297
G2-104	Yaw Actuator Position	+ Blip (Small)	+0, -8	0.324	0.323
H1-101	Pitch Actuator Valve Current	- Blip	+0, -8	0.359	0.359
H1-102	Pitch Actuator Valve Current		±20	0.342	0.341
H1-103	Pitch Actuator Valve Current		±20	0.337	0.336
H1-104	Pitch Actuator Valve Current		±20	0.355	0.354
H2-101	Yaw Actuator Valve Current	+ Blip	+0, -8	0.294	0.293
H2-102	Yaw Actuator Valve Current		±20	0.335	0.334
H2-103	Yaw Actuator Valve Current		±20	0.300	0.299
H2-104	Yaw Actuator Valve Current		±20	0.310	0.309
H10-603	ST-124 Z Accelerometer Pickup	Rings	+2, -8	0.282	0.281
H11-603	ST-124 X Accelerometer Pickup	Rings	+2, -8	0.291	0.290
H12-603	ST-124 Y Accelerometer Pickup	Rings	+2, -8	0.283	0.282
H13-603	ST-124 Z Accelerometer Servo	- Blip	+50	0.283	0.282
H14-603	ST-124 X Accelerometer Servo	- Blip	±50	0.281	0.280
H15-603	ST-124 Y Accelerometer Servo	+ Blip	±50	0.282	0.280
H16-603	Z Accelerometer, A1	Signal Changed	±5	0.284	0.283
H20-603	X Accelerometer, A1	Signal Changed	±5	0.286	0.285
H24-603	Y Accelerometer, A1	Signal Changed	±5	0.306	0.297
H25-603	Y Accelerometer, B1	Signal Changed	±5	0.298	0.290
H26-603	Y Accelerometer, A2	Vibration Pulses	±5	0.290	0.289
H27-603	Y Accelerometer, B2	Vibration Pulses	±5	0.289	0.288
H35-603	4.8 KHZ Platform	- Blip	+2, -83	0.360	0.359
H36-603	Volt 4.8 KHZ, Servo Amp Supply	+ Blip	+50, -100	0.3	0.3
H40-603	Z Gyro Pickup, ST-124M	+ Excursion	+2, -8	0.350	0.349
H41-603	X Gyro Pickup, ST-124M	+ Excursion	+2, -8	0.329	0.328
H42-603	Y Gyro Pickup, ST-124M	+ Blip	+2, -8	0.305	0.304
H44-603	Output Z Gyro Servo	Rings 75Hz	±20	0.280	0.276
H45-603	Output X Gyro Servo	Rings 80Hz	±10	0.282	0.280
H46-603	Output Y Gyro Servo	Rings 80Hz	±20	0.285	0.283
J25-602	RF Power Output, F1 Telemeter	- (Stayed Down)	+2 -83	0.517	0.516

Table 9A-1. List of IU Measurements With 133 Second Response (Continued)

MEASUREMENT NUMBER	MEASUREMENT NAME	INDICATION	TOLERANCE (MSFC)	RAW DATA TIME (133 SEC+)	ADJUSTED TIME (133 SEC+)
J26-602	RF Reflective Power, F1 Telemeter	+(Stayed Up)	+2, -83	0.358	0.357
J27-602	RF Power Output, F2 Telemeter	- Blip	+2, -83	0.375	0.374
J28-602	RF Reflective Power, F2 Telemeter	- Blip	+2, -83	0.383	0.382
J29-602	RF Power Output, P1 Telemeter	+ Offset	+2, -83	0.4	0.4
J30-602	RF Reflective Power, P1 Telemeter	+ Offset	+2, -83	0.393	0.392
J31-602	RF Power Output, S1 Telemeter	+ Offset	+2, -83	0.343	0.342
J32-602	RF Reflective Power, S1 Telemeter	- Blip	+50, -100	0.310	0.309
J75-603	Static Phase Error	+ Blip	+2, -83	0.257	0.256
J76-603	Command and Communication System (CCS) Automatic Gain Control (AGC) (0-5 V)	+ Blip	+2, -83	0.548	0.547
K61-603	Summation Gyro Currents (5T-124H)	+ Blip	+2, -83	0.327	0.326
K62-603	Summation Accelerometer Currents (5T-124H)	+ Blip	+2, -83	0.335	0.334
M3-603	Volt, 56 VDC Supply	+ Blip	+2, -83	0.441	0.440
M6-603	Volt, 250 Volt Ampere (VA) Inverter, Phase AB	- Blip	+2, -83	0.311	0.310
M6-603	Volt, 250 VA inverter, Phase CA	+ Blip	+2, -83	0.365	0.364
M12-601	6011 Bus Voltage	- Blip	+2, -83	0.320	0.319
M13-601	6021 Bus Voltage	+ Blip	+50, -100	0.3	0.3
M14-601	6031 Bus Voltage	- Blip	+50, -100	0.3	0.3
M16-601	6010 Battery Current	+ Blip	+2, -83	0.345	0.344
M17-601	6020 Battery Current	+ Blip	+50, -100	0.3	0.3
M18-601	6030 Battery Current	+ Blip	+2, -83	0.361	0.360
M19-601	6041 Bus Voltage	- Offset	+50, -100	0.3	0.3
M20-601	6040 Battery Current	+ Blip	+2, -83	0.295	0.294
M27-603	Data Adapter 3V Supply	- Blip	+5, -83	0.377	0.376
R4-602	Angular Velocity Pitch Control	+ Blip	±5	0.316	0.313
R5-602	Angular Velocity Yaw Control	- Blip	±5	0.308	0.305
R6-602	Angular Velocity Roll Control	- Blip	±5	0.297	0.295
R7-602	Angular Velocity Pitch Emergency Detection System (FDS) Group Number 1 Spare	+ Blip	+50 -100	0.3	0.3
R8-602	Angular Velocity Yaw EDS Group Number 1	+ Blip	±5	0.322	0.321
R11-602	Angular Velocity Yaw EDS Group Number 2 (Spare)	+ Blip	±100	0.3	0.3
R12-602	Angular Velocity Roll EDS Group Number 2 (Reference)	+ Blip	±5	0.309	0.305
R13-602	Angular Velocity Pitch EDS Group Number 3 (Reference)	+ Blip	±5	0.320	0.316
R14-602	Angular Velocity Yaw EDS Group Number 3 (Command)	Noisy	±50	0.416	0.415
R15-602	Angular Velocity Roll EDS Group Number 3 (Spare)	+ Blip	+2, -83	0.341	0.340
R33-602	EDS Monitor, Angular Velocity R Group Number 1	- Blip	-2, -83	0.286	0.285
R34-602	EDS Monitor, Angular Velocity R Group Number 2	- Blip	+2, -83	0.330	0.329

Table 9A-1. List of IU Measurements With 133 Second Response (Continued)

MEASUREMENT NUMBER	MEASUREMENT NAME	INDICATION	TOLERANCE (NSFC)	RAW DATA TIME (133 SEC+)	ADJUSTED TIME (133 SEC+)
R35-602	EDS Monitor, Angular Velocity R Group Number 3	+ Blip	+2, -83	0.339	0.338
R36-602	Angular Velocity, Pitch (EDS Input)	+ Blip	±5	0.324	0.323
R37-602	Angular Velocity, Roll (EDS Input)	+ Blip	±5	0.315	0.314
R38-602	Angular Velocity, Yaw (EDS Input)	+ Blip	±5	0.328	0.327
D1-900	EDS ΔP Q-Ball	Goes NEG Then Returns	-2, -8	0.280	0.285
D3-900	EDS ΔP Q-Ball	Goes NEG Then Returns	-2, -8	0.286	0.285
D35-900	EDS Q-Ball Summation	Goes NEG Then Returns	+2, -83	0.381	0.380
H60-603	Guidance Computer Operators Fine Sinal Angles				
	X (Roll)	-4.7 Arc Min Oscillates	±50	0.280*	0.280*
	Y (Pitch)	+0.8 Arc Min Offset	±50	0.262*	0.262*
	Z (Yaw)	-5.5 Arc Min Offset	±50	0.350*	0.350*
	Ladders				
	Roll	Pulses	±50	0.265*	0.265*
	Pitch	Pulses	±50	0.695*	0.695*
	Yaw	Pulses	±50	0.280*	0.280*
*Times not accurate due to difficulty in timing LVDA data.					

Table 9A-2. 133 Second Transient Survey, IU Stage

MEASUREMENT		FREQUENCY	
NUMBER	NAME	RESONANT (HERTZ)	133 SECOND (HERTZ)
A6-603	Pitch Body Fixed Accelerometer	100	*
A7-603	Yaw Body Fixed Accelerometer	100	*
E7-603	ST-124 Leg Vibration, Longitudinal	100	100
E9-603	ST-124 Leg Vibration Tangential (Stiffened in Radial Direction)	About 140	140
H10-603	Z Accelerometer Pickup	40	30-40
H11-603	X Accelerometer Pickup	40	30-40
H12-603	Y Accelerometer Pickup	40	30-40
R4-502	Pitch Rate Gyro	17-21	17
R5-602	Yaw Rate Gyro	17-21	17
R6-602	Roll Rate Gyro	17-21	17
*Measurement Bandwidth Limited at 25 Hertz.			

6D10 bus. A momentary short in the 6D91 bus may have also contributed to the problem (see paragraph 9A.6). These could result in transient electrical effects throughout the IU and may account for some measurement changes that were small and unrelated to the mechanical disturbance.

Analysis of the 56 volt power supply regulation and efficiency factor proves that a surge of greater than 10 amperes on the 6D10 battery can easily happen. Worst case condition of ST-124M-3 servo loop drain on the supply would be close to 9 amperes. Normal system operation shows approximately a 1.4 ampere drain. With a 65 percent efficiency, the input current to the 56 volt power supply from the 6D10 bus would be 4.3 amperes.

For normal operation there is an input current of 4.34 amperes at 28 VDC assuming 65 percent efficient output current.

$$I_o = \frac{(28)(4.3)}{56} (0.65) = 1.4 \text{ amperes}$$

Assuming the input current did go to 14 amperes at 28 VDC, the output current was:

$$I_o = \frac{(28)(14)}{56} (0.65) = 4.55 \text{ amperes at } 56 \text{ VDC}$$

Therefore, this is normal operation under vibration conditions.

When the current surge on the 6D10 bus with its consequent voltage drop occurred, there were excursions of a lesser nature noted on the 6D30 and 6D40 buses. These fluctuations were apparently caused by other IU power supplies reacting to the changing voltage on the 6D10 bus. As a result of these fluctuations, transients were induced throughout the IU as evidenced by fluctuations in many measurements.

To discount the possibility of a measuring system problem causing the indications observed, an analysis of the various measurement paths was performed. It was proven that no commonality of measurement discrepancies exists. Measurements are powered by various buses, and are not signal-conditioned in any one measuring rack. Multiple cables, multiplexers, and telemetry transmitting equipments are involved.

Figure 9A-3 is a composite of various electrical indications in response to the disturbance. The electrical effects are first noted on the 6D40 bus at 133.211 seconds. Also, it can be noted that an electrical disturbance occurred at 133.261 seconds at the 6D10 bus.

The 6D30 and 6D40 bus current increases are considered to be due to load sharing in the Launch Vehicle Data Adapter (LVDA) and Flight Control Computer (FCC). When the 6D11 bus voltage dropped, the 6D30 and 6D40 buses assumed the load momentarily but returned to normal when the 6D11 voltage came back up.

9A.2.2 Pressure, Flowrate, and Temperature Measurements

All of the 11 flowrate measurements and 5 of the pressure measurements indicated a change at the time of the disturbance. The threshold for the flow measurements is low enough that they would readily measure acceleration changes due to the hammer effect. The pressure measurements also are susceptible to G-level changes of the magnitude noted.

It is not known whether the temperature measurements that changed were real temperature fluctuations or tertiary electrical effects. The levels involved were so small they are negligible.

The sublimator inlet water pressure transducer, D43-601, sensed a sudden change in pressure beginning at 133.307 seconds. This change was either a plus pressure applied to the positive pressure port connected to the

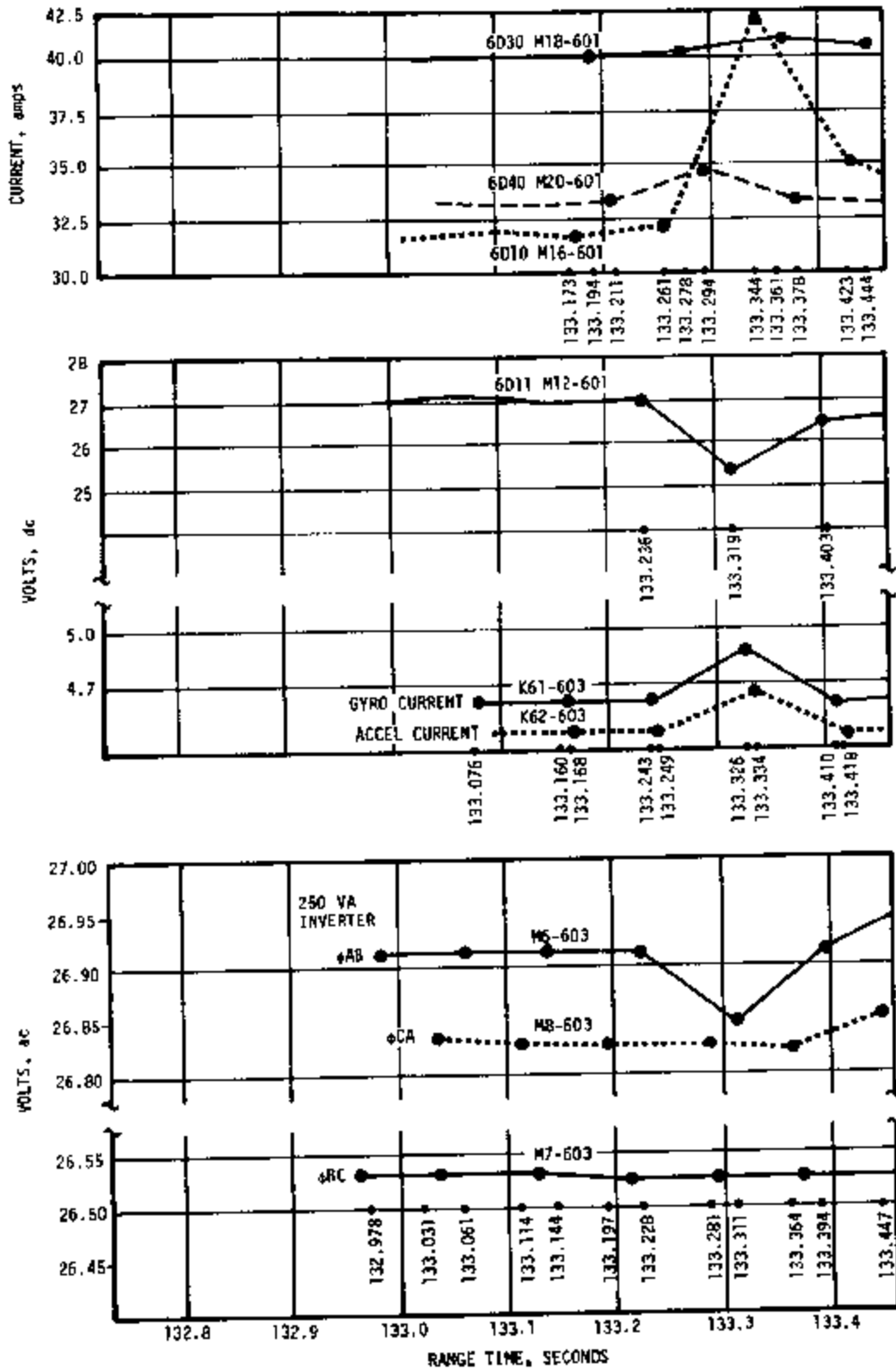


Figure 9A-3. Composite Electrical Effects

water system or a negative change in pressure applied to the minus pressure port which was open to the internal IU compartment. The pressure increased 0.069 N/cm² (0.1 psid) from 133.3 to 133.8 seconds as shown in Figure 9A-4.

Since the IU compartment shares a common pressure environment with the S-IVB forward skirt and the SLA; and ALOTS film showed pieces separating from the area of the SLA, the question of measurement validity was raised. The conclusion that the measurement was valid and did in fact detect a pressure change at about 133 seconds was based on the following facts.

- a. The 0.5 psid pressure transducer has been used previously on seven Saturn I missions (SA-4 through SA-10) with seven transducers used per vehicle. It was also used on the uprated Saturn I first stage on AS-201 through AS-204 with at least four transducers used per vehicle. Failure occurred on only one transducer. It is suspected that the transducer may have been electrically unconnected.
- b. The transducer has been tested by MSFC under vibration and shock levels which significantly exceeded any IU vibration and shock requirements. No DC shift occurred during any of these tests.
- c. The maximum friction between wiper and pot would be two resolutions or 0.66 percent full scale or 0.03 psi; however, friction between wiper and pot is never considered to be a contributing error when there is a known vibration present on the transducer.
- d. The effect of temperature and acceleration would not have produced any measurable amount of error. The smallest measurable error would be 0.33 percent full scale or 0.015 psi representing one resolution (wire turn) of the transducer's potentiometer.

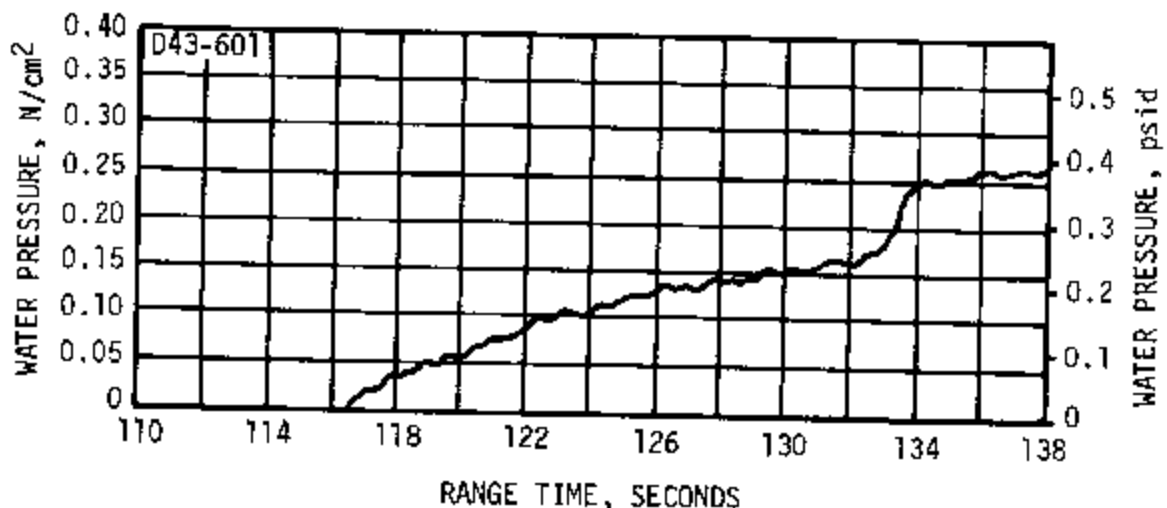


Figure 9A-4. Sublimator Inlet Water Differential Pressure

- e. Vibration is not considered a contributing error because vibration will not produce a change in DC level.

9A.2.3 Radio Frequency (RF) Measurements

Several telemetry system power measurements exhibited level changes at approximately 133 seconds range time. The DS1, DP1, and DF1 power outputs changed by approximately 0.8, 0.15, and -0.15 watts, respectively. The corresponding reflected powers changed 0, 0.05, and 0.1 watts, respectively. The DF2 power measurement levels did not change even though they showed a slight transient.

Only DF1 showed a characteristic which may be directly attributed to a slight impedance change causing an electrical mismatch in RF components beyond the transmitter output; however, the same impedance change could have improved the Voltage Standing Wave Ratio (VSWR) on DS1 and DP1 resulting in the observed changes. Acoustic noise, vibration, or antenna structural stress changes could have caused a slight impedance change.

The causes of the observed level changes and transients have not been identified.

9A.2.4 ST-124M-3 Stabilized Platform Subsystem and Control Subsystem Analysis

9A.2.4.1 Platform. Of the data available, the accelerometer pickup measurements seem to provide very significant insight into the phenomenon. These measurements indicate that a disturbance began at approximately 133.3 seconds and continued for a period of about 100 milliseconds. The nature of the deflection indicates an impulse type disturbance; however because of the short duration of the input, the accelerometer response would be of a transient type regardless of the nature of the input.

Factors that indicate a physical disturbance in the platform area are:

- a. The platform required additional current load with servo disturbances seen. At least part of the additional current drawn from the 6D10 bus was due to increased requirements of servo loops.
- b. Platform accelerometers showed disturbances of approximately the same ratios as seen during vibration. This would be highly improbable in the case of an electrical disturbance.
- c. Phasing was not the same for the three accelerometer loops. For an electrical disturbance, the phasing would very likely be the same.
- d. There was no irregularity on the 56 volt power supply that would have caused the servo disturbance seen.

The platform gimbal angle analysis indicates the following changes:

- a. Pitch. An approximate 0.8 arc-minute shift at 133.280 seconds.
- b. Yaw. An approximate 4.5 arc-minute shift at 133.350 seconds.
- c. Roll. An approximate -4.7 arc-minute oscillation at 133.262 seconds returning to null.

NOTE: LVDA times on these parameters cannot be accepted as factual due to the problems in establishing LVDA times.

The yaw and pitch transients responding to vehicle movement corroborate the angle-of-attack changes that occurred as measured by the Q-Ball. The delta pressure changes indicate that the vehicle nose moved in both pitch and yaw attitudes and then returned to null. The ladder outputs and gimbal angles indicate vehicle movement in pitch, yaw, and roll. (The Q-Ball does not measure roll.)

In both pitch and yaw the vehicle assumed a slight offset; whereas in roll, there were oscillations after which the vehicle and gimbal showed realignment. The offsets in pitch and yaw did not affect guidance and navigation as evidenced by nominal S-IC stage cutoff conditions.

9A.2.4.2 Control Rate Gyros. All of the rate gyros that were not too noisy to evaluate exhibited a response at the time of the disturbance. The effects on the rate gyros at this time are summarized below:

- a. Pitch. A slow buildup of 0.7 degree peak-to-peak signal level at 5 hertz beginning at approximately 120 seconds range time until 133.32 seconds. The signal level reached 4.1 degrees peak-to-peak over 0.7 seconds tapering off to less than 0.5 degree by 136 seconds. A 17-21 hertz gyro resonance noise was superimposed on the 5 hertz signals of 0.5 degree peak-to-peak during this period.
- b. Yaw. Steady-state 0.25 degree peak-to-peak signal level at 5 hertz before the disturbance becoming negligible afterward. The signal level reached 1.4 degrees peak-to-peak over 0.4 seconds of the disturbance. A 17-21 hertz noise was evidenced but hardly discernible.
- c. Roll. Slow buildup of 2.0 degrees peak-to-peak signal level at 5 hertz from 120 seconds until the observed disturbance. The signal level peaked at 8.2 degrees peak-to-peak over 0.4 second diminishing to 1.0 degree peak-to-peak after 136 seconds. A 17-21 hertz noise was evident throughout this period of 0.6 degree peak-to-peak.

Rate gyro signal indications at 133.3 seconds tend to indicate the disturbance to be a physical vibration and/or resonance close to the rate gyro package as opposed to an electrical transient. The initial disturbance is seen as a buildup and not an immediate peak as an electrical transient would produce.

9A.2.5 Structures and Dynamics

Because the IU was not instrumented with strain gauges, a conventional strain analysis cannot be performed; however by deductive reasoning, the structural integrity of the IU during the 133 second transient can be determined.

- a. Any IU structural collapse would result in a catastrophic failure. This has been demonstrated by structural testing.
- b. The IU is an entanglement of electrical cables and Environmental Control Subsystem (ECS) plumbing. Any structural failure would most likely break an electrical connector or cause a leak in the ECS plumbing. Since no malfunction occurred in the IU during the expected lifetime, no structural failure occurred.
- c. The vehicle trajectory performance was nominal assuring that no abnormal structural deformation occurred which would influence the ST-124M-3 stabilized platform subsystem.
- d. The IU structure has been qualified for vehicle loads which exceeded those experienced on AS-502.
- e. Vibrational responses experienced during the 133 second transient were of shorter duration and no worse than those occurring during the maximum inflight load condition of AS-501 or AS-502.

In conclusion, no IU structural failure occurred on AS-502 since it would have been detected in the electrical or ECS areas, and no known anomalies existed.

9A.3 S-IVB STAGE

The S-IVB stage experienced an unusual load distribution at 133 seconds as indicated by strain gage measurements at forward skirt stringers.

Thirty two axial strain gages were installed on external hat stringers. The gages were located at vehicle station 3145 of the forward skirt and station 2821 of the aft skirt as indicated in Figure 9A-5. Eight measurement locations at each station were approximately equally spaced around the circumference. The recorded data from the strain gages were determined to be valid by the S-IVB Data Qualification Review Board. These data were reviewed thoroughly and in detail and no electrical anomalies were detected. In particular, the unusual strain changes which occurred at 133 seconds and which remained through IECO at about 145 seconds were found to be valid by the Review Board.

The strain histories for the eight side-mounted gages on the aft skirt are presented in Figure 9A-6. At range time zero seconds, all measured strains were adjusted to the computed correct strain corresponding to the

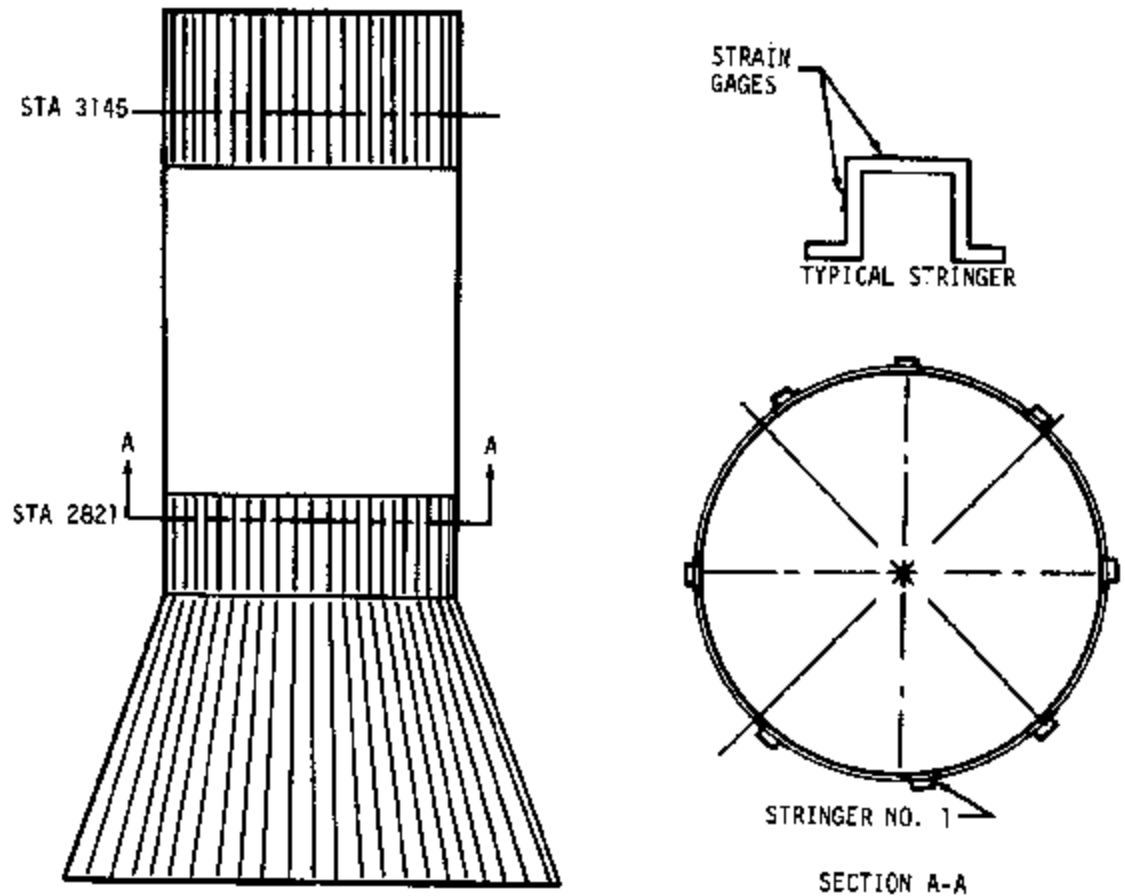


Figure 9A-5. S-IVB Strain Gage Locations

1 g axial load condition preceding liftoff. The maximum and minimum design strain envelopes shown in Figure 9A-6 were calculated from design conditions and include the effects of maximum expected aerodynamic gusts and wind shears. It is to be noted that the aft skirt strain traces indicate no unusual strain changes at 133 seconds. It appears that the structure distributed loads from the forward skirt uniformly to the aft skirt.

The strain histories for the eight side-mounted gages on the forward skirt are presented in Figure 9A-7. The histories for the eight top-mounted gages are shown in Figure 9A-8. A number of strain measurements experienced load shifts at 133 seconds. These strain shifts at 133 seconds are summarized in the polar bar chart of Figure 9A-9. In the chart, negative values indicate increases in compression; positive values indicate decreases in compression. The shift at stringer 81 was 0.00120 in./in. which corresponds to an increase of the stringer axial compression load of approximately 15,124 Newtons (3400 lbf). Stringer 95 experienced an

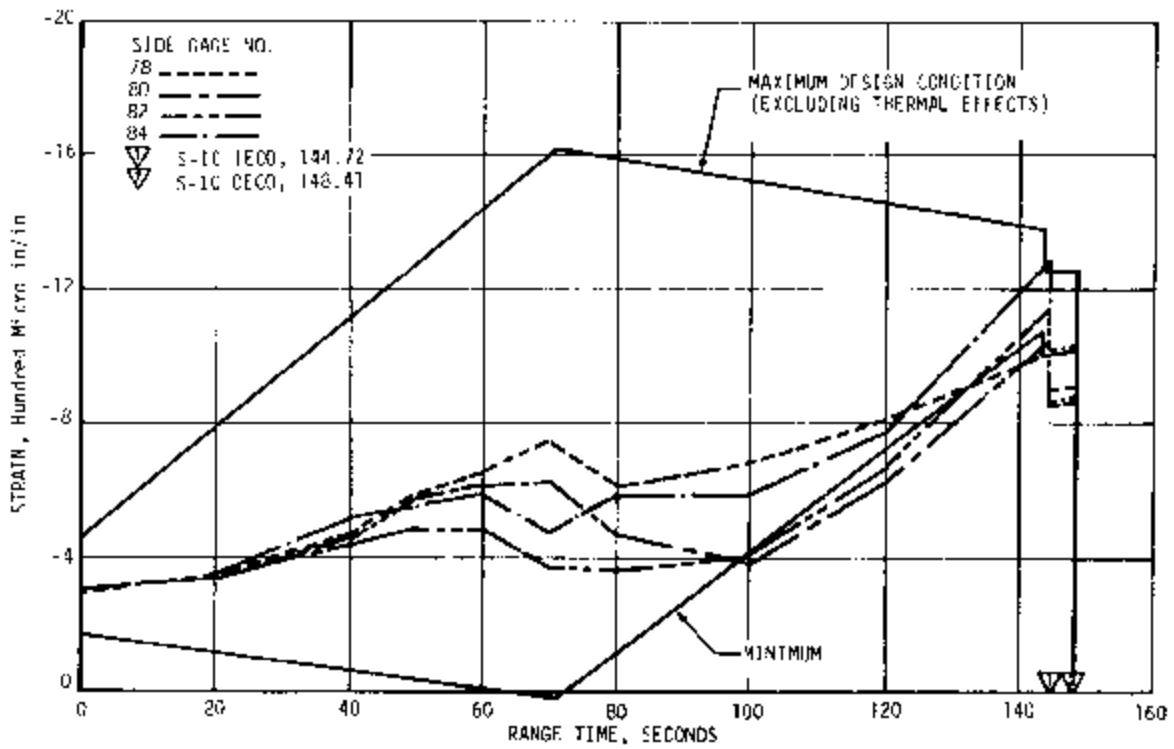
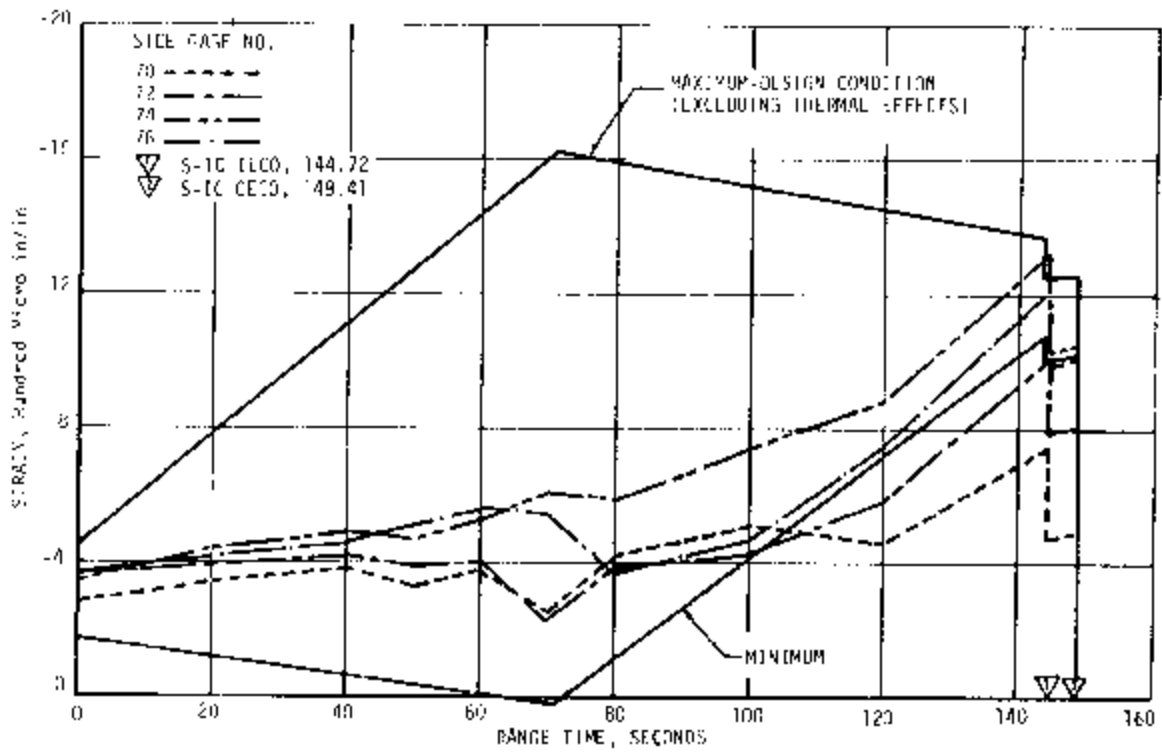


Figure 9A-6. Axial Strain, Aft Skirt Station 2821

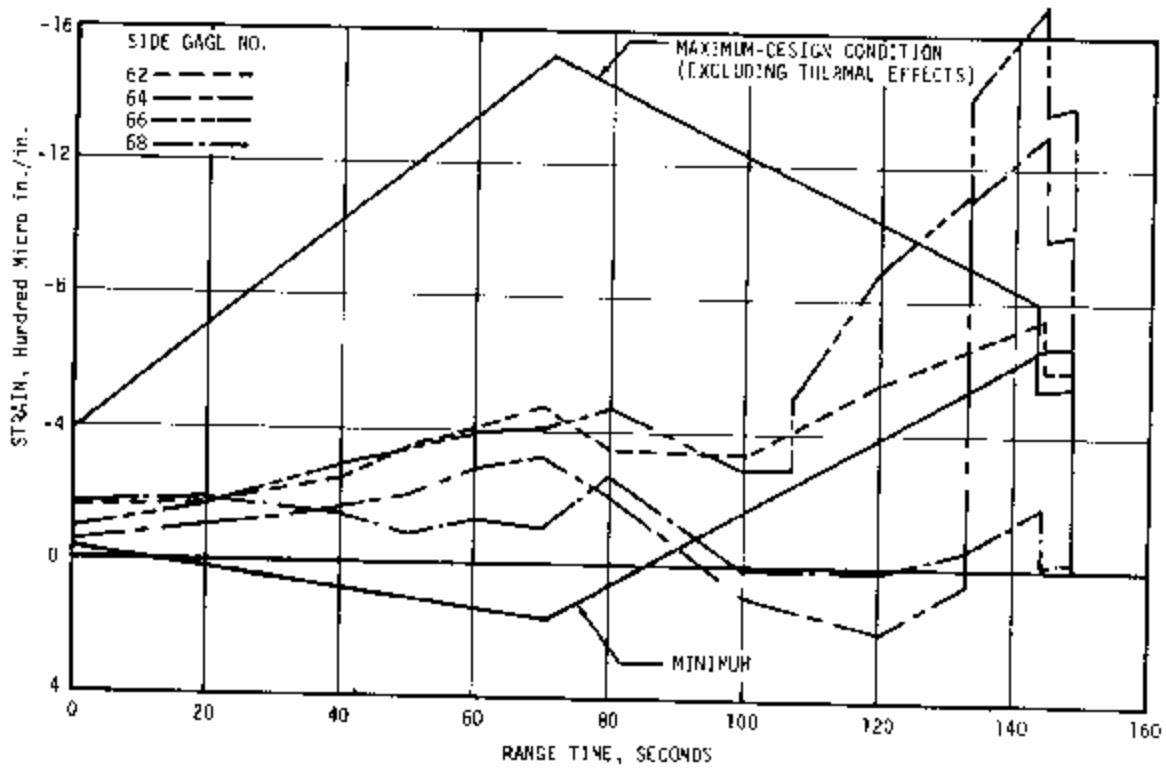
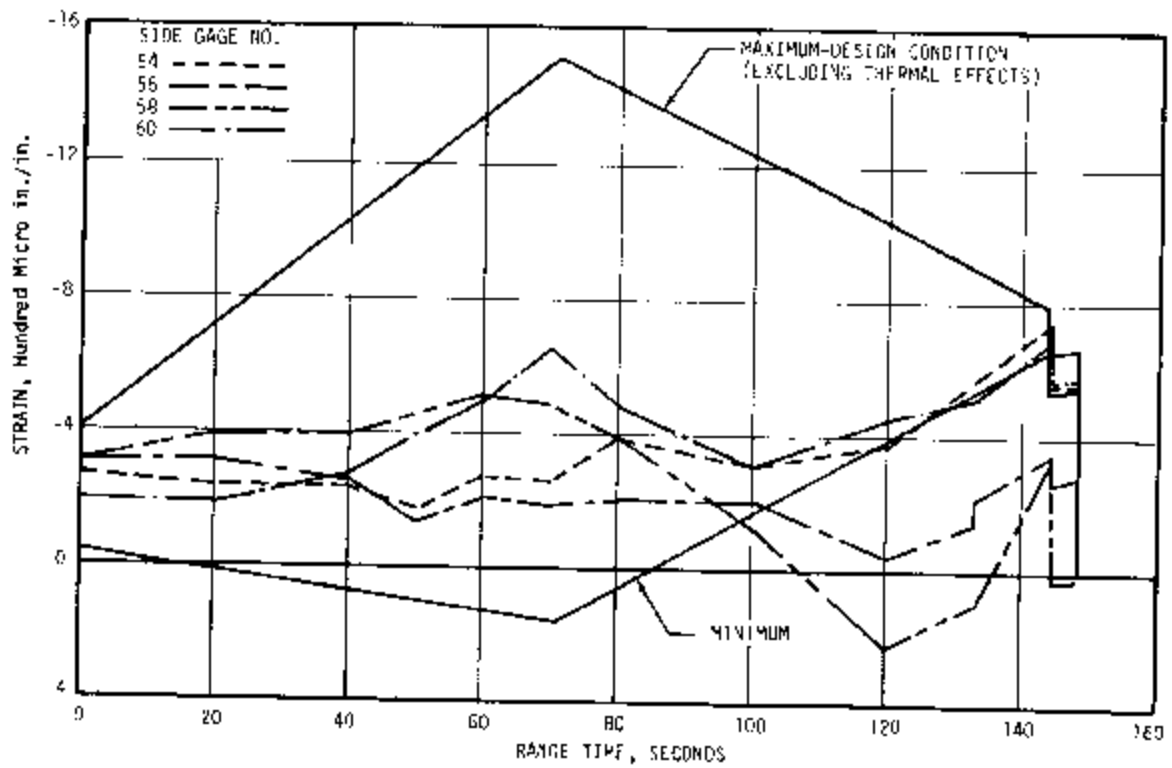


Figure 9A-7. Axial Strain, Forward Skirt Station 3145, Side Gages

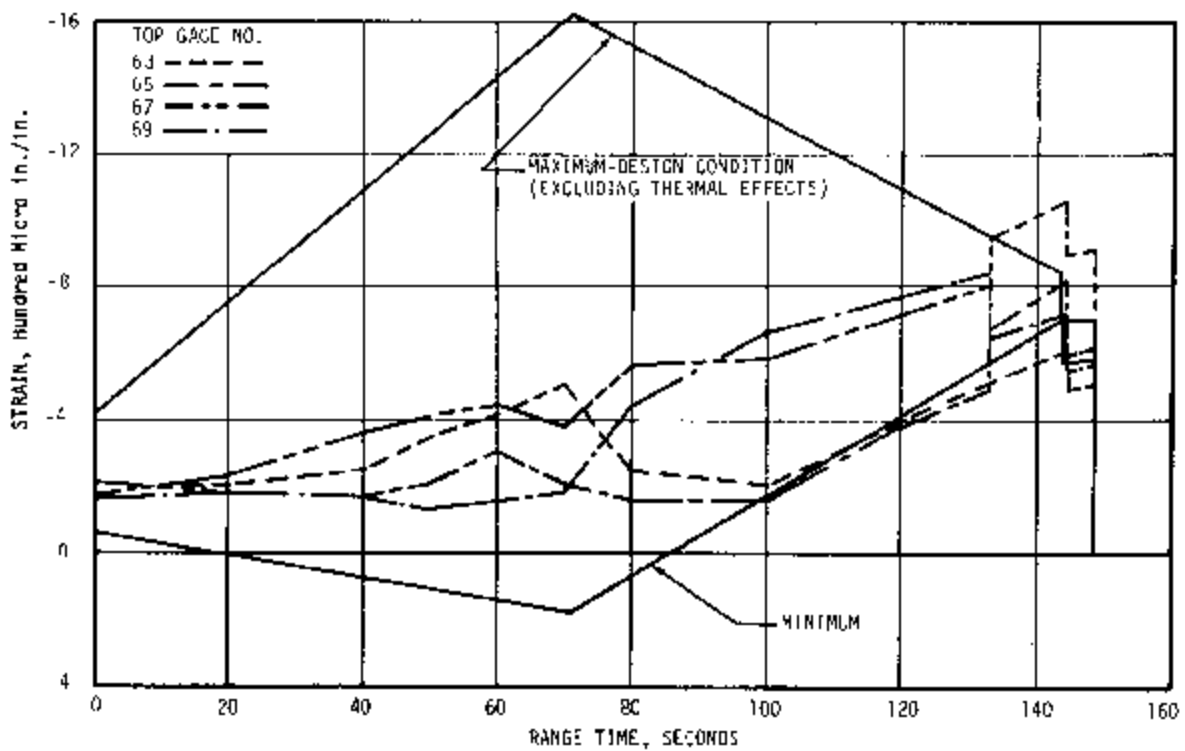
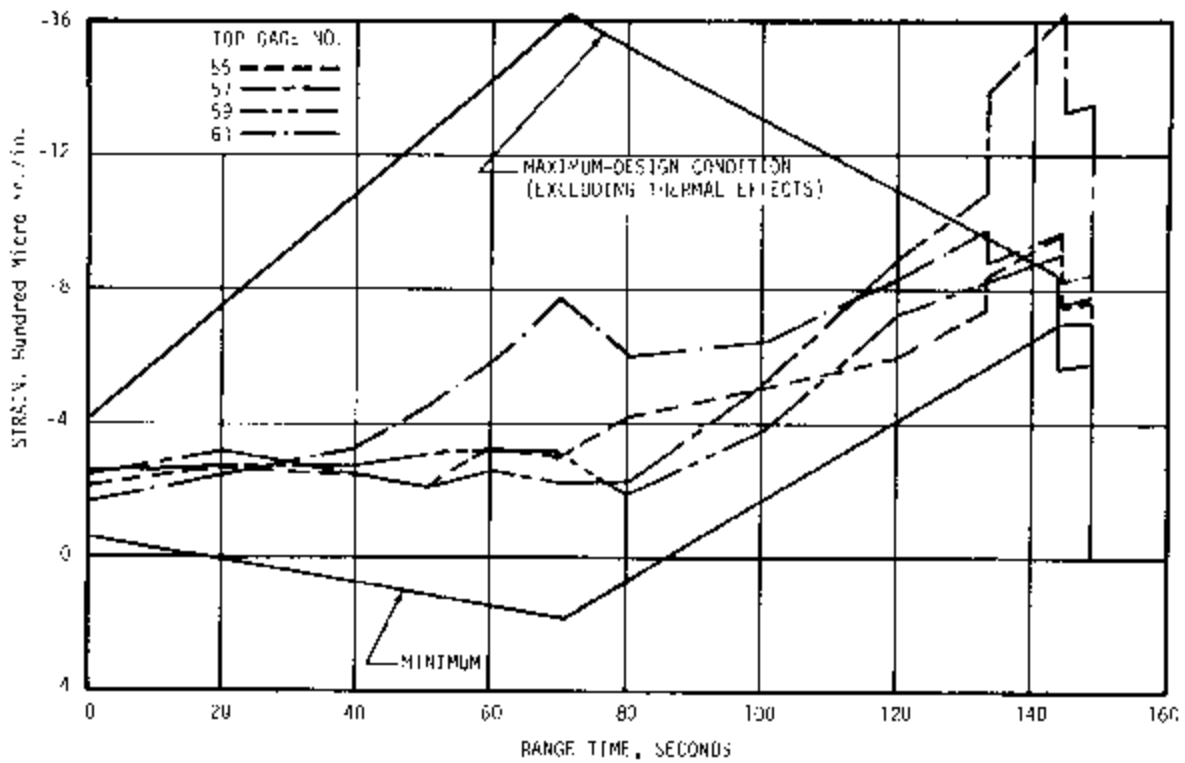


Figure 9A-8. Axial Strain, Forward Skirt Station 3145, Top Gages

- a. The strain changes were not thermally induced because:
 - (1) The changes were too rapid to be from thermal effects.
 - (2) Ten temperature transducers in the forward skirt did not reveal any sudden or drastic changes in skirt temperatures.
- b. The strain changes were not inertially induced since vehicle accelerometer recordings were normal at 133 seconds.
- c. The strain changes were not induced by sudden changes in gross mass or engine thrust as indicated by the continuity and constant slope of the plotted curve from accelerometer readings.
- d. The strain changes were not induced by sudden changes in body bending moments because:
 - (1) Airloads were negligible at 133 seconds.
 - (2) Engine gimbaling was negligible at 133 seconds.
 - (3) Body bending would be transient from engine gimbaling; whereas, the strain disturbances were substantially steady state from 133 seconds to IECO.
- e. The strain changes were not induced by faulty strain gage system electronics because:
 - (1) The data were carefully reviewed by electronic specialists with respect to steady voltages, shorts, gage debonding, wiring identifications, data transmission, data reduction, etc. The data were evaluated as being valid.
 - (2) The pattern of strain changes at 133 seconds was not the type expected of faulty electronics which would produce offscale or zero readings, or result in all similarly wired gages shifting in the same direction by the same amount.
- f. The S-IVB stage forward skirt did not fail and cause the strain changes observed at 133 seconds because:
 - (1) The strain gages continued to respond in normal manner throughout the remainder of powered flight.
 - (2) The applied flight loads and temperatures did not exceed design loads and temperatures.
 - (3) A detailed stress analysis using measured total strains in the forward skirt stringers indicated a minimum margin of safety of 78 percent.

- g. The strain changes at 133 seconds in the S-IVB forward skirt stringers appear to be due to a change in load path through the skirt.
- h. The strain changes at 133 seconds involved eight strain gages; however at 107 seconds, there was an indication of a similar sudden shift of strain from the single measurement of side gage 66 at stringer 95. This strain shift is shown in Figure 9A-9. The cause of this localized incident remains to be determined.

Causes of these strain changes have been investigated by a joint task group at the MSC where all relevant telemetry data from the AS-502 vehicle and spacecraft were reviewed and analyzed. The results of that investigation will be published in a separate report by MSC.

9A.4 S-II STAGE

The S-II stage vibration and acoustic measurements do not indicate a general response to shocks near 133 seconds as has been observed on the Instrument Unit. Only two measurements, E83-219 at vehicle station 63.348 meters (2494 in.), and E81-219 at vehicle station 62.433 meters (2458 in.), on the forward skirt, showed appreciable shocks occurring at 133.8 and 134.1 seconds. The energy appeared to be concentrated at frequencies of approximately 400 and 800 hertz.

9A.5 RF SYSTEMS

A transient in RF signal level at approximately 133.3 seconds was observed at Grand Bahama Islands on IU VHF telemetry links DF1, DF2, DS1, and DP1 as shown in Figures 19-1 and 19-2, Section 19.5. No effects were noted at this time on the Cape Tel 4 (TEL 4) recorded data. The most likely cause for these transients was that a piece of debris from the SLA, shown by the ALOTS film, fell past the IU at this time and momentarily shielded the antennas from the ground receivers. To be effective, this piece would have to:

- a. Be fairly large; at least 0.186 to 0.279 m² (2 to 3 ft²).
- b. Fall fairly close to the antenna.
- c. Be of a conductive material.

Figure 9A-10 shows how passage of a piece of debris from the spacecraft coincides with these transients. Times on this figure were derived from the ALOTS film.

9A.6 EMERGENCY DETECTION SYSTEM (EDS)

Although launch vehicle EDS indications were normal, there are reports of anomalies indicated in the spacecraft. Most significant of these spacecraft anomalies was an indication that one of the three abort lines noted automatic

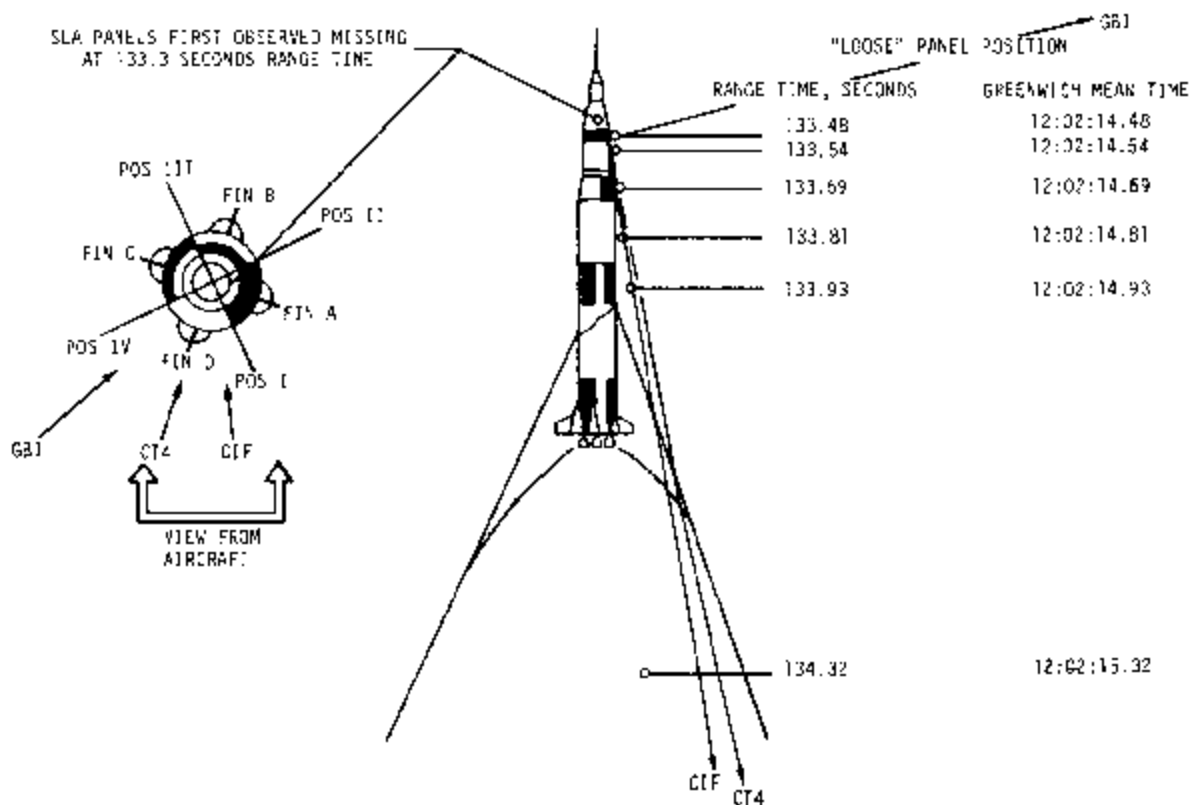


Figure 9A-10. "Quick Look" Assessment, ALOTS 70 MM Film, 133 to 135 Seconds

abort in the EDS logic. Two of the three circuits must give this indication before an automatic abort is initiated. This single abort indication occurred at the time of the 133 second transient and remained throughout the duration of the flight. There were other apparently erratic indications in the spacecraft which occurred subsequent to the transient primarily during the period from 133 seconds to S-II ignition. All functions in these cables are not monitored.

Figure 9A-11 is a simplified diagram to illustrate the interrelationship between the IU and spacecraft EDS power and auto abort interfaces.

Power to operate the IU relays is always derived from IU batteries, although the signal to actuate the relay may come from the spacecraft. The same philosophy holds for spacecraft networks. As a result, the launch vehicle EDS buses 6D91, 6D92, and 6D93 are fed to the spacecraft. Conversely, spacecraft EDS buses No. 1, 2, and 3 are fed to the IU. Since the launch vehicle buses are powered by the three operational IU batteries, a short on an EDS bus would be reflected in the measurements associated with the IU bus which furnishes power to that particular EDS bus. A current spike measured in the 6D10 battery bus which occurred at 133.3 seconds (Figure 13-19, Section 13), could be attributed to a momentary short in the 6D91

bus; however, a more likely cause was the additional current drawn by the platform servo system to stabilize the platform (see paragraph 9A.2.1). Since the 6D91 bus power is transmitted to the spacecraft through the same cable that contains the line which indicated an abort condition, it is conceivable that the same disturbance which caused an abort indication could have caused a momentary short on the 6D91 bus and the resultant transient in the 6D10 battery.

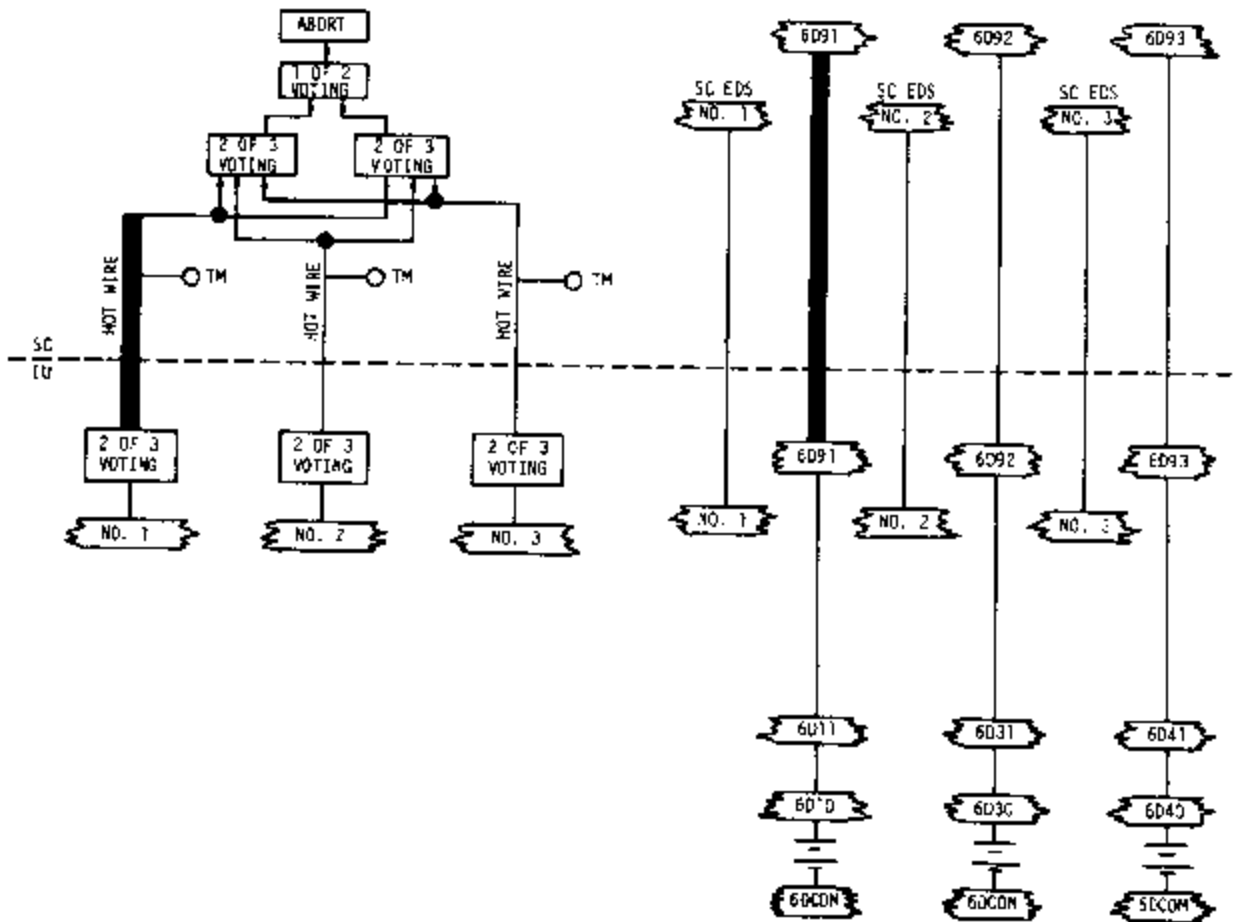


Figure 9A-11. Simplified EDS Power and Auto-Abort Interface

SECTION 10
GUIDANCE AND NAVIGATION

10.1 SUMMARY

10.1.1 Flight Program

The performance of the guidance and navigation system was as predicted from liftoff to 412.92 seconds. S-II engine No. 2 cutoff at 412.92 seconds was followed by cutoff of S-II engine No. 3 at 414.18 seconds. When engine No. 2 cut off a discrete signal was recognized by the IU indicating an engine failure. However, due to a ground rule that only single engine failures be considered, no program action was taken for engine No. 3 failure. The change of vehicle acceleration was detected. With the discrete signal and loss in acceleration the program entered a guidance mode where guidance and navigation computations were made based on a thrust change which was 50 percent of the total actual change. This mode (artificial tau) lasted until the IU sensed an acceleration change due to S-II Programmed Mixture Ratio (PMR) shift. Guidance computations responded to variations in altitude and velocity caused by the decrease in thrust during the S-II burn period. The control system responded well to the guidance commands for the remainder of the boost period. Due to the two-engine-out perturbation, flight path angle and velocity were not optimum at the time guidance commanded S-IVB Engine Cutoff (ECO). This resulted in an overspeed of 48.9 m/s (160 ft/s). A parking orbit which was acceptable though off nominal was achieved.

All orbital guidance maneuvers were satisfactorily performed. IU commands were properly executed for S-IVB restart, but the engine did not reignite. Since acceleration test conditions were not met, Time Base 7 (T7) was initiated and a cutoff command was issued to the S-IVB stage.

10.1.2 Instrument Unit Components

The Launch Vehicle Data Adapter (LVDA) and the Launch Vehicle Digital Computer (LVDC) performed as expected for the AS-502 flight. The ST-124M-3 inertial platform and associated equipment performed as designed. A transient occurred in dynamics at approximately 133 seconds (see Section 9A). Outputs of the servo loops indicated the

disturbance at this time and that the platform responded properly to all transients. Outputs of the accelerometer servo loops indicated nominal performance. The accelerometers correctly measured vehicle acceleration throughout the boost phase. Telemetry signals from the gyro servo loops indicated that the inertial reference was maintained throughout flight until the yaw gimbal reached its limit (± 60 degrees) at 22,112.4 seconds as a result of the loss of vehicle attitude control at 22,023 seconds. Loss of attitude control was due to fuel depletion in the Auxiliary Propulsion System (APS) module at position I at 21,953 seconds and in the module at position III at 22,602 seconds. The module at position III was not able to offset the LOX venting forces after 22,023 seconds.

10.2 GUIDANCE AND NAVIGATION SYSTEM DESCRIPTION

This subsection describes the function of the IU components and the basic flight program.

10.2.1 Instrument Unit System Description

A block diagram of the Navigation, Guidance, and Control System is shown in Figure 10-1.

The LVDC is a high-reliability general-purpose random-access digital computer which contains the logic circuits, memory, and timing system required to perform arithmetical operations necessary for navigation, guidance, and vehicle flight sequencing. The LVDC is also used for prelaunch and orbital checkout.

The LVDA is the input/output device for the LVDC. It is designed to transform signals to be compatible with the receiving equipment, perform minor computations, and provide temporary data storage. The LVDA contains the power supplies used by the LVDC.

The ST-124M-3 platform system is a three-gimbal configuration with gas bearing gyros and pendulous integrating gyro accelerometers mounted on the stable element to provide an inertial space-fixed coordinate reference frame for attitude control and navigation measurements (see Figure 10-2). Vehicle accelerations and rotations are sensed relative to the stable element. Gimbal angles are measured by resolvers which have both fine and coarse outputs. Inertial velocity is obtained from measurements of the angular rotation of the accelerometer measuring head. The data are in the form of encoder outputs which have redundant channels.

10.2.2 Flight Program Description

The flight program controls the LVDC from Guidance Reference Release (GRR) or initiation of T_0 until the end of the mission. The program

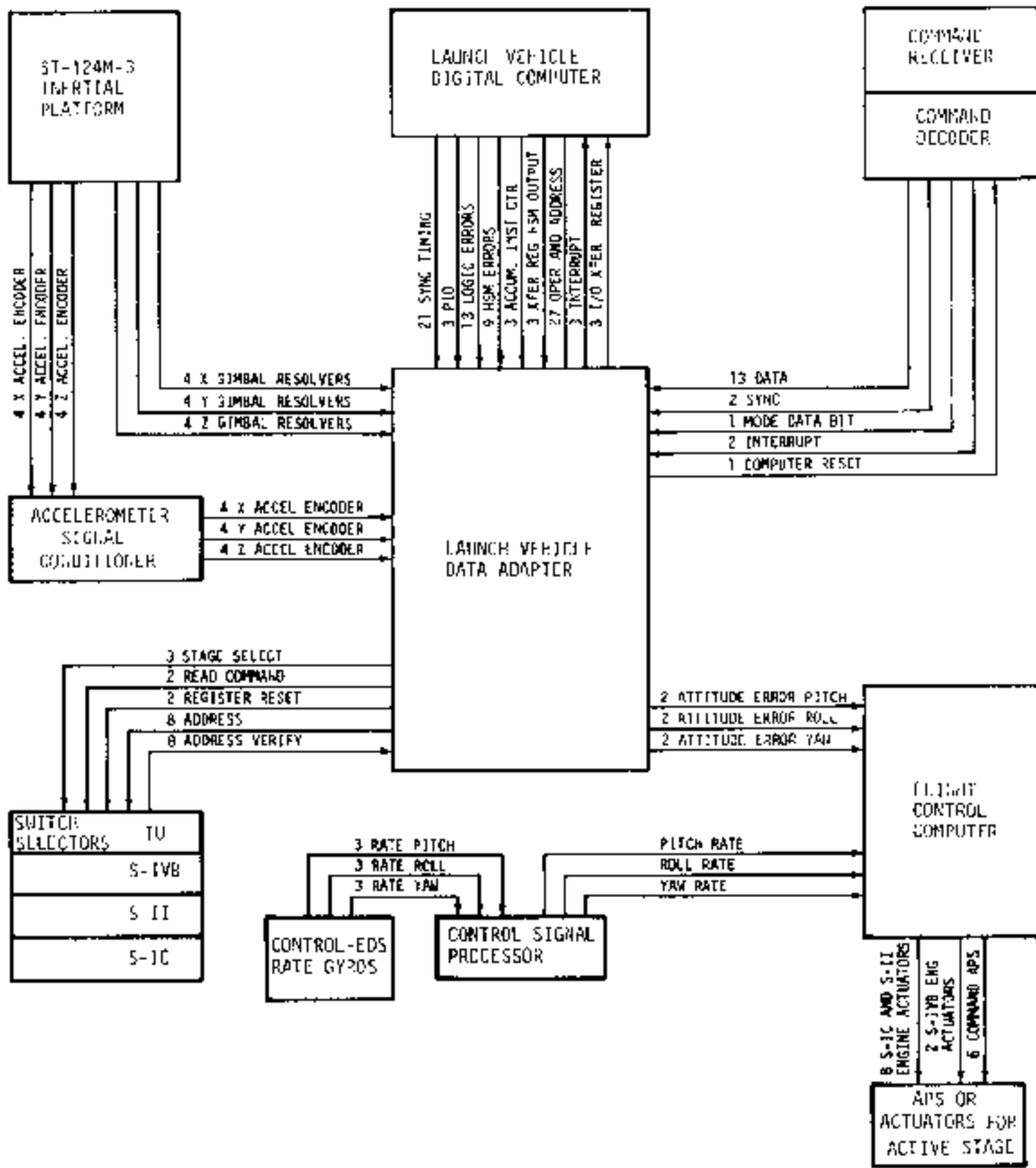


Figure 10-1. Navigation, Guidance, and Control System Block Diagram

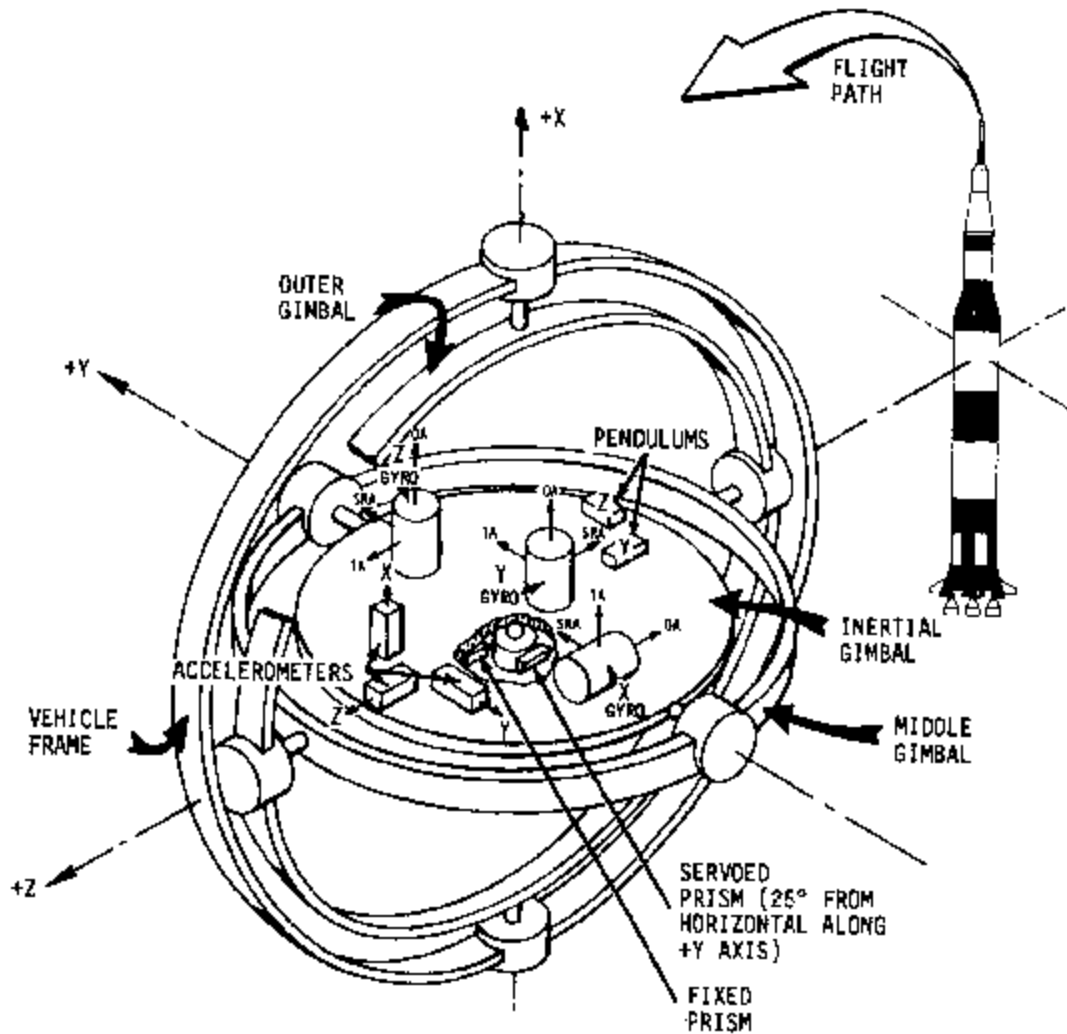


Figure 10-2. Platform Gimbal Configuration

performs seven primary functions: navigation, guidance, event sequencing, attitude control, data management, ground command processing, and hardware evaluation. The program can be described in two parts, boost routines and orbital routines.

10.2.2.1 Boost Routines. In general, the boost routines perform navigation and guidance, event sequencing, and attitude control. Boost navigation encompasses the computations and logic necessary to determine position, velocity, and acceleration of the vehicle during powered flight phases.

The boost guidance is divided into two distinct modes, pre-Iterative Guidance Mode (pre-IGM) and Iterative Guidance Mode (IGM). Pre-IGM is used from initiation of T_1 to S-IC OEEO plus 42 seconds. Programmed commands include a yaw maneuver for tower clearance, roll to align the vehicle to the flight azimuth, and tilt commands. The yaw maneuver is initiated at IU umbilical disconnect sensed by LVDC (T_1) plus 1.0 second. Roll and tilt are initiated when the vertical component of space-fixed position changes by 137 meters (449.5 ft) approximately 11 seconds after T_1 . A time backup of T_1 plus 13 seconds is provided in case of an accelerometer failure. After the tower is cleared and the vehicle fin-I/fin III axis is aligned to the flight azimuth, the roll and yaw commands are set to zero for the remainder of pre-IGM. Tilt commands are computed from one of four third-degree time-tilt polynomials. Nominally, tilt arrest time is T_1 plus a preset time and guidance commands are frozen until initiation of IGM.

The IGM guidance scheme is a modification of the multi-stage, three-dimensional form of IGM. IGM is a near optimal scheme based on a flat earth optimum steering function for planar motion of a point-mass vehicle. The approximate thrust vector steering function is implemented in both the pitch and yaw planes. IGM is implemented in two flight modes, boost-to-parking-orbit IGM and out-of-orbit IGM. However, only the boost-to-parking-orbit mode is applicable to AS-502, since the S-IVB stage engine did not reignite. IGM is initiated at T_3 (S-IC OEEO) plus 42 seconds. Based on the state vector at initiation of IGM, guidance commands are computed and implemented to steer the vehicle to preset terminal conditions. Alternate logic and backup procedures are provided for thrust level shifts and vehicle staging. These procedures are discussed in more detail in paragraph 10.4.2 along with applicable portions of the Flight Program Evaluation.

The Steering Misalignment Correction (SMC) compensates for the misalignment of the thrust vector and for the time lags in output of the steering commands. The SMC terms are only used during active IGM guidance. SMC is not used for any computation cycle in which the reasonableness test on both velocity words fails, turning rates are limited, or when both crossover detectors for the gimbal angle readings are determined to be bad.

Event sequencing is accomplished by the switch selector routine on a stored table basis. The routine determines if it is time to issue a switch selector command, verifies that no switch selector stage was hung, verifies that the correct address is sent to the stage switch selector, and issues the read commands.

Attitude control is accomplished in the minor loop support section of the major loop on an interrupt basis. The minor loop support routine includes calculations of such parameters as steering rates to be applied in the minor loop. Limiting of the ladder outputs is accomplished when necessary, and backup and failure paths are provided in case gimbal angle discrepancies occur.

10.2.2.2 Orbital Routines. The orbital program consists of two interruptible monitor routines. The first is the Instrument Unit Hardware Evaluation Program (HEP), and the second is the Telemetry Executive Program (TEP). Navigation, guidance, event sequencing, attitude control, and ground command processing are initiated on an interrupt basis from either HEP or TEP. During orbital flight and when the vehicle is not over a ground station, the HEP routine is exercised. That is, the computer will be engaged in addressing the Computer Interface Unit (CIU), compressing CIU and LVDC data, and executing computer self-test. Once the vehicle acquires a ground station, TEP is entered as the program major loop. This routine provides time sharing telemetry of compressed and real time data. In addition, command system data and various special data are telemetered on an interrupt basis. Data from the LVDA are telemetered automatically. The orbital guidance routine controls the computation of the commanded vehicle attitudes. This routine is initiated at T₅ (LVDC sensed first S-IVB engine cutoff) plus 15 seconds for the parking orbit and reentered at T₇ for the waiting orbit. Orbital navigation encompasses the computations necessary to determine position, velocity, and acceleration in the space-fixed coordinate system during earth orbit. These computations are carried out in an indirect fashion, making use of mathematical models of the earth, its atmosphere, and the vehicle. A routine for switching the C-band antenna as a function of position is included. This routine is also entered upon exit from the minor loop at 8-second intervals.

Event sequencing in orbit is accomplished in exactly the same manner as in the boost phase but with the added capability to receive time base updates and special output sequence commands from ground stations.

Attitude control for orbital operation is accomplished in the same manner as in the boost phase with the exception of the rate of entry into the minor loop. The orbital minor loop is entered 10 times per second. The first and fifth pass are the attitude update passes (cycled through twice per second), and the remaining eight passes are for attitude hold (cycled through eight times per second) to minimize drift problems.

Ground command processing is accomplished by the Command Receiver interrupt with the Digital Command Subsystem (DCS) routine. The DCS routine processes all ground commands, provides data and mode verification, and supplies the necessary information to the various affected routines. Flight program differences between the AS-501 and AS-502 flights are described below:

- a. One M/F smoothing filter was used for all stages on AS-502.
- b. A new curve fit for the orbital vent model was incorporated.

- c. New orbital guidance maneuvers were planned for T_5 .
- d. T_2 was initiated by the inboard engine cutoff interrupt instead of a fixed time in T_1 .
- e. Five additional CCS commands were provided.
- f. The Apollo Standard Coordinate System was implemented.
- g. The second S-IVB cutoff parameters were representative of translunar trajectories.
- h. No artificial tau steering mode was used for the second S-IVB burn period.
- i. The roll ladder limit was 7 degrees from $T_7 +0$ to $T_7 +600$ seconds, and 15.3 degrees for all other flight times. The pitch and yaw ladder limits were increased from 2.5 to 7 degrees from $T_7 +15$ to $T_7 +600$ seconds.

10.3 GUIDANCE INTELLIGENCE ERRORS

The postflight guidance hardware error analysis is based on comparisons of the ST-124M-3 platform measured velocities with the postflight trajectory established by tracking. Figure 10-3 presents comparisons of the platform measured velocities with corresponding values from the final postflight trajectory (OMPT). Comparisons were made by subtracting guidance values from trajectory values. The differences shown for the pitch plane, (range and altitude) are well within the accuracy of the data compared. The range velocity difference was within ± 0.1 m/s (0.3 ft/s) for the S-IC and S-II flight period. At S-IVB velocity cutoff command the difference was -0.3 m/s (-0.98 ft/s). The altitude velocity difference increased to a maximum of 0.45 m/s (1.48 ft/s) at about 280 seconds and changed slope. At S-IVB cutoff the difference was -0.7 m/s (-2.3 ft/s).

The crossrange velocity difference was well within the accuracy of the data and 3 sigma hardware errors. At S-IVB velocity cutoff command the crossrange velocity difference was -1.85 m/s (-6.07 ft/s). Several attempts have been made to establish error terms that would produce the velocity differences shown. The curves have been simulated to within ± 0.1 m/s (0.3 ft/s) for all three components. A more complete error analysis will be performed and published as a classified memorandum for limited distribution. An estimate of acceleration bias associated with the guidance accelerometers was made using plots of the telemetered velocity outputs during orbit. Although venting was essentially continuous, the general slope of the oscillating curve gives a reasonable estimate of the acceleration bias. Bias errors determined by this method and by calculations in the postflight Orbital Correction Program (OCP) indicate error magnitudes within $\pm 1.0 \times 10^{-4}$ m/s² (3.3×10^{-4} ft/s²) of the preflight measurements for the platform S/N 13.

▽ S-1C OEEO SENSED BY LVDC, 148.41
 ▽ S-II EEO SENSED BY LVDC, 576.33
 ▽ S-IVB VELOCITY CUTOFF COMMAND, 747.04

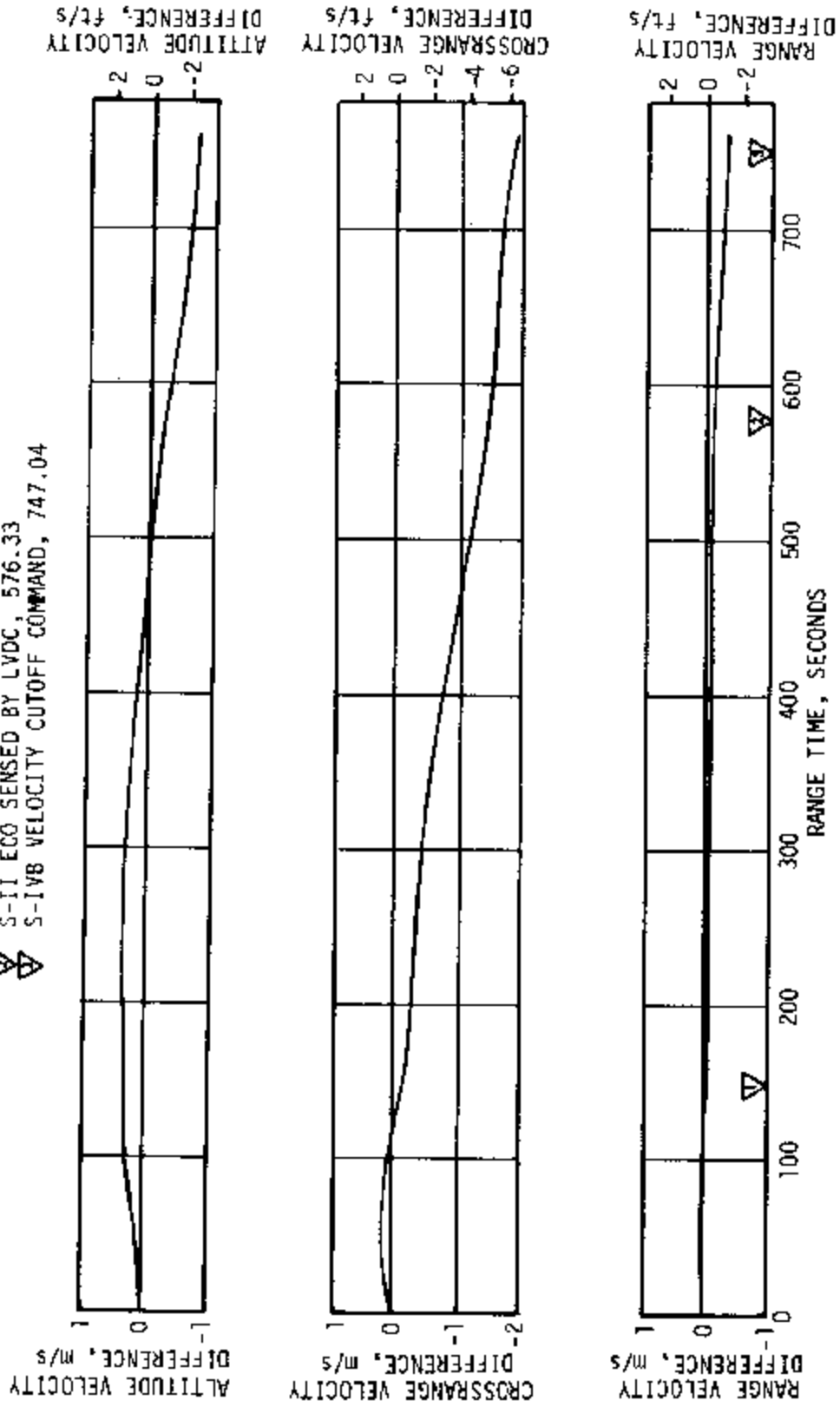


Figure 10-3. Velocity From Postflight Trajectory Minus ST-124M-3 Platform Measured Velocity

10.4 NAVIGATION AND GUIDANCE SCHEME EVALUATION

10.4.1 Inertial Platform and Navigation Parameter Comparisons

ST-124M-3 platform measured velocities and LVDC velocities at several flight event times are shown in Table 10-1, along with corresponding values computed from the postflight trajectory data. Trajectory data were smoothed through the transient areas to be compatible with the velocity differences shown in Figure 10-3. No discrepancy was noted between data telemetered from the accelerometer pickoffs and the accumulated velocities from the LVDC.

Table 10-1. Inertial Platform Velocity Comparisons

EVENTS	VELOCITY*	TELEMETERED ACCELEROMETER m/s (ft/s)	GUIDANCE COMPUTER m/s (ft/s)	POSTFLIGHT TRAJECTORY m/s (ft/s)
S-IC OECO Sensed by LVDC 148.41 sec	\dot{X}	2482.00 (8143.04)	2482.00 (8143.04)	2482.35 (8144.19)
	\dot{Y}	-12.95 (-42.49)	-12.95 (-42.49)	-13.12 (-43.04)
	\dot{Z}	2232.75 (7325.30)	2232.75 (7325.30)	2232.68 (7325.07)
S-II Cutoff Sensed by LVDC, 576.33 sec	\dot{X}	3627.50 (11901.25)	3627.50 (11901.25)	3627.29 (11900.56)
	\dot{Y}	-10.80 (-35.43)	-10.80 (-35.43)	-12.25 (-40.19)
	\dot{Z}	6648.95 (21814.14)	6648.95 (21814.14)	6648.87 (21813.88)
S-IVB Velocity Cutoff Command 747.04 sec	\dot{X}	3144.85 (10317.75)	3144.85 (10317.75)	3144.15 (10315.45)
	\dot{Y}	1.75 (5.74)	1.75 (5.74)	-0.26 (-0.85)
	\dot{Z}	7659.05 (25128.12)	7659.05 (25128.12)	7658.77 (25127.20)
Parking Orbit Insertion, 757.04 sec	\dot{X}	3145.75 (10320.70)	3145.75 (10320.70)	3144.97 (10318.14)
	\dot{Y}	1.75 (5.74)	1.75 (5.74)	-0.27 (-0.89)
	\dot{Z}	7661.45 (25135.99)	7661.45 (25135.99)	7661.17 (25135.07)

*These coordinates are as defined in the Apollo 13 coordinate system:

- \dot{X} = Altitude velocity
- \dot{Y} = Crossrange velocity
- \dot{Z} = Downrange velocity

Navigational positions and velocities determined from the preflight trajectory, postflight trajectory, and telemetered LVDC data are shown in Table 10-2. At S-IC/S-II separation, the guidance data were in very good agreement with the postflight trajectory values. The differences between the actual and preflight data reflect nonstandard flight conditions and S-IC performance. An apparent yaw bias that built up during S-IC burn contributed significantly to the 21.94 m/s difference in crossrange velocity at S-IC (LVDC sensed) OECO. The vehicle drift in yaw resulted from a small thrust misalignment and slight off-nominal engine performance. It should be noted that pre-IGM guidance does not provide path guidance and that the relatively large crossrange velocity difference posed no problem for IGM guidance.

There was good agreement between guidance and postflight trajectory at S-II/S-IVB separation, S-IVB cutoff, and parking orbit insertion. However, due to the perturbation caused by premature cutoff of S-II engines No. 2 and 3, the agreement between preflight trajectory positions and velocities and either guidance or postflight trajectory values is not as good. Measured velocity gain due to thrust decay after first cutoff of the S-IVB stage engine was 2.50 m/s (8.20 ft/s) compared to a predicted value of 2.26 m/s (7.41 ft/s) (see Section 7.4). The velocity outputs of the guidance accelerometers from orbital insertion to T_6 were curve-fitted with time polynomials. The velocity polynomials were differentiated and then evaluated to determine measured accelerations. A Root-Sum-Square (RSS) of the acceleration components is shown as a solid line in Figure 10-4 along with the predicted acceleration (dashed line), taken from the final operational trajectory (preflight predicted), and the programmed vent model. The guidance acceleration components were also adjusted for estimated bias, and the circled points represent adjusted accelerations. The thrust produced by the Continuous Vent System (CVS) based on venting parameters is shown in Figure 7-7 (Section 7.5).

Oscillations of the measured accelerations appeared to be out of phase with the predicted values. This was probably due to some combination of inaccuracies in the predicted values, curve fits of measured data, off-nominal propellants onboard at insertion, and off-nominal orbit. Further investigations are being made to verify the predicted accelerations. The measured accelerations, with minor adjustments for bias, were used in establishing the postflight orbital trajectory (see Figure 4-6 and paragraph 4.3.2). Figure 4-5 is similar to Figure 10-4 in its comparisons of accelerations in parking orbit, except that Figure 4-6 includes an adjustment for predicted drag.

10.4.2 Flight Program Evaluation

The flight program performance was as expected for the flight perturbations experienced. The navigation scheme functioned correctly in all phases of flight, control calculations were correct, and orbital operation

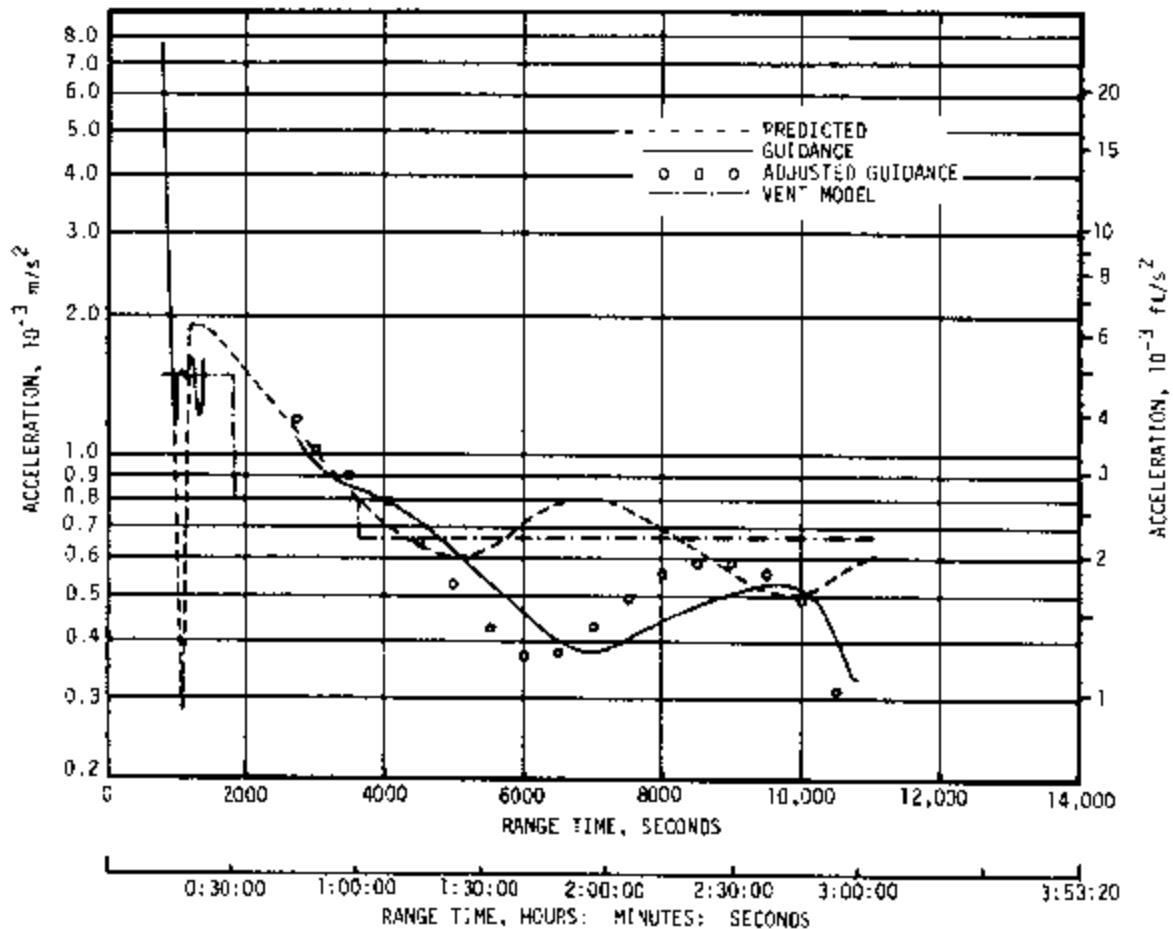


Figure 10-4. Predicted and Measured Accelerations in Parking Orbit

was as expected. Guidance schemes functioned as designed. Investigations have demonstrated that an overspeed of 48.9 m/s (160 ft/s) was a direct result of premature shutdown of the two S-II stage engines.

When the premature S-II outboard engine shutdown was detected by the flight program, bit 15 was set in mode code word 25 (MC25). This bit was improperly identified as inboard engine out in the program documentation. Since this bit is not used in any of the program logic flow, the improper description had no effect on the operation of the flight program; only an erroneous indication in real time telemetry resulted. This problem has been corrected for future flight programs.

Pre-IGM guidance was nominal. The yaw maneuver for tower clearance was initiated at 1.9 seconds and properly executed before pitch and roll commands were initiated at 11.1 seconds. The vehicle was rolled from its 90 degree launch azimuth to the 72 degree flight azimuth by 31.3 seconds. Upon completion of the yaw and roll maneuvers these guidance commands were set to zero for the remainder of pre-IGM guidance mode. No backup modes were required for the S-IC stage, and tilt arrest occurred at 140.9 seconds. From this time the pitch command ($\text{Chi } Y$) was frozen until IGM initiation at 191.0 seconds.

A roll bias of -0.5 degree was observed from approximately 30 seconds to Inboard Engine Cutoff (IECO). A negative yaw bias was noted at approximately 15 seconds and slowly reduced to zero by 70 seconds, then gradually increased from 88 seconds to IECO. The yaw and roll biases were probably the result of allowable thrust deviations during S-IC burn. The pre-IGM guidance does not provide path guidance corrections and the vehicle yaw drift was the major contributor to the 21.94 m/s (71.98 ft/s) off-nominal crossrange velocity at S-IC (LVDC sensed) OECO.

The performance of closed loop guidance (IGM) was nominal until 412.92 seconds, when the S-II stage engine No. 2 shut down, followed by cutoff of engine No. 3 at 414.18 seconds. The flight program detected an S-II outboard engine failure based on both an external discrete and an acceleration test. Although the engine failures occurred in the same computation cycle that the PMR shift was expected, the program properly identified the change in acceleration as an engine out. At this time two modifications were made to the nominal S-II guidance equations:

- a. An artificial tau mode was entered in which preset (versus measured) acceleration values were used as guidance inputs. Tau is a calculated IGM parameter representing time-to-go required to burn all remaining vehicle mass at a constant mass flow rate. Tau is the product of average exhaust velocity (preset value) and the reciprocal of total acceleration.
- b. All parameters based on time of S-II fuel depletion were adjusted to reflect the longer burn time expected on four engines. This modification resulted in a change of the time-to-go to S-II stage cutoff from 101.0 seconds to 126.3 seconds.

The second engine failure that occurred was not acted upon because a basic ground rule in designing flight program backup modes for hardware failures was to protect only against single engine failures. No logic was provided to check for multiple engine failures through acceleration changes. Thus the guidance parameter adjustments which revised time-to-go for S-II stage cutoff underestimated the time by approximately 45 seconds. Vehicle guidance remained in the artificial tau mode until Programmed Mixture Ratio (PMR) shift occurred at 490.8 seconds. At PMR shift, a second artificial tau mode was entered to smooth the transition to the lower thrust level. At termination of the second artificial tau mode (510.2 seconds), due to guidance sensed PMR shift, the measured accelerations were lower than the artificial values used. Guidance commanded nose-up attitude in response to the lower acceleration. Seven and one-half seconds later, a chi freeze was properly initiated in preparation for S-II/S-IVB staging.

Because of control considerations at S-II/S-IVB staging, the flight program normally freezes the guidance commands 5 seconds prior to S-II stage cutoff. For AS-502 the freeze period was entered as specified, but the actual remaining burn time exceeded the time-to-go, which resulted in a 58 second period of constant attitude hold rather than the nominal 5 seconds. This constant vehicle attitude led to a buildup in radial velocity which, in turn, caused an altitude overshoot.

The perturbation due to loss of two S-II engines had two effects on the vehicle performance: the reduced acceleration resulted in lower than nominal velocities, and the lengthened attitude freeze led to higher than nominal altitude. Thus at 28.2 seconds after initiation of guidance in the S-IVB stage, velocity was 172.1 m/s (564.6 ft/s) lower than nominal and altitude was 9.1 kilometers (29,850 ft) higher than nominal.

The IGM flight program normally steers the S-IVB stage to preset end conditions of radius and vector velocity optimally. Steering angles to achieve the vector velocity end conditions are added to steering angles to satisfy the radius constraint in order to form the total commanded vehicle attitude. For AS-502, the highly perturbed state vector which resulted from the two S-II stage engine failures led to inconsistent steering angles to achieve velocity and radius end conditions. The composite of the two pitch steering angles is shown in Figure 10-5. This total commanded vehicle pitch attitude is not rate limited. The corresponding rate limited commands are presented later. As can be seen from Figure 10-5, the commanded attitude on AS-502 was a pitch down to reduce the radius. The radius was corrected, but a resultant negative radial velocity was achieved. A nose-up pitch command was given to compensate for the excess radial velocity. By 712.3 seconds, when terminal guidance mode was entered, pitch attitude had changed 46 degrees nose-up to 13 degrees above the local horizontal. The sensitivity of IGM to changes in acceleration increases as the desired terminal parameters are approached. A terminal guidance scheme (chi bar steering) is required which uses only the velocity constraints. During chi bar steering, altitude constraints are set to zero.

With IGM calculations now constrained only to component velocity in the terminal guidance mode, a continued nose-up pitch was commanded to achieve the desired radial velocity. Chi commands increased +96 degrees until S-IVB stage cutoff. Vehicle pitch attitude was rate limited through the 35-second duration of terminal guidance. S-IVB stage cutoff occurred with pitch attitude approximately 49 degrees above the local horizontal. S-IVB stage cutoff occurred 88.01 seconds later than the nominal predicted time and with total velocity 48.9 m/s (160 ft/s) greater than desired terminal velocity.

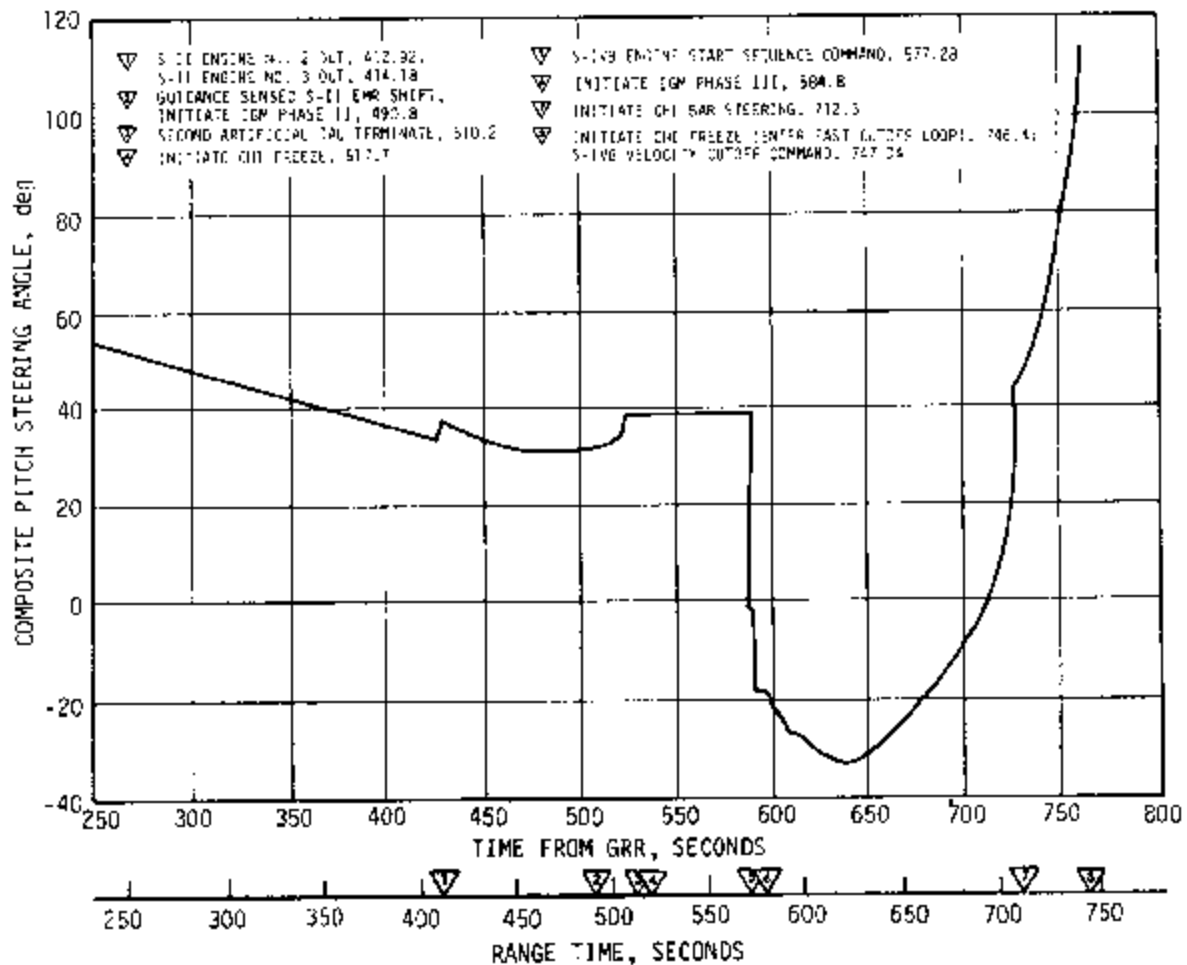


Figure 10-5. Composite Pitch Steering Angle (Not Rate Limited) Referenced to Local Horizontal

Figure 10-6 is a plot of the radial velocity ($\Delta\dot{X}_V$) to-be-gained versus the horizontal velocity ($\Delta\dot{Z}_V$) to-be-gained. The circle about the origin represents the cutoff loop which is entered when total velocity-to-be-gained falls below approximately 65 m/s (213 ft/s). Entry into the cutoff loop is made only from calculations of component velocity-to-be-gained. Once in the loop, cutoff is effected as a function of the magnitude of total velocity. The difference in the actual and nominal velocities-to-be-gained is a result of pitch down attitude commands to correct altitude during the initial portion of S-IVB guidance. The pitch down attitude tended to increase the radial velocity-to-be-gained rather than decrease it. This increase led to an inconsistency in the components of velocity-to-be-gained, and, as a result, both could not be driven to zero simultaneously. The radical attitude changes near S-IVB cutoff finally reduced the velocities-to-be-gained sufficiently to cause entry into the cutoff loop.

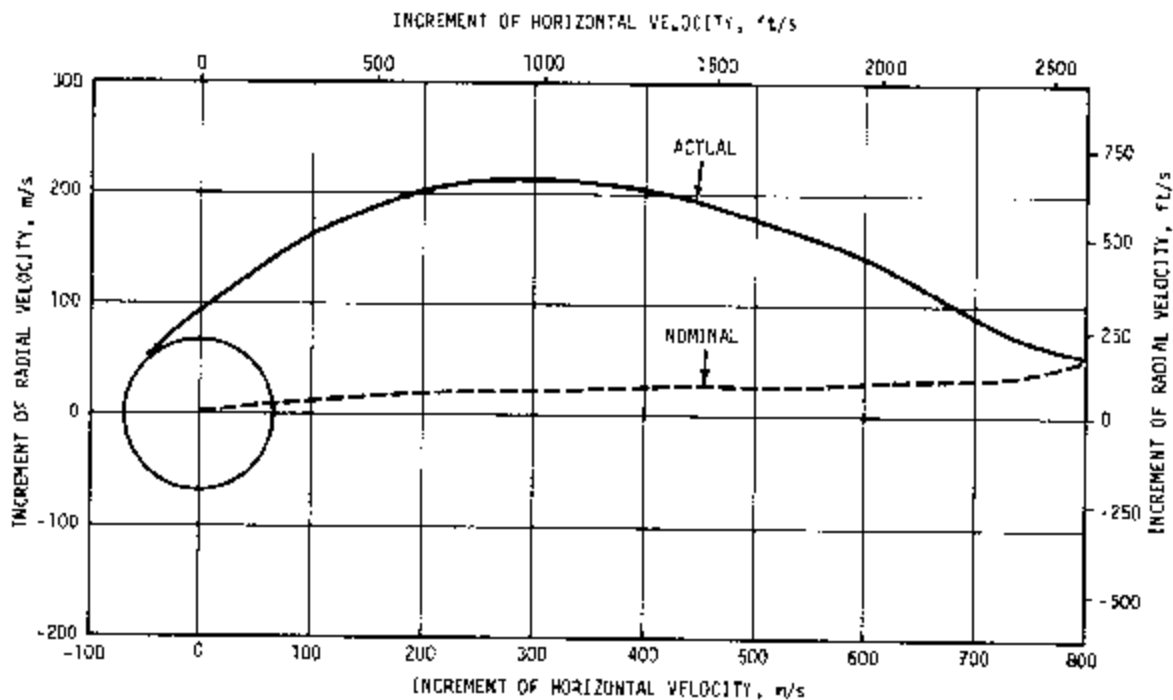


Figure 10-6. Actual and Nominal Velocities-to-be-Gained

On entering the cutoff loop, the AS-502 total velocity was in excess of the desired value of 7790.9 m/s (25,560.7 ft/s), and cutoff signal was immediately given at 747.04 seconds with an overspeed of 48.9 m/s (160 ft/s). This overspeed did not represent an error in the guidance program operation but merely reflected the radial velocity-to-be-gained constraint which had to be satisfied before entry into the high speed cutoff loop.

All commanded attitude outputs were rate limited to 1.0 deg/s. This limit serves to make the vehicle less responsive to program attitude commands. Table 10-3 gives the times the commands were rate limited. Note that they were limited for about two-thirds of the S-IVB active guidance.

Table 10-4 summarizes the start and stop times of the modes used to compute guidance commands. Note that from the S-II-engines-out until S-IVB cutoff, the guidance was either in an artificial tau mode, rate limited, or frozen for all but 62 seconds.

Commanded attitude angles (rate limited) during the boost phase of flight are summarized in Figure 10-7. Both actual and commanded attitude (rate limited) angles during S-IC burn, S-II burn, and S-IVB first burn are shown on expanded scales in Section 11.

Table 10-3. Rate Limited Steering Command Times

START TIME SEC	STOP TIME SEC
415.4	419.1
510.2	514.0
582.9	644.1
699.0	747.0

Table 10-4. Start and Stop Guidance Commands

EVENT	IGM PHASES (SEC)		ARTIFICIAL TAU (SEC)		CHI BAR STEERING (SEC)		CHI FREEZE (SEC)	
	START	STOP	START	STOP	START	STOP	START	STOP
First IGM	191.0	415.4	415.4	490.8	---	---	---	---
Second IGM	490.8	517.7	490.8	510.2	---	---	517.7	582.9
Third IGM	584.8	747.0	584.8	594.3	712.3	746.4	746.4	762.3
Fourth IGM	11628.4	11630.3						

IU commands were properly executed for S-IVB restart but the engine did not reignite. The flight program immediately initiated T₇ through negative results from the acceleration test as programmed. The first event scheduled in T₇ was a cutoff command to the S-IVB stage; this was executed. A simulation using actual AS-502 flight data and a nominal S-IVB second burn thrust revealed that an acceptable waiting orbit could have been achieved from the perturbed parking orbit had the S-IVB engine reignited.

10.4.3 Orbital Guidance

All orbital guidance and sequencing functions were performed correctly. The vehicle response to the guidance commands in T₇ was sluggish because of the inertial characteristics of the vehicle resulting from no second burn of the S-IVB stage and early separation of the spacecraft on ground command. The predicted attitude timeline for the AS-502 flight is shown in Figure 10-8. Comparison of parking orbit attitude commands shown in Section 11 with the attitude timeline yields good agreement.

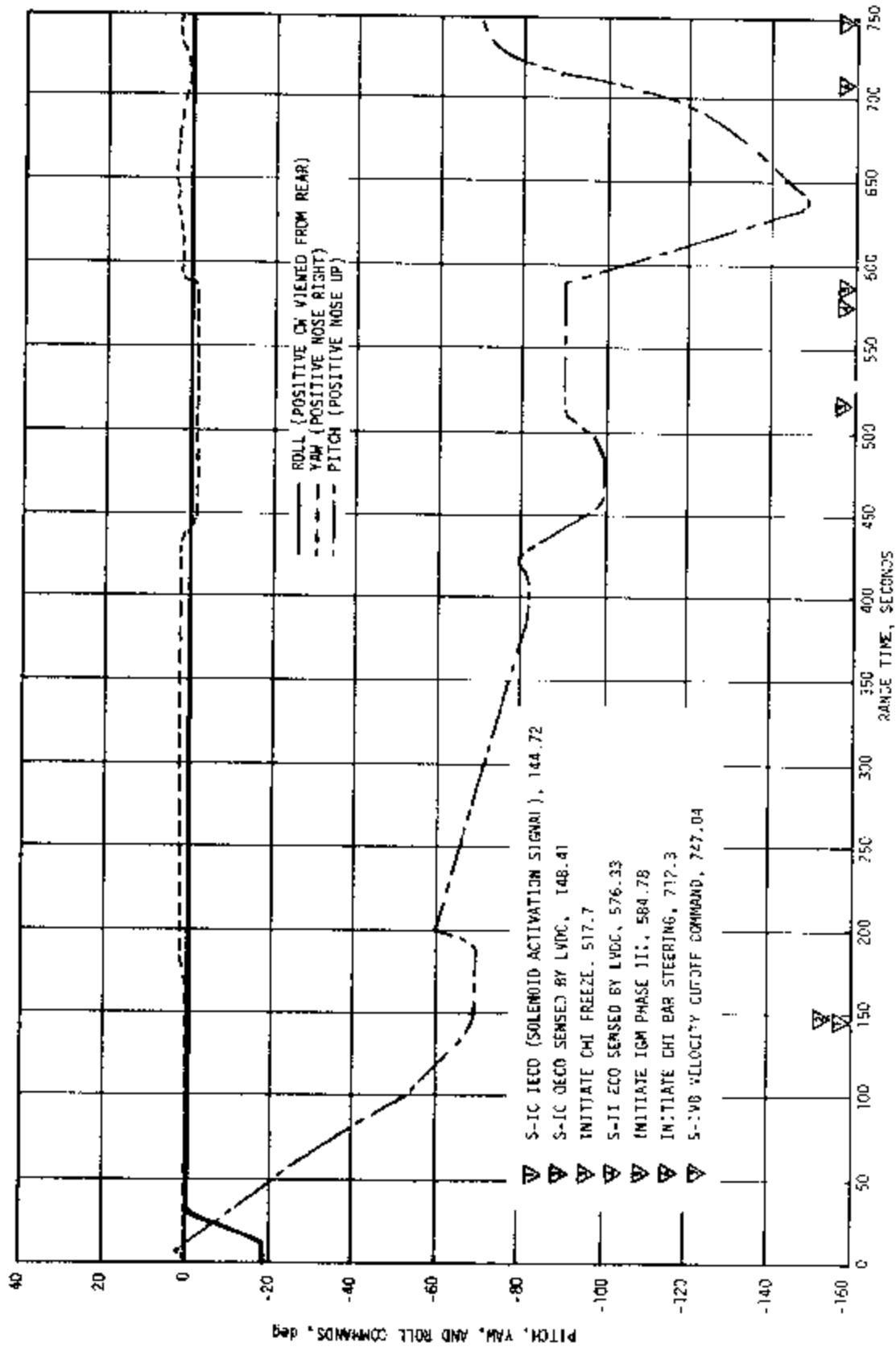


Figure 10-7. Commanded Attitude Angles (Rate Limited) During Boost Phase

- ▽ PARKING ORBIT INSERTION, 669 (PREDICTED)
- ▽ INITIATE 180° ROLL TO PLACE POSITION III DOWN ($T_5 + 90$), 749 (PREDICTED)
- ▽ INITIATE 20° PITCH DOWN MANEUVER ($T_5 + 2460$), 3119 (PREDICTED)
- ▽ INITIATE 20° PITCH UP MANEUVER ($T_5 + 4680$), 5339 (PREDICTED)
- ▽ INITIATE 80° ROLL TO PLACE POSITION I DOWN ($T_5 + 5040$), 5699 (PREDICTED)
- ▽ INITIATE RESTART SEQUENCE AND START OF T_6 , 11,076 (PREDICTED)
- ▽ INITIATE MANEUVER TO SEPARATION ATTITUDE ($T_7 + 20$), 11,478 (PREDICTED)
- ▽ LV-LTA/CSM PHYSICAL SEPARATION, 11,908 (PREDICTED)
- ▽ INITIATE MANEUVER TO POST SEPARATION INERTIAL ATTITUDE ($T_7 + 600$), 12,328 (PREDICTED)

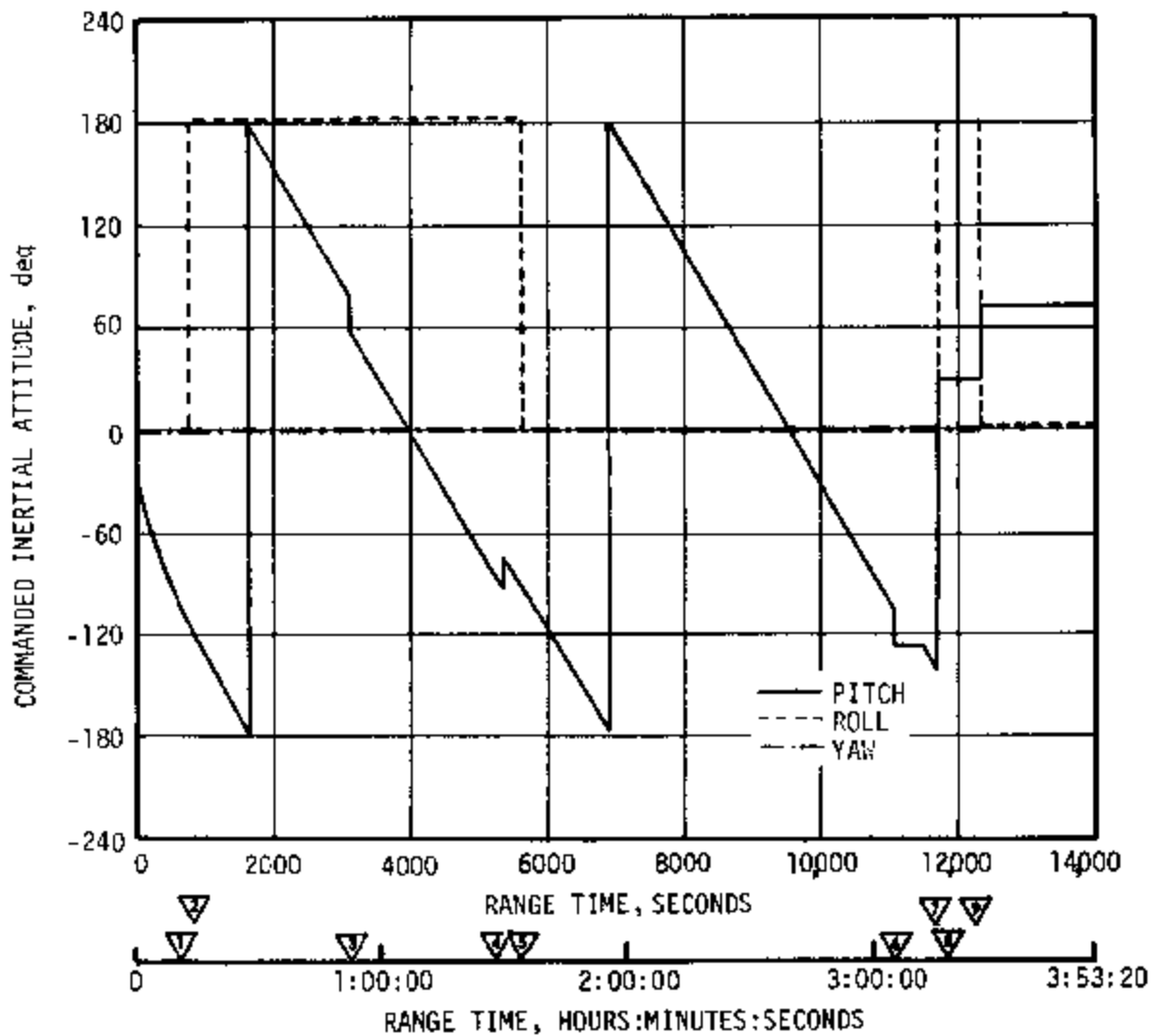


Figure 10-8. Attitude Timeline - Liftoff to Spacecraft Separation

Vehicle control was exercised until 22,112.4 seconds, at which time attitude reference was lost. Partial control was lost at 21,953 seconds due to loss of fuel in the APS module at position I. The opening of the LOX vent valve at 22,023 seconds produced a thrust which overcame the remaining thrust capability of the APS module at position III. Loss of fuel in the APS module at position III occurred at 22,602 seconds.

The minor loop performed as expected during flight. The rate at which the yaw gimbal changed when the APS ran out of fuel was insufficient to cause the program to switch to backups or set the guidance failure discrete.

10.4.4 Orbital Routines

The TEP routines performed as expected. This was proven by the real time and compressed data telemetry which has been reduced. No problems were found with the LVDC self-test or in CIU processing. All DCS commands received by the flight program were processed correctly.

10.4.5 Event Sequencing

All program sequencing was proper. All switch selectors were issued in tolerance. The Environmental Control System logic monitored the thermal switches and opened and closed the control valve properly.

10.5 GUIDANCE SYSTEM COMPONENT EVALUATION

10.5.1 LVDC Performance

Data analysis indicated the LVDC performed as predicted for the AS-502 mission. No valid error monitor words and no self-test error data have been observed that indicate any deviation from correct operation.

10.5.2 LVDA Performance

The LVDA performed satisfactorily for the AS-502 mission. With the exception of the error monitor word related to the interrupt processor no deviations from correct operation have been found. Two error monitor words were observed which indicated apparent disagreements in the Triple Modular Redundant (TMR) Orbital Check Ready (OCR) latch. One disagreement occurred within 0 to 30 seconds prior to 8618.2 seconds and the other at approximately 9218 seconds. For each OCR latch disagreement a TMR Interrupt Control (INTC) error monitor word indication might also be expected. However, the flight program inhibits the OCR interrupt and processes it on a cyclic basis. Since the OCR interrupt is inhibited, no disagreement between logic channels can be sent to the INTC latch. The apparent disagreement in the OCR latch was attributed to a difference between rise delay times for the TMR interrupt input logic channels. Two error monitor words were observed

in compressed data which indicated apparent disagreements in the INTC latch. These disagreements occurred within 0 to 30 seconds prior to 14,984.7 and 15,044.7 seconds.

The real time and interrupt countdown processors performed satisfactorily.

10.5.3 Ladder Outputs

The ladder networks and converter amplifiers performed satisfactorily. No data have been observed that indicate an out-of-tolerance condition between channel A and the reference channel converter-amplifiers.

10.5.4 Telemetry Outputs

Analysis of the available analog telemetry buffer and flight control computer attitude error plots indicated symmetry between the buffer outputs and the ladder outputs. The analysis of the available LVDC power supply plots indicated satisfactory performance of the power supply telemetry buffers.

10.5.5 Discrete Outputs

No valid discrete output register words (TAGS 043 and 052) were observed to indicate guidance or simultaneous memory failure.

10.5.6 Switch Selector Functions

Switch selector data indicate that the LVDA switch selector functions were performed satisfactorily. No error monitor words were observed that indicate disagreement in the TMR switch selector register positions or in the switch selector feedback circuits. No mode code 24 words or switch selector feedback words were observed that indicated a switch selector feedback was in error. In addition, no indications were observed to suggest that the B channel input gates to the switch selector register positions were selected.

10.5.7 ST-124M-3 Inertial Platform Performance

The inertial platform system performed as expected with the only deviation being in the gasbearing supply system. This deviation is described in Section 18.5.

The X, Y, and Z accelerometer servo loops maintained the accelerometer float within the measuring head stops (± 6 degrees) throughout liftoff and MAX Q (see Figure 10-9). The accelerometer encoder outputs indicated that the accelerometers measured the vehicle acceleration properly.

The X, Y, and Z gyro servo loops for the stable element functioned as designed. At no time during liftoff and MAX Q were the operational limits reached. There were several perturbations observed in the servo

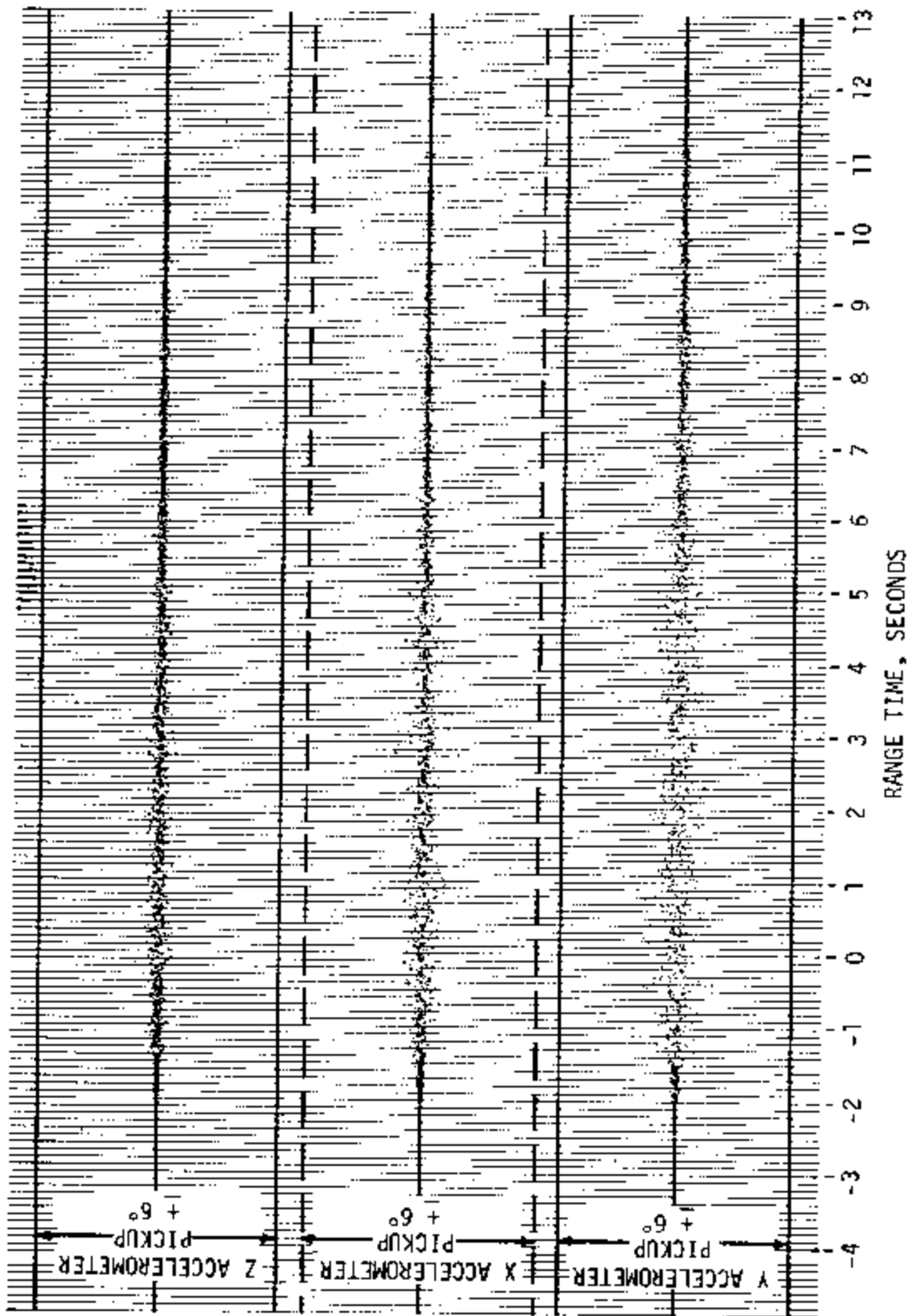


Figure 10-9. Accelerometer Pickup Signals During Liftoff

gyro loops which cannot be fully explained at this time; however, the servo loops responded to these perturbations in the proper manner and maintained the stable reference. Periodic level changes in the servo signals are attributed to servo loop deadband limit cycling associated with vehicle attitude changes.

The fine backup gimbal angle resolver output indicated nominal performance.

There were no vibration-induced malfunctions of the ST-124M-3 Inertial Platform on AS-502. The effects of vibration on the gyro and accelerometer servo output signals are illustrated by the graphs of maximum voltage variations shown in Figure 10-10. These voltages were sufficient to maintain inertial reference and prevent a vibration-induced malfunction of any accelerometer or gyro. This figure also illustrates the large vibration experienced at 133.3 seconds.

Available data indicate that the ST-124M-3 composite vibration levels at liftoff on AS-502 were very near those of AS-501 on the inertial gimbal. However, the structural vibration was lower on AS-502. The vibrations at Mach 1 and MAX Q were higher on AS-502. The composite levels of the inertial gimbal vibrations are shown in Figure 9-34 in Section 9. The vibration experienced at 133.3 seconds is not shown due to its short duration.

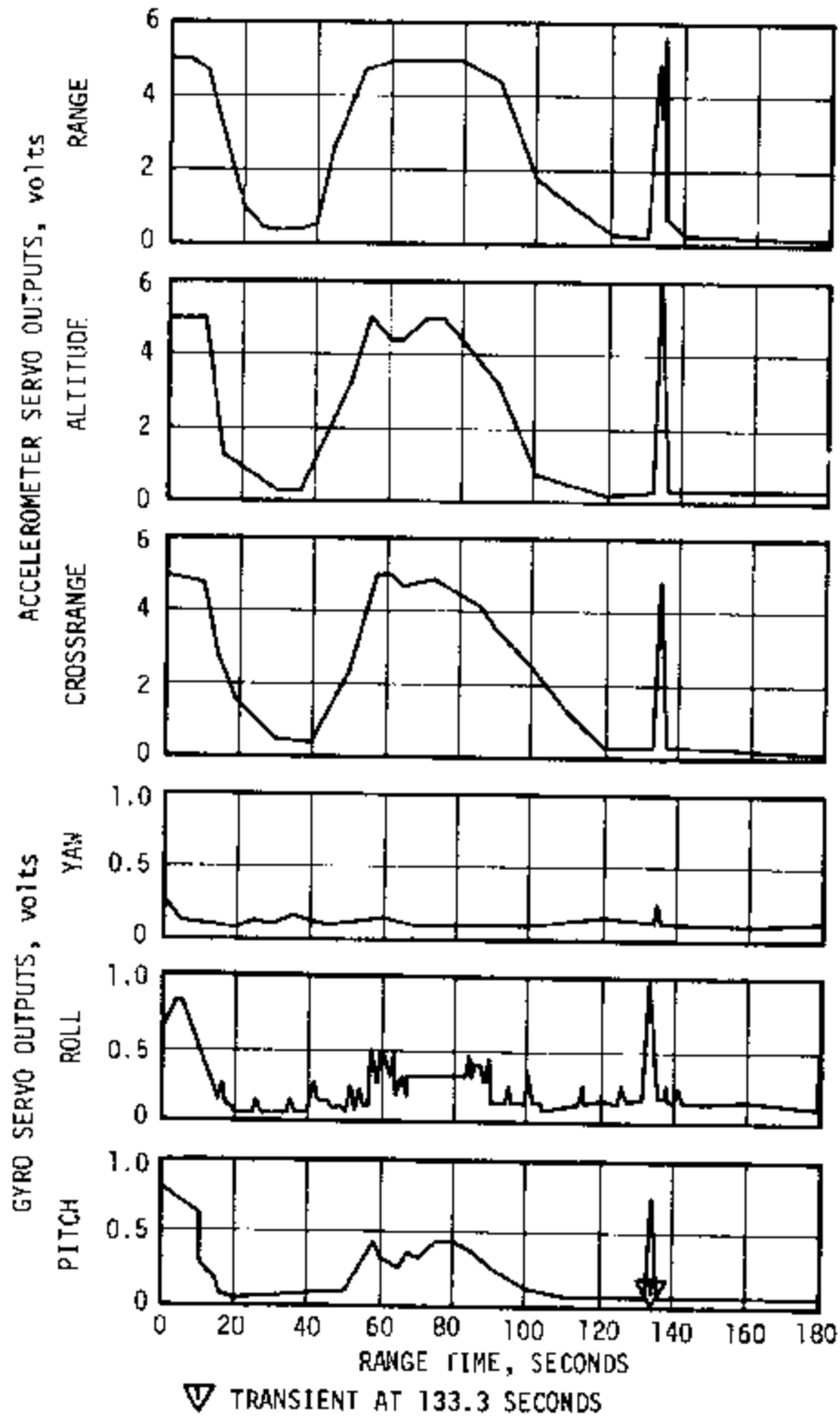


Figure 10-10. Envelope of Maximum Deviations of the Gyro and Accelerometer Servo Amplifier Outputs

SECTION 11

CONTROL SYSTEM

11.1 SUMMARY

The AS-502 Flight Control Computer (FCC), Thrust Vector Control (TVC), and Auxiliary Propulsion System (APS) satisfied all requirements for attitude control and stability of bending and propellant slosh modes in both the boost and orbital coast modes of operation. During liftoff, all vehicle clearance requirements were met satisfactorily with less than 20 percent of the clearance margins being required. The programmed 1.25 degrees yaw maneuver to provide adequate tower clearance and the 18 degrees roll maneuver to the 72 degree flight azimuth were satisfactorily initiated and executed.

The wind-biased pitch tilt program was satisfactorily initiated and executed. The control system was required to correct for a steady-state roll attitude error of approximately -0.5 degree through first stage boost. This roll torque was not observed on AS-501, as the attitude error was essentially null after about 60 seconds.

S-IC/S-II separation was satisfactorily accomplished, as was second plane separation. Control system performance was consistent with events which occurred during S-II boost. The performance shift of engine No. 2 at 319 seconds was evidenced in the TVC as well as in the FCC parameters. However, this performance shift caused no control problems and resulted only in a new steady-state trim condition.

The Steering Misalignment Correction (SMC) was initiated at 212.0 seconds. The performance shift at 319 seconds had a negligible effect on SMC, and the maximum SMC's in pitch and yaw prior to engines No. 2 and 3 shutdown were -0.7 and 0.2 degree in pitch and yaw, respectively. The FCC and TVC responded satisfactorily to the perturbations caused by the shutdown of engines No. 2 and 3 at 412.92 and 414.18 seconds, respectively. This shutdown resulted primarily in a large pitch plane disturbance during which the pitch rate built up to a maximum of 2.8 deg/s (nose-up) and the pitch attitude error reached a maximum of 13.4 degrees. A maximum engine deflection of 5.95 degrees was required to stabilize the attitude excursions. The maximum SMC's required at this time to compensate for the thrust vector misalignment were -13.2 degrees in pitch and -0.6 degree in yaw. The nose-up trim condition resulted in a 7.4 degree pitch attitude error at separation.

At S-II/S-IVB separation, the guidance computer switched to the S-IVB coast mode for 0.3 second. The 7.4 degrees pitch attitude error caused a full-on APS pitch-engine firing of 0.3 second duration to correct the attitude. At 0.3 second after separation, the guidance computer switched to the S-IVB burn mode. The pitch attitude error was trimmed out by the TVC after S-IVB stage J-2 engine ignition. Control system performance was nominal for the remainder of S-IVB first burn.

Orbital attitude control requirements required considerably more APS activity than anticipated. The APS system was required to overcome a 50 degrees nose-up from local horizontal attitude and a 1 deg/s nose-up angular rate to align the vehicle along the local horizontal. The vehicle was subsequently exercised through a sequence of four maneuvers as follows: 180 degrees roll, 20 degrees pitch down, 20 degrees pitch up, and 180 degrees roll. The pitch and roll maneuvers were planned to produce information on the S-IVB restart bottle repressurization and propellant slosh excitation while qualifying these maneuvers for manned flight. Each maneuver was executed as planned. LH₂ sloshing was not appreciable during any of the maneuvers. Significant LOX sloshing existed at the initiation of each pitch maneuver; however, the initial amplitude was not sustained due to high damping.

An auxiliary hydraulic pump failure prevented the S-IVB stage J-2 engine from being centered at the time of S-IVB Engine Start Command (ESC). The engine position at ESC was approximately 1.5 degrees in pitch and -2.3 degrees in yaw. Appreciable attitude errors resulted from this engine position during restart attempt; however, vehicle control was maintained by the APS system following the switch from thrust vector to coast mode control.

Subsequent to spacecraft separation (Section 12) the APS system maintained control until module I fuel depletion at approximately 21,953 seconds. Vehicle attitude rates began to build up significantly following module III fuel depletion (22,602 seconds) and continued to increase as indicated by reduced radar data until a tumble rate of 180 deg/s was recorded by the ninth day following launch.

11.2 CONTROL SYSTEM DESCRIPTION

Figure 10-1 (Section 10) shows the interconnection and signal flow paths of the control components as they relate to the guidance components.

Vehicle attitude correction is accomplished in accordance with the requirements of the guidance system through attitude error signals. These signals are generated by the Launch Vehicle Digital Computer (LVDC) and Launch Vehicle Data Adapter (LVDA). During S-IC stage burn, attitude steering commands are the result of the preprogrammed yaw and roll maneuvers and the time tilt pitch program. At the initiation of Iterative Guidance Mode (IGM), attitude steering commands become the result of guidance system computations.

Angular rate inputs are present when the control system has responded to attitude error commands or forces acting on the vehicle. Commanded vehicle attitude changes during powered flight are limited to rates of 1 deg/s or less, depending upon requirements of the guidance system.

Control system outputs are valve currents (I_v) to first, second, and third stage engine actuators and relay currents to the APS.

The vehicle engine, actuator, and nozzle arrangements and axis definitions are shown in Figure 11-1.

The AS-502 Flight Control Computer, which is essentially identical to the AS-501 FCC, is an analog computer which generates the proper commands for the S-IC, S-II, and S-IVB stage engine actuators and S-IVB stage APS. In generating the engine commands, the FCC processes and combines attitude error signals from the LVDA and angular velocity signals from the Control-EDS Rate Gyros/Control Signal Processor (CSP). Two input channels accept the control signals. Each channel amplifies, scales, and filters its respective signal according to a predetermined time-variable set of gain factors.

The FCC also provides S-IVB stage attitude control commands to the APS. This control is provided to the roll axis during S-IVB stage burn and to all three control axes during coast.

The Control-EDS Rate Gyros/CSP used on AS-502 were essentially identical to those used on AS-501. The Control-EDS Rate Gyros/CSP combination provides angular velocity signals to the FCC for dynamic feedback. The Control-EDS Rate Gyros contain nine rate gyros, three in each axis.

11.3 S-IC CONTROL SYSTEM EVALUATION

The AS-502 control system performed satisfactorily during S-IC powered flight with most parameters near predicted. The 1.25 degree yaw bias tower clearance maneuver was executed as planned and resulted in adequate tower clearance.

Vehicle liftoff acceleration was greater than that of AS-501. Simulation with measured slow release forces and thrust verified this result. Acceleration was greater than AS-501 because 12 lubricated slow release rods were used instead of 16 non-lubricated rods. Less than 20 percent of the available clearances were used during liftoff.

The vehicle performed within flight dynamic constraints throughout flight. In the region of high dynamic pressure, pitch angle-of-attack peaked at 3.1 degrees, and pitch engine deflection peaked at 0.47 degree. Absence of any divergent bending or sloshing frequencies in vehicle motion indicates that the bending and slosh dynamics were adequately stabilized. The control system sufficiently rejected two prominent disturbances near the end of S-IC flight: the 5.3 hertz longitudinal oscillation that coupled into pitch (see Section 9.2.3.1), and the transient at approximately

133 seconds (see Section 9A). Vehicle dynamics prior to S-IC/S-II first plane separation were well within required levels.

11.3.1 Liftoff Clearances

Positive clearance existed between the vehicle and the mobile launcher structure, as shown in Table 11-1. Vehicle clearances were at least 80 percent of those available. Positive clearances resulted from a favorable combination of vehicle-system misalignments. The ground wind direction was 132 degrees east of north, and the magnitude was approximately 53 percent of the design wind. The launch ground wind is compared with the design ground wind in Figure 11-2. The launch ground wind had a steady state magnitude of 7.5 m/s (24.6 ft/s) at the 18.3 meters (60 ft) level, and 12.5 m/s (41.0 ft/s) at the top of the launch tower. The combination of offset center of gravity, thrust imbalance, and thrust misalignment in yaw cancelled the yaw moment from inboard engine cant. Table 11-2 compares the vehicle misalignments measured during flight with preflight measurements.

Liftoff vertical motion and soft release forces are shown in Figure 11-3. Liftoff accelerations were greater than predicted. The slow release forces reduced from continuous analog recorder measurement provide an excellent match between simulated vertical motion and the vertical motion observed by the liftoff cameras. The AS-502 vertical rise was about 0.5 second faster than the AS-501 because the AS-502 had 12 lubricated slow release rods as compared to 16 non-lubricated rods on the AS-501. Figure 11-4 shows that the actual (photographed) trajectory of the S-IC thrust

Table 11-1. Summary of Liftoff Clearances

POTENTIAL INTERFERENCE		AVAILABLE CLEARANCE cm(in.)	PREDICTED MIN CLEARANCE cm(in.)	ACTUAL CLEARANCES cm(in.)
VEHICLE	GROUND EQUIPMENT			
Thrust Structure	Holddown Post	7.54 (2.97)	4.32 (1.7)	7.54 (2.97)
Thrust Structure	Holddown Post Hood	24.13 (9.5)	20.16 (4.0)	22.86 (9.0)
Thrust Structure Insulation	Liftoff Switches	Variable	*	12.7 (5.0)
Engine Bell	Holddown Post	118.11 (46.5)	38.10 (15.0)	109.22 (43.0)
Service Module	SM Swing Arm	Variable	101.6 (40.0)	**
S-IVB Stage	S-IVB Forward Swing Arm	Variable	101.6 (40.0)	**
S-II/S-IVB Interstage	S-IVB Aft Swing Arm	Variable	17.28 (7.0)	**
S-II Stage	S-II Forward Swing Arm	Variable	116.84 (46.0)	**
S-II Stage	S-II Intermediate Swing Arm	Variable	116.84 (46.0)	**
Fin Tip	Swing Arm	862.79 (339.68)	449.58 (177.0)	701.04 (276.0)

* Switch remains on striker plate for 3-sigma conditions.
 ** Camera data indicates clearance - no quantitative data available.

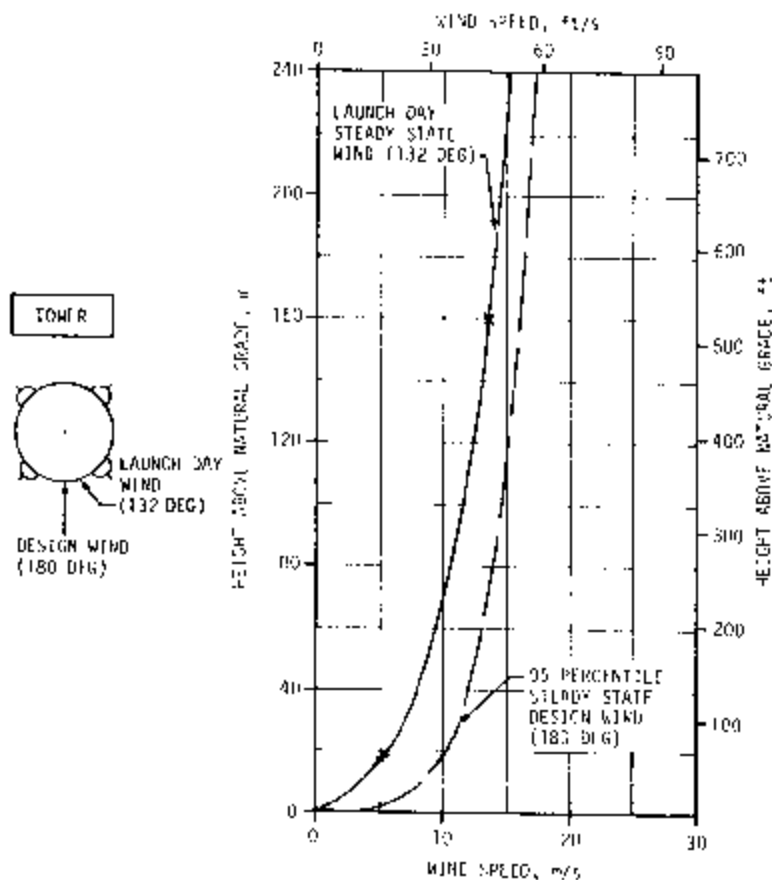
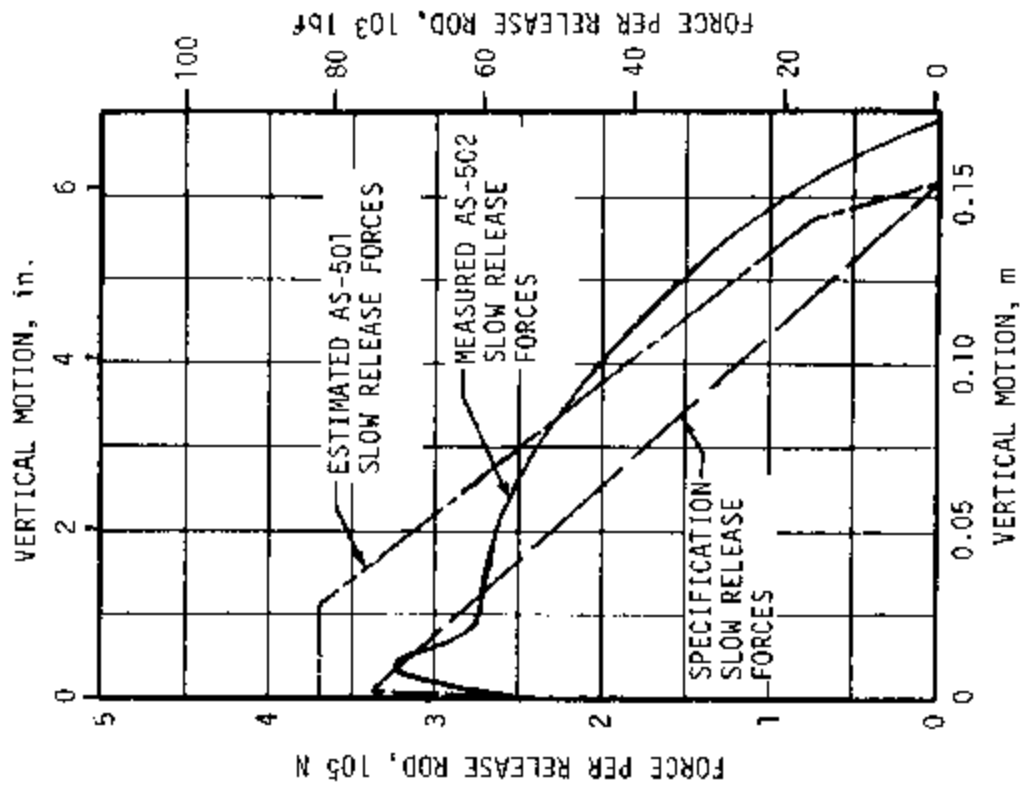


Figure 11-2. Surface Wind Speeds

Table 11-2. AS-502 Misalignment Summary

PARAMETER	PRE-LAUNCH MEASURED			LAUNCH		
	PITCH	YAW	ROLL	PITCH	YAW	ROLL
Thrust Misalignment, deg	+0.20*	+0.20* **	+0.20*	0.0	+0.17	-0.093
Inboard Engine Cant, deg	-0.357	-0.234	-	-0.35	-0.26	-
Servo Amp Offset deg/eng	-0.018	0.0	-	-	-	-
Vehicle Stacking and Pad Misalignment, deg	-0.04	-0.02	-0.18	-0.020	-0.049	-0.278
Peak Soft Release Force per Rod, N (lbf)	348,000 (78,200)l			326,000 (73,300)		
Wind	95 Percentile Envelope			7.5 m/s (24.6 ft/s) at 18.3 m (60 ft)		
Thrust-to-Weight Ratio	1.249			1.249		
* Thrust vector measurement uncertainty.						
** A positive polarity was used to determine minimum fin tip/umbilical tower clearance. A negative polarity was used to determine vehicle/GSE clearances.						



▽ HOLDDOWN ARM RELEASE, 0.36

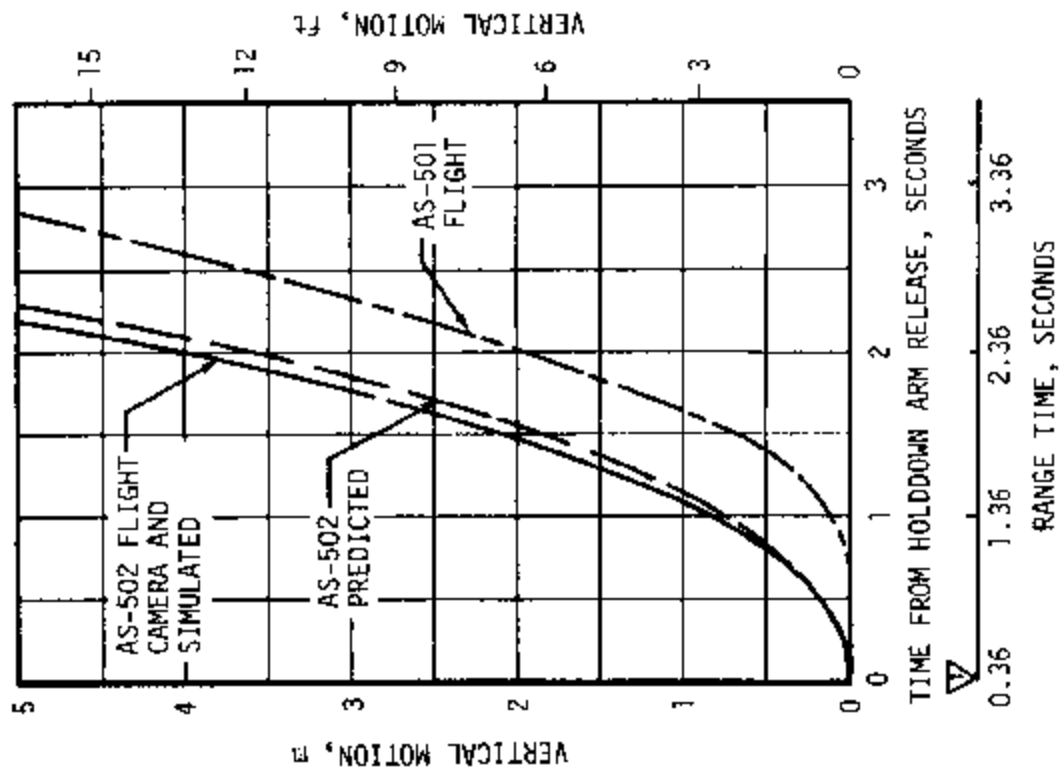


Figure 11-3. Liftoff Vertical Motion and Soft Release Forces

structure (position I) was almost vertical, with a maximum lateral drift of less than 20 centimeters (7.9 in.) after 150 centimeters (59 in.) vertical rise. The simulated data also shown compare favorably with the camera data.

Figure 11-4 also presents the clearance between engine bell 4 and the holddown post at position I and shows that the simulated vertical motion of the bell is almost a duplicate of the actual motion. The motion picture camera monitoring Ground Support Equipment (GSE) operation confirmed that the horizontal motion of engine bell 4 was less than 15 centimeters (5.9 in.) after 600 centimeters (236 in.) vertical rise.

Figure 11-5 shows that the combination of the yaw bias and wind blowing toward the tower resulted in a clearance of 10.0 meters (32.8 ft) between S-IC fin tip A and the top of the tower. Flight data were taken from a tower camera located 426.7 meters (1400 ft) due east of the mobile launcher.

Center engine translation and the exhaust plume angles for each of the five S-IC engines during the first 220 meters (722 ft) of vertical flight are shown in Figure 11-6. Center engine translation was a maximum of 7 meters (23 ft) south and 1 meter (3.3 ft) west. Maximum deviations of the plume were 1.5 degrees north and 0.6 degree east for engines No. 1 through 4 and 1 degree north and 0.7 degree west for engine No. 5. The exhaust plume angle is the angle between the exhaust plume of an engine and the vertical, taken at the engine gimbal point. For both translation and plume angle, positive motion is considered to occur toward the north and the east.

11.3.2 S-IC Flight Dynamics

Table 11-3 lists maximum control parameters during S-IC burn. Dynamics in the region between liftoff and 30 seconds occurred primarily from the yaw bias maneuver, the start of the pitch tilt and roll maneuver, and the end of the roll maneuver. As shown in Figure 11-7, during this time span, maximum pitch attitude error of 1.07 degrees and engine position of 0.52 degree occurred at 13.3 seconds and 12.9 seconds, respectively. The maximum yaw attitude error of -1.28 degrees and engine position of -0.49 degree occurred at 3.5 and 3.2 seconds, as shown in Figure 11-8. These were the largest yaw dynamics encountered during S-IC flight. Figure 11-9 shows the maximum roll dynamics during S-IC flight were -1.37 degrees attitude error at 13.0 seconds and 1.44 deg/s attitude rate at 13.4 seconds. Dynamics in this region occurred as predicted.

In the region between 30 seconds and 140 seconds, maximum dynamics were caused by the pitch tilt program, differences between the wind-bias wind and actual wind magnitude, and wind shears. Figure 11-7 shows that maximum pitch dynamics were 1.14 degrees attitude error at 70.5 seconds, -1.03 deg/s attitude rate at 60.2 seconds, and 0.47 degree engine position at 70.9 seconds. The maximum pitch angle-of-attack of 3.1 degrees occurred at 51.7 seconds, the time of maximum difference between the wind-

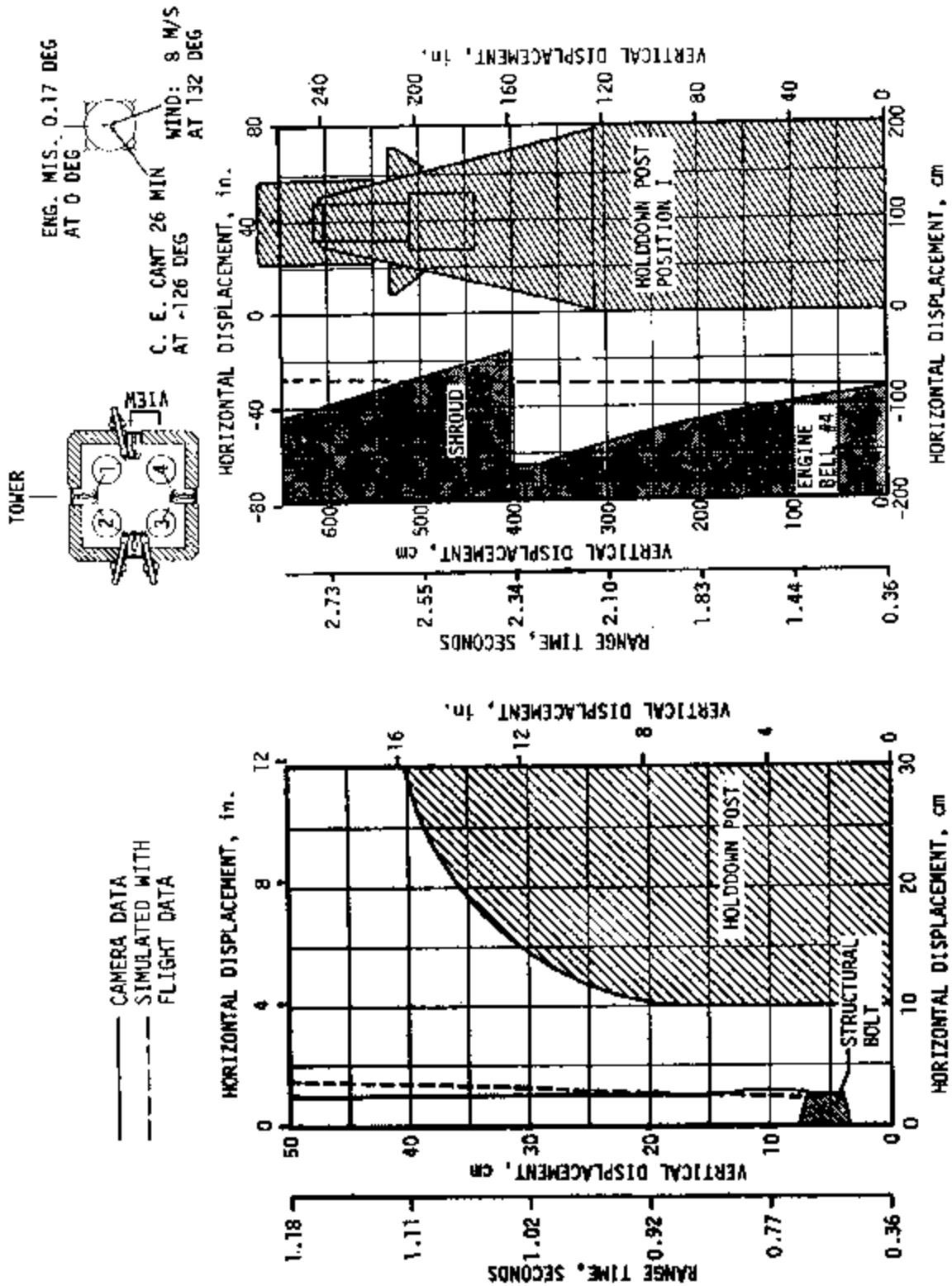


Figure 11-4. Holddown Post Clearances (Position I)

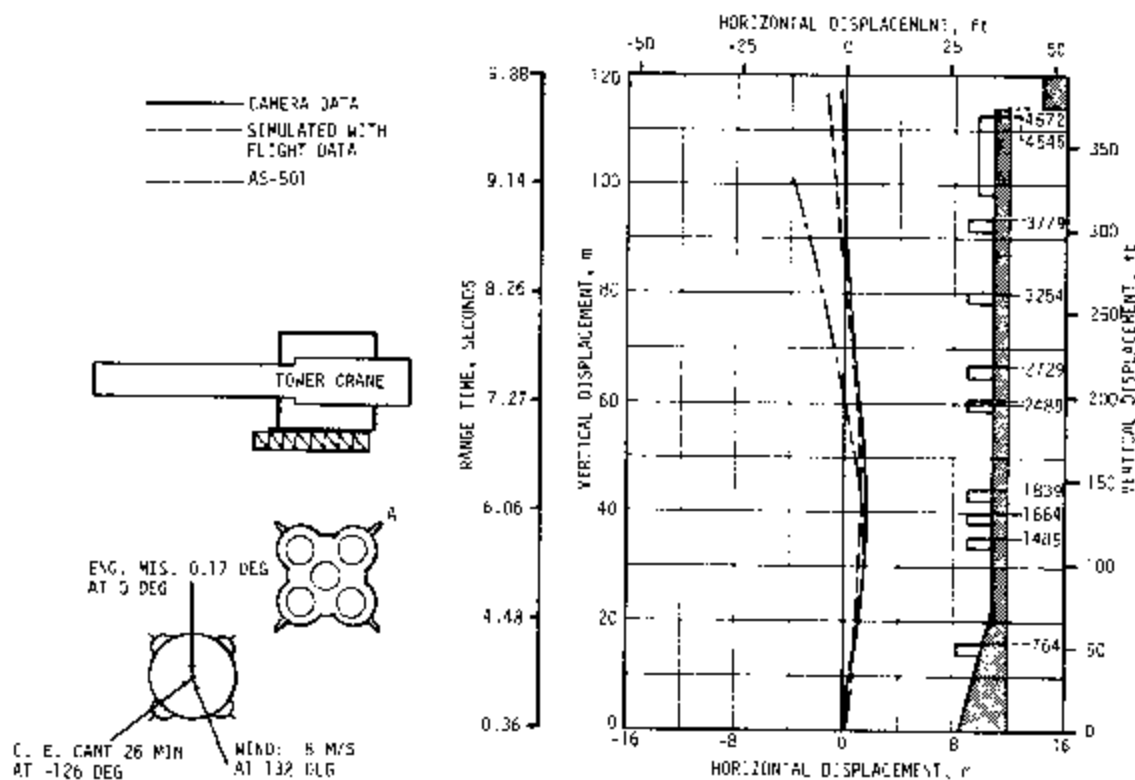


Figure 11-5. Liftoff Trajectories of Fin Tip A

Table 11-3. Maximum Control Parameters During S-IC Burn

PARAMETER	UNITS	PITCH	TIME	YAW	TIME	ROLL	TIME	CONSTRAINT
Attitude Error	deg	1.3	75.5	-1.28	3.5	-1.37	13.0	15.3
Angular Rate	deg/s	-1.03	60.2	0.58	5.2	1.44	13.4	10.0
Engine Deflection (Average)	deg	0.52	12.9	-0.49	3.2	-0.16	3.1	5.16
Angle-of-Attack (in MAX-Q Region)	deg	3.1	51.7	1.6	84.5	-	-	-
Normal Acceleration	m/s ² (ft/s ²)	-0.59 (1.94)	73.6 (241.47)	1.33 (4.36)	81.9 (268.5)	-	-	-
Dynamic Pressure (Q)	N/cm ² (lb _f /in ²)	3.76 (5.45) at 75.2 seconds						
Q= Product	N-deg/cm ² (lb _f -deg/in ²)	10.2 (14.8) at 66.5 seconds						

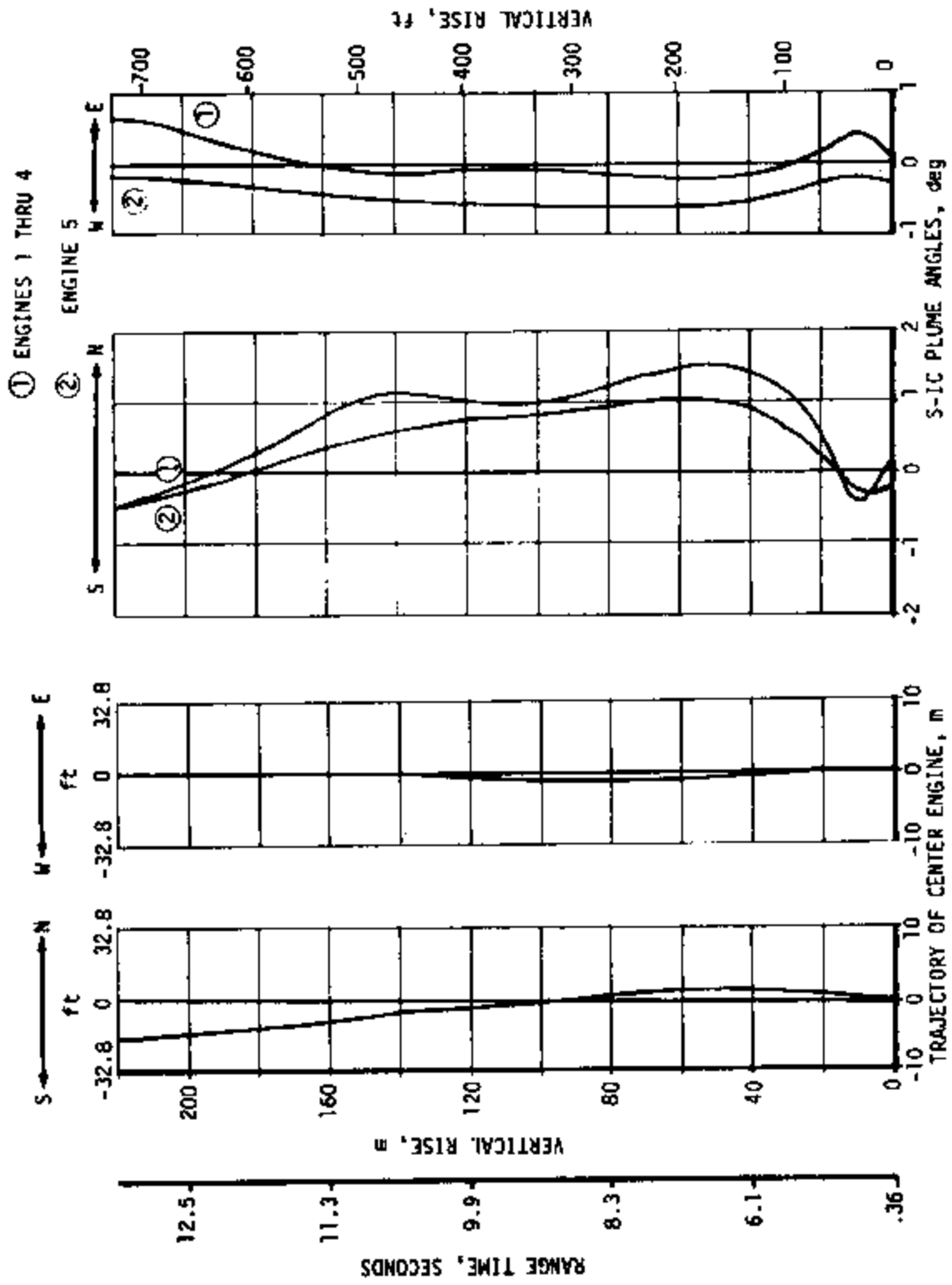


Figure 11-6. S-IC Center Engine Trajectories and Plume Angles

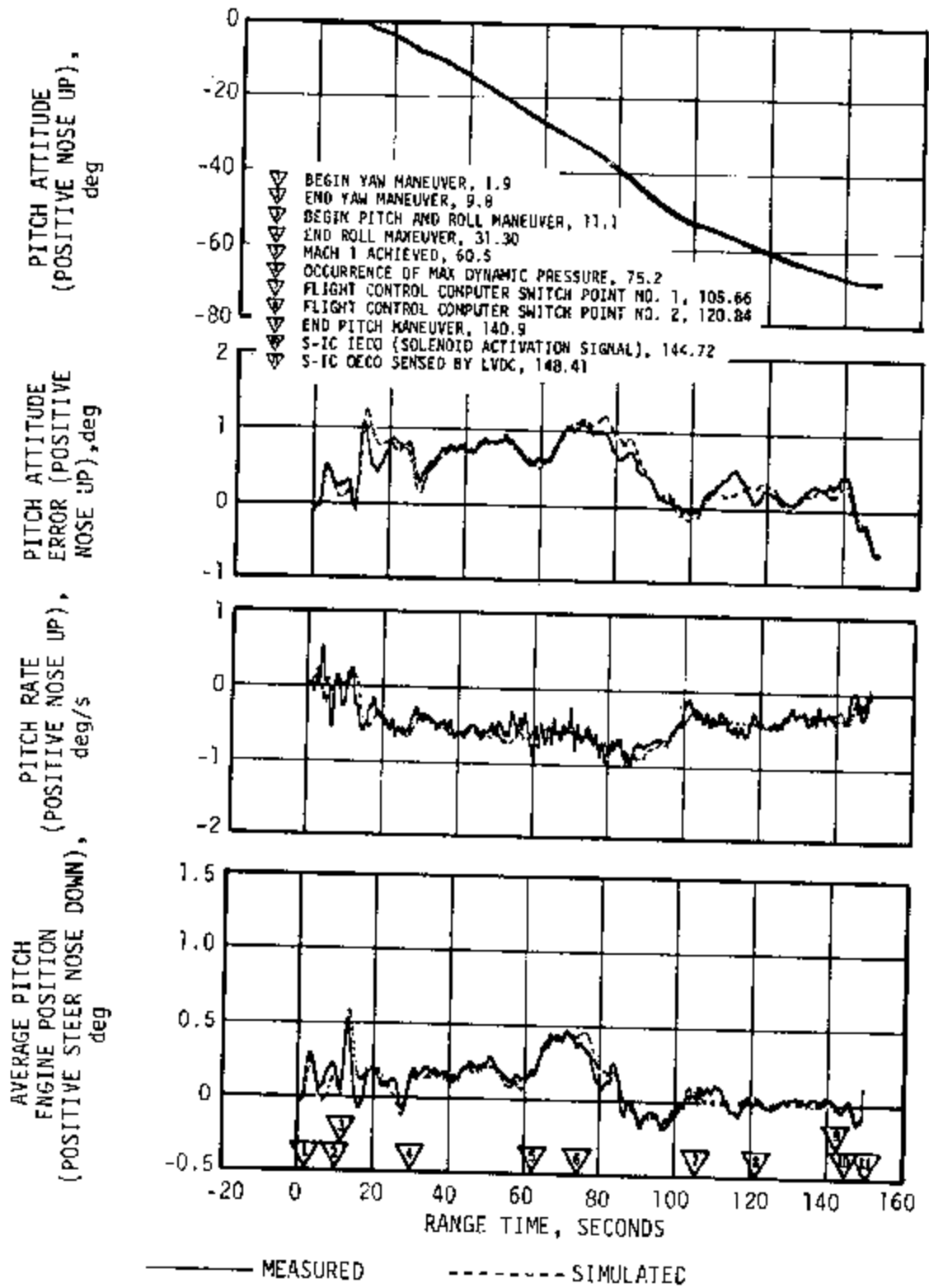


Figure 11-7. Pitch Plane Dynamics During S-IC Burn

- ▽ BEGIN YAW MANEUVER, 1.9
- ▽ END YAW MANEUVER, 9.8
- ▽ BEGIN PITCH AND ROLL MANEUVER, 11.1
- ▽ END ROLL MANEUVER, 31.30
- ▽ MACH 1 ACHIEVED, 60.5
- ▽ OCCURRENCE OF MAX DYNAMIC PRESSURE, 75.2
- ▽ FLIGHT CONTROL COMPUTER SWITCH POINT NO. 1, 105.66
- ▽ FLIGHT CONTROL COMPUTER SWITCH POINT NO. 2, 120.84
- ▽ END PITCH MANEUVER, 140.9
- ▽ S-IC IECCO (SOLENOID ACTIVATION SIGNAL), 144.72
- ▽ S-IC OECCO SENSED BY LVDC, 148.41

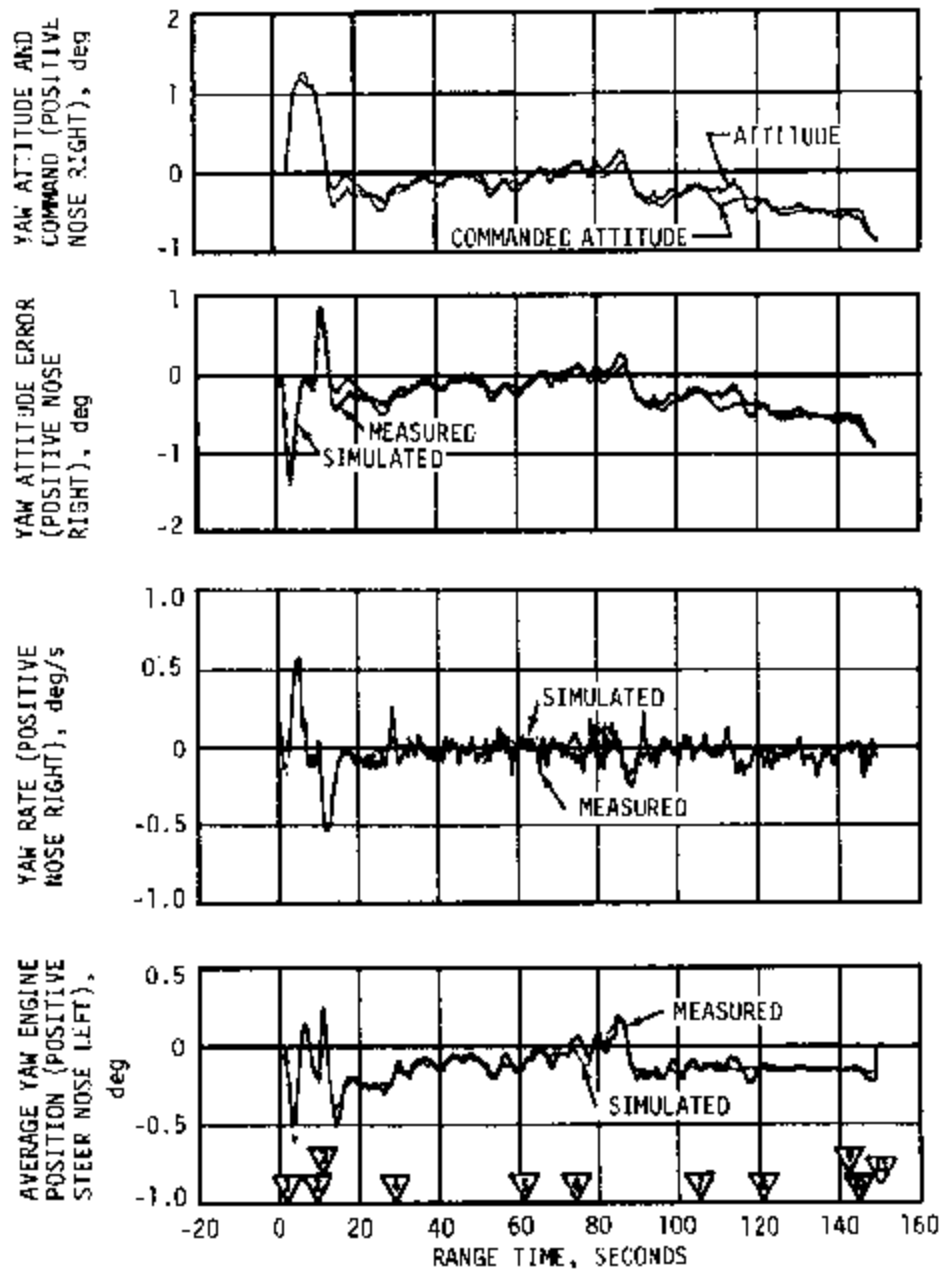


Figure 11-8. Yaw Plane Dynamics During S-IC Burn

- ▽ BEGIN YAW MANEUVER, 1.9
- ▽ END YAW MANEUVER, 9.8
- ▽ BEGIN PITCH AND ROLL MANEUVER, 11.1
- ▽ END ROLL MANEUVER, 31.30
- ▽ MACH 1 ACHIEVED, 60.5
- ▽ OCCURRENCE OF MAX DYNAMIC PRESSURE, 75.2
- ▽ FLIGHT CONTROL COMPUTER SWITCH POINT NO. 1, 105.66
- ▽ FLIGHT CONTROL COMPUTER SWITCH POINT NO. 2, 120.84
- ▽ END PITCH MANEUVER, 140.9
- ▽ S-IC IECC (SOLENOID ACTIVATION SIGNAL), 144.72
- ▽ S-IC OECC SENSED BY LVDC, 148.41

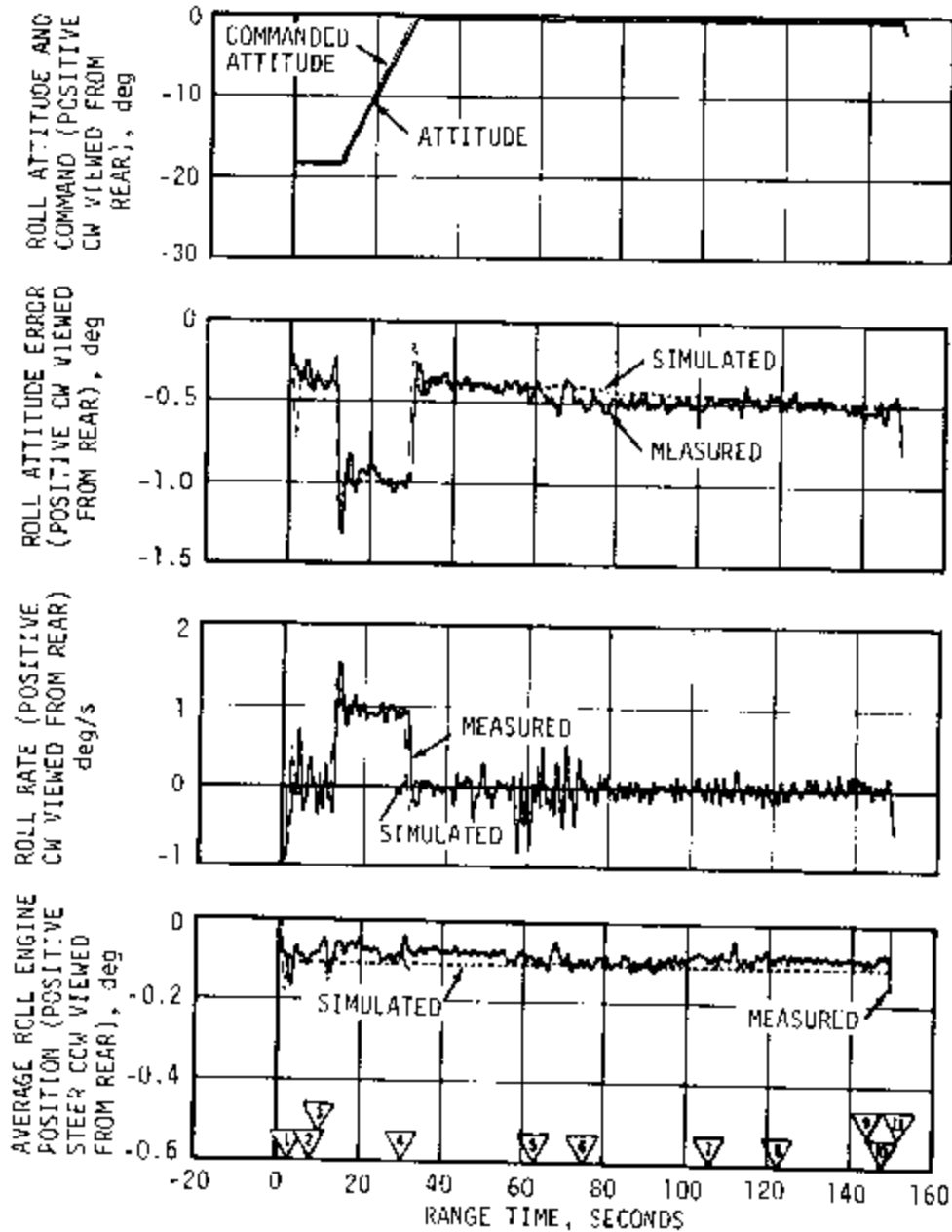


Figure 11-9. Roll Plane Dynamics During S-IC Burn

bias wind and actual wind. Yaw dynamics during this region were caused by the wind. The maximum yaw plane component of angle-of-attack shown in Figure 11-10 was 1.6 degrees at 84.5 seconds, the time of maximum yaw wind. Figure 11-11 shows winds encountered during flight as given by JIMSPHERE and Q-Ball reduced data. Q-Ball reduced winds were determined using Q-Ball angles-of-attack in pitch and yaw, Observed Mass Point Trajectory (OMPT) data, and vehicle characteristics data. Maximum pitch winds in the high dynamic pressure region were 26.8 m/s (87.9 ft/s) at 77.8 seconds from JIMSPHERE data as compared to 20.2 m/s (66.3 ft/s) at 77.8 seconds from Q-Ball reduced data. Yaw winds were 12.9 m/s (42.3 ft/s) at 84.3 seconds from JIMSPHERE data as compared to 13.5 m/s (44.3 ft/s) at 84.5 seconds from Q-Ball reduced data. It is necessary to introduce a time varying roll moment into the simulation to match the flight data. The roll moment would have to reach a value of 228,000 N-m (168,200 lbf-ft) at S-IC Outboard Engine Cutoff (OECO).

Significant longitudinal oscillations occurred during the latter part of S-IC flight. These oscillations were coupled into the pitch, yaw, and roll planes. The largest coupling occurred in the pitch plane, as evidenced by the pitch accelerometer and pitch rate gyro outputs. Frequency spectrum analyses of pitch rate, command to the actuator, and actuator position indicate that the 5.3 hertz oscillation was present in the rate gyro signal but was absent from the command to the actuator. Control system attenuation of 32.4 decibels at this frequency effectively reduced the signal sent to the actuator magnetic amplifiers. The small response of the engine position at the 5.3 hertz frequency was due to direct vibration of the actuator by the engines. Maximum vibration of the actuator was 0.0085 degree peak-to-peak.

A transient occurred in dynamics at approximately 133 seconds as discussed in Section 9A. Oscillogram traces shown in Figures 11-12 and 11-13 show the effect on the control system. The transient was observed in pitch and yaw IU accelerations and rates but not in the pitch and yaw engine positions. The transient was not obvious in pitch acceleration and rate measured in the S-IC stage.

The transient due to Inboard Engine Cutoff (IECO) was used to determine the inboard engine cant of -0.35 degree in pitch and -0.26 degree in yaw. Other misalignments were thrust vector angles required to match flight data. The equivalent thrust vector misalignments were 0.0 degree in pitch, 0.17 degree in yaw, and 0.093 degree in roll. Table 11-2 summarizes AS-502 misalignments.

Dynamics from 140 seconds to separation were caused by tilt arrest and IECO. Table 11-4 lists S-IC dynamic end conditions.

Observed and predicted slosh frequencies are shown in Figure 11-14. Predicted slosh frequencies are system modes associated with slosh in the closed loop control system. Because the tanks are coupled through the vehicle and control system, it is difficult to associate them with a

- ▽ BEGIN YAW MANEUVER, 1.9
- ▽ END YAW MANEUVER, 9.8
- ▽ BEGIN PITCH AND ROLL MANEUVER, 11.1
- ▽ END ROLL MANEUVER, 31.30
- ▽ MACH 1 ACHIEVED, 60.5
- ▽ OCCURRENCE OF MAX DYNAMIC PRESSURE, 75.2
- ▽ FLIGHT CONTROL COMPUTER SWITCH POINT NO. 1, 105.66
- ▽ FLIGHT CONTROL COMPUTER SWITCH POINT NO. 2, 120.84
- ▽ END PITCH MANEUVER, 140.9
- ▽ S-IC IECC (SOLENOID ACTIVATION SIGNAL), 144.72
- ▽ S-IC OECC SENSED BY LVDC, 148.41

----- MEASURED (JIMSPHERE) ——— MEASURED (Q-BALL)

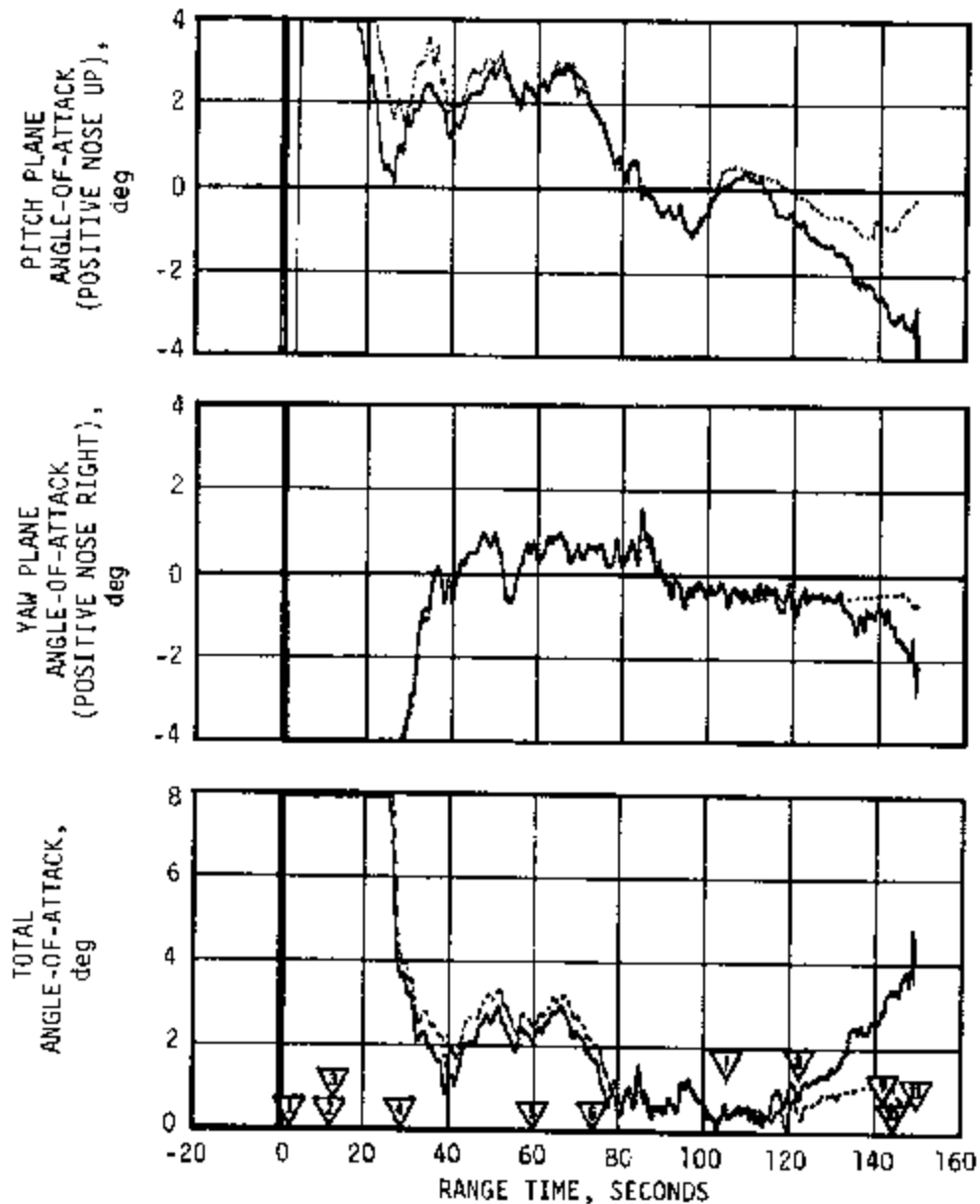


Figure 11-10. Free Stream Angle-of-Attack During S-IC Burn

- ▽ BEGIN YAW MANEUVER, 1.9
- ▽ END YAW MANEUVER, 9.8
- ▽ BEGIN PITCH AND ROLL MANEUVER, 11.1
- ▽ END ROLL MANEUVER, 31.30
- ▽ MACH 1 ACHIEVED, 60.5
- ▽ OCCURRENCE OF MAX DYNAMIC PRESSURE, 75.2
- ▽ FLIGHT CONTROL COMPUTER SWITCH POINT NO. 1, 105.66
- ▽ FLIGHT CONTROL COMPUTER SWITCH POINT NO. 2, 120.84
- ▽ END PITCH MANEUVER, 140.9
- ▽ S-IC IECD (SOLENOID ACTIVATION SIGNAL), 144.72
- ▽ S-IC DECO SENSED BY LVDC, 148.41

————— MEASURED (JIMSPHERE)
 - - - - - CALCULATED FROM ONBOARD DATA - Q-BALL

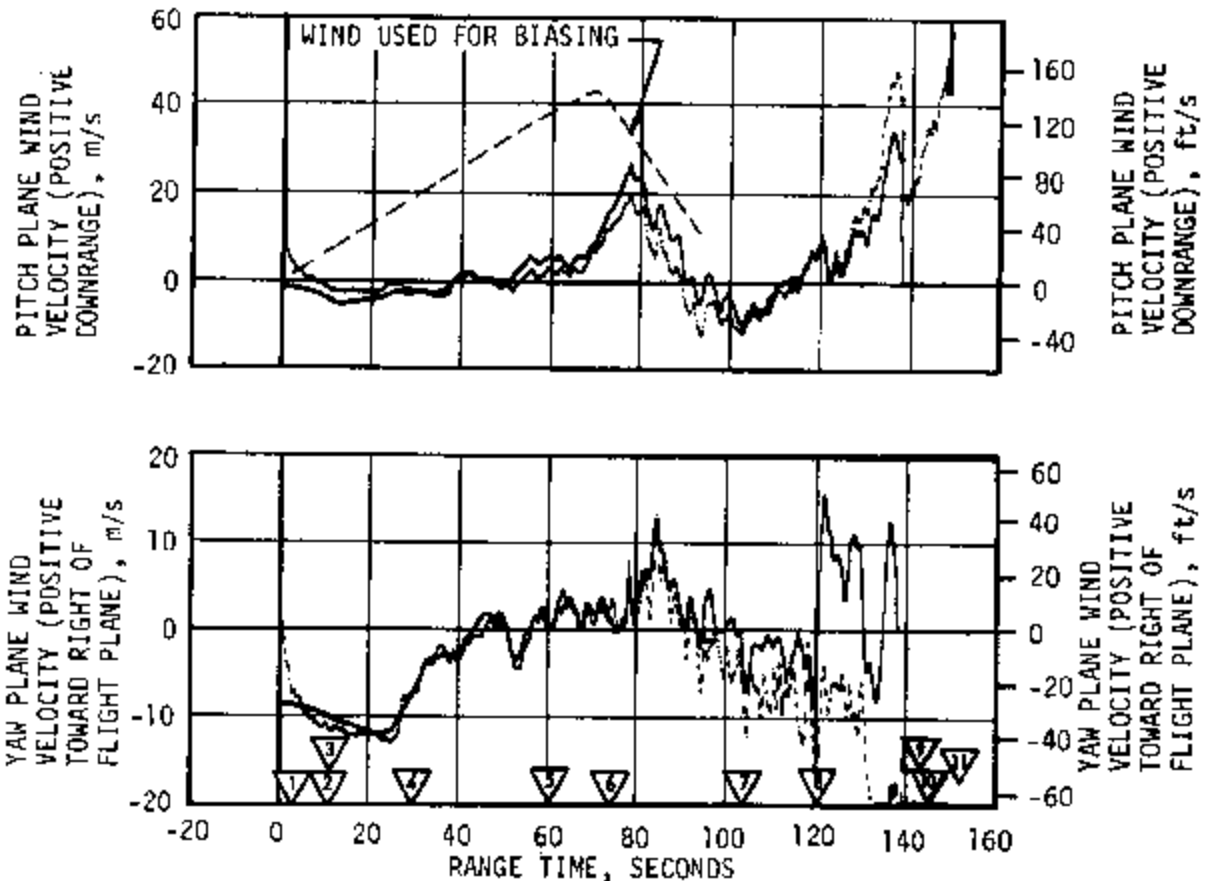


Figure 11-11. Pitch and Yaw Plane Wind Velocity During S-IC Burn

NOTE: FULL SCALE CORRESPONDS APPROXIMATELY TO
MAXIMUM SENSOR READING (+0.5g; +10 deg/s)

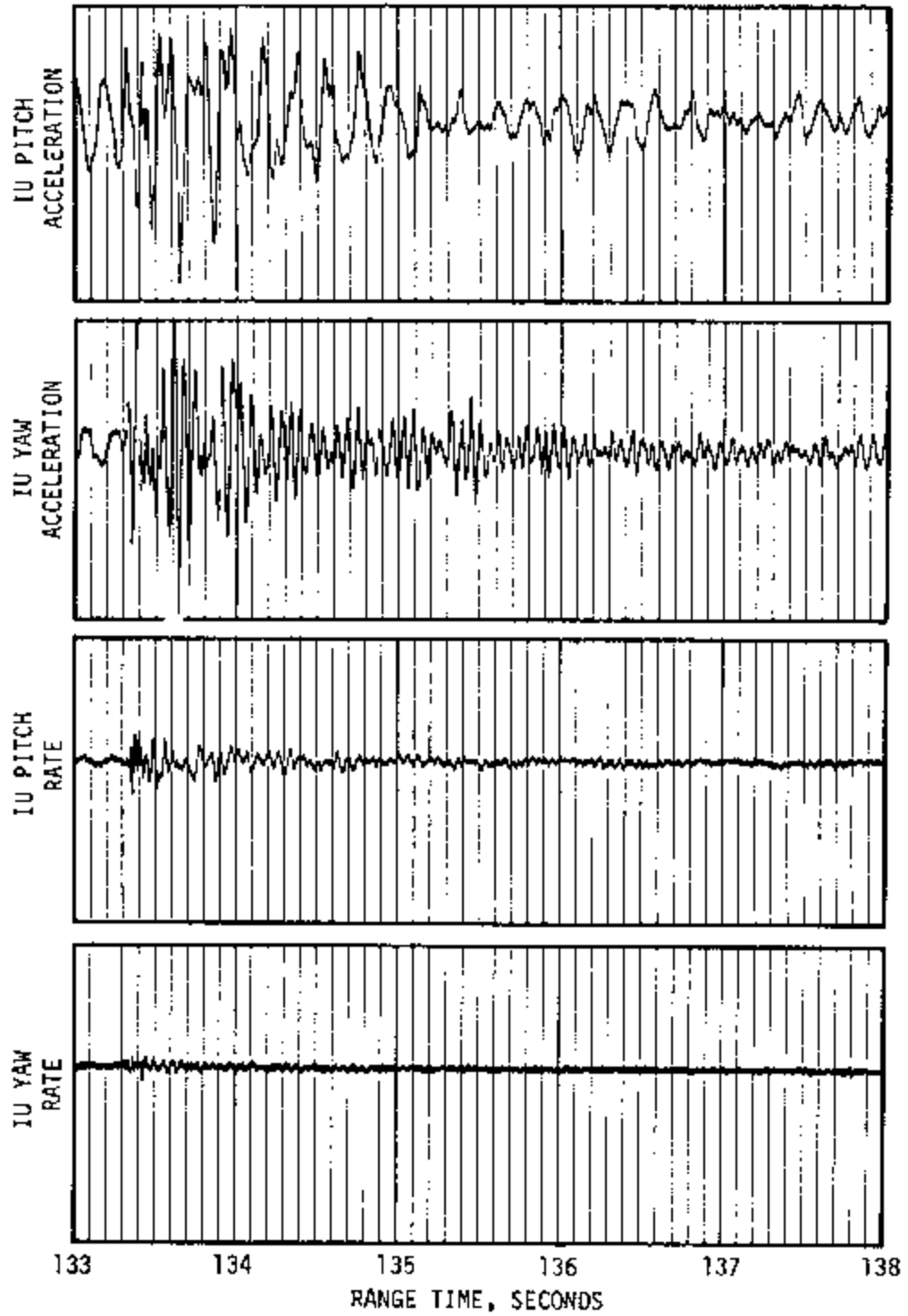


Figure 11-12. Oscillograms of IU Control Sensors
During S-IC Transient

NOTE: FULL SCALE CORRESPONDS APPROXIMATELY TO MAXIMUM SENSOR
READING (± 5 deg; ± 0.5 g; ± 10 deg/s)

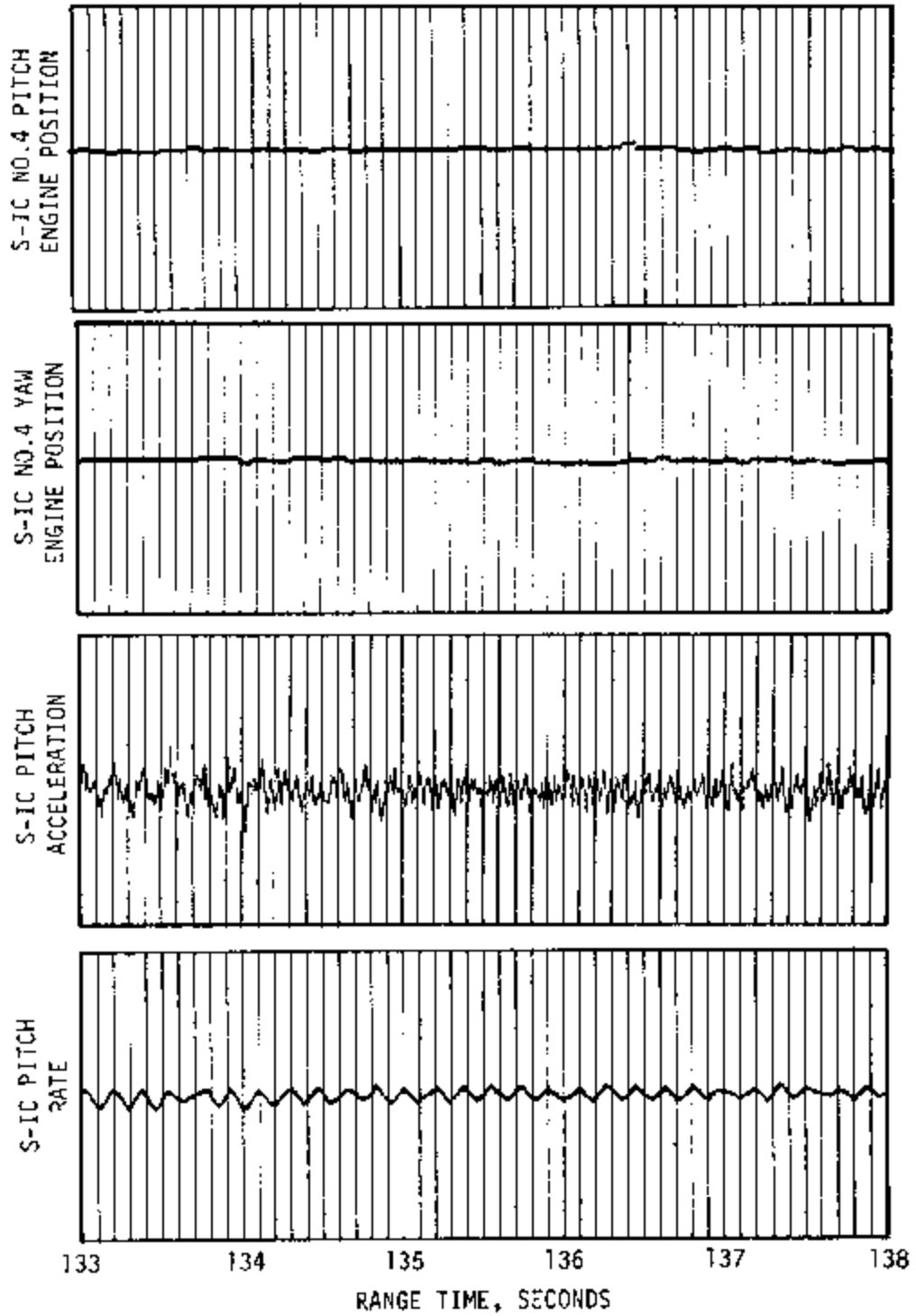


Figure 11-13. Oscillograms of Engine Position and S-IC Sensors During S-IC Transient

Table 11-4. S-IC Dynamic End Conditions*

PARAMETER	UNITS	PITCH	YAW	ROLL
Attitude Error	deg	-0.42	-0.84	-0.75
Attitude Rate	deg/s	0.06	-0.005	-0.70
Average Actuator Position	deg	-0.04	-0.16	-0.10

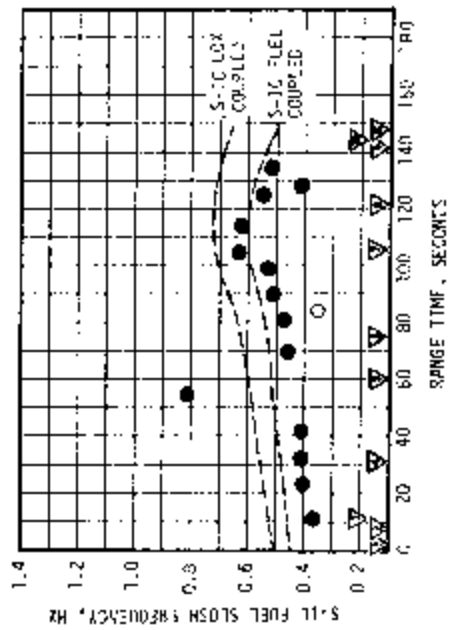
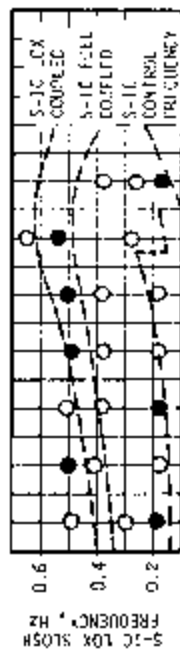
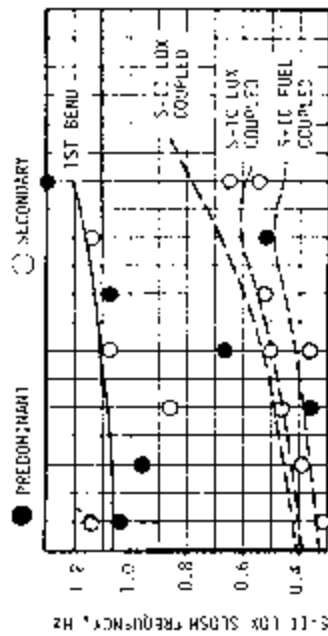
* Conditions at separation command, 149.08 seconds.

particular tank. An attempt was made to do this, and so they are labeled "coupled". They are different from the individual tank frequencies which should not be present during flight. Presence of other modes was detected in the tanks, as was expected. These were bending and control system modes. Predicted curves for these are also shown where required.

Propellant slosh amplitudes in the S-IC tanks are shown in Figure 11-15. Measured peak-to-peak amplitudes were derived from opposing pairs of liquid level probes in the pitch and yaw planes. Simulated data shown as a comparison were derived using first mode slosh models in the pitch and yaw planes. The figure shows the oscillating slosh wave peak-to-peak magnitudes in addition to low frequency effects due to non-zero lateral accelerations during flight. Maximum peak-to-peak slosh amplitudes in the fuel tank were -0.3 meter (-0.98 ft) in pitch at 65 seconds and 0.25 meter (0.82 ft) in yaw at 2.5 seconds. S-IC LOX peak-to-peak amplitudes reached -0.3 meter (-0.98 ft) in pitch at 72 seconds and 0.15 meter (0.49 ft) in yaw at 19, 28, and 85 seconds. Simulated data for the S-IC tanks showed close agreement in phasing but measured slosh amplitudes were larger, which may indicate less slosh damping than predicted. Figure 11-16 shows propellant slosh in the S-II and S-IVB tanks. Amplitudes shown for the S-II slosh give only the oscillating slosh wave peak-to-peak amplitudes. Static, or low frequency oscillations, have been removed from the data. Only S-IVB LH₂ slosh data are available. There was poor agreement between measured and simulated slosh amplitudes in the S-II LOX and S-IVB LH₂ tanks. Because the S-II LOX probe was located very near the center of the tank, it was difficult to correlate measured and simulated data using only first mode simulation data. Maximum peak-to-peak amplitudes in the plane of the Propellant Utilization (PU) probes were 2.7 degrees at 90 seconds for the S-II LOX tank and 1.4 degrees at 95 seconds for the S-II LH₂ tank. Maximum S-IVB LH₂ slosh was 0.084 meter (3.30 in.) peak-to-peak at 85 seconds. There was no evidence of unstable buildup.

Peak-to-peak engine response to propellant slosh is shown in Figure 11-17. The response was derived by passing measured and simulated engine deflection time histories through bandpass filters, retrieving only slosh

- ▽ BEGIN YAW MANEUVER, 1.9
- ▽ END YAW MANEUVER, 9.8
- ▽ BEGIN PITCH AND ROLL MANEUVER, 11.1
- ▽ END ROLL MANEUVER, 31.30
- ▽ MACH 1 ACHIEVED, 60.5



- ▽ OCCURRENCE OF MAX DYNAMIC PRESSURE, 75.2
- ▽ FLIGHT CONTROL COMPUTER SWITCH POINT NO. 1, 105.66
- ▽ FLIGHT CONTROL COMPUTER SWITCH POINT NO. 2, 120.84
- ▽ END PITCH MANEUVER, 140.9
- ▽ S-11 1EGD (SOLENOID ACTIVATION SIGNAL), 144.72
- ▽ S-11 0EGD SENSED BY LVGX, 148.41

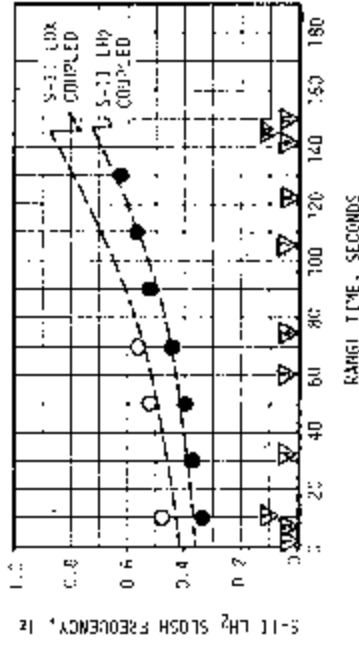
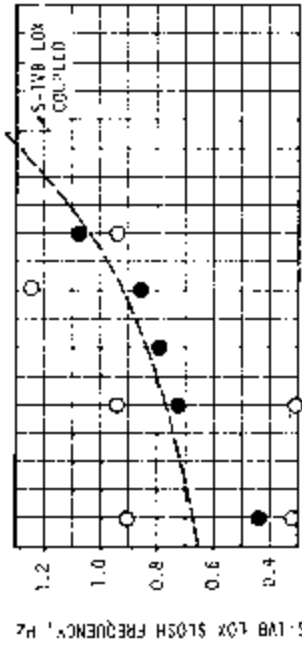
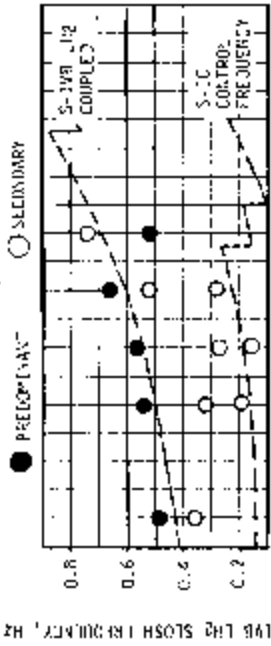
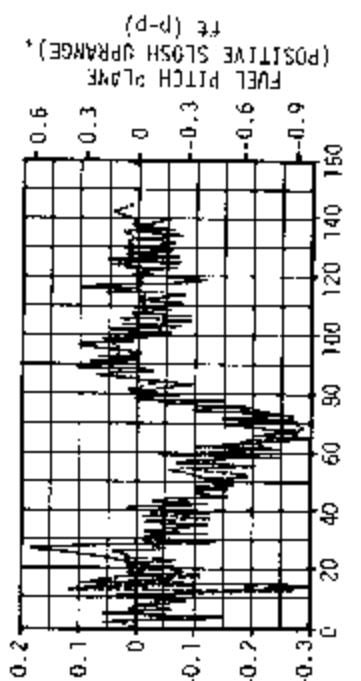
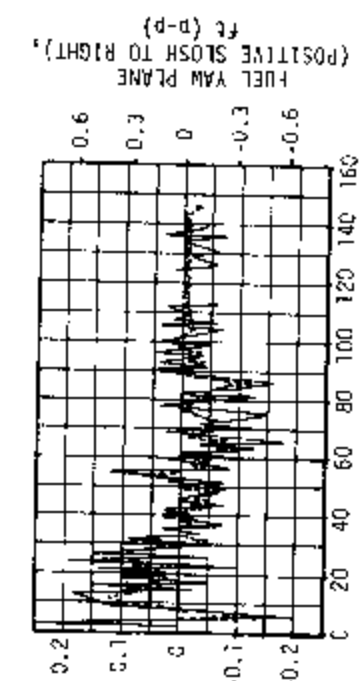
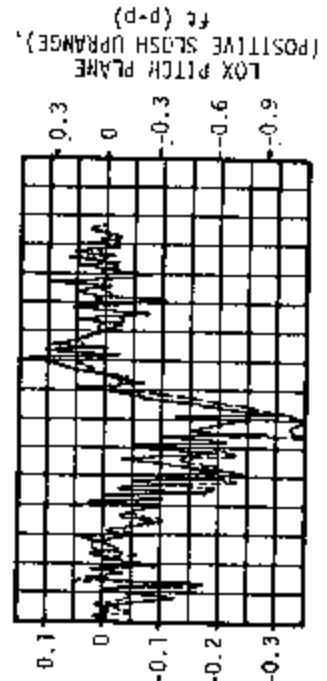
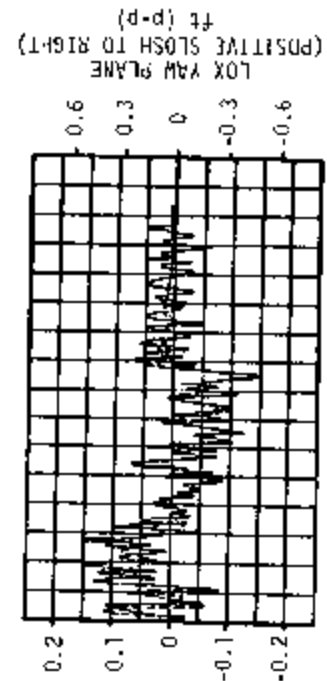


Figure 11-14. Predominant SLOSH Frequencies During S-11 Burn



RANGE TIME, SECONDS

RANGE TIME, SECONDS

Figure 11-15. S-IC Propellant Sesh Amplitudes at the Wall During S-IC Burn

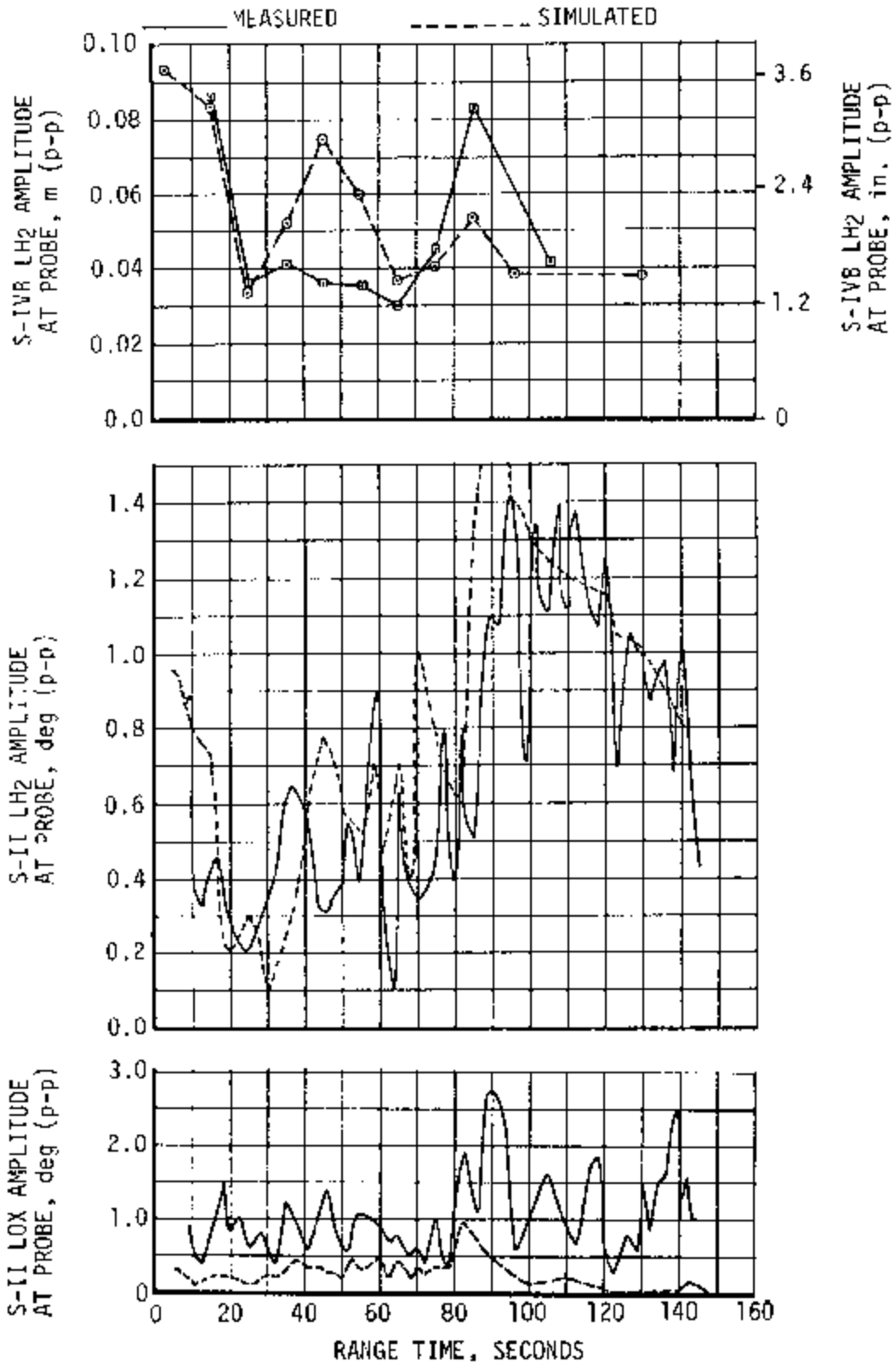
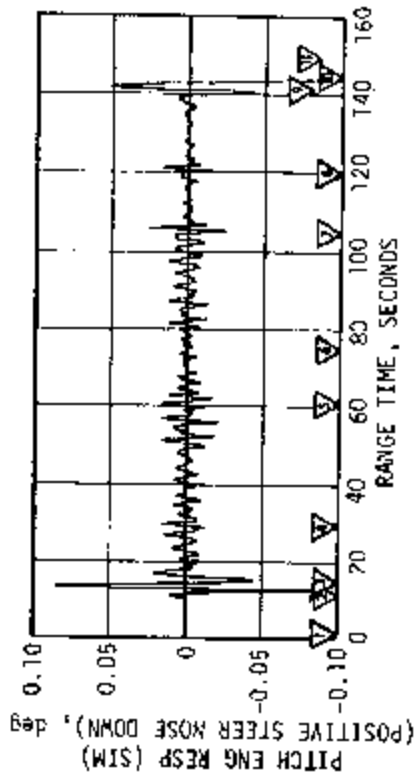
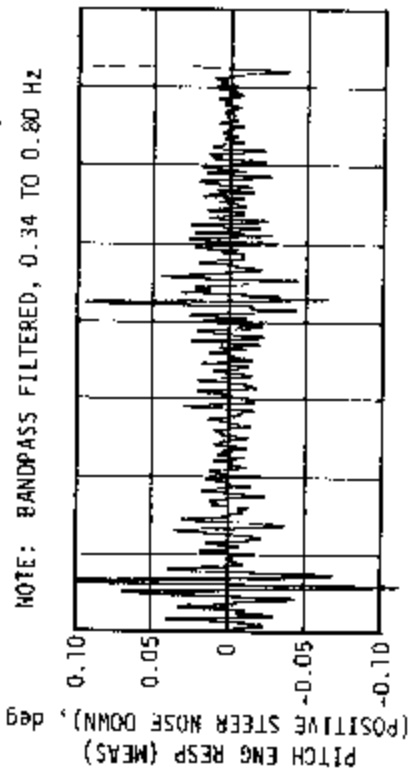


Figure 11-16. S-II and S-IVB Propellant Slosh Amplitudes During S-IC Burn

▽ BEGIN YAW MANEUVER, 1.9
 ▽ END YAW MANEUVER, 9.8
 ▽ BEGIN PITCH AND ROLL MANEUVER, 11.1
 ▽ END ROLL MANEUVER, 31.30
 ▽ MACH 1 ACHIEVED, 60.5
 ▽ OCCURRENCE OF MAX DYNAMIC PRESSURE, 75.2



▽ FLIGHT CONTROL COMPUTER SWITCH POINT NO. 1, 105.66
 ▽ FLIGHT CONTROL COMPUTER SWITCH POINT NO. 2, 120.84
 ▽ END PITCH MANEUVER, 140.9
 ▽ S-IC IECC (SOLENOID ACTIVATION SIGNAL), 144.72
 ▽ S-IC DECO SENSED BY LVDC, 148.41

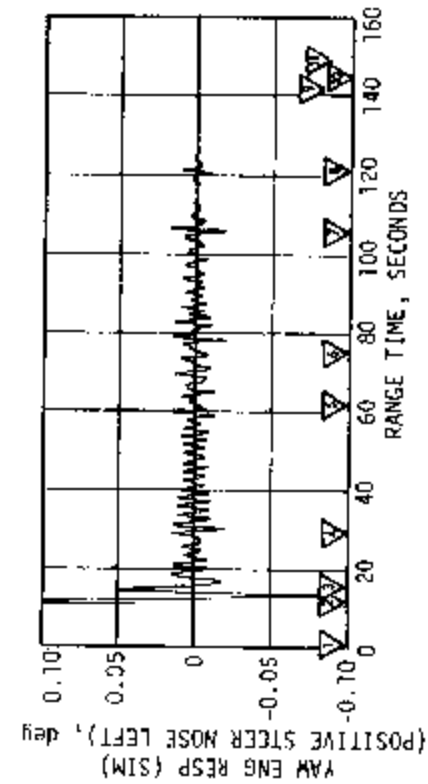
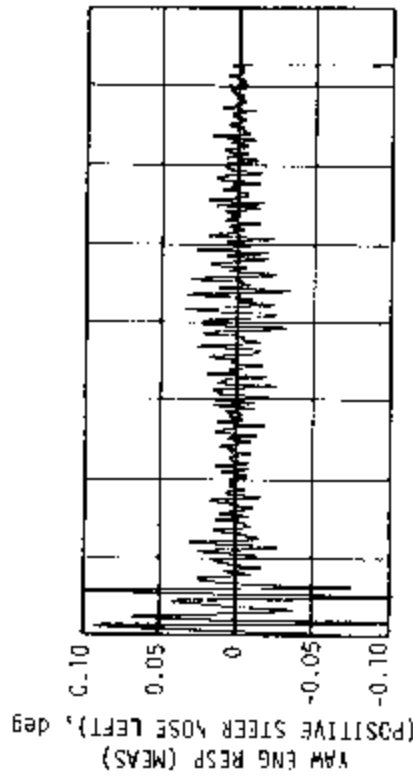


Figure 11-17. S-IC Engine Deflection Response to Propellant Slosh

frequency components. Since frequencies of significant slosh modes lay within a relatively narrow band, the engine responses shown were due to all tanks collectively. Maximum pitch engine response to slosh was -0.12 degree at 13 seconds. Maximum yaw engine response to slosh was 0.1 degree at 11 seconds. The disagreement between measured and simulated engine response to slosh shown on Figure 11-17 tends to support the indication of smaller slosh damping than predicted. The small actuator activity at slosh frequencies other than at the time of known disturbances confirmed that slosh was adequately stabilized.

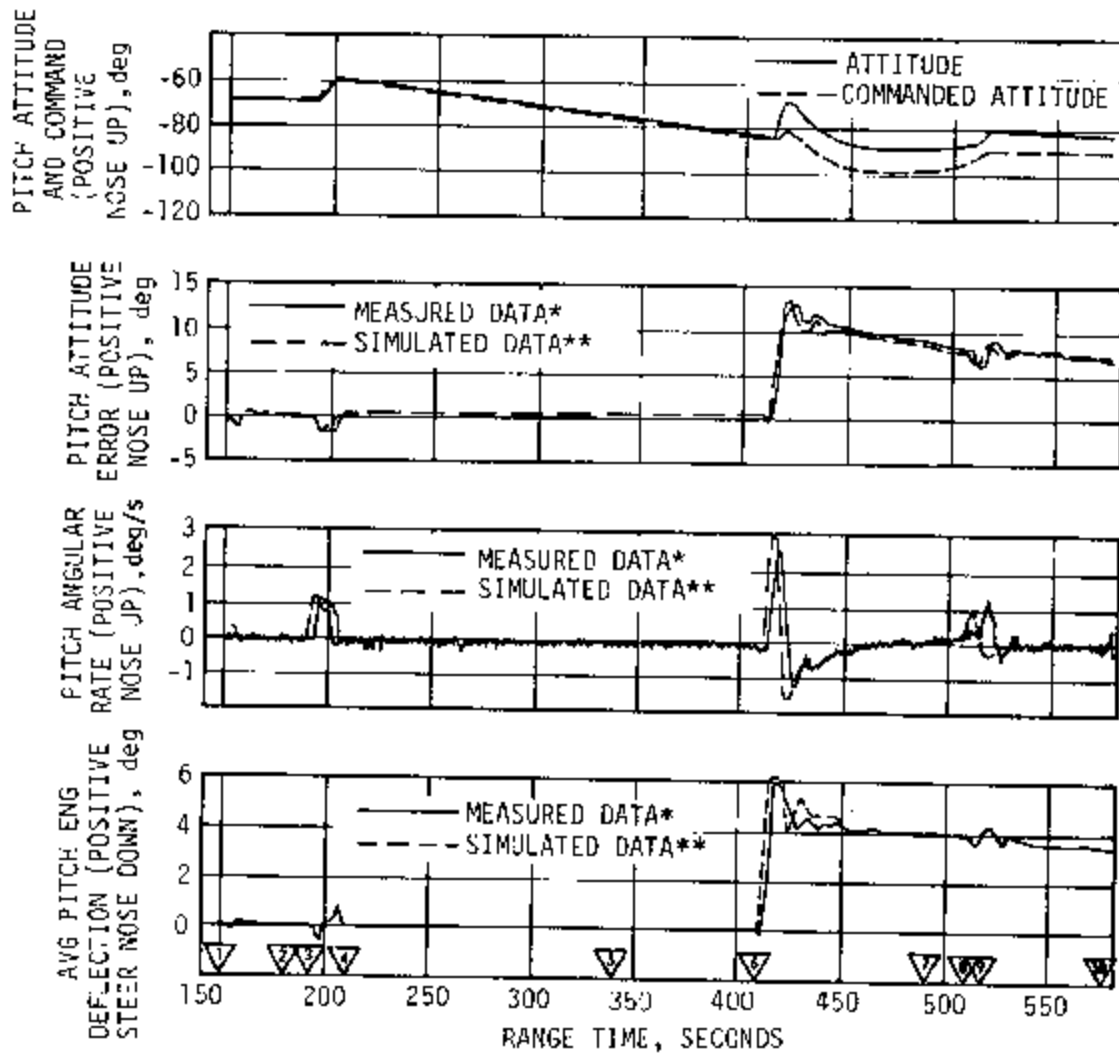
Peak-to-peak engine response to first bending mode was determined by passing measured and simulated engine deflection time histories through bandpass filters, retrieving only bending frequency components. Maximum response to first bending was 0.025 degree at 85 seconds in pitch and 0.02 degree at 90 seconds in yaw. Results indicate that bending dynamics were adequately stabilized throughout flight.

11.4 S-II CONTROL SYSTEM EVALUATION

The S-II stage attitude control system performance was satisfactory. Analysis of the magnitude of modal components in engine deflections revealed that vehicle structural bending and propellant sloshing had negligible effect on control system performance prior to cutoff of engines No. 2 and 3. The maximum values of control parameters occurred in response to shutdown of engines No. 2 and 3. The shutdown of engines No. 2 and 3 caused attitude errors of 13.4 degrees in pitch, 2.7 degrees in yaw, and 4.2 degrees in roll. Attitude rates for pitch, yaw, and roll were 2.8 deg/s, -0.8 deg/s, and -2.2 deg/s, respectively. The response at other times (such as S-IC/S-II separation and initiation of IGM guidance) were within expectations.

11.4.1 Attitude Control Dynamics and Stability

Attitude control commands were computed in the minor loop section of the LVDC. For 42 seconds following S-IC OECO these commands were held constant. Significant events occurring during that interval were S-IC/S-II separation, S-II stage J-2 engine start, second plane separation, and Launch Escape Tower (LET) jettison. The attitude control dynamics throughout this interval indicated stable operation (see Figures 11-18 through 11-20). Simulated data shown for comparison in these figures generally leads actual data by about 2.6 seconds because of a 2-second bias in telemetry data used as input commands to the simulation and a 0.6-second bias in the actual data. The maximum control excursions occurred in the roll axis following S-IC/S-II separation when 2.0 deg/s attitude rate and -2.3 degrees attitude error occurred, as shown in Table 11-5. Steady state attitudes were achieved within 10 seconds from S-IC/S-II separation. The principal attitude error of approximately 0.5 degree for the roll axis was maintained until cutoff of engines No. 2 and 3. Absence of roll rate during this time indicates a combination of center of gravity offsets and thrust or engine misalignments producing a constant roll torque. Similar roll offsets existed during AS-501 S-II stage flight.



* NOT CORRECTED FOR A 0.6 SECOND TIME BIAS IN THE TELEMETRY DATA
 ** NOT CORRECTED FOR A 2.0 SECOND TIME BIAS IN THE SIMULATION INPUT

- ▽ S-IC/S-II SEPARATION COMMAND, 149.08
- ▽ S-II SECOND PLANE SEPARATION COMMAND, 179.06
- ▽ INITIATE IGM PHASE I, 190.95
- ▽ FLIGHT CONTROL COMPUTER SWITCH POINT NO. 3, 209.76
- ▽ FLIGHT CONTROL COMPUTER SWITCH POINT NO. 4, 339.76
- ▽ S-II ENG NO. 2 OUT, 412.92;
- S-II ENG NO. 3 OUT, 414.18;
- FIRST ARTIFICIAL TAU INITIATE, 415.4
- ▽ FIRST ARTIFICIAL TAU TERMINATE,
- SECOND ARTIFICIAL TAU INITIATE, 490.8
- SECOND ARTIFICIAL TAU TERMINATE, 510.2
- ▽ INITIATE CHI FREEZE, 517.7
- ▽ S-II ECO SENSED BY LVDC, 576.33

Figure 11-18. Pitch Plane Dynamics During S-II Burn

- ▽ S-1C/S-II SEPARATION COMMAND, 149.08
- ▽ S-II SECOND PLANE SEPARATION COMMAND, 179.06
- ▽ INITIATE IGM PHASE I, 190.95
- ▽ FLIGHT CONTROL COMPUTER SWITCH POINT NO. 3, 209.76
- ▽ FLIGHT CONTROL COMPUTER SWITCH POINT NO. 4, 339.76
- ▽ S-II ENG NO. 2 OUT, 412.92;
- S-II ENG NO. 3 OUT, 414.18;
- FIRST ARTIFICIAL TAU INITIATE, 415.4
- ▽ FIRST ARTIFICIAL TAU TERMINATE,
- SECOND ARTIFICIAL TAU INITIATE, 490.8
- ▽ SECOND ARTIFICIAL TAU TERMINATE, 510.2
- ▽ INITIATE CHI FREEZE, 517.7
- ▽ S-II ECO SENSED BY LVOC, 576.33

* NOT CORRECTED FOR A 0.6 SECOND TIME BIAS IN TELEMETRY DATA
 ** NOT CORRECTED FOR A 2.0 SECOND TIME BIAS IN SIMULATION INPUT

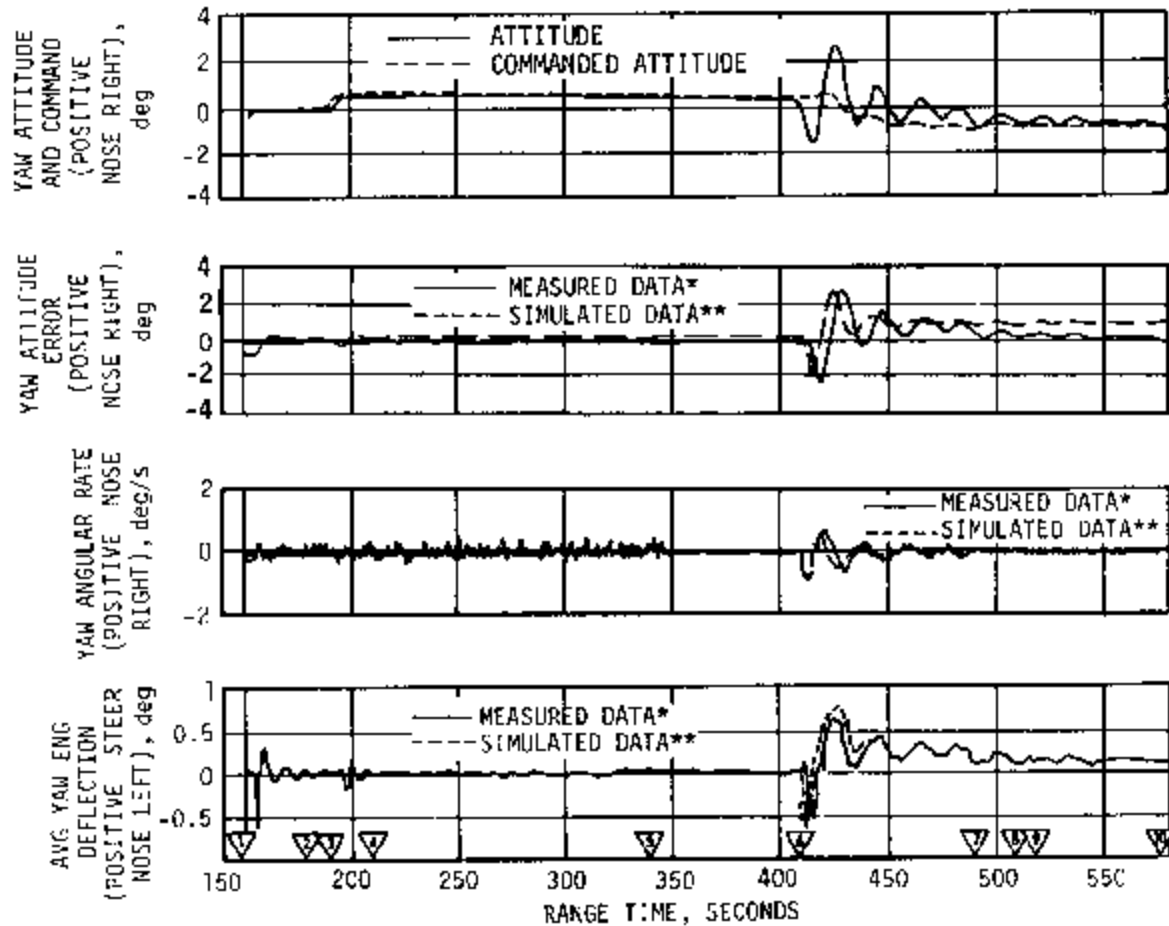


Figure 11-19. Yaw Plane Dynamics During S-II Burn

- ▽ S-IC/S-II SEPARATION COMMAND, 149.08
- ▽ S-II SECOND PLANE SEPARATION COMMAND, 179.06
- ▽ INITIATE JSM PHASE I, 190.95
- ▽ FLIGHT CONTROL COMPUTER SWITCH POINT NO. 3, 209.76
- ▽ FLIGHT CONTROL COMPUTER SWITCH POINT NO. 4, 339.76
- ▽ S-II ENG NO. 2 OUT, 412.92;
- ▽ S-II ENG NO. 3 OUT, 414.18;
- ▽ FIRST ARTIFICIAL TAU INITIATE, 415.4
- ▽ FIRST ARTIFICIAL TAU TERMINATE,
- ▽ SECOND ARTIFICIAL TAU INITIATE, 490.8
- ▽ SECOND ARTIFICIAL TAU TERMINATE, 510.2
- ▽ INITIATE CH1 FREEZE, 517.7
- ▽ S-II ECO SENSED BY LVDC, 576.33

— MEASURED DATA (NOT CORRECTED FOR A 0.6 SECOND TIME BIAS IN TELEMETRY DATA)

- - - SIMULATED DATA (NOT CORRECTED FOR A 2.0 SECOND TIME BIAS IN SIMULATION INPUT)

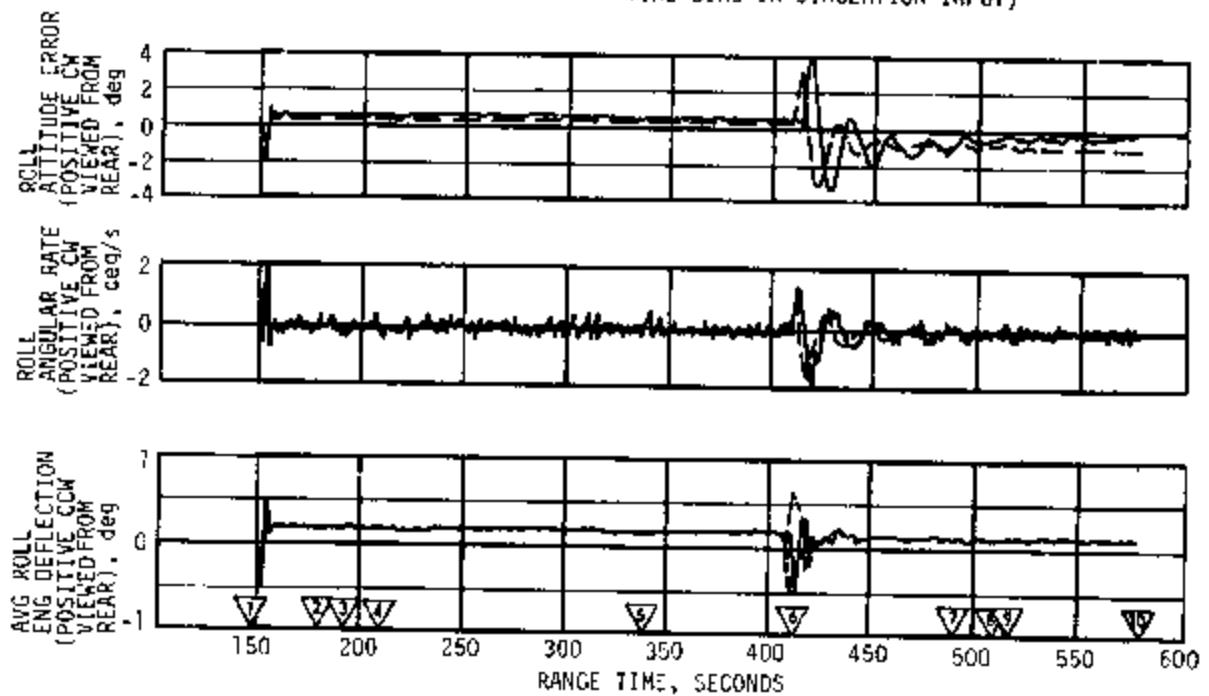


Figure 11-20. Roll Plane Dynamics During S-II Burn

Table 11-5. Maximum Control Parameters During S-II Burn

PARAMETER	S-IC/S-II SEPARATION	1ST PHASE IGM INITIATION	NO. 2 & 3 ENG FAIL	TERMINATE 2ND ARTIFICIAL TAU	S-II CUTOFF
<u>Pitch Plane</u>					
Attitude Error, deg	-0.5	-1.9	13.4	8.2	7.4
Body Rate, deg/s	0.3	1.0	2.3	1.0	0.1
Average Gimbal Angle, deg	0.24	0.9	5.95	4.37	3.5
Slosh Component of Average Gimbal Angle, deg	0.01	0.06	0.15	0.02	-
<u>Yaw Plane</u>					
Attitude Error, deg	-0.8	-0.4	2.7	0.2	0.0
Body Rate, deg/s	0.3	0.1	-0.8	-0.15	-0.2
Average Gimbal Angle, deg	-0.83	-0.23	0.62	0.19	0.11
Slosh Component of Average Gimbal Angle, deg	0.03	0.05	0.18	0.01	-
<u>Roll Plane</u>					
Attitude Error, deg	-2.3	0.5	4.2	-0.7	-0.2
Body Rate, deg/s	2.0	-0.1	-2.2	0.1	0.2
Average Gimbal Angle, deg	-0.49	-0.23	0.39	0.15	-0.14

IGM was initiated at 190.95 seconds, and the flight control computer received thrust vector control commands to pitch the vehicle up. Following IGM initiation, a -1.9 degrees pitch attitude error, 1.0 deg/s pitch rate, and 0.9 degree pitch gimbal deflection occurred. These responses were similar to those obtained during AS-501 flight. The effects of steering misalignment corrections (initiated at 212.0 seconds) and flight control gain switch point 3 had no noticeable effect upon attitude control performance. The thrust reduction on engine No. 2 at 319 seconds (see Section 6.3) had a minor effect on attitude control.

Subsequent to a drop in thrust in engine No. 2 a discrete signal was received by the IU from the S-II stage that indicated thrust not OK on at least one engine. During successive LVDC computation cycles, acceleration decrease due to cutoff of engines No. 2 and 3 was confirmed. This confirmation and the external discrete caused the guidance system to enter an engine-failure-mode artificial tau. The principal dynamics following cutoff of engines No. 2 and 3 occurred in the pitch axis and were attributable to a pitch disturbance moment which acted on the vehicle as a result of the two engines out. The pitch rate built up to a maximum of 2.8 deg/s before the control engines could be repositioned to counteract this moment.

Pitch axis control was stabilized within 10 seconds from time of the engine cutoff. The pitch attitude error reached a maximum of 13.4 degrees and remained above 6 degrees until final engine cutoff prior to S-II/S-IVB separation. This attitude error was required by the control system in order to keep the control engines positioned to counteract the effects of engines No. 2 and 3 being inoperative. With only two outboard engines (engines No. 1 and 4) operating, the yaw and roll axes control systems interacted. A dominant mode with a period of 20 seconds and damping factor of 0.1 was apparent in their responses following the shutdown of engines No. 2 and 3.

The effects of terminating the second artificial tau mode at 510.2 seconds were most apparent in the pitch axis when a 1 deg/s pitch-up response rate occurred. This was a consequence of the change in command angle at this time. Seven seconds later a chi-freeze mode was entered. After this time the vehicle rates were reduced to less than 0.2 deg/s for the remaining 40 seconds of the S-II stage flight. At S-II stage engine cutoff (prior to S-IVB separation), the vehicle attitude errors (except pitch), and attitude rates were at or near null.

Steering Misalignment Correction mode became operative at 212.0 seconds, as shown in Figure 11-21. Its principal effect upon the control system was to introduce a low frequency mode (approximately 0.05 hertz) below the rigid body control mode (approximately 0.11 hertz). During steady state attitude control operation the magnitude of SMC is a measure of thrust misalignment and center of gravity offsets. Following cutoff of engines No. 2 and 3 the SMC angles increased to a maximum of -0.55 and -13 degrees for the yaw and pitch axes, respectively. The low frequency mode present in the yaw and roll axes vehicle responses shown in Figures 11-19 and 11-20 is also apparent in the SMC yaw command angle corrections shown in Figure 11-21.

At 319 seconds a load increase of 32,000 Newtons (7000 lbf) appeared on both the pitch and yaw actuators of engine No. 2 (see Section 8.3). This was precisely the time engine No. 2 chamber pressure dropped, signifying a reduction of thrust in the engine of 33,806 Newtons (7600 lbf). (See Section 6.3.) Figure 11-22 shows the load pressures, input command currents, and the actuator positions for the pitch and yaw actuators of

▽ S-II ENGINE START COMMAND, 149.76
 ▽ SMC INITIATE, 212.0
 ▽ S-II ENG NO. 2 & 3 OUT, 412.92, 414.18;
 ▽ FIRST ARTIFICIAL TAU INITIATE, 415.4
 ▽ FIRST ARTIFICIAL TAU TERMINATE AND
 SECOND ARTIFICIAL TAU INITIATE, 490.8
 ▽ SECOND ARTIFICIAL TAU TERMINATE, 510.2
 ▽ SMC COMPUTATION INHIBIT (516.0 SEC);
 ▽ INITIATE CHI FREEZE, 517.7
 ▽ S-II ECO SENSED BY LVDC, 576.33

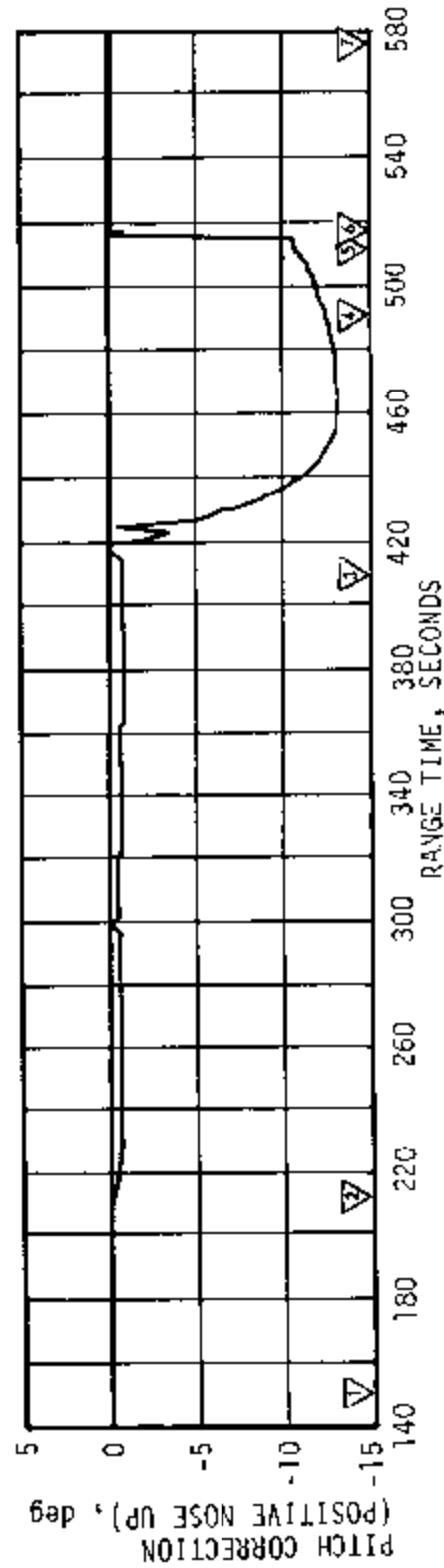
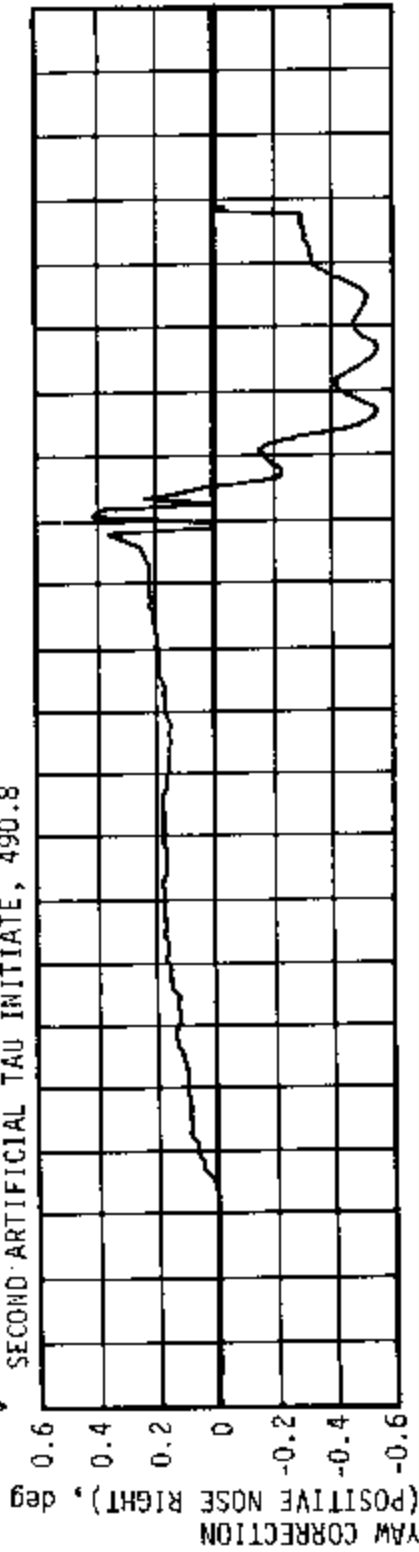


Figure 11-21. Pitch and Yaw Steering Misalignment Correction During S-II Burn

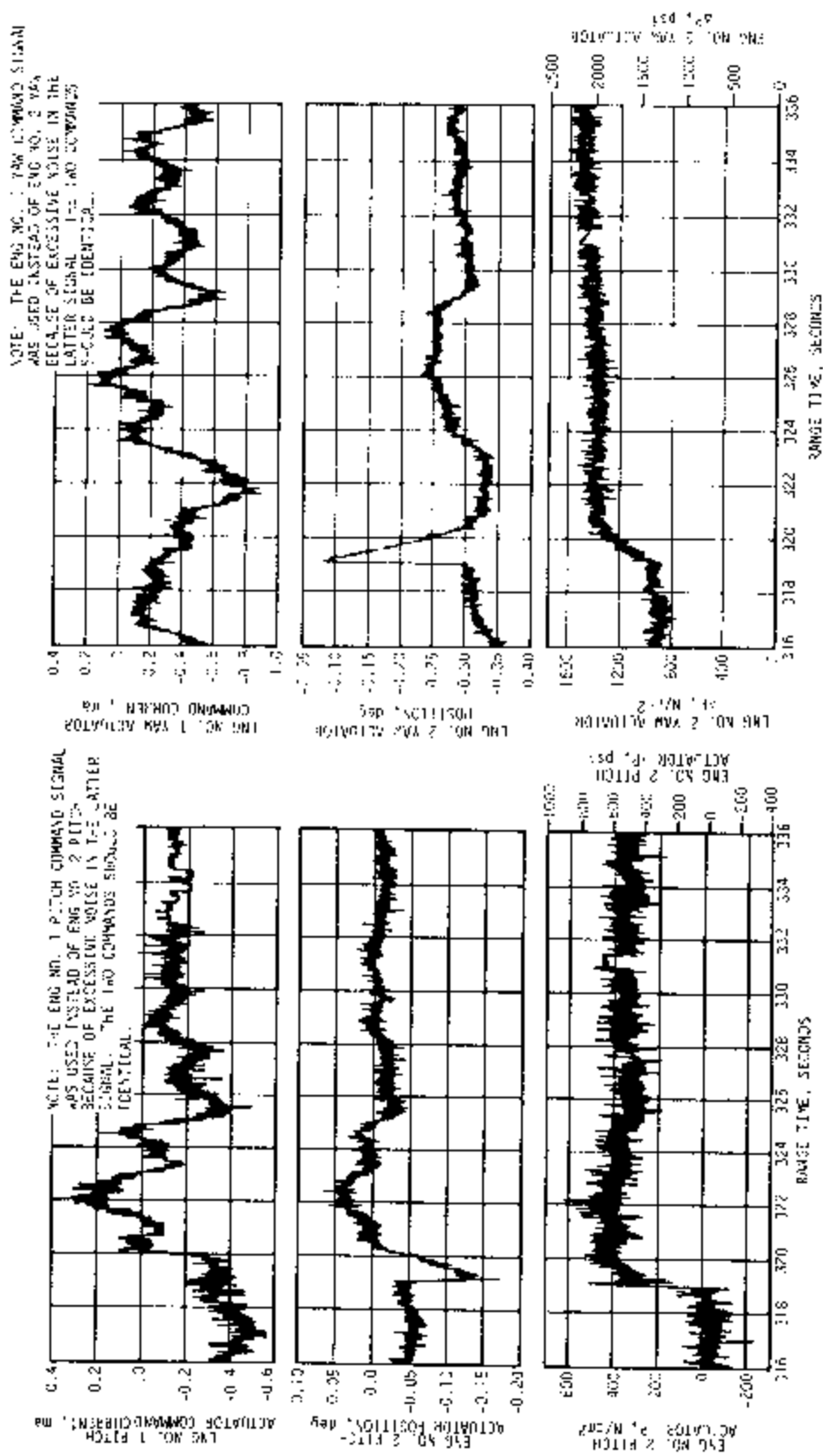


Figure 11-22. S-II Engine No. 2 Pitch and Yaw Actuator Response to the External Compression Load at 319 Seconds and to the Consequent Command at 320 Seconds

engine No. 2. These data show the reactions of these actuators to the loads. The engine No. 2 pitch actuator retracted a maximum of about 0.12 degree and the engine No. 2 yaw actuator retracted a maximum of about 0.2 degree. The actuators retracted with no input command because of applied compression loads. A nozzle side load generated during a test firing with a hole in the thrust chamber nozzle resulting from an ASI fuel line failure (reference MSFC memo R-P&VE-PA-68-M-367) very closely simulated the 414 N/cm² (600 psi) change in differential pressure measured on both pitch and yaw actuators. A moment of 16,380 N-m (145,000 lbf-in.) was measured on the test firing, compared to 14,970 N-m (132,500 lbf-in.) on the S-II engine. Vehicle control parameters confirm that a side load, as indicated from the test, was in evidence subsequent to the S-II engine performance shift at 319 seconds.

After cutoff of S-II engine No. 2, the yaw actuator no longer responded to commands (reference Section 8, Figure 8-5).

11.4.2 Liquid Propellant Dynamics and Their Effects on Flight Control

Estimates of liquid propellant dynamics were extracted from the fine mass probe liquid sensor measurements. Assuming planar wave propellant slosh, the LOX probe measures 98 percent of the pitch component and 20 percent of the yaw component. The LH₂ probe measures 16 percent of the pitch component and 99 percent of the yaw component.

Estimated LOX and LH₂ slosh amplitudes during S-II boost are shown in Figure 11-23. These data were extracted from the fine mass probe liquid sensor measurements by a data processing technique specially developed for this purpose. The amplitude plots show periodic biasing (non-sinusoidal) which should be ignored because it is a consequence of the processing technique. The top two plots are for the LH₂ slosh amplitudes at the probe and wall, respectively. The bottom plot is for the LOX surface angle. The slosh modes were excited after S-II stage J-2 engine start, IGM initiation, cutoff of engines No. 2 and 3, and termination of artificial tau guidance mode, as indicated in the figure. The largest LH₂ slosh amplitude was 15 centimeters (6 in.) at the probe, and occurred after cutoff of engines No. 2 and 3. The LOX slosh amplitude was more sustained than LH₂ sloshing throughout S-II boost.

S-IVB stage slosh data are shown in Figure 11-24. LH₂ sloshing was discernible at S-II engine ignition (149.8 seconds) and at engines No. 2 and 3 cutoff (412.9 and 414.2 seconds). The LH₂ slosh quickly damped out (within 15 seconds). This corresponds to an estimated damping factor of 0.26. The S-IVB LH₂ slosh frequencies were near the natural uncoupled frequency as shown in Figure 11-25. LOX sloshing in the S-IVB tanks was not discernible.

The slosh data were also analyzed for frequency content. Figure 11-25 depicts slosh frequencies estimated from fine mass probe measurements in the S-II stage liquid oxygen and liquid hydrogen tanks. The LH₂ frequency plots show that sloshing occurred near the natural (uncoupled) LH₂ slosh

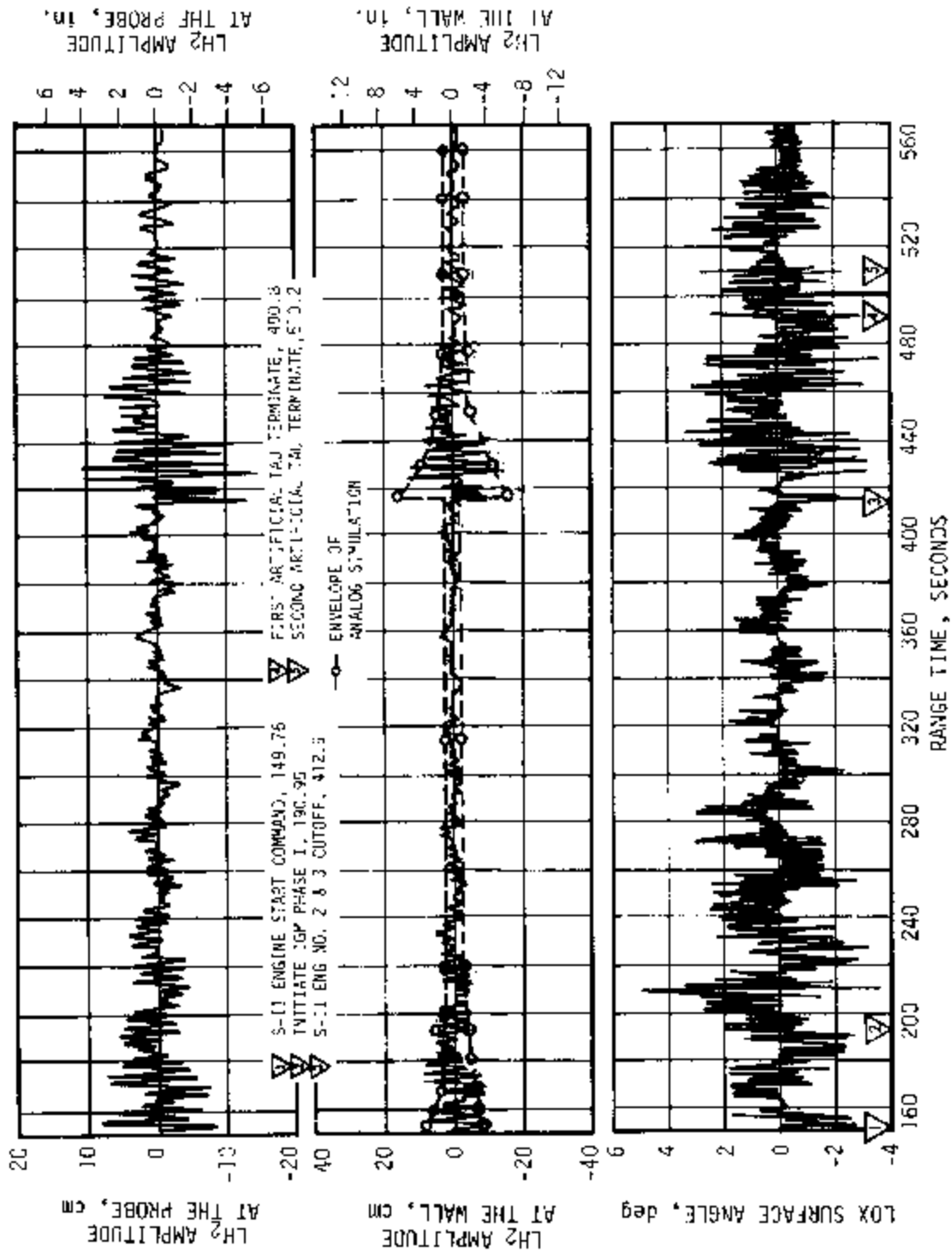


Figure 11-23. S-II LH₂ and LOX Slosh Amplitudes During S-II Burn

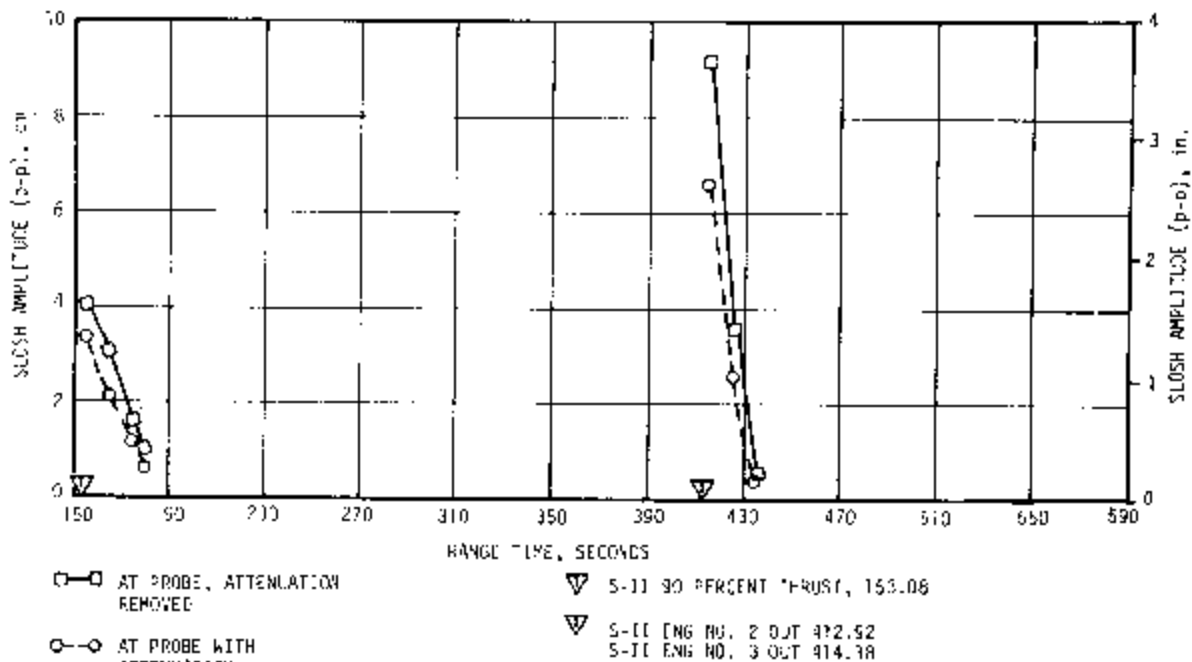


Figure 11-24. S-IVB LH₂ SLOSH Amplitude at the Probe During S-II Burn

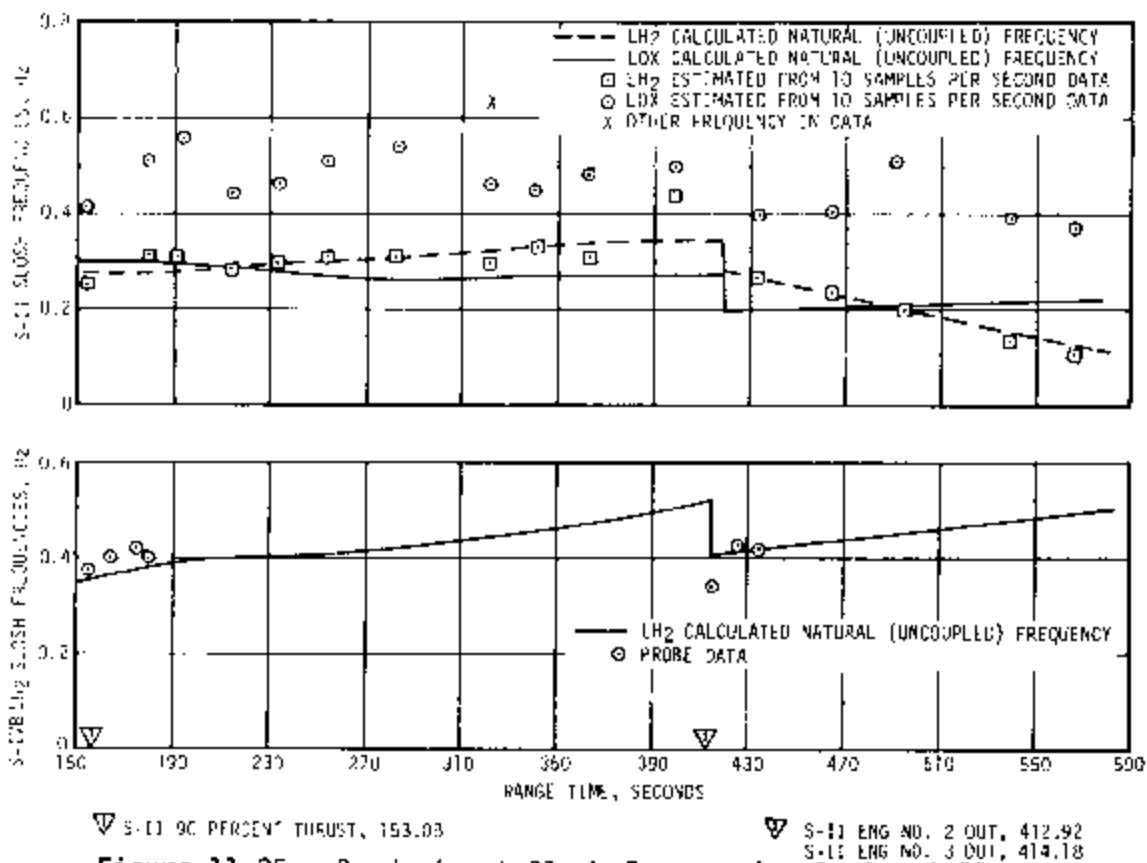


Figure 11-25. Predominant SLOSH Frequencies During S-II Burn

frequencies. The LH₂ sloshing was initially excited during S-II stage J-2 engine ignition (149.8 seconds) and initiation of IGM (191.0 seconds) and then oscillated independently with slow decay due to damping. The observed LOX frequencies were in the range of 0.4 to 0.6 hertz. These frequencies were also evident in the S-II pitch and yaw gyros. The LOX sloshing was apparently coupled with the flight control system response. It is theorized that small amplitude (less than 0.02 degree) attitude limit cycling of the flight control system was forcing the LOX slosh dynamics. A small amplitude attitude limit cycle was predicted by the analog simulation of the S-II stage flight dynamics control system. Attitude control limit cycling is possible because of the quantization of flight control data by the LVDA and the non-linearity of the LVDA-LVDC. The results of simulation of LH₂ amplitude at the wall are plotted in Figure 11-23 for comparison with flight data. The comparison indicates good agreement during the initial excitation of the slosh modes; however, the decay characteristics of the simulation show more attenuation. This indicates that less damping of the slosh modes occurred in flight than anticipated by the simulated flight dynamics.

The effect of liquid propellant slosh upon the control system was estimated from the component of the slosh modes in the engine deflections, presented in Figure 11-26. The engine deflections were analyzed using bandpass filtering.

The largest slosh component magnitudes of 0.18 and 0.15 degree occurred with the yaw and pitch gimbal angles following cutoff of engines No. 2 and 3. The yaw magnitude was approximately 30 percent of the total yaw gimbal angle at this time (see Table 11-5).

S-II stage J-2 engine No. 1 pitch and yaw actuators position data were bandpass filtered at five selected flight times to detect the presence of any structural bending mode frequency components. The results indicate negligible engine deflection due to structural bending of the vehicle. This result was to be expected and indicates the flight control computer electronic filters were effectively attenuating any bending mode effects in the rate gyro or other control system inputs.

11.5 S-IVB CONTROL SYSTEM EVALUATION

The S-IVB Thrust Vector Control System and APS provided satisfactory pitch, yaw, and roll control during S-IVB first burn and parking orbit. During restart attempt the auxiliary and main hydraulic pump cavitated, precluding operation of the TVC system. With this exception, the vehicle attitudes correlated well with actual commanded attitudes, and demands on the control system were well within the capabilities of the system.

11.5.1 S-IVB Control System Evaluation Before and During First Burn

From 118 to 133 seconds during S-IC burn, a 5.5 hertz oscillation at approximately 276 N/cm² (400 psid) peak-to-peak was observed on the S-IVB pitch actuator differential pressure. Figure 11-27 presents a comparison

- ▽ S-IC/S-II SEPARATION COMMAND, 149.08
- ▽ S-II SECOND PLANE SEPARATION COMMAND, 179.1
- ▽ INITIATE IGM PHASE I, 190.95
- ▽ FLIGHT CONTROL COMPUTER SWITCH POINT NO. 3, 209.76
- ▽ FLIGHT CONTROL COMPUTER SWITCH POINT NO. 4, 339.76

- ▽ S-II ENG NO. 2 & 3 OUT, 412.92, 414.18; FIRST ARTIFICIAL TAU INITIATE, 415.4
- ▽ FIRST ARTIFICIAL TAU TERMINATE, SECOND ARTIFICIAL TAU INITIATE, 490.8
- ▽ SECOND ARTIFICIAL TAU TERMINATE, 510.2
- ▽ INITIATE CHI-FREEZE, 517.7
- ▽ S-II ECO SENSED BY LVDC, 576.33

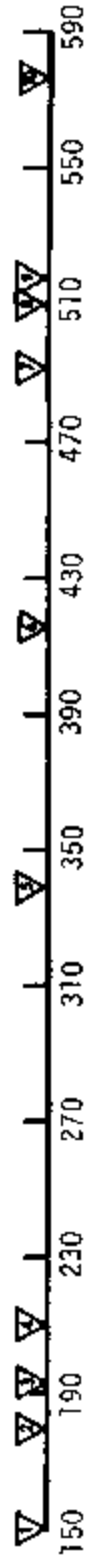
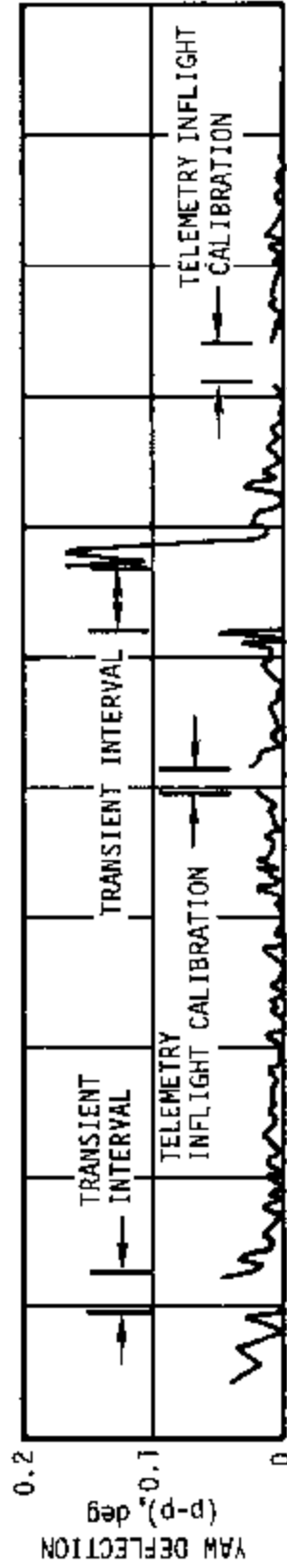
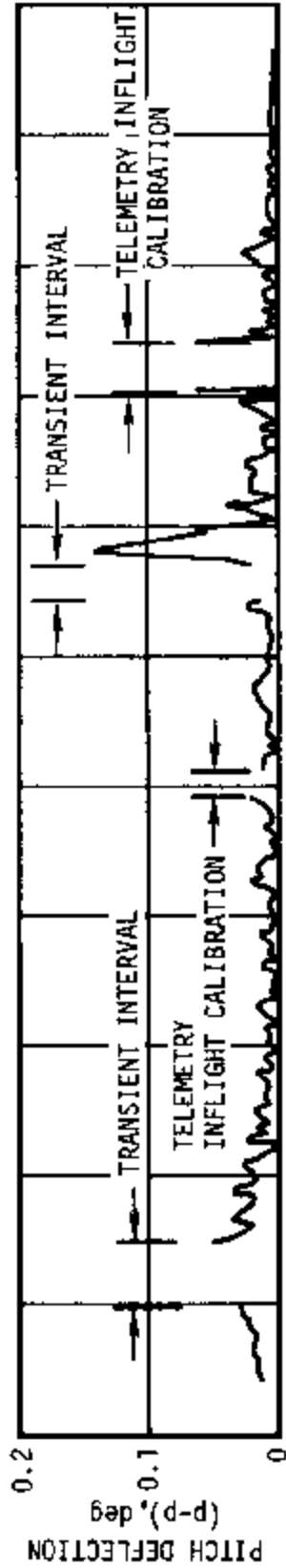


Figure 11-26. S-II Engine Deflection Response to Propellant Slosh

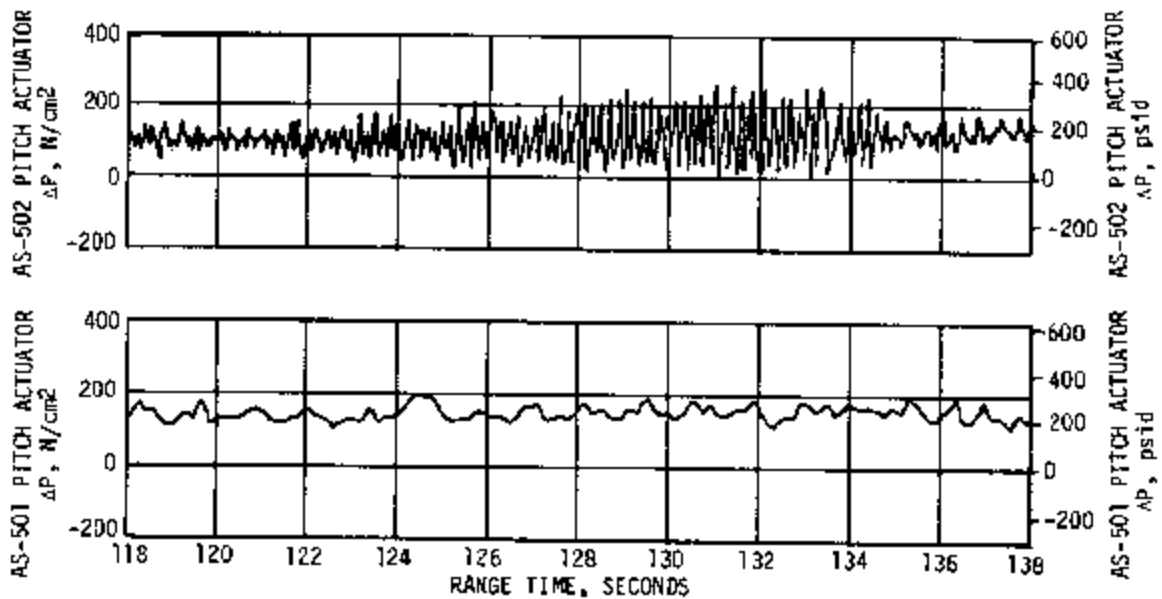


Figure 11-27. S-IVB Pitch Actuator Excitation During S-IC Burn

of AS-502 and AS-501 pitch actuator differential pressure during this time interval. The 5.5 hertz oscillation was not evident on the yaw actuator differential pressure data. Section 9 contains a discussion of the POGO phenomenon which caused this.

At 577.1 seconds (S-II/S-IVB separation command), there was a 0.3 second APS firing by the pitch engine at position I (I_p). The pulse was terminated at approximately 577.4 seconds by the S-IVB Burn Mode ON switch selector command. This command places the flight control computer in the S-IVB burn mode, which enables J-2 engine gimbaling for pitch and yaw control during S-IVB burn, and enables the APS to control in roll. Because the flight control computer was in the S-IVB coast mode for this 0.3 second interval and the pitch attitude error signal was of sufficient magnitude, the I_p engine fired as commanded. This is a normal occurrence on Saturn V. AS-501 had a similar unsynchronized yaw/roll pulse on the APS engine No. 4 at position I (I_{IV}) during staging.

The conditions on Saturn V are not the same as on Saturn IB, in which the flight control computer goes directly into S-IVB burn mode from S-IB burn mode and cannot go to coast mode and trigger the APS unless commanded to coast mode.

The TVC responded satisfactorily to flight control computer commands during first burn. The maximum attitude errors and rates occurred at S-II/S-IVB separation. A summary of the maximum values of critical flight control parameters is presented in Table 11-5.

Table 11-6. Maximum Control Parameters During S-IVB Burn

PARAMETER	S-II/S-IVB SEPARATION, GUID. INITIATION, AND ART. TAU	BEGIN CHI BAR	S-IVB FIRST CUTOFF
Pitch Attitude Error, deg	7.9	-1.0	-0.9
Yaw Attitude Error, deg	-2.3	-1.0	-0.8
Roll Attitude Error, deg	-0.9	0.5	0.4
Pitch Rate, deg/sec	-3.5	1.1	1.0
Yaw Rate, deg/sec	1.1	-0.2	0.1
Roll Rate, deg/sec	-0.6	0.0	0.0
Pitch Actuator Pos., deg	6.7	0.2	0.2
Yaw Actuator Pos., deg	-1.3	-0.5	-0.6

The large attitude error at S-II/S-IVB separation resulted in a pitch actuation position requirement of 6.7 degrees, but the separation transient was within the capabilities of the TVC system. The S-IVB pitch, yaw, and roll dynamics, including command angles, attitude errors, angular rates, and actuator positions, are presented in Figures 11-28, 11-29, and 11-30, respectively. The pitch and yaw effective thrust vector misalignments were +0.25 degree in pitch and -0.4 degree in yaw. The steady-state roll torque was 54 N-m (40 lbf-ft). The powered flight APS impulse requirements are included in Table 11-7.

LOX and LH₂ slosh parameters are presented in Figures 11-31 and 11-32, respectively. LOX sloshing exhibited the coupling found in previous flight data. LH₂ sloshing indicated a large slosh wave following S-II/S-IVB separation due to the large control system transient which occurred at that time. The slosh wave was highly damped by the deflector located in the area of quiescent surface level. Variations in LH₂ sloshing parameters were also noted at approximately 645 seconds, due to the nose-up command which occurred at that time. The LOX and LH₂ sloshing did not significantly affect the control system operation during S-IVB burn.

- ▽ S-IVB ENGINE START SEQUENCE COMMAND, 577.28
- ▽ INITIATE IGM, PHASE III, 584.78
- ▽ ARTIFICIAL TAU TERMINATE, 594.3
- ▽ PITCH COMMAND NOSE UP ATTITUDE, 644.02
- ▽ INITIATE CHI FREEZE, 746.4
- ▽ S-IVB VELOCITY CUTOFF COMMAND, 747.04

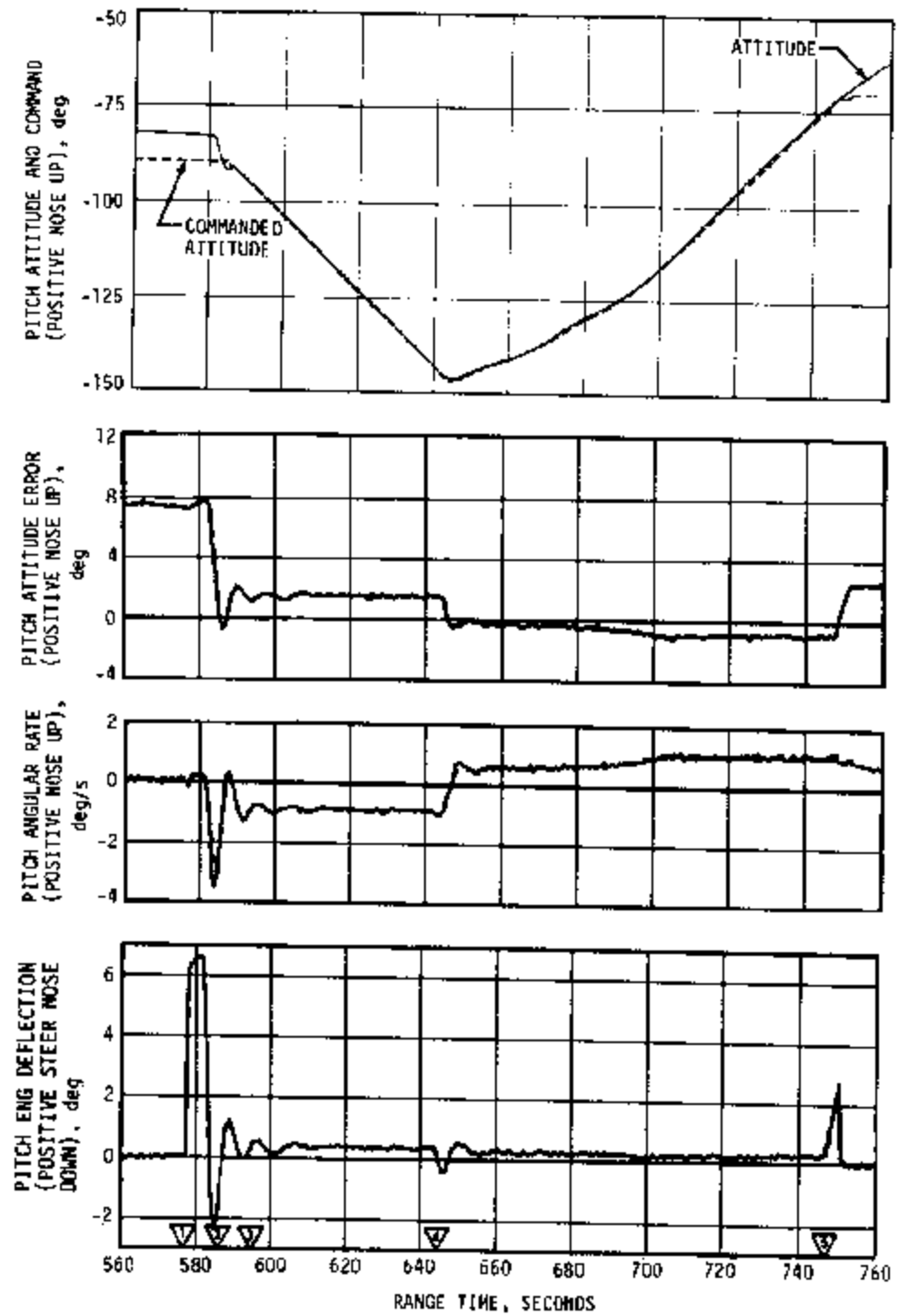


Figure 11-28. Pitch Plane Dynamics During S-IVB First Burn

- ▽ S-IVB ENGINE START SEQUENCE COMMAND, 577.28
- ▽ INITIATE IGM PHASE III, 584.78
- ▽ ARTIFICIAL TAU TERMINATE, 594.3
- ▽ PITCH COMMAND NOSE UP ATTITUDE, 644.02
- ▽ INITIATE CHI BAR STEERING, 712.3
- ▽ INITIATE CHI FREEZE, 746.4;
- ▽ S-IVB VELOCITY CUTOFF COMMAND, 747.04

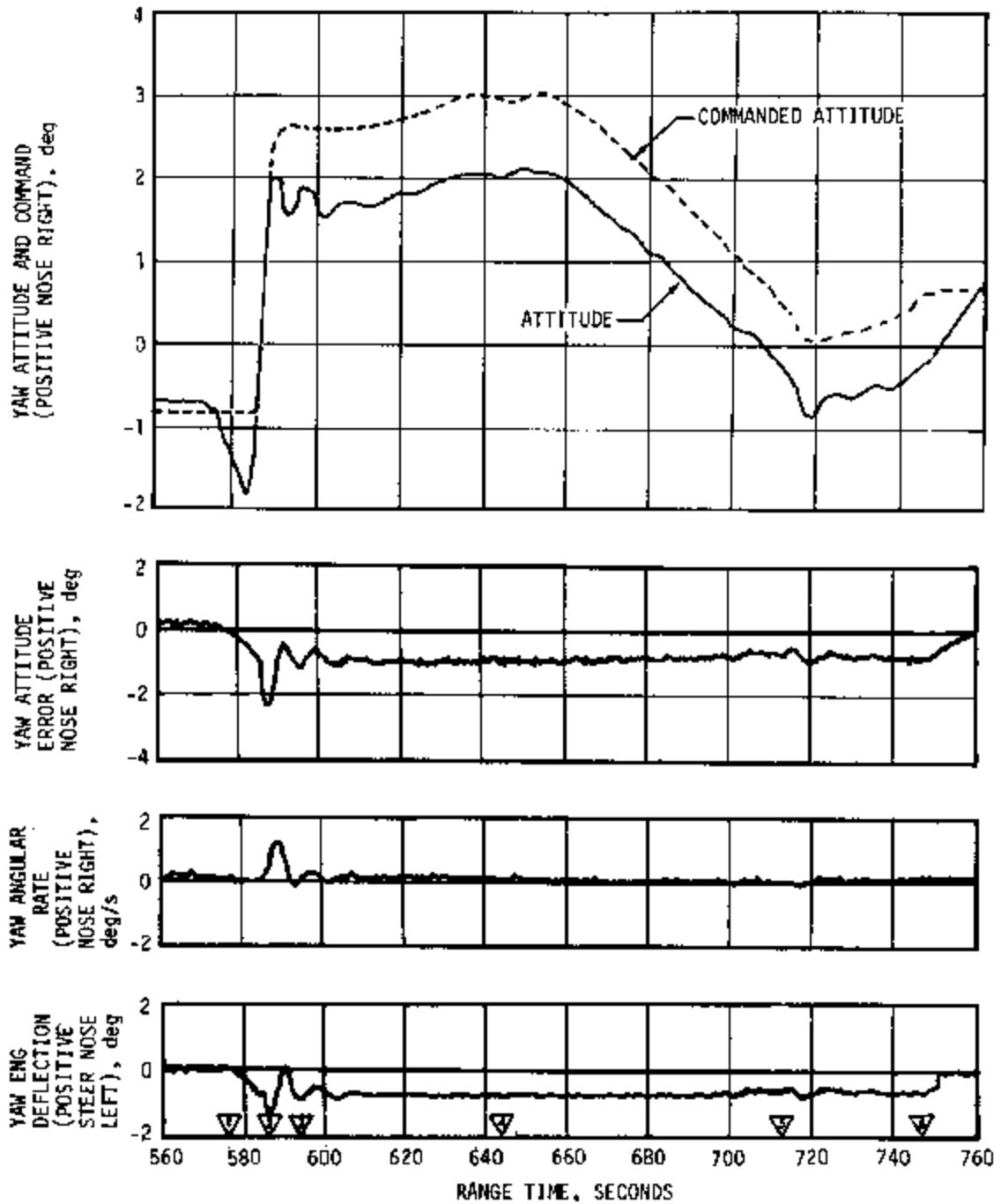


Figure 11-29. Yaw Plane Dynamics During S-IVB First Burn

▽ S-IVB ENGINE START SEQUENCE COMMAND, 577.28
 ▽ INITIATE IGM PHASE III, 584.78
 ▽ ARTIFICIAL TAU TERMINATE, 594.3
 ▽ PITCH COMMAND NOSE UP ATTITUDE, 644.02
 ▽ INITIATE CHI BAR STEERING, 712.3
 ▽ INITIATE CHI FREEZE, 746.4;
 ▽ S-IVB VELOCITY CUTOFF COMMAND, 747.04

▽ S-IVB ENGINE START SEQUENCE COMMAND, 577.28
 ▽ INITIATE IGM PHASE III, 584.78
 ▽ ARTIFICIAL TAU TERMINATE, 594.3

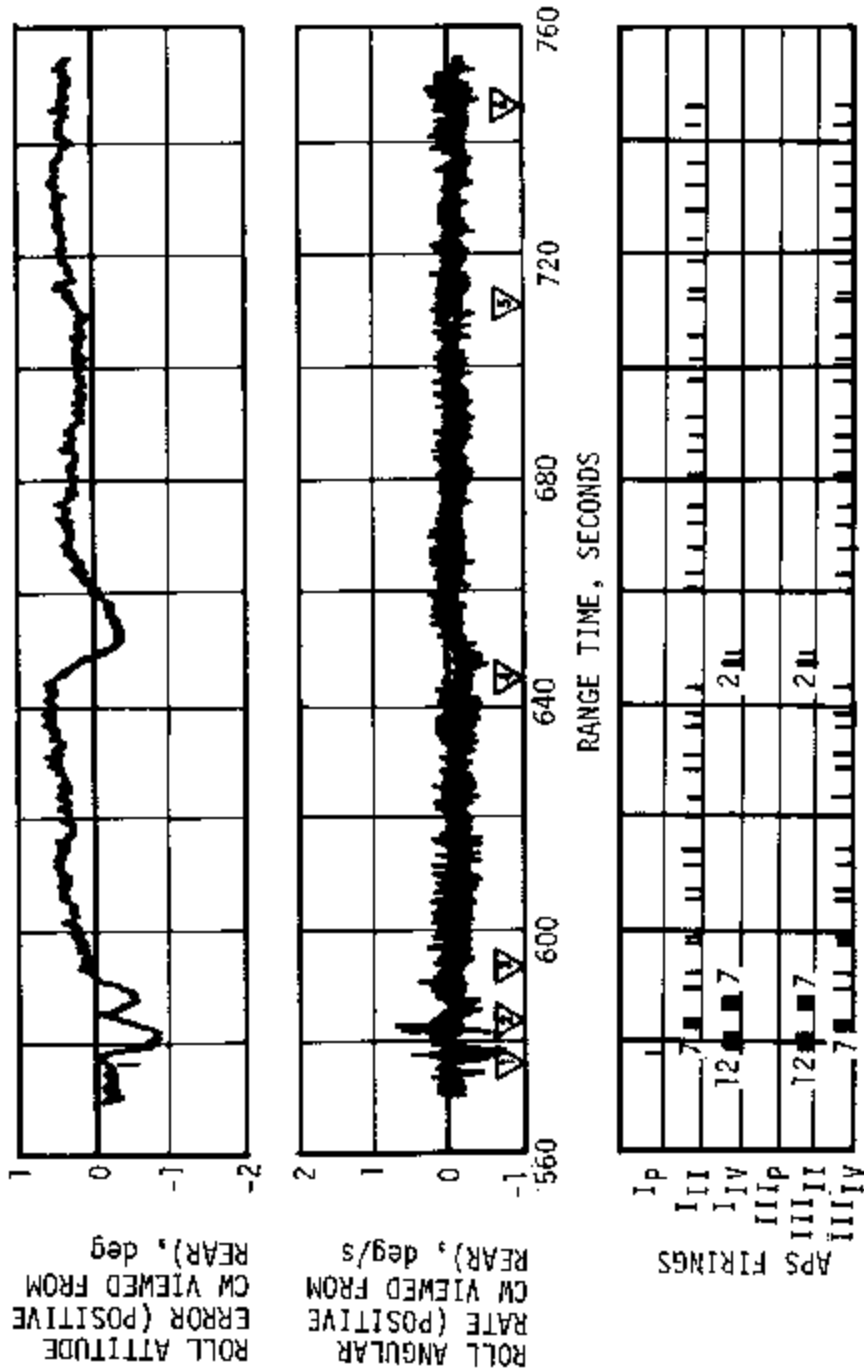


Figure 11-30. Roll Plane Dynamics During S-IVB First Burn

Table 11-7. APS Impulse Requirements

EVENT	UNITS	MODULE		APS ENGINE									
		POSITION I	POSITION II	I _{IV}	I _P	I _{II}	I _{III}	I _{IIp}	I _{III}				
Powered Flight:													
Separation, guidance initiation, & ullage motor jettison (577 to 600 sec)	N-s (1bf-s)	1625.8 (365.5)	1415.3 (318.4)	963.9 (216.7)	70.4 (38.3)	491.5 (110.5)	923.9 (207.7)	0 (0)	492.4 (110.7)				
Limit cycle operation for remainder of first burn (600 to 747 sec)	N-s (1bf-s)	1129.4 (253.9)	1119.2 (251.6)	106.3 (23.9)	0 (0)	1022.6 (229.3)	100.5 (22.6)	0 (0)	1018.6 (229.0)				
*Initial recovery after first burn and alignment to local horizontal including pitch and 180° roll maneuver plus settling usage; continuous vent system (CVS) on (750 to 1230 sec)	N-s (1bf-s)	52,159.8 (11,726.0)	21,860.3 (4914.4)	6445.5 (1449.0)	40,576.7 (9144.5)	5038.5 (1132.7)	6064.7 (1363.4)	10,381.2 (2333.8)	5414.8 (1217.3)				
Pitch down 20° below local horizontal; CVS is on (3210 to 3475 sec)	N-s (1bf-s)	5935.2 (1334.3)	5365.9 (1206.3)	496.0 (111.5)	5438.8 (1222.7)	0 (0)	135.7 (30.5)	4727.6 (1062.8)	502.6 (113.0)				
Pitch up maneuver to align with local horizontal; CVS is on (5426 to 5520 sec)	N-s (1bf-s)	9339.5 (2099.6)	10,290.5 (2313.4)	29.8 (6.7)	9309.2 (2092.8)	0 (0)	0 (0)	10,158.0 (2283.6)	132.6 (29.8)				
Roll 180° to position I down; CVS is on (5785 to 6110 sec)	N-s (1bf-s)	2494.1 (560.7)	888.8 (199.8)	649.9 (146.1)	1576.0 (364.3)	268.2 (60.3)	231.3 (52.0)	0 (0)	657.4 (147.8)				
Pitch and yaw maneuver for restart orientation (11,485 to 11,600 sec)	N-s (1bf-s)	6286.7 (1413.3)	9652.1 (2147.4)	434.6 (97.7)	5633.4 (1266.0)	220.6 (49.6)	131.7 (29.6)	8994.7 (2022.1)	425.1 (95.8)				
Recovery following second burn attempt, maneuver to spacecraft separation attitude, spacecraft separation and settling; 10 sec LOX tank venting, 120 sec LHe tank venting (11,630 to 11,970 sec)	N-s (1bf-s)	65,412.4 (14,930.1)	121,519.1 (27,318.6)	7187.9 (1615.9)	37,011.4 (8320.5)	22,213.1 (4993.7)	22,392.3 (5034.0)	92,611.0 (20,819.8)	6515.8 (1464.8)				

* Does not include 965 to 1010 second time slice because data is not available.

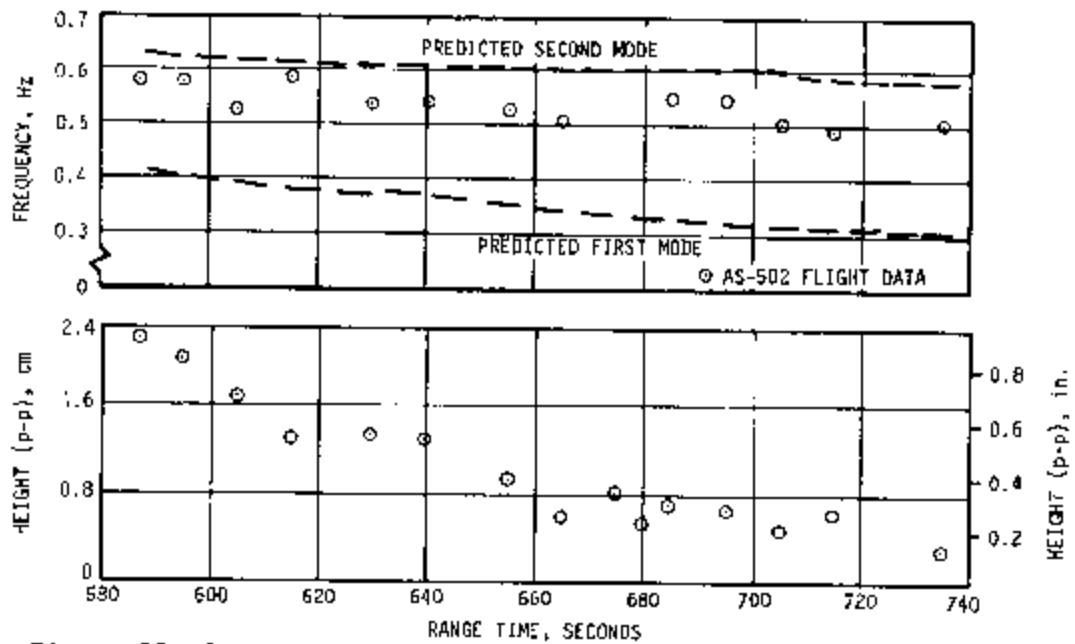


Figure 11-31. S-IVB LOX SLOSH Frequency and Height at the Probe

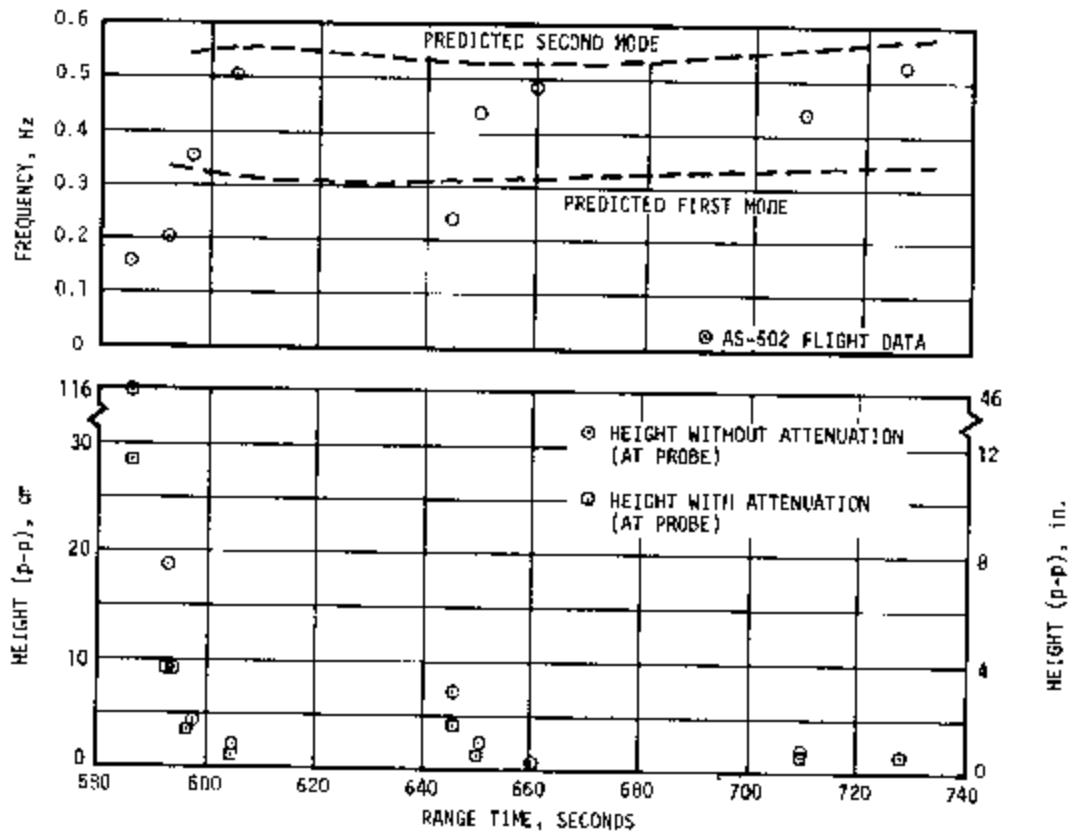


Figure 11-32. S-IVB LH₂ SLOSH Frequency and Height

11.5.2 Control System Evaluation During Parking Orbit

Evaluation of existing orbital data indicates that the APS attitude control performed satisfactorily during orbit.

Pitch, yaw, and roll control attitude errors, angular rates, and APS pulses following first burn are shown in Figures 11-33, 11-34 and 11-35, respectively.

Orbital attitude control requirements were much larger than on previous flights, which can be attributed primarily to initial conditions existing at S-IVB first and second cutoff.

Initial conditions at S-IVB first cutoff (50 degrees nose-up from the local horizontal and 1 deg/s nose-up angular rate) required considerably more APS activity than anticipated. Following activation of the APS, the pitch engine fired full on for approximately 43 seconds primarily to correct for the rate condition. At 762 seconds ($T_5 + 15$ seconds) the pitch engine was commanded to perform the relatively large maneuver of aligning the vehicle with the local horizontal. At 837 seconds ($T_5 + 90$ seconds) the S-IVB began a series of maneuvers planned to produce information on the S-IVB restart bottle repressurization (Section 7.5 and Figure 10-8) and propellant slosh excitation while qualifying these maneuvers for manned flight (see Mission Plan). This sequence of maneuvers consisted of a 180 degree roll, 20 degree pitch down, 20 degree pitch up, and a 180 degree roll. At 837 seconds ($T_5 + 90$ seconds) the S-IVB was commanded to roll counterclockwise 180 degrees to align position III toward earth.

The 20 degree pitch down maneuver was initiated at 3207 seconds ($T_5 + 2460$ seconds) for the purpose of evaluating propellant sloshing during a maneuvering period. The commanded and actual vehicle attitudes, attitude errors, angular rates, and APS pulses for pitch are shown in Figure 11-36. Following initiation of the maneuver, the pitch attitude error increased, as expected, to the -2.5 degree attitude error limit, which established a maneuvering rate of 0.3 deg/s. APS engine III₅ fired to establish the required maneuvering rate, which was maintained until the vehicle attitude approached the commanded attitude, when engine I_p fired to reduce the angular rate to the desired orbital pitch rate.

High frequency (19.5 to 22 hertz) rate signals having a maximum amplitude of 0.5 deg/s peak-to-peak were experienced, particularly on the roll rate gyro, commencing at 3311 seconds and terminating approximately 15 seconds later. This time correlates with the time period of high frequency (approximately 5 to 6 firings per second) APS engine firings required to terminate the pitch maneuver. The high frequency rate signals appeared to terminate as the APS engine firing frequency reduced to a lower level (less than 4 firings per second). Correlation of the high frequency rates and APS firings indicates that the high frequency signals were related to the APS engine firings. The high frequency rate signals,

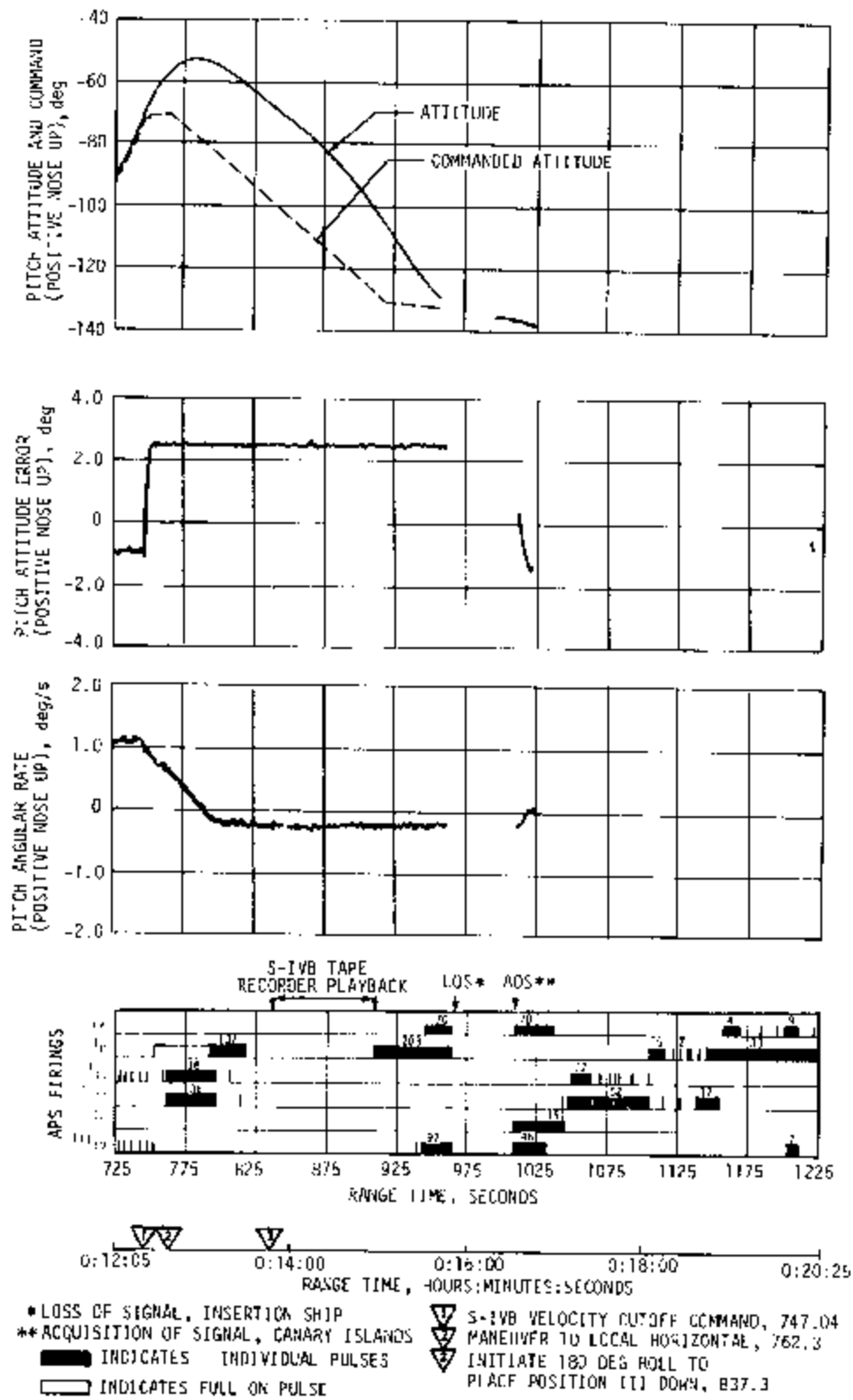


Figure 11-33. Pitch Control Dynamics Following S-IVB First Burn

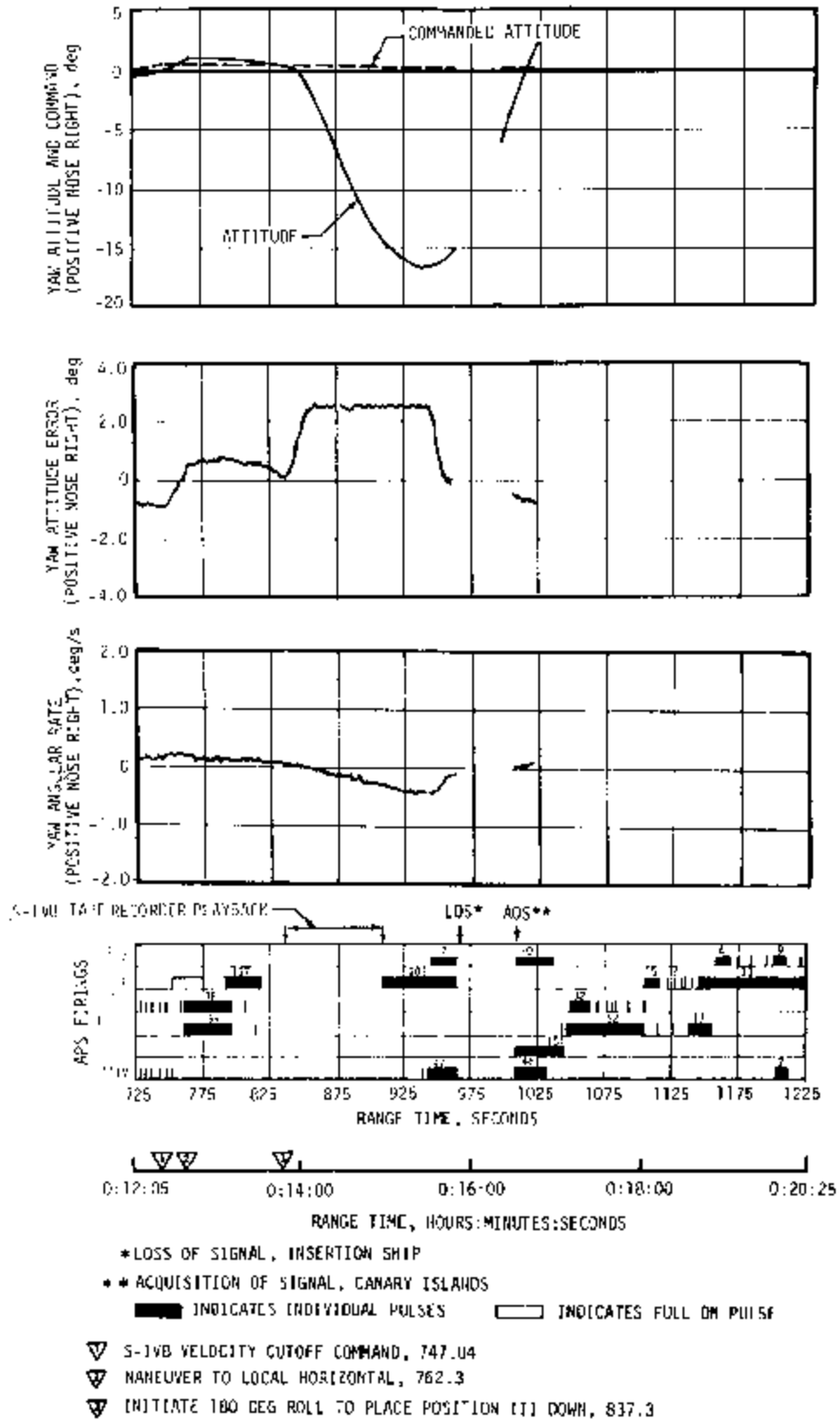


Figure 11-34. Yaw Control Dynamics Following S-IVB First Burn

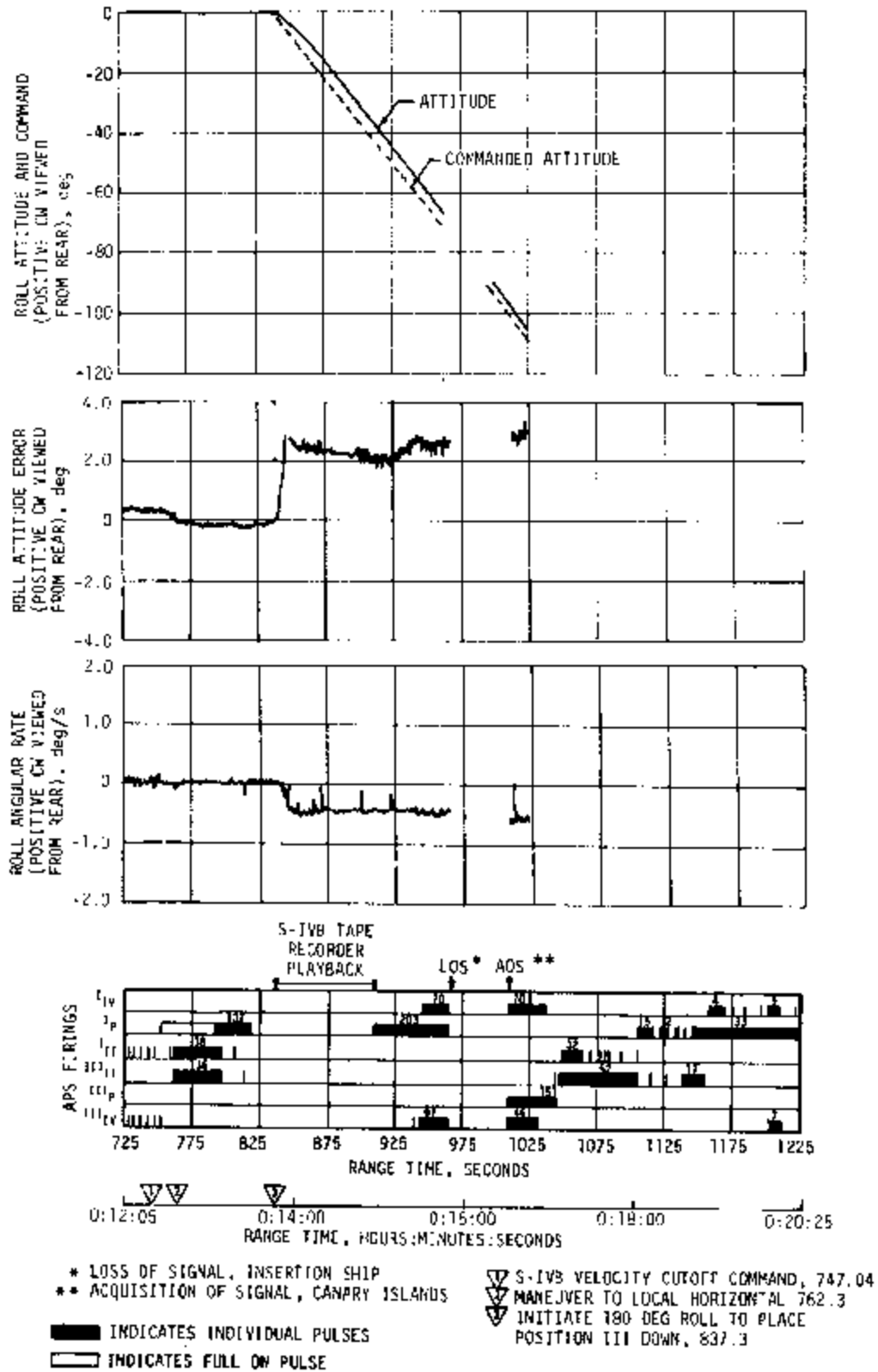


Figure 11-35. Roll Control Dynamics Following S-IVB First Burn

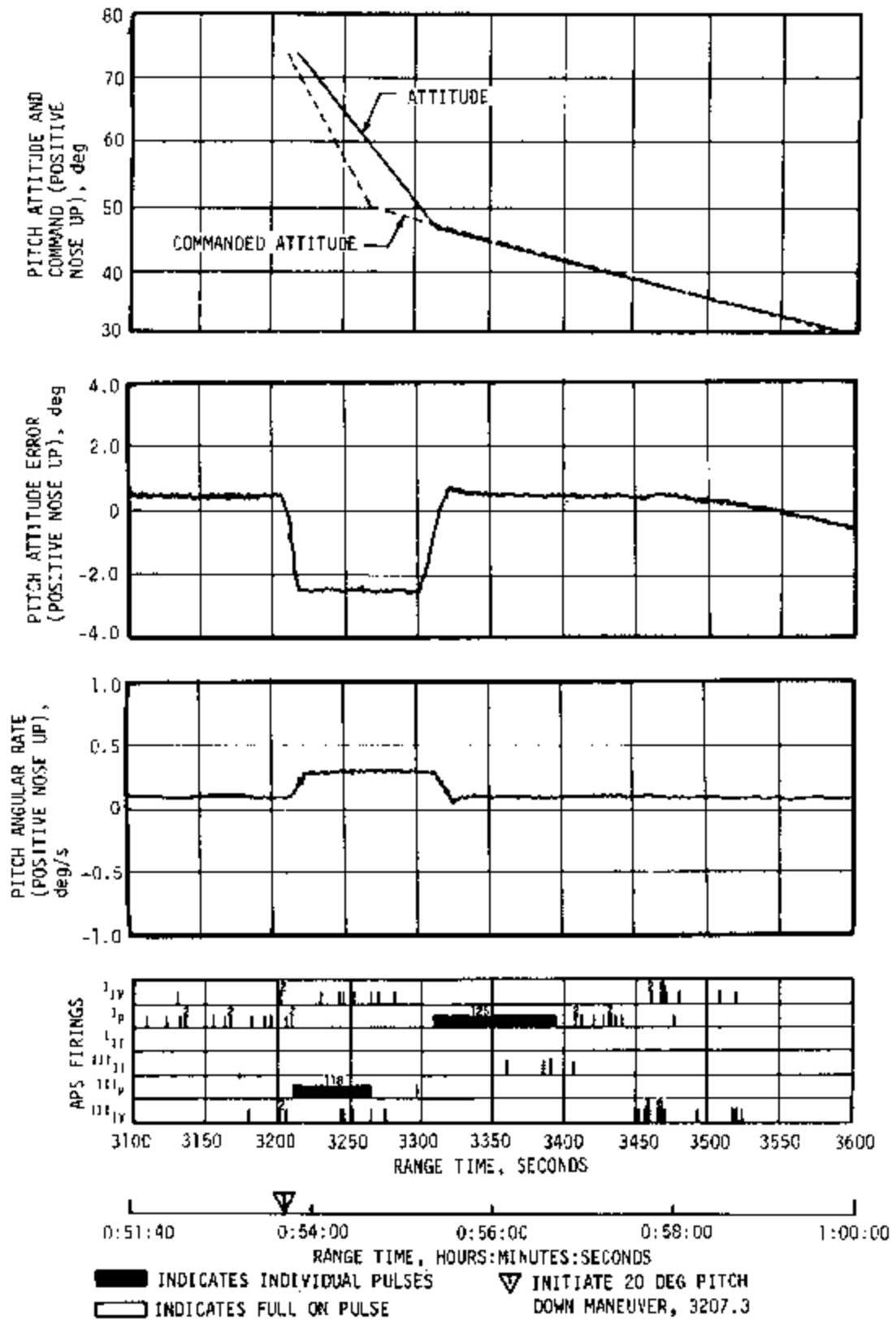


Figure 11-36. Pitch Control Dynamics During 20 Degree Pitch Down Maneuver

which were not of sufficient magnitude to affect attitude control system operation, appeared to be similar to those experienced on previous flights and during other intervals of the AS-502 mission. The APS response appeared normal during this maneuver.

LH₂ sloshing was not appreciable during the 20 degree pitch down maneuver. Significant LOX slosh existed at the initiation of the maneuver; however, LOX sloshing was not sustained due to the high LOX damping.

The 20 degree pitch up maneuver to the local horizontal was initiated at 5427 seconds (T₅ +4680 seconds). The commanded and actual vehicle attitudes, attitude errors, angular rates, and APS pulses are presented in Figures 11-37, 11-38, and 11-39. APS pitch engine I_p fired to remove the existing orbital pitch rate and establish a pitch up rate. The pitch attitude error increased to the attitude error limit of 2.5 degrees, establishing a maneuvering rate of -0.3 deg/s. As the actual vehicle attitude approached the commanded attitude, APS engine III_p fired to remove the maneuver rate and establish an orbital pitch rate (nose down). High frequency oscillations were also observed during this maneuver, particularly on the pitch and roll rate gyros. Again, the high frequency rate signal (0.2 deg/s peak-to-peak for approximately 25 seconds) existed predominantly during intervals of high frequency APS engine firings (approximately 5 firings per second) and damped out at approximately 4 firings per second. The APS operation appeared normal during the 20 degree pitch up maneuver.

LH₂ sloshing was negligible during the 20 degree pitch up maneuver, as was true during the pitch down maneuver. Significant LOX sloshing occurred at the maneuver initiation but was not sustained due to large LOX damping.

A distinct difference in pitch attitude errors was noted between the pitch down and pitch up maneuvers (see Figures 11-36 and 11-37). The pitch up maneuver exhibited considerably more overshoot than the pitch down maneuver. This was attributed to the greater impulse required to terminate the pitch up maneuver and establish the orbital pitch rate than for the pitch down maneuver. Only part of the maneuvering rate during the pitch down maneuver must be removed due to the requirement for the orbital pitch rate, whereas all of the maneuvering rate must be removed and an orbital rate established in the opposite direction for the pitch up maneuver. APS impulse requirements to initiate and terminate each of the pitch maneuvers were as follows:

Pitch Down

Initiate		Terminate	
Module at	4715 N-s	Module at	5026 N-s
Position III	(1060 lbf-s)	Position I	(1130 lbf-s)

Pitch Up

Initiate		Terminate	
Module at	10,097 N-s	Module at	9875 N-s
Position I	(2270 lbf-s)	Position III	(2220 lbf-s)

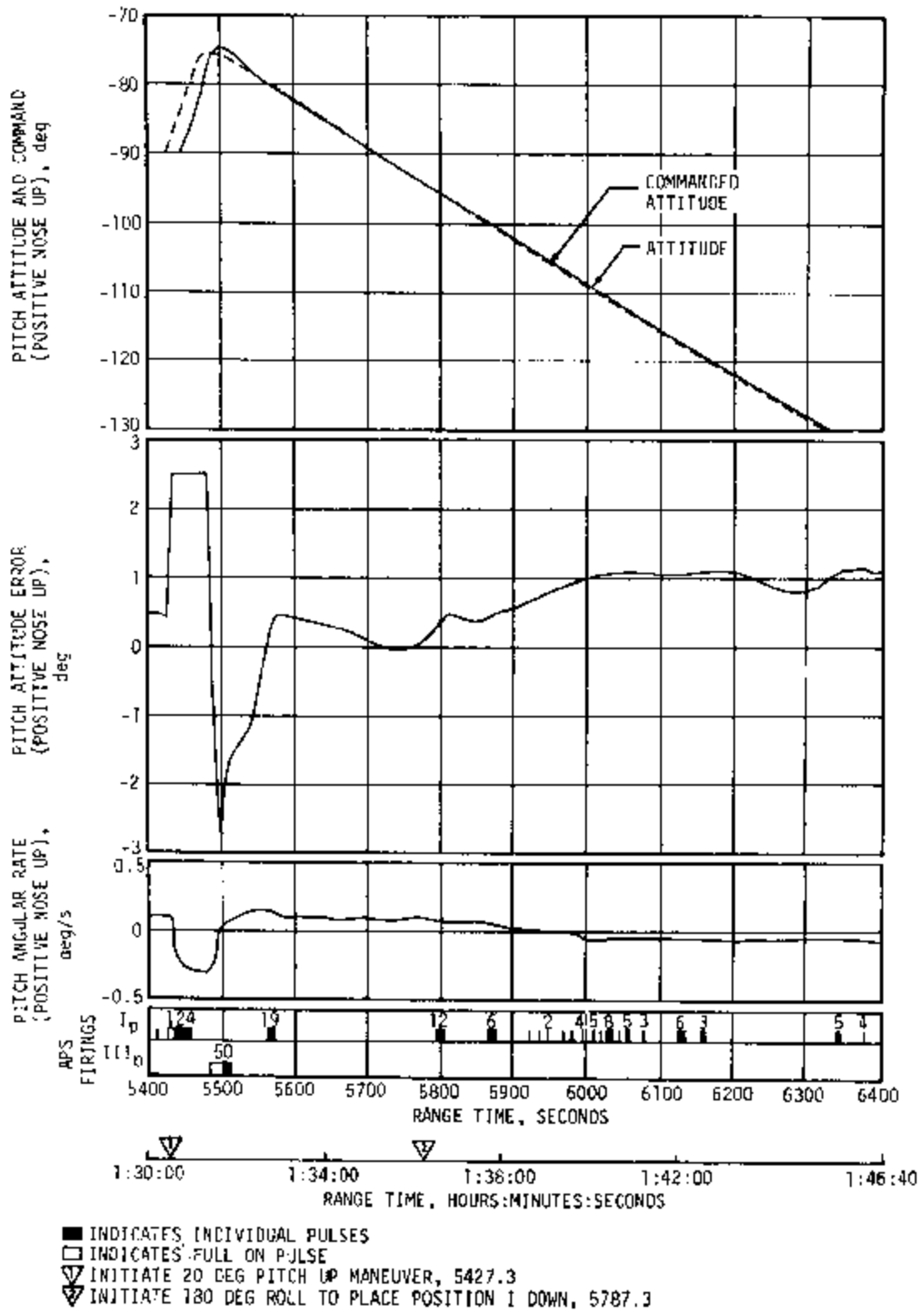


Figure 11-37. Pitch Control Dynamics During Pitch and Roll Maneuvers

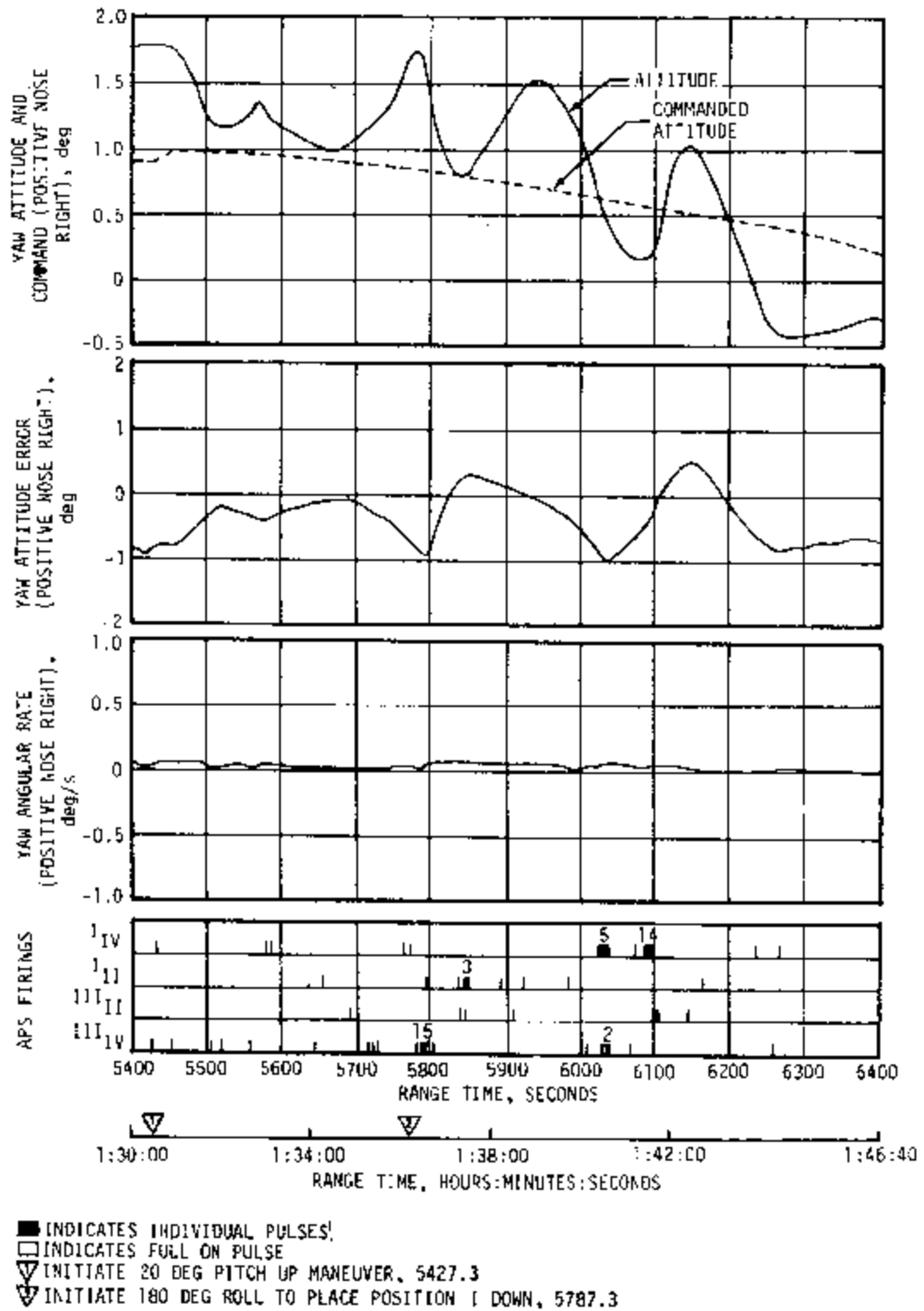


Figure 11-38. Yaw Control Dynamics During Pitch and Roll Maneuvers

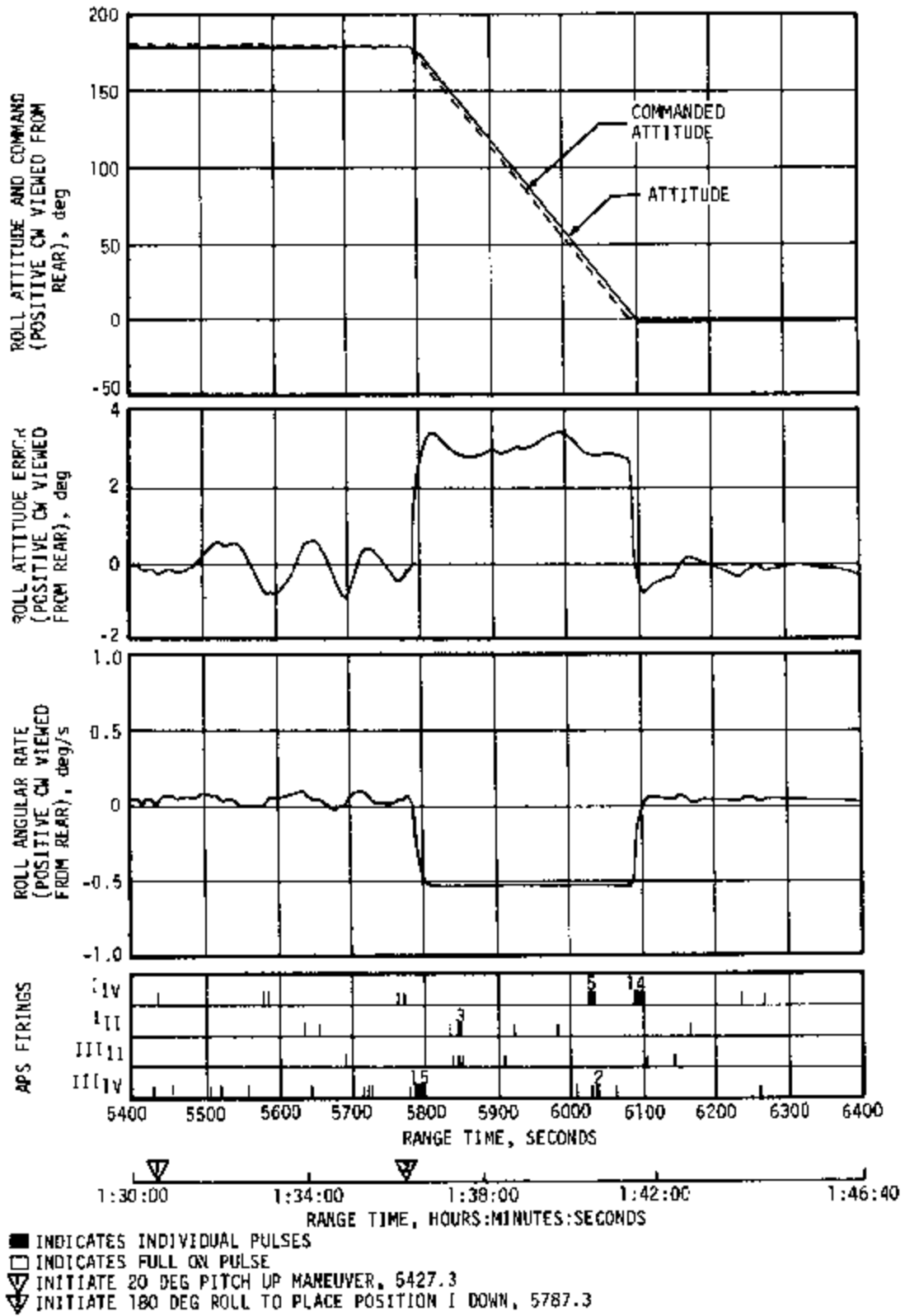


Figure 11-39. Roll Control Dynamics During Pitch and Roll Maneuvers

Figures 11-37, 11-38, and 11-39 show pitch, yaw, and roll control dynamics, respectively, during the 180 degrees counterclockwise roll maneuver to realign position I toward earth at 5787 seconds ($T_5 + 5040$ seconds). No high frequency (19.5 to 22 hertz) oscillations were experienced during initiation or recovery phases of this maneuver.

11.5.3 Control System Evaluation During Restart Attempt

Pitch and yaw commanded and actual attitudes, attitude errors, angular rates, and actuator positions during S-IVB restart are shown in Figures 11-40 and 11-41. The roll attitude error, angular rate, and attitude control system engine firings during this interval are shown in Figure 11-42. An auxiliary hydraulic system failure (see Section 8.6) prevented the J-2 engine from being centered at the time of S-IVB engine start command. The engine position at ESC was approximately 1.5 degrees in pitch and -2.3 degrees in yaw. Disturbances experienced during chill-down were relatively small but increased to a significant magnitude during a short time interval when the thrust built up to approximately 44,482 Newtons (10,000 lbf). This can be seen on both pitch and yaw rates at 11,626 seconds. The apparent discontinuities in yaw and pitch attitude errors at 11,630.33 seconds were due to the shift from T_6 to T_7 . At T_7 initiation the commanded attitude was set at the instantaneous cutoff attitude, thus nullifying any attitude errors which were present at S-IVB main engine cutoff. The thrust vector control system did not provide pitch and yaw control during the short time interval that this system was active due to the aforementioned lack of hydraulic system pressure.

11.5.4 Control System Evaluation After Restart Attempt

With failure to achieve restart, the LVDC went into T_7 and initiated the planned maneuver to the attitude desired for spacecraft separation. The spacecraft was actually separated by ground command to the spacecraft just after initiation of the maneuver. This caused the S-IVB/IU center of gravity to move further aft than normal due to the large LOX mass still onboard. This condition reduced the available APS control moment, thus requiring longer APS firings and greater propellant consumption than normal to complete the separation maneuver and to control propellant sloshing.

The pitch and yaw channels of the APS were activated at approximately 11,633.8 seconds ($T_7 + 3.5$ seconds) after which the pitch engine at position III (III_P) and yaw engines I_{II} and III_{II} came full on. The pitch engine remained on for approximately 67 seconds. The extended control engine firings were attributed to initial rates at S-IVB cutoff (pitch -0.5 deg/s, yaw 0.45 deg/s), the spacecraft separation maneuver (11,650 seconds), spacecraft separation, propellant sloshing, and LOX venting. The attitudes, attitude errors, and body rates about the three axes are shown in Figures 11-40, 11-41, and 11-42.

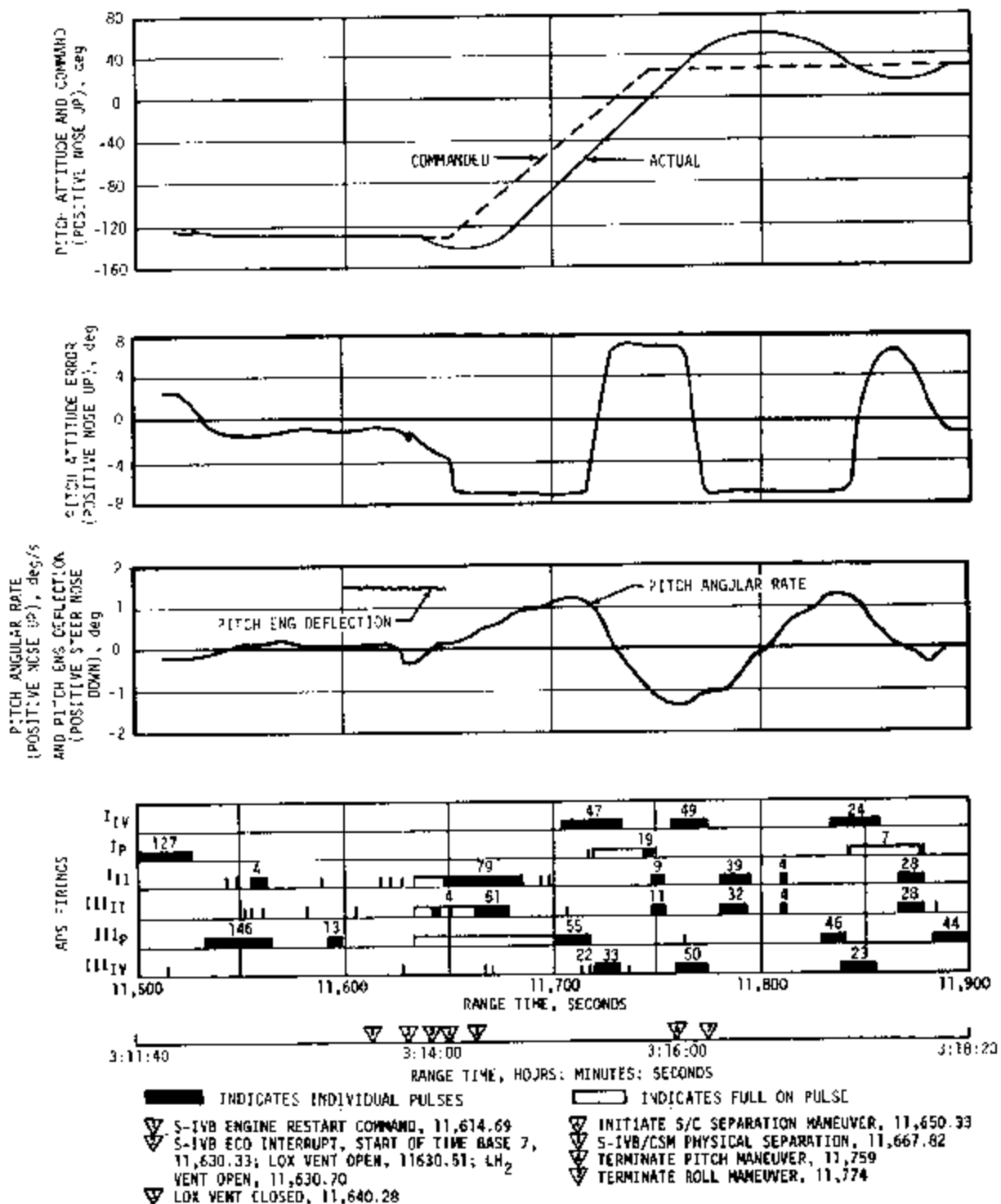


Figure 11-40. S-IVB Pitch Attitude Errors and Rates During Attempted Second Burn

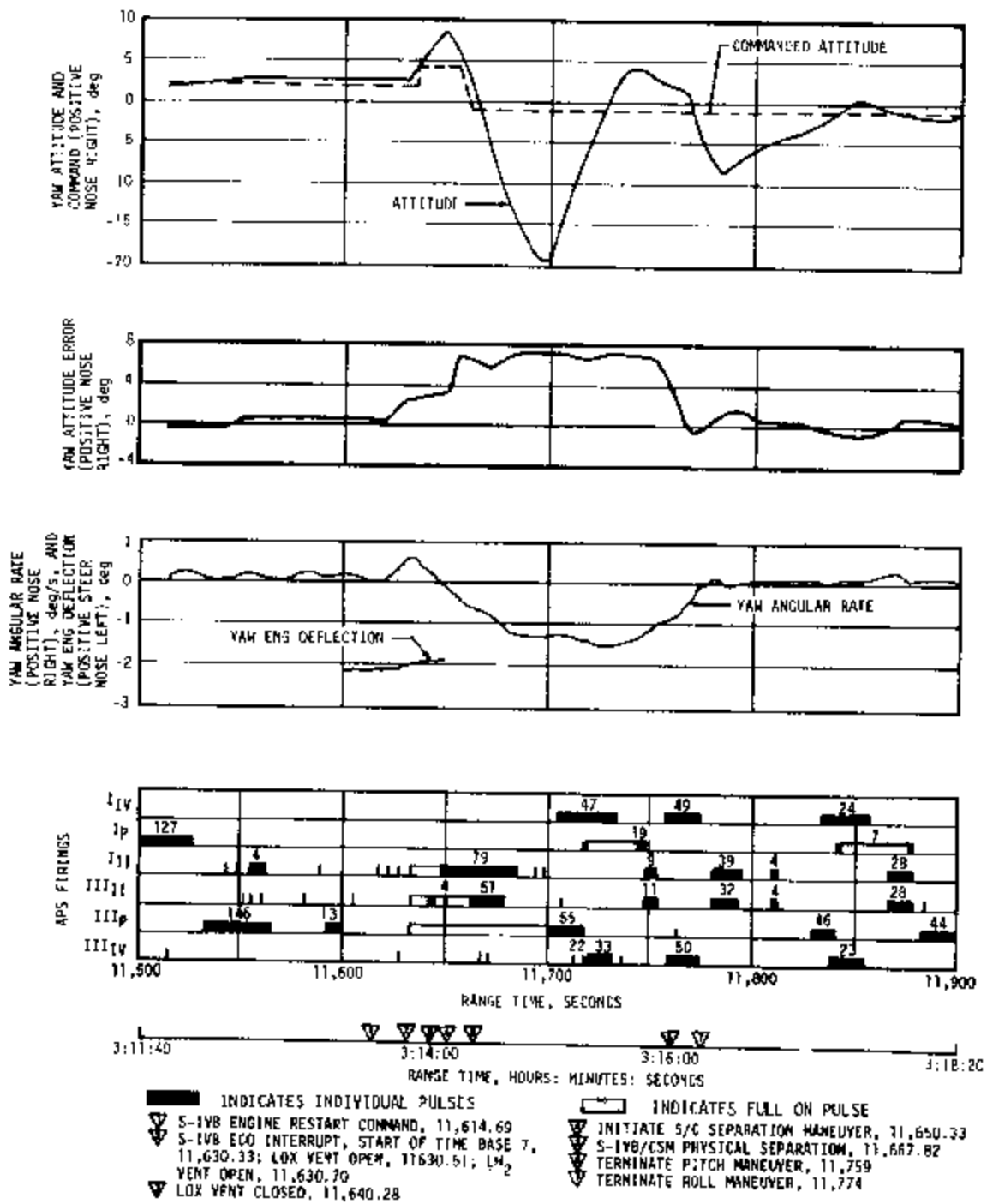


Figure 11-41. S-IVB Yaw Attitude Errors and Rates During Attempted Second Burn

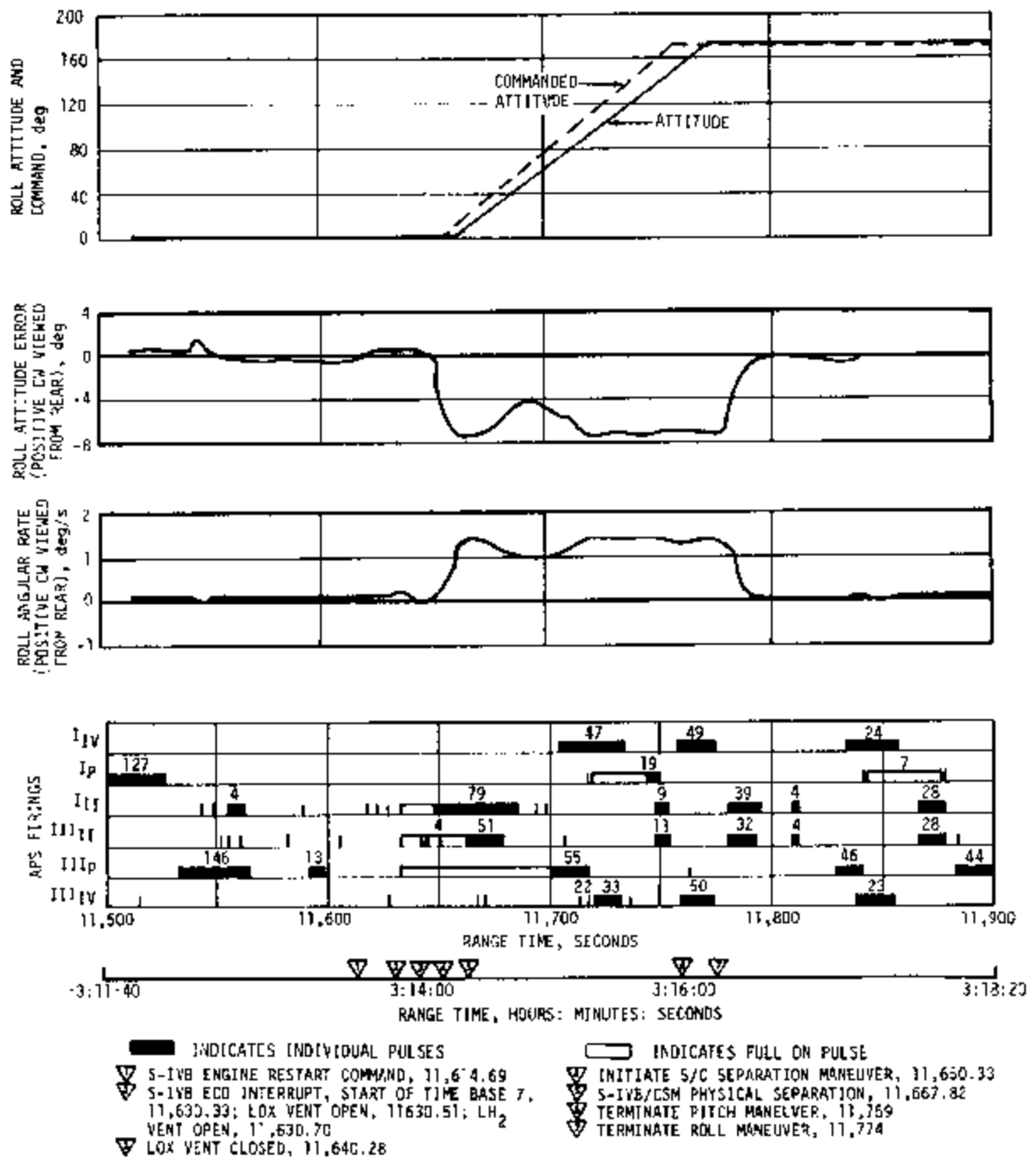


Figure 11-42. S-IVB Roll Attitude Errors and Rates During Attempted Second Burn

APS engine chamber pressure was used to determine the times when the APS modules ceased to function. At 21,953 seconds, the APS module at position I showed total fuel depletion, followed by oxidizer depletion at 22,053 seconds. At 22,053 seconds, the yaw angular rate began to diverge due to a LOX vent initiated at 22,023 seconds. Fuel depletion occurred in the module at position III at 22,602 seconds; oxidizer depletion occurred at 22,634 seconds. At this time the pitch and roll rates began to increase and reached approximately -8.5 deg/s and 1.0 deg/s, respectively, at 22,800 seconds. The vehicle continued to roll, resulting in oscillating pitch and yaw angular rates. Depletion of the APS propellants and subsequent loss of attitude control is reasonable when considering the relatively large and unexpected demands on the control system, particularly following S-IVB first cutoff and following the attempted restart and spacecraft separation. The large LOX mass remaining following spacecraft separation reduced the APS control moment arm which resulted in greater propellant consumption for maneuvers and slosh induced disturbances. The attitude dynamics for this time period are shown in Figure 11-43. The offscale measurements in pitch, yaw, and roll shown in Figure 11-43 are due to LYDC software limitations.

Pitch and yaw attitude rates began to increase after depletion of propellant in the APS module at position III as shown at the top of Figure 11-44. Corresponding APS firing commands during the propellant depletion in this module are shown in the center of Figure 11-44. S-IVB/IU tumble rates obtained from reduction of radar tracking data for a period of nine days following launch are presented at the bottom of Figure 11-44. The rate buildup to 180 deg/s as indicated on the ninth day is attributed to propellant venting.

11.6 INSTRUMENT UNIT CONTROL COMPONENTS EVALUATION

11.6.1 Control-EDS Rate Gyros/Control Signal Processor Analysis

The analysis of the Control-EDS Rate Gyros/CSP indicated that the performance of this combination was normal. The highest detected rates occurred between 59 and 61 seconds and were excursions of approximately 18 hertz which reached peak amplitudes of -3.5 and -5.1 deg/s in the pitch and roll axes, respectively. Analysis indicated that the rate switch filters in the CSP performed nominally.

11.6.2 Flight Control Computer Analysis

The FCC performed normally throughout boost and coast phases of flight. Analysis of the angular velocity and attitude error signals indicated that these signals, as telemetered from the FCC, were similar to the same signals telemetered from the originating component.

The maximum FCC output current was 46.5 milliamps and occurred at 419 seconds, as evidenced on the four pitch 50-milliamps servo amplifier telemetry signals. This resulted from the premature cutoff of two S-II stage engines. This value represents 93 percent of the current available from the FCC servo amplifiers.

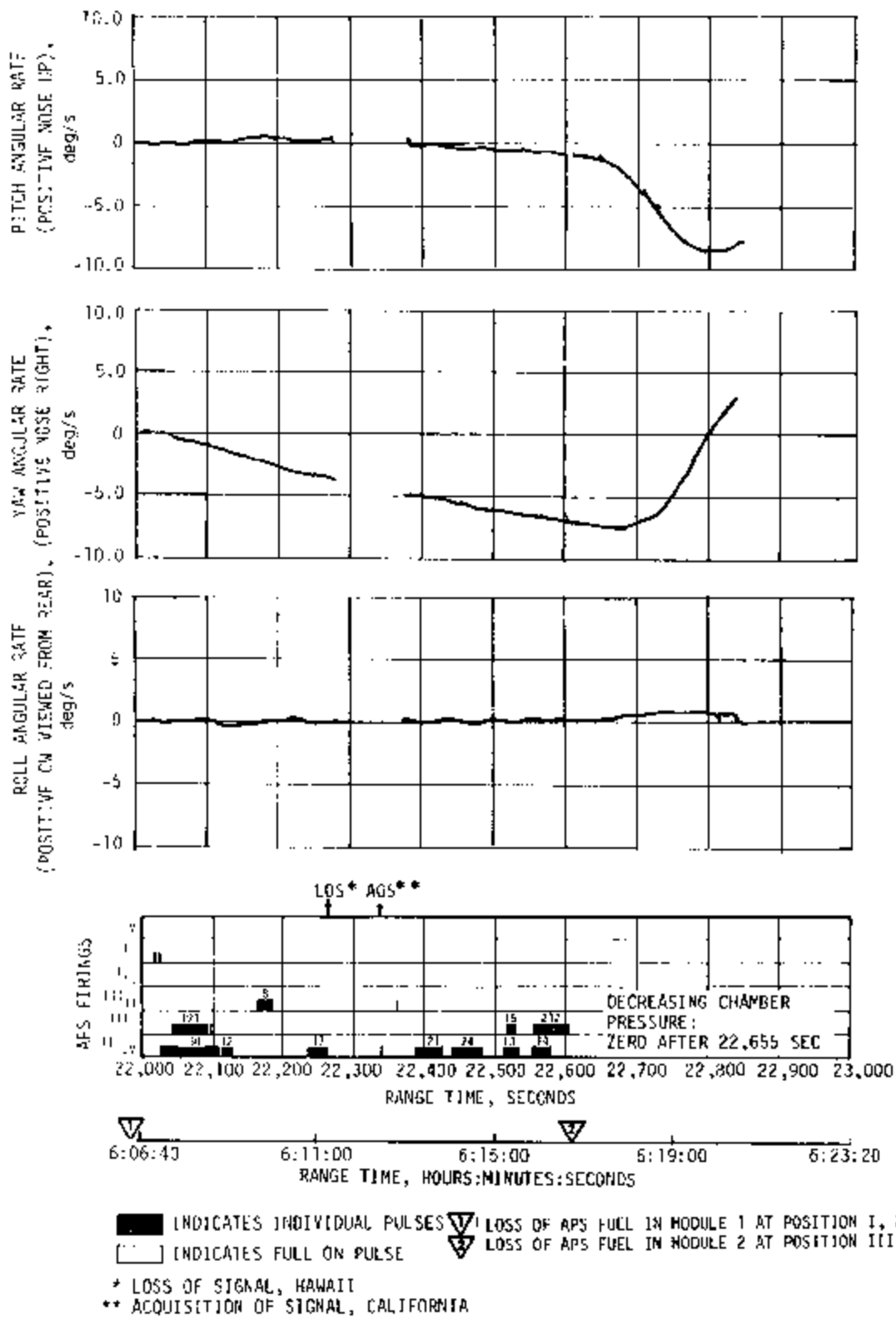


Figure 11-43. Pitch, Yaw, and Roll Dynamics at Loss of Control

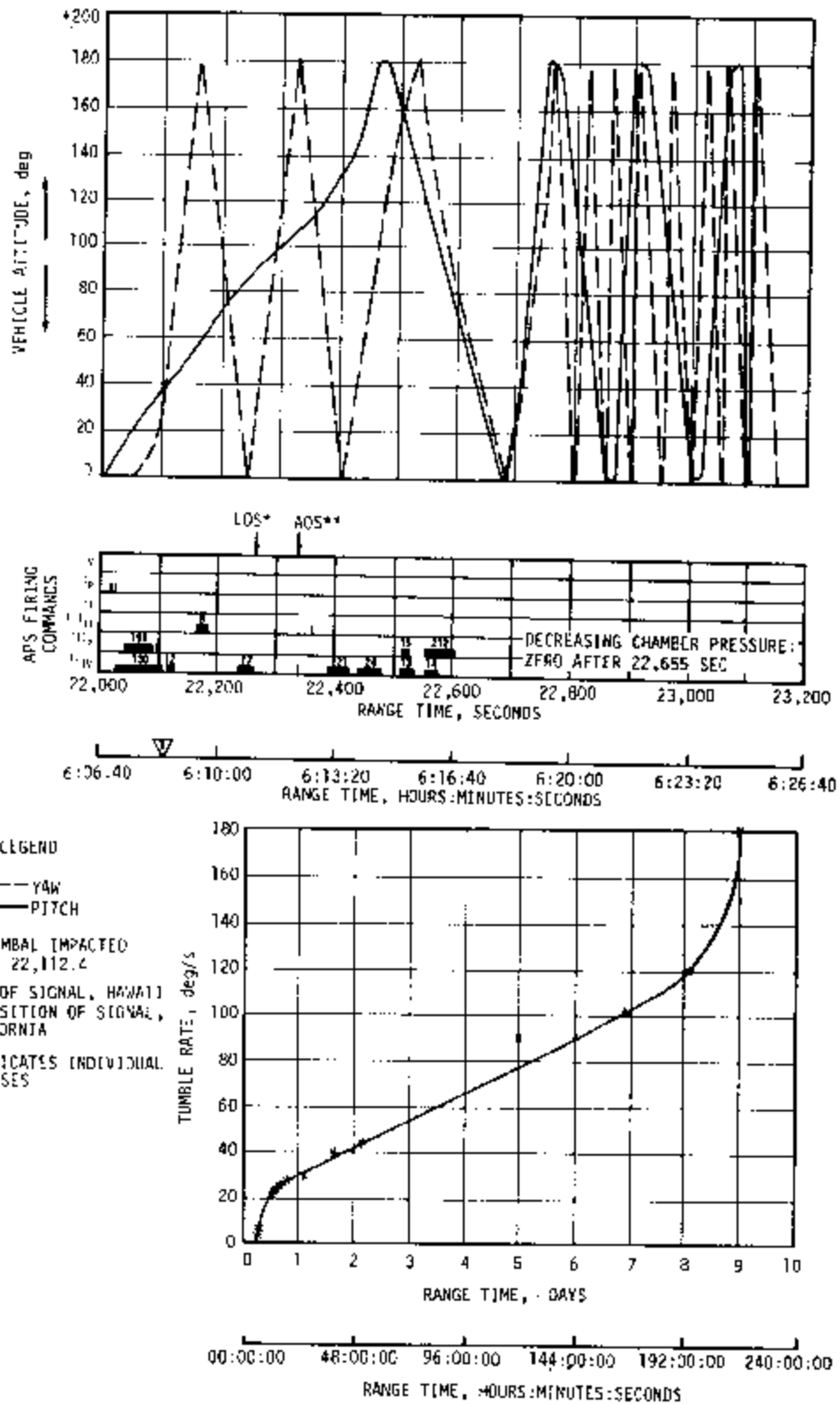


Figure 11-44. S-IVB/IU Tumble Rate History

SECTION 12

SEPARATION

12.1 SUMMARY

S-IC retro motor performance was satisfactory with negligible thrust imbalance in the pitch and yaw planes. The S-IC retro motor data indicate that some parameters were either above normal or possibly above the maximum limits but caused no problem. S-IC/S-II separation and associated sequencing occurred as planned with adequate clearance between stages.

Available data indicated that the S-II ullage motors operated as expected. The loss of S-II main engines No. 2 and 3, with a consequent longer stage burn time, caused loss of ullage motor data on the post S-II cutoff on-board tape recorder playback. Photographic coverage and simulation analysis showed that no problems were encountered during second plane separation.

The S-II retro motors performed as desired; minor deviations from nominal performance in no way impaired their function. The S-IVB ullage motors performed satisfactorily, with performance values very close to those predicted and within design specifications.

The S-IVB separated from the S-II faster than predicted, primarily because of the 40 percent loss of S-II tailoff thrust. The loss of tailoff thrust resulted in a moment on the separating S-II stage. The pitch attitude error caused the S-IVB engine to be gimballed 6.5 degrees during separation; however, this resulted in no clearance or control problems.

Spacecraft separation was initiated by ground command to the spacecraft during the maneuver to separation attitude. There were no Service Module Propulsion System (SPS) engine bell clearance problems during spacecraft separation; however, there may have been a momentary interference between the Command and Service Modules (CSM) and the Spacecraft Lunar Module Adapter (SLA) panel at the separation plane. Any momentary interference was not detrimental to the separation. Therefore, initiation of spacecraft separation during the maneuver to separation attitude did not result in any significant problems.

A summary of separation events and times of occurrence is given in Table 12-1.

Table 12-1. Separation Event Times

EVENT	ACTUAL TIME (SEC)		PREDICTED TIME (SEC)	
	RANGE TIME	TIME BASE +	RANGE TIME	TIME BASE +
LVDC Interrupt (S-IC OECO Sensed), Start of Time Base 3 (T ₃)	148.41	--	147.56	--
S-II Ullage Motor Fire Signal	148.87	0.45	148.06	0.50
S-IC/S-II Separation Command	149.08	0.67	148.26	0.70
S-IC Retro Motor EBW Fire Signal	149.10	0.59	148.43	0.87
S-IC/S-II Physical Separation	149.14	0.73		
S-II Engine Start Command	149.76	1.35	148.96	1.40
S-II Second Plane Separation Command	179.06	30.65	178.26	30.70
LVDC Interrupt (S-II ECO Sensed), Start of Time Base 4 (T ₄)	576.33	--	517.69	--
S-IVB Ullage Motor Burn Time Initiation (Avg. of 2)	576.98	0.65	518.39	0.70
75 Percent Ullage Thrust	577.07	0.74		
S-II/S-IVB Separation Command	577.08	0.75	518.49	0.80
S-II Retro Motor Fire Command	577.08	0.75	518.49	0.80
10 Percent Retro Thrust	577.11	0.78		
S-II/S-IVB Physical Separation	577.13	0.80		
90 Percent Retro Thrust	577.13	0.80		
S-IVB Engine Start Sequence Command	577.28	0.95	518.69	1.00
S-II/S-IVB Separation Complete	578.07	1.74		
S-IVB ECO Interrupt, Start of Time Base 7 (T ₇)	11,630.33	--	11,728.09	--
Spacecraft Separation Command	11,666.02	35.69		
S-IVB-IU/CSM Physical Separation Complete	11,667.82	37.49	11,908.09	180.00

12.2 S-IC/S-II SEPARATION EVALUATION

12.2.1 S-IC Retro Motor Performance

Ignition signal to the retro motors occurred at 149.10 seconds. The performance of all S-IC retro motors was satisfactory, although a review of the data, shown in Table 12-2, indicates that some parameters were either above normal or possibly above the maximum limit. Computed effective impulse values based on combustion pressure data were apparently above the maximum limit shown in the model specification but caused no problems. The average effective pressure and average effective thrust were generally higher than normal, although all were within the upper limit allowable according to the model specification. These higher than normal data are being given further study but are believed to be caused, at least partially, by differences between static and flight measurement conditions which could cause higher than "real" pressure records. If, on the other hand, the pressure transducers were reading actual chamber pressure, the retro motors and the stage attachment hardware were structurally adequate to withstand the higher loads. A test program has been initiated to compare the chamber pressure transducer used in flight and its environment with the transducer used and environment encountered during the qualification testing. The qualification testing established nominal performance and 3 sigma limits.

Thrust imbalance in the pitch and yaw plane was negligible. Figure 12-1 shows thrust versus time for the retro motor with the highest maximum thrust (fin D, position IV) and for the retro motor with lowest maximum thrust (fin B, position III).

12.2.2 S-II Ullage Motor Performance

The S-IC onboard camera system which viewed the S-IC/S-II separation provided evidence that all four S-II ullage motors fired.

This evidence agrees with the thrust buildup observed from S-II telemetry data. No additional information about performance can be determined from telemetry data, since the quality of S-II ullage motor chamber pressure data was inadequate for detailed analysis because of telemetry attenuation. This attenuation was due to S-IC retro motor firing. The ullage motor data is normally obtained from onboard tape recorder playback after S-II cutoff. Due to the longer than planned burn time, this taped information was not played back.

12.2.3 S-IC/S-II Separation Dynamics

S-IC/S-II separation and associated sequencing was accomplished as planned. Subsequent S-IC and S-II dynamics provided adequate positive clearance between the stages. The predicted and measured dynamic pressures at separation were 0.1123 and 0.1189 N/cm², (23.46 and 24.84 lbf/ft²), respectively. Dynamic conditions at separation fell within estimated end conditions and well within staging limits.

Table 12-2. S-1C Retro Motor Performance

RETRO MOTOR	PARAMETER				
	EFFECTIVE BURN TIME (sec) ¹	AVG EFFECTIVE PRESSURE N/cm ² (psia) ²	TOTAL IMPULSE N-s (lbf-s) ³	EFFECTIVE IMPULSE N-s (lbf-s) ⁴	AVG EFFECTIVE THRUST N (lbf) ⁵
Fin A - Pos I	0.669	1161 (1684)	289,935 (65,180)	266,831 (59,986)	398,969 (89,692)
Pos II	0.648	1194 (1732)	288,894 (64,946)	262,294 (58,966)	405,024 (91,053)
Fin B - Pos II	0.646	1196 (1734)	292,373 (65,728)	262,098 (58,966)	405,851 (91,239)
Pos III	0.648	1163 (1687)	278,254 (62,554)	255,991 (57,549)	395,109 (88,824)
Fin C - Pos III	0.560	1191 (1727)	298,818 (67,177)	265,750 (59,743)	402,955 (90,588)
Pos IV	0.567	1149 (1667)	283,369 (63,704)	258,811 (58,183)	388,023 (87,231)
Fin D - Pos IV	0.656	1207 (1751)	298,182 (67,034)	266,947 (60,012)	406,994 (91,496)
Pos I	0.645	1173 (1701)	281,621 (63,511)	257,005 (57,777)	398,765 (89,646)
Average	0.655	1179 (1710)	288,930 (64,554)	261,965 (58,892)	400,211 (89,971)
Nominal 294.1°K (70°F) Motor	0.633	1128 (1636)	No Spec	247,342 (55,605)	391,055 (87,913)
-3σ Limit 271.9°K (30°F) Motor	0.661*	1000 (1451)	No Spec	242,173 (54,443)	352,426 (79,229)
+3σ Limit 321.9°K (120°F) Motor	0.698**	1284 (1862)	No Spec	252,507 (56,766)	440,096 (98,938)
		* At 321.9°K (120°F)			
		** At 271.9°K (30°F)			
¹ Effective Burning Time - The effective burning time is the interval from attainment of the initial 75 percent of maximum pressure on the ascending portion of the pressure trace to the same level on the decay portion of the pressure trace. ² Average Effective Pressure - The average effective pressure is the pressure-time integral between the limits of effective burning time divided by the effective burning time. ³ Total Impulse - Total impulse is the area under the thrust-time trace from zero time until the thrust returns to zero. ⁴ Effective Impulse - The effective impulse is the area under the thrust-time curve, between the limits of effective burning time. ⁵ Average Effective Thrust - The average effective thrust is the effective impulse divided by the effective burning time.					

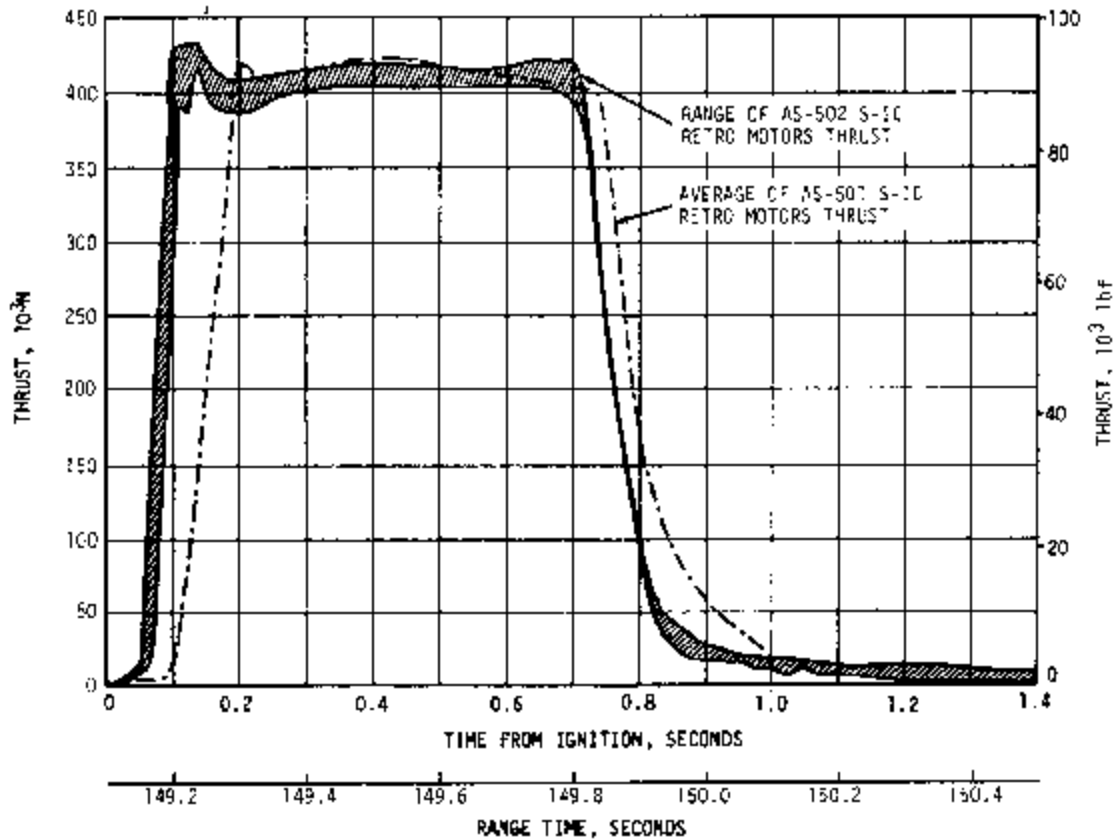


Figure 12-1. S-IC Retro Motor Thrust

The first plane separation was monitored by accelerometers and rate gyros on each of the two stages. Separation rate transducers (extensometers) provided relative separation rate and distance data. In addition, motion picture film provided a visual indication of the clearance between the two stages as they separated. For evaluation purposes, first plane separation dynamics were calculated using a computer program which took into account F-1 thrust decay, S-IC retro motor thrust, S-II ullage motor thrust, initial trajectory conditions, engine gimbal angles, and mass properties. The simulated first plane separation dynamics and separation distances agreed very well with the actual data.

Figure 12-2 shows separation distances and relative velocities of the two stages and their respective contributions to the total. These velocities are changes in velocity magnitudes from time of physical separation. The plot for separation distance also shows the point where the S-IC stage clears the J-2 engines, which extend beyond the separation plane by 0.41 meter (16 in.). Very close agreement between the AS-501 and AS-502 flights is seen. The separation time for the AS-502 flight was slightly longer than for AS-501 because only four ullage motors were used on AS-502 instead of the eight motors used on AS-501.

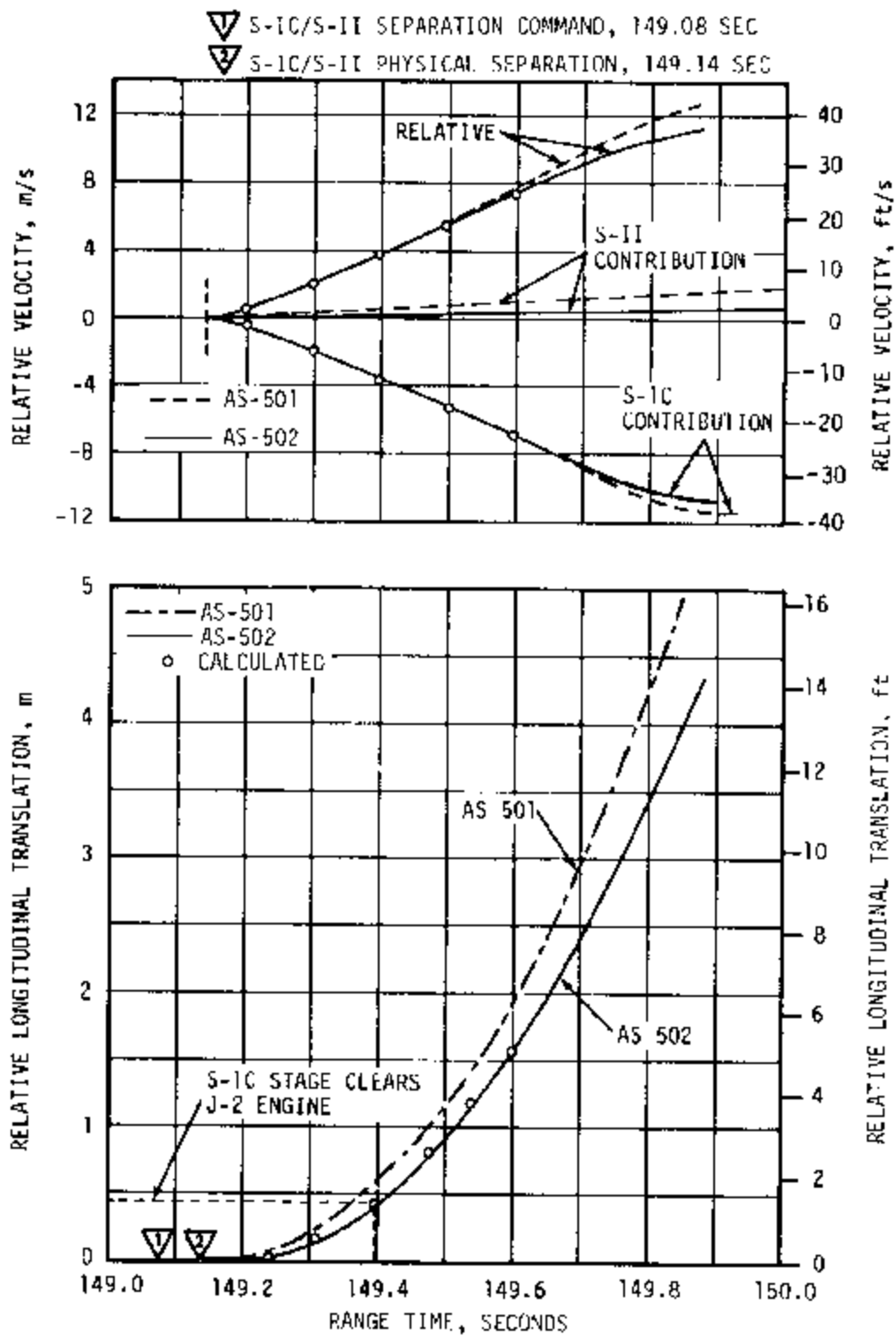


Figure 12-2. S-IC/S-II Relative Velocity and Separation Distance During First Plane Separation

Figure 12-3 shows lateral clearance and longitudinal accelerations for the separation. The minimum clearance was calculated to be 1.33 meters (52.4 in.) between engine No. 1 and the S-IC stage. The longitudinal acceleration indicated that physical separation occurred approximately 0.1 second earlier than AS-501. This was due to the retro motor thrust rising to full thrust 0.1 second earlier. Good agreement between calculated results and flight data existed for this flight.

S-IC angular dispersions during S-IC/S-II separation are shown in Figure 12-4. S-IC attitude deviations after separation were derived by integrating the measured angular rate. Figure 12-5 presents the angular dispersions of the S-II stage during separation. No significant difference existed between the AS-501 and AS-502 flights.

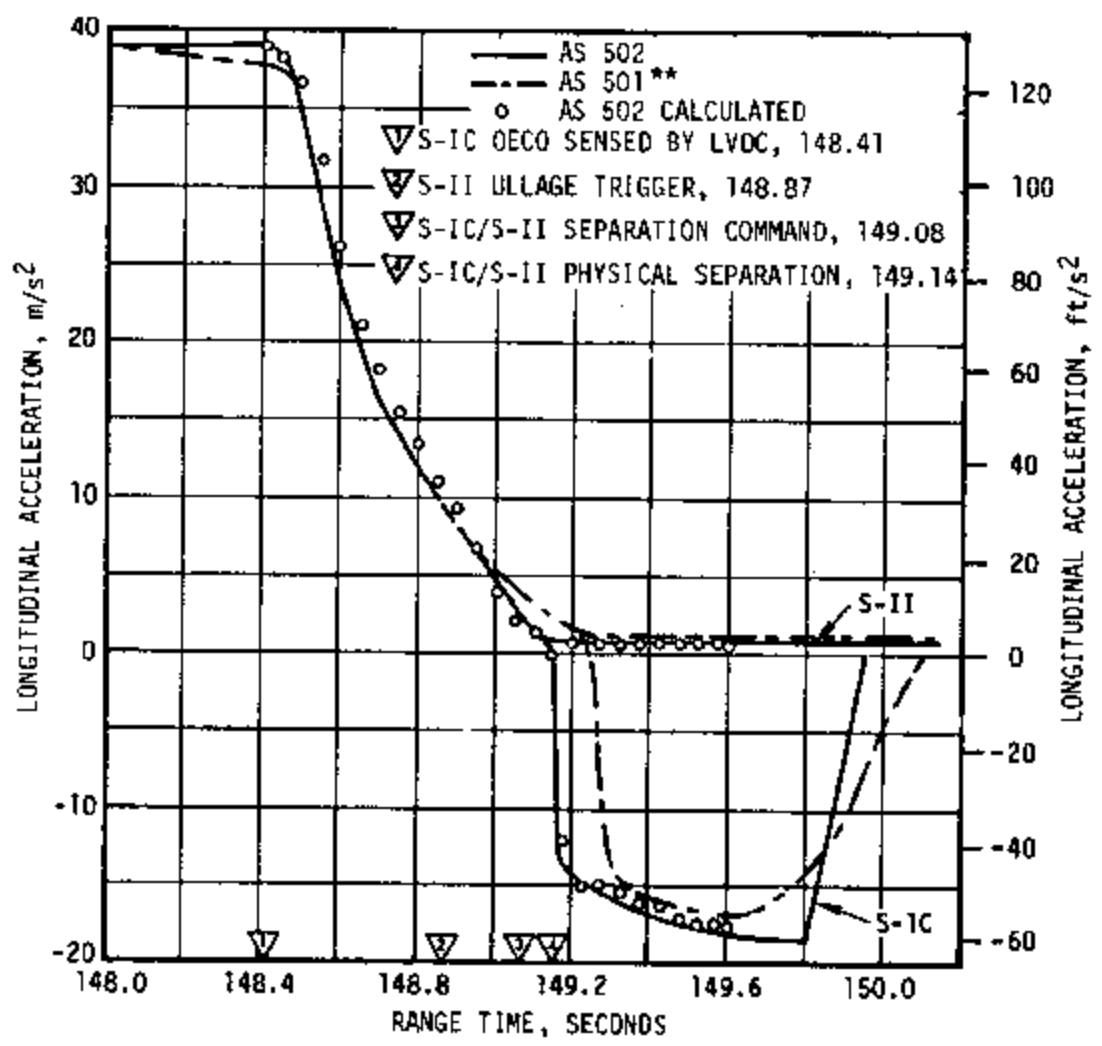
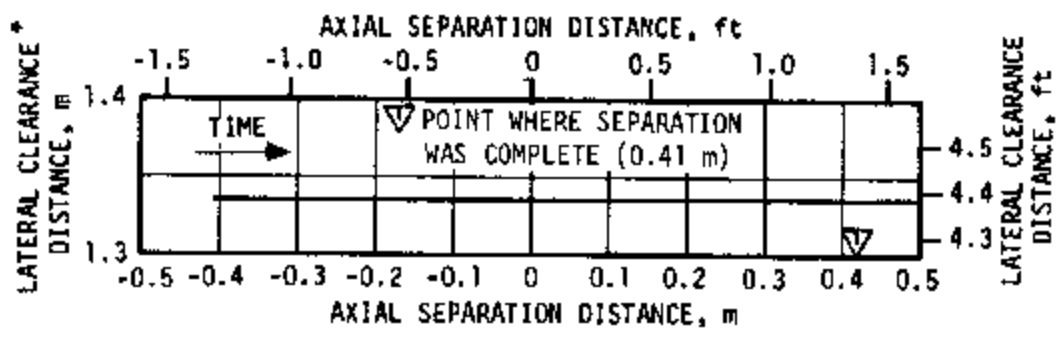
12.3 S-II SECOND PLANE SEPARATION EVALUATION

Photographic coverage provided the only means of adequately monitoring second plane separation. However, the dynamics of both the second stage and the separating interstage were calculated using a computer. These calculations utilized appropriate initial trajectory data, postflight mass characteristics, and J-2 engine plume characteristics obtained from flight data. The only flight data from film analysis available were relative velocity and relative displacement. All other data are calculated results.

The relative separation velocities, the relative velocity contribution of each body to the total, and relative separation distance between the two bodies are shown in Figure 12-6. Very good agreement is seen between AS-502 and AS-501 flight data. The velocities are the changes in velocities from time of physical separation and are calculated results. As was the case for the AS-501 flight, better agreement in relative velocity data between calculated and flight data was obtained by using an electrical disconnect force of zero pound. The relative separation data also indicate very good agreement between AS-501 and AS-502 flight data. The separation was complete when the interstage passed the bottom of the J-2 engines and was calculated to have occurred at approximately 180.12 seconds.

Figure 12-7 presents the angular dispersions of the S-II stage during separation. Attitude errors remained near zero for both flights during second plane separation.

The lateral clearance between the interstage and the engines was computed and is shown for each engine in Figure 12-8. The figure shows the lateral clearance, i.e., the clearance projected in the Y-Z plane, versus the body station on the interstage at which the least distance occurred. An arrow indicates direction of increasing time. There was a minimum clearance of 1.07 meters (42 in.) between engine No. 1 and the interstage rings at vehicle station 43.79 meters (1724 in.). The separation plane is located at vehicle station 44.70 meters (1760 in.). Figure 12-8 also presents the calculated body rates of the separating interstage, which are compared with those calculated for AS-501.



* THE DISTANCE BETWEEN SEPARATING S-IC STAGE AND THE J-2 ENGINE NOZZLE
 ** AS-501 IS COMPARED TO AS-502 FROM S-IC DECO SENSED BY LVDC

Figure 12-3. S-IC/S-II Clearance Distance and Longitudinal Acceleration During First Plane Separation

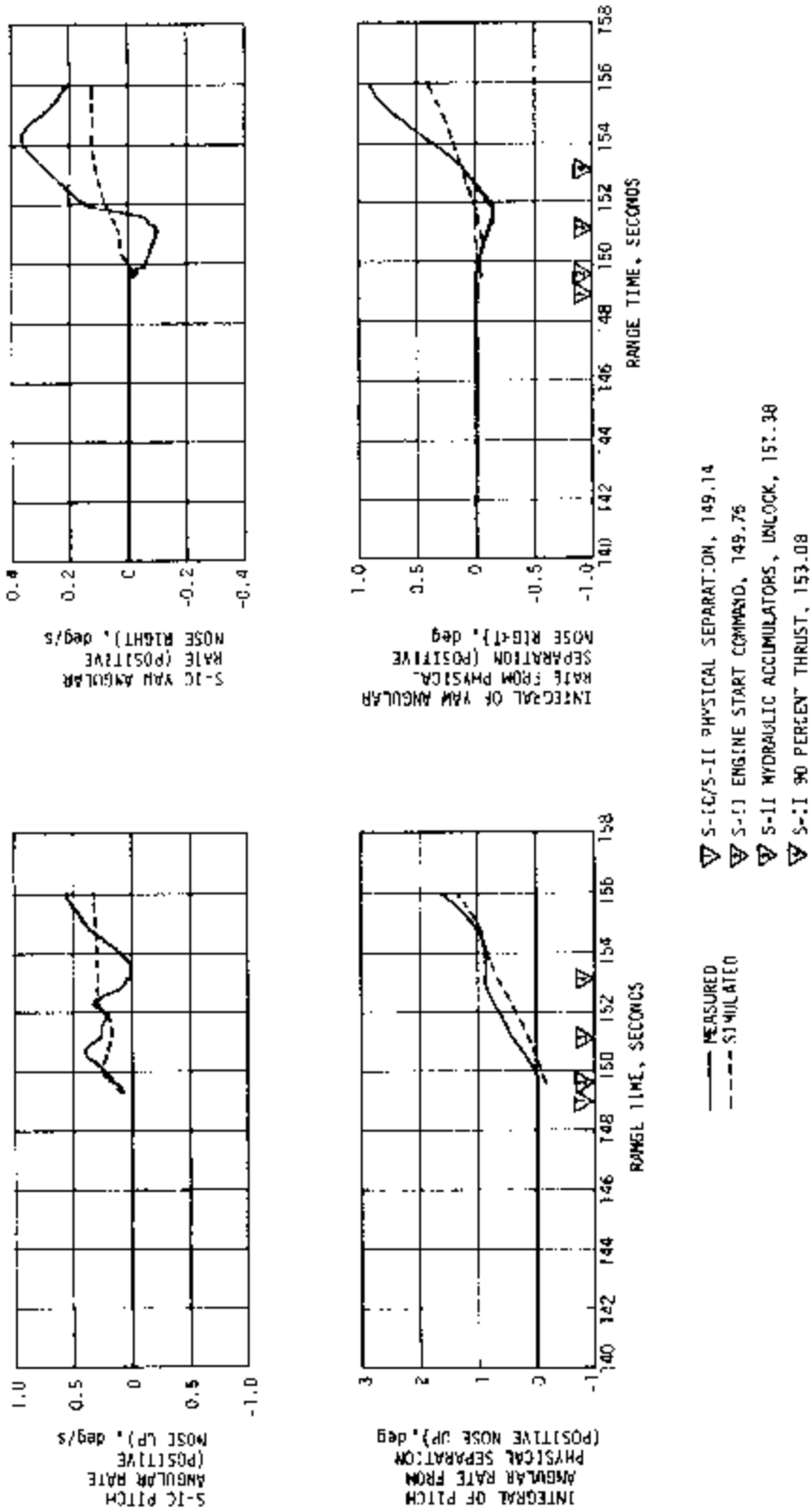
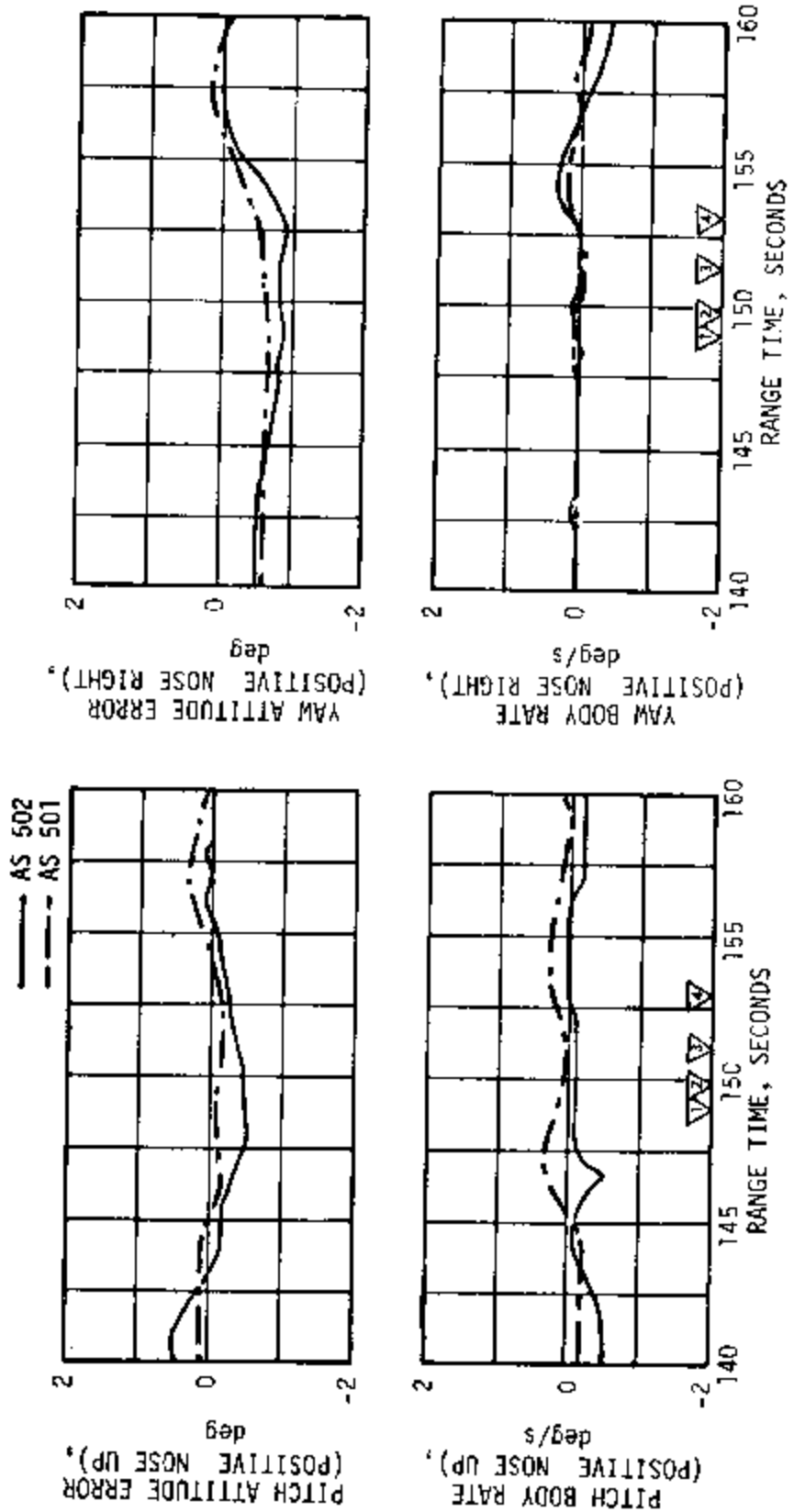


Figure 12-4. S-IC Pitch and Yaw Angular Dynamics Following S-IC/S-II Separation



▽ S-IC/S-II PHYSICAL SEPARATION, 149.14
 ▽ S-II ENGINE START COMMAND, 149.76
 ▽ S-II HYDRAULIC ACCUMULATORS, UNLOCK, 151.38
 ▽ S-II 90 PERCENT THRUST, 153.08

Figure 12-5. S-II Angular Dispersions During S-IC/S-II First Plane Separation

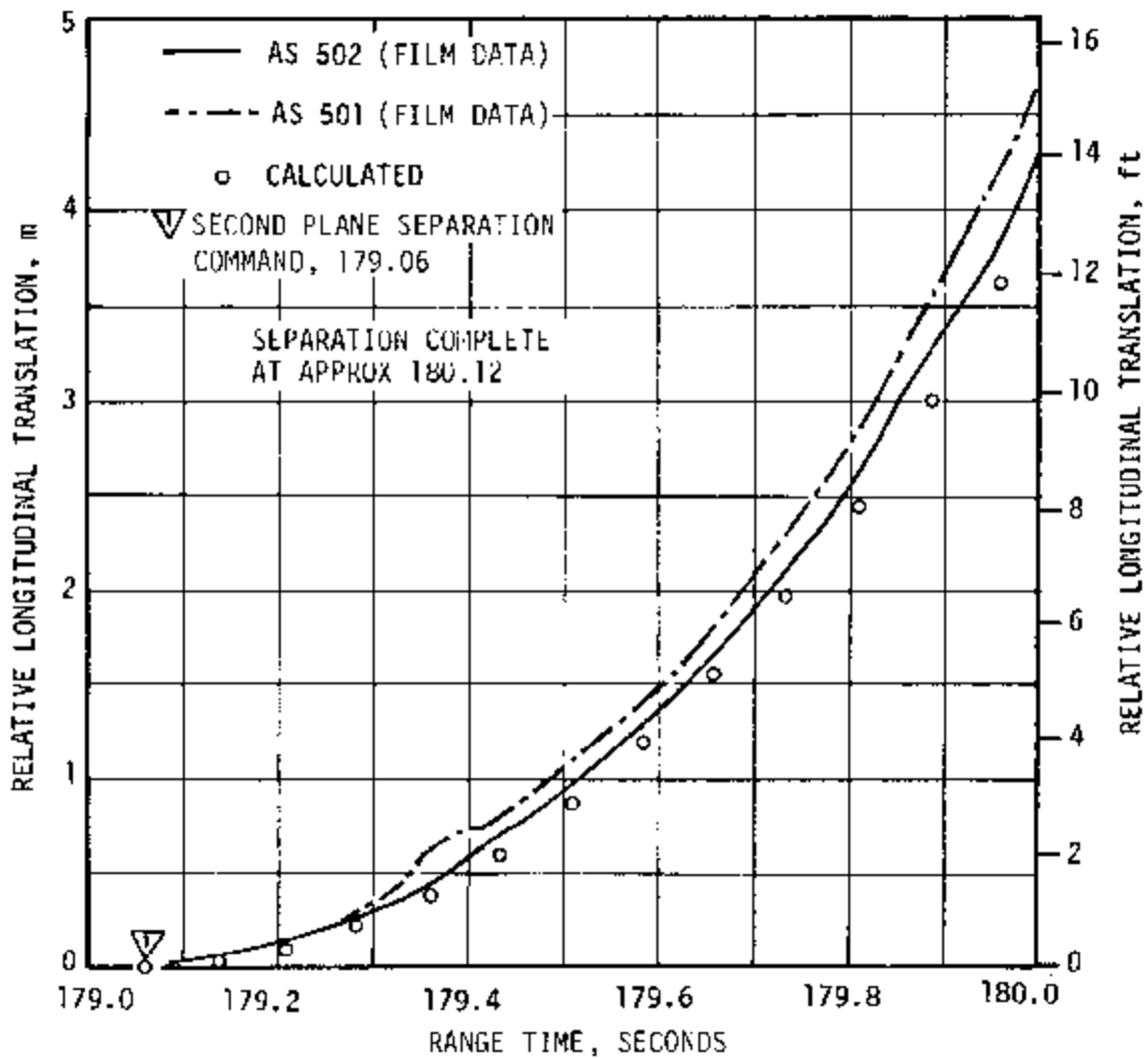
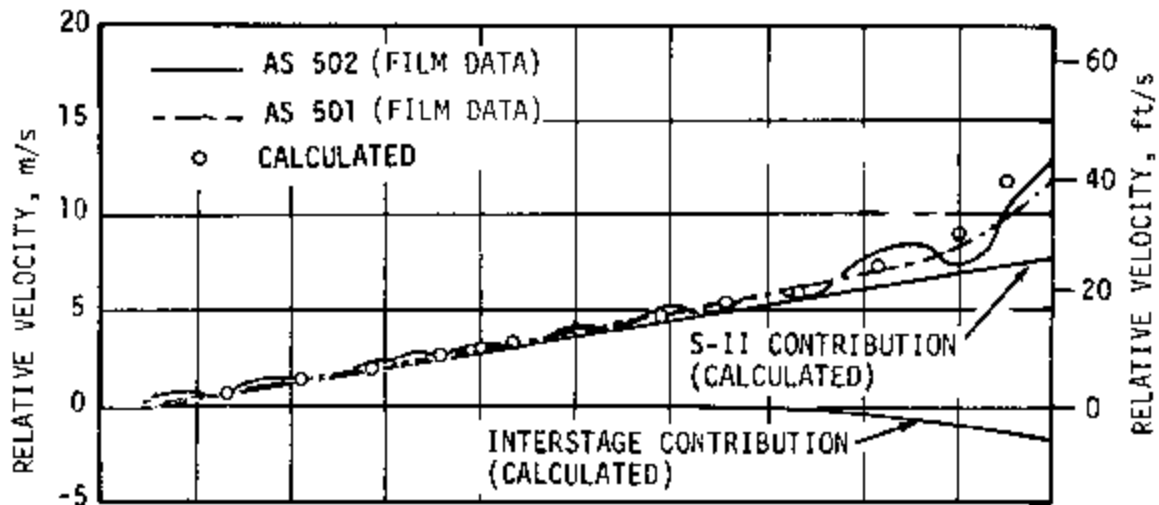


Figure 12-6. Interstage/S-II Relative Velocity and Separation Distance During Second Plane Separation

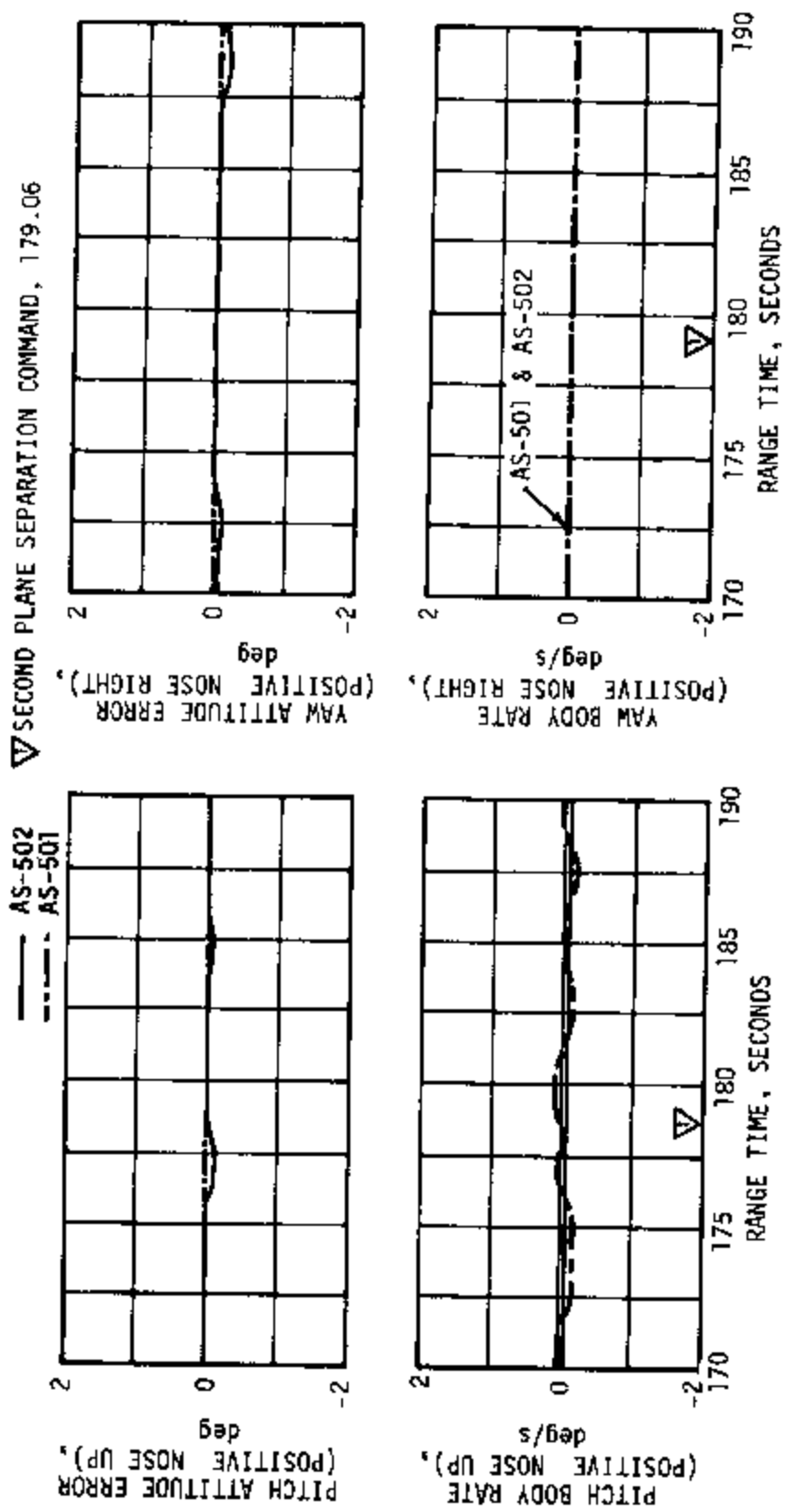
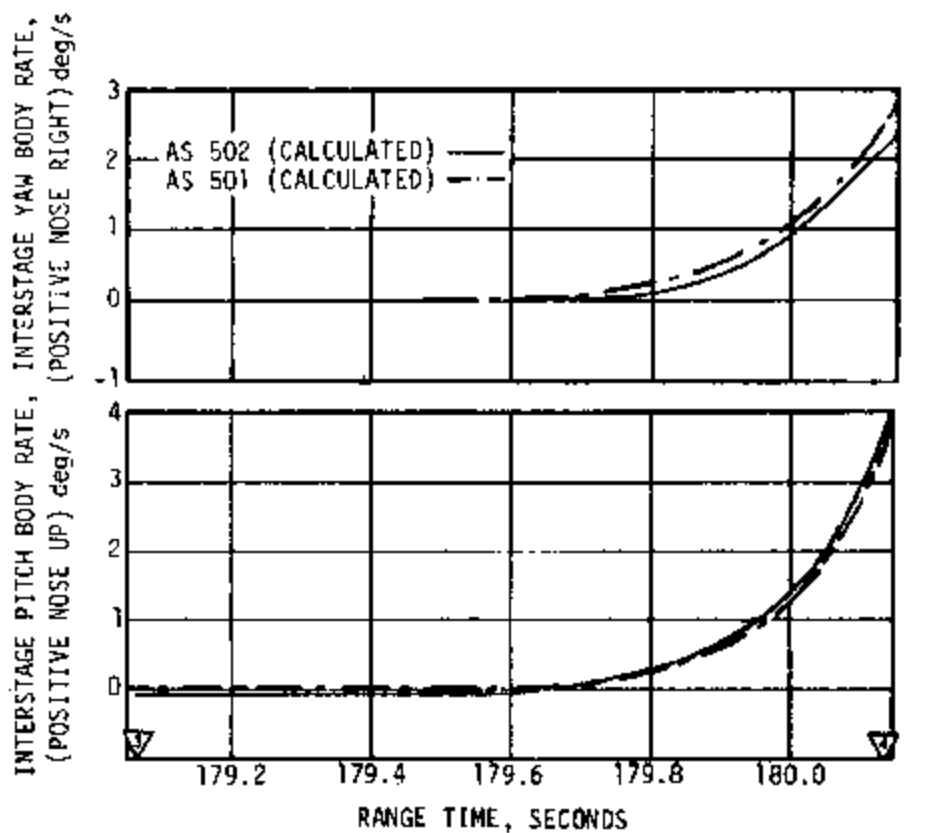
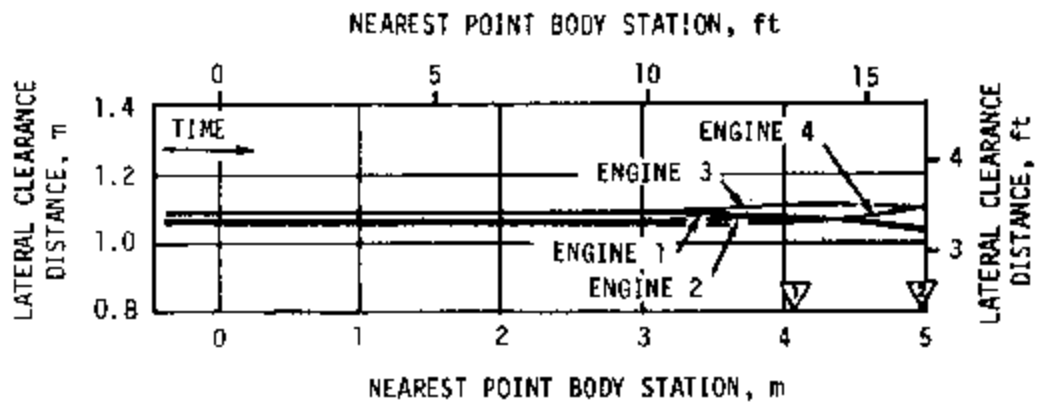


Figure 12-7. S-II Angular Dispersions During Second Plane Separation



- ▽ LOCATION OF INTERSTAGE RING, 4.05 m (13.3 ft)
- ▽ POINT WHERE SEPARATION WAS COMPLETE, 4.98 m (16.3 ft)
- ▽ SECOND PLANE SEPARATION COMMAND, 179.06
- ▽ SEPARATION COMPLETE, 180.12

Figure 12-8. Lateral Clearance Distance and Interstage Body Rates During Second Plane Separation

12.4 S-II/S-IVB SEPARATION EVALUATION

12.4.1 S-II Retro Motor Performance

The four retro motors mounted on the S-II stage performed satisfactorily and separated the S-II stage from the S-IVB stage. The pressure buildup for all four retro motors began within 0.02 second of each other at 577.08 seconds. The thrust and chamber pressure profiles for the four motors were very similar, and the maximum difference in burn times was 0.04 second. Prior to the flight a correlation between thrust and chamber pressure had been obtained from previous ground tests of similar retro motors. This correlation was used in a computer program to determine the retro motor thrust from the chamber pressure data during the AS-502 flight.

Table 12-3 presents the performance parameters for the individual motors. All parameters were within the nominal performance limits except for the burn time total impulse for motor A, which was slightly greater than the nominal maximum value but which had no detrimental effect on motor performance.

Table 12-3. S-II Retro Motor Performance

PARAMETER	MOTOR					SPECIFICATION LIMITS AT 288.9 °K (60 °F)	
	A POS [1-1]	B POS [1-1]	C POS [1-1]	D POS [1-1]	AVERAGE	MAXIMUM	MINIMUM
Burn Time ¹ , sec	1.56	1.52	1.51	1.54	1.53	1.67	1.38
Average Burn Time Chamber Pressure ² , N/cm ² (psia)	1196 (1734)	1180 (1711)	1182 (1715)	1206 (1749)	1191 (1727)	1293 (1875)	1065 (1545)
Maximum Thrust ³ , N (lbf)	181,487 (40,800)	174,370 (39,200)	174,815 (39,300)	181,043 (40,700)	177,929 (40,000)	193,142 (43,420)	152,129 (34,200)
Average Burn Time Thrust ⁴ , N (lbf)	161,786 (36,371)	157,885 (35,494)	157,271 (35,356)	152,520 (34,536)	159,865 (35,939)	134,232 (30,190)	175,416 (39,435)
Burn Time Total Impulse ⁵ , N-s (lbf-s)	250,768 (56,375)	239,986 (53,951)	237,477 (53,387)	250,279 (56,265)	244,630 (54,995)	250,435 (56,300)	232,597 (52,290)

¹ Burn Time - Defined in Section 6.2.1.30 of Thiokol Model Specification TEMS-11.

² Burn Time Average Chamber Pressure - The average chamber pressure during burn time is the area under the pressure time curve over the burn time, divided by the burn time.

³ Maximum Thrust - The highest thrust developed by the rocket motor under any normal operating condition excluding ignition.

⁴ Burn Time Average Thrust - The average thrust during burn time is the burn time total impulse divided by the burn time.

⁵ Burn Time Total Impulse - The area under the thrust-time curve over the burn time.

A thrust profile for the retro motors is shown in Figure 12-9. The smoothness of the thrust traces for motor B and motor D is due to the fact that the chamber pressure data for these two motors were not good on the tape used for the computer program and therefore had to be entered in tabular form from other telemetered data.

12.4.2 S-IVB Ullage Motors

Ullage motor performance was satisfactory. The ullage motor ignition command was given at 576.98 seconds, with the jettison command at 589.08 seconds. These times, relative to engine start command, were very close to predicted. Table 12-4 presents the individual motor performance parameters. A comparison of these data with nominal performance limits indicates that both motors performed within design specifications. Figure 12-10 presents the thrust profiles during burn.

12.4.3 S-II/S-IVB Separation Dynamics

Separation of the S-IVB stage from the S-II stage was accomplished 0.07 second faster than predicted time for a nominal separation (0.99 second). This was caused by lower than nominal S-II tailoff thrust level due to two engines out. Physical separation occurred 0.05 second after the separation command (established from extensometer data). Engines No. 2 and 3 out resulted in a moment on the separation S-II stage which caused a positive S-II pitch rate and caused the critical separation point to be on the position I side of the S-IVB thrust structure. This moment reduced the clearance distance to approximately 15.2 centimeters (6 in.) in the direction of position I.

Table 12-1 contains significant times and events for the S-II/S-IVB separation. Figure 12-11 presents the axial separation history and relative velocities between the two stages during S-II/S-IVB separation. Also shown are the predicted and actual AS-501 separation histories.

Figure 12-12 shows the longitudinal acceleration for the S-II and S-IVB stages. The reconstructed acceleration histories were obtained from S-II and S-IVB accelerometer data.

The angular rates for both the S-II and the S-IVB stages are presented in Figures 12-13 and 12-14. The S-II rates were all approximately zero at physical separation. The S-II pitch rate increased to almost 2 deg/s by separation complete. The yaw rate increased to 0.95 deg/s by separation complete and the roll rate remained approximately zero throughout separation. The S-IVB rates were all small with pitch and yaw rates less than ± 0.2 deg/s.

The path of the interstage lip during separation is shown in Figure 12-15. The closest approach point was a point on the S-IVB engine bell at position I. The 7.6 degree pitch attitude error existing at S-II/S-IVB separation caused the S-IVB engine to be gimballed 6.5 degrees in the direction

Table 12-4. S-IVB Ullage Motor Performance

PARAMETER	UNIT	MOTOR A (POS II - III)	MOTOR B (POS IV - I)	SPECIFICATION LIMITS AT 294.1°K (70°F)	
				MAXIMUM	MINIMUM
Burn Time ¹	sec	3.81	3.80	4.10	3.54
Average Burn Time Chamber Pressure ²	N/cm ² (psia)	672 (975)	690 (1001)	741 (1075)	627 (910)
Maximum Thrust ³	N (lbf)	15,684 (3526)	15,916 (3578)	17,344 (3899)	14,185 (3189)
Average Burn Time Thrust ⁴	N (lbf)	15,048 (3383)	15,449 (3473)	16,841 (3786)	13,745 (3090)
Burn Time Total Impulse ⁵	N-s (lbf-s)	57,333 (12,889)	58,703 (13,197)	60,451 (13,590)	55,603 (12,500)
<p>¹ Burn Time - Time beginning when the pressure has risen to 10 percent of the maximum chamber pressure and ending when the pressure has dropped to 75 percent of the maximum chamber pressure.</p> <p>² Average Burn Time Chamber Pressure - The area under the pressure-time curve during burn time divided by burn time.</p> <p>³ Maximum Thrust - The highest thrust developed by the rocket motor under any normal operating condition excluding the first 0.20 seconds of operation.</p> <p>⁴ Average Burn Time Thrust - The burn time total impulse divided by the burn time.</p> <p>⁵ Burn Time Total Impulse - The integral of thrust with respect to time between the burn time limits.</p>					

of position I during separation. The gimbaleed engine and S-11 moment resulted in a total clearance of approximately 1.60 meters (63 in.) out of a total available clearance of 2.06 meters (81 in.), presenting no clearance or control problems.

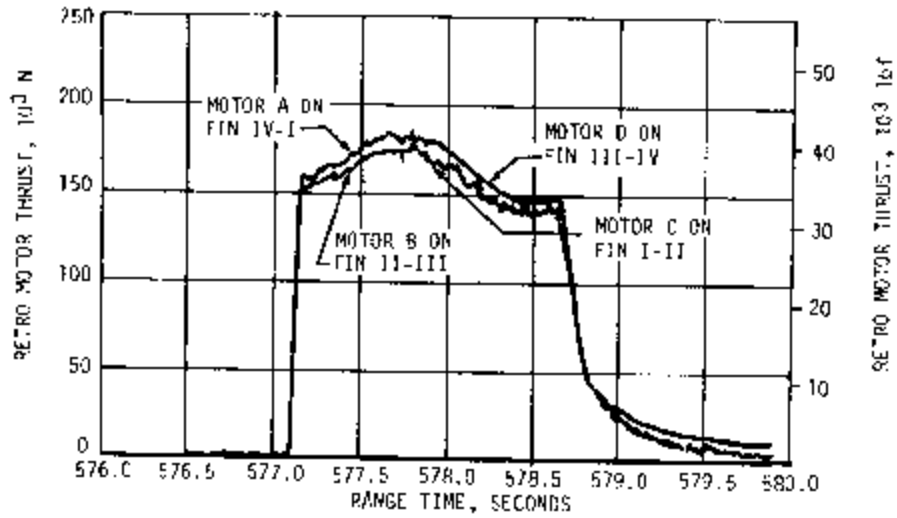


Figure 12-9. S-II Retro Motor Thrust

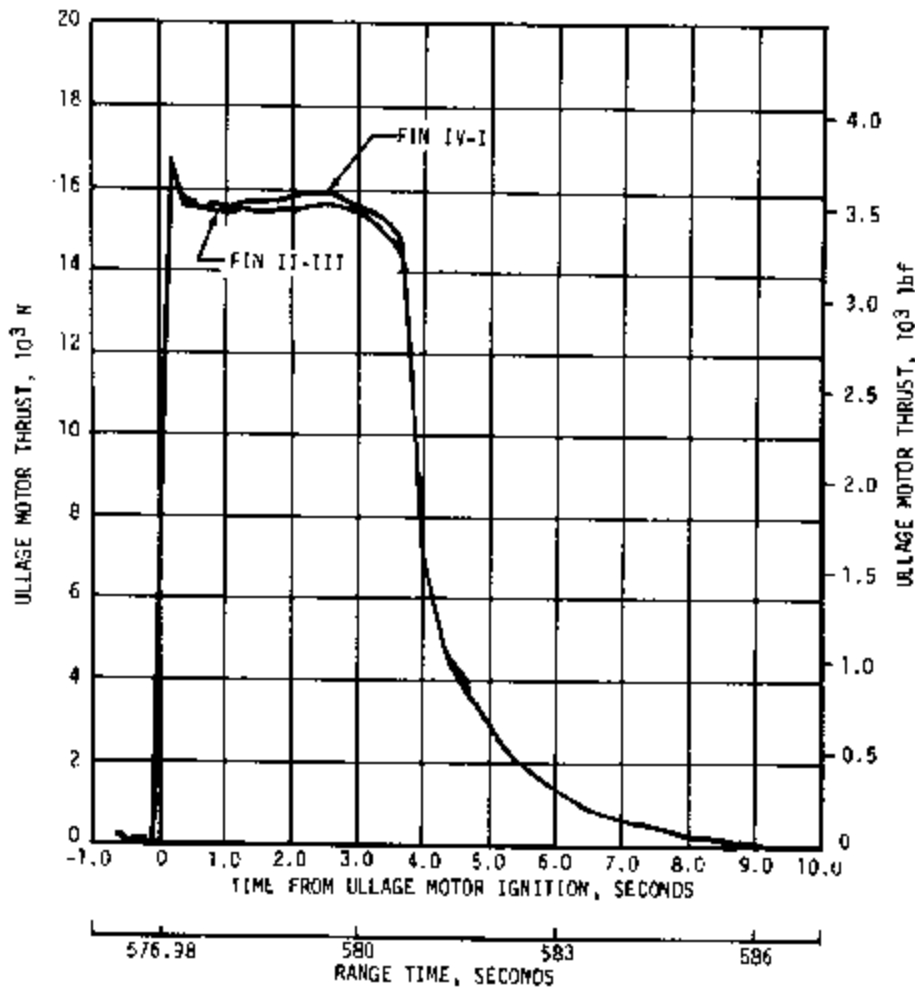


Figure 12-10. S-IVB Ullage Motor Thrust

- ▽ S-II ECD SENSED BY LVDC, 576.33
- ▽ S-II/S-IVB SEPARATION COMMAND, 577.08
- ▽ S-IVB ENGINE START SEQUENCE COMMAND, 577.28

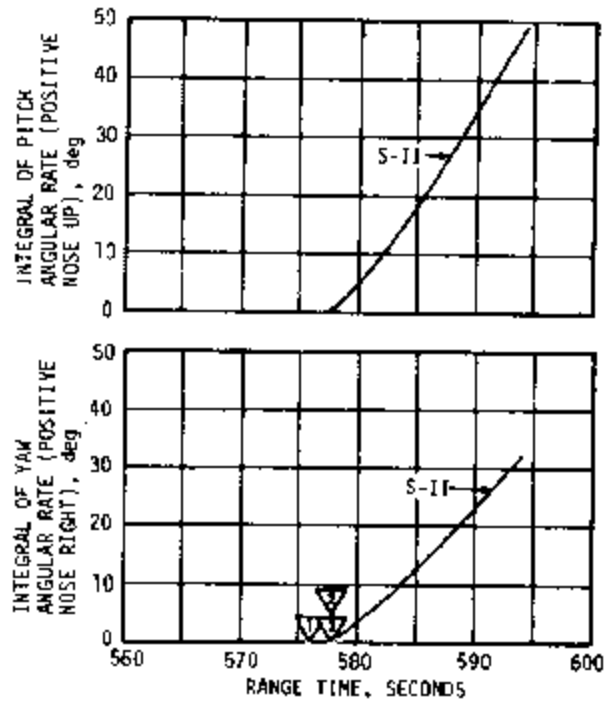


Figure 12-13. S-II Angular Dispersions During S-II/S-IVB Separation

- ▽ S-II/S-IVB PHYSICAL SEPARATION, 577.13
- ▽ S-IVB ENGINE START SEQUENCE COMMAND, 577.28
- ▽ S-II/S-IVB SEPARATION COMPLETE, 578.07

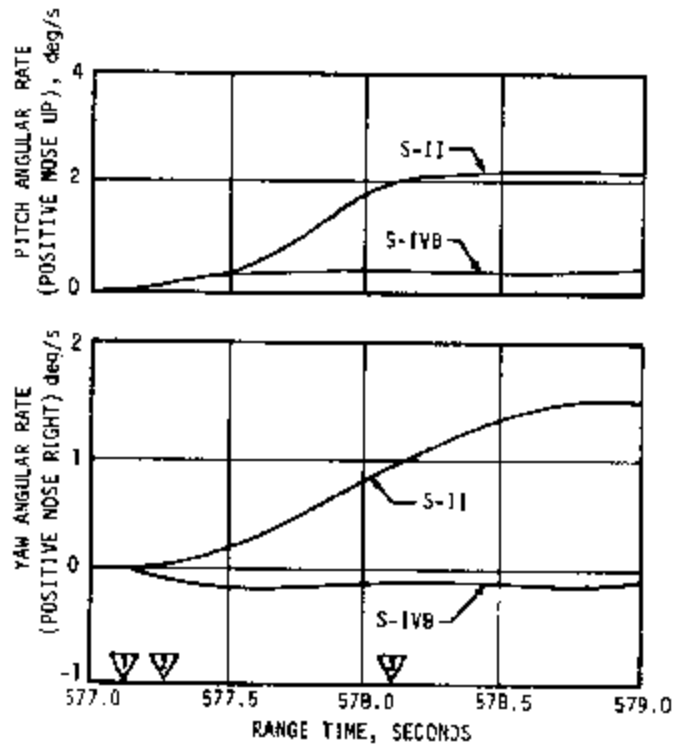


Figure 12-14. S-II and S-IVB Angular Dispersions During S-II/S-IVB Separation

2.5 S-IVB/IU/SPACECRAFT SEPARATION EVALUATION

T₇ was established at 11,630.33 seconds. At T₇ +20 seconds the preprogrammed maneuvers to separation attitude were initiated. However, at 11,666.02 seconds spacecraft separation was initiated by ground command to the spacecraft.

The S-IVB attitude errors and rates during S-IVB/IU/Spacecraft separation are shown in Figures 11-40, 11-41, and 11-42 for pitch, yaw, and roll, respectively. The S-IVB pitch, yaw, and roll attitude errors at spacecraft separation were -7.0, +6.5, and -7.0 degrees, respectively. The S-IVB pitch, yaw, and roll angular rates during spacecraft separation were +0.4, -0.8, and +1.3 deg/s.

Telemetry from the spacecraft and the S-IVB/IU indicated that unexpected disturbances were applied to both vehicles immediately following physical separation. The spacecraft pitch rate increased from 0.3 deg/s to 1.83 deg/s in the nose-up direction over a period of 0.1 second following physical separation. The 1.53 deg/s rate change may be attributed to a momentary interference between the Spacecraft Lunar Module Adapter (SLA) panel located at position I and the spacecraft at the separation plane. The S-IVB/IU pitch rate decreased from 0.38 deg/s to 0.1 deg/s nose-up pitch rate in the same time interval. This rate change may be attributed to the above momentary interference between the vehicles coupled with asymmetrical forces and moments resulting from delayed deployment of the SLA panel located at position I. The S-IVB/IU pitch rate increased from 0.1 deg/s to 0.4 deg/s nose-up 1.0 second after physical separation. This may result from the deceleration of the SLA panel at position III on hitting the deployment position stop prior to the SLA panel at position I. The SLA panels reach an angular rate of approximately 40 deg/s within 0.09 second of physical separation and are fully deployed by 1.3 seconds. Longitudinal acceleration impulses in the aft direction were detected by the IU accelerometer immediately following physical separation and 1.0 second later.

Spacecraft attitude rates and linear acceleration data provided by MSC were utilized to reconstruct the relative motion of the service module engine bell with respect to the S-IVB/IU during spacecraft separation. The resultant relative motion as a function of time from physical separation is shown in Figure 12-16.

Even though there were no SPS engine bell clearance problems there may have been a momentary interference between the CSM and a SLA panel at the separation plane as discussed above. However, the momentary interference was not detrimental to the separation. Therefore, initiation of spacecraft separation during the maneuver to separation attitude did not result in any significant problems.

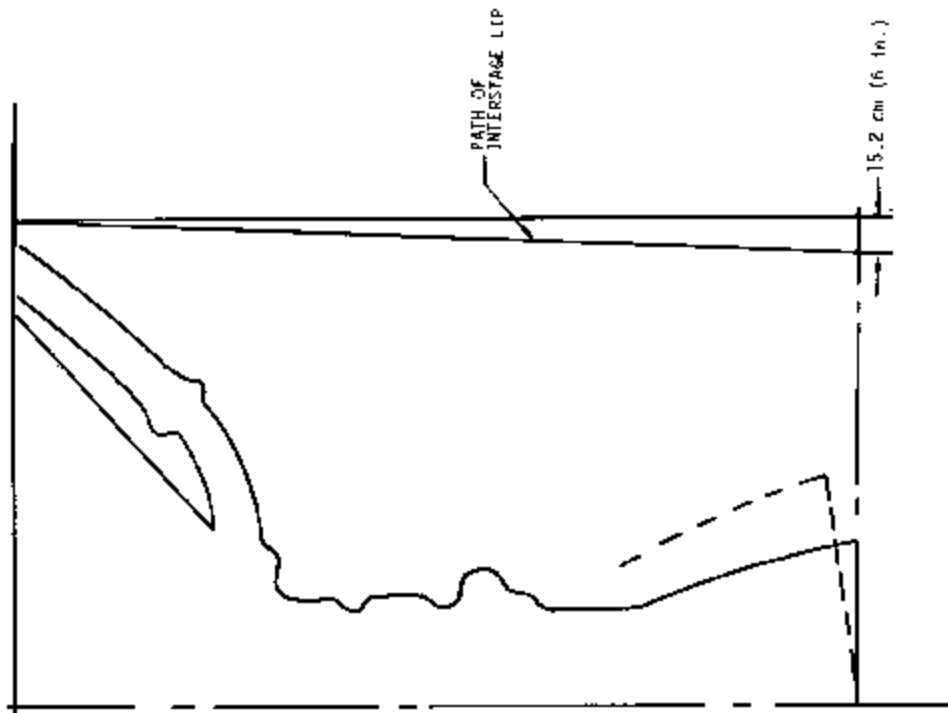


Figure 12-15. S-II/S-IVB Separation Clearance

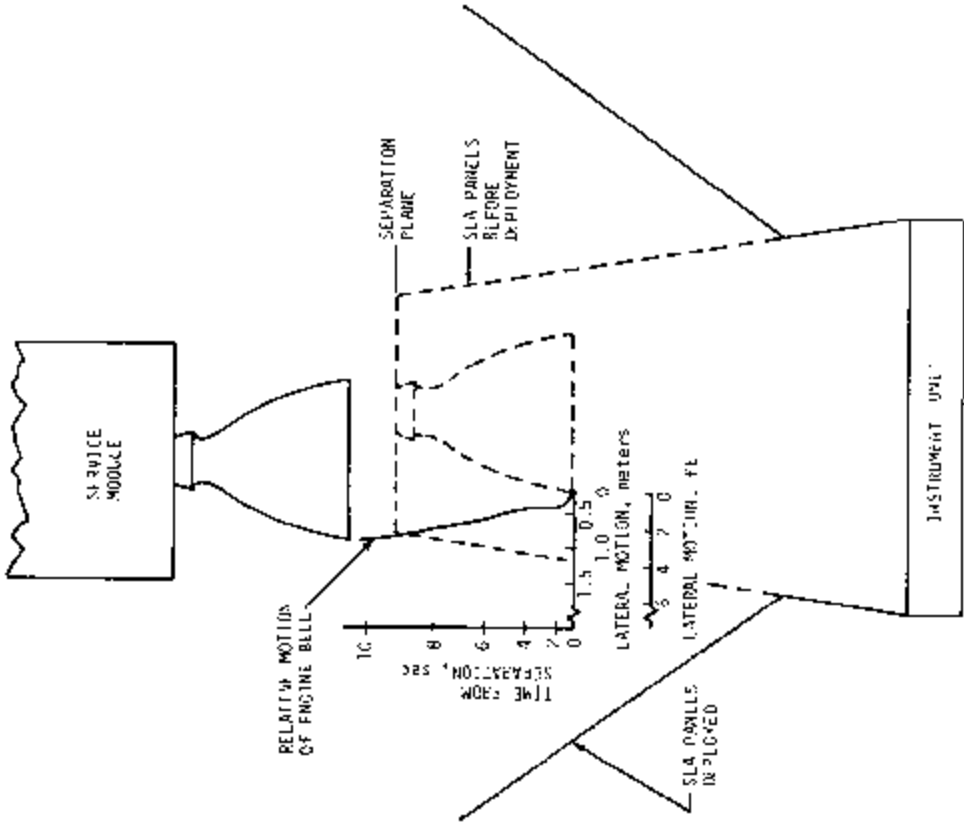


Figure 12-16. Relative Motion During Spacecraft Separation

SECTION 13
ELECTRICAL NETWORKS

13.1 SUMMARY

Each stage has its own electrical system which includes the battery power supply, power distribution systems, switch selector, etc. The stage electrical system supplies and distributes power to all electrical/electronic equipment on the stage. Details of stage electrical systems are presented in the individual stage descriptions.

In general, launch vehicle electrical systems performed satisfactorily during powered flight. Stage deviations are detailed in the individual stage descriptions.

S-IC stage deviations included:

- a. Battery No. 2 voltage drop at about 168 seconds which continued for 11 seconds.
- b. Power supply bus 1D86 voltage drop from a nominal 5 vdc to zero vdc lasting from 160 seconds until loss of telemetry signal.

S-II stage deviations included:

- a. A 34-ampere current spike at 412.7 seconds on the main battery.
- b. Instrumentation battery positive current spikes of 47 and 37 amperes with corresponding voltage drops of 1.2 and 0.5 volts beginning at 414.2 seconds.

The only S-IVB stage electrical deviation was that the PU static inverter/converter 5 vdc exceeded the upper limit of 5.1 vdc by from 30 to 90 millivolts; however, no adverse effects resulted from this deviation.

Instrument Unit deviations included:

- a. A current surge of 9.5 amperes, lasting 400 milliseconds, at 133.3 seconds on the 6D11 bus, with a corresponding voltage drop of 1.5 volts in the 6D10 battery.
- b. A current step of 1 ampere at 22,112.4 seconds on the 6D11 bus.

13.2 S-IC STAGE ELECTRICAL SYSTEM

The S-IC stage electrical system is composed of five 28 vdc batteries which supply the various systems and components through the power distribution system as shown in Figure 13-1. The system includes seven 5 vdc instrumentation measuring power supplies, distributors, and a switch selector.

The electrical system performed satisfactorily during S-IC powered flight. Battery voltages and currents are shown in Figures 13-2 and 13-3. Both battery No. 1 and battery No. 2 stayed within design limits of 26.5 to 32 vdc (as read on buses 1D10 and 1D20, respectively), and below 64 amperes for battery No. 1 and 125 amperes for battery No. 2 (as read at each battery), until approximately 168 seconds. At this time, approximately 19 seconds after S-IC/S-II stage separation, battery No. 2 voltage dropped to 25.8 vdc and the current rose above 175 amperes, the upper limit of range on the ammeter. After 11 seconds

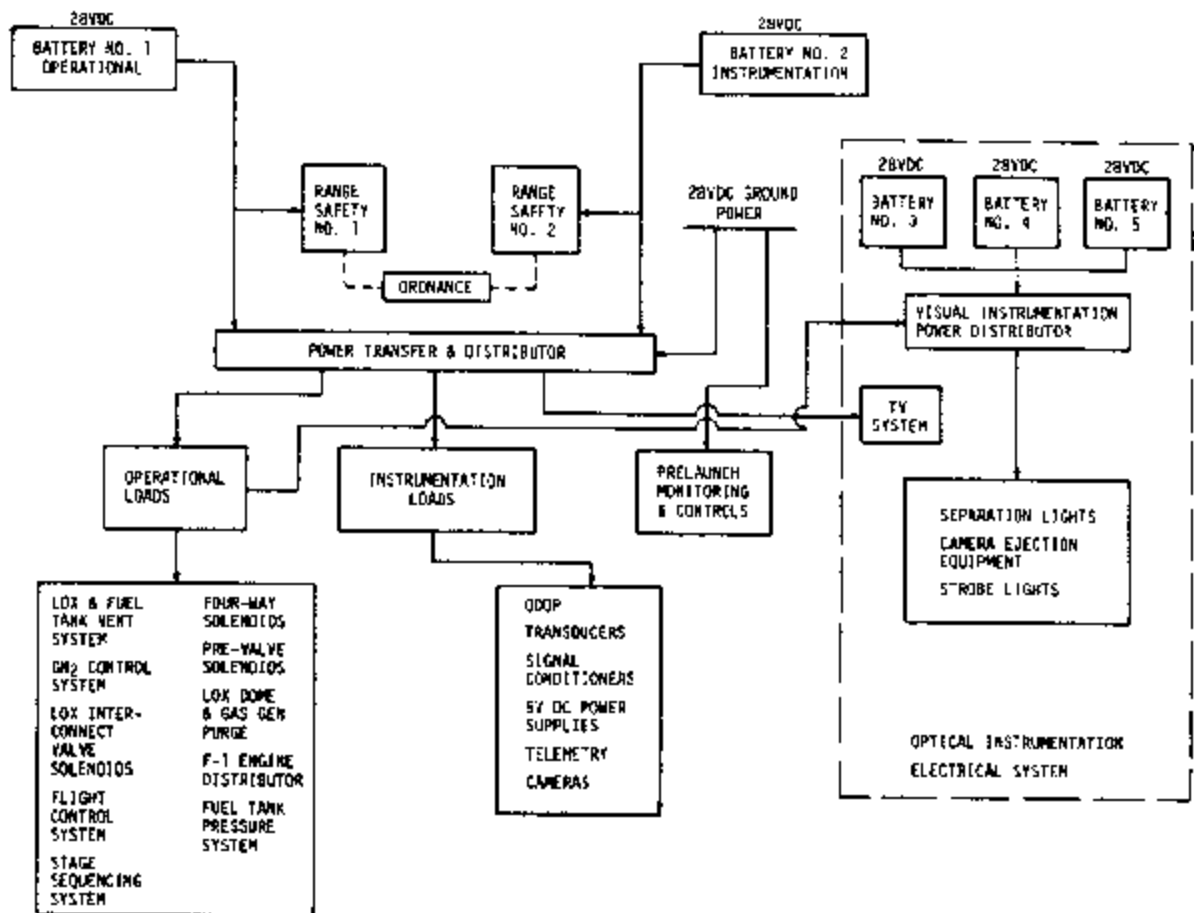


Figure 13-1. S-IC Power Generation and Distribution Systems Block Diagram

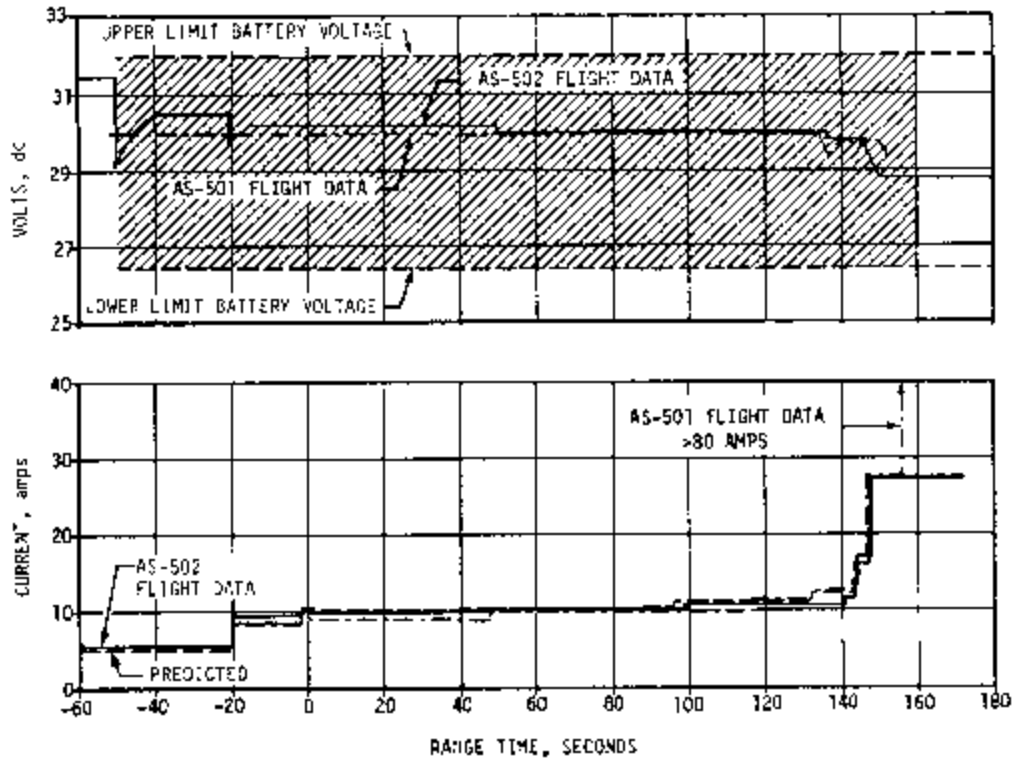


Figure 13-2. S-IC Stage Voltage (on Bus 1D10) and Current (at the Battery)

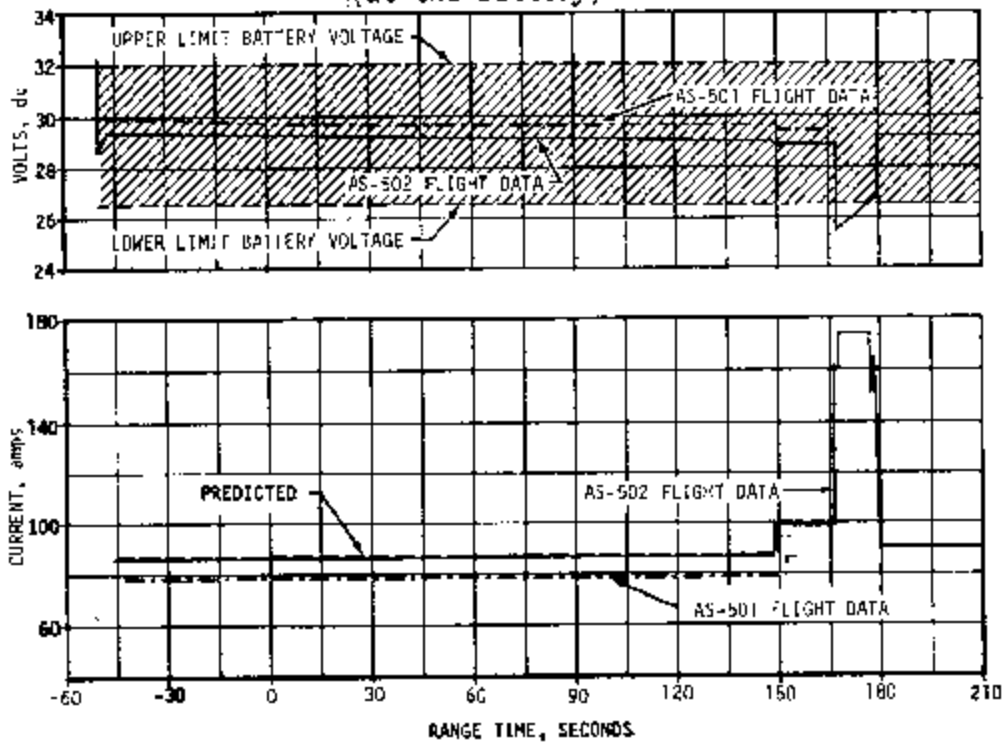


Figure 13-3. S-IC Stage Voltage (on Bus 1D20) and Current (at the Battery)

the battery voltage and amperage returned to normal. A somewhat similar situation occurred on AS-501 S-IC battery No. 1 immediately after S-IC/S-II separation. Tape recorder performance was not affected since the voltage remained above the minimum required by the tape recorder. Investigation is underway to determine probable cause of this deviation, and corrective action to be taken.

S-IC stage batteries No. 1 and 2 outputs in ampere-minutes and as a percent of rated capacity were well within design limits, as shown in Table 13-1. Batteries No. 3, 4, and 5 were not instrumented to give this information.

The seven 5 vdc measuring power supply voltages for instrumentation varied from 4.96 to 5.04 vdc during powered flight. This was within design parameters of 5 ± 0.05 vdc. At approximately 160 seconds, 11 seconds after S-IC/S-II separation, measuring voltage power supply bus 1D86 dropped from a nominal 5 vdc to almost zero vdc and remained at this level until loss of telemetry signal. This deviation is being investigated.

All S-IC switch selector channels functioned as commanded by the Instrument Unit.

Separation and retro motor Exploding Bridgewire (EBW) firing units were armed and triggered. Charging time and voltage characteristics of the EBW firing units were within design specifications. Separation and retro motor ignition charging time and voltage characteristics were within required parameters.

Table 13-1. S-IC Stage Electrical System Battery Performance During Flight

BATTERY	CAPACITY* (AMP-MINS)	CONSUMPTION (AMP-MINS)		PERCENT USAGE
		MAXIMUM EXPECTED	ACTUAL	
Battery No. 1 (Operational)	640	31.4	32.0**	5.0
Battery No. 2 (Instrumentation)	1250	384.2	394.6***	31.6
Batteries No. 3, 4, 5 (Optical Instrumentation)	1250 1250 640	Not instrumented to give consumption data		

* Ampere-minutes ratings are approximate values.

** 0 to S-IC/S-II separation.

*** 0 to 210 seconds.

13.3 S-II STAGE ELECTRICAL SYSTEM

The S-II stage electrical system contains four 28 vdc batteries, two of which are connected in series to furnish 56 vdc to the recirculation inverters. The batteries furnish power to the various stage systems and components through the power distribution system, as shown in Figure 13-4. Five 5 vdc power supplies furnish measuring voltage to the telemetry and other instrumentation. The five LH₂ recirculation pump inverters convert 56 vdc to 42 vac, 3-phase, 400 hertz power for the ac induction motors on the LH₂ recirculation pumps. The system includes various controllers and a stage selector switch.

The S-II electrical power system performed satisfactorily throughout all phases of the AS-502 flight. Operation of the batteries, power transfer switches, and LH₂ recirculation inverters was normal.

All bus voltages stayed within specified limits during the prelaunch and flight periods. Voltage and current profiles for the main bus are shown in Figure 13-5. Main bus current stayed within specified limits except

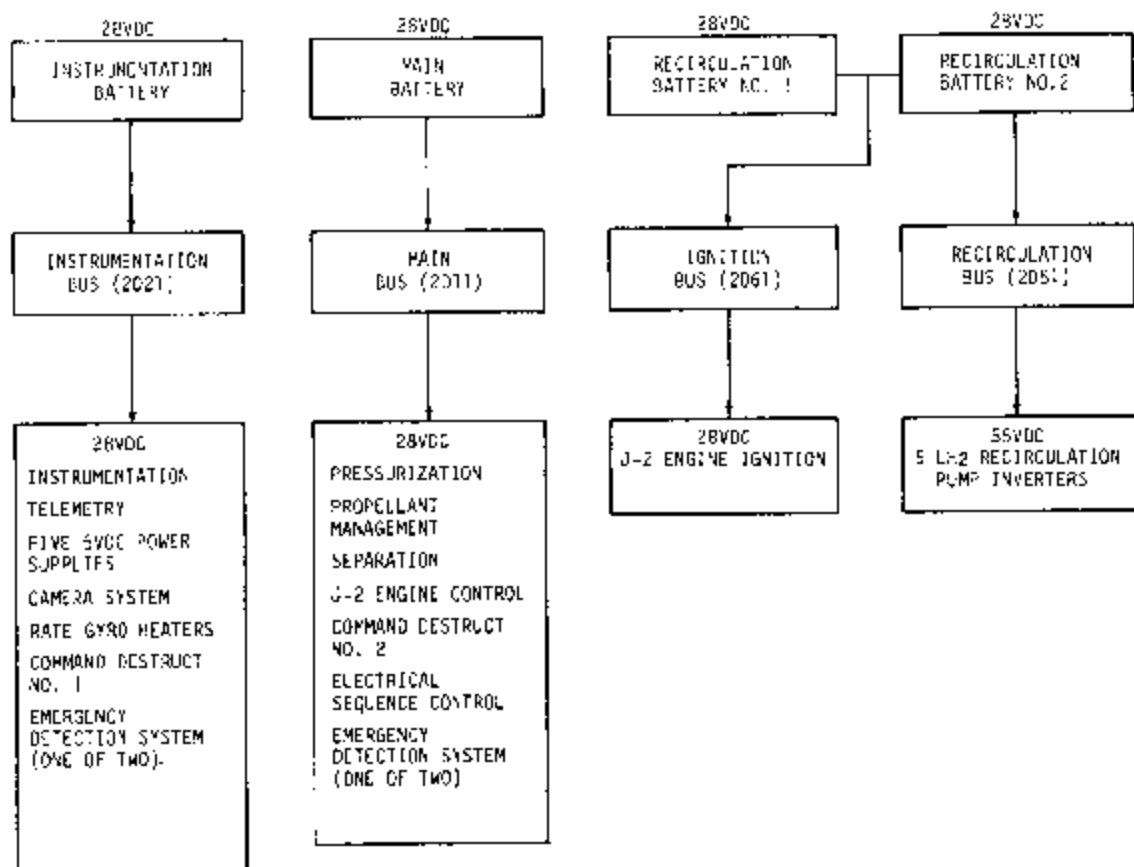


Figure 13-4. S-II Power Generation and Distribution Systems Block Diagram

for an instantaneous current spike of 34 amperes at 412.7 seconds, approximately the time given for J-2 engine No. 2 cutoff. Since there was no significant change in bus voltage at this time, the spike was probably caused by one of the following:

- a. A wild data spike, indicating false data.
- b. Instantaneous short in the stage wiring or bus loads. The possibility of wire damage in this area is indicated by voltage spikes on other measurements and loss of measurements routed by vehicle station 42.57 meters (1676 in.) and stringer 108.

Instrumentation bus voltage and current are shown in Figure 13-6. Instrumentation bus current stayed within specified limits except for a 47-ampere positive spike at 414.2 seconds which lasted for 1.2 seconds and a subsequent 37-ampere spike of shorter duration, with corresponding voltage decreases of 1.2 and 0.5 volts. The time of this deviation corresponded approximately with cutoff of J-2 engine No. 3. The cause was probably shorting of distribution wires in the region of vehicle station 42.57 meters (1676 in.) and stringer 108, where loss of measurements indicates damage to wire cables.

Voltages and currents profiles for recirculation and ignition busses are presented in Figures 13-7 and 13-8. Recirculation and ignition bus current stayed within specified limits.

Battery temperatures (see Table 13-2) remained well within the predicted range. S-II stage batteries consumption, in ampere-hours and as a percent of rated capacity are given in Table 13-2. All four battery ampere-hour outputs were well within design limits. The five 5 vdc power supplies provided proper measuring voltage to the telemetry and other instrumentation.

Table 13-2. S-II Stage Battery Consumption.

BATTERY	DESIGNATION (REFERENCE)	CAPACITY (AMP-HR)*	CONSUMPTION (AMP-HR)	PERCENT CONSUMED	TEMPERATURE	
					MAX	MIN
Main	2D11	35	8.53	24.4	310°K (98°F)	304°K (88°F)
Instrumentation	2D21	35	10.60	30.3	311°K (101°F)	303.5°K (87°F)
Recirculation No. 1	2D51	35	5.17	14.8	302°K (85°F)	300°K (80°F)
Recirculation No. 2	2D51 and 2D61	35	5.21	14.9	301°K (83°F)	298.5°K (78°F)

* Ampere-hour ratings are approximate values.

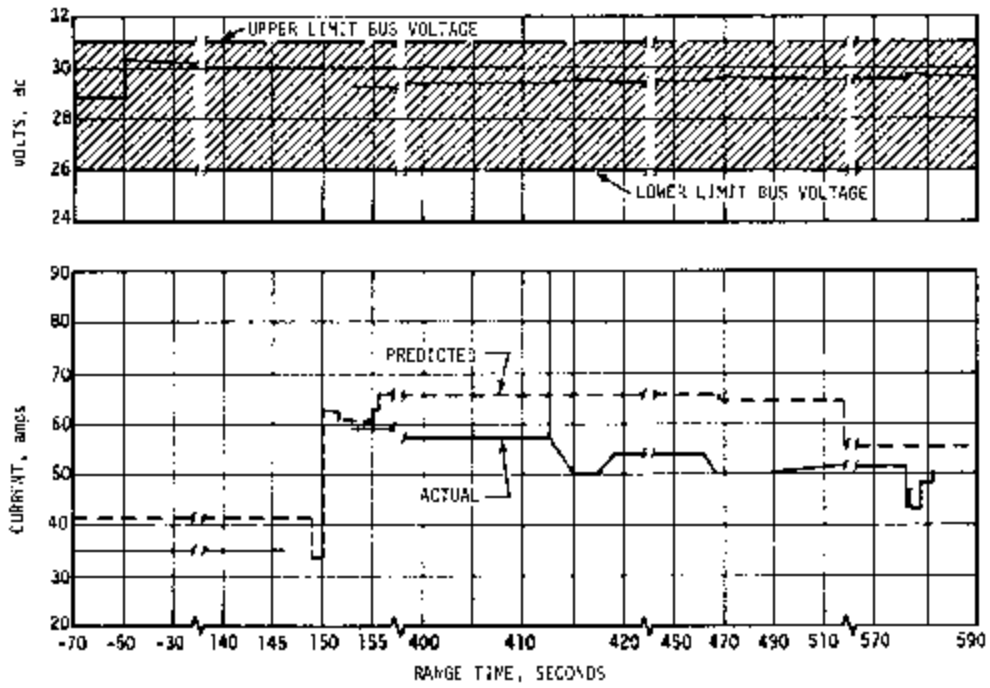


Figure 13-5. S-II Stage Main DC Bus Voltage and Current

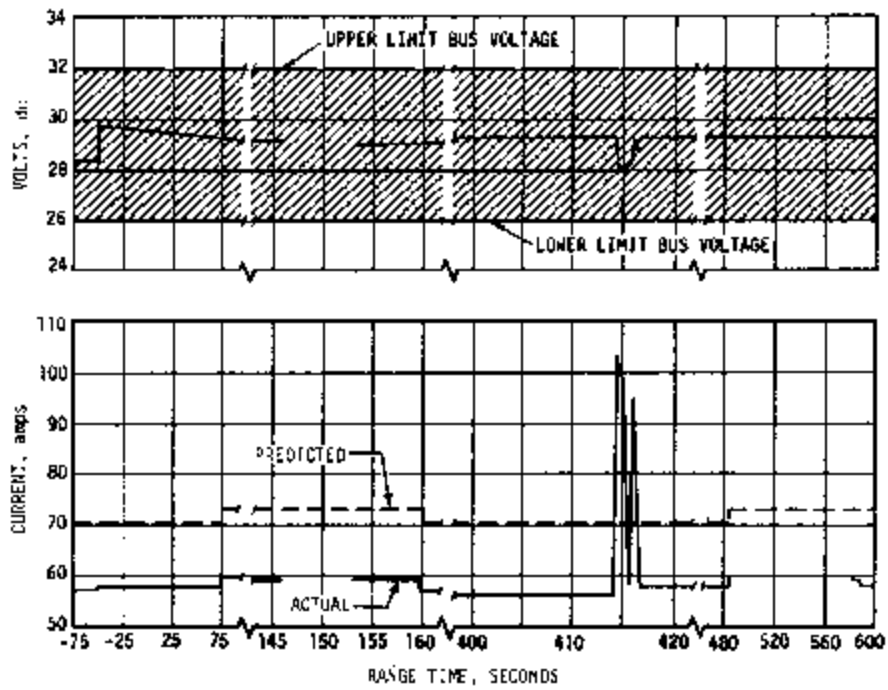


Figure 13-6. S-II Stage Instrumentation Bus Voltage and Current

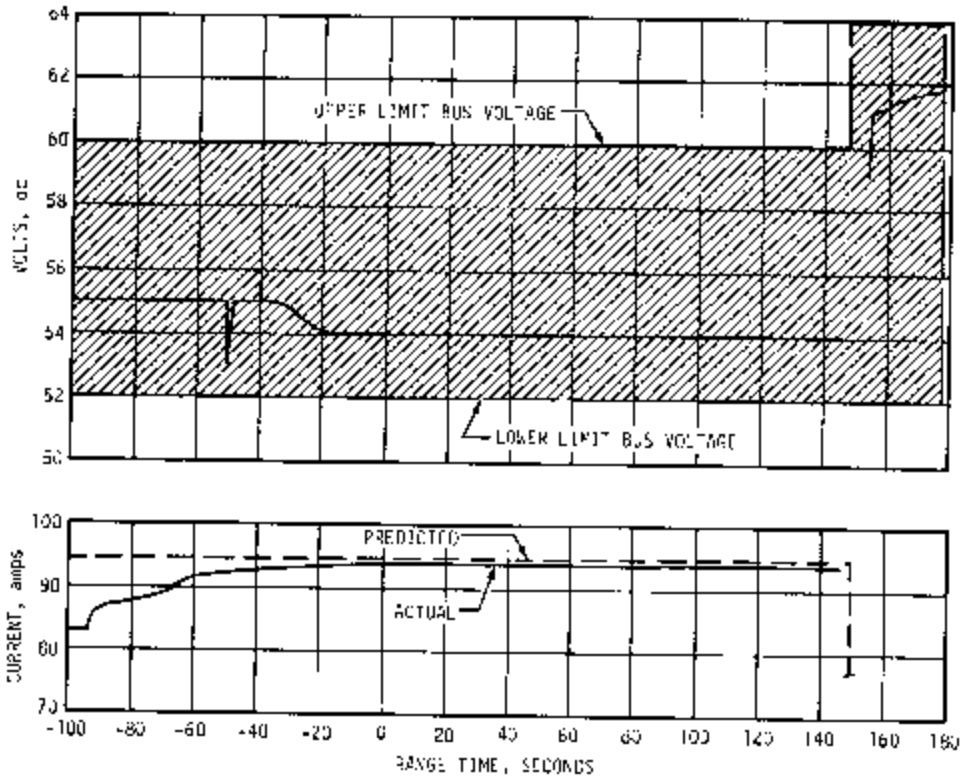


Figure 13-7. S-II Stage Recirculation DC Bus Voltage and Current

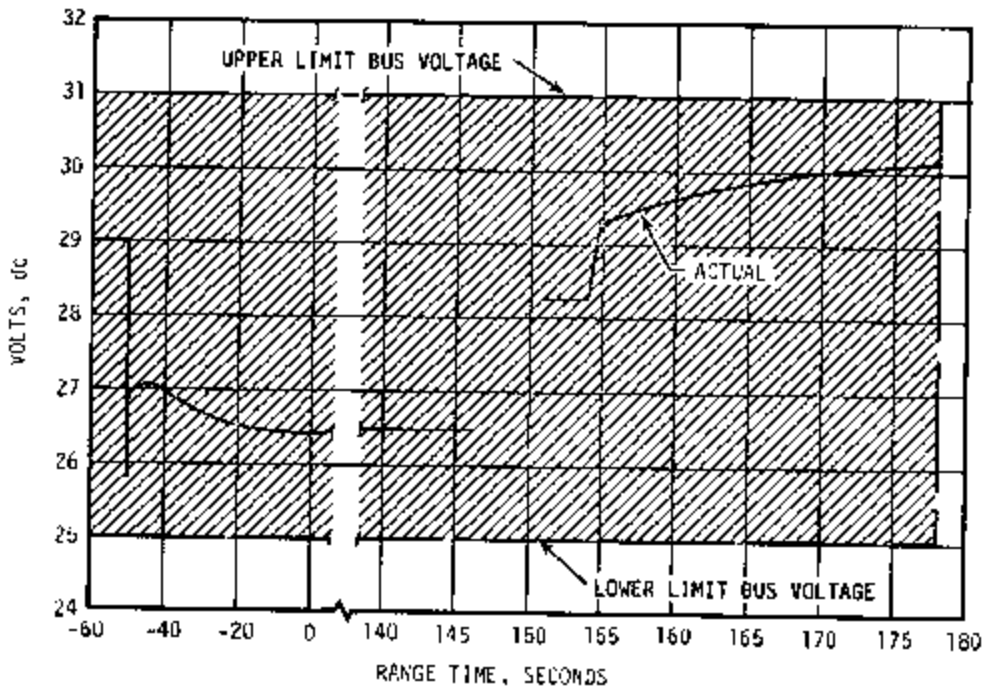


Figure 13-8. S-II Stage Ignition DC Voltage

Performance of the switch selector was satisfactory during the flight. The switch selector telemetry output measurement was not available during portions of the flight due to a malfunction in the measurement; however, events indicated that the switch selector correctly sequenced the S-II stage as commanded by the IU computer. The LH₂ recirculation inverters operated satisfactorily within acceptable limits during the J-2 engine chilldown period.

Performance of the electrical portion of the separation system was satisfactory during the flight. EBW firing units charge and discharge responses were within the predicted time and voltage limits.

13.4 S-IVB STAGE ELECTRICAL SYSTEM

The S-IVB stage electrical system is composed of three 28-vdc and one 56-vdc batteries which supply the various stage systems and components through the power distribution system, as shown in Figure 13-9. Two 5-vdc excitation modules furnish measuring voltage to instrumentation measurement transducers and signal conditioners. Seventeen 20-volt excitation modules supply signal conditioning power for event measurements, excitation power for temperature and voltage measurements, and amplifier power to various measurements that use a dc amplifier. The static inverter/converter converts 28 vdc from

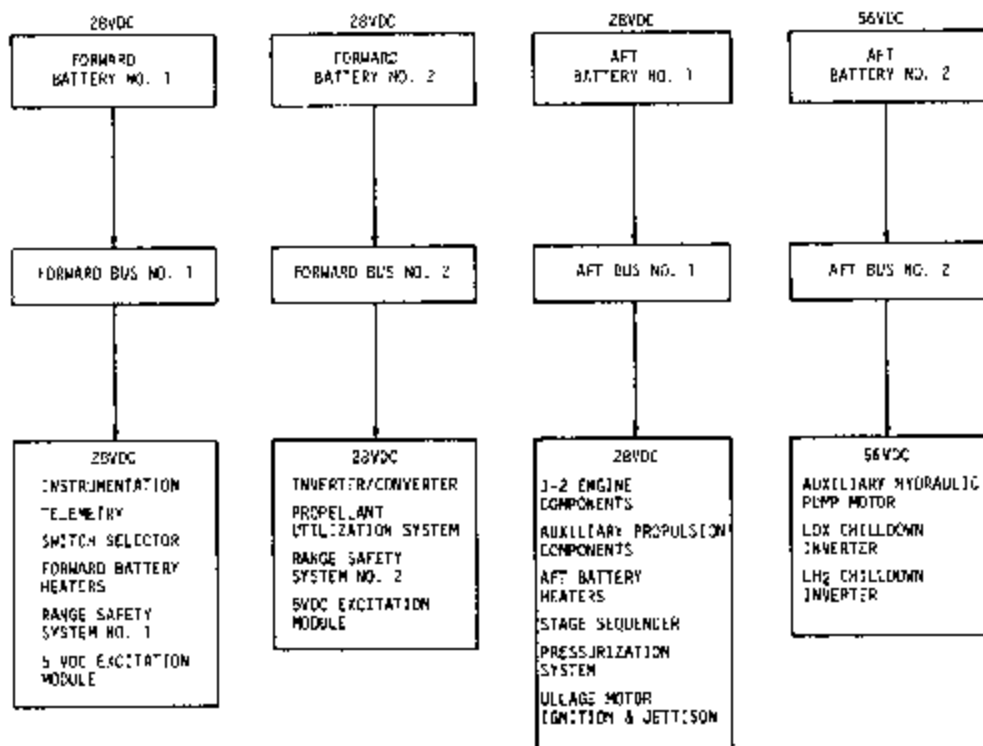


Figure 13-9. S-IVB Power Generation and Distribution Systems Block Diagram

forward battery No. 2 to 115 and 2 vac, 400 hertz, single phase, and to 5, 22, and 117 vdc power for the propellant utilization system. The LOX and LH₂ chilldown inverters convert 56 vdc from aft battery No. 2 to 56 vac 400 hertz for the chilldown pump motors. Power is routed through various distributors and a switch selector.

The S-IVB stage electrical system performed satisfactorily during first burn and through restart attempt. All systems responded normally to the Instrument Unit commands.

Battery voltages, currents, and temperatures are presented in Figures 13-10 through 13-13. Battery temperatures stayed below the 347°K (165°F) limits for the powered portion of the flight (the 347°K limit does not apply after insertion into orbit). The highest temperature reached was 341°K (154°F) on forward battery 1, unit 2, during the sixth revolution, as observed on PCM data from Hawaii (see Figure 13-10). All battery temperatures were within their specified limits through the sixth revolution.

The output voltage of forward battery No. 1 was 18 vdc and decreasing according to sixth revolution Hawaii data. The other three battery voltages were nominal through the sixth revolution. S-IVB stage battery consumption in ampere-hours and as a percent of rated capacity are given in Table 13-3. Forward battery No. 1 furnished 6 percent more ampere-hours than the battery was rated for. The other three battery ampere-hour outputs were well within design limits.

The two 5-vdc excitation modules provided proper excitation voltage at 5 ± 0.03 vdc to the transducers through fifth revolution Hawaii data (27,650 seconds). The sixth revolution Hawaii data (33,380 seconds) showed both voltages offscale high at 5.50 vdc. However, this is attributed to a signal conditioning drift rather than an actual out-of-range condition. The 17 20-vdc excitation modules performed satisfactorily.

The switch selector decoded the Instrument Unit signals properly and activated the desired relays, valves, etc. at the proper times, through the sequencer. The LOX and LH₂ chilldown inverters performed satisfactorily and met their load requirements. The 5 vdc PU static inverter/converter exceeded the upper limit of 5.1 vdc and ranged from 5.13 to 5.19 vdc. However, no degradation of mass calculation occurred since ratios of voltage levels are utilized in the calculations.

All EBW firing units responded as expected to their respective commands. The ullage motor ignition EBW firing units were charged at 482.88 seconds and fired at 576.98 seconds. The ullage motor jettison EBW firing units were charged at 586.09 seconds and fired at 589.08 seconds, to jettison both ullage motors. The Secure Range Safety EBW firing units were not charged or fired, since they were not required for AS-502.

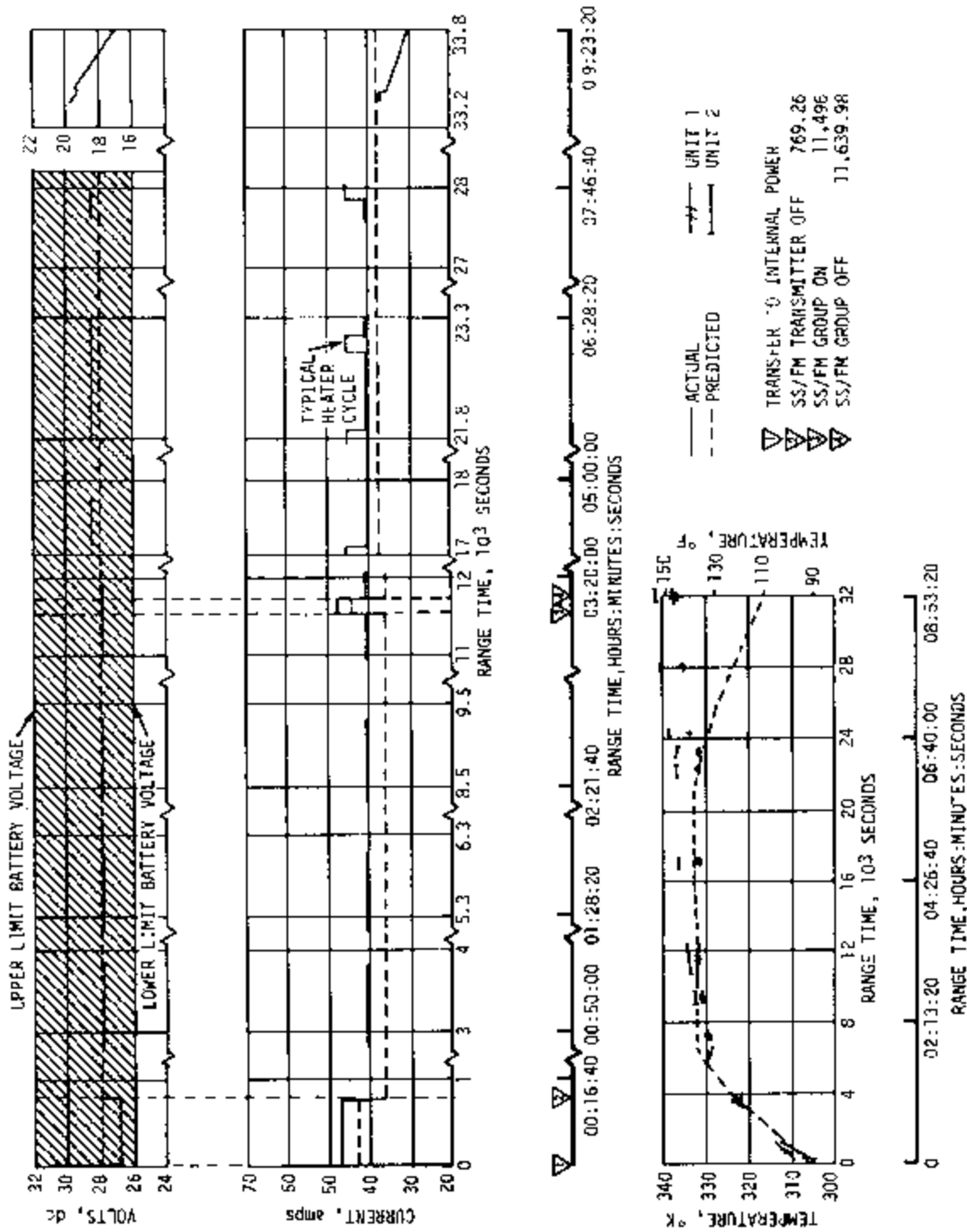
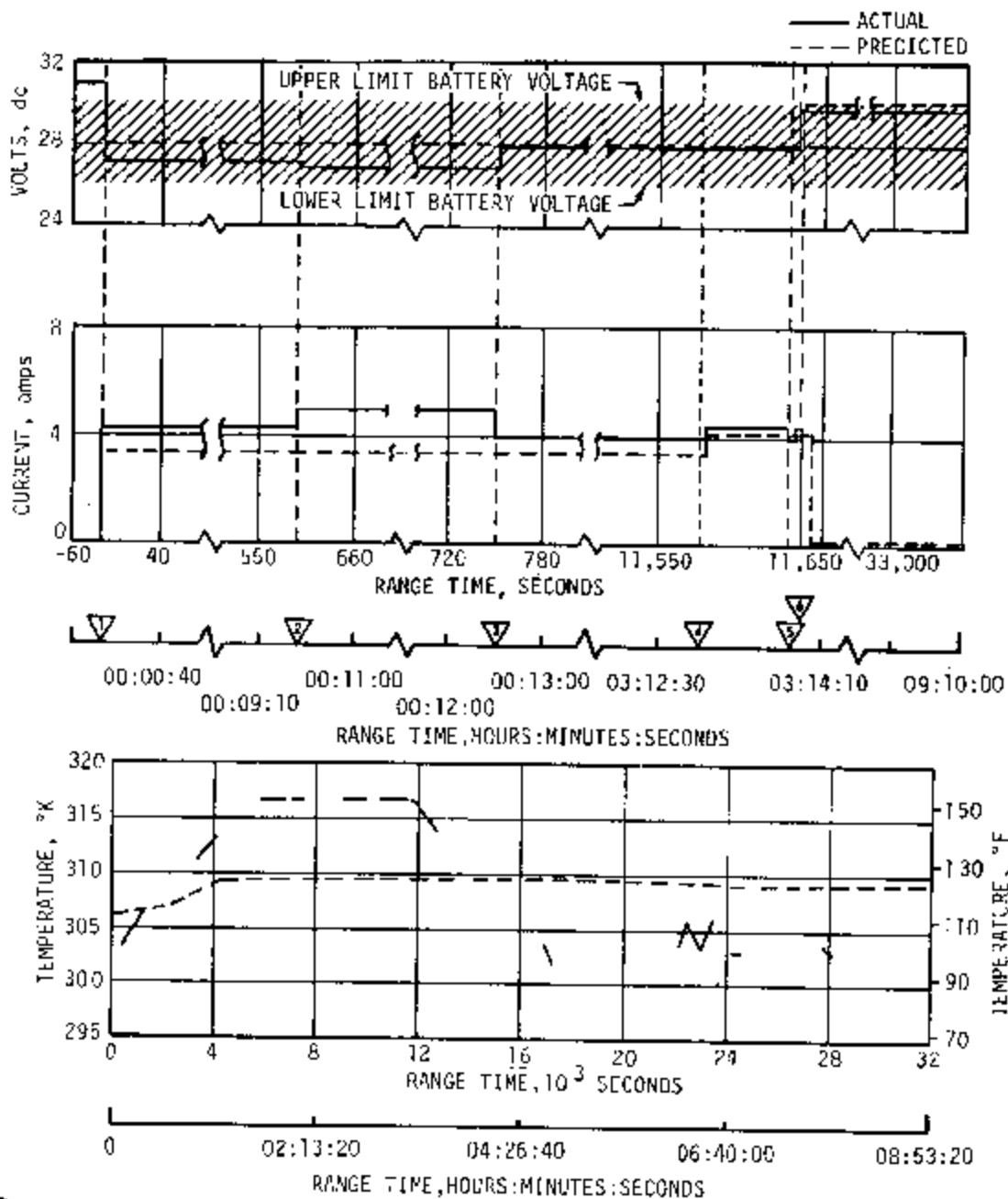


Figure 13-10. S-IVB Stage Forward Battery No. 1 Voltage, Current, and Temperature



- ▽ TRANSFER TO INTERNAL POWER
- ▽ PU ACTIVATE ON 585.30
- ▽ PU ACTIVATE OFF 748.15
- ▽ PU VALVE HARDOVER POSITION ON 11,574.69
- ▽ PU VALVE HARDOVER POSITION OFF 11,627.59
- ▽ PU ACTIVATE ON 11,627.50
- ▽ PU ACTIVATE OFF 11,631.70
- ▽ PU INVERTER AND DC POWER OFF 11,631.80

Figure 13-11. S-IVB Stage Forward Battery No. 2 Voltage, Current, and Temperature

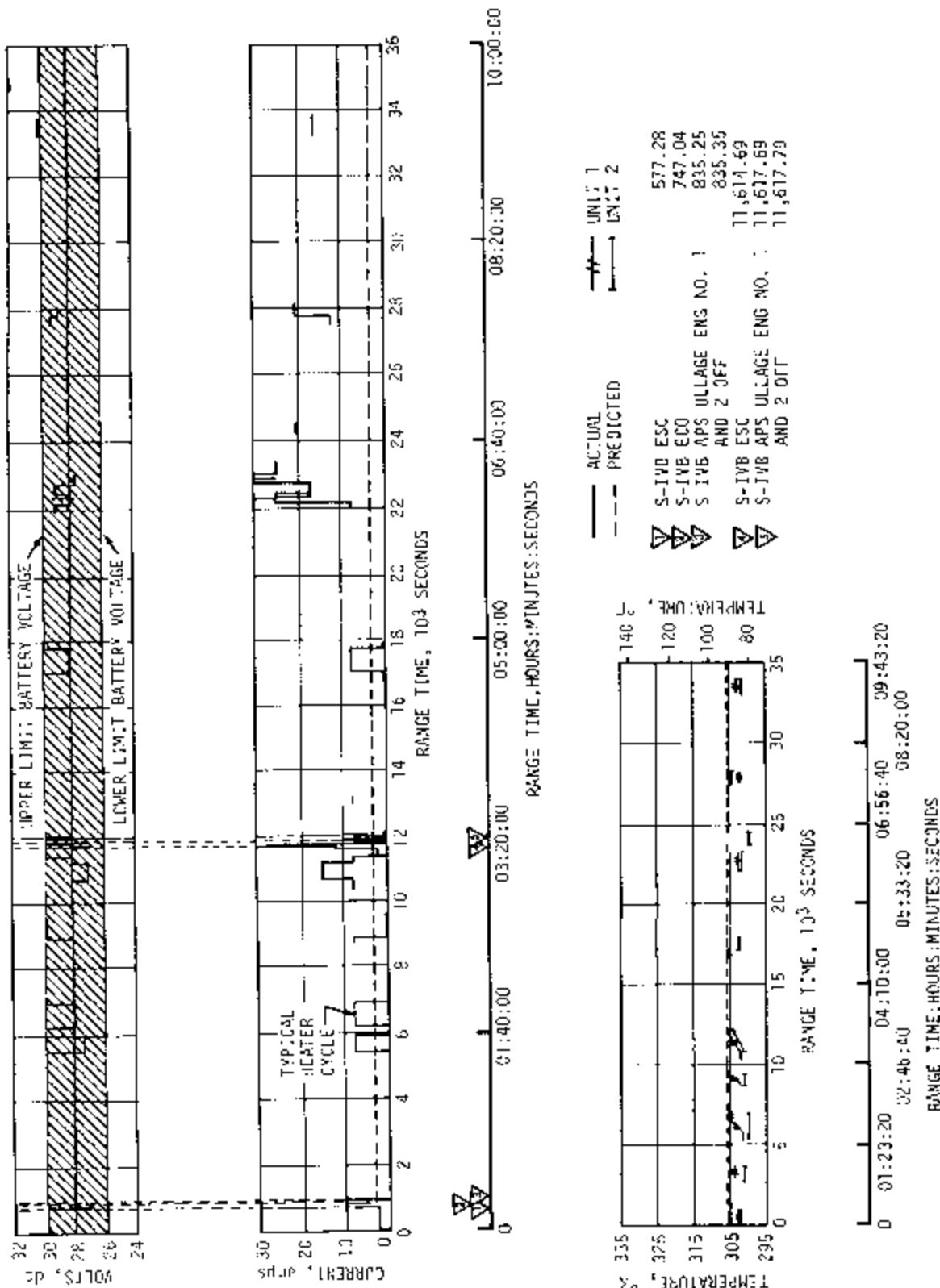


Figure 13-12. S-IVB Stage Aft Battery No. 1 Voltage, Current and Temperature

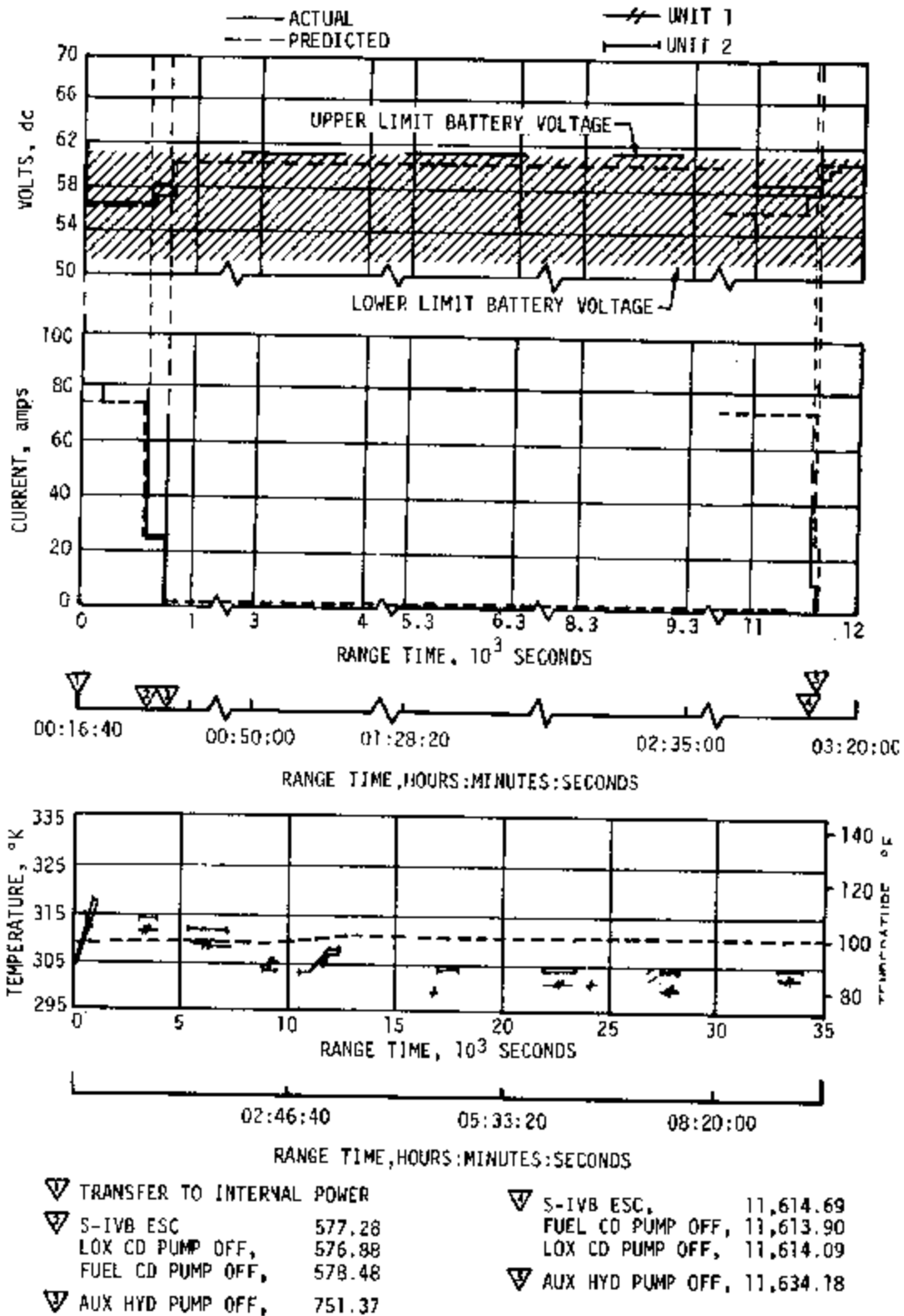


Figure 13-13. S-IVB Stage Aft Battery No. 2 Voltage, Current and Temperature

Table 13-3. S-IV3 Stage Battery Consumption

BATTERY	CAPACITY (AMP-HRS) ¹	CONSUMPTION (AMP-HRS)			PERCENT USAGE
		MAXIMUM EXPECTED ²	ACTUAL HRS		
			6.5 ³	9.3 ⁴	
Fwd No. 1	350	279	265	370	106
Fwd No. 2	25	13	13.1	13.1	52.4
Aft No. 1	300	55	63	137	45.7
Aft No. 2	78	44	20.6	20.6	26.4

- NOTES: 1. Ampere-hour ratings are approximate values.
 2. Predicted usage based on maximum expected values for 6.5 hour flight.
 3. Actual usage for 6.5 hours based on available flight data.
 4. Total usage through sixth revolution (9.3 hours).

13.5 INSTRUMENT UNIT ELECTRICAL SYSTEM

The Instrument Unit electrical system includes four 28-vdc batteries which supply the various IU systems and components through the power distribution system, as shown in Figure 13-14. A 5-vdc power supply converts 28 vdc from an auxiliary power distributor to closely regulated 5 vdc for use as a signal conditioning reference voltage and also to supply various IU transducers. The 56-volt power supply converts 28 vdc from battery 6D10 to 56 vdc for the ST-124-M gyro and accelerometer servoloops and for the accelerometer signal conditioner. The platform ac power supply converts 28 vdc from battery 6D10 to 26 vac, 400 hertz, 3 phase and 20 vac, 4.8 kilohertz for the ST-124-M gyro, and to 20 vac at both 1.92 kilohertz and 1.6 kilohertz for electrical support equipment. Power is routed through six distributors. The switch selector activates the circuits necessary to execute commands received.

IU battery voltages, currents, and temperatures are presented in Figures 13-15 through 13-18. In general the IU electrical system performed satisfactorily during the flight. The only major difference from AS-501 data was the 133 second anomaly mentioned below.

The 6D10 battery performed as predicted except for a current spike at 133.3 seconds and a current step at 22,112.4 seconds. The 133.3 second anomaly involved a 400 millisecond current increase of 9.5 amperes with

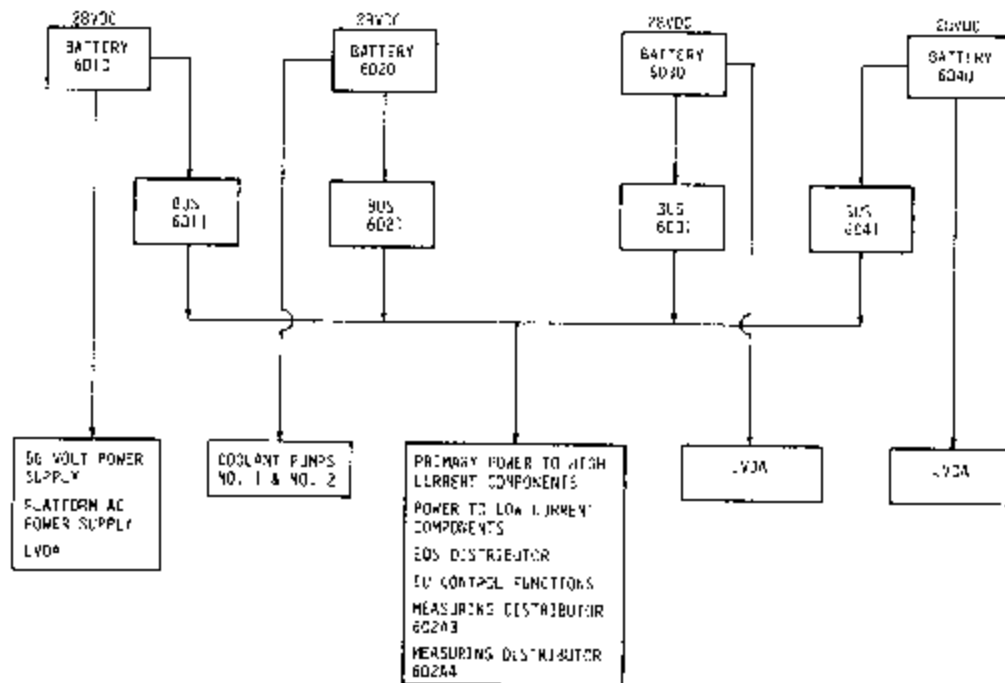


Figure 13-14. Instrument Unit Power Generation and Distribution Systems Block Diagram

a corresponding 1.5-vdc voltage drop, as shown in Figure 13-19. See Section 9A, "133 Second Transient," for a discussion of this anomaly and its implications. The 22,112.4 second current step of 1 ampere resulted from the gimbal torquer motor trying to drive the yaw gimbal off the 60 degree mechanical stops, where it had hit due to loss of effectiveness of one auxiliary propulsion system module in combination with the opening of the LOX vent.

The 6D20, 6D30 and 6D40 battery performance was normal, although 6D30 current was somewhat higher than predicted.

All battery temperatures were within normal limits. The maximum observed temperature was 321°K (118.4°F) on the 6D30 battery at 9.4 hours.

Instrument Unit battery consumption in ampere-hours and as a percent of rated capacity is given in Table 13-4. At the time data were lost, battery 6D30 had furnished 1 ampere-hour more than the battery was rated for, and the other three battery ampere-hour outputs were well within rated limits.

The 5-vdc power supply operation was satisfactory. The 56 volt power supply operation was nominal except for the effect of the 6D10 battery

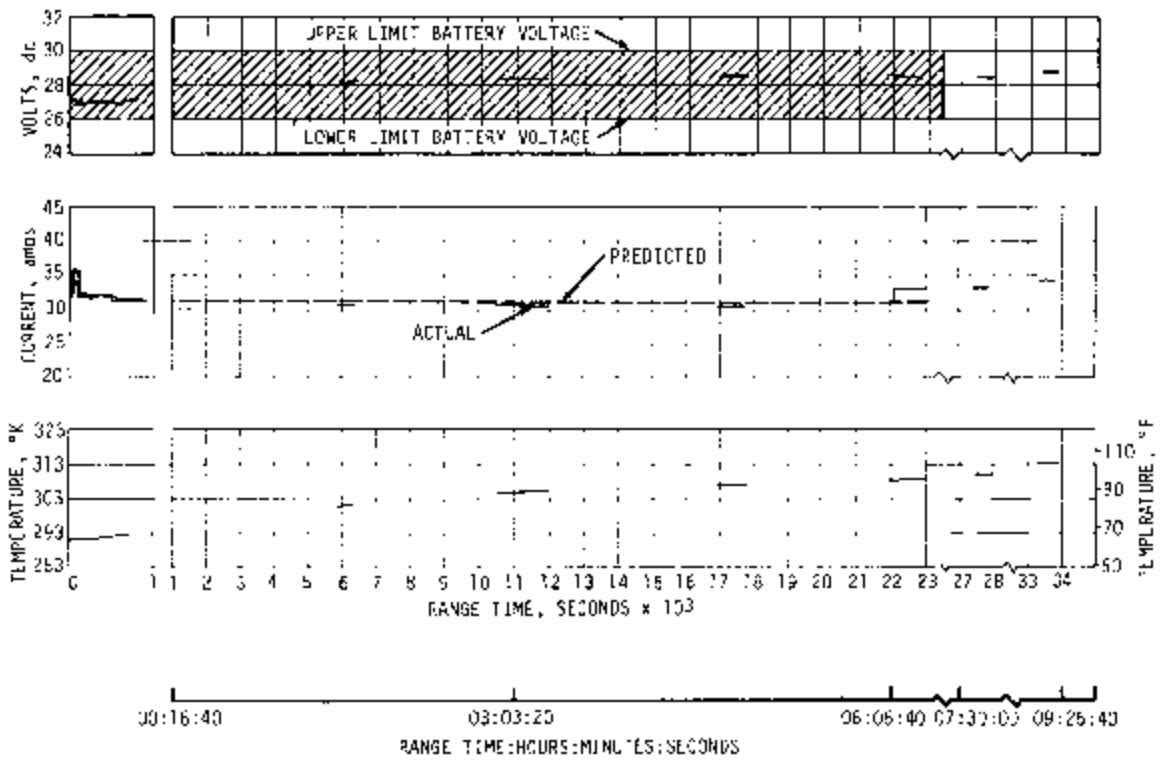


Figure 13-15. IU Battery 6D10 Voltage, Current, and Temperature

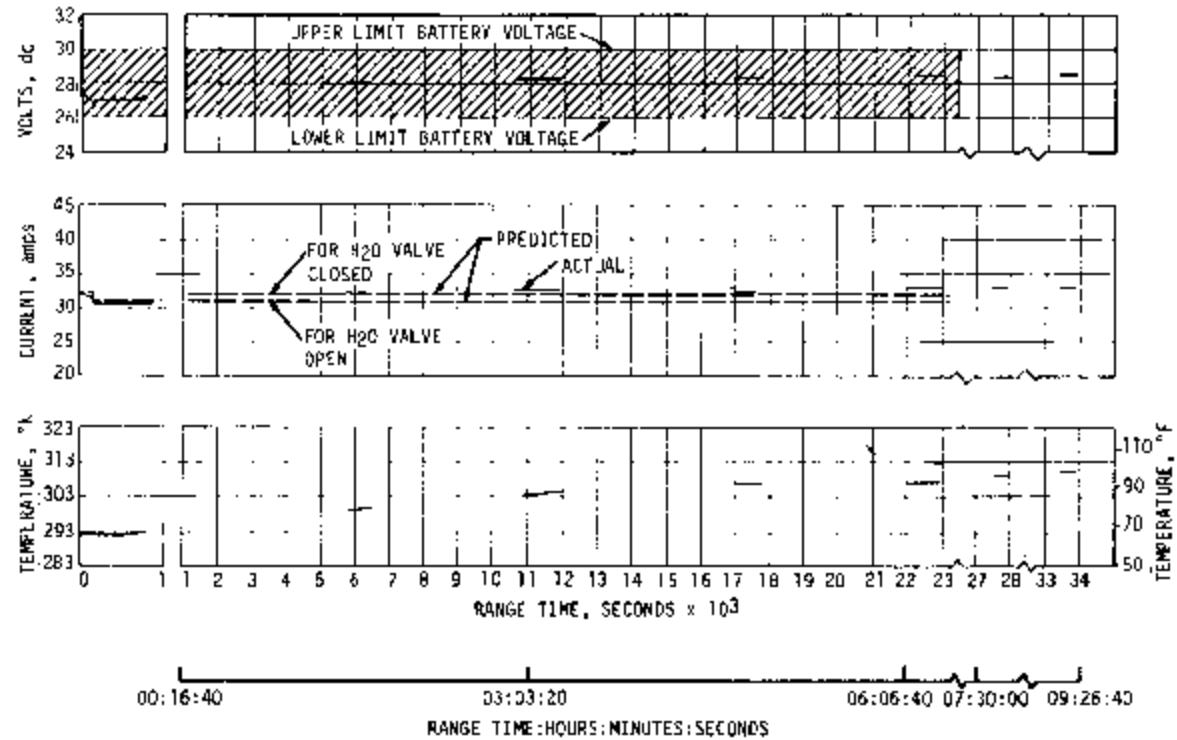


Figure 13-16. IU Battery 6D20 Voltage, Current, and Temperature

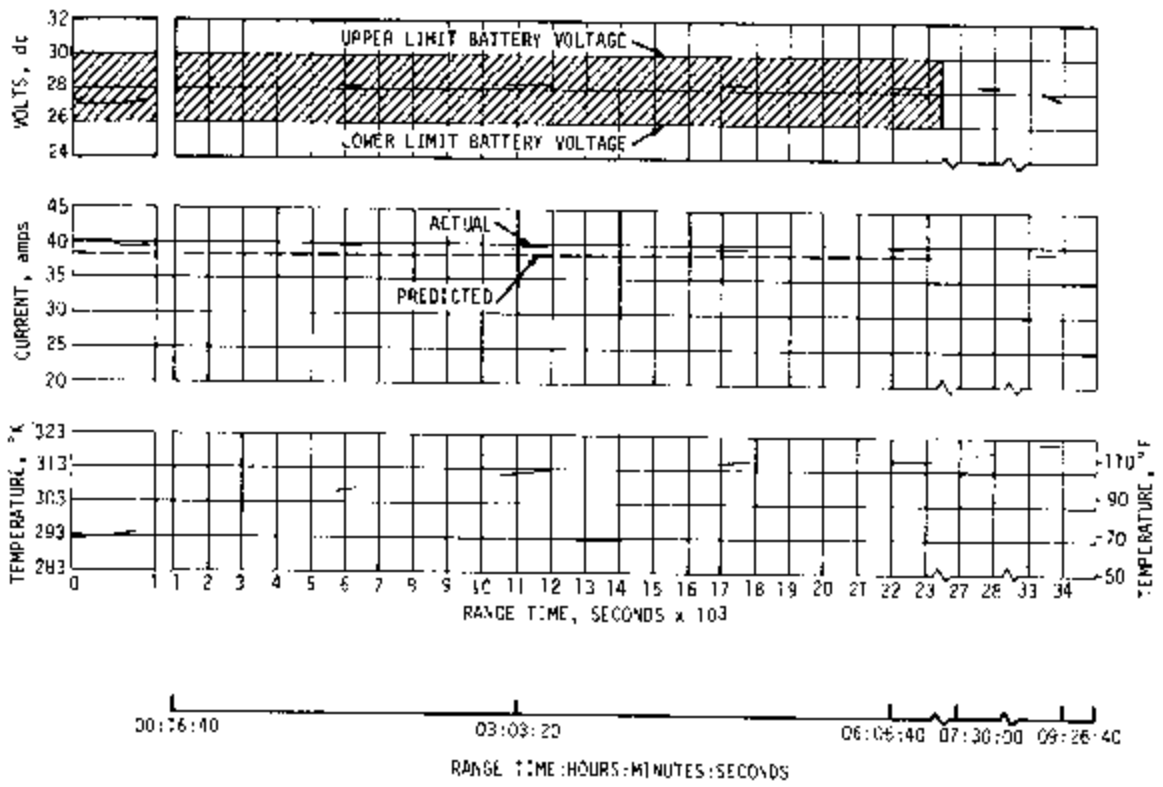


Figure 13-17. IU Battery 6D30 Voltage, Current, and Temperature

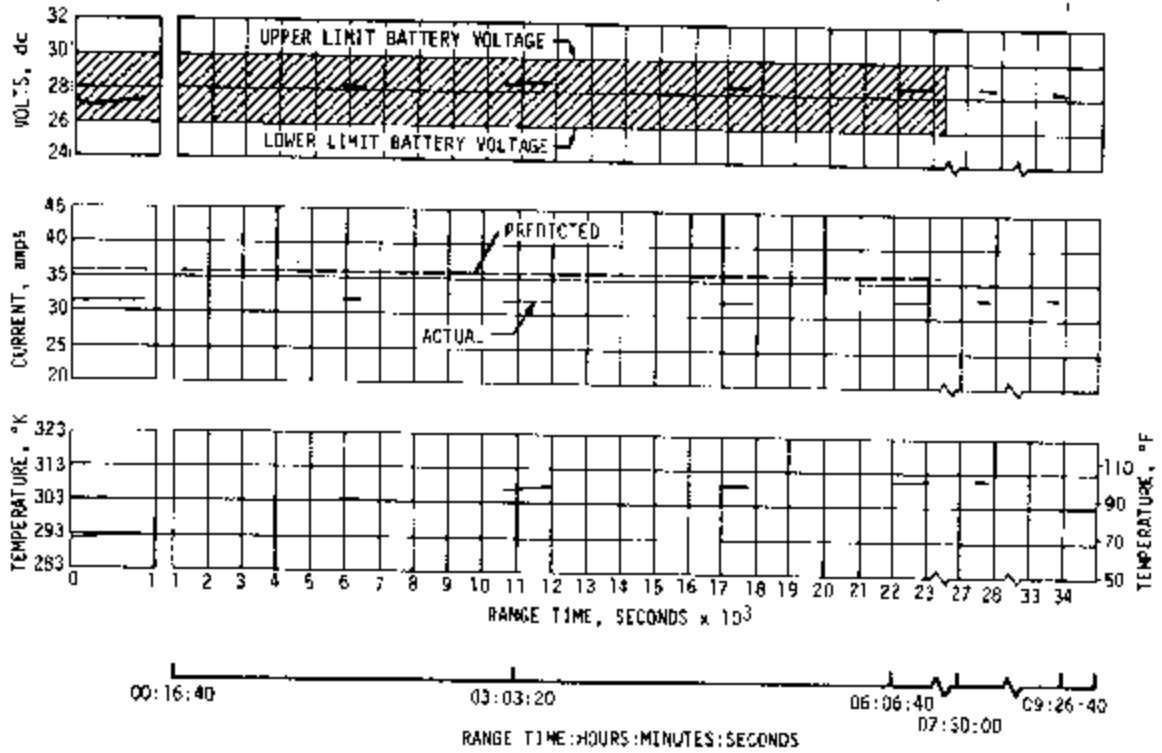


Figure 13-18. IU Battery 6D40 Voltage, Current, and Temperature

spike already discussed (see Figure 13-19). The effect of the 6D10 battery spike was also felt on the platform ac power supply (see Section 9A).

There is no indication of any discrepancy in distributor performance.

The switch selector functioned in a satisfactory manner throughout the flight. All commands to the switch selector were received properly and no complement commands were necessary.

Table 13-4. Instrument Unit Battery Consumption

BATTERY	CAPACITY * (AMP-HRS)	CONSUMPTION (AMP-HRS)			PERCENT USAGE
		MAXIMUM EXPECTED	ACTUAL HRS		
			6.5	9.4**	
6D10	350	NA	NA	295	84
6D20	350	NA	NA	310	88.5
6D30	350	NA	NA	361	100***
6D40	350	NA	NA	305	87.2

* Based on 350 ampere-hours at a 35 ampere discharge rate.

** Total usage through 9.4 hours.

*** Based on the decrease in terminal voltage.

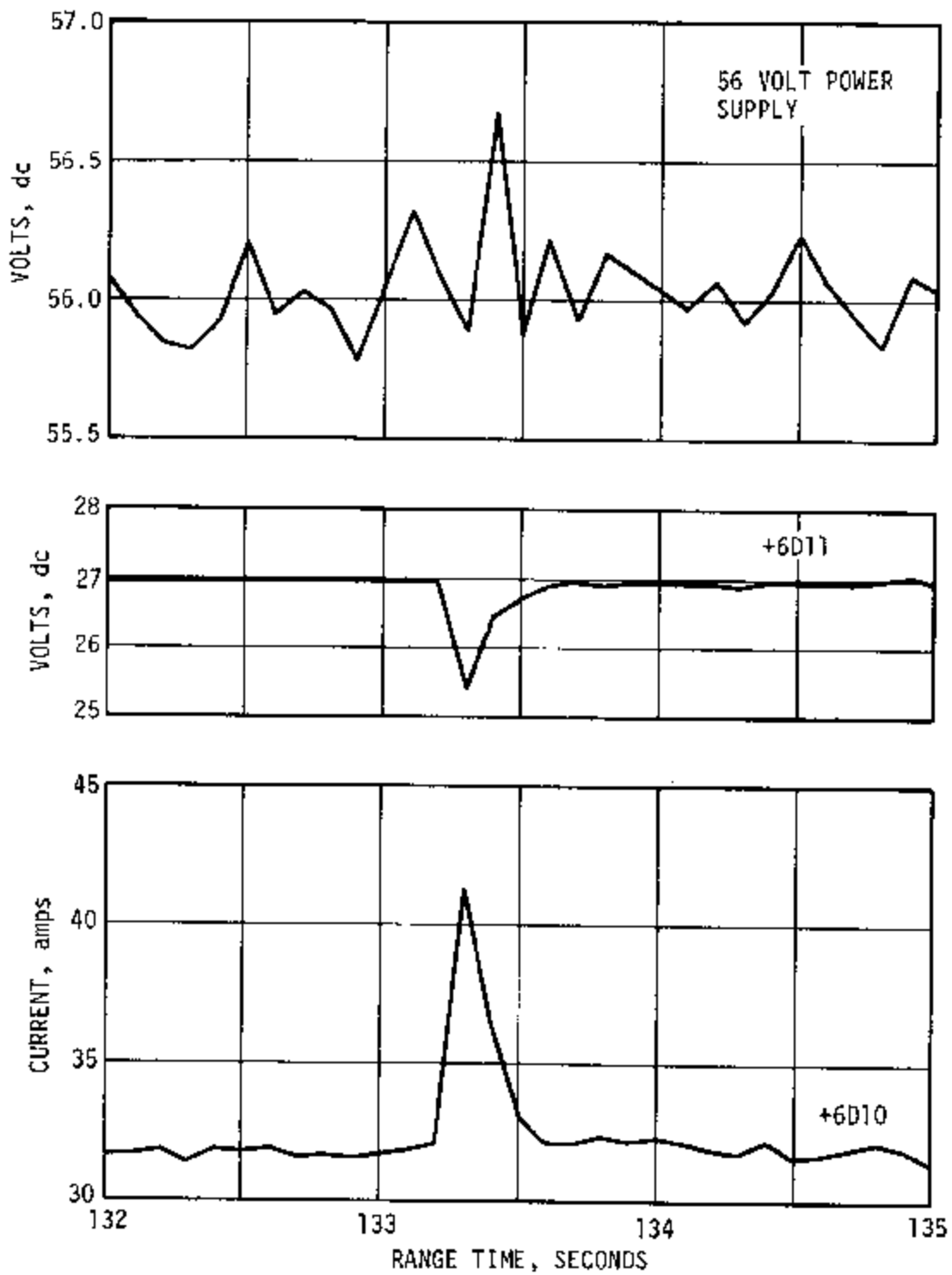


Figure 13-19. Currents and Voltages Associated with 133.3 Second Transient

SECTION 14

RANGE SAFETY AND COMMAND SYSTEMS

14.1 SUMMARY

Data indicated that the redundant Secure Range Safety Command Systems (SRSCS) on the S-IC, S-II, and S-IVB stages were ready to perform their functions properly on command if flight conditions during the launch phase had required vehicle destruct. The system properly safed the S-IVB SRSCS on command from Kennedy Space Center (KSC). The performance of the command and communications system in the Instrument Unit (IU) was very good.

14.2 RANGE SAFETY COMMAND SYSTEMS

The SRSCS provides a means to terminate the flight of the vehicle by radio command from the ground in case of emergency situations in accordance with range safety requirements. After successful insertion into earth orbit, the system is deactivated (safed) by ground command. Each powered stage of the vehicle was equipped with two command receivers/decoders and necessary antennas. The SRSCS in each stage was completely independent of those in other stages.

Three types of SRSCS commands were required for this unmanned flight as follows:

- a. Arm/fuel cutoff - Charging of the Exploding Bridge Wire (EBW) firing unit and thrust termination.
- b. Destruct - Propellant dispersion by firing of the EBW.
- c. Safe - Command system switched off.

During flight, telemetry indicated that the command antennas, receivers/decoders, and destruct controllers functioned properly and were in the required state of readiness if needed. Since no arm/cutoff or destruct commands were required, all data except receiver signal strength remained unchanged during the flight. At 5889 seconds the safing command was initiated, deactivating the system. Both S-IVB stage systems, the only systems in operation at this time, responded properly to the safing command.

The Launch Vehicle-Lunar Module Test Article/Command Service Module (LV-L_{TM}/CSM) was inserted in earth orbit with the range safety system armed, which is normal. The safing command which normally follows shortly after insertion was not sent, however, since the S-II and S-IVB extended burn periods resulted in insertion occurring further downrange, leaving insufficient time before Loss of Signal (LOS) to safe the vehicle at the normal post insertion time. The system was safed during the first orbital pass over KSC.

RF performance of the system is discussed in paragraph 19.5.3.1.

14.3 COMMAND AND COMMUNICATIONS SYSTEM

The IU Command and Communication System (CCS) is a phase-coherent receiver-transmitter system capable of establishing a communication link between the Unified S-Band (USB) ground stations and the IU of the Saturn V launch vehicle. The operational requirements of the CCS include command up-data and downlink telemetry. Turnaround ranging, although not mandatory, can be performed. Specifically, the CCS receives and demodulates command up-data for the guidance computers in the IU, transmits Pulse Code Modulated (PCM) mission control measurements originating in the S-IVB and the IU to the USB ground stations for processing, and coherently retransmits the pseudo random noise range code that is received from the USB ground stations. The CCS physically consists of a transponder, power amplifier, and antenna system.

The performance of the CCS command functions was, in general, very good, despite the vehicle anomalies.

The command portion of the CCS transponder performed flawlessly, as indicated in Table 14-1. Fifty-two flight commands and 600 test words were transmitted by the ground station, and all were received by the vehicle.

The Mission Control Center-Houston (MCC-H) Command History shows that attempts were made to send two additional flight commands from Carnarvon during revolution 3. The first occurred at 16:12:16 Greenwich Mean Time (GMT) and the second at 16:12:30 GMT.

Records indicate that Carnarvon was unable to transmit either command. The 70 KHz subcarrier was off when the first attempt was made (Carnarvon was sweeping in order to acquire the downlink), and the transmitter was off during the second attempt.

Table 14-1. CCS Command History, AS-502

STATION	PASS	FLIGHT COMMANDS		TEST WORDS	
		SENT	RECEIVED AND VERIFIED	SENT	RECEIVED AND VERIFIED
Bermuda	2			340	340
Carnarvon	3	21	21		
Canberra	1			133	133
Hawaii	3	7	7		
	4	15	15		
Guaymas	1			127	127
	3	9	9		
Total		52	52	600	600

Adequate signal strength for good telemetry was achieved throughout most of the mission. Exceptions occurred at:

- a. Bermuda during passes 2, 3, and 4, where it appears that the CCS receiver remained connected to the acquisition antenna, causing low signal strength.
- b. Carnarvon during pass 3, as previously described.
- c. Handover problems at several stations caused some data loss. The most notable example occurred during Guaymas first pass, when handover was attempted before Texas was ready.

RF performance of the system is discussed in paragraph 19.5.3.1.

SECTION 15

EMERGENCY DETECTION SYSTEM

15.1 SUMMARY

The space vehicle Emergency Detection System (EDS) was flight tested in the automatic abort closed-loop configuration on AS-502. Launch vehicle measurements indicated that no EDS limits were exceeded and the system functioned properly. There were some anomalies indicated in the spacecraft. (See paragraph 15.4.)

15.2 SYSTEM DESCRIPTION

The AS-502 EDS configuration was the same as AS-501, with the exception that the automatic abort mode was active. There are two parameters which are monitored for automatic abort. These are: angular overrate and two or more S-IC engines out. These are deactivated by the Instrument Unit (IU) switch selector prior to S-IC inboard cutoff. After automatic abort deactivation, overrate and S-IC thrust are manual abort parameters. The remaining manual abort parameters are:

- a. Angle-of-attack (ΔP).
- b. Launch vehicle attitude reference failure.
- c. S-II thrust.
- d. S-IVB thrust.
- e. S-IVB propellant tank pressures (orbital phase only).
- f. Vehicle attitude, attitude rates, and attitude error (spacecraft sensed).

Figure 15-1 is a functional diagram of the AS-502 EDS.

15.3 SYSTEM EVALUATION

15.3.1 General Performance

The excursion of the parameters monitored by the EDS sensors remained within EDS limits for proper time periods throughout flight, with the exception of premature cutoff of S-II engines No. 2 and 3.

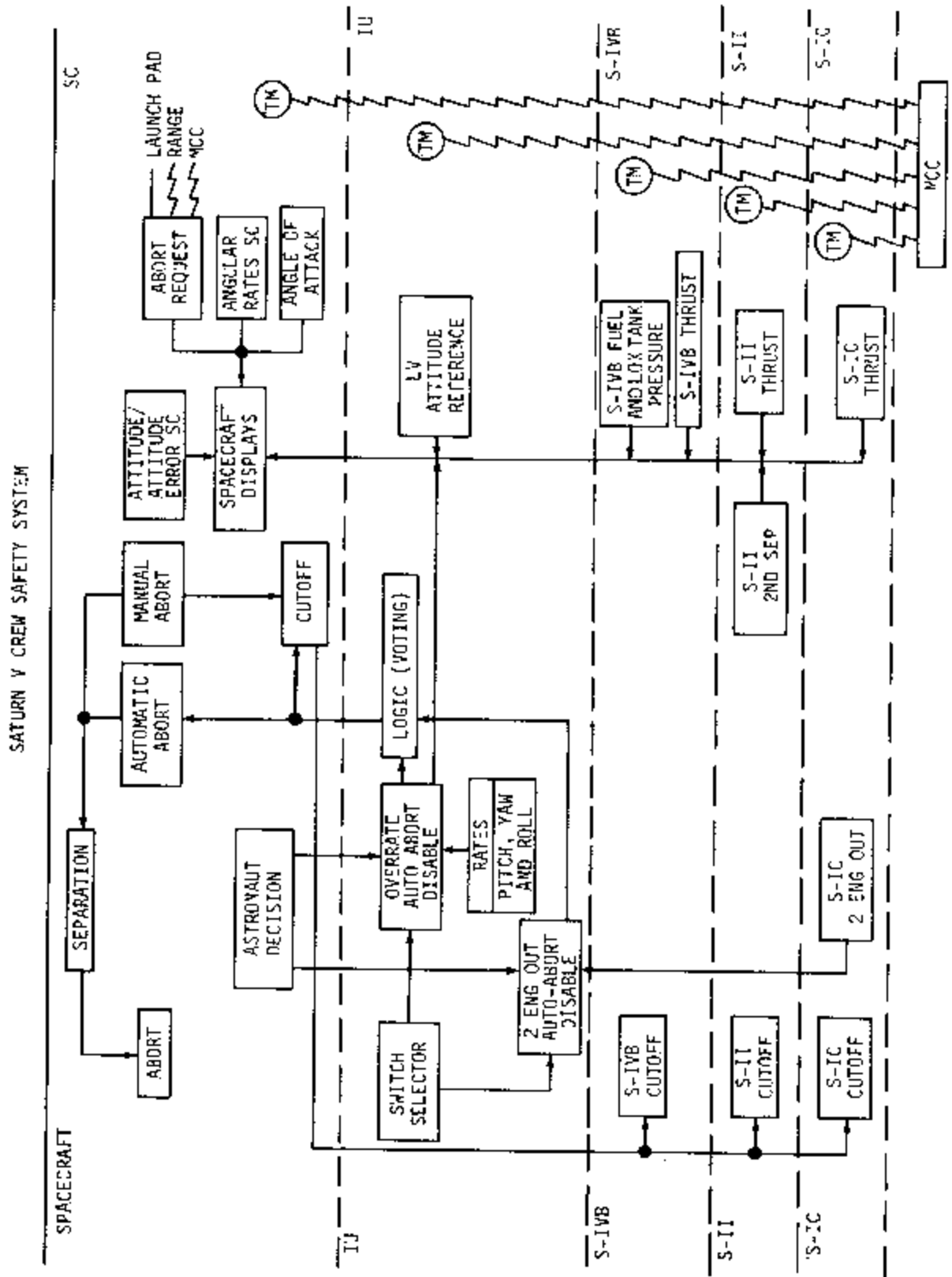


Figure 15-1. EDS Functional Diagram

15.3.2 Propulsion System Sensors

Three thrust OK sensors are used in each of the F-1 engines and two are used on each of the J-2 engines. The F-1 thrust OK switches are voted two out of three to give indication of engine out, and the J-2 thrust OK switches are voted one out of two in the logic circuitry. All thrust measurements from the launch vehicle indicated proper operation of the thrust OK logic. Table 15-1 shows the thrust switch operation times.

On manned Saturn V vehicles the S-IVB propellant tank pressures will be monitored by the flight crew during the orbital phase of flight. Although no provision was made for pressure display in the Block I spacecraft, the sensors functioned properly and the tank pressures remained within acceptable limits.

15.3.3 Flight Dynamics and Control Sensors

The angle-of-attack dynamic pressure product is sensed by a redundant Q-Ball mounted atop the Launch Escape Tower (LET). One output is displayed in the command module and telemetered from the spacecraft; the other output is routed to the IU from which it is telemetered. The maximum ΔP recorded during the AS-502 flight was 0.60 N/cm^2 (0.86 psi) at 66.5 seconds. The preliminary Saturn V abort limit is 2.21 N/cm^2 (3.2 psi), Figure 15-2.

A failure of the launch vehicle inertial reference is indicated when the platform gimbal angles are displaced excessively for a given increment of time. The limits for AS-502 were such that an angular displacement in excess of 0.4 degree must occur in at least three minor computation cycles of a major computation cycle. Reasonableness test failures must then occur 15 times during the next second before an inertial reference failure is considered to exist. The maximum gimbal displacement during a single minor computation cycle for AS-502 powered flight was 0.144 degree. This represents 36 percent of the rate required for a failure indication as stated above.

Angular rates are sensed by three rate gyros in each axis. The outputs of the gyros are fed through filters to rate switches. The rate switch settings for AS-502 were $\pm 4 \pm 0.49 \text{ deg/s}$ in the pitch and yaw axes and $\pm 20 \pm 1.5 \text{ deg/s}$ in the roll axis. When two of three rate switches in any one axis indicate an overrate, an overrate indication is given to the spacecraft; and, prior to overrate auto abort disable, an automatic abort is initiated. The maximum angular rates (unfiltered) measured on AS-502 during the period in which the overrate automatic abort was active were as follows: $\pm 2.5 \text{ deg/s}$ in the pitch axis, $\pm 0.5 \text{ deg/s}$ in the yaw axis, and $\pm 5.0 \text{ deg/s}$ in the roll axis. There was no indication of any rate switch closures on flight records.

Table 15-1. Performance Summary of Thrust OK Pressure Switches

STAGE	ENGINE	SWITCH	TIME CLOSED (RANGE TIME, SEC)	TIME OPENED (RANGE TIME, SEC)
S-IC	1	1	-1.64	148.60
	1	2	-1.64	148.60
	1	3	-1.73	148.60
	2	1	-1.31	148.60
	2	2	-1.31	148.60
	2	3	-1.23	148.60
	3	1	-1.64	148.60
	3	2	-1.64	148.60
	3	3	-1.56	148.60
	4	1	-1.31	148.60
	4	2	-1.33	148.57
	4	3	-1.33	148.57
	5	1	-2.00	144.90
	5	2	-1.92	144.90
5	3	-2.00	144.90	
S-II	1	1	153.70	576.49
	1	2	153.79	576.43
	2	1	153.77	412.84
	2	2	153.74	412.92
	3	1	153.77	414.18
	3	2	153.74	414.13
	4	1	153.70	576.49
	4	2	153.74	576.45
	5	1	153.70	576.49
	5	2	153.71	576.51
S-IVB 1ST BURN	1	1	582.03	747.27
	1	2	582.03	747.27

15.3.4 EDS Sequential Events

The sequential events pertinent to the operation of the EDS were normal. Table 15-2 lists the discrete event times for AS-502 and Table 15-3 lists the switch selector event times for AS-502.

15.4 INTERFACE CONSIDERATIONS

Although launch vehicle EDS indications were normal, there were reports of anomalies in the spacecraft. These anomalies apparently are related to the transient events which occurred at approximately 133 seconds and are discussed in Section 9A.

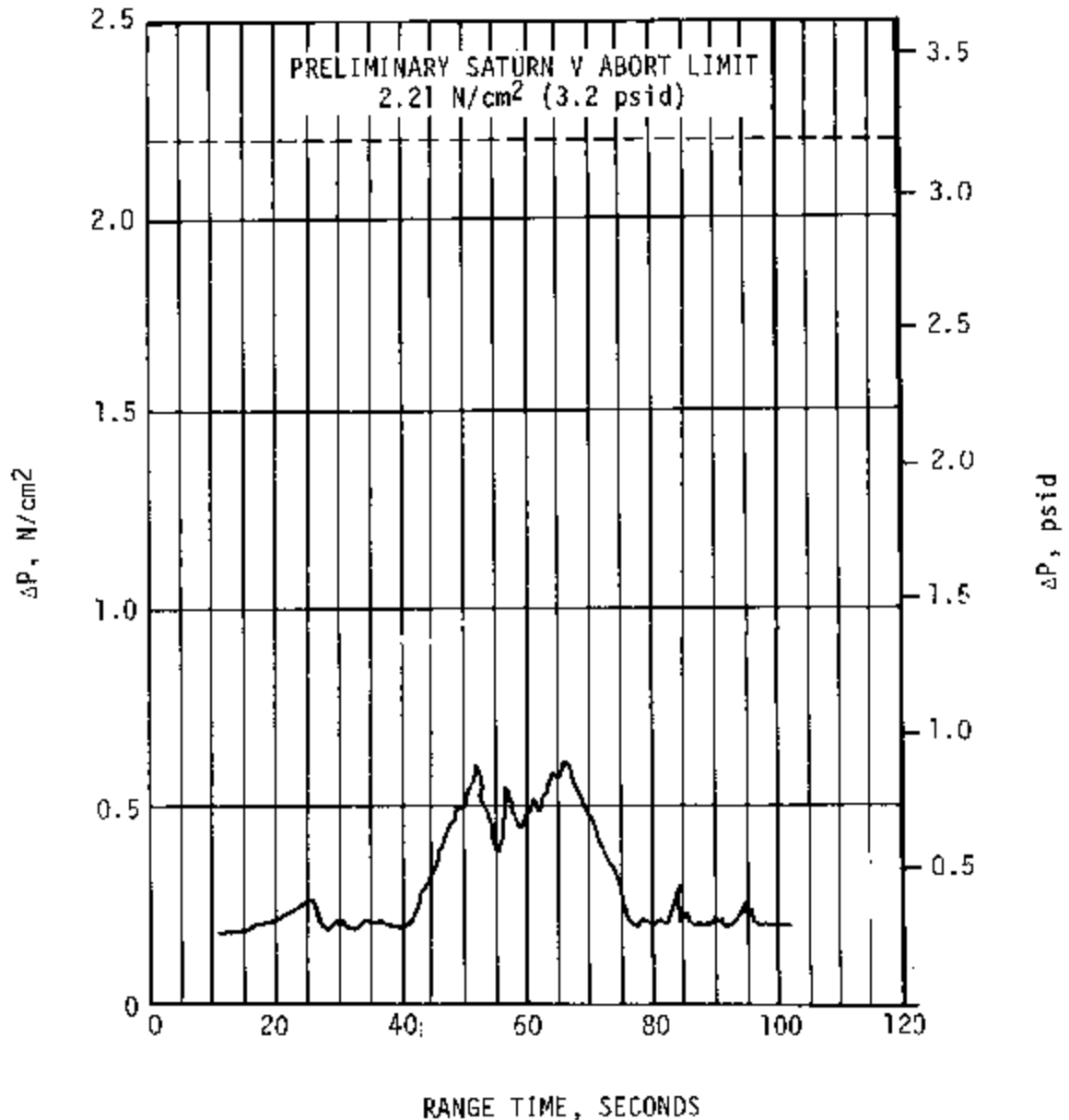


Figure 15-2. Q Ball ΔP Versus Flight Time

Table 15-2. Discrete EDS Events

DISCRETE MEASUREMENT	DISCRETE EVENT	ON/OFF	RANGE TIME (SEC)
K73-602	EDS or MAN. Cutoff of LV Engines Armed	On	30.71
K74-602	EDS or MAN. Cutoff of LV Engines Armed	On	40.95
K81-602	EDS S-IC One Engine Out	On	144.89
K82-602	EDS S-IC One Engine Out	On	144.89
K79-602	EDS S-IC Two Engines Out	On	148.64
K80-602	EDS S-IC Two Engines Out	On	148.64
K88-602	S-IC Stage Separation	Off	149.99
K57-603	Q-Ball on Indication (+6D21)	Off	150.76
K58-603	Q-Ball on Indication (+6D41)	Off	150.76
K87-602	LET Jettison "A"	On	184.78
	LET Jettison "A"	Off	184.81
K87-602	LET Jettison "B"	On	184.98
	LET Jettison "B"	Off	185.30
K75-602	EDS or MAN. Cutoff of LV Engines from S/C	On	11,666.1
K76-602	EDS or MAN. Cutoff of LV Engines from S/C	On	11,666.1

Table 15-3. Switch Selector EDS Events

FUNCTION	STAGE	RANGE TIME (SEC)	TIME FROM BASE (SEC)		
			NOMINAL	ACTUAL	DEVIATION
Start of Time Base 1	--	0.69	T ₁ +0.0	---	---
Auto-Abort Enable Relays Reset	IU	5.64	T ₁ +5.0	4.95	-0.05
Multiple Engine Cutoff Enable	S-IC	14.65	T ₁ +14.0	13.96	-0.04
Launch Vehicle Engines EDS Cutoff Enable	IU	30.66	T ₁ +30.0	29.97	-0.03
S-IC Two Engines Out Auto-Abort Inhibit Enable	IU	135.95	T ₁ +135.3	135.26	-0.04
S-IC Two Engines Out Auto-Abort Inhibit	IU	136.17	T ₁ +135.5	135.48	-0.02
Excess Rate (P, Y, R) Auto- Abort Inhibit Enable	IU	136.34	T ₁ +135.7	135.65	-0.05
Excess Rate (P, Y, R) Auto- Abort Inhibit	IU	136.54	T ₁ -135.9	135.85	-0.05
Start of Time Base 2	--	144.95	T ₂ +0.0	---	---
Start of Time Base 3	--	148.41	T ₃ +0.0	---	---
Q-Ball Power Off	IU	150.76	T ₃ +2.4	2.35	-0.05
LET Jettison "A" On	IU	184.77	T ₃ +36.4	36.36	-0.04
LET Jettison "B" On	IU	184.98	T ₃ +36.6	36.57	-0.03

SECTION 16

VEHICLE PRESSURE AND ACOUSTIC ENVIRONMENT

16.1 SUMMARY

The vehicle internal, external and base region pressure environment was monitored by a series of differential and absolute pressure gages. These measurements were used in confirming the vehicle design external, internal, and base region pressure environments. The flight data were generally in good agreement with the predictions and compared well with the AS-501 data. The pressure environment was well below the design level.

The vehicle internal and external acoustic environment was monitored by a series of microphones positioned to measure both the rocket engine and aerodynamically induced fluctuating pressure levels. The measured acoustic levels were generally in good agreement with the liftoff and inflight predictions and with AS-501 data. The S-IC stage internal acoustic levels at liftoff and during flight were somewhat lower than static firing levels. No detrimental effects due to the acoustic levels have been determined at this time.

16.2 SURFACE PRESSURE AND COMPARTMENT VENTING

16.2.1 S-IC Stage

External and internal pressure environments on the S-IC stage were recorded by 43 measurements which were located on and inside the engine fairings, aft skirt, intertank, and forward skirt. Representative data from a portion of these instruments are compared with the AS-501 flight data and predictions in Figures 16-1 through 16-4. The ambient pressure history of the AS-502 flight is approximately 0.10 N/cm^2 (0.15 psi) greater than the history based on AS-501. The predictions are based on available wind tunnel data and the 48-hour Observed Mass Point Trajectory (OMPT).

The AS-502 S-IC engine fairing compartment pressure differentials are shown in Figure 16-1. The AS-502 pressure data were generally less than the data for AS-501. This was expected as a result of removing the base flow deflectors on AS-502. However, the agreement is good and the trends are the same.

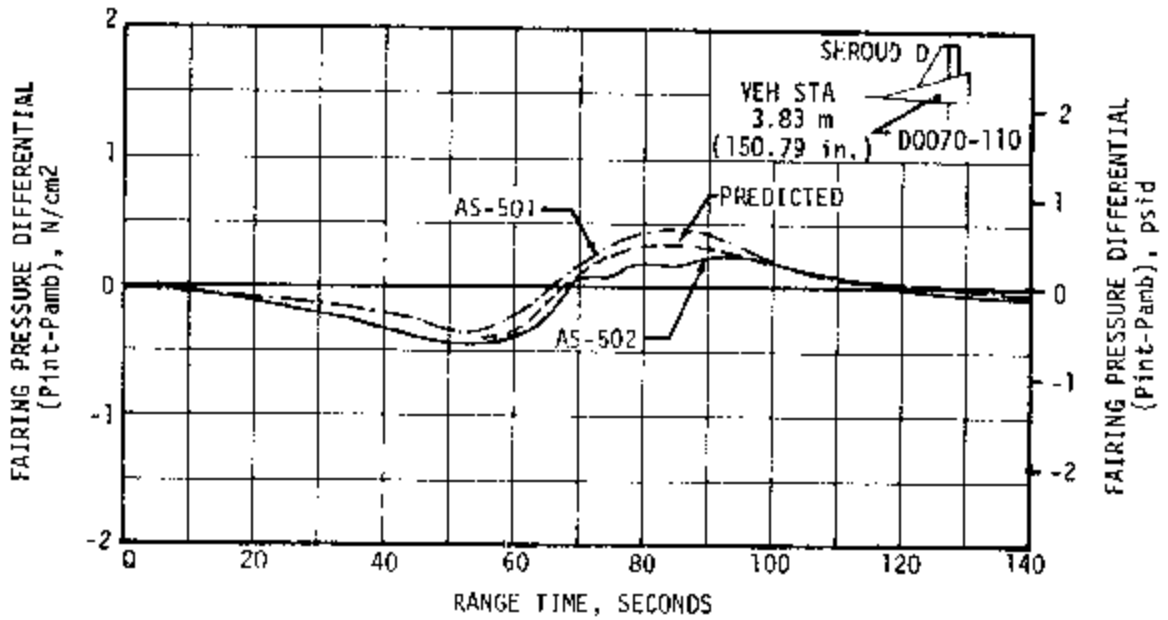
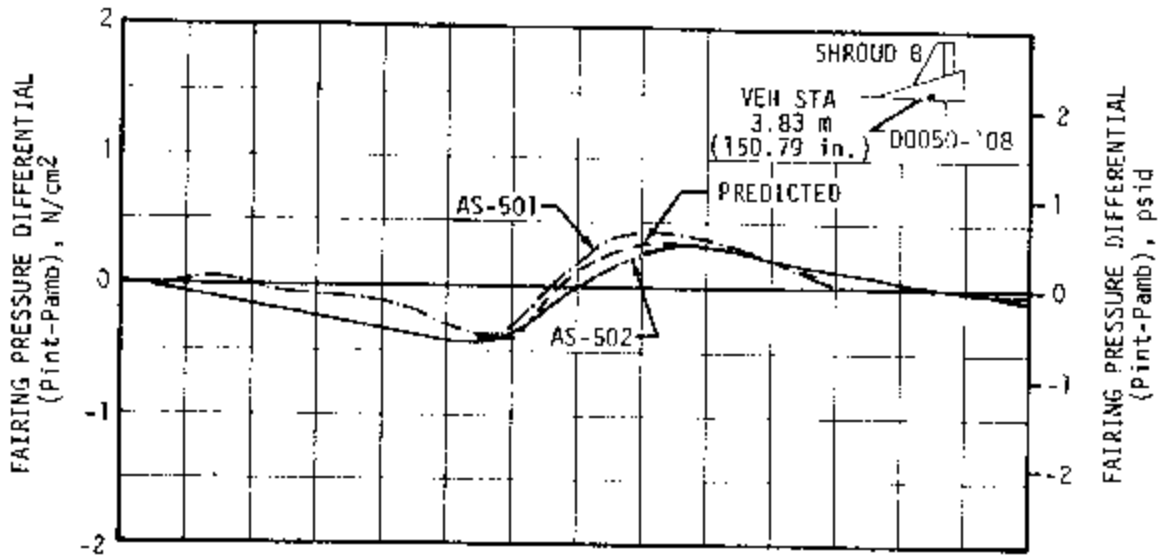


Figure 16-1. S-IC Engine Fairing Compartment Pressure Differential

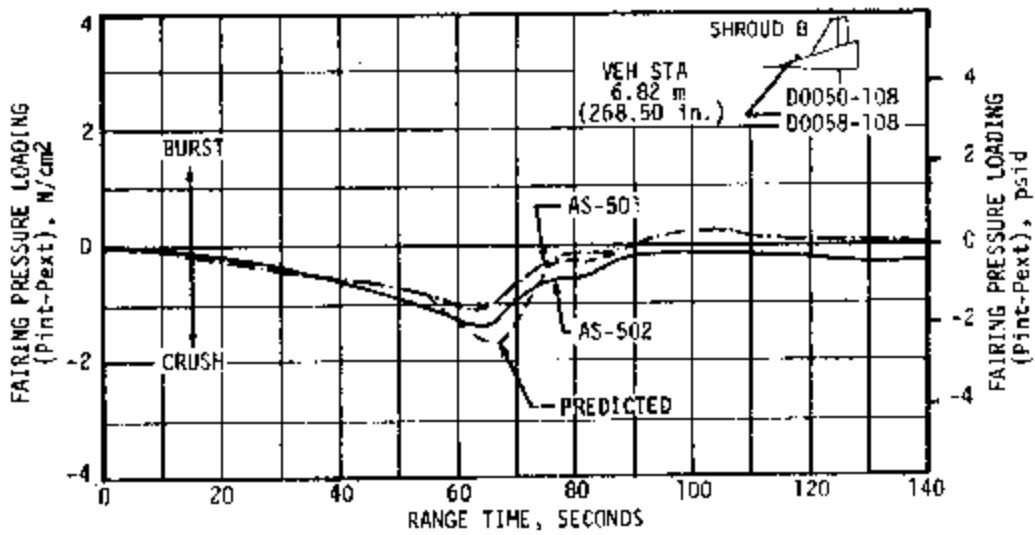
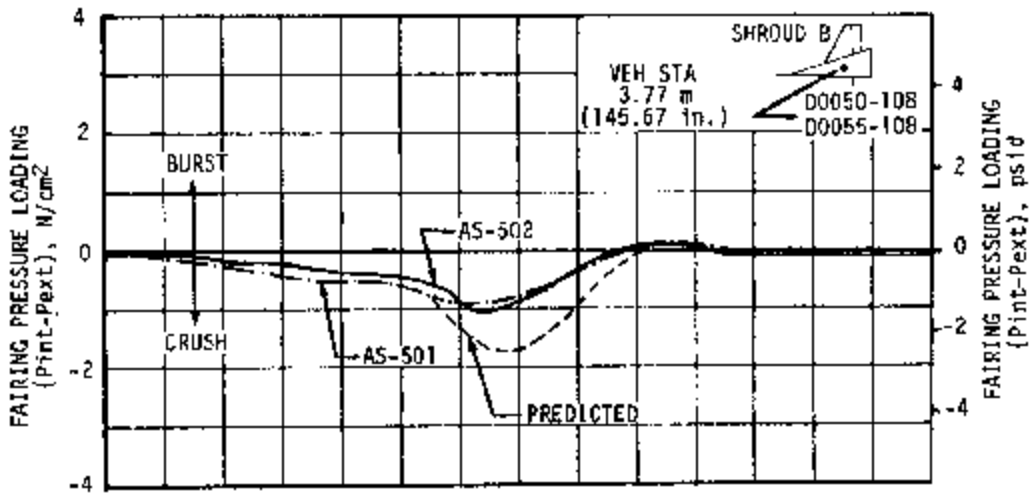
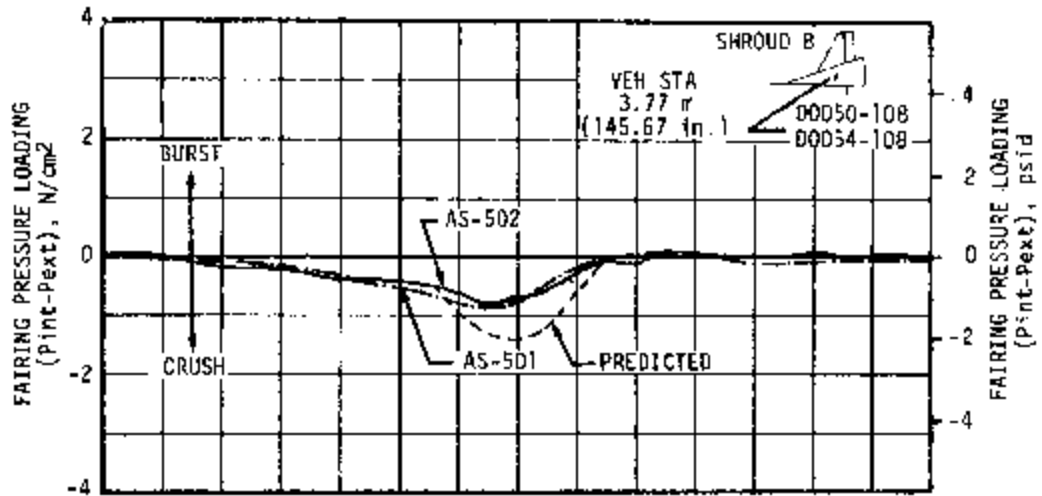


Figure 16-2. S-IC Engine Fairing Pressure Loading, Sheet 1 of 2

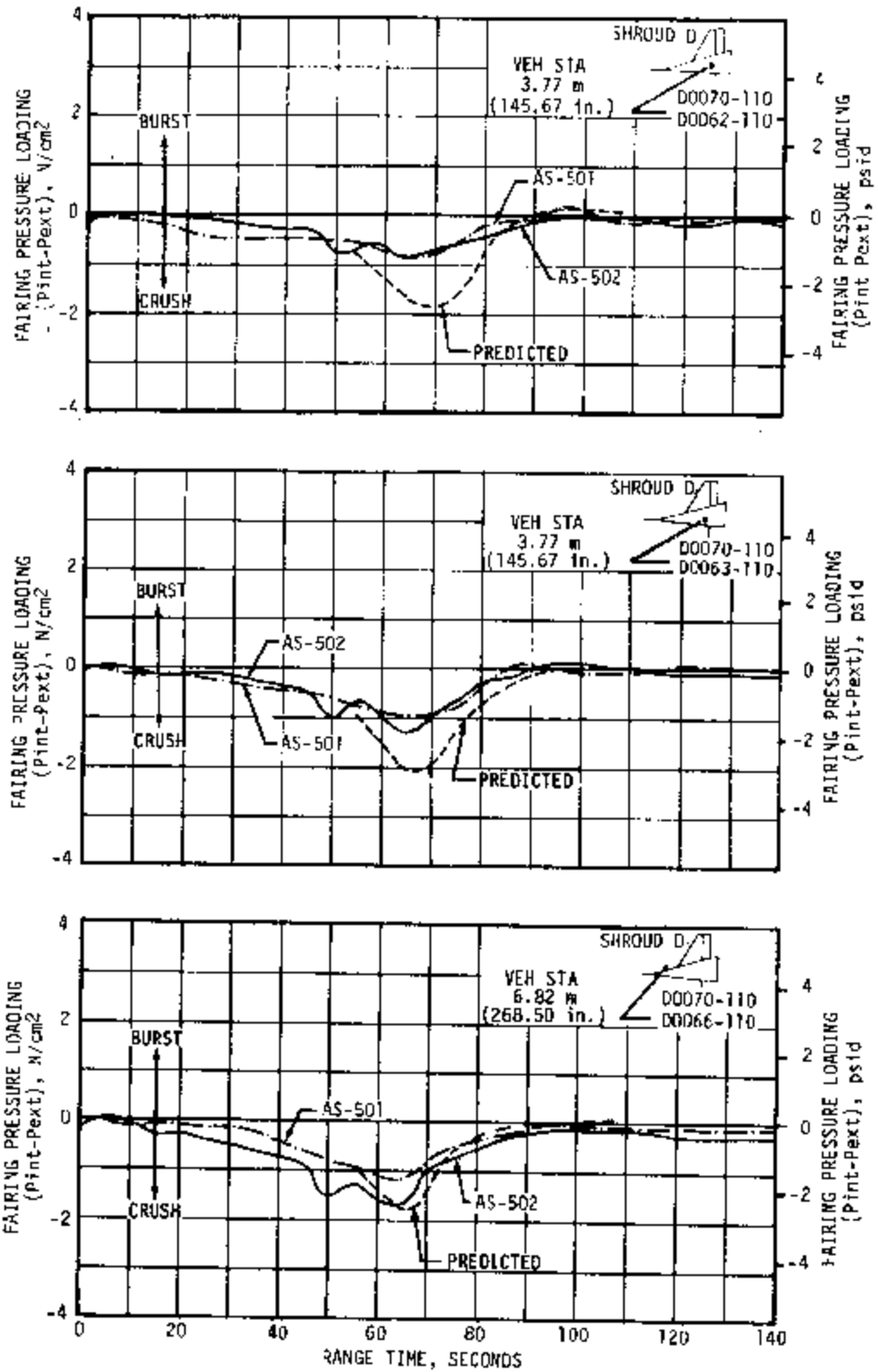


Figure 16-2. S-IC Engine Fairing Pressure Loading, Sheet 2 of 2

The S-IC engine fairing pressure loading is shown in Figure 16-2. The AS-502 and AS-501 data agree very well in magnitude and trend. The shrouds experienced a crush loading over almost the entire flight because their geometry is intended to deflect the air stream away from the S-IC engines.

The S-IC engine, intertank, and forward skirt compartment pressure differentials are shown in Figure 16-3 as a function of range time. Due to the flow deflector removal the AS-502 engine compartment pressure differential was less than that experienced on AS-501 throughout flight. This resulted from the compartment being vented into the shroud base region, which also experienced slightly lower pressures on AS-502 as compared to AS-501, as will be shown in paragraph 16.3. The intertank and forward skirt pressure differentials show good agreement as a function of range time. The predicted bands were derived analytically using maximum and minimum leakage areas. The intertank and forward skirt pressure differentials show a drop between 60 and 70 seconds on both flights. This was associated with the vehicle passing through Mach 1 and was probably the result of a normal shock moving rapidly down the side of the S-II and S-IC stages. On each flight Mach 1 occurred between 60 and 61 seconds.

The S-IC engine, intertank, and forward skirt compartment pressure loadings are shown in Figure 16-4. The engine and intertank pressure loadings agree well with the AS-501 data. The forward skirt loading was greater on AS-502 throughout flight but presented no problem since the maximum value of approximately 0.25 N/cm^2 (0.36 psi) was well below the aerodynamic design value of 1.38 N/cm^2 (2.0 psi). The predictions were based on wind tunnel data and predicted internal pressures.

16.2.2 S-II Stage

Surface pressure and compartment venting analyses were conducted using the AS-502 final OMPT and angle-of-attack data obtained from the S-IC Flight Control Conditioned Data Tape (Q-ball). Atmospheric data were obtained from the final Meteorological Data Tape (Met Tape).

The external flow field at a discrete point on the S-II stage was analyzed by means of the semi-empirical digital computer flow field program. Since the flow field program assumes that the vehicle has a clean configuration the flow disturbances created by the existence of multiple protuberances cannot be predicted. The internal pressure was analyzed by means of a multiple venting digital computer program.

Comparison plots of the pressure loading, acting across the forward skirt wall, are presented in Figure 16-5. The design, AS-502 flight, and post-flight prediction data are presented in the form of maximum-minimum data bands. AS-501 flight data are also shown for comparison. Both flight and predicted pressure loadings were obtained by taking the difference between the respective external pressure values and an internal pressure which was measured at vehicle station 74.53 meters (2934.25 in.) and

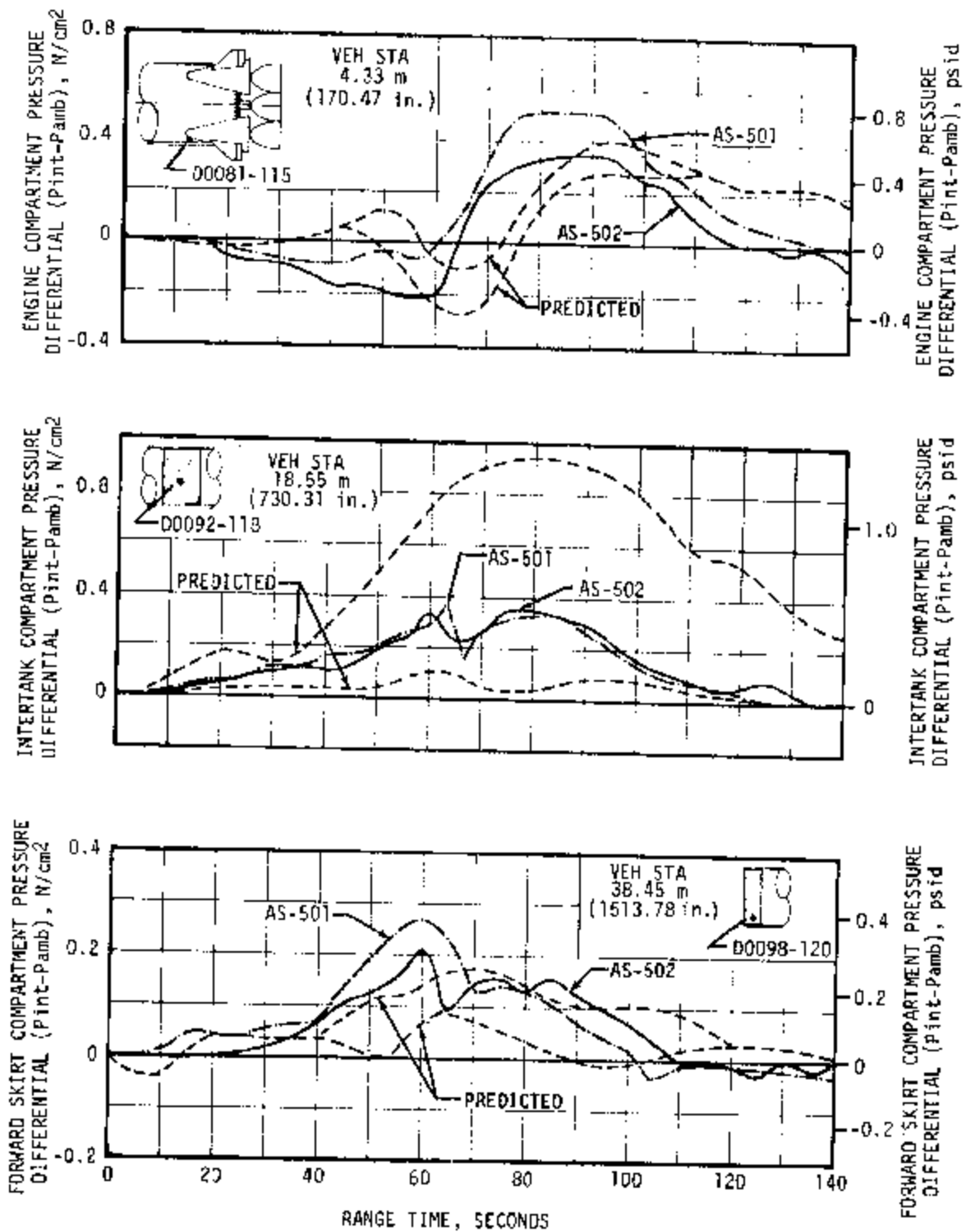


Figure 16-3. S-IC Compartment Pressure Differential

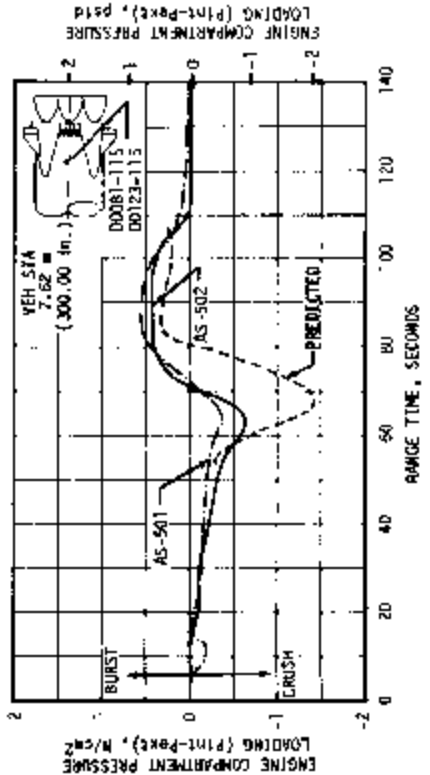
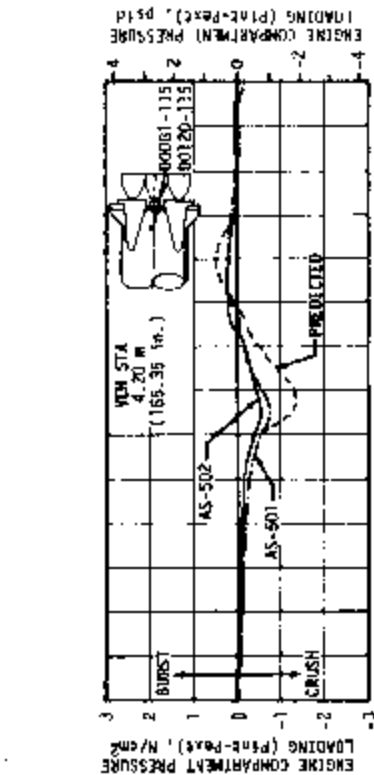
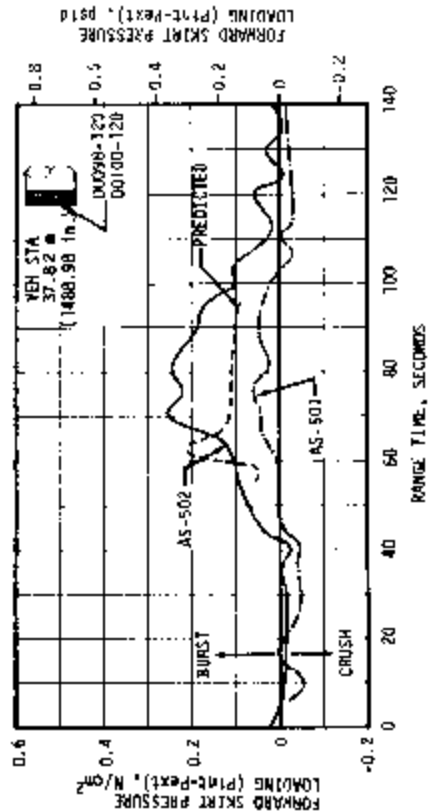
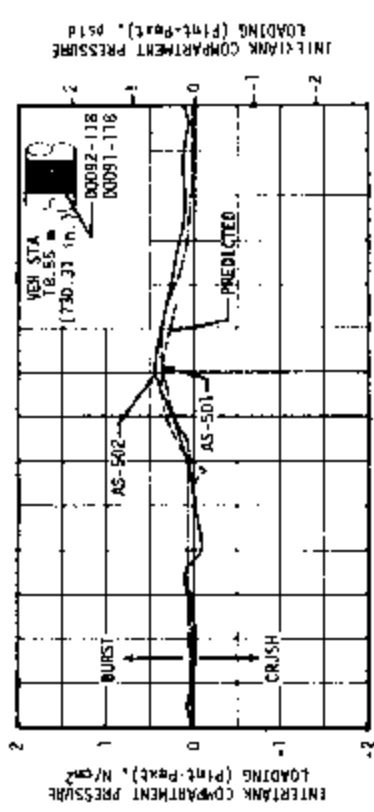


Figure 16-4. S-1C Compartment Pressure Loading

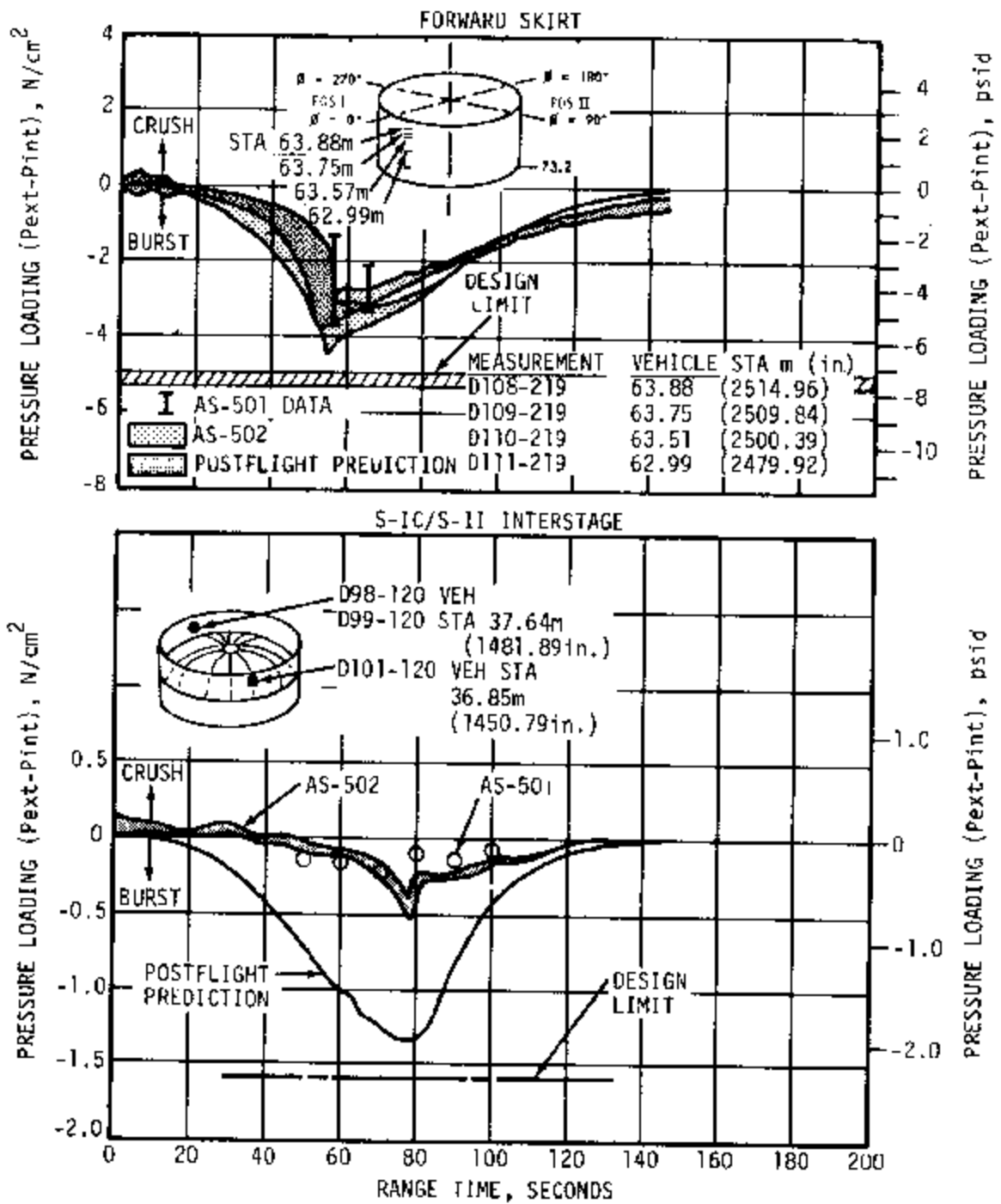


Figure 16-5. S-II Compartment Pressure Loading

assumed to be uniform within the interstage. The flight and predicted values were in fairly good agreement and well within design limits.

Comparison plots of the pressure loading, acting across the interstage wall, are also presented in Figure 16-5. The design, AS-502 flight, and predicted data as well as the AS-501 flight data are shown. The predicted loadings were approximately 1.0 N/cm^2 (1.5 psi) higher than the corresponding flight values, however, both fell within the design limits. This apparently large discrepancy was primarily due to the method and value of the discharge coefficient used to predict the internal pressure. The method was identical to that used for the forward skirt analysis where fairly good agreement was obtained. However, since the boundary layer is considerably thicker on the aft skirt region an increase in the venting efficiency, with a corresponding lower internal pressure, may result. Note also that a uniform internal pressure was assumed to exist throughout the aft skirt compartment for purposes of inflight venting analysis.

Comparison of the AS-502 flight and postflight predicted pressure loading acting across the LH₂ sidewall insulation at vehicle stations 54.2 and 59.8 meters (2133.86 and 2354.33 in.) is presented in Figure 16-6. The flight data for vehicle station 48.0 meters (1889.76 in.) is to be considered unreliable pending further investigation and is shown in this figure for reference only. AS-501 flight measurements for vehicle station 59.8 meters (2354.3 in.) are also shown and compare well with the corresponding AS-502 measurement.

The predicted internal pressure histories were computed by means of the multiple venting digital computer program using a math model to simulate the LH₂ sidewall insulation venting. The math model was developed empirically by matching S-II-1, S-II-3 and S-II-4 ambient blow down test data.

16.2.3 S-IVB Stage

Pressures on the S-IVB stage were measured by one internal transducer in the forward compartment and 21 external and 3 internal measurements for the aft compartment.

Figure 16-7 shows the predicted internal minus ambient pressure differentials for the forward compartment together with flight data for both AS-501 and AS-502. The vent area for AS-502 was 0.097 m^2 (150 in.²) as compared to 0.129 m^2 (200 in.²) for AS-501. With the trajectories flown, the smaller vent area on AS-502 should have resulted in higher internal pressures than AS-501 and correspondingly higher pressure differentials. The lower internal pressures for the first 60 seconds of the AS-502 flight, 0.034 N/cm^2 (0.05 psid), are attributed to instrumentation accuracy ($\pm 0.52 \text{ N/cm}^2$, $\pm 0.75 \text{ psi}$).

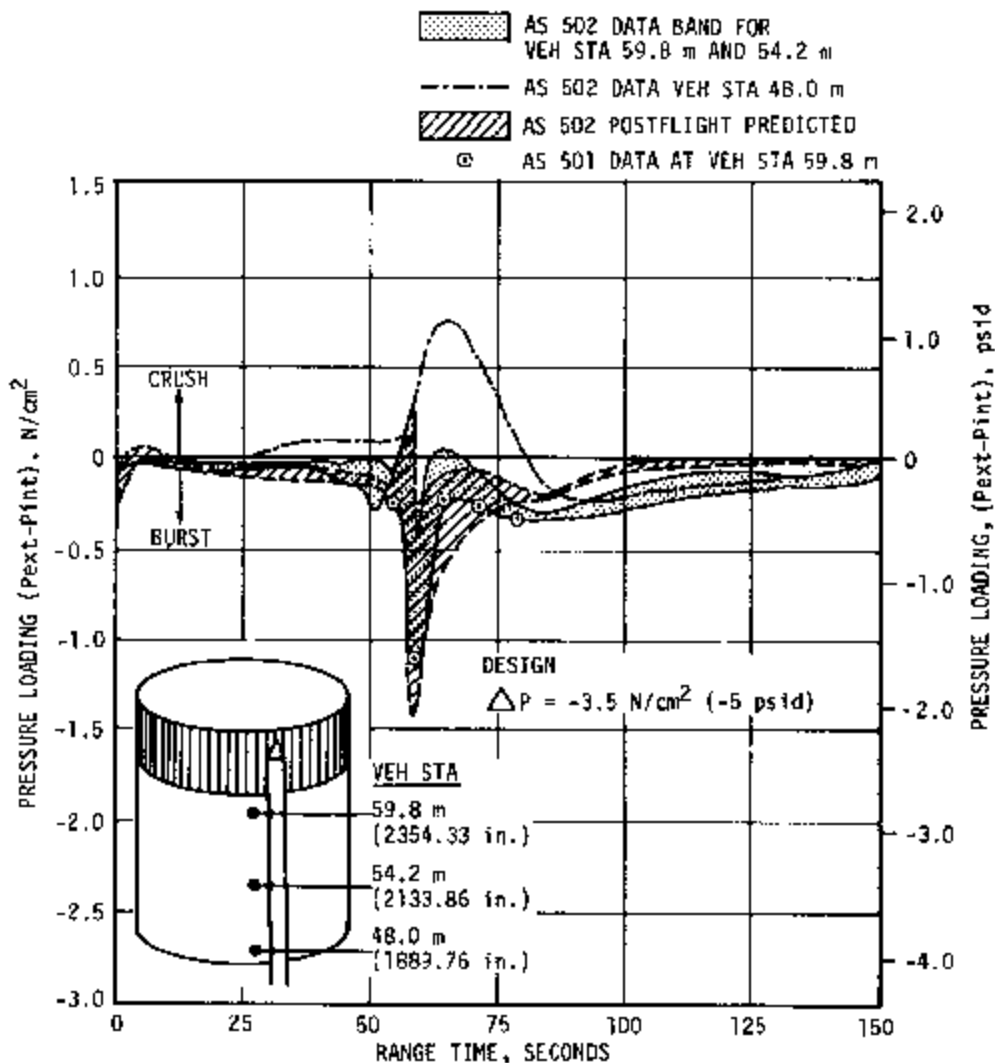


Figure 16-6. S-II LH₂ Sidewall Insulation Differential Pressure

Figure 16-7 also shows the absolute pressure history in the forward skirt for a time interval centered on 133 seconds. The abrupt pressure drop at this time is thought to be associated with the 133 second anomaly as discussed in paragraph 9A.2.1.

Figures 16-8 and 16-9 show predicted and measured pressure differentials and pressure loadings for the aft compartment as internal-minus-ambient and internal-minus-external respectively. The flight data fell within the predicted band during the critical flight period and the maximum bursting and crushing pressures, 2.0 and 0.55 N/cm², (2.9 and 0.8 psid respectively) are well below the design values, 3.23 and 1.54 N/cm² (4.69 and 2.24 psid).

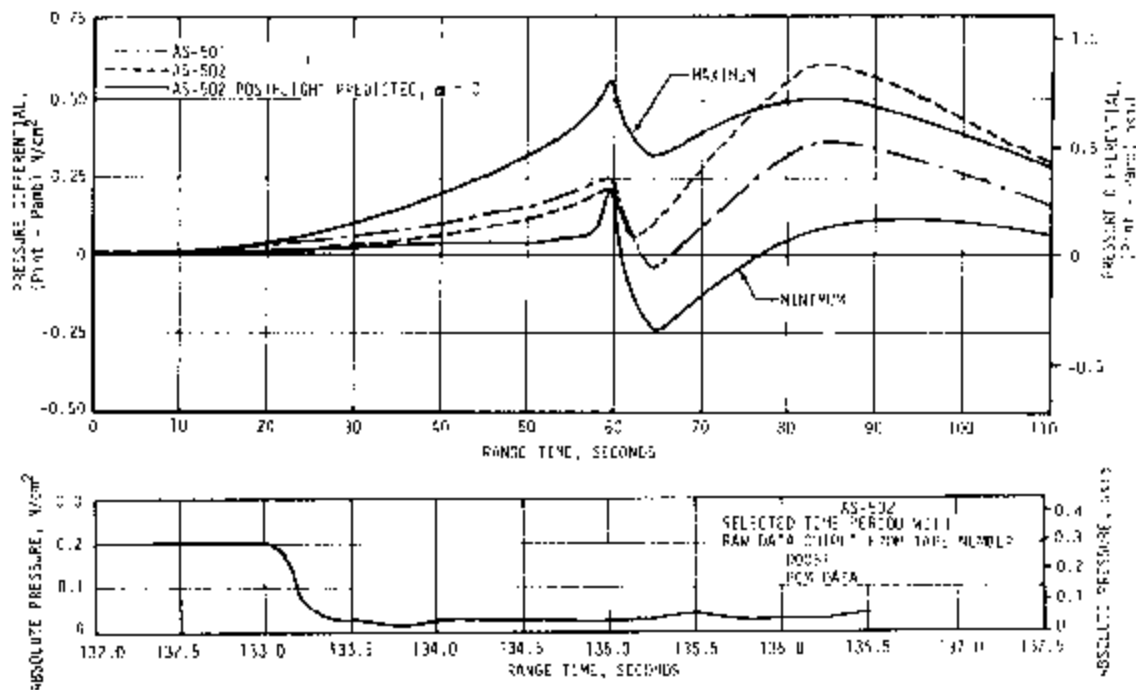


Figure 16-7. S-IVB Forward Compartment Differential Pressure

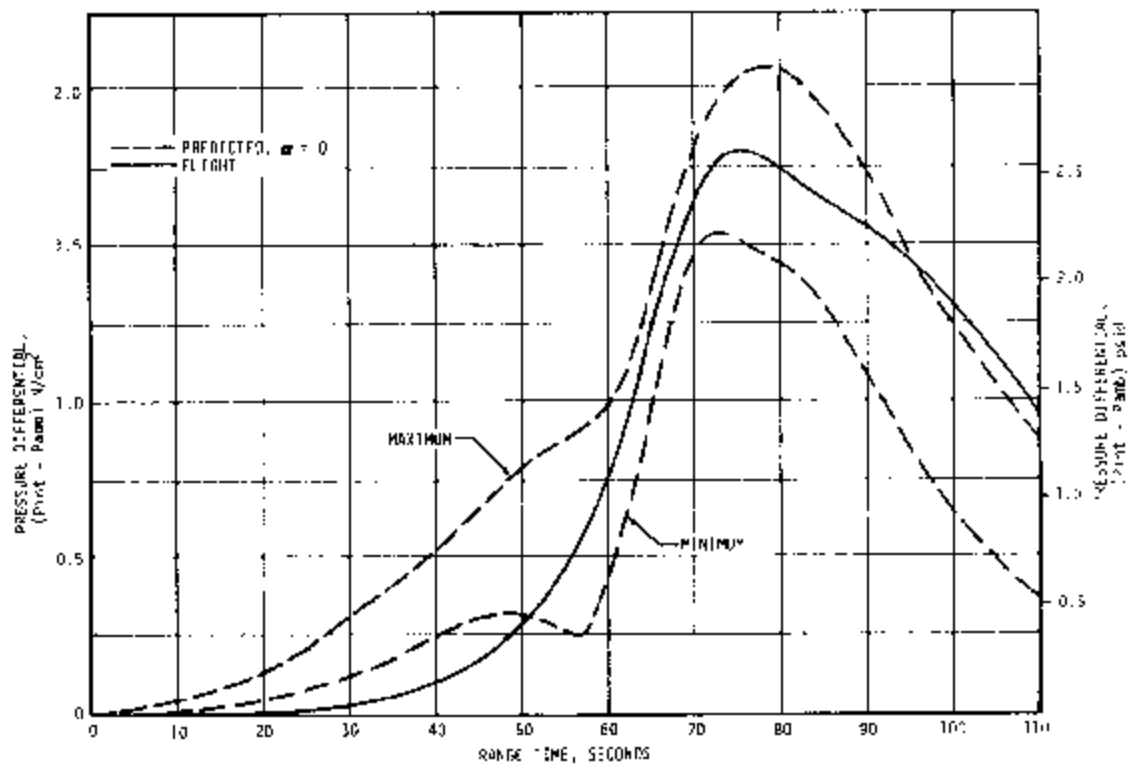


Figure 16-8. S-IVB Aft Skirt and Interstage Differential Pressure

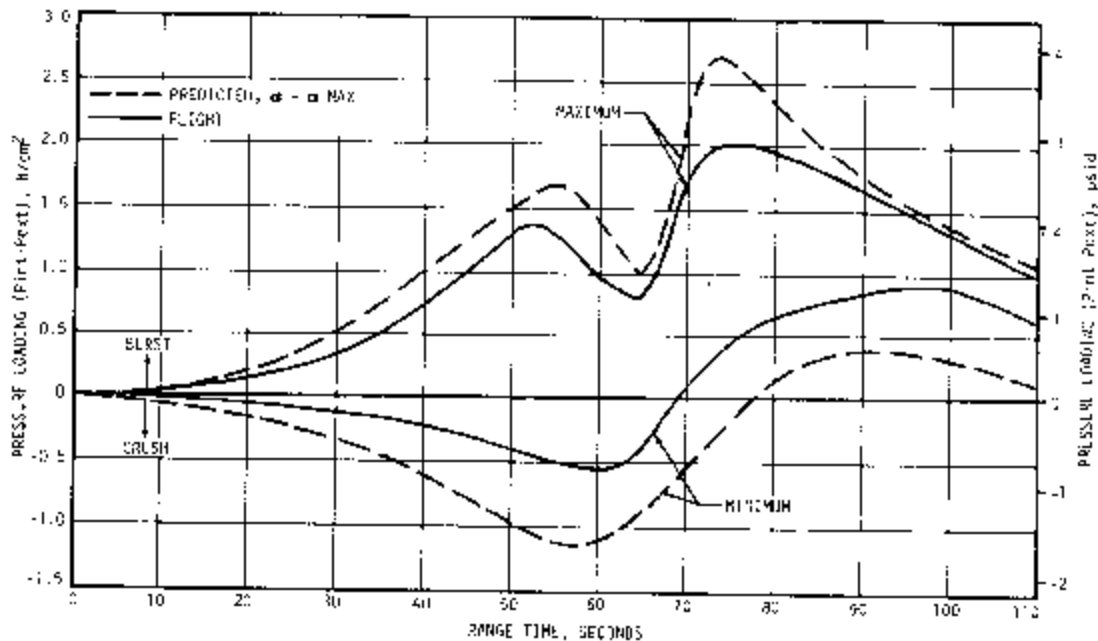


Figure 16-9. S-IVB Aft Skirt and Interstage Pressure Loading

16.3 BASE PRESSURES

16.3.1 S-IC Base Pressures

Static pressures on the S-IC base heat shield were recorded by 11 measurements, 2 of which were heat shield differential pressures. Representative data from a portion of these instruments are compared with AS-501 flight data and predictions based on the 48-hour OMPT. The predictions include the effects of the base flow deflectors since wind tunnel data on a configuration without flow deflectors were not available.

The S-IC base pressure differentials are shown in Figure 16-10. In general, the agreement is good. The AS-502 base pressures were slightly less than AS-501 up to approximately 20 kilometers (10.8 n mi) altitude. Beyond this altitude only small differences existed. The lower pressure below 20 kilometers (10.8 n mi) was a result of removing the base flow deflectors on AS-502.

The S-IC base heat shield pressure loadings are shown in Figure 16-11. Again the AS-502 data were less than AS-501 below 20 kilometers (10.8 n mi). The flow deflector removal on AS-502 lowered the base pressure to which the engine compartment vents. These heat shield differentials were well within the $1.38 N/cm^2$ ($2.0 psid$) design differential.

16.3.2 S-II Base Pressures

The postflight predictions of the S-II base heat shield aft face static pressures are evaluated from a semi-empirical correlation of base

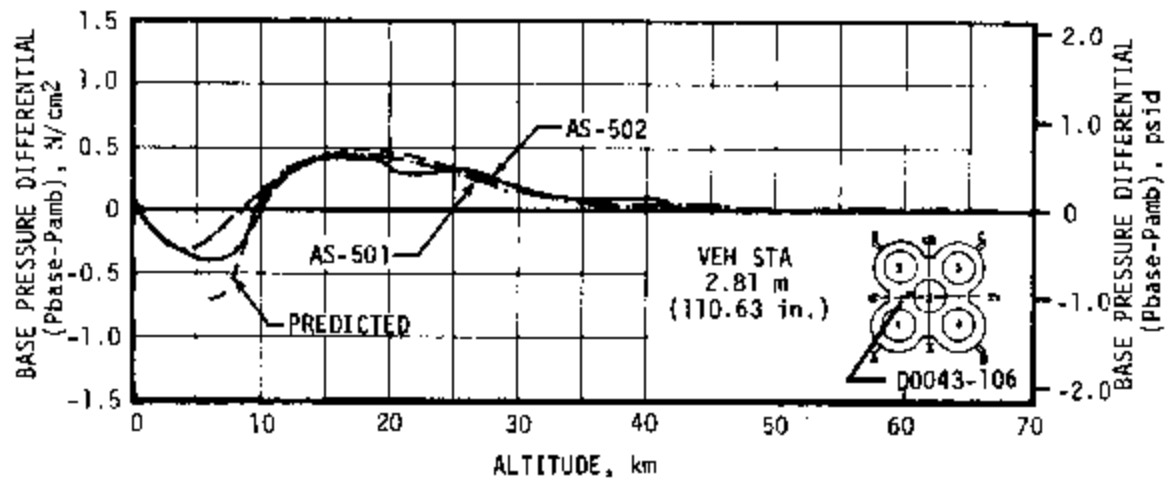
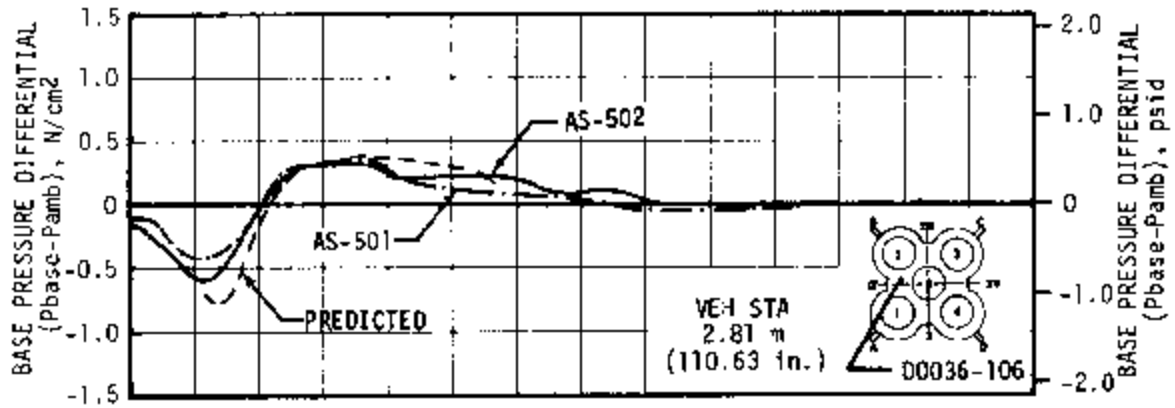
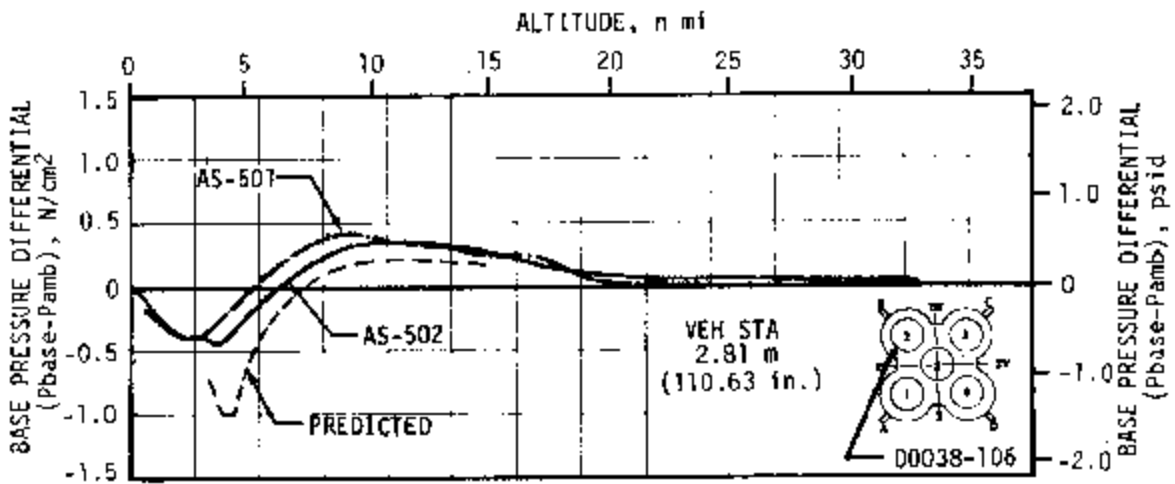


Figure 16-10. S-IC Base Pressure Differentials

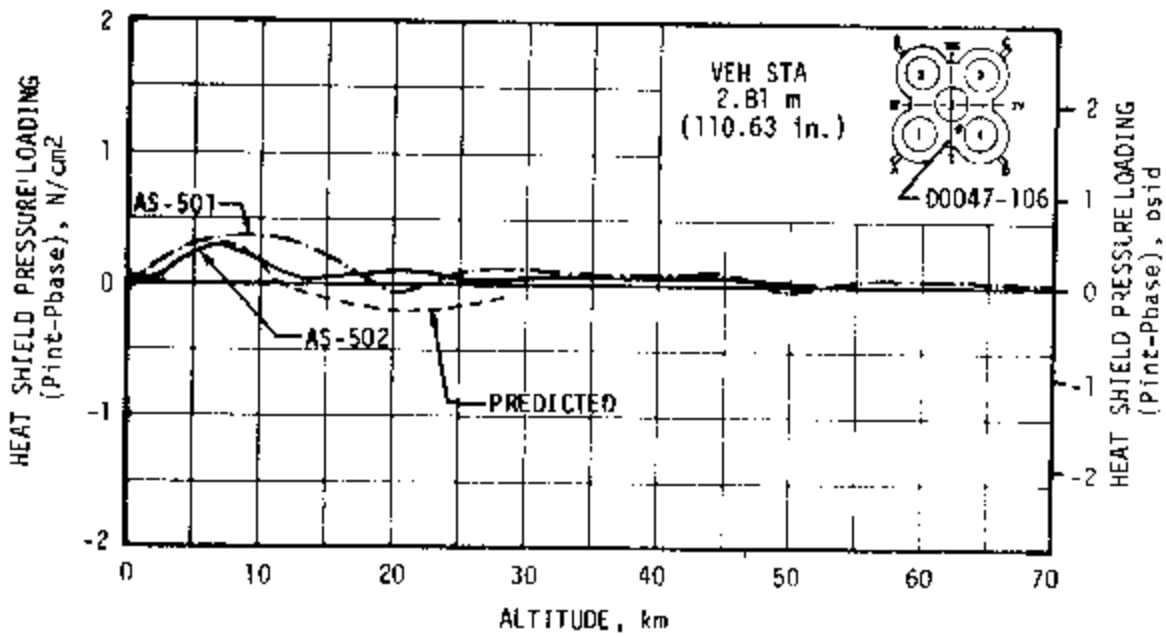
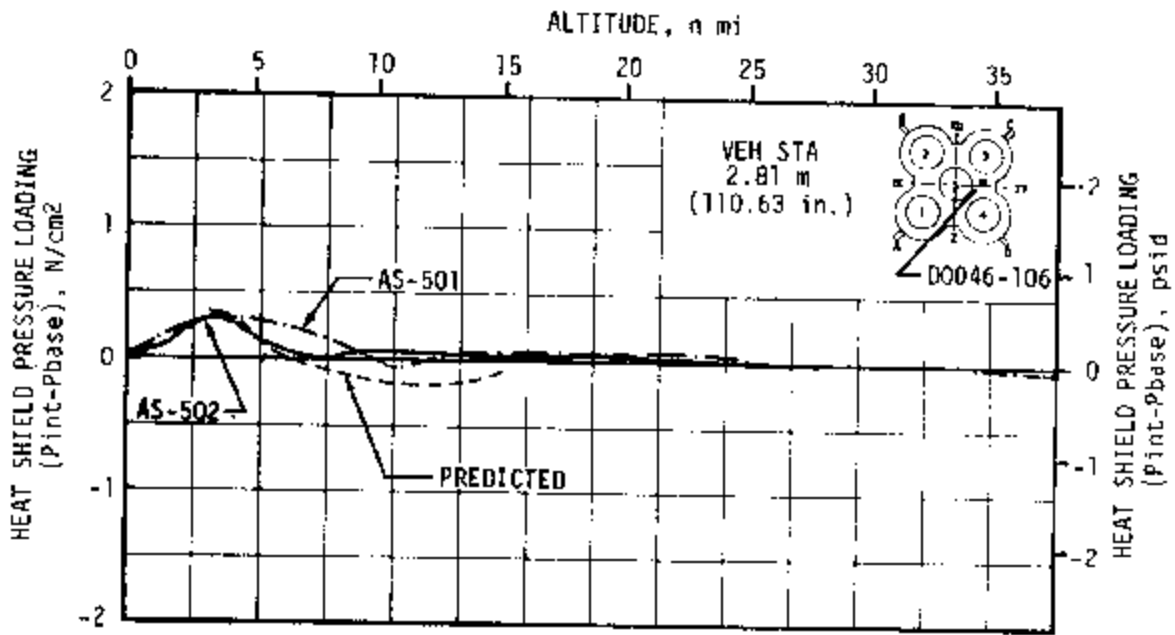


Figure 16-11. S-IC Base Heat Shield Pressure Loading

pressures and heating rates derived from the hot flow scale model test results and AS-501 flight data. The effects of the interstage on the base pressures are accounted for in the analysis. The postflight predictions of the thrust cone region pressures were based on the AS-501 flight data.

Figure 16-12 presents the predicted and measured static pressures on the aft face of the base heat shield. It is noted that the pressure distribution on the base heat shield was more uniform prior to second plane separation. The pressure reached a peak value during interstage separation because the J-2 exhaust plumes were confined by the interstage resulting in high impingement pressures and increased reverse mass flow rates.

After engines No. 2 and 3 cutoff, the pressure distribution on the base heat shield aft face became highly unsymmetrical. This was because positions II, III and IV on the heat shield no longer experienced direct reverse flow impingement. The pressures at these positions dropped to the ambient level while the reverse flow impingement pressure was maintained in position I quadrant.

Figure 16-13 presents the predicted and measured static pressure on the heat shield forward face and on the thrust cone surface. The pressure distribution was more uniform in this region as compared to that on the heat shield aft face. The pressure rise resulting from S-IC/S-II interstage separation was also apparent in the thrust cone region; however, it was not as pronounced as that on the base heat shield aft face. Note that the pressure in the thrust cone region dropped by a factor of 20 after interstage separation.

Figure 16-13 also shows that a considerable pressure rise existed in the thrust cone and heat shield forward face region immediately prior to and during J-2 engine No. 2 cutoff at 412.92 seconds. Note that the maximum indicated pressures were above the pressure transducer range of 0.0689 N/cm² (0.1 psi) and that they were also above the pressures recorded prior to and during interstage separation. Therefore, it is concluded that the measured pressure rises could not result from the J-2 engine exhaust reverse flow. Since the base heat shield aft face/thrust cone region is open to the atmosphere, and because the measured pressure rise appears to be uniform through the base heat shield forward face region, it appears that a very sudden and substantial mass injection into this region occurred causing the measured pressure rise. For further details see paragraph 6.3.

Figures 16-14 and 16-15 present an overall view of base region pressure instrumentation together with the flight data recorded prior to and during the engines No. 2 and 3 cutoff time interval. It is seen that the recorded pressure rise on the thrust cone surface was considerably smaller than the pressure rise on the base heat shield forward surface and that a relatively small pressure rise was also recorded on the heat shield aft surface at this time. This was probably due to engine gimbaling associated with the cutoff of engines No. 2 and 3.

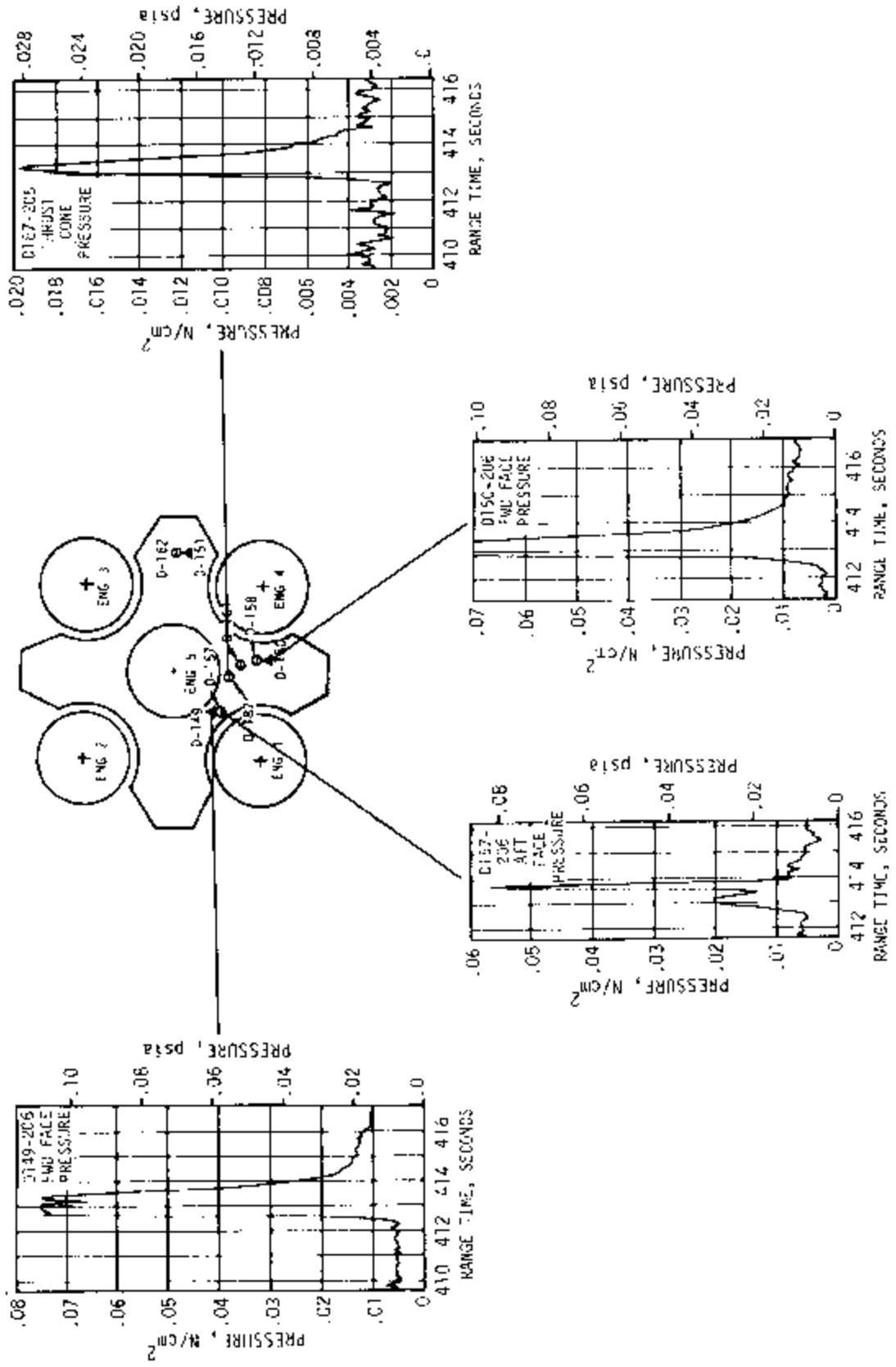


Figure 16-14. S-II Base Heat Shield and Thrust Cone Pressures

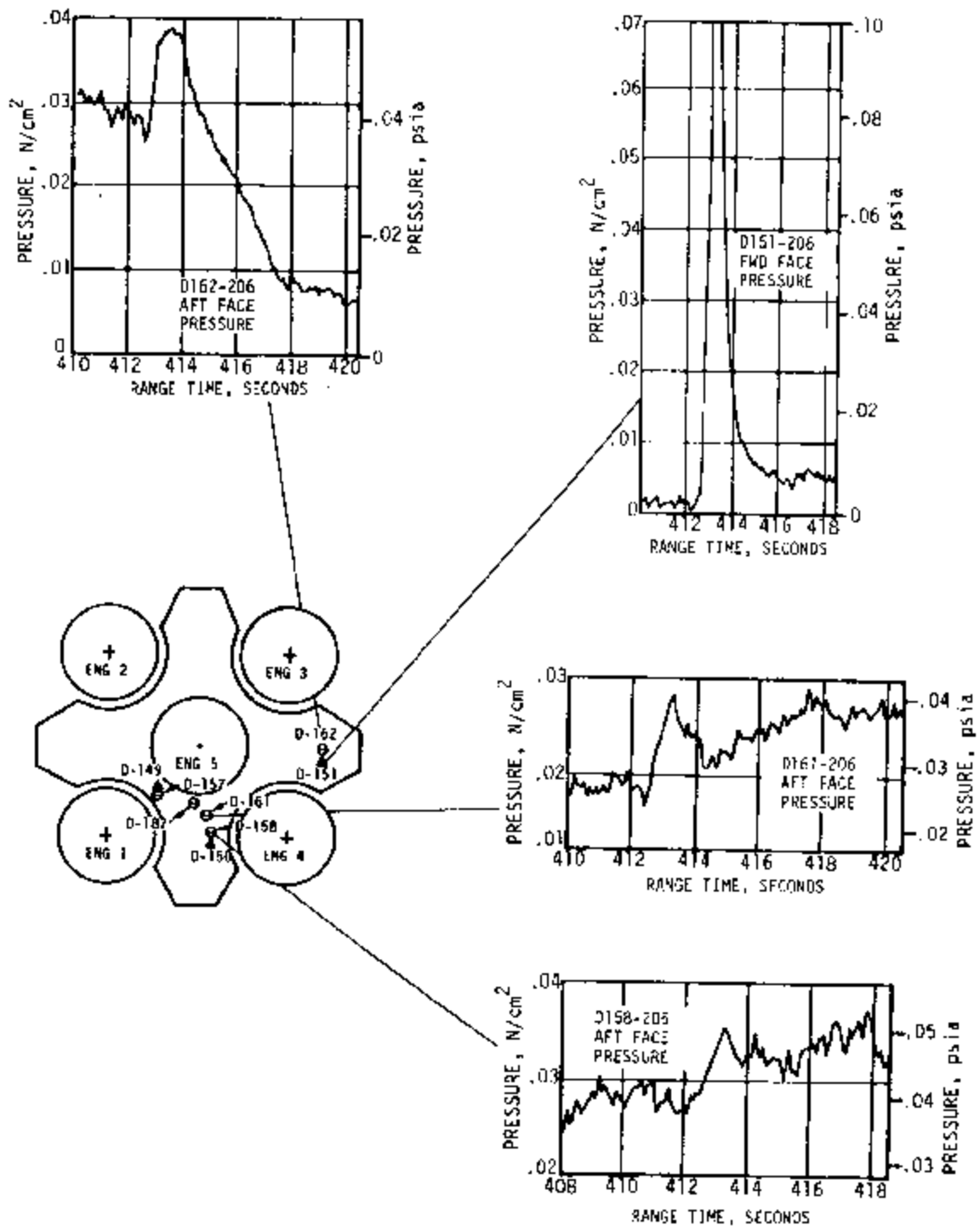


Figure 16-15. S-II Base Heat Shield Pressures

16.4 ACOUSTIC ENVIRONMENT

16.4.1 External Acoustics

The external fluctuating pressure environments for the AS-502 vehicle were recorded by nine instruments located on the instrument unit, S-IVB forward and aft skirts, S-II forward and aft skirts, and S-IC intertank, aft skirt and fin D. Representative data for these instruments along with AS-501 data and applicable prediction curves are shown in Figures 16-16 through 16-19.

Both the Digital Spectral Analysis's program (Ravan) and acoustic analyzer data have been used in determining the plots shown in Figures 16-16 through 16-19. Due to incomplete data, overall pressure levels were obtained by integrating the 1/3 octave band fluctuating pressure level time histories for each instrument. Ravan data have primarily been used to determine time slices where maximum aerodynamic fluctuating pressure occurs. Acoustic analyzer overall levels were computed at these time slices to verify the Ravan results. These data remain relatively quick-look and may be revised after further analysis.

The AS-502 external acoustic environment at liftoff is shown in Figure 16-16. Both Ravan and acoustic analyzer data are plotted for comparison with predicted and AS-501 curves. Agreement is generally good. The scatter of Ravan, acoustic analyzer, and AS-501 data points is below 6 decibels except at vehicle stations 2.06 and 63.98 meters (81.10 and 2518.90 in.) where an approximate difference of 10 decibels existed. These differences are still under investigation.

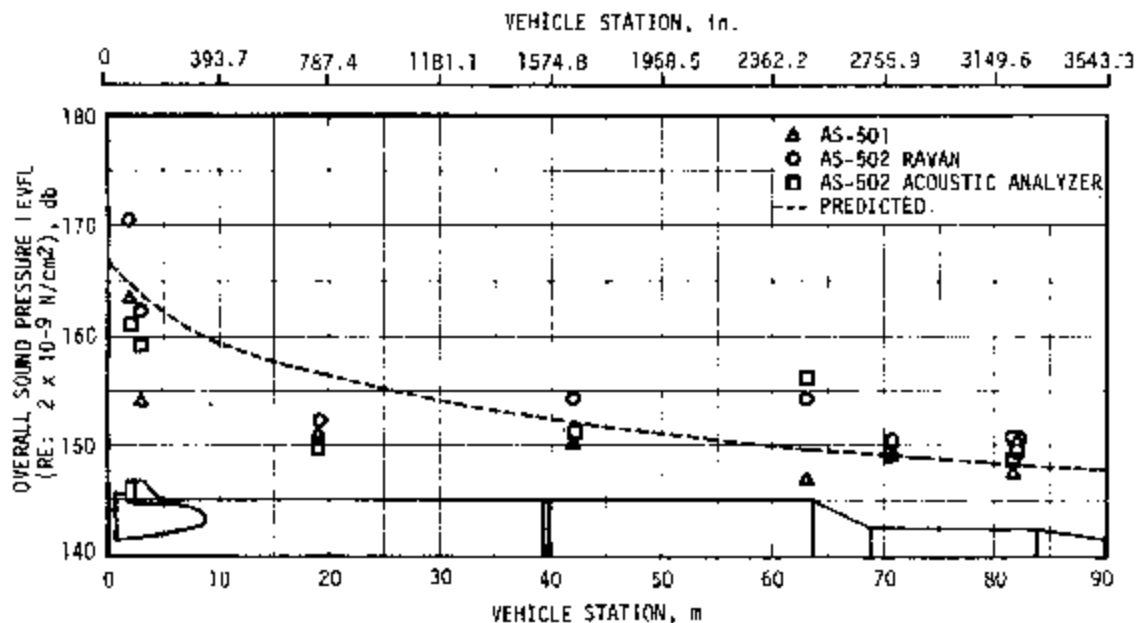


Figure 16-16. Vehicle External Overall Sound Pressure Level at Liftoff

Liftoff sound pressure spectral densities are compared with AS-501 data in Figure 16-17. Frequency characteristics appear similar for both AS-501 and AS-502 with the exception of an apparent level shift in three of the S-IC stage instruments. Instruments B0005-200 and E0004-200 are located at the same vehicle station but on opposite sides of the S-II stage. Data from both measurements were similar. The maximum levels indicated at launch were 148 decibels and 153 decibels for B0005-200 and B0004-200 respectively. Therefore, data are shown for B0004-200 only. In this report B0013-426 on the AS-501 is compared with B0025-426 on the AS-502 flight, since they are at the same location, and appear to indicate normal operation.

Overall fluctuating pressure levels are shown in Figure 16-18. AS-502 acoustic analyzer and Ravan data are both compared with predicted and AS-501 data. Generally higher levels are indicated on the AS-502. Notably excepted is the IU instrument which shows pointwise drops of up to 10 decibels. Further analysis appears necessary. The AS-501 overall level for instrument B0002-115 terminated at 90 seconds due to instrument failure.

A 5 hertz component showed up in the data for two measurements on the S-II aft skirt and S-IC intertank section, shown in Figure 16-19. The appearance of this 5 hertz component requires investigation because the lower frequency limit, where the telemetry system began to attenuate the data signal, was 50 hertz.

The occurrence of the 133-second transient in the acoustic data channels is similar to other data records which are discussed in Section 9A. The signal increase at this time was significant and requires further analysis.

Pressure Spectral Densities (PSD) for AS-502 at maximum aerodynamic fluctuating pressures are shown in Figure 16-19. Acoustic analyzer data was used in the PSD calculations while Ravan data fixed the time at which maximums occurred. Similar distributions are evident between AS-501 and AS-502 data with some level shifts noted.

16.4.2 Internal Acoustics

16.4.2.1 S-IC Stage. The S-IC stage intertank internal acoustic data from a single measurement is shown in Figure 16-20. Liftoff levels were somewhat lower than those for static firing and were similar to those for AS-501. Flight levels were much lower than static firing levels and generally the same as flight levels on AS-501.

16.4.2.2 S-II Stage. Two internal microphones were located on the S-II stage as follows:

Measurement Number	Area	Saturn V Station m	Station (in.)	Azimuth (deg)	Radius m (in.)
B001-206	Thrust Cone	42.6	(1677.2)	013	3.50 (138)
B002-219	Forward Skirt	63.3	(2492.1)	174	4.52 (178)

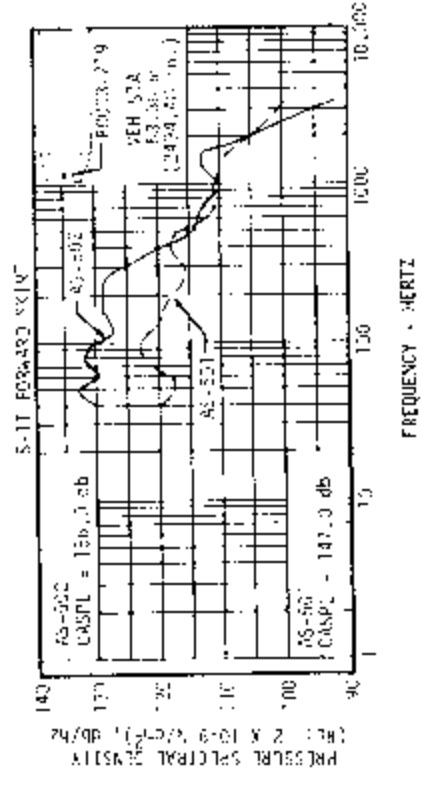
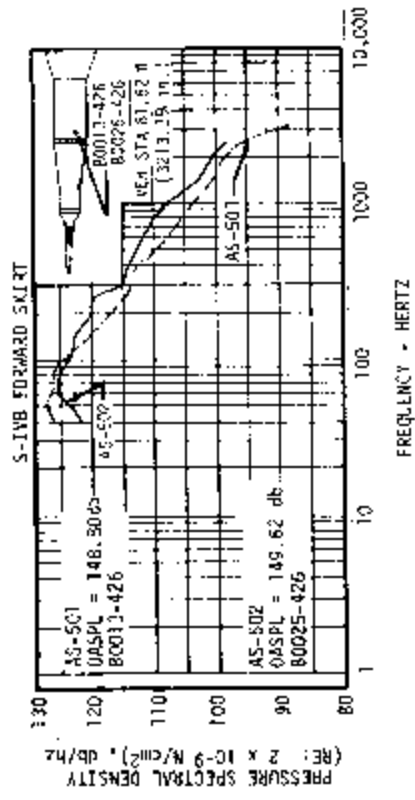
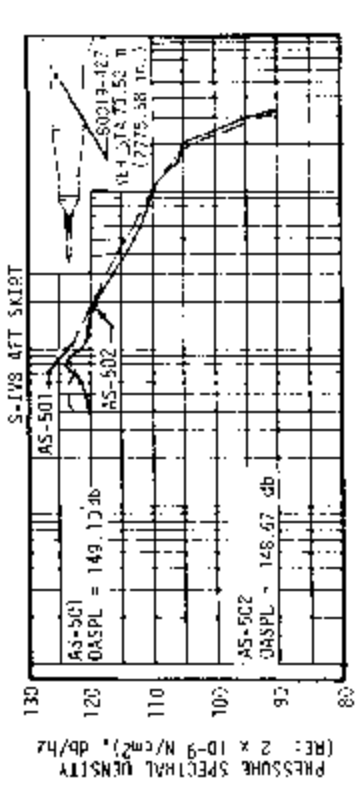
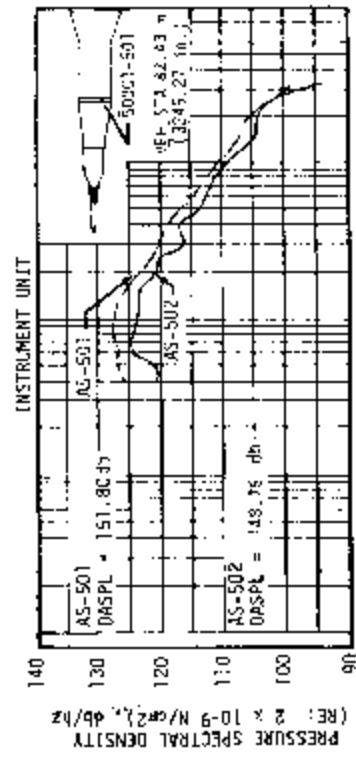


Figure 16-17. Vehicle External Sound Pressure Spectral Densities, Sheet 1 of 2

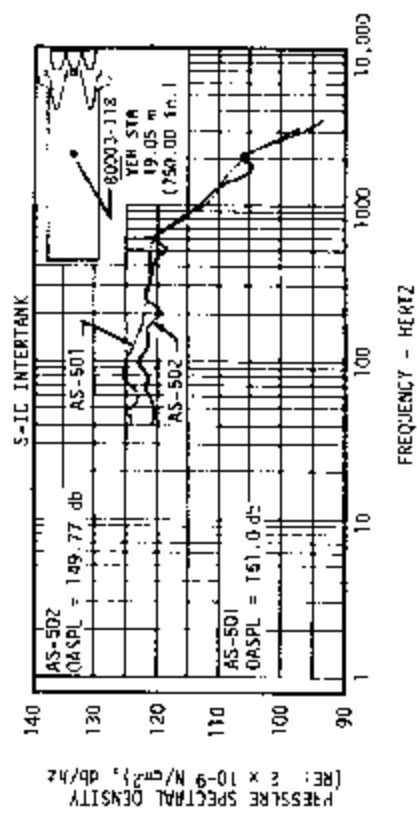
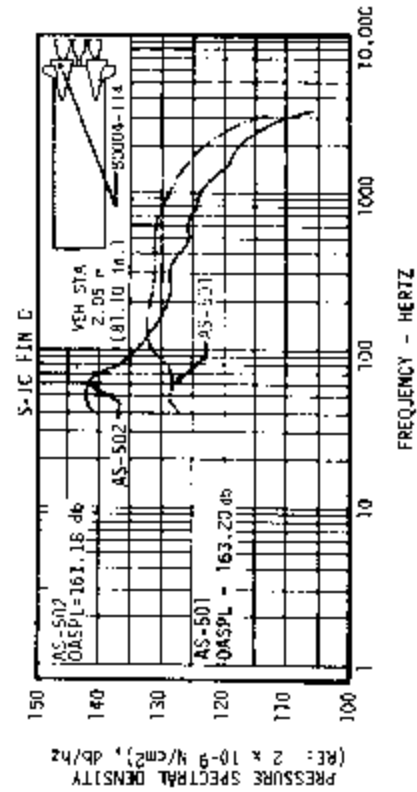
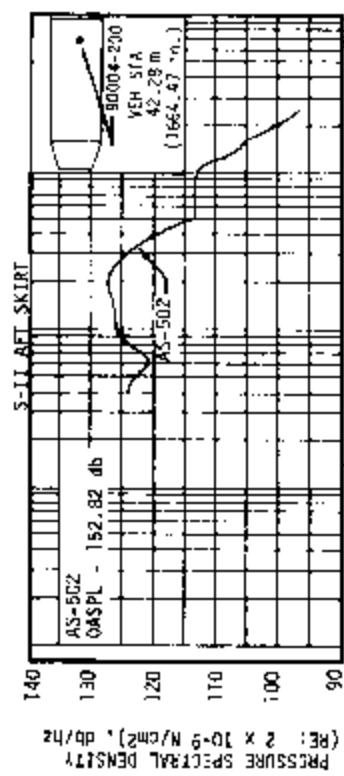
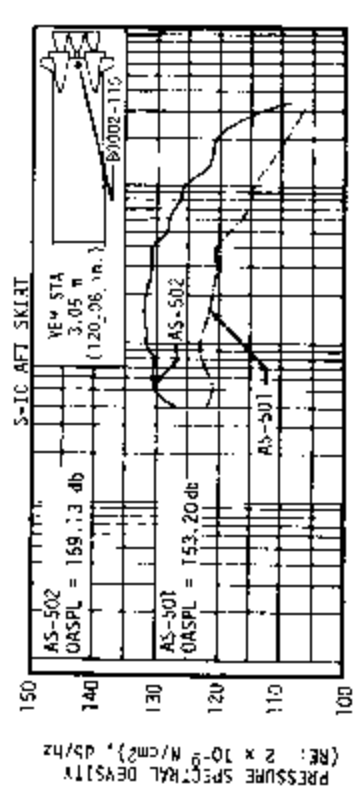


Figure 16-17. Vehicle External Sound Pressure Spectral Densities, Sheet 2 of 2

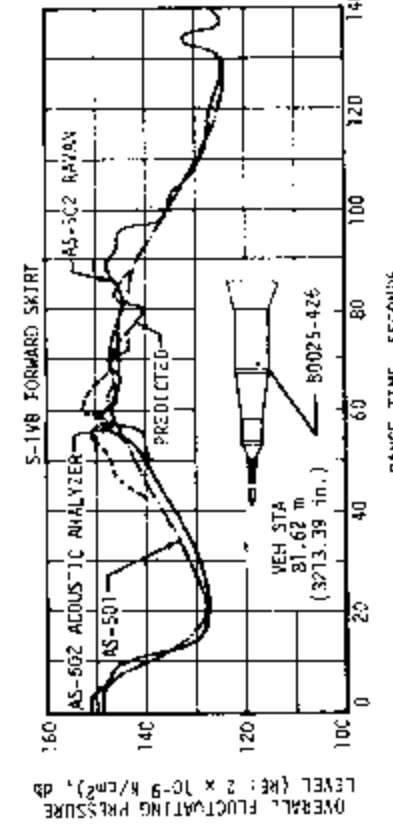
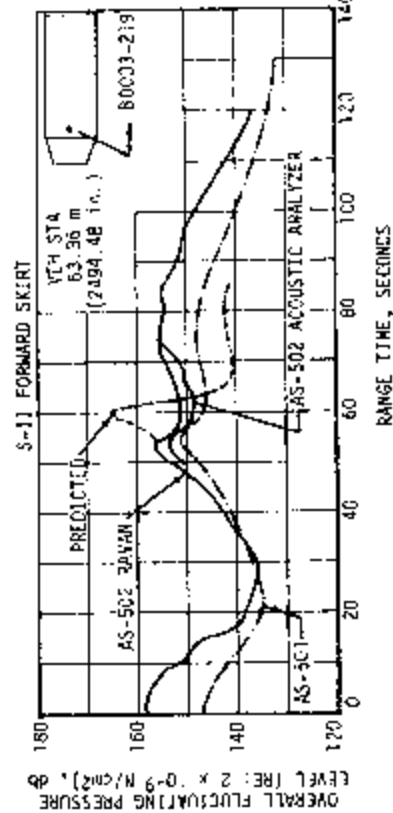
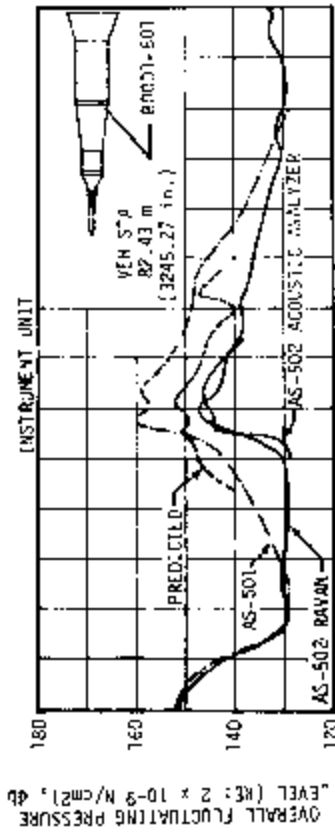
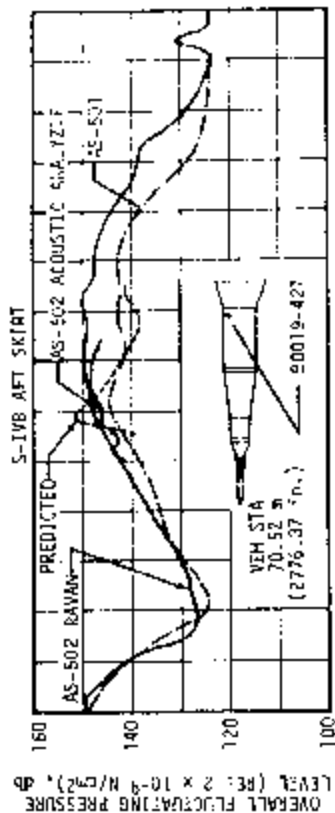


Figure 16-18. Vehicle External Overall Fluctuating Pressure Level, Sheet 1 of 2

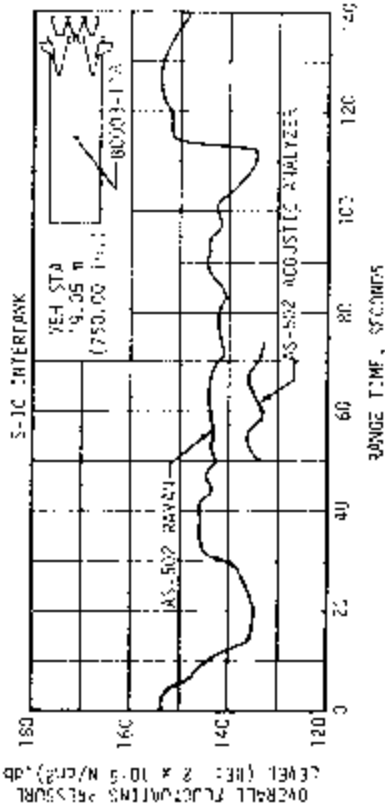
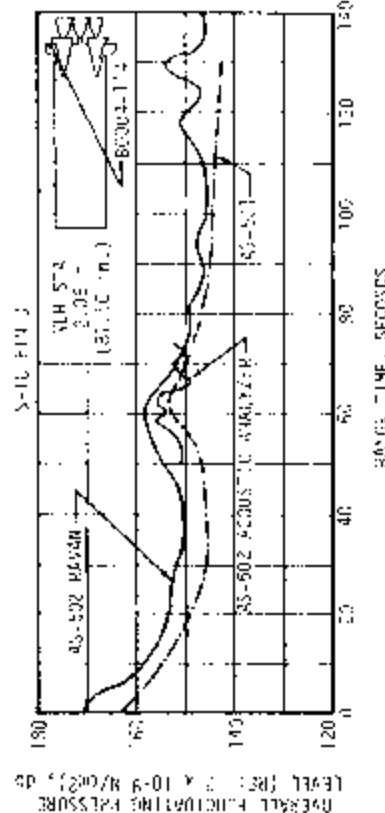
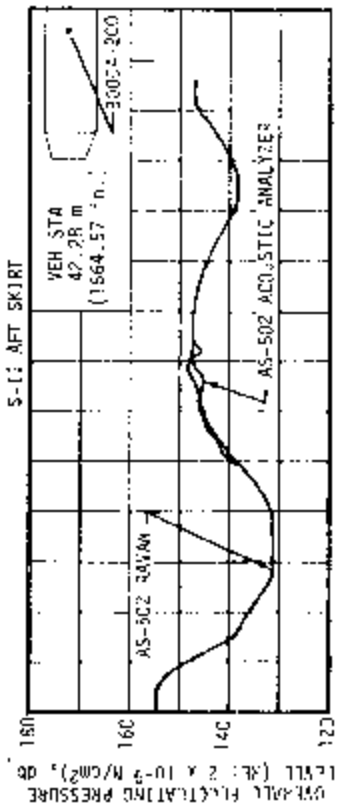
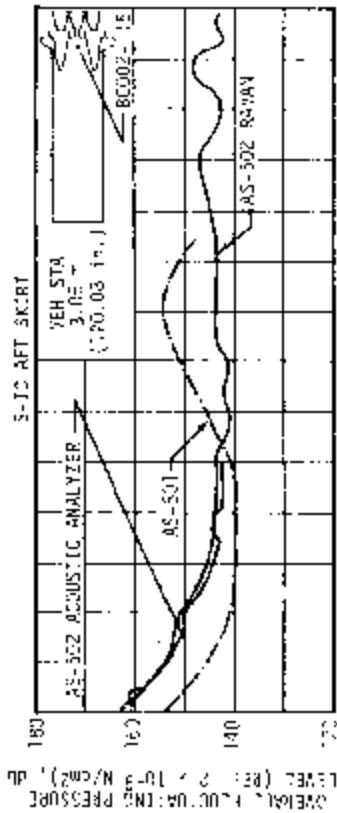


Figure 16-18. Vehicle External Overall Fluctuating Pressure Level, Sheet 2 of 2

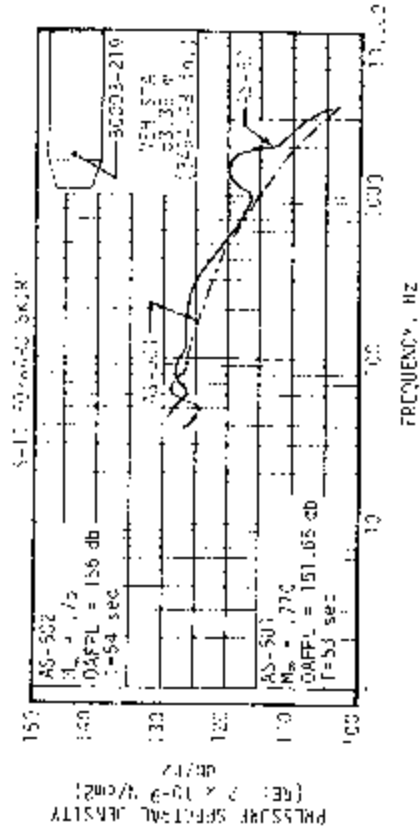
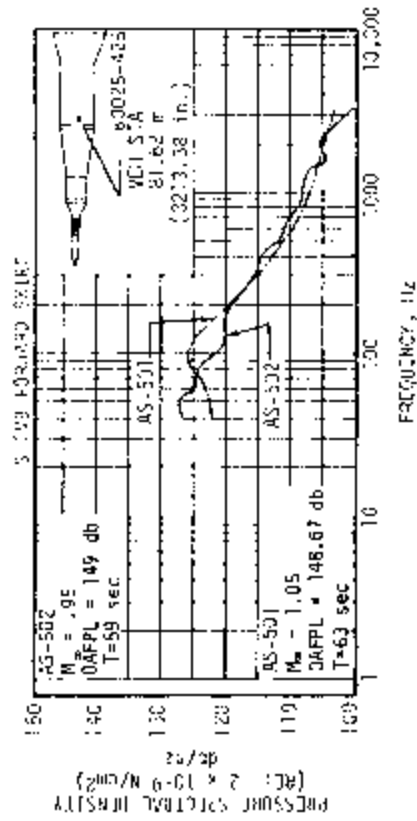
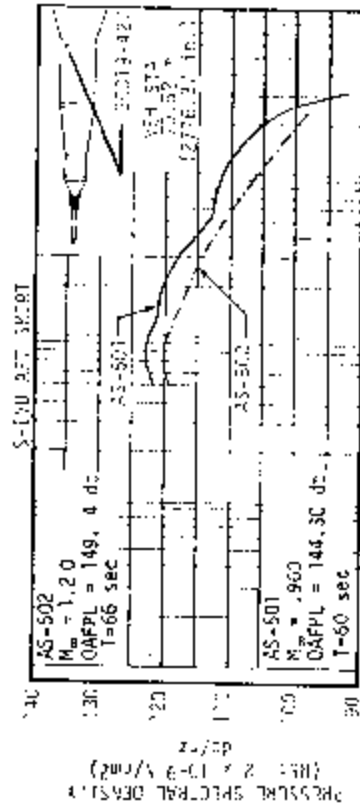
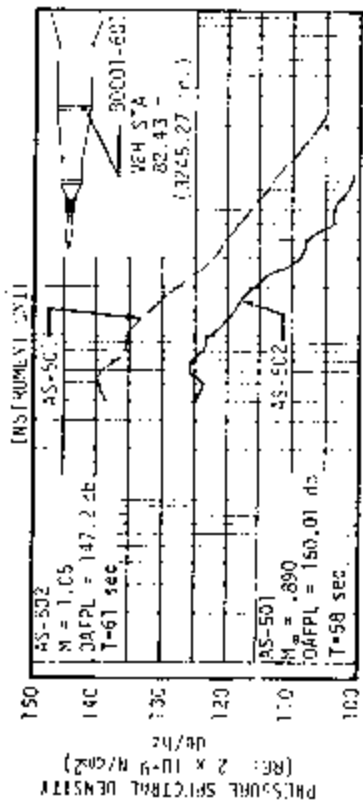


Figure 16-19. Vehicle External Fluctuating Pressure Spectral Densities, Sheet 1 of 2

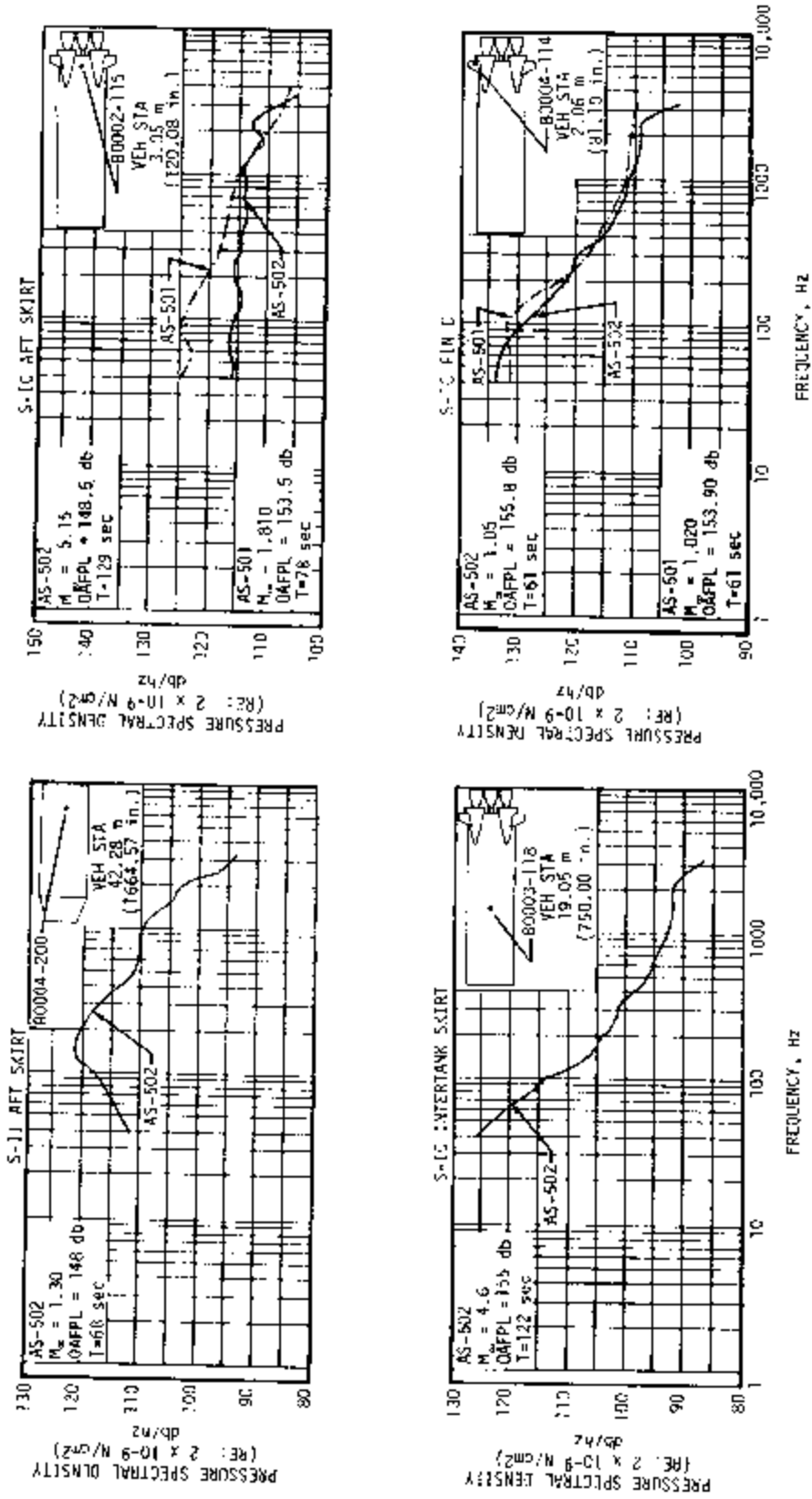


Figure 16-19. Vehicle External Fluctuating Pressure Spectral Densities, Sheet 2 of 2

MEASUREMENT INCLUDED	MAXIMUM SPL, dB (0-3000 CPS)			SPL DESIGN MAXIMUM, dB	LEGEND
	STATIC FIRING	AS-501	AS-502		
S-IC INTERTANK INTERNAL BOD1-15B	145.1 145.4	142.38T+0.6	140.28T+3	157.0	STATIC FIRING DATA ENVELOPE AS-501 FLIGHT DATA ENVELOPE AS-502 FLIGHT DATA ENVELOPE

DECIBEL REFERENCED TO 2×10^{-5} W/M²

THE TWO VALUES ARE THE AVERAGE AND MAXIMUM OVERALL RMS MEASURED DURING ALL THE S-IC FLIGHT STAGE STATIC FIRINGS

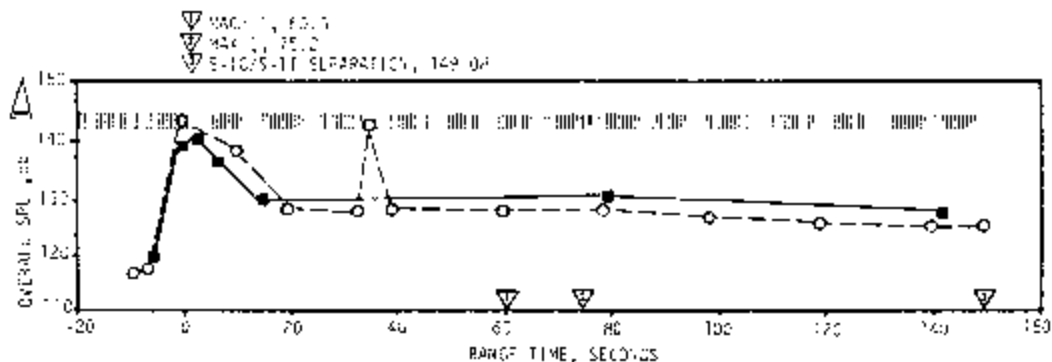


Figure 16-20. S-IC Internal Acoustic Environment

Figure 16-21 presents the measured overall decibel levels versus range time. Also indicated in the figure are the maximum expected levels for liftoff and inflight acoustics, which are values obtained from Saturn V Vehicle Acoustic Environment, R-P&VE-SVE-64-191, August 10, 1963.

The measured acoustic levels were well under the maximum expected values, particularly in the thrust cone area. The thrust cone internal acoustic level was also well under the external acoustics measured on the interstage, as indicated in Table 16-1. The differential at liftoff was 13 to 19 decibels between the aft external and internal measurements. This differential was somewhat larger than expected and is under investigation.

The forward internal measurement is considered valid. The forward external measurement is considered questionable, and is under investigation.

16.4.2.3 S-IVB Stage. The S-IVB acoustic environment was measured at four positions, internal and external on the forward skirt and internal and external on the aft skirt.

Envelopes of the composite, 50 to 3000 hertz levels time histories are presented in Figures 16-22 and 16-23. The shading between the external and internal responses indicates the structural transmittability for

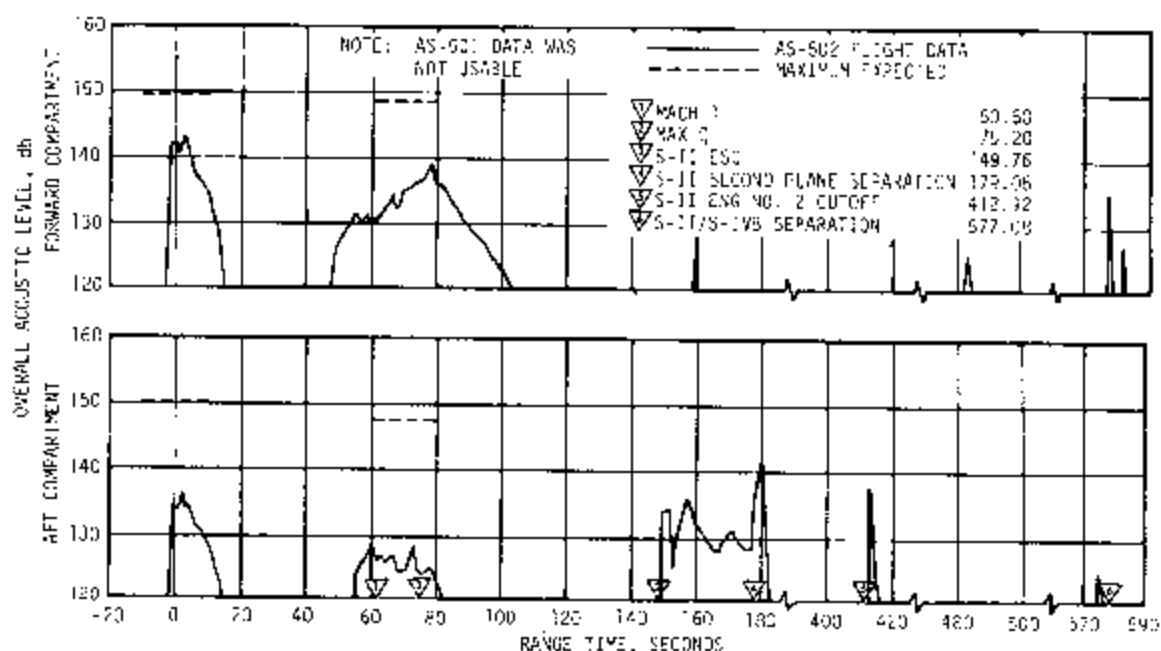


Figure 16-21. S-II Internal Acoustics

sound pressures at liftoff and for boundary layer pressure fluctuations in the transonic portion of flight. Also presented are data from the S-IVB acoustic measurements of the AS-501 flight.

The AS-502 forward skirt levels were in general equal to or less than the AS-501 levels. Also the transmission loss for the AS-502 forward structure was greater than for the AS-501.

Table 16-1. S-II Acoustic Noise Levels Comparison of AS-501 and AS-502 Data

EVENT	OVERALL db							
	FORWARD SKIRT				AFT INTERSTAGE/AFT SKIRT			
	EXTERNAL (R003-219)		INTERNAL (3002-219)		EXTERNAL (B004 & 5003-200)		INTERNAL (3001-200)	
	AS-502	AS-501	AS-502	AS-501	AS-502	AS-501	AS-502	AS-501
Liftoff	*	150	142	No Data	148.9-154.8	152.7	136	No Data
Transonic	*	149.3	131	No Data	142.3-144.0	144.5	125	No Data
Max Q	*	150.3	137	No Data	143.5-147.4	146.5	127	No Data
Static Fring	136	136.0	130	125	150	150	155	155

*Questionable data, under investigation

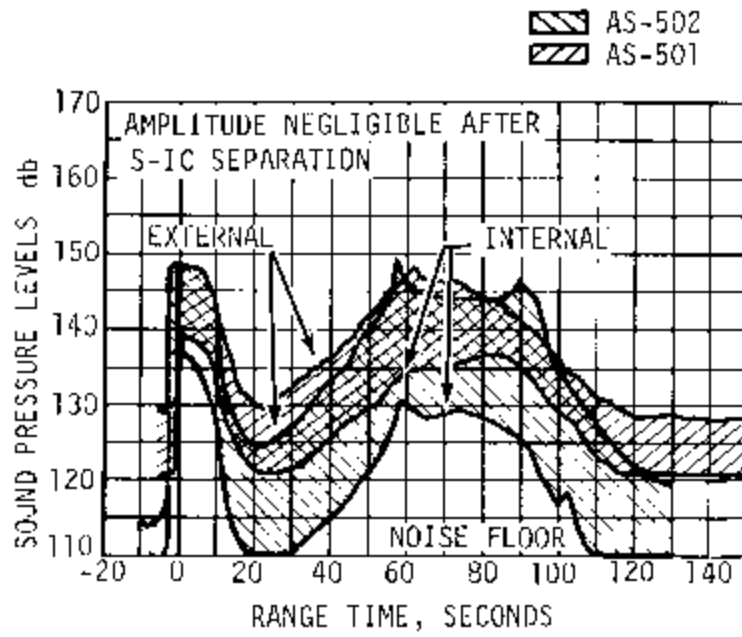


Figure 16-22. S-IVB Forward Skirt Acoustic Levels

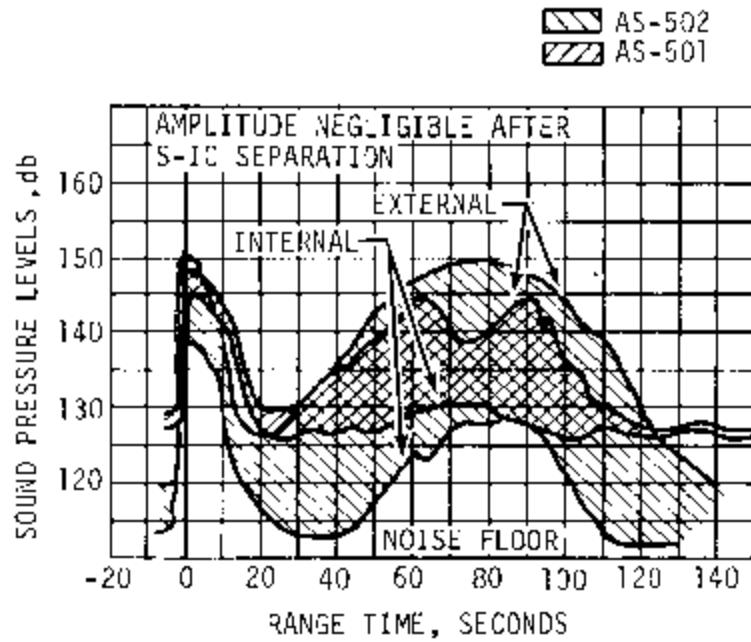


Figure 16-23. S-IVB Aft Skirt Acoustic Levels

SECTION 17

VEHICLE THERMAL ENVIRONMENT

17.1 SUMMARY

The AS-502 S-IC base region radiation and total heating rates were more severe than those measured on AS-501 flight; also the base heat shield and engine gas temperatures were greater and increased more rapidly. Loss of M-31 to the level of the crushed core on the base heat shield was visually observed on this flight via the television cameras which viewed the heat shield. The S-IC forward skirt thermal environment after S-IC/S-II separation was higher than design.

The aerodynamic heating environment on the S-IC forward skirt, inter-tank, engine fairings and fins was slightly higher than AS-501 data but within the predicted bands. The AS-502 trajectory was a higher heating trajectory than that flown by AS-501.

The effect of the premature shutdown of engines No. 2 and 3 on the S-II heat shield and base region environment was minor. With the exception of abrupt spikes due to the engine anomalies, the base region thermal data compared favorably with AS-501 data.

Protuberance induced heating effects on the S-II stage were generally below the design and postflight predictions. The temperature data from AS-502 was in general very similar but slightly higher than that for AS-501.

The AS-502 S-IVB aerodynamic heating environment was slightly more severe than the AS-501 but temperatures were well below the design values.

17.2 S-IC BASE HEATING AND SEPARATION ENVIRONMENT

Thermal environments in the base region of the S-IC stage were recorded by 39 measurements which were located on the heat shield, F-1 engines, and base of fin D. This instrumentation included 6 radiation calorimeters, 19 total calorimeters, and 14 gas temperature probes. Representative data from a portion of these instruments are compared with AS-501 flight data in Figures 17-1 through 17-3.

The calorimeter radiation and total heating rates measured in the base region were more severe than those measured during the AS-501 flight. This increase is attributed to the removal of the flow deflectors on the

AS-502 vehicle. The removal of these flow deflectors allowed the exhaust gases to recirculate into the base at a lower altitude. An increase in heating had been anticipated from model test results.

The radiation hump which was observed at about 30 kilometers (16 n mi) altitude in the AS-501 base flight data was also present in the AS-502 flight data. The AS-501 flight evaluation indicated that the radiation hump may have been caused by a combination of increasing view factors, diminishing afterburning with increase in altitude, plume interaction regions and hot gas recirculation. AS-502 video tapes from S-1C base TV cameras indicate that the hot gas recirculation was the main cause of the radiation hump. The TV data shows that hot recirculated gas reached the base heat shield at an altitude of 12.2 kilometers (6.59 n mi) which correlated with the rise in the radiation heating rates as shown in Figure 17-1. This recirculated exhaust flow is fully established in the base region at 18.5 kilometers (9.99 n mi) which correlates with the peak in the radiation heating rate data. The TV data also indicated that after 36.6 kilometers (19.8 n mi), the base region was clear, indicating a significant reduction in the burning of the fuel rich exhaust gases in the area. This fact correlates with the dropoff in measured heating rates.

Results from the total and radiation calorimeters indicate that a convective cooling rate was measured by the base heat shield instruments to an altitude of 19.8 kilometers (10.7 n mi) and then changed to a small convective heating rate at the higher altitudes (Figure 17-1). However, the average calorimeter effective wall temperature is 350°K (170°F) which, when compared with the lower gas temperature curve in Figure 17-1, indicates that the calorimeters should experience convective heating at altitudes above 10 kilometers (5.4 n mi). A different trend is noted in Figure 17-2 for the F-1 engine nozzle extension calorimeters near the nozzle lip, where convective heating was present from liftoff to a maximum value of 11.35 watt/cm² (10.0 Btu/ft²-s) at an altitude of 18.3 kilometers (9.88 n mi). Comparison of the average calorimeter wall temperature with the gas temperature curve in Figure 17-2 also indicates that the engine nozzle extension calorimeters received convective heating throughout the flight but at altitudes above 24.4 kilometers (13.7 n mi) was negligible. No appreciable difference was noted in the convective heating measured by the calorimeters on the heat shield or engines when comparing the two Saturn V flights. The base heat shield and engine gas temperatures were greater and rose more rapidly than those measured on the AS-501. This, however, is not reflected in the total and radiation calorimeter data.

The total heating rates measured by the calorimeter on the base of fin D are compared with the AS-501 flight data in Figure 17-3 and show the two to be approximately the same. The initial rise in heating occurred at 12.2 kilometers (6.59 n mi) which correlated with the recirculated exhaust gases reaching the heat shield as observed on the TV cameras. The second rise and peak in the curves occurred at about the time that flow separation occurred and was probably caused by the hot gas from the plume moving up the side of the vehicle.

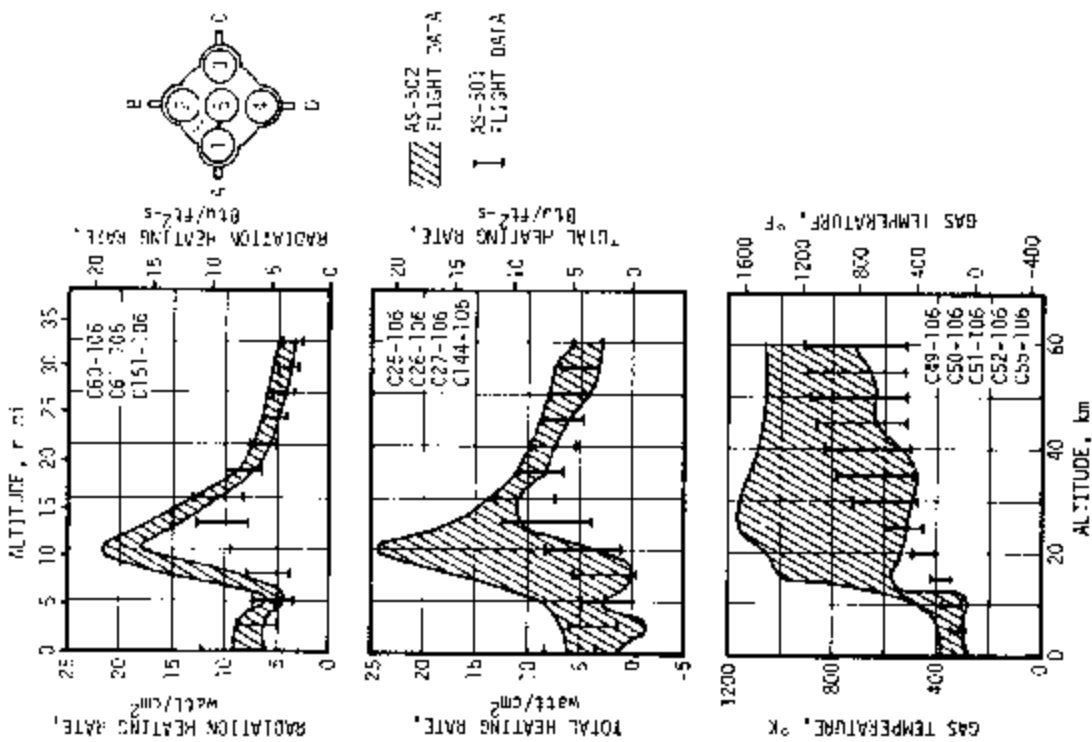


Figure 17-1. S-1C Base Heat Shield Thermal Environment

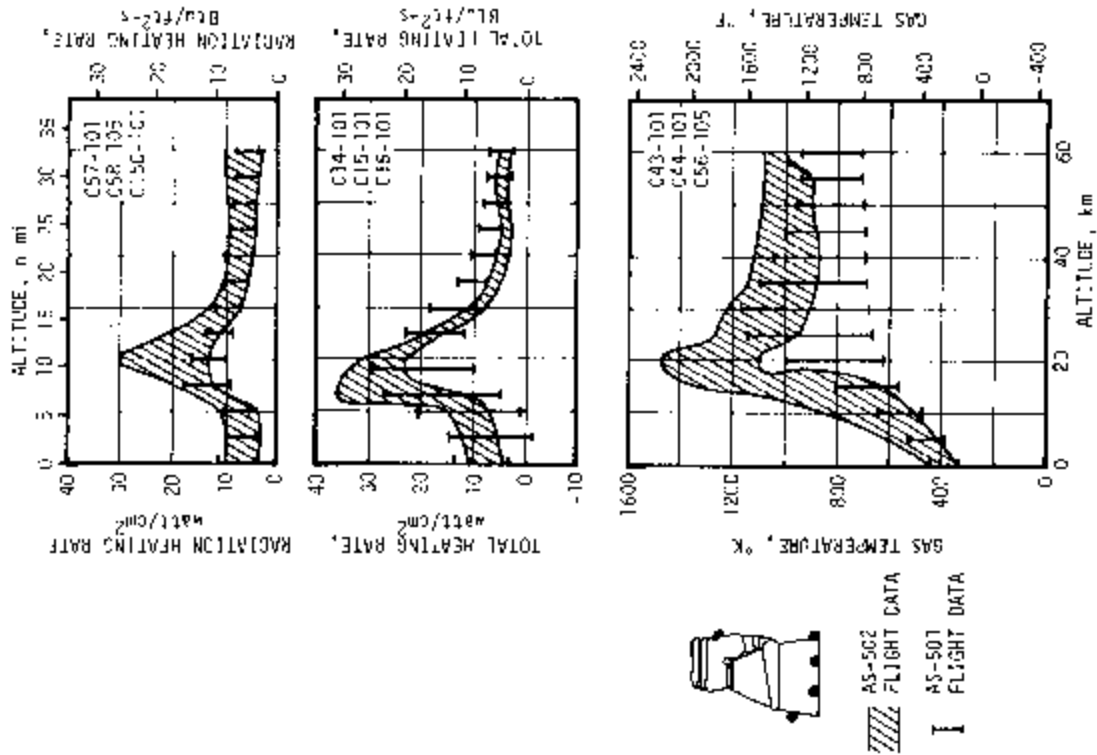


Figure 17-2. F-1 Engine Thermal Environment

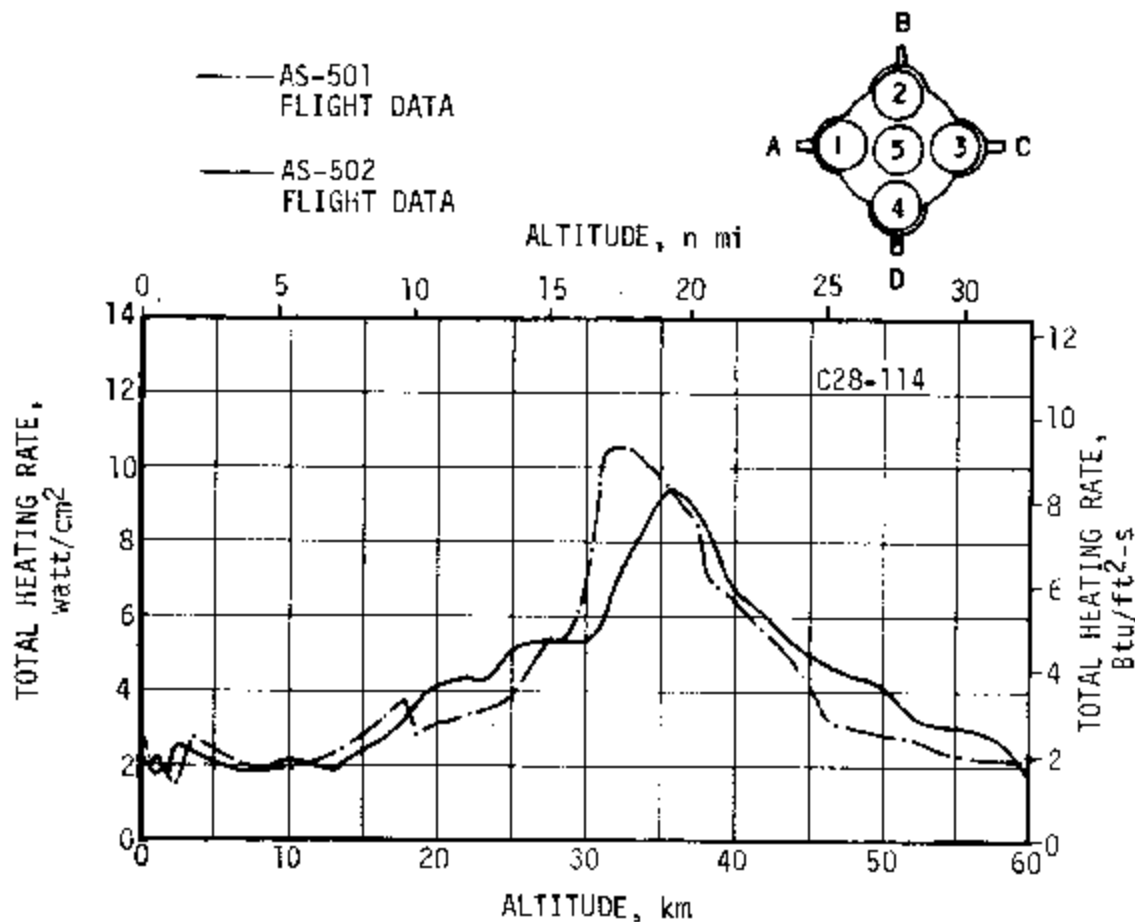


Figure 17-3. S-IC Base of Fin D Total Heating Rate

The heat shield temperature history is illustrated in Figure 17-4. Average cold side and bondline (honeycomb/M-31 interface) temperatures were 345 and 458°K (161 and 364°F), respectively, versus 333 and 380°K (139 and 224°F) for the AS-501 flight. This increase may be attributed to the deletion of the base flow deflectors on the AS-502 vehicle resulting in higher total heating. However, as indicated by the dashed lines showing predicted maximums, the data is well within design limits except for the measurements C032-106 and C033-106. These two thermocouples were located 4.22 meters (166 in.) radially from the heat shield center on Position Line II. At 96 seconds, the sudden increase in temperature could be caused by local loss of M-31 to the level of the crushed core. A similar failure occurred on the AS-501 vehicle. Note the response of C033-106 in Figure 17-4 indicating that it suddenly became exposed to the base region gas but did not fail. Loss of M-31 is substantiated by the correlation of the output from C032-106 compared in Figure 17-4 to a reconstructed curve. This curve was computed using the AS-502 radiation and gas temperature data and the design heat transfer coefficient assuming 0.407 centimeters (0.16 in.) of M-31 was lost

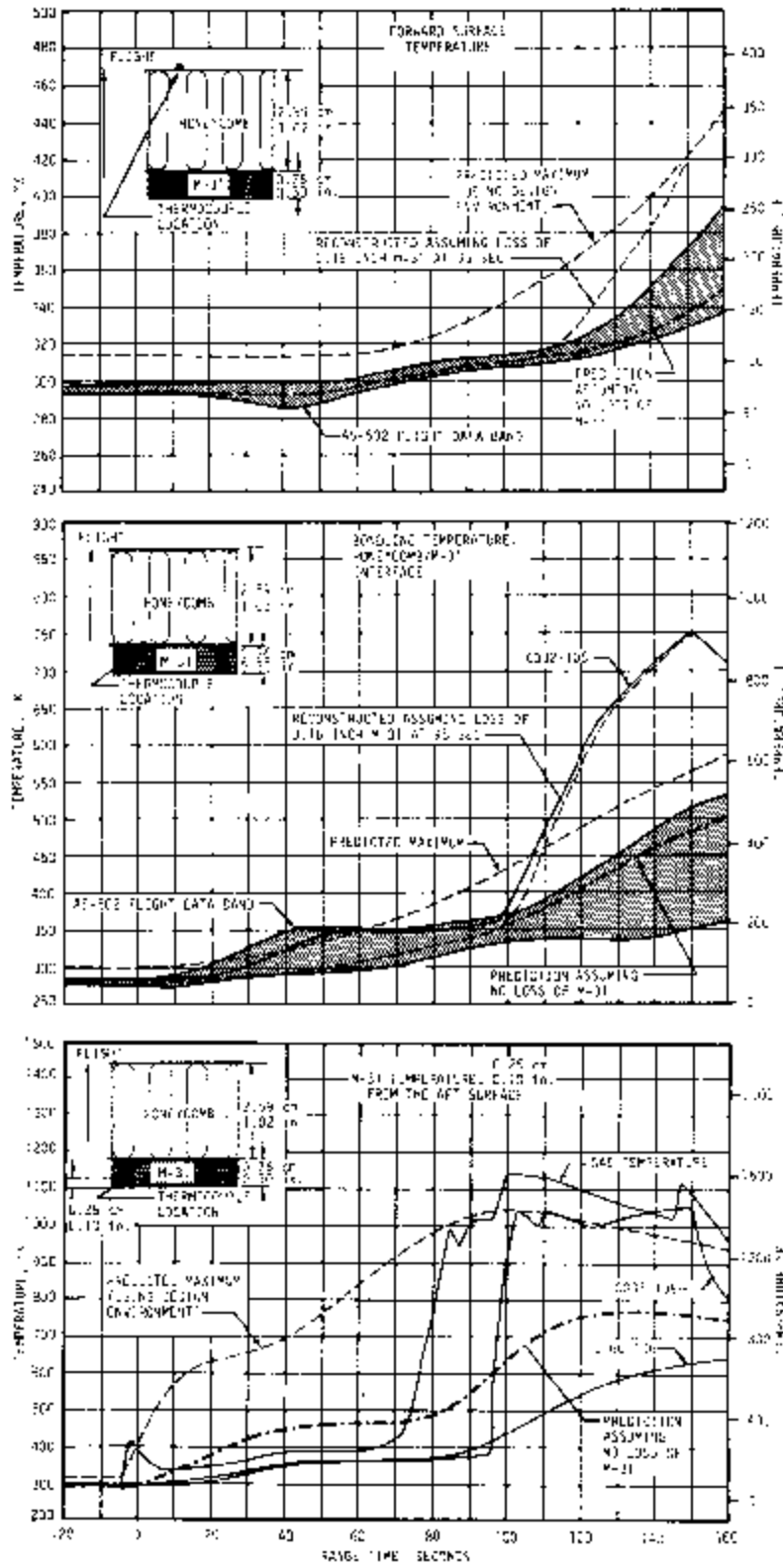


Figure 17-4. S-IC Heat Shield Thermal Environment

from the aft surface (to the level of the crushed core) at 95 seconds. The reconstructed temperature of the forward surface using the same assumptions is also shown in Figure 17-4. M-31 loss to approximately the level of the crushed core was visually observed on AS-502 via the television cameras which viewed the heat shield. These cameras also showed tearing of the inboard flame curtain fiberglass cloth protective covering. This was expected and does not indicate flame curtain degradation.

M-31 insulation loss occurred at 110 seconds on AS-501 and 95 seconds on AS-502 which appears to be a random process and may occur at almost any time during flight. The effects of this loss at various times was computed and the results presented in Figure 17-5. Note that the loss of M-31 at 20 seconds would result in outboard engine cutoff temperatures of 863°K (1094°F) at the aft honeycomb face sheet and 535°K (504°F) at the forward honeycomb face sheet. The maximum allowable temperature for the forward face sheet is 423°K (302°F). However, this is interpreted as a design goal and testing showed the heat shield capable of withstanding temperatures above this level. Actual limits for either face sheet are not defined at this time but are being examined to determine whether a potential problem exists.

Correlation of computed temperatures with heat shield data, as shown in Figure 17-4, for the first 70 or 80 seconds of flight was not good. Examination of the data indicated that the actual M-31 conductivity must differ from the published data. Laboratory testing has shown that the M-31 insulation is hygroscopic and the wet conductivity would therefore differ from the published dry value. The heat shield temperature at the M-31-honeycomb interface for both AS-501 and AS-502 increased rapidly after engine ignition to approximately the boiling point of water. Thereafter, the temperature followed the saturation curve for water as ambient pressure decreased with altitude until about 70 seconds, and then the temperature increased as would be expected when the water was completely boiled away. The fast rise time of the interface temperature early in flight is only partially accounted for by the increased conductivity of the wet M-31. If it is assumed that the transmissivity of the M-31 is greater than zero, this difficulty can be resolved. Hence, there are four factors that acting together could account for the observed temperature history.

- a. Increased conductivity early in flight due to the presence of water in the M-31.
- b. Transpiration cooling due to water boiloff in the M-31.
- c. M-31 transmissivity greater than zero.
- d. Decrease in conductivity later in flight due to outgassing as altitude is gained.

Analytical verification of these factors is now under way.

It is apparent that the heat shield is capable of withstanding the thermal environment with the flow deflectors removed. The bondline and cold side temperatures were below levels to which the panels have been subjected in combined thermal-acoustic qualification testing.

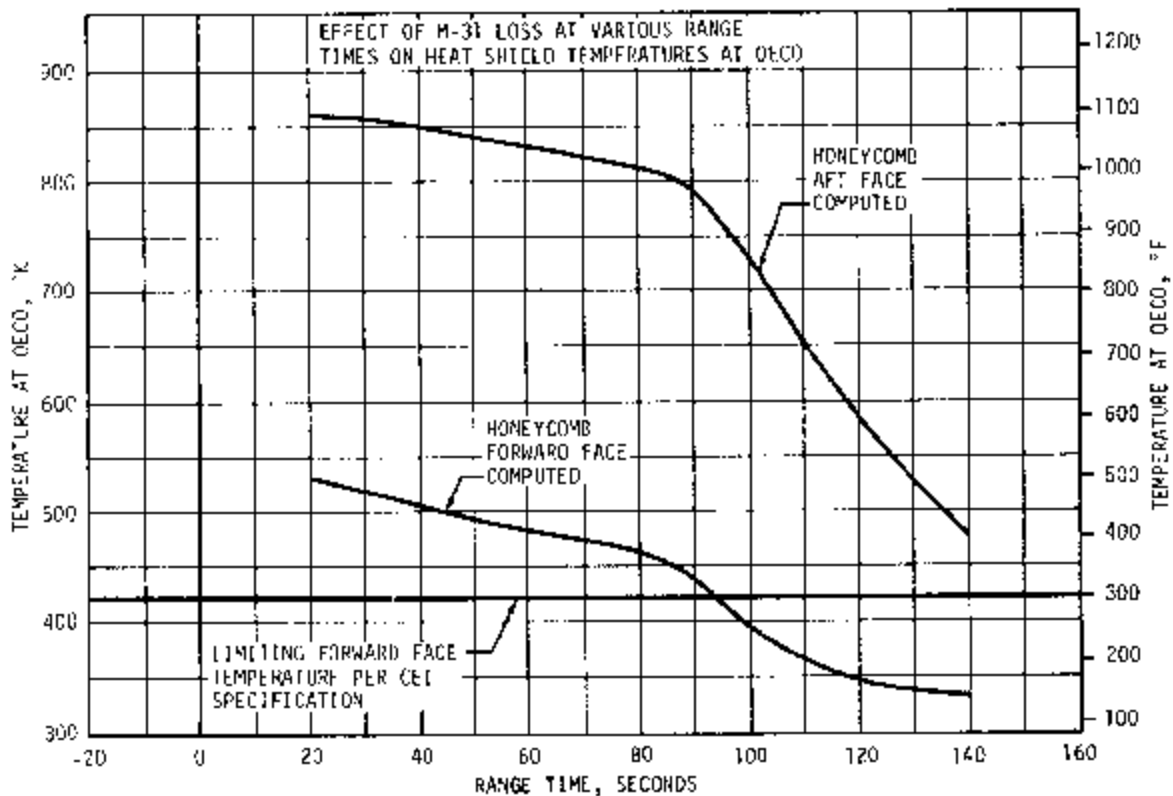


Figure 17-5. S-IC Thermal Environment Effect of M-31 Loss on Heat Shield Temperatures at OECD

Temperatures measured on the engines were very close to the AS-501 flight data. Temperatures under the insulation on the gimbal actuator and on an outrigger remained below 313°K (104°F). Temperature on a fuel discharge line reached 315°K (107°F) and the ambient air temperature under the engine cocoons ranged from 293 to 328°K (68 to 131°F) at the end of flight. The time-temperature data from the thermocouples located on the heat exchanger bellows, turbine exhaust manifold, and nozzle are plotted in Figure 17-6 for both flights.

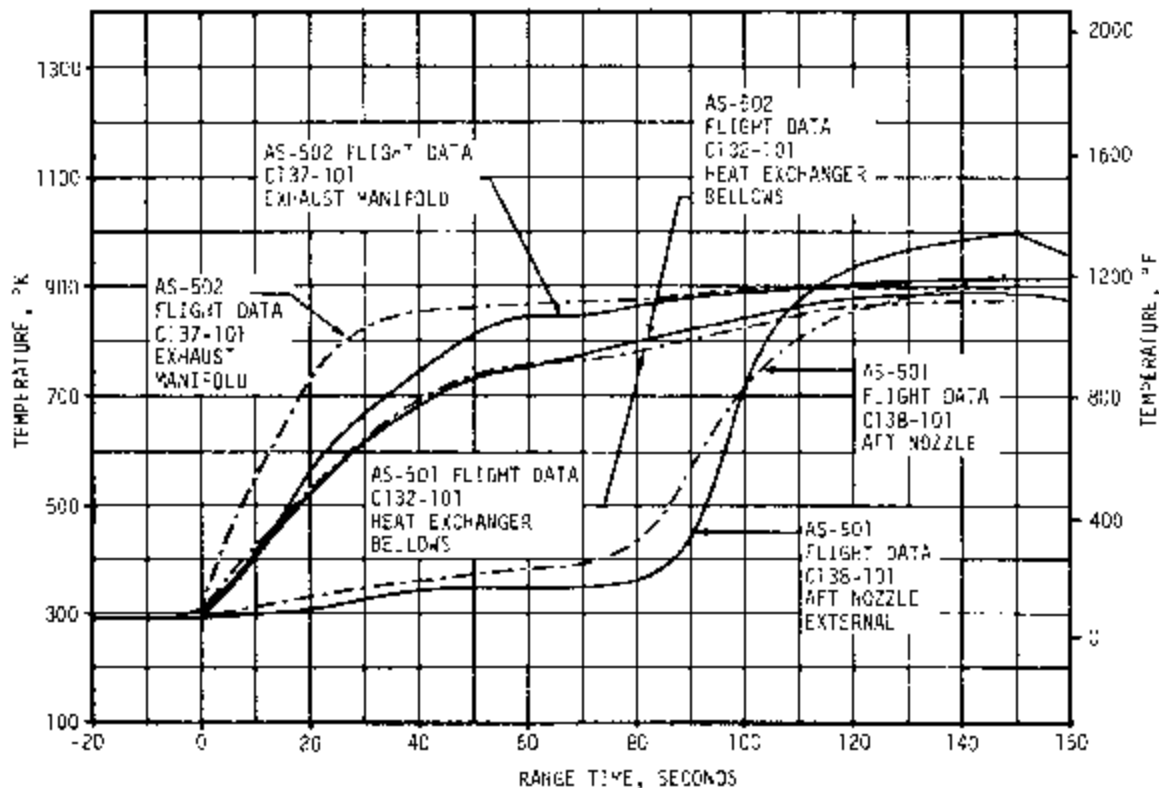


Figure 17-6. Thermal Environment, Temperature Under Insulation On Inboard Side of Engine No.1

17.2.1 S-IC/SII SEPARATION

As shown in Figure 17-7, gas temperatures during separation were similar to those measured on AS-501. Two spikes in gas temperature were present, corresponding to separation and J-2 engine ignition. The fact that the first spike peaked at a lower temperature on AS-502 than on AS-501 may be due to the elimination of four of the eight S-II ullage motors on AS-502. The second spike is related to J-2 engine ignition. Data from the separation extensometers indicate that the separation rate for AS-502 was slightly slower than for AS-501.

The forward skirt skin temperatures measured during separation are shown in Figure 17-7 and are similar to those experienced during the AS-501 flight. The LOX tank dome temperatures during separation are shown in Figure 17-7. These temperatures were considerably lower than those measured on AS-501 which were as high as 473°K (392°F). This is primarily due to the fact that the LOX dome thermocouples were covered with an insulating material on AS-502 thereby isolating them from the thermal environment causing them to read near the actual dome temperature. Three of the four measurements show a temperature drop at separation which is attributed to residual LOX impinging on the

dome. Most of the pressure data in the forward skirt area during separation was lost due to the Radio Frequency (RF) blackout, however, pressures of 0.857 N/cm² (1.243 psia) were measured as compared to a 5.18 N/cm² (7.52 psia) maximum on AS-501.

Several minor failures occurred after separation on both AS-501 and AS-502 which are attributed to the separation environment. These include a shorted cable on AS-501, loss of two LOX tank ullage pressure measurements on both AS-501 and AS-502, failure of a LOX vent and relief control pressure line on AS-502, and failure to eject three of the four S-IC cameras on AS-502 as discussed in paragraph 5.9. Sufficient instrumentation was not available on AS-502 to determine the severity of this environment.

Assuming that these failures were due solely to overheating, extensive studies were made that indicate a separation environment of about twice the design values would be required to cause failure of the aluminum tubing associated with the LOX tank ullage pressure measurements and

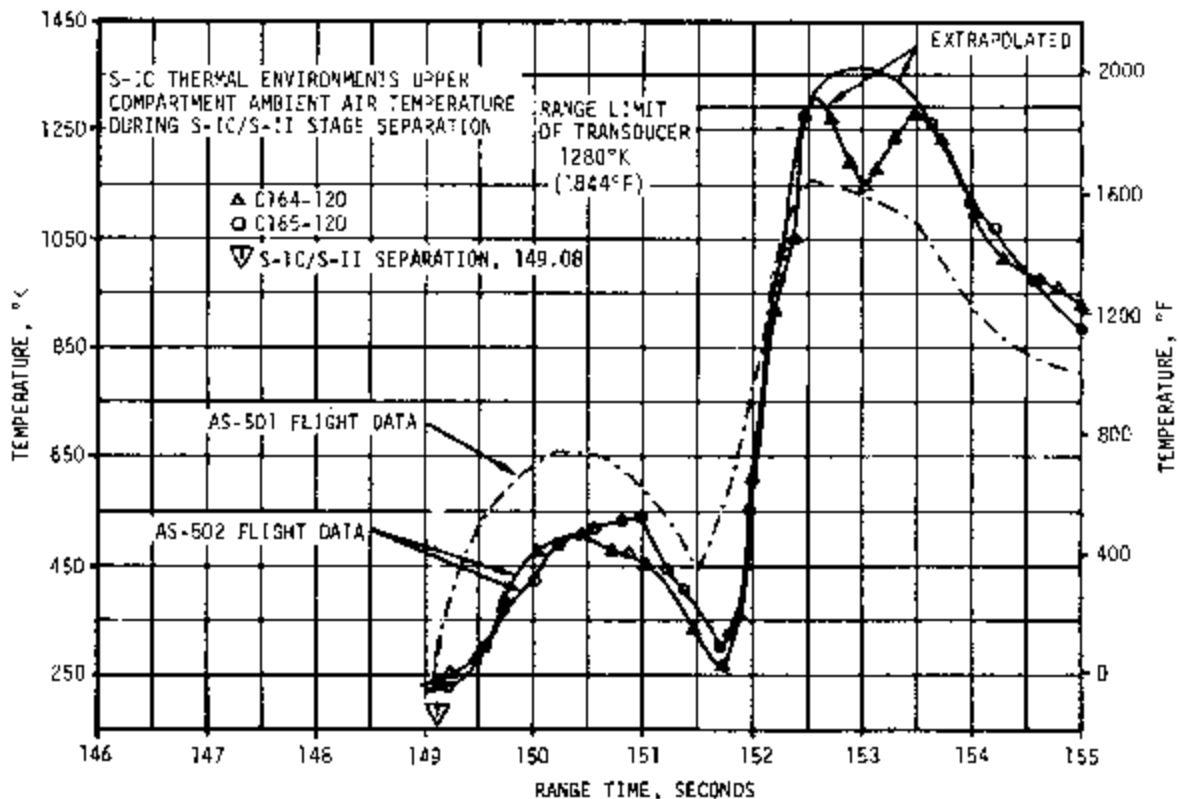


Figure 17-7. S-IC/S-II Separation Thermal Environment, Sheet 1 of 2

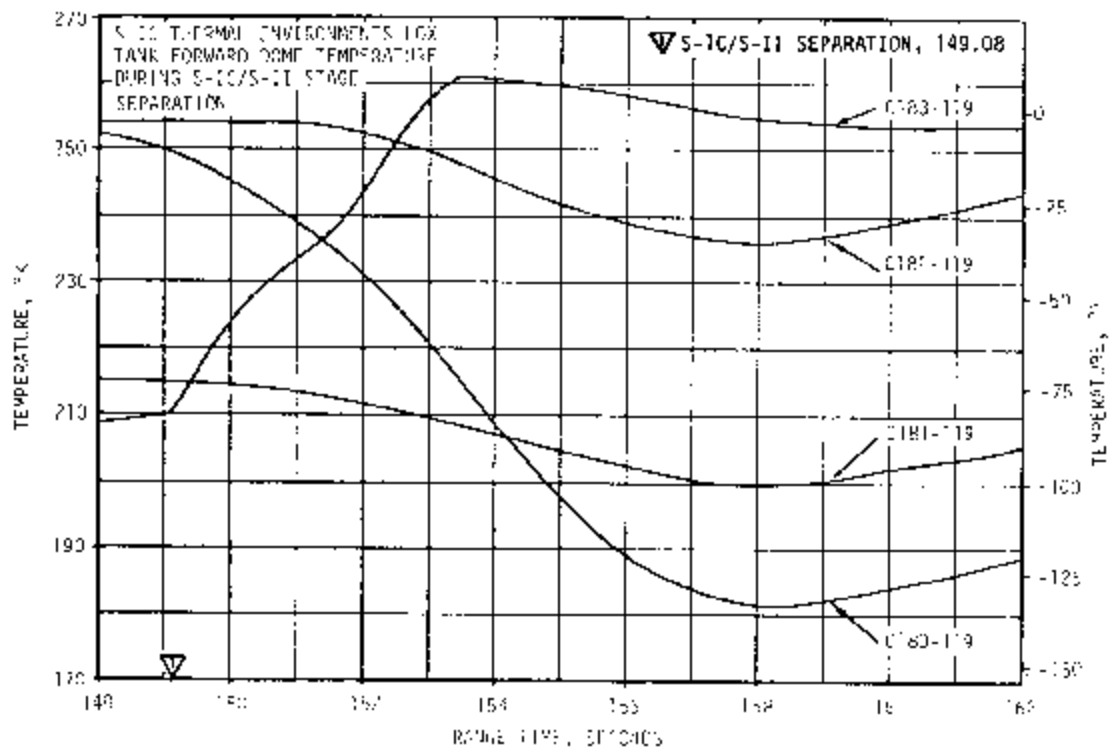
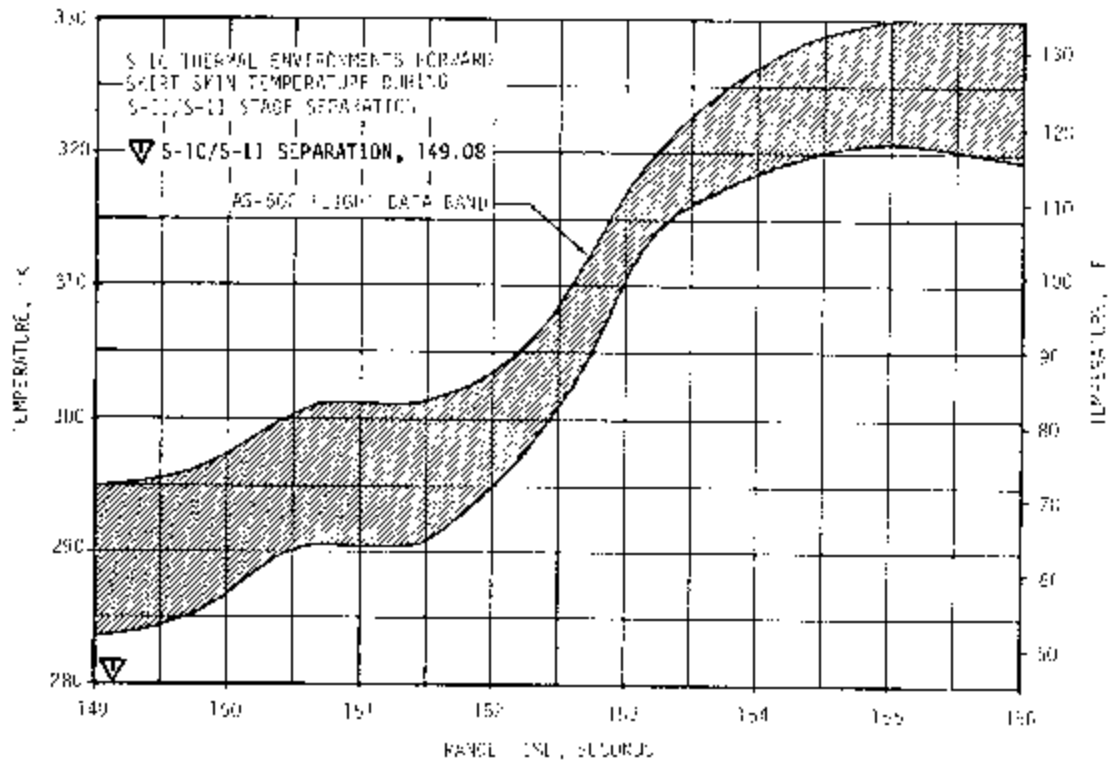


Figure 17-7. S-IC/S-II Separation Thermal Environment, Sheet 2 of 2

the control pressure line. This closely correlates with the environment required to match LOX dome thermocouple data from AS-501. This severe environment may exist only in isolated locations in the S-IC forward skirt. This condition could explain the fact that only a few failures occurred. Efforts to more accurately define the separation environment are continuing.

17.3 S-II BASE HEAT SHIELD AND SEPARATION ENVIRONMENT

The post flight predicted total heating rate values are based on hot flow scale model test data. These data include the effects of the cold turbopump exhaust gas injection in the J-2 nozzle on base heat shield total heating rates. The postflight predicted radiation heating rates were analytically obtained by means of a digital computer program, which uses the method of total hemispherical emissivity derivatives, to compute the incident radiation. Engine performance, i.e., Engine Mixture Ratio (EMR), chamber pressure, temperature, and gimbaling effects on convective heating rates are taken into account.

The AS-502 flight base region total heating rates have been normalized to the 295°K (71°F) cold wall condition.

Figure 17-8 shows the maximum-minimum band of total heating rates to the aft face of the base heat shield throughout S-II boost. The post-flight prediction and AS-501 flight data are also shown for comparison. It is seen that, initially, the postflight prediction heating rates are higher than the flight data, otherwise, good agreement was obtained. Initially, the AS-501 actual heating rates were higher than the corresponding AS-502 values. The sharp increase in heating rates during interstage separation was due to the interstage-exhaust plume impingement which resulted in a higher reverse mass flow rate, increased gas temperatures, pressures, and hence heating rates.

A small abrupt increase of base heat shield total heating rates was observed at approximately 319 seconds in the vicinity of the No. 2 engine, as shown in Figure 17-8, Sheet 2. This figure shows that at the same time the heat shield temperature gradient also increased in this region. It should be noted that at 319 seconds a slight drop in No. 2 engine chamber pressure occurred. Since no changes in engine gimbaling were observed during this time period, it appears that the only possible cause for this increased heating could be an abnormal change of the engine performance, for example, an increase in the EMR. Under normal operations this would result in a corresponding increase in chamber pressure. The opposite trend was observed in this case. For further details see paragraph 6.3.

Figure 17-8, sheet 2, shows the AS-502 flight radiation heating rate to the base heat shield in the vicinity of No. 2 engine. It is seen that a slight abrupt increase in heat rate occurred at approximately 319 seconds. This increase is insignificant with respect to the base heat shield total heating rate. However, it is noteworthy that this

increase occurred at the time when:

- a. No. 2 engine chamber pressure registered a slight decrease.
- b. One surface temperature transducer and two total heating rate transducers in the same region showed an increase.

Analysis of engine performance and gimbaling data for this time period indicates that an EMR increase is the most probable cause for the increased radiation heating rate.

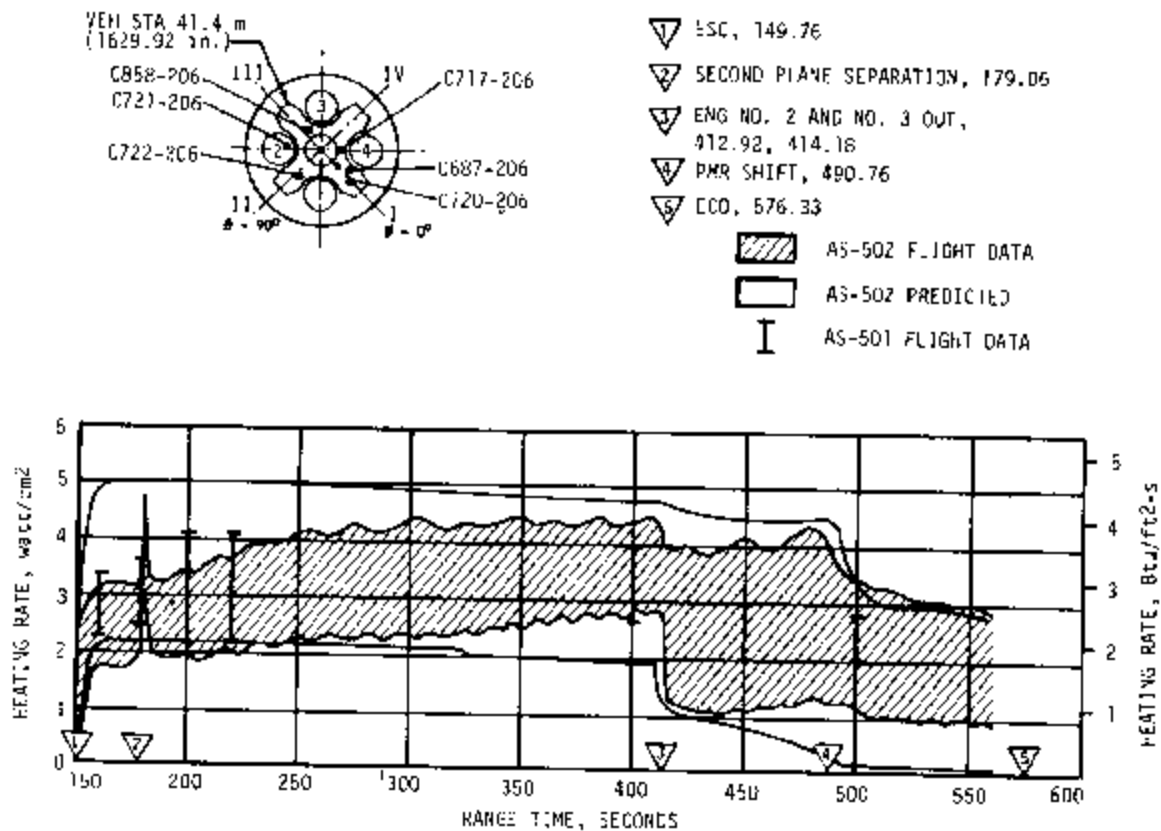


Figure 17-8. S-II Heat Shield Aft Face Heating Rates and System Temperature, Sheet 1 of 2

Figure 17-9 presents the AS-502 flight and postflight total heating rates to the thrust cone surface. AS-501 flight data is indicated for comparison. It is seen that the postflight predicted total heating rates are in very good agreement with flight data. Prior to second plane separation, the AS-501 heating rates were slightly lower than the corresponding AS-502 values, however, the basic heating rate trend is repeated very closely during both flights.

Figure 17-9, sheet 2, has a comparison plot for three individual thrust cone total heating rate measurements for the AS-501 and AS-502 flights. It is seen that at approximately 225 seconds the AS-502 flight total heating rate transducers indicate a gradual heating rate decrease, as compared to the AS-501 data. Since no change of the J-2 engine deflections or performance was noted during this time in flight which could cause this reduction in heating rate, it is believed that this was caused by a cryogenic leak in the base region.

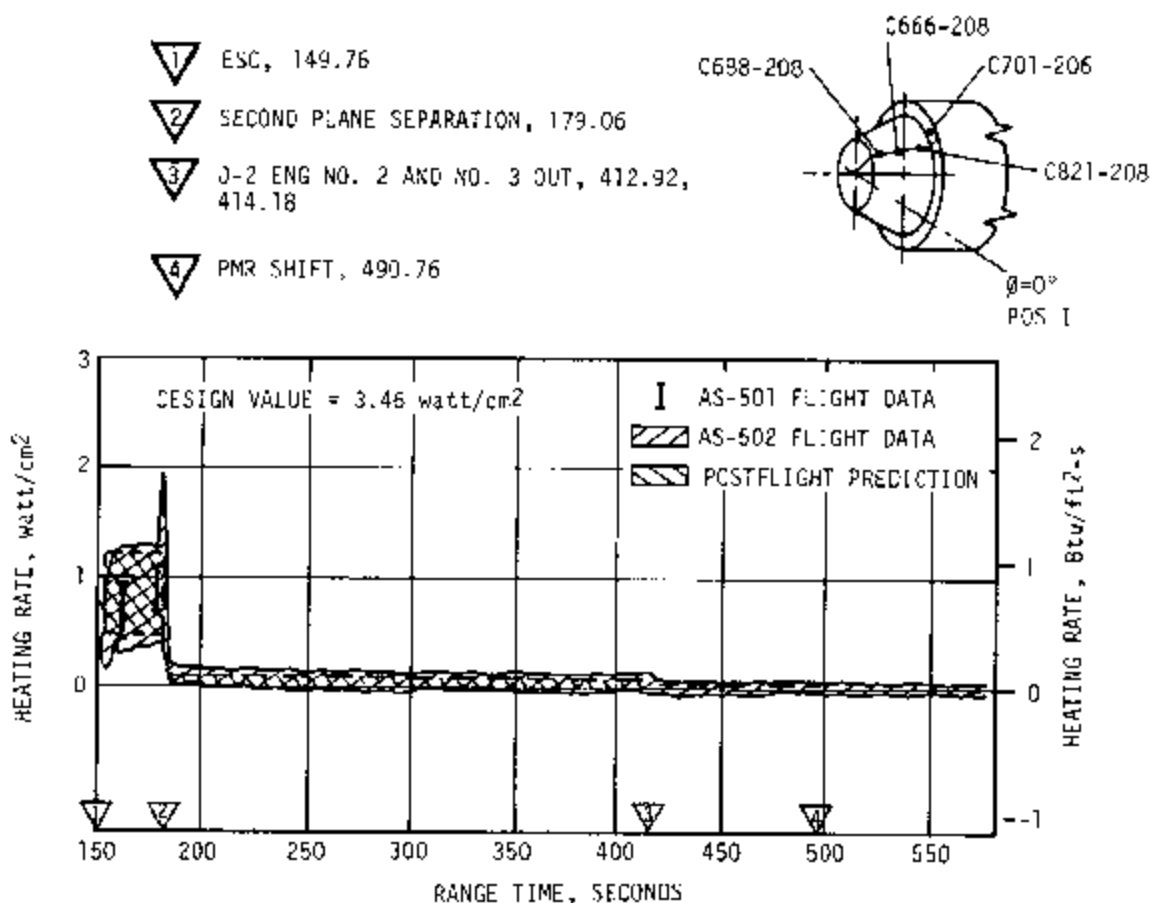


Figure 17-9. S-II Thrust Cone Total Heating Rates, Sheet 1 of 2

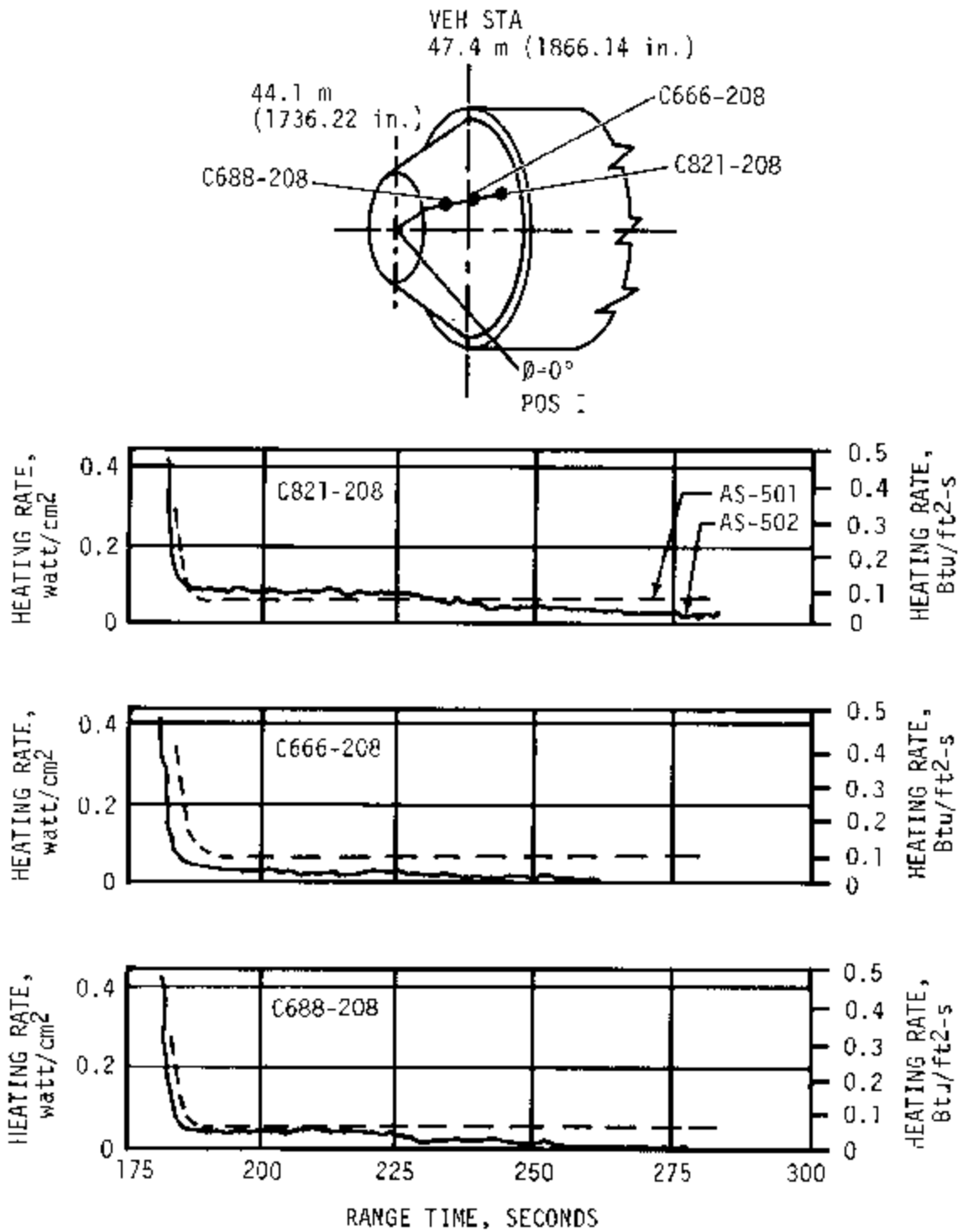


Figure 17-9. S-11 Thrust Cone Total Heating Rates, Sheet 2 of 2

Figure 17-10 presents an overall view of the thrust cone heating rate measurement locations and their performance during the time period prior to and after engine No. 2 cutoff. All the instruments indicate that the thrust cone experienced a sudden increase in heating rates and temperatures during a very short interval at the time of engine No. 2 cutoff. The increase appears to be spread over a very wide region and is unrelated to the location of the instrument with respect to engine No. 2.

A corresponding plot of engine curtain gas temperatures and base heat shield forward face surface temperatures is shown in Figure 17-11. It is seen that all but one of the gas temperature transducers exceeded their maximum range of 422°K (300°F). Several discrepancies are observed in Figure 17-11. These are:

- a. The indicated heat shield surface temperature in the vicinity of engine No. 3 exceeded the recorded gas temperature value in that region.
- b. The surface temperatures appear to "peak out" at approximately 370°K (206°F) while the transducer is set for a maximum value of 590°K (482°F).
- c. The "peaks" have a different duration, and several of the indicated values finally drop below the value recorded prior to engine No. 2 failure.

A similar trend was exhibited by the base region pressure instrumentation, as shown in Figures 16-13 and 16-14. Therefore, it appears that the base heat shield forward face temperature transducers indicate the correct trend, if not the correct level.

In general, base region temperatures at liftoff were colder for AS-502 than for AS-501. This was due to controlling the operation of the engine compartment conditioning system to a lower temperature during prelaunch operation. AS-502 ambient, structural, and component temperature characteristics were similar to those for AS-501 for the first 225 seconds of flight. After 225 seconds, data from AS-502 ambient, structural and component temperature transducers located in the region forward of the heat shield and outboard of engine No. 2, as noted in Figure 17-12, show an abnormal cooling trend indicating a cryogenic leak near No. 2 engine.

The normal S-II boost temperature history trend for ambient temperatures in the region forward of the heat shield is shown by the AS-501 temperature data in Figure 17-12. The ambient temperatures increase with the interstage on and then decrease after interstage separation along with a decrease in base heating. Ambient temperatures forward of the heat shield leveled out and began increasing 250 seconds after AS-501 liftoff. On AS-502, the temperatures followed the same trends as the AS-501 temperature data until 225 seconds after liftoff when,

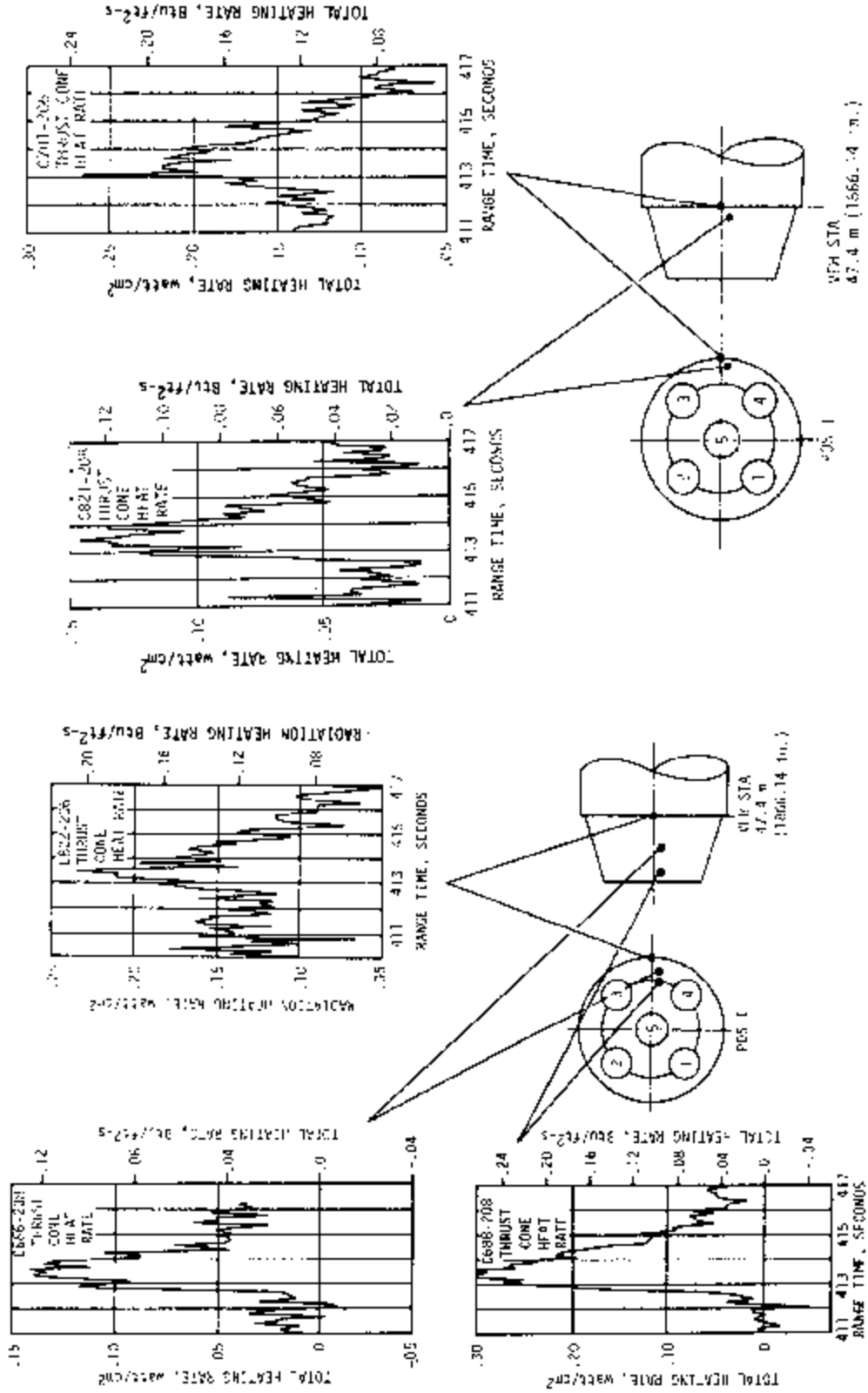


Figure 17-10. S-II Thrust Cone Total and Radiation Heating Rates

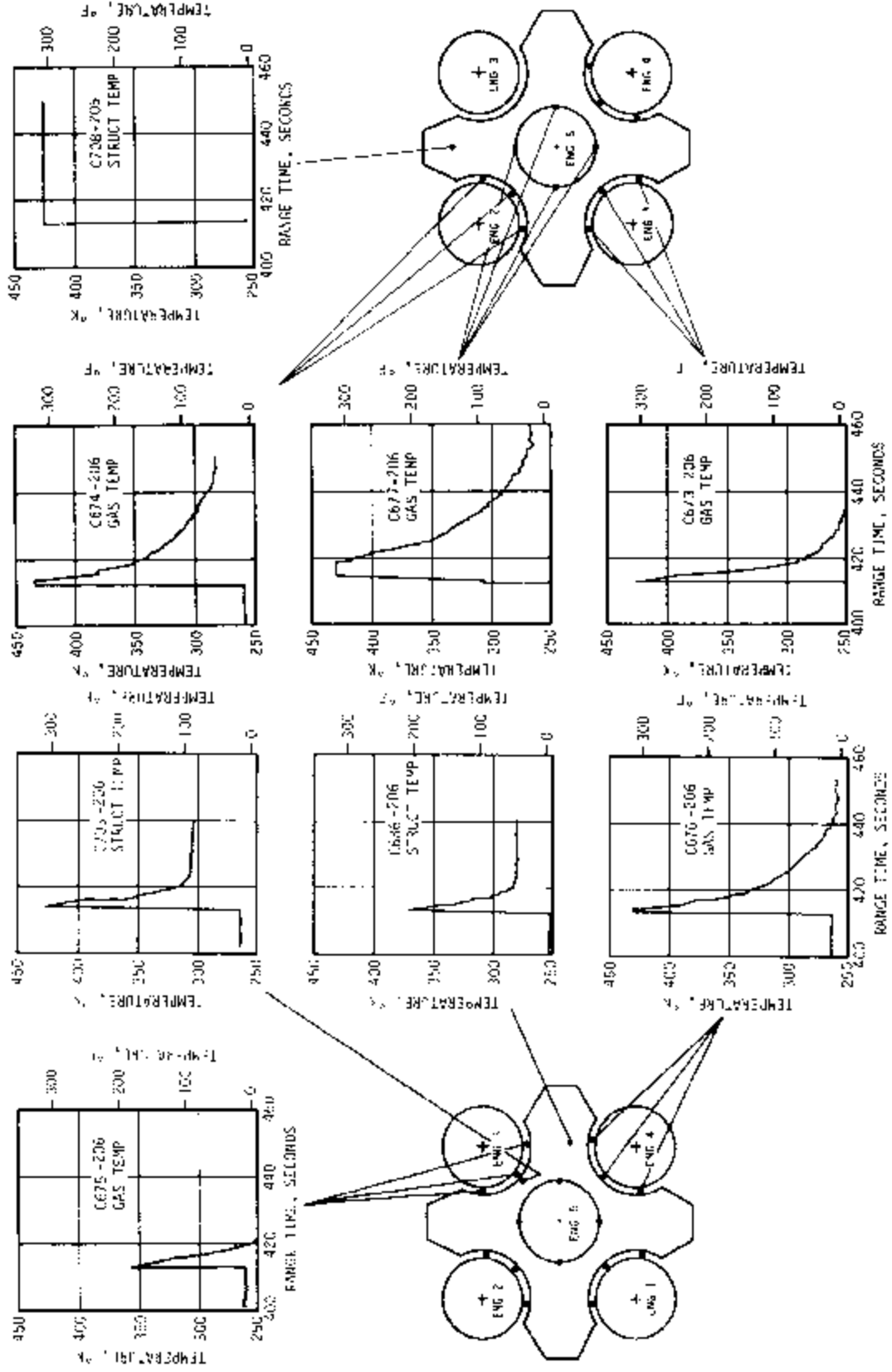
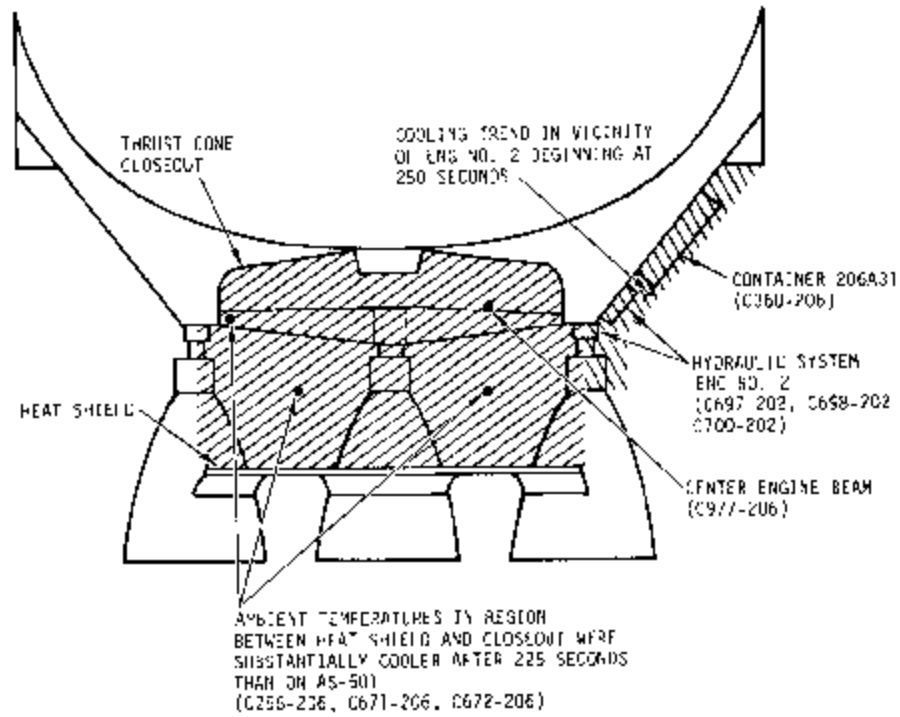


Figure 17-11. S-II Heat Shield Forward Face Temperature

CHILDDOWN OF ENGINE COMPARTMENT



- | | |
|------------------------------------|--|
| 1 ESC, 149.75 | 4 ENG NO. 2 CUTOFF, 412.92
ENG NO. 3 CUTOFF, 474.78 |
| 2 SECOND PLANE SEPARATION, 179.06 | 5 PMR SHIFT, 430.76 |
| 3 ENG NO. 2 PERFORMANCE SHIFT, 319 | 6 ENG NO. 1, 4, & 5 CUTOFF, 578.33 |

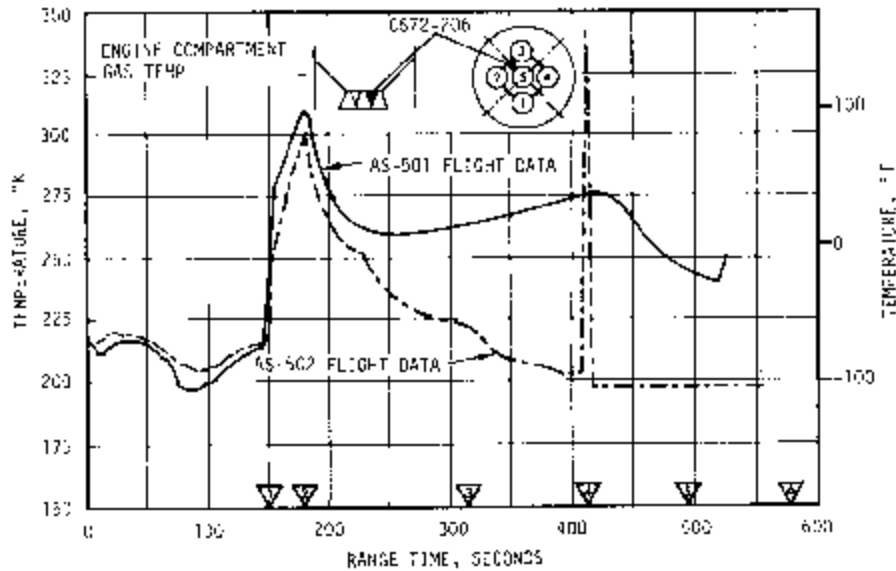


Figure 17-12. Engine Compartment Gas Temperature

instead of leveling out and increasing, they began decreasing at an increasing rate as shown in Figure 17-12. AS-502 hydraulic system temperatures for engine No. 2, container 206A31 equipment mount temperature and center engine beam temperature also showed cooling trends between 250 and 290 seconds when compared with respective AS-501 data. Since AS-502 hydraulic system temperatures for all engines except engine No. 2 appeared normal and the only container temperature which appeared abnormal was a container located on the thrust cone over engine No. 2, it is believed that a cryogenic leak occurred near this engine during the flight.

In the region forward of the heat shield and below the thrust cone and LOX tank, flight data show spikes occurring in the heat shield forward face temperature. The ambient temperature in this region, shown in Figure 17-12, exhibits a spike at 412.6 seconds, just prior to the time of engines No. 2 and 3 cutoff. These temperature spikes correspond to the time of pressure increases discussed earlier in paragraph 16.3.2. Smaller temperature spikes were noted on the thrust cone. These temperature spikes are believed to have been caused by release of hot gases from engine No. 2 just prior to its shutdown. Thrust cone temperatures also spiked at second plane separation due to the increase in base heating explained earlier in this section.

The temperature spikes indicated by structural temperature measurements were probably more of an indication of transducer temperature rather than actual structural temperatures.

Center engine beam temperature, and LOX tank external skin temperature appeared to erratically fluctuate between 412 and 455 seconds. Since the heat capacities of these structures are large, it is doubtful that the recorded temperatures were actual structural temperatures. It is possible that the transducers separated from the structure to which they were originally bonded, in which case, a very small change in heating and cooling would cause the fluctuations and these transducers would then indicate ambient temperature after debonding.

Temperatures recorded during the AS-502 flight on the aft face of the base heat shield are compared in Figure 17-13 with design, AS-501 actual and AS-502 postflight predicted temperatures. The AS-502 data were well below the design and compared favorably with the AS-501 data and AS-502 postflight predictions. The lower temperatures in the AS-501 band were due to the added heat capacitance of a special steel transducer mount used on AS-501. The actual AS-502 temperatures deviated from the actual AS-501 data at the time of engines No. 2 and 3 shutdown (approximately 413 seconds) due to a decrease in base heat rates presented earlier in this section. The maximum AS-502 actual temperature of 736°K (865°F) occurred at 413 seconds, and is in agreement with the maximum of 741°K (875°F) recorded on AS-501. The design temperatures were calculated using the maximum design environment, and the postflight predictions were based on postflight predicted heating rates.

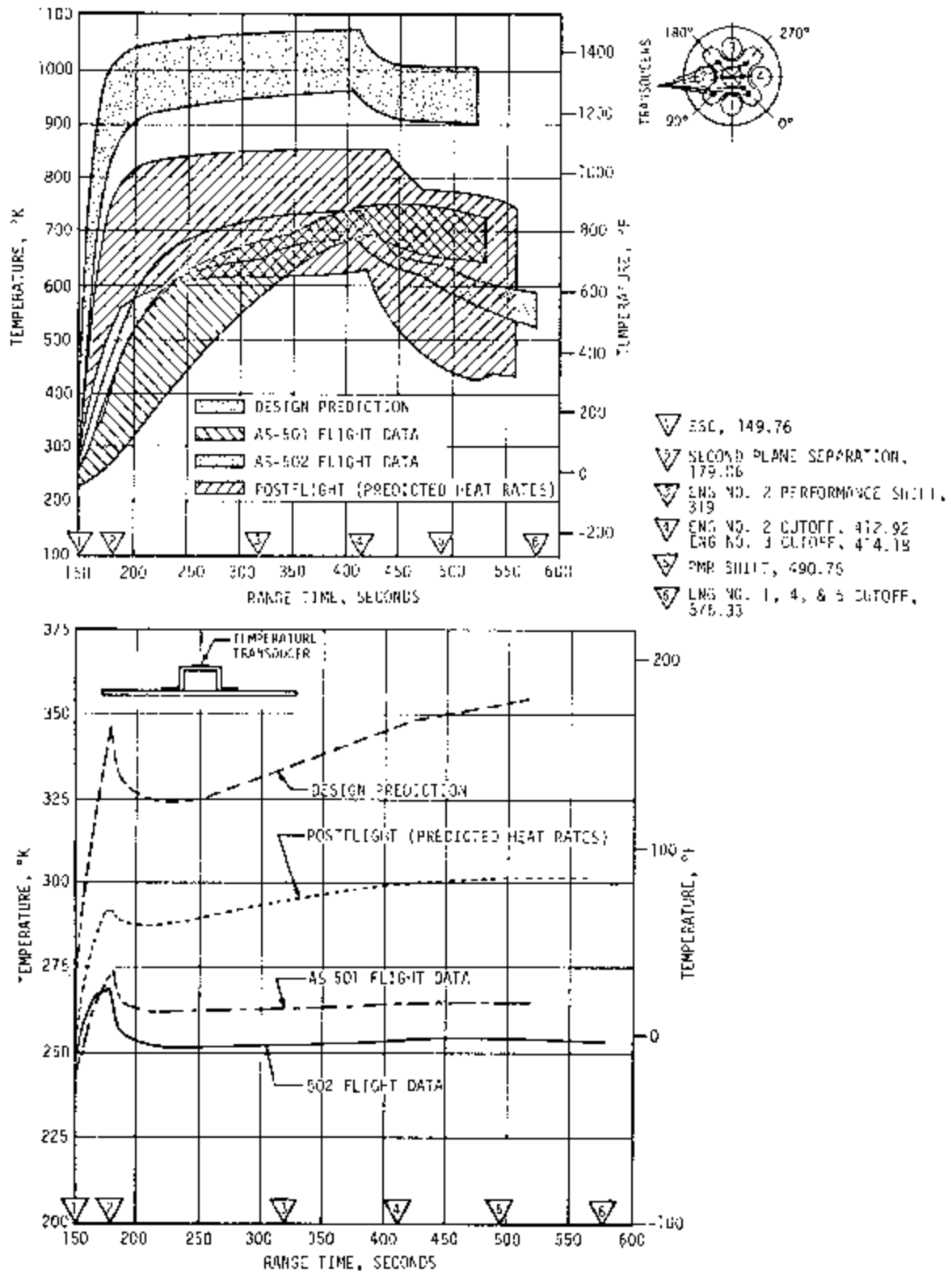


Figure 17-13. S-II heat shield aft face and thrust cone surface temperatures

Thrust cone temperatures were slightly lower on AS-502 than on AS-501 as shown in Figure 17-13 which presents a typical thrust cone surface temperature measurement. This was due to lower base heat rates on AS-502. Design and AS-502 postflight predicted temperatures are also shown in this figure, and were based on the maximum design environment and postflight predicted heat rates.

17.4 S-II/S-IVB SEPARATION ENVIRONMENT

During separation, the retro motor heating rates of the S-IVB structure for AS-501 and AS-502, listed in Table 17-1 were similar, indicating only small differences in the plume impingement environment. Data from the calorimeters indicate that the heat flux to the J-2 engine was somewhat higher on the AS-502 than on AS-501 (but three to six times lower than that experienced on uprated Saturn 1 flights). Predicted heat fluxes are also shown in Table 17-1 and indicate that they were within the maximum envelope expected.

Table 17-1. Retro Motor Plume Heating

TITLE	MEASUREMENT NUMBER	TEMPERATURE RISE, °K (°F)			REMARKS		
		501		502			
Thrust Structure	C07	257 (2)		258 (5)	Position Plane I Halfway between Position Planes I & II and under H ₂ feedline		
Thrust Structure	C08	267 (20)		269 (25)			
Aft Engine Area Ambient	C10	262 (12)		264 (15)	Position Plane I; 0 Gimbal Station		
Aft Skirt	C115	264 (15)		275 (35)	Just off Position Plane I toward IV		
APS Fairing	C207	264 (15)		261 (10)	APS body Position Plane III		
Electrical Tunnel	C227	260 (8)		260 (8)	Just off Position Plane II toward III		
		HEAT FLUX, Watt/cm ² (Btu/ft ² .s)					
		202		501	502		
Engine Nozzle	C2000	7.033 (6.2)		0.454 (0.4)	2.61* (2.3)*	0.624 (0.55)	45° from III toward IV Position Plane III
Heat Flux	C2004	4.05 (3.6)	11.34* (10)*	0.397 (0.35)	1.26* (1.1)*	1.24 (1.10)	
*Analytically predicted maximums							

17.5 VEHICLE AEROHEATING THERMAL ENVIRONMENT

17.5.1 S-IC Stage Aeroheating Environment

The aerodynamic heating environments were measured using thermocouples attached to the backside of the structural skin on the S-IC forward skirt, intertank, engine fairings and fins. Generally, the aerodynamic heating environments and, consequently, the skin temperatures were within prediction bands, below design limits and slightly higher than AS-501 flight data.

Figures 17-14 through 17-16 show comparisons of AS-501 and AS-502 skin temperatures and the heating rates derived from these temperatures. Post-flight simulated skin temperatures are included for comparison. The simulation of the fin skin temperatures includes 0.284 watt/cm^2 ($0.25 \text{ Btu/ft}^2\text{-s}$) for plume radiation, but did not consider effects of flow separation. Skin temperatures on the forward skirt remained at a nearly constant level throughout powered flight as seen in Figure 17-17. The slight downward trend of skin temperature until about 80 seconds follows the trend of the forward skirt compartment gas temperature. At 80 seconds, the free stream recovery temperature begins to rise rapidly causing the slight upward trend in skin temperatures from this point on.

Intertank temperatures closely followed the trend of AS-501 flight data. As shown in Figure 17-17, intertank temperatures were within predicted values throughout flight, and initial temperatures were slightly less than ambient due to the cooling effect of the gas in the intertank compartment. The cooling during the first 70 seconds of flight followed the trend of compartment and free stream ambient gas temperatures. At 70 seconds, the intertank area started to respond to aerodynamic heating and temperatures continuously increased until separation, reaching a maximum 343°K (158°F). The results of an integration of the calculated heating rates on the intertank and fin indicate that the AS-502 vehicle received a slightly higher total heat input than AS-501.

The aerodynamic heating to the body, fins, and engine fairings was interrupted at approximately 110 seconds by flow separation. The flow separation results from expansion of the F-1 engine plumes and, consequently, hot gases are recirculated up the vehicle side. The gas temperature and heat-transfer coefficient in the separated region are expected to be less than those which would have been experienced if separation had not occurred. The temperature increases during separation were most likely caused by the radiation from the hot recirculated gas. The hot gas radiates energy because of the high emissivity of the carbon particles present in the recirculated flow. The resulting change in the heating rates can be noted in Figure 17-14 through 17-16 between 110 and 135 seconds. The increased heating due to flow separation did not constitute a detrimental heating environment. Flow separation and subsequent hot gas recirculation up the side of the vehicle has been

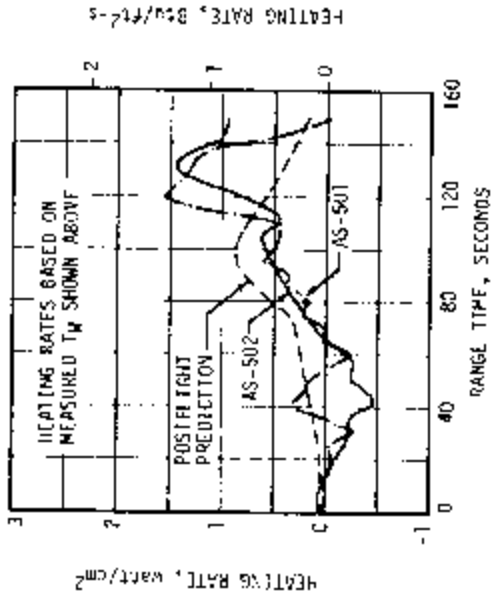
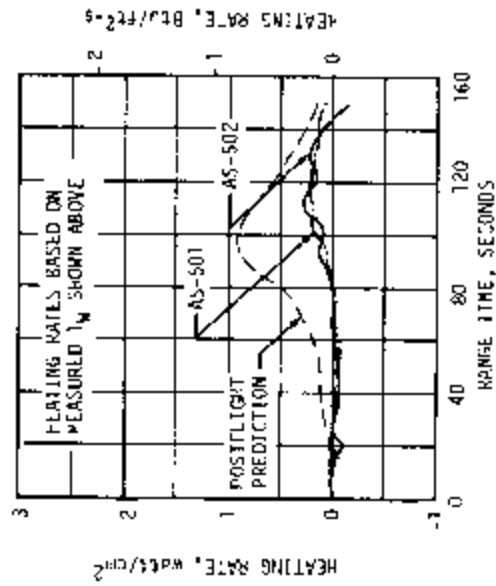
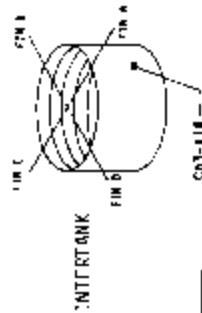
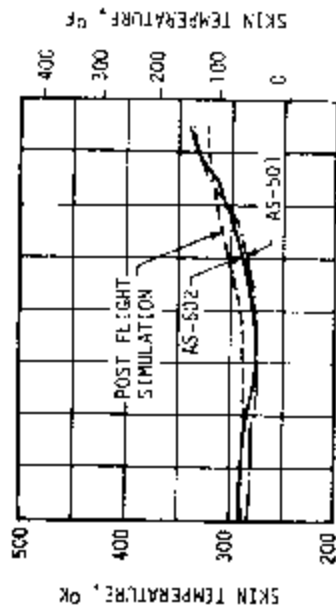
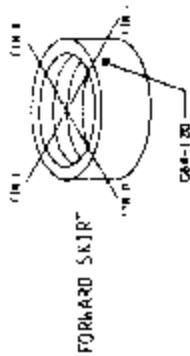
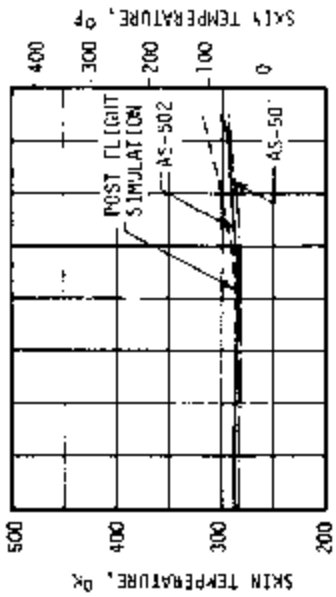


Figure 17-14. S-IC Aerodynamic Heating

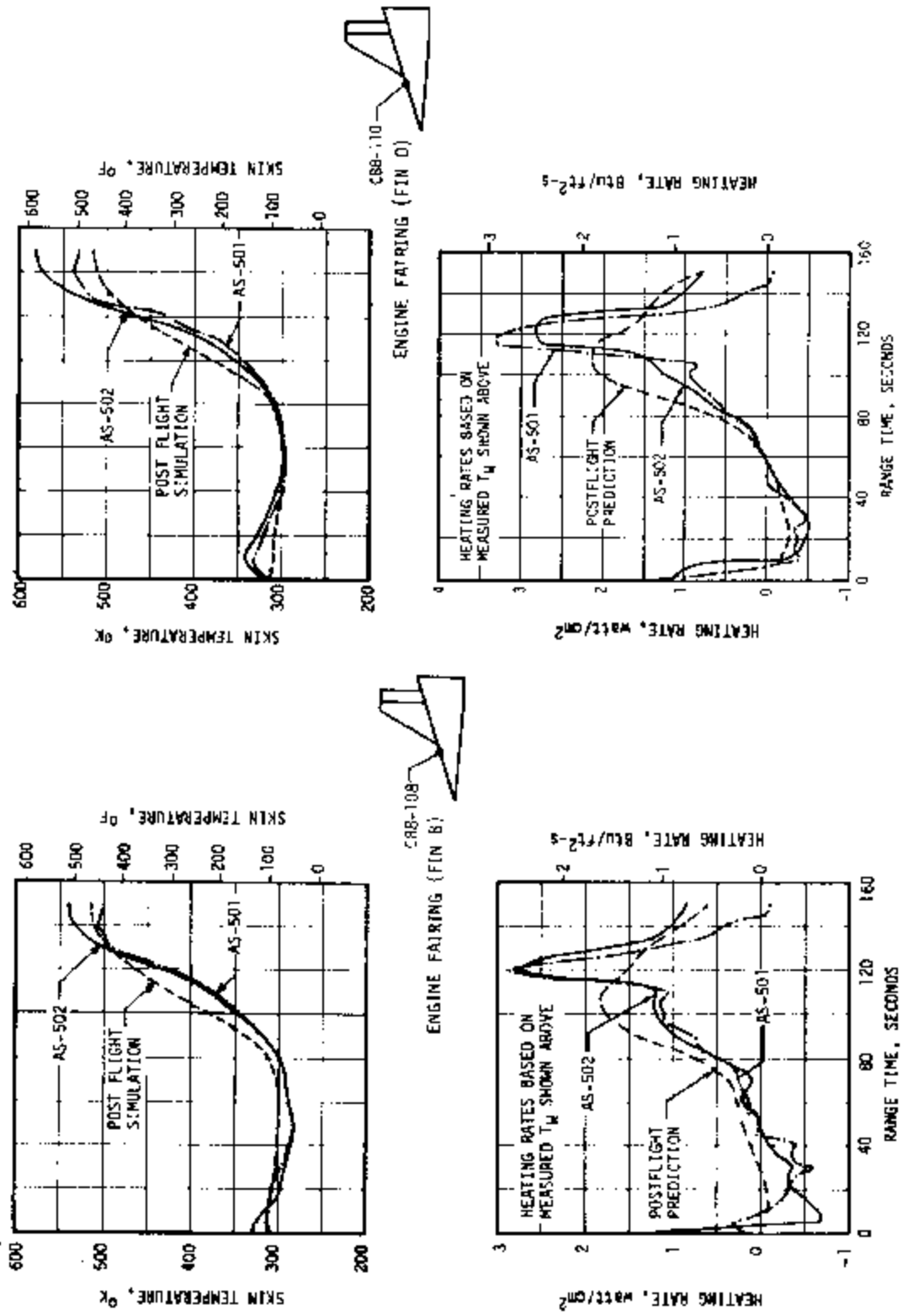


Figure 17-15. S-1C Engine Fairing Aerodynamic Heating

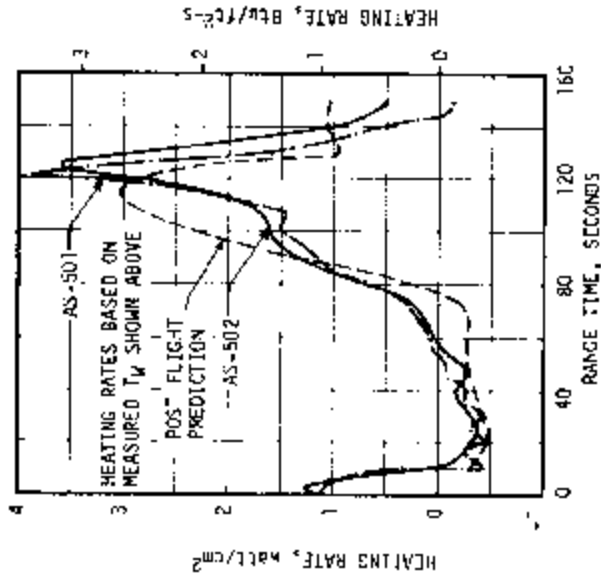
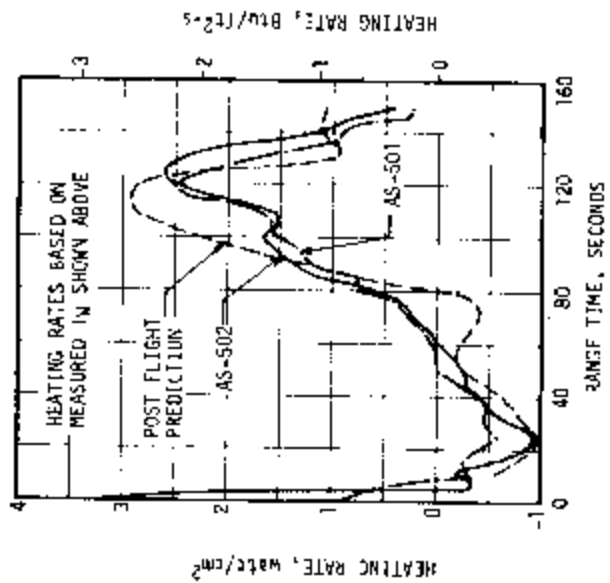
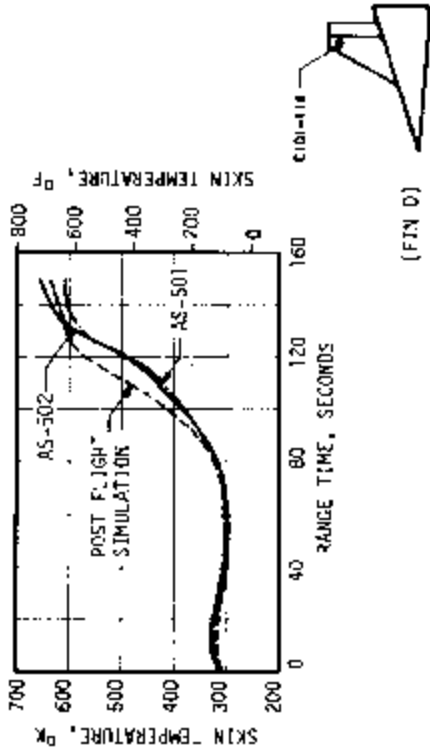
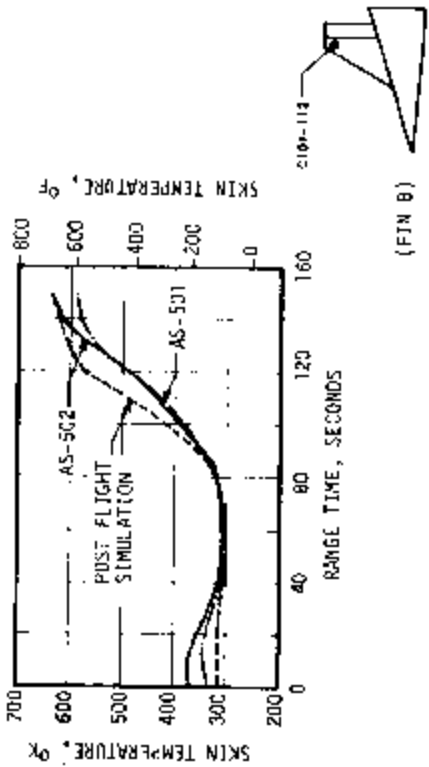


Figure 17-16. S-IC Fin Aerodynamic Heating

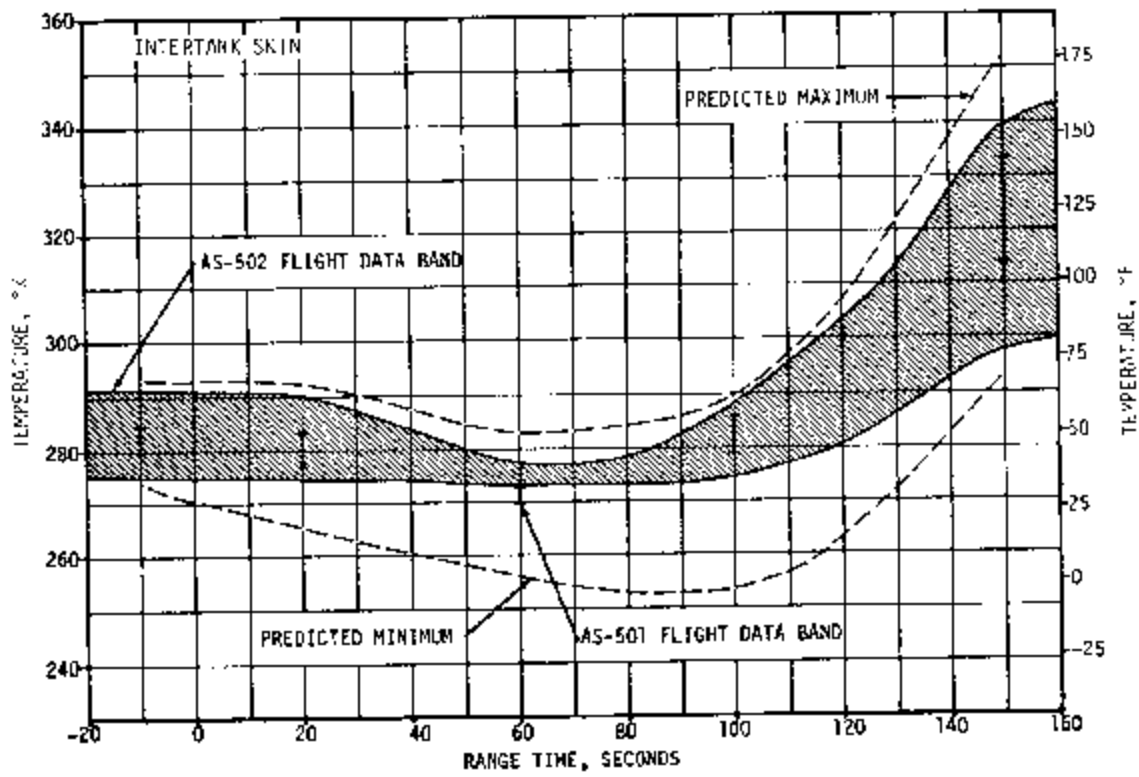
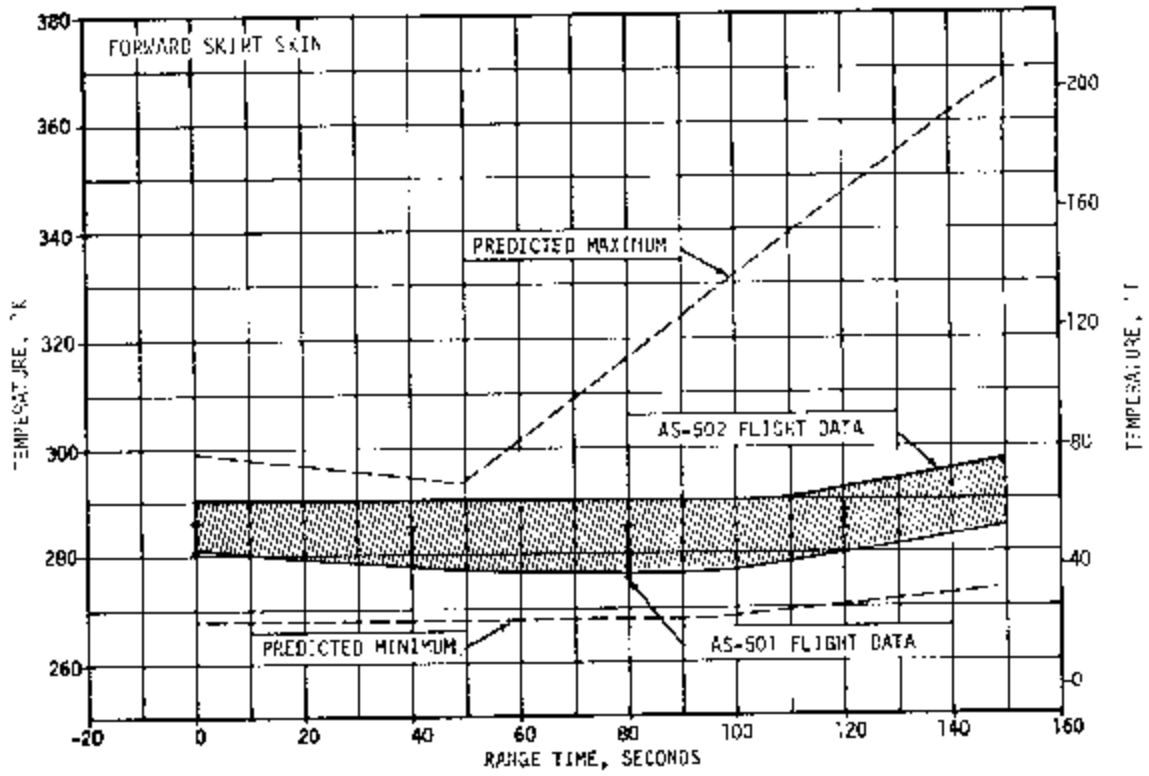


Figure 17-17. S-IC Body Aerodynamic Heating

noted in AS-501 and AS-502 flight optical data. Flow separation was observed on the Saturn I and IB flights and was anticipated on the Saturn V.

Flow separation results from the expansion of the F-1 engine plumes at the higher altitude. The plumes create what could be considered a solid wall to the oncoming free stream. At the lower altitudes, the free stream flow can be deflected around the exhaust plume by the external plume shock; but as the plumes increase in size, the free stream flow can no longer turn near the plume surface. Consequently, the flow on the side of the vehicle separates or begins to turn before it reaches the plumes. Figure 17-18 illustrates the flow field which is obtained after separation occurs. Hot gas is fed into the separated region from the base region and plume interface. The base region hot gas results from the engine exhaust flows impinging upon one another and forcing some of the exhaust gases toward the base heat shield. Separation, once induced, will continue until outboard engine shutdown. As the plume diameter expands with altitude, the point of flow separation moves forward along the vehicle.

Flow separation on the AS-501 and AS-502 flights was first observed between 105 and 110 seconds. Measurements have been made of the point of flow separation for various flight times and are shown in Figure 17-18. It is noted in this figure that the separation region extended beyond the top of the S-1C forward skirt just prior to stage separation. The observed blackness on the stage may be a carbon deposit rather than paint being burned.

Temperatures on the aluminum portion of the fairings (forward of the heat shield) fell within a narrow band reaching a maximum of 573°K (572°F) at the end of powered flight as seen in Figure 17-19. Temperatures at the end of flight were about 40°K (72°F) higher than those attained on AS-501. This was due to the higher heating trajectory flown by AS-502 as seen in Figure 17-20 which compares aerodynamic heating indicator for AS-501 and AS-502. The initial rise in temperature at zero seconds is attributed to initial incident plume radiation. Predicted maximum temperatures were not exceeded on the forward fairing and no severe temperature gradients were observed.

Temperatures on the titanium portion of the fairing are shown in the lower graph of Figure 17-19. Temperatures followed the expected trend and are well below the predicted maximum. The slightly higher temperatures experienced on AS-502 compared to AS-501 were to be expected due to the higher aerodynamic heating trajectory flown by AS-502 and the slightly more severe base environment. The narrow flight data band indicates the lack of any severe temperature gradients on the aft fairing.

Temperatures on the thrust structure followed the expected trend and although the prediction was slightly exceeded at 125 seconds, this presented no problem as the temperatures were within design capability. Since aerodynamic heating effects in this area are thought to be less

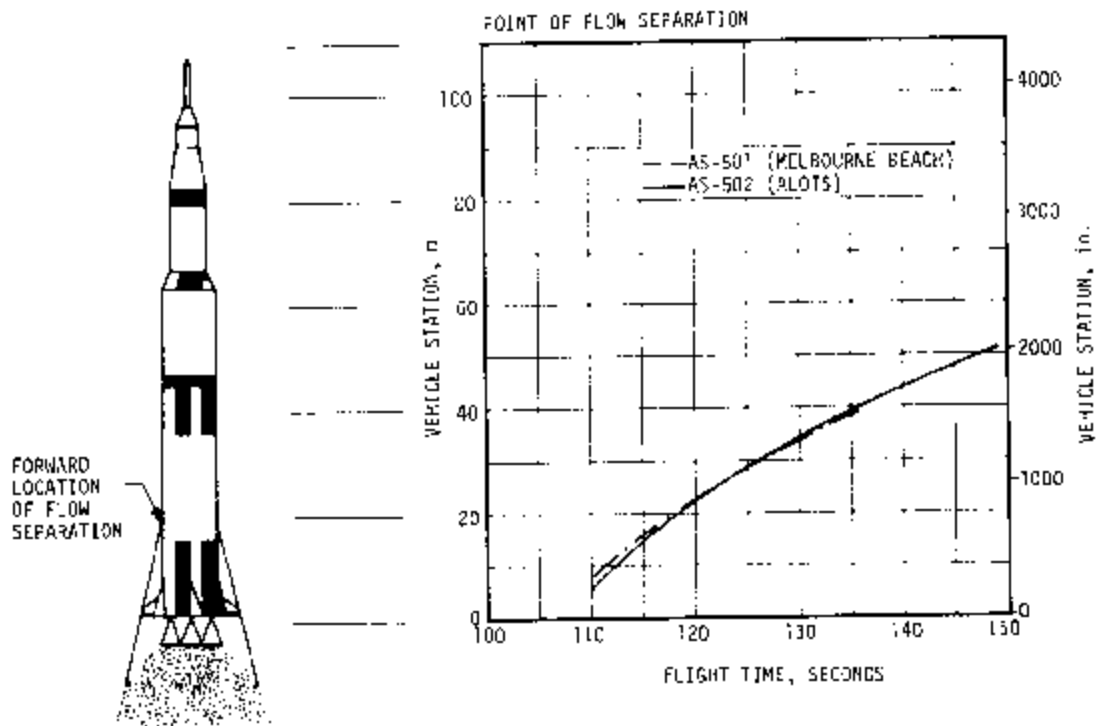
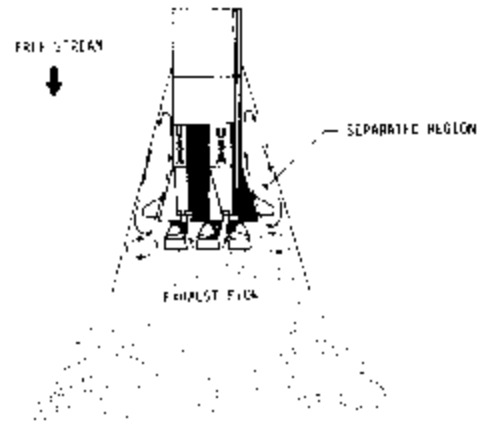


Figure 17-18. Forward Location of Separated Flow

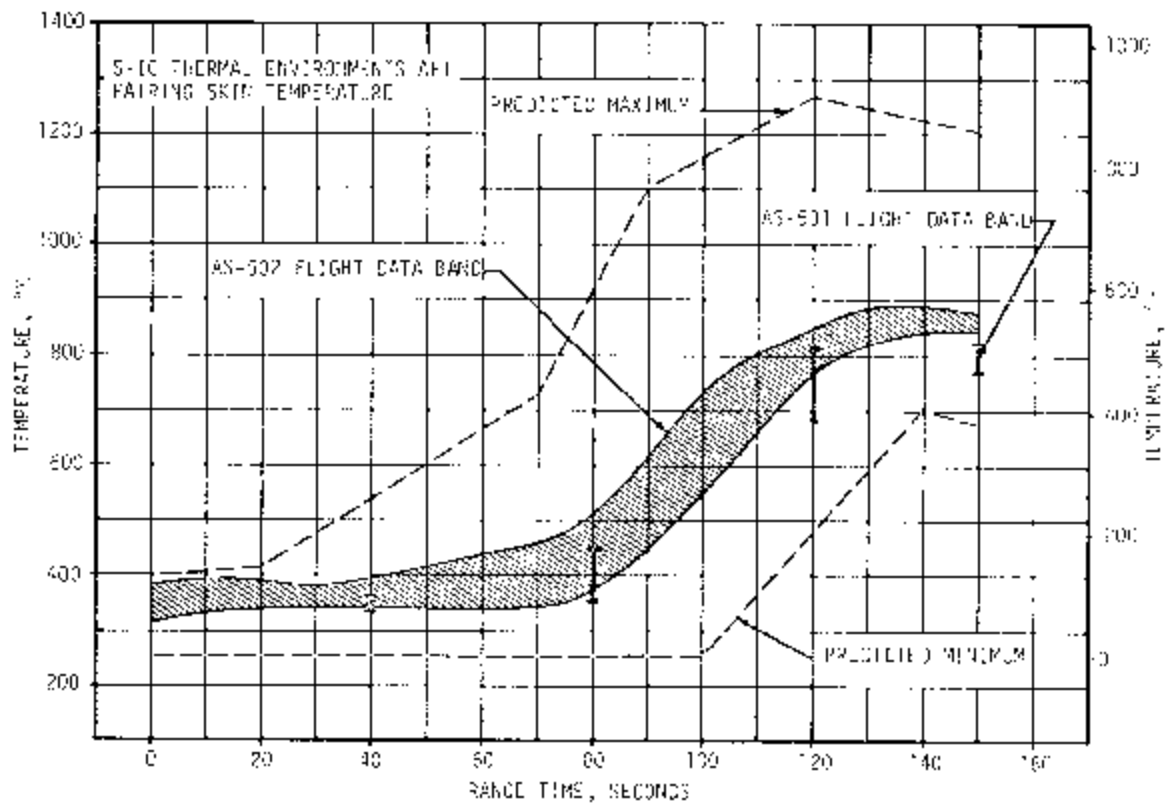
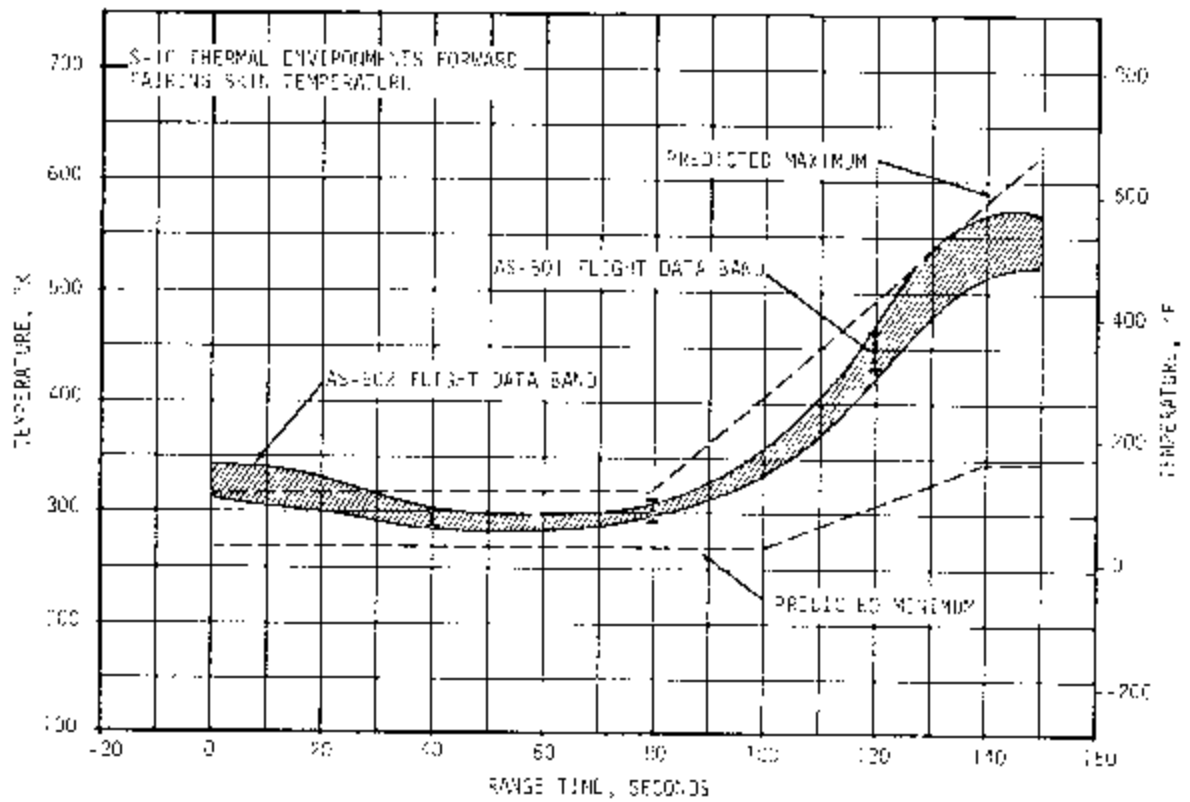


Figure 17-19. S-IC Thermal Environment

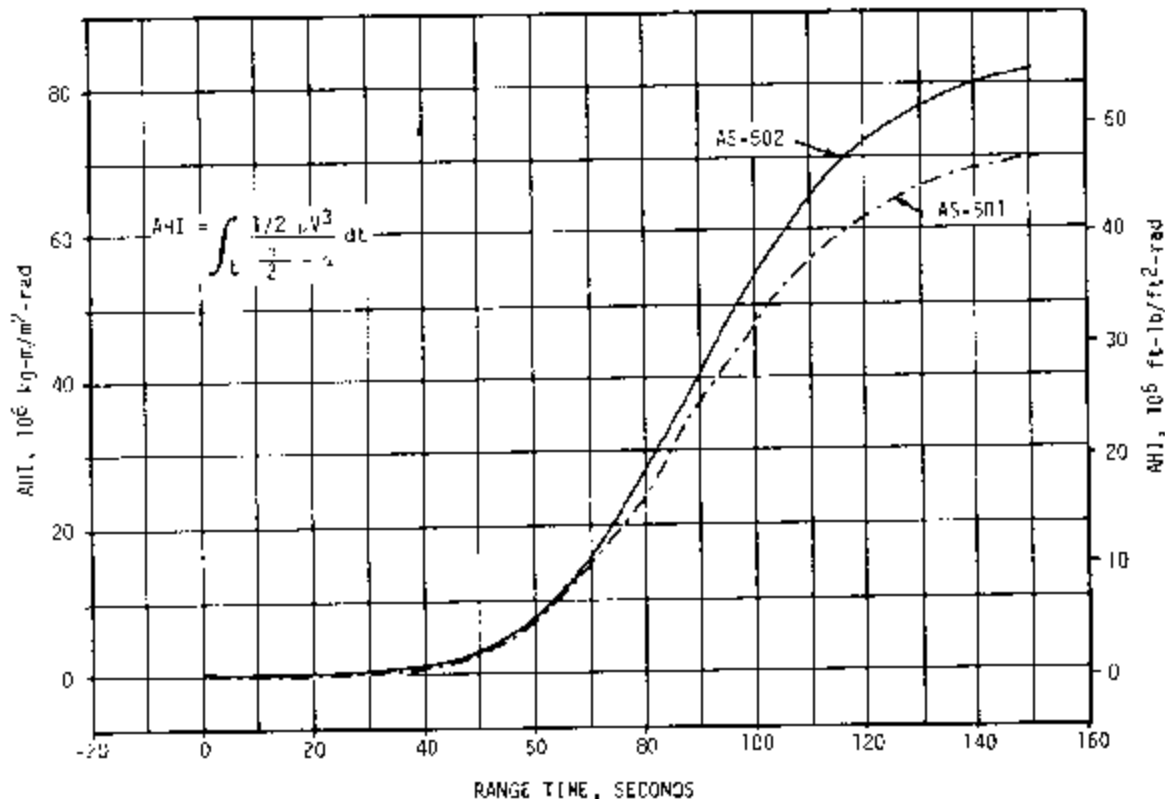


Figure 17-20. S-IC Thermal Environments Aerodynamic Heating Indicator (AHI)

severe than the design levels it is concluded that radiation from the plume and burning gases in the separated flow region accounted for the fact that temperatures exceeded the predictions in this area.

Temperatures on the wedge section of the fins were about 60°K (108°F) higher on AS-502 than on AS-501 as shown in Figure 17-21) due to the higher heating trajectory. However, the predicted maximum temperature was not exceeded and the relatively narrow flight data band indicates an absence of any severe temperature gradients on the fin wedge section. The initial rise in temperature at liftoff was due to burning exhaust gases and initial plume radiation.

Temperatures on the flat section of the fins were of the same order of magnitude as those on the wedge section reaching 633°K (680°F) at the end of flight as shown in Figure 17-21). Predicted maximums were exceeded only near liftoff where a sharp rise in temperature was observed due to burning exhaust gases and plume radiation. Convective cooling occurred until about 70 seconds when recovery temperature began to rise and aerodynamic heating effects caused a skin temperature rise. For the most part, higher temperatures were obtained on the fin flat section on AS-502 than on AS-501 again due to the higher heating trajectory flown by AS-502. No harmful temperature gradients were observed on the flat section of the fins.

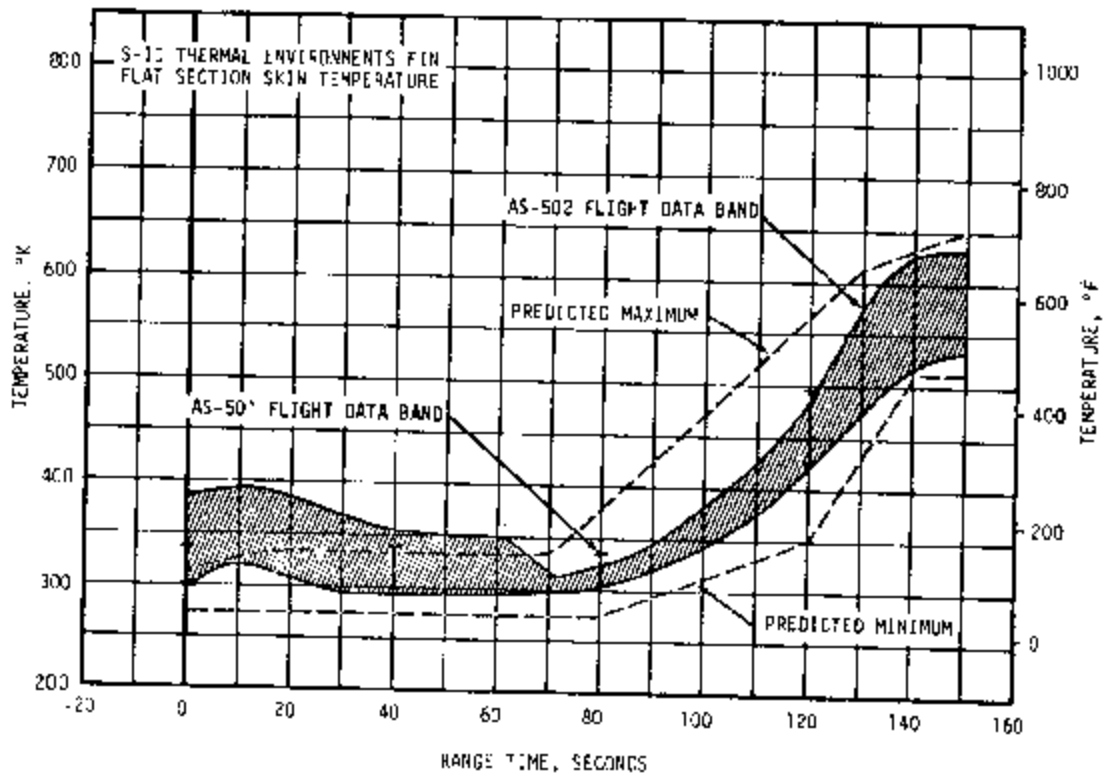
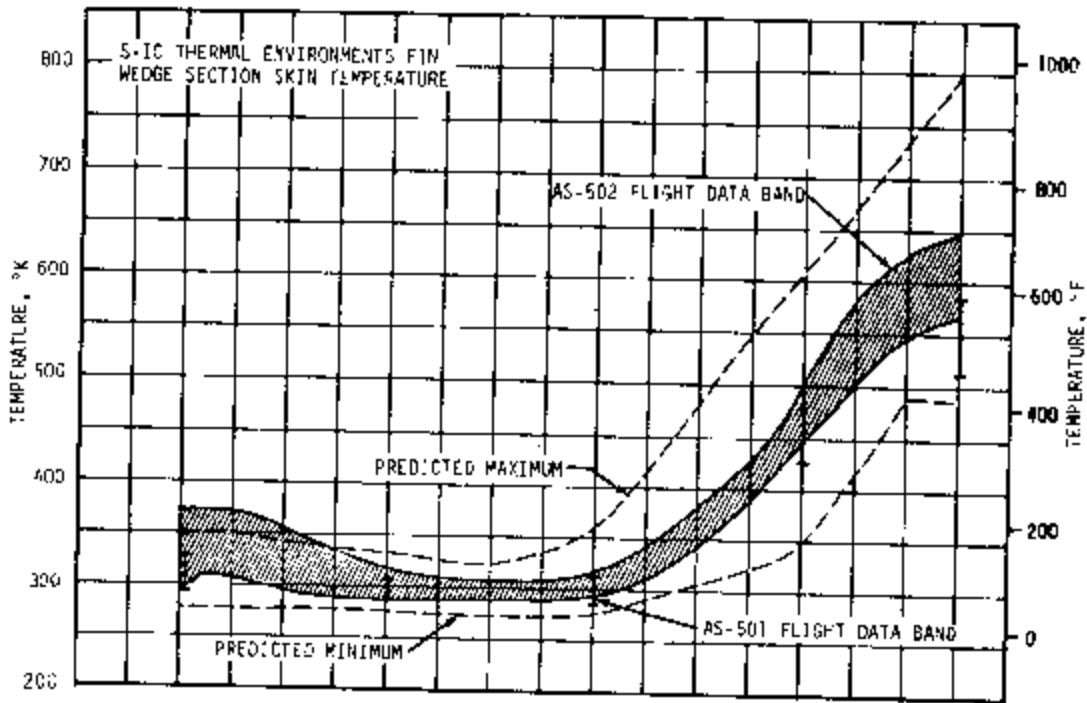


Figure 17-21. S-IC Thermal Environment Fin Skin Temperatures

7.5.2 S-II Stage Aeroheating Environment

Aeroheating rates on S-II stage and its protuberances were analyzed using the AS-502 Final Observed Mass Point Trajectory (OMPT) and angle-of-attack data obtained from the S-IC Flight Control Conditioned Data Tape (Q-ball). Atmospheric data were obtained from the final meteorological data tape.

The aeroheating rates on the S-II stage cylindrical surface and its protuberances were calculated by means of an aeroheating digital computer program. The program includes turbulent flow flat plate heating rate theory and real gas thermodynamic and transport properties for air.

The heating rates to the protuberances were obtained by increasing the basic flat plate heat flux by the appropriate experimentally determined protuberance factors. The predicted aeroheating rates were corrected to the calorimeter conditions for purposes of direct comparison. These transient calorimeter heating rates were determined by first computing the sensor temperature corresponding to the nominal aeroheating rates and then applying the temperature mismatch correction to obtain the final sensor temperature. The final indicated calorimeter heating rates were obtained from the calorimeter sensor-body temperature differentials and the calorimeter calibration curves.

In general, the postflight prediction transient heating rates were higher than the corresponding flight values. The validity of protuberance factors used, which may have contributed to these discrepancies, are under investigation in order to improve the prediction techniques.

The heating rate design values are omitted from these presentations because they are not corrected to the calorimeter conditions. Since the structural surface temperature response plays a key role in transient heat flux predictions, the comparison of design heating rate values for the structure with the calorimeter indicated heat flux is meaningless. However, it has been established that the AS-502 flight aeroheating rates were considerably lower than the design values.

The comparison of AS-502 flight and postflight prediction of the aeroheating rates experienced by the calorimeters mounted on the LH₂ feed-line fairings are presented in Figure 17-22. AS-501 flight data is also indicated and it is seen that it is enveloped by the AS-502 flight data. Reasonably good agreement of flight and postflight prediction was obtained for the measurements installed on the fairing boattail section. However, the predicted heating rates to the fairing nose cone section are considerably higher than the corresponding measured values. Therefore, the experimentally obtained wind tunnel model test protuberance factors will require further modification in order to obtain improved correlation.

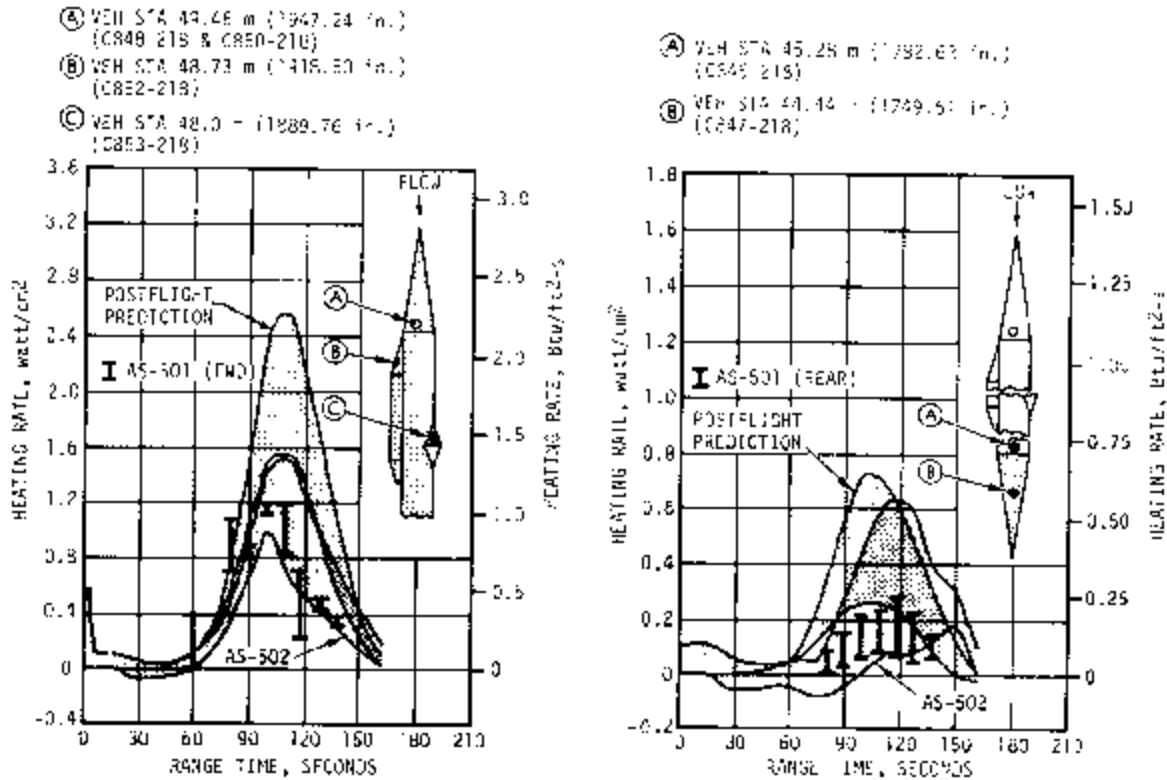


Figure 17-22. S-II LH₂ Feedline Fairing Total Heating Rates

The comparisons of AS-502 flight and postflight predicted aeroh heating rates experienced by the calorimeters mounted on the fairing conical nose sections are presented in Figure 17-23. AS-501 flight data are also shown for comparison. Again, the predicted data are considerably higher than the corresponding flight values as was shown to be the case for the LH₂ feedline fairings.

The comparisons of AS-502 flight and postflight predicted values of the aerodynamic heating rates sensed by the calorimeters installed on the interstage structure and first plane separation fairing are presented in Figure 17-23. AS-501 flight data, which envelopes the AS-502 flight data, are also included. The predicted values are higher than the corresponding flight values during the maximum heating portion of the flight. A qualitative disagreement exists between flight and predicted data beyond 125 seconds. The flight data at this time shows decreasing heating rates which approach a constant level. It is believed that this phenomenon was caused by the scorching of the surrounding cork insulation. The scorching of cork insulation, due to the aeroh heating, was also observed in the photographic coverage of insulation tests performed on the X-15 flights. This phenomena was not accounted for in the analytical postflight prediction, hence the resulting discrepancy. It should be noted that the same trend was observed in the AS-501 flight data.

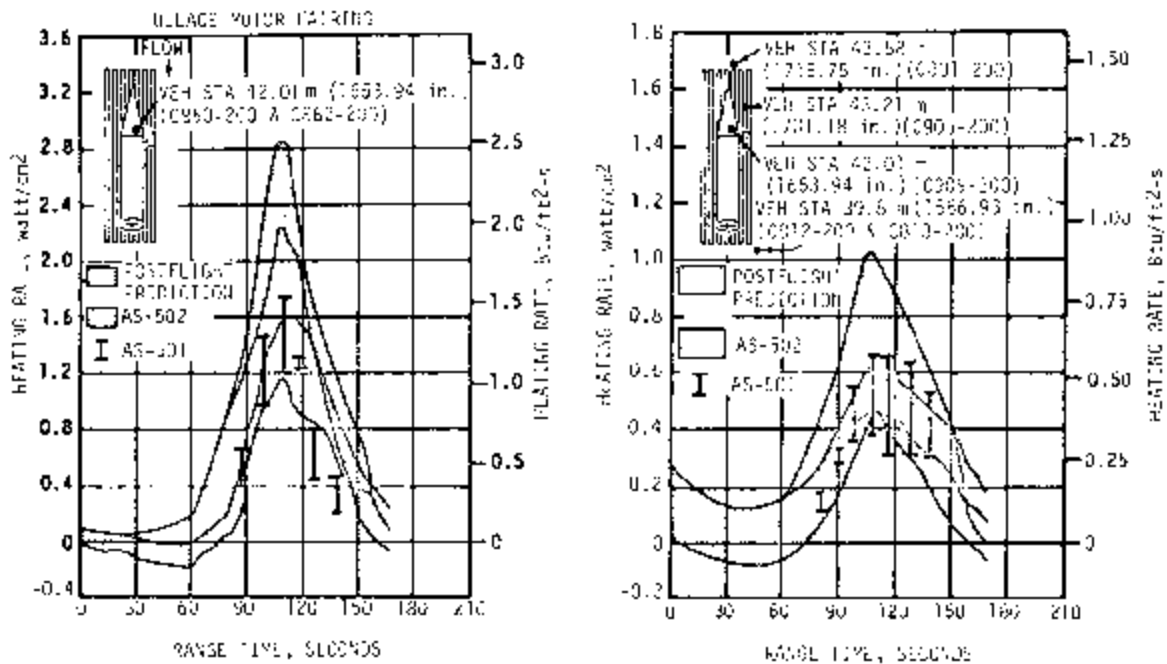


Figure 17-23. S-II Ullage Motor Fairing and Aft Skirt Total Heating Rates

Representative structural, fairing, and surface temperature measurements influenced by AS-502 aerodynamic heating are shown in Figures 17-24 and 17-25. Each plot gives the actual flight data along with design and postflight predictions. AS-501 flight data is included, where appropriate, for comparison. Design predictions are based on S-II stage contractor design heating trajectory with a high angle-of-attack. The postflight predictions were based on the heating rates discussed earlier in this section.

The temperature data from AS-502 are in general very similar to that from AS-501. A slightly higher temperature environment and slightly more severe trajectory resulted in higher temperature and a larger temperature rise for AS-502.

Figure 17-24 presents typical interstage structural temperatures. Postflight predicted and flight values are in good agreement.

Feedline fairing temperature and ullage motor fairing temperature data are presented in Figure 17-24. The postflight predictions of temperature for both these fairings are higher than flight data. Revisions in the protuberance factors used to calculate the aerodynamic heating are expected to result in predictions that will more closely match the flight data.

Figure 17-25 presents the data together with design and postflight predictions for C027-219 forward skirt skin temperature. The postflight prediction is only slightly lower than the flight data.

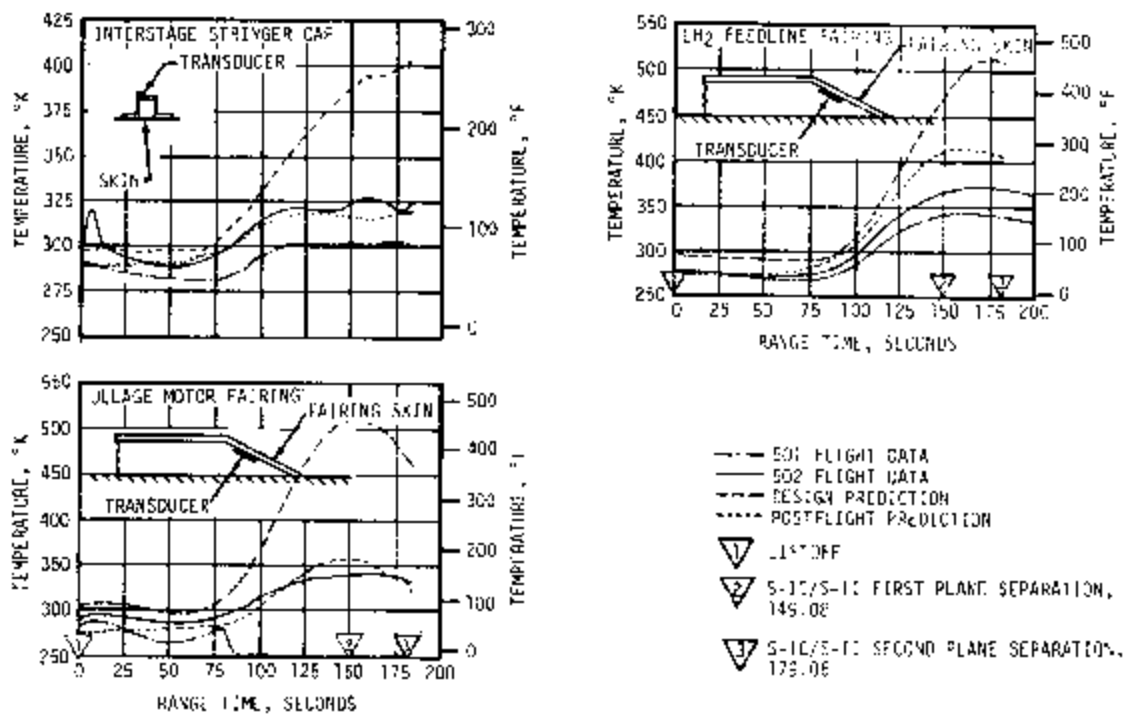


Figure 17-24. S-II Structural Temperatures

LH₂ tank insulation surface temperature measurements for five different locations are presented in Figure 17-25. The abrupt shift in the measured values after the data dropout at approximately 150 seconds is unexplained so far. Up to this shift the postflight prediction and measured values were in good agreement. The significantly lower values obtained from measurement C893-218 were similar to data recorded on AS-501 and may be attributed to cooling due to venting of cold helium gas within the insulation. Investigation into this and other anomalies is continuing.

17.5.3 S-IVB Stage Aeroheating Environment

The AS-502 aerodynamic heating environment was slightly more severe than AS-501. All temperatures were well below the design values for the maximum heating trajectory. Figure 17-26 shows the data and postflight simulation for four skin sensors and one stringer sensor on the forward skirt and data correlations for the LH₂ tank measurements. All simulations use the design method of analysis except that boundary layer transition is determined as the time at which $T_{wall}/T_{recovery} = 0.5$. The maximum recorded temperature was 384°K (232°F). The LH₂ tank measurements were noted to have frost or ice to some degree at liftoff. Unlike AS-501, the frost appears to have persisted for this flight with the exception of one measurement which recorded the maximum temperature of 301°K (82°F).

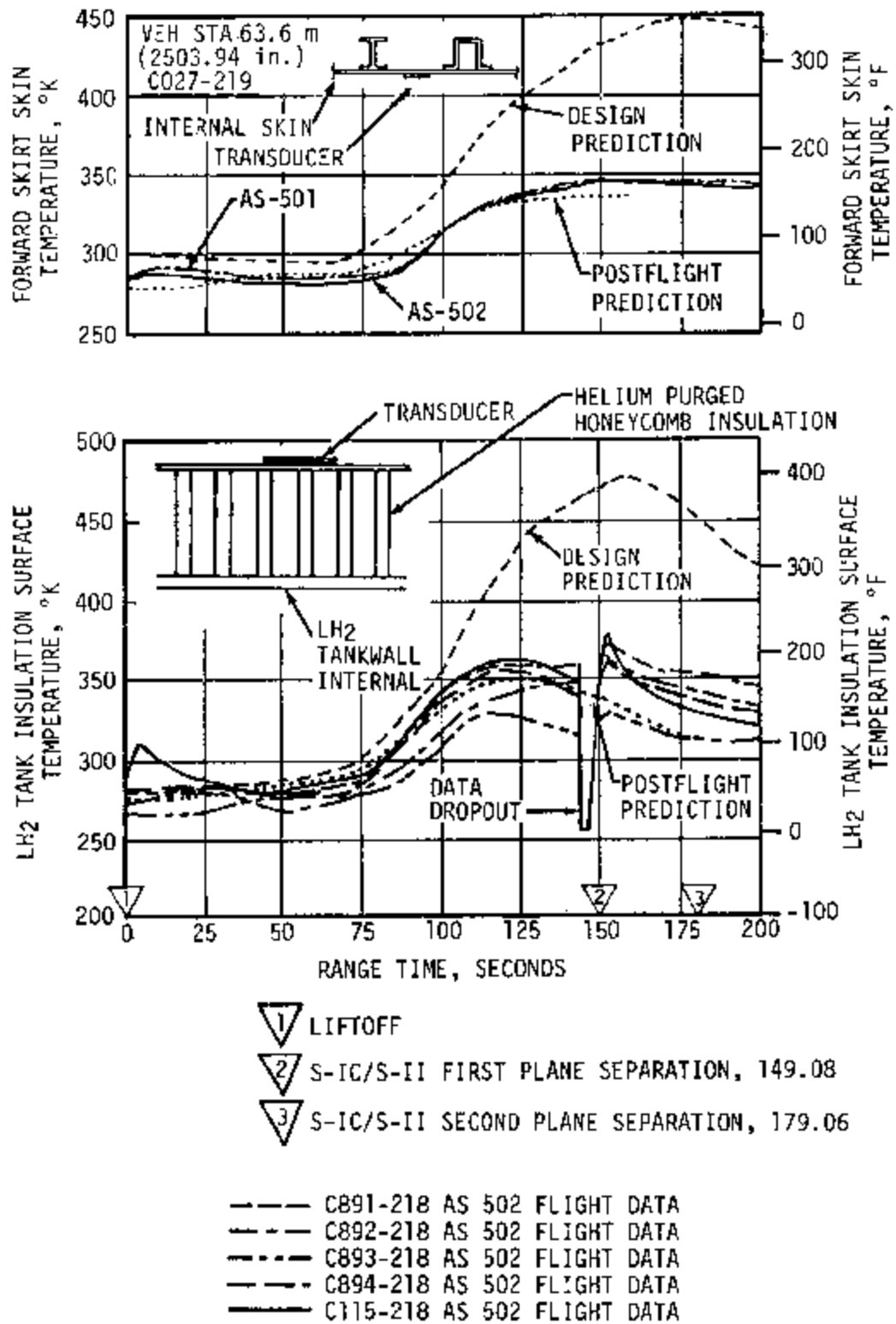


Figure 17-25. S-II Forward Skirt Skin and Insulation Temperatures

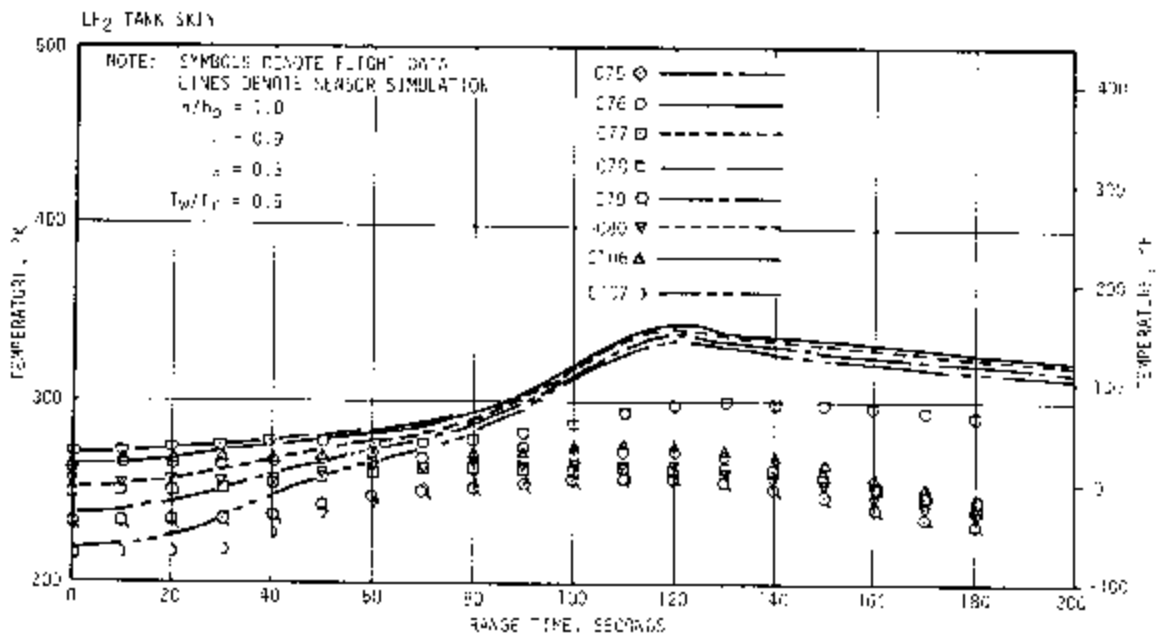
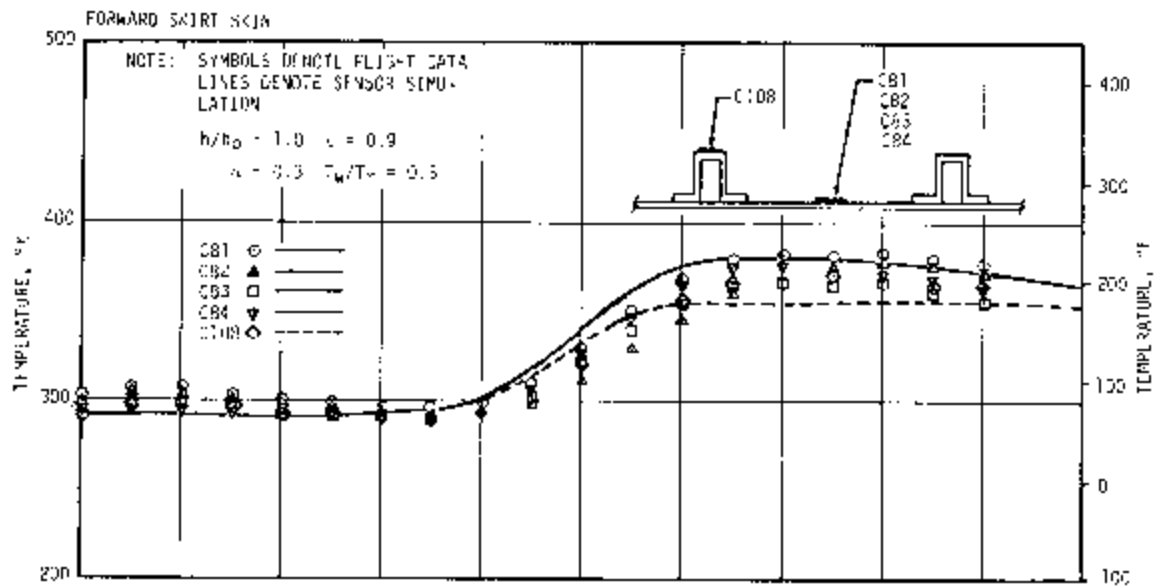


Figure 17-26. S-IVB Aeroheating Environment

Figure 17-27 shows data and correlations for selected skin and stringer temperatures on the aft skirt. All measurements were covered with Korotherm and the analysis assumed a protuberance heating factor of 1.5. The maximum temperature recorded was 353°K (176°F) on the skin. The data and correlation for two adjacent measurements on the aft interstage, one on a stringer and one on the skin are also presented. These measurements were also covered with Korotherm and the maximum recorded temperature was 360°K (187°F). The data and correlation for the measurement on the feedline fairing forebody is also shown. The maximum recorded temperature was 411°K (280°F).

The net heat transferred to the LH₂ during boost was analytically determined by two methods. A comparison between the results obtained from these two methods and the maximum and minimum design heating values is shown in Figure 17-28. Curve A is a simulation using the recovery temperature and tank wall heat transfer coefficient histories based on the flight trajectory. Initial LH₂ tank skin temperatures from flight data and maximum values of insulation thermal conductivity (k) as a function of temperature, as determined from S-IVB loading and acceptance firing test data, were used. The maximum and minimum design values of LH₂ heating are also based on the maximum and minimum k curves. The heat transferred through heat shorts (i.e., heating paths other than the cylindrical tank) was taken from a recent S-IVB propellant heating analysis. Curve B was calculated by integrating LH₂ bulk temperature change resulting from aerodynamic heating during ascent. The LH₂ heating values fall within the design range.

17.5.4 Instrument Unit Aeroheating Environment

The Instrument Unit (IU) aeroheating environment was monitored by eight thermocouples mounted on the inner surface of the honeycomb structure on the low density, 49.7 kg/m³ (3.1 lbf/ft³), core. Seven of the eight measurements indicated temperature rises due probably to internal radiation or local convective heating during the first 30 seconds of flight. This is shown in Figure 17-29. The two sensors located near position IV at station 82.47 meters (3247 in.) and station 82.14 meters (3234 in.) indicated increases of 5°K (9°F) and 8°K (14°F), respectively.

After 30 seconds, these measurements indicated a cooling trend. The IU compartment ambient gas temperature dropped to 283°K (50°F) at 80 seconds. After that time the sensor output was somewhat meaningless since the compartment pressure was approaching 2.1 N/cm² (3.0 psia). The inner skin temperature indicated a maximum 360°K (189°F) at approximately 190 seconds at the sensor located near position I and a minimum of 339°K (151°F) near position II. The simulation in Figure 17-29 indicated a maximum external temperature approximately 24°K (76°F) higher than the inner sensor temperature for the no solar heating case. From 160 to 550 seconds, the effects of solar radiation could be noted in the measured data. The simulation of the data was for no solar heating. The sensors located at positions I and IV would have experienced the greatest solar heat flux; this was indicated in the measured data. These trends due to solar heating were noted in the AS-501 data.

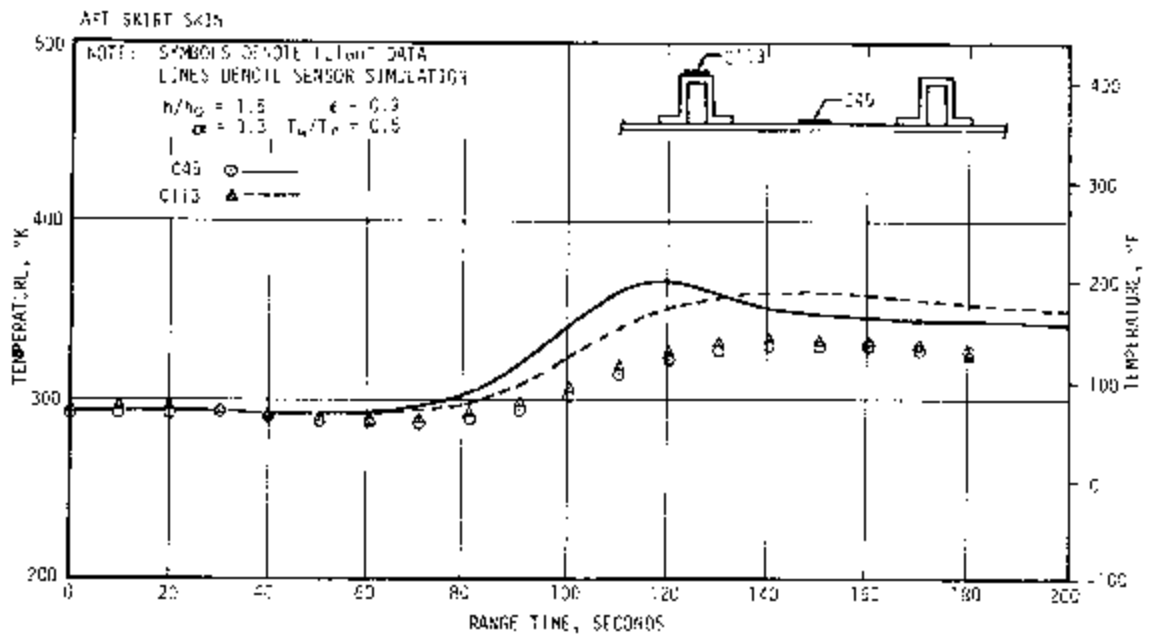
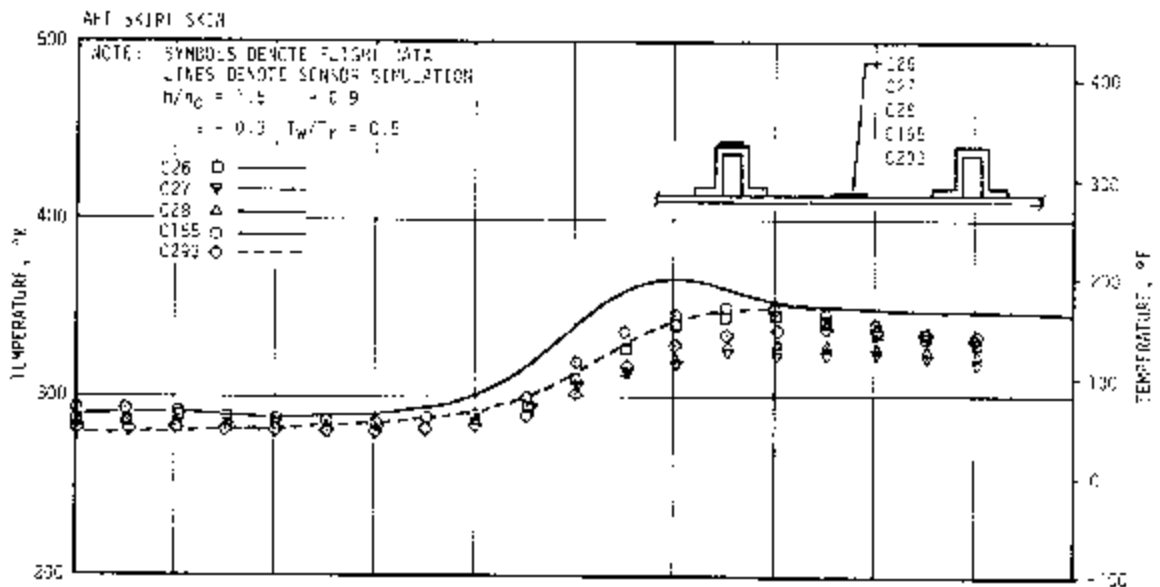


Figure 17-27. S-IVB Protuberance Aeroheating Environment, Sheet 1 of 2

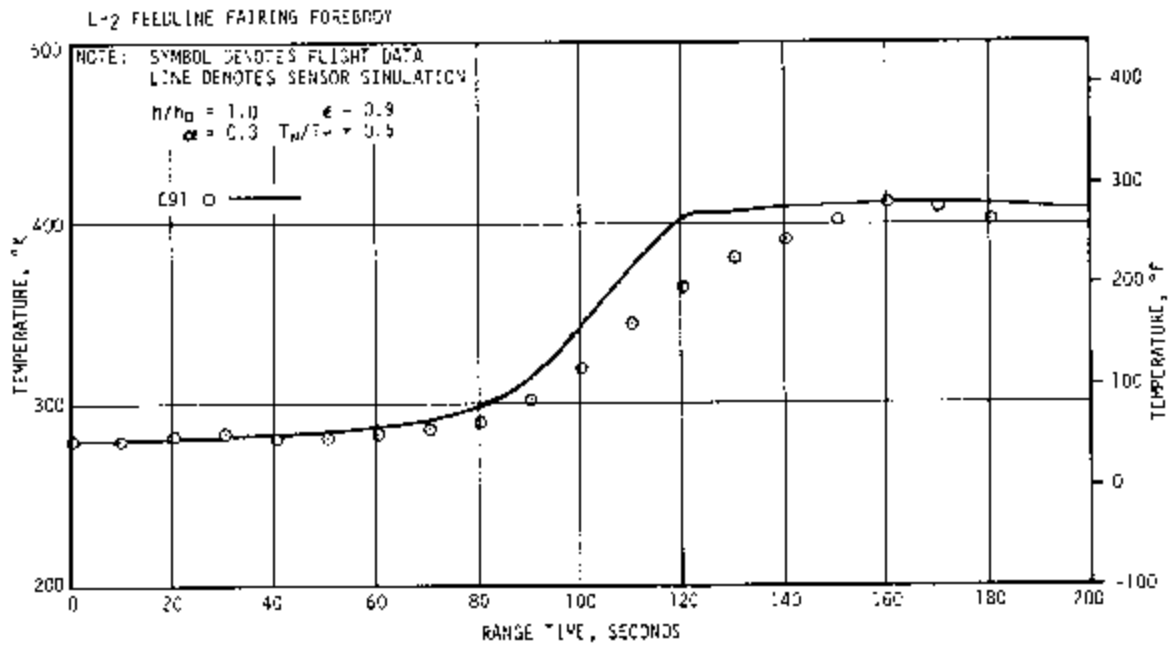
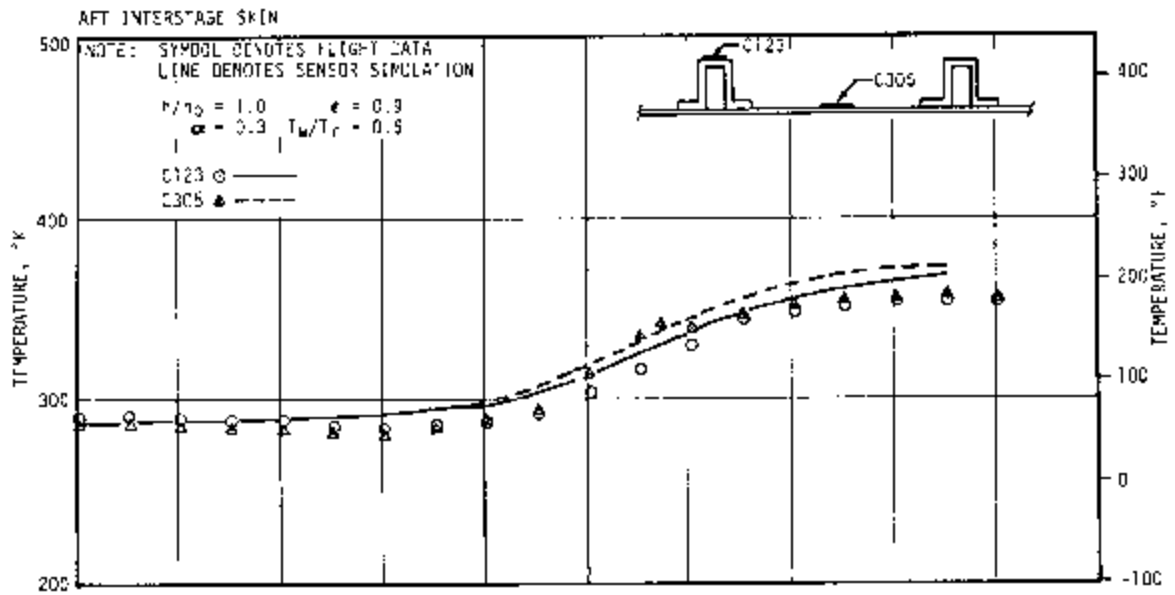


Figure 17-27. S-IVB Protuberance Aeroheating Environment, Sheet 2 of 2

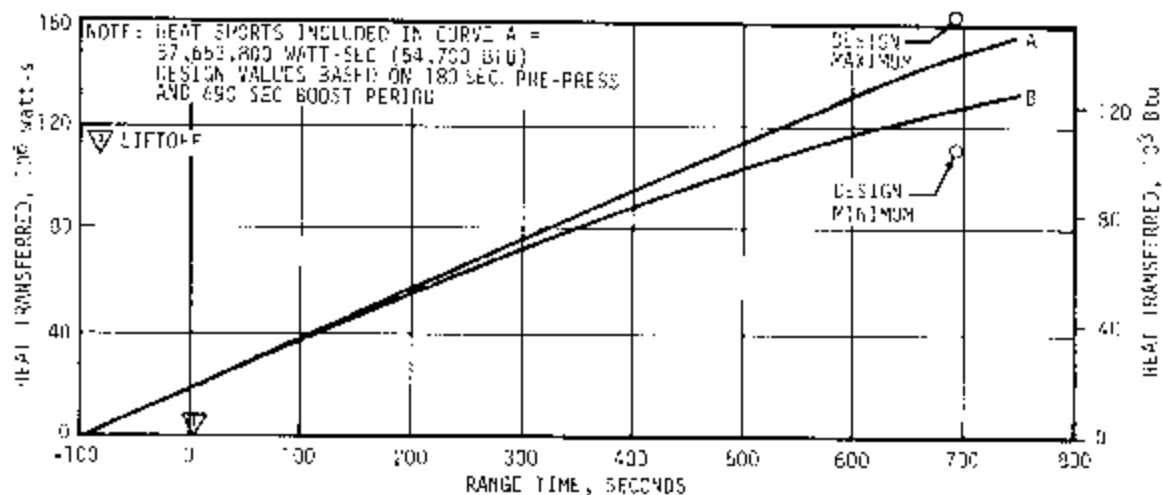


Figure 17-28. S-IVB LH₂ Heating During Boost

17.6 VEHICLE ORBITAL HEATING ENVIRONMENT

17.6.1 S-IVB Orbital Heating

The orbital temperatures for the Auxiliary Propulsion System (APS) were determined by ten sensors mounted internally to the APS fairing on various components and propellant transfer lines and four sensors mounted on the fairing.

Table 17-2 lists the maximum and minimum temperatures during the flight for the APS measurements. The values for the AS-501 flight are included for comparison. It can be seen that all components, with the exception of the propellant transfer lines, remained within their allowable limits during the mission. Thermal radiation from the APS engines caused four line measurements to exceed the maximum allowable temperature of 324°K (125°F). Greater than expected APS engine operation was required due to anomalous flight conditions which occurred about the time of the attempted restart of the S-IVB J-2 engines.

Figure 17-30 shows a comparison of the fairing flight data with respect to the predicted design temperature envelope. The fairing data fall within the analytically predicted maximum and minimum values. A correlation of a measurement located on the APS fairing is also shown. Fairly good correlation was achieved for the first two revolutions. After this time, it is believed that the flight simulation parameters used to establish the vehicle orientation did not match the actual flight parameters.

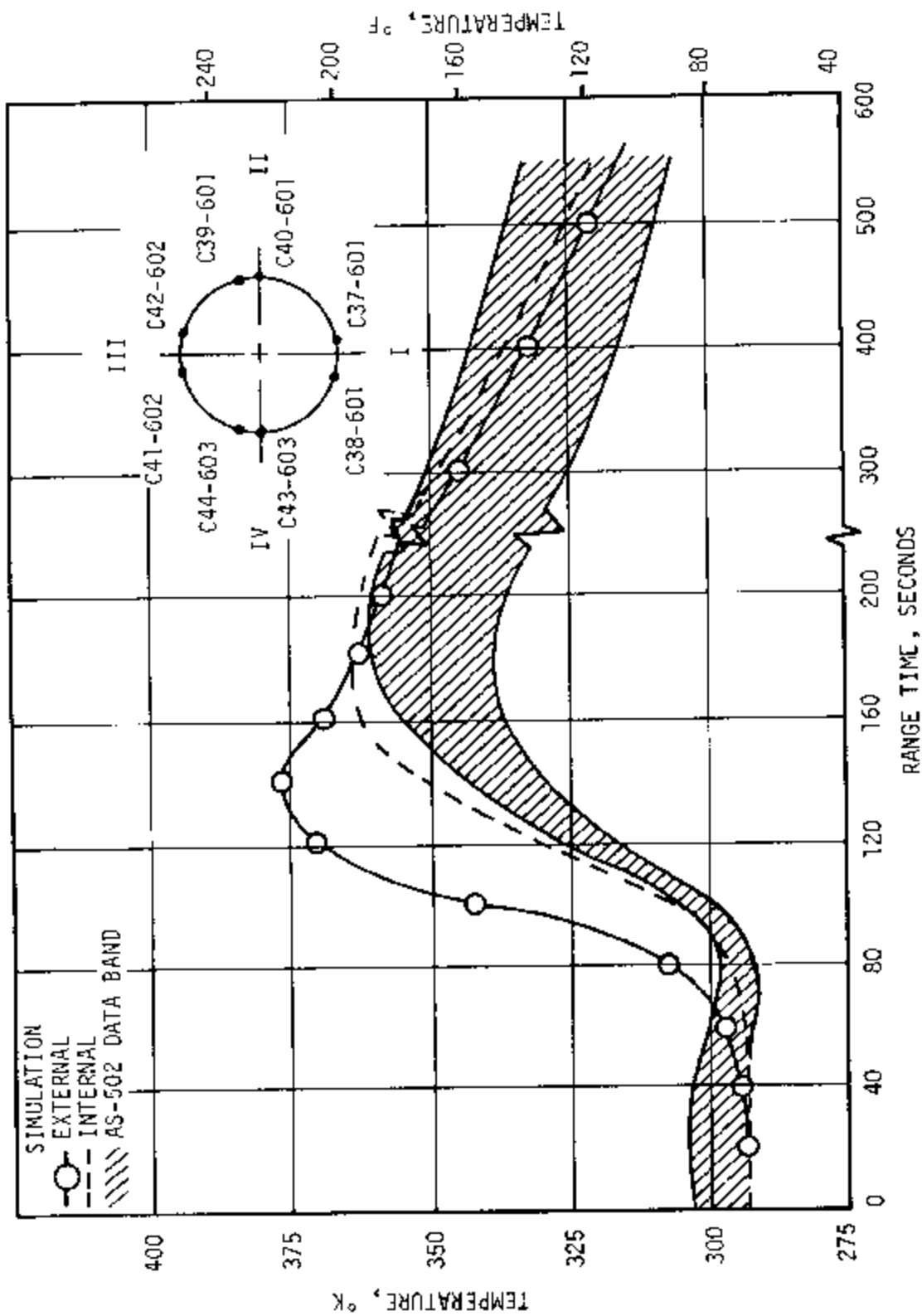


Figure 17-29. IU Inner Skin Temperatures for Ascent

Table 17-2. APS Orbital Temperatures

MEASUREMENT NO. AND DESCRIPTION OR LOCATION	LAUNCH TEMPERATURE °K (°F)		MAXIMUM TEMPERATURE IN FLIGHT °K(°F)		MINIMUM TEMPERATURE IN FLIGHT °K (°F)		EXCEED TIME*	MIN LIMIT	MEASURED		EXCEED TIME*		
	EXPECTED	MEASURED		MAX LIMIT	MEASURED				AS-501	AS-502		AS-501	AS-502
		AS-501	AS-502		AS-501	AS-502							
FAIRING													
C0286 Forebody		296(73)	296(73)	324(125)	319(115)	335(143)	16,500	266(20)	269(25)	274(34)			
C0287 Right Side		301(82)	303(85)	324(125)	314(106)	326(127)	16,850	266(20)	273(32)	272(30)			
C0288 Top		298(77)	300(80)	324(125)	310(97)	320(116)		266(20)	286(55)	280(44)			
C0289 Left Side		298(77)	301(82)	324(125)	305(90)	334(141)	16,500	266(20)	258(5)	264(15)			
INTERNAL													
C0294 Fuel Line	303 ± 4 (85 ± 7)	304(88)	303(86)	324(125)	319(115)	335(143)	16,500	266(20)	303(86)	305(90)			
C0295 Fuel Inlet (Right Side)	303 ± 4 (85 ± 7)	303(86)	303(86)	324(125)	314(106)	326(127)	16,850	266(20)	303(86)	305(90)			
C0296 Fuel Inlet (Left Side)	303 ± 4 (85 ± 7)	303(86)	303(86)	324(125)	310(97)	320(116)		266(20)	300(80)	304(88)			
C0297 Ox Line	303 ± 4 (85 ± 7)	303(86)	303(86)	324(125)	305(90)	334(141)	16,500	266(20)	303(86)	305(90)			
C0298 Ox Line (Left Side)	303 ± 4 (85 ± 7)	303(86)	303(86)	324(125)	311(100)	328(130)	16,850	266(20)	302(84)	304(88)			
C0299 Ox Inlet (Right Side)	303 ± 4 (85 ± 7)	303(86)	303(86)	324(125)	314(106)	316(110)		266(20)	302(84)	305(90)			
C0300 Fuel Tank Support	303 ± 4 (85 ± 7)	303(86)	304(88)	324(125)	313(103)	311(100)		266(20)	305(90)	305(90)			
C0301 Ox Tank Support	303 ± 4 (85 ± 7)	303(86)	+	324(125)	308(95)	+		266(20)	300(80)				
C0302 Fuel Cont. Mod.	303 ± 4 (85 ± 7)	303(86)	303(86)	324(125)	316(110)	313(103)		266(20)	305(90)	304(88)			
C0303 Dx Cont. Mod.	303 ± 4 (85 ± 7)	303(86)	303(86)	324(125)	305(90)	308(95)		266(20)	293(68)	304(88)			

*Time at which temperature limit is exceeded (available data)

†No Data

**Apparent failure during boost

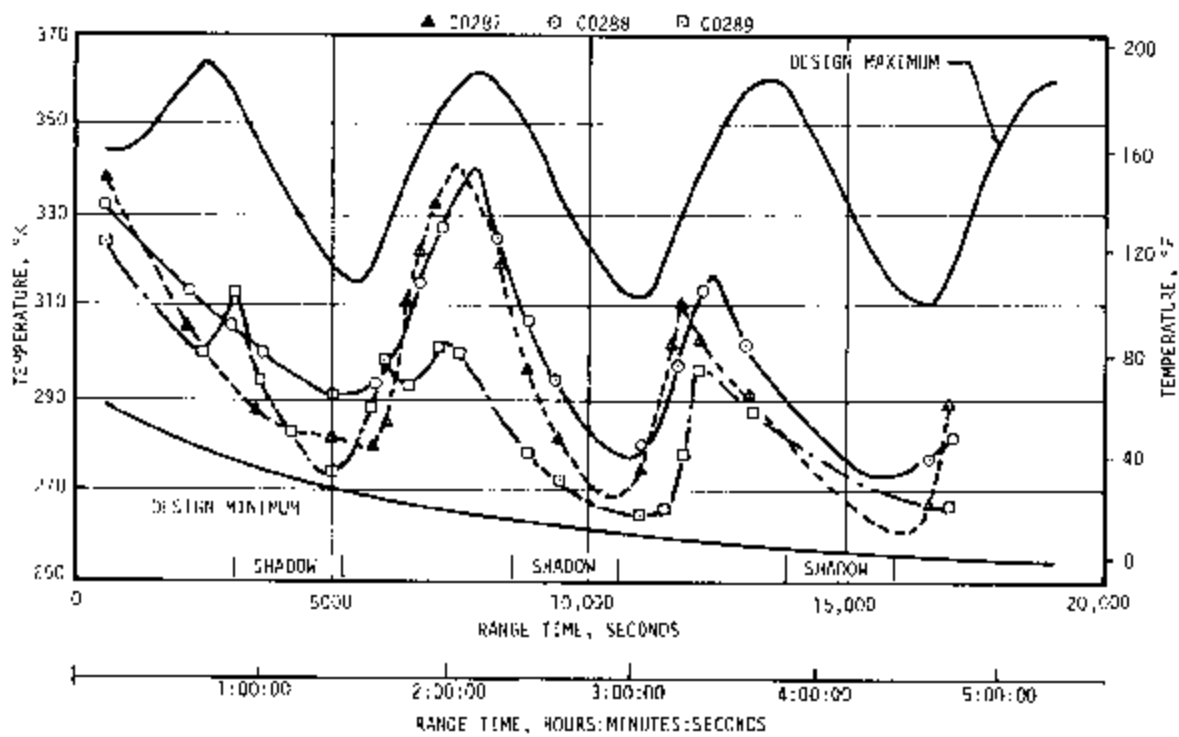
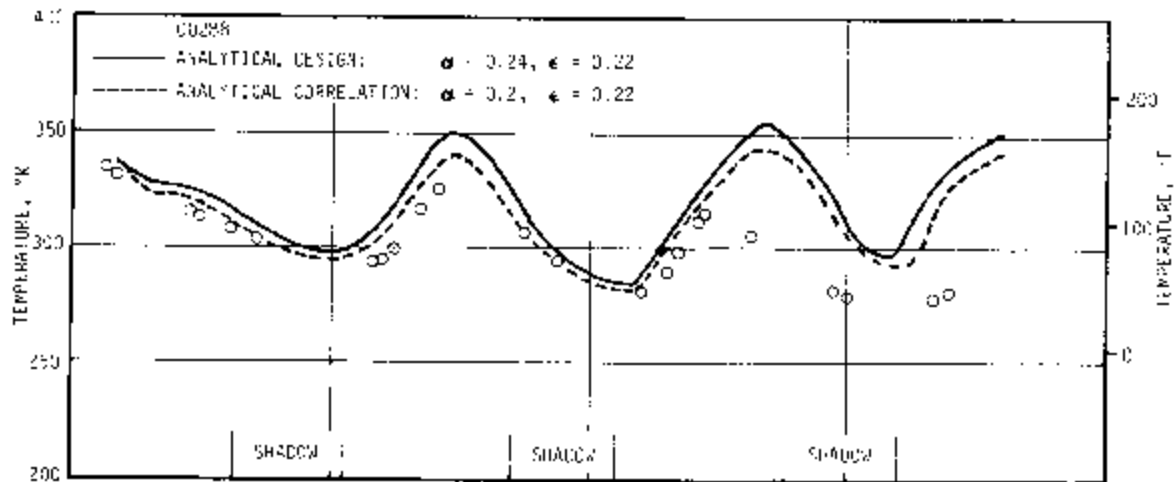


Figure 17-30. S-IVB APS Fairing Temperature

Figure 17-31 shows a correlation of a measurement located on the oxidizer control module filter body housing. The measured and predicted values compare fairly well and were within the operational limits for the component. Thermal radiation from the APS engines (brought about by the heavy duty cycle imposed by the anomalous flight conditions mentioned previously) caused the flight data and analytical values to diverge during the portion of the mission after 13,000 seconds.

17.6.2 IU Orbital Heating

The IU inner skin temperatures are shown in Figure 17-32 for the first 36,000 seconds. The time spent in the earth's shadow is shown by the vertical shaded bars. The highest skin temperature experienced during ascent was 15°K (27°F) higher than that of AS-501. This was primarily caused by a 25 percent higher atmospheric density at the higher altitudes during AS-502 ascent. Also contributing to this heating effect were the higher initial temperatures and a 4 percent higher velocity for AS-502 from 60 to 150 seconds.

Based on the time of year for launch, AS-502 was predicted to be in a somewhat colder orbit than AS-501. The maximum inner-skin temperature measured in orbit for AS-502 was 325°K (125.6°F) compared with 363°K (194°F) for AS-501. Figure 16-29 shows the inner-skin temperatures for AS-502. The large temperature excursions prior to 22,112 seconds were normal. After 22,112 seconds, APS control was lost and LOX venting caused high pitch and yaw rates. This motion of the vehicle tended to damp out these temperature excursions.

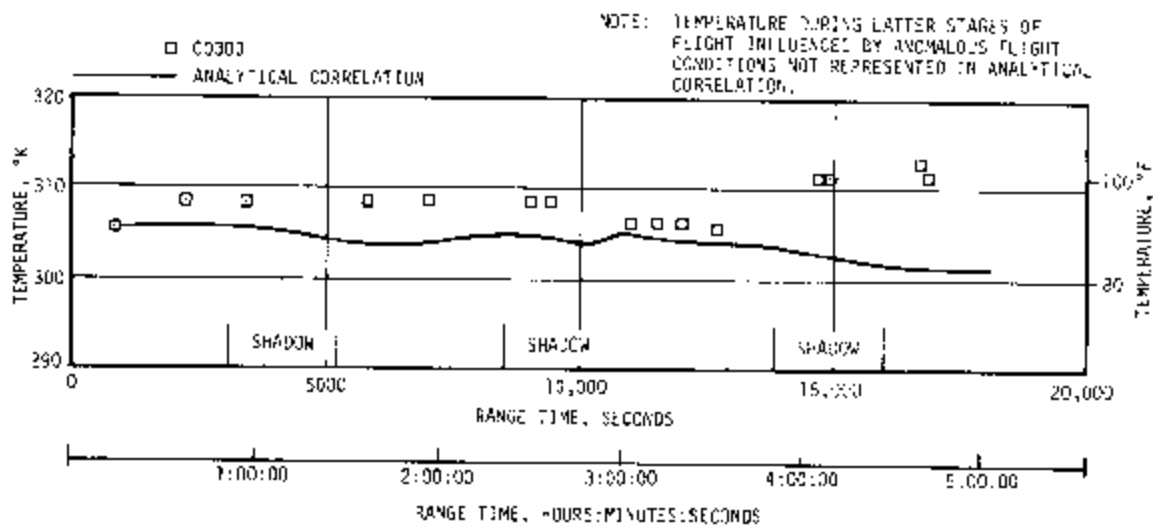


Figure 17-31. S-IVB APS Propellant Control Module Temperature

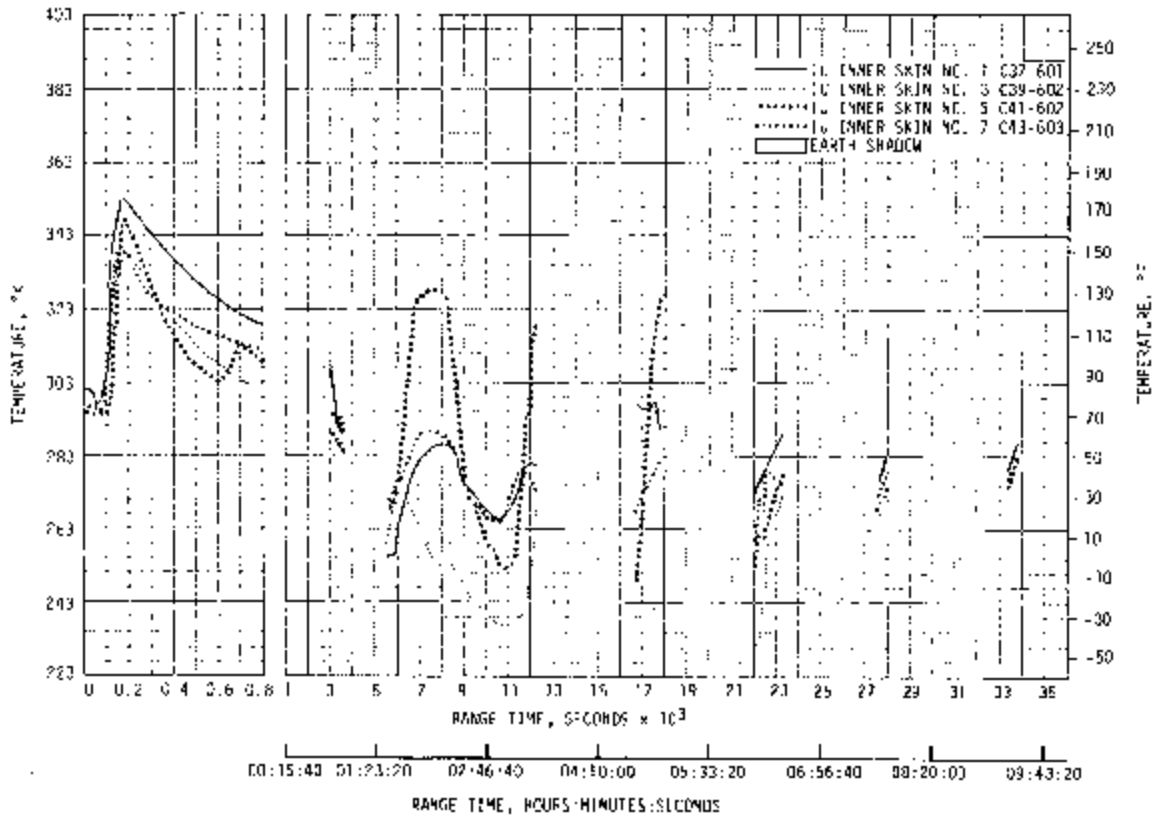
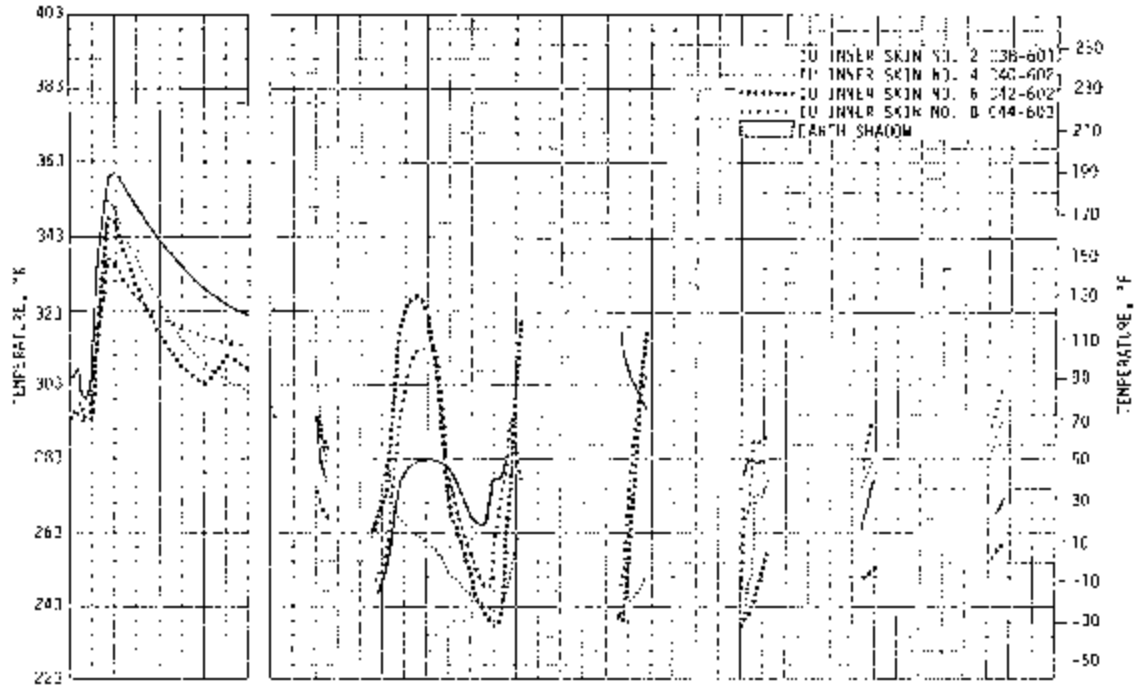


Figure 17-32. IU Inner Skin Temperature in Earth Orbit

SECTION 18

ENVIRONMENTAL CONTROL SYSTEM

18.1 SUMMARY

The S-1C canister conditioning system and the aft environmental conditioning system performed satisfactorily during the AS-502 countdown with only one canister and one ambient temperature measurement dropping below the minimum requirement.

The S-1I thermal control and compartment conditioning system maintained temperatures within the design limits throughout the prelaunch operations.

Temperatures monitored on the S-1VB aft skirt components were slightly cooler than on the AS-501 flight but within design limits. Temperatures of all components mounted on the forward skirt cold plates were within design limits at liftoff.

The IU Environmental Control System (ECS) performed well throughout the flight. Coolant temperatures, pressures, and flowrates remained within the predicted ranges and design limits for the duration of the flight data. One specification deviation was observed which was expected. At 11,670 seconds, the platform gas bearing pressure differential was 0.069 N/cm² (0.1 psid) above the 10.7 N/cm² (15.5 psid) maximum allowable and remained there throughout the remainder of the flight period for which data is available (33,780 seconds).

18.2 S-1C ENVIRONMENTAL CONTROL

The S-1C stage ECS is used to control temperature in the instrumentation canisters of the forward skirt compartment, and thrust structure compartment during preflight operations. The conditioning and purge agent (air until -8 hours and 30 minutes, GN₂ thereafter) is provided to the stage from a central ground supply.

The S-1C canister temperatures remained within the required limits during the countdown except for canister No. 6. The temperature in this canister dropped slightly below 288.7°K (60°F) during the last minute of the countdown. It reached a minimum of 287.9°K (58.5°F) at -16.7 seconds (forward umbilical disconnect).

The other canister temperatures varied from a maximum of 300.7°K (81.5°F) to a minimum of 289.2°K (60.8°F) during prelaunch activities as shown in Table 18-1.

Table 18-1. S-IC Environmental Control System Canister Temperatures

	MAXIMUM TEMPERATURE °K (°F)		MINIMUM TEMPERATURE °K (°F)	
	Canister No. 1 C212-120	296.2	(73.4)	289.2
Canister No. 2 C213-120	295.2	(71.6)	291.2	(64.4)
Canister No. 3 C214-120	300.7	(81.5)	298.9	(78.4)
Canister No. 4 C215-120	299.2	(78.8)	295.4	(72.0)
Canister No. 6 C217-120	294.7	(70.7)	287.9	(58.5)
Extremes from -20 min to -16.7 sec				

The most difficult control condition occurs during J-2 engine chilldown which starts at -8 minutes and continues until umbilical disconnect. Within this time period the ambient temperature in the interstage (forward compartment) area dropped as shown in Figure 18-1. All the temperatures were above the 205.4°K (-90°F) predicted minimum except for C207-120 which reached a minimum of 168.2°K (-157°F). This temperature probe is located under a J-2 engine and receives the maximum effect of the cold helium.

Temperature plots during flight are not presented because the compartment and canisters are only conditioned until -16.7 seconds. A band of canister temperatures versus time is shown in Figure 18-2.

A characteristic aft compartment temperature is shown in Figure 18-3. Temperature extremes for all measurements are given in Table 18-2. All temperatures were within the required limits of 299.8 ±11.2°K (80 ±20°F) except that C-202-115 was 3.5°K (6.5°F) below the minimum requirement prior to liftoff. This instrument is located at Position III facing Position IV. This quadrant has two LOX suction ducts passing through it and C-202 is near the inboard suction duct. The maximum temperature recorded was 301°K (82.4°F) at instrument location C204-115.

The flight batteries are located 28.5 degrees from Position I toward Position II. There is no telemetered instrumentation in this quadrant.

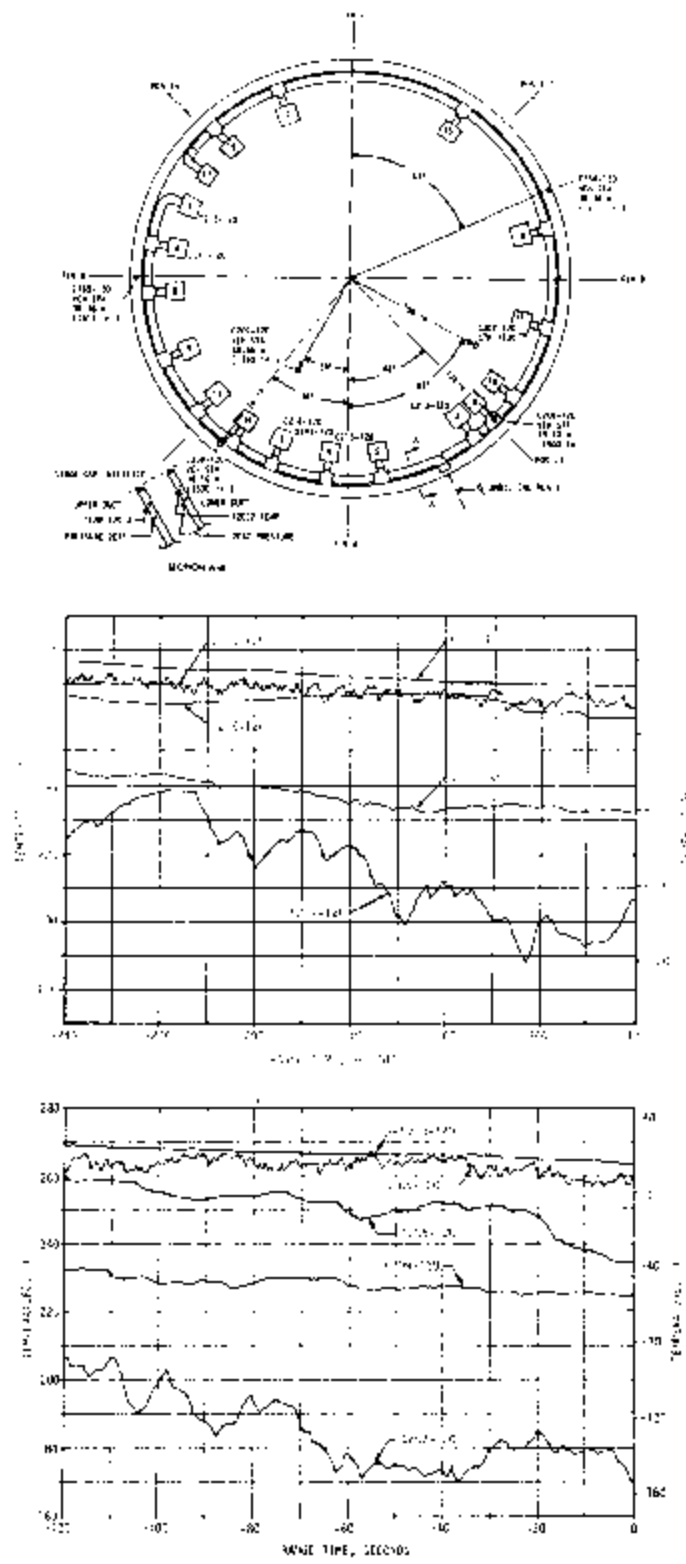


Figure 18-1. S-IC Environmental Control Systems Forward Compartment Canister Conditioning System

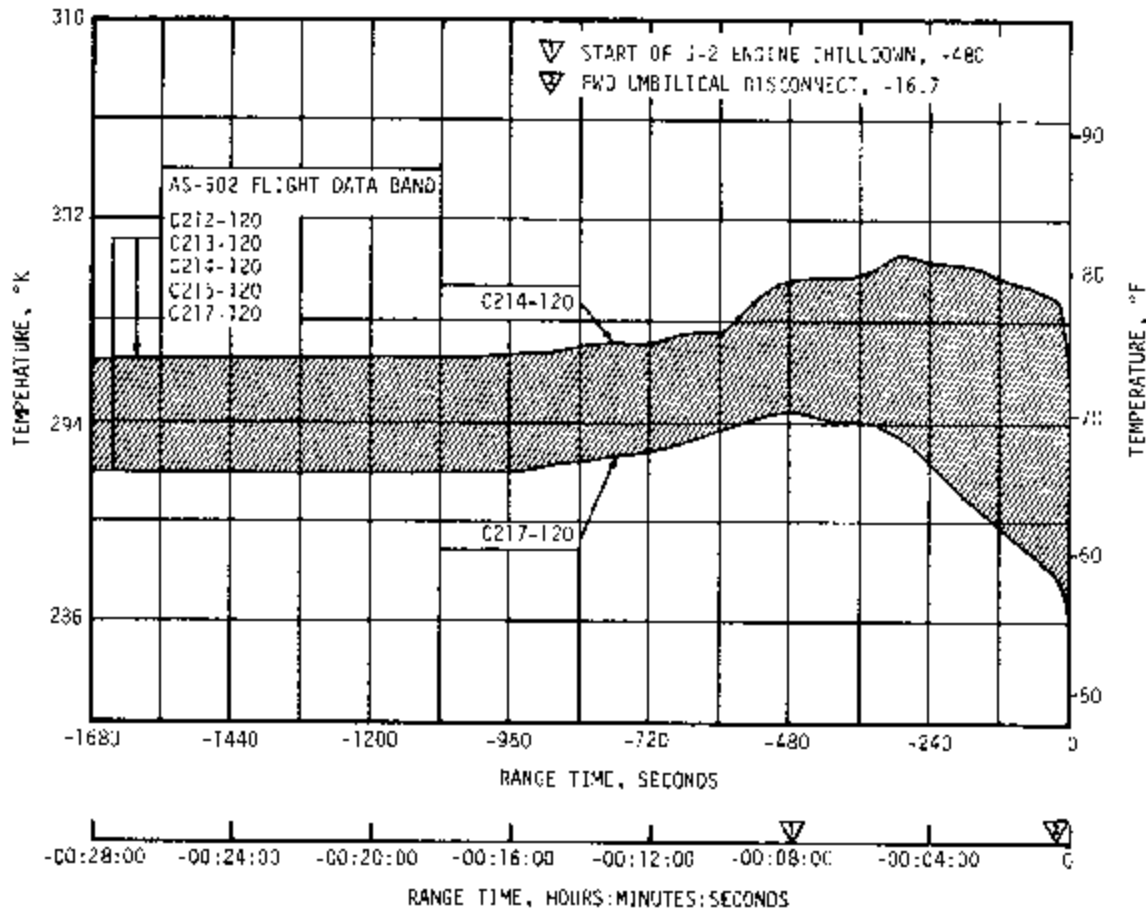


Figure 18-2. S-IC Forward Skirt Canister Temperatures

Table 18-2. S-IC Environmental Control System
Aft Compartment Temperatures

TIME SECONDS	AFT COMPARTMENT TEMPERATURES °K (°F)					
	C107	C108	C202	C203	C204	C205
-240	298(77.0)	293(68.0)	285.5(54.5)	290.5(63.5)	301(82.4)	298.5(77.9)
0	298(77.0)	293(68.0)	285.0(53.6)	290.5(63.5)	301(82.4)	298.5(77.9)
63			268.0(23.0)			
65				275.5(36.5)		
70					288(59.0)	
75						283.0(50.0)
80	283(50.0)	278(41.0)				

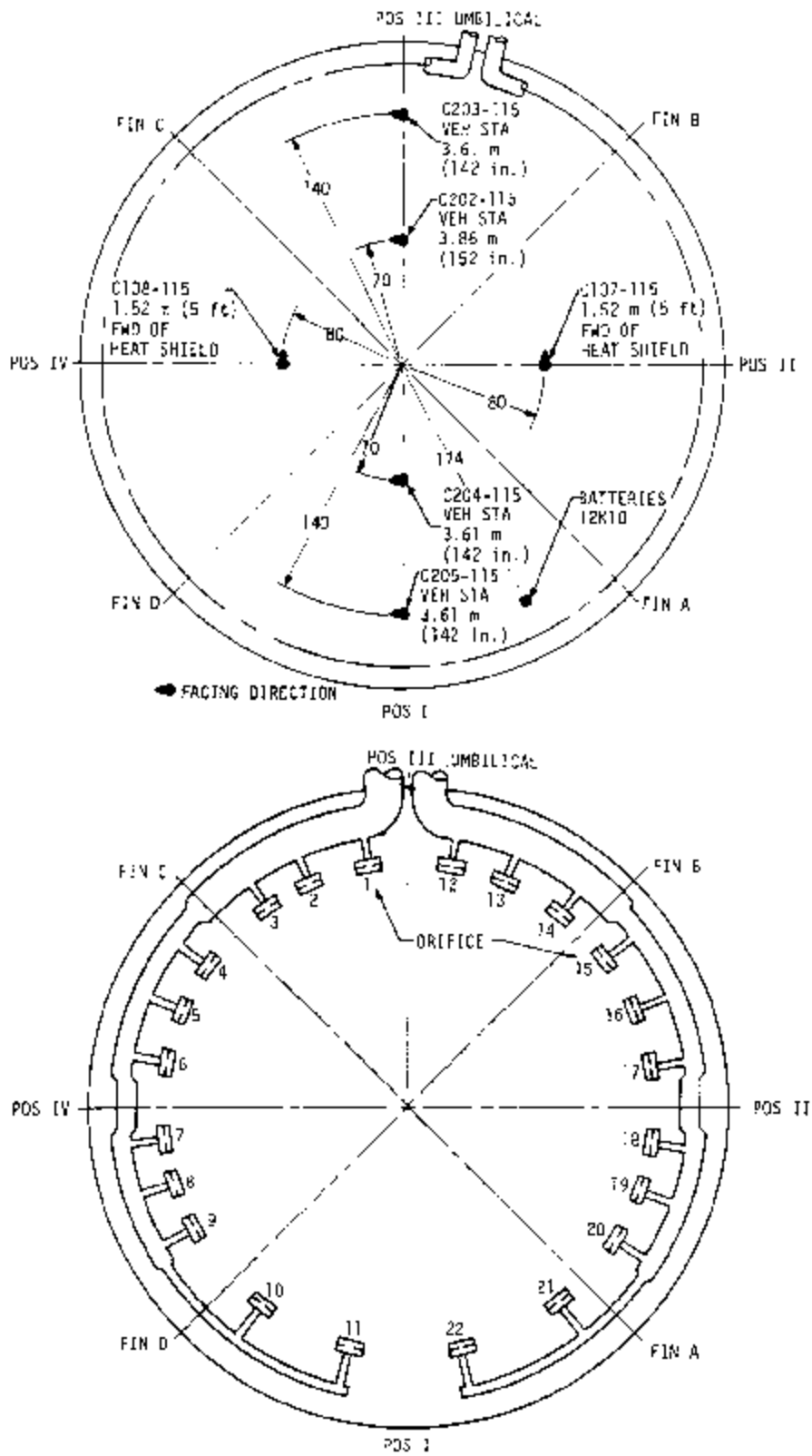


Figure 18-3. S-IC Environmental Control System and Compartment Temperatures, Sheet 1 of 2

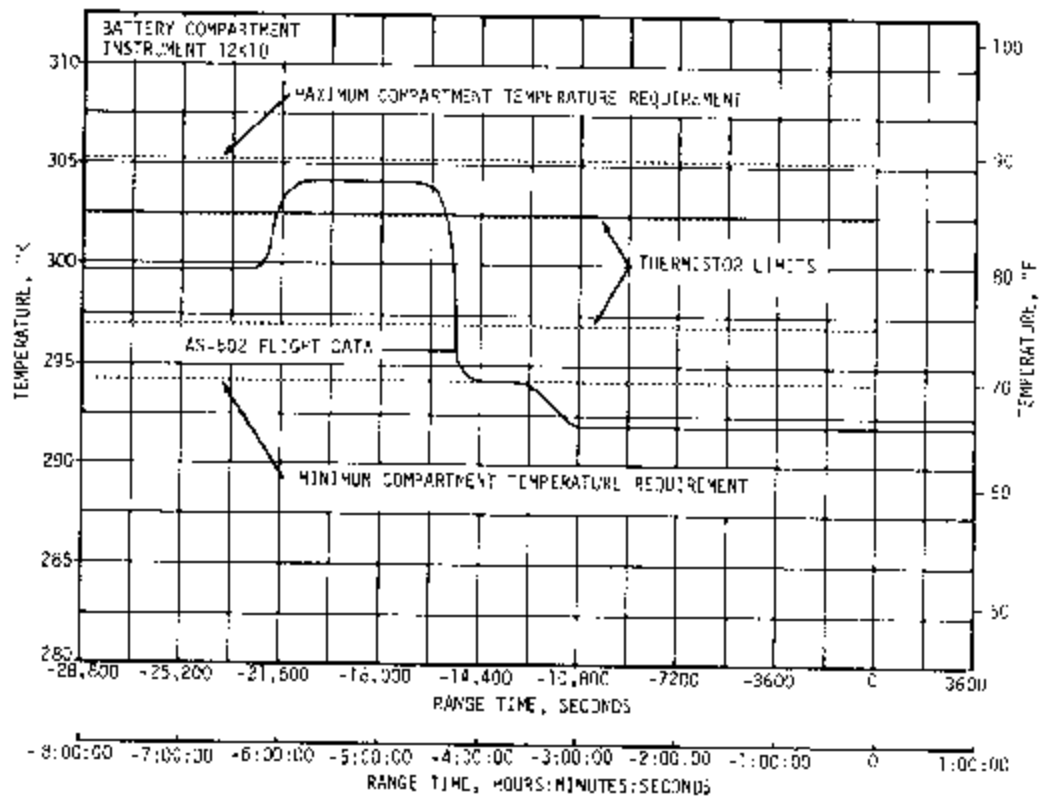
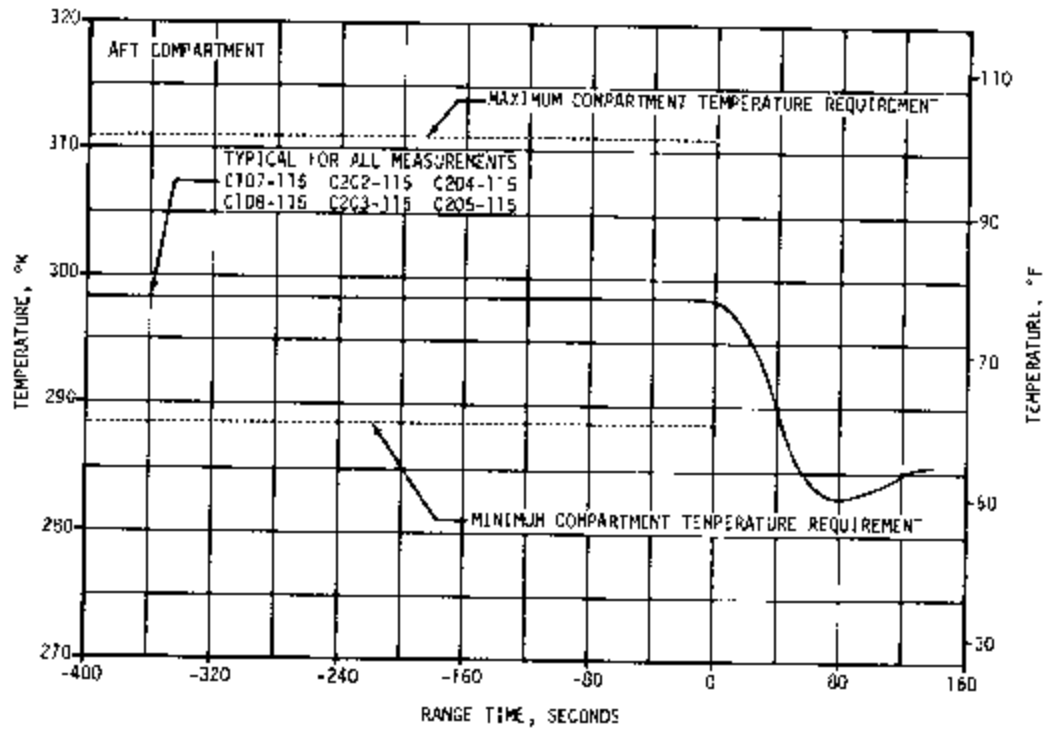


Figure 18-3. S-IC Environmental Control System and Compartment Temperatures, Sheet 2 of 2

Located on the battery container are four thermistors which control the ambient temperature, near the batteries, within the limits of $299.8 \pm 2.8^\circ\text{K}$ ($80 \pm 5^\circ\text{F}$). Figure 18-3 presents the temperature recorded at instrument location 12K10, which is a hardwire measurement. The compartment temperature was maintained within the required limits until LOX loading. After LOX loading until umbilical disconnect, the temperature decreased to 291.9°K (66.0°F). This is 2.2°K (4.0°F) below the compartment requirements of $299.8 \pm 5.6^\circ\text{K}$ ($80 \pm 10^\circ\text{F}$). All interface requirements of flowrate, pressure, and temperature were met by the ground support equipment.

18.3 S-II ENVIRONMENTAL CONTROL

The S-II stage Environmental Control System consists of two parts.

- a. The engine compartment conditioning system provides a means of purging the engine and aft interstage area of explosive mixtures during propellant loading operations, and maintaining proper temperature control for stage components. The compartment purge is effected by means of warm GN_2 and is operational only during the prelaunch period. The compartment vents have been designed to meet these objectives and to relieve internal pressure during S-IC boost.
- b. The thermal control system is designed to provide both temperature control and an inert atmosphere for the electronic equipment containers in the aft compartment. Ground equipment provides conditioned air for cooling during ground checkout, and GN_2 for purging and heating during and after propellant loading. The conditioned gas is directed to the equipment containers through ducting and exhausts to the interstage area. The flow is fixed by orifices and is continuous until terminated at umbilical disconnect. During flight, thermal inertia and container insulation will preclude out-of-tolerance equipment temperatures.

To verify that the thermal control system provided adequate temperature control in the electrical equipment containers, measurements of the equipment mounting surface temperature were made in all the containers. As shown in Tables 18-3 and 18-4, all the equipment mount temperatures were well within the required temperature limits during both the prelaunch and launch operations.

Equipment mount temperatures in the forward and aft systems were within 7°K (13°F) of their corresponding liftoff temperatures on the AS-501 flight and showed the same type of temperature profiles throughout the AS-502 flight with the exception of container 206A31. The equipment mount temperature of this container was very similar to the AS-501 flight up to approximately 325 seconds. From 325 to 425 seconds, the container equipment mount temperature dropped approximately 7°K (13°F) and continued

Table 18-3. S-II Forward Thermal Control System AS-501 and AS-502 Prelaunch and Flight Data

EQUIPMENT MOUNT TEMP. MEASUREMENT AND NUMBER	S-II-1 LAUNCH AS-501					
	DESIGN TEMP. LIMITS		TEMP. AT START OF ENG. CHILL	TEMP. AT LAUNCH	TEMP. AT END OF S-IC BOOST	TEMP. AT END OF S-II BOOST
	MAXIMUM	MINIMUM				
Container 220, C355-200 °K (°F)	334 (140)	256 (0)	290 (62)	290 (62)	287 (57)	283 (61)
Container 221, C356-221 °K (°F)	334 (140)	256 (0)	292 (65)	292 (65)	289 (61)	287 (57)
Container 222, C361-222 °K (°F)	334 (140)	256 (0)	286 (55)	286 (55)	286 (55)	286 (55)
Container 223, C511-223 °K (°F)	334 (140)	245 (-20)	289 (61)	289 (61)	287 (57)	286 (55)
Container 225, C359-225 °K (°F)	334 (140)	256 (0)	304 (88)	304 (88)	303 (86)	305 (89)
Container 227, C509-227 °K (°F)	334 (140)	256 (0)	284 (52)	284 (52)	283 (60)	284 (52)
Container 228, C510-228 °K (°F)	326 (125)	256 (0)	290 (62)	290 (62)	288 (59)	287 (57)
GN ₂ Temp. at Disconnect °K (°F)	320 (115)	314 (105)	--	--	--	--
Sys. G ₂ Flow kg/s (lbm/s)	302 (.666)	257 (.567)	318 (.700)	318 (.700)	--	--
S-II-2 LAUNCH AS-502						
Container 220, C355-220 °K (°F)	334 (140)	256 (0)	289 (61)	289 (61)	289 (61)	290 (62)
Container 221, C356-221 °K (°F)	334 (140)	256 (0)	284 (52)	285 (53)	282 (50)	282 (50)
Container 222, C361-222 °K (°F)	334 (140)	256 (0)	283 (50)	283 (50)	282 (50)	282 (48)
Container 223, C511-223 °K (°F)	334 (140)	245 (-20)	282 (48)	282 (48)	281 (46)	280 (44)
Container 224, C358-224 °K (°F)	334 (140)	256 (0)	278 (41)	278 (41)	277 (39)	277 (39)
Container 225, C359-225 °K (°F)	334 (140)	256 (0)	302 (84)	303 (86)	303 (86)	306 (89)
Container 227, C509-227 °K (°F)	334 (140)	256 (0)	279 (43)	280 (44)	279 (43)	279 (43)
Container 228, C510-228 °K (°F)	326 (125)	256 (0)	287 (57)	287 (57)	285 (53)	285 (53)
GN ₂ Temp. at Disconnect °K (°F)	320 (115)	314 (105)	316 (109)	316 (109)	--	--
Sys. G ₂ Flow kg/s (lbm/s)	302 (.666)	257 (.567)	284 (.625)	276 (.608)	--	--

to drop another 4°K (7°F) during the remainder of the flight. This compared to a drop of only 1°K (2°F) for the same measurement over the same time span on the AS-501 flight indicates the presence of cryogenics in the container area. Considering the proximity of container 206A31 to engine No. 2, together with the fact that none of the other containers were affected, would indicate a cryogenic line failure in the engine No. 2 area. Plots of container 206A31 equipment mount temperatures during both AS-501 and AS-502 flights are shown in Figure 18-4.

The engine compartment conditioning system maintained the compartment temperature within the design limit throughout the prelaunch operations. The thrust structure was below 256°K (0°F) at launch which met the design requirements. A comparison of AS-501 and AS-502 engine compartment temperatures at three time frames during both prelaunch and flight periods is presented in Table 18-5. The measurement locations employed throughout the engine compartment are given in Figure 18-5. The interstage temperature control thermistors were set to control to 275°K (35°F) in comparison to the 278°K (40°F) value employed for the AS-501 launch. This resulted in slightly lower temperatures throughout the interstage at the start of engine chill for AS-502 than during the AS-501 launch; however, the temperature history characteristics through engine chill and S-IC boost were quite similar to the AS-501 flight data. There were no indications of abnormalities through S-IC boost.

From the initiation of tanking through launch, there were no indications of hydrogen or oxygen in the engine compartment.

Table 18-4. S-II Aft Thermal Control System AS-501 and AS-502 Prelaunch and Flight Data

CONTAINER AND MEASUREMENT NUMBER	Design Temperature °K (°F) Limits Minimum °K (°F)	206A31	206A84	206A85	207A1	207A2	208	209	210	211	212	213	214	GN2 Supply Temp.	GN2 Supply Flow (kg/s)
		334 (140) 267 (20)	334 (140) 256 (0)	334 (140) 256 (0)	326 (125) 256 (0)	344 (160) 256 (0)	334 (140) 256 (0)	334 (140) 256 (0)	334 (140) 256 (0)	334 (140) 256 (0)	339 (150) 220 (-55)	334 (140) 256 (0)	334 (140) 256 (0)		
AS-501 LAUNCH															
Temp.															
Event Start of Engine Chill	°K (°F)	292 (67)	291 (64)	300 (80)	304 (88)	293 (68)	301 (82)	297 (75)	292 (66)	289 (61)	304 (88)	293 (68)	295 (71)	319 (115)	.246
Launch	°K (°F)	286 (55)	287 (57)	295 (71)	301 (82)	292 (66)	297 (75)	293 (68)	286 (55)	278 (41)	299 (79)	289 (61)	296 (55)	319 (115)	.246
End of S-IC Boost	°K (°F)	282 (48)	283 (50)	292 (66)	301 (82)	288 (59)	294 (70)	290 (62)	283 (50)	276 (37)	296 (73)	286 (55)	290 (44)	--	--
End of S-II Boost	°K (°F)	279 (43)	280 (44)	290 (62)	301 (82)	287 (57)	294 (70)	292 (66)	283 (50)	276 (37)	296 (73)	284 (52)	275 (35)	--	--
AS-502 LAUNCH															
Temp.															
Event Start of Engine Chill	°K (°F)	290 (52)	286 (55)	295 (71)	303 (86)	289 (61)	305 (89)	303 (86)	293 (58)	284 (52)	300 (80)	293 (68)	295 (71)	317 (111)	.257
Launch	°K (°F)	285 (53)	283 (50)	293 (68)	300 (80)	288 (59)	302 (84)	298 (77)	288 (59)	273 (32)	295 (71)	289 (61)	288 (59)	316 (109)	.257
End of S-IC Boost	°K (°F)	282 (48)	279 (43)	289 (61)	300 (80)	285 (53)	298 (77)	295 (71)	284 (52)	271 (28)	293 (68)	287 (57)	282 (48)	--	--
End of S-II Boost	°K (°F)	270 (26)	278 (41)	287 (57)	300 (80)	285 (53)	298 (77)	294 (70)	283 (50)	269 (25)	292 (65)	285 (53)	275 (35)	--	--

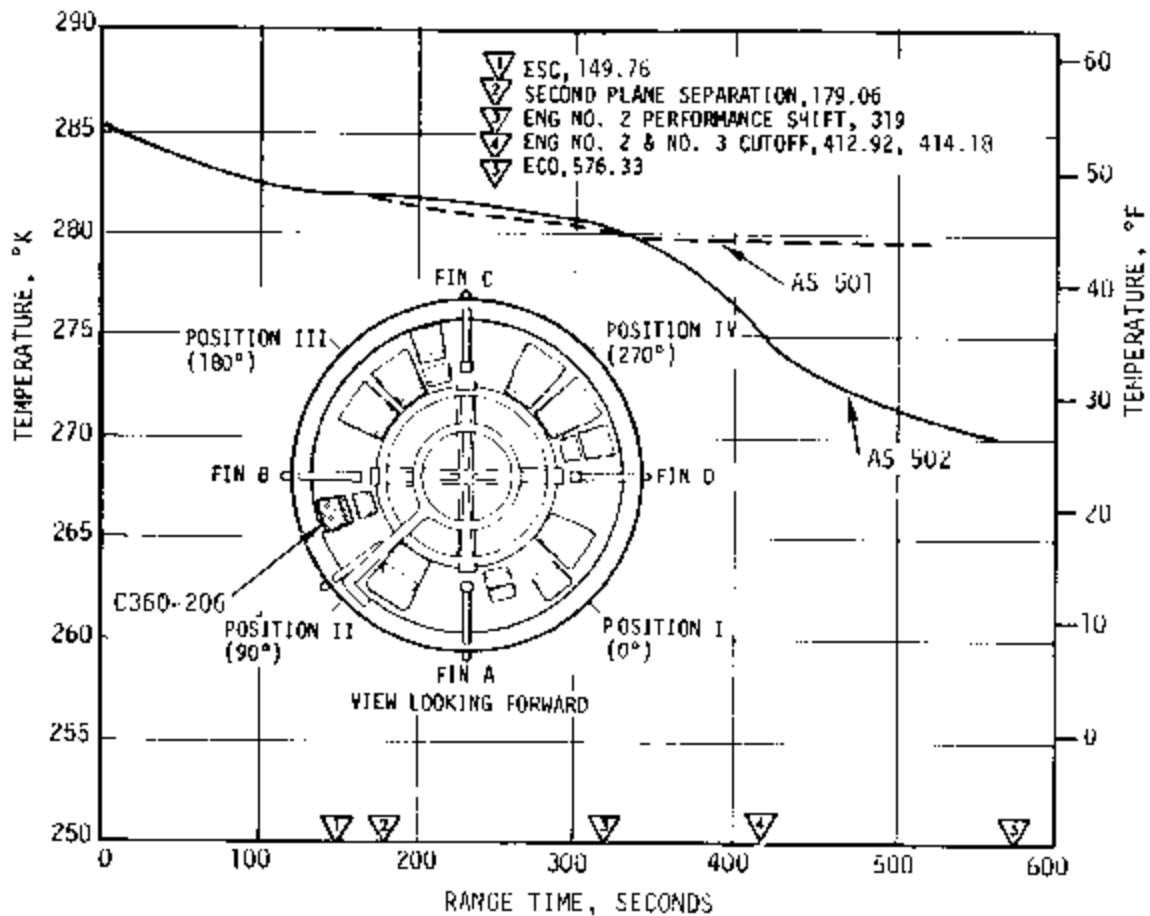


Figure 18-4. Container Equipment Mount Temperature

Table 18-5. S-II Engine Compartment Temperature Data Comparison of AS-501 and AS-502 Flights

MEASUREMENT	AS-501 RANGE TIME			AS-502 RANGE TIME		
	480 SEC TEMPERATURE °K (°F)	ZERO SEC TEMPERATURE °K (°F)	90 SEC TEMPERATURE °K (°F)	480 SEC TEMPERATURE °K (°F)	ZERO SEC TEMPERATURE °K (°F)	90 SEC TEMPERATURE °K (°F)
C172-206	204 (-92)	157 (-105)	171 (-152)	217 (-69)	185 (-127)	172 (-150)
C200-200	299 (79)	247 (-5)	232 (-42)	295 (71)	244 (-20)	229 (-47)
C206-200	294 (70)	270 (26)	260 (8)	253 (68)	270 (26)	263 (14)
C223-206	286 (55)	234 (-30)	226 (-53)	287 (57)	234 (-38)	229 (-47)
C232-206	268 (23)	252 (-6)	243 (-22)	256 (7)	242 (-24)	238 (-31)
C240-206	286 (55)	245 (-20)	236 (-35)	282 (48)	250 (-10)	234 (-38)
C256-206	287 (46)	227 (-51)	215 (-73)	266 (19)	212 (-78)	207 (-87)
C671-206	296 (73)	236 (-35)	210 (-82)	292 (66)	208 (-85)	198* (-103)*
C672-206	290 (62)	218 (-67)	205 (-91)	287 (57)	219 (-65)	197* (-105)*
C206-120	289 (61)	221 (-62)	196* (-107)*	-- --	235 (-37)	198 (-103)
C208-120	-- --	242 (-24)	196* (-107)*	-- --	256 (79)	210 (-82)

*Off Scale

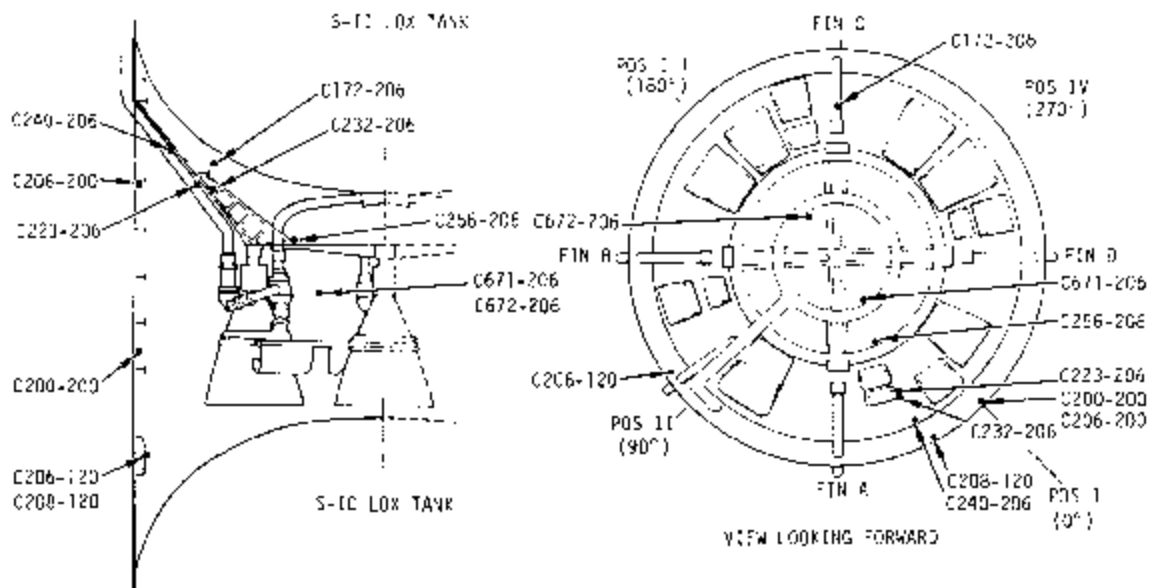


Figure 18-5. S-II Engine Compartment Conditioning System Transducer Locations

18.4 S-IVB ENVIRONMENTAL CONTROL

The forward skirt area of the S-IVB is conditioned by the IU ECS. The aft skirt and interstage ECS provide the following:

- a. Thermal conditioning of the atmosphere, during ground operations, around electrical equipment in the aft skirt.
- b. Thermal conditioning of the Auxiliary Propulsion System (APS), hydraulic accumulator reservoir, and ambient helium bottle.
- c. Purging of the aft skirt, aft interstage and thrust structure, and the S-II stage forward skirt of oxygen and combustible gases.

Temperature-controlled air or GN₂ is supplied at the rate of 3500 SCFM to accomplish the thermal conditioning. The GN₂ purge is initiated at LOX loading and is continued until umbilical disconnect.

18.4.1 Ascent Powered Flight Phase

The temperatures monitored at launch for the aft skirt components, mounted on fiberglass panels, ranged from 5.6 to 11.1°K (10 to 20°F) cooler than those recorded on AS-501. The forward skirt components, mounted on cold plates, ranged up to 9°K (16°F) warmer than those on AS-501. All temperatures at liftoff were well within the components' upper and lower temperature limits.

18.4.2 Parking Orbit Phase

The data monitored throughout the flight for the bridge modules, propellant utilization, and static inverter assemblies appear to be valid. The temperature extremes recorded during the first 33,800 seconds of flight are presented in Table 18-6.

During orbit, all components remained within their temperature limits during the first 24,000 seconds of flight. The chilldown inverters exceeded their lower temperature limit at this time. This is not considered to be a problem because the chilldown inverters' normal operation period extends only over the first 16,200 seconds of a nominal Saturn V flight. The propellant utilization assembly exceeded its low temperature limit at 33,400 seconds. This is attributed to the cold plates being inoperative at this time and is not considered to be a problem.

Table 18-6. Forward and Aft Skirt Component Temperature*

MEASUREMENT NO. AND DESCRIPTION OR LOCATION	LAUNCH TEMP °K (°F)		MAX FLIGHT TEMP °K (°F)				MIN FLIGHT TEMP °K (°F)		
	EXPECTED	MEASURED		LIMIT	MEASURED		LIMIT	MEASURED	
		AS-501	AS-502		AS-501	AS-502		AS-501	AS-502
LOX Chilldown Inverter C0139	275 - 300 (35) (80)	294 (70)	286 (55)	339 (151)	298 (77)	291 (64)	261 (10)	278 (41)	242 (-24)
	275 - 300 (35) (80)	--	281 (46)	--	--	287 (57)	--	--	247 (-15)
LH ₂ Chilldown Inverter C0140	275 - 300 (35) (80)	297 (75)	286 (55)	339 (151)	303 (86)	293 (68)	261 (10)	283 (50)	244 (-20)
	275 - 300 (35) (80)	--	281 (46)	--	--	287 (57)	--	--	243 (-13)
Bridge Modules									
Forward									
C0233	278 - 300 (41) (80)	287 (57)	292 (66)	344 (160)	291 (64)	294 (70)	219 (-65)	287 (57)	272 (30)
C0234	278 - 300 (41) (80)	287 (57)	291 (64)	344 (160)	291 (64)	292 (66)	219 (-65)	287 (57)	272 (30)
C0235	278 - 300 (41) (80)	287 (57)	287 (57)	344 (160)	297 (64)	291 (64)	219 (-65)	287 (57)	271 (28)
Aft									
C0236	256 - 300 (1) (80)	282 (48)	277 (39)	344 (160)	282 (48)	277 (39)	219 (-65)	259 (7)	236 (-35)
C0237	256 - 300 (1) (80)	281 (46)	272 (30)	344 (160)	281 (46)	272 (30)	219 (-65)	263 (14)	228 (-49)
C0238	256 - 300 (1) (80)	292 (66)	284 (52)	344 (160)	292 (56)	284 (52)	219 (-65)	241 (-26)	234 (-38)
PU Assembly C0017	275 - 311 (35) (100)	293 (68)	293 (68)	317 (111)	298 (77)	294 (70)	278 (41)	289 (61)	274 (34)
Static Inverter- Converter C0061	278 - 311 (41) (100)	296 (73)	301 (82)	317 (111)	298 (77)	303 (86)	278 (41)	286 (55)	281 (46)

*During First 33,800 Seconds of Flight.

Ground hold and orbital data, through the first 16,000 seconds of flight, are presented in Figure 18-6 for the chilldown inverters. The results of the postflight analysis, simulating the environment experienced by the LOX inverter, are also presented. As indicated in this figure there is satisfactory correlation between the flight data and the analytical results.

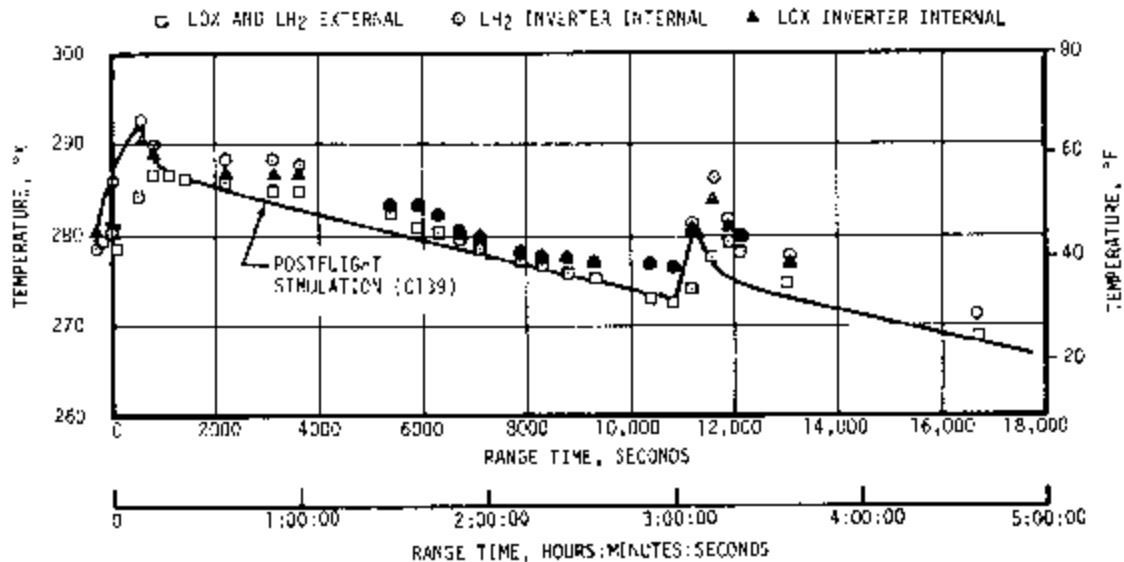


Figure 18-6. LOX and LH₂ Chilldown Inverter Temperatures

18.5 IU ENVIRONMENTAL CONTROL

Prior to launch, a purge duct, located circumferentially above the IU/ spacecraft interface, uniformly distributes temperature-conditioned air from a ground supply prior to fueling, and temperature-conditioned GN₂ subsequent to fueling. Four sensors, located in the IU, monitor the compartment temperature and feed a signal to the ground equipment to control the inlet gas temperature which maintains the compartment temperature within the specified limits, 290.2 to 295.8°K (63 to 73°F).

The Thermal Conditioning Subsystem (TCS) provides temperature-controlled heat sinks to which the electronics reject waste heat. A coolant pump circulates the 60 percent methanol-40 percent water by weight coolant fluid Methanol/Water (M/W) to the IU and S-IVB TCS. Coolant distribution is controlled by fixed orifices within the IU to 16 coldplates and 4 internally cooled components: the ST-124M-3 Inertial Platform Assembly, Flight Control Computer (FCC), Launch Vehicle Data Adapter (LVDA), and Launch Vehicle Digital Computer (LVDC). The IU and S-IVB stage return flows converge before entering a heat exchanger assembly, which is composed of a preflight heat exchanger and a sublimator as shown in Figure 18-7.

Pressure is supplied to the TCS through regulators and filters to a M/W accumulator from a 2068 N/cm² (3000 psi), 2700 cm³ (165 in.³) sphere. The M/W accumulator provides for fluid expansion and contraction, compensates for fluid losses due to leakage, and maintains coolant pump inlet pressure. An orifice regulator further reduces the GN₂ pressure to an acceptable range. This pressure expels water from the water accumulator to the sublimator. The GN₂ continually vents to the vehicle compartment through the orifice regulator.

During prelaunch operation, M/W from a Ground Support Cooling Unit (GSCU) circulates to and from the preflight heat exchanger through the umbilical. A Modulating Flow Control Valve (MFCV) controls the onboard fluid temperature by varying the amount of coolant flowing through or around the heat exchanger. Continuous valve operation maintains a stable M/W temperature of 288 ± 0.56°K (59 ± 1°F).

In flight, heat expulsion is achieved in the sublimator. Water, which is supplied under pressure from the water accumulator, freezes upon exposure to the space environment and then sublimates, removing heat from the M/W coolant.

At T₁ +5 seconds, a switch selector command enables the sensor bias. This command places R1, shown in Figure 18-8, in parallel with the electronic controller assembly input, causing the MFCV to be driven to zero bypass, and all coolant is forced to flow through the sublimator. At T₁ +75 seconds, a switch selector command disables the electronic controller assembly. The M/W temperature is measured by two thermal switches whose outputs are sensed by the LVDA/LVDC. The LVDC is programmed to sense the condition of these discretes once every 300 seconds, starting at T₁ +180 seconds. This allows sufficient time to elapse after liftoff for the ambient pressure to drop low enough for the water sublimator to function. If the temperature of the coolant is above the upper temperature setting, 288.3°K (59.55°F), a switch selector command is issued to open the water solenoid valve to allow sublimator cooling. If the coolant temperature falls below the lower limit 288.1°K (59.16°F), a switch selector command is issued which closes the water solenoid valve, halting sublimator operation.

AS-502 was the first vehicle to utilize sublimator water-feed regulation for temperature control from liftoff. The system was verified on AS-204 as an after-mission experiment. Previous vehicles utilized M/W modulation, as described for ground operation. The change was made to eliminate the undesirable minimum sublimator cooling rate. AS-502 also had seven 140-watt heaters, flown previously on AS-501, as a temporary fix to improve the ECS heat balance.

18.5.1 Thermal Conditioning System

Higher prelaunch purge-gas temperatures were provided on AS-502 to eliminate the low compartment ambient temperature experienced on AS-501

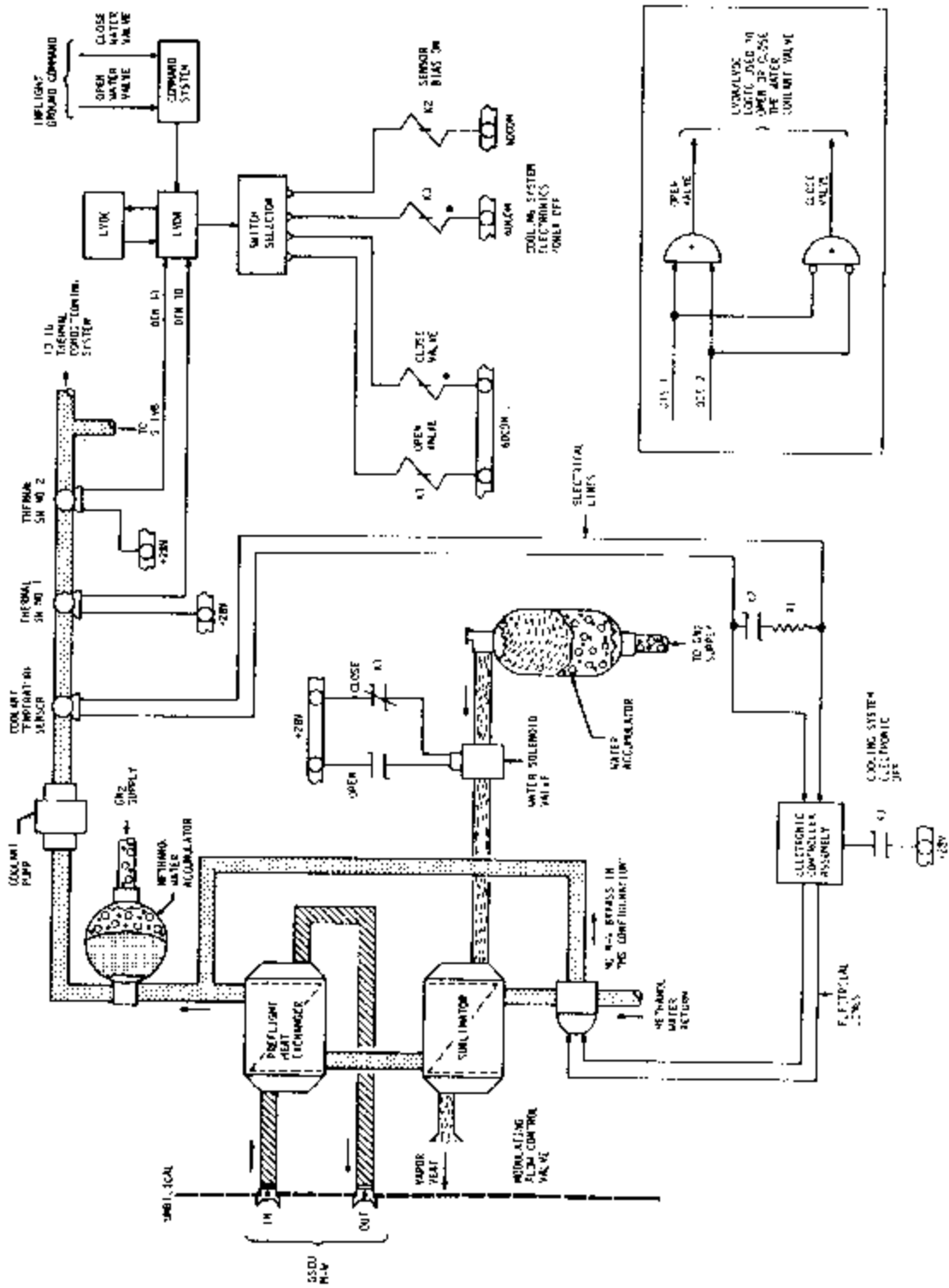


Figure 18-8. Schematic of Thermal Control Using Water Coolant Valve

following S-IVB LH₂ loading. This higher purge-gas temperature, coupled with higher skin temperatures, resulted in a compartment temperature at launch of 295°K (71.6°F) for AS-502, as compared with 287.4°K (58°F) for AS-501. The average skin temperature at launch on AS-502 was 6.12°K (11°F) above the AS-501 average.

The available data shows proper functioning of the TCS, as shown in Figure 18-9. The present indications are that the M/W control temperature remained within the 280.2 to 293.0°K (45 to 68°F) control band.

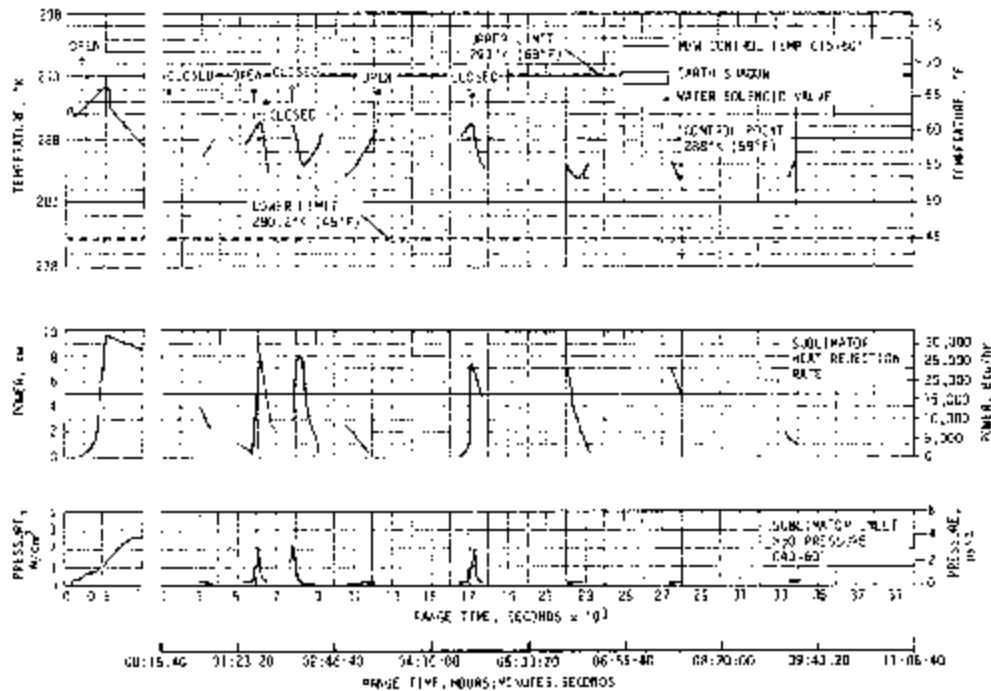


Figure 18-9. Temperature Control Parameters

Figure 18-10 shows a sublimator water inlet temperature rise at 111 seconds. This was 71 seconds prior to sublimator startup and was related to a pressure differential (D43-601) increase at 116.6 seconds. This performance deviation has been attributed to water droplets trapped in the tubing on the sublimator side of the water solenoid valve. By 111 seconds, the IU compartment pressure and sublimator cavity pressure, as indicated by the zero differential reading of D43-601, had decreased to 0.276 N/cm² (0.4 psia). This was approaching the vapor pressure of water at the temperature within the cavity. The warmest water droplets in the sublimator and line cavity would be those adjacent to the water valve which dissipates heat during the time it is closed. As these droplets changed phase, the warm vapor was sensed by the temperature measurement and finally by the pressure differential measurement as the gaseous

molecules filled the sublimator cavity. Water, at the pressure and temperature indicated, will experience a volume increase of approximately 50,000 times as it changes into the gaseous state. The pressure differential increase shown by D43-601 in Figure 18-10 resulted from a constant vapor pressure in the sublimator and tubing while the decreasing IU ambient pressure was approaching zero.

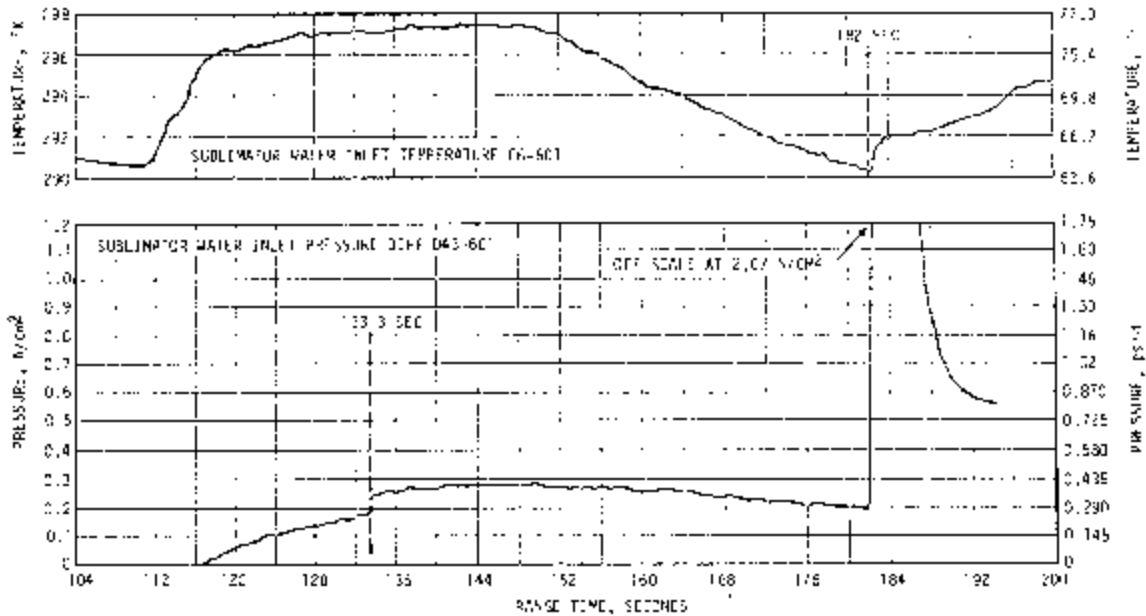


Figure 18-10. Sublimator Water Inlet Performance

A step increase in the differential pressure measurement is noticeable at 133 seconds, which consequently represents a corresponding decrease in the IU internal ambient pressure. If no change had occurred in the IU ambient pressure, a temperature increase of 4.4 to 5°K (9 to 10°F) would have had to occur at this time if the vapor pressure within the water line had increased by the magnitude shown in Figure 18-10. The temperature and pressure decrease after 149 seconds indicated that all the water within the tube had vaporized. This pressure decay is characteristic of the sublimator normal crying cycle. At 182 seconds, when the water solenoid valve opened, the pressure differential response led the temperature response as the vapor bled out of the water line.

Figure 18-11 shows the sublimator start-up characteristics during ascent. Not shown is the position of the MFCV, which began driving to the full sublimator flow at $T_1 + 5$ seconds as programmed. Full heat sink flow was achieved at $T_1 + 16$ seconds.

At 182.29 seconds (first interrogation of the thermal switches), the coolant temperature was 290.2°K (63°F), which was 1.94°K (3.5°F) above

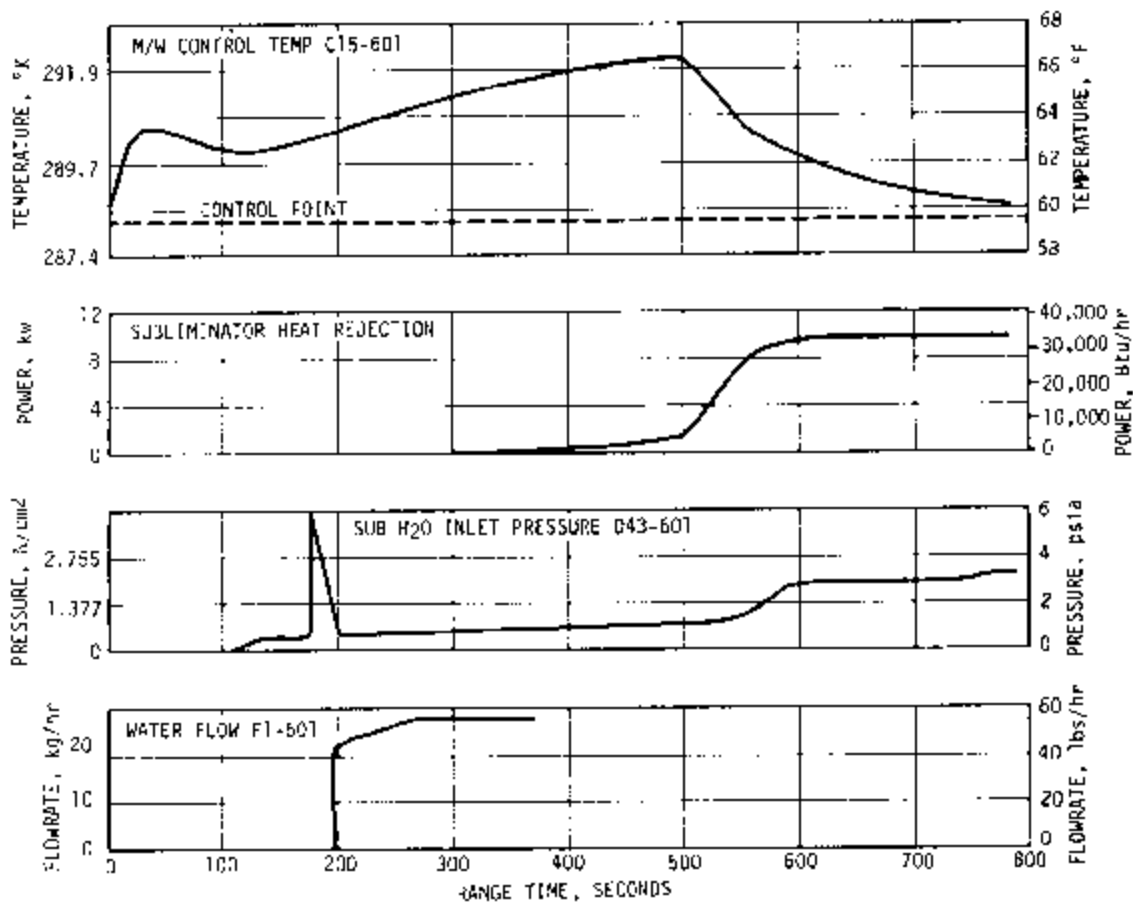


Figure 18-11. IU AS-502 Sublimator Startup Characteristics

the control point, and the water valve opened. This was verified by the valve position, increasing water inlet pressure, and water flowrate measurements. The sublimator inlet temperature reached a calculated 293°K (68°F) during ascent, and a 10 kw (34,140 Btu/hr) heat rejection rate was required to bring the coolant temperature back to the control level. Subsequent sublimator cycling can be identified from the curves in Figure 18-9. Seven water coolant switch selector operations in Section 2, Table 2-3, verify proper operation of the thermal control switching system.

None of the water system deviations (i.e., erratic low-level water flowrates and pressures) experienced on AS-204 were present in the AS-502 data. Fluid pressures and flowrates were within the desired ranges, considering the 5 percent possible measurement error, as shown in Table 18-7. Pump outlet pressure, D17-601, was erratic. However, this was a transducer problem and the measurement was waived prior to launch.

Table 18-7. IU TCS Flowrates and Coolant Pressure Data

FLOWRATES	MEASUREMENT NUMBER	FLIGHT VALUE				SPECIFICATION	
		MINIMUM		MAXIMUM			
		m ³ /s	(gpm)	m ³ /s	(gpm)	m ³ /s	(gpm)
Coldplate 5	F3-601	0.0000297	(0.47)	0.0000316	(0.50)	0.0000281	(0.445)
Coldplate 20	F4-603	0.0000303	(0.48)	0.0000322	(0.51)	0.0000281	(0.445)
ST-124M-3 Shroud	F5-603	0.0000131	(*0.207)	0.0000139	(0.22)	0.0000140	(0.222)
Flight Control Computer	F6-602	0.0000309	(0.49)	0.0000328	(0.52)	0.0000281	(0.445)
Coldplate 4	F7-601	0.00003	(0.475)	0.0000316	(0.50)	0.0000281	(0.445)
LVDA/LVDC	F8-603	0.0000448	(*0.71)	0.0000473	(0.75)	0.0000463	(0.734)
IU	F9-602	0.000593	(*9.4)	0.000619	(9.8)	0.000602	(9.55)
S-IVB	F10-601	0.000495	(7.85)	0.00052	(8.25*)	0.00049 ± 0.0002 (7.77 ± 0.39)	
ST-124M-3 Shroud	F11-603	0.0000126	(*0.200)	0.0000132	(0.21)	0.0000140	(0.222)
Total System	F9+F10	0.00109	(*17.25)	0.00114	(18.05)	0.00109 ± 0.00052 -0 (17.3 ± 0.83) -0	
Pressures		N/cm ²	(psia)	N/cm ²	(psia)	N/cm ²	(psia)
Pump Inlet	D24-601	11.2	(16.2)	11.4	(16.5)	11.4 ± 0.35 (16.5 ± 0.5)	
Pump Outlet	D17-601	28.2	(41)	30.7	(44.5) (Erratic)	17.2 to 22.8 (25 to 33) Above Inlet	
S-IVB Exit	D18-601	18.3	(26.5)	20.7	(30)	9.3 to 10.7 (13.5 to 15.5) Below Pump Outlet At Specified Flowrate	
*Within 5 percent possible measurement error							

The TCS GN₂ sphere pressure decay is seen to be nominal and the excessive GN₂ consumption rate of AS-204 was not observed, as shown in Figure 18-12.

Figure 18-13 shows selected component temperatures for AS-502. There were greater fluctuations in component temperatures for AS-502 than AS-501 during the orbital phase of the flight. This was caused by the water-feed control method of temperature control used on AS-502 which allowed 5°K (9°F) variations in the M/W temperature. The continuous control method employed on AS-501 allowed variations of less than 1°K (1.8°F) in the M/W temperature. The variations in the component temperatures on AS-502 had no detrimental effect on the operation of any of the components.

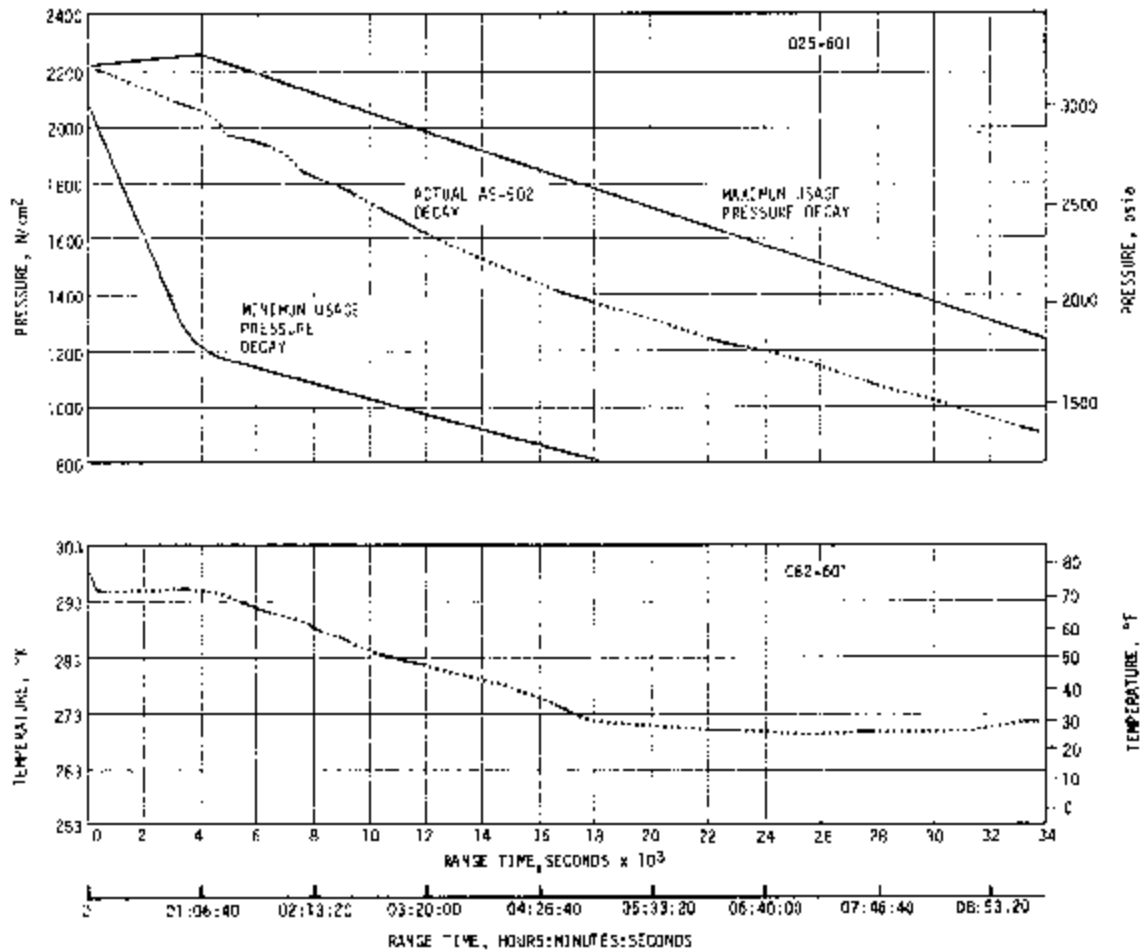


Figure 18-12. TCS GN₂ Supply Pressure and Temperature

18.5.2 Gas Bearing Supply System

The Gas Bearing System (GBS) supplies regulated Gaseous Nitrogen (GN₂) to the ST-124M-3 Inertial Platform Assembly for lubrication of the gas bearings during preflight and flight operation as shown in Figure 18-7. During preflight operations, GN₂ at 2068 N/cm² (3000 psig) flows from a ground source through the GN₂ fill coupling on the umbilical and through the open GN₂ solenoid valve to the 0.057 m³ (2.0 ft³) sphere. Should the GN₂ storage sphere pressure drop below 637.3 N/cm² (925 psig) during prelaunch subsystem operation, a signal from the low-pressure switch would be initiated to shut off electrical power to the platform. The low-pressure switch is inactive during flight.

During system operation, GN₂ flows from the storage sphere at an initial pressure of 2068 N/cm² (3000 psig). After the GN₂ is filtered, the gas

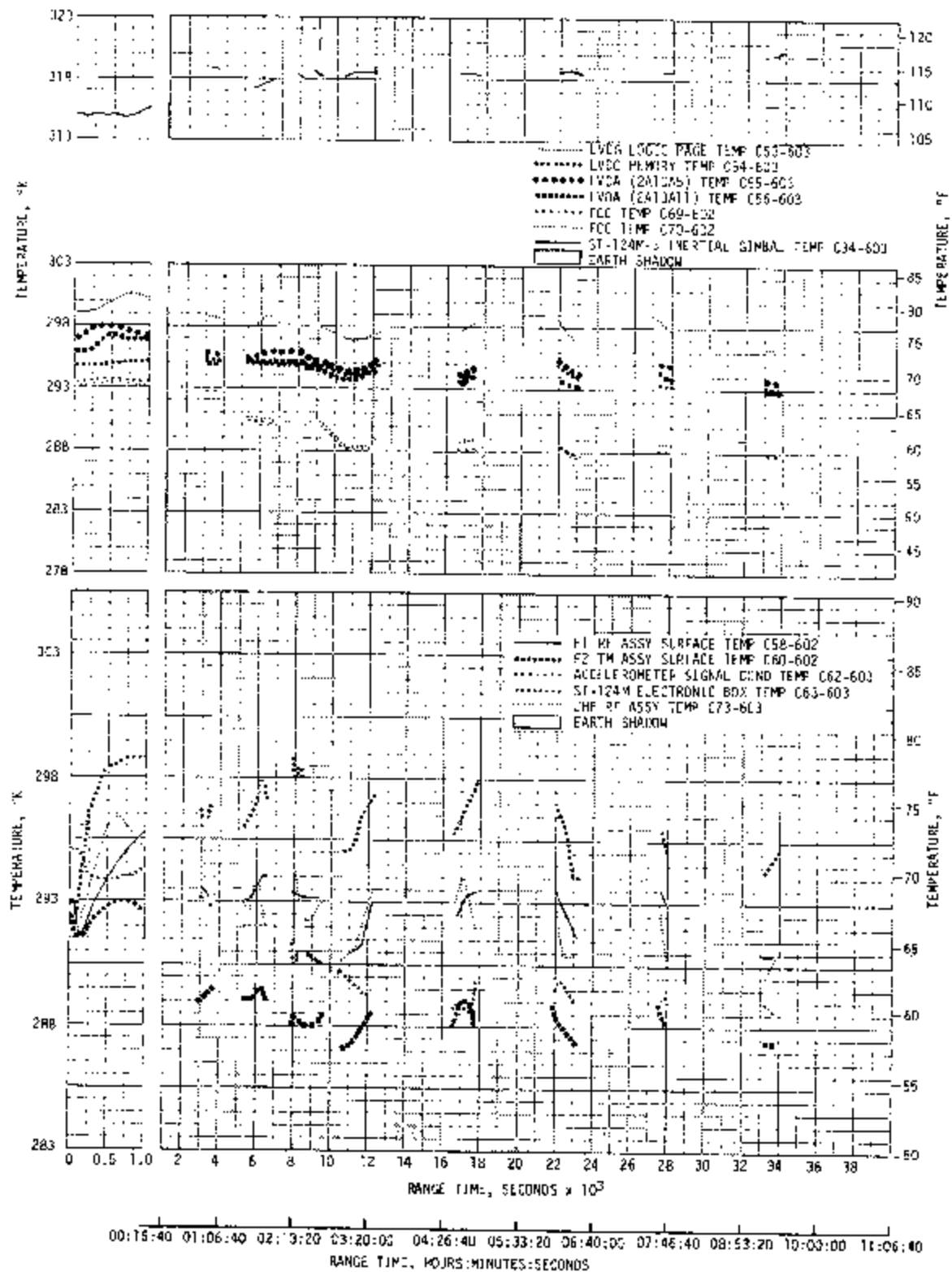


Figure 18-13. Component Temperatures

bearing pressure regulator drops the pressure to the acceptable value for gas bearing operation. The GN₂ flows through the heat exchanger and a second filter to the platform gas bearing inlet. The heat exchanger thermally conditions the GN₂. A line from the platform to the dome of the pressure regulator supplies the reference pressure required to control the pressure differential across the gas bearings.

The GBS pressure differential drifted above the $10.35 \pm 0.345 \text{ N/cm}^2$ ($15 \pm 0.5 \text{ psid}$) specification as expected. Figure 18-14 shows the differential pressure to be 0.069 N/cm^2 (0.1 psi) above the maximum specification value after 11,670 seconds. The gas bearing pressure regulator is sensitive to a changing reference pressure, requiring a series of calibration curves for each different reference pressure. The calibration curves generated during component acceptance testing (to modify the flight data) yield the following result:

- The 10.35 N/cm^2 (15.0 psid) at launch became 10.24 N/cm^2 (14.85 psid).
- The 10.76 N/cm^2 (15.6 psid) at 33,780 seconds became 10.85 N/cm^2 (15.725 psid).

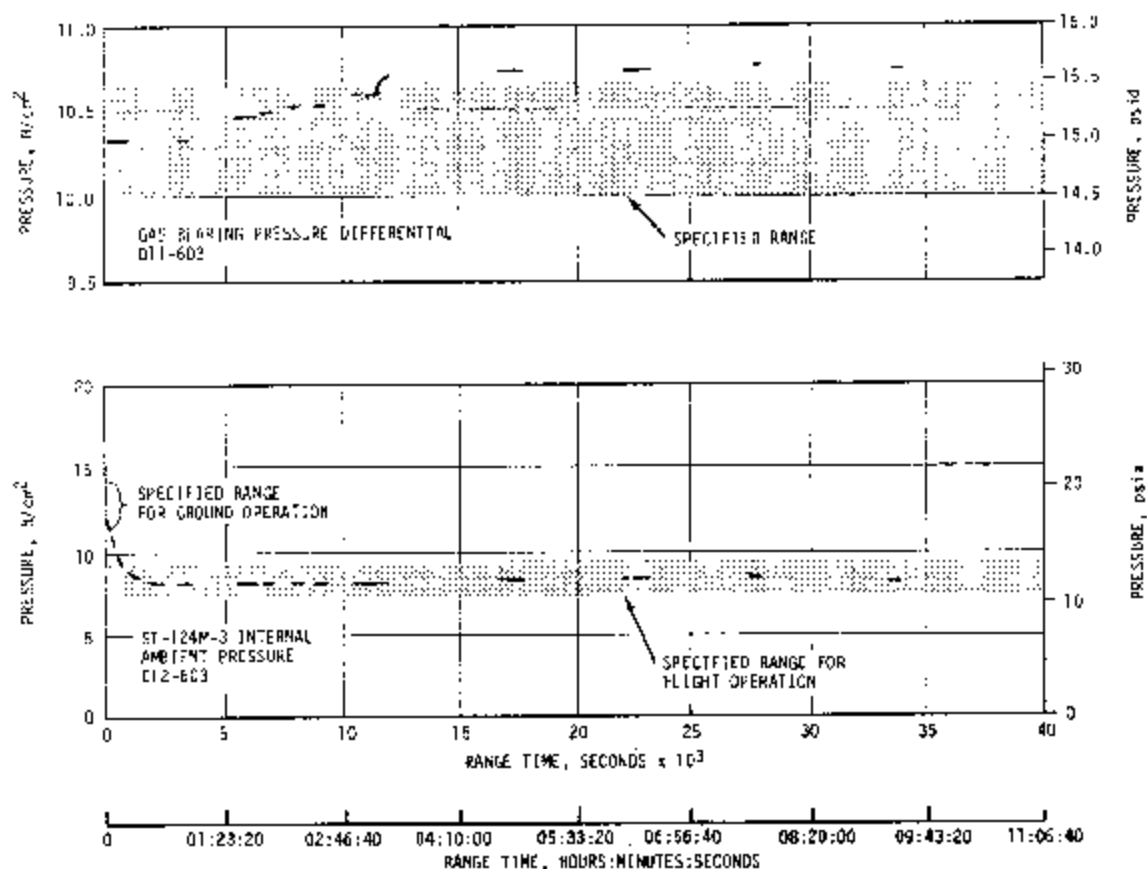


Figure 18-14. GBS Pressure Regulation Performance

The fact that the 5 percent possible measurement error can account for a 0.69 N/cm² (1.0 psid) correction further obscures the actual flight performance data. The following facts should be noted:

- The pressure differential was predicted to drift to 11.04 N/cm² (16.0 psid).
- The desired 10.35 N/cm² (15.0 psid) regulator set point is consistently in error because of the transducer sensitivity to the reference pressure.
- No conclusion about regulator performance can be reached until the flight data can be accurately assessed and transducer problems resolved.

The GN₂ delivered to the platform was well within the 274.7 to 310.8°K (35 to 100°F) temperature requirement. The GBS GN₂ sphere pressure decay as shown in Figure 18-15 is seen to be near nominal. Calculations indicate a 0.388 SCFM usage rate (within the 0.3 to 0.5 SCFM allowable range).

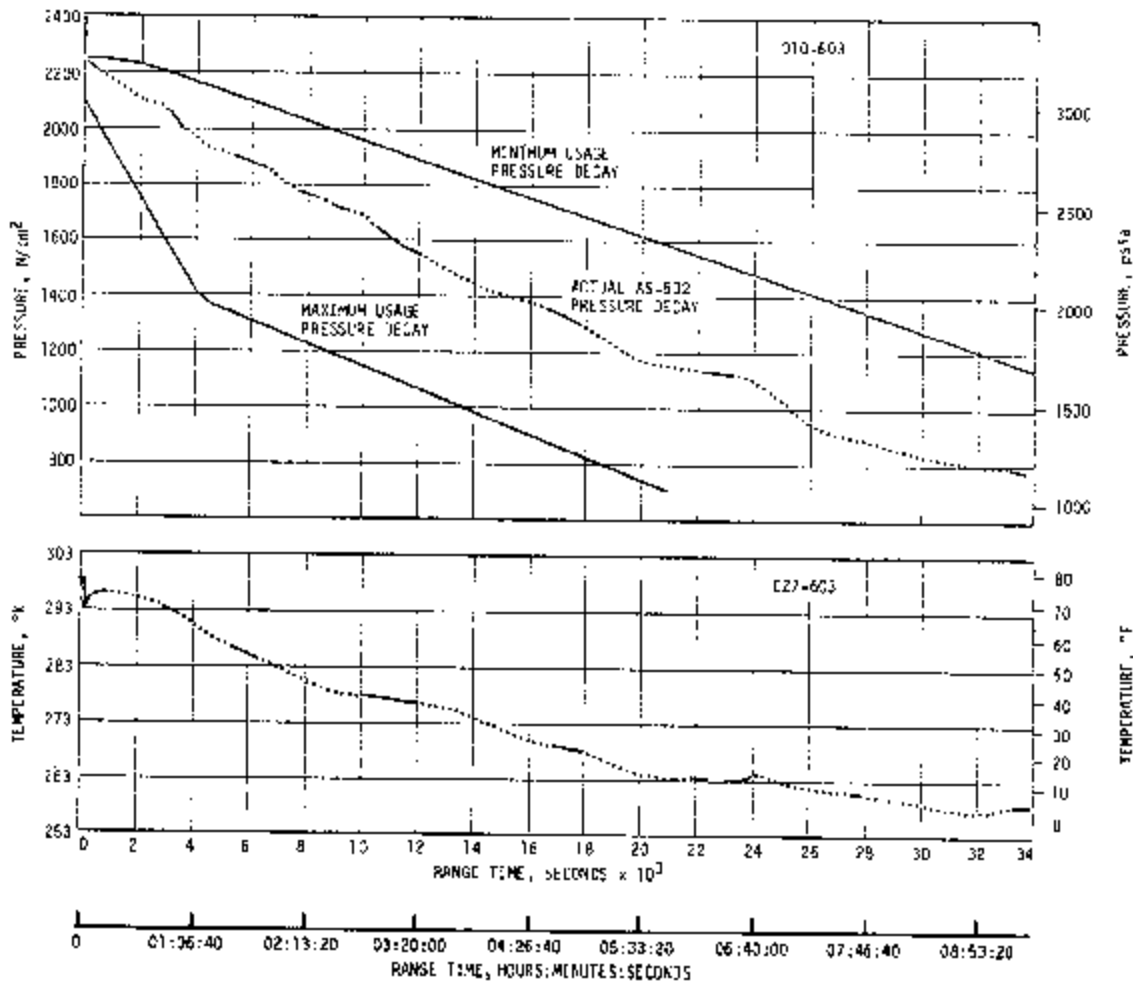


Figure 18-15. GBS GN₂ Supply Pressure and Temperature

SECTION 19

DATA SYSTEMS

19.1 SUMMARY

The data system consists of the measurement systems, telemetry systems, tape recorders, RF systems and optical instrumentation. There were 2758 telemetered measurements active at the start of the AS-502 automatic countdown sequence. Of the 2758 measurements, 58 failed in flight, resulting in an overall system reliability of 97.9 percent.

The Airborne Telemetry System operated satisfactorily, including preflight calibrations and inflight calibration.

Tape recorder performance was good; however, due to the extended burn time of the S-II and S-IVB stages, the S-IC/S-II separation data playback was not recovered from the S-II, S-IVB, and IU recorders. This was because insufficient playback time was programmed to cover the anomalous situation caused by the S-II two-engines-out condition.

Performance of the RF systems was good. Approximately 2 seconds of real time data on all S-IC stage telemetry links were lost due to a data dropout at 146.0 seconds. This condition was also noted on AS-501 and appears to be related to S-IC inboard engine cutoff (IECO).

Ground camera coverage was good as evidenced by 84 percent system efficiency. However, only two of the six onboard film cameras were recovered. Three of the cameras on the S-IC stage failed to eject and one of the S-II cameras was not recovered due to a weak recovery beacon signal.

19.2 VEHICLE MEASUREMENTS EVALUATION

The measurement system is composed of the transducers, signal conditioners and power supplies necessary to transform the physical quantities being measured into electrical signals suitable for telemetering, and of the measuring distributors necessary to route these signals to the proper telemetry channels.

The AS-502 measurement systems operated satisfactorily. Lost measurements did not adversely affect vehicle postflight evaluation, except in isolated cases such as J-2 engine vibrations, since sufficient data were acquired to complete the evaluations.

There were 2788 measurements scheduled for AS-502. Twenty-six measurements were waived/scrubbed prior to start of the automatic countdown sequence and 4 measurements were not considered in determining measurement reliability. Of the remaining 2758 measurements which were used for reliability determinations, 880 were on the S-IC stage, 951 on the S-II stage, 591 on the S-IVB and 336 on the IU. Fifty-eight measurements failed in flight, resulting in an overall measuring system reliability of 97.9 percent. In addition to the failed measurements there were 54 partially successful measurements, 57 measurements with improper range and 2 questionable measurements. Fourteen of the waived/scrubbed measurements provided good data during flight. A summary of vehicle measurements is presented in Table 19-1.

19.2.1 S-IC Stage Measurement Analysis

There were 888 flight measurements scheduled for the S-IC stage. Of these 8 measurements were waived/scrubbed prior to the automatic countdown sequence, 15 failed in flight, 21 were partially successful, and 19 had improper range. Five of the waived/scrubbed measurements provided useful data during flight. Based upon 880 measurements active at the start of automatic countdown and 15 failures during flight, the reliability was 98.3 percent.

Measurements waived/scrubbed prior to launch, measurement failures (including partial failures), and measurements of improper range are summarized in Tables 19-2, 19-3, and 19-4, respectively.

Table 19-1. Vehicle Measurements Summary

	S-IC STAGE	S-II STAGE	S-IVB STAGE		INSTRUMENT UNIT	TOTAL VEHICLE
			PHASE I	PHASE II		
No. Scheduled	888	958	604***	604***	338	2788***
No. Waived/ Scrubbed	8	7	9	9	2	26**
No. Failures	15	24	10	19*	0	58
No. Partial Successes	21	33*	0	0	0	54
No. Improper Range	19	24	8	8	6	57
No. Questionable	0	0	2	1	0	2
Measurement Reliability	98.3%	97.5%	98.3%	96.8%	100%	97.9%

* Includes measurement failures which were a consequence of engine malfunctions.

** Fourteen of these measurements provided useful data during flight.

*** Four of these measurements are not wholly on the stage and are not used in calculating measurement reliability.

Table 19-2. Measurements Waived/Scrubbed Prior to Launch

MEASUREMENT NUMBER	MEASUREMENT TITLE	NATURE OF FAILURE	REMARKS
S-1C STAGE			
AC01-118	Acceleration, Longitudinal	Installation not per drawing.	Waiver LIA-I-22, valid data at separation.
CO41-115	Temperature, Helium Inlet Manifold	Transducer failed at helium manifold.	Waiver LIA-I-31, invalid data.
EO55-115	Vibration, Bending, Pitch	Transducer failed.	Waiver LIA-I-34, invalid data during flight.
EO80-115	ECM Control Unit Switch Output 3, Engine 5	Failed in the ON position.	Waiver LIA-I-35, valid data during flight.
LO18-117	Fuel Slosh, Delta Level Fine, Pos II and IV	Measurement pegged at full scale.	Waiver LIA-I-32, valid data during flight.
LO18-117	Fuel Slosh, Delta Level Coarse, Pos II and IV	Measurement pegged at full scale.	Waiver LIA-I-32, valid data during flight.
NO70-120	11mm Camera Trigger Operation Indicator	Time code not per specification.	Waiver LIA-I-26, partly valid data during flight.
NO22-120	Strobe Light Operation Indicator	Narrow angle strobe light not operative.	Waiver LIA-I-33, invalid data.
S-11 STAGE			
SO15-219	STR 38 Side Longitudinal Strain	Open strain element	Defective installation
SO16-219	STR 38 Top Longitudinal Strain	Open strain element	Defective installation
SO17-219	STR 56 Side Longitudinal Strain	Open strain element	Defective installation
SO23-219	STR 110 Side Longitudinal Strain	Open strain element	Defective installation
SO24-219	STR 110 Top Longitudinal Strain	Open strain element	Defective installation
C171-206	L102 Tank Insulation Surface Temp	Noise out of specification	Received data during flight
C237-206	Thrust Cone Forward Surface Temp	Noise out of specification	Received data during flight
S-1VB STAGE			
CO41-406	Temp-Oxidizer Tank Position 2	Offscale high	Produced data during flight
CO56-406	Temp-LOX Tank Usage Gas 20 Percent	Offscale low	Produced data from 60 to 580 seconds in flight
C150-401	Temp-Engine L102 Pump Surface	Remained at 119.4°K (-244.67°F)	No response to temperature changes
C155-404	Temp-L102 Prevalve Bypass Line	Remained at 237.8°K (-31.67°F)	No response to temperature changes
C205-403	Temp-Helium Recross Sphere No. 4 Gas	Declared inoperative at Cape	Data reverified to be good
C301-415	Temp-APS Oxidizer Tank-2	Offscale low	Shorted out during FRT
GO18-401	Pressure-Engine Regulator Outlet	Offscale low	Data reverified to be good
GO58-401	Pressure-PII Valve Inlet	Erratic data	Had 34.5 N/cm ² (50 psia) fluctuations prior to liftoff. Looked good during second burn attempt.
SO87-426	Strain-Dynamic, Forward Skirt Panel 17	No response to calibration	Unable to verify RAC'S calibration

Table 19-2. Measurements Waived/Scrubbed Prior to Launch (Continued)

MEASUREMENT NUMBER	MEASUREMENT TITLE	NATURE OF FAILURE	REMARKS
10			
FD04-603	Flow Rate Colocate Inlet Coolant (Loc 20) 1.58 to 6.31×10^{-3} m ³ /s (0.25 to 1.0 gpm)	Flowmeter indicated zero flow prior to liftoff	Flowmeter commenced to operate properly at liftoff and provided good data for remainder of flight.
0017-601	Pressure Coolant Manifold Inlet 0 to 47.36 N/cm ² (0 to 60 psia)	Measurement signal intermittent	Measurement provided useful data during flight.

The crystal accelerometers and emitter followers used on AS-501 for 17 engine area vibration measurements were replaced with crystal accelerometers with integral emitter followers for this flight. This change did not completely eliminate high amplitude, low frequency noise problems noted on AS-501. However, a significant improvement was noted in the amount of useful data obtained.

19.2.2 S-II Stage Measurement Analysis

There were 958 flight measurements scheduled for the S-II stage. Of these, 7 measurements were waived/scrubbed prior to the automatic countdown sequence, 24 failed in flight, 33 were partially successful, and 24 had improper range. Two of the waived/scrubbed measurements provided useful data during flight. Based upon 951 measurements active at the start of automatic countdown and 24 failures during flight, the reliability was 97.5 percent.

Measurements waived/scrubbed prior to launch, measurement failures (including partial failures), and measurements of improper range are summarized in Tables 19-2, 19-3, and 19-4, respectively.

Eleven temperature measurements which failed during flight indicated a possible bonding problem. The bonding technique for these transducers is being investigated.

Erratic behavior of two temperature measurements on fuel turbine inlets was suspected to have been caused by melting of solder in the transducer connector, resulting in an open circuit to the dc amplifier. ECP J2-422, effective on engines installed on AS-504 and subs, has been released, requiring that these wires be brazed to the connector.

Interaction between measurements on a common power supply which had been noted on AS-501 was not present on AS-502 even though events similar to those which caused the interaction on AS-501 were experienced. This and static firing data from S-II-4 at Mississippi Test Facility (MTF) demonstrated the effectiveness of the design change to eliminate interactions.

Several vibration measurements experienced short transients. These transients were sufficient to invalidate the data on two measurements. Extensive tests are under way with individual components and a complete stage system configuration to determine the cause. Transients similar to those noted on the flight data have been reproduced in a number of different ways; however, no conclusions as to the specific cause have been formulated.

It was also determined that all engine vibration measurements saturated their respective measurement channels. As a result, an engineering change is being processed to change the range on all of these measurements.

The camera light battery monitor measurement decreased to 88 amperes at interstage separation instead of the expected zero amperes. The probable cause was a cable short to the structure at interstage separation. Since cameras will not be flown on future missions and this measurement will not be used, no changes are contemplated.

The high percentage of strain measurement failures experienced, with five scrubbed measurements and one inflight failure, indicated a possible installation problem. Investigation indicated that the present installation was highly susceptible to moisture absorption, which could create the failure mode experienced by these measurements. An engineering change is presently being processed to moisture-proof these installations.

A number of measurements malfunctioned as a result of the failure mode of engine No. 2. Tests are being conducted in an attempt to determine the particular failure mode of the transducers and signal conditioning equipment. Thus far, it has been determined that similar failure indications could be obtained with a diverse number of unexpected environmental or failure conditions.

Fifteen temperature measurements failed as a result of the engine No. 2 failure mode at approximately 412.9 seconds. Of these, 12 hydraulic temperature measurements were believed lost due to at least one wire from the common ± 28 vdc regulated power supply being shorted to its shield or to the structure. Some of the wires from the power supply to the transducers were located in the area of vehicle station 42.57 meters (1676 in.), stringer 108, where damage to wire bundles was considered to have occurred. The other failures were considered to have been caused by transducer open circuits.

In addition to the 15 temperature measurement failures discussed above, four pressure measurements did not exhibit normal shutdown characteristics at engine No. 2 shutdown. These measurements provided good data until engine No. 2 shutdown; however, after engine cutoff, they did not indicate expected values. Data indicated possible open transducers or open circuits.

An apparent failure occurred on the measurement monitoring switch selector telemetry output. Investigation of the problem indicated that the wiring between the switch selector and the telemetry package, which runs by vehicle station 42.57 meters (1676 in.), stringer 108, probably caused an

open circuit and was associated with the engine No. 2 failure. Switch selector operation was verified using another measurement.

All measurement failures associated with the engine No. 2 failure mode are grouped separately in Table 19-3.

19.2.3 S-IVB Stage Measurement Analysis

There were 604 flight measurements scheduled for the S-IVB stage. Of these, four measurements were not wholly on the S-IVB stage and nine measurements were waived/scrubbed prior to the automatic countdown sequence.

During Phase I (liftoff to parking orbit insertion) there were ten measurement failures in flight. During Phase II (liftoff to S-IVB/Spacecraft separation) there were nine additional failures. One measurement which failed in Phase II is considered questionable in Phase I. Eight measurements had improper range and two were questionable. Five of the waived/scrubbed measurements provided useful data during flight. Based upon 591 measurements active at the start of automatic countdown and wholly on the S-IVB stage and ten failures during Phase I, the measurement reliability was 98.3 percent. Based upon 591 measurements active at the start of automatic sequence and 19 failures during Phase II (including the 10 Phase I failures), the measurement reliability for this period was 96.8 percent.

Measurements waived/scrubbed prior to launch, measurement failures, measurements of improper range, and questionable measurements are summarized in Tables 19-2, 19-3, 19-4, and 19-5, respectively.

Failure of measurements C10-403, C152-403, and E209-401 is considered to be associated with the engine failure to restart anomaly, and these measurements are grouped separately in Table 19-3.

19.2.4 Instrument Unit Measurement Analysis

There were 338 flight measurements scheduled for the Instrument Unit. Of these, two measurements were waived/scrubbed prior to the automatic countdown sequence. There were no failures in flight, either partial or total. Six measurements had improper range. Both of the waived/scrubbed measurements provided useful data during flight.

Based upon 336 measurements active at the start of launch and no failures during flight, the reliability was 100 percent. Measurements waived/scrubbed prior to launch and measurements with improper range are summarized in Tables 19-2 and 19-4, respectively.

19.3 AIRBORNE TELEMETRY SYSTEMS

The telemetry systems of each stage of the vehicle operate independently of the other stages. These systems modulate the signals from the measurement system onto RF carriers for transmission to ground stations. The

Table 19-3. Measurement Malfunctions During Flight

WING NUMBER SUFFIX	TRANS DUCEMENT TITLE	NATURE OF FAILURE	TIME OF FAILURE (RANGE TIME)	CALIBRATION SATISFACTORY OPERATION	REMARKS
TOTAL MEASUREMENT FAILURES, SDC STAGE					
0024-114	Attitude, Rear Fin Q	Data had large transients	-1 second	None	Failure cause unknown.
0015-101	Temp, Engine, Total Calorimeter	Data level shifts abruptly at +5 seconds	+5 seconds	None	Apparent wire failure or fail to lead wire.
0047-100	Temp, Inlet, Inflow, Internal	Data level shifts abruptly at +1 second	+1 second	None	Failure cause unknown
0007-105	Press., 100 Control Valve, 100 Inlet	Data trend excessive high	+2 seconds	None	Apparent transducer failure.
0017-100	Press., Surface Forward Exit	Data does not follow normal trend	0 second	None	Apparent clogged sensing port.
0016-101	Press., Diff. Inlet, Strain System Malicious	Data level shifts below zero at liftoff	-1 second	None	Apparent bias shift of transducer
0016-104	Press., 10A Pump Inlet, High Frequency	Data level shifts at lift- off and goes off-scale at 47 seconds	-1 second	None	Apparent transducer failure.
0017-105	Press., 10F Pump Inlet, High Frequency	Data shifts at liftoff and goes off-scale at 47 seconds	-1 second	None	Apparent transducer failure.
0024-101	Vibration, 100 Ulna, Radial	Data 75 percent of expected level	+7 seconds	None	
0026-100	Vibration, Combustion Chamber Inlet, Longitudinal	High amplitude, low frequency noise	+5 seconds	None	
0026-101	Vibration, 100 Pump Inlet Flange, Radial	Data 200 percent of expected level	-1 second	None	
0047-101	Vibration, Fuel Pump Inlet Flange, Radial	Spectrogram does not agree with accelerometer data	-1 second	None	
0047-105	Vibration, Fuel Pump Flange, Radial	High amplitude, low frequency noise	-1 second	None	
0050-104	Vibration, Retain Motor Attach Point	Intermittent high amplitude, low frequency noise	0 second	None	Some usable data.
0054-105	Vibration, Retain Motor Attach Point	Intermittent high amplitude, low frequency noise	0 second	None	Some usable data.
TOTAL MEASUREMENT FAILURES, SDC STAGE					
0001-200	Fwd Boundary Layer Acoust.	No data	Prior to launch	None	Calibration problem.
0001-201	Fwd Skirt Heat Rate	No data	Prior to launch	None	Transducer covered
0001-200	A Inlet Meter 4 Fwd Fin Q	No data	Prior to launch	None	Transducer covered.
0001-200	B Inlet Meter 5 Fwd Fin Q	No data	Prior to launch	None	Transducer covered.
0066-200	F1 Kaw Activator Delta P	No data	Prior to launch	None	Transducer failure
0007-201	01 Long. Vib. Combust. Cone	Channel saturation	5-11 boost	None	
0007-202	02 Long. Vib. Combust. Cone	Channel saturation	5-11 boost	None	
0007-203	03 Radial Vib. Combust. Cone	Channel saturation	5-11 boost	None	
0007-204	04 Long. Vib. Combust. Cone	Channel saturation	5-11 boost	None	
0007-205	05 Long. Vib. Combust. Cone	Channel saturation	5-11 boost	None	
0007-201	01 Radial Vib. 100 Pump	Channel saturation	5-17 boost	None	
0007-202	02 Radial Vib. 100 Pump	Channel saturation	5-17 boost	None	
0007-203	03 Radial Vib. 100 Pump	Channel saturation	5-17 boost	None	
0007-204	04 Radial Vib. 100 Pump	Channel saturation	5-17 boost	None	
0007-205	05 Radial Vib. 100 Pump	Channel saturation	5-17 boost	None	
0007-201	01 Radial Vib. Fuel Pump	Channel saturation	5-17 boost	None	
0007-202	02 Radial Vib. Fuel Pump	Channel saturation	5-17 boost	None	
0007-203	03 Radial Vib. Fuel Pump	Channel saturation	5-17 boost	None	
0007-204	04 Radial Vib. Fuel Pump	Channel saturation	5-17 boost	None	
0007-205	05 Radial Vib. Fuel Pump	Channel saturation	5-17 boost	None	
0074-205	Lang. Vib. E1 Beam at Ctr.	No data	Prior to launch	None	Possible open cable.
0076-206	Lang. Vib. E1 Beam at E5	Numerous transients	Prior to launch	None	Under investigation
0083-210	Rad. Vib. Fwd Skt Stranger	Numerous transients	Prior to launch	None	Under investigation.
0029-219	Str. 14 Top Long. Strain	No data	Prior to launch	None	Defective install.

Table 19-3. Measurement Malfunctions During Flight (Continued)

MEASUREMENT NUMBER	MEASUREMENT TITLE	NATURE OF FAILURE	TIME OF FAILURE (SPACE TIME)	DURATION SATISFACTORY OPERATION	REMARKS
TOTAL MEASUREMENT FAILURES, S-108 STAGE, PHASE I					
8023-404	Acoustic Aft (2400-4800 Hertz) Internal	No activity	Liftoff	None	Suspected shift of gain adjustment to the filter.
0030-403	Temperature Heat Exchanger MB1 Inlet	Offscale, high	Liftoff	None	Prober RADS calibration
0149-426	Temperature-Electric Tunnel 1	Offscale, high	70 seconds	70 seconds	Debonding
0326-476	Temperature-OX In L1 Stage Gas 90 Percent	Data low	Liftoff	None	Bridge balance shift appeared to recover when probe was uncovered.
1111-426	Temperature-Fwd Skirt B	Offscale, high	Liftoff	None	Offscale, high between liftoff and 118 seconds, erratic at 522 seconds, and ultimate failure at 712 seconds. Bonding problem.
0121-431	Temperature-Engine LH2 Pump Purge	Offscale, high	Liftoff	None	Debonding.
0296-416	Temperature-APS Fairing 2-4	No valid data during time of interest		None	Partial debonding.
0100-403	Press.-LOX TK Press. In Gas Wnd.	No valid data during launch - offscale, high at 32 seconds	Launch phase	None	Returned to scale during restart phase
0114-411	Vib. Fwd Skirt EDW E/S Panel - Axial	Vibration erratic	Liftoff	None	Loose no-axial connector
0210-401*	Vib.-LH2 Turbo Pump, Lateral	Low range	S-1VB Burn	None	
TOTAL MEASUREMENT FAILURES, S-108 STAGE, PHASE II					
0100-414	Temp-APS Inj. Wall, Eng. 1 2	Offscale, high	Coast phase	Launch phase	Debonding
0215-401	Temp-Crossover Inlet Exit Wall 1	Offscale, high	722 seconds	722 seconds	During coast phase, several data excursions indicate unusual failure mode. Further investigation will be made.
0224-401	Press.-LH2 Pump Interstage Outlet	Offscale, low	Coast phase	Launch phase	Investigation continuing
0003-403	Press.-LOX Pump Inlet	Offscale, high	Coast phase	Launch phase	Investigation continuing.
4003-411*	PU System-LOX Coarse Mass Voltage	Offscale, high	10,610 seconds	Launch phase	Short between inner and outer elements of probe due to metallic debris.
NB04-411*	PU System-LOX Fine Mass Voltage	Offscale, high	10,610 seconds	Launch phase	Short between inner and outer elements of probe due to metallic debris.
S-108 FAILURES ASSOCIATED WITH ENGINE ANOMALY					
0019-403*	Temp Engine Area Ambient	Short circuit	699 seconds	699 seconds	Associated with engine anomaly. Temp went above spec. limit.
0152-403*	Temp-LOX Main Line Flange Wall	Open circuit	696 seconds	696 seconds	Associated with engine anomaly. Temp went above spec. limit.
1209-401*	Vib-Combustion Chamber Dome-Long	Oversignal to multiolexer	694 seconds	694 seconds	Location and cause not yet determined. Associated with engine anomaly.
PARTIAL MEASUREMENT FAILURES, S-108 STAGE					
8001-118	Acoustic, Skin, Flush Mounted	Intermittent high amplitude, low frequency noise	20 seconds	20 seconds	Some usable data.

* Considered valid measurements by stage contractor

Table 19-3. Measurement Malfunctions During Flight (Continued)

MEASUREMENT NUMBER	MEASUREMENT TITLE	NATURE OF FAILURE	TIME OF FAILURE (RANGE) (SEC)	DURATION SATISFACTORY OPERATION	REMARKS
PARTIAL MEASUREMENT FAILURES, S-10 STAGE (Continued)					
0081-101	Temp, Ambient Engine Compartment	Data drops abruptly off-scale at 93 seconds	93 seconds	93 seconds	Apparent transducer failure.
0090-108	Temp, Skin, Shroud Outer Surface	Data erratic after 28 seconds	28 seconds	29 seconds	Apparent transducer failure.
0105-112	Temp, Skin, Internal, Fin 8	Data erratic after 60 seconds	60 seconds	60 seconds	Apparent transducer failure.
0120-119	Temp, LOX Tank Jilage	Data erratic from 78 to 88 seconds	78 seconds	78 seconds	Apparent connector chatter.
0174-119	Temp, LOX Tank Skin	Data erratic after 23 seconds	23 seconds	23 seconds	Apparent transducer failure.
0176-119	Temp, LOX Tank Skin	Data erratic after 60 seconds	60 seconds	60 seconds	Apparent transducer failure.
0176-119	Temp, LOX Tank Skin	Data erratic after 24 seconds	24 seconds	24 seconds	Apparent transducer failure.
0177-119	Temp, LOX Tank Skin	Data level shifts abruptly at 33 seconds	33 seconds	33 seconds	Probable transducer/tank bond failure.
0178-119	Temp, LOX Tank Skin	Data noisy from 30 to 45 seconds	30 to 45 seconds	134 seconds	Probable connector chatter.
0179-119	Temp, LOX Tank Skin	Data level shifts abruptly at 42 seconds	42 seconds	42 seconds	Probable transducer/tank bond failure.
0225-118	Vibration, LOX Suction Line, Longitudinal	Data spectrum not as expected	50 seconds	60 seconds	
0225-118	Vibration, LOX Suction Line, Radial	Data spectrum not as expected	50 seconds	60 seconds	
0041-101	Vibration, Fuel Pump Flange, Longitudinal	High amplitude, low frequency noise	0 to 60 seconds	30 seconds	
0042-101	Vibration, Fuel Pump Flange, Radial	High amplitude, low frequency noise	0 seconds		Some usable data.
0050-116	Vibration, External, Helium Line	High amplitude, low frequency noise	2 to 4 seconds	147 seconds	
0034-116	Position, O2 Flow Control Valve	Data shift due to temperature	0 to 120 seconds	30 seconds	Apparent calibration shift due to temperature.
0038-116	Thrust OK Press. Switch 3, Eng 2	Cycled 7 times after 22 seconds	22 seconds	22 seconds	Apparent pressure switch chatter.
0044-116	Thrust OK Press. Switch 3, Eng 4	Cycled 7 times after 0 second	0 seconds		Apparent pressure switch chatter.
0045-116	Thrust OK Press. Switch 1, Eng 5	Cycled 6 times after 48 seconds	48 seconds	48 seconds	Apparent pressure switch chatter.
0023-118	Strain, Intertank Skirt, Longitudinal	Data trend not as expected after 100 seconds	100 seconds	100 seconds	Temperature compensation cannot be accomplished.
PARTIAL MEASUREMENT FAILURES, S-11 STAGE					
0033-204	E4 Fuel Turbine Inlet Temp	Loss of data	260 seconds	260 seconds	Transducer failure.
0003-205	E5 Fuel Turbine Inlet Temp	Loss of data	210 seconds	210 seconds	Transducer failure.
0122-218	E12 Tank Insulation Surface Temp	Loss of data	145 seconds	145 seconds	Transducer failure.
0326-205	F4 LOX Turbine Outlet Temp	Loss of data	367 seconds	367 seconds	Transducer failure.
0648-219	H2 Pressure Regulator Out Temp	Loss of data	288 seconds	288 seconds	Transducer failure.
0710-206	Heat Shield AFT Surf Temp	Loss of data	225 seconds	225 seconds	Transducer failure.
0713-206	Heat Shield AFT Surf Temp	Loss of data	190 seconds	190 seconds	Transducer failure.
0714-206	Heat Shield AFT Surf Temp	Loss of data	190 seconds	190 seconds	Transducer failure.
0059-250	Willage WTR 2 Fair Surf Temp	Loss of data	57 seconds	58 seconds	Transducer failure.
0065-200	Willage WTR 8 Fair Surf Temp	Loss of data	58 seconds	58 seconds	Transducer failure.

Table 19-3. Measurement Malfunctions During Flight (Continued)

MEASUREMENT NUMBER	MEASUREMENT TITLE	NATURE OF FAILURE	TIME OF FAILURE (GMT ± 0.01)	DURATION OF SATISFACTORY OPERATION	REMARKS
PARTIAL MEASUREMENT FAILURES, S-10 STAGE (Continued)					
D111-200	Ullage ATP S Shield Temp	Loss of data	70 seconds	70 seconds	Transducer failure.
D256-201	E1 Fuel Pump Interlock Press	Loss of data	13.46 seconds	200.5 seconds	Transducer failure.
D113-219	Wd. Skt. Static Press.	Loss of data	20 seconds	20 seconds	Transducer failure.
S-11 PARTIAL FAILURES ASSOCIATED WITH S-11 ENGINE ANOMALY					
D649-206	D2 Press. Regulator Outlet	Transducer open	414 seconds	414 seconds	These failures are all associated with the engine hot /2 pre-ignition failure mode.
D664-207	E2 Engine Inlet LO2 Temp	Transducer open	414 seconds	414 seconds	
D697-201	E1 Yaw Actuator Return Fluid Temp	28 vdc power supply short	414 seconds	414 seconds	
D697-202	E2 Yaw Actuator Return Fluid Temp	28 vdc power supply short	414 seconds	414 seconds	
D697-203	E3 Yaw Actuator Return Fluid Temp	28 vdc power supply short	414 seconds	414 seconds	
D697-204	E4 Yaw Actuator Return Fluid Temp	28 vdc power supply short	414 seconds	414 seconds	
D698-201	E1 Pitch Actuator Return Fluid Temp	28 vdc power supply short	414 seconds	414 seconds	
D698-202	E2 Pitch Actuator Return Fluid Temp	28 vdc power supply short	414 seconds	414 seconds	
D698-203	E3 Pitch Actuator Return Fluid Temp	28 vdc power supply short	414 seconds	414 seconds	
D700-204	E4 Pitch Actuator Return Fluid Temp	28 vdc power supply short	414 seconds	414 seconds	
D700-201	E1 Reservoir Out Fluid Temp	28 vdc power supply short	414 seconds	414 seconds	
D700-202	E2 Reservoir Out Fluid Temp	28 vdc power supply short	414 seconds	414 seconds	
D700-203	E3 Reservoir Out Fluid Temp	28 vdc power supply short	414 seconds	414 seconds	
D700-204	E4 Reservoir Out Fluid Temp	28 vdc power supply short	414 seconds	414 seconds	
D704-206	Heat Shield Inlet Temp	Transducer open	414 seconds	414 seconds	
D016-202	E2 Heat Exchanger Inlet Press.	Transducer open or open wire	414 seconds	414 seconds	
D091-202	E2 Engine Inlet LO2 Press.	Transducer open or open wire	414 seconds	414 seconds	
D092-202	E2 Engine Inlet LO2 Press	Transducer open or open wire	414 seconds	414 seconds	
D190-202	E2 PU Valve Inlet Press.	Transducer open or open wire	414 seconds	414 seconds	
M136-206	Switch Selector Telemetry	last output at 361.1 seconds, no output for next event at 421 seconds	421 seconds	414 seconds	

Table 19-4. Measurements With Improper Range

MEASUREMENT NUMBER	MEASUREMENT TITLE	NATURE OF OFFSCALE OUTPUT	TIME	REMARKS
S-10 STAGE				
B002-115	Acoustic, Skin, Flush Mounted	Data level low through liftoff	5 seconds	No valid data after 5 seconds.
C061-106	Temp, Heat Shield Radiation Cal	Offscale, high	93.0 to 93.9 seconds	Valid data except for time noted.
C081-117	Temp, Fuel Tank Skin	Offscale, high	103 seconds	Valid data to 103 seconds.
C157-106	Temp, Heat Shield Radiation Cal	Offscale, high	99 to 94 seconds	Valid data except for time noted.
C096-115	Press Diff, GOX Control Valve	Offscale, high	0.7 to 2 seconds	Valid data except for time noted.
E081-114	Vibration, Fin D, Leading Edge	Offscale, high and low	Liftoff and 120 seconds	Valid data except for time noted.
E094-114	Vibration, Fin D, Trailing Edge	Offscale, high and low	Liftoff, Max Q, and 120 seconds	Valid data except for time noted.
C009-112	Vibration, Fin D, Leading Edge	Offscale, high and low	Liftoff, Max Q, and 120 seconds	Valid data except for time noted.
F010-112	Vibration, Fin B, Trailing Edge	Offscale, high and low	Liftoff, Max Q, and 120 seconds	Valid data except for time noted.
E035-101	Vibration, Yaw Actuator, Longitudinal	Offscale, high and low	80 seconds	Valid data except for time noted.
E037-101	Vibration, LOX Pump Inlet Flange, Longitudinal	Offscale, high and low	0 second	No valid data throughout flight.
E039-101	Vibration, Fuel Pump Inlet Flange, Longitudinal	Offscale, high and low	20 to 60 seconds	Valid data except for time noted.
E041-103	Vibration, Fuel Pump Flange, Longitudinal	Offscale, high and low	0 second	No valid data throughout flight.
E041-104	Vibration, Fuel Pump Flange, Longitudinal	Offscale, high and low	0 through 60 seconds	Valid data except for time noted.
E041-105	Vibration, Fuel Pump Flange, Longitudinal	Offscale, high and low	0 second	No valid data throughout flight.
E051-116	Vibration, External, Helium Line	Offscale, high and low	0 to 4 seconds	Valid data except for time noted.
E059-116	Vibration, Bending, Pitch	Offscale, high	Liftoff	Valid data except at liftoff.
E074-120	Vibration, Structure System Mounting Panel, Longitudinal	Data level low	0 second	No valid data throughout flight.
E095-120	Vibration, Telemetry Equipment Mounting Panel, Longitudinal	Data level low	5 seconds	No valid data after 5 seconds.

Table 19-4. Measurements With Improper Range (Continued)

MEASUREMENT NUMBER	MEASUREMENT TITLE	NATURE OF OFFSCALE OUTPUT	TIME	REMARKS	
S-11 STAGE					
0076-219	FWD SKT Internal Surf Temp	Offscale, low		Range 227.59 to 477.59°K (-50 to 400°F). Range change S-11-3	
0435-217	LOX Tank Utilage Temp	Offscale, low			
0437-217	LOX Tank Utilage Temp	Offscale, low			
0438-217	LOX Tank Utilage Temp	Offscale, low			
0441-217	LOX Tank Utilage Temp	Offscale, low			
0445-217	LOX Tank Utilage Temp	Offscale, low			
0447-217	LOX Tank Utilage Temp	Offscale, low			
0448-217	LOX Tank Utilage Temp	Offscale, low			
0449-217	LOX Tank Utilage Temp	Offscale, low			
0450-217	LOX Tank Utilage Temp	Offscale, low			
0730-206	Heat Shield Gas Recovery Temp	Offscale, low			
0731-206	Heat Shield Gas Recovery Temp	Offscale, low			
0889-218	Li2 Tank Insulation Surf Temp	Saturates between 130/210 seconds	130 to 210 seconds		Range 199.82 to 422.04°K (-100 to 300°F). Deleted from S-11-3 and subs
0922-203	E3 Flat Band 7 Surf Temp	Offscale, low			Range 1088.71 to 2199.82°K (1500 to 3500°F) Range change S-11-3
0018-201	E1 Heat Exchanger Inlet Press.	Saturates at engine start		Range 1088.71 to 2199.82°K (1500 to 3500°F) Range change S-11-3	
0018-202	E2 Heat Exchanger Inlet Press.	Saturates at engine start		Range 19.26 to 310.93°K (-425 to 100°F) No action planned	
0018-203	E3 Heat Exchanger Inlet Press.	Saturates at engine start		Range 227.59 to 588.71°K (-50 to 500°F) No action planned	
0018-204	E4 Heat Exchanger Inlet Press.	Saturates at engine start		Range 0 to 689.48 N/cm ² (0 to 1000 psia) Deleted from S-11-3 and subs	
0018-205	E5 Heat Exchanger Inlet Press.	Saturates at engine start			
0190-201	E1 PU Valve Inlet Press.	Saturates at engine start		Range 0 to 689.48 N/cm ² (0 to 1000 psia) Range change S-11-4 and S-11-5	
0190-202	E2 PU Valve Inlet Press.	Saturates at engine start			
0190-203	E3 PU Valve Inlet Press.	Saturates at engine start			
0190-204	E4 PU Valve Inlet Press.	Saturates at engine start			
0190-205	E5 PU Valve Inlet Press.	Saturates at engine start			

Table 19-4. Measurements With Improper Range (Continued)

MEASUREMENT NUMBER	MEASUREMENT TITLE	NATURE OF OFFSCALE OUTPUT	TIME	REMARKS
S-IVB STAGE				
E041-403	Vib-Thrust Struct. at No Bottle-Thrust	Low level		
E042-403	Vib-Thrust Struct at No Bottle-Pitch	Low level		
E043-403	Vib Thrust Struct at No Bottle-Yaw	Low level		
E051-403	Vib-Lfy Trans Line T/S-Thrust	Low level		
E104-404	Vib-Aft Skirt Sec. Panel-Thrust	Low level		
E106-404	Vib-Aft Skirt Sw. Sel Panel-Thrust	Low level		
E107-404	Vib-Aft Skirt Sw. Sel Panel-Rad.	Low level		
E119-427	Vib-APS Mod. 1 Attach Pt.-Rad.	Low level		
IU STAGE				
E002-603	Vib X Axis Inertial Signal ST-124M	150 percent	Liftoff	
E014-603	Vib Joper Mtg Ring Long	150 percent	84 seconds	
E015-603	Vib Upper Mtg Ring Perp	150 percent	90 seconds	
E026-603	Vib Dig. Comp/Data Adapt Long.	Low data cal.		
E027-603	Vib Dig. Comp/Data Adapt Perp.	Low data cal.		
E028-603	Vib Dig. Comp/Data Adapt Tang.	Low data level		

Table 19-5. Questionable Measurements

MEASUREMENT NUMBER	MEASUREMENT TITLE	REASON QUESTIONED	REMARKS
S-IVB STAGE, PHASE I			
E209-401*	Vib-Combustion Chamber Dome-Long.	Data biased and clipped	Failed during Phase I?
E271-401*	Vib-LOX Turbo Pump-Lateral	Data biased and clipped	Remained questionable during Phase I?

* Considered valid measurements by stage contractor

different modulation techniques employed provide a means for efficient transmission of a large quantity and variety of measured data requiring different bandwidths and accuracy. There were 23 telemetry links used to transmit flight data on the AS-5D2 launch vehicle: six on the S-IC stage, six on the S-II stage, five on the S-IVB stage, and six on the Instrument Unit. Performance of the telemetry systems was generally satisfactory.

There were approximately 4.4 seconds of real time data lost on all S-IC telemetry links due to RF blackouts. Critical data were recovered, however, by airborne tape recorder playback. The S-II stage, S-IVB stage, and IU lost approximately 1 second of data on all telemetry links due to RF blackout during S-IC/S-II staging. None of these data were recovered since tape recorder playback did not reach this time period due to a prolonged recording period brought about by S-II extended burn time and insufficient recorder playback time.

A summary of the telemetry system performance is presented in Table 19-6.

19.3.1 S-IC Stage Telemetry System

There were six telemetry links used to transmit flight data on the S-IC stage: three Pulse Amplitude Modulation/Frequency Modulation/Frequency Modulation (PAM/FM/FM) links; one Pulse Code Modulation/Frequency Modulation (PCM/FM) link; and two Single Sideband/Frequency Modulation (SS/FM) links. Transmission of data from all six links was generally satisfactory during flight with the exception of three significant data dropout periods when data were lost from all links. These data dropouts occurred at approximately 146.0 seconds (2 seconds), 149.2 seconds (1.2 seconds), and 152.3 seconds (1.2 seconds), and corresponded with the RF blackout periods discussed in detail in paragraph 19.5.1. Data from the AF1 and AF2 links were recovered from the airborne tape recorder playback.

The internal calibrator within the 270-channel multiplexer assembly for PAM/FM/FM link AF2 initiated a sixth calibration step, approximately 26 percent of full scale, after completion of each programmed five step calibration sequence. This resulted in 83.3 milliseconds of interrupted data on each PAM channel after each inflight calibration. No further hindrance to data transmission was exhibited. This condition was noted prior to flight and a waiver granted.

During ground checkout, the frequency of the upper and lower band edges of the PCM/FM link RF assembly were found to be above their specified limits by 2 kilohertz and 5 kilohertz, respectively. This out-of-tolerance condition was waived and produced no adverse effect on the PCM data transmitted.

The signal strength from PAM/FM/FM link AF1 became erratic and exhibited a marked reduction in level at approximately 350 seconds. The incident and reflected power measurements for this link indicated an erratic mismatch in impedance between the Voltage Standing Wave Ratio (VSWR) monitor and the RF multicoupler at this time. It is suspected that the problem is associated with the cable interconnecting these two components.

Table 19-6. Launch Vehicle Telemetry Links

LINK	FREQUENCY (Mhz)	MODULATION	STAGE	FLIGHT PERIOD (RANGE TIME, SEC)	PERFORMANCE SUMMARY
AF1	240.2	PAM/FM/FM	S-1C	0-395	Satisfactory Data Dropouts <u>Range Time (sec)</u> <u>Duration (sec)</u> 146.0 2.0 149.2 1.2 152.3 1.2
AF2	252.4	PAM/FM/FM	S-1C	0-395	
AF3	231.9	PAM/FM/FM	S-1C	0-395	
AP1	244.3	PCM/FM	S-1C	0-395	
AS1	235.0	SS/FM	S-1C	0-395	
AS2	255.2	SS/FM	S-1C	0-395	
BF1	241.5	PAM/FM/FM	S-1I	0-796	Satisfactory Data Dropouts <u>Range Time (sec)</u> <u>Duration (sec)</u> 149.2 Approx 1.0
BF2	234.0	PAM/FM/FM	S-1I	0-796	
BF3	229.9	PAM/FM/FM	S-1I	0-796	
BF4	248.6	PCM/FM	S-1I	0-796	
BS1	227.2	SS/FM	S-1I	0-796	
BS2	236.2	SS/FM	S-1I	0-796	
CF1	258.5	PAM/FM/FM	S-1VB	Full duration	Satisfactory Data Dropouts <u>Range Time (sec)</u> <u>Duration (sec)</u> 149.2 Approx 1.0
CF2	246.3	PAM/FM/FM	S-1VB	Full duration	
CF3	253.8	PAM/FM/FM	S-1VB	Full duration	
CP1	232.9	PCM/FM	S-1VB	Full duration	
CS1	226.2	SS/FM	S-1VB	Full duration	
DF1	250.7	FM/FM	IU	Full duration	Satisfactory Data Dropouts <u>Range Time (sec)</u> <u>Duration (sec)</u> 149.2 Approx 1.0
DF2	245.3	PAM/FM/FM	IU	Full duration	
US1	259.7	SS/FM	IU	Full duration	
DP1	255.1	PCM/FM	IU	Full duration	
DP1A	2277.5	PCM/FM	IU	Full duration	
DP1B	2282.5	CCS	IU	Full duration	

Programmed inflight calibrations indicated that all telemeter channels were within the accuracies specified.

19.3.2 S-II Stage Telemetry System

There were six telemetry links used to transmit flight data on the S-II stage: three PAM/FM/FM links, two SS/FM links, and one PCM/FM link. Transmission of data from all six links was generally satisfactory with the exception of expected dropouts during S-IC/S-II staging when all data were lost. These data were not recovered by airborne tape recorder playback for the reasons discussed in paragraph 19.4.2.

Selected measurements and oscillograph recordings were evaluated to determine the proper functional operation of the telemetry equipment to the black-box level. This selective review verified the proper operation of the telemetry equipment.

Four programmed inflight calibrations indicated that all telemeter channels were within the accuracies specified.

Transients were noted on several channels of both SS/FM telemetry links. Comparison of the data processed from all sites verified that the transients were the result of a stage problem and not a data processing problem. Studies are underway to determine the source of these transients.

19.3.3 S-IVB Telemetry System

There were five telemetry links used to transmit flight data on the S-IVB stage: three PAM/FM/FM links, one PCM/FM link, and one SS/FM link. Transmission of data from all five links was generally satisfactory with the exception of expected dropouts during S-IC/S-II staging when all data were lost. These data were not recovered by airborne tape recorder playback for the reasons discussed in paragraph 19.4.

The performance of the PCM system was excellent. All multiplexers were properly synchronized and their outputs properly interlaced as confirmed by the reduced data. PCM was utilized as the prime data acquisition system.

The performance of the PAM system was excellent. There were no system or component malfunctions and synchronization was good.

Performance of the FM system was excellent. The Voltage Controlled Oscillators (VCO) performed well. VCO center and band edge frequencies were well within their specified limits.

The SS/FM systems performed well during the mission. The SS/FM translator calibrated as specified, and all calibration signals were clean and easily distinguishable for evaluation.

19.3.4 Instrument Unit Telemetry Systems

There were six telemetry links used to transmit flight data in the IU: one FM/FM/FM link, one PAM/FM link, one SS/FM link, one PCM/FM link (VHF), one PCM/FM link (UHF), and one PCM/FM link which used the Command and Communications System (CCS) transponder. The three PCM links all transmitted the same data. Examination of available data indicated satisfactory performance of all links with the exception of expected drop out during S-IC/S-II staging when all data were lost. These data were not recovered by airborne tape recorder playback for the reasons discussed in paragraph 19.4. The reflected power in the FM/FM/FM link measured by the VSWR was above the specified 9 percent of the forward power; however, this measurement was above the specification prior to launch. Transmitted data were of good quality and indicated low noise levels.

Performance of the PAM/FM and PCM/FM (VHF) links was nominal. All data transmitted were of good quality. Because of the abnormal flight profile, no satisfactory data were available to check out performance of the redundant UHF and CCS PCM systems.

The performance of the SS/FM link was satisfactory. The reflected power for this link was above the specified limits prior to launch but dropped to within specified limits after approximately 200 seconds of flight.

19.4 AIRBORNE TAPE RECORDERS

The airborne tape recorders recorded and stored for subsequent transmission portions of the data that would otherwise have been lost due to flare effects or visibility constraints at receiving stations. Not all of the recorded data were recovered due to factors discussed below. A summary of vehicle tape recorders is presented in Table 19-7.

19.4.1 S-IC Stage Recorder

One two-channel magnetic tape recorder recorded data from the S-IC stage AF1 and AF2 PAM/FM/FM telemetry links during S-IC/S-II staging. The record and playback commands were initiated on schedule as shown in Table 19-7. Data were recorded for approximately 123.7 seconds. The duration of the airborne timer which initiated playback was 24.7 seconds, falling within the design limits of 24 ± 1.5 seconds. Airborne recorder playback amplifier gain was within specified limits of ± 3 decibels of the corresponding real time data.

The 3 sigma noise errors for recorded links AF1 and AF2 were 2.73 percent and 2.08 percent of full scale, respectively. This compared with respective 3.50 percent and 3.85 percent of full scale noise values for the AS-501 flight.

19.4.2 S-II Stage Recorders

Two two-channel magnetic tape recorders recorded data from the BF1, BF2, and BF3 PAM/FM/FM telemetry links and selected discrete data pertinent to

Table 19-7. Tape Recorder Summary

RECORDER	LINK RECORDED	RECORD TIME (RANGE TIME, SEC)		PLAYBACK TIME (RANGE TIME, SEC)	
		START	STOP	START	STOP
LAUNCH PHASE					
S-IC Recorder	AF1 AF2	50.15	173.82	173.82	298.66
S-II Recorder No. 1	BF1 BF2	74.74 483.67	159.78 587.60	599.35	699.60
S-II Recorder No. 2	BF3 BT1	74.74 483.67	159.78 587.60	599.35	699.60
S-IVB Recorder	CF1 CF2 CF3	135.16 483.46	159.78 584.28	835.75	908.75
IU Recorder	DF1 DF2	135.55 483.46	160.17 595.18	836.45	920.45
ORBITAL PHASE					
S-IVB Recorder Playback at:	CPI				
Tananarive		909.45	2392.75	2392.95	2560.75
Guaymas		2560.95	5417.95	5418.35	5774.75
Tananarive		5775.15	7939.75	7939.97	8210.55
Hawaii		8210.75	10,442.75	10,442.95	10,707.75
Guaymas		10,707.95			
Hawaii		16,929.72*	16,930.62*	21,987.42*	

* Ground command.

the separation sequence. The discrete data were time division multiplexed by the BT1 multiplexer, and the playback was transmitted on the BS1 SS/FM telemetry link.

The record and playback commands were initiated as shown in Table 19-7. The recorders and associated hardware performed as required, with the exception of the record/playback capability due to the extended S-II stage burn time.

Due to the extended S-II burn time the only receiver station to receive playback data was Bermuda; hence, this evaluation was limited to the flight data received from that station.

Several problem areas were encountered because of the prolonged S-II powered flight time. The normal record periods are 85.04 seconds for S-IC/S-II separation and 58 seconds for S-II/S-IVB separation followed by a 100-second playback interval as determined by S-II stage onboard timer 3. This time sequencing was to ensure that the recorded calibrations occurring approximately 18 seconds prior to S-IC engine cutoff and approximately 18 seconds after S-II engine cutoff would be returned in addition to the separation data. However, since the S-II stage burned longer than nominal, the record intervals for recorders 1 and 2 during S-II/S-IVB separation were 103.93 and 99.48 seconds, respectively, rather than the nominal 58 seconds. It should also be noted that recorders 1 and 2 stopped recording 17.2 seconds and 6.82 seconds after S-II engine cutoff, respectively, instead of the nominal 23 seconds. The recorders were stopped at these times because tape on the supply reel was exhausted. Additionally, since the playback interval was limited to approximately 100 seconds and the recorders play back backwards neither the S-IC/S-II separation data nor the calibration 18 seconds prior to S-IC engine cutoff were retrieved during playback. No calibration data, therefore, were retrieved on tape recorder playback for comparison with the corresponding real time data.

To ensure that these problems encountered on AS-502 would not recur on subsequent flights, Master Change Record (MCR) 5669 has been initiated to disable timer 3 by tying back the output from the timer, thereby eliminating the 100-second limited playback interval. Although this would not rectify the failure to record the calibration cycle 18 seconds after S-II engine cutoff, which is a function of the amount of tape in the supply reel, it would ensure retrieval of S-IC/S-II separation data and the calibration cycle 18 seconds prior to S-IC engine cutoff. Presently the tape recorders are equipped with sufficient tape to cover a burn time approximately 40 seconds longer than nominal.

The analysis of the tape recorder system was accomplished by evaluating oscillograph recordings of continuous IRIG channels of BF1, BF2, and BF3 plus certain PAM channels of Multiplexers A1, A2, and A3. The present requirement is that the tape recorder playback shall be within 3 percent of the real time flight data.

The data on the continuous IRIG channels of BF1, BF2, and BF3 varied from the real time data only to the extent that additional noise was present on the signal. The amount of noise present during playback above that present during real time data was 2 percent for BF1 and BF2, and 1 percent for BF3. The PAM data also displayed a nominal data level difference on the order of 2 percent for multiplexers A1, A2, and A3. The comparison of the calibration levels for the IRIG channels plus the PAM channels was not performed since no calibration data were transmitted during playback due to the extended burn time.

The discrete measurements transmitted via the BT1 multiplexer were analyzed utilizing a 3 percent trend tab and oscillograph recordings. These were then compared with the PCM discrete tab for correlation between the two data links. Analysis revealed that the 120 sample per second discrete measurements correlated with the PCM data and the noise content did not exceed the 3 percent figure. The 12 sample per second discrete measurements transmitted via channels 24 through 27 of BT1 multiplexer, however, contained excessive noise not evident on the PCM data. Further analysis is required to resolve the source of the excessive noise. The calibration was not transmitted during playback.

19.4.3 S-IVB Stage Recorder

Three of the fourteen available tracks in the S-IVB tape recorder were utilized to record PAM/FM/FM links CF1, CF2, and CF3 during S-IC/S-II and S-II/S-IVB separation. The recorder was commanded to play back the recorded data after S-IVB first cutoff. Five of the 14 available tracks of the S-IVB tape recorder were utilized to record the PCM/FM telemetry link in orbit.

Tape recorder performance was generally good throughout the mission. S-IC/S-II separation data were not recovered due to the extended S-II burn time for reasons similar to those previously discussed on the S-II stage recorders. The tape recorder recorded all analog data on fast and slow record commands and played it back for the times specified with the exception noted above. Although the orbit was perturbed as a result of the S-IVB overspeed at first burn cutoff, the ground track timeline over receiver sites recording S-IVB tape recorder playback data apparently remained close to nominal since nearly 90 percent of the airborne recorded data was received on the ground.

19.4.4 Instrument Unit Recorder

One two-channel magnetic tape recorder recorded data from the IU DF1 and DF2 telemetry links during S-IC/S-II and S-II/S-IVB staging. The recorder responded properly to record and play back commands. The quality of the playback data received by Apollo Range Instrumented Aircraft (A/RIA) was poor, probably because of poor signal reception. S-IC/S-II staging data were not recovered due to the S-II extended burn time for reasons similar to those previously discussed on the S-II stage recorders.

19.5 RF SYSTEMS EVALUATION

The launch vehicle RF systems consist of telemetry, tracking (including C-Band, ODDP, Azusa/Glotrac and CCS), command, and television systems transmission and reception. Not all of the data required to perform a total RF analysis were available for this evaluation. Based on available data the overall performance of launch vehicle RF systems was good. Measured flight data with few exceptions agreed favorably with expected trends. Telemetry propagation was good, as was tracking performance. Due to the extended S-II burn period tape recorder playback was not accomplished, and data lost during S-IC/S-II staging were not recovered, as discussed in paragraph 19.4. Preliminary data indicated that the Command and Communications System performed well. Insufficient data were received to evaluate the video system.

19.5.1 Telemetry Systems RF Propagation Evaluation

The telemetry transmission system provided the means for transmitting modulated measurement data from the vehicle to the ground receiving stations. The RF carriers were chosen to provide an appropriate balance of data transmission capability to handle the quantities and varieties of data originating on the Saturn V vehicle. The performance of the telemetry systems on AS-502 was excellent.

Gross main engine effects causing attenuation and signal strength fluctuations were observed between 120 and 145 seconds at Cape Telemetry 4 (TEL 4) and Central Instrumentation Facility (CIF) as predicted. Grand Bahama Island (GBI) also experienced these effects due to separation flow up the side of the vehicle. The average attenuation at TEL 4 was about 20 to 25 decibels, which was less than the signal strength fluctuation experienced by Saturn I and IB vehicles and was comparable to AS-501.

A transient in signal level occurred at 133.3 seconds but did not result in any data loss. This transient was observed on the Instrument Unit DF1, DF2, DS1, and DP1 VHF telemetry links at GBI and is shown in Figures 19-1 and 19-2. No effects were observed at this time on the TEL 4 recorded data. This transient is discussed in detail in Section 9A.

A drop of approximately 8 decibels was observed on IU links DF1, DF2, DS1, and DP1 at 141.2 seconds. This drop in signal level was indicative of apparent antenna ionization problems. Antenna recovery on these links was observed at 165.5 seconds. A drop in signal level for 2 seconds similar to that experienced on AS-501 occurred at 146.0 seconds and resulted in loss of signal from the S-IC VHF telemetry at TEL 4, CIF, and GBI. VHF telemetry effects in the other stages were progressively less severe. Tape recorder playback data on the S-IC telemetry links at this time generally indicated an increase in reflected power and a decrease in forward power. The time of this anomaly followed within 1.3 seconds of S-IC inboard engine cutoff and appeared to be directly related to this event.

Staging effects at 149.1 seconds were as expected, resulting in VHF telemetry data loss to all supporting launch sites for approximately 1 second.

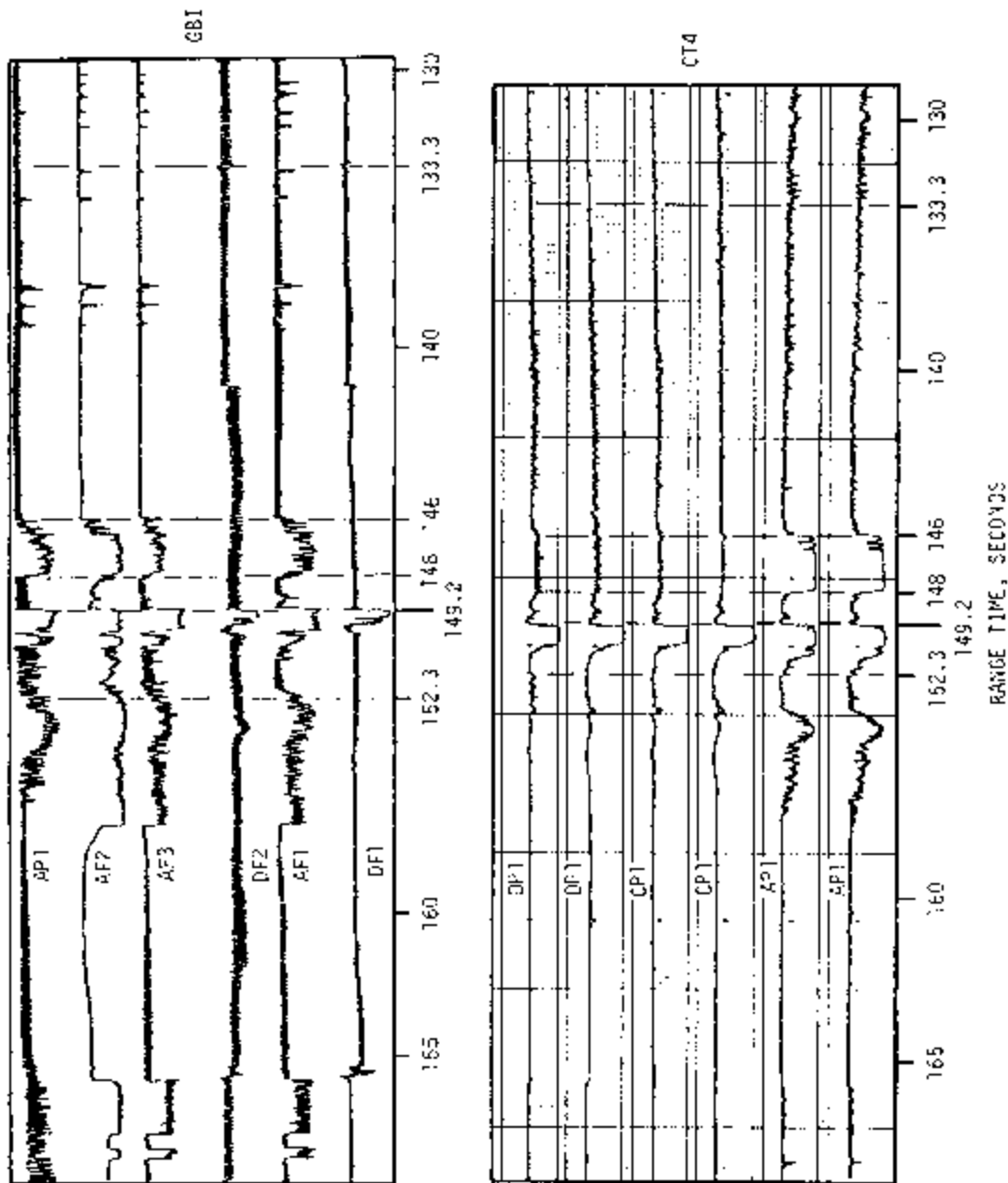


Figure 19-1. CT4 and GBI Telemetry Coverage

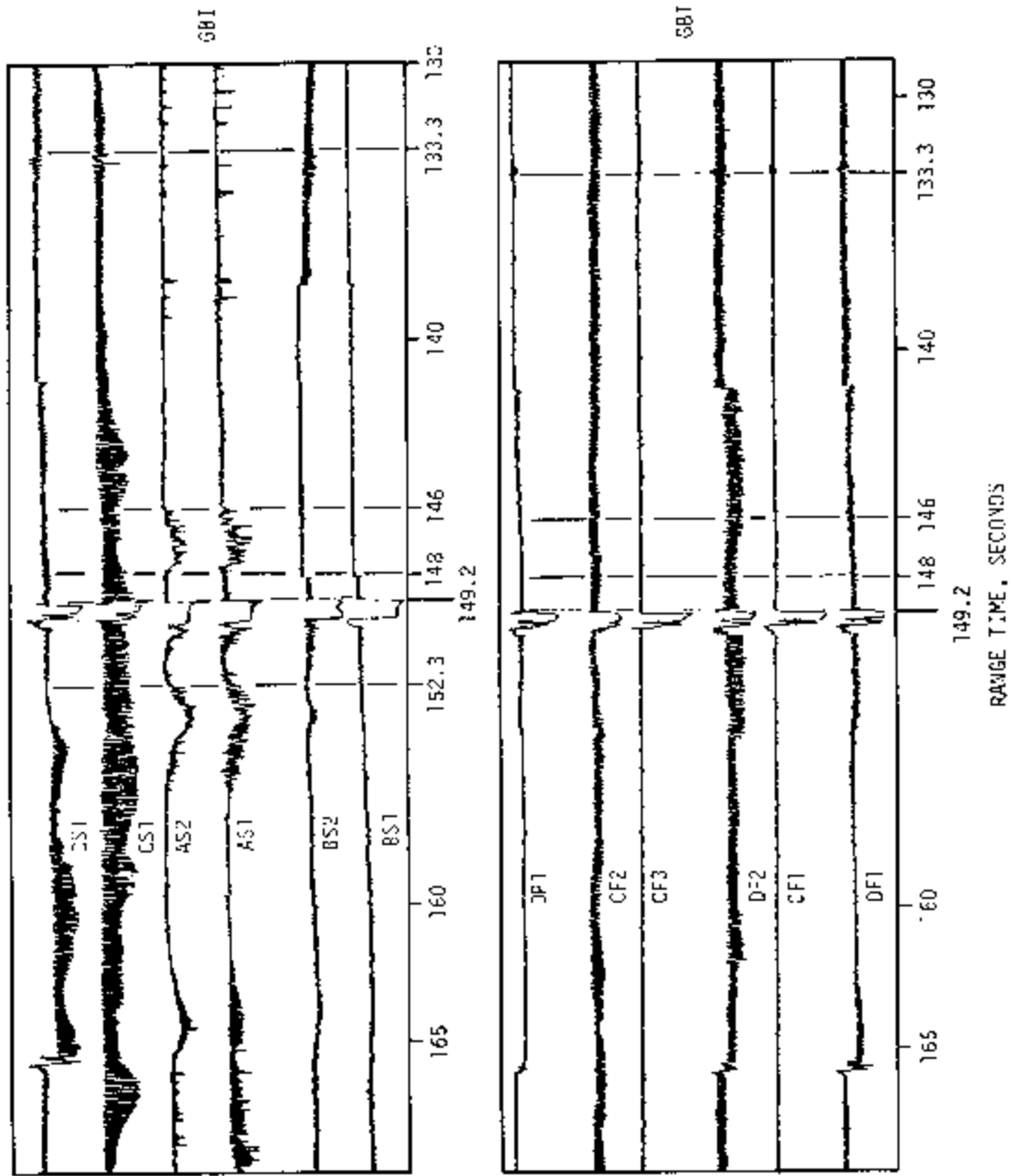


Figure 19-2. GBI Telemetry Coverage

S-II stage ignition effects on the VHF telemetry systems were observed at approximately 152 seconds. S-IC telemetry links experienced greater than 60 decibels attenuation at all sites and approximately 1 second data loss. S-II telemetry experienced attenuation up to 15 decibels, and the Instrument Unit and the S-IVB stage had up to 5 decibels attenuation at TEL 4 and CIF. No effects were observed at GBI for the S-II, S-IVB, and IU telemetry links.

Three drops in RF signal level occurred at 165.7, 168.1, and 169.5 seconds on S-IC links AF1, AF2, and AF3. Duration of these drops were 2, 0.4, and 1.6 seconds, respectively. Since these three links are transmitted through the same antenna system, it appears that this antenna system may have suffered an RF breakdown. This effect did not occur for the other S-IC VHF telemetry antenna system. The drops in signal level did not cause any loss in significant data since recovery to normal level occurred prior to tape recorder playback.

S-II second plane separation at 179 seconds resulted in approximately 25 decibels signal degradation of the S-II, S-IVB, and IU telemetry signal transmission to the Cape sites. Transmission to GBI was not affected.

Launch escape tower jettison did not result in any adverse effects to the RF telemetry transmission.

Ionospheric effects were as observed on previous flights, posing no threat to reception of telemetry data. This phenomenon resulted in signal fluctuation to those ground stations looking through the S-II exhaust plume and was presumed to have been caused by interaction of the plume and ionospheric layers.

Detailed analysis of S-IVB and IU telemetry data during the orbital flight phase was not accomplished because of insufficient orbital flight data at the time of this report.

A summary of telemetry coverage from launch to approximately 28,800 seconds is shown in Figure 19-3.

19.5.2 Tracking Systems RF Propagation Evaluation

The purpose of radio tracking was the determination of the vehicle's trajectory. The AS-502 vehicle carried several tracking transponders, as shown in Table 19-8.

Tracking performance throughout the flight was satisfactory, according to data received to date. No major anomaly occurred, although minor effects were observed which are being evaluated to determine the potential impact on systems performance and possible improvement for subsequent flights.

19.5.2.1 Offset Frequency Doppler (ODOP). The ODOP tracking system is a phase-coherent, multistation doppler tracking system which measures position of the vehicle equipped with the ODOP transponder. The ODOP transponder was carried in the S-IC stage of the vehicle, therefore ODOP tracking

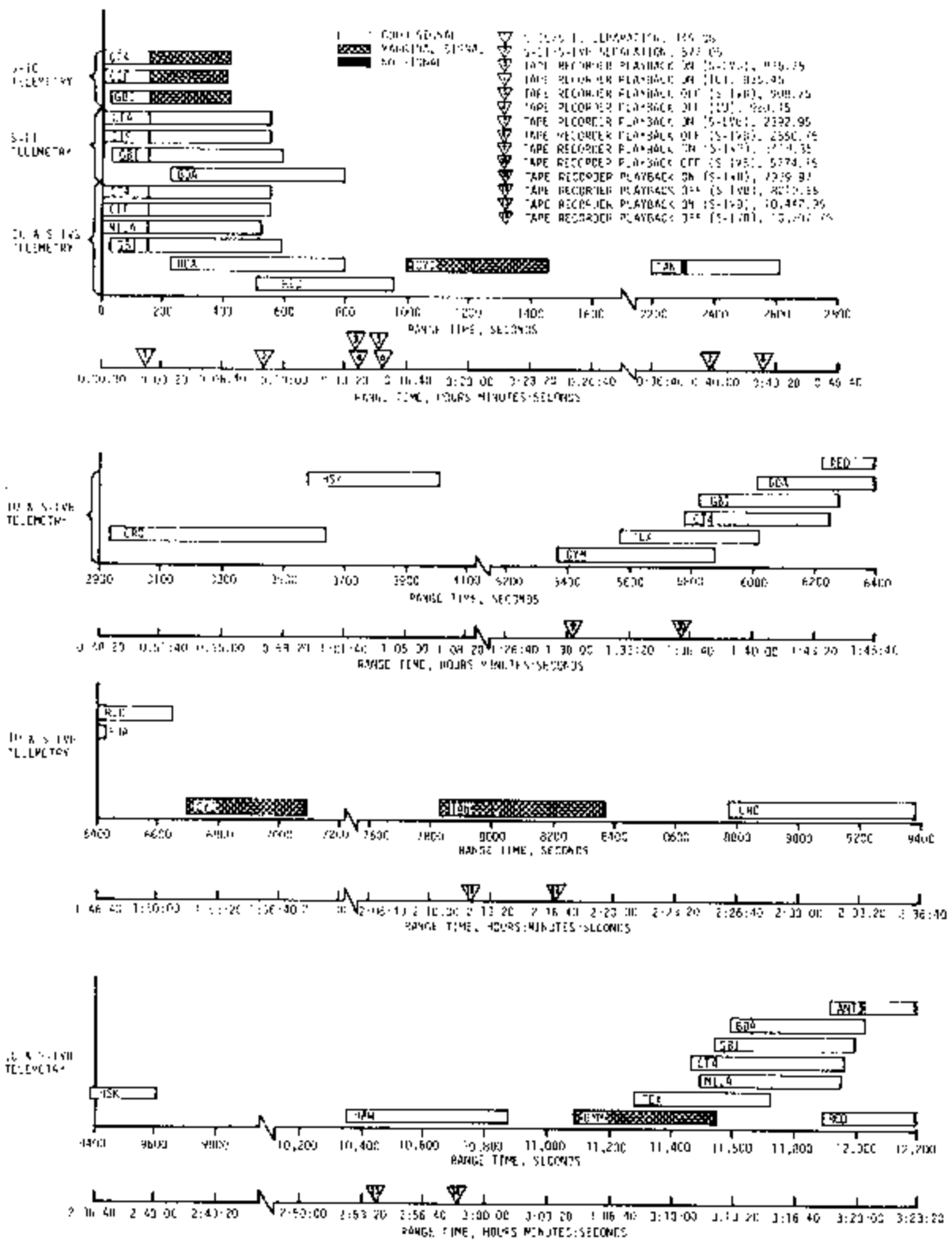


Figure 19-3. VHF Telemetry Coverage Summary, Sheet 1 of 2

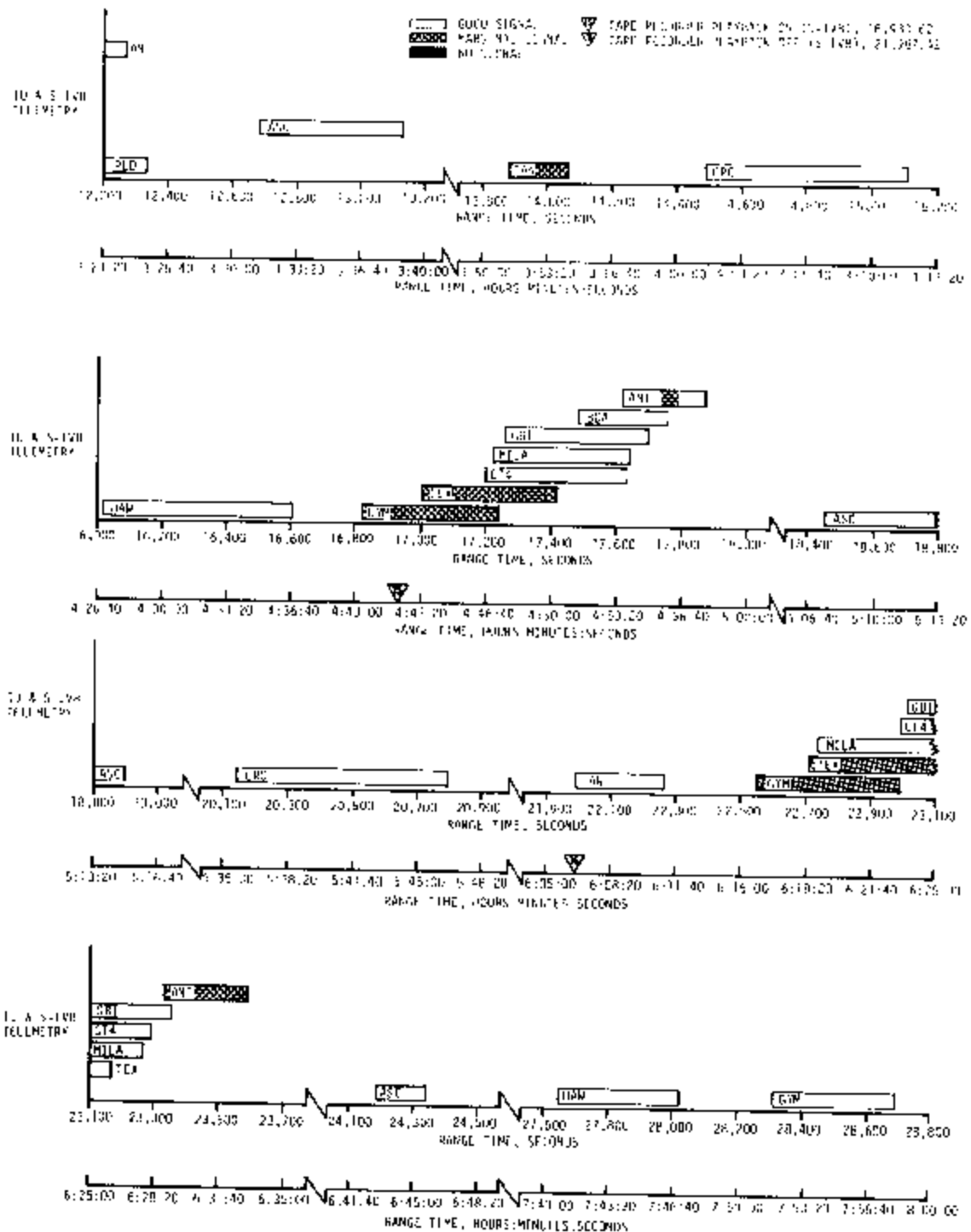


Figure 19-3. VHF Telemetry Coverage Summary, Sheet 2 of 2

Table 19-8. AS-502 Onboard Tracking Systems

VEHICLE LOCATION	SYSTEM	ONBOARD TRANSMITTER FREQUENCY (MEGAHERTZ)	ONBOARD RECEIVER FREQUENCY (MEGAHERTZ)
S-IC	ODOP	960	890
IU	Azusa/Glotrac	5000	5060.194
IU	C-Band Radar	5765	5690
IU	CCS	2282.5	2101.8

was limited to the flight of the first stage only. ODOP evaluation was based on limited data received from the MARGO station and telecon with KSC.

The ODOP tracking system obtained doppler data for trajectory analysis from vehicle liftoff until S-IC/S-II separation at 149 seconds. All ground stations maintained continuous track of the vehicle during this period.

The erratic data and large variation between predicted and actual ODOP transponder received signal strength experienced on AS-501 from 35 to 45 seconds did not recur on this flight.

S-IC main engine flame attenuation on the ODOP transponder up-link signal strength occurred from 80 seconds to S-IC/S-II separation. The flame effects were sufficiently severe during the period from 110 to 145 seconds to cause excessive phase modulation of the interrogator RF signal, thus causing noisy data at the various ODOP receiving stations. This also occurred during the AS-501 flight and resulted in poor ODOP tracking analysis after 110 seconds.

Phase lock between the ground interrogation station and the ODOP transponder was lost at S-IC/S-II separation due to staging flow field. Recovery was made shortly after staging, at approximately 154 seconds, compared to 194 seconds on AS-501.

19.5.2.2 Azusa/Glotrac. The Azusa/Glotrac is an interferometer tracking system using doppler and FM radar techniques to determine position, range, range rate, and range sum data with a high degree of accuracy. Because of the restricted number of ground stations, usage of the system is limited to coverage in the Cape Kennedy area.

The performance of the Azusa/Glotrac system appeared to be satisfactory and in accordance with nominal expectations. The Azusa Mark II station tracked the vehicle from liftoff to 200 seconds. The signal was marginal from 200 to 237 seconds, at which time the onboard transponder broke phase lock. Bermuda accepted active interrogation of the transponder at 253 seconds and maintained track until 724 seconds. About 35 seconds of data were

lost during handover to Bermuda. All data from the Grand Turk Glotrak station were lost because of a local oscillator malfunction at the ground station. Azusa/Glotrak tracking coverage from launch to 11,720 seconds is shown in Figure 19-4.

19.5.2.3 C-Band Radar. C-Band is a pulse radar system which used mono-pulse ground station equipment and was used for precise tracking during launch and orbit phases. Two C-Band radar transponders were carried in the IU to provide radar tracking capability independent of the vehicle attitude. The transponder received coded or single-pulse interrogation from ground stations and transmitted a single-pulse reply in the same frequency band. Each transponder radiated signals over a single transmit/receive antenna.

Insufficient data were received to compile a comprehensive analysis of the C-Band radar system throughout the mission in time for this report. However, available data indicated that performance of the C-Band radar was well within the requirement of the mission with the following exceptions:

- a. Data dropout occurred during second revolution at Bermuda and Redstone because of excessive azimuth rates and at Carnarvon because of site transmitter malfunction.
- b. Undesirable transponder response occurred during third revolution at Grand Turk Island and Redstone, with complete data loss at Bermuda.

The C-Band radar tracking coverage from launch to 17,100 seconds is shown in Figure 19-5.

19.5.3 Command Systems RF Evaluation

The AS-502 Command systems consisted of the Secure Range Safety Command System (SRSCS) and the Command and Communications System (CCS).

19.5.3.1 Secure Range Safety Command System. The SRSCS provided a means to terminate the flight of the vehicle by radio command from the ground in case of emergency situations in accordance with range safety requirements. Each powered stage of the vehicle was equipped with two command receivers/decoders and the necessary antennas to provide omnidirectional receiving characteristics.

Available data indicated that the SRSCS functioned properly during flight, and sufficient signal was received at all onboard receivers to have performed the assigned function had destruct been essential.

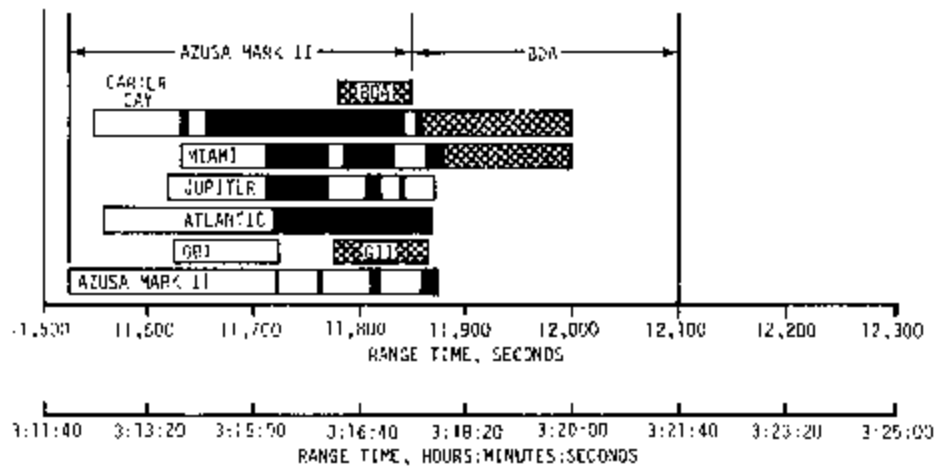
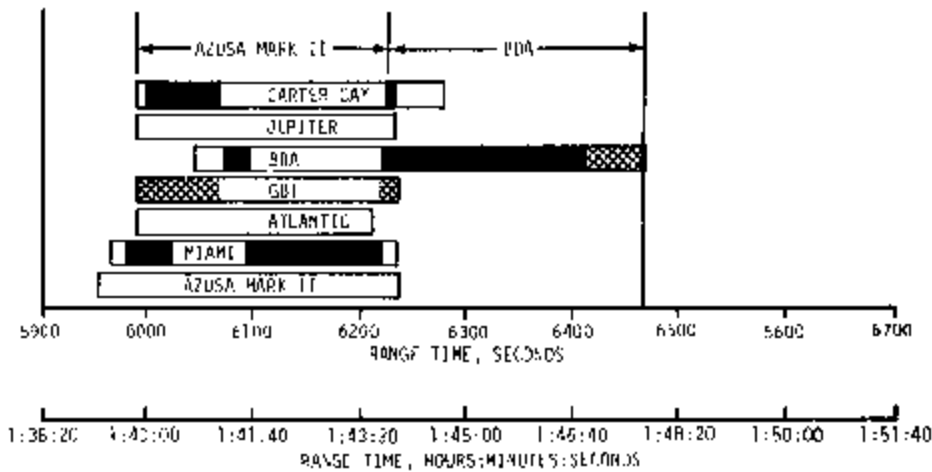
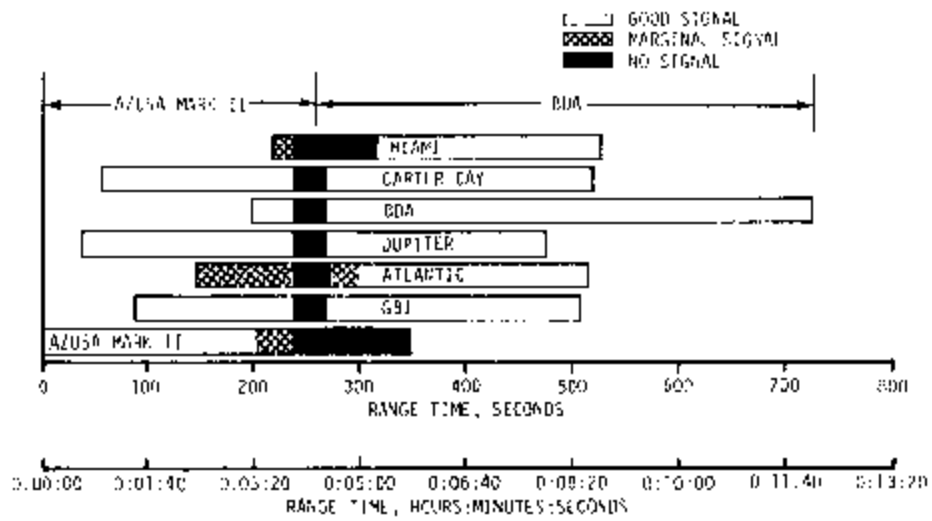


Figure 19-4. Azusa/Glotrac Coverage Summary

The S-IC camera impacted at approximately 7:10 a.m. EST and was recovered at 7:25 a.m. by helicopter from the recovery ship. The capsule was tracked by the SARAH beacon from impact time and recovery was made 46.3 to 55.6 kilometers (25 to 30 n mi) from the ship. Inspection showed that two of the ground planes for the radio beacon antenna were sheared off; three of the shroud lines in the drag skirt were broken; and the connector leaked, allowing water to enter the camera and wet the film. However, the film was still usable.

During recovery of the S-II cameras the beacon signal from one SARAH beacon was not sufficient for radar lock on, resulting in loss of one camera capsule. Drag flap and paraballoon, flashing light beacon, dye marker, and shark repellent operations were all satisfactory on the recovered capsule. The capsule landed within 13.45 kilometers (7.25 n mi) of the predicted impact point. The quartz window of the recovered capsule was shattered due to the impact attitude of the capsule, but there was no apparent damage to film as a result of the broken window. The redesigned antenna deployment performed satisfactorily on this camera.

Films from the TV cameras provided very good coverage.

19.6.2 Ground Engineering Cameras

In general, ground camera coverage was good. Seventy-five films from the Launch Complex 39A camera system were received and evaluated. Six items had unusable timing, one was an unusable track, and one was a bad exposure. In addition, five of the programmed cameras malfunctioned and did not acquire film data. As a result of the above failures, system efficiency was 84 percent.

The Eastern Test Range tracking cameras provided good coverage with the exception of an erratic track of the IGOR camera at Patrick Air Force Base. In addition, these data were provided on 35 mm film rather than on the 70 mm film requested. The tumble rate of the S-IC after separation would be difficult to determine from 35 mm film.

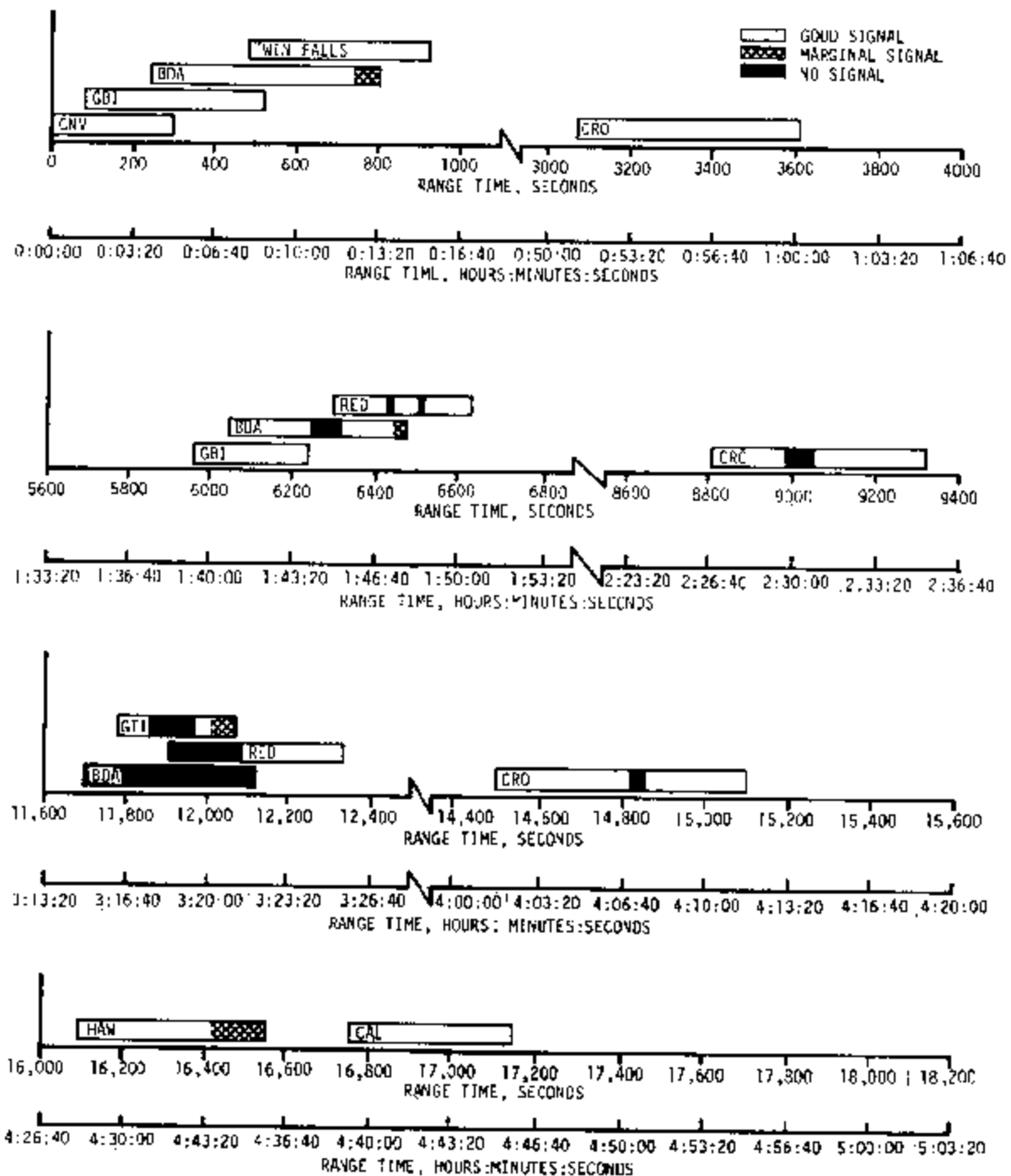


Figure 19-5. C-Band Radar Coverage Summary